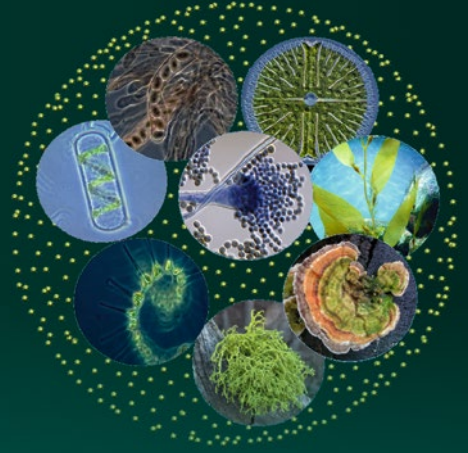


Advances in Environmental Microbiology 10



Christon J. Hurst  
*Editor*

# Microbial Metabolism of Metals and Metalloids

 Springer

# **Advances in Environmental Microbiology**

Volume 10

**Series Editor**

Christon J. Hurst  
Cincinnati, Ohio,  
USA

and

Universidad del Valle  
Santiago de Cali, Valle  
Colombia

This book series addresses the questions of which microbes, microbial genes and gene products are present at particular places and times, as well as the environmental transport and survival capabilities of microbes. The authors define the ways in which microorganisms interact chemically as well as physically with their surroundings, including microbial actions that change our planet's geochemistry. *Advances in Environmental Microbiology* facilitates an understanding of how microbes have contributed towards coevolutionary processes and addresses microbial contributions to the successional colonization of environmental locations. The explorations of topics include a microbiological perspective of public health, animal husbandry and agricultural issues, including consideration of the fact that infectious diseases are often either acquired from environmental reservoirs or transmitted through the environment, plus an explanation of how microbial establishment either on or within a host results in transformation of the colonization site into a microbially modified environment. This series also will include both microbial pest control and microbial diversity, along with insights into industrial production processes that are connected to environmental microbiology.

More information about this series at <https://link.springer.com/bookseries/11961>

Christon J. Hurst  
Editor

# Microbial Metabolism of Metals and Metalloids

 Springer

*Editor*

Christon J. Hurst  
Cincinnati, OH, USA

ISSN 2366-3324

ISSN 2366-3332 (electronic)

Advances in Environmental Microbiology

ISBN 978-3-030-97184-7

ISBN 978-3-030-97185-4 (eBook)

<https://doi.org/10.1007/978-3-030-97185-4>

© Springer Nature Switzerland AG 2022

This work is subject to copyright. All rights are reserved by the Publisher, whether the whole or part of the material is concerned, specifically the rights of translation, reprinting, reuse of illustrations, recitation, broadcasting, reproduction on microfilms or in any other physical way, and transmission or information storage and retrieval, electronic adaptation, computer software, or by similar or dissimilar methodology now known or hereafter developed.

The use of general descriptive names, registered names, trademarks, service marks, etc. in this publication does not imply, even in the absence of a specific statement, that such names are exempt from the relevant protective laws and regulations and therefore free for general use.

The publisher, the authors and the editors are safe to assume that the advice and information in this book are believed to be true and accurate at the date of publication. Neither the publisher nor the authors or the editors give a warranty, expressed or implied, with respect to the material contained herein or for any errors or omissions that may have been made. The publisher remains neutral with regard to jurisdictional claims in published maps and institutional affiliations.

Cover illustration: “Volvox reimagined” is a montage image created in 2015 and is being used with permission of the artist, Christon J. Hurst. Those images incorporated into this montage were: center image “Aspergillus flavus” (author: Hossein Mirhendi, image supplied by and used with author’s permission); clockwise from upper right “Micrasterias” (author: Rogelio Moreno Gill, image supplied by and used with author’s permission), “BrownGiantKelp3600ppx” (author: FASTILY, Creative Commons Attribution Share Alike 3.0 Unported license), “Stumpfungus” (author: Ecornerdropshop, public domain image), “Letharia vulpina JHollinger crop” (author: Jason Hollinger, Creative Commons Attribution-Share Alike 3.0 Unported license), “Phytoplankton - the foundation of the oceanic food chain”, (author: NOAA MESA Project, public domain image), “Spirogyra cell” (author: Jasper Nance, Creative Commons Attribution-Share Alike 3.0 Unported license), “Morelasci” (author: Peter G. Werner, Creative Commons Attribution-Share Alike 3.0 Unported license).

This Springer imprint is published by the registered company Springer Nature Switzerland AG  
The registered company address is: Gewerbestrasse 11, 6330 Cham, Switzerland



This image shows a cube cluster of the mineral pyrite protruding upward from marl matrix. Pyrite has a beautiful metallic luster and its chemical formula is  $\text{FeS}_2$  (iron (II) disulfide). This image is titled "Pyrite from Ampliación a Victoria Mine, Navajún, La Rioja, Spain 2.jpg". Its author is JJ Harrison (<https://www.jjharrison.com.au/>) and the image is being used under a Creative Commons Attribution-Share Alike 3.0 Unported license. Microbial metabolism of pyrite produces acid mine drainage and acid rock drainage

*During this lifetime I have been informally adopted by Ken Reed and Fred Kawahara, two gentleman who perceived me as a son. They helped to shape the person whom I have become and the memory of their presence continues with me as both an honor and a blessing.*

*I met Kenneth E. Reed Jr. in 1968, when I became a member of Boy Scout Troop 433 in Greenhills, Ohio. Ken was the lead Assistant Scoutmaster of that troop. He had been born during 1924 in Millinocket, Maine, and made the Dean's list in 1945 while studying at the University of Maine. Ken graduated from the University of Maine that spring and then came to Cincinnati, Ohio, where he subsequently worked on the development of turbine engines for 42 years at General Electric Aircraft Engines. During his youth, Ken had been an Eagle Scout. Eventually he encouraged 78 young men, including myself, to also earn that rank. Ken received the Silver Beaver Award which is the Boy Scouts of America's distinguished service award for leadership. He also received additional honors for his*

*community service including the Philippe Award from General Electric.*

*My biological father had begun working in South Vietnam at the beginning of 1968, and that left me needing someone who could seem like a father. Ken sensed my need, and I would imagine that during his years as Assistant Scoutmaster Ken informally adopted several scouts. One of the things which Ken did for the troop was to make leather patches for all of our hiking trips and camping trips. Those patches were made from new leather replacement soles for shoes and each boy who went on the trip received a patch for his personal collection. There were many times when Ken would invite me over to his house for making troop patches. He also helped me to cut the plywood pieces when I made a pair of speaker cabinets, and after the cabinets were finished Ken presented me with an album of classical piano music to be enjoyed through those new speakers.*

*There was a time when Ken was laid off from General Electric and that left him feeling tremendously unneeded. He called me on that day, inviting me over to his house to talk. I understood that Ken needed a son to whom he could describe what he was feeling.*

*Eventually, Ken was called back to his job and that helped him to again sense confidence in being useful.*

*Ken had a pottery studio in his basement. Decades later, in 1997, I built a pottery studio in the basement of the house where I still live. I told Ken about my pottery studio. He immediately came to my house, feeling proudly as any father possibly could be, to*



*inspect and approve the studio. During that visit he also gave to me a commemorative coin from the 1969 National Boy Scout Jamboree. He had remembered, through all of those intervening years, that I had gone to the Jamboree in 1969. Ken had been saving that commemorative coin for nearly 30 years in thinking of me. On that day he also gave to me a ceramic paperweight made in his basement pottery studio.*

*Eventually, there was a timepoint long after both of my own biological parents had died, when Father's Day was approaching and I felt tremendously discouraged because I needed a father. I knew exactly what to do! I sent a Father's Day greeting card to Ken and I then called him on Father's Day.*



*Kenneth E. Reed, Jr.*

*I met Fred Katsumi Kawahara in 1980 when I was a newly hired microbiologist at the U.S. Environmental Protection Agency in Cincinnati, Ohio. Fred was a chemist at the EPA. He was Nisei, born in Pennngrove, California, during 1921 to parents who had immigrated from Japan, and he was very proudly an American. Fred was in the middle of his university undergraduate education and living in Berkeley, California, when his family was ordered to spend the second world war*

*interred at Abraham Relocation Center which was a concentration camp in Utah. Their family was given the number 13508, and Fred was assigned 13508E.*

*Fred subsequently resumed his formal education, earning a Bachelor's degree with honors from the University of Texas in 1944. He then earned a Doctor of Philosophy from the University of Wisconsin in 1948, and became a postdoctoral fellow at the University of Chicago. Fred began his professional career as a chemist for the U.S. Department of Agriculture, he then worked for Standard Oil of Indiana, and later he worked for the Environmental Protection Agency, in Cincinnati. One of Fred's research projects was developing a process to precipitate usable metal ions from acid mine drainage contained in the Berkeley Pit, which is a former open pit copper mine in Butte, Montana.*

*Fred always called me Christon, as did my family, and he often said that I reminded him of his son. I still remember that his face would light up with a smile whenever he saw me. Fred always spoke kindly and gently, and I valued the fact that he constantly was encouraging. There were many times when he would ask how my scientific projects were progressing, and on each of those occasions he would remind me that I should be proud of my accomplishments. He certainly was proud of those accomplishments on my behalf.*



*Fred Katsumi Kawahara*

*Ken and Fred lovingly assumed the role of being a father to me. I treasure the fact that each considered me as if I were their son. It is with tremendous pride that I dedicate my efforts on this book to my fathers Kenneth E. Reed, Jr. and Fred Katsumi Kawahara.*

*Christon J. Hurst  
Cincinnati, OH*

# Series Preface

The light of natural philosophy illuminates many subject areas including an understanding that microorganisms represent the foundation stone of our biosphere by having been the origin of life on Earth. Microbes therefore comprise the basis of our biological legacy. Comprehending the role of microbes in this world which together all species must share, studying not only the survival of microorganisms but as well their involvement in environmental processes, and defining their role in the ecology of other species, does represent for many of us the Mount Everest of science. Research in this area of biology dates to the original discovery of microorganisms by Antonie van Leeuwenhoek, when in 1675 and 1676 he used a microscope of his own creation to view what he termed “animalcula,” or the “little animals” which lived and replicated in environmental samples of rainwater, well water, seawater, and water from snow melt. van Leeuwenhoek maintained those environmental samples in his house and observed that the types and relative concentrations of organisms present in his samples changed and fluctuated with respect to time. During the intervening centuries we have expanded our collective knowledge of these subjects which we now term to be environmental microbiology, but easily still recognize that many of the individual topics we have come to better understand and characterize initially were described by van Leeuwenhoek. van Leeuwenhoek was a draper by profession and fortunately for us his academic interests as a hobbyist went far beyond his professional challenges.

It is the goal of this series to present a broadly encompassing perspective regarding the principles of environmental microbiology and general microbial ecology. I am not sure whether Antonie van Leeuwenhoek could have foreseen where his discoveries have led, to the diversity of environmental microbiology subjects that we now study and the wealth of knowledge that we have accumulated. However, just as I always have enjoyed reading his account of environmental microorganisms, I feel that he would enjoy our efforts through this series to summarize what we have learned. I wonder, too, what the microbiologists of still future centuries would think of our efforts in comparison with those now unimaginable discoveries which they will have achieved. While we study the many wonders of microbiology, we also

further our recognition that the microbes are our biological critics, and in the end they undoubtedly will have the final word regarding life on this planet.



Christon J. Hurst in Heidelberg

Indebted with gratitude, I wish to thank the numerous scientists whose collaborative efforts will be creating this series and those giants in microbiology upon whose shoulders we have stood, for we could not accomplish this goal without the advantage that those giants have afforded us. The confidence and very positive encouragement of the editorial staff at Springer DE has been appreciated tremendously and it is through their help that my colleagues and I are able to present this book series to you, our audience.

Cincinnati, OH

Christon J. Hurst

# Preface

My personal introduction to the environmental outcome from microbial metabolism of minerals came when I was an undergraduate student in the laboratory of my science advisor J. Robie Vestal, at the University of Cincinnati. Robie took his research students on a field trip to the Appalachian coal mining region of southeastern Ohio so that we could see what acid mine drainage looked like and thus comprehend the environmental impact of that drainage.

Members of the bacterial genus *Acidithiobacillus* are acidophilic and most are obligate autotrophs in their natural environments. *Acidithiobacillus ferrooxidans* is able to derive energy from iron and sulfur. It can use iron sulfides such as marcasite and pyrite that are present in coal, and this microbe also grows in other natural deposits that include iron sulfides. The microbe produces ferric iron and sulfuric acid by metabolizing those minerals. *Acidithiobacillus thiooxidans* converts hydrogen sulfide into sulfuric acid which notably causes biogenic sulfide corrosion of concrete sewer pipes. Together, these two bacterial species contribute to the acid mine drainage which characteristically emanates from coal mines and iron mines. Acid rock drainage similarly can come from pyrite-rich rock that has been used as fill material for roadworks and mine reclamation. As you might imagine, mining operations for other metals including gold do similarly contribute in this way to acidification of local water sources when mine tailings containing iron sulfide minerals become exposed to a combination of microbes, oxygen, and water.

The pH of such drainage can be in the negative range and may kill virtually everything in its flow path. Those hazards which are associated with acidic drainage include contamination of groundwaters and surface waters. When the pH of that drainage and its receiving waters is increased sufficiently to reach above 3, the soluble iron ions precipitate as yellow-orange iron hydroxide which colloquially is known as yellow boy, and which we also call rust. Acidic drainage from other mineral deposits can contain such metals and metalloids as aluminium, arsenic, cadmium, chromium, cobalt, copper, lead, manganese, mercury, nickel, silver, and zinc. Limestone in the overburden can neutralize that acidity before the drainage emerges.

During that field trip from Cincinnati, Ohio, I saw the most disastrous scene that I could image. The drainage water from abandoned mines was in retention ponds and the pH of that water was so low that the iron still was in solution. The water in those ponds was completely black as were the water saturated standing remains of tree trunks which were visible above the pond water's surface. The leaves and branches of those trees had long since fallen into the water and it seemed as though the tree trunks still were standing only because they could not decay sufficiently to fall over.



This is an image of the Berkeley Pit abandoned mine in Butte, Montana. The image is titled "BerkeleyPit2.jpg" by author [Pahcal123](#) and it is being used under a [Creative Commons Attribution-Share Alike 4.0](#) license. The Berkeley Pit is an abandoned open pit copper mine which has become filled to a depth of 900 feet by groundwater that became acid mine drainage, the water has a pH of 2.5





This is a public domain image titled “Rio tinto river CarolStoker NASA Ames Research Center.jpg” by Carol Stoker at NASA. The description supplied with this image is “[Acid mine drainage](#) causes severe environmental problems in the Rio Tinto, Spain”. For part of its length, the water in this river has a pH of 2. The orange color is precipitated iron hydroxide



This is a public domain image titled “Iron hydroxide precipitate in stream.jpg” by D. Hardesty, USGS Columbia Environmental Research Center. The description supplied with this image is “Iron hydroxide precipitate (orange) in a Missouri stream receiving acid drainage from surface coal mining” and again, the orange color is precipitated iron hydroxide

The vast majority of elements are metals. There also are many additional elements that have been defined as metalloids, and they possess characteristics which are in

between those of metals and non-metals. Some of the metals and metalloids serve as key components for proteins including enzymes and for chlorophylls, with ions of those elements often facilitating electron transfers. Those required ions are needed in specified amounts, and the growth of microorganisms becomes limited when the intracellular availability of their required metal and metalloid ions either is too high or too low. Some of these same metals and metalloids serve as sources of energy when they are metabolized by microbes, including the metabolism that results in formation of acid mine and rock drainage. And yet, others of the metals and metalloids are toxic even to the microbes. The difference between those metals and metalloids which can be useful and even required, versus others which are toxic, depends upon the evolutionary history of the microbe being considered.

This book explains the metabolic processes by which microbes acquire and control the intracellular availability of their required metal and metalloid ions. The book also explains how intracellular concentrations of unwanted metal and metalloid ions successfully are limited. The authors additionally describe how microbes derive metabolic energy by changing the charge states of metal and metalloid ions.

The book is divided into four parts.

Part I provides an introduction to microbes, metals and metalloids.

It also helps our readers to understand the chemical constraints for transition metal cation allocation.

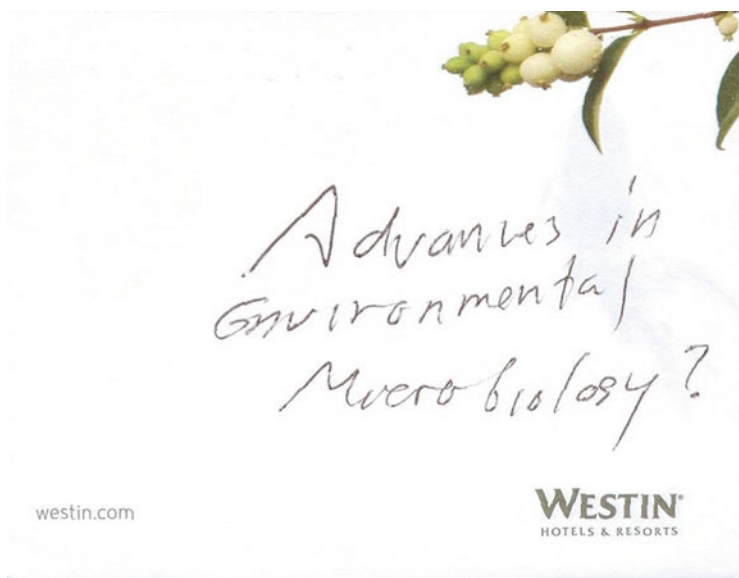
Part II explains that there are many commonalities in the basic processes which microbes use for metal transport. That part also explains the uses, as well as the challenges, associated with metal-based antimicrobials.

Part III gives our readers an understanding that because of microbial capabilities to process metals and metalloids, the microbes have become our best tools for accomplishing many jobs. These applications include the design of microbial consortia for use in bioleaching processes that recover metal and metalloid ions from industrial wastes. The synthesis of metal nanoparticles and similarly the synthesis of metalloid structures also are tasks ideally suited for the microbes.

Part IV explains that while commonalities can guide our understanding of the ways in which microbes process metals and metalloids, progressing through the alphabet from antimony and arsenic to zinc we can find unique attributes associated with the microbiology of these elements.

The first engineering book that I owned was a copy of the 1950 volume *Applied Sedimentation*, edited by Parker D. Trask. I chose that when my parents allowed me to select any book I wanted from a used book sale at my elementary school. Summer was beginning, I had just finished fifth grade, and considering that I then was 10 years old my parents likely were quite surprised by my selection of a book on geological engineering. I spent much of that summer giving my best effort at understanding Trask's book. That summer I also began learning to work with microorganisms by spending my mornings for 2 weeks in the bacteriology laboratory at what was then called Cincinnati General Hospital. That facility now is called University of Cincinnati Medical Center. Finally, at my present age of 67 years, I now have found usage for combining that information by editing this book titled "Microbial Metabolism of Metals and Metalloids".

During the evening of October 31, 2009 I started organizing my plans for beginning this book series. That effort was initiated by writing the planned series title on a piece of adhesive note paper supplied by the hotel in Washington, D.C., where I was staying. In the United States, we celebrate that evening as Halloween and it seemed to be an appropriate time for beginning such a potentially frightening project.



The beginning of *Advances in Environmental Microbiology* with words on a Post-it note, October 31 2009

Hannah Hensler encouraged me in those efforts, and in 2013 the series finally was accepted by Springer Nature. The photograph included in the series preface shows me in Hannah's office on July 19, 2013 as I was signing the contract which formally began this series *Advances in Environmental Microbiology*. Hannah assigned the coordination of this series to Andrea Schlitzberger. With her characteristic kindness, Andrea successfully helped me through the tasks of organizing the initial ten volumes of this series. I wish to thank Andrea Schlitzberger for her encouraging assistance and for her patience during my work on this book series. I frequently will remember Andrea, particularly every September when our common birthday occurs.



Dr. Andrea Schlitzberger

I also am thankful to the authors who very kindly contributed their collective time and knowledge to this book. With the publication of this volume I am retiring from the series *Advances in Environmental Microbiology* that I began those many years ago. My trust is that Springer Nature successfully will find a new series editor to skillfully carry this project into its future.

Cincinnati, OH

Christon J. Hurst

# Contents

## Part I Introduction

- 1 Metal Munching Microbes . . . . . 3**  
John F. Stolz
- 2 Chemical Constraints for Transition Metal Cation Allocation . . . . . 21**  
Dietrich H. Nies

## Part II Understanding Commonality of the Basic Processes

- 3 The Mosaic Landscape of Algal Metal Transport and Usage . . . . . 55**  
Crysten E. Blaby-Haas
- 4 Metal Based Antimicrobials: Uses and Challenges . . . . . 77**  
Daniel A. Salazar-Alemán and Raymond J. Turner

## Part III When Microbes are the Best Tool for the Job

- 5 Microbial Consortium: A Promising Strategy for Bioleaching of Metals from Industrial Wastes . . . . . 109**  
Mital Chakankar and Hocheng Hong
- 6 Molecular Mechanisms that Mediate Microbial Synthesis of Metal Nanoparticles . . . . . 135**  
Ankit Banik, Meyappan Vadivel, Moumita Mondal, and Natarajan Sakthivel
- 7 Bacterial Production of Metal(loid) Nanostructures . . . . . 167**  
Nikhil Pradhan and Raymond J. Turner

## Part IV Uniqueness of the Elements

- 8 Microbes: Key Players of the Arsenic Biogeochemical Cycle . . . . . 197**  
Rimi Biswas and Angana Sarkar

<b>9</b>	<b>Microbial Transformations of Antimony</b> . . . . .	223
	Huaqing Liu, Weimin Sun, and Max M. Häggblom	
<b>10</b>	<b>Microbial Remediation of Chromium</b> . . . . .	255
	M. Gomathy, K. G. Sabarinathan, K. S. Subramaian, T. Sivashankari Devi, K. Ananthi, P. Kalaiselvi, and M. Jeyshee	
<b>11</b>	<b>Microbial Interactions with Gold and Uranium</b> . . . . .	279
	Sadia Ilyas, Hyunjung Kim, and Rajiv Ranjan Srivastava	
<b>12</b>	<b>Prokaryotic Ferrous Iron Transport: Exploiting Pools of Reduced Iron Across Multiple Microbial Environments</b> . . . . .	299
	Alex E. Sestok, Mark A. Lee, and Aaron T. Smith	
<b>13</b>	<b>Pterin-Containing Microbial Molybdenum Enzymes</b> . . . . .	359
	Mikayla C. Metzger and Partha Basu	
<b>14</b>	<b>Microbial Metabolism of Nickel</b> . . . . .	417
	Robert P. Hausinger	
<b>15</b>	<b>Microbial Transformation of Silicon in Soil</b> . . . . .	503
	Kalyanasundaram Geetha Thanuja, V. S. Reddy Kiran Kalyan, Subburamu Karthikeyan, and Savariappan Anthoniraj	
<b>16</b>	<b>Microbial Interactions with Titanium</b> . . . . .	527
	Lori Çobani and Ann M. Valentine	
<b>17</b>	<b>Microbial Tungsten Assimilation</b> . . . . .	545
	Tetyana Milojevic	
<b>18</b>	<b>Vanadium-Based Transformations Effected by Algae and Microbes</b> . . . . .	563
	Dieter Rehder	
<b>19</b>	<b>How is a Zinc Ion Correctly Allocated to a Zinc-dependent Protein?</b> . . . . .	579
	Dietrich H. Nies	

**Part I**  
**Introduction**



# Chapter 1

## Metal Munching Microbes



**John F. Stolz**

**Abstract** Life has been a powerful geologic force, shaping the world as we know it today. Microbes in particular have played a crucial role in this transformation, through their metabolic diversity and mineral interactions. Microbes use over 50 elements, including metals and metalloids, for a variety of cellular functions including structure, energy generation, and metabolism. Starting from a few basic metal centers, namely iron-sulfur clusters, porphyrin, and pyranopterin, microbes developed the great variety of electron transfer components, bacteriochlorophylls and chlorophylls, and enzymes (i.e., dehydrogenases, oxidases, and reductases). Microbe-mineral interactions gave rise to extracellular electron transfer (EET) including direct interspecies electron transfer (DIET) and long-distance electron transfer (LDET). High throughput DNA sequencing projects have revealed a much larger global microbiome with the discovery of “microbial dark matter” and the “rare biosphere”. This review will provide a brief overview of microbes and metals and how their intimate relationship has impacted the evolution of life on Earth.

### 1.1 Introduction

The world we live in today is a far cry from what it was in the ancient past. The composition of the Earth’s lithosphere, atmosphere, and hydrosphere have been changed dramatically over time by life. The current atmosphere is out of chemical equilibrium with the amount of oxygen and the variety of reduced gases present. It is estimated that there exist over 1500 different minerals in the crust due to the coexistence of oxidizing and reducing conditions (Hazen et al. 2008). Microorganisms are the prime culprits due to their long intimate relationship with their environment and especially with minerals (Weiss et al. 2016). It has been postulated that the origin of life itself was the result of a protocell interacting with mineral surfaces,

---

J. F. Stolz (✉)

Duquesne University, Department of Biological Sciences, Center for Environmental Research and Education, Pittsburgh, PA, USA

e-mail: [stolz@duq.edu](mailto:stolz@duq.edu)

especially iron-sulfur, in alkaline hydrothermal systems (Lane and Martin 2012; Jordan et al. 2019). Early microbe-mineral interactions are preserved in Archean aged rocks such as banded iron formations, laminated carbonates, and stromatolites (Fru et al. 2013; Hofmann 2000). Over time, the global microbiome has expanded and exploited the rich diversity of elements present on the planet, creating a plethora of biochemical pathways many mediated by proteins with metal centers. Microbial diversity has been facilitated by modifications of metal-containing cofactors such as porphyrin, heme, iron-sulfur clusters, and pyranopterin, that expanded their functionality. In life's insatiable quest for energy, microbe-mineral interactions have given rise to extracellular electron transfer (EET). Today, the global microbiome may be comprised of over a trillion species (Whitman et al. 1998; Locey and Lennon 2016). Deep sequencing metagenome projects are revealing the true extent of this diversity, exploring "microbial dark matter" and the "rare biosphere" (Rinke et al. 2013; Solden et al. 2016; Sogin et al. 2006). This review will provide a brief overview of how microbes have exploited the elements in the periodic table, examples of metal cofactors that have been modified for functionality, mechanisms of EET, and the implications for the global microbiome with respect to metals in biology and the evolution of life on Earth.

## 1.2 The Microbial View of the Periodic Table

The elements that make up the periodic table can be generally grouped into metals, metalloids, and non-metals. Non-metals include the main constituents of life, C, N, O, S, and P as well as the halogens (e.g., F, Cl, Br, I) and noble gases (e.g., He, Ne, Ar, Kr, Xe, Rn). The metalloids are B, Si, Ge, As, Se, Sb, and Te. There has been some debate whether Se is a non-metal or a metalloid as it has properties of both (Goldsmith 1982; Vernon 2013). Regardless, the recognition of its importance in biology continues to grow (Wells and Stolz 2020; Wells et al. 2021). The radionuclides Po and At have also been considered metalloids. The rest of the elements may be considered metals, with the denser of those being heavy metals. All the elements (with the exception of Tc) with an atomic number up to and including 83 (Bi), are stable and remarkably, more than half of them have a function in biology (Table 1.1). Tc and the elements from 84 (Po) are not stable (Helmenstine 2021). Nevertheless, some radioactive elements, such as U and Pu, are known to undergo microbially mediated oxidation/reduction reactions (Lovley et al. 1991; Icopini et al. 2009). The University of Minnesota Biocatalyst/Biodegradation Database (Wackett et al. 2004; Gao et al. 2010), which is a compendium of pathways and now maintained by the Swiss Federal Institute of Aquatic Science and Technology, currently lists 86 bioactive elements ([eawag-bbd.ethz.ch/periodic/](http://eawag-bbd.ethz.ch/periodic/)). However, 58 elements are indicated as "may be bound, transported, reduced, and/or methylated". Here, Table 1.1 lists 51 elements, an example of an organism and the biological process involved. These include use for cell structure, energy generation (i.e., photosynthesis, fermentation, respiration), anabolism, resistance (i.e., methylation, biosorption), and

**Table 1.1** A microbes view of the periodic table

Non-metals	Element	Microbe	Process/function	References
Non-metals	Hydrogen	<i>Clostridium</i>	Fermentation	Gadd (2010)
	Carbon	<i>Achromatium</i>	Assimilation	Gray et al. (2000)
	Nitrogen	<i>Rhizobium</i>	N <sub>2</sub> fixation	Burke and Burris (1941)
	Oxygen	<i>Anabaena</i> sp.	Photosynthesis	De Las Rivas et al. (2003)
	Sulfur	<i>Shewanella</i> sp.	Respiration	Moser and Nealson (1996)
	Phosphorus	<i>Escherichia coli</i>	Gene regulation	Wanner (2004)
Halogens	Fluoride	<i>Nitrosomonas europaea</i>	Oxidation	Hyman et al. (1994)
	Chloride	<i>Dechloromonas agitata</i>	Chlorate respiration	Achenbach et al. (2001)
	Bromide	<i>Marinomonas mediterranea</i>	Dehalogenation	Gamal et al. (2016)
	Iodine	<i>Roseovarius</i> sp.	Oxidation	Yuliana et al. (2017)
Metalloids	Boron	<i>Vibrio harveyi</i>	Quorum sensing	Chen et al. (2002)
	Silicon	<i>Thalassiosira pseudonana</i> <sup>a</sup>	Structural	Heintze et al. (2020)
	Germanium	<i>Bacillus cereus</i>	Biosorption	Van Dyke et al. (1989)
	Arsenic	<i>Sulfurospirillum arsenophilum</i>	Respiration	Ahmann et al. (1994)
	Selenium	<i>Bacillus selenitireducens</i>	Respiration	Wells et al. (2019)
	Antimony	<i>Stibiobacter senarmonii</i>	Oxidation	Li et al. (2016)
	Tellurium	<i>Shewanella oneidensis</i>	Reduction	Klonowska et al. (2005)
Metals	Lithium	<i>Glutamicibacter nicotianae</i> (formerly <i>Arthrobacter nicotianae</i> )	Biosorption	Tsuruta (2005)
	Sodium	<i>Acidaminococcus fermentans</i>	Decarboxylation	Dimroth (1987)
	Magnesium	<i>Clostridium perfringens</i> (formerly <i>Clostridium welchii</i> )	Cell division	Webb (1953)
	Aluminum	<i>Pseudomonas fluorescens</i>	Detoxification	Appanna and Hamel (2006)
	Potassium	<i>Escherichia coli</i>	Metabolism	Lester (1957)
	Calcium	<i>Emiliania huxleyi</i> <sup>a</sup>	Structural	

(continued)

**Table 1.1** (continued)

Non-metals	Element	Microbe	Process/function	References
				Haunost et al. (2020)
	Vanadium	<i>Pseudomonas isachenkovii</i>	Reduction	Antipov et al. (2000)
	Chromium	<i>Desulfovibrio vulgaris</i>	Reduction	Humphries and Macaskie (2002)
	Manganese	<i>Shewanella oneidensis</i>	Respiration	Myers and Nealson (1988)
	Iron	<i>Geobacter metallireducens</i>	Respiration	Lovley and Phillips (1988)
	Cobalt	<i>Salmonella enterica</i> subsp. <i>enterica</i> serovar <i>Typhimurium</i>	Corrinoid synthesis	Santander et al. (1997)
	Nickle	<i>Methanobacterium thermoautotrophicum</i>	Methanogenesis	Diekert et al. (1981)
	Copper	<i>Achromobacter cycloclastes</i>	Nitrite reductase	Li et al. (2014)
	Zinc	<i>Escherichia coli</i>	Co-factor	Blencowe and Morby (2003)
	Strontium	<i>Closterium moniliferum</i> <sup>a</sup>	Structural	Krejci et al. (2011)
	Molybdenum	<i>Cereibacter sphaeroides</i> (formerly <i>Rhodobacter sphaeroides</i> )	Co-factor	Hille (1996)
	Palladium	<i>Desulfovibrio desulfuricans</i>	Biosorption	Lloyd et al. (1998)
	Silver	<i>Pseudomonas aeruginosa</i>	Biosorption	Mullen et al. (1989)
	Cadmium	<i>Conticribra weissflogii</i> <sup>a</sup> (formerly <i>Thalassiosira weissflogii</i> )	Co-factor	Lane and Morel (2000)
	Tin	Bacteria	Methylation	Hallas et al. (1982)
	Cesium	<i>Synechocystis</i> sp. PCC 6803	Intracellular	Avery et al. (1991)
	Barium	<i>Closterium moniliferum</i> <sup>a</sup>	Structural	Krejci et al. (2011)
	Tungsten	<i>Moorella thermoacetica</i>	Co-factor	Andreesen and Makedssi (2008)
	Platinum	<i>Desulfovibrio desulfuricans</i>	Reduction	de Vargas et al. (2003)
	Gold	<i>Geobacter metallireducens</i>	Reduction	Kashefi et al. (2001)

(continued)

**Table 1.1** (continued)

Non-metals	Element	Microbe	Process/function	References
	Mercury	<i>Desulfovibrio desulfuricans</i>	Methylation	Choi et al. (1994)
	Thallium	Bacteria	Methylation	Schedlbauer and Heumann (2000)
	Lead	<i>Pseudomonas marginalis</i>	Export	Roane (1999)
Radionuclides	Technetium	<i>Shewanella putrefaciens</i>	Respiration	Wildung et al. (2000)
	Polonium	<i>Bacillus</i> sp. strain 6A	Methylation	Bahrou et al. (2012)
	Radium	<i>Citrobacter freundii</i>	Biosorption	Satvatmanesh et al. (2003)
	Uranium	<i>Geobacter metallireducens</i>	Respiration	Lovley et al. (1991)
	Neptunium	<i>Pseudomonas fluorescens</i>	Biosorption	Songkasiri et al. (2002)
	Plutonium	<i>Geobacter metallireducens</i>	Reduction	Icopini et al. (2009)

<sup>a</sup>Protist

biomineralization (Raab and Feldmann 2003). The need for essential elements has led to a diversity of strategies for assimilation, dissimilation, and dismutation (Stolz and Oremland 2011; Staicu and Stolz 2021). An example of a metal, in this case Fe, used for structure and function is the magnetosome of magnetotactic bacteria (Stolz 1993). These bacteria are able to assimilate soluble Fe to precipitate single-domain particles of magnetite (Fe<sub>3</sub>O<sub>4</sub>), often aligned in chains, that allow them to orient in the Earth's magnetic field (Blakemore 1975). The size, shape, and composition of these particles are tightly regulated (Mueller et al. 2020a, b). Large populations (i.e., 10<sup>5</sup> /g) can impart natural magnetic remanence to the sediments in which the reside (Stolz et al. 1986).

Microbes are particularly good at exploiting metals and metalloids for energy generation. Mn and Fe are the most important metals in the environment being used as terminal electron acceptors (TEAs) as reflected in the canonical vertical zonation observed in sediments and stratified water columns: O<sub>2</sub> > NO<sub>3</sub><sup>-</sup> > Mn<sup>4+</sup> > Fe<sup>3+</sup> > SO<sub>4</sub><sup>2-</sup> > CO<sub>2</sub> (Lloyd 2003; Gadd 2010; Lovley 1988). An increasing number of bacteria have been documented to use antimony, arsenic, selenium (both selenate and selenite), and tellurium in anaerobic respiration (Albin and Hollibaugh 2014; Li et al. 2016; Ahmann et al. 1994; Switzer Blum et al. 2016; Baesman et al. 2007). Thus, for a given environment, the consumption of available electron donors and organic matter may be impacted by the presence of other of TEAs such as oxyanions of Cr, As, and Se (Newman et al. 1998). Arsenic is a case in point. Originally, the microbial oxidation, reduction, and methylation of inorganic arsenic was thought to be primarily for resistance and detoxification. We now know however, that arsenic oxyanions can be used in anaerobic respiration with arsenite serving as an electron

donor or with arsenate serving as an electron acceptor (Oremland and Stolz 2003; Stolz et al. 2006). Environments with elevated arsenic concentrations, such as Searles Lake and Mono Lake in California, support an ecology based on arsenic cycling (Oremland et al. 2004, 2005). Mono Lake is home not only to a chemolithoautotrophic arsenite oxidizing bacterium, *Alkalilimnicola ehrlichii*, but also to strains of *Ectothiorhodospira* that are capable of light dependent arsenite oxidation (i.e., arsenite serves as an electron donor to photoautotrophy) (Hoeft et al. 2007; McCann et al. 2017; Kulp et al. 2008; Zargar et al. 2012). On the farm, the organoarsenical, 3-nitro-4-hydroxybenzene arsonic acid (aka roxarsone, a chicken growth hormone and antibiotic) can be respired for growth by the strict anaerobic *Alkaliphilus oremlandii* (Stolz et al. 2007). Some bacteria have even used the toxicity of arsenic to their advantage, warding off other microbes. The methylarsenical arsinothricin [2-amino-4-(hydroxymethylarsinoyl) butanoate], otherwise known as AST, produced by *Burkholderia gladioli* strain GSRB05, has been shown to have broad-spectrum antibiotic activity against both Gram positive and Gram negative bacteria (Chen and Rosen 2020). Over a dozen proteins are now known to be involved in microbial arsenic metabolism including oxidases (Aio, Arx), reductases (Arr, ArsC), methyltransferases (ArsM), efflux pumps (ArsB, ArsJ, ArsK, ArsP), and transcriptional regulators (ArsD, ArsR, AioS, AioR) as well as an As-C lyase (ArsI) (McDermott et al. 2020; Chen and Rosen 2020). A recent survey of arsenic genes in the microbiome of the human gastro-intestinal tract revealed arsenic genes throughout, a finding that may have implications for human health (McDermott et al. 2020). Arsenic has played a role in the evolution of life on Earth and arsenic-based ecosystems have even been proposed for other planetary bodies and their satellites in our solar system (Oremland et al. 2009).

### 1.3 The Biochemist's Tool Box

Microbes are the great inventors of biochemical pathways, whether to synthesize unique compounds in self-defense (e.g., antibiotics), or metabolize a wide range of carbon substrates for cell growth. Metalloproteins and their co-factors play a key role in many of these pathways, especially in energy generation. As illustrated in the previous section, metals are an integral part of the cell and define the “metalloproteome” (Yannone et al. 2012). Metal binding proteins, such as glutathione, are essential for cellular redox balance (Smirnova and Oktyabrsky 2005). Non-heme proteins such as bacterioferritin are important for iron homeostasis and storage (Rivera 2017). Proteins with metal centers, often bound to co-factors, perform critical cell functions. In what has been referred to as the “redox protein construction kit” and the “LEGO brick metaphor” for basic protein structure, the idea is that a group of key metal centers and co-factors serve as the guts, and have through evolution given rise to a diversity of metalloproteins (Baymann et al. 2002; Levy 2017). These metalloproteins can catalyze reactions for catabolism and anabolism, function in oxidation/reduction reactions (e.g., oxygen atom transfer), and

electron transfer. Their substrate specificity and redox potential can be modified by the protein milieu that surrounds the metal center. The Last Universal Common Ancestor (LUCA) to all cell types (Bacteria, Archaea, Eukarya) is believed to have had a simple metabolism similar to the Wood-Ljungdahl (acetyl-CoA) pathway with a number of metalloproteins containing one or more of the following metal centers: flavin, iron-sulfur clusters, porphyrin, pyranopterin (Sousa et al. 2013).

Flavins can be involved in electron transfer in the form of flavin mononucleotide (FMN) and flavin adenine dinucleotide (FAD) often as a co-factor in FMN and FAD dependent reactions (Mansoorabadi et al. 2007). Iron-sulfur clusters, which also function in electron transfer, come in a variety of forms including 2Fe-2S, 3Fe-3S, 3Fe-4S, 4Fe-4S, 8Fe-7S and 8Fe-8S (Johnson et al. 2005; Brzoska et al. 2006; Zanello 2018). They range from the small 2Fe-2S Rieske subunit of arsenite oxidase (AioB), to the large MoFe center of nitrogenase, which has 7Fe and 8S (Ellis et al. 2001; Burges and Lowe 1996). Flavodoxins and ferredoxins can serve as low potential electron carriers (Campbell et al. 2019). Iron-sulfur clusters can be found in catalytic subunits and in electron transfer subunits. For dissimilatory arsenate reductase, Arr, the catalytic subunit, ArrA, contains one 4Fe-4S cluster along with the molybdenum cofactor, while the smaller subunit, ArrB, that transfers electrons from a membrane anchoring subunit (ArrC) to ArrA, has four 4Fe-4S clusters (Glasser et al. 2018). Succinate dehydrogenase has three different iron-sulfur clusters in its beta subunit (SdhB) organized in a linear arrangement 2Fe-2S → 4Fe-4S → 3Fe-4S, each with a different redox potential (Janssen et al. 1997; Zanello 2018).

Porphyrin is a precursor to several cofactors including corrin, heme, and the chlorophylls (Dayan and Dayan 2011). Corrin is used to make vitamin B<sub>12</sub> (Santander et al. 1997). Hemes come in a variety of types and are found in cytochromes including cytochromes a, b, c, d, and o (Reedy and Gibney 2004). The number of hemes can vary dramatically, from monoheme, such as horse heart cytochrome c, to the multiheme cytochrome c involved in nitrate respiration in *Geobacter metallireducens* (Bushnell et al. 1990; Naik et al. 1993). Further, the number of heme proteins in a bacterium can number from just a few to over a hundred. Dissimilatory metal-reducing bacteria are particularly loaded with c-type cytochromes. It's been reported that *Shewanella oneida* may have as many as 42 c-type cytochromes (Heidelberg et al. 2002; Meyer et al. 2004) while *G. metallireducens* and *Geobacter sulfurreducens* number over 100 (Aklujkar et al. 2009; Methe et al. 2003). This overabundance of c-type cytochromes common in *Geobacter* species can lead to an insatiable need for Fe (i.e., μM amounts), as reported for *G. metallireducens* even when nitrate is used as the terminal electron acceptor (Senko and Stolz 2001).

Chlorophylls (Chl) and Bacteriochlorophylls (BChl) have the basic porphyrin structure and a magnesium ion (Scheer 2006). They are an example of how modification of a central core (i.e., porphyrin) can be tuned to absorb a particular wavelength of light by the addition of different side groups as well as the proteins that cradle it (Chew and Bryant 2007). There are six bacteriochlorophylls BChl *a*, BChl *b*, BChl *c*, BChl *d*, BChl *e*, and BChl *g*. While the maximum absorption peak may be similar when extracted, the in vivo absorption maximum is red-shifted.

Methanol extracted BChl *a*, for example, has an absorption maximum of 773 nm, but in vivo it may range from 800 nm to 890 nm depending on the location in the cell and the protein environment that encapsulates it (Ritchie 2018). BChl *a* and *b* are found in the reaction center of purple (either BChl *a* or BChl *b*) and green phototrophic bacteria (BChl *a*) (Stolz 1990). BChl *a* can also be part of the light harvesting structures in both purple and green phototrophic bacteria. BChl *c* (740 nm in vivo), BChl *d* (720 nm in vivo), and BChl *e* (714 nm in vivo) are associated with the light harvesting structure (i.e., chlorosome) of green phototrophic bacteria, while BChl *g* is found only in Heliobacteriaceae (Stolz 1990). Chlorophylls are found in cyanobacteria and chloroxybacteria, and include Chl *a*, Chl *b*, Chl *d*, and Chl *f* (Chen and Blankenship 2011). The typical “Z” scheme for photosynthesis with photosystems I and II uses Chl *a* that absorbs at 680 nm (PS I) and 700 nm (PS II), respectively. Chl *f* can absorb light in the near infrared and is found in red-light adapted cyanobacteria (Chen et al. 2010, 2012). Far-red light adapted cyanobacterial species chromatically adapt their PS I and PS II with Chl *f* that absorbs at 745 nm (PS I) and 727 nm (PS II), respectively (Nuernberg et al. 2018). In natural systems, this diversity of bacteriochlorophylls and chlorophylls allow the coexistence of a variety of phototrophs, each absorbing a particular range of the electromagnetic spectrum. Populations of different species can form distinct layers in the water column or sediment, acting as light filters (Stolz 1990, 2000).

The dimethyl sulfoxide (DMSO) reductase family of mono-nuclear molybdoenzymes is an example of how a metal center can be modified to catalyze different reactions (Hille et al. 2014). The “standard” enzyme in this family has three subunits, a large catalytic subunit that houses the molybdopterin cofactor but may also contain an iron-sulfur cluster, a smaller electron transfer unit comprised of multiple iron-sulfur clusters, and an anchoring subunit that also acts as an electron shuttle and connects to the quinone pool (Rothery et al. 2008). Examples include DMSO reductase, dissimilatory arsenate reductase (Arr), arsenite oxidase (Aio), nitrate reductase (Nar, Nas, Nap), formate hydrogen lyase, and formate dehydrogenase (Stolz and Basu 2002; Wells et al. 2020). The substrate specificity derives from a combination of the size and orientation of the catalytic pocket (as defined by the amino acid sequence), the angle of the pyranoterins, and the co-ordinating ligand to the metal (i.e., cysteine, selenocysteine, serine, aspartate, or OH) (Hille 1996; Hille et al. 2014).

## 1.4 The Microbial Body Electric

The discovery of “electrotrophy” was not unexpected. Extracellular electron transfer (EET) was suggested by demonstration that the dissimilatory iron reducing bacterium *Geobacter metallireducens* could use amorphous ferrioxyhydroxide as a terminal electron acceptor producing magnetite in the process (Lovley et al. 1987). What was unexpected is how common it has been found to be and the different mechanisms by which it occurs. Two tenets of microbiology had been roadblocks to



the concept. The first, is that electron transfer must occur within the confines of the cell wall, between the cytoplasm, cytoplasmic membrane, and periplasm. Second, that proteins involved in electron transport were not part of the outer membrane or cell surface (this author has grant reviews from the early 1990s that attest to this). These conventions were challenged by the discovery of dissimilatory metal-reducing bacteria such as *Shewanella* and *Geobacter* that could grow on solid forms of iron and manganese oxides (Myers and Nealson 1988; Lovley and Phillips 1988). Additionally, both organisms were found to have outer membrane c-type cytochromes (Myers and Myers 1997; Mehta et al. 2005) and could be grown directly on electrodes (Kim et al. 1999; Bond and Lovley 2003). *Shewanella* species can use excreted extracellular compounds such as quinones and flavins as electron shuttles (Newman and Kolter 2000; Kotloski and Gralnick 2013). More recently, the Gram positive bacterium *Listeria monocytogenes* was shown to use a flavinylated fumarate reductase in electron transfer (Light et al. 2019). That observation suggests other extracellular enzymes may be as well, and the possibility exists of a general “flavin-based [extracellular] electron transfer strategy” (Light et al. 2019).

Specialized conductive pili, or “nanowires”, have been implicated in EET for both *Shewanella* and *Geobacter* species (Gorby et al. 2006; Reguera et al. 2005; Lovley and Walker 2019). The purification and crystal structure determination for *Shewanella baltica* revealed a 20-heme electron transfer complex comprised of the decaheme MtrA, transmembrane protein MtrB, and the decaheme MtrC (Edwards et al. 2020). For *Geobacter* it was proposed that its nanowires were composed of a chain of the hexaheme cytochrome OmcS (Wang et al. 2019). Recently though, it has been shown that *G. sulfurreducens* have pili comprised of PilA-N-C that actually push a chain of the outer membrane multiheme OmcS or OmcZ through an outer membrane secretory complex (Gu et al. 2021). The mechanism has been described as an “on-off” switch (Lanese 2021).

EET is not just confined to microbe mineral interactions as there are at least two variations on this theme. These are direct interspecies electron transfer (DIET) and long distance extracellular electron transfer (LDEET). While interspecies hydrogen transfer was a well know phenomenon in microbial physiology, DIET has only been recognized recently (Bryant et al. 1967; Summers et al. 2010; Nagarajan et al. 2013; Walker et al. 2020). Anaerobic methane oxidation via DIET has been demonstrated for a consortium comprised of an anaerobic methanotrophic archaea and a sulfate-reducing bacteria (Wegener et al. 2015). DIET has also been shown between a *Methanobacterium* strain (YSL) and *G. metallireducens* (Zheng et al. 2020). Continuing the theme of microbe-mineral interactions, DIET between *Thiobacillus denitrificans* and *G. sulfurreducens* under denitrifying conditions was mediated by nanoparticles of magnetite (Kato et al. 2012). While EET and DIET are impressive by themselves, the truly remarkable discovery was the existence of cable bacteria and long-distance electron transport (LDET) (Pfeffer et al. 2012). How is it possible for a chain of cells several centimeters long to transfer electrons from one end to the other? It seems to defy physics, and yet it is indeed possible (Teske 2019). Whole new genera have been described, such as *Candidatus Electronema* and *Candidatus Electrothrix*, that appear to be capable of sulfur disproportionation; both oxidizing

and reducing mixed redox sulfur compounds (Kjeldsen et al. 2019; Mueller et al. 2020a, b). Orienting vertically in the sediment between the sulfidic and oxic zones, the chains essentially form electrical cables in the sediment (Nielsen 2016; Teske 2019; Pennisi 2020). This phenomenon is not limited to sulfur metabolizing bacteria as it has also been linked to the oxidation of iron sulfide minerals. Thus, it may play a critical role in maintaining redox in aquatic sediments with implications for the survival of benthic fauna (Seitaj et al. 2015).

## 1.5 Dark Matters Arising

Culture-independent methods using high throughput sequencing, like metagenomics and metatranscriptomics, have opened up a new avenue to explore microbial diversity at a scale not possible before. Deep sequencing projects have revealed a much richer global microbiome and introduced the concepts of “microbial dark matter” and the “rare biosphere” (Rinke et al. 2013; Solden et al. 2016; Jiao et al. 2021; Sogin et al. 2006). Microbial dark matter is made up of Candidate Phyla (CP), organisms that have been identified through these sequences projects but have no known relatives in culture. CP could make up greater than 15% of Bacterial diversity (Brown et al. 2015; Solden et al. 2016). The rare biosphere refers to a large diversity of rare species that are found in low abundance (Sogin et al. 2006). Used in concert with other techniques such as proteomics and metabolomics, we might find out what these organisms are actually doing. A study employing a combination of metagenomics and proteomics was able to attribute fermentation, hydrogen metabolism, sulfur metabolism to uncultured bacteria from an anoxic aquifer in Colorado (Wrighton et al. 2012). Overall, these projects have resulted in a proliferation of data bases such as the Genomic Encyclopedia of Bacteria and Archaea and Archaea-Microbial Dark Matter (GEBA-MDM), the Earth Microbiome Project, and the Global Catalogue of Microorganisms (Jiao et al. 2021). These data bases are a treasure trove of single-amplified genomes and metagenome assembled genomes (aka SAGs and MAGs) waiting to be mined, with the prospect that more microbe-mineral interactions and metal munching microbes await discovery. While the geomicrobiologist’s tool kit now includes an arsenal of culture-independent methods the old adage is still true: “to truly know them is to grow them”.

**Dedication and Acknowledgement** This review is dedicated to the late Ronald S. Oremland for his inspiration, our years of collaboration on microbial metal and metalloid metabolism, and friendship. A heartfelt thanks to Partha Basu, who shares a similar love of molybdoenzymes and whose attention to details made me a better scientist. And to my students, without whom much of this work would not have been accomplished.



Ronald S. Oremland

## References

- Achenbach LA, Michaelidou U, Bruce RA et al (2001) *Dechloromonas agitata* gen. nov., sp. nov. and *Dechlorosoma suillum* gen. nov., sp. nov., two novel environmentally dominant (per)chlorate-reducing bacteria and their phylogenetic position. *Int J Syst Evol Microbiol* 51: 527–533. <https://doi.org/10.1099/00207713-51-2-527>
- Ahmann D, Roberts AL, Krumholz LR, Morel FMM (1994) Microbe grows by reducing arsenic. *Nature* 371:750
- Aklujkar M, Krushkal J, BiBartolo G et al (2009) The genome sequence of *Geobacter metallireducens*: features of metabolism, physiology and regulation common and dissimilar to *Geobacter sulfurreducens*. *BMC Microbiol* 9:109. <https://doi.org/10.1186/1471-2180-9-109>

- Albin CA, Hollibaugh JT (2014) Dissimilatory antimonite reduction and production of antimony trioxide microcrystals by a novel microorganism. *Environ Sci Technol* 48:681–688
- Andreesen JR, Makdessi K (2008) Tungsten, a surprisingly positively acting heavy metal element for prokaryotes. *Ann N Y Acad Sci* 1125:215–229. <https://doi.org/10.1196/annals.1419.003>
- Antipov AN, Lyalikova NN, L'vov NP (2000) Vanadium-binding protein excreted by vanadate-reducing bacteria. *IUBMB Life* 49:137–141
- Appanna VD, Hamel R (2006) Aluminum detoxification mechanism in *Pseudomonas fluorescens* is dependent on iron. *FEMS Microbiol Lett* 143:223–228
- Avery SV, Codd GA, Gadd GM (1991) Caesium accumulation and interactions with other monovalent cations in the cyanobacterium *Synechocystis* PCC 6803. *Gen Microbiol* 137:405–413. <https://doi.org/10.1099/00221287-137-2-40>
- Baesman SM, Bullen TD, Dewald J et al (2007) Formation of tellurium nanocrystals during anaerobic growth of bacteria that use Te oxyanions as respiratory electron acceptors. *Appl Environ Microbiol* 73:2135–2143. <https://doi.org/10.1128/AEM.02558-06>
- Bahrou AS, Olliver PR, Hanson TE et al (2012) Volatile dimethyl polonium produced by aerobic marine organisms. *Environ Sci Technol* 46:11402–11407. <https://doi.org/10.1021/es3006546>
- Baymann F, Lebrun E, Brugna M et al (2002) The redox protein construction kit: pre-last universal common ancestor evolution of energy-conserving enzymes. *Philos Trans R Soc Lond B* 358: 267–274. <https://doi.org/10.1098/rstb.2002.1184>
- Blakemore R (1975) Magnetotactic bacteria. *Science* 190:377–379
- Blencowe DK, Morby AP (2003) Zn(II) metabolism in prokaryotes. *FEMS Microbiol Rev* 27:291–311
- Bond DR, Lovley DR (2003) Electricity production by *Geobacter sulfurreducens* attached to electrodes. *Appl Environ Microbiol* 69:1548–1555. <https://doi.org/10.1128/AEM.69.3.1548-1555.2003>
- Brown CT, Hug LA, Thomas BC et al (2015) Unusual biology across a group comprising more than 15% of domain bacteria. *Nature* 523:208–211. <https://doi.org/10.1038/nature14486>
- Bryant MP, Wolin EA, Wolin MJ, Wolfe RS (1967) *Methanobacillus omelianskii*, a symbiotic association of two species of bacteria. *Arch Microbiol* 59:20–31
- Brzoska K, Meczynska S, Kruszewski M (2006) Iron-sulfur cluster proteins: electron transfer and beyond. *Acta Biochim Pol* 53:685–691
- Burges BK, Lowe DJ (1996) Mechanism of molybdenum nitrogenase. *Chem Rev* 96:2983–3011. <https://doi.org/10.1021/cr950055x>
- Burke D, Burris RH (1941) Biochemical nitrogen fixation. *Ann Rev Biochem* 10:587–618
- Bushnell GW, Louie GV, Brayer GD (1990) High-resolution three-dimensional structure of horse-heart cytochrome c. *J Mol Biol* 214:585–595. [https://doi.org/10.1016/0022-2836\(90\)90200-6](https://doi.org/10.1016/0022-2836(90)90200-6)
- Campbell IJ, Bennett GN, Silberg JJ (2019) Evolutionary relationships between low potential ferredoxin and flavodoxin electron carriers. *Front Energy Res*. <https://doi.org/10.3389/fenrg.2019.00079>
- Chen M, Blankenship RE (2011) Expanding the solar spectrum used by photosynthesis. *Trends Plant Sci* 16:427–431. <https://doi.org/10.1016/j.tplants.2011.03.011>
- Chen J, Rosen BP (2020) The arsenic methylation cycle: how microbial communities adapted methylarsenicals for use as weapons in the continuing war for dominance. *Front Environ Sci*. <https://doi.org/10.3389/fenvs.2020.00043>
- Chen X, Schauder S, Potier N et al (2002) Structural identification of a bacterial quorum-sensing signal containing boron. *Nature* 415:545–549
- Chen M, Schliep M, Willows RD et al (2010) A red-shifted chlorophyll. *Science* 328:1318–1319. <https://doi.org/10.1126/science.1191127>
- Chen M, Li Y, Birch D, Willows RD (2012) A cyanobacterium that contains chlorophyll f – a red-adsorbing photopigment. *FEBS Lett* 586:3249–3254. <https://doi.org/10.1016/j.febslet.2012.06.045>
- Chew AGM, Bryant DA (2007) Chlorophyll biosynthesis in bacteria: the origins of structural and functional diversity. *Annu Rev Microbiol* 61:113–129. <https://doi.org/10.1146/annurev.micro.61.080706.093242>

- Choi SC, Chase TJ, Bartha R (1994) Metabolic pathways leading to mercury methylation in *Desulfovibrio desulfuricans* LS. *Appl Environ Microbiol* 60:4072–4077
- Dayan FE, Dayan EA (2011) Porphyrins: one ring in the colors of life. *Am Sci* 99:236–243. <https://doi.org/10.1511/2011.90.236>
- De Las Rivas J, Balsera M, Barber J (2003) Evolution of oxygenic photosynthesis: genome-wide analysis of the OEC extrinsic proteins. *Trends Plant Sci* 9:18–25
- de Vargas I, Macaskie LE, Guibal E (2003) Biosorption of palladium and platinum by sulfate-reducing bacteria. *J Chem Technol Biotechnol* 79:49–56
- Diekert G, Konheiser U, Piechulla K, Thauer RK (1981) Nickel requirement and factor F430 content of methanogenic bacteria. *J Bacteriol* 148:459–464
- Dimroth P (1987) Sodium ion transport decarboxylases and other aspects of sodium ion cycling in bacteria. *Microbiol Rev* 51:320–340
- Edwards MJ, White GF, Butt JN et al (2020) The crystal structure of a biological insulated transmembrane molecular wire. *Cell* 181:665–673. <https://doi.org/10.1016/j.cell.2020.03.032>
- Ellis PJ, Conrads T, Hille R, Kuhn P (2001) Crystal structure of the 100 kDa arsenite oxidase from *Alcaligenes faecalis* in two crystal forms at 1.64 Å and 2.03 Å. *Structure* 9:125–132
- Fru EC, Ivarsson M, Kiliyas SP et al (2013) Fossilized iron bacteria reveal a pathway to the biological origin of banded iron formation. *Nat Commun* 4:2050. <https://doi.org/10.1038/ncomms3050>
- Gadd MG (2010) Metals, minerals and microbes: geomicrobiology and bioremediation. *Microbiology (Reading)* 156:609–643
- Gamal AE, Agarwal V, Rahman I, Moore BS (2016) Enzymatic reductive dehalogenation controls the biosynthesis of marine bacterial pyrroles. *J Am Chem Soc* 138:13167–13170. <https://doi.org/10.1021/jacs.6b08512>
- Gao J, Ellis LBM, Wackett LP (2010) The University of Minnesota Biocatalysis/Biodegradation Database: improving public access. *Nucleic Acids Res* 38:D488–D491
- Glasser NR, Oyala PH, Osborne TH et al (2018) Structural and mechanistic analysis of the arsenate respiratory reductase provides insight into environmental arsenic transformations. *Proc Natl Acad Sci U S A* 115(37):E8614–E8623. <https://doi.org/10.1073/pnas.1807984115>
- Goldsmith RH (1982) Metalloids. *J Chem Ed* 59:526–527. <https://doi.org/10.1021/ed059p526>
- Gorby YA, Yanina S, McLean JS et al (2006) Electrically conductive bacterial nanowires produced by *Shewanella oneidensis* strain MR-1 and other microorganisms. *Proc Natl Acad Sci* 103:11358–11363. <https://doi.org/10.1073/pnas.0604517103>
- Gray ND, Howarth R, Pickup RW et al (2000) Use of combined microautoradiography and fluorescence *in situ* hybridization to determine carbon metabolism in mixed natural communities of uncultured bacteria from the genus *Achromatium*. *Appl Environ Microbiol* 66:4518–4522
- Gu Y, Srikanth V, Salazar-Morales AI et al (2021) Structure of *Geobacter* pili reveals secretory rather than nanowire behaviour. *Nature* 597:430–434. <https://doi.org/10.1038/s41586-021-03857-w>
- Hallas LE, Means JC, Cooney JJ (1982) Methylation of tin by estuarine microorganisms. *Science* 215:1505–1507. <https://doi.org/10.1126/science.215.4539.1505>
- Haunost M, Riebesell U, Bach LT (2020) The calcium carbonate shell of *Emiliania huxleyi* provides limited protection against viral infection. *Front Mar Sci* 7:530757. <https://doi.org/10.3389/fmars.2020.530757>
- Hazen RM, Papineau D, Bleeker W et al (2008) Mineral evolution. *Am Mineral* 93:1693–1720. <https://doi.org/10.2138/am.2008.2955>
- Heidelberg JF, Paulsen IT, Nelson KE et al (2002) Genome sequence of the dissimilatory metal ion-reducing bacterium *Shewanella oneidensis*. *Nat Biotech* 20:1118–1123. <https://doi.org/10.1038/nbt749>
- Heintze C, Formanke P, Pohl D et al (2020) An intimate view into the silica deposition vesicles of diatoms. *BMC Mater* 2:11. <https://doi.org/10.1186/S42833-020-00017-8>

- Helmenstine T (2021) What are the radioactive elements? Science Notes Posts. <https://sciencenotes.org/what-are-the-radioactive-elements/>. Accessed 24 Aug 2021
- Hille R (1996) The mononuclear molybdenum enzymes. Chem Rev 7:2757–2816. <https://doi.org/10.1021/CR950061T>
- Hille R, Hall J, Basu P (2014) The mononuclear molybdenum enzymes. Chem Rev 114:3963–4038. <https://doi.org/10.1021/cr400443z>
- Hoefl SE, Switzer Blum J, Stolz JF et al (2007) *Alkalilimnicola ehrlichii*, sp. nov. a novel arsenite-oxidizing halophilic gamma proteobacterium capable of chemoautotrophic or heterotrophic growth with nitrate or oxygen as the electron acceptor. Int J Syst Evol Microbiol 57:504–512
- Hofmann HJ (2000) Archean stromatolites as microbial archives. In: Riding RE, Awramik SM (eds) Microbial sediments. Springer, Heidelberg, pp 315–327. [https://doi.org/10.1007/978-3-662-04036-2\\_34](https://doi.org/10.1007/978-3-662-04036-2_34)
- Humphries AC, Macaskie LE (2002) Reduction of Cr(VI) by *Desulfovibrio vulgaris* and *Microbacterium* sp. Biotechnol Lett 24:1261–1267
- Hyman MR, Page CL, Arp DJ (1994) Oxidation of methyl fluoride and dimethyl ether by ammonia monoxygenase in *Nitrosomonas europaea*. Appl Environ Microbiol 60:3033–3035
- Icopini GA, Lack JG, Hersman LE et al (2009) Plutonium(V/VI) reduction by the metal-reducing bacteria *Geobacter metallireducens* GS-15 and *Shewanella oneidensis* MR-1. Appl Environ Microbiol 75:3641–3647
- Janssen S, Schaefer G, Anemueller S et al (1997) A succinate dehydrogenase with novel structure and properties from hyperthermophilic Archaeon Sulfolobus acidocaldarius: genetic and biophysical characterization. J Bacteriol 179:5560–5569
- Jiao J-Y, Liu L, Hua Z-S et al (2021) Microbial dark matter coming to light: challenges and opportunities. Natl Sci Rev 8:nwaa280. <https://doi.org/10.1093/nsr/nwaa280>
- Johnson DC, Dean DR, Smith AD, Johnson MK (2005) Structure, function, and formation of biological iron-sulfur clusters. Annu Rev Biochem 74:247–281
- Jordan SF, Ramm H, Zheludev IN et al (2019) Promotion of protocell self-assembly from mixed amphiphiles at the origin of life. Nat Ecol Evol 3:1705–1714. <https://doi.org/10.1038/s41559-019-1015-y>
- Kashefi K, Tor JM, Nevin KP, Lovley DR (2001) Reductive precipitation of gold by dissimilatory Fe(III)-reducing *Bacteria* and *Archaea*. Appl Environ Microbiol 67:3275–3279
- Kato S, Hashimoto K, Watanabe K (2012) Microbial interspecies electron transfer via electric currents through conductive minerals. Proc Natl Acad Sci 109:10042–10046. <https://doi.org/10.1073/pnas.1117592109>
- Kim B-H, Kim H-J, Hyun M-S, Park D-H (1999) Direct electrode reaction of Fe(III)-reducing bacterium *Shewanella putrefaciens*. J Microbiol Biotechnol 9:127–131
- Kjeldsen KU, Schreiber L, Thorup CA et al (2019) On the evolution and physiology of cable bacteria. Proc Natl Acad Sci U S A 116:19116–19125
- Klonowska A, Heulin T, Vermeglio A (2005) Selenite and tellurite reduction by *Shewanella oneidensis*. Appl Environ Microbiol 71:5607–5609
- Kotloski NJ, Gralnick JA (2013) Flavin electron shuttles dominate extracellular electron transfer by *Shewanella oneidensis*. mBio 4:e00553-12. <https://doi.org/10.1128/mBio.00553-12>
- Krejci MR, Wasserman B, Finney L et al (2011) Selectivity in biomineralization of barium and strontium. J Struct Biol 176:192–202
- Kulp TR, Hoefl SE, Madigan M et al (2008) Arsenic(III) fuels anoxygenic photosynthesis in hot spring biofilms from Mono Lake, California. Science 321:967–970
- Lane N, Martin WF (2012) The origin of membrane bioenergetics. Cell 151:1406–1416. <https://doi.org/10.1016/j.cell.2012.11.050>
- Lane TW, Morel FM (2000) A biological function for cadmium in marine diatoms. Proc Natl Acad Sci U S A 97:4627–4631
- Lanese N (2021) Scientists discover on-off switch for bacteria that breathe electricity. <https://www.livescience.com/bacteria-breathe-electricity-on-off-switch.html>. Accessed 3 Sept 2021
- Lester G (1957) Requirement for potassium by bacteria. J Bacteriol 75:426–428

- Levy Y (2017) Protein assembly and building blocks: beyond the limits of the LEGO brick metaphor. *Biochemist* 56:5040–5048. <https://doi.org/10.1021/acs.biochem.7b00666>
- Li Y, Hodak M, Bernholm J (2014) Enzymatic mechanism of copper-containing nitrite reductase. *Biochemistry* 54:1233–1242. <https://doi.org/10.1021/bi5007767>
- Li J, Wang O, Oremland RS et al (2016) Microbial antimony biogeochemistry: enzymes, regulation, and related metabolic pathways. *Appl Environ Microbiol* 15:5482–5495. <https://doi.org/10.1128/AEM.01375-16>
- Light SH, Meheust R, Ferrell JL et al (2019) Extracellular electron transfer powers flavinylated extracellular reductases in Gram-positive bacteria. *Proc Natl Acad Sci* 116:26892–26899. <https://doi.org/10.1073/pnas.1915678116>
- Lloyd JR (2003) Microbial reduction of metals and radionuclides. *FEMS Microbiol Rev* 27:411–425. [https://doi.org/10.1016/S0168-6445\(03\)00044-5](https://doi.org/10.1016/S0168-6445(03)00044-5)
- Lloyd JR, Yong P, Macaskie LE (1998) Enzymatic recovery of elemental palladium by using sulfate-reducing bacteria. *Appl Environ Microbiol* 64:4607–4609. <https://doi.org/10.1128/AEM.64.11.4607-4609>
- Locey KJ, Lennon JT (2016) Scaling laws predict global microbial diversity. *Proc Natl Acad Sci* 113:5970–5975
- Lovley DR (1988) Hydrogen concentrations as an indicator of the predominant terminal electron-accepting reactions in aquatic sediments. *Geochim Cosmochim Acta* 52:2993–3003. [https://doi.org/10.1016/0016-7037\(88\)90163-9](https://doi.org/10.1016/0016-7037(88)90163-9)
- Lovley DR, Phillips EJP (1988) Novel mode of microbial energy metabolism: organic carbon oxidation coupled to dissimilatory reduction of iron and manganese. *Appl Environ Microbiol* 56:1472–1480
- Lovley DR, Walker DJF (2019) *Geobacter* protein nanowires. *Front Microbiol* 10:2078. <https://doi.org/10.3389/fmicb.2019.02078>
- Lovley DR, Stolz JF, Nord GL, Phillips EJ (1987) Anaerobic production of magnetite by a dissimilatory iron-reducing microorganism. *Nature* 330:242–254
- Lovley DR, Phillips EJP, Gorby Y (1991) Microbial reduction of uranium. *Nature* 350:413–416
- Mansoorabadi SO, Thibodeaux CJ, Liu H-W (2007) The diverse roles of flavin coenzymes: nature's most versatile thespians. *J Org Chem* 72:6329–6342. <https://doi.org/10.1021/jo0703092>
- McCann SH, Conrad A, Hernandez-Maldonado J et al (2017) Arsenite as an electron donor for anoxygenic photosynthesis: description of three strains of *Ectothiorhodospira* from Mono Lake, California and Big Soda Lake, Nevada. *Life* 7:1. <https://doi.org/10.3390/life7010001>
- McDermott T, Stolz JF, Oremland RS (2020) Arsenic and the intestinal tract microbiome. *Environ Microbiol Rep* 12:136–159
- Mehta T, Coppi MV, Childers SE, Lovley DR (2005) Outer membrane c-type cytochromes required for Fe(III) and Mn(IV) oxide reduction in *Geobacter sulfurreducens*. *Appl Environ Microbiol* 71:8634–8641. <https://doi.org/10.1128/AEM.71.12.8634-8641.2005>
- Methe BA, Nelson KE, Eisen JA et al (2003) Genome of *Geobacter sulfurreducens* metal reduction in subsurface environments. *Science* 302:1967–1969. <https://doi.org/10.1126/science.1088727>
- Meyer TE, Tsapin AI, Vandenbergh I et al (2004) Identification of 42 possible cytochrome c genes in *Shewanella oneidensis* genome and characterization of six soluble cytochromes. *OMICS* 8:57–77. <https://doi.org/10.1089/153623104773547499>
- Moser DP, Nealson KH (1996) Growth of the facultative anaerobe *Shewanella putrefaciens* by elemental sulfur reduction. *Appl Environ Microbiol* 62:2100–2105
- Mueller F-D, Schueler D, Pfeiffer D (2020a) A compass to boost navigation: cell biology of bacterial magnetotaxis. *J Bacteriol* 202. <https://doi.org/10.1128/JB.00398-20>
- Mueller H, Marozava S, Probst AJ, Meckenstock RU (2020b) Groundwater cable bacteria conserve energy by sulfur disproportionation. *ISME J* 14:623–634. <https://doi.org/10.1038/s41396-019-0554-1>
- Mullen MD, Wolf DC, Ferris FG et al (1989) Bacterial sorption of heavy metals. *Appl Environ Microbiol* 55:3143–3149

- Myers CR, Myers JM (1997) Outer membrane cytochromes of *Shewanella putrefaciens* MR-1: spectral analysis, and purification of the 83-kDa *c*-type cytochrome. *Biochim Biophys Acta* 1326:307–318
- Myers CR, Nealson KH (1988) Bacterial manganese reduction and growth with manganese oxide as the sole electron acceptor. *Science* 240:1319–1321. <https://doi.org/10.1126/science.240.4857.1319>
- Nagarajan H, Embree M, Rotaru A-E et al (2013) Characterization and modelling of interspecies electron transfer mechanisms and microbial community dynamics of a syntrophic association. *Nat Commun* 4:2809. <https://doi.org/10.1038/ncomms3809>
- Naik RN, Murillo FM, Stolz JF (1993) Evidence for a novel nitrate reductase in *Geobacter metallireducens*. *FEMS Microbiol Lett* 106:53–58
- Newman DK, Kolter R (2000) A role for excreted quinones in extracellular electron transfer. *Nature* 405:94–97. <https://doi.org/10.1038/35011098>
- Newman DK, Ahmann D, Morel FMM (1998) A brief review of microbial arsenate respiration. *Geomicrobiol J* 15:255–268. <https://doi.org/10.1080/01490459809378082>
- Nielsen LP (2016) Ecology: electrical cable bacteria save marine life. *Curr Microbiol* 26:R32–R33. <https://doi.org/10.1016/j.cub.2015.11.014>
- Nuernberg DJ, Morton J, Santabarbara S et al (2018) Photochemistry beyond the red limit in chlorophyll *f*-containing photosystems. *Science* 360:1210–1213. <https://doi.org/10.1126/science.aar8313>
- Oremland RS, Stolz JF (2003) The ecology of arsenic. *Science* 300:939–944
- Oremland RS, Stolz JF, Hollibaugh JT (2004) The microbial arsenic cycle in Mono Lake, California. *FEMS Microbiol Ecol* 48:15–27
- Oremland RS, Kulp TR, Switzer Blum J et al (2005) A microbial arsenic cycle in a salt-saturated, extreme environment: Searles Lake, California. *Science* 308:1305–1308
- Oremland RS, Saltikov CW, Wolfe-Simon F, Stolz JF (2009) Arsenic in the evolution of Earth and extraterrestrial ecosystems. *Geomicrobiol J* 26:1–15
- Pennisi E (2020) The mud is electric. *Science* 369:902–905. <https://doi.org/10.1126/science.369.6506.902>
- Pfeffer C, Larsen S, Song J et al (2012) Filamentous bacteria transport electrons over centimeter distances. *Nature* 491:218–221. <https://doi.org/10.1038/nature11586>
- Raab A, Feldmann J (2003) Microbial transformation of metals and metalloids. *Sci Prog* 86:179–202
- Reedy CJ, Gibney BR (2004) Heme protein assemblies. *Chem Rev* 104:617–649. <https://doi.org/10.1021/cr0206115>
- Reguera G, McCarthy KD, Mehta T et al (2005) Extracellular electron transfer via microbial nanowires. *Nature* 435:1098–1101. <https://doi.org/10.1038/nature03661>
- Rinke C, Schwientek P, Sczyrba A et al (2013) Insights into the phylogeny and coding potential of microbial dark matter. *Nature* 499:431–436. <https://doi.org/10.1038/nature12352>
- Ritchie RJ (2018) Measurement of chlorophylls *a* and *b* and bacteriochlorophyll *a* in organisms from hypereutrophic auxinic waters. *J Appl Phycol* 30:3075–3087. <https://doi.org/10.1007/s10811-1431-4>
- Rivera M (2017) Bacterioferritin: structure, dynamics, and protein-protein interactions at play in iron storage and mobilization. *Acc Chem Res* 50:331–340. <https://doi.org/10.1021/acs.accounts.6b00514>
- Roane TM (1999) Lead resistance in two bacterial isolates from heavy metal-contaminated soils. *Microb Ecol* 37:218–224
- Rothery RA, Workun GJ, Weiner JH (2008) The prokaryotic complex iron-sulfur molybdoenzyme family. *Biochim Biophys Acta* 1778:1897–1929. <https://doi.org/10.1016/j.bbamem.2007.09.002>
- Santander PJ, Roessner CA, Stolorowich NJ et al (1997) How corrinoids are synthesized without oxygen: nature's first pathway to vitamin B12. *Chem Biol* 4:659–666



- Satvatmanesh DF, Siavoshi F, Beitollahi MM et al (2003) Biosorption of  $^{226}\text{Ra}$  in high level natural radiation areas of Ramsar, Iran. *J Radioanal Nucl Chem* 258:483–486
- Schedlbauer OF, Heumann KG (2000) Biomethylation of thallium by bacteria and first determination of biogenic dimethylthallium in the ocean. *Appl Organomet Chem* 14:330–340
- Scheer H (2006) An overview of chlorophylls and bacteriochlorophylls: biochemistry, biophysics, functions and applications. *Adv Photosyn Res* 25:1–26. [https://doi.org/10.1007/1-4020-4516-6\\_1](https://doi.org/10.1007/1-4020-4516-6_1)
- Seitaj D, Schauer R, Sulu-Gambari F et al (2015) Cable bacteria generate a firewall against euxinia in seasonally hypoxic basins. *Proc Natl Acad Sci* 112:13278–13282
- Senko J, Stolz JF (2001) Evidence for iron-dependent nitrate reduction in the dissimilatory iron-reducing bacterium *Geobacter metallireducens*. *Appl Environ Microbiol* 67:3750–3752
- Smirnova GV, Oktyabrsky ON (2005) Glutathione in bacteria. *Biochem (Moscow)* 70:1199–1211
- Sogin ML, Morrison HG, Huber JA et al (2006) Microbial diversity in the deep sea and the underexplored “rare biosphere”. *Proc Natl Acad Sci* 103:12115–12120. <https://doi.org/10.1073/pnas.0605127103>
- Solden L, Lloyd K, Wrighton K (2016) The bright side of microbial dark matter: lessons learned from the uncultivated majority. *Curr Opin Microbiol* 31:217–226. <https://doi.org/10.1016/j.mib.2016.04.020>
- Songkasiri W, Reed DT, Rittmann BE (2002) Biosorption of neptunium(V) by *Pseudomonas fluorescens*. *Radiochim Acta* 90:785–789
- Sousa FL, Thiergart T, Landan G et al (2013) Early bioenergetic evolution. *Philos Trans R Soc* 368: 20130088. <https://doi.org/10.1098/rstb.2013.0088>
- Staicu LC, Stolz JF (2021) Editorial: microbes vs. metals: harvest and recycle. *FEMS Microbiol Ecol* 97:fiab056. <https://doi.org/10.1093/femsec/fiab056>
- Stolz JF (1990) Structure of phototrophic prokaryotes. CRC Press, Boca Raton
- Stolz JF (1993) Magnetosomes: a review. *J Gen Microbiol* 139:1663–1670
- Stolz JF (2000) Structure of microbial mats and biofilms. In: Riding RE, Awramik SM (eds) *Microbial sediments*. Springer, Heidelberg, pp 1–8. [https://doi.org/10.1007/978-3-662-04036-2\\_1](https://doi.org/10.1007/978-3-662-04036-2_1)
- Stolz JF, Basu P (2002) Evolution of nitrate reductase: molecular and structural variations on a common function. *Chem Biol Chem* 3:101–109. [https://doi.org/10.1002/1439-7633\(20020301\)3:2/3<198::AID-CBIC198>3.0.CO;2-C](https://doi.org/10.1002/1439-7633(20020301)3:2/3<198::AID-CBIC198>3.0.CO;2-C)
- Stolz JF, Oremland RS (eds) (2011) *Microbial metabolism of metal and metalloids: advances and applications*. ASM Press, Washington DC
- Stolz JF, Chang S-BR, Kirschvink JL (1986) Magnetotactic bacteria and single domain magnetite in hemipelagic sediments. *Nature* 321:849–851
- Stolz JF, Basu P, Santini JM, Oremland RS (2006) Selenium and arsenic in microbial metabolism. *Annu Rev Microbiol* 60:107–130
- Stolz JF, Perera E, Kilonzo B et al (2007) Biotransformation of 3-nitro-4-hydroxybenzene arsonic acid and release of inorganic arsenic by *Clostridium* species. *Environ Sci Technol* 41:818–823
- Summers ZM, Fogarty HE, Leang C et al (2010) Direct exchange of electrons within aggregates of an evolved syntrophic coculture of anaerobic bacteria. *Science* 330:1413–1415. <https://doi.org/10.1126/science.1196526>
- Switzer Blum J, Hoefft McCann S, Bennett S et al (2016) A microbial arsenic cycle in sediments of an acidic mine impoundment: Herman Pit, Clear Lake, California. *Geomicrobiology*. <https://doi.org/10.1080/01490451.2015.1080323>
- Teske A (2019) Cable bacteria, living electrical conduits in the microbial world. *Proc Natl Acad Sci U S A* 116:19759–18761
- Tsuruta T (2005) Removal and recovery of lithium using various microorganisms. *J Biosci Bioeng* 100:562–566. <https://doi.org/10.1263/jbb.100.562>
- Van Dyke MI, Lee H, Trevors JT (1989) Germanium accumulation by bacteria. *Arch Microbiol* 152:533–538

- Vernon RE (2013) Which elements are metalloids? *J Chem Ed* 90:1703–1707. <https://doi.org/10.1021/ed3008457>
- Wackett LP, Dodge AG, Ellis LBM (2004) Microbial genomics and the periodic table. *Appl Environ Microbiol* 70:647–655. <https://doi.org/10.1128/AEM.70.2.647-655.2004>
- Walker DJ, Nevin KP, Holmes DE et al (2020) *Syntrophus* conductive pili demonstrate that common hydrogen-donating syntrophs can have a direct electron transfer option. *ISME J* 14: 837–846. <https://doi.org/10.1038/s1396-019-0575-9>
- Wang F, Gu Y, O'Brien JP (2019) Structure of microbial nanowires reveals stacked hemes that transport electrons over micrometers. *Cell* 177:361–369. <https://doi.org/10.1016/j.cell.2019.03.029>
- Wanner BL (2004) Gene regulation by phosphate in enteric bacteria. *J Cell Biochem* 51:47–54
- Webb M (1953) Effects of magnesium on cell division. *Science* 118:607–611
- Wegener G, Krukenberg V, Riedel D et al (2015) Intercellular wiring enables electron transfer between methanotrophic archaea and bacteria. *Nature* 526:587–590
- Weiss MC, Sousa FL, Mrnjavac N et al (2016) The physiology and habitat of the last universal common ancestor. *Nat Microbiol* 1:16116. <https://doi.org/10.1038/nmicrobiol.2016.116>
- Wells MB, Stolz JF (2020) Microbial selenium metabolism: a brief history, biogeochemistry, and ecophysiology. *FEMS Microbiol Ecol* 96:faa209. <https://doi.org/10.1093/femsec/faa209>
- Wells MB, McGary J, Gaye MM et al (2019) The respiratory selenite reductase from *Bacillus selenitireducens* strain MLS10. *J Bacteriol* 201:e00614–e00618. <https://doi.org/10.1128/JB.00614-18>
- Wells MB, Jeganathar Kanmanii J, Al Zadjali AM et al (2020) Methane, arsenic, selenium and the origins of the DMSO reductase family. *Sci Rep* 10:10946. <https://doi.org/10.1038/s41598-020-67892-9>
- Wells MB, Basu P, Stolz JF (2021) The physiology and evolution of selenium metabolism in bacteria and archaea. *Metalomics* 13:mfab024. <https://doi.org/10.1093/mtomcs/mfab024>
- Whitman WB, Coleman DC, Wiebe WJ (1998) Prokaryotes: the unseen majority. *Proc Natl Acad Sci* 95:6578–6583
- Wildung RE, Gorby YA, Krupka KM et al (2000) Effect of electron donor and solution chemistry on products of dissimilatory reduction of technetium by *Shewanella putrefaciens*. *Appl Environ Microbiol* 66:2451–2460. <https://doi.org/10.1128/AEM.66.6.2451-2460.2000>
- Wrighton KC, Thomas BC, Sharon I et al (2012) Fermentation, hydrogen, and sulfur metabolism in multiple uncultivated bacterial phyla. *Science* 337:1661–1665
- Yannone SM, Hartung S, Menon AL et al (2012) Metals in biology: defining metalloproteomes. *Curr Opin Biotechnol* 23:89–95. <https://doi.org/10.1016/j.copbio.2011.11.005>
- Yuliana T, Nakajima N, Yamamura S et al (2017) Draft genome sequence of *Roseovarius* sp. A-2, an iodide-oxidizing bacterium isolated from natural gas brine water, Chiba, Japan. *J Genomics* 5:51–53. <https://doi.org/10.7150/jgen.19846>
- Zanello P (2018) Structure and electrochemistry of proteins harboring iron-sulfur clusters of different nuclearities. Part III [4Fe-4S], [3Fe-4S], and [2Fe-2S] iron-sulfur proteins. *J Struct Biol* 202:264–274. <https://doi.org/10.1016/j.jsb.2018.03.008>
- Zargar K, Conrad A, Bernick DL et al (2012) ArxA, a new clade of arsenite oxidase within the DMSO reductase family of molybdenum oxidoreductases. *Environ Microbiol* 14:1635–1645. <https://doi.org/10.1111/j.1462-2920.2012.02722.x>
- Zheng S, Liu F, Wang B et al (2020) *Methanobacterium* capable of direct interspecies electron transfer. *Environ Sci Technol* 54:15347–15354. <https://doi.org/10.1021/acs.est.0c05525>

# Chapter 2

## Chemical Constraints for Transition Metal Cation Allocation



Dietrich H. Nies

**Abstract** The aim of this book is to understand cellular handling of transition metals and metalloids. These may occur in oxidation states from (I), as in case of the monovalent cation Cu(I), via (II), (III), and so on to (VI) as in case of Cr(VI), Mo (VI), and W(VI) and even beyond this oxidation state. Metals with a high oxidation state usually form oxyanions such as chromate, arsenate, or molybdate. Sometimes, the oxy-anionic and the cationic form are both important to the cell, for instance arsenite and the As(III) cation. Transition metal oxyanions as minor bioelements are rare but may serve as electron acceptors in anaerobic respiration events or could be substrate and electron donor for chemolithoautotrophic microorganisms. Compared to the oxy-anionic minor bioelements Mo, W, and V, the mono- to trivalent transition metal cations of Mn, Fe, Co, Ni, Cu, and Zn are of much higher importance for living cells. They occur in higher number of atoms per cell, in more metal-dependent proteins and biochemical reactions. This chapter concerns the chemical constraints for correct allocation of transition metal cations to the respective metal-dependent enzyme. These are the basis for a deep understanding of multiple transition metal homeostasis – from the number of electrons in the 3d shell all the way to molecular clockwork of the cellular metal allocation, discrimination, and distribution network in crowded bacterial cells.

### 2.1 Introduction: Life Can Hardly Exist without Metals

Musing about all kinds of biological processes may start with the work of Erwin Schrödinger, who explained thermodynamics of life (Schrödinger 1992, first published 1944). The life process depends on the existence of cells, delimited special volumes with a border between outside and inside (Fig. 2.1). To obey the first and second law of thermodynamics, cells transform energy into negentropy (or order) inside of the cell at the cost of an even larger, overcompensating increase in entropy

---

D. H. Nies (✉)

Martin-Luther-University Halle-Wittenberg, Molecular Microbiology, Halle (Saale), Germany  
e-mail: [d.nies@mikrobiologie.uni-halle.de](mailto:d.nies@mikrobiologie.uni-halle.de)

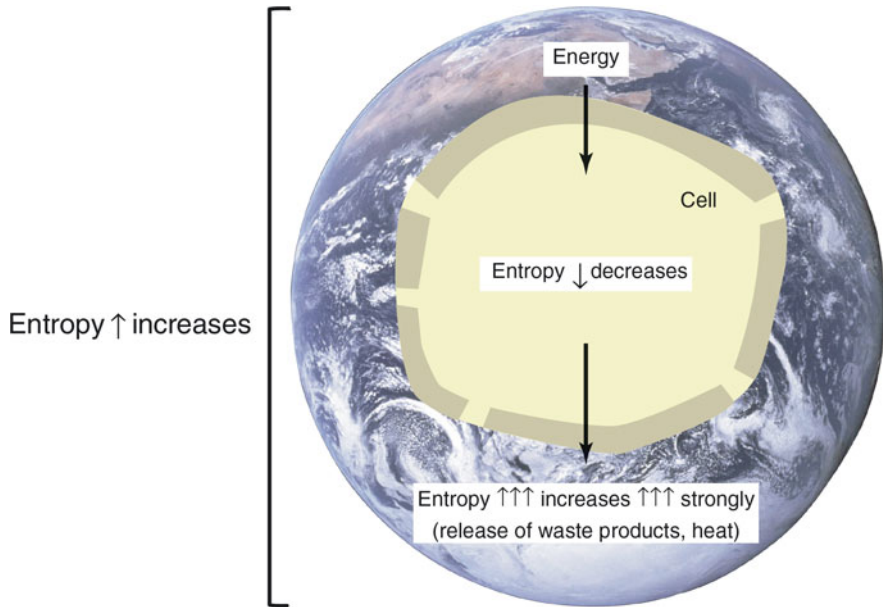


**Fig. 2.1** Definition of life according to Schrödinger. To build order inside an organism, cells continuously use energy to decrease the intracellular entropy (or increase the intracellular negentropy = order) and overcompensate this by increasing the entropy in the environment by the release of waste products and heat. Thus, in the total system composed of a cell and its environment, the entropy increases steadily during the chemical reactions in a cell, and the second law of thermodynamics is kept. Energy can be light energy or chemical energy. Intracellular order means macromolecules (Nies 2014)

outside. The energy being transformed could originate from light, an exergonic chemical reaction, energy forms previously stored inside the cell, or, in rare cases of dormancy, the energy transformation process can be postponed for some time {further reading chapter S1.1, (Nies 2014)}.

This energy transformation process is the result of a network of chemical reactions. The interacting molecules are composed of atoms and chemical elements arranged neatly in the periodic table of the elements (PSE). The number of protons in the atomic nucleus increases by one from one element to the next, consequently also the number of electrons in the electron shell of an electric neutral atom. The electrons reside in electron orbitals defined by the principal (e.g., 1, 2, 3, 4, ...), the azimuthal (e.g., s, p, d, f, g), and the magnetic quantum numbers (e.g.,  $p_x$ ,  $p_y$ ,  $p_z$ ) with two electrons with different spins fitting into one orbital (Nies 2014; Housecroft and Constable 2006). The orbitals of most chemical elements can be derived from that of hydrogen, and the orbitals of this simplest element can be calculated by solving the Schrödinger equation, making Erwin Schrödinger the godfather of both, modern chemistry and biology.

Entropy of a system increases with the number of components, particles and sub-systems plus their translational and rotation degrees of freedom. Consequently,

negentropy means a decrease in the number of components and limitation of their movement. This condition is fulfilled by macromolecules. Living cells thus transform energy to produce and repair macromolecules (Fig. 2.1). This can only happen in the liquid physicochemical state, not in the gaseous and solid states. Existence of macromolecules in solution requires a solvent, which also allows the formation of a border between the inside and outside of a cell. Formation of macromolecules depends on an element able to form polymers (Nies 2014).

Except for the primordial hydrogen and some helium, the remaining chemical elements were synthesized by atomic fusion in ancient stars, first from hydrogen to helium as our sun is doing right now, followed by fusion of helium to carbon, nitrogen, and oxygen, and so on, until formation of iron is reached. Iron is the element with the highest atomic number that can be produced by an exergonic atomic fusion event. All these elements are released by dying stars in supernova events, mix with the primordial hydrogen clouds and form new stars surrounded by planets. As outlined elsewhere (Nies 2014, 2016), this elemental array, plus the planet-formation process, the redox potential and solubility of ions, resulted in the principal availability of elements, atoms, and ions which allowed for evolution of a living cell. An enormous amount of H and He is followed by a lack of Li, Be, and B because these three elements are consumed again during element formation, a large availability of C, N, O, a declining amount of the following elements but with an availability peak of iron and neighbors, because iron is the element with the highest atomic number that can be produced exergonically (Fig. 2.2).

Possible solvents for life processes are those with the highest availability, these would be the hydrogenated compounds of C, N, and O, which are methane, ammoniac, or water, respectively. Among these, water has a polarity of 39 that adequately allows the existence of macromolecules and a cellular border. Ammoniac is less suitable (polarity 19) and has much lower melting and boiling points of  $-33\text{ }^{\circ}\text{C}$  and  $-77.7\text{ }^{\circ}\text{C}$ , respectively, which would make life process that are very slow. Methane as an a-polar substance (polarity 4) is not suited at all (Nies 2014). Carbon is an ideal building block for polymers such as macromolecules. Thermodynamics of life, the PSE and the availability of chemical elements lead to the hypothesis that life can be expected to be a carbon-based and water-bound process, not only on our planet but also on most other ones harboring life.

The carbon atom possesses two inner electrons in the 1 s orbital, two electrons in the 2 s and two in the 2p orbitals. The 2 s and three 2p orbitals with the principal quantum number 2 can hybridize to form four  $sp^3$  orbitals for four bonding partners in sigma bonds, or three  $sp^2$  orbitals leaving one  $2p_z$  orbital for a double bond, or even two sp orbitals leaving  $2p_y$  and  $2p_z$  orbitals for two double bonds. Carbon is the element most suited to form polymers by stable covalent C-C simple sigma bonds, or additionally pi double bonds (Housecroft and Constable 2006). This leaves in  $sp^3$  carbon two “arms” free for covalent bonds with the other frequently occurring non-metals, H, N, and O. Completely hydrogenated carbon polymers such as fatty acids or isoprenoids are very hydrophobic. These are ideal for the formation of a cellular border between inside and outside in water-based life; a pre-requisite for the life process according to Schrödinger. On the other hand, introduction of

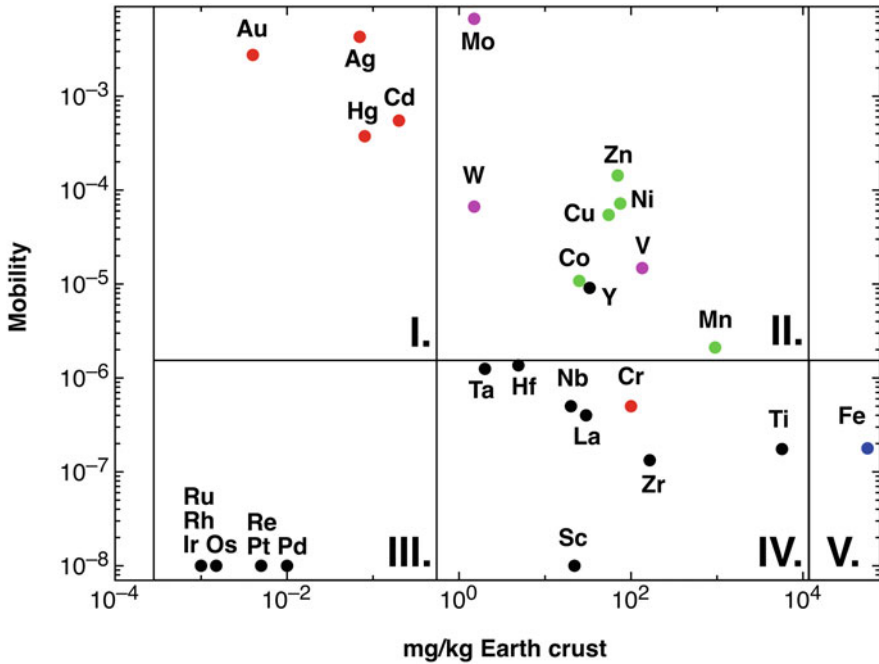


**Fig. 2.2** Availability of transition metals. The figure plots the content of a transition metal against the mobility, calculated as sea water content of this metal divided by the content of the earth's crust (Weast 1984). This clearly defines five sets of transition metals: (I) those with high mobility despite a low content in the earth's crust; (II) with high availability; (III) with extremely limited availability; (IV) with a high content in the earth's crust but low availability; and (V) iron. Group II contains all essential oxyanions (purple), essential-but-toxic cations (green) plus Y but except iron (blue) and group I the toxic-only transition metals (red). With the exception of Cr or La, the metals in groups III and IV are of no relevance for bacteria (Nies 2016)

hydrogenated N as amino- and O as alcohol, carbonyl, or carboxyl groups results in polar molecules or building blocks of macromolecules. Moreover, carboxylic groups are negatively charged under cytosolic pH values, and ammonium groups positively charged. This allows bonding between parts of macromolecules using ionic interactions. The strength of ionic interactions is comparable to that of covalent bonds. Finally, O and N-containing side chains may interact by formation of hydrogen bonds, which have a lower energy than covalent or ionic bonds but can occur in a high number within one or between two macromolecules. Together with hydrophobic and van der Waals interactions, these forces are fundamental for structure, function, and interaction of macromolecules within a living cell.

Cells can use different processes to harvest external energy and use this energy to synthesize macromolecules (Fig. 2.3). Phototrophic cells absorb photons as short-living excitons and transform these excitons into a concentration gradient across a biological membrane, in most cases a proton gradient (proton motive force, pmf). Chemolithoautotrophic bacteria transfer electrons from a reduced electron donor

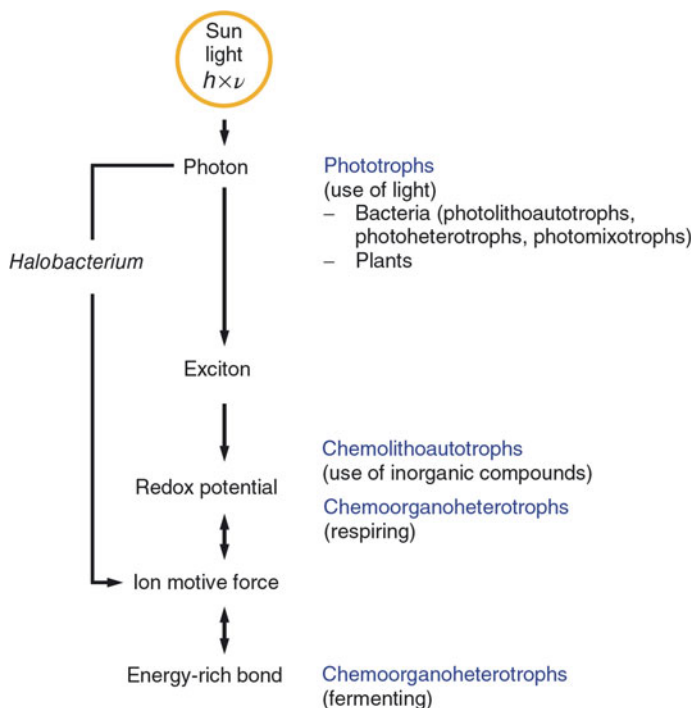


**Fig. 2.3** An universal roadmap of energy conservation. Phototrophs use light energy (photons) to create an exciton that is subsequently used to change the redox potential of a redox carrier to a lower potential (= higher energy). Electron transport from the resulting low redox potential to a more positive one drives ion transport to form an ion motive force, mostly in the form of a proton motive force pmf. Finally, the ion motive force is used to generate a compound containing an energy-rich bond such as ATP. To be brief, some archaea such as *Halobacterium* use a protein named bacteriorhodopsin to create an ion motive force directly from an exciton. Chemolithoautotrophic bacteria use the difference in redox potential of inorganic compounds to conserve energy, respiring chemoorganoheterotrophic bacteria transfer electrons from organic compounds to external electron acceptors that are mostly also inorganic compounds. Fermenting organisms are also chemoorganoheterotrophs that use biochemical reactions for a direct formation of energy-rich bonds. Some phototrophs can grow photolithoautotrophically, others photoheterotrophically or photomixotrophically. Note that energy-rich bonds can also be used to build an ion motive force, for example, for transport processes, and an ion motive force to drive electrons toward a low redox potential (reverse electron transport.) From (Nies 2014)

such as molecular hydrogen to an oxidized electron acceptor such as molecular oxygen, and transform this energy stemming from a redox reaction into a proton gradient. Respiring cells degrade organic material and transfer the electrons from these compounds again onto an external electron acceptor, again forming a proton or other gradient. But the pmf or other forms of energy stored in a gradient cannot be efficiently harnessed to synthesize macromolecules or their building blocks because synthesis of macromolecules from building blocks needs an activation of these precursors. With C, H, O, N alone and the exception of rare acid anhydrides between

carboxylic groups, only ester or amide bonds can be realized, which are low-energy bonds.

To produce high-energy, activating bonds, two other chemical elements are needed. S is needed for energy-rich thiol esters and subsequently for maintenance of a reduced redox state inside the cellular cytoplasm, which is a pre-requisite for the existence of free thiol groups as educts of thiol ester formation. Secondly, P in phosphate forms high-energy anhydrides or mixed anhydrides. Examples are the thiol bonds in acetyl-coenzyme A, the mixed anhydride at the C1 group of 1,3 bis-phospho-glycerate (the C3-bound phosphate is in a low-energy ester bond), and the phosphate anhydride between the alpha- and beta- as well as between the beta- and gamma-phosphate groups of adenosine-triphosphate ATP. I have not yet mentioned fermentation as energy-conservation process, it gains most of the conserved energy directly from the formation of high-energy bonds such as 1,3-bis-phospho-glycerate from the  $\text{NAD}^+$ -dependent oxidation of glyceralaldehyde-3-phosphate.

This leads to a chemical composition of the dry mass of most cells on the average of about 50% C, 8% H (with a 12-times lower atomic mass so that the molar excess of C:H is about 1:2), 20% O, 14% N, 3% P, and 1% S. Composed of these elements are the macromolecules, again about 50% proteins, 20% nucleic acids, 20% carbohydrates (in bacteria as cell wall and storage compound), and 10% lipids in the membrane or membranes (Nies 2014). At a neutral pH value, each phosphate moiety of the backbone of the nucleic acids, the phospholipids and teichoic acids of the Gram-positive bacteria carry a negative charge. Negative charges are also contributed by the side-chain carboxylic groups of glutamate and aspartate. All these negative charges are compensated by the positive charges of the side chains of asparagine and lysine, so that in bacterial and other cells the macromolecules in their totality carry a negative charge. Theoretically, these negative charges could be compensated by mobile ammonium ions  $\text{NH}_4^+$  or nitrogen in amine compounds such as spermidine but ammonium- or amine-N is much too valuable to be wasted as positively charged counterion, because N is needed for synthesis of proteins, the cell wall, and nucleic acids.

Transformation of energy by cells needs negatively charged phosphate-containing compounds. Energy transformation creates negentropy inside the cells in the form of information-containing macromolecules so that phosphate residues are a coupling factor between cellular energy transformation and information flow, which essentially defines the life process. Metal cations neutralize the negative charges of phosphate and allow the life process: life can hardly exist without metals.

Available in most ecosystems are the monovalent alkali metal cations of Na and K, the divalent earth alkali metals of Mg and Ca, and, since exergonic synthesis of elements stops at Fe, this metal and others of the first transition period of the PSE plus the oxyanions of molybdenum and tungsten (Fig. 2.2). While Na, K, Mg, and Ca make up most of the missing 4% of the cellular dry mass, the content of the transition metals is much lower. They are considered as minor bioelements in contrast to the “big ten” major bioelements (C, H, O, N, P, S, K, Mg, Ca, Na) (Nies 2014).



The metal cations among the “big ten” have different functions in the cell (Nies 2014). The monovalent cation of K for rapid-response osmo-regulation, of Na for formation of gradients and both as general cationic counterions. The divalent cation of Mg is the main charge-bridging ion in the cytoplasm. The redox-active iron serves as the one-electron transferring metal in iron-sulfur clusters, heme compounds, mononuclear nonheme and other iron-containing protein-bound clusters. The Ni and Co cations split, re-arrange, and form bonds in a very limited number of enzymes, and copper is of course found in copper-dependent oxidases which mostly interact with molecular oxygen. Zn serves as Lewis acid in some enzymes and organizes the domains of many proteins into a defined structure (Nies 2016).

Bacterial and other cells are confronted with an ever-changing concentration of these metal cations from the pM to the mM range, and also the composition of the metal mélange is changing, depending on the environment and competition with other organisms for essential metals. Moreover, the transition metal cations all have similar ionic radii. How is it, that cells are nevertheless able to get the correct metal into the correct center of a metal-depending protein, without causing toxic effect, and without interfering too much with the allocation of other metal cations with a similar size?

## 2.2 Constraints for an Allocation Model

### 2.2.1 Metals, PSE, and Complex Compounds

Living cells use three kinds of metals. I would group these as alkali metal cations, earth alkali metal cations, both used as major bioelements, and transition metal cations and oxyanions. In general, transition metals that are present as trivalent and tetravalent metal cations form highly insoluble hydroxide complexes at neutral pH values in aqueous environments. Metals that are predominantly present in these oxidation states (e.g., Sc, Ti, Y, Zr) are not used by living cells (Fig. 2.2). Rare exceptions are La(III) in some bacteria and Cr(III) in eukaryotes. Another important exception is Fe(III), a highly abundant metal that was available as Fe(II) to living cells before the first oxygenation event 2.4 billion years ago (Lyons et al. 2014; Parnell et al. 2010). When molecular oxygen, produced by cyanobacteria, increased in the atmosphere and aquatic ecosystems on earth, Fe(II) was oxidized to Fe(III) in oxic environments and cells had to evolve a way to obtain the now nearly un-available transition metal (Nies 2016).

Alkali metals have one electron in the valence orbital  $3s$  (Na) and  $4s$  (K) (Housecroft and Constable 2006). Their monovalent cations are stable in aqueous solutions due to the low energy of the completely filled electron shell with the principal quantum number 2 (Na) and 3 (K). For the same reason, the earth alkali metals Mg ( $3s^2$ ) and Ca ( $4s^2$ ) form stable divalent cations in water. The transition metal oxyanions vanadate and chromate are structural analogs of phosphate and sulfate, respectively. They interfere with the uptake and metabolism of

these species of the major bioelements P and S, and are used only under exceptional conditions (Nies 2016). The biologically important oxyanions molybdate and tungstate, on the other hand, are less-toxic species compared to the cationic forms of Mo and W, they have a higher solubility and availability as these forms, leading to a high importance of these metals. Nevertheless, these transition metal oxyanions are immediately captured in different kinds of nucleotide-based cofactors to prevent any “accidental” reduction of molybdate and tungstate inside the cell (Nies and Silver 2007). Together with Se, the halogens Br and I, and an exceptional use of Cd and La, Mo and W are the only elements with a higher atomic number than Zn that are known as constituents of enzymes, cofactors or other molecules produced by living cells.

Allocation of the divalent zinc cation occurs in the presence of the divalent cations of Mg and Ca, as well as the other cations of the first transition period, Mn, Fe, Co, Ni, and Cu, and of Cd, which accompanies Zn in most environments. The zinc cation has to be discriminated with respect to these metal ions. The ionic radii of the divalent transition metal cations are very similar and decrease from Mn (80 pm) via Fe (76 pm), Co (74 pm), Ni (72 pm) to Cu (69 pm) before it increases again with Zn (74 pm) due to the presence of completely filled 3d orbitals (Weast 1984). The divalent Mg ion (65 pm) is also close to these values while Ca (99 pm) and in most cases the toxic-only Cd (97 pm) are larger. Among the monovalent cations, Cu (96 pm) is close to Na (95 pm) but smaller than K (133 pm). This provides a similar charge-volume ratio to the divalent transition metal cations and Mg (Fig. 2.4).

During the first transition period of the PSE, the transition metals fill up their five 3d orbitals with up to five pairs of electrons. All of them except Zn(II) and Cu(I) have unoccupied 3d orbitals. This allows especially the transition metal cations to form stable complex compounds. Up to six ligands are able to bind to a central transition metal cation by donating a free electron pair into an orbital provided by this metal. According to the molecule orbital theory (Housecroft and Constable 2006), metal orbitals and ligand orbitals hybridize to form molecule orbitals. Since orbitals have to follow the law of energy conservation, hybridization of two atomic orbitals must result in the formation of two molecule orbitals. A bonding molecule orbital has a lower energy than the parent atomic orbital, an antibonding molecule a higher energy. The sum of the energy states of both molecule orbitals equals that of the parent atomic orbitals. If two electrons from different atoms form a chemical bond, they together occupy the bonding molecule orbital and the energy difference between bonding molecule orbital and the atomic orbitals minus the energy needed to pair two electrons (pairing energy  $P$ ) is released as entropy. The antibonding molecule orbital remains empty. When it becomes occupied, the atoms quit bonding and separate.

All unoccupied orbitals of a metal can be used to form a complex compound (Housecroft and Constable 2006). These are in case of the metal cations of the first transition row the empty 3d, 4s, 4p and even the 4d orbitals. A chemical bond in a complex compound is formed when a ligand supplies an electron pair, which has the advantage that no pairing energy needs to be considered. In hex-aquo complexes,

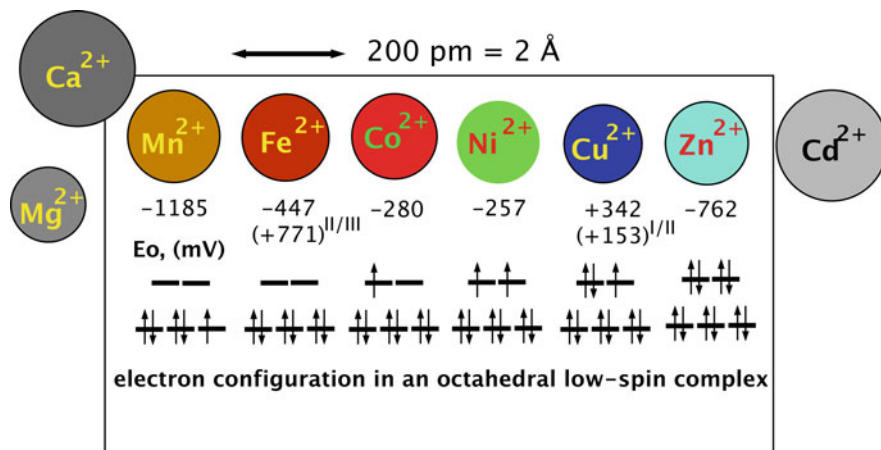


**Fig. 2.4** The essential transition metal cations of the first transition period. The essential divalent transition metal cations all have similar radii and can only be discriminated if variations in the complex-forming and redox abilities are considered. The diameter is indicated by the size of the circles that represent the metal. The half-cell redox potential  $E_0$  and electron configuration of a theoretical octahedral low-spin complex are indicated below these symbols (Weast 1984). An electron spin of  $+1/2$  is indicated by an arrow pointing up, and in a  $-1/2$  spin the arrow points down. The three lines in the lower part of the electron configuration represent the nonbonding  $3d t_{2g}$  orbitals, and the two lines above represent the antibonding  $d$  orbitals. The  $\Delta_o$  energetic distance between both is not drawn to the scale. During the formation of the six ligand bonds in this example, six free electron pairs residing in six different ligand orbitals recruit six metal orbitals, namely the empty  $4s$  valence orbital, the three  $4p$  orbitals and the two  $3d e_g$  bonding orbitals. This forms six new complex orbitals for bonds between ligands and the metal cation. Because the total number of orbitals in a system has to remain constant, a consequence of the first law of thermodynamics (energy conservation), six antibonding complex orbitals come into existence to compensate for the six complex bonds, one  $s^*$ , three  $p^*$  of very high energy (not shown) plus the two antibonding  $3d^*$  orbitals. Reproduced with permission from (Nies 2012) (Copyright 2012, American Society for Microbiology)

which is the species of most transition metal cations in water without further ingredients, the six water molecules are bound using the  $4s$ , three  $4p$  and two  $4d$  orbitals, without using the  $3d$  orbitals. Because the energy of the  $4p$  orbitals is higher than that of the  $3d$  orbitals, the energy of bonding molecule orbitals stemming from  $4p$  orbitals is higher than that of those that originated from  $3d$  orbitals. With other words,  $4p$  complexes are energetically less favorable and thermodynamically less stable than  $3d$  complexes.

The  $Mg(II)$  cation has a completely filled electron shell with the principal quantum number 2 and unoccupied  $3s$ ,  $3p$ , and  $3d$  orbitals. Since there are only one  $3s$  and three  $3p$  orbitals, bonding more than four ligands needs to use  $3d$  orbitals, which have an energy even higher than the  $4s$  orbitals of the next principal quantum number. The  $Mg(II)$  cation may be able to occupy empty, pre-formed ligand fields in biological macromolecules, however, incoming transition metal cations should be easily able to displace magnesium if the respective site is accessible. In chlorophyll

(Fiedor et al. 2008; Kania and Fiedor 2006), the most important biological substance to transfer photons into an exciton state using the conjugated double bonds of a tetrapyrrole ring, the central magnesium ion forms a charge-transfer complex with the tetrapyrrole, which stabilizes the exciton so that it can be transferred to another molecule. The 3 s, three 3p, and two 3d orbitals are used for an octahedral conformation but only four electron pairs from N atoms of the flat tetrapyrrole are accepted while axial ligands are not bound. This does not disturb the conjugated double bonds of the tetrapyrrole but allows an easy transfer of the exciton to a stacked second chlorophyll, until the electron in the exciton state is finally separated from an electron-donating molecule to an acceptor (Fig. 2.3), which is now in a reduced state of very high energy (or very negative redox potential).

Individual transition metal cations can be discriminated against each other because they are able to accept a different number of ligands. Up to six ligands can be bound, forming an octahedral complex as in chlorophyll. The metal cation is in the center, four ligands form a square in a plane. In case of octahedral complexes of transition metal cations, also the two axial ligands above and below the plane are used. To accept six electron pairs from ligands, again six empty metal orbitals are needed to form the molecule orbitals, in case of the transition metal cations of the first transition period these are the 4 s orbital, the three 4p orbitals plus two empty 3d orbitals, which have a lower energy than do the 4p orbitals. In octahedral complexes, these are the two 3d orbitals oriented toward the ligand, the  $3d_{x^2-y^2}$  and the  $3d_{z^2}$  or  $e_g$  orbitals, rather than the remaining three  $t_{2g}$  orbitals  $3d_{xy}$ ,  $3d_{yz}$ ,  $3d_{xz}$ . The six unoccupied 4 s,  $4p_x$ ,  $4p_y$ ,  $4p_z$ ,  $3d_{x^2-y^2}$ , and  $3d_{z^2}$  orbitals hybridize to form bonding molecule orbitals for the complex compounds by accepting free electron pairs from the ligands. For reasons of energy conservation, this also results in the formation of six antibonding complex orbitals or “\*” orbitals, two  $3d^*$ , one  $4s^*$  with higher energy than the two  $3d^*$  orbitals, and three  $4p^*$  orbitals with even higher energy (Housecroft and Constable 2006).

Since only two 3d  $e_g$  orbitals are used to produce the six ligand-accepting metal orbitals in an octahedral complex, three 3d  $t_{2g}$  orbitals are left to harbor the 3d electrons of the metal (Fig. 2.4). These nonbonding 3d orbitals, which are not involved in the formation of the complex, have a lower energy than the two  $3d^*$  orbitals and are occupied first. When theoretical octahedral complexes of the metals of the first transition period of the PSE from Sc to Zn are being considered, the only 3d electron of a theoretical Sc(II) would occupy one nonbonding 3d orbital and would have a spin of +1/2. This electron would be visible in an electron spin resonance (ESR) as a duplet state, however, Sc usually occurs as Sc(III) with a very low solubility of the hydroxides (Fig. 2.2). In a theoretical Ti(II), the second electron would occupy a second nonbonding d-orbital with a spin of +1/2 due to Hund's rule of the largest multiplicity, leading to a triplet state. Again, Ti mainly occurs as Ti(IV), again with a low solubility of the hydroxides. Likewise, the third electron of V(II) would occupy the third and last nonbonding d-orbital, leading to the low-energy state of a half-occupied nonbonding 3d electron shell. V is mainly present as V(V) in an oxy-anionic species (Fig. 2.2).

Cr mainly exists in the Cr(VI) oxidation state chromate or di-chromate, or as Cr(III) with a similar half-filled nonbonding 3d electron shell of a theoretical complex. For a Cr(II) complex, two possibilities would exist. Either electron number four has a  $-1/2$  spin and pairs with an electron in one of the nonbonding 3d orbitals, which increases the energetic state due to the needed pairing energy  $P$ , or it enters antibonding 3d\* orbitals, which have a higher energy  $\Delta_o$  compared to the nonbonding 3d orbitals (Housecroft and Constable 2006). If  $\Delta_o < P$ , the electron resides in the antibonding orbital, the number of electrons with a positive  $+1/2$  spin is high and the complex is a high-spin complex with a high multiplicity of, in this example 5, a quintet state. On the other hand, if  $\Delta_o > P$ , the electron pairs with a spin of  $-1/2$  with another electron in a nonbonding 3d orbital, and the number of electrons with a spin of  $+1/2$  is by a factor of 2 smaller than that of the comparable high-spin complex, the multiplicity is 3, a triplet state. In the high-spin state, the electron residing in the antibonding orbital decreases the strength of the bond of one ligand resulting in a weak ligand field compared to a strong ligand field of the corresponding low-spin complex.

The pairing energy  $P$  is a function of the electrostatic repulsion of two electrons in the same orbital according to Coulomb, the energetic consequences of the pairing process, and the difference in energy of an electron with a  $-1/2$  spin compared to the  $+1/2$  spin (Housecroft and Constable 2006). The energy  $\Delta_o$  increases with the oxidation state of the central metal cation, the principal quantum number of the considered d-orbital (compared to 3d: factor 1.5 for 4d and 2 for 5d), and the ligand. With respect to the individual metal,  $\Delta_o$  increases from Mn(II) to Ni(II), Co(II), and from Fe(II) via Fe(III), Cr(III), Co(III), Mn(IV), Mo(III) to Pt(IV). With respect of the ligands,  $\Delta_o$  increases from  $I^-$  via  $Br^-$ ,  $S^{2-}$ ,  $Cl^-$ ,  $F^-$ ,  $OH^-$ ,  $H_2O$ , and  $NH_3$  ultimately to  $CN^-$  and CO (Beyer and Cornejo 2012).

Mn(II) may form a high-spin complex with three single electrons in the three nonbonding 3d orbitals and two single electrons in the two antibonding 3d\* orbitals, or a low-spin complex with two nonbonding 3d orbitals possessing an electron pair and the third one a single electron (Fig. 2.4). Due to the low  $\Delta_o$ , Mn(II) is prone to form weak ligand field, high-spin complexes (not shown in Fig. 2.4). The hydrated Mn(II) cation in water possesses a half-filled 3d shell with five single electrons in the five 3d orbitals, which is a favorable state of low energy. When Mn(II) binds ligands, this stable half-filled 3d shell has to be transformed into a weak ligand field, high-spin complex. Mn(II) complexes are consequently less stable than the complexes of the transition metal cations following Mn in the PSE but Mn(II) complexes can be stabilized by oxidizing Mn(II) such as in Mn-dependent superoxide dismutases or the water-splitting complex of the photosynthetic reaction center II of the cyanobacteria. This increases  $\Delta_o$  and would result in the formation of low-spin complexes of Mn(III). In Mn(IV), all electrons reside in the nonbonding 3d orbitals (Nies 2016).

For iron, octahedral complexes of Fe(III) and Fe(II) may exist. A low-spin Fe(II) complex with three electron pairs filling the nonbonding 3d orbitals completely has a very low energetic state (Fig. 2.4) while a high-spin Fe(II) complex has four electrons in the nonbonding 3d orbitals plus two single electrons in the antibonding

3d\* orbitals (not shown in Fig. 2.4), weakening the bond to two ligands. On the other hand, a low-spin Fe(III) complex has five electrons in the nonbonding 3d orbitals but a high-spin Fe(III) complex has five single electrons in the three nonbonding 3d and two antibonding 3d\* orbitals, which results in a half-filled 3d shell, again a state of low energy. This feature allows the existence of iron-containing complexes with a wide range of half-cell redox potentials for a single electron transfer reaction such as iron–sulfur clusters, cytochromes, or mononuclear iron centers. Moreover, by changing the arrangements of the ligands, for instance, in an enzyme, the energetic differences  $\Delta_o$  between the non- and antibonding 3d orbitals and the pairing energy may be altered so that an enzyme with an iron complex may switch between an electron-accepting and -donating form, which couples the electron transfer process with a conformational change of the respective enzyme (Nies 2016).

These features make iron the most important minor bio-element and transition metal cations, and there are only very few organisms that do not need this metal. Among the metal cations of the first transition period of the PSE, only Fe, Mn, and Cu ions can change their oxidation state outside of complex compounds within the physiological redox range (Fig. 2.4), which is between the half-cell potentials of the constituents of water, molecular hydrogen ( $E_o' = -420$  mV), and molecular oxygen ( $E_o' = +816$  mV), and among the divalent cations, only Mn(II) and Fe(II) are able to fully accept six ligands in complexes that use the 3d, 4s, and 4p orbitals for ligand-accepting molecule orbitals (Fig. 2.4). All divalent metal cations following Fe in the PSE either accept a lower number of ligands, a lower bonding energy of one or two ligands, or use the less favorable 4d orbitals.

Both differences can be used to discriminate Fe against these metals. On the other hand, Fe(II) and Fe(III) interact with reactive oxygen species to form even more dangerous reactive oxygen species in the Fenton reaction as described by Haber and Weiss (Haber and Weiss 1932; Liochev and Fridovich 2002). This was not a problem for living cells before the first oxygenation event but after the concentration of molecular oxygen started to increase on earth, it was very important to protect cellular Fe against reactive oxygen species. One solution of this problem was to use Zn(II) instead of Fe(II) in reactions where a one-electron transferring redox reaction was not needed. A zinc delivering pathway had to evolve to supply Zn(II) to these compounds and to keep other metal cations away, especially Fe(II).

Continuing within the first transition period of the PSE (Fig. 2.4), the Co (II) cation with 7 electrons in the d orbitals may form a high-spin complex with two electrons in 3d\* and five in the nonbonding 3d orbitals or a low-spin complex with the nonbonding 3d orbitals completely filled and a single electron in the 3d\* antibonding orbital. In both forms, one or two ligands are only loosely bound. In contrast, Co(III) with six electrons and a larger  $\Delta_o$  than Co(II), may form a low-spin complex with a low energy due to a completely filled nonbonding 3d shell, plus a less likely high-spin complex with two electrons in 3d\* and four electrons in the nonbonding 3d orbitals. This provides low-spin Co(III) complexes with a low energetic state due to the half-filled 3d orbitals so that Co(III) complexes are kinetically stable. Most of the cell-bound Co thus resides in cobalamin complexes, which sequester cobalt ions and prevent them from interfering with the iron and zinc

metabolism. Derivatives of cobalamin are even used to exchange cobalt between cells, allowing them to keep the concentration of unbound Co(II) in the cytoplasm very low (Nies 2016).

There are no high- and low-spin complexes of Ni(II) (Fig. 2.4). The eight electrons fill the three nonbonding 3d complexes completely with six electrons and two more electrons reside in the two antibonding 3d\* orbitals. Consequently, Ni(II) is not able to accept six ligands in a stable bond in octahedral complex compounds using 3d orbitals. Two ligands are formally only half-bonded with the ligand electron pairs forming the bond and one anti-bond each provided by a single electron in the nonbonding 3d\* orbital. Alternatively, the two electrons in the antibonding 3d orbitals pair, which needs addition of the pairing energy, and five ligands can be bound. Octahedral Co(II) complexes could be formally discriminated against similar Ni(II) complexes by the energy of one additional half-bond, and Fe(II) by two additional half-bonds.

Cu(II) complexes would not be able to accommodate six ligands at all because the nonbonding 3d complexes would be completely filled, one antibonding 3d\* orbital too, and the second antibonding 3d\* orbital with a single electron (Fig. 2.4). Cu(II) is also smaller than the other transition metal cations. The Cu(I) ion has a completely filled 3d orbital, can only bind four ligands by using the 4s and three 4p orbitals. Octahedral copper complexes would have to use 4d orbitals. The redox potential of the Cu(II)/Cu(I) of  $E_o' = -267$  mV allows a rapid, thiol-mediated reduction of any incoming Cu(II) in the cytoplasm (Rigo et al. 2004). Since free thiols are needed in the cytoplasm to allow the formation of high-energy thiol ester compounds, Cu(II) immediately reacts with cysteine residues in proteins, glutathione, other cellular thiols, or free cysteine to form cystine and Cu(I). The large size of the Cu(I) cation plus a charge-volume ratio different from that of the divalent transition metal cations is one contributor of the discrimination process of copper against the other transition metal cations.

Zn(II) finally with 3d<sup>10</sup> is also only able to accept four ligands if the 4d orbitals are not used (Fig. 2.4). Zn(II) is redox-inactive under physiological conditions. From the ionic sizes and ability to form complex compounds, Zn(II) could be discriminated against Cd(II) by its smaller ionic diameter, against Cu(I) due to the differences in the charge-surface ratios, and against Ni(II), Co(II), and Fe(II) by an increasing number of ligands bound, two half-bonds for Ni(II), three for Co(II), and four for Fe(II). Consequently, Fe(II) could most easily be removed from a Zn(II) allocation pathway using the lower energetic state of octahedral Fe(II) complexes compared to tetrahedral Zn(II) complexes, Co(II) less easily and Ni(II) with even more problems. Let us now add the ligands to the picture.

In summary, the ionic radii of the divalent transition metal cations are very similar and not useful for discrimination. Discrimination processes, however, may use differences in the redox potentials. These allow an easy change in the oxidation states of iron and copper but forbid reduction or oxidation of Zn(II) in living cells. Secondly, Zn(II) - > Ni(II) - > Co(II) - > Fe(II) can accept an increasing number of 4, 5, 5.5, and 6 stable ligands, respectively, in a complex compound, so that the bonding energy of the respective additional ligand can be used for discrimination.

Mn(II) forms weak ligand field-, high-spin complexes due to the small energetic difference between non- and antibonding d-orbitals. Mn(II) usually does not out-compete Fe(II), Co(II), Ni(II), or Zn(II) from their complexes.

### 2.2.2 *Metal Cations Are Lewis Acids Interacting with Lewis Bases*

When a metal complex is being formed, a free electron pair of a ligand is donated into an empty orbital of the metal (Housecroft and Constable 2006). The Lewis theory of acids and bases describes a Lewis acid as an atom or molecule that contains an empty orbital and accepts an electron pair from a Lewis base to form a Lewis adduct. A proton is a Lewis acid and a metal cation, too. Formation of a metal complex thus fits into the scope of the Lewis acid and base theory. Free electron pairs can be lone, nonbonding electron pairs from oxygen, e.g. in water, alcoholic, or carbonyl groups, or non-protonated nitrogen atoms or sulfur, e.g. in the sidechains of histidine or methionine, respectively.

Compared to ligands donating a lone electron pair, the complex bond is stronger when an electron pair from a negatively charged molecule is provided, because the electron density at the metal cation is higher. Examples are the monovalent anions of the halides, oxygen atoms in carboxylic acids, carbonate, hydroxide, phosphate, sulfate, or a de-protonated thiol group. These substances also bind protons, they are strong or weak acids. Release of a proton, which is accepted by a water molecule to form a hydronium  $\text{H}_3\text{O}^+$ , is described by the reaction (A, anion):  $\text{AH} + \text{H}_2\text{O} \rightarrow \text{A}^- + \text{H}_3\text{O}^+$ . The equilibrium constant is  $K = [\text{A}^-][\text{H}_3\text{O}^+]/[\text{AH}]$  or simply  $K = [\text{A}^-][\text{H}^+]/[\text{AH}]$ . Water as solvent is not considered. This equation can be transformed into  $\text{pH} = \text{p}K_a + \lg([\text{A}^-]/[\text{AH}])$ , the Henderson–Hasselbalch equation useful to design pH buffers. The  $\text{p}K_a$  is consequently the pH value with  $[\text{AH}] = [\text{A}^-]$  with an identical concentration of the protonated and de-protonated form of the anion. The free Gibbs energy of this reaction is  $\Delta G = -RT \ln K$ ,  $K = e^{(-\Delta G/RT)}$ ,  $\text{p}K_a = -\lg(e^{(-\Delta G/RT)}) = +\Delta G/RT * \lg(e)$ , or  $\Delta G = +\text{p}K_a * RT * \lg(e)$  for the release of the proton. With increasing  $\text{p}K_a$ , release of a proton is an endergonic process with increasing positive free Gibbs energy because the proton is bound more and more tightly, compared to the hydronium ion. On the other hand, bonding of a proton is an exergonic process with increasing  $\text{p}K_a$  value with a value of  $-\text{p}K_a * RT * \lg(e)$  or  $-1.094 \text{ kJ/mol} * \text{p}K_a$ , roughly  $-1.1 * \text{p}K_a \text{ kJ/mol}$ .

Since metal cations and protons are both Lewis acids, this relationship should describe also the energy released by bonding of a ligand to a metal in a complex compound. Strong acids such as halogens consequently are less suitable to form metal complexes than weak acids such as the side chains of glutamate and aspartate, and suitability to form complexes should increase with the  $\text{p}K_a$  value until a ligand is protonated at physiological pH values and is no longer able to provide a free electron pair, e.g. in the protonated side chains of arginine and lysine.



Histidine is a special case. It has  $pK_a$ -values of 1.82, 6.05, and 9.17 with respect to the de-protonation of the carboxy-group, of the imidazole ring, and the amino-group, respectively (Dawson et al. 1969). At a cellular pH value of 7.6 (Zilberstein et al. 1984), protein-incorporated His is 97% de-protonated at the imidazole ring. This ring contains one nitrogen atom in a  $sp^2$ -hybridization and a double bond with the carbon atom at the tip of the imidazole ring and the second in a  $sp^3$ -hybridization and a bound hydrogen atom. Both N atoms exchange the proton in a tautomerization, thereby switching the hybridization state. The imidazole ring can be best described as an aromatic ring system with a de-localized negative charge that is neutralized by a proton switching between the two nitrogen atoms. Metal cations are usually complexed by the free electron pair from the  $sp^2$ -hybridized N atom (Babor et al. 2008; Ebert and Altman 2008), so that the resulting positive partial charge of the nitrogen atom decreases the de-localized negative charge of the aromatic ring system. In a few instances, the migrating proton can be partially subtracted: a negatively charged amino acid such as Asp or Glu in the direct vicinity of the His residue can form a hydrogen bond with the migrating proton so that part of the positive charge of the metal-N-bond is neutralized. Histidine residues, especially with an adjacent Asp or Glu residue that increases the electron density of the imidazole ring system, are therefore excellent ligands for transition metal cations although the free electron pair originates from a formally electric neutral nitrogen atom.

Lewis acids and bases can be sorted into (i) a “class A,” “hard,” or “nonpolarizable”; (ii) a “class B”, “soft,” or “polarizable”; and (iii) a borderline category depending upon various degrees of ionic versus covalent sigma-bonding, pi-bonding, and other effects (Pearson 1963). Hard Lewis acids are protons, the cations of the alkali and earth alkali elements, trivalent and tetravalent metal cations and Mn(II). Soft Lewis acids are Cu(I), Ag(I), Au(I), Hg(II), and Cd(II). Borderline Lewis acids are the divalent metal cation of the first transition group from Fe(II) to Zn(II) (Pearson 1963). Hard Lewis acids have a high charge-volume ratio, whereas soft Lewis acids a lower one. Hard Lewis acids prefer to interact with hard Lewis bases, which are  $H_2O$ ,  $OH^-$ ,  $NH_3$ ,  $F^-$ ,  $Cl^-$ , phosphate, sulfate, carbonate, and acetate. Soft Lewis acids interact preferentially with soft Lewis bases, de-protonated and protonated thiols, sulfide, and other reduced sulfur-containing compounds plus cyanide and CO.

The thermodynamic stability of complexes of hard metal cations is governed by electrostatic interactions and dominated by the charge/volume ratio of the cation. Complex stability increases with increasing charge from monovalent via divalent to tri- and tetravalent metal cations but decreases with the ionic radius, for instance within the group of the alkali metals and within the group of the earth alkaline metals. The stability of the borderline transition metal cation complexes is described by the Irving–Williams series (Irving and Williams 1948) as  $Cu(II) > Ni(II) > Co(II) > Fe(II) > Mn(II)$  and  $Cu(II) > Zn(II)$ . This famous basis for understanding transition metal homeostasis can be nicely visualized by plotting the solubility product of transition metal sulfides ( $S^{2-}$  is a soft Lewis base) against that of the respective hydroxide ( $OH^-$  is a hard Lewis base) (Nies 2016). The hard Mn(II) and

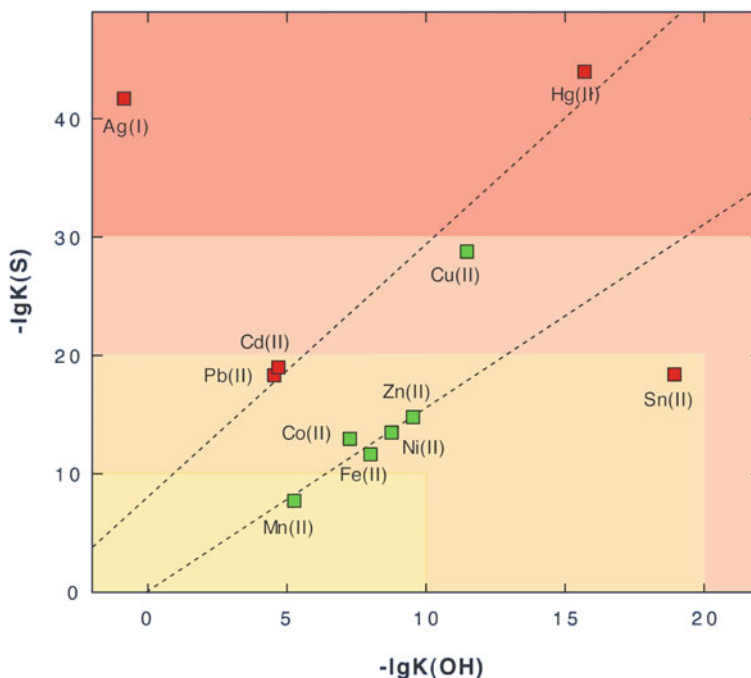


**Fig. 2.5** Solubility product of metal sulfides and metal hydroxides as a measure of affinity to sulfur and oxygen, assigning them to the groups of soft or borderline metals. The negative logarithm of the solubility products of divalent heavy metal cations plus Ag(I)36 was plotted against each other to illustrate the Irving–Williams series of the order of stability of metal complexes (Irving and Williams 1948). Essential trace elements are green and toxic elements red. With the exception of tin and the monovalent cation Ag(I), the data points are located on two lines. The essential elements except copper are on one line, and the “toxic-only” elements due to their high affinity to sulfur are on the other line. Reproduced from (Nies 2007) with permission. Copyright 2007, Springer

the borderline metals Fe(II), Co(II), Ni(II), and Zn(II) are on one line of increasing affinity to both ligand classes (Fig. 2.5). In the order Zn(II) > Ni(II) > Co(II) > Fe(II) >> Mn(II) the metal cations would out-compete each other. Cd(II) and Pb(II) would out-compete all borderline metal cations in the presence of soft Lewis bases as ligands and Cu(II) all of these metals cations.

One facet for cellular transition metal allocation was described above: removal of other, competing transition metal cations by using their ability to bind either more or fewer ligands to octahedral complexes using 3d orbitals. A second constituent comes from the hard and soft acids and bases concept. Since the redox potential of the cytoplasm needs to maintain reduced thiol compounds to allow high-energy thioesters, Cu(II) and accessible Fe(III) ions are reduced to Cu(I) and Fe(II), respectively. Cu(I) as well as the toxic-only Cd(II) and Pb(II) ions are soft Lewis acids, bind strongly to soft, thiol-containing soft Lewis bases, which can be used to discriminate these metals, for regulatory purposes, sequestration, or export reactions. Iron can be discriminated using its ability to alter between the Fe(II) and Fe(III)

oxidation state, high-spin octahedral Fe(III) complexes with six hard ligands, or low-spin octahedral Fe(II) complexes with six soft ligands. Once these metals have been removed, Zn(II) can out-compete the other borderline transition metal cations Co(II), Ni(II) and misplaced Fe(II) in tetrahedral complexes with a mixture of soft and hard ligands. The Sect. 2.2.3 describes how the electrons in the complex bond are distributed between the first-shell ligand atom of the Lewis base and the central metal cationic Lewis acid.

In summary, cations and protons are Lewis acids that interact with free electron pairs in negatively charged or neutral Lewis bases, and in the case of transition metal cations these also form complex compounds. Examples for Lewis bases as complex ligands are the side chains of Glu, Asp, His, and Cys residues of proteins. Hard Lewis acids are small, nonpolarizable ions that prefer ionic bonding and interact with hard Lewis bases such as an oxygen or nitrogen atom as first-shell ligand. Soft Lewis acids are polarizable larger ions with a tendency to form covalent sigma bonds and interact with soft Lewis bases such as thiol groups. The transition metal cations are mostly borderline Lewis acids and the stability of their complexes decreases from soft copper via the borderline cations to the hard Lewis acid manganese.

### 2.2.3 *Electronegativity and Electron Affinity*

Chemical bonds in complex compounds stand between ionic and covalent bonds. Covalent bonds are stable in water. Compounds in ionic bonds may dissolve in water because the hydrated Lewis acids and bases represent a lower state of energy. When this is not the case, on the other hand, such compounds may not dissolve in water or precipitate. Whether two atoms tend to form a covalent or an ionic bond can be predicted from their electronegativity, for instance, according to Linus Pauling, who predicted electronegativity  $\chi_P$  of elements from dissociation energies of chemical bonds to other elements (IUPAC 1997). Electronegativity can also be used to describe complex compounds.

In reality, chemical bonds are never exclusively ionic or covalent bonds, but intermediates. A difference in electronegativity of  $\Delta\chi_P = 1.7$  means 50% ionic and 50% covalent bond so that above this value, the respective Lewis acid and base may dissolve in water if it is soluble at all. The percentage of the covalent character of a bond can be perceived as the period of time that a cation–anion pair is stable before it breaks apart and solvent molecules separate both ions; the higher the covalent character, the longer the cation–anion pair stays in direct contact.

The atoms O and N which donate electrons in many hard Lewis acids have a  $\chi_P$  of 3.0 (N) or 3.5 (O) while S of soft Lewis acids has an  $\chi_P$  of 2.5. The  $\chi_P$  of the alkali metals Na, K, and the earth alkali metals Mg and Ca is 0.9, 0.8, 1.3, and 1.0, respectively, so that these hard Lewis acids form mainly ionic bonds with hard Lewis acids containing O and N first-shell atoms. The bonds of these metal cations to O with  $\Delta\chi_P$  between 2.3 and 1.9 are 59% to 74% ionic, to N with  $\Delta\chi_P$  between 1.8 and 1.4 are 39% to 55% ionic with a higher ionic character of the alkali cation bond

compared to the earth alkali metal bond. Interaction with S may form a covalent bond but hard Lewis acids do not likely interact with soft Lewis bases: the small radius of the respective mono- or divalent cations (65 pm Mg(II), 99 pm Ca(II), 95 pm Na(I) and 133 pm K(I)) does not fit to that of the large S atom (184 pm); the orbital geometry does not efficiently overlap to form molecule orbitals of sufficient low energy to compete with smaller orbitals from O in water (Weast 1984; Housecroft and Constable 2006).

The  $\chi_P$  of the transition metals is  $1.5 \text{ Mn} < 1.6 \text{ Zn} < 1.7 \text{ Cd} < 1.8 \text{ Fe} = \text{Co} = \text{Ni} < 1.9 \text{ Cu} = \text{Ag} = \text{Hg} < 2.4 \text{ Au}$  (IUPAC 1997), so that the Au–S bond is 99.5% covalent, the Cu/Ag/Hg–S bond 91%, the Fe/Co/Ni–S bond 88%, the Cd–S bond 85%, and the Zn–S bond 81%. This high covalent character of chemical bonds to sulfur is the reason for the low solubility of the sulfides especially of the soft Cu(I) and Ag(I) ions but also for the sulfides of the borderline metal cations, and the high stability of their bond to de-protonated cysteine residue. Starting with Fe, all transition metals except the lanthanides and actinides have such a high electronegativity that they form covalent and very stable bonds to cellular thiol compounds. All these cations are thiol poisons if their cytoplasmic concentration is not strictly controlled. By bonding to thiols, they disturb conformations of proteins, with an outcome similar to heat stress, and the thiol-based cellular redox homeostasis, which is essential to allow energy-rich thiol esters (Nies 2007). Soft and borderline cations may also interfere with the formation of iron–sulfur clusters or destroy them (Helbig et al. 2008b; Helbig et al. 2008a; Macomber and Hausinger 2011; Fantino et al. 2010; Majtan et al. 2011), subsequently releasing un-controlled iron. In addition to the formation of reactive oxygen species by Fe(II)/Fe(III) and Cu(I)/Cu(II), this is the second reason for the toxicity of all transition metal cations. The soft Lewis acids such as Cu(I), Cd(II), Ag(I), Pb(II) are more toxic than the borderline metals (Nies 2000).

Even the Mn–S bond would be 78% covalent but Mn(II) is again a hard Lewis acid due to its half-filled 3d orbitals and does not interact strongly with S. In contrast, the Mn–O bond is a hard Lewis acid–base interaction that would be 63% ionic, Zn–O 59%, Cd–O 55%, and Fe–O 51%. Bonds coming from N in hard Lewis acids are in-between S and O with respect to the ionic/covalent character of the bond: Zn–N is 61% covalent, Co–N 70%, and Mn–N 57%. Such a bond could come from a nitrogen atom of histidine.

The electronegativity  $\chi_P$  according to Pauling can also be calculated from the electronegativity  $\chi_M$  according to Mulliken (Atkins and de Paula 2013):  $\chi_P = 1.35 * (\chi_M)^{0.5} - 1.37$  with  $\chi_M = (E_{ca} + E_i)/2$ .  $E_i$  is the first ionization energy needed to remove the out-most valence electron and  $E_{ca}$  the electron affinity, which is the energetic difference between the first anion and the neutral atom, all in eV per atom. Electronegativity  $\chi_P$  according to Pauling is therefore a direct linear function of the square root of the mean value of both energies. The ionization energy  $E_i$  increases with the atomic number but decreases with  $1/n^2$ , the reciprocal square of the principal quantum number  $n$ . For most metals,  $E_i$  is between 5 eV per atom and 10 eV per atom. The value is low for the s-, d-, f- and the first p-elements of each period, reaching the highest value for He with 25 eV/atom. The  $E_i$  for the elements

**Table 2.1** Ionization energies and electron affinities (kJ/mol)<sup>a</sup>

Element	Mn	Fe	Co	Ni	Cu	Zn
1st	717	763	760	737	746	906
2nd	1509	1562	1648	1753	1958	1733
electrAff	-50.0	15.7	63.7	112.0	118.4	-58.0
2nd/1st	2.10	2.05	2.17	2.38	2.63	1.91
eleAff/1st	-6.97%	2.06%	8.38%	15.19%	15.88%	-6.40%

<sup>a</sup>The table shows the first and second ionization energy and electron affinities (Weast 1984; Kramida et al. 2019). The ionization energies are the energies needed to remove the first or second electron from the atom in the gaseous state, respectively. “elecAff” is the electron affinity, the energy released when an additional electron is bound by the neutral atom, yielding the first anionic state. Please note that this value is negative for Mn and Zn, meaning that addition of an electron to the neutral atom is an endergonic event. Two ratios follow, the second divided by the first ionization energy, and the electron affinity divided by the first ionization energy

from Sc to Cr is about 6 eV/atom, for Mn to Cu about 7.5 eV/atom, and nearly 10 eV in case of Zn. This calculates into first ionization energies in kJ/mol of 717 kJ/mol for Mn, 737 kJ/mol and 763 kJ/mol for Fe to Cu, respectively, and 906 kJ/mol for Zn (Table 2.1).

Electron affinities were determined with single atoms using laser photo-detachment threshold studies or laser photo-detached electron spectrometry (Scheer et al. 1998). The alkali metals have an  $E_{ea}$  between 0.5 eV/atom and 0.6 eV/atom, the earth alkali metals an  $E_{ea}$  of 0 eV. Their low electronegativity results from a low electron affinity because these electrons would occupy the s-orbital of a new electron shell with the next principal quantum number. Calculated into kJ/mol (Table 2.1), the electron affinities are between +15.7 kJ/mol for removal of an additional electron from the  $Fe^-$  anion up to +118 kJ/mol for  $Cu^-$ . Due to the half-filled or filled 3d orbital, respectively, the electron affinities for  $Mn^-$  is -50 kJ/mol and for  $Zn^-$  -58 kJ/mol: adding electrons to neutral transition metal cations is exergonic for Co, Ni, Cu, exergonic with a comparable low energy released for Fe but endergonic for Mn and Zn.

The  $E_{ea}$  values are small compared to the ionization energy  $E_i$ , between 2% and 16% for Fe, Co, Ni, Cu; and -6 to -7% for Mn and Zn (Table 2.1). The low first ionization energy plus negative electron affinity results in a small electronegativity of Mn and Zn, despite the high first ionization energy of Zn (Table 2.1). Although the electronegativity  $\chi_P$  of the transition metals,  $1.5 Mn < 1.6 Zn < 1.8 Fe = Co = Ni < 1.9 Cu$ , increases only 25% from Mn to Cu and is identical for Fe, Co, and Ni, the underlying electron affinities are very different, negative for Mn and Zn, weak for Fe, and positive for Co, Ni, Cu. When the respective metal cations accept electrons from ligands in a complex compound, which has a strong covalent attitude as can be derived from the differences in electronegativity, the residence probability of the electrons in the bonding molecule orbitals increases with the difference in electronegativity and the number of ligands. Providing electrons from ligands to the central metal cation should be an exergonic process for all divalent metal cations until the two positive charges are neutralized. When more electron

probabilities are added, it continues to be an exergonic process for Co(II), Ni(II), Cu(II), has not much benefit for Fe(II) until it is oxidized to Fe(III), and is an endergonic process for Mn(II) and Zn(II).

In summary, hard Lewis acids (Na, K, Mg, Ca) have a low electronegativity while the electron pair donors of hard Lewis bases (O, N) have a high electronegativity. This makes bonds between them predominantly ionic. On the contrary, the difference in electronegativity of soft and borderline Lewis acids and bases is smaller, leading to bonds with a more covalent character. The electronegativity can be calculated from the first ionization energy and electron affinity of an element, which is the respective energy needed to remove the first electron from the neutral atom, or to supply one electron to yield the first anionic state. Due to the half-filled or completely filled, respectively, 3d orbitals, the electron affinity of Mn and Zn is negative. In contrast to other transition metal cations, a negative net charge at the metal atom is thus an endergonic state for Mn and Zn.

### 2.2.4 Bonding Energies for Two Ligands

Calculated from the difference in electronegativity, all bonds between the transition metal cations and O, N, S are less than 100% covalent. In a purely 100% covalent bond, the bonding electron pair in the bonding molecule orbital resides exactly in the middle between the two bonding atoms, with each atom receiving on the average the residence probability of one electron. In case of a bond that is <100% covalent, less than one electron probability resides at the metal cation per ligand, and the two positive charges of the divalent metal cation are not neutralized when two ligands were accepted. In case of all divalent transition metal cations, bonding of two Lewis bases as ligands should be an exergonic process because the positive charge of the central cation would not even be fully neutralized in a purely covalent bond with two ligands. The negative electron affinities of Mn(II) and Zn(II) must not be considered for two ligands.

When a metal cation is entering a bacterial cell, it is confronted with a variety of possible ligands. Phosphate as a hard Lewis base and a first  $pK_a$  of 2.49 is less suitable than the carboxy-groups of the amino acid residues of aspartate (terminal carboxy-group  $pK_a = 3.7$ ) or glutamate ( $pK_a = 4.3$ ) as ligand for hard or borderline metal cations (Dawson et al. 1969). Tyrosine (OH group at the aromatic ring  $pK_a = 9.19$ ) should be largely protonated at a cytoplasmic pH value and not ready to accept a metal cation, although Tyr may be a ligand in the metal-site of a protein. The concentration of  $OH^-$  ions is very low. At  $pH_i$  7.6 (Zilberstein et al. 1984), the  $pOH$  is consequently 6.4 and the concentration is 398 nM, so that the primary hard Lewis base ligands should be Asp and Glu. Histidine residues (imidazole  $pK_a = 6.05$ ) should be largely neutral and ideal ligands for borderline metals. Cysteine residues (thiol  $pK_a = 8.48$ ) should be 13% de-protonated at pH 7.6 (Zilberstein et al. 1984) according to the Henderson–Hasselbalch equation. Cys and  $S^{2-}$  released as intermediates during synthesis of cysteine and iron–sulfur clusters are soft Lewis bases

not only for soft metal cations such as Cu(I), Cd(II), and Pb(II) but also for borderline metals.

The stability constants of metal complexes can be used to calculate the free energy released during formation of the complex with one or two ligands (Table 2.2). From these, Boltzmann distribution statistics allows us to predict competition between the metals for the ligands. Mg(II) and Ca(II) as hard Lewis acids bind to the hard Lewis bases in the terminal carboxy-groups of Asp and Glu and could be out-competed by a thousand-fold lower concentration of Zn(II). However, the stability constant of the  $\text{Ca}_3(\text{PO}_4)_2$  complex is  $1.3 \times 10^{-32}$ , so that cytoplasmic Ca(II) would immediately precipitate cytoplasmic ortho-phosphate. Consequently, cytoplasmic Ca(II) is only allowed under extraordinary circumstances, e.g. as a signaling substance, and Ca(II) is not further considered here. Mn(II) as hard divalent transition metal cation binds only weakly to Cys and can be out-competed easily by the other transition metal cations at all four ligands Cys, His, Asp, and Glu (Table 2.2). Nevertheless, even alkali metal cations form complexes with histidine and their complexation energies decrease in the order  $\text{Mg(II)} > \text{Ca(II)} > \text{Na(I)} > \text{K(I)}$  (Hashemian 2011; Kumar et al. 2015) so that all inorganic cytoplasmic cations should interact with the Asp, Glu, and His side chains of the resident proteins.

The  $\Delta G$  values in Table 2.2 should only be taken as proxy for the real interaction energies in vivo. They are much more negative than values measured experimentally, for instance by isothermal calorimetry (ITC). Bonding of a Cu(II) to a region with two His residues at pH 7 would release a free energy of  $-57.9$  kJ/mol for the first bond and  $-48.25$  kJ/mol for the second bond, summing up to  $-106.15$  kJ/mol (Table 2.2). Experimental values determined for bonding of Cu(II) to a peptide with 2 His and 2 Lys residues are between  $-20.08$  kJ/mol and  $-29.29$  kJ/mol, depending on the position of the Lys residues and the spacing of the His residues (Wang et al. 2020). These differences result from the difference between the experimental reality and theoretical consideration. For instance, ITC experiments measure the difference in energy between a metal bound to a given substance minus the energy needed to release the metal from the buffer used in the ITC experiment, plus energy stemming from a release or bonding of protons to the complex ligand and the buffer. The ITC experiment used as an example was performed in the presence of MES (2-(*N*-morpholino)ethanesulfonic acid) as buffer (Wang et al. 2020). Buffers are Lewis bases and also bind Lewis acids such as metal cations with a bonding energy of around  $-42$  kJ/mol for Zn(II) (Bou-Abdallah and Giffune 2016), and a higher value expected for Cu(II). ITC results and the prediction of bonding energies from the stability of metal complexes are thus different proxies for the condition in the cytoplasm and cannot be directly compared.

As shown in Table 2.2, the soft Lewis acid Cu(II) would strongly interact with all ligands and could out-compete all other metal cations even at very low concentrations. This metal must be kept away from all metal sorting pathway or it would out-compete every other metal from its metal bonding site. This task can be easily accomplished since Cu(I) is the predominant form of copper in the cytoplasm, has a larger ionic diameter, is a soft Lewis acid and binds strongly to thiol group, for

**Table 2.2** Free energy released during the first and second bonding of a ligand (kJ/mol)<sup>a</sup>

	$\Delta G_o(K_1)$				$\Delta G_o(K_2)$				S <sup>2-</sup>	OH <sup>-</sup>	
	Cys	His	Asp	Glu	Cys	His	Asp	Glu			
Mg(II)			-13.92	-11.02							-64.10
Ca(II)			-9.28	-8.12							-34.14
Mn(II)	-23.78	-23.20	-21.46	-19.14	-20.68	-21.46	-16.26	-14.72	-87.91	-73.66	
Fe(II)	-35.96	-29.42	-28.05	-26.68	-32.48	-24.52	-21.25	-20.53	-106.72	-85.53	
Co(II)	-53.95	-43.98	-34.22	-26.56	-44.08	-36.65	-24.94	-20.43	-123.56	-90.50	
Ni(II)	-59.88	-50.31	-41.18	-34.22	-52.07	-41.92	-30.74	-25.52	-119.05	-91.63	
Cu(II)	<b>n, v.<sup>b</sup></b>	-57.90	-49.89	-45.82	<b>n, v.<sup>b</sup></b>	-48.25	-39.44	-38.86	-209.38	-109.03	
Zn(II)	-57.43	-38.86	-33.64	-31.90	-51.05	-29.58	-25.52	-23.20	-125.31	-94.82	
<b>Boltzmann distribution compared to Zn(II)</b>											
Mg(II)			2512	3981							197.778
Ca(II)			15,849	12,589							2.89E+10
Mn(II)	630,957	501	126	158	171,705	25	40	29	2,800,000	4444	
Fe(II)	5012	42.4	9.20	7.94	1585	7.46	5.45	2.89	1600	40.0	
Co(II)	3.98	0.131	0.794	8.35	15.85	0.0605	1.26	3.01	2.00	5.56	
Ni(II)	0.377	0.0106	0.0501	0.398	0.666	0.00746	0.126	0.398	12.0	3.56	
Cu(II)		5.23E-04	1.58E-03	3.98E-03		6.05E-04	3.98E-03	2.00E-03	3.20E-15	3.56E-03	

<sup>a</sup>The stability constants of metal complexes (Dawson et al. 1969) were transformed into free energies according to  $\Delta G_o = -RT \ln(K)$  with  $K_1$  being the stability constant of the metal cation with the first ligand. The constant  $K_2$  was taken from  $b_2 = K_1 * K_2$ . For some complexes, either  $b_2$  or  $K_1$  were provided. Since the energy of the first bonding was  $25\% \pm 11\%$  higher than that of the second ( $15\% \pm 6\%$  for Cys,  $20\% \pm 16\%$  for His,  $32\% \pm 5\%$  for Asp, and  $30\% \pm 10\%$  for Glu), the amino acid-specific values were used to calculate the respectively missing energy. These values are in italics. No values are available for Cu(II) and Cys since the metal cation is reduced rapidly by the thiol residue of the amino acid. In the second part, the Boltzmann distribution of metal cations compared to Zn(II) is shown according to  $N_1/N_2 = e^{\Delta} \{-(E_1-E_2)/RT\}$ . This shows which concentration of the other metal cation is needed to compete with an equimolar concentration of Zn(II)

<sup>b</sup>No value (**n,v.**) exists for Cu(II) and cysteine since Cu(II) ions are reduced by cysteine to cystine and Cu(I), which is subsequently bound by remaining free cysteines with a lg  $K_1$  of 10, calculating to  $-58$  kJ/mol (Rigo et al. 2004)



instance in copper chaperones (O'Halloran and Culotta 2000). Iron, on the other hand, would only at a 5000-fold higher concentration be able to out-compete Zn (II) for the first Cys ligand (Table 2.2). The bonding energies for Co(II) and Zn (II) are very similar to those for Zn(II). They would also be able to out-compete Fe (II). After copper ions were removed up-front every metal allocation and sorting pathway as Cu(I), a Fe(II) allocation pathway had to be shielded against Co(II), Ni (II), and Zn(II). In a last step, Co(II) and Ni(II) had to be ushered away from zinc allocation pathways.

To discriminate the metal cations Fe(II), Co(II), Ni(II), and Zn(II) against each other, the different redox potentials, electron affinities, number of accepted ligands, and concentrations inside the cell can be used. While the redox potential of Fe(III)/Fe (II) is  $E_o' = +771$  mV and thus within the redox range of living cells (Weast 1984), oxidation states of Co and Ni other than (II) are only possible in special metal complexes. Zn(II) cannot be oxidized or reduced at all by living cells. The possibility of an easy change of the redox potential can be used to discriminate Fe(II) against the other divalent metal cations. The different electron affinities influence the effect when more than two ligands are being bound. This is considered in the next section (Sect. 2.2.5).

In summary, two negatively charged Lewis base ligands will not fully neutralize the positive net charge of a divalent metal cation so that the electron affinity of the metal is of no concern. The free energy of bonding two ligands mirrors the Irvine–Williams series for metal cations, but not completely for the most prominent ligands Cys, His, Asp, and Glu. According to Irvine–Williams and demonstrated here, Cu (II) always forms the strongest complexes, Ni(II) is second, and Mn(II) the weakest complexes. The ranking of Zn(II), Co(II), and Fe(II) depends on the ligand. For Cys, Zn(II) > Co(II) > Fe(II); for His and Asp, Co(II) > Zn(II) > Fe(II), and for Glu, Zn (II) > Fe(II) > Co(II). This opens another possibility for discrimination. Cu (II) complexes with Cys are not stable and lead to a rapid reduction of Cu(II) to Cu(I).

### 2.2.5 *Net Charges for More than Two Ligands*

According to Table 2.2, bonding of Zn(II) to two Cys plus 2 His (CCHH), three Cys plus 1 His (CCCH), or four Cys (CCCC) should release an energy of  $-177$  kJ/mol,  $-198$  kJ/mol, or  $-211$  kJ/mol, if the bonding of ligand number 3 or 4 releases a similar amount of energy as does ligand number 2. ITC experiments that determine distribution of Zn(II) from HEPES buffer at a neutral pH value to CCHH, CCCH, and CCCC environments measured a release of free energy of about  $-42$  kJ/mol with not much difference between the environments (Bou-Abdallah and Giffune 2016). Although different values are measured here, free energy calculated from the stability of complex compound versus exchange of Zn(II) between a substance and a buffer in the ITC experiments, the free energy of Zn(II)-bonding should increase from the CCHH to the CCCC environment because Cys bonds with an higher release

of energy than does His. This indicates that the negative electron affinity of zinc may indeed have an influence on the formation of zinc complexes with more than two ligands.

The negative electron affinity of zinc should have an influence when the net charge of the central Zn(II) becomes a negative value. For each ligand that provides a bonding electron pair to the central metal cation, the residence probability of the electron pair in a covalent bond would be in the middle between both atoms, adding formally one electron to the metal and one to the first-shell ligand atom. In a purely ionic bond, both electrons would reside close to the first-shell ligand atom and no negative charge would be contributed to the metal. Consequently, the percentage of the covalent bond character between both atoms can be calculated from the difference in electronegativity between metal and first-shell ligand atom. This value equals the negative charge actually provided from the ligand to the metal. Since the charge provided by the first-shell ligand atom is influenced by the other atoms of the ligands, this value was corrected by the ratio of the bonding energy of the first-shell atom in a ligand (e.g., the S in Cys) divided by the bonding energy of the lone atom (e.g.,  $S^{2-}$ ). From these data, the charge of the central atom in complexes with one to four ligands was estimated for hypothetical Mn(II) to Zn(II) complexes (Table 2.3).

These data (Table 2.3) are rough extrapolations and ignore mesomeric forms of complex compounds, kinetics, an inadequate position of the ligand, accessibility of the site, conformation changes of the bonding macromolecules, and so on. They represent a simple model and allow us to estimate the effect of the different electron affinities of the transition metal cations on the formation of complex compounds and derive consequences for the metal distribution and discrimination in the cytoplasm.

As expected, all metal complexes with only one or two ligands still carry a positive net charge of the central metal atom (Table 2.3) so that the electron affinity has no influence. Among the complexes with three ligands, CCC complexes of Cu(II) and Ni(II), Ni(II)-CCH and Cu(II)-CCD would have a negative net charge ("D" in Table 2.3 standing for Asp or Glu). Nearly all complexes between Co(II), Ni(II), Cu(II), and Zn(II) with two or more Cys residue carry a negative net charge but only two iron complexes (CCCC and CCCH) and no Mn complex. Only few complexes with one Cys only or more than two His residues but without Cys lead to a formal negative charge of the central metal atom. These are in most cases Ni(II) complexes (Table 2.3).

Complexes of Cu(II) and Mn(II) with two or more Cys residues are not relevant in the cytoplasm. Complexes of Cu(II) with two or more Cys residues immediately lead to the formation of cystine and Cu(I) (Rigo et al. 2004), and this Cu(I) would be bound to a third Cys ligand. The hard Lewis acid Mn(II) binds only weakly to Cys (Table 2.2). The Co(II) and Ni(II) complexes with two or more Cys should be stabilized by the positive electron affinities while the respective Zn(II) complexes should be de-stabilized: formation of tetrahedral Zn(II) complexes with many Cys residues should be an endergonic process. The energy needed to stabilize such complexes could be generated in a metal-protein by conformational re-arrangements that lead to the formation of additional ionic or hydrogen bonds.

**Table 2.3** Net charge of a divalent transition metal cation with one, two, three, or four amino acid residues as ligands<sup>a</sup>

Metal	Mn(II)	Fe(II)	Co(II)	Ni(II)	Cu(II)	Zn(II)
D (= D or E)	1.82	1.72	1.71	1.65	1.58	1.75
H	1.72	1.58	1.52	1.42	1.70	1.55
C	1.61	1.44	1.30	1.17	1.09	1.30
CC	1.21	0.87	0.60	0.34	0.18	0.60
CH	1.32	1.01	0.82	0.59	0.79	0.85
CD	1.43	1.16	1.01	0.82	0.67	1.05
HH	1.43	1.16	1.03	0.84	1.41	1.10
HD	1.54	1.30	1.23	1.07	1.28	1.31
DD	1.64	1.45	1.43	1.30	1.15	1.51
CCC	0.82	0.31	<b>-0.09</b>	<b>-0.48</b>	<b>-0.73</b>	<b>-0.10</b>
CCH	0.93	0.45	0.12	<b>-0.24</b>	<b>-0.12</b>	0.15
CCD	1.03	0.59	0.32	<b>-0.01</b>	<b>-0.24</b>	0.35
CHH	1.04	0.59	0.34	0.01	0.50	0.40
CHD	1.14	0.74	0.53	0.24	0.37	0.60
CDD	1.25	0.88	0.73	0.47	0.24	0.80
HHH	1.15	0.73	0.55	0.26	1.11	0.66
HHD	1.25	0.88	0.75	0.49	0.99	0.86
HDD	1.36	1.03	0.94	0.72	0.86	1.06
DDD	1.46	1.17	1.14	0.94	0.73	1.26
CCCC	0.42	<b>-0.26</b>	<b>-0.79</b>	<b>-1.31</b>	<b>-1.64</b>	<b>-0.80</b>
CCCH	0.53	<b>-0.12</b>	<b>-0.58</b>	<b>-1.06</b>	<b>-1.03</b>	<b>-0.55</b>
CCCD	0.64	0.03	<b>-0.38</b>	<b>-0.83</b>	<b>-1.15</b>	<b>-0.35</b>
CCHH	0.65	0.03	<b>-0.36</b>	<b>-0.82</b>	<b>-0.41</b>	<b>-0.30</b>
CCHD	0.75	0.17	<b>-0.17</b>	<b>-0.59</b>	<b>-0.54</b>	<b>-0.10</b>
CCDD	0.85	0.32	0.03	<b>-0.36</b>	<b>-0.67</b>	0.10
CHHH	0.76	0.17	<b>-0.15</b>	<b>-0.57</b>	0.20	<b>-0.04</b>
CHHD	0.86	0.32	0.05	<b>-0.34</b>	0.08	0.16
CHDD	0.96	0.46	0.24	<b>-0.11</b>	<b>-0.05</b>	0.36
CDDD	1.07	0.61	0.44	0.12	<b>-0.18</b>	0.56
HHHH	0.87	0.31	0.07	<b>-0.32</b>	0.82	0.21
HHHD	0.97	0.46	0.26	<b>-0.09</b>	0.69	0.41
HHDD	1.08	0.60	0.46	0.13	0.56	0.61
HDDD	1.18	0.75	0.65	0.36	0.44	0.81
DDDD	1.28	0.89	0.85	0.59	0.31	1.01
CCSS(II) <sup>b</sup>	<b>-0.35</b>	<b>-0.89</b>	<b>-1.16</b>	<b>-1.42</b>	<b>-1.64</b>	<b>-1.02</b>
CCSS(III) <sup>b</sup>	0.65	0.11	<b>-0.16</b>	<b>-0.42</b>		
HHHEE <sup>c</sup>	0.79	0.18	<b>-0.02</b>	<b>-0.45</b>		
HHHHHCy(II) <sup>d</sup>	<b>-0.13</b>	<b>-0.69</b>	<b>-0.93</b>			
HHHHHCy(III) <sup>d</sup>	0.87	0.31	<b>0.07</b>			

<sup>a</sup>First, the residence probability of bonding electrons was calculated from the difference in electronegativity according to Pauling between the central metal and the first-shell ligand O (D or E), N (H), or S (C). This value was corrected with the ratio of the bonding energies 0.5(OH<sup>-</sup>/

(continued)

2Asp + OH<sup>-</sup>/2Glu), S<sup>2-</sup>/2Cys, or a mean value used for His. The bonding energies for OH<sup>-</sup> and S<sup>2-</sup> result from the solubility constants of the hydroxides and sulfides. These compounds precipitate when the O or S atoms bind at least to two metal cations. Therefore, the bonding energies for the hydroxides were divided by the bonding energies of two of the respective amino acyl residues. This first step yielded an approximation of the charge provided by each ligand. In the second step, the net charge was calculated as: +2 minus the sum of the charges provided by the ligands in the field. D stands for Asp or Glu, H for His, C for Cys, S for a sulfide, and Cy for cyanide

<sup>b</sup>Iron–sulfur cluster with a divalent or trivalent metal cation

<sup>c</sup>Bonding site of CnrX (Trepreau et al. 2014). Here, a methionine is also involved and the “EE” indicates oxygen atoms coming from glutamate residue E63. Charges from the S of the Met residue were not calculated

<sup>d</sup>Net charge of cyano-cobalamin with a divalent or trivalent metal cation in the center. Negative net charges in bold

Although Cys residues bind more strongly to Zn(II) than His residues, exchanging His for Cys does not increase the amount of energy released during bonding (Bou-Abdallah and Giffune 2016) due to the “electron overload” of Zn(II) in ligand fields with more than two Cys residues (Table 2.3). Moreover, the conformation change that needs to occur during zinc-binding to such complexes may close a zinc site against access from the outside. Releasing the Zn(II) again would require another conformation change or proteolytic degradation of the protein, raising a barrier against the exchange of the metal. The totality of zinc ions bound to such complexes would represent a pool of firmly bound zinc ions. Zinc bound here would have a conformational function, for instance in the center of the beta-prime subunit of the bacterial RNA-polymerase (King et al. 2004; Markov et al. 1999; Wu et al. 1992). Zn(II) is here in a CCCC ligand field.

Conformational Zn(II) ions in a CCCX or CCHH ligand field do not simply stabilize the respective polypeptide chain due to an especially low energetic state. This would stabilize only the position of the ligands surrounding the zinc ion while other amino acids are still mobile. The energy needed to override the negative electron affinity of Zn(II) in CCCX/CCHH ligand fields forces also the formation of ionic, hydrophobic interactions or hydrogen bonds in other parts of the zinc-polypeptide so that Zn(II) has a long-distance effect on the conformation of the respective protein. These proteins with their firmly bound zinc ion form the dead-end of the zinc allocation pathway, firmly bound and not accessible zinc ions. Zinc should be inserted into such proteins immediately following translation. Consequently, zinc must be delivered to the ribosome, stored here and delivered to the folding protein (Akanuma et al. 2006; Hensley et al. 2011; Kaczanowska and Ryden-Aulin 2007).

None of the zinc complexes with a maximum of three ligands carries a net negative charge (that of Zn(II)CCC is very small, Table 2.3). These complexes have a solute-accessible fourth ligand position, allowing catalysis with Zn(II) acting as Lewis acid, exchange of zinc ions against other metals, or migration of zinc ions from one site to another one. The totality of these zinc complexes would form a pool of still accessible zinc ions. The bonding energy and complex stability should increase from a Zn(II)DDD to a Zn(II)CCC complex. In the middle between

loosely bound and firmly bound zinc ions would be those in tetrahedral complexes with only one Cys or without Cys such as a His-rich ligand field. In these cases, accessibility of the site and the conformational stability of the zinc-macromolecule would decide if the Zn(II) is shielded and part of the firmly bound zinc pool or still part of the mobile, loosely bound zinc pool.

In summary, tetrahedral sites with more than three Cys or a Cys<sub>2</sub>His<sub>2</sub> (CCHH) site are endergonic sites for zinc. This 3d<sup>10</sup> metal has a negative electron affinity and the electron pairs donated by the Cys sulfur atoms in the nearly covalent bond to Zn (II) result in an overcompensation of the two positive charges of the metal. On the one hand, such sites could be employed to counter-select against Zn(II), for instance during formation of iron–sulfur clusters in a Cys<sub>2</sub>S<sub>2</sub><sup>2-</sup> environment. On the other hand, the energies released during formation of ionic or hydrogen bonds of the protein harboring such a site can be used to overcompensate the endergonic zinc-process. This would not only strongly stabilize the conformation of the zinc site but also that of all bonds allowing zinc bonding, stabilizing the protein conformation on a higher level. This fact and the redox-inactivity make zinc into an ideal structure-determining component of proteins. Probably, such a zinc-stabilized conformation has to be generated immediately after protein synthesis at the ribosome, which needs to receive and store a constant supply with zinc.

### 2.2.6 *Transition Metal Cations and Glutathione*

When Zn(II) or another transition metal cation enters the cytoplasm of a Gram-negative bacterial cell, it is confronted by a concentration of about 5 mM glutathione (GSH) (Apontoweil and Berends 1975; Fahey et al. 1978; Helbig et al. 2008a). Due to the high affinity of Zn(II) to Cys (Table 2.2) and the fact that about 13% of the Cys residue of GSH should be de-protonated at a cytoplasmic pH of 7.6 (Zilberstein et al. 1984) according to Henderson–Hasselbalch, Zn(II) could be bound by two GSH forming a zinc-bis-glutathionato-complex (Dominey and Kustin 1983). This bonding should also protect accessible Cys residues or sulfides released during Cys biosynthesis or synthesis of iron–sulfur centers against bonding by Zn(II). GSH may even “wash” Zn(II) away from exposed Cys residues. Bonding of zinc to these thiols would disturb redox homeostasis of the cell and energy transformation using thiol esters so that the protecting effect of GSH may be based on its ability to shield thiols against transition metal cations. Nevertheless, the bis-glutathionato-complexes of transition metal cations (or Cu(I)-GS) react with molecular oxygen to oxidized glutathione GSSG, superoxide radicals, H<sub>2</sub>O<sub>2</sub>, and also the released metal cation, which immediately binds again to GSH. This catalytic function of transition metal cations is the reason for redox stress caused by cations such as Zn(II) or Cd(II), which cannot be reduced or oxidized. In case of Cu(I), this even causes the Fenton-type production of reactive oxygen species (Aliaga et al. 2012; Bishop et al. 2007; Corazza et al. 1996; Kachur et al. 1998).

In Gram-negative bacteria, GSH can be transported into the periplasm and from the periplasm into the cytoplasm so that interaction of metal cation with GSH also occurs in the periplasm (Pittman et al. 2005; Suzuki et al. 2005). Gram-positive bacteria are able to import GSH or contain other main cellular thiol compounds such as mycothiol (Fahey et al. 1978; Newton et al. 1996; Newton and Fahey 2002; Sherrill and Fahey 1998). Consequently, the interaction of cytoplasmic Zn(II) that occurs in Gram-negative bacteria also occurs in a similar manner in Gram-positive bacteria, in the periplasm of Gram-negative bacteria, and similar interactions also exist with other transition metal cations.

Zn(II) and other transition metal cations thus cannot stay within the GSH pool. The best goal would be to prevent these metals from entering the pool at all. Bonding of a Zn(II)-(GS)<sub>2</sub>-complex to a pair of His residues would form a CCHH ligand field with a negative net charge of  $-0.30$  (Table 2.3), which is against the negative electron affinity of zinc. Displacement of one GSH-Cys by a third amino acid residue would result in a CHHH or CHHD field and lower the negative net charge of the Zn (II) ion. Bonding of a His, Glu, or Asp yields a lower amount of energy than bonding of a GSH-Cys (Table 2.2), however, the negative electron affinity of Zn(II) may lower the energetic barrier for such an exchange. After release of the first GSH, the danger of oxidation of the two GSH to GSSG is avoided. Release of the second GSH could be accomplished by a Cys residue of the protein. Double-His sites with an adjacent Asp and Glu and a Cys in the vicinity should be fully sufficient to clear the GSH pool from Zn(II). The bonding energy of Zn(II) to a HD, HE, HH, EE, ED, or DD site is more negative than bonding to a single Cys (Table 2.2). Three His would even bind more strongly than 2 Cys.

In summary, small His-rich regions at the surface of proteins may play an important role in keeping Zn(II) away from the GSH pool or to remove any zinc from here. Ni(II) and Co(II) have an even more negative bonding energy to His (Table 2.2) so that the His-rich sites in proteins may play a similar function for these two metals.

### ***2.2.7 Conclusion: Cellular Transition Metal Cation Allocation Pathways***

As stated above, all numbers in Tables 2.2 and 2.3 for Cu(II) are only theoretical values because Cu(II) is immediately reduced to Cu(I), which binds to GSH and may cause Fenton reactions (Rigo et al. 2004; Aliaga et al. 2012; Freedman et al. 1989; Kachur et al. 1998; Speisky et al. 2009). The first rule of cytoplasmic multiple transition metal homeostasis would thus be to either sequester or remove Cu(I) from the cytoplasm.

The bonding energy of Fe(II) to Cys is much lower than that of Ni(II), Co(II), and Zn(II) (Table 2.2). In a ligand field with two Cys and two sulfides (CCSS, Table 2.3), the negative net charge and negative electron affinity would prevent bonding of Zn

(II). Ni(II) and Co(II) would acquire more than one negative net charge, which would be beyond their otherwise positive electron affinity. These ions are not stable central ions for such a complex but inhibit its assembly (Fantino et al. 2010; Ranquet et al. 2007; Davidson et al. 2005; Macomber and Hausinger 2011). Only Fe(II) has a net charge in such a complex that is below  $-1$  and Fe(II) can also be oxidized to Fe(III), which is not a possible step for the other metal cations. Synthesis of iron–sulfur clusters could be an important discrimination process for iron. A second unique reaction for iron would be the oxidation of cytoplasmic Fe(II) to Fe(III) and subsequent precipitation in ferritin-like proteins.

Co(II) and Ni(II) have to be kept away from synthesis of iron–sulfur clusters. Misplaced Ni(II) might cause inhibition of enzymes depending on a catalytic Zn(II) as Lewis acid (Macomber et al. 2011; Macomber and Hausinger 2011). Co(II) and Ni(II) are highly competitive compared to Zn(II) with respect to bonding of Asp, Glu, and Cys, but even more to His (Table 2.2). Co(II) could be removed by cobalamin biosynthesis. As modeled for cyano-cobalamin (Table 2.3), Co(II) is here in an octahedral complex. Oxidation of the central Co(II) to Co(III) yields a metal with completely filled nonbonding 3d orbitals, a very stable configuration. On the other hand, Co(II) may be able to substitute so some extend in metal-promiscuous proteins, especially under zinc-limiting conditions (Ammendola et al. 2020).

A model for a Ni(II)-sorting ligand field, HHHEE, comes from the nickel sensor CnrX (Maillard et al. 2015; Trepreau et al. 2014; Pompidor et al. 2008; Trepreau et al. 2011). The Ni(II) ion is bound by three His residues H<sub>42</sub>, H<sub>46</sub>, H<sub>119</sub>, Met residue M<sub>123</sub> plus the two oxygen atoms of the terminal carboxylic group of the same Glu residue E<sub>63</sub>. This six ligand field strongly discriminates against Zn(II), which cannot accommodate 5 or 6 ligands easily (Nies et al. 2017). The negative net charge of the Ni(II)-HHHEE complex (Met not calculated) in combination with the high electron affinity of Ni(II) should discriminate against bonding of Co(II), Fe(II), and Mn(II), in addition to the highly competitive bonding of Ni(II) to these ligands (Tables 2.2 and 2.3). His-, Asp-, and Glu-rich sites could be suitable to retard and discriminate Ni(II).

In summary describing briefly the overall principles of cellular transition metal homeostasis, after Cu(I) has been removed from the cytoplasm and Fe(II) by synthesis of iron–sulfur clusters or storage as Fe(III) within ferritin-like proteins, Co(II) and Ni(II) may move along with Zn(II) for a while within the cytoplasmic allocation pathways. The concentrations of Co(II) and Ni(II) have to be kept low to avoid interference with zinc and iron homeostasis. At the end, Ni(II) and Co(II) have to be kept away from the actual step that supplies Zn(II) to a structural or catalytic site. Co(II) and Ni(II) allocation pathways have to branch off before such an event occurs.

## References

- Akanuma G, Nanamiya H, Natori Y, Nomura N, Kawamura F (2006) Liberation of zinc-containing L31 (RpmE) from ribosomes by its paralogous gene product, YtiA, in *Bacillus subtilis*. *J Bacteriol* 188:2715–2720
- Aliaga ME, Lopez-Alarcon C, Garcia-Rio L, Martin-Pastor M, Speisky H (2012) Redox-changes associated with the glutathione-dependent ability of the cu(II)-GSSG complex to generate superoxide. *Bioorgan Med Chem* 20(9):2869–2876. <https://doi.org/10.1016/j.bmc.2012.03.027>
- Ammendola S, Ciavardelli D, Consalvo A, Battistoni A (2020) Cobalt can fully recover the phenotypes related to zinc deficiency in *Salmonella typhimurium*. *Metallomics* 12(12): 2021–2031. <https://doi.org/10.1039/d0mt00145g>
- Apontowiel P, Berends W (1975) Glutathione biosynthesis in *Escherichia coli* K 12. Properties of the enzymes and regulation. *Biochim Biophys Acta* 17:1–9
- Atkins PW, de Paula J (2013) *Physikalische Chemie*. Wiley-VCH-Verlag, Weinheim
- Babor M, Gerzon S, Raveh B, Sobolev V, Edelman M (2008) Prediction of transition metal-sites from apo protein structures. *Proteins* 70(1):208–217
- Beyer L, Cornejo J (2012) *Koordinationschemie*. Studienbücher Chemie. Vieweg+Teubner Verlag, Wiesbaden
- Bishop GM, Dringen R, Robinson SR (2007) Zinc stimulates the production of toxic reactive oxygen species (ROS) and inhibits glutathione reductase in astrocytes. *Free Radic Biol Med* 42(8):1222–1230. <https://doi.org/10.1016/j.freeradbiomed.2007.01.022>
- Bou-Abdallah F, Giffune TR (2016) The thermodynamics of protein interactions with essential first row transition metals. *Biochim Biophys Acta* 5:879–891. <https://doi.org/10.1016/j.bbagen.2015.11.005>
- Corazza A, Harvey I, Sadler PJ (1996) <sup>1</sup>H, <sup>13</sup>C-NMR and X-ray absorption studies of copper (I) glutathione complexes. *Eur J Biochem* 236:697–704
- Davidson T, Chen HB, Garrick MD, D'Angelo G, Costa M (2005) Soluble nickel interferes with cellular iron homeostasis. *Mol Cell Biochem* 279(1–2):157–162
- Dawson RMC, Elliott DC, Elliott WH, Jones KM (1969) *Data for biochemical research*, 2nd edn. At The Clarendon Press, Oxford
- Dominey LA, Kustin K (1983) Kinetics and mechanism of Zn(II) complexation with reduced glutathione. *J Inorg Biochem* 18:153–160
- Ebert JC, Altman RB (2008) Robust recognition of zinc sites in proteins. *Protein Sci* 17(1):54–65
- Fahey RC, Brown WC, Adams WB, Worsham MB (1978) Occurrence of glutathione in bacteria. *J Bacteriol* 133:1126–1129
- Fantino JR, Py B, Fontecave M, Barras F (2010) A genetic analysis of the response of *Escherichia coli* to cobalt stress. *Environ Microbiol* 12(10):2846–2857. <https://doi.org/10.1111/j.1462-2920.2010.02265.x>
- Fiedor L, Kania A, Mysliwa-Kurdziel B, Orzel L, Stochel G (2008) Understanding chlorophylls: central magnesium ion and phytol as structural determinants. *Biochim Biophys Acta* 1777(12): 1491–1500. <https://doi.org/10.1016/j.bbabi.2008.09.005>
- Freedman JH, Ciriolo MR, Peisach J (1989) The role of glutathione in copper metabolism and toxicity. *J Biol Chem* 264(10):5598–5605
- Haber F, Weiss J (1932) Über die Katalyse des Hydroperoxydes. *Naturwissenschaften* 20:948–950. <https://doi.org/10.1007/BF0150471>
- Hashemian S (2011) Interaction energies of histidine with cations (H<sup>+</sup>, Li<sup>+</sup>, Na<sup>+</sup>, K<sup>+</sup>, Mg<sup>2+</sup>, Ca<sup>2+</sup>). *Russ J Inorg Chem* 56(3):397–401. <https://doi.org/10.1134/s0036023611020082>
- Helbig K, Bleuel C, Krauss GJ, Nies DH (2008a) Glutathione and transition metal homeostasis in *Escherichia coli*. *J Bacteriol* 190(15):5431–5438
- Helbig K, Grosse C, Nies DH (2008b) Cadmium toxicity in glutathione mutants of *Escherichia coli*. *J Bacteriol* 190(15):5439–5454
- Hensley MP, Tierney DL, Crowder MW (2011) Zn(II) to *Escherichia coli* 70S ribosomes. *Biochemistry* 50(46):9937–9939. <https://doi.org/10.1021/bi200619w>



- Housecroft CE, Constable EC (2006) Chemistry, 3rd edn. Pearson Education Limited, Essex
- Irving H, Williams RJP (1948) Order of stability of metal complexes. *Nature* 162:746–747
- IUPAC (1997) Compendium of chemical terminology (the “gold book”). International Union of Pure and Applied Chemistry, Cambridge. <https://doi.org/10.1351/goldbook.E01990>
- Kachur AV, Koch CJ, Biaglow JE (1998) Mechanism of copper-catalyzed oxidation of glutathione. *Free Radic Res* 28(3):259–269. <https://doi.org/10.3109/10715769809069278>
- Kaczanowska M, Ryden-Aulin M (2007) Ribosome biogenesis and the translation process in *Escherichia coli*. *Microbiol Mol Biol Rev* 71(3):477–494. <https://doi.org/10.1128/MMBR.00013-07>
- Kania A, Fiedor L (2006) Steric control of bacteriochlorophyll ligation. *J Amer Chem Soc* 128(2): 454–458. <https://doi.org/10.1021/ja055537x>
- King RA, Markov D, Sen R, Severinov K, Weisberg RA (2004) A conserved zinc domain in the largest subunit of DNA-dependent RNA polymerase modulates intrinsic transcription termination and antitermination but does not stabilize the elongation complex. *J Mol Biol* 342(4): 1143–1154. <https://doi.org/10.1016/j.jmb.2004.07.072>
- Kramida A, Ralchenko Y, Reader J, NIST ASD Team (2019) NIST Atomic Spectra Database (version 5.7.1). <https://doi.org/10.18434/T4W30F>
- Kumar BA, Naik KB, Raju S, Rao GN (2015) Formation and confirmation of binary complexes of calcium(II), magnesium(II) and zinc(II) with L-histidine in dioxan-water media. *Chem Spec Bioavailab* 24(3):139–146. <https://doi.org/10.3184/095422912x13406452149755>
- Liochev SI, Fridovich I (2002) The Haber-Weiss cycle - 70 years later: an alternative view. *Redox Rep* 7(1):55–57. <https://doi.org/10.1179/135100002125000190>
- Lyons TW, Reinhard CT, Planavsky NJ (2014) The rise of oxygen in Earth's early ocean and atmosphere. *Nature* 506(7488):307–315. <https://doi.org/10.1038/nature13068>
- Macomber L, Hausinger RP (2011) Mechanisms of nickel toxicity in microorganisms. *Metallomics* 3(11):1153–1162. <https://doi.org/10.1039/C1mt00063b>
- Macomber L, Elsey SP, Hausinger RP (2011) Fructose-1,6-bisphosphate aldolase (class II) is the primary site of nickel toxicity in *Escherichia coli*. *Mol Microbiol* 82(5):1291–1300. <https://doi.org/10.1111/j.1365-2958.2011.07891.x>
- Maillard AP, Kuennemann S, Grosse C, Volbeda A, Schleuder G, Petit-Härtlein I, de Rosny E, Nies DH, Coves J (2015) Response of CnrX from *Cupriavidus metallidurans* CH34 to nickel binding. *Metallomics* 7:622–631. <https://doi.org/10.1039/c4mt00293h>
- Majtan T, Frerman FE, Kraus JP (2011) Effect of cobalt on *Escherichia coli* metabolism and metalloporphyrin formation. *Biometals* 24(2):335–347. <https://doi.org/10.1007/s10534-010-9400-7>
- Markov D, Naryshkina T, Mustaev A, Severinov K (1999) A zinc-site in the largest subunit of DNA-dependent RNA polymerase is involved in enzyme assembly. *Genes Dev* 13(18): 2439–2448
- Newton GL, Fahey RC (2002) Mycothiol biochemistry. *Arch Microbiol* 178(6):388–394
- Newton GL, Arnold K, Price MS, Sherrill C, Delcardayre SB, Aharonowitz Y, Cohen G, Davies J, Fahey RC, Davis C (1996) Distribution of thiols in microorganisms: mycothiol is a major thiol in most actinomycetes. *J Bacteriol* 178:1990–1995
- Nies DH (2000) Heavy metal resistant bacteria as extremophiles: molecular physiology and biotechnological use of *Ralstonia spec.* CH34. *Extremophiles* 4(2):77–82
- Nies DH (2007) Bacterial transition metal homeostasis. In: Nies DH, Silver S (eds) *Molecular microbiology of heavy metals*, Microbiology monographs, vol 6. Springer-Verlag, Berlin, pp 118–142
- Nies DH (2012) Zinc starvation response in a cyanobacterium revealed. *J Bacteriol* 194(10): 2407–2412. <https://doi.org/10.1128/jb.00257-12>
- Nies DH (2014) Basic biochemical roots. *Ecological Biochemistry: Environmental and Interspecies Interactions*. Wiley-VCH, Weinheim
- Nies DH (2016) The biological chemistry of the transition metal “transportome” of *Cupriavidus metallidurans*. *Metallomics* 8:481–507. <https://doi.org/10.1039/C5MT00320B>

- Nies DH, Silver S (eds) (2007) Molecular microbiology of heavy metals, vol 6. Microbiology Monographs. Springer Verlag, Berlin
- Nies DH, Coves J, Sawers G (2017) Cross-talk between nickel and other metals in microbial systems. In: Kozłowski H, Zamble D, Rowińska-Zyrek M (eds) The biochemistry of nickel. The Royal Society of Chemistry, London, pp 306–338
- O'Halloran TV, Culotta VC (2000) Metallochaperones, an intracellular shuttle service for metal ions. *J Biol Chem* 275(33):25057–25060
- Parnell J, Boyce AJ, Mark D, Bowden S, Spinks S (2010) Early oxygenation of the terrestrial environment during the Mesoproterozoic. *Nature* 468:290–293
- Pearson RG (1963) Hard and soft acids and bases. *J Amer Chem Soc* 85(22):3533. <https://doi.org/10.1021/ja00905a001>
- Pittman MS, Robinson HC, Poole RK (2005) A bacterial glutathione transporter (*Escherichia coli* CytDC) exports reductant to the periplasm. *J Biol Chem* 280:32254–32261
- Pompidor G, Maillard AP, Girard E, Gambarelli S, Kahn R, Coves J (2008) X-ray structure of the metal-sensor CnrX in both the apo- and copper-bound forms. *FEBS Lett* 582(28):3954–3958. <https://doi.org/10.1016/j.febslet.2008.10.042>
- Ranquet C, Ollagnier-de-Choudens S, Loiseau L, Barras F, Fontecave M (2007) Cobalt stress in *Escherichia coli*. *J Biol Chem* 282:30442–30451
- Rigo A, Corazza A, di Paolo ML, Rossetto M, Ugolini R, Scarpa M (2004) Interaction of copper with cysteine: stability of cuprous complexes and catalytic role of cupric ions in anaerobic thiol oxidation. *J Inorg Biochem* 98(9):1495–1501. <https://doi.org/10.1016/j.jinorgbio.2004.06.008>
- Scheer M, Brodie CA, Bilodeau RC, Haugen HK (1998) Laser spectroscopic measurements of energies and fine-structure splittings of co-, Ni-, Rh-, and Pd. *Phys Rev A* 58(3):2051–2062. <https://doi.org/10.1103/PhysRevA.58.2051>
- Schrödinger E (1992, First published 1944) What is life?: the physical aspect of the living cell. Cambridge University Press, New York
- Sherrill C, Fahey RC (1998) Import and metabolism of glutathione by *Streptococcus mutans*. *J Bacteriol* 180:1454–1459
- Speisky H, Gomez M, Burgos-Bravo F, Lopez-Alarcon C, Jullian C, Olea-Azar C, Aliaga ME (2009) Generation of superoxide radicals by copper-glutathione complexes: redox-consequences associated with their interaction with reduced glutathione. *Bioorgan Med Chem* 17(5):1803–1810. <https://doi.org/10.1016/J.Bmc.2009.01.069>
- Suzuki H, Koyanagi T, Izuka S, Onishi A, Kumagai H (2005) The *yliA*, *-B*, *-C*, and *-D* genes of *Escherichia coli* K-12 encode a novel glutathione importer with an ATP-cassette. *J Bacteriol* 187:5861–5867
- Trepreau J, Girard E, Maillard AP, de Rosny E, Petit-Haertlein I, Kahn R, Coves J (2011) Structural basis for metal sensing by CnrX. *J Mol Biol* 408(4):766–779. <https://doi.org/10.1016/j.jmb.2011.03.014>
- Trepreau J, Grosse C, Mouesca J-M, Sarret G, Girard E, Petit-Haertlein I, Kuennemann S, Desbourdes C, de Rosny E, Maillard AP, Nies DH, Coves J (2014) Metal sensing and signal transduction by CnrX from *Cupriavidus metallidurans* CH34: role of the only methionine assessed by a functional, spectroscopic, and theoretical study. *Metallomics* 6:263–273
- Wang J, Wang C, Ge Y, Sun Y, Wang D, Xu H (2020) Self-assembly of hairpin peptides mediated by Cu(II) ion: effect of amino acid sequence. *Pept Sci* 113:e24208. <https://doi.org/10.1002/pep2.24208>
- Weast RC (1984) CRC handbook of chemistry and physics, 64th edn. CRC Press, Inc., Boca Raton, FL
- Wu FYH, Huang WJ, Sinclair RB, Powers L (1992) The structure of the zinc sites of *Escherichia coli* DNA-dependent RNA polymerase. *J Biol Chem* 267(35):25560–25567
- Zilberstein D, Agmon V, Schuldiner S, Padan E (1984) *Escherichia coli* intracellular pH, membrane potential, and cell growth. *J Bacteriol* 158:246–252

**Part II**  
**Understanding Commonality of the Basic**  
**Processes**

# Chapter 3

## The Mosaic Landscape of Algal Metal Transport and Usage



Crysten E. Blaby-Haas

**Abstract** Like all other eukaryotes, metal ions are essential nutrients for algae, which must be assimilated from the environment. At the same time, in excess, metal ions are inherently toxic. Reflecting the complex evolutionary relationships among the algal groups, algal genomes encode a variety of widely conserved and unique transport proteins to handle the balance between nutrient and toxin. Each genomic repertoire enables algal species to thrive in environments with unique biogeochemical characteristics compared to non-algal species commonly used as reference organisms for metal homeostasis. As a result, the study of algal metal homeostasis broadens our understanding of how phenotypically and taxonomically divergent eukaryotes have evolved to perform photosynthesis in disparate environments. These niches are as varied as marine versus freshwater, aquatic versus deserts, polar versus tropical, and free-living versus endosymbiotic. While access to genome sequences and predicted gene models is increasing, enabling identification of characterized proteins through computational genomics analyses, the next stage is developing transformation approaches and RNA-guided endonuclease systems for understanding the molecular and biological function of metal-regulated genes unique to algae.

### 3.1 Introduction

In the early 1900s, to sum his observations of animal behavior, Victor Shelford wrote “. . .the habitat is the mold into which the organism fits” (Shelford 1913). This statement holds true across scales from learned behavior down to the selective pressures imparted by environments on genomes. Indeed, the habitat is the mold into which the genome fits. Any organisms that fail to fit that mold are outcompeted and fade from existence in the niche. With the development of whole-genome

---

C. E. Blaby-Haas (✉)

Biology Department, Brookhaven National Laboratory, Upton, NY, USA

Department of Biochemistry and Cell Biology, Stony Brook University, Stony Brook, NY, USA

e-mail: [cblaby@bnl.gov](mailto:cblaby@bnl.gov)

sequencing technologies, those inherited adaptations that passed the filter of natural selection can be elucidated and compared across lineages and environments. The rise of RNA-guided endonucleases as genetic tools is opening the door to experimental validation of those genome-based insights, providing a means to erase individual adaptative strategies and quantify the impact on condition-specific fitness.

For metal ions, two filters exist: competition for metal ions and avoidance of their toxicity. Metals provide proteins with chemistry or folding properties that are not easily achieved with just the amino acid sidechains of polypeptides. As a result, metals are essential nutrients. At the same time, metal ions are inherently toxic to biology. Transition metals can accept and donate electrons, a function that biology has capitalized on, but if allowed to react with oxygen or reactive oxygen species, these metals can catalyze oxidative damage to membranes and proteins. Zinc, although not redox active, can bind indiscriminately to proteins either inactivating them by replacing the cognate catalytic metal or by generating protein aggregates. Therefore, metal ions have left their mark on genomes as protein cofactors, and multi-layered strategies for handling deficiency and toxicity exist.

The guiding principle underlying metal homeostasis is to ensure a supply of metal ions to metal-dependent proteins while avoiding potential toxicity of excess metal ions. Subsequently, both global and local metal bioavailabilities across time have shaped gene repertoires reflected in the resulting lifestyles and metabolism of different algal species. The ability of individual algae to thrive in environments with unique geochemistry, compared to non-algal species commonly used as reference organisms for metal homeostasis, combined with access to their gene and protein sequences, provides an opportunity to broaden our understanding of metal transport and usage across the eukaryotic tree of life. The availability of omics technologies, such as transcriptomics and proteomics, enables genome-wide surveys of gene-specific responses to metal deficiency and excess. These datasets often reveal both conserved responses across algal and non-algal lineages and organism-specific or lineage-specific adaptations. Those genes found to be highly differentially expressed then often become targets for follow-on experimental characterization, largely through reverse genetics and molecular biology techniques. As discussed in this chapter, these studies have revealed commonalities in metal homeostasis with non-algal lineages, including land plants, fungi and animals, and novelty that has contributed to the success of algae in complex and competitive habitats.

## **3.2 What Are Algae and Where Can They Be Found?**

An alga is any eukaryotic organism that can perform photosynthesis and is not a land plant. Because of this pre-molecular (i.e. pre-genome sequencing) definition, the algal group is unified based on phenotype, not molecular phylogenetics. Algae are distributed throughout the eukaryotic tree of life; they do not have a single common ancestor in the traditional sense. Instead, the proverbial saying ‘You are what you eat’ could never be truer. The major lineages of algae are related through

independent instances of endosymbiosis during which a eukaryotic host engulfs and retains either a cyanobacterium, producing a primary plastid, or an established alga, producing a secondary (or tertiary or more complex) plastid. The distinguishing feature of primary plastids compared to the more complex plastids is the number of membranes surrounding the plastid. Primary plastids have two membranes, while complex plastids, with a few exceptions (Wetherbee et al. 2019), have three to four membranes. Many of the stolen genes from the endosymbiont are ultimately transferred to and incorporated into the host's nuclear genome; a process often referred to as endosymbiotic gene transfer. The algal group is, therefore, polyphyletic, because the most recent common ancestor of all eukaryotic algae was not an alga, and many algae are more closely related to non-photosynthetic protists than they are to other algae.

There are also grey areas in the use of the terms alga and algae. With the advent of DNA sequencing and molecular phylogenetics, the term “non-photosynthetic algae” can now be found in the literature referring to organisms that are phylogenetically embedded in algal lineages but have colorless plastids, because they have lost the ability to perform photosynthesis. These types of algae provide insightful comparator species for phylogenetically profiling gene sets important for photosynthesis (Hadariová et al. 2017; Gawryluk et al. 2019). There are also several organisms that are sometimes referred to as algae but do not have a self-replicating plastid. These acquired phototrophs either have a symbiotic relationship with an alga, such as *Paramecium bursaria* with endosymbiotic *Chlorella* spp. (Karakashian 1975), or are able to engulf and steal plastids from algae (kleptoplasty), such as *Mesodinium rubra* (previously named as *Myrionecta rubra*), which acquires plastids from cryptophyte algal prey (Johnson and Stoecker 2005). In these cases, feeding on algae is needed to replenish their supply of plastids.

Because of these complex evolutionary histories and deep evolutionary roots, the gene repertoires of algae are diverse. The green, red and glaucophyte algae, like their sister lineage the land plants, share genes from their shared last common ancestor, including both genes from the last common ancestor of Archaeplastida and genes from the cyanobacterium-like endosymbiont that became the shared primary chloroplast. This lineage likely dates back to an algal ancestor that existed at least 1.5 billion years ago (Blaby-Haas and Merchant 2019). Algae that do not have a primary plastid, such as diatoms or Euglena, share genes from an ancient protist-like ancestor and genes from a red-alga-like or green-alga-like endosymbiont, respectively, that became their chloroplast. The spread of plastids across the eukaryotic tree of life through endosymbiosis, retention, and endosymbiotic gene transfer has occurred multiple independent times, with some cases of complex serial endosymbiosis (Stiller et al. 2014).

The lifestyles, environments, and morphology of individual algal subgroups are as diverse as their evolutionary relationships. As an example, the Chlorophyte lineage (also known as the green algae, which share a relatively recent common ancestor with the land plants) contains both the smallest and largest known free-living single-celled eukaryotes, *Ostreococcus tauri* (Courties et al. 1994) and *Caulerpa taxifolia* (Ranjan et al. 2015), respectively. Multicellular green algal

species can range from 20  $\mu\text{M}$  [the colonial alga *Tetrabaena socialis* (Arakaki et al. 2013)] to 3 feet in size [the seaweed *Ulva lactuca* (Steffensen 1976)]. The largest alga, *Macrocystis pyrifera* (North 1971), a brown alga in the SAR supergroup, can reach 200 feet in length. Algae can be found in temperate and tropical soil, fresh water, and the oceans, as well as extreme environments. The halophilic green alga *Dunaliella salina* inhabits the Northern arm of the Great Salt Lake, Utah, where the NaCl concentration is oversaturated (Brock 1975). Red algae in the order *Cyanidiales* thrive at pH 0.5–3 and high temperature (50–55 °C) (Castenholz and McDermott 2010). Psychrophilic green algae, such as *Chlamydomonas raudensis* (UWO 241), inhabit permanently ice-covered lakes in Antarctica (Pocock et al. 2004), while snow algae often cover glaciers like pink Kool-Aid (because of a red carotenoid pigment) (Bidigare et al. 1993) and diatoms inhabit brine channels in sea ice (Mock and Junge 2007). Because of these and other drastically different algal species, unique adaptations involving metal homeostasis are expected but remain under investigated.

### 3.3 Metal Usage

Because of their role in enzyme catalysis and protein folding, metal ions are essential nutrients, but which metals and at what concentrations are needed by an individual algal species can vary. Based on studies of reference algal species with sequenced nuclear genomes (Table 3.1), algae have a relatively large requirement for iron as the most abundant and irreplaceable inorganic cofactor for linear electron transport during photosynthesis and respiration. In addition to iron, algae require several metals from the d-block of the periodic table, specifically zinc, copper, manganese, and molybdenum. Some algae, such as the prasinophytes, use nickel for urease (Collier et al. 2009), while cobalt, in the form of cobalamin (vitamin B<sub>12</sub>), is needed for one of two classes of methionine synthase (Helliwell et al. 2011). Since no alga is known to be able to synthesize B<sub>12</sub>, this vitamin must be acquired from bacteria (Croft et al. 2005).

**Table 3.1** Common reference algal species for metal homeostasis with sequenced nuclear genomes

Species	Lineage	Environment	Type of plastid	Genome
<i>Chlamydomonas reinhardtii</i>	Plant	Freshwater/ soil	Primary	Merchant et al. (2007) and Blaby et al. (2014)
<i>Ostreococcus tauri</i>	Plant	Marine	Primary	Derelle et al. (2006)
<i>Phaeodactylum tricorutum</i>	Diatom	Marine	Complex	Bowler et al. (2008) and Rastogi et al. (2018)
<i>Thalassiosira pseudonana</i>	Diatom	Marine	Complex	Armbrust et al. (2004)

The types of reactions and classes of proteins that bind and utilize specific metal ions is determined by the inherent chemistry of each metal ion. In nature, the zinc ion exhibits a single oxidation state (+2) and is often used as a cofactor to stabilize protein structure or in hydrolytic reactions where it serves as an electrophile. Depending on the specific ligand environment, copper, iron, and manganese ions, which can exist in different oxidation states, are also employed for hydrolytic reactions but, unlike zinc, can function in electron transfer reactions. Molybdenum has only been found in eukaryotes as the constituent of a tricyclic pyranopterin compound named the molybdenum cofactor (Moco) and functions in electron transfer within a small number of proteins. Typically, zinc, copper and manganese are not associated with prosthetic groups. Iron, on the other hand, is versatile, being directly associated with amino acids in some enzymes, as in Fe-dependent superoxide dismutase, and incorporated into organic or inorganic cofactors like heme and Fe-S clusters, as found in the photosynthetic complexes. These iron-bound cofactors associate with proteins as prosthetic groups and provide an additional means for tuning the redox potential of the iron atom to catalyze electron transfer.

Because individual proteins have evolved to harness the chemistry of specific metal ions, substitution of metal ions for one another is not a common occurrence. Nevertheless, such adaptive mechanisms have been described for algae and examples of nutritive substitution phenomena involving replacement of one metal ion for another are available. In some cases, the underlying genetics is understood. Carbonic anhydrase in eukaryotes is characterized as a zinc-dependent enzyme, but during growth under low zinc conditions with cadmium supplementation, the carbonic anhydrase CDCA1 from the marine diatom *Conticribra weissflogii* (previously *Thalassiosira weissflogii*) is active with cadmium instead of zinc (Lane et al. 2005). The cambialistic (capable of functioning with multiple metal atoms) nature of this enzyme is thought to represent a zinc-sparing mechanism that provides a selective advantage for diatoms growing in zinc-poor ocean waters. In contrast to such promiscuous proteins, interchangeable proteins that require different metal cofactors have also been characterized in algae. The copper-regulated switch between Cu-dependent plastocyanin and Fe-dependent cytochrome  $c_6$  is a well-characterized strategy for recycling and sparing copper (Kropat et al. 2015). In contrast to these examples, a cobalt/zinc nutritive substitution has been widely described for different types of algae (Sunda and Huntsman 1995; Intwala et al. 2008; Saito and Goepfert 2008), but the underlying genetics and mechanism for this phenotype are not known. Based on the previous examples, zinc and cobalt may be interchangeable cofactors because of the existence of cambialistic proteins, or some algae may have interchangeable sets of zinc-dependent and cobalt-dependent protein isoforms. Discovering the proteins that are responsible for this type of cofactor switch promises to reveal novel proteins and homeostatic regulation unique to algae.



## 3.4 Metal Transport

Like all other eukaryotes, algal cells are surrounded by a plasma membrane with intracellular membranes delineating sub-compartments and organelles. Metal-dependent proteins are found throughout the cell and are typically translocated into organelles as unfolded polypeptides. As such, transporters are needed for passing metals across multiple membranes, either to correct deficiency or toxicity. However, our understanding of metal transporters in the plasma membrane is far more advanced than our understanding of metal transport across the membranes of organelles. Two main types of transport have been described in algae, endocytosis-mediated and permease-mediated.

### 3.4.1 Endocytosis-Mediated Iron Transport

Endocytosis is a process by which the plasma membrane surrounds a target by invagination to form a vesicle in the cytosol. The cargo is then sorted, often associated with endosomal acidification (Elkin et al. 2016). Although endocytosis may be responsible for the uptake of other metal ions or metal-chelate molecules, only iron uptake by endocytosis has been described for algae. Four separate families of algal proteins have been implicated in endocytosis-mediated iron assimilation: transferrin, phytoferritin, ISIP1 (iron starvation-induced protein 1), and ferrichrome-binding protein (FBP).

An animal-like transferrin was first discovered in the unicellular green alga *D. salina* as a salt-induced, 150 kDa, plasma membrane bound protein and was initially referred to as p150 (Sadka et al. 1991). Cloning and sequencing of the corresponding cDNA revealed sequence similarity to animal transferrin (Fisher et al. 1996). While animal transferrins are composed of two homologous domains, the *D. salina* transferrin has three homologous domains and is often referred to as TTf for triplicated transferrin (Fisher et al. 1998). Like animal transferrins, expression is induced by iron deficiency, and TTf binds and facilitates assimilation of the oxidized ion of iron,  $\text{Fe}^{3+}$  (Fisher et al. 1998). Unlike animals, TTf forms a complex with a multi-copper ferroxidase (D-Fox), p130b and a second transferrin-like protein, DTf (*D. salina* transferrin) (Paz et al. 2007a). D-Fox is likely responsible for oxidation of  $\text{Fe}^{2+}$  prior to binding to TTf, as has been suggested for ceruloplasmin (Eid et al. 2014). The function of DTf is unknown since the protein does not bind iron (Schwarz et al. 2003). The function of p130b is also unknown, but it is structurally similar to ISIP1 from the diatom *Phaeodactylum tricorutum*, which is also induced by iron deficiency (Allen et al. 2008). Shared structural features with the low-density lipoprotein receptor LDLR, a cell-surface receptor in humans, led to the original hypothesis that p130b and ISIP1 are iron-deficiency-responsive receptors (Lommer et al. 2012). Subsequent characterization in *P. tricorutum* led to the conclusion that ISIP1 is involved in the endocytosis-mediated assimilation of siderophores by FBPI,

a protein with sequence similarity to the periplasmic component of the bacterial  $\text{Fe}^{3+}$ -hydroxamate transport system (Sutak et al. 2012; Kazamia et al. 2018). Therefore, by analogy, p130b may function in the endocytosis of TTF in *D. salina*. However, while multiple algal and land plant genomes encode transferrin-like proteins, only diatoms and *D. salina* have a protein similar to p130b or ISIP1 (Fig. 3.1).

Not only was *D. salina* the first alga for which an animal-like transferrin was found, but this family is also uniquely expanded. At least 10 separate genes encoding proteins with similarity to the transferrin Pfam domain PF00405 are present in the available genome assembly (Polle et al. 2020). When other algae and land plants have transferrin, there typically are only one or two. A similarly sized expansion (7 animal-like transferrins) is also found in the genome of the macroalga *Caulerpa lentillifera*, an edible seaweed commonly referred to as sea grapes (Arimoto et al. 2019). For *D. salina*, the unusual number of transferrins may relate to its unique tolerance of hypersaline environments where iron bioavailability is relatively low. *C. lentillifera*, however, is not an extremophile and is often found throughout the coastal Asia-Pacific region. What is unique about *C. lentillifera* and other members of the *Caulerpa* genus is that they appear to be complex plant-like seaweeds with structures analogous to leaves, stems and roots but are actually composed of a single cell with multiple nuclei (Coneva and Chitwood 2015). The absence of compartmentalization afforded by being multi-cellular must come with its own challenges, such as having to rely on diffusion and cytoplasmic streaming for distribution of metal ions across relatively large distances. By assimilating iron with transferrin and endocytosis, these siphonous macroalgae may be able to selectively shuttle iron throughout the expansive cytoplasm with vesicle-mediated trafficking, releasing the iron where and when needed.

Animal-like transferrins have only been identified in plants and green algae in the chlorophyte and streptophyte lineages (Bai et al. 2016; Blaby-Haas and Merchant 2017), while most algae contain proteins similar to phytotransferrin (pTF) from *P. tricornutum* (Fig. 3.1). The use of the “phyto” prefix may be confusing since this family is not found in land plants. Instead, phytotransferrin homologs are specific to algae and can be found as soluble proteins, such as the FEA (*Fe*-assimilating) proteins in the green alga *Chlamydomonas reinhardtii* (Allen et al. 2007), or membrane-bound proteins, such as Ot-*FEA1* in the green alga *O. tauri* (Lelandais et al. 2016; Scheiber et al. 2019). The first member of this alga-specific family to be discovered was *HCR1* from *Alvikia littoralis* (previously *Chlorococcum littorale*), a marine green alga from the chlorophyte lineage. The gene was isolated as a high- $\text{CO}_2$  and iron-deficiency induced transcript (Sasaki et al. 1998). Subsequently, a homolog from the freshwater/soil green alga *C. reinhardtii*, originally named *H43*, was identified as a cadmium- and iron-deficiency induced transcript (Rubinelli et al. 2002). After the identification of a second iron-deficiency-induced *H43*-like gene in *C. reinhardtii*, these proteins were renamed FEA (Merchant et al. 2006; Allen et al. 2007). In *C. reinhardtii*, the FEA proteins are secreted, and in a cell-wall-less strain, *FEA1/FEA2* are lost to the supernatant correlating with increased sensitivity to iron deficiency (Allen et al. 2007). The mechanism responsible for FEA-mediated iron assimilation is uncharacterized, but recombinant expression of *FEA1* in *Arabidopsis*

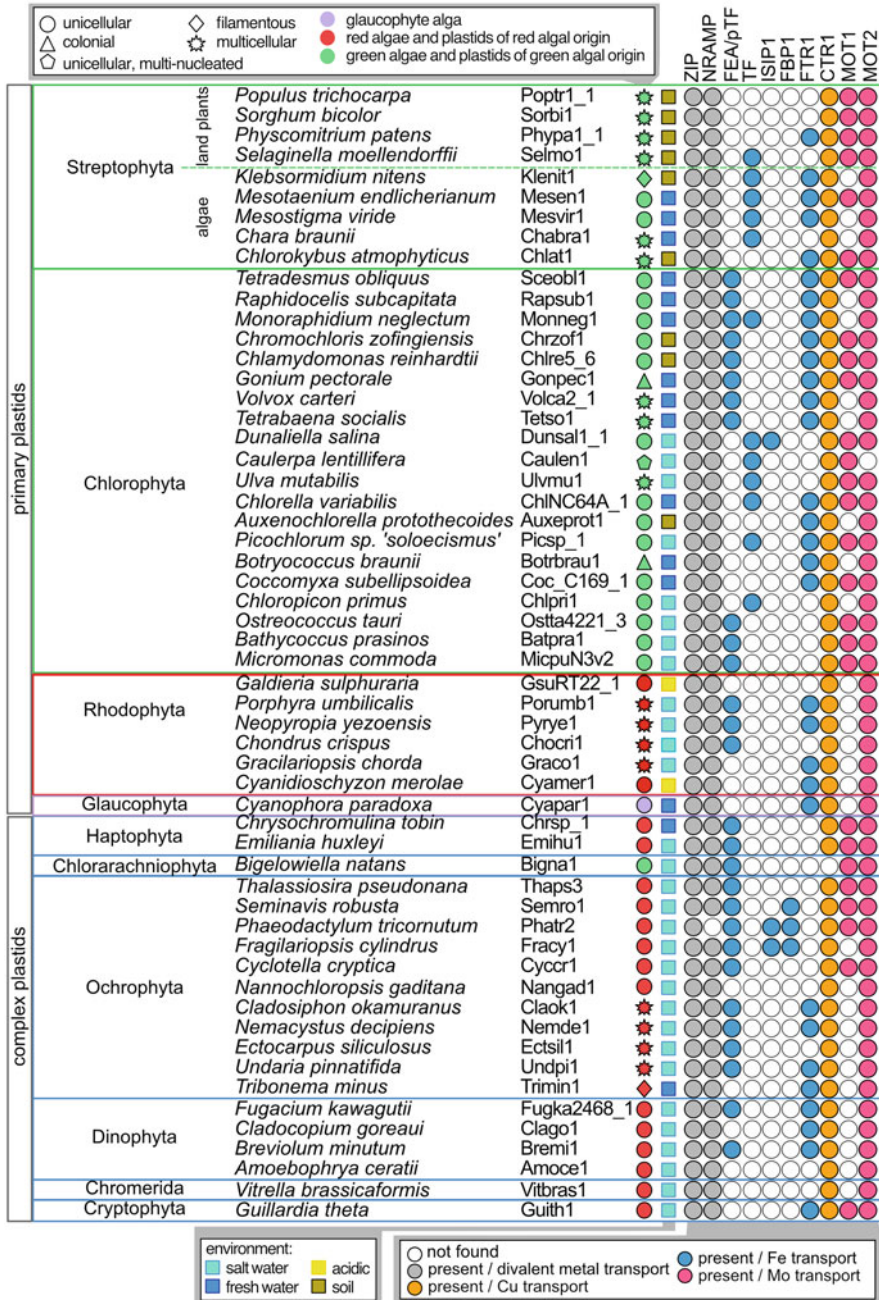


**Fig. 3.1** Presence of genes predicted to encode homologs of known metal transport proteins. Proteins were identified using either presence of a corresponding Pfam domain or sequence similarity. The taxonomic class, genome identifiers from the Phycocosm database, physiological characteristics and environment are indicated

*thaliana* and cassava leads to increased root iron content (Narayanan et al. 2011; Ihemere et al. 2012).

Phytotransferrin was originally named ISIP2 and was discovered in an iron-responsive transcriptomics study in *P. tricornutum* (Allen et al. 2008). Follow-on characterization of this protein resulted in increasing evidence for a function analogous to transferrin leading to the name phytotransferrin (Morrissey et al. 2015; McQuaid et al. 2018). Recent analysis of protein-protein interactions and microscopy suggests that after endocytosis phytotransferrin may be directly sorted to the chloroplast with vesicle trafficking together with ISIP1 and FBP1 (Turnšek et al. 2021). Whether such vesicle-mediated transport of iron and potentially other metal ions to the chloroplast exists outside diatoms is currently unknown. *D. salina*, which has a primary plastid like other chlorophytes, appears to internalize iron into acidic compartments, which are thought to act as an intermediary storage station, as in animals (Paz et al. 2007b). Therefore, the functional analogy between transferrins and phytotransferrins in algae may end after internalization. In contrast to land plants and algae with primary plastids, the chloroplast of diatoms is surrounded by four membranes, where the outer envelope (called the chloroplast endoplasmic reticulum (CER)) is continuous with the nuclear envelope and is proposed to have originated from the host endomembrane. Vesicle-mediated iron transport within the endomembrane system may have been an adaptation necessary for supplying nutrients to the engulfed alga ancestor of the plastid, and this strategy has been maintained.

### 3.4.2 *Metal Permeases*

Metal permeases are membrane-spanning proteins that provide routes for metal ions to cross biological membranes. Some permeases form a selective channel for metal ions to travel through the membrane while leveraging concentration gradients to drive transport. Other permeases leverage ATP hydrolysis or protonmotive force. Based largely on characterization of non-algal homologs, metal permeases can be divided into two main functional groups based on their predicted direction of transport relative to the cytosol. Transporter families typically fall into one group or the other, but exceptions to such broad classifications often occur in the literature. These exceptions may be due to functional divergence within a transporter family or, in some cases, may be a consequence of relying solely on phenotypes of gene knockouts without additional information, such as transporter localization or orientation in the membrane, with which to contextualize reverse-genetics data. Therefore, the following generalizations are a useful jumping-off point for functional annotation, but experimentation is critical for establishing functional capabilities, since diversification is central to the evolution of adaptive mechanisms.

### 3.4.2.1 An Overview of Assimilation

Members of group A typically transport metal ions into the cytoplasm, either across the plasma membrane during assimilation or across intracellular membranes for release of intracellular stores. Expression of the corresponding genes often, but not always, increases during metal deficiency. Group A permeases include the NRAMP, ZIP, FTR, CTR, MOT1, and MOT2 families (Fig. 3.2). The NRAMP family was named after the first member to be studied, *Natural-Resistance-Associated Macrophage Protein 1*, from mouse (Vidal et al. 1993). NRAMPs are most often found to function in iron and manganese uptake as proton-metal symporters. The ZIP (*Zrt-, Irt-like Proteins*) family is named after the first members to be characterized, the zinc transporters *Zrt1p* (Zhao and Eide 1996a) and *Zrt2p* (Zhao and Eide 1996b) from the yeast *Saccharomyces cerevisiae* and *IRT1*, the major iron-uptake protein in *A. thaliana* roots (Eide et al. 1996). Those ZIP transporters characterized to date transport divalent metal ions, and most play biological roles in either zinc or iron transport. The FTR (*Fe transporter*) family was first identified as part of a high-affinity iron transport complex containing *Fet3p*, a multi-copper oxidase (MCO), in *S. cerevisiae* (Stearman et al. 1996). Unlike NRAMP and ZIP, which can transport

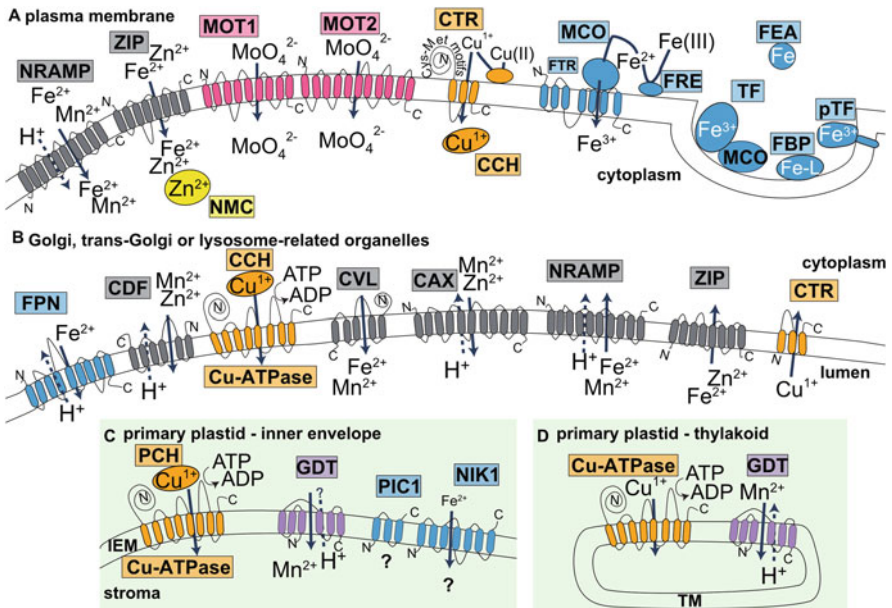


**Fig. 3.2** Metal transport proteins found in algae. (a) Transport proteins often found to localize to the plasma membrane. (b) Transporters often found to localize to intracellular membranes of the endomembrane system. (c, d) Transporters identified in the land plant *Arabidopsis* that are conserved in the green algae. Abbreviations not found in the text: CCH Cu chaperone, PCH plastid Cu chaperone, FRE ferric reductase, CVL Ccc1/VIT1-like, PIC1 permease in chloroplasts 1, NIK1 nickel transporter family, CAX cation/proton exchanger

ferrous iron, FTR transports ferric iron. CTR (*Cu transporter*) was also first discovered in *S. cerevisiae* (Dancis et al. 1994). Unlike the three transporters described so far, CTRs transport monovalent cations. MOT1 and MOT2 (*Molybdenum transporters*) are independent families of oxianion molybdate ( $\text{MoO}_4^{-2}$ ) transporters (Tejada-Jiménez et al. 2007, 2011).

### 3.4.2.2 An Overview of Export

Members of group B typically transport metal ions out of the cytoplasm. Within this group are distributive transporters, which provide metal for organelle-localized metalloproteins that are either synthesized in organelles or imported as unfolded polypeptides. When present in the endomembrane system, group B transporters pump metal into membrane-delineated compartments for storage or efflux out of the cell. These families are also often found in the vacuole's boundary membrane. Since not all algae have vacuoles as described for yeast and plants, these transporters may be found in other lysosome-like organelles that function to detoxify and store metal ions (Blaby-Haas and Merchant 2014). Expression of the corresponding genes often, but not always, increases during metal excess. Exceptions are the distributive transporters PAA1 (P-type ATPase of Arabidopsis 1) and PAA2 (P-type ATPase of Arabidopsis 2) from the Cu-ATPase family, which supply copper for the biogenesis of plastocyanin in the chloroplast. The genes encoding these transporters are down-regulated in the shoots of *A. thaliana* plants when exposed to excess copper (del Pozo et al. 2010). Members of group B include the CDF, P<sub>1B</sub>-type ATPases, GDT1, ferroportin, and Ccc1/VIT1 families (Fig. 3.2). The first member of the CDF (Cation Diffusion Facilitator) family was identified in *S. cerevisiae* as a gene responsible for zinc tolerance, *ZRC1* (zinc resistance conferring) (Kamizono et al. 1989). Comparison of this protein with a second protein from yeast responsible for cobalt tolerance, Cot1p (Conklin et al. 1992), and a bacterial protein involved in tolerance to multiple metals, CzcD (Nies 1992), led to the hypothesis that these make up a family of metal transporters responsible for metal resistance (Nies and Silver 1995). P<sub>1B</sub>-type ATPases couple ATP hydrolysis to monovalent (copper) or divalent metal transport (zinc, cadmium, or iron) depending on the specific subfamily and sequence determinants (Purohit et al. 2018). Members of the GDT1 family (formerly named UPF0016) were first described as  $\text{Ca}^{2+}$  effluxers (Demaegd et al. 2013; Wang et al. 2016), but were later found to also function as  $\text{Mn}^{2+}$  transporters in different organisms and different cellular compartments (Fisher et al. 2016; Schneider et al. 2016; Potelle et al. 2016). Ferroportins (Fpn) are most often described as iron exporters, but a plant homolog, IREG2 is thought to detoxify  $\text{Ni}^{2+}$  (Schaaf et al. 2006). Ccc1p, the founding member from *S. cerevisiae*, and VIT1, the founding member from *A. thaliana*, both mediate transport of  $\text{Fe}^{2+}$  into the vacuole (Li et al. 2001; Kim et al. 2006).

### 3.4.2.3 Permease Substrates

Unlike endocytosis-mediated transport that appears to be specific to iron, metal permeases are often able to transport multiple different metal ions. For instance, although characterized members of the NRAMP family have specificity against  $\text{Ca}^{2+}$  and  $\text{Mg}^{2+}$ , they can transport several d-block divalent metal ions with a preference for  $\text{Fe}^{2+}$  and  $\text{Mn}^{2+}$  over  $\text{Zn}^{2+}$  (Illing et al. 2012; Bozzi et al. 2016). Other metal permeases that transport divalent metal ions have an analogous lack of selectivity when comparing first row transition metals and zinc. Ferroportin is best known as a  $\text{H}^+/\text{Fe}^{2+}$  antiporter (Pan et al. 2020), but can also transport  $\text{Co}^{2+}$ ,  $\text{Zn}^{2+}$  and  $\text{Ni}^{2+}$  (Schaaf et al. 2006; Mitchell et al. 2014). Since these permeases often have a broad spectrum of substrates, the biologically relevant substrate is typically predicted based on the conditions under which the permease is expressed. For instance, members of the ZIP family are predicted to be responsible for zinc transport when the gene is expressed during zinc deficiency, or iron when expressed during iron deficiency. However, even though structural and mechanistic models are now available for the ZIPs, sequence determinants for substrate preference or whether a preference exists are unknown (Hu 2020). Since the assimilation of non-limiting metal ions during zinc- or iron-deficiencies would lead to mis-metallation of apo-proteins, such knowledge gaps point to the possibility that additional factors, such as periplasmic metal-binding proteins, exist in the cell to mediate substrate specificity.

Indeed, such proteins are co-expressed with ZIPs during zinc deficiency in algae. In *C. reinhardtii*, a protein structurally similar to AztD, a WD40-like periplasmic zinc chaperone characterized in bacteria (Handali et al. 2015; Neupane et al. 2019), is induced during zinc limitation (Malasarn et al. 2013). Based on the recent reference genome assembly (Goodstein et al. 2012; Blaby et al. 2014), the gene encoding this protein is head-to-head with *ZRT1* that encodes one of the main zinc transporters from the ZIP family in *C. reinhardtii*. This proximity suggests that the two genes could share a bi-directional promoter, and evolution has selected for tight co-regulation of this putative zinc chaperone and the zinc transporter. A protein similar to TroA, a zinc-binding component of a bacterial ATP-binding cassette transport system (Lee et al. 1999), is expressed during zinc limitation in *Emiliania huxleyi*, a unicellular alga from the haptophyte lineage, which is commonly found in zinc-depleted open-ocean waters (Shire and Kustka 2021). Whether these algal proteins function in an analogous way to their bacterial counterparts is unknown. Like other eukaryotes, algae do not contain multi-subunit ABC transport complexes, such as ZnuABC from bacteria. Therefore, if these proteins do function as secreted zinc chaperones in algae, they may interact with and lend substrate specificity to the ZIPs.

Selectivity of metal ion transport has been achieved to a certain extent by the CTR family and Cu-ATPases that transport  $\text{Cu}^{1+}$  and the MCO/FTR complex that transports  $\text{Fe}^{3+}$  (Fig. 3.2). These transporters can electrochemically separate the monovalent cuprous ion and trivalent ferric ion, respectively, from the other potentially

competing divalent metal ions, such as zinc that only exists in nature as a divalent ion. However, the CTR family can also transport  $\text{Ag}^{1+}$ , and, as a result, under conditions that these transporters are expressed, such as copper-deficiency, cells are sensitive to  $\text{Ag}^{1+}$  toxicity (Howe and Merchant 1992). Presumably, from the point-of-view of natural selection, the cost associated with increased  $\text{Ag}^{1+}$  toxicity is offset by the benefit afforded by excluding divalent metal ions. A similar bargain likely exists for the MCO/FTR transporter, since analogous ferric transporters from bacteria can also transport  $\text{Ga}^{3+}$  and  $\text{Al}^{3+}$  (Anderson et al. 2004).

#### 3.4.2.4 Metal Permease Families in Algae

With some notable exceptions, much of our understanding of algal metal permeases is derived from bioinformatic analyses. Membrane-spanning transporters are often difficult to work with in vitro and, for those algae that are genetically tractable, genetic redundancy due to overlapping gene functions often obfuscates phenotypes of gene-specific mutants. Robust bioinformatic analyses rely on the availability of high-quality algal genome sequences and gene models (Blaby-Haas and Merchant 2019; Hanschen and Starkenburg 2020). With these resources in hand, sequence similarity and phylogenetics of metal permease families can be used to leverage experimentally defined knowledge from reference organisms, such as *S. cerevisiae* and *A. thaliana*, for understanding metal transport in algae. One consequence is that much of our understanding of algal metal transport comes from experimental results with similar proteins in non-algal species. Therefore, a key step in leveraging protein family knowledge derived from other organisms is contextualizing that information with experimentation in algae and shedding light on functional divergence and tailoring that has occurred during evolution. Depending on the genetic tractability and culturability of a target algal species, such experimentation could be as simple as assaying condition-specific gene expression or as complex as reverse genetic analyses. Algal genomes also encode metal transport proteins that have yet to be found in non-algal genomes. These proteins are often found through metal-responsive transcriptome and proteome analyses. The algal-specific FEA (Rubinelli et al. 2002; Allen et al. 2007) and phytotransferrin families (McQuaid et al. 2018) discussed above, highlight the need for experimentation in algae beyond omics-based technologies.

Genes encoding ancient metal transport families shared with other eukaryotes or with bacteria are found in algal genomes. As a result, close homologs may be found in either the plant, fungal, animal, protist or bacterial lineages (Hanikenne et al. 2005; Blaby-Haas and Merchant 2012). Even within the same transporter family, algal genomes often encode some members that are closely related to fungal sequences and other members that are more closely related to plant sequences, reflecting the complex evolution that has resulted in modern-day algal genomes. An example is the CTR family in the green alga *C. reinhardtii*. Two homologs, CTR1 and CTR2, are similar to available fungal sequences, while the homolog COPT1 is similar to land plant sequences (Page et al. 2009). *C. reinhardtii* also has



members of transport families that are more similar to bacterial sequences, such as the divalent metal ion permeases, NRAMP1 and NRAMP2, which are members of the MntH-like subfamily (Blaby-Haas and Merchant 2012). Because of such evolutionary relationships at the protein family level, an understanding of protein phylogeny can help determine which functional knowledge, for instance derived from fungal, bacterial, or plant homologs, may be more relevant to understanding the function of a particular algal protein.

### 3.4.3 Metallochaperones

In addition to membrane-bound transporters, soluble proteins are responsible for transporting metal ions. These proteins, referred to as metal chaperones or metallochaperones, ensure that the correct metals are delivered to the right proteins. Like other eukaryotes, algal genomes encode Atx1-like copper chaperones (Pufahl et al. 1997; Merchant et al. 2020) and, for those algae that have a Cu-Zn superoxide dismutase, a CCS-like copper chaperone (Culotta et al. 1997; Foflonker and Blaby-Haas 2020). Green algae also share a plant-specific copper chaperone that delivers copper to the chloroplast (Blaby-Haas et al. 2014). Unlike other eukaryotes, algae have an unusually large number of nucleotide-dependent metallochaperones (NMCs) that are often expressed only during zinc limitation.

The molecular function of the NMC family [also referred to as CobW or COG0523 (Haas et al. 2009)] is not yet fully resolved. Most homologs contain conserved GTPase and metal-binding motifs. This family has shared ancestry with HypB and UreG, two GTPases involved in nickel insertion in Ni-Fe hydrogenase and Ni-urease, respectively (Haas et al. 2009). This shared ancestry plus the conservation of GTPase and metal-binding suggests that these putative chaperones also function in metalloprotein biogenesis. Most eukaryotic genomes only contain one homolog, with some gene expansion in human (5 homologs) and plants (3–4 homologs). Algal genomes, however, can encode upwards of 27 NMCs as found for *E. huxleyi*. Three of these NMCs are significantly increased in abundance during zinc deficiency (Shire and Kustka 2021). The *C. reinhardtii* genome encodes 12 NMCs. Of these, *ZCP1* and *ZCP2* respond specifically to zinc, and these two proteins are the two most abundant soluble proteins during zinc limitation (Haas et al. 2009; Hsieh et al. 2013; Malasarn et al. 2013). Although *E. huxleyi* and *C. reinhardtii* are both algae and share some genes, because of endosymbiotic gene transfer from a red alga in an ancestor of *E. huxleyi*, their last common ancestor likely dates to the first eukaryotes, suggesting that the large number of NMCs in these algae is due to convergent evolution. Clearly, the NMCs are providing important metal-related functions for algae from different environments and with different evolutionary backgrounds.

### 3.5 Conclusions

Largely through omics-based experiments, significant progress has been made in identifying conserved and unique metal-transport strategies in algae. Transporters encoded in these genomes can be identified by similarity based techniques, aided by high-quality genome assemblies and gene model predictions. Likewise, technologies, such as RNAseq and iTRAQ-based proteomics, are available to quantify gene expression at the genome-wide scale in response to metal ion availability. However, the intracellular location of most metal transporters and substrate preferences are unknown. Development of reverse-genetic techniques enabled by RNA-guided endonucleases, such as CRISPR-Cas9, and the characterization of mutants defective in genes identified in omics experiments are expected to yield considerable new discoveries. Insights into novel functional capabilities and adaptations that have evolved are critical for understanding the role of taxonomically diverse algae in distinct ecosystems. There are notable interactions between metals, such as the need for increased copper transport to metallate FOX1 during iron deficiency, which can complicate the interpretation of loss-of-function phenotypes for ascribing molecular function. Therefore, inter-disciplinary studies are needed to understand the role of predicted algal proteins at both the molecular and biological levels. The number of genes of unknown or uncertain function that are predicted in algae genomes points to yet-to-be discovered strategies (Blaby-Haas and Merchant 2019). As algae are increasingly the focus of biotechnological innovation in bioenergy and bioproduction, understanding these processes will also provide novel resources for engineering algal metabolism.

**Acknowledgments** CB is supported by the US Department of Energy, Office of Science, Office of Biological, and Environmental Research, as part of the Quantitative Plant Science Initiative SFA at Brookhaven National Laboratory and under Award Number DE-SC0018301.

### References

- Allen MD, Del Campo JA, Kropat J, Merchant SS (2007) FEA1, FEA2, and FRE1, encoding two homologous secreted proteins and a candidate ferrireductase, are expressed coordinately with FOX1 and FTR1 in iron-deficient *Chlamydomonas reinhardtii*. *Eukaryot Cell* 6:1841–1852. <https://doi.org/10.1128/EC.00205-07>
- Allen AE, LaRoche J, Maheswari U et al (2008) Whole-cell response of the pennate diatom *Phaeodactylum tricorutum* to iron starvation. *Proc Natl Acad Sci U S A* 105:10438–10443. <https://doi.org/10.1073/pnas.0711370105>
- Anderson DS, Adhikari P, Nowalk AJ et al (2004) The hFbpABC transporter from *Haemophilus influenzae* functions as a binding-protein-dependent ABC transporter with high specificity and affinity for ferric iron. *J Bacteriol* 186:6220–6229. <https://doi.org/10.1128/JB.186.18.6220-6229.2004>
- Arakaki Y, Kawai-Toyooka H, Hamamura Y et al (2013) The simplest integrated multicellular organism unveiled. *PLoS One* 8:e81641

- Arimoto A, Nishitsuji K, Higa Y et al (2019) A siphonous macroalgal genome suggests convergent functions of homeobox genes in algae and land plants. *DNA Res* 26:183–192. <https://doi.org/10.1093/dnares/dsz002>
- Armbrust EV, Berges JA, Bowler C et al (2004) The genome of the diatom *Thalassiosira Pseudonana*: ecology, evolution, and metabolism. *Science* 306:79–86. <https://doi.org/10.1126/science.1101156>
- Bai L, Qiao M, Zheng R et al (2016) Phylogenomic analysis of transferrin family from animals and plants. *Comp Biochem Physiol Part D Genomics Proteomics* 17:1–8
- Bigdare RR, Ondrusek ME, Kennicutt MC et al (1993) Evidence a photoprotective for secondary carotenoids of snow algae. *J Phycol* 29:427–434. <https://doi.org/10.1111/j.1529-8817.1993.tb00143.x>
- Blaby IK, Blaby-Haas CE, Tourasse N et al (2014) The *Chlamydomonas* genome project: a decade on. *Trends Plant Sci* 19. <https://doi.org/10.1016/j.tplants.2014.05.008>
- Blaby-Haas CE, Merchant SS (2012) The ins and outs of algal metal transport. *Biochim Biophys Acta, Mol Cell Res* 1823:1531–1552. <https://doi.org/10.1016/j.bbamcr.2012.04.010>
- Blaby-Haas CE, Merchant SSS (2014) Lysosome-related organelles as mediators of metal homeostasis. *J Biol Chem* 289:28129–28136. <https://doi.org/10.1074/jbc.R114.592618>
- Blaby-Haas CE, Merchant SS (2017) Regulating cellular trace metal economy in algae. *Curr Opin Plant Biol* 39:88–96. <https://doi.org/10.1016/j.pbi.2017.06.005>
- Blaby-Haas CE, Merchant SS (2019) Comparative and functional algal genomics. *Annu Rev Plant Biol* 70:605–638
- Blaby-Haas CE, Padilla-Benavides T, Stübe R et al (2014) Evolution of a plant-specific copper chaperone family for chloroplast copper homeostasis. *Proc Natl Acad Sci U S A* 111:E5480–E5487. <https://doi.org/10.1073/pnas.1421545111>
- Bowler C, Allen AE, Badger JH et al (2008) The *Phaeodactylum* genome reveals the evolutionary history of diatom genomes. *Nature* 456:239–244. <https://doi.org/10.1038/nature07410>
- Bozzi AT, Bane LB, Weihofen WA et al (2016) Conserved methionine dictates substrate preference in Nramp-family divalent metal transporters. *Proc Natl Acad Sci U S A* 113:10310–10315. <https://doi.org/10.1073/pnas.1607734113>
- Brock TD (1975) Salinity and the ecology of *Dunaliella* from Great Salt Lake. *Microbiology* 89:285–292
- Castenholz RW, McDermott TR (2010) The Cyanidiales: ecology, biodiversity, and biogeography. In: *Red algae in the genomic age*. Springer, pp 357–371
- Collier JL, Baker KM, Bell SL (2009) Diversity of urea-degrading microorganisms in open-ocean and estuarine planktonic communities. *Environ Microbiol* 11:3118–3131
- Coneva V, Chitwood DH (2015) Plant architecture without multicellularity: quandaries over patterning and the soma-germline divide in siphonous algae. *Front Plant Sci* 0:287. <https://doi.org/10.3389/FPLS.2015.00287>
- Conklin DS, McMaster JA, Culbertson MR, Kung C (1992) COT1, a gene involved in cobalt accumulation in *Saccharomyces cerevisiae*. *Mol Cell Biol* 12:3678–3688. <https://doi.org/10.1128/MCB.12.9.3678-3688.1992>
- Courties C, Vaquer A, Troussellier M et al (1994) Smallest eukaryotic organism. *Nature* 370:255
- Croft MT, Lawrence AD, Raux-Deery E et al (2005) Algae acquire vitamin B<sub>12</sub> through a symbiotic relationship with bacteria. *Nature* 438:90–93
- Culotta VC, Klomp LW, Strain J, Casareno RL, Krems B, Gitlin JD et al (1997) The copper chaperone for superoxide dismutase. *J Biol Chem* 272:23469–23472. <https://doi.org/10.1074/JBC.272.38.23469>
- Dancis A, Yuan DS, Haile D et al (1994) Molecular characterization of a copper transport protein in *S. cerevisiae*: an unexpected role for copper in iron transport. *Cell* 76:393–402. [https://doi.org/10.1016/0092-8674\(94\)90345-X](https://doi.org/10.1016/0092-8674(94)90345-X)

- del Pozo T, Cambiazo V, González M (2010) Gene expression profiling analysis of copper homeostasis in *Arabidopsis thaliana*. *Biochem Biophys Res Commun* 393:248–252. <https://doi.org/10.1016/j.bbrc.2010.01.111>
- Demaegd D, Foulquier F, Colinet AS et al (2013) Newly characterized Golgi-localized family of proteins is involved in calcium and pH homeostasis in yeast and human cells. *Proc Natl Acad Sci U S A* 110:6859–6864. <https://doi.org/10.1073/pnas.1219871110>
- Derelle E, Ferraz C, Rombauts S et al (2006) Genome analysis of the smallest free-living eukaryote *Ostreococcus tauri* unveils many unique features. *Proc Natl Acad Sci* 103:11647–11652. <https://doi.org/10.1073/PNAS.0604795103>
- Eid C, Hémadi M, Ha-Duong NT, El Hage Chahine JM (2014) Iron uptake and transfer from ceruloplasmin to transferrin. *Biochim Biophys Acta* 1840:1771–1781. <https://doi.org/10.1016/J.BBAGEN.2014.01.011>
- Eide D, Broderius M, Fett J, Guerinot ML (1996) A novel iron-regulated metal transporter from plants identified by functional expression in yeast. *Proc Natl Acad Sci U S A* 93:5624–5628. <https://doi.org/10.1073/pnas.93.11.5624>
- Elkin SR, Lakoduk AM, Schmid SL (2016) Endocytic pathways and endosomal trafficking: a primer. *Wien Med Wochenschr* 166(166):196–204. <https://doi.org/10.1007/S10354-016-0432-7>
- Fisher M, Gokhman I, Pick U, Zamir A (1996) A structurally novel transferrin-like protein accumulates in the plasma membrane of the unicellular green alga *Dunaliella salina* grown in high salinities. *J Biol Chem* 272:1565–1570
- Fisher M, Zamir A, Pick U (1998) Iron uptake by the halotolerant alga *Dunaliella* is mediated by a plasma membrane transferrin. *J Biol Chem* 273:17553–17558
- Fisher CR, Wyckoff EE, Peng ED, Payne SM (2016) Identification and characterization of a putative manganese export protein in *Vibrio cholerae*. *J Bacteriol* 198:2810–2817. <https://doi.org/10.1128/JB.00215-16>
- Foflonker F, Blaby-Haas CE (2020) Co-locality to co-functionality: eukaryotic gene neighborhoods as a resource for function discovery. *Mol Biol Evol*. <https://doi.org/10.1093/molbev/msaa221>
- Gawryluk RMR, Tikhonenkov DV, Hehenberger E et al (2019) Non-photosynthetic predators are sister to red algae. *Nature* 572(7768):240–243. <https://doi.org/10.1038/s41586-019-1398-6>
- Goodstein DM, Shu S, Howson R et al (2012) Phytozome: a comparative platform for green plant genomics. *Nucleic Acids Res* 40. <https://doi.org/10.1093/nar/gkr944>
- Haas CE, Rodionov DA, Kropat J et al (2009) A subset of the diverse COG0523 family of putative metal chaperones is linked to zinc homeostasis in all kingdoms of life. *BMC Genomics* 10:1–21. <https://doi.org/10.1186/1471-2164-10-470>
- Hadariová L, Vesteg M, Hampl V, Krajčovič J (2017) Reductive evolution of chloroplasts in non-photosynthetic plants, algae and protists. *Curr Genet* 64(64):365–387. <https://doi.org/10.1007/S00294-017-0761-0>
- Handali M, Roychowdhury H, Neupane DP, Yukl ET (2015) AztD, a periplasmic zinc metallochaperone to an ATP-binding cassette (ABC) transporter system in *Paracoccus denitrificans*. *J Biol Chem* 290:29984–29992. <https://doi.org/10.1074/JBC.M115.684506>
- Hanikenne M, Krämer U, Demoulin V, Baurain D (2005) A comparative inventory of metal transporters in the green alga *Chlamydomonas reinhardtii* and the red alga *Cyanidioschizon merolae*. *Plant Physiol* 137:428–446. <https://doi.org/10.1104/pp.104.054189>
- Hanschen ER, Starckenburg SR (2020) The state of algal genome quality and diversity. *Algal Res* 50:101968. <https://doi.org/10.1016/J.ALGAL.2020.101968>
- Helliwell KE, Wheeler GL, Leptos KC et al (2011) Insights into the evolution of vitamin B12 auxotrophy from sequenced algal genomes. *Mol Biol Evol* 28:2921–2933
- Howe G, Merchant S (1992) Heavy metal-activated synthesis of peptides in *Chlamydomonas reinhardtii*. *Plant Physiol* 98:127–136. <https://doi.org/10.1104/pp.98.1.127>
- Hsieh SI, Castruita M, Malasam D et al (2013) The proteome of copper, iron, zinc, and manganese micronutrient deficiency in *Chlamydomonas reinhardtii*. *Mol Cell Proteomics* 12:65–86. <https://doi.org/10.1074/mcp.M112.021840>

- Hu J (2020) Toward unzipping the ZIP metal transporters: structure, evolution, and implications on drug discovery against cancer. *FEBS J*. <https://doi.org/10.1111/FEBS.15658>
- Ihemere UE, Narayanan NN, Sayre RT (2012) Iron biofortification and homeostasis in transgenic cassava roots expressing the algal iron assimilatory gene, *FEA1*. *Front Plant Sci* 3:171. <https://doi.org/10.3389/fpls.2012.00171>
- Illing AC, Shawki A, Cunningham CL, Mackenzie B (2012) Substrate profile and metal-ion selectivity of human divalent metal-ion transporter-1. *J Biol Chem* 287:30485–30496. <https://doi.org/10.1074/jbc.M112.364208>
- Intwala A, Patey TD, Polet DM, Twiss MR (2008) Nutritive substitution of zinc by cadmium and cobalt in phytoplankton isolated from the Lower Great Lakes. *J Great Lakes Res* 34:1–11
- Johnson MD, Stoecker DK (2005) Role of feeding in growth and photophysiology of *Myrionecta rubra*. *Aquat Microb Ecol* 39:303–312
- Kamizono A, Nishizawa M, Teranishi Y et al (1989) Identification of a gene conferring resistance to zinc and cadmium ions in the yeast *Saccharomyces cerevisiae*. *Mol Gen Genet MGG* 219(1/2):161–167. <https://doi.org/10.1007/BF00261172>
- Karakashian MW (1975) Symbiosis in *Paramecium bursaria*. *Symp Soc Exp Biol*:145–173
- Kazamia E, Sutak R, Paz-Yepes J et al (2018) Endocytosis-mediated siderophore uptake as a strategy for Fe acquisition in diatoms. *Sci Adv* 4:eaar4536. <https://doi.org/10.1126/SCIADV.AAR4536>
- Kim SA, Punshon T, Lanzirotti A et al (2006) Localization of iron in Arabidopsis seed requires the vacuolar membrane transporter VIT1. *Science* 314:1295–1298. <https://doi.org/10.1126/science.1132563>
- Kropat J, Gallaher SD, Urzica EI et al (2015) Copper economy in Chlamydomonas: prioritized allocation and reallocation of copper to respiration vs. photosynthesis. *Proc Natl Acad Sci U S A* 112:2644–2651. <https://doi.org/10.1073/pnas.1422492112>
- Lane TW, Saito MA, George GN et al (2005) A cadmium enzyme from a marine diatom. *Nature* 435:42
- Lee Y-H, Deka RK, Norgard MV et al (1999) *Treponema pallidum* TroA is a periplasmic zinc-binding protein with a helical backbone. *Nat Struct Biol* 6(6):628–633. <https://doi.org/10.1038/10677>
- Lelandais G, Scheiber I, Paz-Yepes J et al (2016) *Ostreococcus tauri* is a new model green alga for studying iron metabolism in eukaryotic phytoplankton. *BMC Genomics* 17:1–23
- Li L, Chen OS, Ward DMV, Kaplan J (2001) CCC1 is a transporter that mediates vacuolar iron storage in yeast. *J Biol Chem* 276:29515–29519. <https://doi.org/10.1074/jbc.M103944200>
- Lommer M, Specht M, Roy A-S et al (2012) Genome and low-iron response of an oceanic diatom adapted to chronic iron limitation. *Genome Biol* 13(13):1–21. <https://doi.org/10.1186/GB-2012-13-7-R66>
- Malasarn D, Kropat J, Hsieh SI et al (2013) Zinc deficiency impacts CO<sub>2</sub> assimilation and disrupts copper homeostasis in *Chlamydomonas reinhardtii*. *J Biol Chem* 288:10672–10683. <https://doi.org/10.1074/jbc.M113.455105>
- McQuaid JB, Kustka AB, Oborník M et al (2018) Carbonate-sensitive phytoferritin controls high-affinity iron uptake in diatoms. *Nature* 555:543–537. <https://doi.org/10.1038/nature25982>
- Merchant SS, Allen MD, Kropat J et al (2006) Between a rock and a hard place: trace element nutrition in Chlamydomonas. *Biochim Biophys Acta, Mol Cell Res* 1763:578–594. <https://doi.org/10.1016/j.bbamcr.2006.04.007>
- Merchant SS, Prochnik SE, Vallon O et al (2007) The Chlamydomonas genome reveals the evolution of key animal and plant functions. *Science* 318:245–250
- Merchant SS, Schmollinger S, Strenkert D et al (2020) From economy to luxury: copper homeostasis in Chlamydomonas and other algae. *Biochim Biophys Acta, Mol Cell Res* 1867:118822. <https://doi.org/10.1016/j.bbamcr.2020.118822>
- Mitchell CJ, Shawki A, Ganz T et al (2014) Functional properties of human ferroportin, a cellular iron exporter reactive also with cobalt and zinc. *Am J Physiol Cell Physiol* 306:C450–C459. <https://doi.org/10.1152/ajpcell.00348.2013>

- Mock T, Junge K (2007) Psychrophilic diatoms. Springer, Dordrecht, pp 343–364
- Morrissey J, Sutak R, Paz-Yepes J et al (2015) A novel protein, ubiquitous in marine phytoplankton, concentrates iron at the cell surface and facilitates uptake. *Curr Biol* 25:364–371. <https://doi.org/10.1016/j.cub.2014.12.004>
- Narayanan NN, Ihemere U, Chiu W et al (2011) The iron assimilatory protein, FEA1, from *Chlamydomonas reinhardtii* facilitates iron-specific metal uptake in yeast and plants. *Front Plant Sci* 2:67. <https://doi.org/10.3389/fpls.2011.00067>
- Neupane DP, Fullam SH, Chacón KN, Yukl ET (2019) Crystal structures of AztD provide mechanistic insights into direct zinc transfer between proteins. *Commun Biol* 2(2):1–12. <https://doi.org/10.1038/s42003-019-0542-z>
- Nies DH (1992) CzcR and CzcD, gene products affecting regulation of resistance to cobalt, zinc, and cadmium (czc system) in *Alcaligenes eutrophus*. *J Bacteriol* 174:8102–8110. <https://doi.org/10.1128/JB.174.24.8102-8110.1992>
- Nies DH, Silver S (1995) Ion efflux systems involved in bacterial metal resistances. *J Ind Microbiol* 142(14):186–199. <https://doi.org/10.1007/BF01569902>
- North WJ (1971) Growth of individual fronds of the mature giant kelp, *Macrocystis*. *Nov hedwigia Beihefte*
- Page MD, Kropat J, Hamel PP, Merchant SS (2009) Two *Chlamydomonas* CTR copper transporters with a novel cys-met motif are localized to the plasma membrane and function in copper assimilation. *Plant Cell* 21:928–943. <https://doi.org/10.1105/tpc.108.064907>
- Pan Y, Ren Z, Gao S et al (2020) Structural basis of ion transport and inhibition in ferroportin. *Nat Commun* 11:1–11. <https://doi.org/10.1038/s41467-020-19458-6>
- Paz Y, Katz A, Pick U (2007a) A multicopper ferroxidase involved in iron binding to transferrins in *Dunaliella salina* plasma membranes. *J Biol Chem* 282:8658–8666. <https://doi.org/10.1074/jbc.M609756200>
- Paz Y, Shimoni E, Weiss M, Pick U (2007b) Effects of iron deficiency on iron binding and internalization into acidic vacuoles in *Dunaliella salina*. *Plant Physiol* 144:1407–1415. <https://doi.org/10.1104/PP.107.100644>
- Pocock T, Lachance M-A, Pröschold T et al (2004) Identification of a psychrophilic green alga from Lake Bonney Antarctica: *Chlamydomonas raudensis* Ettl. (UWO 241) *Chlorophyceae*. *J Phycol* 40:1138–1148
- Polle JEW, Calhoun S, McKie-Krisberg Z et al (2020) Genomic adaptations of the green alga *Dunaliella salina* to life under high salinity. *Algal Res* 50:101990. <https://doi.org/10.1016/j.ALGAL.2020.101990>
- Potelle S, Morelle W, Dulary E et al (2016) Glycosylation abnormalities in Gdt1p/TMEM165 deficient cells result from a defect in Golgi manganese homeostasis. *Hum Mol Genet* 25:1489–1500. <https://doi.org/10.1093/hmg/ddw026>
- Pufahl RA, Singer CP, Peariso KL et al (1997) Metal ion chaperone function of the soluble Cu (I) receptor Atx1. *Science* 278:853–856. <https://doi.org/10.1126/science.278.5339.853>
- Purohit R, Ross MO, Batelu S et al (2018) Cu<sup>+</sup>-specific CopB transporter: revising P1B-type ATPase classification. *Proc Natl Acad Sci* 115:2108–2113. <https://doi.org/10.1073/PNAS.1721783115>
- Ranjan A, Townsley BT, Ichihashi Y et al (2015) An intracellular transcriptomic atlas of the giant coenocyte *Caulerpa taxifolia*. *PLoS Genet* 11:e1004900
- Rastogi A, Maheswari U, Dorrell RG et al (2018) Integrative analysis of large scale transcriptome data draws a comprehensive landscape of *Phaeodactylum tricoratum* genome and evolutionary origin of diatoms. *Sci Rep* 8(8):1–14. <https://doi.org/10.1038/s41598-018-23106-x>
- Rubinelli P, Siripornadulsil S, Gao-Rubinelli F, Sayre RT (2002) Cadmium- and iron-stress-inducible gene expression in the green alga *Chlamydomonas reinhardtii*: evidence for H43 protein function in iron assimilation. *Planta* 215:1–13. <https://doi.org/10.1007/s00425-001-0711-3>
- Sadka A, Himmelhoch S, Zamir A (1991) A 150 kilodalton cell surface protein is induced by salt in the halotolerant green alga *Dunaliella salina*. *Plant Physiol* 95:822–831

- Saito MA, Goepfert TJ (2008) Zinc-cobalt colimitation of *Phaeocystis antarctica*. *Limnol Oceanogr* 53:266–275
- Sasaki T, Kurano N, Miyachi S (1998) Cloning and characterization of high-CO<sub>2</sub>-specific cDNAs from a marine microalga, *Chlorococcum littorale*, and effect of CO<sub>2</sub> concentration and iron deficiency on the gene expression. *Plant Cell Physiol* 39:131–138. <https://doi.org/10.1093/oxfordjournals.pcp.a029349>
- Schaaf G, Honsbein A, Meda AR et al (2006) AtIREG2 encodes a tonoplast transport protein involved in iron-dependent nickel detoxification in *Arabidopsis thaliana* roots. *J Biol Chem* 281:25532–25540. <https://doi.org/10.1074/jbc.M601062200>
- Scheiber IF, Pilátová J, Malych R et al (2019) Copper and iron metabolism in *Ostreococcus tauri* – the role of phytoferritin, plastocyanin and a chloroplast copper-transporting ATPase. *Metallomics* 11:1657–1666. <https://doi.org/10.1039/C9MT00078J>
- Schneider A, Steinberger I, Herdean A et al (2016) The evolutionarily conserved protein PHOTO-SYNTHESIS AFFECTED MUTANT71 is required for efficient manganese uptake at the thylakoid membrane in *Arabidopsis*. *Plant Cell* 28:892–910. <https://doi.org/10.1105/tpc.15.00812>
- Schwarz M, Sal-Man N, Zamir A, Pick U (2003) A transferrin-like protein that does not bind iron is induced by iron deficiency in the alga *Dunaliella salina*. *Biochim Biophys Acta* 1649:190–200. [https://doi.org/10.1016/S1570-9639\(03\)00185-7](https://doi.org/10.1016/S1570-9639(03)00185-7)
- Shelford VE (1913) Animal communities in temperate America: as illustrated in the Chicago region: a study in animal ecology, 2nd edn. The University of Chicago Press, Chicago
- Shire DM, Kustka AB (2021) Proteomic responses of the coccolithophore *Emiliania huxleyi* to zinc limitation and trace metal substitution. *Environ Microbiol*. <https://doi.org/10.1111/1462-2920.15644>
- Stearman R, Yuan DS, Yamaguchi-Iwai Y et al (1996) A permease-oxidase complex involved in high-affinity iron uptake in yeast. *Science* 271:1552–1557. <https://doi.org/10.1126/SCIENCE.271.5255.1552>
- Steffensen DA (1976) Morphological variation of *Ulva* in the Avon-Heathcote Estuary, Christchurch. *N Z J Mar Freshw Res* 10:329–341
- Stiller JW, Schreiber J, Yue J et al (2014) The evolution of photosynthesis in chromist algae through serial endosymbioses. *Nat Commun* 5(1):1–7. <https://doi.org/10.1038/ncomms6764>
- Sunda WG, Huntsman SA (1995) Cobalt and zinc interreplacement in marine phytoplankton: biological and geochemical implications. *Limnol Oceanogr* 40:1404–1417
- Sutak R, Botebol H, Blaiseau P-L et al (2012) A comparative study of iron uptake mechanisms in marine microalgae: iron binding at the cell surface is a critical step. *Plant Physiol* 160:2271–2284. <https://doi.org/10.1104/PP.112.204156>
- Tejada-Jiménez M, Llamas Á, Sanz-Luque E et al (2007) A high-affinity molybdate transporter in eukaryotes. *Proc Natl Acad Sci U S A* 104:20126–20130. <https://doi.org/10.1073/pnas.0704646104>
- Tejada-Jiménez M, Galván A, Fernández E (2011) Algae and humans share a molybdate transporter. *Proc Natl Acad Sci U S A* 108:6420–6425. <https://doi.org/10.1073/pnas.1100700108>
- Turnšek J, Brunson JK, Martínez Viedma MDP et al (2021) Proximity proteomics in a marine diatom reveals a putative cell surface-to-chloroplast iron trafficking pathway. *elife* 10:1–113. <https://doi.org/10.7554/ELIFE.52770>
- Vidal SM, Malo D, Vogan K et al (1993) Natural resistance to infection with intracellular parasites: isolation of a candidate for Bcg. *Cell* 73:469–486. [https://doi.org/10.1016/0092-8674\(93\)90135-D](https://doi.org/10.1016/0092-8674(93)90135-D)

- Wang C, Xu W, Jin H et al (2016) A putative chloroplast-localized  $\text{Ca}^{2+}/\text{H}^{+}$  antiporter CCHA1 is involved in calcium and pH homeostasis and required for PSII function in Arabidopsis. *Mol Plant* 9:1183–1196. <https://doi.org/10.1016/j.molp.2016.05.015>
- Wetherbee R, Jackson CJ, Repetti SI et al (2019) The golden paradox – a new heterokont lineage with chloroplasts surrounded by two membranes. *J Phycol* 55:257–278. <https://doi.org/10.1111/JPY.12822>
- Zhao H, Eide D (1996a) The yeast ZRT1 gene encodes the zinc transporter protein of a high-affinity uptake system induced by zinc limitation. *Proc Natl Acad Sci U S A* 93:2454–2458. <https://doi.org/10.1073/pnas.93.6.2454>
- Zhao H, Eide D (1996b) The ZRT2 gene encodes the low affinity zinc transporter in *Saccharomyces cerevisiae*. *J Biol Chem* 271:23203–23210. <https://doi.org/10.1074/jbc.271.38.23203>



# Chapter 4

## Metal Based Antimicrobials: Uses and Challenges



Daniel A. Salazar-Alemán and Raymond J. Turner

**Abstract** In this antimicrobial resistance era, where resistance to most antibiotics is commonplace, metals and metalloid based antimicrobials (MBA) have emerged as an alternative to treat pathogenic agents. A variety of MBAs are under research for their antimicrobial activities, with copper, silver and zinc leading the charge. MBAs are toxic to microorganisms through a variety of mechanisms. Many MBAs attack thiol redox balance and compete out iron in redox enzymes freeing it to carry out Fenton reactions producing reactive oxygen species. Other toxic sites include the cell wall and membrane as well as competing out essential metal transport and their role in essential enzymatic activities. Whether these mechanisms are solely responsible for cell death has yet to be fully elucidated as the majority of molecular mechanistic research has studied specific genes mediating resistance. Still, what is understood is that MBAs demonstrate broad-spectrum activity when compared to conventional antimicrobials. Applications of metals as antimicrobials are concentrated in the biomedical field in the form of: coatings for medical devices, contact-killing surfaces, impregnation of fabrics, among others. Other applications are found in agriculture and industries like food and cosmetics. Novel technologies, like metal-based nanomaterials, metal-organic frameworks, metal-biocide co-crystals and solid metal surfaces, further enlarge the repertoire of metals as a viable alternative against multidrug resistant bacteria. Several challenges lie in the future, including how the current linear-economy model of consumption may eventually lead to a proliferation of resistance to these MBAs. Thus careful stewardship is required, less metals follow the same fate as organic antibiotics.

---

D. A. Salazar-Alemán · R. J. Turner (✉)  
Department of Biological Sciences, University of Calgary, Calgary, AB, Canada  
e-mail: [danielarmando.salaza@ucalgary.ca](mailto:danielarmando.salaza@ucalgary.ca); [turnerr@ucalgary.ca](mailto:turnerr@ucalgary.ca)

## 4.1 Introduction

As indicated in the Global Priority Pathogens List, published in 2017 by the World Health Organization (2017), bacterial infections that reflect antibiotic resistance are a great concern to public health. This reflects that the research and development of new alternatives for antimicrobials should be a high priority for researchers; consequently, several initiatives around the globe are pushing to provide incentives for all types of involved parties with the aim of stimulating the pipeline of different types of antimicrobials (Ardal et al. 2018).

Given our present state of challenges to control infectious organisms in this state of the AMR era, a push for new antimicrobial compounds is evolving out of academic laboratories. Considerations towards using Phage (Brives and Pourraz 2020), Natural and synthetic Cationic Peptides (Magana et al. 2020; Cowan 1999), so called natural compounds mainly extracts of plants, such as alkaloids (Khameneh et al. 2019) and flavonoids (Sarbu et al. 2019), polymers (Kamaruzzaman et al. 2019), nanomaterials (Bernardos et al. 2019; Khan et al. 2020) and metal and metalloid [referred to as ‘metal(loid)s’ hereafter to indicate both groups]—based antimicrobials (MBAs) (Turner 2017). Here we will overview the types of elements one sees as MBA’s and their mechanisms, uses and challenges.

For convenience all soft, hard, and other elements with ‘metal’ properties are grouped together into the term MBA. Another point that needs to be understood in the context of a discussion of MBA’s, is that in biology there are several essential metals. Metals provide biochemical activities that cannot be satisfied by organic molecules alone. Essential metals primarily include iron (Fe), copper (Cu), zinc (Zn), nickel (Ni), magnesium (Mg), calcium (Ca), manganese (Mn), cobalt (Co), molybdenum (Mo), and selenium (Se) plus a few other elements used in extreme environments for unique organisms. Life’s selectivity towards what metals are used in biochemistry is a reflection of evolution and corresponds to stages of our planet’s biological development (Dupont et al. 2006). Although non-essential metal(loid) elements tend to be toxic, essential elements at higher concentrations or presented in different redox speciation states are also toxic. Finally, the reader should also recognize that there are other inorganic elements, particularly the halogens, that are also essential, but with antimicrobial properties i.e.: chlorine, bromine and iodine (Koski et al. 1966). However, halogens will not be discussed here. For practical reasons, although some radioactive elements are antimicrobial, those will also not be discussed. Thus, here in this chapter the focus is on the metal(loid)s shown to have antimicrobial properties.

## 4.2 History of Metals as Antimicrobials

Historical uses have led to the current idea of metals and metalloids now considered as an alternative for addressing the ongoing antibiotic resistance debacle. Metals, along with natural plant extracts (an example being the usage of ground plant homogenate as a poultice), have been used since antiquity and likely earlier for treatments of disease and infection. It was the work of Sir Alexander Fleming discovering penicillin in 1928 that changed infection control in the twentieth century (Fleming 1929). Following his initial discovery and the realization that microbes produce molecules to ‘attack’ each other, there was an explosion of new antibiotic discoveries (Aminov 2010), leading metals to take a back seat in relation to these new antibiotics (Gould 2016).

For thousands of years, metals have been used for their antibacterial properties. Persians used vessels made of copper and silver to prevent water fouling and help preserve food. Such practices were adapted by subsequent civilizations of the Phoenicians, Greeks, Romans, and Egyptians (Alexander 2009). Even towards modern times North American settlers added silver coins into containers to preserve water, wine, milk and vinegar. Soldiers in world wars in the twentieth century and earlier would also add silver to water to prevent dysentery (Borkow and Gabbay 2009).

Metals as antimicrobials were also explored early in agriculture. One of the first known specific uses was that of the Bordeaux mixture (mix of copper sulfate and slaked lime) to prevent downy mildew on grape vines (Dixon 2004). In the eighteenth century copper salts were used to protect grain and grape crops against bacterial and fungal infections (Russell 2005) and are still used to date on crops as diverse as tomatoes, peaches and apples. Copper compounds have been used in agriculture since the late 1700s to control fungi on grain seeds. Of course, Cu was also used as a fertilizer additive as it is an essential element and promotes crop growth.

Metals as antimicrobials have been widely used throughout history as a medical treatment. Copper was used as an astringent by the Egyptians around 1500 B.C. This was documented in the Edwin Smith Papyrus, the oldest known surgical text. Metals as an antiseptic for the treatment of wounds and infections have been continuously explored since. Diseases like leprosy, tuberculosis, gonorrhoea, syphilis, anaemia were treated by tellurite, arsenate/arsenite, copper and mercury (Pereira 1836; Hodges 1889).

Overall, the noble metal Silver (Ag) and to a lesser extent gold (Au) have received the greatest attention over the millennia for their antimicrobial activities. Some applications from the eighteenth century for the use of silver include silver sutures (Sims 1852), silver to prevent gonorrhoeal eye infections in newborns (Crede 1881), and silver foils to prevent infection from burn wounds (Silver et al. 2006).

Diseases like syphilis and tuberculosis were commonly treated with Cu in the seventeenth to nineteenth century (Borkow and Gabbay 2009) and then later tellurium was explored (Frazer and Edin 1930). Syphilis was a serious problem and

people were desperate to try anything for relief. Mercury (Hg) and then Arsenic (As) were both explored for the treatment of syphilis (O'Shea 1990; Williams 2009). In fact, the organoarsenic compound salvarsan was termed the 'Magic Bullet' by Paul Ehrlich and was the world's most widely prescribed drug in the early 1900s (Ferrie 2014). Mercury found many uses as a disinfectant (Hodges 1889) and was still being used late into the twentieth century as an antiseptic applied to minor cuts in the form of mercurochrome. Bismuth (Bi) was later found to be a very good antimicrobial and largely displaced the usage of Hg until the discovery of penicillin in 1943 (Ros-Vivancos et al. 2018).

Metals have also been used in other industries to control microbes. For example, many metals have been utilized as wood preservatives. From the late 1960s well into the 2000s most of the wood used in outdoor residential settings was treated with a chromate–arsenic mixture or a chromated copper arsenate (CCA) (Townsend and Sololo-Gabriele 2006). Mercury has also been added to the Cr-As mixture or used alone as HgS (cinnabar) for preserving wood in some regions or as a 'slimicide' in pulp and paper manufacturing (Hylander and Meili 2005). Ancient paintings often used pigments made from metals and metal gildings on murals in the Middle Ages. One can speculate that these metals may have helped preserve these ancient artists' work but certainly poisoned the artists.

Thus, we see that the use of metals and metalloids as antimicrobials is nothing new, they just lost their throne with organic chemistry advancements and discovery of antibiotics. However, with the concern of organic pollutants and our antimicrobial resistance era, we see metals having a renaissance of interest over the past decade.

### 4.3 Metals and Metalloids as Antimicrobials

Here we will overview the mechanisms of toxicity and resistance of MBA's. There are several good reviews the reader is directed to for more in-depth discussions (Hobman and Crossman 2015; Lemire et al. 2013; Silver and Phung 2005; Nies 1999; Silver and Misra 1988). However, the reader should not get the impression that everything is fully understood on this topic. The study of the genes responsible for resistance garnered more attention in the past, particularly those gene (s) providing resistance to specific metal(loid)s (Silver and Phung 1996; Silver 1996). Such resistance determinants are typically carried on mobile genetic elements and provide resistance to:  $\text{Ag}^+$ ,  $\text{AsO}_4^{3-}$ ,  $\text{AsO}_4^{3-}$ ,  $\text{Cd}^{2+}$ ,  $\text{Co}^{2+}$ ,  $\text{CrO}_4^{2-}$ ,  $\text{Cu}^{2+}$ ,  $\text{Hg}^{2+}$ ,  $\text{Ni}^{2+}$ ,  $\text{Pb}^{2+}$ ,  $\text{Sb}^{3+}$ ,  $\text{TeO}_3^{2-}$  and  $\text{Zn}^{2+}$ . Resistance mechanisms can be categorized as generally falling into a limited number of processes that include: effluxing the metal out of the cell; changes to the inorganic ion import systems; repair of damage; changes to essential metal binding sites to avoid exchange; and chemical modification of metal to fewer toxic species. The specific gene systems that have evolved to provide bacteria resistance to metal(oids) are summarized for each metal in Table 4.1. This table reflects the findings from many research groups over several decades. However, the understanding of the biochemical molecular mechanism

**Table 4.1** Specific gene resistance mechanisms of metals and metalloids

Element	Gene and function
Ag	<i>sil</i> ; binding and efflux
As, (Sb)	<i>ars, aso</i> ; arsenate reduction, arsenite oxidation, efflux <i>arr</i> ; arsenate respiratory reductase
Cu	<i>cop, cus, pco</i> ; binding and efflux <i>cueO/corA</i> ; Cu <sup>+</sup> oxidation to Cu <sup>2+</sup>
Cd	<i>cad</i> ; efflux
Cd, Co, Zn	<i>czc</i> ; efflux
Co, Ni	<i>cnr</i> ; efflux
Cr	<i>chr</i> ; efflux
Ni, Co, Cd	<i>ncc</i> ; efflux
Ni	<i>nre</i> ; efflux
Cd, Ni, Cu, Cd	<i>smt</i> ; metallothionein metal binding protein
Pb	<i>pbr</i> ; efflux
Te	<i>tel, ter, teh, ars</i> ; reductase and efflux are proposed, but mechanisms not fully defined
Zn,	<i>zit, znt</i> ; efflux
Hg	<i>mer</i> ; import and reduction of Hg <sup>2+</sup> to Hg <sup>0</sup> giving volatilization

responsible for processes giving sensitivity or tolerance of bacteria towards metal and metalloid ions is still an active field of interest.

Antimicrobials are active in two fundamental ways. (1) Bacteriostatic where cells do not die but their physiology is disrupted so that they cannot replicate, they may also have little biochemical activity. Thus, defining a minimum inhibitory concentration (MIC), is where there is no killing but preventing growth, this is the effect of most preservatives and some antibiotics and antiseptics. (2) Bactericidal leads to cell death and one obtains a minimal biocidal concentration (MBC), which is the amount required for killing of the cells. These values typically refer to activity against the free-swimming planktonic form of the bacteria, yet most microbes spend most of their lifestyle as sessile organisms attached to surfaces, and often as a community referred to as a biofilm. Biofilms tend to be far more tolerant to antibiotics and other stresses, but can still be sensitive to metal ion stress, albeit at higher concentrations than the MIC (Harrison et al. 2007). An unfortunate failure of the study of metal (loid) tolerance/resistance or sensitivity/toxicity towards microbes is that the antimicrobial challenge conditions are not standardized in the field. This is important as the speciation of the metal can be different in different media conditions and thus potentially changing their efficacy. Additionally, different media lead to different physiological fitness states of the bacteria potentially setting them differently to tolerate a challenge. This has been highlighted in the comparative study of challenging different bacteria to different metals in different media conditions (Pormohammad and Turner 2020).

Speciation is only one aspect to the toxicity of metal(oids). One needs to consider the fundamental chemistry of the metals as well. Physico-chemical analysis of the

**Table 4.2** Overview of biochemical toxicity mechanisms of metal and metalloid based antimicrobials

Element	Cell and biochemical targets
Au	Oxidizes thiols, imbalance of cell oxidative status
Ag	Cell membrane; [Fe-S] centres; released Fe gives ROS
Al	Replaces Ca, Mg, Fe; interacts with phosphate binds carboxyls in proteins
As <sup>a</sup>	Competes with phosphate, reactions with reactive thiols
Bi	Cell wall; replaces Zn in metallo-beta-lactamases
Cd <sup>a</sup>	Cell membrane; thiol groups; protein damage
Cu	Competing out other metals; thiol groups; [Fe-S] centres; Fenton active-ROS
Co	Replaces Fe; disrupting Fe-S centres, sulfur assimilation and oxidizes thiols
Cr <sup>a</sup>	Binds to peptides; competes with sulfate transport; protein damage
Fe	Fenton reactions producing ROS
Ga	Competing with Fe transport; [Fe-S] centres; replacing Fe in redox enzymes
Hg <sup>a</sup>	Reactions with thiols; affects membrane fluidity, binds DNA
Ni	Highly reactive; reacts with thiols
Pb <sup>a</sup>	Cell membrane; binds DNA
Sb <sup>a</sup>	Similar to As but less toxic
Se	Oxidising reactive thiols—glutathione
Te	Oxidizing reactive thiols, uncouples electron transport chain.
Ti	Catalyzes ROS production in presence of light.
V <sup>a</sup>	Vanadate places phosphate; inhibitor of ATPases
W	Competes with Mo in anaerobic respiratory enzymes.
Zn	Reactions with reduced thiols

<sup>a</sup> Historically used MBAs that due to high toxicity are less used

elements has shown a good correlation of toxicity with its standard redox potential or the solubility product of the corresponding metal-sulfide complex (Workentine et al. 2008). Other parameters such as electronegativity, Pearsons softness index, electron density and covalent index were found particularly relevant for those elements with d-electron shells. Correlations were different for biofilms compared to planktonic cells suggesting biochemistry is different in the two growth states. Further analysis suggests toxicity generally follows Hard-Soft Acid-Base theory (Lemire et al. 2013). Generally, cell toxicity and resistance of a bacterium to MBAs falls into a fixed set of biochemical process categories.

The toxicity of various metal ions range from micromolar to tens of mM for their MICs. Roughly the order of most to least toxic metal(loid) ions when assessed towards the model organism *Escherichia coli* is:  $\text{TeO}_3^{2-} > \text{Hg}^{2+} > \text{Ag}^+, \text{Au}^{3+} > \text{CrO}_4^{2-}, \text{Pd}^{2+}, \text{Pt}^{4+}, \text{Cd}^{2+} > \text{Co}^{2+}, \text{Ni}^{2+}, \text{Cu}^{2+}, \text{Zn}^{2+} > \text{Al}^{3+}$ , various lanthanides  $> \text{Pb}^{2+}, \text{Sb}^{3+}, \text{Ga}^{3+}, \text{Cr}^{3+}, \text{V}^{3+}, \text{Ti}^{3+} > \text{SeO}_3^{2-}$  (Nies 1999). The toxicity mechanisms are summarized in Table 4.2 for each of the metals, and include: interacting with the cell membrane affecting lipid properties (Sule et al. 2020); competing with essential metal transporters and ion channels; replacing catalytic metals in enzymes; replacing redox active metals in enzymes and electron transfer systems, and catalysing Fenton reactions producing reactive oxygen species (ROS) (Lemire et al. 2013).

A cautionary comment regarding ROS production is important. Essentially all antimicrobial challenges lead to ROS production (Monych et al. 2019). This results in part from a discontinuity of the electron transfer chain such that transfer of electrons between electron carrying components (iron sulfur centers, cytochromes, quinones) leads to reactions with water, oxygen, nitrates and sulfates to give reactive oxygen, nitrogen and sulfur compounds (RONS). In the case of MBA's many studies report ROS production and attribute it to the metal itself, which is often incorrect if the metal is not redox active, for example Ag. Ag exposure leads to ROS because it disrupts Fe-S clusters, releasing the Fe to carry out the Fenton reaction for exposure (Sect. 4.3.2). A comparative study of metals ability to be thiol active or ROS producers nicely showed that not all metals produced ROS which was assumed in the literature at the time (Harrison et al. 2009). That study also showed not all metals induced antioxidant genes.

A significant difference of metal ions as antimicrobials compared to organic antibiotics is that the modes of action by metal ions is more pleiotropic. Antibiotics tend to affect very specific enzymes involved in the central dogma of biology—replication, transcription, translation—or in central metabolism. Metals ions tend to interact with multiple enzymes and biological processes. The mechanisms described in Table 4.2 are quite general. Below provides more detail for each of the primary metal(oids) used or with potential for use.

### **4.3.1 Noble Metals: Silver and Gold**

The metals Ag and Au are very effective MBAs. Despite silver being perhaps the most popular and researched MBA (Barillo and Marx 2014), its precise toxicity mechanism(s) are less documented than those of copper. Speciation of Ag has been suggested to be of substantial influence on toxicity (Lemire et al. 2015). It is often observed that like Cu, Ag exposure induces an increase of intracellular ROS by means of iron release after interaction with cysteine residues of [Fe-S] clusters. This will cause the decomposition of the electron transfer chain as well as interfering with a cell's antioxidant molecules such as the oxidation of glutathione (Xu and Imlay 2012). Interactions with membrane-bound proteins involved in the electron transport chain leads to uncoupling the proton motive force which can also lead to increased membrane permeability (Gugala and Turner 2018). Silver causes a loss of lipopolysaccharides (LPS) in bacteria, although the exact process behind this effect remains unclear (Jung et al. 2008; Li et al. 2016). Certainly, the cell wall barrier becomes compromised, and one observes in electron micrographs deformed cells and membrane blebbing. Additionally, even though DNA may be another cell target for metals, genotoxicity hasn't been confirmed for Ag (Asakura et al. 2009). A recent genomics study confirmed that silver's intracellular toxic activity extends to other cellular processes, encompassing genes involved in cell wall maintenance, quinone metabolism and sulfur assimilation (Gugala et al. 2018).

Gold ( $\text{Au}^{1+}$ ), just like silver ( $\text{Ag}^{1+}$ ), is considered a soft acid according to Pearson's acid base theory (Pearson 1963). An oxidative imbalance is observed with thiol oxidation and increased superoxide concentration inducing dismutases and catalases (Muñoz-Villagrán et al. 2020). Thus, a toxicity path of destruction of [Fe-S] centres leading to ROS and depletion of antioxidant reserves is assumed; but there is a lack of specific studies that confirms these mechanisms. However, its antimicrobial effect is not in doubt, as it has delivered positive results inhibiting planktonic and biofilm growth on different types of bacteria (Vaidya et al. 2017).

Gold nanoparticles (NPs) majorly depend on direct adherence onto the bacterial surface to cause cytotoxicity, resulting in alterations of membrane potential. Additionally, inhibition of ATP synthesis and inhibition of tRNA binding in ribosomes have also been proposed (Abdel-Kareem and Zohri 2018). Silver NPs are thought to bind to the surface of the bacteria as well. The change in physicochemical environment on the cell surface is thought to decompose the NP and oxidize the metal atoms thus releasing a localized dose of  $\text{Ag}^{1+}$  ions to the cell (Dakal et al. 2016).

### 4.3.2 Copper

Cu is a biologically essential element as it serves as a cofactor in major oxidation/reduction enzymes, such as cytochrome c oxidase and NADH dehydrogenase (Gugala and Turner 2018). It can switch from the less toxic form  $\text{Cu}^{2+}$  to  $\text{Cu}^{1+}$  and vice versa under cellular redox potentials (Karlin 1993). Copper, as a soft acid, binds readily to many biochemical functional groups and can out compete other metal ions in protein binding sites.

The damage caused by copper has been usually attributed to the appearance of ROS through Fenton reactions from copper competing out and releasing iron from [Fe-S] centres; in addition, Cu can catalyze Fenton and Haber-Weiss reactions by itself (Solioz et al. 2010; Valko et al. 2005). The -SH group of cysteine residues within proteins are a target for copper binding, but copper also binds to the nitrogen of histidine, which can lead to protein damage and dysfunction (Dupont et al. 2011; Xu and Imlay 2012). A study in *Rubrivivax gelatinosus* also confirmed that Cu interferes with the electron transport chain (Durand et al. 2015). Works that demonstrate an increase of the hydroxyl radical within the periplasm of *E. coli* and an increase in gene regulation of proteins involved in ROS stress further reinforce this (Macomber et al. 2007; Teitzel et al. 2006). However, recognizing copper's superior binding affinity and promiscuity to sites, there must be a presumption that it has multiple targets within the cell, even perhaps the cell membrane and other metal transport activities. Copper (Cu NPs) and copper oxide ( $\text{CuO}$  and  $\text{CuO}_2$  NPs) nanoparticles are suggested to take an active role as electron acceptors as they aggregate along the bacterial membrane, contributing to its degradation. Release of  $\text{Cu}^{2+}$  ions and excited electron-holes pairs in  $\text{CuO}$  NPs due to light irradiation are also believed to be toxicity sources (Sánchez-López et al. 2020).



### 4.3.3 Zinc

Zinc is an essential metal ion that plays an active role as an effective catalytic centre in bond breaking and formation reactions (Król et al. 2017).  $Zn^{2+}$  is the only chemical species present at physiological reduction potentials and has the ability to perform catalysis because of its Lewis acid properties (Wu and Wu 1987). According to the Hard-Soft Acid-Base theory, zinc falls in the borderline acids category displaying neither a pure hard nor soft behavior. This allows it to react with both hard and soft bases; if present in an excess concentration, it may displace other metals from their original arrangements (Lemire et al. 2013).

When it comes to antimicrobial activity, Zn is more of a bacteriostatic agent rather than a bactericide. Phan et al. (2004) demonstrate some of the (reversible) effects of zinc against oral *Streptococci* variants, including inhibition of acid production, F-Type Adenosine Triphosphate Synthases and several glycolytic enzymes. Harrison et al. (2009) showed the oxidation of cellular thiols upon  $Zn^{2+}$  exposure. Zinc oxide nanoparticles (ZnO NPs) have been popularly trending during the past decade because of their bactericidal activity (Sánchez-López et al. 2020). Zinc NPs aggregation blockades  $K^{1+}$  ion channels in the bacterial membrane, changing the membrane potential and overall improving cell permeability; this allows the entrance of destabilizing agents, one of them being freshly released  $Zn^{2+}$  ions from the NPs themselves (Happy et al. 2019).

### 4.3.4 Gallium

Due to its physicochemical similarities to iron, gallium-based compounds have promise as a possible antimicrobial agent. Its mechanism of action relies on the ability of  $Ga^{3+}$  to act as an  $Fe^{3+}$  mimetic, which alters bacterial growth by disrupting iron homeostasis: Ga substitution for Fe changes the ability for physiological redox chemistry in numerous metabolic and electron transfer pathways. This is because  $Ga^{3+}$  cannot be reduced under physiological conditions (Chitambar 2016; Vinuesa and McConnell 2021). Genomics research confirmed the complex relationship between Fe and Ga metabolism; it also revealed that Ga toxicity is enhanced by proteins involved in cellular processes such as response to oxidative stress, DNA or [Fe-S] cluster repair and nucleotide biosynthesis (Gugala et al. 2019).

Multiple types of Ga compounds have been explored to test their antimicrobial potential. Examples include: gallium nitrate ( $Ga(NO_3)_3$ ) (Runci et al. 2016), gallium-protoporphyrin IX (GaPPIX) (Hijazi et al. 2017), gallium maltolate (GaM) (Thompson et al. 2015) and gallium citrate (GaCi) (Hijazi et al. 2018) with some of these showing exciting results against different antibiotic resistant nosocomial pathogens under in vitro conditions (Choi et al. 2019).

### 4.3.5 Selenium & Tellurium

Selenium can exist in multiple valence states: elemental selenium ( $\text{Se}^0$ ), selenide ( $\text{Se}^{2-}$ ), selenite ( $\text{Se}^{4+}$ ) and selenate ( $\text{Se}^{6+}$ ) (Barceloux 1999). Its cytotoxicity will depend strongly on the chemical speciation, with the selenite ( $\text{SeO}_3^{2-}$ ) and selenate ( $\text{SeO}_4^{2-}$ ) oxyanions being two of the most prevalent forms in nature (Wu 2004). Selenium is an essential micronutrient for many organisms in the form of selenocysteine, which is considered the 21st amino acid providing different reactivity than the thiol group. Thus, we see many selenoproteins, like glutathione peroxidases (GPx) and thioredoxin reductase (TrxR), which are heavily involved in antioxidant processes in both eukaryotes and various microorganisms (Filipović et al. 2021).

Selenite is the most toxic form and it has the ability to oxidize reactive thiol groups in the cells, with antioxidant molecules like mycothiol, bacillithiol, and glutathione found to be a primary target. While selenite can oxidize these and other thiol biochemicals, they are readily repaired by glutathione reductases and NAD(P)H, thus selenite is mostly bacteriostatic rather than bactericidal and requires millimolar concentrations to be effective. Because of this, selenium wasn't considered as a competitive alternative in the antimicrobial field when compared to other more effective metals. It was only until the past decade that the rise of nanoscience brought to light that elemental selenium nanoparticles (Se NPs) could significantly inhibit *Staphylococcus aureus* growth (Webster and Tran 2011). This discovery has sparked a surge in interest on the antimicrobial potential that this metal could have. Recent developments in the field include the production and testing of Se NPs by traditional chemical methods (Filipović et al. 2021), as well as microbial challenges using biogenically produced Se NPs (Piacenza et al. 2017).

Tellurium has not been defined as an essential element although it has similar oxyanion forms as selenium. In fact, the oxyanion of tellurium (Te), tellurite  $\text{TeO}_3^{2-}$  is overall the most toxic metal(loid) to most Gram-negative bacteria (Taylor 1999). It has been used in clinical work to identify pathogenic *E. coli* strains, as the Te resistance determinant *ter* is found on the pathogenicity island (Taylor et al. 2002). The biochemistry of the toxicity of tellurite has been recently reviewed (Presentato et al. 2019). Briefly, similar to selenium oxyanions, tellurium oxyanions (primary work done on  $\text{TeO}_3^{2-}$ ) react with cell thiols. However, they are less likely to be reduced again and recovered making tellurite quite bactericidal (Turner et al. 1999). Subsequent effects include decomposition of [Fe-S] centers and subsequent ROS levels increase (in some but not all bacteria), plus carbonylation and lipid peroxidation levels increase. Additionally, tellurite is able to pull electrons away from cytochromes, the disulfide bond isomerase systems of DsbAB, and from various complex iron-sulfur molybdoenzymes such as nitrate reductase. This electron transport chain damage leads to decreased ATP levels (Lohmeier-Vogel et al. 2004).

Although, both selenium and tellurium oxyanions are quite toxic to bacteria, it is remarkable that in various extreme environments, bacteria have evolved to respire using these anions as terminal electron acceptors in the same way other bacteria use

nitrate or sulfate (Maltman and Yurkov 2018). Here and in sensitive bacteria, the primary general resistance response is thiol mediated reduction to  $\text{Se}^0$  or  $\text{Te}^0$  which precipitates out as nanomaterial, crystals or larger atom aggregates (Presentato et al. 2019).

### 4.3.6 Mechanisms of Other Less Studied Metals

#### 4.3.6.1 Aluminium

Aluminium can mimic essential metals such as calcium, magnesium and iron (Lemire et al. 2013) and has a binding preference to phosphates and carboxylate groups. Substitution of Fe is of special interest, as this produces an ROS by means of Fenton chemistry (Exley 2004; Caillet et al. 2007). A perturbed iron homeostasis may affect essential processes like the tricarboxylic acid cycle and electron transport chain (Chenier et al. 2008; Heidari et al. 2009). A study from Booth et al. (2013) identified the most toxic speciation state to *Pseudomonas fluorescens* is  $\text{Al}_3(\text{OH})_4^{5+}$ .

#### 4.3.6.2 Bismuth

Bismuth, in its  $\text{Bi}^{3+}$  form, is considered a borderline acid (Lemire et al. 2013). Its mechanism of action is the replacement of Zn in enzymes, particularly metallo-beta-lactamases, thus leading to cell wall disruption and a significantly weaker response to carbapenem antibiotics (Wang et al. 2018).

#### 4.3.6.3 Cobalt

Cobalt is an important metal cofactor.  $\text{Co}^{3+}$  is a hard acid and  $\text{Co}^{2+}$  behaves like a borderline acid, according to Pearson's (1963) acid base theory. Overall, it can replace iron, affecting [Fe-S] centres, sulfur assimilation, and reduction of free thiol pool (Majtan et al. 2011). Both redox states have been explored as part of complexes that could be applied for antibacterial and antiviral purposes (Chang et al. 2010), although their exact mechanisms of action within the cell are not fully clear. An inkling under very specific conditions is provided by a couple of studies that demonstrate the stability of  $\text{Co}^{3+}$ -histidine complexes (Takeuchi et al. 1999; Schwartz et al. 2001). Another feature is the catalyzation of Fenton reactions by itself (Valko et al. 2005). Some cobalt ions impact bacterial membrane melting temperature and lateral mobility of lipids (Kerek et al. 2017). Cobalt has become popular with some of the novel antimicrobial approaches, with recent studies exploring multiple types of cobalt nanoparticles (Anwar et al. 2019; Moradpoor et al. 2019; Gheidari et al. 2020) and metal-organic frameworks (Aguado et al.

2014), with the steady release of ions serving as the principal metal-related toxicity mechanism of the latter (Yang and Yang 2020).

#### 4.3.6.4 Titanium

Titanium has been demonstrated to fend off planktonic and biofilm growth when tested against *E. coli*, *S. aureus* and *Pseudomonas aeruginosa* (Gugala et al. 2017), but the precise toxicity mechanisms for this metal remain unclear. Titanium dioxide nanoparticles (TiO<sub>2</sub>-NPs) are also another alternative. Their antimicrobial action hails from their UV radiation-dependent nature, as they can produce ROS that affect all types of cellular structures (Reddy et al. 2007; Jiang et al. 2010).

### 4.3.7 Mechanisms of Toxic Heavy Metals

The term ‘heavy metals’ is a chemically inaccurate term and was coined by the toxicology field to describe a group of metals on the periodic table with higher molecular weights that were found to be toxic to eukaryotes (Järup 2003). In this context this group includes the elements: arsenic (As), mercury (Hg), cadmium (Cd), lead (Pb) and chromium (Cr).

#### 4.3.7.1 Arsenic

Arsenic toxicity depends to a large degree on its chemical species. Arsenate (As<sup>5+</sup>) seems to be treated in a similar way as phosphate, given that it makes its way into cells through phosphate uptake systems and obstructs metabolic pathways involving phosphate ions. At the same time, arsenite (As<sup>3+</sup>) may bind to thiol groups and inactivate enzymes that carry these functional groups (Valko et al. 2005).

#### 4.3.7.2 Cadmium and Lead

Cadmium and Lead tend to be toxic via competing out essential metals like Zn and Ni (Jaishankar et al. 2014). Cadmium additionally shows an affinity to react with functionally important thiol groups which are present in glutathione, thioredoxin, glutaredoxin and related enzymes (Xu and Imlay 2012). Cadmium ions influence cell membrane melting temperature and lipid mobility (Kerek et al. 2017). Meanwhile, Pb is also known for causing surges in intracellular ROS levels and antioxidant depletion (Jaishankar et al. 2014). Both Cd and Pb will bind to negative charged lipids and affect membrane fluidity.

### 4.3.7.3 Chromium

Chromate ( $\text{Cr}^{6+}$ ) is in the hard acids category (Pearson 1963). Like copper and cobalt, it can also catalyze Fenton reactions by itself (Valko et al. 2005).  $\text{Cr}^{6+}$  ions have been reported for their mutagenic ability (Arlauskas et al. 1985). Chromate will inhibit sulfate transport and catalysis, and causes oxidative damage to various biomolecules particularly proteins (Ramírez-Díaz et al. 2008).

### 4.3.7.4 Mercury

Mercury works in a similar way to Ag, in the sense that thiol and imine nitrogen groups will be involved in coordination. The bacteriostatic effect of mercury can be attributed to interaction and inactivation of enzymes due to this ligation binding, like the case of dehydratases (Xu and Imlay 2012). Moreover, organic mercury compounds have an enhanced lipid solubility and can pass through membranes quite rapidly (Clarkson and Magos 2007). These mercurial compounds tend to bind to DNA, causing genotoxicity.

## 4.4 Applications

Here we will briefly cover some of the modern day uses of metal(loid)s as antimicrobials in several industries to highlight their widespread use. As pointed out in the introduction, we are in the AMR era and the need to control microbial growth is key to sustainability in health, agriculture, and economy. The economic cost of microbial biofouling in distribution infrastructure systems of wastewater, drinking water, cooling and heating, and as well in petroleum energy systems, is in the 10's of billions Euros worldwide. Marine fouling alone in the USA is ~6 billion US dollars annually which originates from microbes forming a biofilm on the surface that attracts larger lifeforms to feed on them (Yebra et al. 2004). Thus there is a huge demand for novel biocides to control biofilms. There are many examples of the use of MBAs in this regard, here we highlight several present-day examples, but in no way is this a comprehensive listing.

### 4.4.1 Medical Applications

A recent trend in the past decades has been the rise in the use of metals as antimicrobials in the medical field. There is an increasing number and wide variety of applications, and certainly silver and copper have enjoyed the majority of the spotlight. Beyond the text here common applications are mentioned in Table 4.3.

**Table 4.3** Examples of MBAs applied in the medical field

Metal	Medical applications
Silver (Ag)	<p>Silver sulfadiazine, silver-chlorhexidine silver nitrate and Ag-NPs as a topical antimicrobial for burn infections.</p> <p>Implants composed of Ag-doped hydroxyapatite.</p> <p>Used as an antimicrobial in an abundance of wound dressing variations, including hydrogels, polymers and biocomposites.</p> <p>Impregnation/coatings on textile fabrics such as nylon, polyester and cotton.</p> <p>Coatings on medical indwelling devices such as endotracheal tubes and catheters.</p> <p>Ag NPs in combination therapy with beta-lactam antibiotics.</p> <p>Dental plaque prevention by silver nano-coating on dentine.</p> <p>Silver-embedded glass for wall covering in health centres.</p> <p>Ag-nodes in metal organic frameworks that act as carriers and synergistic antimicrobial compounds.</p>
Copper (Cu)	<p>Copper and copper-based alloys as coatings for high touch surfaces based on contact-killing.</p> <p>Copper oxide-containing respiratory face masks with antiviral protection.</p> <p>Adsorption in fibers, latex and polyester for its biocide properties.</p> <p>Applied as an antibacterial in bioactive wound healing dressings.</p> <p>Impregnation in clothing to improve wound healing.</p> <p>Formulations to combat hospital-acquired infections (HAI)-causing pathogens.</p> <p>Mg-Cu alloy implants for treatment of osteomyelitis.</p> <p>Cu involved as a synergistic antimicrobial in metal organic frameworks.</p>
Zinc (Zn)	<p>Everyday dental hygiene products such as mouth rinses and toothpaste.</p> <p>Explored for tandem antimicrobial applications with silver nitrate.</p> <p>Zinc oxide as a sunscreen and is added to ointments for infection control of minor cuts.</p> <p>Dandruff-treatment shampoos' usage of zinc pyrithione.</p> <p>Antimicrobial Zn-chitosan complexes.</p> <p>Zn as a synergistic antimicrobial agent in metal organic frameworks.</p>
Gold (Au)	<p>Gold teeth are effective to prevent plaque build up and are increasingly used in the form of caps to generally control gingivitis.</p> <p>Burn wound dressings—but expensive.</p> <p>Dental caries treatment with Au NPs.</p> <p>Drug delivery nanostructures.</p>
Others	<p>Iron-chelating agents &amp; gallium in combination therapy, with and without antibiotics.</p> <p>Gallium compounds as potential antimicrobials in burn wound dressings.</p> <p>Antimicrobial gallium-doped phosphate-based glasses.</p> <p>Bismuth complexes as an enhancer of antibiotics in combination therapies against pathogenic bacteria.</p> <p>Titanium implants and endotracheal tubes coated with TiO<sub>2</sub>.</p> <p>TiO<sub>2</sub> NPs used as antimicrobials in skin-care products.</p> <p>Ethylmercury in vaccines and cosmetics as a preservative.</p>

One of the main applications is as protective coatings for medical devices to combat traditional and particularly drug-resistant pathogens, with the latter becoming an increasingly dangerous source of nosocomial infections.

Silver coatings have been demonstrated to be successful in applications as diverse as urinary catheters and wound dressings while displaying limited cytotoxicity to

human cells and tissues (Boonkaew et al. 2014; Saint et al. 1998; Rupp et al. 2004; Ewald et al. 2006). Copper usages for high touch surfaces in hospitals have been examined for their potential in decreasing the viability of pathogenic microorganisms (Curtis 2008). Particularly of concern are methicillin-resistant *S. aureus* (MRSA), vancomycin-resistant *Enterococci* (VRE), and spores of *Clostridioides difficile*, against which copper surfaces have shown control (Curtis 2008). We are seeing Cu emerging as a competitive alternative over antibiotics, antiseptics and silver, in the light of positive results against several disease causing organisms such as *Listeria monocytogenes*, *Escherichia coli* (including a verocytotoxigenic *E. coli*), *Mycobacterium tuberculosis*, *Salmonella enterica*, *Campylobacter jejuni*, VRE, MRSA, *Bacillus cereus*, and *Deinococcus radiodurans* (Wilks et al. 2005; Wilks et al. 2006; Mehtar et al. 2008; Faúndez et al. 2004; Warnes and Keevil 2011; Noyce et al. 2006; Santo et al. 2011). Other medical applications of copper include its use in face masks and other materials (like fibers, latex and polyester) as a biocide to control pathogen spread (Borkow et al. 2010; Borkow and Gabbay 2004). Copper, like Ag, is also found impregnated in clothing or bandages to improve the healing of minor wounds in diabetic patients (Borkow et al. 2009).

Zinc is considered as one of the safest metals for human consumption by the FDA, and as such, it is being used to replace Cu and Ag in applications where their effective concentration has started to reach cytotoxic levels. Copper and Ag should be avoided for ingestion. Thus, Zn is found in such products as mouth rinses and toothpaste to control dental plaque and reduce halitosis (Lynch 2011).

Various groups are exploring delivering metals as organo-chelated complexes. The chelator may be a key metabolite to facilitate uptake of the metal into the bacteria (an example being citrate chelate of Zn). Siderophores also fall into this category, with the primary example being the Ga loaded siderophore bringing in Ga rather than Fe as trojan horse antimicrobial (Kircheva and Dudev 2020). Another approach is the use of an organic compound acting as an adjuvant facilitating permeation into the cell, with the organic compound alone having no biological relevance. Finally, the organic may be an organic antibiotic or antiseptic that provides synergistic biocidal activity with the metals. Time will tell if organo metal chelates are superior to metal nanomaterials or metal salts in different applications.

A timely observation on the subject would be to indicate that metal(loid) based nano-antimicrobials are gaining strength in this field, due to their ability to deliver metal loads. Metal nanomaterials are antibacterial, antifungal and may have antiviral properties valuable to combat pathogen-related diseases (Sánchez-López et al. 2020). Some of the most relevant metals being currently used in nanoform are silver, titanium, zinc, nickel, copper, gold, palladium, selenium and iron (Makvandi et al. 2020).

#### 4.4.2 *Agricultural Applications*

Copper salts are the most used MBA in agriculture and used equally in both advanced and developing nations. Usage of the Bordeaux mixture is very well known in vineyards, where it is highly effective as a fungicide (Lamichhane et al. 2018). Crops may also benefit from other fungicides based on copper in the forms of hydroxide, oxychloride, oxide and octanoate (Coelho et al. 2020). A recent study confirmed the prevalence of copper usage in crops like hops, grapes, potatoes, apples, squash, and pears; whilst also highlighting the significantly higher use of Cu in organic farming in relation to conventional farming (Kuhne et al. 2017). Plant diseases controlled by copper include grape downy mildew, caused by the *Plasmopara viticola*; apple scab, caused by the *Venturia inaequalis*; and potato late blight, caused by the *Phytophthora infestans* (Andrivon et al. 2018). The nanomaterials field has made advancements in using the antifungal and antibacterial activity of certain metal NPs such as Ag NPs, Cu NPs, Ni NPs and Zn NPs, among others.

Zinc and copper are also used directly in animal husbandry. Hoof rot is caused by the synergistic effect of multiple bacteria, and it affects sheep and cattle. Copper sulfate was found to be one of the best solutions to this problem (Van Metre 2017). Copper sulfate is an effective bactericidal agent but it can stain the wool and, if applied incorrectly, can be a source of acute poisoning (Ortolani et al. 2004), so the less-toxic zinc sulfate is now preferred (Kimberling and Ellis 1990). Footbaths are the default treatment, but topical medications and oral therapy (for ZnSO<sub>4</sub>) are other alternatives.

#### 4.4.3 *Other Industries*

In order to get away from issues of using As in wood preservatives, we see Cu being actively explored in a number of different formulations with organic preservatives. Some examples include acid copper chromate mixture, alkaline copper mix with quaternary cation antiseptics, Cu naphthenate to name a few (EPA 2021).

The cosmetics industry requires preservation compounds to guarantee a safe usage and a prolonged shelf-life. Zinc pyrithione is crucial for many varieties of dandruff-treating shampoos (Doose et al. 2004). Silver chloride and mercury in the form of ethylmercury (or other organomercurials) is used in a wide range of present-day cosmetics including mascara and moisturizers, ear, eye, and nose drops, contact lens solutions, a variety of topical medications and in most influenza and tetanus vaccines (Halla et al. 2018; Magos 2001).

Metal based antimicrobials such as copper can also be added to paints to prevent fouling (Lagerström et al. 2020), which expands the working life of salmon cages in aquaculture (Braithwaite et al. 2006). However, there are concerns of such practices



that will leach the metals into marine and aquatic environments and affect other organisms.

Water treatment applications can also be attained with metals. Drinking water purification and wastewater handling are seeing the application of silver (and or copper) ionizers used as water sterilization agents (Moustafa 2017). Another promising application is the deployment of a TiO<sub>2</sub> nanocomposite for the breakdown of organic contaminants such as methylene blue dye (Rahimdokht et al. 2019).

Food packaging is an area that is evolving as new technology arises, with the aim of improved food quality and safety. Active packaging involves the steady release of substances into the packaged food from its surroundings (Arora and Padua 2010). Silver salts-agar composites have been explored and suggested for these purposes (Rhim et al. 2013). A plethora of metal nanoparticles have been researched during the past decade for this application based on (see below) their antimicrobial activity including copper, silver, zinc and titanium (Silvestre et al. 2011).

#### ***4.4.4 Metals in Antimicrobial Nanomaterials***

An intriguing alternative to the growing resistance to traditional antibiotics through the use of metal(loid)s, is the use of metal-based nanomaterials (M-NMs). At a fundamental level, nanomaterials are defined as particles within the size range of 1–100 nm; having an external dimension at the nanoscale range ( $10^{-9}$  m), which bestows them with unique and special mechanical, electromagnetic and chemical properties. It is these very features what differentiate them from the same components that have bigger size ranges or the metal salts (Sánchez-López et al. 2020). The most influential factors that affect the antibacterial mechanisms of M-NMs include size, surface charge, surface morphology and crystalline structure. These define how M-NMs interact with the cell wall of bacteria and how toxic they will ultimately be (Wang et al. 2017). Although there are several structures that can be produced as a NM including rods, wires, sheets, cubes, etc., the sphere tends to be favored as an antimicrobial and often referred to as a nanoparticle (NP). A key feature of nanomaterial is the material of the coating of the metal core which can strongly influence their antimicrobial properties as seen for example with Se-NPs (Piacenza et al. 2017).

Both Gram-positive and Gram-negative bacteria have negatively charged regions on their cell walls: in the former's case, teichoic acids—which are abundant in phosphate groups—extend from within the thick peptidoglycan cell wall to their surface, while partially phosphorylated lipopolysaccharides (LPS) bring that property to the latter (Lesniak et al. 2013). Given this feature, positive charged nanoparticles usually have a higher toxicity level than negative charged ones or even neutral charged NPs (Silva et al. 2014; Abbaszadegan et al. 2015), making surface charge a key element when comparing the efficiency between different types of NPs. Nonetheless, Gram-negative bacteria usually pose a greater challenge because of the complex barrier formed of secreted LPS, while Gram-positive

bacteria allow an easier entrance pathway by means of stronger negative charges, their possession of only a thin peptidoglycan layer and an increased number of pores (Sarwar et al. 2015).

Right now, some of the metal NPs most widely used as antimicrobials are silver, gold, zinc oxide, copper, iron oxide and titanium dioxide, with selenium, mercury and zirconium used to a lesser degree (Iravani et al. 2014; Kandi and Kandi 2015; Piacenza et al. 2017; Bottagisio et al. 2019). Some examples include Ag-NPs are widely used as coatings for medical devices, bandages, fabrics and clothing (Zhang et al. 2016); Cu NPs used as a coating for surfaces (Lewis Oscar et al. 2015); ZnO and TiO<sub>2</sub> NPs can be photo-activated and have shown effectiveness against *Xanthomonas perforans*, which causes spot disease in tomato plants (Paret et al. 2013).

#### 4.4.5 *Metal Organic Frameworks & Metal-Biocide Cocrystals*

A novel antimicrobial approach that has surfaced over the past decade is the use of metal-organic frameworks (MOFs). These are hybrid, low-density compounds that combine metal nodes (ions or clusters) and organic ligands, together forming versatile, low-density structures that can be customized to fit multiple applications (Furukawa et al. 2013). One highlight is the possibility to combine bactericidal metal ions with other organic or natural antimicrobials. Tuning the MOF structure can define the rate at which they decompose to release the metal ions and organic. This can be controlled under certain stimulus conditions, such as lowering pH and laser irradiation (Lin et al. 2017; Nasrabadi et al. 2019; Song et al. 2018; Zhang et al. 2019; Qiu et al. 2019; Huang et al. 2020). There are many options to choose their components, manipulate their large surface areas and tune the pore sizes. MOFs are appealing as they tend to have low cytotoxicity and excellent biodegradability, which has extended their applications to medicine and biology (Horcajada et al. 2012; Yang and Yang 2020). Silver, copper, zinc and cobalt ions constitute some of the most relevant metals being researched for MOFs (Li et al. 2021).

Metal-biocide cocrystals aim to apply a similar principle. Cocrystallization, which is an application of crystal engineering principles (Almarsson and Zaworotko 2004), is under exploration in the pharmaceutical field as it allows for association of active ingredients and co-formers, which just like in MOFs, may also be an active component. These combinations may produce new formulations or change the physicochemical and pharmacokinetic properties of already known pharmaceuticals (Schultheiss and Newman 2009). Recent research on the subject has shown that silver, zinc and copper show promise as part of cocrystal complexes when coupled with antiseptic quaternary ammonium compounds like proflavine or methyl viologen (Shemchuk et al. 2020; Fiore et al. 2021).

#### 4.4.6 Solid Metal Surfaces

This chapter was written while the COVID-19 pandemic was underway, which highlighted the need for infection propagation control procedures. Infectious agents possess the ability to propagate through different methods: touch, aerosol, intravenous, etc. Some viruses and bacteria possess the ability to live and survive for extended periods of time under adverse living conditions such as on dry surfaces (Weber et al. 2013). Thus, it is natural to think of commonly used objects or surfaces as hotspots—places that are under constant contact by many different people and represent a point where infectious agents can accumulate and subsequently spread between interactors (Otter and French 2009). Examples of high touch hotspots include digital devices, toilets, sinks, door handles, light switches, public telephones, handrails, and hospital surfaces in general. Healthcare centers are one of the main places of interest for this, as Hospital Acquired Infections (HAI) represent a problem even in developed countries. Every year in the European Union alone, it is estimated that four million patients acquire an HAI (Querido et al. 2019).

In response, techniques to provide surfaces with coatings of compounds that employ mechanisms to kill microorganisms are emerging over repetitive cleaning protocols. For the most part, current research focuses on coatings applied over touch surfaces or development of specific potentially antimicrobial metal alloys. It is also possible to incorporate antimicrobial substances into ingredients during the production phase, with the aim of manufacturing a homogenous mixture of the base material containing the antimicrobial. As an example, an antibacterial glass that incorporates silver ions within their structure claims to eliminate “99% of all bacteria that form on its surface whilst also preventing the spread of fungi” (AGC 2017).

Another approach is by using surfaces entirely composed of intrinsically active antimicrobial metals. Copper based alloys (e.g. Brass) lead the metals, followed by silver and zinc (Villapún et al. 2016). A 3-year study was performed where copper alloy door handles and handrails replaced previously existing surfaces which resulted in a significant decrease in colonization rates of MRSA (Colin et al. 2018). Furthermore, Warnes and Keevil (2016) demonstrated that (1) significant lethality could be achieved within the first 15 min of exposure—crucial for contact hotspots, and (2) possibilities of horizontal gene transfer are reduced as DNA destruction is unleashed by the sudden oxidative environment.

Alternatively, the photocatalytic properties of TiO<sub>2</sub> NPs provide yet another method. As mentioned in the previous section, formation of ROS will ensue after surfaces coated with TiO<sub>2</sub> NPs are irradiated by specific photon energy. Experiments involving thin films with TiO<sub>2</sub> NPs proved to be totally lethal against *E. coli* after a 20-min exposure to UV light, with evidence of peroxidation to membrane lipids confirming that cytotoxic effect (Joost et al. 2015).

#### **4.4.7 Misuse of Metal(loid) Based Antimicrobials**

Above sections of this chapter list uses of MBA's in a variety of applications. However, there are applications that are troubling and that will dilute their efficacy. Silver and copper are perhaps the most abused MBAs. In societies where new technologies are being applied in novel ways to bring new products we see their misuse and exploitation in the constant consumerism goal to make more money. In the case of silver, we see it being used as an antimicrobial to control body odor in athletic clothing, socks, footwear as well as sleepwear. We even see clothing washing machines with silver ionizers used to extend the 'freshness' of clothing and bedding. Personal care products such as deodorants, toothbrushes, and feminine hygiene products also are subject to this misuse of technology. Although these Ag products work as advertised, we should ask the question "Is it worth controlling body odor in this way, while at the same time promoting Ag resistance?". Then you can find yourself with a bad wound and silver bandages will not help in controlling infection.

The use of copper based antimicrobial compounds (CBACs) in agriculture has been a saviour for many farmers for various crops and for animal husbandry, and in many situations become the mainstay. However, there are issues around sustainable use. Effects on soil biota and food quality have led to pressures towards restrictions first put in place by the European Union and slowly beginning to be adapted worldwide. Applied prediction models suggest that Cu and Zn concentrations will reach alarming levels in some soil and water systems within the next 10–50 years (Monteiro et al. 2010). Moreover, agriculture was identified as the main source of Cu- and Zn-contamination of arable soil in England and Wales (Nicholson et al. 2003), so further action is needed to prevent these levels of bioaccumulation in soil and water bodies (Seiler and Berendonk 2012).

### **4.5 Challenges in Using Metals as Antimicrobials**

There are now a remarkable number of MBA products on the market, either as salts, chelate mixtures or nanomaterials. In the case of Ag, there has been tremendous market growth (Sim et al. 2018). This on the surface gives a strong impression of MBA success. However, the growth has not been kept in check by critical thinking policies. For example, there is very little evidence that Ag and other elements *actually* improve wound healing outcomes (Pormohammad et al. 2021). Even with the strong antimicrobial properties of Ag, what is the logic of adding Ag to one's athletic clothing to prevent odor, when continued exposure will lead to Ag resistance (Silver 2003) and thus nullify any practical use in burn wound bandages (Klasen 2000)?

An issue that is just starting to be considered for pharmaceuticals is that their activities do not stop with the human consumer. They find contaminating products

washing down toilets and drains along with disposed human waste and landing up in water treatment plants. In the case of MBAs, it is critical to appreciate that as opposed to organic chemistry-based medicines that may break down, the metal element of MBA's will not be destroyed, although their speciation states will change based on different physicochemical characteristics of the environmental niches. This then gives a high MBA load to treatment plants that can get poisoned and lose processing efficacy. Additionally, the MBAs will wash out to the river, similarly MBA formulations added to crops will also find their way into aquatic systems. Further the metals released into the environment will lead to bioaccumulation into the periphyton and thus the food chain. What are the consequences to the microbes and organisms in ravine and marine periphytons, and movement through the food chain?

It is now recognized that several MBAs can select for multidrug resistance efflux transporters (MDREP) thus presenting antibiotic resistance as collateral damage to their use, an issue first highlighted in 2006 (Baker-Austin et al. 2006). For example,  $\text{Cu}^{2+}$  or  $\text{Zn}^{2+}$  can induce the MDREPs Mdt or Acr (Chen et al. 2015).  $\text{Cu}^{2+}$  and  $\text{Cr}_2\text{O}_7^{2-}$  can regulate the SoxRS system, and  $\text{Cu}^{2+}$  the MarR system, both leading to a variety of MDREPs. For another example, livestock additives containing Zn and Co have led to the induction of MdrL providing Zn, Co and Cr resistance accompanied by resistance to the antibiotics cefoximine, clindamycin, erythromycin and Josamycin in *Listeria monocytogenes* in a food processing plant; for this and other examples see review by Yu et al. (2017). Therefore, MBA use in the agriculture industry which can improve crops and livestock health can have consequences for infection control in the human population with antibiotics. Is this an acceptable cost to have perfect looking fruit and tender meat on the dinner table? Yet, knowing the food may be laced with MDR pathogens (Wales and Davies 2015).

It must be remembered that resistance determinants exist for all metal ions used as antimicrobials and often are carried on mobile genetic elements. Thus, it is clear any misuse or overuse will lead to a proliferation of resistance to these MBA's. Although it was once thought that their incorporation into nanomaterial form will avoid resistance, resistance to metal(loid) nanoparticles already exists (Niño-Martínez et al. 2019).

Regardless of the challenges of use and lack of policies around MBA implementations, MBA's provide an effective alternative in our AMR era.

## References

- Abbaszadegan A, Ghahramani Y, Gholami A, Hemmateenejad B, Dorostkar S, Nabavizadeh M, Sharghi H (2015) The effect of charge at the surface of silver nanoparticles on antimicrobial activity against Gram-positive and Gram-negative bacteria: a preliminary study. *J Nanomater* 2015:720654
- Abdel-Kareem MM, Zohri AA (2018) Extracellular mycosynthesis of gold nanoparticles using *Trichoderma hamatum*: optimization, characterization and antimicrobial activity. *Lett Appl Microbiol* 67:465–475

- AGC (2017) ANTIBACTERIAL GLASS™. AGC Glass Europe. [https://www.agc-yourglass.com/sites/default/files/brochures/original/antibacterial\\_glass\\_2017\\_en.pdf](https://www.agc-yourglass.com/sites/default/files/brochures/original/antibacterial_glass_2017_en.pdf). Accessed 01 June 2021
- Aguado S, Quirós J, Canivet J, Farrusseng D, Boltes K, Rosal R (2014) Antimicrobial activity of cobalt imidazolate metal–organic frameworks. *Chemosphere* 113:188–192
- Alexander JW (2009) History of the medical use of silver. *Surg Infect* 10:289–292
- Almarsson O, Zaworotko MJ (2004) Crystal engineering of the composition of pharmaceutical phases. Do pharmaceutical co-crystals represent a new path to improved medicines? *Chem Commun* 2004:1889–1896
- Aminov RI (2010) A brief history of the antibiotic era: lessons learned and challenges for the future. *Front Microbiol* 1:134
- Andrivo D, Bardin M, Bertrand C, Brun L, Daire X, Fabre F, Gary C, Montarry J, Nicot P, Reignault P, Tamm L, Savini I (2018) Can organic agriculture cope without copper for disease control? Synthesis of the collective scientific assessment report, INRA (France), 64 p. hal-02944872f
- Anwar A, Numan A, Siddiqui R, Khalid M, Khan NA (2019) Cobalt nanoparticles as novel nanotherapeutics against *Acanthamoeba castellanii*. *Parasit Vectors* 12:280
- Ardal C, Findlay D, Savic M, Carmeli Y, Gyssens I, Laxminarayan R, Outtersson K, Rex J (2018) Revitalizing the antibiotic pipeline: stimulating innovation while driving sustainable use and global access. *Drive-Ab Rep.* 2018
- Arlauskas A, Baker RSU, Bonin AM, Tandon RK, Crisp PT, Ellis J (1985) Mutagenicity of metal ions in bacteria. *Environ Res* 36:379–388
- Arora A, Padua GW (2010) Review: nanocomposites in food packaging. *J Food Sci* 75(1):R43–R49
- Asakura K, Satoh H, Chiba M, Okamoto M, Serizawa K, Nakano M, Omae K (2009) Genotoxicity studies of heavy metals: lead bismuth indium silver and antimony. *J Occup Health* 51(6):498–512. <https://doi.org/10.1539/joh.L9080>
- Baker-Austin C, Wright MS, Stepanauskas R, McArthur JV (2006) Co-selection of antibiotic and metal resistance. *Trends Microbiol* 14:176–182
- Barceloux DG (1999) Selenium. *J Toxicol Clin Toxicol* 37(2):145–172
- Barillo DJ, Marx DE (2014) Silver in medicine: a brief history BC 335 to present. *Burns* 40:S3–S8
- Bernardos A, Piacenza E, Sancenon F, Mehrdad H, Maleki A, Turner RJ, Martinez-Manez R (2019) Mesoporous silica-based materials with bactericidal properties. *Small* 15:1900669
- Boonkaew B, Kempf M, Kimble R, Supaphol P, Cuttle L (2014) Antimicrobial efficacy of a novel silver hydrogel dressing compared to two common silver burn wound dressings: Acticoat and PolyMem Silver. *Burns* 40:89–96
- Booth SC, George IF, Zannoni D, Cappelletti M, Duggan GE, Ceri H, Turner RJ (2013) Effect of aluminium and copper on biofilm development of *Pseudomonas pseudoalcaligenes* KF707 and *P. fluorescens* as a function of different media compositions. *Metallomics* 5:723–735
- Borkow G, Gabbay J (2004) Putting copper into action: copper-impregnated products with potent biocidal activities. *FASEB J* 18:1–20
- Borkow G, Gabbay J (2009) Copper, an ancient remedy returning to fight microbial, fungal and viral infections. *Curr Chem Biol* 3:272–278
- Borkow G, Zatcoff RC, Gabbay J (2009) Reducing the risk of skin pathologies in diabetics by using copper impregnated socks. *Med Hypotheses* 73:883–886
- Borkow G, Zhou SS, Page T, Gabbay J (2010) A novel anti-influenza copper oxide containing respiratory face mask. *PLoS One* 5(6):e11295
- Bottagisio M, Lovati AB, Galbusera F, Drago L, Banfi G (2019) A precautionary approach to guide the use of transition metal-based nanotechnology to prevent orthopedic infections. *Materials* 12(2):314
- Braithwaite RA, Carracosa MC, McEvoy LA (2006) Biofouling of salmon cage netting and the efficacy of a typical copper-based antifoulant. *Aquaculture* 262:219–226
- Brives C, Pourraz J (2020) Phage therapy as a potential solution in the fight against AMR: obstacles and possible futures. *Palgrave Commun* 6:100

- Caillet S, Yu H, Lessard S, Lamoureux G, Ajdukovic D, Lacroix M (2007) Fenton reaction applied for screening natural antioxidants. *Food Chem* 100(2):542–552. <https://doi.org/10.1016/j.foodchem.2005.10.009>
- Chang EL, Simmers C, Knight DA (2010) Cobalt complexes as antiviral and antibacterial agents. *Pharmaceuticals (Basel)* 3(6):1711–1728
- Chen S, Li X, Sun G, Zhang Y, Su Y, Ye J (2015) Heavy metal induced antibiotic resistance in bacterium LSJC7. *Int J Mol Sci* 16(10):23390–23404
- Chenier D, Beriault R, Mailloux R, Baquie M, Abramia G, Lemire J, Appanna V (2008) Involvement of fumarase C and NADH oxidase in metabolic adaptation of *Pseudomonas fluorescens* cells evoked by aluminum and gallium toxicity. *Appl Environ Microbiol* 74:3977–3984
- Chitambar CR (2016) Gallium and its competing roles with iron in biological systems. *Biochim Biophys Acta* 1863(8):2044–2053
- Choi SR, Britigan BE, Narayanasamy P (2019) Dual inhibition of *Klebsiella pneumoniae* and *Pseudomonas aeruginosa* iron metabolism using gallium porphyrin and gallium nitrate. *ACS Infect Dis* 5:1559–1569
- Clarkson T, Magos L (2007) The toxicology of mercury and its chemical compounds. *Crit Rev Toxicol* 36:609–662
- Coelho FC, Squitti R, Ventriglia M, Cerchiaro G, Daher JP, Rocha JG, Rongioletti M, Moonen AC (2020) Agricultural use of copper and its link to Alzheimer’s disease. *Biomol Ther* 10(6):897
- Colin M, Klingelschmitt F, Charpentier E, Josse J, Kanagaratnam L, De Champs C, Gangloff SC (2018) Copper alloy touch surfaces in healthcare facilities: an effective solution to prevent bacterial spreading. *Materials* 11(12):2479
- Cowan MM (1999) Plant products as antimicrobial agents. *Clin Microbiol Rev* 12(4):564–582
- Crede CSF (1881) Die verhütung der augenentzündung der neugeborenen. *Arch Gynakol* 17:50–53
- Curtis LT (2008) Prevention of hospital-acquired infections: review of non-pharmacological interventions. *J Hosp Infect* 69:204–219
- Dakal TC, Kumar A, Majumdar RS, Yadav V (2016) Mechanistic basis of antimicrobial actions of silver nanoparticles. *Front Microbiol* 7:1831
- Dixon B (2004) Pushing Bordeaux mixture. *Lancet Infect Dis* 4:594
- Doose CA, Ranke J, Stock F, Bottin-Weber U, Jastorff B (2004) Structure–activity relationships of pyrithiones–IPC-81 toxicity tests with the antifouling biocide zinc pyrithione and structural analogs. *Green Chem* 6:259–266
- Dupont CL, Yang S, Palenik B, Bourne PE (2006) Modern proteomes contain putative imprints of ancient shifts in trace metal geochemistry. *Proc Natl Acad Sci* 103:17822–17827
- Dupont CL, Grass G, Rensing C (2011) Copper toxicity and the origin of bacterial resistance - new insights and applications. *Metallomics* 3:1109–1118
- Durand A, Azzouzi A, Bourbon ML, Steunou AS, Liotenberg S, Maeshima A, Astier C, Argentini M, Saito S, Ouchane S (2015) C-type cytochrome assembly is a key target of copper toxicity within the bacterial periplasm. *MBio* 6:1–10
- EPA (2021) Overview of wood preservative chemicals. United States Environmental Protection Agency. <https://www.epa.gov/ingredients-used-pesticide-products/overview-wood-preservative-chemicals>. Accessed 22 May 2021
- Ewald A, Glückermann SK, Thull R, Gbureck U (2006) Antimicrobial titanium/silver PVD coatings on titanium. *Biomed Eng* 5:22
- Exley C (2004) The pro-oxidant activity of aluminum. *Free Radic Biol Med* 36:380–387
- Faúndez G, Troncoso M, Navarrete P, Figueroa G (2004) Antimicrobial activity of copper surfaces against suspensions of *Salmonella enterica* and *Campylobacter jejuni*. *BMC Microbiol* 4:1–7
- Ferrie JE (2014) Arsenic, antibiotics and interventions. *Int J Epidemiol* 43(4):977–982
- Filipović N, Ušjak D, Milenković MT, Zheng K, Liverani L, Boccaccini AR, Stevanović MM (2021) Comparative study of the antimicrobial activity of selenium nanoparticles with different surface chemistry and structure. *Front Bioeng Biotechnol* 8:624621
- Fiore C, Shemchuk O, Grepioni F, Turner R, Braga D (2021) Proflavine and zinc chloride “team chemistry”: combining antibacterial agents via solid-state interaction. *CrystEngComm* 23:4494

- Fleming A (1929) On antibacterial action of culture of penicillium, with special reference to their use in isolation of *B. influenzae*. Br J Exp Pathol 10:226–236
- Frazer AD, Edin MB (1930) Tellurium in the treatment of syphilis. Lancet 216:133–134
- Furukawa H, Cordova KE, O’Keeffe M, Yaghi OM (2013) The chemistry and applications of metal–organic frameworks. Science 341:1230444
- Gheidari D, Mehrdad M, Maleki S, Hosseini S (2020) Synthesis and potent antimicrobial activity of CoFe<sub>2</sub>O<sub>4</sub> nanoparticles under visible light. Heliyon 6:e05058
- Gould K (2016) Antibiotic: from prehistory to present day. J Antimicrob Chemother 71:572–575
- Gugala N, Turner RJ (2018) The potential of metals in combating bacterial pathogens. In: Rai M, Ingle A, Medici S (eds) Biomedical applications of metals. Springer, Cham, pp 129–150
- Gugala N, Lemire JA, Turner RJ (2017) The efficacy of different anti-microbial metals at preventing the formation of, and eradicating bacterial biofilms of pathogenic indicator strains. J Antibiot 70(6):775–780
- Gugala N, Lemire J, Chatfield-Reed K, Yan Y, Chua G, Turner R (2018) Using a chemical genetic screen to enhance our understanding of the antibacterial properties of silver. Genes 9:344
- Gugala N, Chatfield-Reed K, Turner RJ, Chua G (2019) Using a chemical genetic screen to enhance our understanding of the antimicrobial properties of gallium against *Escherichia coli*. Genes 10: 34
- Halla N, Fernandes I, Heleno S, Costa P, Boucherit-Otmani Z, Boucherit K, Rodrigues A, Ferreira I, Barreiro M (2018) Cosmetics preservation: a review on present strategies. Molecules 23(7): 1571
- Happy A, Soumyaa M, Kumara V, Rajeshkumar S, Sheba DR, Lakshmi T, Nallaswamy VD (2019) Phyto-assisted synthesis of zinc oxide nanoparticles using *Cassia alata* and its antibacterial activity against *Escherichia coli*. Biochem Biophys Rep 17:208–211
- Harrison JJ, Ceri H, Turner RJ (2007) Multimetal resistance and tolerance in microbial biofilms. Nat Rev Microbiol 5(12):928–938
- Harrison JJ, Tremaroli V, Stan MA, Chan CS, Vacchi-Suzzi C, Heyne BJ, Parsek MR, Ceri H, Turner RJ (2009) Chromosomal antioxidant genes have metal ion-specific roles as determinants of bacterial metal tolerance. Environ Microbiol 11(10):2491–2509
- Heidari MM, Houshmand M, Hosseinkhani S, Nafissi S, Khatami M (2009) Complex I and ATP content deficiency in lymphocytes from Friedreich’s ataxia. Can J Neurol Sci 36:26–31
- Hijazi S, Visca P, Frangipani E (2017) Gallium-protoporphyrin IX inhibits *Pseudomonas aeruginosa* growth by targeting cytochromes. Front Cell Infect Microbiol 7:12
- Hijazi S, Visaggio D, Pirollo M, Frangipani E, Bernstein L, Visca P (2018) Antimicrobial activity of gallium compounds on ESKAPE pathogens. Front Cell Infect Microbiol 8:316
- Hobman JL, Crossman LC (2015) Bacterial antimicrobial metal ion resistance. J Med Microbiol 64: 471–497
- Hodges NDC (1889) The value of mercuric chloride as a disinfectant. Science 13:62–64
- Horcajada P, Gref R, Baati T, Allan PK, Maurin G, Couvreur P, Ferey G, Morris RE, Serre C (2012) Metal–organic frameworks in biomedicine. Chem Rev 112:1232–1268
- Huang G, Li Y, Qin Z, Liang Q, Xu C, Lin B (2020) Hybridization of carboxymethyl chitosan with MOFs to construct recyclable, long-acting and intelligent antibacterial agent carrier. Carbohydr Polym 233:115848
- Hylander LD, Meili M (2005) The rise and fall of mercury: converting a resource to refuse after 500 years of mining and pollution. Crit Rev Environ Sci Technol 35:1–36
- Iravani S, Korbekandi H, Vahid MS, Zolfaghari B (2014) Synthesis of silver nanoparticles: chemical, physical and biological methods. Res Pharm Sci 9:385–406
- Jaishankar M, Tseten T, Anbalagan N, Mathew BB, Beeregowda KN (2014) Toxicity, mechanism and health effects of some heavy metals. Interdiscip Toxicol 7(2):60–72
- Järup L (2003) Hazards of heavy metal contamination. Br Med Bull 68(1):167–182
- Jiang X, Yang L, Liu P, Li X, Shen J (2010) The photocatalytic and antibacterial activities of neodymium and iodine doped TiO<sub>2</sub> nanoparticles. Colloids Surf B Biointerfaces 79:69–74



- Joost U, Juganson K, Visnapuu M, Mortimer M, Kahru A, Nömmiste E, Joost U, Kisand V, Ivask A (2015) Photocatalytic antibacterial activity of nano-TiO<sub>2</sub> (anatase)-based thin films: effects on *Escherichia coli* cells and fatty acids. *J Photochem Photobiol B Biol* 142:178–185
- Jung WK, Koo HC, Kim KW, Shin S, Kim SH, Park YH (2008) Antibacterial activity and mechanism of action of the silver ion in *Staphylococcus aureus* and *Escherichia coli*. *Appl Environ Microbiol* 74:2171–2178
- Kamaruzzaman NF, Tan LP, Hamdan RH, Choong SS, Wong WK, Gibson AJ, Chivu A, Pina MF (2019) Antimicrobial polymers: the potential replacement of existing antibiotics? *Int J Mol Sci* 20(11):2747
- Kandi V, Kandi S (2015) Antimicrobial properties of nanomolecules: potential candidates as antibiotics in the era of multi-drug resistance. *Epidemiol Health* 37:e2015020
- Karlin KD (1993) Metalloenzymes, structural motifs, and inorganic models. *Science* 261:701–708
- Kerek E, Hassanin M, Zhang W, Prenner EJ (2017) Preferential binding of inorganic mercury to specific lipid classes and its competition with cadmium. *Biochim Biophys Acta Biomembr* 1859(7):1211–1221
- Khameneh B, Iranshahy M, Soheili V, Fazly Bazzaz BS (2019) Review on plant antimicrobials: a mechanistic viewpoint. *Antimicrob Resist Infect Control* 8:118
- Khan MR, Fromm KM, Rizvi TF, Giese B, Ahmad F, Turner RJ, Füeg M, Marsili E (2020) Metal nanoparticle-microbe interactions: synthesis and antimicrobial effects. *Part Syst Charact* 37(5):1900419
- Kimberling CV, Ellis RP (1990) Advances in the control of foot rot in sheep. *Vet Clin North Am Food Anim Pract* 6(3):671–681
- Kircheva N, Dudev T (2020) Gallium as an antibacterial agent: a DFT/SMD study of the Ga<sup>3+</sup>/Fe<sup>3+</sup> competition for binding bacterial siderophores. *Inorg Chem* 59(9):6242–6254
- Klasen HJ (2000) Historical review of the use of silver in the treatment of burns. I. Early uses. *Burns* 26(2):117–130
- Koski TA, Stuart LS, Ortenzio LF (1966) Comparison of chlorine, bromine, iodine as disinfectants for swimming pool water. *Appl Microbiol* 14(2):276–279
- Król A, Pomastowski P, Rafińska K, Railean-Plugaru V, Buszewski B (2017) Zinc oxide nanoparticles: synthesis, antiseptic activity and toxicity mechanism. *Adv Colloid Interf Sci* 249:37–52
- Kuhne S, Roßberg D, Rohrig P, Mering F, Weihrauch F, Kanthak S, Kienzle J, Patzwahl W, Reiners E, Gitzel J (2017) The use of copper pesticides in Germany and the search for minimization and replacement strategies. *Org Farming* 3:66–75
- Lagerström M, Ytreberg E, Wiklund AE, Granhag L (2020) Antifouling paints leach copper in excess - study of metal release rates and efficacy along a salinity gradient. *Water Res* 186:116383
- Lamichhane JR, Osdaghi E, Behlau F, Köhl J, Jones JB, Aubertot JN (2018) Thirteen decades of antimicrobial copper compounds applied in agriculture. A review. *Agron Sustain Dev* 38:1–18
- Lemire J, Harrison JJ, Turner RJ (2013) Antimicrobial activity of metals: mechanisms, molecular targets and applications. *Nat Rev Microbiol* 11:371–384
- Lemire JA, Kalan L, Bradu A, Turner RJ (2015) Silver oxynitrate, an unexplored silver compound with antimicrobial and antibiofilm activity. *Antimicrob Agents Chemother* 59:4031–4039
- Lesniak A, Salvati A, Santos-Martinez MJ, Radomski MW, Dawson KA, Åberg C (2013) Nanoparticle adhesion to the cell membrane and its effect on nano-particle uptake efficiency. *J Am Chem Soc* 135(4):1438–1444
- Lewis Oscar F, Mubarak Ali D, Nithya C, Priyanka R, Gopinath V, Alharbi NS, Thajuddin N (2015) One pot synthesis and anti-biofilm potential of copper nanoparticles (CuNPs) against clinical strains of *Pseudomonas aeruginosa*. *Biofouling* 31(4):379–391
- Li H, Gao Y, Li C, Ma G, Shang Y, Sun Y (2016) A comparative study of the antibacterial mechanisms of silver ion and silver nanoparticles by Fourier transform infrared spectroscopy. *J Vib Spec* 85:112–121

- Li R, Chen T, Pan X (2021) Metal–organic-framework-based materials for antimicrobial applications. *ACS Nano* 15(3):3808–3848
- Lin S, Liu X, Tan L, Cui Z, Yang X, Yeung KWK, Pan H, Wu S (2017) Porous iron-carboxylate metal–organic framework: a novel bioplatfrom with sustained antibacterial efficacy and nontoxicity. *ACS Appl Mater Interfaces* 9:19248–19257
- Lohmeier-Vogel EM, Ung S, Turner RJ (2004) In vivo <sup>31</sup>P nuclear magnetic resonance investigation of tellurite toxicity in *Escherichia coli*. *Appl Environ Microbiol* 70:7342–7347
- Lynch RJ (2011) Zinc in the mouth its interactions with dental enamel and possible effects on caries; a review of the literature. *Int Dent J* 61:46–54. <https://doi.org/10.1111/j.1875-595X.2011.00049.x>
- Macomber L, Rensing C, Imlay JA (2007) Intracellular copper does not catalyze the formation of oxidative DNA damage in *Escherichia coli*. *J Bacteriol* 189:1616–1626
- Magana M, Pushpanathan M, Santos AL, Leanse L, Fernandez M, Ioannidis A, Giulianotti MA, Apidianakis Y, Bradfute S, Ferguson AL, Cherkasov A, Seleem MN, Pinilla C, de la Fuente-Nunez C, Lazaridis T, Dai T, Houghten RA, Hancock REW, Tegos GP (2020) The value of antimicrobial peptides in the age of resistance. *Lancet Infect Dis* 20(9):e216–e230
- Magos L (2001) Review on the toxicity of ethylmercury including its presence as a preservative in biological and pharmaceutical products. *J Appl Toxicol* 21(1):1–5
- Majtan T, Frerman FE, Kraus JP (2011) Effect of cobalt on *Escherichia coli* metabolism and metalloporphyrin formation. *Biometals* 24(2):335–347
- Makvandi P, Wang CY, Zare EN, Borzacchiello A, Niu L-n, Tay FR (2020) Metal-based nanomaterials in biomedical applications: antimicrobial activity and cytotoxicity aspects. *Adv Funct Mater* 30(22):1910021
- Maltman C, Yurkov V (2018) Bioremediation potential of bacteria able to reduce high levels of selenium and tellurium oxyanions. *Arch Microbiol* 200:1411–1417
- Mehtar S, Wiid I, Todorov SD (2008) The antimicrobial activity of copper and copper alloys against nosocomial pathogens and *Mycobacterium tuberculosis* isolated from healthcare facilities in the Western Cape: an in vitro study. *J Hosp Infect* 68:45–51
- Monteiro SC, Lofts S, Boxall ABA (2010) Pre-assessment of environmental impact of zinc and copper used in animal nutrition. European Food Safety Authority EFSA-Q-2008-04980
- Monych NK, Gugala N, Turner R (2019) Metal-based antimicrobials. In: Domb AJ, Kunduru KR, Farah S (eds) Antimicrobial materials for biomedical applications, vol 5. Royal Society of Chemistry, pp 252–276
- Moradpoor H, Safaei M, Rezaei F, Golshah A, Jamshidy L, Hatam R, Abdullah RS (2019) Optimisation of cobalt oxide nanoparticles synthesis as bactericidal agents. *Open Access Maced J Med Sci* 7(17):2757–2762
- Moustafa MT (2017) Removal of pathogenic bacteria from wastewater using silver nanoparticles synthesized by two fungal species. *Water Sci* 31:164–176
- Muñoz-Villagrán C, Contreras F, Cornejo F, Figueroa M, Valenzuela-Bezanilla D, Luraschi R, Reinoso C, Rivas-Pardo J, Vásquez C, Castro M, Arenas F (2020) Understanding gold toxicity in aerobically-grown *Escherichia coli*. *Biol Res* 53:26
- Nasrabadi M, Ghasemzadeh MA, Monfared MRZ (2019) The preparation and characterization of UiO-66 metal–organic frameworks for the delivery of the drug ciprofloxacin and an evaluation of their antibacterial activities. *New J Chem* 43:16033–16040
- Nicholson FA, Smith SR, Alloway BJ, Carlton-Smith C, Chambers BJ (2003) An inventory of heavy metals inputs to agricultural soils in England and Wales. *Sci Total Environ* 311:205–219
- Nies NH (1999) Microbial heavy-metal resistance. *Appl Microbiol Biotechnol* 51:730–750
- Niño-Martínez N, Salas Orozco MF, Martínez-Castañón GA, Torres Méndez F, Ruiz F (2019) Molecular mechanisms of bacterial resistance to metal and metal oxide nanoparticles. *Int Mol J Sci* 20(11):2808
- Noyce JO, Michels H, Keevil CW (2006) Potential use of copper surfaces to reduce survival of epidemic meticillin-resistant *Staphylococcus aureus* in the healthcare environment. *J Hosp Infect* 63:289–297

- O'Shea JG (1990) "Two minutes with venus, two years with mercury" mercury as an antisiphilitic chemotherapeutic agent. *J R Soc Med* 83:392–395
- Otolani EL, Antonelli AC, de Souza Sarkis JE (2004) Acute sheep poisoning from a copper sulfate footbath. *Vet Hum Toxicol* 46(6):315–318
- Otter JA, French GL (2009) Bacterial contamination on touch surfaces in the public transport system and in public areas of a hospital in London. *Lett Appl Microbiol* 49:803–805
- Paret ML, Vallad GE, Averett DR, Jones JB, Olson SM (2013) Photocatalysis: effect of light-activated nanoscale formulations of TiO<sub>2</sub> on *Xanthomonas perforans* and control of bacterial spot of tomato. *Phytopathology* 103(3):228–236
- Pearson RG (1963) Hard and soft acids and bases. *J Am Chem Soc* 85:3533–3539
- Pereira J (1836) *Materia medica or pharmacology and general therapeutics*. *Lond Med Gaz* 18:305–314
- Phan TN, Buckner T, Sheng J, Baldeck JD, Marquis RE (2004) Physiologic actions of zinc related to inhibition of acid and alkali production by oral *streptococci* in suspensions and biofilms. *Oral Microbiol Immunol* 19(1):31–38
- Piacenza E, Presentato A, Zonaro E, Lemire JA, Demeter M, Vallini G, Turner RJ, Lampis S (2017) Antimicrobial activity of biogenically produced spherical Se-nanomaterials embedded in organic material against *Pseudomonas aeruginosa* and *Staphylococcus aureus* strains on hydroxyapatite-coated surfaces. *Microb Biotechnol* 10(4):804–818
- Pormohammad A, Turner RJ (2020) Silver antibacterial synergism activities with eight other metal (loid)-based antimicrobials against *Escherichia coli*, *Pseudomonas aeruginosa*, and *Staphylococcus aureus*. *Antibiotics* 9:853
- Pormohammad A, Monych NK, Ghosh S, Turner DL, Turner RJ (2021) Nanomaterials in wound healing and infection control. *Antibiotics* 10:473
- Presentato A, Turner RJ, Vasquez CC, Yurkov V, Zannoni D (2019) Tellurite-dependent blackening of bacteria emerges from the dark ages. *Environ Chem* 16(4):266–288
- Qiu H, Pu F, Liu Z, Deng Q, Sun P, Ren J, Qu X (2019) Depriving bacterial adhesion-related molecule to inhibit biofilm formation using CeO<sub>2</sub>-decorated metal–organic frameworks. *Small* 15(36):1902522
- Querido MM, Aguiar L, Neves P, Pereira CC, Teixeira JP (2019) Self-disinfecting surfaces and infection control. *Colloids Surf B: Biointerfaces* 178:8–21. <https://doi.org/10.1016/j.colsurfb.2019.02.00>
- Rahimdokht M, Pajootan E, Ranjbar-Mohammadi M (2019) Titania/gum tragacanth nanohydrogel for methylene blue dye removal from textile wastewater using response surface methodology. *Polym Int* 68(1):134–140
- Ramírez-Díaz MI, Díaz-Pérez C, Vargas E, Riveros-Rosas H, Campos-Ragcia J (2008) Mechanisms of bacterial resistance to chromium compounds. *Biometals* 21:321–332
- Reddy MP, Venugopal A, Subrahmanyam M (2007) Hydroxyapatite-supported Ag-TiO<sub>2</sub> as *Escherichia coli* disinfection photocatalyst. *Water Res* 41:379–386
- Rhim JW, Wang LF, Hong SI (2013) Preparation and characterization of agar/silver nanoparticles composite films with antimicrobial activity. *Food Hydrocoll* 33(2):327–335
- Ros-Vivancos C, González-Hernández M, Navarro-Gracia JF, Sánchez-Payá J, González-Torga A, Portilla-Sogorb J (2018) Evolución del tratamiento de la sífilis a lo largo de la historia (Evolution of treatment of syphilis through history). *Rev Esp Quimioter* 31(6):485–492
- Runci F, Bonchi C, Frangipani E, Visaggio D, Visca P (2016) *Acinetobacter baumannii* biofilm formation in human serum and disruption by gallium. *Antimicrob Agents Chemother* 61(1):e01563–e01516
- Rupp ME, Fitzgerald T, Marion N, Helget V, Puumala S, Anderson JR, Fey PD (2004) Effect of silver-coated urinary catheters: efficacy, cost-effectiveness, and antimicrobial resistance. *Am J Infect Control* 32:445–450
- Russell PE (2005) A century of fungicide evolution. *J Agric Sci* 143:11–25

- Saint S, Elmore JG, Sullivan SD, Emerson SS, Koepsell TD (1998) The efficacy of silver alloy-coated urinary catheters in preventing urinary tract infection: a meta-analysis. *Am J Med* 105: 236–241
- Sánchez-López E, Gomes D, Esteruelas G, Bonilla L, Lopez-Machado AL, Galindo R, Cano A, Espina M, Ettcheto M, Camins A, Silva AM, Durazzo A, Santini A, Garcia ML, Souto EB (2020) Metal-based nanoparticles as antimicrobial agents: an overview. *Nano* 10(2):292
- Santo CE, Lam EW, Elowsky CG, Quaranta D, Domaille DW, Chang CJ, Grass G (2011) Bacterial killing by dry metallic copper surfaces. *Appl Environ Microbiol* 77:794–802
- Sarbu LG, Bahrin LG, Babii C, Stefan M, Birsa ML (2019) Synthetic flavonoids with antimicrobial activity: a review. *J Appl Microbiol* 127(5):1282–1290
- Sarwar A, Katas H, Samsudin SN, Zin NM (2015) Regioselective sequential modification of chitosan via azide-alkyne click reaction: synthesis, characterization, and antimicrobial activity of chitosan derivatives and nanoparticles. *PLoS One* 10(4):e0123084
- Schultheiss N, Newman A (2009) Pharmaceutical cocrystals and their physicochemical properties. *Cryst Growth Des* 9(6):2950–2967
- Schwartz JA, Lium EK, Silverstein SJ (2001) Herpes simplex virus type 1 entry is inhibited by the cobalt chelate complex CTC-96. *J Virol* 75(9):4117–4128
- Seiler C, Berendonk TU (2012) Heavy metal driven co-selection of antibiotic resistance in soil and water bodies impacted by agriculture and aquaculture. *Front Microbiol* 3:399
- Shemchuk O, Braga D, Grepioni F, Turner R (2020) Co-crystallization of antibacterials with inorganic salts: paving the way to activity enhancement. *RSC Adv* 10(4):2146–2149
- Silva T, Pokhrel LR, Dubey B, Tolaymat TM, Maier KJ, Liu X (2014) Particle size, surface charge and concentration dependent ecotoxicity of three organo-coated silver nanoparticles: comparison between general linear model-predicted and observed toxicity. *Sci Total Environ* 468–469: 968–976
- Silver S (1996) Bacterial resistances to toxic metal ions—a review. *Gene* 179(1):9–19
- Silver S (2003) Bacterial silver resistance: molecular biology and uses and misuses of silver compounds. *FEMS Microbiol Rev* 27:341–353
- Silver S, Misra TK (1988) Plasmid-mediated heavy metal resistances. *Annu Rev Microbiol* 42:717–743
- Silver S, Phung LT (1996) Bacterial heavy metal resistance: new surprises. *Annu Rev Microbiol* 50: 753–789
- Silver S, Phung LT (2005) A bacterial view of the periodic table: genes and proteins for toxic inorganic ions. *J Ind Microbiol Biotechnol* 32:587–605
- Silver S, Phung LT, Silver G (2006) Silver as biocides in burn and wound dressings and bacterial resistance to silver compounds. *J Ind Microbiol Biotechnol* 33:627–634
- Silvestre C, Duraccio D, Cimmino S (2011) Food packaging based on polymer nanomaterials. *Prog Polym Sci* 36(12):1766–1782
- Sim S, Barnard RT, Blaskovich MAT, Ziora ZM (2018) Antimicrobial silver in medicinal and consumer applications: a patent review of the past decade (2007–2017). *Antibiotics* 7:93
- Sims JM (1852) On the treatment of vesicovaginal fistula. *Am J Med Sci* 45:59–82
- Soloz M, Abicht HK, Mermod M, Mancini S (2010) Response of Gram-positive bacteria to copper stress. *J Biol Inorg Chem* 15:3–14
- Song Z, Wu Y, Cao Q, Wang H, Wang X, Han H (2018) pH responsive, light-triggered on-demand antibiotic release from functional metal–organic framework for bacterial infection combination therapy. *Adv Funct Mater* 28:1800011
- Sule K, Umbsaar J, Prenner EJ (2020) Mechanisms of Co, Ni, and Mn toxicity: from exposure and homeostasis to their interactions with and impact on lipids and biomembranes. *Biochim Biophys Acta Biomembr* 1862(8):183250
- Takeuchi T, Böttcher A, Quezada CM, Meade TJ, Gray HB (1999) Inhibition of thermolysin and human alpha-thrombin by cobalt(III) Schiff base complexes. *Bioorg Med Chem* 7(5):815–819
- Taylor DE (1999) Bacterial tellurite resistance. *Trends Microbiol* 7:111–115

- Taylor DE, Rooker M, Keelan M, Ng LK, Martin I, Perna NT, Burland NT, Blattner FR (2002) Genomic variability of O islands encoding tellurite resistance in enterohemorrhagic *Escherichia coli* O157:H7 isolates. *J Bacteriol* 184:4690–4698
- Teitzel GM, Geddie A, De Long SK, Kirisits MJ, Whiteley M, Parsek MR (2006) Survival and growth in the presence of elevated copper: transcriptional profiling of copper-stressed *Pseudomonas aeruginosa*. *J Bacteriol* 188:7242–7256
- Thompson MG, Truong-Le V, Alameh YA, Black CC, Anderl J, Honnold CL, Pavlicek RL, Abu-Taleb R, Wise MC, Hall ER, Wagar EJ, Patzer E, Zurawski DV (2015) Evaluation of gallium citrate formulations against a multidrug-resistant strain of *Klebsiella pneumoniae* in a murine wound model of infection. *Antimicrob Agents Chemother* 59(10):6484–6493
- Townsend T, Sololo-Gabriele H (eds) (2006) Environmental impacts of treated wood. CRC Press, Taylor and Francis Group, Florida
- Turner RJ (2017) Metal-based antimicrobial strategies. *Microb Biotechnol* 10:1062–1065
- Turner RJ, Weiner JH, Taylor DE (1999) Tellurite-mediated thiol oxidation in *Escherichia coli*. *Microbiology* 145:2549–2557
- Vaidya MY, McBain AJ, Butler JA, Banks CE, Whitehead KA (2017) Antimicrobial efficacy and synergy of metal ions against *enterococcus faecium*, *Klebsiella pneumoniae* and *Acinetobacter baumannii* in planktonic and biofilm phenotypes. *Sci Rep* 7(1):5911
- Valko M, Morris H, Cronin M (2005) Metals, toxicity and oxidative stress. *Curr Med Chem* 12: 1161–1208
- Van Metre DC (2017) Pathogenesis and treatment of bovine foot rot. *Vet Clin North Am Food Anim Pract* 33(2):183–194
- Villapún VM, Dover LG, Cross A, González S (2016) Antibacterial metallic touch surfaces. *Materials (Basel)* 9(9):736
- Vinuesa V, McConnell MJ (2021) Recent advances in iron chelation and gallium-based therapies for antibiotic resistant bacterial infections. *Int J Mol Sci* 22(6):2876
- Wales AD, Davies RH (2015) Co-selection of resistance to antibiotics, biocides and heavy metals, and its relevance to foodborne pathogens. *Antibiotics* 4:567–604
- Wang L, Hu C, Shao L (2017) The antimicrobial activity of nanoparticles: present situation and prospects for the future. *Int J Nanomedicine* 12:1227–1249
- Wang RM, Lai TP, Gao P, Zhang HM, Ho PL, Ma GX, Woo PCY, Kao YT, Li H, Sun HZ (2018) Bismuth antimicrobial drugs serve as broad-spectrum metallo- $\beta$ -lactamase inhibitors. *Nat Commun* 9(1):439
- Warnes SL, Keevil CW (2011) Mechanism of copper surface toxicity in vancomycin-resistant enterococci following wet or dry surface contact. *Appl Environ Microbiol* 77:6049–6059
- Warnes SL, Keevil CW (2016) Lack of involvement of Fenton chemistry in death of methicillin-resistant and methicillin-sensitive strains of *Staphylococcus aureus* and destruction of their genomes on wet or dry copper alloy surfaces. *Appl Environ Microbiol* 82(7):2132–2136
- Weber DJ, Anderson D, Rutala WA (2013) The role of the surface environment in healthcare associated infections. *Curr Opin Infect Dis* 26:345–351
- Webster TJ, Tran PA (2011) Selenium nanoparticles inhibit *Staphylococcus aureus* growth. *Int J Nanomedicine* 6:1553–1558
- WHO (2017) Global priority list of antibiotic resistant bacteria to guide research, discovery, and development of new antibiotics. World Health Organization. <https://www.who.int/medicines/publications/global-priority-list-antibiotic-resistant-bacteria/en/>. Accessed 22 May 2021
- Wilks SA, Michels H, Keevil CW (2005) The survival of *Escherichia coli* O157 on a range of metal surfaces. *Int J Food Microbiol* 105:445–454
- Wilks SA, Michels HT, Keevil CW (2006) Survival of *Listeria monocytogenes* Scott A on metal surfaces: implications for cross-contamination. *Int J Food Microbiol* 111:93–98
- Williams KJ (2009) The introduction of ‘chemotherapy’ using arsphenamine - the first magic bullet. *J R Soc Med* 102(8):343–348
- Workentine ML, Harrison JJ, Stenroos PU, Ceri H, Turner RJ (2008) *Pseudomonas fluorescens* view of the periodic table. *Environ Microbiol* 10(1):238–250

- Wu L (2004) Review of 15 years of research on ecotoxicology and remediation of land contaminated by agricultural drainage sediment rich in selenium. *Ecotoxicol Environ Saf* 57(3):257–269
- Wu FYH, Wu CW (1987) Zinc in DNA replication and transcription. *Annu Rev Nutr* 7:251–257
- Xu FF, Imlay JA (2012) Silver(I), mercury(II), cadmium(II), and zinc(II) target exposed enzymic iron-sulfur clusters when they toxify *Escherichia coli*. *Appl Environ Microbiol* 78:3614–3621
- Yang J, Yang YW (2020) Metal–organic frameworks for biomedical applications. *Small* 16: 1906846
- Yebra DM, Kiil S, Johansen KD (2004) Antifouling technology-past, present and future steps toward efficient and environmentally friendly antifouling coatings. *Prog Org Coat* 50(2):75–104
- Yu Z, Gunn L, Wall P, Fanning S (2017) Antimicrobial resistance and its association with tolerance to heavy metals in agriculture production. *Food Microbiol* 64:23–32
- Zhang XF, Liu ZG, Shen W, Gurunathan S (2016) Silver nanoparticles: synthesis, characterization, properties, applications, and therapeutic approaches. *Int J Mol Sci* 17:9
- Zhang Y, Sun P, Zhang L, Wang Z, Wang F, Dong K, Liu Z, Ren J, Qu X (2019) Silver-infused porphyrinic metal–organic framework: surface-adaptive, on-demand nanopatform for synergistic bacteria killing and wound disinfection. *Adv Funct Mater* 29:1808594

**Part III**  
**When Microbes are the Best Tool**  
**for the Job**

# Chapter 5

## Microbial Consortium: A Promising Strategy for Bioleaching of Metals from Industrial Wastes



Mital Chakankar and Hocheng Hong

**Abstract** Advances in biohydrometallurgical technology have made it possible to utilize the microorganisms and their metabolites in the recovery and resource recycling of metals from secondary sources like industrial wastes. Various strategies have been developed to apply these microorganisms to improve the efficiency of the method. Use of microbial consortia is one of the promising strategies. Microbial consortia can be applied in various approaches and this chapter discusses the current applications and some promising emerging technologies that can assist in enhancing the bioleaching performance. Furthermore, interesting applications of microbial consortia for metal recovery from different industrial wastes are described along with the role of consortia and mechanisms involved.

### 5.1 Introduction

Microorganisms are known to perform a number of astonishing tasks in nature including bio weathering and metal dissolutions. They excel in these tasks owing to their diverse metabolic functionalities. Biohydrometallurgical processes involving the use of microorganisms for recovery of metals from ores or wastes are mostly based on and similar to their role in nature. Harnessing the potential of these microorganisms may help to make resource recovery and recycling processes more green. However, limiting factors like slow leaching rate, low recovery, and toxicity due to high metal contents make it difficult to employ the bioleaching

---

M. Chakankar (✉)

Department of Power Mechanical Engineering, National Tsing Hua University, Hsinchu, Taiwan

Department of Biotechnology, Helmholtz Institute Freiberg for Resource Technology, Dresden, Germany

H. Hong

Department of Power Mechanical Engineering, National Tsing Hua University, Hsinchu, Taiwan



processes at industrial scale. One of the ways to address these limitations is the use of a microbial consortium.

A microbial consortium is comprised of more than one microbial strain or species. Microbial consortia, also termed as mixed populations, typically emphasize using microbes as a black box technology, wherein there is a group of naturally occurring microorganisms, in the given habitat, and that group is composed of various different taxa's, or species, or different strains of the same species. Organization of microbial consortium in a nature is such that they work together in a manner where they exchange their metabolites or molecular signalling molecules and respond to each other (Keller and Surette 2006), this in turn helps them to communicate within the members of the consortium. In other words, members of consortia have complimentary metabolic functions that enable them to perform the tasks which are not possible for individual organisms. This behaviour helps in division of labour, wherein they can perform various tasks in combination. Such a communication and division of labour further enhances their ability to perform complex tasks or functions. Moreover, during such actions, members in consortia can exhibit the control over each other's activity either positively or negatively with respect to exchange of intermediate metabolites that will or can promote or inhibit the metabolic activity or growth of other members (Brenner et al. 2008; Kato et al. 2005). These consortia not only can better perform tasks that are complicated but can also better endure robust environmental conditions or fluctuations in those conditions as compared to single strains.

Omnipresence of microbial consortia in nature and the ecologically important role that they play encompasses many natural aspects. These are now increasingly being included in various processes like food and drug manufacturing, wastewater treatment, environmental bioremediation, etc., both in therapeutic and industrial settings and beyond (Rosero-Chasoy et al. 2021).

Consortia bear broader metabolic capacities, as compared to single species, and enable the division of labour. Such a division of labour distributes the functions among the consortia members, which possibly helps improve the overall efficiency. The vast features of natural consortia can be harnessed to solve the real-world problems like green resource recycling from industrial wastes. In addition, it is possible to modify the constituents of the consortia with respect to the desired functions by changing the ratio of strains or the constituent strains (Qian et al. 2020).

Biohydrometallurgical recovery of metals is an efficient and environmentally friendly way for resource recovery of metals from primary as well as secondary sources. This chapter focuses on the environmental applications of microbial consortia with an emphasis on their role in biohydrometallurgical recovery of metals from industrial wastes. Microbial consortia, whether natural or synthetic or engineered are a powerful and versatile tool that can be employed to exhibit complex functions like bioleaching of complex or heterogeneous industrial wastes (Brenner et al. 2008).

### ***5.1.1 Types of Interactions in Consortia***

There exist different kinds of interaction mechanisms between various members of microbial consortia. In-depth understanding of these interactions could be beneficial in constructing the consortia for various applications. Resource partitioning is an interaction where each member of the consortium utilizes different nutrients than the other and hence there is no competition for the same nutrients between the members of the consortium. In symbiotic interactions, different chemicals like metabolites or signalling molecules are exchanged between the members. Symbiotic relationships can be commensalism where one member benefits from the other and does not receive any return benefit or harm from the other member. Alternatively, the relationship can be mutualism where members depend on each other for survival as they exchange the metabolites (Tsoi et al. 2019).

## **5.2 Types of Consortia**

### ***5.2.1 Natural Consortia***

Natural consortia or undefined consortia are obtained from environmental samples wherein, microbial communities have an unknown number of constituents. Natural consortia are most widely applied in bio mining where microbes and their metabolites play a major role in the recovery of minerals from ores (Rebello et al. 2021). Most of the research on utilizing consortia in prospect of biohydrometallurgy is centred around bio mining. However, it is beyond the scope of this chapter to include this aspect. Yet, there are some reports where natural consortia are used for metal recovery from industrial wastes and those are discussed in the next sections.

### ***5.2.2 Synthetic Consortia***

The naturally occurring microbial consortia or communities can perform an amazing variety of functions. Yet, their effectiveness, which is often sufficient in the natural context, might be less efficient when it comes to specific applications in industrial environment. Thus, there is a need to optimize the conditions for their performance or construct the depictive synthetic consortia having improved capabilities (Eng and Borenstein 2019). Defined or synthetic consortia, also termed as being engineered consortia, can have a different composition than do naturally occurring consortia. These differences offer a unique opportunity to improve existing community functions and expanding the range of their applications. Such microbial communities can be obtained or designed by various methods like enrichment, community reduction, and combinatorial evaluation employing computational methods that use

**Fig. 5.1** Flowchart of types of consortia and methods used for application

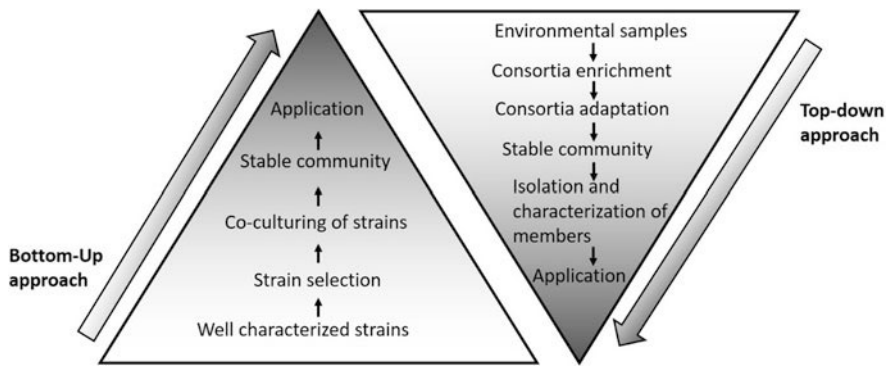
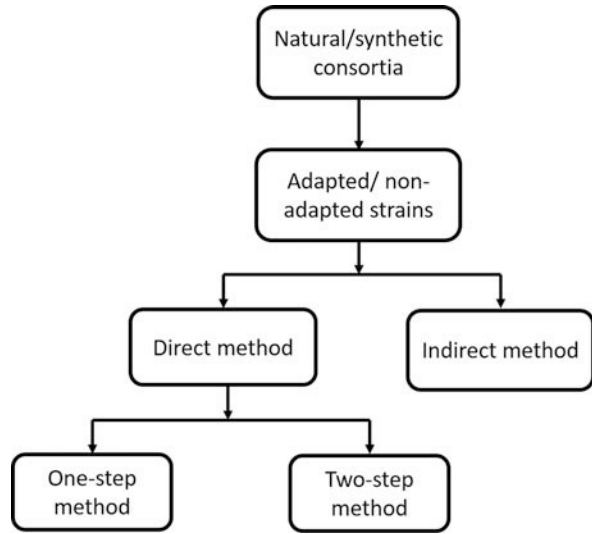


**Fig. 5.2** A comparison of top-down and bottom-up approaches to construct microbial consortia

mechanistic microbial function models and ecological models of community dynamics (Eng and Borenstein 2019). Figure 5.1 shows the flowchart of various types of consortia and methods used for their applications, which are discussed in detail in further sections.

Assembling or construction of the microbial consortium can be done by two different approaches, i.e. ‘bottom-up’ approach and ‘top-down’ approach. Figure 5.2 shows a comparison of top-down and bottom-up approaches used to construct microbial consortia.

### 5.2.2.1 Top-Down Approach

This approach relies on the consortia development from diverse environmental samples. Where, strains are enriched and adapted for a specific function and those that adapt survive the enrichment whereas others disappear. In a top-down approach, a stable microbial community having unknown composition is enriched first and the members are then isolated and characterized.

Top-down consortia are often black boxes with unknown composition. Enriching the consortia from environmental samples provides us with the reduced yet suitable number as well as type of microorganisms. These enriched population members can further be isolated, identified, and characterized. However, it might be difficult to control such consortia due to limited knowledge about the community and variables influencing their efficiency and reliability (Peng et al. 2016). Hence, it is necessary to explore the microbial constituents of the natural consortium and undertake their further characterization. By so doing it is possible to determine the extent and compositional nature of their diversity. It could become possible to decipher this knowledge in the coming years by using research tools developed in bioinformatics, metabolic engineering, etc.

Another attractive strategy as suggested by Peng et al. (2016) could be combining the top-down and bottom-up approaches to develop a defined consortium from already existing consortium. The main advantage of such a strategy is their significant stability. This stability arises from the interaction between members of consortium and diversity in species as well as their metabolic functionality. In such communities, even though there are changes in population due to environmental fluctuations, redundant members act positively and keep up the function for entire consortium.

### 5.2.2.2 Bottom-Up Approach

Synthetic biology allows use of the bottom-up approach to build microbial communities (Hays et al. 2015). In a bottom-up approach, consortia comprising different taxonomies and metabolic functions and having high stability and efficiency are enriched together (Ibrar and Zhang 2020). Most defined consortia are generally designed using a bottom-up approach, wherein two or more isolated and characterized strains are co-cultured. Most studies reporting the use of consortia for bioleaching of metals from wastes employ bottom-up approach, where synthetic microbial communities are constructed for such tasks. Populations in this consortium generally have a commensal or syntrophic relation, and the metabolites or products of one member are beneficial or used as substrate by the other (Peng et al. 2016).

Many synthetic consortia have shown high efficiency as compared to their subcomponent pure cultures. Synthetic microbial consortia designed in a bottom-up way do have potential to go forward in bioleaching yet, many challenges like difficulties in co-culturing the microorganisms that can form stable and

metabolically diverse consortia, set it back. Moreover, only well-characterized strains are employed in developing such consortia and a plethora of unidentified and uncharacterized microorganisms remain unexplored for their use in this approach. Besides, it is not feasible to test all possible permutations and combinations with respect to a large number of organisms to find suitable members for the consortia.

There are several challenges in constructing the model consortia, some that include stable coexistence of various strains or species, defining optimum growth and processing parameters when working with different species such as pH, temperature, dissolved oxygen, growth substrates, etc.

### 5.3 Application Approach

Microbial consortia are known to cooperate and synergistically recover metals (Latorre et al. 2016). Along with the type of microorganisms used, various factors influence the bioleaching efficiency including pH, temperature,  $\text{Fe}^{3+}$  concentration, pulp density, etc. (Bayat and Sari 2010; Rastegar et al. 2014; Gu et al. 2018; Zhou et al. 2019). To improve the bioleaching efficiency, microbial consortia are applied in various ways. In the direct leaching method, members of consortia are grown in the presence of waste for metal recovery. Here, the applied consortia may be non-adapted wherein the naturally occurring microbes are grown in presence of waste or adapted consortia where either the members individually or as a whole consortia are acclimatized to increasing concentration of wastes. Direct leaching is also termed as contact leaching as microorganisms come in direct contact with the ore or waste to be bioleached. The microbes typically then attach to the available surfaces and form biofilms. Metabolites formed in the biofilm leach the metals. E.g. In case of acidophiles, the  $\text{Fe}^{2+}$  is oxidized in the biofilm to  $\text{Fe}^{3+}$ , which helps in metal dissolution. Again, these adapted or non-adapted consortia can be used in direct or indirect leaching methods. Direct leaching can be one-step, where waste is added to the bioleaching medium along with microbial inoculum; or it could be two-step where the bacterial growth process is separated from the bioleaching process, and waste is added after maximum growth of the bacterial culture (Heydarian et al. 2018).

In an indirect method, microbial cultures are grown in specific medium to produce lixivants required for leaching, and the microbial growth is then separated to obtain the spent medium which is used for the bioleaching (Jadhav and Hocheng 2013). Such a use of spent media for bioleaching is desirable from the point of view of industrial application to increase the leaching efficiency (Hocheng et al. 2012). Moreover, the major advantage of this approach is that separation of lixiviant generation or growth phase and leaching phase allows us to optimize these processes independently to maximize productivity. Another approach that could be very useful is the synergistic or sequential approach where one or more microorganisms are used to recover some metals from the waste followed by the use of other microorganisms

that could recover remaining metals. Sometimes a single strain or type of strains alone are not sufficient to leach the metals in a given waste. In such a case, employing another type of strain to synergistically leach the metals could significantly increase the leaching efficiency as well as yield. If we employ the different microorganisms with known characteristics in such an approach for the metal recovery, then it can be defined as a division of labour using synthetic biology approaches.

## 5.4 Recovery of Metals from Industrial Wastes by Consortia

The use of microbial consortia in environmental applications is as complex as its applications in other fields and various aspects need to be considered before application. For example, during applications for bioremediation of pollutants, the consortia may need to be repurposed or engineered to clean up the pollutants in such a way that important divisions of labour are established. Because the complexity and toxicity of industrial waste compounds often requires several steps for their degradation, the employed strains must be robust when exposed to such wastes, making the use of consortia an ideal solution (Hays et al. 2015). A variety of microorganisms are involved in bioleaching of metals from industrial wastes, but there exist some limitations when it comes to leaching of industrial wastes which are very complex and heterogeneous in nature. Moreover, bioleaching has many advantages like high efficiency, low operating costs and energy consumptions, easy management and implementation of operating conditions, environmental friendliness, and less heavily industrialized requirements (Baniasadi et al. 2019). Literature about this subject suggests that the usage of consortia has increased bioleaching efficiency as compared to single strains (Ilyas et al. 2007, Xia et al. 2018, Ghassa et al. 2020a).

Thus, the goal of developing microbial consortia provides us with new prospects for applying our technology of biological community synthesis and our understanding of community collaboration, where the ability of individual microbes can be harnessed and brought together creatively to focus on specific applications. Table 5.1 summarizes uses of consortia in bioleaching of various industrial wastes.

## 5.5 Types of Industrial Waste

### 5.5.1 E-Waste

E-waste or electronic waste is the fastest growing waste around the world. Recycling of e-waste is important from the point of view of its high toxicity due to heavy metals as well as the high amount of precious, rare, and base metal content, and considering

**Table 5.1** Studies using consortia for bioleaching of industrial wastes

Waste	Type of consortia	Construction approach	Bioleaching method	Reference
Electronic scrap	Natural—adapted from environmental samples—moderately thermophilic bacteria	Top-down	Direct	Ilyas et al. (2007); Ilyas et al. (2010); Ilyas et al. (2013)
Spent Li-ion batteries	Natural—environmental samples	Bottom-up	Direct—two-step	Xin et al. (2009)
PCB	Natural—environmental samples	Top-down	Direct—two-step	Xiang et al. (2010)
Metal concentrates of PCBs	Natural—acidophilic bacteria	Top-down	Direct—two-step	Zhu et al. (2011)
PCBs	Defined	Bottom-up	Direct—two-step	Pradhan and Kumar (2012)
Spent Zn-Mn batteries	Defined	Bottom-up	Direct	Xin et al. (2012)
Manufacturing scrap TV circuit boards	Natural—non-adapted mesophilic bacteria	Top-down	Direct	Bas et al. (2013)
PCBs	Defined—adapted	Bottom-up	Direct	Liang et al. (2013)
Electronic waste	Natural—adapted from environmental samples—moderately thermophilic bacteria	Top-down	Direct	Ilyas et al. (2014)
PCBs	Defined	Bottom-up	Direct—two-step and sequential	Isildar et al. (2016)
PCBs	Natural—adapted from environmental samples—moderately thermophilic bacteria	Top-down	Direct	Xia et al. (2017)
Low-grade waste PCB	Natural—adapted from environmental samples—fungal consortium	Top-down	Direct	Xia et al. (2018)
PCBs	Natural	Top-down	Indirect	Wu et al. (2018)
Electroplating sludge	Defined—moderately thermophilic acidophiles	Bottom-up	Direct—two-step	Zhou et al. (2019)
Spent Li-ion batteries	Natural—adapted—moderately thermophilic bacteria	Top-down	Direct—two-step	Ghassa et al. (2020a)
Electroplating sludge	Defined—enriched and adapted	Bottom-up	Direct—two-step	Zhang et al. (2020)
Comminuted spent PCBs	Natural—adapted	Top-down	Direct—two-step	Hubau et al. (2020)
Electroplating sludge	Defines—adapted	Bottom-up	Direct	Sun et al. (2021)

that we face depleting natural sources of these metals. Large amounts of literature have reported upon the use of *Acidithiobacillus ferrooxidans* (as Fe oxidizer), *Acidithiobacillus thiooxidans* (as S oxidizer), or Fe and S oxidizer alone or in consortium for bioleaching of metals from the electronic waste by direct or indirect leaching mechanisms (Ilyas et al. 2021).

### 5.5.1.1 Low-Grade Scrap TV Circuit Board

In a series of studies, Ilyas et al. (2007, 2010 and 2013) investigated the potential of using adapted moderately thermophilic consortia to recover metals from electronic scrap followed by column studies and further process optimization, and additionally studied the introduction of a pre-treatment process.

In their initial studies, Ilyas et al. (2007) employed an adapted consortium made up of *Sulfobacillus thermosulfidooxidans* and an unidentified acidophilic heterotroph isolated from environmental samples, to recover metals from electronic scrap. Efficiency of bioleaching was associated with the growth of consortia members. High growth rate resulting in high metal removal rate. External addition of sulphur in order to generate the acid and avoid pH adjustments helped in improving bioleaching efficiency as the added sulphur acted as an additional energy source and improved bacterial growth. *S. thermosulfidooxidans* alone was not able to leach the metals efficiently; yet high leaching rates could be explained by the synergistic effect of acidophilic heterotrophs in concert with the growth of *S. thermosulfidooxidans* (Ilyas et al. 2007).

In their next study, Ilyas et al. (2010) explored the practicability of using column bioleaching for metal recovery from electronic scrap using defined moderately thermophilic consortia. Consortia of *S. thermosulfidooxidans* and *Thermoplasma acidophilum* were adapted to mixed metal solutions prior to their use in bioleaching. In order to stabilize the pH, scrap was pre-leached with sulphuric acid before bioleaching. Cu, Ni, and Zn were predominantly recovered by bioleaching whereas Al was recovered as result of both acid leaching and bioleaching. Initial supply of a carbon source is essential for the growth of *S. thermosulfidooxidans* and achieving a high leaching rate in consortia can be attributed to microbial population growth, which was supported by the acidophilic heterotroph present in the consortia (Ilyas et al. 2010).

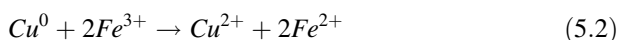
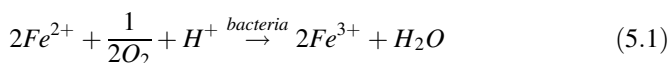
Furthermore, providing some additional energy source in the form of  $\text{FeS}_2$  and  $\text{S}^0$  enhanced the bioleaching performance of consortia as oxidation of that  $\text{S}^0$  partially compensated the acid consumption, improving the leaching conditions for the consortia (Ilyas et al. 2013).

Bas et al. (2013), through their studies emphasized the importance of initial iron availability in the wastes to be treated for improved leaching efficiency. They also highlighted the use of pyrite as a potential alternate source of iron and sulphur for microorganisms during e-waste bioleaching. MES1 is a microbial consortium composed of mesophilic bacteria like *A. ferrooxidans*, *A. thiooxidans*, *L. ferrooxidans* and it was used for recovery of copper from the manufacturing scrap of TV circuit



boards (STVB) employing direct leaching method. Initial iron content of the waste, which was nearly 43 g/ton, played an important role during the leaching process where it helped to promote the bacterial growth by providing the iron and sulphur during the lag phase. External addition of Fe (II) (1–8 g/l) improved the extraction by 54%. However, in view of the low iron content of the waste, a new approach of pyrite addition in the form of pyrite concentrate (PyC) (5–50 g/l) was tested as an iron and sulphur source. The addition of 50 g/l PyC improved the Cu recovery from 24 to 84% and the consumption of biological sulphuric acid was lowered to 62%. Furthermore, the bioleaching rate was also enhanced by increase in the microbial inoculum size from initial 10% v/v to final 50%v/v.

The iron oxidizing acidophiles in the consortium oxidize Fe(II) under suitable conditions generating Fe(III) which acts as powerful oxidant (Eq. 5.1) (Nemati et al. 1998). Metal extraction efficiency depends on maintenance of the oxidative leaching conditions. Metals in e-waste are present either in native form or as alloys. Ferric iron generated during the oxidation of ferrous iron by bacteria acts as oxidizing agent during Cu leaching (Eq. 5.2). Thus, Cu leaching rate is dependent on the availability and the rate of biooxidation of ferrous iron in the bioleaching environment. Many studies have reported enhanced Cu extraction during external addition of Fe(II)/Fe (III), whereas others have reported low extraction due to limited availability of initial soluble iron in the samples used for bioleaching. Fe (II) acted as an inherent energy-yielding substrate to support the bacterial growth. Hence, external iron addition markedly enhanced the Cu recovery rate. The increased availability of soluble iron improved the growth of consortia members along with their capacity for the generation of ferric iron in the bioleaching environment. When pyrite was added as iron and acid source, biooxidation of pyrite generated acid with concurrent release of iron. Further increasing inoculum size increases the ratio of active members in consortia, thereby enhancing and improving the bioleaching rate and extent. This enhancement in turn can be attributed to the rapid conversion of Fe(II) to Fe(III) again due to increased bacterial population (Bas et al. 2013).



In this leaching process, the members of natural consortium are in a symbiotic mutual relationship where they exchange metabolites among their members. Moreover, external factors like addition of a nutrient source in the form of PyC can enhance the performance of the consortium.

Recovery of heavy metals from recycling industry electronic waste using microbial consortium was studied by Ilyas et al. (2014). A moderately thermophilic microbial consortium of *Sulfobacillus thermosulfidooxidans* and *Thermoplasma acidophilum* was used. Commercial S<sup>0</sup> powder and biogenic S<sup>0</sup> sludge were used as the substrates for the consortium. Results of their stirred tank reactor studies revealed a high metal removal efficiency of 92 and 82% at 1% biogenic S<sup>0</sup> sludge

and 2% commercial  $S^0$  powder, respectively, at 15% pulp density and 150 mm particle size with an intermittent addition of inoculum at low concentration.  $S^0$  oxidation was higher (95%) in 12 days in case of biogenic sludge as compared to 82% for commercial  $S^0$  powder in 24 days, making the use of biogenic  $S^0$  sludge cost effective. Achieving that high degree of biogenic  $S^0$  oxidation could have been due to the higher specific surface area of the particles and their possessing lower hydrophobicity (Steudel 1989). Moreover, the fact of biogenic  $S^0$  sludge being a by-product of bio-based metal refinery operations and desulphurization plants, offers added advantage for using it as a substrate (Ilyas et al. 2014).

### 5.5.1.2 Printed Circuit Boards

Printed circuit boards (PCBs) are an important component of electronic waste, comprising various precious and base metals. These boards are one of the most studied wastes for metal recovery (Ilyas et al. 2007). Yet, heterogeneous and complex composition limits their recycling rate (Lee et al. 2007). PCBs are composed of nearly 28% metals, 19% plastic, 4% bromine, plus 49% glass and ceramics (Ilyas et al. 2007). Waste PCBs pose an environmental threat due to heavy metals and would also result in the loss of other valuable metals.

In a top-down approach, an enriched bacterial consortium from natural acid mine drainage was used to recover Cu from waste PCBs followed by optimization of the process parameters (Xiang et al. 2010). In an indirect process, Cu was mainly extracted through oxidation by ferric ions. The population analysis of enriched AMD sample revealed the presence of *Acidithiobacillus* and *Gallionella* in addition to small amounts of *Leptospirillum* spp. The synergistic effect of microbial consortia improves the bioleaching efficiency as compared to the use of pure cultures. Iron and sulphur oxidizers cooperate to dissolve the metals and acidophilic heterotrophs promote their own growth by removing the organic products of their metabolism (Zeng et al. 2010; Ilyas et al. 2007; Marhual et al. 2008). Initial pH and  $Fe^{2+}$  concentration as well as low pulp density of PCB powder play a crucial role in Cu extraction and precipitate formation. In a two-step process, PCB was added to the culture medium when  $Fe^{2+}$  concentration reached at 6.25 g/l. Cu was removed at 95% in 5 days at initial pH of 1.5, 9 g/l initial  $Fe^{2+}$  and 20 g/l PCB powder dosage. Moreover, use of a consortium significantly reduced the bioleaching time by 7 days. Yet, the studies were negatively impacted by the ferric iron precipitate even under optimum conditions. That precipitation resulted in low availability of ferric ions causing low oxidation. Furthermore, ferric iron precipitation may limit the biomass amount and either create a kinetic barrier or slow down the mass transfer by forming a layer of precipitate on the PCB particles. As pH levels below 1.8 are known to limit such precipitation, one solution to evade this problem could be achievement of microbial adaptation to that lower pH environment (Jensen and Webb 1995).

Increased toxicity of electronic scraps and PCBs towards microbes is attributed to the non-metallic components of this waste (Brandl et al. 2001). Hence, Zhu et al.

(2011) used the metal concentrates of PCBs to recover metals using acidophilic consortia. The consortia were obtained from natural acid mine drainage. Influence of various factors like initial pH,  $\text{Fe}^{2+}$  concentration, pulp density, particle size, and inoculation quantity on bioleaching efficiency were assessed to optimize the process parameters. Initial pH and  $\text{Fe}^{2+}$  concentration had significant impact on Cu recovery and precipitate formation. Moreover, indirect bioleaching of copper by biogenic ferric ions was more effective in metal removal as compared to chemical leaching. In a two-step process, a consortium was pre-cultured in absence of metal concentrate, followed by its addition when the desired concentration of  $\text{Fe}^{2+}$  was reached. Resultingly, 96.8% Cu was recovered in 45 h, followed by 88.2% Al and 91.6% Zn by the end of 98 h. That recovery was achieved under the optimum process conditions of pH 2.0, initial  $\text{Fe}^{2+}$  concentration of 12 g/l, metal concentrate dosage of 12 g/l, microbial inoculum size of 10% v/v, and particle size of 60–80 mesh. Thus, use of microbial consortia with optimized process parameters not only improved the bioleaching efficiency but also reduced the time significantly (Zhu et al. 2011).

Three different strains of *Chromobacterium violaceum*, *Pseudomonas fluorescens*, and *Pseudomonas aeruginosa* have been used alone as well as in a consortium to evaluate their metal extraction efficiency from waste PCBs (Pradhan and Kumar 2012). In a two-step method, microorganisms alone as well as in consortia were used for the process. Cu (79%), Au (69%), and Zn (46%) were leached by *C. violaceum* alone, whereas the consortium of three organisms could leach Cu (83%), Au (73%), and Zn (49%). High metal recovery by *C. violaceum* was attributed to high growth rate, high tolerance towards metal toxicity, and formation of stable metal complexes.

Research by Liang et al. (2013) was subjected to optimizing the consortia of two acidophiles, *A. ferrooxidans* and *A. thiooxidans*, for improved Cu leaching from PCBs and increased pulp density. The effect of varied inoculum ratios on the microbial growth was studied along with the optimization of process parameters like pH, concentrations of  $\text{Fe}^{2+}$  and  $\text{S}^0$ , by response surface methodology. Addition of PCB during the initial growth stages inhibits the microbial growth, lowering the leaching efficiency due to toxicity. Hence, a multiple point PCBs addition approach was employed, where PCB was added at low concentration during the initial stage and higher concentration at the later stage, to minimize the toxic impact of PCBs on the growth as well increase step-by-step increase in pulp density. High Cu leaching of 94% was obtained after 240 h with step wise addition of PCB at the concentration of 18 g/l in total (Liang et al. 2013). In continuation to this study, changing the ratios of microbes in the inoculum had significant effect on the growth of both acidophiles and the initial inoculum ratio (Af:At) 1:2 was found to be the most efficient resulting in 92.6% Cu recovery at pH 1.56,  $\text{FeSO}_4 \cdot 7\text{H}_2\text{O}$  and  $\text{S}^0$  at 16.88 and 5.44 g/l, and PCB addition of 28.8 g/l (Liang et al. 2013).

Isildar et al. (2016) experimented with the two-step bioleaching process for effective recovery of Cu and Au from PCBs. *Acidithiobacillus ferrivorans* and *A. thiooxidans*, both chemolithotrophic acidophiles, were used in the first step. Whereafter, *P. fluorescens* and *Pseudomonas putida*, both of which are cyanide producing heterotrophs, were used in the second step. Biogenic sulphuric acid and

ferric iron produced by iron and sulphur oxidizing bacteria play a major role in metal recovery via acidolysis and redoxolysis (Lee and Pandey 2012). The sentence should be as follows: Whereas, free cyanide produced by heterotrophs complexes and mobilizes the metals by complexolysis (Brandl et al. 2008). Growth phase of the consortium was separated from the bioleaching phase to reduce the toxicity, wherein PCB was added at the later stage of the growth. Increase in Cu extraction in the first step without any lag phase can be attributed to the pre-growth strategy and co-operative bioleaching. Respectively, 98.4 and 44% of Cu and Au were recovered. Although Au bioleaching using biogenic cyanide was effective, the Au mobilization efficiency was low as compared to use of a chemical process (Isildar et al. 2016). That study is an excellent example of sequential leaching.

To improve the feasibility and efficiency of PCBs recycling, Xia et al. (2017) employed a pre-treatment process prior to applying the bioleaching method. The powdered PCB was pre-treated by table separation and was then bioleached using moderately thermophilic consortia in a stirred tank reactor. An environmental sample of acid mine drainage was obtained from a copper mine and enriched in a mineral medium, cultured at 45 °C for enrichment of the moderately thermophilic microorganisms. Furthermore, the resulting enriched consortium was acclimatized to the increasing concentration of PCB to improve the metal tolerance. The adapted consortium could tolerate up to 80 g/l PPCBs and was able to recover Zn (85.23%), Cu (76.59%), and Al (70.16%) in 7 days. Further, the authors also studied the community structure during bioleaching to get an overview of the effect of high concentration of PPCBs on growth of consortium members as well as to study the shift in microbial communities during the process. Compositional analysis of adapted and acclimatized consortia showed the presence of *Leptospirillum ferriphilum* (iron oxidizer), *Acidithiobacillus caldus* (sulphur oxidizer), and an uncultured *Thermoplasmatales archaeon* (heterotroph). This is an excellent example of synergistic relationship in the consortium where, the iron oxidizer performs a major role in metal dissolution by oxidation of  $Fe^{2+}$  to  $Fe^{3+}$ , the acidic environment required for the bioleaching process is created by a sulphur oxidizer, and the heterotroph indirectly participates in iron oxidation by providing stability for the consortium by consuming organic metabolites produced by the autotrophs (Giaveno and Donati 2001; Xia et al. 2008; Gurung and Chakraborty 2009). During the later phase of this process, when elemental sulphur became a primary energy source, growth of *A. caldus* was accelerated and dominated the population. Further comparisons of moderately thermophiles, mesophiles and their mixtures, revealed that where the leaching efficiency was found to be low for mesophiles as compared to others, the reason for that low efficiency was resistance of moderate thermophiles to high pulp density (80 g/l in this study) and metal concentration (Zhou et al. 2009; Zeng et al. 2010; Wang et al. 2013; Xia et al. 2017).

In another study by the same group, a fungal consortium was employed for the recovery of metals from low-grade waste PCB (Xia et al. 2018). There are very few reports on the use of the fungal consortia in such a process. In a top-down approach, three fungal consortia were collected from a multi-metal contaminated soil. A group of consortia was selected from these on the basis of high resistance to the metal

extract from waste PCBs during initial adaptation. The adapted consortium was able to recover 56.1% Cu, 15.7% Al, 20.5% Pb, 49.5% Zn, and 8.1% Sn from the PCBs at 8% (w/v) pulp density in the stirred tank reactor. The general mechanism of bioleaching using fungi involves an indirect leaching process, with an involvement of fungal metabolites like organic acids, amino acids, and others. Metal recovery by fungi occurs via complexolysis, acidolysis, redoxolysis, and bioaccumulation. In acidolysis, a mechanism performed by organic acids plays a major role, there is rapid protonation of the oxygen on the metal surface followed by combination of metal with water which results in separation of metal atoms from the surface (Rezza et al. 2001). Further extraction of these dissolved metals is reinforced by the complexolysis, a significant character of fungal leaching (Burgstaller and Schinner 1993).

SEM and FTIR studies have helped in investigating the interaction between fungal mycelium and PCB particles. Fungal mycelium have been seen wound around and penetrating through the PCB particles. FTIR analysis revealed that the toxic PCB components like epoxy and cyanate resin from polymer matrix, brominated flame-retardants and metals damaged the critical groups on mycelium, hampered the bioleaching efficiency. Further community composition of the consortia was analysed. The results suggested the dominance of *Purpureocillium lilacinum* and *Aspergillus niger* with those two species having 71.9% and 27.9% relative abundance at the end of the bioleaching process. *A. niger* is reported widely for its application in metal recovery with regard to high production of organic acids. Whereas *P. lilacinum* was found to have high tolerance to heavy metals and acidity (Oggerin et al. 2014; Oggerin et al. 2013). Such studies revealing the community structure of consortia are useful to understand the basis not only for the consortium regulation but also to improve the efficiency of consortia (Xia et al. 2018).

The toxic impact of high concentrations of metals in PCB, as compared to the toxicity of most any other type of waste, is well known. To overcome this negative effect, researchers have been using various approaches like use of low pulp density, adaptation of microorganisms, and two-step methods where waste is added after the growth of microorganisms. Another approach to evade this problem of metal toxicity is the use of indirect leaching methods in which spent bacterial medium that contains only the metabolites of bacteria is used to leach the metals. This indirect approach completely avoids the direct metal toxicity towards the bacteria. Wu et al. (2018) applied such an indirect strategy to recover metals from PCBs. Their bacterial consortium was dominated by *L. ferriphilum* and *Sulfobacillus thermosulfidooxidans*. That consortium was grown until the complete oxidation of  $\text{Fe}^{2+}$  to  $\text{Fe}^{3+}$  had occurred and the bacteria-free culture supernatant or spent medium was then used for leaching the metals from the PCB. Nearly 93.4% of Cu was recovered in 9 days from 100 g/l PCB. Their study demonstrated the feasibility of using spent medium from a consortium for bioleaching of metals with an advantage of high recovery as well as mitigation of toxic effects of PCB towards bacteria. Furthermore, the authors also succeeded in developing a continuous bio oxidation–leaching–separation cycle with high leaching efficiency. They determined that pyrite aided in establishing continuous culture of consortia where, on the one hand, the

pyrite acted as a carrier material for microbes and on the other hand, the pyrite acted as an energy source. After removal of supernatant from this biooxidation process, bacteria attached to the pyrite surface were used for the next cycle of biooxidation. In addition, when the  $\text{Fe}^{2+}$  in the growth medium was exhausted, pyrite served as an energy source (Wu et al. 2018).

Recently bioleaching of metals from comminuted spent printed circuit boards (PCBs) was investigated in a stirred tank reactor (Hubau et al. 2020). The kinetics of metal dissolution was compared between a batch mode and double-stage continuous mode of bioreactor operation. A BRGM-KCC acidophilic consortium employed in this study originated from BRGM culture collection. This consortium is composed of iron oxidizers, sulphur oxidizers, as well as both iron and sulphur oxidizers like *L. ferrophilum*, *Acidithiobacillus*, and *Sulfobacillus benefaciens*. The batch mode studies were carried out in 2.25 L glass bioreactors to evaluate the effect of presence of bacteria and the impact of initial Fe (III) concentration. The operating conditions used were 10%v/v microbial consortium inoculum size; stirring speed of 600 rpm; temperature maintained either at 35 °C (to obtain high Fe (II) oxidation rate) or 40 °C (optimum temperature for consortium); PCB concentration of 1%w/v and 5% w/v; initial Fe (III) concentrations of 0, 1, and 8 g/l; gas flow rate of 8 and 60 l/hr. and CO<sub>2</sub> enrichment of 0% and 1%, and hydraulic retention time (HRT) of 3.2 hours. Although the results of batch mode were promising, they did not show the impact of microbial bioleaching as the lag phase of microbial growth was longer than the time required for chemical dissolution of metals.

In the double-stage continuous mode, two separate stages were involved in the process. In the first phase consortium was used to oxidize Fe (II) to Fe (III) and in the second stage this liquor was used to leach metals from PCBs. Bubble column reactor (200 ml capacity) was used in the first stage to obtain the optimum growth of consortium. The column was first inoculated with 10%v/v inoculum size at 35 °C in a medium containing 1 g/l of Fe (II) concentration from ferrous sulphate at pH 1.1 and 15 g activated charcoal. Stirring was performed by continuous airflow rate of 20–30 L/hr. with 1% CO<sub>2</sub> enrichment. The second stage reactor was similar to that used in batch mode that was fed continuously with a liquor from first stage with an incoming flow rate of 47 ml/hr. so as to obtain HRT of 48 hr. In addition the column was fed with comminuted PCBs with the pulp density varying from 1% to 1.8% at the flow rate of 0.5–0.85 g/hr. The pH was kept at 1.5 with the addition of sulphuric acid. Other operating conditions like temperature 35 °C, stirring speed 600 rpm, and air flow rate of 60 l/hr. with 1% CO<sub>2</sub> enrichment were constantly maintained. Cu 96%, Ni 73%, Zn 85%, and Co 93% were recovered at 1% (w/v) pulp density, respectively. The pulp density was further increased to 1.8% in the double-stage bioreactor, without hampering the bioleaching rate. Moreover, once the bioleaching reaction was established, bacteria were able to grow in the second stage. As the Fe in the PCBs was sufficient for bacterial growth, the external addition of Fe (II) was no longer required.

The separation of two stages reduced the toxic impact of metals from PCB on microbial growth, allowed the consortium the time required for the adaptation and resulted in improved recovery yields.

Changes in microbial community over time in the double-stage continuous mode process were examined by 16S rRNA gene CE-SSCP fingerprints. Both liquid and solid phases from two stages (activated charcoal from bubble column of first stage and comminuted PCBs residues from second stage) were used for this analysis. Results revealed the presence of iron oxidizer *L. ferriphilum* in solid and liquid phase along with sulphur and iron oxidizer *S. benefaciens* and an unknown strain in the first stage of bioreactor. Whereas, only *L. ferriphilum* was detected at the second stage and other typical members of consortium like *At. caldus* and *Sulfobacillus thermosulfidooxidans* were not detected, likely due to unsuitable growth conditions (Hubau et al. 2018). Absence of reduced sulphur compounds in the bioreactor (stopping of ferrous sulphate feeding) could have been the reason for absence of *At. caldus*, which is a sulphur oxidizing bacteria. Similarly, the 35 °C temperature of the reactor was too low for *Sulfobacillus thermosulfidooxidans*, whose optimum growth temperature is 51 °C (Watling et al. 2008). Dominance of *L. ferriphilum* could be explained with the observation of Guezennec et al. (2017) that large proportions of *L. ferriphilum* growth on solid fractions than in plankton form.

### 5.5.1.3 Li-Ion Batteries

The extensive use of batteries as energy storage devices has led to increased production and consequently increased amounts of spent batteries. Spent batteries are classified as hazardous waste due to their heavy metal content and toxicity (Nan et al. 2005). There remains a gap between production and recycling rates of batteries due to different regulations, inefficient collection, and unavailability of suitable recycling techniques (Velázquez-Martínez et al. 2019). Considering the increasing demand, depleting natural reservoirs, and loss of valuable metals from the batteries, it is necessary to develop a recycling process that will allow the resource utilization as well as environmental conservation (Xin et al. 2012).

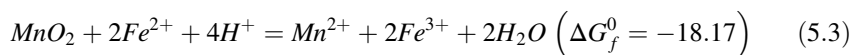
Xin et al. (2009) examined the bioleaching mechanism for metal recovery from spent Li-ion batteries by microbial consortium. The consortium was designed using a bottom-up approach, however the members of the consortia were isolated from an old mining site and initially grown independently. An iron oxidizer was grown until the formation of  $\text{Fe}^{3+}$ , a sulphur oxidizer was grown until the pH of growth media dropped below 2.0 due to production of biogenic sulphuric acid, and together those two microbes were used as inoculant for the bioleaching experiments. The combination of these two microbes was experimentally provided with different energy sources. In a two-step process, the consortium was allowed to grow first and then electrode powder from Li-ion batteries was added in the second step. Li dissolution was highest when elemental sulphur was the energy source and the lowest pH was 1.54. Li dissolution was lowest with  $\text{FeS}_2$  as the energy source and with the highest pH being 1.69. Contrary to this, Co dissolution was highest with  $\text{S} + \text{FeS}_2$  as energy source and at high pH with varied ORP. Co dissolution was lowest with elemental sulphur as energy source and unchanged ORP. These results suggested that, independent of supplied energy source, acid dissolution played a major role in Li

bioleaching, yet  $\text{Fe}^{2+}$  reduction did take part in the process.  $\text{Fe}^{2+}$  played a role in reducing insoluble  $\text{Co}^{3+}$  into soluble  $\text{Co}^{2+}$  followed by  $\text{Co}^{2+}$  release mediated by acid dissolution in presence of both  $\text{FeS}_2$  and  $\text{FeS}_2 + \text{S}$  as energy sources. The suggested mechanism was confirmed by further chemical simulation of bioleaching process.

Non-contact mechanism is predominant in the bioleaching of spent batteries, as  $\text{Fe}^{3+}$  does not play a direct role in release of metals from the spent batteries (Zhao et al. 2008b; Zhao et al. 2008a). The results of a study by Xin et al. indicated that different metal species and various energy sources influence the mechanism of bioleaching (Xin et al. 2009).

In their next studies, Xin et al. (2012) employed pure cultures and consortia of *Alicyclobacillus* sp., as sulphur oxidizer and *Sulfobacillus* sp. as iron oxidizer for recovery of metals from spent Zn-Mn batteries. In this work as well, influence of various energy sources on difference in metal recovery and mechanism was investigated. Irrespective of employed bacterial species and type of energy source provided, 96% of Zn recovery was obtained within 24. However, higher initial pH values resulted in lower Zn recovery. Zn dissolution was a result of non-contact leaching due to acid dissolution and biogenic sulphuric acid played a major role. As pH values of all the studied bioleaching systems were very low, it was enough for the Zn dissolution which is generally in the form of ZnO in the batteries and hence the type of bacteria used did not hamper the process (Sayilgan et al. 2009).

However, Mn recovery has been seen to be influenced by process parameters. Highest recovery of 97% was obtained for Mn with consortium and the use of mixed energy sources. In the case of Mn extraction, it is known that contact, non-contact, and biological leaching play roles. Contact of microbial cells with battery powder contributed to the direct bioleaching whereas a combination of acidic dissolution of soluble  $\text{Mn}^{2+}$  mediated by biogenic  $\text{H}_2\text{SO}_4$  and reductive dissolution of insoluble  $\text{Mn}^{4+}$  mediated by  $\text{Fe}^{2+}$  contributed to the non-contact bioleaching. The reason behind consortia having high Mn extraction values is that Mn usually exists as  $\text{Mn}_2\text{O}_3$  and  $\text{Mn}_3\text{O}_4$  in batteries (Sayilgan et al. 2009). Partial dissolution of  $\text{Mn}_2\text{O}_3$  and  $\text{Mn}_3\text{O}_4$  by biogenic sulphuric acids extracts  $\text{Mn}^{2+}$  and produces  $\text{Mn}^{4+}$  in the form of insoluble precipitate of  $\text{MnO}_2$ .  $\text{FeS}_2$  is utilized by iron oxidizing bacteria to produce biogenic sulphuric acid as well as biogenic  $\text{Fe}^{2+}$ . Further oxidation of  $\text{Fe}^{2+}$  to  $\text{Fe}^{3+}$  contributes in generation of chemical  $\text{Fe}^{2+}$ . Combined action of biogenic and chemical  $\text{Fe}^{2+}$  aid in the formation of soluble  $\text{Mn}^{2+}$  (Eq.5.3). Moreover, low pH of a consortia medium boosts the formation of  $\text{Fe}^{3+}$  by iron oxidizers (Xin et al. 2009).



The feasibility of bioleaching to recover valuable metals like Li, Co, Ni, and Mn from spent electric vehicle Li-ion batteries was investigated by Xin et al. (2016). In a bottom-up approach, microbial consortia of sulphur oxidizing *A. thiooxidans* (A.t.) and iron oxidizing *L. ferriphilum* (L.f.) were employed in a two-step bioleaching approach, wherein the battery powder was added after sufficient growth of the



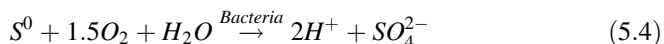
consortium. Several different aspects were considered and those were: use of different cathodes like  $\text{LiMn}_2\text{O}_4$ ,  $\text{LiFePO}_4$ , and  $\text{LiNi}_x\text{Co}_y\text{Mn}_{1-x-y}\text{O}_2$ ; treatment by pure microbial cultures versus consortia; respective energy sources (sulphur-A.t., pyrite-L.f., and MS-MC), bioleaching mechanism for resistant  $\text{LiNi}_x\text{Co}_y\text{Mn}_{1-x-y}\text{O}_2$ ; and influence of pH on the bioleaching of  $\text{LiNi}_x\text{Co}_y\text{Mn}_{1-x-y}\text{O}_2$ .

Xin et al. (2016) found that their sulphur-A.t. system showed high Li recovery with regard to the acid dissolution by biogenic acid in a non-contact mechanism. High recovery of Co, Ni, and Mn was observed for their mixed energy source-mixed culture system (MS-MC) as a result of combined action of acid dissolution and  $\text{Fe}^{2+}$  reduction in a contact mechanism. Further adjusting the pH of bioleaching medium enhanced the metal recovery from resistant  $\text{LiNi}_x\text{Co}_y\text{Mn}_{1-x-y}\text{O}_2$  reaching more than 95%, especially improving Co and Ni extraction.  $\text{LiNi}_x\text{Co}_y\text{Mn}_{1-x-y}\text{O}_2$  is to some extent resistant to bioleaching as compared to easily leachable  $\text{LiMn}_2\text{O}_4$  and  $\text{LiFePO}_4$ . Although the treatment of  $\text{LiNi}_x\text{Co}_y\text{Mn}_{1-x-y}\text{O}_2$  by consortia resulted in efficient Li and Mn recovery, it was low for Co and Ni. To overcome this hurdle, pH of the growth medium was adjusted which improved efficiency. This in turn suggested that poor microbial growth disturbed both biogenic acid production and  $\text{Fe}^{2+}/\text{Fe}^{3+}$  oxidation cycle. The factor that added to the increased pH value was the alkaline oxides or hydroxide in spent batteries that consumes more acid than usual during the leaching process. The produced biogenic sulphuric acid was not enough for this process and resulted in increased pH values hampering the growth of consortia.

The study by Xin et al. (2016) revealed that pure cultures were efficient in bioleaching of certain metals. However, they are not sufficient for recovery of several metals that require various bioleaching mechanisms acting in conjunction and in such cases microbial consortia play a vital role (Xin et al. 2016).

One of the drawbacks of using a biohydrometallurgical approach for metal recovery from wastes is the slow leaching rate. This can be improved by using thermophiles as shown in the recent study of Ghassa (Ghassa et al. 2020a). Their group studied the bioleaching of waste lithium ion batteries using a consortium of moderately thermophilic microorganisms including *A. caldus*, *L. ferriphilum*, *Sulfobacillus* spp., and *Ferroplasma* spp. provided by Sarcheshmeh Copper Complex (Ahmadi et al. 2011). Prior to the experiments, their consortium was adapted to the LIBs using a two-step adaptation process (Heydarian et al. 2018). Influence of three different additives was explored including iron scrap as a substitute for  $\text{FeSO}_4 \cdot 7\text{H}_2\text{O}$ . Addition of external sulphur ( $\text{S}^0$ ), to increase its concentration in the bioleaching environment, improved Li recovery but had no significant effect on the dissolution of Co and Ni. More sulphuric acid was produced due to increased  $\text{S}^0$  concentration (Eq. 5.4), suggesting the role of acid leaching. LIBs cathode materials,  $\text{LiCoO}_2$  and  $\text{LiNiO}_2$ , are known to dissolve in acidic environments (Wu et al. 2018). Further comparison of SEM images for bioleaching and control leaching tests by authors has shown an extremely corroded surface of particles in the bioleaching residue as compared to the smooth surface of residue in control tests. This corrosion can be attributed to either bacterial attachment to the surface and direct bioleaching, or indirect bioleaching due to reaction of bacterial metabolites, or products like

extracellular polymeric substances interacting with the surface (Watling 2006; Wang 2018).



Furthermore, addition of  $FeSO_4 \cdot 7H_2O$  increased Co recovery as well as leaching kinetics significantly, where  $Fe^{2+}$  acted as reducing agent improving Co recovery. During 2 days of bioleaching in presence of  $FeSO_4 \cdot 7H_2O$ , 99.9% Co, 99.7% Ni, and 84% Li were recovered (Ghassa et al. 2020a). In addition, high leaching kinetics of the process can be associated with increased process temperature as a result of employing thermophilic microorganisms. As suggested by Valdes et al. (2008), ferrous ions act as an electron donor and thus increase the metabolism of acidophiles in the consortium. Chemically, these ferrous ions act as reducing agent and increased metal dissolution from LIBs, especially Co (Ghassa et al. 2020b). A previous study from this group (Ghassa et al. 2020b) showed increased Li leaching by ferrous ions due to removal of an unsolvable Co layer from the surface and concurrent increase in reagent diffusion to Li atoms. Similarly, increase in Co dissolution consequently increased Ni dissolution due to increase in reagent diffusion (Ghassa et al. 2020b).

Furthermore, having an iron source replaced with iron scrap was a cost-effective approach, which increased the leaching time by 4 days (Ghassa et al. 2020a). In this process, iron from the scraps is dissolved in sulphuric acid producing  $FeSO_4$  which then aids Co dissolution. Formation of a jarosite layer on the surface of scrap particles can hamper the release of ferrous ions. Oxidization of scrap particles becomes favoured over LIBs particles by microorganisms seeking to release the necessary ferrous ions, and thus increasing the leaching time. Results of bioleaching and leaching tests have revealed that acid leaching resulted in dissolution of Li and oxidation–reduction reactions dissolved Co, whereas Ni was dissolved due to direct bioleaching mechanism (Ghassa et al. 2020a). Here again, symbiotic mutual relationships in the consortium can be enhanced by external factors like nutrient source as well as temperature (Ghassa et al. 2020a).

#### 5.5.1.4 Electroplating Sludge

Another type of industrial waste is an electroplating sludge which is generated by electroplating processes that are widely used including technological and decorative applications (Zhou et al. 2018). Large volumes of wastewater containing various heavy metals is generated during these processes (Yue et al. 2019). Treatment of these wastewaters for removing their metals results in precipitate formation thereby producing the secondary waste which is termed electroplating sludge (Scarazzato et al. 2017). These efforts at reducing the toxicity of treatment effluents by means of precipitation procedures nevertheless make this sludge waste more complex as now it contains the mixture of metal species which are not usually present in ores, thereby making it difficult to process (Twidwell and Dahnke 2001).

In a very interesting study, bioleaching of electroplating sludge was carried out on a semi-pilot scale using consortium of moderately thermophilic acidophiles (Zhou et al. 2019). Consortium used for that project was assembled in a bottom-up approach, and consisted of *L. ferriphilum* CS13, *A. caldus* S2 and *Sulfobacillus acidophilus* CS5. In a first step of that process, the consortium was cultivated to obtain a biological suspension in a bioreactor. In the next step, this suspension was mixed with the sludge in a stirred tank reactor for the bioleaching process. The microbial suspension was able to leach metals efficiently at pH 1.5, 45 °C temperature, 40% bacterial liquid ratio, 4:1 l/kg, and 5 h leaching time. Dividing the process into two steps, microbial cultivation as a first step and then bioleaching as a second step prevented the toxic effect of sludge and particle shear force from being deleterious upon the microbial growth. Comparison of chemical and biological leaching revealed the combined effect of ferric iron and microorganisms (Zhou et al. 2019).

In a different approach, Zhang et al. (2020) used a two-step bioleaching method to recover metals from an electroplating sludge using a bottom-up approach for the construction of microbial consortia. Various known strains like *A. ferrooxidans*, *A. thiooxidans*, *A. ferrivorans*, *A. caldus*, *L. ferriphilum*, *Sulfobacillus* sp. TPY, *Ferroplasma thermophilum*, *Acidiplasma cupricumulans*, and *Acidiphilium* were grown in the presence of electroplating wastewater and sludge. This mixture was further enriched and adapted in the presence of increasing concentration of electroplating sludge to increase the metal tolerance. Population analysis of consortia after that adaptation process showed the dominance of *A. ferrooxidans* followed by *Acidiphilium* sp. and small amounts of *A. ferrivorans* and *A. thiooxidans*. In a two-step leaching process, electroplating sludge was added to the bioleaching medium after growth of the microbial consortium. Recovery of Cu, Ni, Zn, and Cr was investigated while studying the influence of various process parameters like bulk pH, pulp density, and  $\text{Fe}^{2+}$  concentration. Comparison of chemical leaching and bioleaching revealed the superior performance of consortia and hence bioleaching. Consortia played a crucial role in dissolution of metals from the residual fraction by both contact and non-contact leaching mechanisms. Biogenic acid provided protons that not only aided in the recovery of target metals but also avoided Fe precipitation that would have otherwise hampered the bioleaching efficiency.  $\text{H}^+$  ions were primarily responsible for recovery of Cu, Ni, and Zn present in the acid soluble fraction and Fe and Mn oxyhydroxides in bound fractions. Further Cr recovery was due to the combinatorial actions of  $\text{H}^+$ ,  $\text{Fe}^{3+}$ , and microorganisms. Optimized conditions with bulk pH 2.0,  $\text{Fe}^{2+}$  concentration of 9 g/l and 15% (w/v) pulp density resulted in recovery of more than 95% Cu, Zn, and Ni and nearly 90% Cr (Zhang et al. 2020).

Chemical leaching and bioleaching using microbial consortium were used for recovery of Cu from Cu containing electroplating sludge by Sun et al. (2021). The defined consortium was developed in a bottom-up approach and was composed of iron oxidizing, sulphur oxidizing as well as iron and sulphur oxidizing microorganisms like *Leptospirillum ferriphilum* CS13, *At. caldus* S2, and *Sulfobacillus acidophilus* TPY. The pure cultures were first acclimatized in order to improve the

metal tolerance and used later to construct the consortium. Bioleaching showed higher leaching efficiency of 94.3% on 7th day as compared to chemical leaching using sulphuric acid, which was lower than 21.1% that of bioleaching. Further significant change in surface morphology of the sludge was observed through SEM and EDX. Not only was the amount of residual Cu in the bioleached sludge very much less, but the leached residue was also considered to be non-hazardous after the Toxicity Characteristic leaching Procedure (TCLP) test. High bioleaching efficiency could be attributed to the combined metabolic functionalities of the members involved in the consortia. Biogenic ferric iron generated by oxidation of ferrous iron and conversion of elemental sulphur to biogenic sulphuric acid by consortium enhanced the metal dissolution rate (Sun et al. 2021).

## 5.6 Conclusion and Future Outlook

Characteristics like robustness and broad metabolic capacities of the microbial consortia are attractive for applications in environmental biotechnology. Microbial consortia will support the movement towards green and circular economy. The best approach to enhance the metal recovery from industrial waste not only depends on the type, complexity, and toxicity of the waste but also the approach used for leaching. Further combinatorial approaches as well as use of advanced bioinformatics and metabolic modelling can be consolidated to help and improve the designing of stable microbial consortia. A top-down approach for consortia design should be employed when the output and stability of the consortia are the main focus as compared to control over individual members of consortia, whereas a bottom-up approach should be considered when the ability to manipulate and emphasize control over the individual members is required. Also, the limited knowledge of intercellular communications and exchange, change in the structure of microbial population, and culture conditions over time, etc., may still hinder the success of consortia after the construction and over the course of time. To overcome this scenario of hindrance, studies with respect to deciphering the mechanisms of interactions within the consortia, and developments of predictable computational models, etc., are necessary.

Though microbial consortia are known to perform well as compared to pure cultures, their use for bioleaching is not yet established for application at an industrial scale in a cost-efficient way. Microbiome engineering is one of the recent approaches that is being investigated in order to improve the utilization or embrace fully the potential of consortia in different fields. In this approach, naturally occurring microbial communities are manipulated or synthetic communities are constructed in a way so as to provide specific function. This could be a promising and innovative approach to employ in the bioleaching of industrial wastes.

**Acknowledgement** Mital Chakankar thankfully acknowledges the European Commission for the Marie-Curie Individual fellowship on 'BioFlot' project (Project number 841437).

## References

- Ahmadi A, Schaffie M, Petersen J, Schippers A, Ranjbar M (2011) Conventional and electrochemical bioleaching of chalcopyrite concentrates by moderately thermophilic bacteria at high pulp density. *Hydrometallurgy* 106(1):84–92. <https://doi.org/10.1016/j.hydromet.2010.12.007>
- Baniasadi M, Vakilchah F, Bahaloo-Horeh N, Mousavi SM, Farnaud S (2019) Advances in bioleaching as a sustainable method for metal recovery from e-waste: a review. *J Ind Eng Chem* 76:75–90. <https://doi.org/10.1016/j.jiec.2019.03.047>
- Bas AD, Deveci H, Yazici EY (2013) Bioleaching of copper from low grade scrap TV circuit boards using mesophilic bacteria. *Hydrometallurgy* 138:65–70. <https://doi.org/10.1016/j.hydromet.2013.06.015>
- Bayat B, Sari B (2010) Comparative evaluation of microbial and chemical leaching processes for heavy metal removal from dewatered metal plating sludge. *J Hazard Mater* 174(1):763–769. <https://doi.org/10.1016/j.jhazmat.2009.09.117>
- Brandl H, Bosshard R, Wegmann M (2001) Computer-munching microbes: metal leaching from electronic scrap by bacteria and fungi. *Hydrometallurgy* 59(2):319–326. [https://doi.org/10.1016/S0304-386X\(00\)00188-2](https://doi.org/10.1016/S0304-386X(00)00188-2)
- Brandl H, Lehmann S, Faramarzi MA, Martinelli D (2008) Biomobilization of silver, gold, and platinum from solid waste materials by HCN-forming microorganisms. *Hydrometallurgy* 94(1): 14–17. <https://doi.org/10.1016/j.hydromet.2008.05.016>
- Brenner K, You L, Arnold FH (2008) Engineering microbial consortia: a new frontier in synthetic biology. *Trends Biotechnol* 26(9):483–489. <https://doi.org/10.1016/j.tibtech.2008.05.004>
- Burgstaller W, Schinner F (1993) Leaching of metals with fungi. *J Biotechnol* 27(2):91–116. [https://doi.org/10.1016/0168-1656\(93\)90101-R](https://doi.org/10.1016/0168-1656(93)90101-R)
- Eng A, Borenstein E (2019) Microbial community design: methods, applications, and opportunities. *Curr Opin Biotechnol* 58:117–128. <https://doi.org/10.1016/j.copbio.2019.03.002>
- Ghassa S, Farzanegan A, Gharabaghi M, Abdollahi H (2020a) Novel bioleaching of waste lithium ion batteries by mixed moderate thermophilic microorganisms, using iron scrap as energy source and reducing agent. *Hydrometallurgy* 197:105465. <https://doi.org/10.1016/j.hydromet.2020.105465>
- Ghassa S, Farzanegan A, Gharabaghi M, Abdollahi H (2020b) The reductive leaching of waste lithium ion batteries in presence of iron ions: process optimization and kinetics modelling. *J Clean Prod* 262:121312. <https://doi.org/10.1016/j.jclepro.2020.121312>
- Giaveno A, Donati EJPB (2001) Bioleaching of heazlewoodite by *Thiobacillus* spp. *Process Biochem* 36:955–962
- Gu T, Rastegar SO, Mousavi SM, Li M, Zhou M (2018) Advances in bioleaching for recovery of metals and bioremediation of fuel ash and sewage sludge. *Bioresour Technol* 261:428–440. <https://doi.org/10.1016/j.biortech.2018.04.033>
- Guezennec A-G, Joulain C, Jacob J, Archane A, Ibarra D, de Buyer R, Bodéan F, d'Hugues P (2017) Influence of dissolved oxygen on the bioleaching efficiency under oxygen enriched atmosphere. *Miner Eng* 106:64–70. <https://doi.org/10.1016/j.mineng.2016.10.016>
- Gurung A, Chakraborty R (2009) The role of *Acidithiobacillus ferrooxidans* in alleviating the inhibitory effect of thiosulfate on the growth of acidophilic *Acidiphilium* species isolated from acid mine drainage samples from Gorubathan, India. *Can J Microbiol* 55(9):1040–1048. <https://doi.org/10.1139/w09-062>
- Hays SG, Patrick WG, Ziesack M, Oxman N, Silver PA (2015) Better together: engineering and application of microbial symbioses. *Curr Opin Biotechnol* 36:40–49. <https://doi.org/10.1016/j.copbio.2015.08.008>
- Heydarian A, Mousavi SM, Vakilchah F, Baniasadi M (2018) Application of a mixed culture of adapted acidophilic bacteria in two-step bioleaching of spent lithium-ion laptop batteries. *J Power Sources* 378:19–30. <https://doi.org/10.1016/j.jpowsour.2017.12.009>

- Hocheng H, Chang J-H, Jadhav UU (2012) Micromachining of various metals by using *Acidithiobacillus ferrooxidans* 13820 culture supernatant experiments. *J Clean Prod* 20(1): 180–185. <https://doi.org/10.1016/j.jclepro.2011.07.019>
- Hubau A, Minier M, Chagnes A, Jouliau C, Perez C, Guezennec AG (2018) Continuous production of a biogenic ferric iron lixiviant for the bioleaching of printed circuit boards (PCBs). *Hydrometallurgy* 180:180–191
- Hubau A, Minier M, Chagnes A, Jouliau C, Silvente C, Guezennec A-G (2020) Recovery of metals in a double-stage continuous bioreactor for acidic bioleaching of printed circuit boards (PCBs). *Sep Purif Technol* 238. <https://doi.org/10.1016/j.seppur.2019.116481>
- Ibrar M, Zhang H (2020) Construction of a hydrocarbon-degrading consortium and characterization of two new lipopeptides biosurfactants. *Sci Total Environ* 714:136400. <https://doi.org/10.1016/j.scitotenv.2019.136400>
- Ilyas S, Anwar MA, Niazi SB, Afzal Ghauri M (2007) Bioleaching of metals from electronic scrap by moderately thermophilic acidophilic bacteria. *Hydrometallurgy* 88(1):180–188. <https://doi.org/10.1016/j.hydromet.2007.04.007>
- Ilyas S, Ruan C, Bhatti HN, Ghauri MA, Anwar MA (2010) Column bioleaching of metals from electronic scrap. *Hydrometallurgy* 101(3):135–140. <https://doi.org/10.1016/j.hydromet.2009.12.007>
- Ilyas S, Lee J-c, Chi R-a (2013) Bioleaching of metals from electronic scrap and its potential for commercial exploitation. *Hydrometallurgy* 131-132:138–143. <https://doi.org/10.1016/j.hydromet.2012.11.010>
- Ilyas S, Lee J-c, Kim B-s (2014) Bioremoval of heavy metals from recycling industry electronic waste by a consortium of moderate thermophiles: process development and optimization. *J Clean Prod* 70:194–202. <https://doi.org/10.1016/j.jclepro.2014.02.019>
- Ilyas S, Srivastava RR, Kim H, Das S, Singh VK (2021) Circular bioeconomy and environmental benignness through microbial recycling of e-waste: a case study on copper and gold restoration. *Waste Manag* 121:175–185. <https://doi.org/10.1016/j.wasman.2020.12.013>
- Isildar A, van de Vossenberg J, Rene ER, van Hullebusch ED, Lens PN (2016) Two-step bioleaching of copper and gold from discarded printed circuit boards (PCB). *Waste Manag* 57:149–157. <https://doi.org/10.1016/j.wasman.2015.11.033>
- Jadhav U, Hocheng H (2013) Extraction of silver from spent silver oxide–zinc button cells by using *Acidithiobacillus ferrooxidans* culture supernatant. *J Clean Prod* 44:39–44. <https://doi.org/10.1016/j.jclepro.2012.11.035>
- Jensen AB, Webb C (1995) Ferrous sulphate oxidation using thiobacillus ferrooxidans: a review. *Process Biochem* 30(3):225–236. [https://doi.org/10.1016/0032-9592\(95\)85003-1](https://doi.org/10.1016/0032-9592(95)85003-1)
- Kato S, Haruta S, Cui ZJ, Ishii M, Igarashi Y (2005) Stable coexistence of five bacterial strains as a cellulose-degrading community. *Appl Environ Microbiol* 71(11):7099–7106. <https://doi.org/10.1128/AEM.71.11.7099-7106.2005>
- Keller L, Surette MG (2006) Communication in bacteria: an ecological and evolutionary perspective. *Nat Rev Microbiol* 4(4):249–258. <https://doi.org/10.1038/nrmicro1383>
- Latorre M, Cortés MP, Travisany D, Di Genova A, Budinich M, Reyes-Jara A, Hödar C, González M, Parada P, Bobadilla-Fazzini RA, Cambiazo V, Maass A (2016) The bioleaching potential of a bacterial consortium. *Bioresour Technol* 218:659–666. <https://doi.org/10.1016/j.biortech.2016.07.012>
- Lee J-c, Pandey BD (2012) Bio-processing of solid wastes and secondary resources for metal extraction – a review. *Waste Manag* 32(1):3–18. <https://doi.org/10.1016/j.wasman.2011.08.010>
- Lee J-c, Song HT, Yoo J-M (2007) Present status of the recycling of waste electrical and electronic equipment in Korea. *Resour Conserv Recycl* 50(4):380–397. <https://doi.org/10.1016/j.resconrec.2007.01.010>
- Liang G, Tang J, Liu W, Zhou Q (2013) Optimizing mixed culture of two acidophiles to improve copper recovery from printed circuit boards (PCBs). *J Hazard Mater* 250-251:238–245. <https://doi.org/10.1016/j.jhazmat.2013.01.077>

- Marhual NP, Pradhan N, Kar RN, Sukla LB, Mishra BK (2008) Differential bioleaching of copper by mesophilic and moderately thermophilic acidophilic consortium enriched from same copper mine water sample. *Bioresour Technol* 99(17):8331–8336. <https://doi.org/10.1016/j.biortech.2008.03.003>
- Nan J, Han D, Zuo X (2005) Recovery of metal values from spent lithium-ion batteries with chemical deposition and solvent extraction. *J Power Sources* 152:278–284. <https://doi.org/10.1016/j.jpowsour.2005.03.134>
- Nemati M, Harrison STL, Hansford GS, Webb C (1998) Biological oxidation of ferrous sulphate by *Thiobacillus ferrooxidans*: a review on the kinetic aspects. *Biochem Eng J* 1(3):171–190. [https://doi.org/10.1016/S1369-703X\(98\)00006-0](https://doi.org/10.1016/S1369-703X(98)00006-0)
- Oggerin M, Tornos F, Rodríguez N, del Moral C, Sánchez-Román M, Amils R (2013) Specific jarosite biomineralization by *Purpureocillium lilacinum*, an acidophilic fungi isolated from Río Tinto. *Environ Microbiol* 15(8):2228–2237. <https://doi.org/10.1111/1462-2920.12094>
- Oggerin M, Rodríguez N, del Moral C, Amils R (2014) Fungal jarosite biomineralization in Río Tinto. *Res Microbiol* 165(9):719–725. <https://doi.org/10.1016/j.resmic.2014.10.001>
- Peng XN, Gilmore SP, O'Malley MA (2016) Microbial communities for bioprocessing: lessons learned from nature. *Curr Opin Chem Eng* 14:103–109. <https://doi.org/10.1016/j.coche.2016.09.003>
- Pradhan JK, Kumar S (2012) Metals bioleaching from electronic waste by *Chromobacterium violaceum* and pseudomonads sp. *Waste Manag Res* 30(11):1151–1159. <https://doi.org/10.1177/0734242X12437565>
- Qian X, Chen L, Sui Y, Chen C, Zhang W, Zhou J, Dong W, Jiang M, Xin F, Ochsenreither K (2020) Biotechnological potential and applications of microbial consortia. *Biotechnol Adv* 40:107500. <https://doi.org/10.1016/j.biotechadv.2019.107500>
- Rastegar SO, Mousavi SM, Shojaosadati SA (2014) Cr and Ni recovery during bioleaching of dewatered metal-plating sludge using *Acidithiobacillus ferrooxidans*. *Bioresour Technol* 167:61–68. <https://doi.org/10.1016/j.biortech.2014.05.107>
- Rebello S, Anoopkumar AN, Aneesh EM, Sindhu R, Binod P, Kim SH, Pandey A (2021) Hazardous minerals mining: challenges and solutions. *J Hazard Mater* 402:123474. <https://doi.org/10.1016/j.jhazmat.2020.123474>
- Rezza I, Salinas E, Elorza M, Sanz de Tosetti M, Donati E (2001) Mechanisms involved in bioleaching of an aluminosilicate by heterotrophic microorganisms. *Process Biochem* 36(6):495–500. [https://doi.org/10.1016/S0032-9592\(00\)00164-3](https://doi.org/10.1016/S0032-9592(00)00164-3)
- Rosero-Chasoy G, Rodriguez-Jasso RM, Aguilar CN, Buitron G, Chairez I, Ruiz HA (2021) Microbial co-culturing strategies for the production high value compounds, a reliable framework towards sustainable biorefinery implementation - an overview. *Bioresour Technol* 321:124458. <https://doi.org/10.1016/j.biortech.2020.124458>
- Sayilgan E, Kukrer T, Civelekoglu G, Ferella F, Akcil A, Veglio F, Kitis M (2009) A review of technologies for the recovery of metals from spent alkaline and zinc-carbon batteries. *Hydrometallurgy* 97(3):158–166. <https://doi.org/10.1016/j.hydromet.2009.02.008>
- Scarazzato T, Panossian Z, Tenório JAS, Pérez-Herranz V, Espinosa DCR (2017) A review of cleaner production in electroplating industries using electrodialysis. *J Clean Prod* 168:1590–1602. <https://doi.org/10.1016/j.jclepro.2017.03.152>
- Stuedel R (1989) On the nature elemental sulfur (S<sub>0</sub>) reduced by sulfur-oxidizing bacteria e a model for S<sub>0</sub> globules. In: Schlegel HG, Bowien B (eds) *Autotrophic bacteria*. Science Technology Publishers, Madison, WI, pp 289–303
- Sun S, Jin C, He W, Li G, Zhu H, Huang J (2021) Management status of waste lithium-ion batteries in China and a complete closed-circuit recycling process. *Sci Total Environ* 776:145913. <https://doi.org/10.1016/j.scitotenv.2021.145913>
- Tsoi R, Dai Z, You L (2019) Emerging strategies for engineering microbial communities. *Biotechnol Adv* 37(6):107372. <https://doi.org/10.1016/j.biotechadv.2019.03.011>
- Twidwell LG, Dahnke DR (2001) Treatment of metal finishing sludge for detoxification and metal value. *Eur J Miner Process Environ Prot* 1:76–88

- Valdés J, Pedroso I, Quatrini R, Dodson RJ, Tettelin H, Blake R, Eisen JA, Holmes DS (2008) *Acidithiobacillus ferrooxidans* metabolism: from genome sequence to industrial applications. *BMC Genomics* 9(1):597. <https://doi.org/10.1186/1471-2164-9-597>
- Velázquez-Martínez O, Valio J, Santasalo-Aarnio A, Reuter M, Serna-Guerrero R (2019) A critical review of lithium-ion battery recycling processes from a circular economy perspective. *Batteries* 5:68
- Wang J (2018) Reuse of heavy metal from industrial effluent water. *IOP Conference Series: Earth and Environmental Science* 199. <https://doi.org/10.1088/1755-1315/199/4/042002>
- Wang J, Zhao H-b, Zhuang T, Qin W-q, Zhu S, Qiu G-z (2013) Bioleaching of Pb–Zn–Sn chalcopyrite concentrate in tank bioreactor and microbial community succession analysis. *Trans Nonferrous Metals Soc China* 23(12):3758–3762. [https://doi.org/10.1016/S1003-6326\(13\)62926-X](https://doi.org/10.1016/S1003-6326(13)62926-X)
- Watling HR (2006) The bioleaching of sulphide minerals with emphasis on copper sulphides — a review. *Hydrometallurgy* 84(1):81–108. <https://doi.org/10.1016/j.hydromet.2006.05.001>
- Watling HR, Perrot FA, Shiers DW (2008) Comparison of selected characteristics of *Sulfobacillus* species and review of their occurrence in acidic and bioleaching environments. *Hydrometallurgy* 93(1):57–65. <https://doi.org/10.1016/j.hydromet.2008.03.001>
- Wu W, Liu X, Zhang X, Zhu M, Tan W (2018) Bioleaching of copper from waste printed circuit boards by bacteria-free cultural supernatant of iron–sulfur-oxidizing bacteria. *Bioresources and Bioprocessing* 5(1):10. <https://doi.org/10.1186/s40643-018-0196-6>
- Xia L-x, Liu J-s, Xiao L, Zeng J, Li B-m, Geng M-m, Qiu G-z (2008) Single and cooperative bioleaching of sphalerite by two kinds of bacteria—*Acidithiobacillus ferrooxidans* and *Acidithiobacillus thiooxidans*. *Trans Nonferrous Metals Soc China* 18(1):190–195. [https://doi.org/10.1016/S1003-6326\(08\)60034-5](https://doi.org/10.1016/S1003-6326(08)60034-5)
- Xia MC, Wang YP, Peng TJ, Shen L, Yu RL, Liu YD, Chen M, Li JK, Wu XL, Zeng WM (2017) Recycling of metals from pretreated waste printed circuit boards effectively in stirred tank reactor by a moderately thermophilic culture. *J Biosci Bioeng* 123(6):714–721. <https://doi.org/10.1016/j.jbiosc.2016.12.017>
- Xia M, Bao P, Liu A, Wang M, Shen L, Yu R, Liu Y, Chen M, Li J, Wu X, Qiu G, Zeng W (2018) Bioleaching of low-grade waste printed circuit boards by mixed fungal culture and its community structure analysis. *Resour Conserv Recycl* 136:267–275. <https://doi.org/10.1016/j.resconrec.2018.05.001>
- Xiang Y, Wu P, Zhu N, Zhang T, Liu W, Wu J, Li P (2010) Bioleaching of copper from waste printed circuit boards by bacterial consortium enriched from acid mine drainage. *J Hazard Mater* 184(1):812–818. <https://doi.org/10.1016/j.jhazmat.2010.08.113>
- Xin B, Zhang D, Zhang X, Xia Y, Wu F, Chen S, Li L (2009) Bioleaching mechanism of Co and Li from spent lithium-ion battery by the mixed culture of acidophilic sulfur-oxidizing and iron-oxidizing bacteria. *Bioresour Technol* 100(24):6163–6169. <https://doi.org/10.1016/j.biortech.2009.06.086>
- Xin B, Jiang W, Aslam H, Zhang K, Liu C, Wang R, Wang Y (2012) Bioleaching of zinc and manganese from spent Zn–Mn batteries and mechanism exploration. *Bioresour Technol* 106:147–153. <https://doi.org/10.1016/j.biortech.2011.12.013>
- Xin Y, Guo X, Chen S, Wang J, Wu F, Xin B (2016) Bioleaching of valuable metals Li, Co, Ni and Mn from spent electric vehicle Li-ion batteries for the purpose of recovery. *J Clean Prod* 116:249–258
- Yue Y, Zhang J, Sun F, Wu S, Pan Y, Zhou J, Qian G (2019) Heavy metal leaching and distribution in glass products from the co-melting treatment of electroplating sludge and MSWI fly ash. *J Environ Manag* 232:226–235. <https://doi.org/10.1016/j.jenvman.2018.11.053>
- Zeng W, Qiu G, Zhou H, Peng J, Chen M, Tan SN, Chao W, Liu X, Zhang Y (2010) Community structure and dynamics of the free and attached microorganisms during moderately thermophilic bioleaching of chalcopyrite concentrate. *Bioresour Technol* 101(18):7079–7086. <https://doi.org/10.1016/j.biortech.2010.04.003>



- Zhang L, Zhou W, Liu Y, Jia H, Zhou J, Wei P, Zhou H (2020) Bioleaching of dewatered electroplating sludge for the extraction of base metals using an adapted microbial consortium: process optimization and kinetics. *Hydrometallurgy* 191:105227. <https://doi.org/10.1016/j.hydromet.2019.105227>
- Zhao L, Yang D, Zhu N-W (2008a) Bioleaching of spent Ni–Cd batteries by continuous flow system: effect of hydraulic retention time and process load. *J Hazard Mater* 160(2):648–654. <https://doi.org/10.1016/j.jhazmat.2008.03.048>
- Zhao L, Zhu N-W, Wang X-H (2008b) Comparison of bio-dissolution of spent Ni–Cd batteries by sewage sludge using ferrous ions and elemental sulfur as substrate. *Chemosphere* 70(6): 974–981. <https://doi.org/10.1016/j.chemosphere.2007.08.011>
- Zhou H-B, Zeng W-M, Yang Z-F, Xie Y-J, Qiu G-Z (2009) Bioleaching of chalcopyrite concentrate by a moderately thermophilic culture in a stirred tank reactor. *Bioresour Technol* 100(2): 515–520. <https://doi.org/10.1016/j.biortech.2008.06.033>
- Zhou C, Ge S, Yu H, Zhang T, Cheng H, Sun Q, Xiao R (2018) Environmental risk assessment of pyrometallurgical residues derived from electroplating and pickling sludges. *J Clean Prod* 177: 699–707. <https://doi.org/10.1016/j.jclepro.2017.12.285>
- Zhou W, Zhang L, Peng J, Ge Y, Tian Z, Sun J, Cheng H, Zhou H (2019) Cleaner utilization of electroplating sludge by bioleaching with a moderately thermophilic consortium: a pilot study. *Chemosphere* 232:345–355. <https://doi.org/10.1016/j.chemosphere.2019.05.185>
- Zhu N, Xiang Y, Zhang T, Wu P, Dang Z, Li P, Wu J (2011) Bioleaching of metal concentrates of waste printed circuit boards by mixed culture of acidophilic bacteria. *J Hazard Mater* 192(2): 614–619. <https://doi.org/10.1016/j.jhazmat.2011.05.062>

# Chapter 6

## Molecular Mechanisms that Mediate Microbial Synthesis of Metal Nanoparticles



Ankit Banik, Meyappan Vadivel, Moumita Mondal,  
and Natarajan Sakthivel

**Abstract** Microbe-assisted synthesis of nanoparticles is a promising approach that provides a green, rapid, and ecologically sound strategy to fabricate potentially biogenic nanoparticles. These nanoparticles possess innate physicochemical and optoelectronic properties that render them effective in various fields of technology including biomedical, industrial, cosmetics, textiles, agricultural as well as in drug delivery. Biological synthesis routes employ various microbes such as bacteria, viruses, yeasts, actinomycetes, and fungi for the synthesis of different nanoparticles such as silver, gold, silicon, iron, zinc, platinum, and palladium. Microbial flora can generate metallic nanoparticles by either intracellular or extracellular synthesis routes. The future challenges include optimal production of nanoparticles with minimization of generation time and preferred nanoparticle structural attributes. Thus, comprehending the underlying cellular and biochemical synthesis mechanisms is imperative to designing tailor-made processes for generating optimized nanoparticles. A goal is that enhanced large-scale production and possible industrial exploitation of these generative processes will become possible. This chapter provides insights on the molecular mechanisms that encompass enzymatic and nonenzymatic production of different types of nanoparticles along with the physicochemical factors involved in the process.

### 6.1 Introduction

Intensive research and exploration of new applicability of nanomaterials with technological innovations have opened gates to successful nanotechnology. It involves creating particles that belong to the order of 100 nm or less (Thakkar et al. 2010). Nanoparticles with specific size, shape, different compositions, and other important features have wide application in various fields such as agriculture, food, medicine, and in environment (Oza et al. 2012).

---

A. Banik · M. Vadivel · M. Mondal · N. Sakthivel (✉)  
Department of Biotechnology, School of Life Sciences, Pondicherry University, Kalapet,  
Puducherry, India

Nanoparticles can be synthesized chemically, or by biological sources such as microbes or plants. Nanoparticles synthesized through the use of biogenic enzymatic processes have been found to be better than those created by chemical methods in several ways. These include elimination of expensive chemicals and hazardous toxic wastes, creation of particles with potentially higher catalytic activity, and the greater specific surface area of the particles produced by microbes (Bhattacharya and Mukherjee 2008; Simkiss and Wilbur 2012). This green synthesis route is efficient, clean, and economical. Microbial nanoparticle synthesis takes place when the microbes collect certain metallic ions from the surroundings and then convert those into elemental metal forms by processes like cellular enzymatic activities. Among the groups of microbes, several bacteria, fungi, actinomycetes, yeast, and viruses have been exploited for nanoparticle synthesis and this route is categorized as a bottom-up process (Narayanan and Sakthivel 2010). Nanoparticle synthesis can be also grouped into extracellular and intracellular processes on the basis of location where the particles are produced (Simkiss and Wilbur 2012; Mann 2001). The extracellular mechanisms involve capturing metal ions on the cellular surface via enzymatic reduction, while the intracellular mechanisms involve ion mobilization inside the microbial cell to synthesize nanoparticles with the help of specific enzymes (Zhang et al. 2011). Various factors such as reaction time, pH, temperature, concentration of salt, and biomass affect the biosynthesis process.

Varying the unique physicochemical properties can be accomplished, with nanoparticles being tuned to optimum applicability owing to their catalytic, optoelectronic, magnetic, and chemical properties (Hulkoti and Taranath 2014). These nanoparticles have found their utility in fields of agriculture, pharmaceuticals, food industry, electronics, cosmetics, environmental health, and optics (Kumar et al. 2019). This chapter is focused on the factors involved and the mechanistic aspects for the biosynthesis of various types of metal nanoparticles such as silver (Ag), gold (Au), silicon (Si), titanium (Ti), zinc (Zn), palladium (Pd), platinum (Pt), cadmium (Cd), and iron (Fe).

## 6.2 Factors Responsible for the Synthesis of Nanoparticles

Various factors are involved in the control and manipulation of the microbial synthesis of metallic nanoparticles. Some of the parameter values that need to be optimized during the synthesis of nanoparticles include pH, temperature, pressure, time, and the surrounding environment which influence the composition of the capping and shape of nanoparticles (Ajayan 2004; Somorjai and Park 2008).

### 6.2.1 pH

The pH is a critical factor that needs to be optimized for better synthesis of nanoparticles. The pre-solution state of the nanoparticle formulation requires an optimum pH set up for the desired texture and size of the nanoparticle (Gardea-Torresdey et al. 1999; Armendariz et al. 2004). Previous studies reported that variation in the size of silver nanoparticles (AgNPs) using *Chrysosporium tropicum* and *Fusarium oxysporum* could be obtained by conferring different pH levels to the pre-solution (Soni and Prakash 2011). In another report, it was also observed that a decrease in pH resulted in increased absorption and bigger-sized nanoparticles (Prakash et al. 2011).

### 6.2.2 Temperature

The temperature is one of the factors that play an imperative role in the formation of nanoparticles. Optimum temperature is needed for the desirable synthesis of nanoparticles. While the other routes of synthesis of the nanoparticles require temperature conditions to be above 100 °C, the microbial pathway for the same is best achieved at a temperature preferably much lower than 100 °C. One example of this is that Rai et al. (2006) reported the temperature maintained in solution media affected the morphology of synthesized nanoparticles (Rai et al. 2006). Broadening of SPR peak of nanoparticles at low temperatures indicated the formation of bigger-sized nanoparticles and vice versa as identified from several reports (Vanaja et al. 2013).

### 6.2.3 Pressure

The morphological properties of the nanoparticles are greatly influenced by the imposed pressure on the solution media (Pandey 2012). Previous reports suggested that microbial synthesis was much more rapid at optimum pressure conditions (Tran and Le 2013).

### 6.2.4 Time

Time and tide wait for none. But here, for the desirable synthesis of the nanoparticles, the time has to wait or rather the duration of the time utilized for the reaction mechanism to synthesize the nanoparticles, majorly affects the type and the quality of the nanoparticles (Darroudi et al. 2011). Time variations have been

highly influential in determining the formation of nanoparticles in aggregate form, expanded or shrunk form (Baer 2011). Instances have been seen where microbes belonging to a cyanobacterial group, like *Cylindrospermum stagnale* successfully were utilized for the synthesis of AgNPs. The size of the produced nanoparticles showed variations from 38 to 88 nm as temperature conditions were modulated and synthesis time was varied from 30 hours to 360 hours (Husain et al. 2015).

### **6.2.5 Environment**

The surrounding environmental conditions have a vital role to play in deciding the morphological features of the formed nanoparticles. These nanoparticles can form clusters by utilizing the components in the surrounding habitat as their substrates and, after that, undergo different reactions (Sarathy et al. 2008; Lynch et al. 2007). The surrounding conditions also have an impact on the physical chemistry of the nanoparticles. Previously it was reported that *Lysinibacillus sphaericus* was involved in bio-remediating uranium contamination through the activity of proteins found in the S-layer of its cellular walls. This S-layer was majorly found to be responsible for adhering to the heavy metal ions from the surrounding environment and transforming those ions into elemental forms (Pollmann et al. 2006).

### **6.2.6 Other Factors**

Various microbes are known to release secondary metabolites that reduce the metal ions to nanoparticles and provide stability or capping to them. Also, the metabolites secreted into the medium have different components such as enzymes, ions, and polysaccharides, which may assist in the synthesis of nanoparticles (Park et al. 2011). Concentration of metal ions also plays an important role in optimization of synthesis (Mondal et al. 2021). Employing photo-irradiation, microwave (Manikprabhu and Lingappa 2013), gamma-irradiation (El-Sayyad et al. 2018) also aid in microbial extracellular synthesis.

## **6.3 Localization of the Synthesis of Nanoparticles**

Microbes produce nanoparticles either intra- or extracellularly and the synthesis mechanism is different with different biological agents. The synthesis routes are largely mediated by enzymes, sugars, proteins, and other biomolecules that participate in the bioreduction of metal salts to nanoparticles. A rough outline of this process has been formulated as presented in Fig. 6.1.

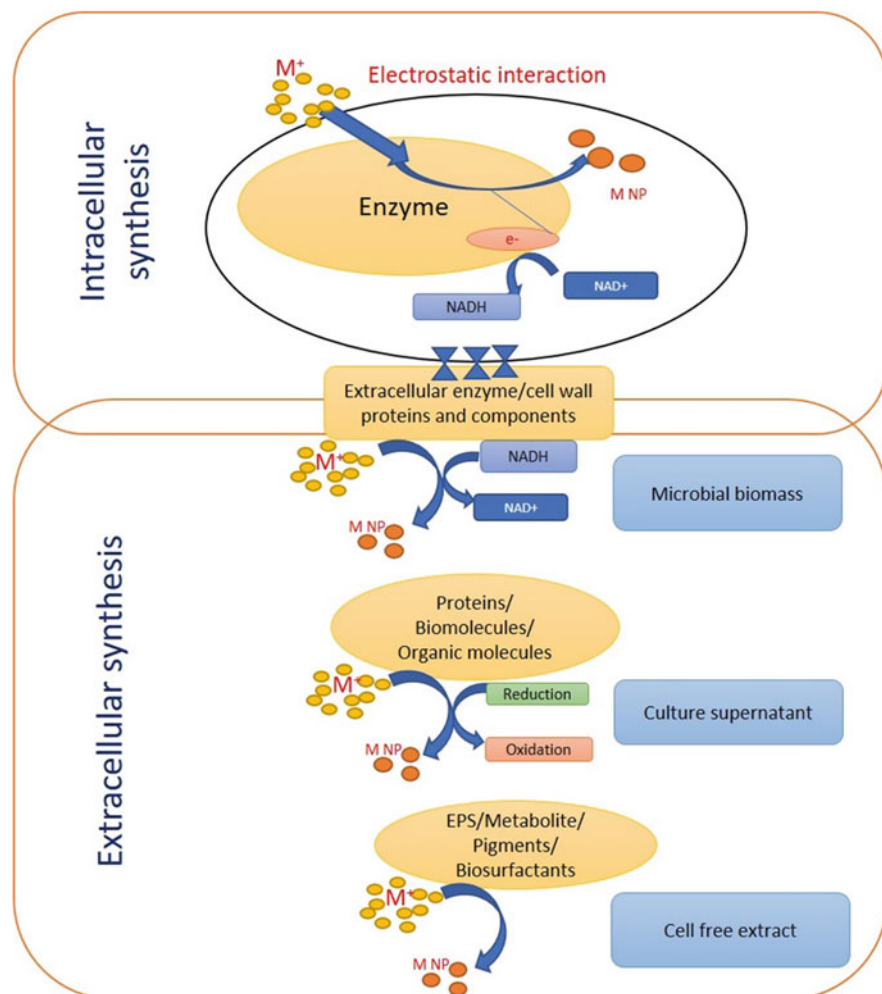


**Fig. 6.1** Microbial intra- and extracellular synthesis routes of nanoparticles

### 6.3.1 Intracellular Synthesis

The ionic charges deposited on the cellular wall of the microbes are an important aspect in the synthesis of nanoparticles, which is carried over by ionic mobility in the microbes, accompanied by various factors such as enzymes and other proteins. The metallic ions adhere to the cellular wall due to active site promotion by the cellular wall composition including its various proteins and polysaccharides (Slavin et al. 2017). Metal ions are known to exhibit more affinity to the cell wall due to the presence of negative charge from the carboxylate groups in many polypeptides (Zhang et al. 2011). Hence, the microbes face a huge risk when it comes to heavy

metals since the ions are trapped electrostatically in the cell wall through microbial gripping (Selvarajan and Mohanasrinivasan 2013). Thereafter, the trapped ions undergo reduction into their elemental form via NADH-dependent reductase activity, localized in the cell membrane, and eventually transform into nanoparticles to be aggregated in either the cell wall or the cytoplasm. Different types of macromolecules such as proteins and amino acids contribute to the stabilization of nanoparticles (Iravani 2014; Shedbalkar et al. 2014).

### 6.3.2 Extracellular Synthesis

Microbial extracellular synthesis is generally known to involve three major role players, such as (a) microbial biomass-cell surface and enzyme, (b) microbial supernatant, and (c) microbial cell-free extract (Singh et al. 2013b). In microbial biomass, extracellular enzyme activity such as NADH-dependent nitrate reductase has been reported (Durán et al. 2005). Microbial supernatants have been harvested from microbes grown for 24–48 h under sterile conditions. These were then reacted with metal salts at optimum conditions for the synthesis of nanoparticles. Biomolecules in the supernatant were reported to play the role of reducing and stabilizing agents. Shivaji et al. (2011) observed that supernatants of *Pseudomonas antarctica*, *Pseudomonas proteolytica*, *Pseudomonas meridiana*, *Paeniglutamicibacter kerguelensis*, *Paeniglutamicibacter gangotriensis*, *Metabacillus indicus*, and *Bacillus cecembensis* readily reduced silver ions when compared to the microbial biomass cell surface. This evidenced that other than the extracellular enzyme activity of the microbial cell surface, the biomolecules in the supernatant were involved in the bioreduction process (Shivaji et al. 2011). Secondary metabolites (Mohanta and Behera 2014), biosurfactants (Palanisamy 2008) and pigments present in microbial cell free extract also assist in nanoparticle synthesis.

## 6.4 Mechanistic Routes of Nanoparticle Synthesis in Microbes

In the process of microbial synthesis of nanoparticles, metallic ions are initially captured on the surface or inside the microbial cells. The captured ions are then reduced to form nanoparticles aided by enzymatic action. Several defense mechanisms have been built by microbes such as metallic ion reduction, precipitation, complex formation, and dissimilatory oxidation to fight against metal toxicity (Tanzil et al. 2016). Some previous reports suggested a significant role of NADH-dependent nitrate reductases in nanoparticle formation (Ahmad et al. 2003; Hulkoti and Taranath 2014).

### 6.4.1 Enzymes Involved in the Biosynthesis of Nanoparticles

The bioremediation of metallic wastes and contaminants can be carried out in situ as well as ex situ with the help of microbial metal reduction. For understanding the link between biorecovery, bioremediation, bioreduction, and biosynthesis of metallic nanoparticles, scientists have looked into the aspect of reducing agents in bacteria like enzymes, proteins, and several other factors, and the various pathways contributing toward the reduction of metallic ions. The ability of the microbes to mobilize metal substrates and their bioreduction play a huge role in the precipitation of metals at nanometer scale (Stephen and Macnaughton 1999). This has urged the scientists to dwell into the matter of bioremediation of radionuclide-burdened lands and other toxic metals mediated by microbial mechanistic pathways. Scientists are also checking the operational viability of using selectively modified microbes and genetically engineered microbes that can cause overexpression of certain reducing agents, thereby controlling the yield, shape, stability, and size of nanoparticles that can be formed.

#### 6.4.1.1 Nitrate Reductase

The biological reduction of metal ions is mediated by the enzyme NADH-dependent reductase which is responsible for the transfer of electrons from NADH (Hulkoti and Taranath 2014). Thereafter, the ions are reduced to elemental form upon gaining the electrons resulting in the formation of metallic nanoparticles. The concerned enzyme nitrate reductase has been found bound to the membrane as well as in periplasmic regions in several microbes such as *Cereibacter sphaeroides*, *Paracoccus pantotrophus*, *Pseudomonas denitrificans*, *Cupriavidus necator*, and *Escherichia coli*. This enzyme has exhibited the ability to reduce metal ions such as tellurite to synthesize the corresponding metallic nanoparticles in vitro (Avazéri et al. 1997; Sabaty et al. 2001).

Ahmad et al. (2003) were the first to report the involvement of NADH-dependent reductase in extracellular reduction of cadmium ions to form cadmium nanoparticles (CdNPs) by *F. oxysporum*. This was confirmed by protein examination and identification. AgNPs have been synthesized extracellularly by adding different concentrations of silver nitrate ( $\text{AgNO}_3$ ) solution to bacterial cultures. During this process, the enzymes (oxidases and reductases) further converted silver ions into oxides of silver (Ahmad et al. 2003; Mukherjee et al. 2018). The bacterium *Bacillus cereus* has provided another wonderful example of using NADH as the carrier of electrons which upon transfer with the help of the concerned enzyme, gave way for the production of AgNPs (Prakash et al. 2011). A similar case was observed in *Bacillus licheniformis* where the nitrate reductase enzyme was considered to be the main factor responsible for the synthesis of AgNPs (Kalimuthu et al. 2008; Kalishwaralal et al. 2010). AgNPs were reported to be efficiently formulated when peptides were ligated to the surface of AgNPs. This attachment stimulated reduction of silver ions



at a much higher pace (Naik et al. 2002). He et al. (2007) also reported the role of nitrate reductase in the extracellular synthesis of gold nanoparticles (AuNPs) using *Rhodobacter capsulatus* that released cofactor NADH and NADH-dependent enzymes.

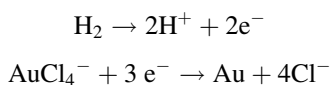
Scientists have worked on the production of AgNPs by using *Streptomyces* sp. LK-3 (Lengke et al. 2007). Their work led to the conclusion that the enzyme nitrate reductase of actinomycetes was responsible for the bioreduction phenomenon. There was a reduction of nitrate molecule to gaseous nitrogen through a chain of conversions. The AgNPs were nearly 5 nm in size and were stable without any aggregation, even without the presence of any capping agent (Karthik et al. 2014). Narasimha and coworkers (Narasimha et al. 2013) also synthesized AgNPs using actinomycetes. They demonstrated that the rate of nitrate reductase production by the organisms, which took part in silver ion reduction, was around 120 nmol/hr./ml. The rate of synthesis of AgNPs by *Klebsiella* sp. has been found to vary and show multiple production rates when the combination of *Klebsiella* culture and silver nitrate was exposed to visible light (Mokhtari et al. 2009). It was reported that *Pseudomonas* sp. accumulated silver on its cell membrane through interaction with hydrogen sulfide (H<sub>2</sub>S) resulting in its nontoxic form of silver (Klaus et al. 1999). The enzymes involved in the synthesis of AgNPs have been determined as mainly nitrate reductases, whereupon NADH acted as a coenzyme (Ali et al. 2017). This same reductase enzyme was also reported to be involved in reducing gold ions in order to synthesize AuNPs in *Stenotrophomonas maltophilia*. The formation of AuNPs was confirmed by intensity analysis of the reaction suspension as well as readings observed by means of the spectrophotometer that performed the analysis, based on color change of the solution with variant NADPH concentrations (Nangia et al. 2009). This further indicated that NADPH and biomass are imperative factors in the AuNPs synthesis process.

Acetate permease (AcP) activity toward the synthesis of nanoparticles was well observed in the bacterium *Rhodobacter capsulatus*. A cascade of reactions occurs when bacterial cells get exposed to tellurite and those reactions respond to changes in pH. When the AcP shuttle gets switched on, it propels tellurite to mobilize into the cytoplasmic region (Borghese and Zannoni 2010). The enzyme nitrate reductase which adheres to the cell membrane is believed to play its part in reducing the tellurite to its elemental form, thereby leading to the synthesis of tellurium nanoparticles, TeNPs (Sabaty et al. 2001).

An experiment was designed to search for an indicative of possible involvement of any enzyme or proteinaceous factor responsible for the synthesis of zinc oxide nanoparticles (ZnO-NPs) in the bacterium *Rhodococcus pyridinivorans* NT2 (Kundu et al. 2014). The bacterial biomass was provided an exposure to zinc ions. Profiling of protein expression followed by protein assays showed that the extracellular protein concentration was twofold higher following zinc ion exposure as compared to the protein concentration which existed prior to exposure with Zn ions. This, along with SDS PAGE, further confirmed the involvement of NADH-dependent reductase in the synthesis of ZnO-NPs.

### 6.4.1.2 Hydrogenase

The hydrogenase enzyme involved in metal reduction is another type of enzyme that has been reported to be present in the cytoplasmic as well as periplasmic regions. Hydrogenase majorly plays a critical role in the reduction of different compounds of gold and palladium to convert them into their elemental forms. It had been reported previously that hydrogenase was involved in the formation of selenium, technetium, chromium, and nickel nanocomposites, although their mechanisms are not quite clear. The hydrogenase enzyme acted as a catalyst in *Shewanella algae* during the biosynthesis of AuNPs, activating the molecular hydrogen and using the molecule as the electron donor according to the following reaction (Konishi et al. 2006):



Hence, the *S. algae* cells were involved in reduction of Au from  $\text{AuCl}_4^-$  ions via transfer of electrons forming 10–20 nm-sized AuNPs. There was no observed decrease in the concentration of  $\text{Au}^{3+}$  ions upon utilizing citrate or lactate as an electron donor, leading to a conclusion that an enzyme having hydrogenase activity was responsible for the reduction of  $\text{AuCl}_4^-$  ions in presence of  $\text{H}_2$  by *S. algae*.

AuNP synthesis was also seen in *E. coli* and *Desulfovibrio desulfuricans*, where hydrogen acted as an electron donor and hydrogenase enzyme located in the periplasmic region was involved in the reduction of  $\text{Au}^{3+}$  ions and accumulation of AuNPs. Transmission electron microscopy (TEM) studies indicated the presence of AuNPs between the cell membrane and the cell wall, which further suggested that the enzyme involved in the reduction of  $\text{Au}^{3+}$  ions was situated in the periplasmic space (Deplanche and Macaskie 2008).

### 6.4.1.3 Iron Reductase

The bacteria *Acinetobacter* sp. was reportedly found as a residual biomass in a container having  $\text{Fe}^{2+}/\text{Fe}^{3+}$  ions, which indicated that when the bacteria came across  $\text{Fe}^{2+}/\text{Fe}^{3+}$  ions, they were able to produce iron reductase and iron oxidase enzymes (Bharde et al. 2005). The reductase enzyme supposedly exhibits a siderophore kind of activity, which confers the extracellular reduction of  $\text{Fe}^{3+}$ . Thereafter, formation of magnetite ( $\text{Fe}_3\text{O}_4$ ) or maghemite ( $\gamma\text{-Fe}_2\text{O}_3$ ) was evident (Bharde et al. 2008). This formation was promoted by a compound known to be iron oxyhydroxide, which was catalyzed by iron oxidase. PCR analysis and BLAST results suggested that iron reductase was present in the concerned species and was responsible for the synthesis of iron nanoparticles (FeNPs).

#### 6.4.1.4 Cysteine Desulfhydrase

Cadmium sulfide nanoparticles (CdS-NPs) have been reported to be produced by *Rhodospseudomonas palustris* with the help of the enzyme cysteine desulfhydrase that can convert sulfate to sulfide. The bacterium, when incubated with cadmium sulfate, produced  $S^{2-}$  in the cytoplasm, and simultaneously the bacterium secreted proteins that were able to stabilize the CdS-NPs (Bai et al. 2009). This reducing pathway was brought about by the reciprocity of the sulfhydryl groups on cysteine bearing negative charge with the metallic ions bearing the positive charge. This process is energy-dependent and needs cysteine/imidazole rings on histidine residues for the interactivity of sulfhydryl groups with Cd ions.

#### 6.4.1.5 Superoxide Dismutase

In a particular experiment involving *Lactobacillus acidophilus* for the synthesis of selenium nanoparticles (SeNPs), several assays for analysis of enzymatic activity indicated the production of reactive oxygen species (ROS) in the elemental solution. That discovery presumably served as being indicative of the production of the ROS under a very minimal amount of stress, caused mainly due to the enhanced activity of superoxide dismutase (SOD) (Alam et al. 2020). Interestingly, in *F. oxysporum*, cadmium-selenium (Cd-Se) nanoparticles were synthesized in a heterogeneous mixture where analysis by SDS PAGE revealed that there was a decline in the relative concentration of the SOD enzyme in the heterogeneous solution of Se and Cd. However, fluorescence microscopy analysis revealed that cytosolic SOD increased at the time of Cd-Se nanoparticle formation indicating the crucial role of the enzyme during the synthesis (Kato and Suzuki 2020). Metals such as tellurite also have been shown to augment the enzymatic activity of SOD during TeNP synthesis. SOD inactivated ROS generation and resulted in the reduction of tellurite (Borsetti et al. 2005).

#### 6.4.1.6 Phenol Oxidase

One of the commonly known fungal enzymes, phenol oxidase, is active when fungi or fungal extracts are utilized for obtaining metal nanoparticles. In earlier reports, the formation of nanoparticles was mediated by exposing a metal solution to fungal cell extracts containing different proteins and enzymes which reduced the compounds to their elementary form (Vetchinkina et al. 2018). This redox system in fungi was observed to be brought about by phenol oxidases such as tyrosinases, laccases, and manganese peroxidases (Vetchinkina et al. 2018). These enzymes presumably took part in the nanoparticle formation by those fungal extracts. Phenol oxidase activity was checked during this process and it was found to be considerably high in extracts prepared from most of the examined fungal species (Vetchinkina et al. 2018).

AgNPs (average size 5–20 nm) and AuNPs (average size 5–15 nm) were also synthesized with these phenol oxidase enzymes playing a crucial role in the process (Vetchinkina et al. 2017).

#### 6.4.2 Biomolecules Involved in Biosynthesis of Nanoparticles

When metal ions come in contact with the cell surface of microbes, biomolecules such as proteins, amino acids, and sugars in the local environment of those microbes reduce the metal ions as evidenced using dried biomass of bacteria (Parikh et al. 2011). pH and temperature have been reported as major factors responsible for this bioreduction. Many reports have predicted that groups of biomolecules could be responsible for the reduction of nanoparticles and their coating with biomolecules for stabilization (Hulkoti and Taranath 2014). Several studies reported the biosynthesis of nanoparticles using microbial biomass cell pellets of *B. licheniformis* (Kalimuthu et al. 2008), filamentous cyanobacterium, *Leptolyngbya boryana* (Lengke et al. 2007), *Lactobacillus* strains, several strains of the fungus *F. oxysporum* (Durán et al. 2005), and *Aspergillus flavus* (Vigneshwaran et al. 2007).

Functional groups such as  $-OH$ ,  $-NH_2$ ,  $-SH_2$ ,  $-CHO$ , and  $-COOH$  in proteins present on the cell wall or periplasmic space provide binding sites to metal ions and stabilize those metal ions while leading to the reduction which produces nanoparticles (Lahiri et al. 2021). Proteins of the fungus, *Trametes versicolor* have been observed to play an active part in the reduction of metal ions, without the addition of any surfactant or linking agent under optimum conditions. This inferred that surface-bound peptides or protein molecules were involved in the stabilization and reduction that produced the nanoparticles. Usage of Fourier-transform infrared spectroscopy (FTIR) to examine supernatants from cultures of different fungal species showed spectrum patterns corresponding to amide I, II, and III groups. The FTIR peaks revealed that the bioreduction of metal ions was due to the protein involvement which corresponded to amide I and amide II groups, and the associated protein activity also stabilized the nanoparticles (Sanghi and Verma 2009). Culture supernatant of *Cladosporium cladosporioides* has been used for extracellular synthesis of AgNPs (Balaji et al. 2009). It was reported that biomolecules (proteins, polysaccharides, and organic acids) in the supernatant were able to reduce the ions and form nanoparticles with crystal shapes (Balaji et al. 2009). Iravani (2014) stated that the *Cladosporium cladosporioides* bacterial supernatant was composed of growth media nutrients and organic molecules released by the microbes during their growth, which made the supernatant an ideal source for bioreduction of metal ions to metal nanoparticles. However, it was noted that nanoparticles obtained from microbial supernatant were embed in the organic matrix of the media components, which negatively affects their colloidal dispersion, characterization and recovery.

Species such as *Geobacter* sp. and *Magnetospirillum magnetotacticum* have intracellular magnetosomes that encapsulate ferric oxide nanoparticles ( $Fe_2O_3$ -NPs) with the aid of ferritin that accumulates Fe in its soluble form within the

vesicles (Kuzajewska et al. 2020). The outer layer of cell wall of *Priestia megaterium* is composed of a proteinaceous surface layer (S-layer), in addition to a thick peptidoglycan layer. The S-layer is believed to play a crucial role in metal interactions (Prakash et al. 2010). In another report, cell surface protein and pilin proteins were found to play a role in biomineralization of uranium nanoparticles in *Geobacter sulfurreducens* (Cologgi et al. 2011).

Lactic acid bacteria (LAB) have been found to produce AgNPs by a different kind of technique. Authors (Sintubin et al. 2009) have reported that this activity by LAB is associated with a cyclic ring of monosaccharides, and a protonated anionic functional group in their cell wall. The observed production of AgNPs trended toward higher pH, the corresponding deprotonation took place, and negatively charged  $\text{Ag}^+$  absorption sites were formed. Simultaneously, the cyclic ring converted into the open ring form. The AgNPs transformation from  $\text{Ag}^+$  was mediated by oxidation of the rings aldehyde functional group.

Bacterial exopolysaccharides (EPS) are biopolymers that act as reducing and stabilizing agents. EPS played a key role (Adebayo-Tayo and Popoola 2017) in the biosynthesis of AgNPs by the EPS-producing *Lacticaseibacillus casei* (LPW2E) and *Limosilactobacillus fermentum*. The nanoparticles ranged from 0.2 to 10 and 0.0 to 10 nm from the two species, respectively. Spectral analysis of the produced nanoparticles by FTIR revealed the presence of groups such as hydroxyl, carboxyl, ester, and aldehydes that were involved in reduction, capping, and stabilization of the nanoparticles. These nanoparticles showed high antibacterial activity (Adebayo-Tayo and Popoola 2017). Saravanan et al. (2017) reported the formation of EPS-stabilized AgNPs using *Leuconostoc lactis*. FTIR spectrum analysis revealed that polysaccharides stabilized the nanoparticles. Transmission electron microscopy (TEM) and scanning electron microscopy (SEM) analyses revealed that the nanoparticles were stabilized by EPS that formed a thin biofilm of 35 nm. One kind of EPS, obtained from *Komagataeibacter xylinus* was levan that acted as both a reducing and capping agent in synthesis of AgNPs and AuNPs. Those nanoparticles were tested for catalytic activity (Ahmed et al. 2014). Succinoglycan of *Sinorhizobium meliloti* also has been reported to be involved in synthesis of AgNPs (Sathiyarayanan et al. 2017).

Several amino acids play a vital role in the formation of nanoparticles. Maruyama et al. (2015) reported that L-histidine concentration affected the size of synthesized AuNPs and their aggregates. The  $-\text{NH}_2$  and  $-\text{COOH}$  groups were responsible for both the reduction of tetra auric acid and coating the nanoparticle surface. Shu et al. (2020) reported the synthesis of 13.8 nm average-sized AgNPs from yeast extract. The authors implied the role of carbohydrates, amino acids,  $\alpha$ -linolenic acid, and aminobutyric acid in the bioreduction process.

### 6.4.3 Secondary Metabolites Involved in Biosynthesis of Nanoparticles

Mohanta and Behera (2014) reported the role of a secondary metabolite in the fermented extract of *Streptomyces* sp. SS2 was involved in reduction and stabilization of AgNPs. Microbial pigments that have potent biological and industrial applications also have been utilized for synthesis of nanoparticles. An example of this would be that *Penicillium chrysogenum* produced melanin, which is a pigment known to serve as a proto-protective polymer (Vasanthakumar et al. 2015). This melanin pigment produced magnesium oxide nanoparticles (MgO-NPs) when it was reacted with 4 mM magnesium nitrate solution and exposed to gamma radiation. The possible mechanism behind melanin-doped synthesis of MgO-NPs is that hydrated electrons and free radicals generated from melanin, when exposed to gamma radiation, reduced  $Mg^{2+}$  ions to form MgO-NPs (El-Sayyad et al. 2018). It was also reported that melanin was found to assist in the synthesis of SeNPs and bismuth nanoparticles (Bi-NPs) (El-Batal et al. 2017). Manikprabhu and Lingappa (2014) reported that the green pigment synthesized by extended-spectrum beta-lactamase (ESBL) present in *E. coli* produced biologically active AgNPs when photo-irradiated for 20 min. *Talaromyces purpurogenus* had produced monascus-like pigments which contained azaphilone mixtures of highly soluble yellow, orange, and red pigments (Bhatnagar et al. 2019). These pigments reduced silver ion to AgNPs without any irradiation and the generated AgNPs showed high bactericidal and anticancer activities against HeLa and HepG2 cancer cells (Bhatnagar et al. 2019). Pink pigment of *Streptomyces fulvissimus* assisted the synthesis of AgNP that exhibited potential antibacterial activity against both Gram-positive and Gram-negative bacteria (Singh et al. 2021). In another report, the pigment gamma actinorhodin produced by the *Streptomyces coelicolor* assisted in synthesis of AgNPs when kept in microwave oven (Manikprabhu and Lingappa 2013).

Biosurfactants are produced by the living cells mostly by microbes on their surfaces or are extracellularly secreted. These compounds are amphiphilic containing both polar and nonpolar functional groups. Polar group can be a carbohydrate, amino acid, cyclic peptide, phosphate, carboxylic acid, or an alcohol whereas the nonpolar group is a long-chain fatty acid, hydroxyl fatty acid or  $\alpha$ -alkyl  $\beta$ -hydroxy fatty acid. Rhamnolipid as a biosurfactant assisted the synthesis of nickel oxide (NiO-NPs) (Palanisamy 2008). Rhamnolipids of *P. aeruginosa* were employed in the synthesis of AgNPs (Kumar et al. 2010) and ZnS NPs (Narayanan et al. 2010). Uncharacterized glycolipid produced by *Brevibacterium casei* MSA19 acted as a suitable stabilizer in AgNP biosynthesis under solid-state fermentation (Kiran et al. 2010). Hazra et al. (2013) noted that nanoparticles capped with biosurfactants showed reduced toxicity and high efficiency of dye degradation by ZnS nanoparticles in brown textile. *Starmarella bombycolia* secreted sophorolipids, oleic/linoleic acid that aided in the synthesis of cobalt nanoparticles that showed paramagnetic property. It was also reported that oleic acid sophorolipids produced smaller nanoparticles while linoleic acid sophorolipids produced larger

nanoparticles (Kasture et al. 2008). Surfactin, lipopeptide biosurfactant of *B. subtilis* (Reddy et al. 2009) and *Bacillus amyloliquifaciens* (Singh et al. 2011) was assisted in the synthesis of AuNPs and CdS-NPs, respectively.

#### 6.4.4 Role of Electron Shuttle or Redox Mediators

Some metal ions can be reduced to less toxic oxidative states. This is possible via efflux systems, where the compound is detoxified by reduction, and export of the detoxified product can promote the conversion of metal ions to metals nanoparticles (Durán et al. 2005). An electron shuttle is a mobile pathway that includes mobilization of molecules like NADH and ubiquinol. Microbial resistance to toxic metal ions seemingly has been conferred in this way, possibly owing to the functionality of efflux pumps and cellular transporters in the cells (Prakash et al. 2010).

Molecules such as metal ions present on the cell wall surface have been suggested to justify the role of electron seekers. Presumably, by accepting electrons mobilized to the outer wall, with involvement via the inner membrane and periplasm, these contribute to the extracellular synthesis of metallic nanoparticles (Shi et al. 2012). Microbial cells, upon exposure to heavy metals, tend to adsorb as well as intake the heavy metal ions (Husseiny et al. 2007). At a certain time, the cells then reach the threshold point beyond which they cannot accumulate any more ionic particles. Thereafter, the cells utilize their transporter system or pumping mechanism to eliminate the toxic metal ions (Velásquez and Dussan 2009) whereupon the ions are reduced most of the time and get deposited on the surface of the cells in the form of nanoparticles (Thatheyus and Ramya 2016; Shamim 2018).

Various redox compounds, such as cytochrome c and members of the quinone family, which are produced by microbial cells have the capability to shuttle electrons and these compounds can act as causative effectors of metal reduction (Newman and Kolter 2000). Several redox mediators like cytochrome c interact with metallic ions for mediating the shuttle system (Bewley et al. 2013; Ng et al. 2013). This shuttling provides for the synthesis of the metallic nanoparticles extracellularly. It was reportedly suggested that the study of the MR-1 strain of *Shewanella oneidensis* (Shi et al. 2012) and also *G. sulfurreducens* (Liu et al. 2014; Liu et al. 2015; Vasylevskyi et al. 2017) might help to elucidate the mechanistic cascade of mobilizing an electron from quinol to the cellular surface with the participation of a cytochrome c molecule. The major striking factor in that consideration was the effective transportation of electrons from  $\text{Fe}^{2+}$  component to  $\text{F}^{3+}$  of the cytochrome c (Vasylevskyi et al. 2017). Kumar et al. (2007) postulated that nitrate reductase was the NADH- and NADPH-dependent factor which was actively involved in the bioreduction process, and that like quinone, hydroxyquinoline acted as an electron carrier shuttle which moved electrons during the oxidoreduction reaction which then resulted in synthesis of AgNPs by the fungus *F. oxysporum*.

## 6.5 Types of Nanoparticles Synthesized by Microbes

Microbes such as bacteria, fungi, yeast, actinomycetes, and virus have been utilized in the biogenic synthesis of various metal and metal oxide nanoparticles as listed in Table 6.1.

### 6.5.1 Silver Nanoparticles

AgNP is one of the most synthesized types of nanoparticle and with wide applicability. Among microbes, bacteria have been widely exploited for intra- and extracellular production of AgNPs. Singh et al. (2013b) reported extracellular AgNP synthesis by *Acinetobacter calcoaceticus* LRVP54 isolated from wheat rhizosphere. The bacteria produced monodispersed spherical 8–12 nm ranged AgNPs that exhibited synergistic antibacterial potential against seven pathogens. Deepak et al. (2011) evidenced the role of a fibrinolytic enzyme (URAK) in the biosynthesis of 50–80 nm-sized spherical AgNPs from *B. cereus* NK1. *Proteus mirabilis* was exploited for both extra- and intracellular synthesis of AgNPs that resulted in 10–20 nm average-sized spherical nanoparticles (Samadi et al. 2009). A report suggested that *Leptolyngbya boryana* UTEX 485 was able to synthesize AgNPs, as indicated by the grayish-black coloration produced by the cultured microorganisms (Lengke et al. 2006). The metabolic process of reducing nitrate promoted Ag<sup>+</sup> reduction, besides reducing nitrate to nitrite and ammonium, in the cyanobacterial cell (Lengke et al. 2007). An aqueous solution of *Azospirillum brasilense* has been found to produce spherical AgNPs ranging from 10 to 50 nm after 12 h of incubation (Vetchinkina et al. 2019).

AgNPs also have been synthesized using endophytic fungi, specifically *Penicillium* sp. isolated from *Curcuma longa*. The produced nanoparticles were an average size of 25 nm and showed a SPR band at 425 nm. These were spherical in shape and exhibited antibacterial activity (Singh et al. 2013a). A cell-free filtrate of phytopathogenic fungi, *Macrophomina phaseolina* has been used to synthesize protein capped AgNPs of 5–40 nm size after 24 h of incubation (Chowdhury et al. 2014).

*Streptacidiphilus griseoplanus* was able to produce AgNPs of average size 20 nm after 96 h of incubation (Vijayabharathi et al. 2018). Korbekandi et al. (2016) reported the synthesis of AgNPs from yeast *Saccharomyces cerevisiae* that was spherical and 2 to 20 nm in size.

### 6.5.2 Gold Nanoparticles

Beveridge and Murray (1980) have reported the synthesis of AuNPs using *Bacillus subtilis*. Those authors determined that under conditions, when the cells were



**Table 6.1** Microbe-mediated different types of nanoparticles, their sizes and shapes

Type of microbe	Species	Type of nanoparticles	Size (nm)	Shape	References	
Bacteria	<i>Aeromonas hydrophila</i>	Zn; Ti	57.72; 40.5	Spherical, oval, spherical	(Jayaseelan et al. 2012, 2013)	
	<i>Bacillus licheniformis</i>	Zn; Ag; Au	200 for nanoparticles; 18.69–63.4; 10–100	Nanoflower; spherical; nanocubes	(Tripathi et al. 2014; Shamthi et al. 2016; Kalimuthu et al. 2008)	
	<i>Bacillus subtilis</i>	Ag; Au; Fe	20, 3–20; 40–60; 37.4	Spherical, hexagonal; Hexagonal; Blade	(El-Bendary et al. 2021; Alsamary 2020; Rane et al. 2017; Daneshvar and Hosseini 2018)	
	<i>Escherichia coli</i>	Ag; Au; Cds; Pd, Pt	50; 10; 2–10; 2–5	Spherical; Spherical; Cubical; Spherical	(Gurunathan et al. 2009; Gholami-Shabani et al. 2015; Alsagaf et al. 2020; Deplanche et al. 2010)	
	<i>Klebsiella pneumoniae</i>	Ag; Au; Cu	15–37; 35–65	Spherical; Spherical; Spherical	(Kalpana and Lee 2013; Malarkodi et al. 2013; Noman et al. 2020)	
	<i>Proteus mirabilis</i>	Ag; Fe	10–20; 11.7–60.8	Spherical; Spider web-like	(Samadi et al. 2009; Zaki et al. 2019)	
	<i>Pseudomonas aeruginosa</i>	Ag; Pd, Zn; Se	8–24; 22.1; 35–80; ND	Spherical; Polygonal, spherical; Spherical, contour	(Kumar et al. 2010; Srivastava and Constanti 2012; Singh et al. 2014; Yadav et al. 2008)	
	<i>Vibrio alginolyticus</i>	Ag; Au	50–100; 50–100	Spherical; Irregular	(Rajeshkumar et al. 2013; Shummugam et al. 2021)	
	Fungus	<i>Aspergillus oryzae</i>	Ag; Fe; Se; Si	16.7; 10–24.6; 55; 90	Spherical; Spherical; Spherical; Spherical	(Phanjom and Ahmed 2015; Tarafdar and Raihya 2013; Mosallam et al. 2018; Wu et al. 2013)
		<i>Aspergillus flavus</i>	Ag-Au; Ag; Zn	>120; 8.92; 12–24	Spherical; Spherical; Spherical	(Chen et al. 2003; Vigneshwaran et al. 2007; Uddandarao et al. 2019)
<i>Aspergillus niger</i>		Zn; Ag; Au	53–69; 20; 12.8	Spherical; Spherical; Spherical, elliptical	(Kalpana et al. 2018; Gade et al. 2008; Bhambare et al. 2009)	
<i>Fusarium oxysporum</i>		Au, Ni; Ag; Fe; Pt	40.3, 25–50; 5.8; 5–30; 15–30	Spherical, spherical; Spherical; Spherical; Spherical	(Costa et al. 2013; Hussein et al. 2015; Abdeen et al. 2013; Syed and Ahmad 2012)	
<i>Trichoderma viride</i>		Ag, Cds; Ti	10–15; 60–87	Spherical; Spherical	(Mukherjee et al. 2001; Chinnaperumal et al. 2018)	

Yeast	<i>Saccharomyces cerevisiae</i>	Au; Ag; Fe; Pd; Se	13; 2–20; 8–9; 32; 75	Spherical; Spherical; Spherical; Hexagonal; Spherical	(Attia et al. 2016; Korbekandi et al. 2016; Vainshtein et al. 2014; Srimulu and Sumathi 2018; Faramarzi et al. 2020)
	<i>Candida albicans</i>	Ag; Zn	50–100; 20	Spherical; Quasi-spherical	(Marchiol 2012; Mashrai et al. 2017)
	<i>Candida glabrata</i>	Cds	110–130	Spherical	(Dameron et al. 1989)
	<i>Pichia kudriavzevii</i>	Zn; Ag	10–61; 20.7	Hexagonal; Spherical, cubical	(Moghaddam et al. 2017; Ammar et al. 2021)
Actinomycete	<i>Yarrowia lipolytica</i>	Au; Ag	15; 5–12	Hexagonal; Spherical	(Agnihotri et al. 2009; Kathiresan et al. 2009)
	<i>Streptomyces</i> sp.	Zn; Fe; Cu	20–50; 65–87; 78–80	Spherical; Quasi-spherical; Spherical	(Balraj et al. 2017; Rajeswaran et al. 2020; Korbekandi et al. 2016)
	<i>Streptomyces viridogenes</i>	Au	18–20	Spherical, rod	(Balagurunathan et al. 2011)
	<i>Rhodococcus</i> sp.	Au; Ag	5–10; 10	Spherical, rod; Spherical	(Sastry et al. 2003; Otari et al. 2012)
	<i>Thermomonospora</i> sp.	Au	12–20	Spherical	(Ahmad et al. 2003)
Virus	<i>Tobamovirus Tobacco mosaic virus</i>	Si, Cds, Pbs	<30	Multishaped	(Kashyap et al. 2013)
	<i>Escherichia virus M13</i>	Cds, Zn	10–25	Spherical	(Sweeney et al. 2004)

incubated with  $\text{Au}^{3+}$  ions and organic phosphates that aided as a supplement, there occurred successful promotion of the bacteria–Au complex. The produced AuNPs were octahedral in shape and 5–25 nm in size.

*Pseudomonas denitrificans* is a Gram-negative bacterium typically involved in the denitrification process. The bacterium was reported to release NADH-dependent enzymes such as nitrate reductases, which could have been responsible for the conversion of Au ions to AuNPs. This same reduction process has led to the production of AuNPs of 15–20 nm at an optimum temperature of 37 °C and pH 3 (Mewada et al. 2012). Flower-shaped AuNPs have been biosynthesized using *Bhargavaea indica* DC1 isolated from *Panax ginseng* rhizosphere soil. Those AuNPs were monodispersed and crystalline in nature with an average diameter of 106 nm. The flower shape was reported to uphold beneficial optical and electrical applicability (Singh et al. 2015).

In filamentous cyanobacterium, *Leptolyngbya boryana* UTEX 485 when interacted with aqueous gold chloride, promoted gold sulfide deposition in the cell walls and metallic gold accumulation on the cell surfaces. The association of various elements like nitrogen, phosphorous, and sulfur with the deposited gold as observed by TEM suggests the involvement of these ligands in the bioreduction of gold sulfide (Lengke et al. 2006). Biosynthesized AuNPs from *Aspergillus foetidus* have been found to be polydispersed and spherical shape with sizes ranging from 10 to 40 nm (Roy et al. 2016).

Attia et al. (2016) reported the synthesis of spherical and 13 nm average-sized AuNPs from yeast *S. cerevisiae* that showed anticancer activity. The use of actinomycetes was also reported to be successful for the biosynthesis of AuNPs. *Gordonia amarae* was used for the bioformulation of 20–40 nm ranged spherical AuNPs that showed applicability in copper detection (Bennur et al. 2016).

### 6.5.3 Silicon Nanoparticles

The biosynthesis of Si or silicon dioxide ( $\text{SiO}_2$ ) nanocomposites by *Actinobacter* sp. using a potassium fluorosilicate ( $\text{K}_2\text{SiF}_6$ ) precursor has been determined to involve the action of several nonspecific reductases and oxidizing enzymes (Singh et al. 2008). The released reductase enzyme was responsible for mediating the reduction of  $\text{Si}^{4+}$  ions to  $\text{Si}^0$  form. Since it is well known that the Si surface is reactive and gets layered with its native oxide, the elemental form of silicon formation presumably also followed the same pattern, leading to the formation of Si/ $\text{SiO}_2$ –NPs, and their size was around 10 nm (Singh et al. 2008).

In another report, SiNPs were synthesized using intra- and extracellular fungal extracts and sodium silicate ( $\text{Na}_2\text{SiO}_3$ ) that led to nanoparticles with zeta potentials ranging from –10 to –15 mV. Large individual particles were obtained with *Lentinula edodes* and *Ganoderma lucidum* whereas small aggregates were retrieved using *Pleurotus ostreatus* and *Grifola frondosa* (Vetchinkina et al. 2018).

*F. oxysporum* species also have been used to synthesize SiO<sub>2</sub>-NPs (Bansal et al. 2005). Those authors reported the involvement of proteins that could have hydrolyzed the anionic complex, SiF<sub>6</sub><sup>2-</sup> at room temperature (RT). Using K<sub>2</sub>SiF<sub>6</sub> as a precursor, SiO<sub>2</sub>-NPs ranging from 50 to 100 nm were identified in the frustules which form the silica exoskeleton of diatom algae (Dhillon et al. 2012) suggesting that algae can be hence utilized to monitor the formation and assembly of SiNPs.

#### 6.5.4 Titanium Nanoparticles

It has been reported that a *B. subtilis* culture could aid in the synthesis of titanium (Ti) NPs (Kirthi et al. 2011). The morphological characteristics of the produced titanium NPs were found to be spherical in shape with an average size of 66–77 nm. X-ray diffraction analysis (XRD) indicated predominance of TiO<sub>2</sub> in the obtained nanoparticle structure.

Using a culture filtrate of *Lactobacillus* sp., spherical TiNPs of about 40 to 60 nm were synthesized extracellularly by different fermented food materials at room temperature (Prasad et al. 2007). These nanoparticles might find their applications in cancer therapy, automobiles, submarines, and airplanes, among other usages due to their lightweight and high thermal resistance capacity (Waghmode et al. 2019). pH-sensitive oxidoreductases in culture medium have resulted in the synthesis of n-TiO<sub>2</sub> (Babitha and Korrapati 2013). It has been reported that a metal resistant, Gram positive, pleomorphic bacterium *Acidipropionibacterium jensenii* having high G + C content, had the potential to synthesize TiO<sub>2</sub> NPs (Babitha and Korrapati 2013). Synthesized Ti nanoparticles found to be spherical in shape ranging in size from 15 to 80 nm were synthesized using 25 mM TiO(OH)<sub>2</sub> solution at 60 °C for 10 min.

Using 14 fungal isolates of species that included *A. flavus*, *Aspergillus terreus*, *Aspergillus tubingensis*, *A. niger*, *Aspergillus fumigatus*, *A. oryzae*, and *M. phaseolina*, have been found to produce TiNPs with sizes ranging from 1.5 to 30 nm at pH 5.5 at 28 °C after 72 h of incubation (Raliya and Tarafdar 2014).

#### 6.5.5 Zinc Nanoparticles

Biogenic synthesis of zinc oxide (ZnO) NPs was reported, using *Aeromonas hydrophila*. The nanoparticles were crystalline in nature and atomic force microscopy (AFM) images displayed spherical and oval morphology with an average size of 57.72 nm (Jayaseelan et al. 2012). The membrane-bound oxidoreductases of *Bacillus coagulans* which are pH dependent were observed to produce ZnO NPs ranging from 5 to 10 nm size under low pH conditions suggesting that lower pH ambience was needed for the synthesis of nanoparticles (Prasad and Jha 2009).

An average size of 8.2 nm ZnNPs having a surface charge of  $-5.70$  mV was synthesized using 14 fungal isolates of species that included *Aspergillus* species and *M. phaseolina*. The synthesis was optimized using 0.01 mM of zinc oxide, zinc sulfate, zinc chloride, and zinc nitrate as precursor compound precursor salts at pH 5.5 at 28 °C for 72 h of incubation (Raliya and Tarafdar 2014). ZnNPs were also synthesized using *Streptomyces* sp. that rendered spherical nanoparticles of 20–50 nm in size and showed promising antibacterial and anticancer properties (Balraj et al. 2017).

Yeast has also been reported to produce ZnNPs. In one report, quasi-spherical-shaped nanoparticles with 20 nm average size were reported from *Candida albicans* and those NPs showed effective catalytic activity (Mashrai et al. 2017). *P. kudriavzevii* has been used to obtain hexagonal nanoparticles ranging from 10 to 61 nm with antibacterial and antioxidant activities (Moghaddam et al. 2017).

### 6.5.6 Palladium Nanoparticles

Palladium has found its usefulness in applications ranging from catalysts to automobiles. PdNPs have been obtained by conversion of soluble  $\text{Pd}^{2+}$  to  $\text{Pd}^0$ , which turned out to be a sustainable and effective process (Ahmed et al. 2018). *G. sulfurreducens* has been reported to reduce Pd ions to PdNPs extracellularly, which aided in recovering pre-consumed metal catalysts (Yates et al. 2013). *S. oneidensis* MR-1 has been identified to produce PdNPs through electrocatalysis and also molecular oxidation of biofuel (Wu et al. 2018).

*S. oneidensis* and *D. desulfuricans* (Yong et al. 2002; Lloyd et al. 1998) reportedly have been able to convert soluble  $\text{Pd}^{2+}$  into insoluble  $\text{Pd}^0$ , with either lactate, pyruvate, formate, or  $\text{H}_2$  as the electron donor (Windt et al. 2005). PdNPs have been evidenced to be synthesized on the bacterial cell envelope as reported from studies on *Pseudomonas* sp. (Schlüter et al. 2014) and *E. coli* (Lloyd et al. 1998). *S. cerevisiae* has been used to synthesize hexagonal PdNPs with an average size of 32 nm and those particles possessed photocatalytic degradation potentials (Sriramulu and Sumathi 2018).

### 6.5.7 Platinum Nanoparticles

Platinum nanoparticles reportedly have been formed by reduction of  $\text{Pt}^{4+}$  ions mediated by hydrogenase enzyme obtained from sulfate-reducing bacterium *Desulfovibrio vulgaris* (Martins et al. 2017), *Acinetobacter calcoaceticus* (Gaidhani et al. 2014), *Leptolyngbya boryana* UTEX 485 (Lengke et al. 2006), and *D. desulfuricans* (Yong et al. 2002).

A *Shewanella* sp. has been reported to produce PtNPs intracellularly (Martins et al. 2017) through reduction of  $\text{PtCl}_6^{2-}$ , localized in the periplasmic space.

Occurrence of blackish coloration and decrease in the amount of  $\text{PtCl}_6^{2-}$  ions act as indicators for the formation of PtNPs. The reduction could not take place in the presence of lactate (Konishi et al. 2007).

*Neurospora crassa* has been used to synthesize monodispersed PtNPs of 4–35 nm in size and agglomerates of 20–110 nm intracellularly (Castro-Longoria et al. 2012). *F. oxysporum* also has been used to produce PtNPs both extra- and intracellularly with varying sizes of 10–100 nm and shapes by response surface methodology (Riddin et al. 2006). *Saccharomyces boulardii* (*nom. Inval.*) has been reported to form spherical PtNPs of 120 nm in average size having anticancer properties (Borse et al. 2015).

### 6.5.8 Cadmium Nanoparticles

CdS-NPs were reported to be produced by *R. palustris* using the help of the enzyme cysteine desulfhydrase that can convert sulfate to sulfide (Bai et al. 2009). The bacterium secreted proteins that stabilized the produced CdS-NPs. A previous report suggested that *Klebsiella aerogenes* produced CdS-NPs in the presence of  $\text{Cd}(\text{NO}_3)_2$  and optimum pH conditions (Holmes et al. 1995). *B. licheniformis* has been found to be efficient in producing 20–40 nm-sized crystalline Cds-NPs that showed effective antimicrobial activities against foodborne pathogens (Shivashankarappa and Sanjay 2015). *C. versicolor* fungus has been reported to bioremediate cadmium ions in a continuous column mode by enzymatic process synthesize 5–9 nm-sized stable cadmium nanoparticles in aqueous state with no external sulfur usage required for the nanoparticle transformation (Sanghi and Verma 2009).

### 6.5.9 Iron Nanoparticles

Iron oxide nanoparticles ( $\text{Fe}_3\text{O}_4$ -NPs) were reported to be synthesized using *B. subtilis* isolated from rhizosphere soil (Sundaram et al. 2012). An extracellular synthesis resulted in the formation of 60–80 nm-sized stable  $\text{Fe}_3\text{O}_4$  nanoparticles. In another report, *Priestia megaterium* has been utilized to synthesize cuboid-shaped iron nanoparticles ranging from 40 to 60 nm in size (Ghani et al. 2017). Additionally, the nanoparticles showed antibacterial properties. Stable spherical-shaped  $\text{Fe}_3\text{O}_4$ -NPs with an average size of 23 nm were obtained from *B. cereus* strain HMH1 (Fatemi et al. 2018). Those nanoparticles were reported to have super paramagnetic properties and displayed in vitro cytotoxicity against breast cancer (MCF-7) cell line. Vainshtein et al. (2014) reported the synthesis of magneto-sensitive iron nanoparticles from yeasts such as *S. cerevisiae* and *Vanrija humicola*. Large irregular-shaped nanoparticles were obtained with the former yeast culture whereas the latter produced 8–9 nm uniform-sized nanoparticles. *A. oryzae* has been reported

to synthesize spherical iron nanoparticles in sizes ranging from 10 to 24.6 nm (Tarafdar and Raliya 2013).

## 6.6 Conclusion and Future Prospects

After the advent of research breakthroughs in nanobiotechnology, synthesis of novel microbial nanomaterials has been prioritized owing to the huge potential applications for these materials in the fields of biomedicine, agriculture, and industry. The biogenic mode of nanoparticle synthesis is economical, clean, and environmentally benign. An array of microbes including bacteria, fungi, yeast, actinomycete, and viruses have been employed to synthesize different nanoparticles. Considering their rich diversity, microbes are referred to as potential biofactories for the production of nanomaterials. By modulating the reaction parameters, time duration of microbial synthesis of nanoparticles can be minimized with their dispersivity and particle size tenably controlled. Hence, it is crucial to develop in-depth studies to completely understand the cellular, biochemical, and molecular mechanisms of nanoparticle synthesis and improve the efficacy of synthesis. Exploration of physicochemical, and optoelectronic properties of bionanomaterials will pave the way for implementation of large-scale production and applicability in various fields.

**Acknowledgments** We thank the University Grants Commission, New Delhi and Department of Biotechnology (DBT), Delhi for financial support through MSc Biotechnology CEEB fellowship to Ankit Banik, UGC-JRF fellowship to Meyappan Vadivel, and Rajiv Gandhi National Fellowship to Moumita Mondal. We also thank the DST-FIST program coordinated by Prof. N. Sakthivel for providing infrastructure facilities.

## References

- Abdeen S, Isaac RR, Geo S, Sornalekshmi S, Rose A, Praseetha P (2013) Evaluation of antimicrobial activity of biosynthesized iron and silver nanoparticles using the fungi *Fusarium oxysporum* and *Actinomyces* sp. on human pathogens. *Nano Biomed Eng* 5(1):39–45
- Adebayo-Tayo BC, Popoola AO (2017) Biogenic synthesis and antimicrobial activity of silver nanoparticle using exopolysaccharides from lactic acid bacteria. *Int J Nano Dimens* 8(1):61–69
- Agnihotri M, Joshi S, Kumar AR, Zinjarde S, Kulkarni S (2009) Biosynthesis of gold nanoparticles by the tropical marine yeast *Yarrowia lipolytica* NCIM 358. *Mater Lett* 63(15):1231–1234
- Ahmad A, Senapati S, Khan MI, Kumar R, Sastry M (2003) Extracellular biosynthesis of monodisperse gold nanoparticles by a novel extremophilic actinomycete, *Thermomonospora* sp. *Langmuir* 19(8):3550–3553
- Ahmed KBA, Kalla D, Uppuluri KB, Anbazhagan V (2014) Green synthesis of silver and gold nanoparticles employing Levan, a biopolymer from *Acetobacter xylinum* NCIM 2526, as a reducing agent and capping agent. *Carbohydr Polym* 112:539–545
- Ahmed E, Kalathil S, Shi L, Alharbi O, Wang P (2018) Synthesis of ultra-small platinum, palladium and gold nanoparticles by *Shewanella loihica* PV-4 electrochemically active biofilms and their enhanced catalytic activities. *J Saudi Chem Soc* 22(8):919–929

- Ajayan PM (2004) How does a nanofibre grow? *Nature* 427(6973):402–403
- Alam H, Khatoun N, Khan MA, Husain SA, Saravanan M, Sardar M (2020) Synthesis of selenium nanoparticles using probiotic bacteria *Lactobacillus acidophilus* and their enhanced antimicrobial activity against resistant bacteria. *J Clust Sci* 31(5):1003–1011
- Ali J, Ali N, Jamil SUU, Waseem H, Khan K, Pan G (2017) Insight into eco-friendly fabrication of silver nanoparticles by *Pseudomonas aeruginosa* and its potential impacts. *J Environ Chem Eng* 5(4):3266–3272
- Alsaggaf MS, Elbaz AF, El-baday S, Moussa SH (2020) Anticancer and antibacterial activity of cadmium sulfide nanoparticles by *Aspergillus niger*. *Adv Polym Technol* 2020:1–13
- Alsamhary KI (2020) Eco-friendly synthesis of silver nanoparticles by *Bacillus subtilis* and their antibacterial activity. *Saudi J Biol Sci* 27(8):2185–2191
- Ammar HA, Abd El Aty AA, El Awdan SA (2021) Extracellular myco-synthesis of nano-silver using the fermentable yeasts *Pichia kudriavzevii* HA-NY2 and *Saccharomyces uvarum* HA-NY3, and their effective biomedical applications. *Bioprocess Biosyst Eng* 44(4):841–854
- Armendariz V, Herrera I, Jose-yacaman M, Troiani H, Santiago P, Gardea-Torresdey JL (2004) Size controlled gold nanoparticle formation by *Avena sativa* biomass: use of plants in nanobiotechnology. *J Nanopart Res* 6(4):377–382
- Attia YA, Farag YE, Mohamed YM, Hussien AT, Youssef T (2016) Photo-extracellular synthesis of gold nanoparticles using Baker's yeast and their anticancer evaluation against Ehrlich ascites carcinoma cells. *New J Chem* 40(11):9395–9402
- Avazéri C, Turner RJ, Pommier J, Weiner JH, Giordano G, Verméglio A (1997) Tellurite reductase activity of nitrate reductase is responsible for the basal resistance of *Escherichia coli* to tellurite. *Microbiology* 143(4):1181–1189
- Babitha S, Korrapati PS (2013) Biosynthesis of titanium dioxide nanoparticles using a probiotic from coal fly ash effluent. *Mater Res Bull* 48(11):4738–4742
- Baer DR (2011) Surface characterization of nanoparticles: critical needs and significant challenges. *J Surface Anal* 17:163–169
- Bai H, Zhang Z, Guo Y, Yang G (2009) Biosynthesis of cadmium sulfide nanoparticles by photosynthetic bacteria *Rhodospseudomonas palustris*. *Colloids Surf B: Biointerfaces* 70(1):142–146
- Balagurunathan R, Radhakrishnan M, Rajendran RB, Velmurugan D (2011) Biosynthesis of gold nanoparticles by actinomycete *Streptomyces viridogens* strain HM10. *Indian J Biochem Biophys* 48(5):331–335
- Balaji D, Basavaraja S, Deshpande R, Mahesh DB, Prabhakar B, Venkataraman A (2009) Extracellular biosynthesis of functionalized silver nanoparticles by strains of *Cladosporium cladosporioides* fungus. *Colloids Surf B: Biointerfaces* 68(1):88–92
- Balraj B, Senthilkumar N, Siva C, Krithikadevi R, Julie A, Potheher IV, Arulmozhi M (2017) Synthesis and characterization of zinc oxide nanoparticles using marine *Streptomyces* sp. with its investigations on anticancer and antibacterial activity. *Res Chem Intermed* 43(4):2367–2376
- Bansal V, Rautaray D, Bharde A, Ahire K, Sanyal A, Ahmad A, Sastry M (2005) Fungus-mediated biosynthesis of silica and titania particles. *J Mater Chem* 15(26):2583–2589
- Bennur T, Khan Z, Kshirsagar R, Javdekar V, Zinjarde S (2016) Biogenic gold nanoparticles from the Actinomycete *Gordonia amarae*: application in rapid sensing of copper ions. *Sensors Actuators B Chem* 233:684–690
- Beveridge T, Murray R (1980) Sites of metal deposition in the cell wall of *Bacillus subtilis*. *J Bacteriol* 141(2):876–887
- Bewley KD, Ellis KE, Firer-Sherwood MA, Elliott SJ (2013) Multi-heme proteins: Nature's electronic multi-purpose tool. *Biochim Biophys Acta Bioenerg* 1827(8–9):938–948
- Bhambure R, Bule M, Shaligram N, Kamat M, Singhal R (2009) Extracellular biosynthesis of gold nanoparticles using *Aspergillus niger*—its characterization and stability. *Chem Eng Technol* 32(7):1036–1041
- Bharde A, Wani A, Shouche Y, Joy PA, Prasad BL, Sastry M (2005) Bacterial aerobic synthesis of nanocrystalline magnetite. *J Am Chem Soc* 127(26):9326–9327



- Bharde AA, Parikh RY, Baidakova M, Jouen S, Hannover B, Enoki T, Prasad B, Shouche YS, Ogale S, Sastry M (2008) Bacteria-mediated precursor-dependent biosynthesis of superparamagnetic iron oxide and iron sulfide nanoparticles. *Langmuir* 24(11):5787–5794
- Bhatnagar S, Kabori T, Ganesh D, Ogawa K, Aoyagi H (2019) Biosynthesis of silver nanoparticles mediated by extracellular pigment from *talaromyces purpurogenus* and their biomedical applications. *Nano* 9(7):1042
- Bhattacharya R, Mukherjee P (2008) Biological properties of “naked” metal nanoparticles. *Adv Drug Deliv Rev* 60(11):1289–1306
- Borghese R, Zannoni D (2010) Acetate permease (Act P) is responsible for tellurite (TeO<sub>3</sub><sup>2-</sup>) uptake and resistance in cells of the facultative phototroph *Rhodobacter capsulatus*. *Appl Environ Microbiol* 76(3):942–944
- Borse V, Kaler A, Banerjee UC (2015) Microbial synthesis of platinum nanoparticles and evaluation of their anticancer activity. *Int J Emerg Trends Electr Electron* 11(2):5283
- Borsetti F, Tremaroli V, Michelacci F, Borghese R, Winterstein C, Dalldal F, Zannoni D (2005) Tellurite effects on *Rhodobacter capsulatus* cell viability and superoxide dismutase activity under oxidative stress conditions. *Res Microbiol* 156(7):807–813
- Castro-Longoria E, Moreno-Velasquez SD, Vilchis-Nestor AR, Arenas-Berumen E, Avalos-Borja M (2012) Production of platinum nanoparticles and nanoaggregates using *Neurospora crassa*. *J Microbiol Biotechnol* 22(7):1000–1004
- Chen J, Lin Z, Ma X (2003) Evidence of the production of silver nanoparticles via pretreatment of *Phoma* sp. 3.2883 with silver nitrate. *Lett Appl Microbiol* 37(2):105–108
- Chinnaperumal K, Govindasamy B, Paramasivam D, Dilipkumar A, Dhayalan A, Vadivel A, Sengodan K, Pachiappan P (2018) Bio-pesticidal effects of *Trichoderma viride* formulated titanium dioxide nanoparticle and their physiological and biochemical changes on *Helicoverpa armigera* (hub.). *Pestic Biochem Physiol* 149:26–36
- Chowdhury S, Basu A, Kundu S (2014) Green synthesis of protein capped silver nanoparticles from phytopathogenic fungus *Macrophomina phaseolina* (Tassi) Goid with antimicrobial properties against multidrug-resistant bacteria. *Nanoscale Res Lett* 9(1):1–11
- Cologgi DL, Lampa-Pastirk S, Speers AM, Kelly SD, Reguera G (2011) Extracellular reduction of uranium via *Geobacter* conductive pili as a protective cellular mechanism. *Proc Natl Acad Sci* 108(37):15248–15252
- Costa PM, Cardoso AL, Mendonça LS, Serani A, Custódia C, Conceição M, Simões S, Moreira JN, De Almeida LP, De Lima MCP (2013) Tumor-targeted chlorotoxin-coupled nanoparticles for nucleic acid delivery to glioblastoma cells: a promising system for glioblastoma treatment. *Mol Ther Nucleic Acids* 2:e100
- Dameron C, Reese R, Mehra R, Kortan A, Carroll P, Steigerwald M, Brus L, Winge D (1989) Biosynthesis of cadmium sulphide quantum semiconductor crystallites. *Nature* 338(6216):596–597
- Daneshvar M, Hosseini MR (2018) From the iron boring scraps to superparamagnetic nanoparticles through an aerobic biological route. *J Hazard Mater* 357:393–400
- Darroudi M, Ahmad MB, Zamiri R, Zak A, Abdullah AH, Ibrahim NA (2011) Time-dependent effect in green synthesis of silver nanoparticles. *Int J Nanomedicine* 6:677
- Deepak V, Umamaheshwaran PS, Guhan K, Nanthini RA, Krithiga B, Jaithoon NMH, Gurunathan S (2011) Synthesis of gold and silver nanoparticles using purified URAK. *Colloids Surf B: Biointerfaces* 86(2):353–358
- Deplanche K, Macaskie L (2008) Biorecovery of gold by *Escherichia coli* and *Desulfovibrio desulfuricans*. *Biotechnol Bioeng* 99(5):1055–1064
- Deplanche K, Caldeleri I, Mikheenko IP, Sargent F, Macaskie LE (2010) Involvement of hydrogenases in the formation of highly catalytic Pd (0) nanoparticles by bioreduction of Pd (II) using *Escherichia coli* mutant strains. *Microbiology* 156(9):2630–2640
- Dhillon GS, Brar SK, Kaur S, Verma M (2012) Green approach for nanoparticle biosynthesis by fungi: current trends and applications. *Crit Rev Biotechnol* 32(1):49–73

- Durán N, Marcato PD, Alves OL, De Souza GI, Esposito E (2005) Mechanistic aspects of biosynthesis of silver nanoparticles by several *Fusarium oxysporum* strains. *J Nanobiotechnol* 3(1):1–7
- El-Batal AI, El-Sayyad GS, El-Ghamry A, Agaypi KM, Elsayed MA, Gobara M (2017) Melanin-gamma rays assistants for bismuth oxide nanoparticles synthesis at room temperature for enhancing antimicrobial, and photocatalytic activity. *J Photochem Photobiol B Biol* 173:120–139
- El-Bendary MA, Afifi SS, Moharam ME, Abo El-Ola SM, Salama A, Omara EA, Shaheen MN, Hamed AA, Gawdat NA (2021) Biosynthesis of silver nanoparticles using isolated *Bacillus subtilis*: characterization, antimicrobial activity, cytotoxicity, and their performance as antimicrobial agent for textile materials. *Prep Biochem Biotechnol* 51(1):54–68
- El-Sayyad GS, Mosallam FM, El-Batal AI (2018) One-pot green synthesis of magnesium oxide nanoparticles using *Penicillium chrysogenum* melanin pigment and gamma rays with antimicrobial activity against multidrug-resistant microbes. *Adv Powder Technol* 29(11):2616–2625
- Faramarzi S, Anzabi Y, Jafarizadeh-Malmiri H (2020) Nanobiotechnology approach in intracellular selenium nanoparticle synthesis using *Saccharomyces cerevisiae*—fabrication and characterization. *Arch Microbiol* 202(5):1203–1209
- Fatemi M, Mollania N, Momeni-Moghaddam M, Sadeghifar F (2018) Extracellular biosynthesis of magnetic iron oxide nanoparticles by *Bacillus cereus* strain HMH1: characterization and in vitro cytotoxicity analysis on MCF-7 and 3T3 cell lines. *J Biotechnol* 270:1–11
- Gade A, Bonde P, Ingle A, Marcato P, Duran N, Rai M (2008) Exploitation of *Aspergillus niger* for synthesis of silver nanoparticles. *J Biobaased Mater Bioenergy* 2(3):243–247
- Gaidhani SV, Yeshvekar RK, Shedbalkar UU, Bellare JH, Chopade BA (2014) Bio-reduction of hexachloroplatinic acid to platinum nanoparticles employing *Acinetobacter calcoaceticus*. *Process Biochem* 49(12):2313–2319
- Gardea-Torresdey J, Tiemann K, Dokken K, Pingitore N (1999) Recovery of gold (III) by alfalfa biomass and binding characterization using X-ray microfluorescence. *Adv Environ Res* 34: U7–93
- Ghani S, Rafiee B, Sadeghi D, Ahsani M (2017) Biosynthesis of iron nano-particles by *Bacillus megaterium* and its anti-bacterial properties. *J. Babol Univ Medical Sci* 19(7):13–19
- Gholami-Shabani M, Shams-Ghahfarokhi M, Gholami-Shabani Z, Akbarzadeh A, Riazi G, Ajdari S, Amani A, Razzaghi-Abyaneh M (2015) Enzymatic synthesis of gold nanoparticles using sulfite reductase purified from *Escherichia coli*: a green eco-friendly approach. *Process Biochem* 50(7):1076–1085
- Gurunathan S, Kalishwaralal K, Vaidyanathan R, Venkataraman D, Pandian SRK, Muniyandi J, Hariharan N, Eom SH (2009) Biosynthesis, purification and characterization of silver nanoparticles using *Escherichia coli*. *Colloids Surf B: Biointerfaces* 74(1):328–335
- Hazra C, Kundu D, Chaudhari A, Jana T (2013) Biogenic synthesis, characterization, toxicity and photocatalysis of zinc sulfide nanoparticles using rhamnolipids from *Pseudomonas aeruginosa* BS01 as capping and stabilizing agent. *J Chem Technol Biotechnol* 88(6):1039–1048
- He S, Guo Z, Zhang Y, Zhang S, Wang J, Gu N (2007) Biosynthesis of gold nanoparticles using the bacteria *Rhodospseudomonas capsulata*. *Mater Lett* 61(18):3984–3987
- Holmes JD, Smith PR, Evans-Gowing R, Richardson DJ, Russell DA, Sodeau JR (1995) Energy-dispersive X-ray analysis of the extracellular cadmium sulfide crystallites of *Klebsiella aerogenes*. *Arch Microbiol* 163(2):143–147
- Hulkoti NI, Taranath T (2014) Biosynthesis of nanoparticles using microbes—a review. *Colloids Surf B: Biointerfaces* 121:474–483
- Husain S, Sardar M, Fatma T (2015) Screening of cyanobacterial extracts for synthesis of silver nanoparticles. *World J Microbiol Biotechnol* 31(8):1279–1283
- Hussein M, Abd El-Aziz M, Badr Y, Mahmoud M (2007) Biosynthesis of gold nanoparticles using *Pseudomonas aeruginosa*. *Spectrochim Acta A Mol Biomol Spectrosc* 67(3–4): 1003–1006

- Husseiny SM, Salah TA, Anter HA (2015) Biosynthesis of size controlled silver nanoparticles by *Fusarium oxysporum*, their antibacterial and antitumor activities. *Beni Suef Univ J Basic Appl Sci* 4(3):225–231
- Iravani S (2014) Bacteria in nanoparticle synthesis: current status and future prospects. *Int Sch Res Notices* 2014:1–18
- Jayaseelan C, Rahuman AA, Kirthi AV, Marimuthu S, Santhoshkumar T, Bagavan A, Gaurav K, Karthik L, Rao KB (2012) Novel microbial route to synthesize ZnO nanoparticles using *Aeromonas hydrophila* and their activity against pathogenic bacteria and fungi. *Spectrochim Acta A Mol Biomol Spectrosc* 90:78–84
- Jayaseelan C, Rahuman AA, Roopan SM, Kirthi AV, Venkatesan J, Kim S-K, Iyappan M, Siva C (2013) Biological approach to synthesize TiO<sub>2</sub> nanoparticles using *Aeromonas hydrophila* and its antibacterial activity. *Spectrochim Acta A Mol Biomol Spectrosc* 107:82–89
- Kalimuthu K, Babu RS, Venkataraman D, Bilal M, Gurunathan S (2008) Biosynthesis of silver nanocrystals by *Bacillus licheniformis*. *Colloids Surf B: Biointerfaces* 65(1):150–153
- Kalishwaralal K, Deepak V, Pandian SRK, Kottaisamy M, Barath Mani Kanth S, Kartikeyan B, Gurunathan S (2010) Biosynthesis of silver and gold nanoparticles using *Brevibacterium casei*. *Colloids Surf B: Biointerfaces* 77(2):257–262
- Kalpna D, Lee YS (2013) Synthesis and characterization of bactericidal silver nanoparticles using cultural filtrate of simulated microgravity grown *Klebsiella pneumoniae*. *Enzym Microb Technol* 52(3):151–156
- Kalpna V, Kataru BAS, Sravani N, Vigneshwari T, Panneerselvam A, Rajeswari VD (2018) Biosynthesis of zinc oxide nanoparticles using culture filtrates of *Aspergillus niger*: antimicrobial textiles and dye degradation studies. *Open Nano* 3:48–55
- Karthik L, Kumar G, Kirthi AV, Rahuman A, Rao KB (2014) *Streptomyces* sp. LK3 mediated synthesis of silver nanoparticles and its biomedical application. *Bioprocess Biosyst Eng* 37(2): 261–267
- Kashyap PL, Kumar S, Srivastava AK, Sharma AK (2013) Myconanotechnology in agriculture: a perspective. *World J Microbiol Biotechnol* 29(2):191–207
- Kasture M, Patel P, Prabhune A, Ramana C, Kulkarni A, Prasad B (2008) Synthesis of silver nanoparticles by sophorolipids: effect of temperature and sophorolipid structure on the size of particles. *J Chem Sci* 120(6):515–520
- Kathiresan K, Manivannan S, Nabeel M, Dhivya B (2009) Studies on silver nanoparticles synthesized by a marine fungus, *Penicillium fellutanum* isolated from coastal mangrove sediment. *Colloids Surf B: Biointerfaces* 71(1):133–137
- Kato Y, Suzuki M (2020) Synthesis of metal nanoparticles by microorganisms. *Crystals* 10(7):589
- Kiran GS, Sabu A, Selvin J (2010) Synthesis of silver nanoparticles by glycolipid biosurfactant produced from marine *Brevibacterium casei* MSA1. *J Biotechnol* 148(4):221–225
- Kirthi AV, Rahuman AA, Rajakumar G, Marimuthu S, Santhoshkumar T, Jayaseelan C, Elango G, Zahir AA, Kamaraj C, Bagavan A (2011) Biosynthesis of titanium dioxide nanoparticles using bacterium *Bacillus subtilis*. *Mater Lett* 65(17–18):2745–2747
- Klaus T, Joerger R, Olsson E, Granqvist C-G (1999) Silver-based crystalline nanoparticles, microbially fabricated. *Proc Natl Acad Sci* 96(24):13611–13614
- Konishi Y, Tsukiyama T, Ohno K, Saitoh N, Nomura T, Nagamine S (2006) Intracellular recovery of gold by microbial reduction of AuCl<sub>4</sub><sup>-</sup> ions using the anaerobic bacterium *Shewanella* algae. *Hydrometallurgy* 81(1):24–29
- Konishi Y, Ohno K, Saitoh N, Nomura T, Nagamine S, Hishida H, Takahashi Y, Uruga T (2007) Bioreductive deposition of platinum nanoparticles on the bacterium *Shewanella* algae. *J Biotechnol* 128(3):648–653
- Korbekandi H, Mohseni S, Mardani Jouneghani R, Pourhossein M, Iravani S (2016) Biosynthesis of silver nanoparticles using *Saccharomyces cerevisiae*. *Artif Cells Nanomed Biotechnol* 44(1): 235–239

- Kumar SA, Abyaneh MK, Gosavi S, Kulkarni SK, Pasricha R, Ahmad A, Khan M (2007) Nitrate reductase-mediated synthesis of silver nanoparticles from AgNO<sub>3</sub>. *Biotechnol Lett* 29(3): 439–445
- Kumar CG, Mamidyala SK, Das B, Sridhar B, Devi GS, Karuna MS (2010) Synthesis of biosurfactant-based silver nanoparticles with purified rhamnolipids isolated from *Pseudomonas aeruginosa* BS-161R. *J Microbiol Biotechnol* 20(7):1061–1068
- Kumar I, Mondal M, Sakthivel N (2019) Green synthesis of phyto-genic nanoparticles. In: *Green synthesis, characterization and applications of nanoparticles*. Elsevier, Amsterdam, pp 37–73
- Kundu D, Hazra C, Chatterjee A, Chaudhari A, Mishra S (2014) Extracellular biosynthesis of zinc oxide nanoparticles using *Rhodococcus pyridinivorans* NT2: multifunctional textile finishing, biosafety evaluation and in vitro drug delivery in colon carcinoma. *J Photochem Photobiol B Biol* 140:194–204
- Kuzajewska D, Wszolek A, Żwierzeło W, Kirczuk L, Maruszevska A (2020) Magnetotactic bacteria and magnetosomes as smart drug delivery systems: a new weapon on the battlefield with cancer? *Biology* 9(5):102
- Lahiri D, Nag M, Sheikh HI, Sarkar T, Edinur H, Pati S, Ray R (2021) Microbiologically synthesized nanoparticles and their role in silencing the biofilm signaling cascade. *Front Microbiol* 12:180
- Lengke MF, Fleet ME, Southam G (2006) Morphology of gold nanoparticles synthesized by filamentous cyanobacteria from gold (I)– thiosulfate and gold (III)– chloride complexes. *Langmuir* 22(6):2780–2787
- Lengke MF, Fleet ME, Southam G (2007) Biosynthesis of silver nanoparticles by filamentous cyanobacteria from a silver (I) nitrate complex. *Langmuir* 23(5):2694–2699
- Liu Y, Wang Z, Liu J, Levar C, Edwards MJ, Babauta JT, Kennedy DW, Shi Z, Beyenal H, Bond DR (2014) A trans-outer membrane porin-cytochrome protein complex for extracellular electron transfer by *Geobacter sulfurreducens* PCA. *Environ Microbiol Rep* 6(6):776–785
- Liu Y, Fredrickson JK, Zachara JM, Shi L (2015) Direct involvement of ombB, omaB, and omcB genes in extracellular reduction of Fe (III) by *Geobacter sulfurreducens* PCA. *Front Microbiol* 6: 1075
- Lloyd JR, Yong P, Macaskie LE (1998) Enzymatic recovery of elemental palladium by using sulfate-reducing bacteria. *Appl Environ Microbiol* 64(11):4607–4609
- Lynch I, Cedervall T, Lundqvist M, Cabaleiro-Lago C, Linse S, Dawson KA (2007) The nanoparticle–protein complex as a biological entity; a complex fluids and surface science challenge for the 21st century. *Adv Colloid Interf Sci* 134:167–174
- Malarkodi C, Rajeshkumar S, Vanaja M, Paulkumar K, Gnanajobitha G, Annadurai G (2013) Eco-friendly synthesis and characterization of gold nanoparticles using *Klebsiella pneumoniae*. *J Nanostructure Chem* 3(1):1–7
- Manikprabhu D, Lingappa K (2013) Microwave assisted rapid and green synthesis of silver nanoparticles using a pigment produced by *Streptomyces coelicolor* klmp33. *Bioinorg Chem Appl* 2013:1–5
- Manikprabhu D, Lingappa K (2014) Synthesis of silver nanoparticles using the *Streptomyces coelicolor* klmp33 pigment: an antimicrobial agent against extended-spectrum beta-lactamase (ESBL) producing *Escherichia coli*. *Mater Sci Eng C* 45:434–437
- Mann S (2001) *Biomaterialization: principles and concepts in bioinorganic materials chemistry*, vol 5. Oxford University Press, New York
- Marchiol L (2012) Synthesis of metal nanoparticles in living plants. *Ital J Agron* 7:e37–e37
- Martins M, Mourato C, Sanches S, Noronha JP, Crespo MB, Pereira IA (2017) Biogenic platinum and palladium nanoparticles as new catalysts for the removal of pharmaceutical compounds. *Water Res* 108:160–168
- Maruyama T, Fujimoto Y, Maekawa T (2015) Synthesis of gold nanoparticles using various amino acids. *J Colloid Interface Sci* 447:254–257

- Mashrai A, Khanam H, Aljawfi RN (2017) Biological synthesis of ZnO nanoparticles using *C. albicans* and studying their catalytic performance in the synthesis of steroidal pyrazolines. *Arab J Chem* 10:S1530–S1536
- Mewada A, Oza G, Pandey S, Sharon M (2012) Extracellular synthesis of gold nanoparticles using *Pseudomonas denitrificans* and comprehending its stability. *J Microbiol Biotech Res* 2(4): 493–499
- Moghaddam AB, Moniri M, Azizi S, Rahim RA, Ariff AB, Saad WZ, Namvar F, Navaderi M, Mohamad R (2017) Biosynthesis of ZnO nanoparticles by a new *Pichia kudriavzevii* yeast strain and evaluation of their antimicrobial and antioxidant activities. *Molecules* 22(6):872
- Mohanta YK, Behera SK (2014) Biosynthesis, characterization and antimicrobial activity of silver nanoparticles by *Streptomyces* sp. SS2. *Bioprocess Biosyst Eng* 37(11):2263–2269
- Mokhtari N, Daneshpajouh S, Seyedbagheri S, Atashdehghan R, Abdi K, Sarkar S, Minaian S, Shahverdi HR, Shahverdi AR (2009) Biological synthesis of very small silver nanoparticles by culture supernatant of *Klebsiella pneumoniae*: the effects of visible-light irradiation and the liquid mixing process. *Mater Res Bull* 44(6):1415–1421
- Mondal M, Vadivel M, Louis L, Sakthivel N (2021) Phyto-genic synthesis of gold nanoparticles: mechanisms and applications. In: *Nanobiotechnology*. Elsevier, pp 187–210
- Mosallam FM, El-Sayyad GS, Fathy RM, El-Batal AI (2018) Biomolecules-mediated synthesis of selenium nanoparticles using *Aspergillus oryzae* fermented Lupin extract and gamma radiation for hindering the growth of some multidrug-resistant bacteria and pathogenic fungi. *Microb Pathog* 122:108–116
- Mukherjee P, Ahmad A, Mandal D, Senapati S, Sainkar SR, Khan MI, Parishcha R, Ajaykumar P, Alam M, Kumar R (2001) Fungus-mediated synthesis of silver nanoparticles and their immobilization in the mycelial matrix: a novel biological approach to nanoparticle synthesis. *Nano Lett* 1(10):515–519
- Mukherjee K, Gupta R, Kumar G, Kumari S, Biswas S, Padmanabhan P (2018) Synthesis of silver nanoparticles by *Bacillus clausii* and computational profiling of nitrate reductase enzyme involved in production. *J Genet Eng Biotechnol* 16(2):527–536
- Naik RR, Stringer SJ, Agarwal G, Jones SE, Stone MO (2002) Biomimetic synthesis and patterning of silver nanoparticles. *Nat Mater* 1(3):169–172
- Nangia Y, Wangoo N, Goyal N, Shekhawat G, Suri CR (2009) A novel bacterial isolate *Stenotrophomonas maltophilia* as living factory for synthesis of gold nanoparticles. *Microb Cell Factories* 8(1):1–7
- Narasimha G, Alzohairy M, Khadri H, Mallikarjuna K (2013) Extracellular synthesis, characterization and antibacterial activity of silver nanoparticles by actinomycetes isolate. *Int J Nano Dimens* 4(1):77–83
- Narayanan KB, Sakthivel N (2010) Biological synthesis of metal nanoparticles by microbes. *Adv Colloid Interf Sci* 156(1–2):1–13
- Narayanan J, Ramji R, Sahu H, Gautam P (2010) Synthesis, stabilisation and characterisation of rhamnolipid-capped ZnS nanoparticles in aqueous medium. *IET Nanobiotechnol* 4(2):29–34
- Newman DK, Kolter R (2000) A role for excreted quinones in extracellular electron transfer. *Nature* 405(6782):94–97
- Ng CK, Sivakumar K, Liu X, Madhaiyan M, Ji L, Yang L, Tang C, Song H, Kjelleberg S, Cao B (2013) Influence of outer membrane c-type cytochromes on particle size and activity of extracellular nanoparticles produced by *Shewanella oneidensis*. *Biotechnol Bioeng* 110(7): 1831–1837
- Noman M, Shahid M, Ahmed T, Tahir M, Naqqash T, Muhammad S, Song F, Abid HMA, Aslam Z (2020) Green copper nanoparticles from a native *Klebsiella pneumoniae* strain alleviated oxidative stress impairment of wheat plants by reducing the chromium bioavailability and increasing the growth. *Ecotoxicol Environ Saf* 192:110303
- Otari S, Patil R, Nadaf N, Ghosh S, Pawar S (2012) Green biosynthesis of silver nanoparticles from an actinobacteria *Rhodococcus* sp. *Mater Lett* 72:92–94

- Oza G, Pandey S, Gupta A, Kesarkar R, Sharon M (2012) Biosynthetic reduction of gold ions to gold nanoparticles by *Nocardia farcinica*. *J Microbiol Biotechnol Res* 2(4):511–515
- Palanisamy P (2008) Biosurfactant mediated synthesis of NiO nanorods. *Mater Lett* 62(4–5):743–746
- Pandey B (2012) Synthesis of zinc-based nanomaterials: a biological perspective. *IET Nanobiotechnol* 6(4):144–148
- Parikh RY, Ramanathan R, Coloe PJ, Bhargava SK, Patole MS, Shouche YS, Bansal V (2011) Genus-wide physicochemical evidence of extracellular crystalline silver nanoparticles biosynthesis by *Morganella* spp. *PLoS One* 6(6):e21401
- Park Y, Hong Y, Weyers A, Kim Y, Linhardt R (2011) Polysaccharides and phytochemicals: a natural reservoir for the green synthesis of gold and silver nanoparticles. *IET Nanobiotechnol* 5(3):69–78
- Phanjom P, Ahmed G (2015) Biosynthesis of silver nanoparticles by *Aspergillus oryzae* (MTCC No. 1846) and its characterizations. *Nanosci Nanotechnol* 5(1):14–21
- Pollmann K, Raff J, Merroun M, Fahmy K, Selenska-Pobell S (2006) Metal binding by bacteria from uranium mining waste piles and its technological applications. *Biotechnol Adv* 24(1):58–68
- Prakash A, Sharma S, Ahmad N, Ghosh A, Sinha P (2010) Bacteria mediated extracellular synthesis of metallic nanoparticles. *Int Res J Biotechnol* 1(5):071–079
- Prakash A, Sharma S, Ahmad N, Ghosh A, Sinha P (2011) Synthesis of AgNps by *Bacillus cereus* bacteria and their antimicrobial potential. *J Biomater Nanobiotechnol* 2(02):155
- Prasad K, Jha AK (2009) ZnO nanoparticles: synthesis and adsorption study. *Nat Sci* 1(02):129
- Prasad K, Jha AK, Kulkarni A (2007) *Lactobacillus* assisted synthesis of titanium nanoparticles. *Nanoscale Res Lett* 2(5):248–250
- Rai A, Singh A, Ahmad A, Sastry M (2006) Role of halide ions and temperature on the morphology of biologically synthesized gold nanotriangles. *Langmuir* 22(2):736–741
- Rajeshkumar S, Malarkodi C, Paulkumar K, Vanaja M, Gnanajobitha G, Annadurai G (2013) Intracellular and extracellular biosynthesis of silver nanoparticles by using marine bacteria *Vibrio alginolyticus*. *Nanosci Nanotechnol* 3(1):21–25
- Rajeswaran S, Thirugnanasambandan SS, Dewangan NK, Moorthy RK, Kandasamy S, Vilwanathan R (2020) Multifarious pharmacological applications of green routed eco-friendly iron nanoparticles synthesized by *Streptomyces* Sp.(SRT12). *Biol Trace Elem Res* 194(1):273–283
- Raliya R, Tarafdar J (2014) Biosynthesis and characterization of zinc, magnesium and titanium nanoparticles: an eco-friendly approach. *Int Nano Lett* 4(1):93
- Rane AN, Baikar VV, Ravi Kumar V, Deopurkar RL (2017) Agro-industrial wastes for production of biosurfactant by *Bacillus subtilis* ANR 88 and its application in synthesis of silver and gold nanoparticles. *Front Microbiol* 8:492
- Reddy AS, Chen C-Y, Chen C-C, Jean J-S, Fan C-W, Chen H-R, Wang J-C, Nimje VR (2009) Synthesis of gold nanoparticles via an environmentally benign route using a biosurfactant. *J Nanosci Nanotechnol* 9(11):6693–6699
- Riddin T, Gericke M, Whiteley C (2006) Analysis of the inter- and extracellular formation of platinum nanoparticles by *Fusarium oxysporum* f. sp. *lycopersici* using response surface methodology. *Nanotechnology* 17(14):3482
- Roy S, Das TK, Maiti GP, Basu U (2016) Microbial biosynthesis of nontoxic gold nanoparticles. *Mater Sci Eng B* 203:41–51
- Sabaty M, Avazeri C, Pignol D, Vermiglio A (2001) Characterization of the reduction of selenate and tellurite by nitrate reductases. *Appl Environ Microbiol* 67(11):5122–5126
- Samadi N, Golkaran D, Eslamifard A, Jamalifar H, Fazeli MR, Mohseni FA (2009) Intra/extracellular biosynthesis of silver nanoparticles by an autochthonous strain of *Proteus mirabilis* isolated from photographic waste. *J Biomed Nanotechnol* 5(3):247–253
- Sanghi R, Verma P (2009) A facile green extracellular biosynthesis of CdS nanoparticles by immobilized fungus. *Chem Eng J* 155(3):886–891

- Sarathy V, Tratnyek PG, Nurmi JT, Baer DR, Amonette JE, Chun CL, Penn RL, Reardon EJ (2008) Aging of iron nanoparticles in aqueous solution: effects on structure and reactivity. *J Phys Chem C* 112(7):2286–2293
- Saravanan C, Rajesh R, Kaviarasan T, Muthukumar K, Kavita D, Shetty PH (2017) Synthesis of silver nanoparticles using bacterial exopolysaccharide and its application for degradation of azo-dyes. *Biotechnol Rep* 15:33–40
- Sastry M, Ahmad A, Khan MI, Kumar R (2003) Biosynthesis of metal nanoparticles using fungi and actinomycete. *Curr Sci* 85:162–170
- Sathiyarayanan G, Dineshkumar K, Yang Y-H (2017) Microbial exopolysaccharide-mediated synthesis and stabilization of metal nanoparticles. *Crit Rev Microbiol* 43(6):731–752
- Schlüter M, Hentzel T, Suarez C, Koch M, Lorenz WG, Böhm L, Düring R-A, Koinig KA, Bunge M (2014) Synthesis of novel palladium (0) nanocatalysts by microorganisms from heavy-metal-influenced high-alpine sites for dehalogenation of polychlorinated dioxins. *Chemosphere* 117:462–470
- Selvarajan E, Mohanasrinivasan V (2013) Biosynthesis and characterization of ZnO nanoparticles using *Lactobacillus plantarum* VITES07. *Mater Lett* 112:180–182
- Shamim S (2018) Biosorption of heavy metals. *Biosorption* 2:21–49
- Shanthi S, Jayaseelan BD, Velusamy P, Vijayakumar S, Chih CT, Vaseeharan B (2016) Biosynthesis of silver nanoparticles using a probiotic *Bacillus licheniformis* Dab1 and their antibiofilm activity and toxicity effects in *Ceriodaphnia cornuta*. *Microb Pathog* 93:70–77
- Shedbalkar U, Singh R, Wadhvani S, Gaidhani S, Chopade B (2014) Microbial synthesis of gold nanoparticles: current status and future prospects. *Adv Colloid Interf Sci* 209:40–48
- Shi L, Rosso KM, Clarke TA, Richardson DJ, Zachara JM, Fredrickson JK (2012) Molecular underpinnings of Fe (III) oxide reduction by *Shewanella oneidensis* MR-1. *Front Microbiol* 3:50
- Shivaji S, Madhu S, Singh S (2011) Extracellular synthesis of antibacterial silver nanoparticles using psychrophilic bacteria. *Process Biochem* 46(9):1800–1807
- Shivashankarappa A, Sanjay K (2015) Study on biological synthesis of cadmium sulfide nanoparticles by *Bacillus licheniformis* and its antimicrobial properties against food borne pathogens. *Nanosci Nanotechnol Res* 3(1):6–15
- Shu M, He F, Li Z, Zhu X, Ma Y, Zhou Z, Yang Z, Gao F, Zeng M (2020) Biosynthesis and antibacterial activity of silver nanoparticles using yeast extract as reducing and capping agents. *Nanoscale Res Lett* 15(1):1–9
- Shunmugam R, Balusamy SR, Kumar V, Menon S, Lakshmi T, Perumalsamy H (2021) Biosynthesis of gold nanoparticles using marine microbe (*Vibrio alginolyticus*) and its anticancer and antioxidant analysis. *J King Saud Univ Sci* 33(1):101260
- Simkiss K, Wilbur KM (2012) *Biomaterialization*. Elsevier, Burlington
- Singh S, Bhatta UM, Satyam P, Dhawan A, Sastry M, Prasad B (2008) Bacterial synthesis of silicon/silica nanocomposites. *J Mater Chem* 18(22):2601–2606
- Singh BR, Dwivedi S, Al-Khedhairi AA, Musarrat J (2011) Synthesis of stable cadmium sulfide nanoparticles using surfactin produced by *Bacillus amyloliquifaciens* strain KSU-10. *Colloids Surf B: Biointerfaces* 85(2):207–213
- Singh D, Rathod V, Ninganagouda S, Herimath J, Kulkarni P (2013a) Biosynthesis of silver nanoparticle by endophytic fungi *Penicillium* sp. isolated from *Curcuma longa* (turmeric) and its antibacterial activity against pathogenic gram negative bacteria. *J Pharm Res* 7(5):448–453
- Singh R, Wagh P, Wadhvani S, Gaidhani S, Kumbhar A, Bellare J, Chopade BA (2013b) Synthesis, optimization, and characterization of silver nanoparticles from *Acinetobacter calcoaceticus* and their enhanced antibacterial activity when combined with antibiotics. *Int J Nanomedicine* 8:4277
- Singh BN, Rawat AKS, Khan W, Naqvi AH, Singh BR (2014) Biosynthesis of stable antioxidant ZnO nanoparticles by *Pseudomonas aeruginosa* rhamnolipids. *PLoS One* 9(9):e106937
- Singh P, Kim YJ, Singh H, Mathiyalagan R, Wang C, Yang DC (2015) Biosynthesis of anisotropic silver nanoparticles by *Bhargavaea indica* and their synergistic effect with antibiotics against pathogenic microorganisms. *J Nanomater* 2015:1–10

- Singh N, Naik B, Kumar V, Kumar V, Gupta S (2021) Actinobacterial pigment assisted synthesis of nanoparticles and its biological activity: nanoparticles and its biological activity. *J Microbiol Biotechnol Food Sci* 10(4):604–608
- Sintubin L, De Windt W, Dick J, Mast J, Van Der Ha D, Verstraete W, Boon N (2009) Lactic acid bacteria as reducing and capping agent for the fast and efficient production of silver nanoparticles. *Appl Microbiol Biotechnol* 84(4):741–749
- Slavin YN, Asnis J, Häfeli UO, Bach H (2017) Metal nanoparticles: understanding the mechanisms behind antibacterial activity. *J Nanobiotechnol* 15(1):1–20
- Somorjai GA, Park JY (2008) Colloid science of metal nanoparticle catalysts in 2D and 3D structures. Challenges of nucleation, growth, composition, particle shape, size control and their influence on activity and selectivity. *Top Catal* 49(3–4):126–135
- Soni N, Prakash S (2011) Factors affecting the geometry of silver nanoparticles synthesis in *Chrysosporium tropicum* and *Fusarium oxysporum*. *Am J Nanotechnol* 2(1):112–121
- Sriramulu M, Sumathi S (2018) Biosynthesis of palladium nanoparticles using *Saccharomyces cerevisiae* extract and its photocatalytic degradation behaviour. *Adv Nat Sci Nanosci Nanotechnol* 9(2):025018
- Srivastava SK, Constanti M (2012) Room temperature biogenic synthesis of multiple nanoparticles (Ag, Pd, Fe, Rh, Ni, Ru, Pt, Co, and Li) by *Pseudomonas aeruginosa* SM1. *J Nanopart Res* 14(4):1–10
- Stephen JR, Macnaughtont SJ (1999) Developments in terrestrial bacterial remediation of metals. *Curr Opin Biotechnol* 10(3):230–233
- Sundaram PA, Augustine R, Kannan M (2012) Extracellular biosynthesis of iron oxide nanoparticles by *Bacillus subtilis* strains isolated from rhizosphere soil. *Biotechnol Bioprocess Eng* 17(4):835–840
- Sweeney RY, Mao C, Gao X, Burt JL, Belcher AM, Georgiou G, Iverson BL (2004) Bacterial biosynthesis of cadmium sulfide nanocrystals. *Chem Biol* 11(11):1553–1559
- Syed A, Ahmad A (2012) Extracellular biosynthesis of platinum nanoparticles using the fungus *Fusarium oxysporum*. *Colloids Surf B: Biointerfaces* 97:27–31
- Tanzil AH, Sultana ST, Saunders SR, Shi L, Marsili E, Beyenal H (2016) Biological synthesis of nanoparticles in biofilms. *Enzym Microb Technol* 95:4–12
- Tarafdar JC, Raliya R (2013) Rapid, low-cost, and ecofriendly approach for iron nanoparticle synthesis using *Aspergillus oryzae* TFR. *J Nanoparticles* 2013:4. <https://doi.org/10.1155/2013/141274>
- Thakkar KN, Mhatre SS, Parikh RY (2010) Biological synthesis of metallic nanoparticles. *Nanomedicine* 6(2):257–262
- Thatheyus AJ, Ramya D (2016) Biosorption of chromium using bacteria: an overview. *Sci Int* 4(2):74–79
- Tran QH, Le A-T (2013) Silver nanoparticles: synthesis, properties, toxicology, applications and perspectives. *Adv Nat Sci Nanosci Nanotechnol* 4(3):033001
- Tripathi R, Bhadwal AS, Singh P, Shrivastav A, Singh M, Shrivastav B (2014) Mechanistic aspects of biogenic synthesis of CdS nanoparticles using *Bacillus licheniformis*. *Adv Nat Sci Nanosci Nanotechnol* 5(2):025006
- Uddandarao P, Balakrishnan RM, Ashok A, Swarup S, Sinha P (2019) Bioinspired ZnS: Gd nanoparticles synthesized from an endophytic fungi *Aspergillus flavus* for fluorescence-based metal detection. *Biomimetics* 4(1):11
- Vainshtein M, Belova N, Kulakovskaya T, Suzina N, Sorokin V (2014) Synthesis of magneto-sensitive iron-containing nanoparticles by yeasts. *J Ind Microbiol Biotechnol* 41(4):657–663
- Vanaja M, Rajeshkumar S, Paulkumar K, Gnanajobitha G, Malarkodi C, Annadurai G (2013) Kinetic study on green synthesis of silver nanoparticles using *Coleus aromaticus* leaf extract. *Adv Appl Sci Res* 4(3):50–55
- Vasanthakumar A, DeAraujo A, Mazurek J, Schilling M, Mitchell R (2015) Pyomelanin production in *Penicillium chrysogenum* is stimulated by L-tyrosine. *Microbiology* 161(6):1211–1218



- Vasylevskiy SI, Kracht S, Corcosa P, Fromm KM, Giese B, Füg M (2017) Formation of silver nanoparticles by electron transfer in peptides and c-cytochromes. *Angew Chem Int Ed* 56(21): 5926–5930
- Velásquez L, Dussan J (2009) Biosorption and bioaccumulation of heavy metals on dead and living biomass of *Bacillus sphaericus*. *J Hazard Mater* 167(1–3):713–716
- Vetchinkina EP, Loshchinina EA, Vodolazov IR, Kursky VF, Dykman LA, Nikitina VE (2017) Biosynthesis of nanoparticles of metals and metalloids by basidiomycetes. Preparation of gold nanoparticles by using purified fungal phenol oxidases. *Appl Microbiol Biotechnol* 101(3): 1047–1062
- Vetchinkina E, Loshchinina E, Kupryashina M, Burov A, Pylaev T, Nikitina V (2018) Green synthesis of nanoparticles with extracellular and intracellular extracts of basidiomycetes. *Peer J* 6:e5237
- Vetchinkina E, Loshchinina E, Kupryashina M, Burov A, Nikitina V (2019) Shape and size diversity of gold, silver, selenium, and silica nanoparticles prepared by green synthesis using fungi and bacteria. *Ind Eng Chem Res* 58(37):17207–17218
- Vigneshwaran N, Ashtaputre N, Varadarajan P, Nachane R, Paralikar K, Balasubramanya R (2007) Biological synthesis of silver nanoparticles using the fungus *Aspergillus flavus*. *Mater Lett* 61(6):1413–1418
- Vijayabharathi R, Sathya A, Gopalakrishnan S (2018) Extracellular biosynthesis of silver nanoparticles using *Streptomyces griseoplanus* SAI-25 and its antifungal activity against *Macrophomina phaseolina*, the charcoal rot pathogen of sorghum. *Biocatal Agric Biotechnol* 14:166–171
- Waghmode MS, Gunjal AB, Mulla JA, Patil NN, Nawani NN (2019) Studies on the titanium dioxide nanoparticles: biosynthesis, applications and remediation. *SN Appl Sci* 1(4):1
- Windt WD, Aelterman P, Verstraete W (2005) Bioreductive deposition of palladium (0) nanoparticles on *Shewanella oneidensis* with catalytic activity towards reductive dechlorination of polychlorinated biphenyls. *Environ Microbiol* 7(3):314–325
- Wu Z, Wang Z, Guan B, Wang X, Zhang Y, Xiao Y, Zhi B, Liu Y, Li Z, Huo Q (2013) Improving the properties of  $\beta$ -galactosidase from *Aspergillus oryzae* via encapsulation in aggregated silica nanoparticles. *New J Chem* 37(11):3793–3797
- Wu R, Tian X, Xiao Y, Ulstrup J, Christensen HEM, Zhao F, Zhang J (2018) Selective electrocatalysis of biofuel molecular oxidation using palladium nanoparticles generated on *Shewanella oneidensis* MR-1. *J Mater Chem A* 6(23):10655–10662
- Yadav V, Sharma N, Prakash R, Raina KK, Bharadwaj L, Prakash NT (2008) Generation of selenium containing nano-structures by soil bacterium *Pseudomonas Aeruginosa*. *Biotechnology* 7(2):299–304
- Yates MD, Cusick RD, Logan BE (2013) Extracellular palladium nanoparticle production using *Geobacter sulfurreducens*. *ACS Sustain Chem Eng* 1(9):1165–1171
- Yong P, Rowson NA, Farr JPG, Harris IR, Macaskie LE (2002) Bioreduction and biocrystallization of palladium by *Desulfovibrio desulfuricans* NCIMB 8307. *Biotechnol Bioeng* 80(4):369–379
- Zaki SA, Eltarahony MM, Abd-El-Haleem DA (2019) Disinfection of water and wastewater by biosynthesized magnetite and zerovalent iron nanoparticles via NAP-NAR enzymes of *Proteus mirabilis* 10B. *Environ Sci Pollut Res* 26(23):23661–23678
- Zhang X, Yan S, Tyagi R, Surampalli R (2011) Synthesis of nanoparticles by microorganisms and their application in enhancing microbiological reaction rates. *Chemosphere* 82(4):489–494

# Chapter 7

## Bacterial Production of Metal(loid) Nanostructures



Nikhil Pradhan and Raymond J. Turner

**Abstract** Nanomaterials (NM) are of interest due to their unique properties allowing for widespread applications. Physical and chemical approaches are the standard method of synthesis, but due to the negative aspects of traditional manufacturing protocols that can be energy expensive or use toxic chemicals, interest in biologically produced NMs is gaining traction. While plant-based NM synthesis is currently the most popular, there is a growing interest in using microbes to carry out this task. Bacteria are able to utilize the wide array of reducing and oxidizing powers in the cell to convert metal salts into NMs. Bacteria can produce NMs in a variety of structures including nanocrystals, nanowires, nanoparticles (spheres), and nanorods. These NMs may form extracellularly or intracellularly. NMs produced by bacteria to date have been comprised of silver, gold, selenium, tellurium, zinc, titanium, nickel, arsenic, tin, iron, platinum and cadmium or hetero atom mixtures thereof. There have been advances in controlling the shape and size of the metal(loid) NMs produced using bacteria, which is one of the most important aspects when producing NMs. Further research into those biomolecules that are important for the coating and stabilization of biologically produced nanoparticles is needed, and bacterial coats have been found to offer unique properties over traditional chemically synthesized metal(loid) NMs. Metal(loid) based NM production using microbes is a growing field that has made considerable advances in recent years.

### 7.1 Introduction

Nanoscience is an emerging field with important unique terminology that often gets misused. It is the study of nanomaterial (NM) which describes materials that have a nanoscale dimension (1–100 nm) (Horikoshi and Serpone 2013). Nanomaterials are synthesized at the atom scale and can comprise of various chemicals and elements.

---

N. Pradhan · R. J. Turner (✉)

Department of Biological Sciences, University of Calgary, Calgary, AB, Canada

e-mail: [nikhil.pradhan@ucalgary.ca](mailto:nikhil.pradhan@ucalgary.ca); [turnerr@ucalgary.ca](mailto:turnerr@ucalgary.ca)

© Springer Nature Switzerland AG 2022

C. J. Hurst (ed.), *Microbial Metabolism of Metals and Metalloids*, Advances in Environmental Microbiology 10, [https://doi.org/10.1007/978-3-030-97185-4\\_7](https://doi.org/10.1007/978-3-030-97185-4_7)

167

They can be produced in a variety of structures on the nanoscale. Nanostructures that have three external nanoscale dimensions are referred to as nanoparticles (NP). Different shapes can be found for NPs including spherical, cubic, trigonal, hexagonal, octahedral or even irregular crystalline like shapes. Other nanostructures include: Nanorods (NR), nanowires (NW) and nanosheets also called nanoplates (NP) and are separately defined as they have different lengths in the long and short axes. Nanomaterials may be composed from a variety of materials from metals, inorganic and or organic compounds. For more general information on nanomaterials see these suggested reviews (Mody et al. 2010; Sharma et al. 2015; Bahadar et al. 2016; Slavin et al. 2017; Jeevanandam et al. 2018; Piacenza et al. 2018c; Bernardos et al. 2019; Khan et al. 2019; Yaqoob et al. 2020; Ijaz et al. 2020).

Modern nanomaterial synthesis places a heavy focus on turning sizes and shapes of the synthesized nanostructures. This is because the size and shape dictate their physicochemical properties such as absorbance, fluorescence, and conductance (Dreaden et al. 2012; Mourdikoudis et al. 2018) and their large area to volume ratio leads to excellent properties for catalysis (Xie et al. 2020). The goal is scaled up synthesis protocols that give monodisperse particles of defined size and shape (Khan et al. 2019). Although nanomaterials can be produced using a variety of organic and inorganic starting materials, this review focuses on metal nanomaterials that can be produced by bacteria. We see nanomaterials comprised of metals and metalloids by using such starting elements as: silver, gold, selenium, tellurium, zinc, nickel, arsenic, titanium, tin, iron, platinum, cobalt and cadmium (Wang and Wang 2014; Khan et al. 2019). Due to metal(loid) nanomaterials unique properties, they are found in applications such as catalysts, biocides, electronics, solar panels and bioimaging (Salata 2004; Khan et al. 2019).

Metal nanomaterial functionality is derived from the elemental composition, size and shape. Size and shape of particles can result in changes in the NP functionality, with the photophysical properties being one of the most striking (Banerjee et al. 2016). This is because as the size and shape of the nanoparticle changes, so does the surface plasmon resonance, which is the phenomenon that enables NPs to have enhanced quantum yield characteristics and subsequently very 'bright' fluorescence (Jana et al. 2016). Some metal NPs have been used for drug delivery and cancer therapy (Ahmad et al. 2010). In these cases, the size of the metal nanoparticle needs to be small enough to reach the intended location inside the body (De Jong and Borm 2008). Metal nanomaterials have also been widely explored for their antimicrobial properties (Khan et al. 2020). For any application, it is important to create a uniform population of NPs, and as such a large amount of effort has gone into fine tuning synthesis parameters to do so.

Conventional production of nanoparticles is performed via specific reagent based chemical synthesis or with physical techniques such as high temperatures from lasers, microwaves or ultrasound in either bottom-up or top-down approaches (Schwarz et al. 2014). Through chemical synthesis, metal salts mixed with defined reducing or oxidizing agents, as well as specific capping chemicals, provides focused synthesis of a specified particle (Gudikandula and Charya Maringanti 2016). Physical-chemical synthesis of nanoparticles offers tight control over the size and shape of the synthesized particles by altering concentrations, temperature,

pressure and synthesis time (Lane and Zimmerman 2019). For decades, these physical-chemical methods have been the standard or traditional routes to synthesize nanostructures. However, reducing agents can often be harmful, expensive, and have challenging waste control measures, making them increasingly less desirable when synthesis processes are scaled up (Abdul Salam et al. 2014). This has led to exploring 'green' or 'eco-friendly' synthetic approaches that utilize biological systems to produce nanoparticles.

Eco-friendly synthesis of nanoparticles using biological systems (Biogenic) is typically done with microbes (bacteria, yeasts and fungi), or plants and their extracts (Sharma et al. 2015; Fawcett et al. 2017; Piacenza et al. 2018b). Within these organisms are a large variety of biochemical molecules that are electron rich sources to reduce metal salts and form nanoparticles. Examples include: reducing sugars, reductive enzymes, amino acids, reducing cofactors such as glutathione and NAD (P)H (Hulkoti and Taranath 2014; Keat et al. 2015). This eliminates the use of harsh reductive chemicals (such as borohydrides) leading to a safer manufacturing process and potentially less expensive as well (Abdul Salam et al. 2014).

Early biogenic production primarily used plant material, typically agricultural wastes (examples: banana peels, wheat chafe, various leaf extracts), as source of reducing equivalents (sugars and oxidation/reduction enzymes) (Herlekar et al. 2014; Sharma et al. 2015; Patil and Chandrasekaran 2020). Since about 2010, there has been increased interest in using microbes to synthesis metal(loid) nanomaterials. This has been explored with the idea that one should be able to better control and tune NP production with better reproducibility over plant extracts. This chapter will focus on the synthesis of metal(loid) based nanomaterials using bacteria, which is rapidly becoming the major eco-friendly approach.

## 7.2 Biosynthesis of Metal(loid) Nanostructures by Bacteria

There is a wide array of metal(loid) -based nanostructures that are now produced by biogenic means, each with their own unique functionality. Silver nanoparticles offer strong antimicrobial properties useful for sterilizing medical equipment and wounds (Prasad et al. 2011; Durán et al. 2016; Siddiqi et al. 2018a). Gold nanoparticles have strong conductive properties that make them a strong candidate for use in future electronic chipsets (Elahi et al. 2018). Quantum dots are fluorescent particles that are useful for bioimaging of live cells and targeted drug delivery and are used in the photoelectronic industry (Matea et al. 2017; Cotta 2020). Iron oxide particles are known for strong super-magnetic properties (Ali et al. 2016). Selenium and tellurium particles have excellent fluorescent and conductive properties, respectively (Piacenza et al. 2018c). These particles are not limited to the single functions listed and offer more properties that will be described further in the chapter. As many metals and metalloids are effective antimicrobials (see Chap. 4), their nanomaterial versions are often antimicrobial (Hoseinzadeh et al. 2016; Correa et al. 2020; Khan

et al. 2020). Overall, the Biogenic metal(loid) nanoparticles that are being produced have properties that match or surpass their chemically produced counterparts.

Metal exposure to bacteria is inherently toxic, which is why, over time, microbes have evolved robust defense systems to limit the damage. These include metal efflux pumps (either specific or promiscuous), oxidation/reduction reactions from enzymes or metabolites, metal sequestration proteins, and damage repair systems (Lemire et al. 2013). These systems can be overwhelmed by increasing metal concentrations and metal tolerance levels vary from one species to another. When metals enter a cell, the damage can be exhibited as production of reactive oxygen, nitrogen, sulfur species, damage to cell membranes leading to loss of cell integrity, protein and enzyme dysfunction, DNA damage of base modifications or strand breaks, all of which are lethal to the cells (Lemire et al. 2013; Frankel et al. 2016; Gugala and Turner 2018).

Bacteria are able to prevent metal-associated cellular damage by using energy to reduce or oxidize metal ions into less harmful forms or species. Such biochemistry may occur via intracellular and extracellular processes. It is this processes that is the basis of NP biosynthesis as mediated by bioconversion of the toxic metal species to atom forms. Regardless of the location, biogenic nanomaterials are considered to follow the LaMer model (Presentato et al. 2018a; Lahiri et al. 2021). Reduction of the metal ions enables the nucleation step of nanoparticle formation where the metal atoms clump together to form the start of the NP, which are known as seeds. Once these seeds have formed, through the process referred to as Ostwald ripening, the atoms agglomerate onto the seeds going the NP into larger and structured forms. At some point they become coated with an organic molecule in the reaction chamber (the bacterial cell and growth medium in this case). The biomolecules provide the capping of the NP preventing aggregation and can also control NP shape and functionality, but particularly stability (Piacenza et al. 2018b). These coating molecules, which provide stabilizing and functional properties, are provided by the bacteria and may be either a single biomolecule type or a combination of biomolecules and classes. As such, the coat would contain biopolymers (carbohydrates, nucleic acids, fatty acids and lipids), reducing biochemicals, metal binding proteins, and may include catalytic enzymes involved in the reduction. Unfortunately, exact compositional studies have yet to become popularized to the literature as of yet, but it is clear such compositions vary even between closely related bacterial strains (Bulgarini et al. 2021).

The cellular location of synthesis depends on the metal(loid), the bacterial species, and the physiological state derived from the growth conditions (media type and if aerobic or anaerobic metabolism). Fundamental to the metal is the standard reduction potential of conversion of metal ion to atom form to initiate the NP development. Thus, the match between the bacterial species, growth conditions and metal(loid)s leads to the accurate magic for Biogenic NM synthesis. For some species, the NM production is inherent into the physiology such as bacteria that are respiring off the metal(loid) ions. This is well highlighted in the variety of species that either on purpose or as side reactions biotransform selenium species leading to either intracellular or extracellular NMs (see recent review Ojeda et al. 2020).

### 7.2.1 Extracellular Synthesis

Extracellular synthesis relies on reducing sugars that are present on the surface of the cell as well as enzymes that are present on the surface. The types and amounts of sugars and enzymes present extracellularly will vary depending on the organism, which is why some microbes are better NP producers than others. While the exact mechanisms of synthesis haven't been explored in depth, there are general theories on how they are made (Sharma et al. 2015). Bacteria cell walls are lined with sugar molecules of various compositions. Several species have been shown to secrete enzymes and reducing power molecules such as NAD(P)H in response to metal stress (Li et al. 2011b; Qidwai et al. 2018). Metal ions can get bound along the cell wall allowing the various molecules to reduce the metal ion to atom state that leads to NP formation as described above. The biomolecules used in this process vary depending on the metal used as well as the bacteria strain.

Silver nanoparticles are extremely popular and as such have received a lot of attention when it comes to microbial synthesis. *Escherichia coli*, *Bacillus subtilis*, *Pseudomonas aeruginosa* and many more microbes have been studied and are capable of synthesizing extracellular AgNP. Nitrate reductase and NADH and related cofactors are the two proposed routes of synthesis (Kalishwaralal et al. 2010). Nitrate reductase has been found to play a role in reducing silver, while the cell releases NADH which helps to form the nanoparticles (Kalishwaralal et al. 2010). Although nitrate reductases are periplasmic enzymes, silver exposure compromises the cell membrane, which could release enzymes from this compartment. Detection of NADH and nitrate reductase outside of the cells upon silver exposure suggests that they play a strong role in AgNP production. Biosorption of the  $\text{Ag}^+$  ions to biopolymers on the cell wall traps them to the surface allowing for reduction to occur (Li et al. 2011a).

Gold nanoparticles have been synthesized by *Bacillus subtilis*, *Rhodococcus* sp. *Rhodopseudomonas capsulate* as well as a wide variety of other microorganisms. Optimal bacterial growth conditions are used so that a large quantity of bacterial cells are available for NP synthesis. The cells are exposed to  $\text{Au}^{3+}$  ions where they get trapped on the surface of these Gram positive cells. Enzymatic cofactors such as NAD(P)H and NAD(P)H-dependent enzymes are released extracellularly in response to  $\text{Au}^{3+}$  ion presence (Nangia et al. 2009). The trapped  $\text{Au}^{3+}$  ions are reduced by these enzymes to produce Au atoms leading to AuNPs. This mechanism has been proposed for *Rhodopseudomonas*, *Stentrophomans matophilia* and *Rhizopus oryzae*. The synthesized NPs have been reported to range from 1–100 nm and appear in a wide variety of shapes dependent on the species. For example, *Bacillus cereus* produced 20–50 nm sized particles that ranged in shape from spherical, hexagonal to octagonal (Pourali et al. 2017). A study demonstrated surface proteins of *Bacillus subtilis* adsorb considerable amounts of selenite via the proteins' sulfhydryl sites and they believe this is a crucial step in extracellular SeNP formation (Yu et al. 2018). Amino, sulfhydryl and carboxylic groups are among the main groups that are secreted and could potentially play a role in the production of extracellular AuNP (Singh and Kundu 2014).

Production of nanomaterial extracellularly is typically favored due to the ease to work with as flow, and the use of flow through reactors can be conceptualized. As the nanomaterial is produced, the bacteria solution will often change color due to the production and formation of nanomaterial. For example, the reduction of Ag to Ag<sup>0</sup> will change the color from yellow to a darker brown (Singh et al. 2018a). This colour change is often more intense when the NPs are extracellular. Along with being easier to identify the presence of nanoparticles, it is also easier to separate the cells from those nanoparticles that are extracellular. Simple differential centrifugation and filtering will allow for extracellular NP isolation. The overall ease of extracellular synthesis makes it very appealing for biogenic NP production.

### 7.2.2 Intracellular Synthesis

Bacteria have many reducing molecules inside the cell as part of central and specific metabolism(s), this leads the cytoplasm of bacteria to be a very reducing environment. This is why bacteria can produce NP via an intracellular synthesis route (Ovais et al. 2018). Synthesis via this method can be more controlled, but also makes it much harder to extract the NPs since the cell must be completely disrupted to obtain the nanomaterial. Multiple rounds of centrifugation and ultrasonication are among the typical methods used to break open the cell and then separate the cell material from the desired nanomaterial. This process is time consuming and requires hands-on-time by trained individuals, which can make it less desirable as a commercial process (Ovais et al. 2018). With certain metal(oids)s and bacteria, intracellular synthesis is the only method to produce NPs. For example, *Rhodococcus aetherivorvans* will favor an extracellular synthesis when exposed to selenium but will only reduce tellurium intracellularly (Piacenza et al. 2018c). Tellurium NM tends to be produced intracellularly regardless of the strain used. Tellurite is taken into the cell which allows it to be reduced via intracellular reduced thiols that are part of enzymes inside the cell (Presentato et al. 2018b). This starts the seeding process for the formation of TeNM which remains inside the cell. To extract the NMs, the cells are ultrasonicated to lyse the cell, followed by centrifugation and filtration to isolate the NPs. However, a discovery from the Zannoni group, found that by adding the redox-mediator lawsone, which has a redox couple close to tellurite, one could get extracellular production of Te nanocrystals (Borghese et al. 2014).

Gold nanomaterial has been synthesized inside cells with enzymatic reduction (Khandel and Kumar Shahi 2016). An ion transportation system is required to uptake the gold ions into the cell, which may be the reason some strains of bacteria only reduce gold extracellularly due to potentially lacking the transporter. Adsorption of the gold ions to the cell membrane is needed for the transporter to bring in the gold to the cell (Khandel and Kumar Shahi 2016).

The list for intracellularly produced NM is shorter due to many researchers favoring strains that can extracellularly produce material (Ovais et al. 2018). The mechanisms behind intracellular synthesis rely on enzymatic reduction and

functional biochemistry inside the cell such as reactive reduced thiols. Intracellular synthesis requires a transporter to recognize and uptake the metal ions as well as a cell's tolerance to the metal challenge. Overall, while intracellular synthesis is highly effective at producing nanoparticles, the extra steps needed make it less popular for researchers.

### 7.2.3 Cellular Extract

While nanomaterial is typically produced using live bacterial cells, this is not always needed. Bacterial cells may contain biomolecules that will reduce and oxidize regardless if a cell is alive and metabolizing or not. Many researchers have taken cellular extract, which is a lysed cell containing the cytoplasm and vesicles (remnants of the membrane of the cell), to add to a solution with metal salts and often specific capping agents such as surfactants (Singh et al. 2020). The cellular extract replaces the typical reducing agents that a chemogenic protocol would use, but also removes any variability that biological growth can introduce. Thus, the cellular extract acts as a mixture of catalysts to reduce the metal salts and enable the production of nanomaterial. This method is useful as it can be simpler than using live bacteria as it acts as a hybrid between chemical and biological syntheses.

It is considered that the production of nanoparticles is a biproduct of mechanisms to detoxify the metal ions thus limiting the harm that the metal inflicts. This makes the biochemical route of synthesis dependent on the bacteria species or strain, regardless of whether the nanoparticle synthetic activity is extracellular or intracellular. Therefore, reduction of the metal is an active process done through the biochemistry of a given bacteria strain. Using cellular extracts eliminates that active process and just takes advantage of the reducing biomolecules present inside a cell (Singh et al. 2020). This prevents possible multiple reactions within the cell synthesis and can make the synthesis easier to conduct. Using cellular extract allows for parameters such as temperature, pH and pressure to be changed, as there are few living organisms' survivability that would not be affected by these changes (Singh et al. 2020). There is also an advantage when it comes to scaling up the process as large quantities of cellular extract can be obtained and then added to larger quantities of metal salts in controlled and timed fashion.

## 7.3 Examples of Bacterial Produced Nanostructures

Microbially produced nanoparticles have become increasingly popular and has enabled production of biogenic NP of many compositions. Table 7.1 highlights examples that reflect a wide variety of microbes used to synthesize all types of NPs. While many bacteria can produce NPs, there are certain strains such *E. coli* and *Bacillus* sp., that consistently appear on the table regardless of metal. This may be a



**Table 7.1** Different types of nanostructures produced by various bacteria species. Shape of the produced nanostructure listed as well as the location that the particles accumulate

Metal	Bacteria	Size	Shape	Location	Reference
Ag	<i>Escherichia coli</i>	42.2–89.6 nm	Spherical	Extracellular	Gurunathan et al. (2009)
	<i>Rhodococcus</i> sp.	10–15 nm	Spherical	Extracellular	Otari et al. (2014)
	<i>Bacillus</i> sp.	5–15 nm	–	Extracellular and periplasmic space	Pugazhenthiran et al. (2009)
	<i>Bacillus cereus</i>	4–5 nm	Spherical	Intracellular	Ganesh Babu and Gunasekaran (2009)
	<i>Streptomyces coelicolor</i>	28–50 nm	Irregular	Extracellular	Manikprabhu and Lingappa (2013)
Au	<i>Escherichia coli</i>	25–33 nm	Spherical and triangular	Intracellular	Du et al. (2007)
	<i>Bacillus subtilis</i>	5–25 nm	Octahedral	Intracellular	Reddy et al. (2010)
	<i>Rhodospseudomonas capsulata</i>	10–20 nm	Spherical	Extracellular	
	<i>Bacillus licheniformis</i>	10–100 nm	Cubic	Intracellular	Kalishwaralal et al. (2009)
Se	<i>Pseudomonas aeruginosa</i>	15–30 nm	Spherical	Extracellular	Husseiny et al. (2007)
	<i>Rhodococcus aetherivorans</i>	43–97 nm	Spherical and rods	Extracellular	Presentato et al. (2018a)
	<i>Bacillus cereus</i>	50–150 nm	Spherical	Extracellular	Kora (2018)
Te	<i>Proteus mirabilis</i>	167–190 nm	Spherical	Extracellular	Wang et al. (2018)
	<i>Stenotrophomonas maltophilia</i>	76–78 nm	Spherical	Intracellular	Zonaro et al. (2015)
	<i>Rhodococcus aetherivorans</i>	~781 nm	Rods	Intracellular	Presentato et al. (2018a, b)
	<i>Pseudomonas</i> sp.	~68 nm	Triangular	Intracellular	Pugin et al. (2014)
CdS	<i>Halobacillus</i> sp.	2–5 nm	Spherical	Extracellular	Bruna et al. (2019)
	<i>E. coli</i>	4–10 nm	Spherical	Extracellular	Mi et al. (2011)
	<i>Pleurotus ostreatus</i>	4–5 nm	Spherical	Extracellular	Borovaya et al. (2015)

CdTe	<i>Pseudomonas fragi</i> GC01	2.31–2.59 nm	Spherical	Extracellular	Gallardo-Benavente et al. (2019)
	<i>E. coli</i>	2–3 nm	Spherical	Extracellular	Bao et al. (2010)
Fe <sub>2</sub> O <sub>3</sub>	<i>Proteus vulgaris</i>	19–30 nm	Spherical	Extracellular	Majeed et al. (2020)
TiO <sub>2</sub>	<i>Bacillus mycoides</i>	40–60 nm	Spherical	Extracellular	Órdenes-Aenishanslims et al. (2014)
ZnO	<i>Lactobacillus plantarum</i> TA4	292.6 ± 83.2 nm	Nanoflower	Extracellular	Mohd Yusof et al. (2020)

bias due to a strong understanding of the species' physiology and genetics (e.g. *E. coli*). Other commonly used species are those that have been isolated from environments of high metal pollution challenge. This comes with the idea that the more highly tolerant the cells are to a metal ion, they should be able to survive a higher load and thus give a higher yield of their NPs. The literature continues to be filled with those exploring new strains for better or novel metal nanomaterial production. Figure 7.1 provides microscopy images of examples of biogenic nanomaterials.

### 7.3.1 Silver Nanoparticles

Silver nanoparticles are likely the most popular NP, which has resulted in a large focus being placed on producing silver NPs through biological approaches, typically plant extracts or fungi (Keat et al. 2015). Microbes such as *E. coli*, *Bacillus cereus*, *Bacillus* sp., *Streptomyces coelicolor*, and many more are all commonly used to synthesize Ag NPs as a larger focus has been placed on microbially synthesized NP (Ganesh Babu and Gunasekaran 2009; Gurunathan et al. 2009; Manikprabhu and Lingappa 2013; Otari et al. 2014). The *Bacillus* species has been shown to produce smaller particle sizes and all strains tend to produce spherical particles. Yet there are reports of irregular shapes being produced in the case of *Streptomyces coelicolor*

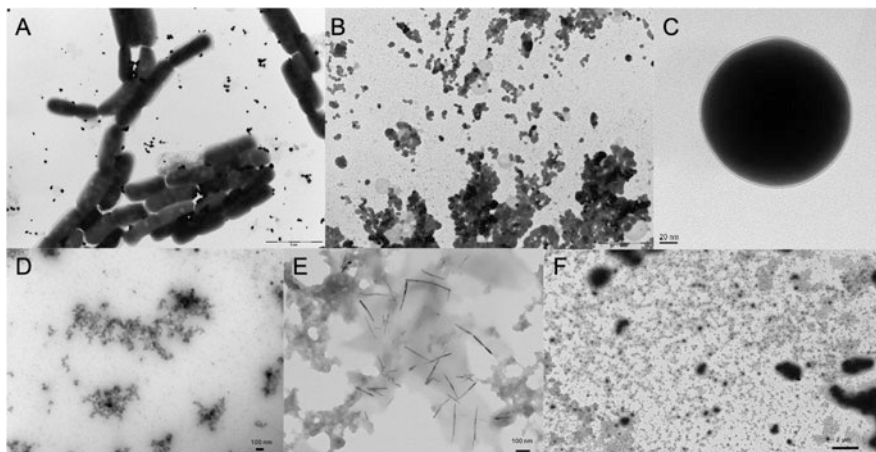


**Fig. 7.1** Transmission electron microscopy photos of biogenic nanomaterial. (a) *Bacillus* sp. producing SeNPs extracellularly after 24 h of growth (Dr. Elena Piacenza). (b) SeNPs separated and extracted from *Bacillus* sp. (Dr. Elena Piacenza). (c) SeNP extracted and purified from *Stenotrophomonas maltophilia* SELTE02, showing a thin less electron dense associated cap layer (Dr. Elena Piacenza). (d) Ag NP produced from *E. coli* showing less electron dense biocorona (Nikhil Pradhan). (e) Extracted Te nanorods produced from *Rhodococcus aetherivorans* BCP1 showing loosely associated EPS layer (Dr. Elena Piacenza). (f) Wide field view of extracted CdSe QD from *Rhodococcus aetherivorans* BCP1 (Nikhil Pradhan)

(Manikprabhu and Lingappa 2013). Silver nanomaterial remains to be one of the most popular and the focus on biological production doesn't look like it will slow down at any point soon. Exploration into reliably producing more diverse shapes and improvements in increasing yields will likely be the focus moving forward.

### 7.3.2 *Gold Nanoparticles*

Gold nanomaterial synthesis using bacteria has yielded spherical, triangular, cubic and octahedral particles using many species of bacteria such as: *Escherichia coli*, *Pseudomonas aeruginosa*, *Rhodopseudomonas capsulate*, *Bacillus licheniformis*, and *Bacillus subtilis* (Du et al. 2007; He et al. 2007; Husseiny et al. 2007; Kalishwaralal et al. 2009; Satyanarayana Reddy et al. 2010). Once again *E. coli* and *Bacillus* strains make an appearance showing their versatility in particle formation. In addition, *Pseudomonas aeruginosa* and *Rhodopseudomonas capsulate* have successfully produced Au NM (He et al. 2007; Husseiny et al. 2007). The Au NPs tend to be obtained in relatively tight size distributions making them useful for potential scaled up syntheses. Gold can be reduced both intracellularly and extracellularly, which means it is dependent on the bacteria strain of choice and the conditions the strain is grown in.

### 7.3.3 *Selenium Nanoparticles*

Selenium nanomaterial has been biogenically synthesized from a variety of bacterial species (Ojeda et al. 2020). This nanomaterial has been made in both spherical particles as well as nanorods. Extracellular synthesis of selenium nanoparticles by *Bacillus cereus* and *Proteus mirabilis* produced spherical particles with wide ranges in size centred at ~100 nm (Kora 2018; Wang et al. 2018). The obtained particles have been characterized and displayed expected properties with absorbance peaks at 300–500 nm. *Rhodococcus aetherivorvans* BCP1 managed to produce selenium nanoparticles ranging from 53–97 nm depending on the conditions. In addition, the production of selenium nanorods of around 444–555 nm was observed (Presentato et al. 2018a). Selenium nanomaterial has also been produced from bacteria such as *E. coli*, *Salmonella enterica*, *Thauera selenatis*, and *Comamonas testosterone* (Dridge and Butler 2010; Yee et al. 2014; Connelly et al. 2016; Tan et al. 2018). Particularly species that can reduce selenium oxyanions such as selenate and selenite to elemental selenium are all potential candidates to produce selenium nanomaterial.

### 7.3.4 Tellurium Nanostructures

Tellurium nanomaterial is produced in many different shapes by bacteria. Spherical particles, nanorods and triangular particles have all been synthesized. Typically, Te NM is synthesized inside cells, with only a few strains being capable of extracellular synthesis. A challenge with this element is that the oxyanion tellurite ( $\text{TeO}_3^{2-}$ ) is very toxic to most bacteria in the 1  $\mu\text{g/ml}$  range (Presentato et al. 2019). Produced particles range from 68–78 nm if of spherical or triangular shape (Pugin et al. 2014; Zonaro et al. 2015). Tellurium nanorods, synthesized using *Rhodococcus aetherivorans* BCP1, are much larger at 781 nm average and as long as 1  $\mu\text{m}$ , thought to occur though capping by natural surfactants produced by this strain (Presentato et al. 2018b). *Pseudomonas* sp. Strain BNF22 was able to synthesize Te NM that ranged between 68–361 nm dependent on the synthesis conditions (Pugin et al. 2014). Glutathione reductase from this strain was identified to have tellurite reductase and when overproduced in *E. coli* (Pugin et al. 2014). *Rhodobacter capsulatus* was used to produce nanorods of around 100 nm (Borsetti et al. 2003). Spherical tellurium nanoparticles were produced by *Pseudomonas pseudoalcaligenes* KF707 as well as *Rhodobacter sphaeroides* (Moore and Kaplan 1992; di Tomaso et al. 2002). While all of the mentioned bacteria produced their NPs intracellularly, there are strains that have produced extracellular material.

*Bacillus selenitireducens* and *Sulfurospirillum barnesii* have both produced Te nano rods and particles, respectively, that localized on the outer cell surface (Baesman et al. 2007; Ramos-Ruiz et al. 2016).

### 7.3.5 Heteroatom Nanomaterial

Heteroatom nanomaterials are comprised of two or more different elements and within this category a very popular material that is synthesized are quantum dots (QD). One of the most popular QD formulations are made of cadmium and are capped with either a zinc sulfide or zinc selenide shell (Javed et al. 2016). CdS QD have been synthesized by *Halobacillus* sp. and were produced in a monodisperse distribution ranging from 2–5 nm (Bruna et al. 2019). The dots were produced in high NaCl concentrations, and these are the first salt stable biologically produced CdS quantum dots to have been created using an extremophile organism (Bruna et al. 2019). *E. coli* has also been reported to produce CdS QD with high fluorescence yields and uniform size distribution as well (Mi et al. 2011). Most reported QD syntheses produce monodisperse populations with tight size distributions.

Cadmium Telluride (CdTe) QDs have been synthesized from an Antarctic bacteria *Pseudomonas fragi* GC01 extracellularly (Gallardo-Benavente et al. 2019). The synthesized particles were measured via Atomic Force Microscopy and displayed size averages below 40 nm depending on the biosynthesis conditions allowing them to produce green, yellow and orange particles (Gallardo-Benavente et al. 2019).

TEM imaging displayed particles that ranged from 2.31–2.59 nm indicating the sample was very polydisperse (Gallardo-Benavente et al. 2019). The synthesis was able to be controlled to adjust the size of the particles, which is a highly valuable aspect. *E. coli* once again displays immense versatility as it has been shown to produce CdTe QD where sizes ranged from 2–3 nm (Bao et al. 2010).

Heteroatom nanomaterial is not limited to just QD. Iron oxide ( $\text{Fe}_2\text{O}_3$ ) nanoparticles are a popular nanomaterial and were synthesized by *Proteus vulgaris* (Majeed et al. 2020). Spherical particles were produced in this synthesis ranging from 19–30 nm in size. *Bacillus mycoides* has been used to successfully synthesize titanium dioxide ( $\text{TiO}_2$ ) nanomaterial extracellularly (Órdenes-Aenishanslins et al. 2014). Zinc oxide (ZnO) NPs have also been synthesized from *Lactobacillus plantarum* TA4 (Mohd Yusof et al. 2020).

## 7.4 Control of Synthesis

The functionality and uniqueness of NM comes from the size and shape of a nanoparticle. Physical-chemical syntheses are carefully tuned to produce particles of the desired size range and specific shape (Wang and Wang 2014; Khan et al. 2019). This is considered easier to do chemically as there are fewer variables that are available to be modified when compared to using microbes to produce NP. In a chemical protocol the initial concentrations, temperature, pressure, etc. can all be effectively adjusted to produce the desired particles. There are now many resources available for protocols for the production of a wide range of nanomaterials (Schwarz et al. 2014).

When using bacteria, there are more variables due to bacteria being living organisms and one must maintain their physiology through their lifecycle. There is typically a narrow range of pH, ionic strength, redox potential, and temperature for each species for survival. This makes production of NPs using bacteria dependent on the species and strain. Even between strains, there can be subtle differences in genotype that lead to different physiology and subsequently different biochemical processes within the cell. These differences can lead to the favoring of specific shapes and or reduction of some metals over others. Tight regulation of bacterial culturing conditions, metal concentrations and incubation times is also needed to ensure the size ranges are small and precise (Singh et al. 2020). Factors such as the type of growth media (carbon and energy source) have also been explored and found to have effects on the shape and size of metal-based NPs (Luo et al. 2018; Presentato et al. 2018a, b). Metal concentrations, incubation time and growth media all have direct effects on how a bacterium cell can grow and react to stressful environments (Luo et al. 2018).

It is important to understand the metal toxicity level to the strain being used as well as understanding the mechanisms of metal ion toxicity and resistance. Readers are directed to a review by Lemire for an overview of this topic (Lemire et al. 2013). The bacteria's ability to produce metal NS's may depend on how it responds to the

metal toxicity stress. Regardless, it is clear that the bacterial strain type and resulting physiology from culturing conditions leads to different biogenic synthetic pathways leading to different nanostructures of varying thermodynamic stability (Piacenza et al. 2019). As such it makes sense that changes to growth and culturing parameters will alter how the bacteria will reduce the metal salt leading to metal atoms with the potential to cluster into nanostructures. Additionally, changes to the growth conditions could also prevent NP formation altogether (Luo et al. 2018). Table 7.2 summarizes parameters to consider when exploiting bacteria for NS synthesis.

## 7.5 Differences of Biosynthesis vs Chemical Nanostructures

Biogenically produced nanomaterials are functionality dependent a number of variables: the type of metal(loid); the size and shape; its capping molecules; and the types of associated biomolecules. The NS core will be comprised of atoms either arranged crystalline or amorphous. This core metal is surrounded by a layer of molecules that coat the particle referred to as the cap. This layer is typically intimately associated with the metal atoms through various modes of bonding (covalent, electrostatic, van der Waals, and hydrophobic) (Khan et al. 2019). Additional biomolecules can be more loosely associated with the biogenic nanostructures. These additional biomolecules are seen in TEM images as less electron dense material that is sometimes referred to as an exopolymeric substance(s) (EPS) (Jain et al. 2015) or as the ‘biocorona’ of the NP (Lin et al. 2017) as seen in examples shown on Fig. 7.1. The recognition that this additional organic material is difficult to totally remove from biogenic preparations of nanomaterial led a group to suggest defining Biogenic as Nanostructures Embedded in Organic material (NEMO-NS) (Piacenza et al. 2017).

The cap can give rise to new properties. Particularly the cap molecules participate in stabilization by producing a surface that provides stability through electrostatic, steric or electrosteric interactions preventing agglomerations of atom cores (Piacenza et al. 2018b). Bacteria have an enormous diversity of biomolecules available for this cap through their diverse metabolism. Even comparing the products from similar environmental isolates gave surprising different physical-chemical properties (Piacenza et al. 2018a). Bulgarini et al. evaluated Se NPs produced by a variety of environmental isolates and evaluated biomolecular cap and biocorona compositions. They found that each strain produced slightly different biogenic Se NPs with different ratios of Lipid: Protein: Carbohydrate, and these differences led to different size and stabilities of the NSs (Bulgarini et al. 2021). This group presented a model to indicate the cap vs the outer layer biocorona in a loose equilibrium with the bulk biomolecules.

Changes in the cap biomolecule can lead to solubility differences. For example, a non-polar coat could make the particles soluble in organic solvents, while a polar coat would make the particles water soluble. It is common also to observe that the biological molecule cap appears to be responsible for the enhanced activity of the

**Table 7.2** Variables that affect nanoparticle synthesis when using bacteria

Biological variable	Comments
Species	~98% of the living species on the planet are bacteria thus providing an astronomical number of possible systems
Strain	Each species has different strains based on subtle genomic variations; of which can lead to different physiologies
Media—carbon source	Not all bacteria grow on the same carbon or energy source, and many species can grow on a surprising number of different types of sources
Metal salt counter ion	Metal(loid) ions may have halogens, sulfate or nitrate as counter ions. Some species will use the counter ion as energy source changing the physiology dramatically
Solution speciation	Metal(loid) ions may not be free, and most will be coordinated/chelated by other molecules in the media and biomolecules once associated with the cell. This will alter their bioavailability and uptake
Media pH, ionic strength, redox potential Oxygen (anoxic vs aerobic growth)	These parameters influence the ion speciation and reduction state of the metal(loid) ion via the Pourbaix chemical equilibrium relationship diagrams
Growth temperature	Most species can grow over quite a wide range of temperatures, but at their extremes they would be stressed and thus have different physiology. The temperature also will affect the kinetics of the biochemical reactions in the cell and thus rate of NS production
Metal concentrations	As with chemical synthesis this is an important parameter as it will define the amount of metal atoms available to cluster per unit time. However, the concentration tolerance level of the species must also be considered
Growth state (log vs stationary phase)	Bacterial cultures go through a growth curve structure consisting of an initial lag phase (adjusting to conditions by expressing key genes), log phase (rapid metabolism and short replication time), stationary phase (feedback from metabolic waste from log phase and decreased nutrients lead to decreased metabolic rate and less cell division), death phase. There are considerable gene expression differences between the different phases and thus very different biochemistry occurring
Physiological state	This relates to how the bacteria are grown, variations of which results in different levels of fitness to withstand stress

nanoparticles. This was observed comparing the antimicrobial activity of biogenic vs chemogenic Se NPs (Piacenza et al. 2017) or the fluorescence intensity of biogenic vs chemogenic Se NPs (Piacenza et al. 2020). A number of studies have demonstrated the higher antimicrobial efficacy of biogenic Ag NPs compared to chemogenic [described in reviews: (Gandhi and Khan 2016; Barros et al. 2018)]. These are just a few examples, yet it is known from chemical processes that the cap molecules can be specifically chosen to tune the NS to the intended function.

Physical-Chemical synthesis sees the particles coated during or after synthesis whereas bacteria coat the NP with biomolecules naturally during synthesis of the



particle. These biomolecular coats provide high thermodynamic stability (Piacenza et al. 2018b). In fact, analysis of biogenic NP coats finds biomolecules considered to have been part of the synthesis to be part of the cap (Lampis et al. 2017; Bulgarini et al. 2021). These biomolecules consist of a mixture of carbohydrates, proteins and lipids that vary in amounts depending on the organism that produced it (Bulgarini et al. 2021). The identity of the molecules that coat biological NP is only started to be explored (Bulgarini et al. 2021). These surface layers may be a single molecule as suggested by the synthesis of Te Nanorods being coated by a biosurfactant produced by the bacterial biofactory involved (Presentato et al. 2018b); or a mixture of biomolecule types as observed by Bulgarini et al. (2021).

## 7.6 Examples of Uses of Biogenic Nanostructures

One of the primary uses of metal(loid) nanoparticles are as antimicrobials. As metal ions are now reasonably established as a defined class of antimicrobial agents (Turner 2017), the nanostructure versions of the metals are also explored and have shown excellent efficacies (Khan et al. 2020). The field of metal(loid)-based nanoparticles as antimicrobial agents has moved from the discovery stage to the application level with thoughts towards real world implementations. This means issues around pharmacokinetics and toxicological risk are to be considered (Sánchez-López et al. 2020). Particularly since microbial produced nanomaterial carries with it biomolecules from the bacterial factory which may carry toxicity and either allergenic or irritant properties of their own (Akter et al. 2018; Zorraquín-Peña et al. 2020). Regardless of their promise as antimicrobial agents, stewardship of use is important, as bacteria are already evolving mechanisms of resistance to metal(loid) nanoparticles (Salas Orozco et al. 2019). Yet, the ecofriendly fashion of bacterial synthesis of metal(loid) nanostructures lends this type of microbial biotechnology towards solutions of the United Nations sustainable development goals (Nakai 2018; Dutta et al. 2020).

The most prevalent application being explored for biogenic nanomaterial is for use as antimicrobials and incorporating NPs can keep surgical equipment sterile and can be used to treat wounds and burns through the integration into bandages (Singh et al. 2018b; Paladini and Pollini 2019; Pormohammad et al. 2021). There is also a developing field in the use of Biogenic metal and non-metal nanomaterials in the agricultural industry (see book edited by Ghorbanpour et al. 2020 and chapters therein). Here we will take a look at a few specific examples of use for some of the nanomaterial that has been synthesized by bacteria. As biogenic NM are comprised of the same metal chemical equivalents, their functionality will be largely similar with some differences in certain properties that will be highlighted if and when applicable.

### 7.6.1 Silver

Silver NPs find uses in the medical field due to the strong antimicrobial effects they exhibit. The antimicrobial effect is assumed to come from Ag NP releasing free silver ions that then perform their toxicity on the cell. The mechanism hypothesis is the delivery via the NP will provide a localized pulse of Ag ions compared to use of silver nitrate (Kędziora et al. 2018). Ag NPs also have unique optical properties, due to the surface plasmon resonance phenomenon, that are controlled via size and shape of the particle (Siddiqi et al. 2018a). Smaller particles absorb at ~400 nm whereas larger particles scatter more light instead and absorbed light will be red shifted due to the larger particle. The optical properties make them useful for biosensors, due to having specific absorption peaks, that are capable of detecting various molecules (Siddiqi et al. 2018a). One such sensor that used chemical Ag NP was used to detect microRNA let-7a (plays a role in cell proliferation), which validates that biogenic versions could be used in such applications (Elhakim et al. 2018). Ag NPs can also be used to catalyze redox reactions. The diversity of potential applications makes biogenic silver nanomaterial appealing and as such they garner a lot of attention.

### 7.6.2 Gold

Gold NP are also widely popular due to unique optical and electronic properties that are present in both chemically and biogenically produced nanomaterial. Au NPs also have a surface plasmon resonance that is affected by the size and shape (Elahi et al. 2018). The biogenically synthesized gold NP, regardless of strain, displayed the expected properties of Au NP such as fluorescence quenching and surface plasmon resonance, the latter of which gives rise to unique optical properties (Yeh et al. 2012). Smaller particles absorb around 450 nm and that value is red shifted the larger the nanomaterial is. Smaller particles give off a red color while larger particles display bluer colors. Due to the surface plasmon resonance Au NPs have, they find uses in sensors and probes (Elahi et al. 2018). For example, a study showed Au NP being used in an optical sensor to detect the presence of biogenic amines in meats (El-Nour et al. 2017). There are also uses in cancer treatment as Au NPs can be directed to tumors and heated to kill the tumor cells (Sztandera et al. 2019). These particles also carry unique electronic properties that allow them to be used in electronic devices to help advance electronic chips (Yang et al. 2016; Menon et al. 2017). Like Ag NPs, Au NPs can be used to catalyze redox reactions (Carabineiro 2019). A study also showed biogenic Au NP exhibiting antibacterial and antibiofilm properties against *Pseudomonas aeruginosa* (Ali et al. 2020).

### 7.6.3 *Metalloids Selenium and Tellurium*

Selenium nanoparticles offer catalytic properties as well as strong fluorescence and antimicrobial properties (Khalid et al. 2016). They display anticancer properties where contact with cancer cells suggests they are able to induce cell cycle arrest and apoptosis while leaving healthy cells relatively unharmed (Wadhvani et al. 2016; Khurana et al. 2019). A study showing the linkage of Se NP and Spiulina polysaccharides allowed for targeted delivery of the NM to the cancer cells (Yang et al. 2012). They find uses in cellular imaging and usefulness for treating oxidative stress and inflammation disorders (Khalid et al. 2016). A study from Piacenza et al. (2019) showed biogenic Se NP that displayed fluorescence and Raman peaks matching chemical equivalents of the same size, and those Se NP did as well act as strong antimicrobial agents (Piacenza et al. 2018a). Chemical Se NP are effective and less toxic than other forms of selenium, however they do display toxicity with a Lethal Dose of 50% of 198.1 mg/kg, therefore limiting potential use (Shakibaie et al. 2013). Biogenic Se NP were shown to be 26-fold less toxic in this comparison, which makes the biogenic synthesis a potentially favorable method (Shakibaie et al. 2013).

Tellurium NM have strong conductivity and photocatalytic properties that make them candidates for applications such as electronics and solar cells (Piacenza et al. 2018c). Chemogenic Te NM has been shown to cover total absorption of solar radiation and there is a good potential that biogenic TeNM might display this same property (Ma et al. 2018). Biogenic Te NPs produced were found to have very good antibacterial activity including efficacy against cultures grown as a biofilm (Zonaro et al. 2015). They also acted as an anti-virulence agent stopping a major virulence factor pyoverdine in *Pseudomonas aeruginosa* (Mohanty et al. 2014). Work was done to look at potential anticancer properties, where Te NPs were shown to target melanoma cells and left healthy cells alone (Brown et al. 2018). Regarding cytotoxicity, (Turner et al. 2012) it was found biogenic Te nanorods were less toxic than the metal salts used to produce them (Forootanfar et al. 2015).

### 7.6.4 *Heteroatom Nanoparticles*

The primary example of heteroatom NPs are quantum dots. These NPs offer strong photophysical properties making them extremely useful in bioimaging, solar cells, and electronics (Matea et al. 2017). Quantum dots such as CdSe are known for their strong optical properties that dependent on their size. Size tunable biogenic CdSe QD have been made which allows for the change in the emission peaks, with smaller particles emitting smaller wavelengths and larger particles emitting larger wavelengths (Tian et al. 2017). Looking at CdTe QD, these have found uses in solar cell coatings due to an optimal direct band gap and a high optical absorption coefficient (Kulkarni et al. 2017). In addition, they have also found uses in sensors of various

types with biogenic CdTe QD showing promise in bioimaging and biosensing (Rodrigues et al. 2017; Tian et al. 2017).

Iron oxide NPs are a type of magnetic NP and used with magnetic fluids, magnetic resonance image, targeted drug delivery and detection of biological material (Wu et al. 2008). Platinum-palladium NPs can be used as catalysts in polymer electrolyte fuel cells (Stephen et al. 2019). Titanium dioxide NPs have a wide variety of uses particularly in photocatalysis, solar cells as well as pollution treatment (Sungur 2020). A study showed biogenic TiO<sub>2</sub> particles displaying these same properties as did equivalent chemogenic products (Meenatchisundaram et al. 2021). The biogenic variants demonstrated comparable electronic properties to their chemical capabilities and were produced within a size range of 40–60 nm (Órdenes-Aenishanslins et al. 2014). Zinc oxide NP display strong antimicrobial properties making them useful in treating injuries and boils, however safety and health hazards prevent widespread use (Siddiqi et al. 2018b). Commercial applications typically see chemogenic zinc oxide NP used in sunscreens and various electronics such as LED, transparent transistors, solar cells and cosmetics (Siddiqi et al. 2018b).

## 7.7 Metal(loid) Nanostructures Produced by Other Microbes

Microbial synthesis of NM is not limited to bacteria as this process can be carried out by fungi, yeasts and algae. A large focus has been placed in producing silver and gold nanoparticles with a variety of bacterial species. However, other metal(loid) NMs have been produced by fungi such as: Selenium, Silicon Dioxide, Lead Sulfide, Copper(II) Oxide, Iron Oxide, Palladium and Zinc Oxide to name a few. Fungi species have produced Ag NM and that has been done by *Verticillium*, *Phanerochaete chrysosporium*, *F. solani*, and many others as mentioned in the following reviews (Dhillon et al. 2012; Moghaddam et al. 2015). All the listed species produced spherical particles ranging anywhere from 3–200 nm depending on strain and synthesis conditions. Triangular particles were synthesized by *Fusarium oxysporum* (Kumar et al. 2007). This fungus is also used to produce both Ag and Au NPs of spherical and triangular shapes, as well as spherical silicon dioxide NPs (Bansal et al. 2005; Rajput et al. 2016; Mukherjee et al. 2002). Selenium NPs were produced by a fungus known as *Alternaria alternata* (Sarkar et al. 2011).

Yeasts such as *Pichia jadinii* sp. and *Yarrowia lipolytica* have been used to synthesize gold particles (Mourato et al. 2011; ben Tahar et al. 2019). Lead sulfide particles have also been produced by *Rhodospiridium diobavatum* showing their ability to produce heteroatom NM (Seshadri et al. 2011). This is further shown by *Saccharomyces cerevisiae* being used to produce both CdSe (Sur et al. 2019) and CdTe quantum dots (Jigyasu et al. 2019).

Eukaryotic algae species have been shown to produce a wide variety of metal (loid) nanomaterial compositions. Experiments with the fungi *Aureobasidium*

*pullulans*, produced both Se and Te NPs of <100 nm in size extracellularly (Nwoko et al. 2021), demonstrating quite a different pattern than most bacterial species. There has been a lot of work on Ag NM production, being produced by *Chlamydomonas reinhardtii*, *Padina pavonica*, *Codium capitatum*, and *Caluerpa racemosa* to name a few (Khanna et al. 2019). Spherical Ag NPs were produced from all listed species, however *Chlamydomonas reinhardtii* was able to produce rectangular particles while *Caluerpa racemose* was capable of producing triangular particles (Barwal et al. 2011; Kathiraven et al. 2015). There is also a large number of species that have been used to produce Au NP where a lot of fungal species show the ability to produce standard spherical particles (Khanna et al. 2019). Of note is the production of triangular particles by *Cosmarium impressulum*, *Anabaena flosaquae*, and *E. gracilis* (Dahoumane et al. 2012). Additionally, in a follow up study, *E. gracilis* was able to produce hexagonal shaped gold particles (Dahoumane et al. 2016). Copper oxide, iron oxide, palladium and zinc oxide NPs are among some of the types of NM produced by algae species demonstrating variety in the metals they can handle (Mahdavi et al. 2013; Azizi et al. 2014; Abboud et al. 2014; Momeni and Nabipour 2015).

## 7.8 Conclusion

Nanoparticle production using bacteria has exploded in popularity in recent years. Advances in understanding the mechanism of synthesis has led to improved synthesis protocols and better control over the size and shape of the produced NP. With this, a large variety of bacterial strains and species have been used to synthesize metal(loid) nanomaterials of various compositions. Initial understanding over the NP coat gives the impression that the biochemical coat offers improved NP properties compared to chemically synthesized particles. While a lot of advances have been made, there are still gaps in the literature. Deeper understandings on biochemical pathways and reactions involved in the synthesized NPs will help improve syntheses. Defining how the biochemicals of the NP coat composition link to NPs size, shape and properties is crucial to modify bacterial strain and bacterial growth conditions to optimize the presence of key biomolecules. Regardless, microbially produced metal(loid) NPs present a technological base offering an eco-friendly economically preferred solution to producing NPs.

## References

- Abboud Y, Saffaj T, Chagraoui A, el Bouari A, Brouzi K, Tanane O, Ihssane B (2014) Biosynthesis, characterization and antimicrobial activity of copper oxide nanoparticles (CONPs) produced using brown alga extract (*Bifurcaria bifurcata*). *Appl Nanosci* 4:571–576
- Abdul Salam H, Sivaraj R, Venkatesh R (2014) Green synthesis and characterization of zinc oxide nanoparticles from *Ocimum basilicum* L. var. *purpurascens* Benth.-Lamiaceae leaf extract. *Mater Lett* 131:16–18

- Ahmad MZ, Akhter S, Jain GK, Rahman M, Pathan SA, Ahmad FJ, Khar RK (2010) Metallic nanoparticles: technology overview and drug delivery applications in oncology. *Expert Opin Drug Deliv* 7:927–942
- Akter M, Sikder MT, Rahman MM, Ullah AKMA, Hossain KFB, Banik S, Hosokawa T, Saito T, Kurasaki M (2018) A systematic review on silver nanoparticles-induced cytotoxicity: physico-chemical properties and perspectives. *J Adv Res* 9:1–16
- Ali A, Zafar H, Zia M, Ul Haq I, Phull AR, Ali JS, Hussain A (2016) Synthesis, characterization, applications, and challenges of iron oxide nanoparticles. *Nanotechnol Sci Appl* 9:49–67
- Ali SG, Ansari MA, Alzohairy MA, Alomary MN, Alyahya S, Jalal M, Khan HM, Asiri SMM, Ahmad W, Mahdi AA, El-Sherbeeney AM, El-Meligy MA (2020) Biogenic gold nanoparticles as potent antibacterial and antibiofilm nano-antibiotics against *Pseudomonas aeruginosa*. *Antibiotics* 9:100
- Azizi S, Ahmad MB, Namvar F, Mohamad R (2014) Green biosynthesis and characterization of zinc oxide nanoparticles using brown marine macroalga *Sargassum muticum* aqueous extract. *Mater Lett* 116:275–277
- Baesman SM, Bullen TD, Dewald J, Zhang D, Curran S, Islam FS, Beveridge TJ, Oremland RS (2007) Formation of tellurium nanocrystals during anaerobic growth of bacteria that use Te oxyanions as respiratory electron acceptors. *Appl Environ Microbiol* 73:2135–2143
- Bahadar H, Maqbool F, Niaz K, Abdollahi M (2016) Toxicity of nanoparticles and an overview of current experimental models. *Iran Biomed J* 20:1–11
- Banerjee A, Qi J, Gogoi R, Wong J, Mitragotri S (2016) Role of nanoparticle size, shape and surface chemistry in oral drug delivery. *J Control Release* 238:176–185
- Bansal V, Sanyal A, Rautaray D, Ahmad A, Sastry M (2005) Bioleaching of sand by the fungus *Fusarium oxysporum* as a means of producing extracellular silica nanoparticles. *Adv Mater* 17: 889–892
- Bao H, Lu Z, Cui X, Qiao Y, Guo J, Anderson JM, Li CM (2010) Extracellular microbial synthesis of biocompatible CdTe quantum dots. *Acta Biomater* 6:3534–3541
- Barros CHN, Fulaz S, Stanisic D, Tasic L (2018) Biogenic nanosilver against multidrug-resistant bacteria (MDRB). *Antibiotics* 7:69
- Barwal I, Ranjan P, Kateriya S, Yadav SC (2011) Cellular oxido-reductive proteins of *Chlamydomonas reinhardtii* control the biosynthesis of silver nanoparticles. *J Nanobiotechnol* 9:1–12
- ben Tahar I, Fickers P, Dziedzic A, Ploch D, Skóra B, Kus-Liśkiewicz M (2019) Green pyomelanin-mediated synthesis of gold nanoparticles: modelling and design, physico-chemical and biological characteristics. *Microb Cell Factories* 18:1–11
- Bernardos A, Piacenza E, Sancenón F, Hamidi M, Maleki A, Turner RJ, Martínez-Mañez R (2019) Mesoporous silica-based materials with bactericidal properties. *Small* 15:1900669
- Borghese R, Baccolini C, Francia F, Sabatino P, Turner RJ, Zannoni D (2014) Reduction of chalcogen oxyanions and generation of nanoprecipitates by the photosynthetic bacterium *Rhodobacter capsulatus*. *J Hazard Mater* 269:24–30
- Borovaya M, Pirkó Y, Krupodorova T, Naumenko A, Blume Y, Yemets A (2015) Biosynthesis of cadmium sulphide quantum dots by using *Pleurotus ostreatus* (Jacq.) P. Kumm. *Biotechnol Bioequip* 29:1156–1163
- Borsetti F, Borghese R, Francia F, Randi MR, Fedi S, Zannoni D (2003) Reduction of potassium tellurite to elemental tellurium and its effect on the plasma membrane redox components of the facultative phototroph *Rhodobacter capsulatus*. In: *Protoplasma*. Springer, vol 221, pp 153–161
- Brown CD, Cruz DM, Roy AK, Webster TJ (2018) Synthesis and characterization of PVP-coated tellurium nanorods and their antibacterial and anticancer properties. *J Nanopart Res* 20:1–13
- Bruna N, Collao B, Tello A, Caravantes P, Díaz-Silva N, Monrás JP, Órdenes-Aenishanslins N, Flores M, Espinoza-Gonzalez R, Bravo D, Pérez-Donoso JM (2019) Synthesis of salt-stable fluorescent nanoparticles (quantum dots) by polyextremophile halophilic bacteria. *Sci Rep* 9:1–13

- Bulgarini A, Lampis S, Turner RJ, Vallini G (2021) Biomolecular composition of capping layer and stability of biogenic selenium nanoparticles synthesized by five bacterial species. *Microb Biotechnol* 14:198–212
- Carabineiro SAC (2019) Supported gold nanoparticles as catalysts for the oxidation of alcohols and alkanes. *Front Chem* 7:702
- Connelly KRS, Stevenson C, Kneuper H, Sargent F (2016) Biosynthesis of selenate reductase in *Salmonella enterica*: critical roles for the signal peptide and DmsD. *Microbiology (United Kingdom)* 162:2136–2146
- Correa MG, Martínez FB, Vidal CP, Streitt C, Escrig J, de Dicastillo CL (2020) Antimicrobial metal-based nanoparticles: a review on their synthesis, types and antimicrobial action. *Beilstein J Nanotechnol* 11:1450–1469
- Cotta MA (2020) Quantum dots and their applications: what lies ahead? *ACS Appl Nano Mater* 3:4920–4924
- Dahoumane SA, Djediat C, Yéprémian C, Couté A, Fiévet F, Coradin T, Brayner R (2012) Species selection for the design of gold nanobioreactor by photosynthetic organisms. *J Nanopart Res* 14:1–17
- Dahoumane SA, Yéprémian C, Djediat C, Couté A, Fiévet F, Coradin T, Brayner R (2016) Improvement of kinetics, yield, and colloidal stability of biogenic gold nanoparticles using living cells of *Euglena gracilis* microalga. *J Nanopart Res* 18:1–12
- De Jong WH, Borm PJA (2008) Drug delivery and nanoparticles: applications and hazards. *Int J Nanomedicine* 3:133–149
- Dhillon GS, Brar SK, Kaur S, Verma M (2012) Green approach for nanoparticle biosynthesis by fungi: current trends and applications. *Crit Rev Biotechnol* 32:49–73
- di Tomaso G, Fedi S, Carnevali M, Manegatti M, Taddei C, Zannoni D (2002) The membrane-bound respiratory chain of *pseudomonas pseudoalcaligenes* KF707 cells grown in the presence or absence of potassium tellurite. *Microbiology* 148:1699–1708
- Dreaden EC, Alkilany AM, Huang X, Murphy CJ, El-Sayed MA (2012) The golden age: gold nanoparticles for biomedicine. *Chem Soc Rev* 41:2740–2779
- Dridge EJ, Butler CS (2010) Thermostable properties of the periplasmic selenate reductase from *Thauera selenatis*. *Biochimie* 92:1268–1273
- Du L, Jiang H, Liu X, Wang E (2007) Biosynthesis of gold nanoparticles assisted by *Escherichia coli* DH5 $\alpha$  and its application on direct electrochemistry of hemoglobin. *Electrochem Commun* 9:1165–1170
- Durán N, Durán M, de Jesus MB, Seabra AB, Fávaro WJ, Nakazato G (2016) Silver nanoparticles: a new view on mechanistic aspects on antimicrobial activity. *Nanomedicine* 12:789–799
- Dutta T, Chattopadhyay AP, Ghosh NN, Khatua S, Acharya K, Kundu S, Mitra D, Das M (2020) Biogenic silver nanoparticle synthesis and stabilization for apoptotic activity; insights from experimental and theoretical studies. *Chem Pap* 74:4089–4101
- Elahi N, Kamali M, Baghersad MH (2018) Recent biomedical applications of gold nanoparticles: a review. *Talanta* 184:537–556
- Elhakim HKA, Azab SM, Fekry AM (2018) A novel simple biosensor containing silver nanoparticles/propolis (bee glue) for microRNA let-7a determination. *Mater Sci Eng C* 92:489–495
- El-Nour KMA, Salam ETA, Soliman HM, Orabi AS (2017) Gold nanoparticles as a direct and rapid sensor for sensitive analytical detection of biogenic amines. *Nanoscale Res Lett* 12:1–11
- Fawcett D, Verduin JJ, Shah M, Sharma SB, Poinern GEJ (2017) A review of current research into the biogenic synthesis of metal and metal oxide nanoparticles via marine algae and seagrasses. *J Nanosci* 2017:1–15
- Forootanfar H, Amirpour-Rostami S, Jafari M, Forootanfar A, Yousefizadeh Z, Shakibaie M (2015) Microbial-assisted synthesis and evaluation of the cytotoxic effect of tellurium nanorods. *Mater Sci Eng C* 49:183–189

- Frankel ML, Booth SC, Turner RJ (2016) How bacteria are affected by toxic metal release. In: Metal sustainability: global challenges, consequences, and prospects. Wiley Blackwell, pp 253–270
- Gallardo-Benavente C, Carrión O, Todd JD, Pieretti JC, Seabra AB, Durán N, Rubilar O, Pérez-Donoso JM, Quiroz A (2019) Biosynthesis of CdS quantum dots mediated by volatile sulfur compounds released by Antarctic *Pseudomonas fragi*. Front Microbiol 10:1866
- Gandhi H, Khan S (2016) Biological synthesis of silver nanoparticles and its antibacterial activity. J Nanomed Nanotechnol 7:366
- Ganesh Babu MM, Gunasekaran P (2009) Production and structural characterization of crystalline silver nanoparticles from *Bacillus cereus* isolate. Colloids Surf B: Biointerfaces 74:191–195
- Ghorbanpour M, Bhargava P, Varma A, Choudhary DK (eds) (2020) Biogenic nano-particles and their use in agro-ecosystems. Springer, Cham
- Gudikandula K, Charya Maringanti S (2016) Synthesis of silver nanoparticles by chemical and biological methods and their antimicrobial properties. J Exp Nanosci 11:714–721
- Gugala N, Turner RJ (2018) The potential of metals in combating bacterial pathogens. In: Bio-medical applications of metals. Springer, pp 129–150
- Gurunathan S, Kalishwaralal K, Vaidyanathan R, Venkataraman D, Pandian SRK, Muniyandi J, Hariharan N, Eom SH (2009) Biosynthesis, purification and characterization of silver nanoparticles using *Escherichia coli*. Colloids Surf B: Biointerfaces 74:328–335
- He S, Guo Z, Zhang Y, Zhang S, Wang J, Gu N (2007) Biosynthesis of gold nanoparticles using the bacteria *Rhodospseudomonas capsulata*. Mater Lett 61:3984–3987
- Herlekar M, Barve S, Kumar R (2014) Plant-mediated green synthesis of iron nanoparticles. J Nanopart 2014:1–9
- Horikoshi S, Serpone N (2013) Introduction to nanoparticles. In: Microwaves in nanoparticle synthesis: fundamentals and applications. Wiley-VCH, pp 1–24
- Hoseinzadeh E, Makhdoumi P, Taha P, Hossini H, Stelling J, Amjad Kamal M, Md Ashraf G (2016) A review on nano-antimicrobials: metal nanoparticles, methods and mechanisms. Curr Drug Metab 18:120–128
- Hulkoti NI, Taranath TC (2014) Biosynthesis of nanoparticles using microbes—a review. Colloids Surf B: Biointerfaces 121:474–483
- Hussey MI, El-Aziz MA, Badr Y, Mahmoud MA (2007) Biosynthesis of gold nanoparticles using *Pseudomonas aeruginosa*. Spectrochim Acta A Mol Biomol Spectrosc 67:1003–1006
- Ijaz I, Gilani E, Nazir A, Bukhari A (2020) Detail review on chemical, physical and green synthesis, classification, characterizations and applications of nanoparticles. Green Chem Lett Rev 13:59–81
- Jain R, Jordan N, Weiss S, Foerstendorf H, Heim K, Kacker R, Hübner R, Kramer H, van Hullebusch ED, Farges F, Lens PNL (2015) Extracellular polymeric substances govern the surface charge of biogenic elemental selenium nanoparticles. Environ Sci Technol 49:1713–1720
- Jana J, Ganguly M, Pal T (2016) Enlightening surface plasmon resonance effect of metal nanoparticles for practical spectroscopic application. RSC Adv 6:86174–86211
- Javed H, Fatima K, Akhter Z, Nadeem MA, Siddiq M, Iqbal A (2016) Fluorescence modulation of cadmium sulfide quantum dots by azobenzene photochromic switches. R Soc 472:20150692
- Jeevanandam J, Barhoum A, Chan YS, Dufresne A, Danquah MK (2018) Review on nanoparticles and nanostructured materials: history, sources, toxicity and regulations. Beilstein J Nanotechnol 9:1050–1074
- Jigyasu AK, Siddiqui S, Jafri A, Arshad M, Lohani M, Khan IA (2019) Biological synthesis of CdTe quantum dots and their anti-proliferative assessment against prostate cancer cell line. J Nanosci Nanotechnol 20:3398–3403
- Kalishwaralal K, Deepak V, Ram Kumar Pandian S, Gurunathan S (2009) Biological synthesis of gold nanocubes from *Bacillus licheniformis*. Bioresour Technol 100:5356–5358



- Kalishwaralal K, Deepak V, Ram Kumar Pandian SB, Kottaisamy M, BarathManiKanth S, Kartikeyan B, Gurunathan S (2010) Biosynthesis of silver and gold nanoparticles using *Brevibacterium casei*. *Colloids Surf B: Biointerfaces* 77:257–262
- Kathiraven T, Sundaramanickam A, Shanmugam N, Balasubramanian T (2015) Green synthesis of silver nanoparticles using marine algae *Caulerpa racemosa* and their antibacterial activity against some human pathogens. *Appl Nanosci (Switzerland)* 5:499–504
- Keat CL, Aziz A, Eid AM, Elmarzugi NA (2015) Biosynthesis of nanoparticles and silver nanoparticles. *Bioresour Bioprocess* 2:47
- Kędziora A, Speruda M, Krzyżewska E, Rybka J, Łukowiak A, Bugla-Płoskońska G (2018) Similarities and differences between silver ions and silver in nanoforms as antibacterial agents. *Int J Mol Sci* 19:444
- Khalid A, Tran PA, Norello R, Simpson DA, O'Connor AJ, Tomljenovic-Hanic S (2016) Intrinsic fluorescence of selenium nanoparticles for cellular imaging applications. *Nanoscale* 8:3376–3385
- Khan I, Saeed K, Khan I (2019) Nanoparticles: properties, applications and toxicities. *Arab J Chem* 12:908–931
- Khan MR, Fromm KM, Rizvi TF, Giese B, Ahamad F, Turner RJ, Füg M, Marsili E (2020) Metal nanoparticle–microbe interactions: synthesis and antimicrobial effects. *Part Part Syst Charact* 37:1900419
- Khandel P, Kumar Shahi S (2016) Microbes mediated synthesis of metal nanoparticles: current status and future prospects. *Int J Nanomater Biostruct* 6:1–24
- Khanna P, Kaur A, Goyal D (2019) Algae-based metallic nanoparticles: synthesis, characterization and applications. *J Microbiol Methods* 163:105656
- Khurana A, Tekula S, Saifi MA, Venkatesh P, Godugu C (2019) Therapeutic applications of selenium nanoparticles. *Biomed Pharmacother* 111:802–812
- Kora AJ (2018) *Bacillus cereus*, selenite-reducing bacterium from contaminated lake of an industrial area: a renewable nanofactory for the synthesis of selenium nanoparticles. *Bioresour Bioprocess* 5:30
- Kulkarni R, Rondiya S, Pawbake A, Waykar R, Jadhavar A, Jadkar V, Bhorde A, Date A, Pathan H, Jadkar S (2017) Structural and optical properties of CdTe thin films deposited using RF magnetron sputtering. *Energy Procedia* 110:188–195
- Kumar SA, Abyaneh MK, Gosavi SW, Kulkarni SK, Pasricha R, Ahmad A, Khan MI (2007) Nitrate reductase-mediated synthesis of silver nanoparticles from AgNO<sub>3</sub>. *Biotechnol Lett* 29:439–445
- Lahiri D, Nag M, Sheikh HI, Sarkar T, Edinur HA, Pati S, Ray RR (2021) Microbiologically-synthesized nanoparticles and their role in silencing the biofilm signaling cascade. *Front Microbiol* 12:636588
- Lampis S, Zonaro E, Bertolini C, Cecconi D, Monti F, Micaroni M, Turner RJ, Butler CS, Vallini G (2017) Selenite biotransformation and detoxification by *Stenotrophomonas maltophilia* SeITE02: novel clues on the route to bacterial biogenesis of selenium nanoparticles. *J Hazard Mater* 324:3–14
- Lane MKM, Zimmerman JB (2019) Controlling metal oxide nanoparticle size and shape with supercritical fluid synthesis. *Green Chem* 21:3769–3781
- Lemire JA, Harrison JJ, Turner RJ (2013) Antimicrobial activity of metals: mechanisms, molecular targets and applications. *Nat Rev Microbiol* 11:371–384
- Li L, Hu Q, Zeng J, Qi H, Zhuang G (2011a) Resistance and biosorption mechanism of silver ions by *Bacillus cereus* biomass. *J Environ Sci* 23:108–111
- Li X, Xu H, Chen ZS, Chen G (2011b) Biosynthesis of nanoparticles by microorganisms and their applications. *J Nanomater* 2011:1–16
- Lin S, Mortimer M, Chen R, Kallinen A, Riviere JE, Davis TP, Ding F, Ke PC (2017) NanoEHS beyond toxicity-focusing on biocorona. *Environ Sci Nano* 4:1433–1454
- Luo K, Jung S, Park KH, Kim YR (2018) Microbial biosynthesis of silver nanoparticles in different culture media. *J Agric Food Chem* 66:957–962

- Ma C, Yan J, Huang Y, Wang C, Yang G (2018) The optical duality of tellurium nanoparticles for broadband solar energy harvesting and efficient photothermal conversion. *Sci Adv* 4:eas9894
- Mahdavi M, Namvar F, Bin Ahmad M, Mohamad R (2013) Green biosynthesis and characterization of magnetic iron oxide (Fe<sub>3</sub>O<sub>4</sub>) nanoparticles using seaweed (*Sargassum muticum*) aqueous extract. *Molecules* 18:5954–5964
- Majeed S, Danish M, Mohamad Ibrahim MN, Sekeri SH, Ansari MT, Nanda A, Ahmad G (2020) Bacteria mediated synthesis of iron oxide nanoparticles and their antibacterial, antioxidant, cytocompatibility properties. *J Clust Sci*:1–12
- Manikprabhu D, Lingappa K (2013) Microwave assisted rapid bio-based synthesis of gold nanorods using pigment produced by *Streptomyces coelicolor* klm33. *Acta Metallurgica Sinica (Eng Lett)* 26:613–617
- Mateo CT, Mocan T, Tabaran F, Pop T, Mosteanu O, Puia C, Iancu C, Mocan L (2017) Quantum dots in imaging, drug delivery and sensor applications. *Int J Nanomedicine* 12:5421–5431
- Meenatchisundaram N, Chellamuthu J, Jeyaraman AR, Arjunan N, Muthuramalingam JB, Karuppuchamy S (2021) Biosynthesized TiO<sub>2</sub> nanoparticles an efficient biogenic material for photocatalytic and antibacterial applications. *Energy Environ* 0:1–22
- Menon S, Rajeshkumar S, Venkat Kumar S (2017) A review on biogenic synthesis of gold nanoparticles, characterization, and its applications. *Resour Efficient Technol* 3:516–527
- Mi C, Wang Y, Zhang J, Huang H, Xu L, Wang S, Fang X, Fang J, Mao C, Xu S (2011) Biosynthesis and characterization of CdS quantum dots in genetically engineered *Escherichia coli*. *J Biotechnol* 153:125–132
- Mody V, Siwale R, Singh A, Mody H (2010) Introduction to metallic nanoparticles. *J Pharm Bioallied Sci* 2:282
- Moghaddam AB, Namvar F, Moniri M, Tahir PM, Azizi S, Mohamad R (2015) Nanoparticles biosynthesized by fungi and yeast: a review of their preparation, properties, and medical applications. *Molecules* 20:16540–16565
- Mohanty A, Kathawala MH, Zhang J, Chen WN, Loo JSC, Kjelleberg S, Yang L, Cao B (2014) Biogenic tellurium nanorods as a novel antivirulence agent inhibiting pyoverdine production in *Pseudomonas aeruginosa*. *Biotechnol Bioeng* 111:858–865
- Mohd Yusof H, Abdul Rahman NA, Mohamad R, Zaidan UH, Samsudin AA (2020) Biosynthesis of zinc oxide nanoparticles by cell-biomass and supernatant of *Lactobacillus plantarum* TA4 and its antibacterial and biocompatibility properties. *Sci Rep* 10:1–13
- Momeni S, Nabipour I (2015) A simple green synthesis of palladium nanoparticles with *Sargassum Alga* and their electrocatalytic activities towards hydrogen peroxide. *Appl Biochem Biotechnol* 176:1937–1949
- Moore MD, Kaplan S (1992) Identification of intrinsic high-level resistance to rare-earth oxides and oxyanions in members of the class proteobacteria: characterization of tellurite, selenite, and rhodium sesquioxide reduction in *Rhodobacter sphaeroides*. *J Bacteriol* 174:1505–1514
- Mourato A, Gadanho M, Lino AR, Tenreiro R (2011) Biosynthesis of crystalline silver and gold nanoparticles by extremophilic yeasts. *Bioinorg Chem Appl* 2011:546074
- Mourdikoudis S, Pallares RM, Thanh NTK (2018) Characterization techniques for nanoparticles: comparison and complementarity upon studying nanoparticle properties. *Nanoscale* 10:12871–12934
- Mukherjee P, Senapati S, Mandal D, Ahmad A, Islam Khan M, Kumar R, Sastry M, Khan MI, Ahmad A, Kumar R, Mukherjee P, Senapati S, Mandal D, Sastry M (2002) Extracellular synthesis of gold nanoparticles by the fungus *Fusarium oxysporum*. *Chembiochem* 3:461–463
- Nakai J (2018) Food and Agriculture Organization of the United Nations and the sustainable development goals. 22
- Nangia Y, Wangoo N, Goyal N, Shekhawat G, Suri CR (2009) A novel bacterial isolate *Stenotrophomonas maltophilia* as living factory for synthesis of gold nanoparticles. *Microb Cell Factories* 8:1–7

- Nwoko KC, Liang X, Perez MA, Krupp E, Gadd GM, Feldmann J (2021) Characterisation of selenium and tellurium nanoparticles produced by *Aureobasidium pullulans* using a multi-method approach. *J Chromatogr A* 1642:462022
- Ojeda JJ, Merroun ML, Tugarova AV, Lampis S, Kamnev AA, Gardiner PHE (2020) Developments in the study and applications of bacterial transformations of selenium species. *Crit Rev Biotechnol* 40:1250–1264
- Órdenes-Aenishanslins NA, Saona LA, Durán-Toro VM, Monrás JP, Bravo DM, Pérez-Donoso JM (2014) Use of titanium dioxide nanoparticles biosynthesized by *Bacillus mycoides* in quantum dot sensitized solar cells. *Microb Cell Factories* 13:1–10
- Otari SV, Patil RM, Nadaf NH, Ghosh SJ, Pawar SH (2014) Green synthesis of silver nanoparticles by microorganism using organic pollutant: its antimicrobial and catalytic application. *Environ Sci Pollut Res* 21:1503–1513
- Ovais M, Khalil AT, Ayaz M, Ahmad I, Nethi SK, Mukherjee S (2018) Biosynthesis of metal nanoparticles via microbial enzymes: a mechanistic approach. *Int J Mol Sci* 19:4100
- Paladini F, Pollini M (2019) Antimicrobial silver nanoparticles for wound healing application: progress and future trends. *Materials* 12:2540
- Patil S, Chandrasekaran R (2020) Biogenic nanoparticles: a comprehensive perspective in synthesis, characterization, application and its challenges. *J Genet Eng Biotechnol* 18:1–23
- Piacenza E, Presentato A, Zonaro E, Lemire JA, Demeter M, Vallini G, Turner RJ, Lampis S (2017) Antimicrobial activity of biogenically produced spherical Se-nanomaterials embedded in organic material against *Pseudomonas aeruginosa* and *Staphylococcus aureus* strains on hydroxyapatite-coated surfaces. *Microb Biotechnol* 10:804–818
- Piacenza E, Presentato A, Ambrosi E, Speghini A, Turner RJ, Vallini G, Lampis S (2018a) Physical–chemical properties of biogenic selenium nanostructures produced by *Stenotrophomonas maltophilia* SeITE02 and *Ochrobactrum* sp. MPV1. *Front Microbiol* 9:3178
- Piacenza E, Presentato A, Turner RJ (2018b) Stability of biogenic metal(loid) nanomaterials related to the colloidal stabilization theory of chemical nanostructures. *Crit Rev Biotechnol* 38:1137–1156
- Piacenza E, Presentato A, Zonaro E, Lampis S, Vallini G, Turner RJ (2018c) Selenium and tellurium nanomaterials. *Phys Sci Rev* 3:16
- Piacenza E, Presentato A, Bardelli M, Lampis S, Vallini G, Turner RJ (2019) Influence of bacterial physiology on processing of selenite, biogenesis of nanomaterials and their thermodynamic stability. *Molecules* 24
- Piacenza E, Presentato A, Heyne B, Turner RJ (2020) Tunable photoluminescence properties of selenium nanoparticles: biogenic versus chemogenic synthesis. *Nano* 9:3615–3628
- Pormohammad A, Monych NK, Ghosh S, Turner DL, Turner RJ (2021) Nanomaterials in wound healing and infection control. *Antibiotics* 10:473
- Pourali P, Badiie SH, Manafi S, Noorani T, Rezaei A, Yahyaie B (2017) Biosynthesis of gold nanoparticles by two bacterial and fungal strains, *Bacillus cereus* and *Fusarium oxysporum*, and assessment and comparison of their nanotoxicity in vitro by direct and indirect assays. *Electron J Biotechnol* 29:86–93
- Prasad TNVKV, Subba Rao Kambala V, Naidu R (2011) A critical review on biogenic silver nanoparticles and their antimicrobial activity. *Curr Nanosci* 7:531–544
- Presentato A, Piacenza E, Anikovskiy M, Cappelletti M, Zannoni D, Turner RJ (2018a) Biosynthesis of selenium-nanoparticles and -nanorods as a product of selenite bioconversion by the aerobic bacterium *Rhodococcus aetherivorans* BCPI. *New Biotechnol* 41:1–8
- Presentato A, Piacenza E, Darbandi A, Anikovskiy M, Cappelletti M, Zannoni D, Turner RJ (2018b) Assembly, growth and conductive properties of tellurium nanorods produced by *Rhodococcus aetherivorans* BCPI. *Sci Rep* 8:1–10
- Presentato A, Turner RJ, Vásquez CC, Yurkov V, Zannoni D (2019) Tellurite-dependent blackening of bacteria emerges from the dark ages. *Environ Chem* 16:266–288

- Pugazhenthiran N, Anandan S, Kathiravan G, Prakash NKU, Crawford S, Ashokkumar M (2009) Microbial synthesis of silver nanoparticles by *Bacillus* sp. *J Nanopart Res* 11:1811–1815
- Pugin B, Cornejo FA, Muñoz-Díaz P, Muñoz-Villagrán CM, Vargas-Pérez JI, Arenas FA, Vásquez CC (2014) Glutathione reductase-mediated synthesis of tellurium-containing nanostructures exhibiting antibacterial properties. *Appl Environ Microbiol* 80:7061–7070
- Qidwai A, Pandey A, Kumar R, Shukla SK, Dikshit A (2018) Advances in biogenic nanoparticles and the mechanisms of antimicrobial effects. *Indian J Pharm Sci* 80:592–603
- Rajput S, Werezuk R, Lange RM, Mcdermott MT (2016) Fungal isolate optimized for biogenesis of silver nanoparticles with enhanced colloidal stability. *Langmuir* 32:8688–8697
- Ramos-Ruiz A, Field JA, Wilkening JV, Sierra-Alvarez R (2016) Recovery of elemental tellurium nanoparticles by the reduction of tellurium oxyanions in a methanogenic microbial consortium. *Environ Sci Technol* 50:1492–1500
- Reddy AS, Chen CY, Chen CC, Jean JS, Chen HR, Tseng MJ, Fan CW, Wang JC (2010) Biological synthesis of gold and silver nanoparticles mediated by the bacteria *Bacillus subtilis*. *J Nanosci Nanotechnol* 10:6567–6574
- Rodrigues SSM, Ribeiro DSM, Soares JX, Passos MLC, Saraiva MLMFS, Santos JLM (2017) Application of nanocrystalline CdTe quantum dots in chemical analysis: implementation of chemo-sensing schemes based on analyte-triggered photoluminescence modulation. *Coord Chem Rev* 330:127–143
- Salas Orozco MF, Niño-Martínez N, Martínez-Castañón GA, Méndez FT, Ruiz F (2019) Molecular mechanisms of bacterial resistance to metal and metal oxide nanoparticles. *Int J Mol Sci* 20:2808
- Salata OV (2004) Applications of nanoparticles in biology and medicine. *J Nanobiotechnol* 2:3
- Sánchez-López E, Gomes D, Esteruelas G, Bonilla L, Lopez-Machado AL, Galindo R, Cano A, Espina M, Ettchetto M, Camins A, Silva AM, Durazzo A, Santini A, Garcia ML, Souto EB (2020) Metal-based nanoparticles as antimicrobial agents: an overview. *Nano* 10
- Sarkar J, Dey P, Saha S, Acharya K (2011) Mycosynthesis of selenium nanoparticles. *Micro Nano Lett* 6:599–602
- Satyanarayana Reddy A, Chen CY, Chen CC, Jean JS, Chen HR, Tseng MJ, Fan CW, Wang JC (2010) Biological synthesis of gold and silver nanoparticles mediated by the bacteria *Bacillus subtilis*. *J Nanosci Nanotechnol* 10:6567–6574
- Schwarz JA, Lyshevski SE, Contescu CI (eds) (2014) Dekker encyclopedia of nanoscience and nanotechnology – seven volume set. CRC Press
- Seshadri S, Saranya K, Kowshik M (2011) Green synthesis of lead sulfide nanoparticles by the lead resistant marine yeast, *Rhodospiridium diobovatum*. *Biotechnol Prog* 27:1464–1469
- Shakibaie M, Shahverdi AR, Faramarzi MA, Hassanzadeh GR, Rahimi HR, Sabzevari O (2013) Acute and subacute toxicity of novel biogenic selenium nanoparticles in mice. *Pharm Biol* 51:58–63
- Sharma D, Kanchi S, Bisetty K (2015) Biogenic synthesis of nanoparticles: a review. *Arab J Chem* 12:3576–3600
- Siddiqi KS, Husen A, Rao RAK (2018a) A review on biosynthesis of silver nanoparticles and their biocidal properties. *J Nanobiotechnol* 16:14
- Siddiqi KS, Ur Rahman A, Tajuddin, Husen A (2018b) Properties of zinc oxide nanoparticles and their activity against microbes. *Nanoscale Res Lett* 13:1–13
- Singh PK, Kundu S (2014) Biosynthesis of gold nanoparticles using bacteria. *Proc Natl Acad Sci India Sect B Biol Sci* 84:331–336
- Singh H, Du J, Singh P, Yi TH (2018a) Role of green silver nanoparticles synthesized from *Symphytum officinale* leaf extract in protection against UVB-induced photoaging. *J Nanostruct Chem* 8:359–368
- Singh P, Garg A, Pandit S, Mokkaipati VRSS, Mijakovic I (2018b) Antimicrobial effects of biogenic nanoparticles. *Nanomaterials* 8:1009

- Singh A, Gautam PK, Verma A, Singh V, Shivapriya PM, Shivalkar S, Sahoo AK, Samanta SK (2020) Green synthesis of metallic nanoparticles as effective alternatives to treat antibiotics resistant bacterial infections: a review. *Biotechnol Rep*:25
- Slavin YN, Asnis J, Häfeli UO, Bach H (2017) Metal nanoparticles: understanding the mechanisms behind antibacterial activity. *J Nanobiotechnol* 15:65
- Stephen AJ, Rees NV, Mikheenko I, Macaskie LE (2019) Platinum and palladium bio-synthesized nanoparticles as sustainable fuel cell catalysts. *Front Energy Res* 7:66
- Sungur Ş (2020) Titanium dioxide nanoparticles. In: *Handbook of nanomaterials and nanocomposites for energy and environmental applications*. Springer, pp 1–18
- Sur VP, Kominkova M, Buchtova Z, Dolezelikova K, Zitka O, Moullick A (2019) CdSe QD biosynthesis in yeast using tryptone-enriched media and their conjugation with a peptide hecate for bacterial detection and killing. *Nano* 9:1463
- Sztandera K, Gorzkiewicz M, Klajnert-Maculewicz B (2019) Gold nanoparticles in cancer treatment. *Mol Pharm* 16:1–23
- Tan Y, Wang Y, Wang Y, Xu D, Huang Y, Wang D, Wang G, Rensing C, Zheng S (2018) Novel mechanisms of selenate and selenite reduction in the obligate aerobic bacterium *Comamonas testosteroni* S44. *J Hazard Mater* 359:129–138
- Tian LJ, Zhou NQ, Liu XW, Liu JH, Zhang X, Huang H, Zhu TT, Li LL, Huang Q, Li WW, Liu YZ, Yu HQ (2017) A sustainable biogenic route to synthesize quantum dots with tunable fluorescence properties for live cell imaging. *Biochem Eng J* 124:130–137
- Turner RJ (2017) Metal-based antimicrobial strategies. *Microb Biotechnol* 10:1062–1065
- Turner RJ, Borghese R, Zannoni D (2012) Microbial processing of tellurium as a tool in biotechnology. *Biotechnol Adv* 30:954–963
- Wadhvani SA, Shedbalkar UU, Singh R, Chopade BA (2016) Biogenic selenium nanoparticles: current status and future prospects. *Appl Microbiol Biotechnol* 100:2555–2566
- Wang EC, Wang AZ (2014) Nanoparticles and their applications in cell and molecular biology. *Integr Biol (Camb)* 6:9–26
- Wang Y, Shu X, Hou J, Lu W, Zhao W, Huang S, Wu L (2018) Selenium nanoparticle synthesized by *Proteus mirabilis* YC801: an efficacious pathway for selenite biotransformation and detoxification. *Int J Mol Sci* 19:3809
- Wu W, He Q, Jiang C (2008) Magnetic iron oxide nanoparticles: synthesis and surface functionalization strategies. *Nanoscale Res Lett* 3:397–415
- Xie C, Niu Z, Kim D, Li M, Yang P (2020) Surface and interface control in nanoparticle catalysis. *Chem Rev* 120:1184–1249
- Yang F, Tang Q, Zhong X, Bai Y, Chen T, Zhang Y, Li Y, Zheng W (2012) Surface decoration by *Spirulina* polysaccharide enhances the cellular uptake and anticancer efficacy of selenium nanoparticles. *Int J Nanomedicine* 7:835–844
- Yang G, Hu L, Keiper TD, Xiong P, Hallinan DT (2016) Gold nanoparticle monolayers with tunable optical and electrical properties. *Langmuir* 32:4022–4033
- Yaqoob AA, Ahmad H, Parveen T, Ahmad A, Oves M, Ismail IMI, Qari HA, Umar K, Mohamad Ibrahim MN (2020) Recent advances in metal decorated nanomaterials and their various biological applications: a review. *Front Chem* 8:341
- Yee N, Choi J, Porter AW, Carey S, Rauschenbach I, Harel A (2014) Selenate reductase activity in *Escherichia coli* requires *Isc* iron-sulfur cluster biosynthesis genes. *FEMS Microbiol Lett* 361:138–143
- Yeh YC, Creran B, Rotello VM (2012) Gold nanoparticles: preparation, properties, and applications in bionanotechnology. *Nanoscale* 4:1871–1880
- Yu Q, Boyanov MI, Liu J, Kemner KM, Fein JB (2018) Adsorption of selenite onto *Bacillus subtilis*: the overlooked role of cell envelope sulfhydryl sites in the microbial conversion of Se (IV). *Environ Sci Technol* 52:10400–10407
- Zonaro E, Lampis S, Turner RJ, Junaid S, Vallini G (2015) Biogenic selenium and tellurium nanoparticles synthesized by environmental microbial isolates efficaciously inhibit bacterial planktonic cultures and biofilms. *Front Microbiol* 6:584
- Zorraquín-Peña I, Cueva C, Bartolomé B, Moreno-Arribas MV (2020) Silver nanoparticles against foodborne bacteria. Effects at intestinal level and health limitations. *Microorganisms* 8:132

**Part IV**  
**Uniqueness of the Elements**

# Chapter 8

## Microbes: Key Players of the Arsenic Biogeochemical Cycle



Rimi Biswas and Angana Sarkar

**Abstract** The arsenic biogeochemical cycle is vastly influenced by the biotransformation of arsenic. The insights within the complexities of this bio-cycle can be determined using microbial community analysis by meta-omics coupled with the identification of microbial pathways influencing the biotransformation of arsenic. The fate of toxic environmental contaminants and nutrients is governed by the microbial arsenic transformations in the biogeochemical cycle. The bioavailability of arsenic species is greatly prejudiced by the microbial redox metabolism of carbon, iron, nitrogen, and sulphur. In this chapter, we exemplify the genes and microbial biogeochemical processes concerned with the biotransformation of arsenic. The importance of deciphering the individual microbial communities using the current and future omic approaches will aid in determining their connections to other cycles of biogeochemical nature. Specific biotechnological solutions could be designed for environmental problems using these microbial metabolic insights. A thorough biochemical modelling integrated with systematic approaches is needed to comprehend the complex nature of organic, inorganic, and environmental arsenic species. Hence, a relation between arsenic biotransformation and the environment could be adjudged which will pave the way for further studies on arsenic biogeochemistry.

### 8.1 Introduction

Biotransformation and redox reactions often interconnect the biogeochemical cycles (Di et al. 2019). Numerous microbes mediate the cycling of a specific element influencing the biogeochemical processes. Arsenite (As(III)) oxidizing and arsenate (As(V)) reducing microbes control the diverse arsenic redox changes. Sulphur, carbon, iron, and nitrogen often couple to the variable processes of arsenic biogeochemical cycle besides controlling the dynamics of ions/elements within the redox arsenic cycle (Gnanaprakasam et al. 2017). Recent attention has been garnered in

---

R. Biswas · A. Sarkar (✉)

Department of Biotechnology and Medical Engineering, National Institute of Technology, Rourkela, India

studies of the coupling reaction between different biogeochemical cycles. In the current scenario, these offer a scientific basis for the prominent environmental and industrial problems (Finzi et al. 2011). There has been a continuous re-development and evolution of chemical species within the biogeochemical cycle affected by various physical, chemical, and geological forces catalysing proteins in living organisms (Table 8.1). Understanding of the basic arsenic biogeochemical cycle requires the indulgence of genetic analysis which acts as the key factor. The influence of microbial metabolism on arsenic biogeochemical cycling is being predicted using the genes involved in the reactions and the effect of environmental signals on varied gene expression. This chapter primarily focuses on the recognized genes concerned with arsenic biotransformations besides studying the arsenic biogeochemistry and the effect of variable elements on it. The recent effect of meta-omic approaches along with microbial metabolism of arsenic has also been deciphered. Finally, the possible combination of biogeochemical models with meta-omic approaches has been studied to envisage the probable transformation of arsenic with former elements.

## 8.2 Arsenic Metabolism Genes and Biochemical Cycling

Since many years, microbes have been transforming arsenic for energy metabolism or detoxification via several approaches.

### 8.2.1 The Arsenic Redox Cycle

Primitive microbes generally evolved within an anoxic or oxygen strained environment, having a minority of reduced As (V), wherein the oxidized As (III) formed the dominant arsenic species. The acquisition and evolution of genes encoding the anaerobic respiratory pathways could be due to the bioavailability of As (III) which acts as a driving force for the primitive anaerobic microbial metabolic processes (Oremland et al. 2009). For instance, *Ectothiorhodospira* PHS-1, a photosynthetic sulphur purple bacterium performs anoxygenic photosynthesis in the dark and the light simultaneously using As (V) and As (III) as an electron acceptor and electron donor, respectively (Hoeft et al. 2010; Hernandez-maldonado et al. 2017). *Alkalilimnicola ehrlichii* MLHE-1, a chemolithoautotrophic oxidizer of As (III), utilizes nitrate as an acceptor of electron along with As (III) as a donor of electron in numerous energy driven respiratory pathways (Oremland et al. 2002). The evolution of microbes having similar metabolic pathways dates back to several million years. In accordance to the primordial biosphere which was mostly anoxic in nature, these microbes survived in intense growth conditions of low oxygen or high As (III) concentrations (Biswas et al. 2019). The foreseeable choice for such microbes to produce energy, was to exploit As (III) as a donor of electron as most



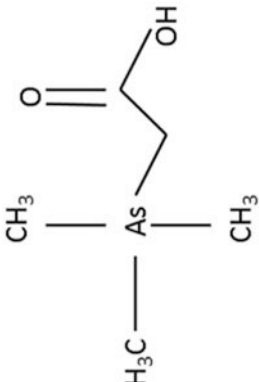
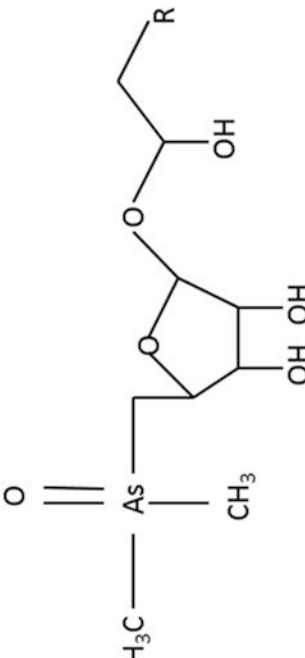
**Table 8.1** Speciation of arsenic in the environment (Ardini et al. 2020)

Sl. No	Species of Arsenic	Structure of arsenic speciation
1	Arsenite (As III)	$\begin{array}{c} \text{HO} - \text{As} - \text{OH} \\   \\ \text{OH} \end{array}$
2	Arsenic acid (As V)	$\begin{array}{c} \text{O} \\    \\ \text{HO} - \text{As} - \text{OH} \\   \\ \text{OH} \end{array}$
3	Trimethylarsine oxide (TMAO)	$\begin{array}{c} \text{O} \\    \\ \text{H}_3\text{C} - \text{As} - \text{CH}_3 \\   \\ \text{CH}_3 \end{array}$

(continued)

Table 8.1 (continued)

Sl. No	Species of Arsenic	Structure of arsenic speciation
4	Dimethylarsenate (DMAS (V))	$  \begin{array}{c}  \text{O} \\  \parallel \\  \text{H}_3\text{C} - \text{As} - \text{OH} \\    \\  \text{CH}_3  \end{array}  $
5	Methylarsenate (MMAs (V))	$  \begin{array}{c}  \text{O} \\  \parallel \\  \text{OH} - \text{As} - \text{OH} \\    \\  \text{CH}_3  \end{array}  $

6	Arsenobetaine (AsB)	 <chem>C[As](C)(C)CCO</chem>
7	Arsenosugars	 <chem>C[As](C)C1OC(O)C(O)C1OCCO</chem>

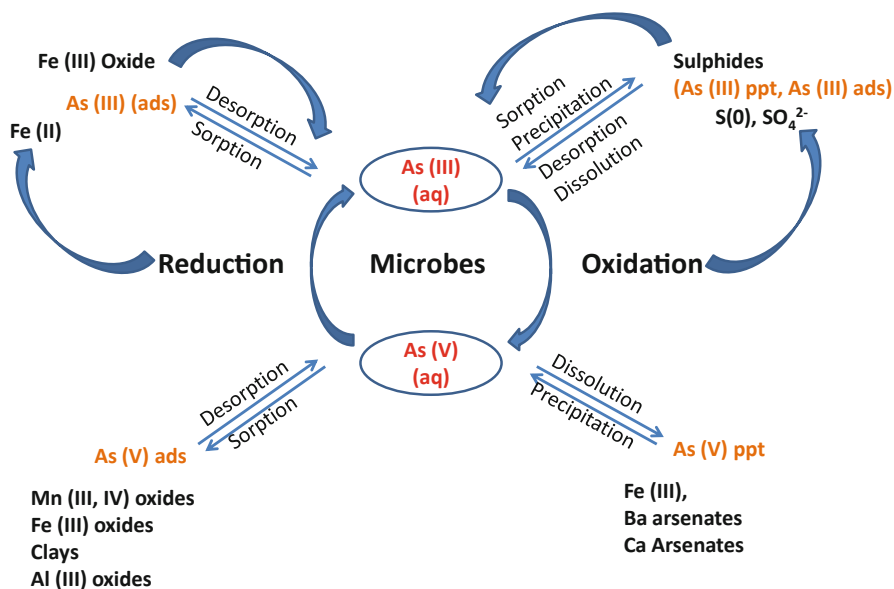


**Fig. 8.1** The arsenic biogeochemical cycle

certainly it was the only bio-available prime arsenic species (Fig. 8.1) (Kulp 2014). The As (III) oxidase enzyme is comprised of dual dissimilar subunits which catalyze the process of As (III) oxidation. The larger subunit ( $\alpha$ ) has a (AioA) [3Fe-4S] cluster and molybdopterin wherein the minor subunit ( $\beta$ ) consists of (AioB) Rieske-type [2Fe-2S] cluster (Stolz et al. 2010). Arsenite is recognized via aio genes, which regulate its expression. A dual-component pair of transduction units regulating its signal is comprised of AioR (transcriptional regulator)/AioS (sensor histidine kinase) which is encoded by aioR and aioS genes of the prime aio operon which is again a huddle of aioA and aioB genes (Table. 8.2) (Chatterjee et al. 2017). The operon sometimes consists of a moeA gene which aids in the synthesis of the molybdenum cofactor of AioAB oxidase encoding protein MoeA (Branco et al. 2009). In recent times, *A. ehrlichii* MLHE-1 exhibited activities such as As (III) oxidase and As (V) reductase in vitro by an ArxA gene encoding As (III) oxidase (Zargar et al. 2010). Sometimes photosynthesis is coupled to As (III) oxidation genes; for instance, in *Ectothiorhodospira sp.* PHS-1 (Hernandez-maldonado et al. 2017). Also, two proteins, namely TorD—molybdoenzyme chaperone, a quinol oxidoreductase—a membrane anchoring subunit comprised of a [4Fe-4S] centre is encoded by arxB, arxB2, arxC, and arxD genes in addition to PHS-1, MLHE-1, and arxA operons, respectively. Genes such as ArxR; a regulator for response, ArxS; a two component sensor of histidine kinase, ArxX; a phosphate specific substrate binding periplasmic protein, arxXSR; a regulatory putative protein comprise a divergent and an adjacent gene cluster (Zargar et al. 2012). The phylogenetic gap between As (V) reductases and As (III) oxidases is filled by ArxA gene which has

**Table 8.2** Genes regulating microbial arsenic transformation

Gene	Protein	Protein Function	References
<b>Oxidation of As (III)</b>			
arxX/ aioX	ArxX/AioX: Binding protein for As (III)	Involved in regulation and signalling of As(III) oxidation	Liu et al. (2012)
arxA	ArxAB: As (III) oxidase	Oxidation of As (III)	Richey et al. (2009)
aioA and aioB	AioAB: As (III) oxidase	Oxidation of As (III)	Sardiwal et al. (2010)
arxB/ arxB2	ArxB/ ArxB2: Iron-sulphur [4Fe-4S] containing protein	Function unknown	Zargar et al. (2012)
arsH	ArsH: Organoarsenical oxidase	Reduction of iron and chromium, oxidation of trivalent aromatic and methylated arsenicals	Chen et al. (2015)
arxD	ArxD: Molybdoenzyme TorD-like chaperone	Oxidation of As (III)	Zargar et al. (2012)
arxC	ArxC: Quinol oxidoreductase subunit aiding in anchoring of membrane	Oxidation of As (III)	Zargar et al. (2012)
arxR/ aioR	ArxR/AioR: Regulator of transcription	Regulate the expression of <i>arx/aio</i> operon	Sardiwal et al. (2010)
arxS/ aioS	ArxS /AioS: Sensor histidine kinase	Part of a dual-component signal transduction system	Zargar et al. (2012)
moeA	MoeA: A biosynthesis protein having a molybdenum cofactor	Synthesize the molybdenum cofactor of AioAB oxidase	Sardiwal et al. (2010)
<b>Reduction of As (V)</b>			
ACR2	ACR2: As(V) reductase	Reduction of As (V)	Chen et al. (2020)
arrA and arrB	ArrAB: Respiratory reductases for As (V)	Reduction of As (V)	Hu et al. (2019)
arsC	ArsC: As(V) reductase	Reduction of As (V)	Mukhopadhyay and Rosen (2002)
arrS	ArrS: Histidine kinase sensor	Controls the expression of arr operon	Van Lis et al. (2013)
arrD	ArrD: Chaperon for As (V) reductase	Reduction of As (V)	Van Lis et al. (2013)
arrC	ArrC: A membranous subunit for As (V) reduction	Reduction of As (V)	Van Lis et al. (2013)
arsN	ArsN: acetyltransferase	Reduction of putative As (V)	Chauhan et al. (2009)
GstB	GstB: Glutathione S-transferase B	Involvement of reduced GSH for the reduction of As (V) to As (III)	Chrysostomou et al. (2015)
arsR/ arrR	ArsR /ArrR: Repressor for arsenic response	The expression of <i>ars/arr</i> operon is regulated	Taleshi et al. (2014)

(continued)

**Table 8.2** (continued)

Gene	Protein	Protein Function	References
ACR1	ACR1: Regulatory transcriptional protein	The expression of ACR1 genes is regulated	Chen et al. (2020)
<b>Methylation and Demethylation of arsenic</b>			
arsI	ArsI: As lyase	The demethylation of trivalent organoarsenicals is catalysed and regulated	Yoshinaga and Rosen (2014)
arsM	ArsM: As(III) S-adenosylmethionine methyltransferases	Aids in the methylation of arsenic	Qin et al. (2006)
<b>Transport of arsenic</b>			
arsA	ArsA: ATPase As (III) pump	The catalytic subunit of an oxyanion-translocating ATPase	Lin et al. (2006)
arsB	ArsB: Protein for pumping of As (III)	Removal of As (III) from the cell	Lin et al. (2006)
apqS	AqpS: Aquaglyceroporin	Removal of As (III) from the cell	Yang et al. (2005)
arsD	ArsD: Metallochaperone for arsenic	Transfer of As (III) to ArsA	Lin et al. (2006)
pgpA P-	PgpA: Protein related to glycoprotein	Identify and transport metal-thiol conjugates	Lin et al. (2006)
arsP	ArsP: Trivalent organoarsenicals specific efflux system	Removal of As (III) from the cell	Chen et al. (2015)
arsJ	ArsJ: Efflux permease for organoarsenicals	Removal of organoarsenicals from the cell	Chen et al. (2016)
Ycf1p	Ycf1p: Cytosolic cadmium factor for yeast protein	Impound cytosolic glutathione or As (III) complexes into vacuoles	Lin et al. (2006)
ACR3	ACR3: Permease protein for As (III)	Removal of As (III) from the cell	Chen et al. (2020)
<b>Unknown functions</b>			
ArsT	ArsT: Thioredoxin reductase	Function unknown	Wang et al. (2006)
arsO	ArsO: Flavin-binding monooxygenase	Function unknown	Wang et al. (2006)

less similarity to AioA and higher similarity to ArrA subunit (Zargar et al. 2010). Preceding the Great Oxidation Event (GOE), the As (V) respiring microbes created a niche for themselves surviving in an anoxic environment due to the oxidation of As (III) by anaerobes (Oremland et al. 2009). DARPs or ‘dissimilatory As (V)-respiring prokaryotes’ utilized As (V) as a terminal acceptor of electrons. Less mobile or toxic As (V) was converted to more toxic and additionally more mobile As (III) via ArrB or respiratory As (V) reductase through the energy producing respiratory chain (Pederick et al. 2007; Héry et al. 2008). ArrAB potentially consists of two subunits called ArrB (smaller subunit) and ArrA (a catalytic larger subunit) (Lin et al. 2019). The arr operon also comprises arrR, arrS, arrD, and arrC. The products of their gene

are a transcriptional regulator (ArrR), a histidine sensor kinase (ArrS), a reductase chaperon of As (V) (ArrD), and reductase membrane bound subunit of As (V) (ArrC), respectively (Van Lis et al. 2013). A new environmental toxin emerged post the GOE, wherein the As (III) was oxidized to As (V) in oceans. Most organisms uptake As (V) via the phosphate systems in their body (Yan et al. 2017). Hence, novel strategies had to be developed in order to cope with the predominantly toxic species of arsenic. In order to detoxify the As (III), most of the microbes developed Acr3 or ArsB efflux permeases. Eventually the cells had to reduce the substrate of Acr3 or ArsB; reduce toxic As (V) to less toxic As (III) to become resistant to more soluble As (V) species. As (V) reductase, a protein of small molecular mass aided in the evolution of several As (V) reductases in a range of organisms. The ars operon encoded by the arsC genes is the most well-known mechanism of arsenic resistance and detoxification (Mukhopadhyay and Rosen 2002). Recently, glutathione S-transferase B (GstB) using glutathione (GSH) or glutaredoxin (Grx) coupled to thioredoxin (Trx) helped in detoxifying the toxic As (V) in mutant cells of *Escherichia coli* lacking arsC genes (Chrysostomou et al. 2015).

### 8.2.2 The Arsenic Methylation Cycle

Organoarsenical degradation includes pathways for biotransformation, methylation, and demethylation of arsenic and reduction or oxidation of inorganic arsenic species within primitive organisms. In the early 1800s, Gosio gas (trimethylarsine) was produced by inorganic arsenic compounds by fungi which were used as wall pigments. Nowadays, protozoa, cyanobacteria, algae, and bacteria in the prevalent environment have shown to perform arsenic methylation (Yin et al. 2011). In order to detoxify arsenic, methylation of arsenic is a predominant mechanism. Methylated pentavalent arsenic species are being rapidly produced non-enzymatically by using the trivalent toxic arsenic species. Also, the product is removed into the air as trimethylarsine which is a gaseous end product. Designated as ArsM and AS3MT in microbes and animals, As (III) S-adenosylmethionine (SAM) methyltransferase catalyses the route of the methylation of arsenic. Similar to the detoxification pathway of arsenic methylation, ArsR, the As (III)-responsive transcriptional repressor regulates the expression of archaeal and prokaryotic arsM genes (Thomas and Rosen 2013). Sometimes microbes use unconventional pathways for detoxification in which arsM is constitutive and is not regulated as in some cyanobacteria (Ye et al. 2012; Xue et al. 2017). In recent times, a dual-step regulated pathway of MSMA demethylation as well as reduction was deciphered (Yoshinaga et al. 2011). Further from environmental isolates such as cyanobacterium *Nostoc sp.* 7120 and bacterium *Bacillus sp.* MD1, an ArsI enzyme was identified and characterized, which catalyses the demethylation of As (III) organoarsenicals (Yan et al. 2015). But to date, there has been no identification of any reductases of As (V) organoarsenicals. Other organisms may also have developed substitute pathways for demethylation of

organoarsenical compounds as only bacterial species incur the ArsI putative orthologs.

### 8.2.3 *The Organoarsenical Cycle*

Marine organisms usually produce complex organoarsenical compounds by transforming inorganic arsenic which is present at a concentration of 1–2 µg/l in sea water. Marine animals host arsenobetaine, which is the most common species of arsenic present in them, whereas marine algae have arsenosugars, which are water soluble species of arsenic (Edmonds and Francesconi 2013). In recent times, analytical techniques help in the identification of more complex organoarsenicals. AsPL has also been reported in cyanobacteria and algae besides its first identification in *Undaria pinnatifida*, a brown alga as an arsenosugar phospholipid (Xue et al. 2014; García-Salgado et al. 2012). Presence of the arsenic-containing fatty acid (AsFA) has been noted in cod liver oil, in several species of fish, and in algae (Taleshi et al. 2010; Raab et al. 2013). Algae and fish also are reported to have arsenic-containing hydrocarbons (AsHC), which was initially identified in capelin oil (Taleshi et al. 2010; Taleshi et al. 2008). From herring caviar, two novel arsenolipid groups, namely arsenic-bearing phosphatidylethanolamine (AsPE) and arsenic-bearing phosphatidylcholines (AsPC) were characterized (Viczeke et al. 2016). Marine organisms surviving in extreme salt and low phosphate environments have been found to possess more than 70 arsenolipids and 20 arsenosugars. Their function is yet not deciphered in marine organisms but they are non-toxic to both animals and plants. Within phosphate limiting environments, As (V) in the form of arsenolipids could also be used as an alternative to the inorganic phosphate, due to possessing more structural similarity in phospholipids than do either nitrates or sulphates such as are in phytoplanktons (Chang et al. 2018). A recent study revealed that under conditions of low phosphate, more arsenosugar phospholipids were produced by *Ectocarpus siliculosus* than occurred under optimum phosphate conditions (Petursdottir et al. 2016). The cytotoxicity of organoarsenicals in vitro was analogous to As (III) for cultured liver cells and bladder cells in humans (Meyer et al. 2014). Organisms which cannot biosynthesize it, may have to bear the toxicity of the arsenic-containing hydrocarbons. In humans, small molecular compounds of arsenic and other dimethylated arsenical species (DMAs) are produced by metabolizing the arsenolipids, followed by their excretion in urine (Schmeisser et al. 2006). Very few genes have been identified in regard to the complex transformation and organoarsenical degradation and further studies are needed to decode the same.



### 8.2.4 *The Thiolation Cycle of Arsenic*

The prevailing species of arsenic in sulphidic, arsenic-loaded, and alkaline rich environments are thioarsenates ( $H_3AsS_nO_{4-n}$ ). They play a prominent role in sulphidic geothermal environments and arsenic biogeochemical cycle (Planer-Friedrich et al. 2010; Planer-Friedrich et al. 2007). Biological oxidation along with desulphidation or abiotic decomposition by sulphur oxidizing bacteria under conditions of increased pH aid in the transformation of thioarsenates to As (III) or As (V) (Saunders et al. 2019). Thioarsenates usually enclose oxidized As (V) or reduced  $S_2$  and can serve as both electron acceptors and donors. In alkaline environments, purple sulphur bacteria use monothioarsenate for anoxygenic photosynthesis whereas *Thermocrinis ruber* OC 14/7/2 uses it as an electron donor (Edwardson et al. 2014).

### 8.2.5 *Efflux Pathways for Arsenic*

A competent efflux system is the finest way to remove toxic arsenicals from cells. There has been an extensive study of As (III) systems in both higher organisms and in plants. In most bacteria such as in *E. coli*, ArsB binds to ArsA by ATP hydrolysis and there is an arsenic specific ATP driven pump, which is an energy dependent process that serves to efflux As (III). Further, in *Sinorhizobium meliloti*, a legume symbiont, As (III) is extruded from the cells by an aquaglyceroporin (AqpS) and not ArsB (Yang et al. 2005). As (III) extrusion from cells in both yeast and bacteria is mediated by Acr3, acting as an efficient efflux transporter for As (III). Comparatively, the genes for arsB are less widespread than Acr3 in both archaea and bacteria. Moreover, microbes such as *Pseudomonas aeruginosa* have revealed novel mechanisms for resistance to As (V) (Chen et al. 2016). Two genes, namely; arsJ, encoding an organoarsenical efflux permease and the other a glyceraldehyde-3-phosphate dehydrogenase (GAPDH) combine together in these bacteria. An exceedingly unstable organoarsenical 1-arseno-3-phosphoglycerate is formed using glyceraldehydes and As (V) by GAPDH. This compound further breaks down to 3-phosphoglycerate and As (V) as soon as ArsJ extrudes it out from the cells. Hence the microbes form resistance to As (V) through these efflux pathways through an effective net reaction. Further, trivalent organoarsenicals have been demonstrated to be effluxed out from *Campylobacter jejuni* using ArsP and bacterial permease (Chen et al. 2015). Hence, trivalent arsenic reductases and transporters have a crucial role to play in the efflux system of the biogeochemical cycle of arsenic.

## 8.3 Effect of Former Elements on Arsenic Biogeochemical Cycling

All elementary processes of biogeochemical cycling such as transformation of a specific element are controlled by several organisms at many levels. Cycling of nitrogen, sulphur, iron, and carbon is often coupled with arsenic biotransformations (Handley et al. 2013).

### 8.3.1 *The Coupling Upshot of Iron on Arsenic Biogeochemical Cycling*

Both pH and redox potential strongly mediate the mobility of arsenic and its chemical speciation within natural environments. Arsenic is predominantly present in the form of As (V) in oxic conditions as  $\text{HAsO}_4^{2-}$  and as  $\text{H}_2\text{AsO}_4^-$  within alkaline and acidic pH conditions. As (III) primarily occurs as  $\text{H}_2\text{AsO}_3^-$  and  $\text{As}(\text{OH})_3$  under conditions of alkaline and neutral pH within anoxic environments. As (V) is also less mobile than As (III) (Carlson et al. 2013). The interaction of arsenic with Fe moreover depends on the pH wherein the As (III) sorption is lesser than As (V) onto goethite and amorphous oxides of iron at a pH level below 5–6. At neutral pH, the sorption rates of both the arsenic species are on the higher side. Further, As (V) is less easily adsorbed than As (III) at a pH level above 7–8 (Dixit and Hering 2003). Redox reactions, dissolution, transformation, and mineral formation between Fe and arsenic cycles directly or indirectly facilitate the arsenic bioavailability within arsenic aquifers and soils (Melton et al. 2014). The mobility of arsenic in the rhizosphere is modulated by several Fe (III)-reducing bacteria (Islam et al. 2004). Dissimilatory iron-reducing bacteria (DIRB) cause dissimilatory Fe (III) oxide reduction to Fe (II) ensuing in As (V) release from the sediment sorption sites, from Fe (II) bound minerals, rice root plaque, rice paddy soils or from ferric crystalline minerals (Wang et al. 2009; Muehe et al. 2016). The addition of acetate enhanced the reduction of Fe (III) as a probable electron donor resulting in the increment of DIRBs, improved rate of As (V) reduction to As (III), and finally the release of arsenic following the Fe (III) reduction (Islam et al. 2004). *Sulfurospirillum barnesii* and *Shewanella sp.* ANA-3 could both release As (III) and Fe (II) from As (V) bearing ferrihydrite by reducing the As (V) solid phase to Fe (III) when used as DARPs. Ultimately, in the presence of adequate organic electron donor, As (III) and Fe (II) could be liberated from the superficial matrix of ferrihydrite (Oremland and Stolz 2005). The earth crust has more aluminium than iron. As previously reported, the dissolution of As (V) bearing aluminium hydroxide by *S. barnesii* was inefficient and hence further studies are needed on understanding how the interaction of arsenic with aluminium affects the biogeochemical cycle (Ngegla et al. 2020). The lower bioavailability and immobilization of arsenic under Fe (II)-oxidizing conditions is due to the development or dissolution of new Fe (III)

or Fe (II) minerals mediating arsenic mobilization or immobilization under geochemical conditions (Hohmann et al. 2010; Hohmann et al. 2011). Also, inefficient arsenic co-precipitation and weak dissolution of Fe (III) containing minerals have been shown by several Fe (II) oxidizing and nitrate reducing bacteria (Omorieg et al. 2013). Arsenic removal using biotechnological applications such as in filters for drinking water could imply the process of microaerophilic oxidation of Fe (II) and nitrate-aided Fe (II) oxidation which significantly influences the mobility of arsenic (Nitzsche et al. 2015). Although, in commercially used filters for drinking water the removal of arsenic is lowered by Fe (II) oxidizing bacteria formation of iron biominerals (Kleinert et al. 2011).

### ***8.3.2 The Coupling Upshot of Sulphur on Arsenic Biogeochemical Cycling***

Sulphosalts and sulphides comprise more than 20% of the earth's crust, and the crust contains more than 200 diverse arsenic-bearing minerals (Mandal and Suzuki 2002). The biological or redox behaviour of sulphur mediates the release of immobilized arsenic (Corkhill et al. 2008). Arsenic solubility is affected by the formation of arsenopyrite (FeAsS), orpiment (As<sub>2</sub>S<sub>3</sub>), realgar (AsS), pyrite (FeS<sub>2</sub>), or affected by mediation with As (V) reduction by a strong reductant called abiotic sulphide under reduced sulphate conditions (Rochette et al. 2000). Generation of hydrogen sulphide causes striking changes in arsenic, sulphide, and Fe species by specific sulphate-reducing bacteria (SRB) (Yang et al. 2020). It also causes release of metal species which have lower solubility such as FeAsS or As<sub>2</sub>S<sub>3</sub> by localized precipitation. Also, As (V) is reduced and may indirectly or directly be produced by activity of thioarsenates or As (III), and by immobilizing arsenic using arsenic-bound or free sulphur by potential sulphur oxidizing bacteria (Hollibaugh et al. 2006). Hence, the upshot of arsenic in the environment is significantly controlled by transformations involving sulphur.

### ***8.3.3 The Coupling Upshot of Nitrogen on Arsenic Biogeochemical Cycling***

Under anoxic environments, the microbial oxidation of As (III) is ecologically supported by significant concentrations of nitrate. Within anoxic columns of lake water, the first linkage of denitrification with anoxic oxidation of As (III) was reported in a field study (Richey et al. 2009). The arsenic redox state was predominantly affected by the presence or absence of nitrate. As (III) and As (V) were the prevailing species within the anoxic rich and poor nitrate periods. The denitrification of nitrate to nitrite was partially coupled to the oxidation of As (III) by *A. ehrlichii*

strain MLHE-1 which is an As (III) oxidation bacterium (Oremland et al. 2002). Absolute denitrification to nitrogen gas from nitrate by oxidizing and fixing As (III) and CO<sub>2</sub> was reported by two chemolithoautotrophic anoxic chains, namely *Sinorhizobium* strain DAO10 and *Azoarcus* strain DAO1 (Zhou et al. 2020). Nitrate prominently plays a key role in the arsenic biogeochemical cycle as the oxidation of As (III) is somewhat nitrate dependent biologically (Sun et al. 2009a; b). The Fe (II) oxidation is often linked to nitrate reduction, indirectly influencing the mobility and bioavailability of arsenic. Paddy soils have reported firm coupling between arsenic, Fe, and N (Chen et al. 2008). The Fe (III) minerals present in the soil co-precipitate arsenic by several Fe (II) oxidizing nitrate dependent bacteria. Also, arsenic mobilization was reduced due to nitrate reduction or inhibition of Fe (III) leading to reduced uptake of arsenic on nitrate addition in paddy soils. Hence, the reduction in the mobility of arsenic in several ecosystems such as in groundwater and marine or freshwater sediments is potentially influenced by nitrate-aided microbial oxidation of Fe (II) (Jiang et al. 2009).

### ***8.3.4 The Coupling Upshot of Organic Matter on Arsenic Biogeochemical Cycling***

There has been a wide distribution of natural organic matter (NOM) even within apparently innate environments. A range of functional and structural properties of various heterogeneous mixtures of NOM controls the fate of arsenic by redox reactions and aggressive adsorption by the formation of mineral colloids and organic metal arsenic-bearing compounds (Thomasarrigo et al. 2014; Sharma et al. 2010a; b). The NOM molecules consist of different combinations of functional groups such as nitroso, esteric, phenolic, hydroxyl, amino, sulphhydryl, and carboxylic (Sharma and Kappler 2011). Under reducing and oxic geochemical conditions, arsenic is efficiently trapped by these functional molecules. NOM is associated with As (III) by formation of bridges between functional NOM, arsenic oxyanions, and Fe (III) as NOM-As (III)-Fe (III) complexes, hydrophobic interactions between NOM-As (III) and hydrogen binding by carboxyl of phenolic OH groups (Sharma et al. 2010a, b). Whereas, the phenolic OH groups or protonated amino groups of NOM react with As (V) in a nucleophile substitution reaction causing immobilization of As (V) (Buschmann et al. 2006). Also, arsenic could be sequestered potentially by NOM sulphhydryl groups and As (III) by the formation of a complex which is trigonal-pyramidal in nature (Langner et al. 2011). The microbial activities or communities are also vastly affected by the change in organic matter (Rowland et al. 2009). The release of arsenic is facilitated by the reductive dissolution and redox transformations of Fe (III) (oxyhydr) oxides and As (V) to As (III) (Bauer and Blodau 2006). The arsenic volatilization and methylation are significantly enhanced in paddy soils on addition of organic matter (Huang et al. 2012). As (V) can also be reduced on addition of humic acids which are a part of NOMs (Palmer et al. 2006).

DARPs use petite organic molecules such as formate, ethanol, glycerol, acetate, citrate, butyrate, succinate, malate, fumarate, pyruvate, and lactate as a donor of electrons for reduction of As (V) (Lear et al. 2007). Sometimes the reduction of As (V) is facilitated by aromatic complex substrates including toluene, benzoate, ferulic acid, syringic acid, and phenol such as in *Desulfosporosinus sp. Y5* (Liu et al. 2012). Nitrite, nitrate, thiosulphate, Fe (III), selenite, and sulphate are also respired by a few DARPs. The coexistence of arsenic with C, S, N, or Fe provides electron donors which benefits the environmental growth of microbes. Environmental interaction of arsenic with compounds that have other physio-chemical properties, including minerals, and inorganic elements that create biologically significant transformations make it necessary to study the genes affecting the arsenic biogeochemical cycle (Bertin et al. 2011). Although As (III) oxidizing and As (V) reducing bacteria are vastly disseminated in the environment, due to restricted availability of suitable primers our ability to study their quantification has been more difficult in natural bacterial communities in contrast to the relative ease of studying pure cultures (Han et al. 2017). Compared to laboratory conditions, biogeochemical transformation, fate and speciation of arsenic are much more intricately in the environment. Hence, the application of intensive, comprehensive, and systematic approaches is required to comprehend the environmental interaction of microbes such as metagenomics, metatranscriptomics, metaproteomics, and metabolomics.

## 8.4 The Application of Omics and Constitutive Modelling Influencing the Arsenic Biogeochemical Cycle

### 8.4.1 Metagenomics

As the majority of micro-organisms cannot be cultured in vitro, metagenomics characterizes such microbes straight from the environmental samples to elucidate their biochemical pathways (Fig. 8.2). Similar to acetyltransferases protein, a unique As (V) resistant gene named *arsN* was identified from two arsenic resistant bacteria from a metagenomic library (Wang et al. 2020). The genes coupled to arsenic transformation were analysed using metagenomic techniques by Xio et al. A protein database was constructed using high-throughput sequencing of arsenic metabolizing genes in five paddy fields containing low arsenic. It was found that even in conditions of low arsenic concentrations, the genes were abundant and ubiquitously affecting the metabolism of arsenic (Xiao et al. 2016). Also among different niches, strong correlation between the transformation of arsenic and microbes was revealed (Luo et al. 2014). Moreover, it is important to understand the limitation that physiological activity is not demonstrated using metagenomics which only reveals the functional and taxonomical profile of a community (Aguar-Pulido et al. 2016). Hence, in order to demarcate the functionally active genes, the study of metatranscriptomics becomes all the more essential.

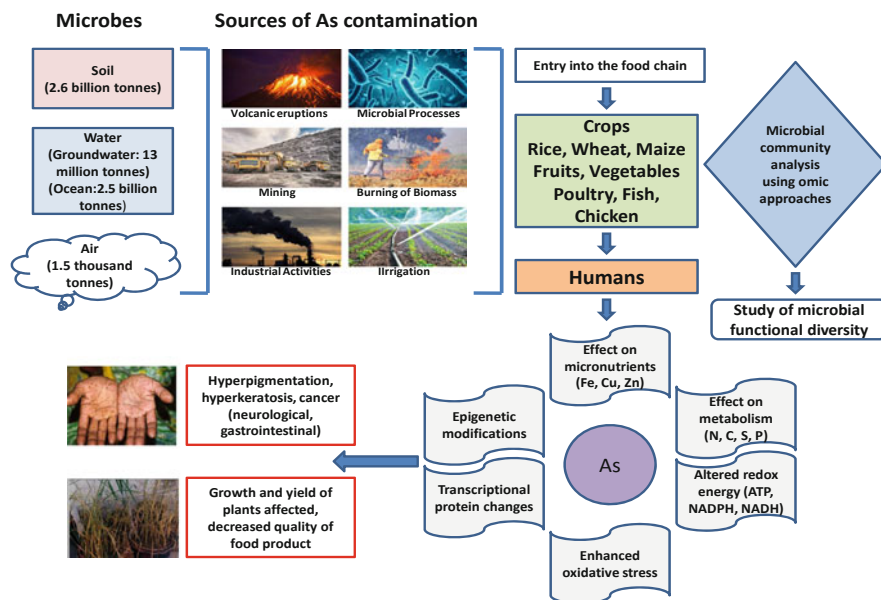


Fig. 8.2 Effect of microbial arsenic transformation on the environment

#### 8.4.2 Metatranscriptomics

Metatranscriptomics is the study of microbial activities and functional gene expression of the complex communities of microbes by their total mRNA sequencing under explicit environmental conditions at a given point of time. Novel genes concerned with the transformation of heavy metals are isolated and characterized using functional metatranscriptomics (Kour 2014). The profile of a functional microbial community along with their interaction with the environment is deciphered using metatranscriptomics (Gilbert et al. 2008). Recent studies have reported the symbiotic interaction between a symbiont *Ensifer* (syn. *Sinorhizobium*) *medicae* MA11 and model legume *Medicago truncatula* and their interaction with As (III) using meta-analytic transcriptomics (Lafuente et al. 2015). The response of a symbiotic bacteria towards arsenic exposure and their response strategies have been identified using this study process. The governing effect of enhanced concentrations of arsenic under changing environmental conditions along with the study of gene regulation by microbes can be examined using the metatranscriptomic approach. In conditions of low protein environments, the mRNA inventories are sensitive and their responsive changes are rapid within microbial environmental communities (Moran et al. 2013). Hence, it has become essential to study the small molecular metabolites and protein repertoires to determine the adaptation strategies of microbes in dynamic and complex environments using microbial metabolomics and metaproteomics.

### 8.4.3 *Metaproteomics and Metabolomics*

Application of an amalgamation of gas or liquid chromatography-dependent separations and mass spectrometry-dependent identification techniques to quantify and characterize the metabolites and proteins released by the microbes into the environment is studied by metabolomics and metaproteomics approaches (Gupta et al. 2020). The microbial community interaction with the environment along with their functional diversities is studied using microbial metabolome and metaproteome (Lankadurai et al. 2013). Compared to metatranscriptomics and metagenomics, less data is generated using metaproteomics when analysed using amplification of 16S rRNA genes within arsenic contained sediments in prokaryotic arsenic-bearing communities (Halter et al. 2011). Hence, when humans, animals, plants, or bacteria are exposed to environmentally saturated stressors, they generate metabolites of low molecular mass within a cell compartment, biofluid, or a tissue which can be studied using metabolomics. Further, arsenic contaminated drinking water filters and mice liver exposed to high cholesterol and fat have been investigated for arsenic-associated metabolites using high-throughput metabolomics (Shi et al. 2014). As the extraction and amplification of small quantities of metabolites and proteins are difficult, their application in real environmental conditions has been a challenge (Bastida et al. 2009).

### 8.4.4 *Integrating Meta-omic Techniques*

A more complete picture of biogeochemical cycles can be provided by the meta-omic approaches, including the examination of genes and the meta-omic datasets, helping us to decipher the complex and dynamic interactions between the environment and its microbial communities. Composite marine microbial communities and their novel genes were detected using metagenomic and metatranscriptomic approaches (Shekhar et al. 2020). Furthermore, the response and interaction of those communities with correspondence to environmental parameters was revealed on integration of metabolomics with metagenomic data sets (Lu et al. 2014). The functional diversity of microbes in biogeochemical cycles, which cannot be cultured in laboratory conditions, is effectively studied using metagenomic technologies. Recently, analysis of microbial alteration of metabolome, proteome, or transcriptome of microbes on exposure to arsenic was termed as arsenomics (Sacheti et al. 2013). Hence, the analysis of microbes exposed to arsenic in real environments can be governed using meta-omic approaches and arsenomics.

### 8.4.5 *Biochemical Modelling Using Meta-omic Approaches*

Microbes vastly influence the biogeochemical cycles and are universal in diverse environmental habitats including within plants or animals, freshwater or marine sediments, or soil niches. Rice plants host several methylated and inorganic species of arsenic in various percentages and concentrations along with the microbes which effect their transformation (Sun et al. 2009a; b). Preceding plant uptake, the microbial methylation of arsenic occurs in soil as the only primary source (Lomax et al. 2012). The prediction and dynamics of arsenic bioavailability in situ provides a detailed knowledge regarding the arsenic contamination in a region. When tested in Mono Lake, California having an inorganic arsenic concentration of 200  $\mu\text{M}$  using radiotracers ( $^{35}\text{S}$  and  $^{73}\text{As}$ ), it was seen that the reduction rate of sulphate and arsenic in monimolimnion waters increased at a depth of 18–28 metre (2.3  $\mu\text{M}/\text{day}$  to 5.9  $\mu\text{M}/\text{day}$ ) (Oremland et al. 2000). This was also tested in Searles Lake and Mono Lake, respectively, having salt concentrations of 340 g/L and 90 g/L. There was significant As (V) reduction in both the lakes while Mono lake showed signs of sulphate reduction as well (Kulp et al. 2006). The sediment microbial communities in these lakes differed when tested using amplified 16S rRNA genes by denatured gradient gel electrophoresis (DGGE). The reduction activity of As (V) was higher in Mono Lake due to the presence of novel *arrA* gene signalling (Kulp et al. 2006). The arsenic status in the environment cannot be predicted by limited information on functional genes (Mitchell et al. 2020). Integration of environmental meta-omic approaches will elucidate the process, characterization, and application of arsenic biotransformation. Integration of genomics into the study of microbial communities, examinations from biochemistry to biogeochemistry and biogeochemical fluxes will aid in the development of in situ biochemical models and help us with the lab to field transition of knowledge (Ji et al. 2020). Several mitigation technologies can be urbanized to foresee the effectiveness of arsenic functional dynamics in the innate environment. Numerous models are being urbanized in low intricate environments. Lately, within the minimum oxygen zone in the Arabian sea, the microbial geochemistry and communities were explored using qPCR and environmental genomics in biogeochemical models (Reed et al. 2014). Thus, such approaches of biochemical modelling pave the way for further prediction of microbial metabolic networks and elemental biogeochemical cycles.

## 8.5 Perspectives

The coupling of elemental biogeochemical cycles such as N, S, along with Fe to diverse enzymes isolated from microbial communities catalyses our understanding of the biotransformation of arsenic. With time, a greater number of genes are being characterized and discovered which indirectly or directly influence the metabolism of arsenic, along with our cataloging of an enhanced number of sequenced genomes.



The complex processes of the environment such as microbial metabolic pathways are governed in ways that we now are discerning by rapid advances in microbiology, analytical chemistry, and genomics. We expect that, in the near future, a deeper prediction of arsenic biogeochemical processes within diverse niches can be determined by integrating biochemical models into meta-omic datasets, along with the usage of spatio-temporal scales of analysis. The global arsenic biogeochemical cycle hosts a complex of metabolic and biochemical pathways and science will be providing geochemical insights into the transformation of arsenic. Lastly, the dynamics of arsenic species in soil, sediments, and water could be predicted by integrating meta-omic datasets to biochemical models influencing the arsenic biogeochemical cycle. Together these almost certainly will provide us with several options for mitigation techniques and help us to limit the human associated pollution of arsenic in the environment.

## References

- Aguiar-pulido V, Huang W, Suarez-ulloa V, Cickovski T, Mathee K, Narasimhan G (2016) Metagenomics, metatranscriptomics, and metabolomics approaches for microbiome analysis. *Evol Bioinforma* 12:5–16
- Ardini F, Dan G, Grotti M (2020) Arsenic speciation analysis of environmental samples. *J Anal At Spectrom* 35:215–237
- Bastida F, Moreno JL, Nicolás C, Hernández T, García C (2009) Soil metaproteomics: a review of an emerging environmental science. Significance, methodology and perspectives. *Eur J Soil Sci* 60:845–859
- Bauer M, Blodau C (2006) Mobilization of arsenic by dissolved organic matter from iron oxides, soils and sediments. *Sci Total Environ* 354:179–190
- Bertin PN, Heinrich-Salmeron A, Pelletier E, Goulhen-Chollet F, Arsène-Ploetze F, Gallien S, Lauga B, Casiot C, Calteau A, Vallenet D, Bonnefoy V (2011) Metabolic diversity among main microorganisms inside an arsenic-rich ecosystem revealed by meta- and proteo-genomics. *ISME J* 5:1735–1747
- Biswas R, Majhi AK, Sarkar A (2019) The role of arsenate reducing bacteria for their prospective application in arsenic contaminated groundwater aquifer system. *Bioact Agri Biotech* 20: 101218
- Branco R, Francisco R, Chung AP, Morais PV (2009) Identification of an aox system that requires cytochrome c in the highly arsenic-resistant bacterium *Ochrobactrum tritici* SCII24. *Appl Environ Microbiol* 75:5141–5147
- Buschmann J, Kappeler A, Lindauer U, Kistler D, Berg M, Sigg L (2006) Arsenite and arsenate binding to dissolved humic acids: influence of pH, type of humic acid, and aluminum. *Environ Sci Technol* 40:6015–6020
- Carlson HK, Clark IC, Blazewicz SJ, Iavarone AT, Coates JD (2013) Fe(II) oxidation is an innate capability of nitrate-reducing bacteria that involves abiotic and biotic reactions. *J Bacteriol* 195: 3260–3268
- Chang JS, Yoon IH, Kim KW (2018) Arsenic biotransformation potential of microbial arseH responses in the biogeochemical cycling of arsenic-contaminated groundwater. *Chemosphere* 191:29–737
- Chatterjee S, Moogoui R, Gupta DK (2017) Arsenic: source, occurrence, cycle, and detection. In: Gupta D, Chatterjee S (eds) *Arsenic contamination in the environment*. Springer, Cham, pp 13–35

- Chauhan NS, Ranjan R, Purohit HJ, Kalia VC, Sharma R (2009) Identification of genes conferring arsenic resistance to *Escherichia coli* from an effluent treatment plant sludge metagenomic library. *FEMS Microbiol Ecol* 67:130–139
- Chen XP, Zhu YG, Hong MN, Kappler A, Xu YX (2008) Effects of different forms of nitrogen fertilizers on arsenic uptake by rice plants. *Environ Toxicol Chem* 27:881–887
- Chen J, Madegowda M, Bhattacharjee H, Rosen BP (2015) ArsP: a methylarsenite efflux permease. *Mol Microbiol* 98:625–635
- Chen J, Yoshinaga M, Garbinski LD, Rosen BP (2016) Synergistic interaction of glyceraldehydes-3-phosphate dehydrogenase and ArsJ, a novel organoarsenical efflux permease, confers arsenate resistance. *Mol Microbiol* 100:945–953
- Chen SC, Sun GX, Yan Y, Konstantinidis KT, Zhang SY, Deng Y, Li XM, Cui HL, Musat F, Popp D, Rosen BP (2020) The great oxidation event expanded the genetic repertoire of arsenic metabolism and cycling. *Proc Natl Acad Sci* 117:10414–10421
- Chrysostomou C, Quandt EM, Marshall NM, Stone E, Georgiou G (2015) An alternate pathway of arsenate resistance in *E. coli* mediated by the glutathione S-transferase GstB. *ACS Chem Biol* 10:875–882
- Corkhill CL, Wincott PL, Lloyd JR, Vaughan DJ (2008) The oxidative dissolution of arsenopyrite (FeAsS) and enargite (Cu<sub>3</sub>As<sub>4</sub>) by *Leptospirillum ferrooxidans*. *Geochim Cosmochim Acta* 72:5616–5633
- Di X, Beesley L, Zhang Z, Zhi S, Jia Y, Ding Y (2019) Microbial arsenic methylation in soil and uptake and metabolism of methylated arsenic in plants: a review. *Int J Environ Res Public Health* 16:5012
- Dixit S, Hering JG (2003) Comparison of arsenic(V) and arsenic(III) sorption onto iron oxide minerals: implications for arsenic mobility. *Environ Sci Technol* 37:4182–4189
- Edmonds JS, Francesconi KA (2013) Organoarsenic compounds in the marine environment. In: Craig PJ (ed) *Organometallic compounds in the environment*. Chichester, Wiley, pp 195–222
- Edwardson CF, Planer-friedrich B, Hollibaugh JT (2014) Transformation of monothioarsenate by haloalkaliphilic, anoxygenic photosynthetic purple sulfur bacteria. *FEMS Microbiol Ecol* 90: 858–868
- Finzi AC, Cole JJ, Doney SC, Holland EA, Jackson RB (2011) Research frontiers in the analysis of coupled biogeochemical cycles. *Front Ecol Environ* 9:74–80
- García-Salgado S, Raber G, Raml R, Magnes C, Francesconi KA (2012) Arsenosugar phospholipids and arsenic hydrocarbons in two species of brown macroalgae. *Environ Chem* 9:63–66
- Gilbert JA, Field D, Huang Y, Edwards R, Li W, Gilna P, Joint I (2008) Detection of large numbers of novel sequences in the Metatranscriptomes of complex marine microbial communities. *PLoS One* 3:e3042
- Gnanaprakasam ET, Lloyd JR, Boothman C, Ahmed KM, Choudhury I, Bostick BC, van Geen A, Mailloux BJ (2017) Microbial community structure and arsenic biogeochemistry in two arsenic-impacted aquifers in Bangladesh. *MBio* 8:e01326–e01317
- Gupta K, Biswas R, Sarkar A (2020) Advancement of omics: prospects for bioremediation of contaminated soils. In: Shah MP (ed) *Microbial Bioremediation & Biodegradation*. Springer, Singapore, pp 113–142
- Halter D, Cordi A, Gribaldo S, Gallien S, Goulhen-Chollet F, Heinrich-Salmeron A, Carapito C, Pagnout C, Montaut D, Seby F, Van Dorsselaer A (2011) Taxonomic and functional prokaryote diversity in mildly arsenic-contaminated sediments. *Res Microbiol* 162:878–887
- Han YH, Fu JW, Xiang P, Cao Y, Rathinasabapathi B, Chen Y, Ma LQ (2017) Arsenic and phosphate rock impacted the abundance and diversity of bacterial arsenic oxidase and reductase genes in rhizosphere of As-hyperaccumulator *Pteris vittata*. *J Hazard Mater* 321:146–153
- Handley KM, McBeth JM, Charnock JM, Vaughan DJ, Wincott PL, Polya DA, Lloyd JR (2013) Effect of iron redox transformations on arsenic solid-phase associations in an arsenic-rich, ferruginous hydrothermal sediment. *Geochim Cosmochim Acta* 102:124–142

- Hernandez-Maldonado J, Sanchez-Sedillo B, Stoneburner B, Boren A, Miller L, McCann S, Rosen M, Oremland RS, Saltikov CW (2017) The genetic basis of anoxygenic photosynthetic Arsenite oxidation. *Environ Microbiol* 19:130–141
- Héry M, Gault AG, Rowland HA, Lear G, Polya DA, Lloyd JR (2008) Molecular and cultivation-dependent analysis of metal-reducing bacteria implicated in arsenic mobilisation in south-east Asian aquifers. *Appl Geochem* 23:3215–3223
- Hoelt SE, Kulp TR, Han S, Lanoil B, Oremland RS (2010) Coupled arsenotrophy in a hot spring photosynthetic biofilm at Mono Lake, California. *Appl Environ Microbiol* 76:4633–4639
- Hohmann C, Winkler E, Morin G, Kappler A (2010) Anaerobic Fe(II)-oxidizing bacteria show as resistance and immobilize as during Fe(III) mineral precipitation. *Environ Sci Technol* 44:94–101
- Hohmann C, Morin G, Ona-Nguema G, Guigner JM, Brown GE Jr, Kappler A (2011) Molecular-level modes of As binding to Fe(III) (oxyhydr) oxides precipitated by the anaerobic nitrate-reducing Fe(II)-oxidizing *Acidovorax* sp. strain BoFeN1. *Geochim Cosmochim Acta* 75:4699–4712
- Hollibaugh JT, Budinoff C, Hollibaugh RA, Ransom B, Bano N (2006) Sulfide oxidation coupled to arsenate reduction by a diverse microbial community in a Soda Lake. *Appl Environ Microbiol* 72:2043–2049
- Hu M, Sun W, Krumins V, Li F (2019) Arsenic contamination influences microbial community structure and putative arsenic metabolism gene abundance in iron plaque on paddy rice root. *Sci Total Environ* 649:405–412
- Huang H, Jia Y, Sun GX, Zhu YG (2012) Arsenic speciation and volatilization from flooded paddy soils amended with different organic matters-supporting information. *Environ Sci Technol* 46:2163–2168
- Islam FS, Gault AG, Boothman C, Polya DA, Charnock JM, Chatterjee D, Lloyd JR (2004) Role of metal-reducing bacteria in arsenic release from Bengal delta sediments. *Nature* 430:68–71
- Ji J, He E, Qiu H, Peijnenburg WJ, Van Gestel CA, Cao X (2020) Effective modeling framework for quantifying the potential impacts of coexisting anions on the toxicity of arsenate, selenite, and vanadate. *Environ Sci Technol* 54:2379–2388
- Jiang J, Bauer I, Paul A, Kappler A (2009) Arsenic redox changes by microbially and chemically formed semiquinone radicals and hydroquinones in a humic substance model quinone. *Environ Sci Technol* 43:3639–3645
- Kleinert S, Muehe EM, Posth NR, Dippon U, Daus B, Kappler A (2011) Biogenic Fe(III) minerals lower the efficiency of iron-mineral-based commercial filter systems for arsenic removal. *Environ Sci Technol* 45:7533–7541
- Kour M (2014) Isolation and characterization of metal resistance genes by using Metatranscriptomic approach. Master Dissertation, Thapar University, Patiala, Punjab
- Kulp TR (2014) Arsenic and primordial life. *Nat Geosci* 7:785–786
- Kulp TR, Hoelt SE, Miller LG, Saltikov C, Murphy JN, Han S, Lanoil B, Oremland RS (2006) Dissimilatory arsenate and sulfate reduction in sediments of two hypersaline, arsenic-rich Soda Lakes: Mono and Searles Lakes, California. *Appl Environ Microbiol* 72:6514–6526
- Lafuente A, Pérez-Palacios P, Doukkali B, Molina-Sánchez MD, Jiménez-Zurdo JI, Caviedes MA, Rodríguez-Llorente ID, Pajuelo E (2015) Unraveling the effect of arsenic on the model *Medicago-Ensifer* interaction: a transcriptomic meta-analysis. *ISME J* 205:255–272
- Langner P, Mikutta C, Kretzschmar R (2011) Arsenic sequestration by organic Sulphur in peat. *Nat Geosci* 5:66–73
- Lankadurai BP, Nagato EG, Simpson MJ (2013) Environmental metabolomics: an emerging approach to study organism responses to environmental stressors. *Environ Rev* 21:180–205
- Lear G, Song B, Gault AG, Polya DA, Lloyd JR (2007) Molecular analysis of arsenate-reducing bacteria within Cambodian sediments following amendment with acetate. *Appl Environ Microbiol* 73:1041–1048
- Lin Y, Walmsley AR, Rosen BP (2006) An arsenic metallochaperone for an arsenic detoxification pump. *Proc Natl Acad Sci* 103:15617–15622

- Lin J, Hu S, Liu T, Li F, Peng L, Lin Z, Dang Z, Liu C, Shi Z (2019) Coupled kinetics model for microbially mediated arsenic reduction and adsorption/desorption on iron oxides: role of arsenic desorption induced by microbes. *Environ Sci Technol* 53:8892–8902
- Liu G, Liu M, Kim EH, Maaty WS, Bothner B, Lei B, Rensing C, Wang G, McDermott TR (2012) A periplasmic arsenite-binding protein involved in regulating arsenite oxidation. *Environ Microbiol* 14:1624–1634
- Lomax C, Liu WJ, Wu L, Xue K, Xiong J, Zhou J, McGrath SP, Meharg AA, Miller AJ, Zhao FJ (2012) Methylated arsenic species in plants originate from soil microorganisms. *New Phytol* 193:665–672
- Lu K, Abo RP, Schlieper KA, Graffam ME, Levine S, Wishnok JS, Swenberg JA, Tannenbaum SR, Fox JG (2014) Arsenic exposure perturbs the gut microbiome and its metabolic profile in mice: an integrated metagenomics and metabolomics analysis. *Environ Health Perspect* 122:284–291
- Luo J, Bai Y, Liang J, Qu J (2014) Metagenomic approach reveals variation of microbes with arsenic and antimony metabolism genes from highly contaminated soil. *PLoS One* 9:e108185
- Mandal BK, Suzuki KT (2002) Arsenic round the world: a review. *Talanta* 58:201–235
- Melton ED, Swanner ED, Behrens S, Schmidt C, Kappler A (2014) The interplay of microbially mediated and abiotic reactions in the biogeochemical Fe cycle. *Nat Rev Microbiol* 12:797–809
- Meyer S, Matissek M, Müller SM, Taleshi MS, Ebert F, Francesconi KA, Schwerdtle T (2014) In vitro toxicological characterisation of three arsenic-containing hydrocarbons. *Metallomics* 6: 1023–1033
- Mitchell K, Moreno-Jimenez E, Jones R, Zheng L, Trakal L, Hough R, Beesley L (2020) Mobility of arsenic, chromium and copper arising from soil application of stabilised aggregates made from contaminated wood ash. *J Hazard Mater* 393:122479
- Moran MA, Satinsky B, Gifford SM, Luo H, Rivers A, Chan LK, Meng J, Durham BP, Shen C, Varaljay VA, Smith CB (2013) Sizing up metatranscriptomics. *ISME J* 7:237–243
- Muehe EM, Morin G, Scheer L, Pape PL, Esteve I, Daus B, Kappler A (2016) Arsenic (V) incorporation in Vivianite during microbial reduction of arsenic(V)-bearing biogenic Fe (III) (Oxyhydr)oxides. *Environ Sci Technol* 50:2281–2291
- Mukhopadhyay R, Rosen BP (2002) Arsenate reductases in prokaryotes and eukaryotes. *Environ Health Perspect* 110:745–748
- Negrel JV, Zhou X, Chen X, Zhu X, Liu Z, Feng J, Zeng XC (2020) Unique diversity and functions of the arsenic-methylating microorganisms from the tailings of Shimen Realgar mine. *Ecotoxicology* 29:86–96
- Nitzsche KS, Weigold P, Lösekann-Behrens T, Kappler A, Behrens S (2015) Microbial community composition of a household sand filter used for arsenic, iron, and manganese removal from groundwater in Vietnam. *Chemosphere* 138:47–59
- Omeregie EO, Couture RM, Van Cappellen P, Corkhill CL, Charnock JM, Polya DA, Vaughan D, Vanbroekhoven K, Lloyd JR (2013) Arsenic bioremediation by biogenic iron oxides and sulfides. *Appl Environ Microbiol* 79:4325–4335
- Oremland RS, Stolz JF (2005) Arsenic, microbes and contaminated aquifers. *Trends Microbiol* 13: 45–49
- Oremland RS, Dowdle PR, Hoelt S, Sharp JO, Schaefer JK, Miller LG, Blum JS, Smith RL, Bloom NS, Wallschläger D (2000) Bacterial dissimilatory reduction of arsenate and sulfate in meromictic Mono Lake, California. *Geochim Cosmochim Acta* 64:3073–3084
- Oremland RS, Hoelt SE, Santini JM, Bano N, Hollibaugh RA, Hollibaugh JT (2002) Anaerobic oxidation of Arsenite in Mono Lake water and by a facultative, Arsenite-oxidizing chemoautotroph, strain MLHE-1. *Appl Environ Microbiol* 68:4795–4802
- Oremland RS, Saltikov CW, Wolfe-Simon F, Stolz JF (2009) Arsenic in the evolution of earth and extraterrestrial ecosystems. *Geomicrobiol J* 26:522–536
- Palmer NE, Freudenthal JH, Wandruszka RV (2006) Reduction of arsenates by humic materials. *Environ Chem* 3:131–136

- Pederick RL, Gault AG, Charnock JM, Polya DA, Lloyd JR (2007) Probing the biogeochemistry of arsenic: response of two contrasting aquifer sediments from Cambodia to stimulation by arsenate and ferric iron. *J Environ Sci Heal Part A* 42:1763–1774
- Petursdottir AH, Fletcher K, Gunnlaugsdottir H, Krupp E, Kupper FC, Feldmann J (2016) Environmental effects on arsenosugars and arsenolipids in *Ectocarpus* (Phaeophyta). *Environ Chem* 13:21–33
- Planer-Friedrich B, London J, Mcleskey RB, Nordstrom DK, Wallschläger D (2007) Thioarsenates in geothermal waters of Yellowstone National Park: determination, preservation, and geochemical importance. *Environ Sci Technol* 41:5245–5251
- Planer-Friedrich B, Suess E, Scheinost AC, Wallschlä D (2010) Arsenic speciation in sulfidic waters: reconciling contradictory spectroscopic and chromatographic evidence. *Anal Chem* 82: 10228–10235
- Qin J, Rosen BP, Zhang Y, Wang G, Franke S, Rensing C (2006) Arsenic detoxification and evolution of trimethylarsine gas by a microbial arsenite S-adenosylmethionine methyltransferase. *Proc Natl Acad Sci* 103:2075–2080
- Raab A, Newcombe C, Pitton D, Ebel R, Feldmann J (2013) Comprehensive analysis of lipophilic arsenic species in a brown alga (*Saccharina latissima*). *Anal Chem* 85:2817–2824
- Reed DC, Algar CK, Huber JA, Dick GJ (2014) Gene-centric approach to integrating environmental genomics and biogeochemical models. *Proc Natl Acad Sci* 111:1879–1884
- Richey C, Chovanec P, Hoelt SE, Oremland RS, Basu P, Stolz JF (2009) Respiratory arsenate reductase as a bidirectional enzyme. *Biochem Biophys Res Commun* 382:298–302
- Rochette EA, Bostick BC, Li G, Fendorf S (2000) Kinetics of arsenate reduction by dissolved sulfide. *Environ Sci Technol* 34:4714–4720
- Rowland HAL, Boothman C, Pancost R, Gault AG, Polya DA, Lloyd JR (2009) The role of indigenous microorganisms in the biodegradation of naturally occurring petroleum, the reduction of iron, and the mobilization of Arsenite from West Bengal. *J Environ Qual* 38:1598–1607
- Sacheti P, Bhonsle H, Patil R, Kulkarni MJ, Srikanth R, Gade W (2013) Arsenomics of *Exiguobacterium* sp. PS (NCIM 5463). *RSC Adv* 3:9705–9713
- Sardiwal S, Santini JM, Osborne TH, Djordjevic S (2010) Characterization of a two-component signal transduction system that controls arsenite oxidation in the chemolithoautotroph NT-26. *FEMS Microbiol Lett* 313:20–28
- Saunders JK, Fuchsman CA, McKay C, Rocap G (2019) Complete arsenic-based respiratory cycle in the marine microbial communities of pelagic oxygen-deficient zones. *Proc Natl Acad Sci* 116: 9925–9930
- Schmeisser E, Goessler W, Francesconi KA (2006) Human metabolism of arsenolipids present in cod liver. *Anal Bioanal Chem* 385:367–376
- Sharma P, Kappler A (2011) Desorption of arsenic from clay and humic acid-coated clay by dissolved phosphate and silicate. *J Contam Hydrol* 126:216–225
- Sharma P, Ofner J, Kappler A (2010a) Formation of binary and ternary colloids and dissolved complexes of organic matter, Fe and As. *Environ Sci Technol* 44:4479–4485
- Sharma P, Rolle M, Kocar BD, Fendorf S, Kappler A (2010b) Influence of natural organic matter on As transport and retention. *Environ Sci Technol* 45:546–553
- Shekhar SK, Godheja J, Modi DR (2020) Molecular Technologies for Assessment of bioremediation and characterization of microbial communities at pollutant-contaminated sites. In: Bharagava RN, Saxena G (eds) *Bioremediation of industrial waste for environmental safety*. Springer, Singapore, pp 437–474
- Shi X, Wei X, Koo I, Schmidt RH, Yin X, Kim SH, Vaughn A, McClain CJ, Arteel GE, Zhang X, Watson WH (2014) Metabolomic analysis of the effects of chronic arsenic exposure in a mouse model of diet-induced fatty liver disease. *J Proteome Res* 13:547–554
- Stolz JF, Basu P, Oremland RS (2010) Microbial arsenic metabolism: new twists on an old poison. *Microbe* 5:53–59

- Sun W, Sierra R, Fernandez N, Sanz JL, Amils R, Legatzki A, Maier RM, Amils R, Field JA (2009a) Molecular characterization and in situ quantification of anoxic Arsenite oxidizing denitrifying enrichment cultures. *FEMS Microbiol Ecol* 68:72–85
- Sun GX, Williams PN, Zhu YG, Deacon C, Carey AM, Raab A, Feldmann J, Meharg AA (2009b) Survey of arsenic and its speciation in rice products such as breakfast cereals, rice crackers and Japanese rice condiments. *Environ Int* 35:473–475
- Taleshi MS, Jensen KB, Raber G, Edmonds JS, Gunnlaugsdottir H, Francesconi KA (2008) Arsenic-containing hydrocarbons: natural compounds in oil from the fish capelin, *Mallotus villosus*. *Chem Commun* 39:4706–4707
- Taleshi MS, Edmonds JS, Goessler W, Ruiz-Chancho MJ, Raber G, Jensen KB, Francesconi KA (2010) Arsenic-containing lipids are natural constituents of sashimi tuna. *Environ Sci Technol* 44:1478–1483
- Taleshi MS, Raber G, Edmonds JS, Jensen KB, Francesconi KA (2014) Arsenolipids in oil from blue whiting *Micromesistius poutassou*—evidence for arsenic-containing esters. *Sci Rep* 4:7492
- Thomas DJ, Rosen BP (2013) Arsenic methyltransferase. In: Uversky VN, Kretsinger RH, Permyakov EA (eds) *Encyclopedia of metalloproteins*. Science+Business Media, New York, pp 138–143
- Thomasarrigo LK, Mikutta C, Byrne J, Barmettler K, Kappler A, Kretzschmar R (2014) Iron and arsenic speciation and distribution in organic flocs from streambeds of an arsenic-enriched peatland. *Environ Sci Technol* 48:13218–13228
- Van Lis R, Nitschke W, Duval S, Schoep-Cothenet B (2013) Arsenics as bioenergetic substrates. *Biochim Biophys Acta Bioenerg* 1827:176–188
- Viczek SA, Jensen KB, Francesconi KA (2016) Arsenic-containing phosphatidylcholines: a new Group of Arsenolipids Discovered in herring caviar. *Angew Chem Int Ed* 55:5259–5262
- Wang L, Chen S, Xiao X, Huang X, You D, Zhou X, Deng Z (2006) arsRBOCT arsenic resistance system encoded by linear plasmid pHZ227 in *Streptomyces* sp. strain FR-008. *Appl Environ Microbiol* 72:3738–3742
- Wang X, Chen X, Yang J, Wang Z, Sun G (2009) Effect of microbial mediated iron plaque reduction on arsenic mobility in paddy soil. *J Environ Sci* 21:1562–1568
- Wang L, Yin Z, Jing C (2020) Metagenomic insights into microbial arsenic metabolism in shallow groundwater of Datong basin, China. *Chemosphere* 245:125603
- Xiao KQ, Li LG, Ma LP, Zhang SY, Bao P, Zhang T, Zhu YG (2016) Metagenomic analysis revealed highly diverse microbial arsenic metabolism genes in paddy soils with low-arsenic contents. *Environ Pollut* 211:1–8
- Xue XM, Raber G, Foster S, Chen SC, Francesconi KA, Zhu YG (2014) Biosynthesis of arsenolipids by the cyanobacterium *Synechocystis* sp. PCC 6803. *Environ Chem* 11:506–513
- Xue XM, Ye J, Raber G, Francesconi KA, Li G, Gao H, Yan Y, Rensing C, Zhu YG (2017) Arsenic methyltransferase is involved in Arsenosugar biosynthesis by providing DMA. *Environ Sci Technol* 51:1224–1230
- Yan Y, Ye J, Xue XM, Zhu YG (2015) Arsenic demethylation by a C<sub>2</sub>-as Lyase in cyanobacterium *Nostoc* sp. PCC 7120. *Environ Sci Technol* 49:14350–14358
- Yan Y, Ding K, Yu X, Ye J, Xue X (2017) Ability of periplasmic phosphate binding proteins from *Synechocystis* sp. PCC 6803 to discriminate phosphate against arsenate. *Water Air Soil Pollut* 228:148
- Yang H, Cheng J, Finan TM, Rosen BP (2005) Novel pathway for arsenic detoxification in the legume symbiont *Sinorhizobium meliloti*. *J Bacteriol* 187:6991–6997
- Yang YP, Tang XJ, Zhang HM, Cheng WD, Duan GL, Zhu YG (2020) The characterization of arsenic biotransformation microbes in paddy soil after straw biochar and straw amendments. *J Hazard Mater* 391:122200
- Ye J, Rensing C, Rosen BP, Zhu YG (2012) Arsenic biomethylation by photosynthetic organisms. *Trends Plant Sci* 17:155–162
- Yin XX, Chen J, Qin J, Sun GX, Rosen BP, Zhu YG (2011) Biotransformation and volatilization of arsenic by three photosynthetic cyanobacteria. *Plant Physiol* 156:1631–1638

- Yoshinaga M, Rosen BP (2014) AC As lyase for degradation of environmental organoarsenical herbicides and animal husbandry growth promoters. *Proc Natl Acad Sci* 111(641):7701–7706
- Yoshinaga M, Cai Y, Rosen BP (2011) Demethylation of methylarsonic acid by a microbial community. *Environ Microbiol* 13:1205–1215
- Zargar K, Hoefl S, Oremland R, Saltikov CW (2010) Identification of a novel arsenite oxidase gene, *arxA*, in the haloalkaliphilic, arsenite-oxidizing bacterium *Alkalilimnicola ehrlichii* strain MLHE-1. *J Bacteriol* 192:3755–3762
- Zargar K, Conrad A, Bernick DL, Lowe TM, Stolc V, Hoefl S, Oremland RS, Stolz J, Saltikov CW (2012) Arx A, a new clade of arsenite oxidase within the DMSO reductase family of molybdenum oxidoreductases. *Environ Microbiol* 14:1635–1645
- Zhou X, Kang F, Qu X, Fu H, Alvarez PJ, Tao S, Zhu D (2020) The role of extracellular polymeric substances (EPS) in microbial reduction of arsenate to arsenite by *Escherichia coli* and *Bacillus subtilis*. *Environ Sci Technol* 54:6185–6193

# Chapter 9

## Microbial Transformations of Antimony



Huaqing Liu, Weimin Sun, and Max M. Häggblom

**Abstract** Antimony (Sb) is a widespread metalloid and Sb contamination has drawn increasing attention. Microorganisms are one of the main drivers of Sb transformation, which is closely associated with its mobility, toxicity and bioavailability. This chapter examines Sb biotransformation processes (i.e., oxidation, reduction and methylation) from the aspects of microorganisms, genes and enzymes. The transformations of Sb are catalyzed by a series of enzymes in diverse environmental microorganisms. Given that Sb has similar chemical properties with arsenic (As), the correlations between Sb and As metabolisms are included.

### 9.1 Introduction

#### 9.1.1 *Sb in the Environment*

Antimony (Sb) is a metalloid belong to Group 15 of the periodic table, positioned directly below arsenic (As), and these two metalloids share similar chemical

---

H. Liu

Department of Biochemistry and Microbiology, School of Environmental and Biological Sciences, Rutgers, The State University of New Jersey, New Brunswick, NJ, USA

National-Regional Joint Engineering Research Center for Soil Pollution Control and Remediation in South China, Guangdong Key Laboratory of Integrated Agro-environmental Pollution Control and Management, Institute of Eco-environmental and Soil Sciences, Guangdong Academy of Sciences, Guangzhou, China

W. Sun

National-Regional Joint Engineering Research Center for Soil Pollution Control and Remediation in South China, Guangdong Key Laboratory of Integrated Agro-environmental Pollution Control and Management, Institute of Eco-environmental and Soil Sciences, Guangdong Academy of Sciences, Guangzhou, China

M. M. Häggblom (✉)

Department of Biochemistry and Microbiology, School of Environmental and Biological Sciences, Rutgers, The State University of New Jersey, New Brunswick, NJ, USA

e-mail: [haggblom@rutgers.edu](mailto:haggblom@rutgers.edu)



properties. The application of Sb can be traced back to 3100 BC, when antimony trisulfide ( $\text{Sb}_2\text{S}_3$ ) was used by Egyptians as a black powder eye pigment, kohl (Dupont et al. 2016). In 1604, the properties and production of Sb were first described by the alchemist Vasily Valentine (Krenev et al. 2015). Later, Sb was listed as a chemical element by Antoine-Laurent Lavoisier in 1789 (Rouvray 2004).

To date, Sb has been largely applied to produce flame retardants, bearing alloys, brake linings, cable coverings, among other applications, with an increasing annual world production currently over 160,000 tons (LePan 2020). Sb naturally co-occurs with about 120 minerals, of which Sb is primarily in the forms of  $\text{Sb}_2\text{S}_3$  and  $\text{Sb}_2\text{O}_3$  (He et al. 2019; Krenev et al. 2015). Frequent mining activities and industrial emissions have inevitably increased Sb release to the surrounding environment. Since Sb and its compounds exhibit toxic properties, the geochemical cycling and environmental behavior of Sb are of great concern (Dupont et al. 2016; Long et al. 2020).

Sb is widespread in the crust surface of the Earth, at  $<10 \text{ mg kg}^{-1}$  and  $<1 \text{ mg L}^{-1}$  in un-contaminated soils and water, respectively (Filella et al. 2002; Tschan et al. 2009). However, elevated concentrations of Sb frequently occur in environments associated with anthropogenic activities, such as mining and smelting, much higher than the guideline values (i.e.,  $36 \text{ mg kg}^{-1}$  Sb in soil,  $20 \text{ } \mu\text{g L}^{-1}$  Sb in drinking water) provided by the World Health Organization (WHO). Even in the Arctic, Sb accumulation has increased by 50% in the past 30 years, mainly from anthropogenic sources (Pierart et al. 2015). Severe Sb contamination has been observed in soils, sediments, surface water and groundwater around the world (Table 9.1). Mining activities usually have extensive and lasting effects on Sb dispersal. For example, Sb concentrations in a creek draining a mine abandoned 85 years ago were still above  $30 \text{ } \mu\text{g L}^{-1}$  (Casiot et al. 2007). Smelting activities can lead to extremely high levels of Sb in the environment, with Sb content in the smelting sites up to  $1.7 \times 10^5 \text{ mg kg}^{-1}$  (Wilson et al. 2004). Sb in mining and smelting sites is sparingly soluble over a wide pH range, and this insoluble Sb fraction has a lower risk to the environment (Flynn et al. 2003).

The metalloid As is also widespread in the environment, with background As concentrations generally higher than that of Sb (Wilson et al. 2010). Some Sb- and As-bearing minerals are closely related, e.g., stibnite ( $\text{Sb}_2\text{S}_3$ ) and orpiment ( $\text{As}_2\text{S}_3$ ), stibodomeykite  $[\text{Cu}_3(\text{Sb,As})]$ , gerstleyite  $[\text{Na}_2(\text{Sb,As})_8\text{S}_{13} \cdot 2\text{H}_2\text{O}]$  (Herath et al. 2017; Multani et al. 2016). Sb frequently co-occurs with As, although the quantitative relations between the two metalloids are irregular (Table 9.1). The mobility of Sb is higher than As under prevailing oxidizing conditions, but lower than As under reducing conditions (Ritchie et al. 2013; Warnken et al. 2017). Nevertheless, the coexistence of Sb and As establishes a connection between the biogeochemical cycles of these two metalloids.

**Table 9.1** Antimony and arsenic occurrence in different environments

Location	Media type	Samples	Sb (ppm)	As (ppm)	Cause of pollution	Reference
Soil/sediment						
Northern New South Wales, Australia	River sediment	107	3–237	3–275,000	Former mining activity	Ashley and Lottermoser (1999)
North-Eastern New South Wales, Australia	Floodplain	72	0–39	2–40	Former mining activity	Tighe et al. (2005)
New South Wales, Australia	Sediment	25	180–554	59–176	Mining activity	Telford et al. (2009)
British Columbia, Canada	Sediment	12	6–105	115–10,726	Mining activity	Beauchemin et al. (2012)
Dushan, China	Soil	26	58–101,689	78–680	Sb smelting activity	Sun et al. (2017)
Guizhou, China	Soil	31	0–233	0–1385	Mining activity	Zhang et al. (2009)
Xikuangshan, China	Soil	60	30–302	5–341	Mining activity	Yu et al. (2021)
Corsica, France	River sediment	24	31–1057	217–9135	Former mining activity	Culioli et al. (2009)
Noyelles-Godault, France	Soil	37	2–175	4–65	Smelting activity	Douay et al. (2008)
Prestea, Ghana	Sediment	39	9–90	942–10,200	Mining activity	Serfor-Armah et al. (2006)
Endeavour Inlet, New Zealand	Soil and tailings	19	18–176,700	14–9120	Former Sb smelting activity	Wilson et al. (2004)
Castelo Branco, Portugal	Soil	24	31–5987	11–651	Former mining activity	Pratas et al. (2005)
Silesia, Poland	Reservoir sediment	24	41–355	41–373	Former mining activity	Michalski et al. (2016)
Glendinning, Scotland	Soil	18	3–1020	0–170	Mining activity	Macgregor et al. (2015)
Western Carpathians, Slovakia	Sediment	25	11–1360	25–9180	Mining activity	Hiller et al. (2012)
Zlata Idka, Slovakia	Soil	46	7–13,610	37–13,040	Former mining activity	Rapant et al. (2006)
Chungcheongnam-do, South Korea	Soil	88	2–21,400	0–186	Sb smelting activity	Park et al. (2021)
Zamora, Spain	Soil	90	14–324	246–758	Former mining activity	Álvarez-Ayuso et al. (2012)
Switzerland	Soil	70	35–17,500	1–14	Shooting range	Johnson et al. (2005)
Alaska, USA	Sediment	51	7–7230	15–10,100	Mining activity	Ritchie et al. (2013)

(continued)

Table 9.1 (continued)

Location	Media type	Samples	Sb (ppm)	As (ppm)	Cause of pollution	Reference
Texas, USA	Sediment	90	0–486	1–14	Sb smelting plant	Baeza et al. (2010)
Water						
British Columbia, Canada	Porewater	12	0–0.36	0–3.63	Mining activity	Beauchemin et al. (2012)
Xikuangshan, China	Groundwater	34	0–39.16	0–1.76	Mining activity	Zhou et al. (2017)
Corsica, France	River water	24	0–0.15	0–2.33	Former mining activity	Culioli et al. (2009)
Ord basin, France	Creek water	7	0–0.03	0–0.01	Former mining activity	Casiot et al. (2007)
Prestea, Ghana	Stream water	39	0–0.75	0.15–8.25	Mining activity	Serfor-Armah et al. (2006)
Sardinia, Italy	Stream water	99	0–30.00	0–16.00	Mining activity	Cidu et al. (2018)
Glendinning, Scotland	Porewater	9	0–0.78	0–1.77	Mining activity	Macgregor et al. (2015)
Western Carpathians, Slovakia	Water	64	0–9.30	0–2.15	Mining activity	Hiller et al. (2012)
Alaska, USA	Porewater	51	0–55.00	0–3.51	Mining activity	Ritchie et al. (2013)
Texas, USA	Creek water	90	0–0.22	0–0.02	Sb smelting activity	Baeza et al. (2010)
Yellowstone National Park, USA	Spring water	23	0.01–0.17	0.16–3.57	Natural origin	Stauffer and Thompson (1984)

### 9.1.2 *Microbes and Sb*

Microorganisms have significant effects on Sb speciation and mobility, and the geochemical cycling of Sb is largely driven by microorganisms. Although Sb can exist in the V, III, 0, and –III valence states, antimonate [Sb(V)] and antimonite [Sb(III)] are the two prevalent oxidation states in the natural environment and biota (Filella et al. 2002). Redox changes of Sb are mediated by diverse Sb-oxidizing and -reducing microorganisms, and the biotransformation of Sb(III) to Sb(V) can minimize the mobility and toxicity of Sb, and vice versa (Li et al. 2016). In addition, Sb oxyanions can be methylated to organic Sb species, which can potentially be released into the atmosphere (Bentley and Chasteen 2002). This chapter explores the diversity of microorganisms responsible for Sb cycling (i.e., Sb(V) reduction, Sb(III) oxidation and Sb methylation) and introduces the genes and enzymes involved in Sb(V) reduction, Sb(III) oxidation and Sb uptake and efflux.

Given the similar properties and reactivities between Sb and As, they are linked in their distribution, oxidation state, mobility, toxicity and bioavailability (Ashley et al. 2007; Wilson et al. 2010). Compared to our knowledge regarding As microbiology, the understanding of microbial mediated Sb cycling is still in its infancy (Li et al. 2016). Nevertheless, the current knowledge demonstrates both the similarities and uniqueness in the biogeochemical cycles of Sb and As. For instance, some microorganisms are capable of transforming both Sb and As, while others are not (Nguyen et al. 2021). Thus, it is of interest to identify the connections and differences in Sb and As biotransformations with regards to the functional microorganisms, genes and enzymes. In this chapter the microbial transformation of Sb metabolism as it relates to As metabolism will be considered.

## 9.2 Microbial Communities in Sb-Contaminated Sites

Both Sb and As are toxic metalloids and with no known essential biological functions. Understanding the effects of Sb contamination on microbiota has progressed over the years. Sb exposure can induce DNA mutagenesis, cause mortality, and decreased survival of culturable bacteria under Sb stress, e.g., *Azospirillum brasilense*, *Staphylococcus aureus*, *Bacillus subtilis* and *Escherichia coli* (An and Kim 2009; Obiakor et al. 2019). A field study showed that Sb and As contamination reduced community diversity although low concentrations of Sb (V) and As(V) enhanced microbial diversity (Sun et al. 2017). Some potential keystone taxa in mining sites, including *Hyphomicrobiaceae* and *Bradyrhizobiaceae*, are inhibited by heavy Sb contamination, which could impair the ecological functions of these members (Sun et al. 2019c). Sb contamination can interfere with soil microbial processes of respiration, carbon mineralization and nitrification (Guillamot et al. 2014; Yu et al. 2021). The adverse impacts of Sb and As pollutants on soil microbial communities is greater on bacteria than fungi (Wang

et al. 2011). The toxicity of Sb strongly depends on its speciation, which generally follows the order: Sb (III) > Sb (V) > organoantimonials (e.g., methylated Sb) (He and Yang 1999). Sb(III) is reported to be ten times more toxic than Sb(V) (Oorts et al. 2008). The toxicity of As species follows the same order: As(III) > As (V) > organoarsenicals (e.g., methylated As) (Wei et al. 2015; Wilson et al. 2010). However, compared with As, our understanding of the mechanism of Sb toxicity to microbiota is still very limited (He et al. 2019).

Due to the toxicity of Sb, polluted environments select for specific indigenous microorganisms with the ability to detoxify or transform Sb. For example, members of the genera *Opitutus*, *Sphingomonas* and *Anaerolinea* were enriched in sites with heavy Sb and As contamination (Sun et al. 2019c). Moreover, a number of microbial taxa in Sb mining sites were found to be positively correlated with different Sb species (Sun et al. 2016; Li et al. 2021). The diversity and abundance of functional genes associated with Sb and As biotransformation showed positive correlation with both Sb and As concentration, suggesting the potential role of these microorganisms and genes in Sb and As metabolism (Luo et al. 2014).

## 9.3 Biochemical Sb Cycle

### 9.3.1 Sb Transformation Pathways

Microorganisms are not only influenced by Sb contamination, they are also extensively involved in Sb transport and transformation. Microbially mediated Sb transformation pathways include Sb(III) oxidation, Sb(V) reduction, Sb(III) reduction and Sb methylation (Fig. 9.1). Typically, Sb(V) is prevalent in oxic environments, while Sb(III) dominates in anoxic environments (Wang et al. 2018). The redox transformations of Sb can be accomplished either by abiotic or biotic reactions. Abiotic Sb(III) oxidation with O<sub>2</sub> as the oxidant is extremely slow, with a half-life of 170 years (Leuz et al. 2006). Some other oxidants (e.g., H<sub>2</sub>O<sub>2</sub>, iodate, birnessite, manganite) show faster Sb(III) oxidation rates, but were barely detectable in natural environments (Sun et al. 2019a; Wang et al. 2012). In comparison, microbial Sb(III) oxidation can occur in both oxic and anoxic environments. The oxidation rate of Sb

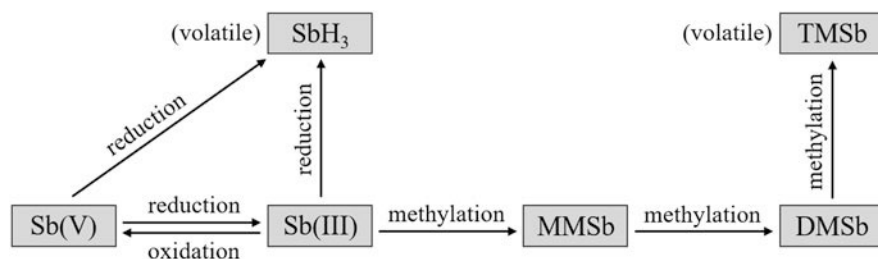


**Fig. 9.1** The identified biotransformation pathways of antimony

(III) by microorganisms can be over  $10 \mu\text{M h}^{-1}$ , suggesting that microorganisms could contribute to Sb(III) oxidation (Choi et al. 2017; Li et al. 2018). Microbial Sb(V) reduction has been observed in various sites, including Sb mining sites (Lai et al. 2016), shooting ranges (Hockmann et al. 2014), rice paddies (Sun et al. 2019b), membrane bioreactors (Lai et al. 2018a), and even aqueous environments without previous Sb exposure (Yang et al. 2021a). Microbial Sb(V) reduction results in accumulation of Sb(III), and this process decreases the mobility and increases the toxicity of Sb (Hockmann et al. 2014). Smith et al. (2002b) showed that microorganisms are capable of reducing Sb(V) directly to stibine ( $\text{SbH}_3$ ) with the valence state of  $-III$ . In addition, microbial  $\text{SbH}_3$  formation could also occur in cultures incubated with Sb(III) (Meyer et al. 2007). The formation of  $\text{SbH}_3$ , as a highly toxic gas, poses a threat of Sb contamination to the atmosphere. Methylated Sb species, including monomethylantimony (MMSb), dimethylantimony (DMSb), and trimethylantimony (TMSb), have been widely observed in soil, sediment, sewage, fresh water, seawater and landfill gas (Andreae and Froelich Jr 1984; He et al. 2019; Wilson et al. 2010). Sb biomethylation in these environments is mainly mediated by microorganisms. The mechanism of Sb biomethylation has been summarized by Filella (2010), who suggested the methylation process occurs from MMSb to DMSb and TMSb.

### 9.3.2 Sb-Oxidizing Microorganisms

More than 70 Sb(III) oxidizers have been identified over the past decades, most of them are isolated from mining sites (Table 9.2). Lialikova (1967) reported that Sb(III) was oxidized by a culture of *Thiobacterium*, which is one of the earliest, if not the earliest discovery of a Sb transforming microorganism. *Acidithiobacillus ferrooxidans* has been found to fix  $\text{CO}_2$  in the presence of  $\text{Sb}_2\text{S}_3$ , and enhance leaching of  $\text{Sb}_2\text{S}_3$  (Hoffman and Hendrix 1976; Silver and Torma 1974). Sb(III) oxidation by chemoautotrophs was demonstrated with the isolation of *Stibiobacter senarmontii*, which is capable of chemoautotrophic growth using the energy from Sb(III) oxidation (Lialikova 1974). Terry et al. (2015) isolated two other Sb(III)-oxidizing chemoautotrophs, *Hydrogenophaga* sp. IDSBO-1 and *Variovorax* sp. IDSBO-4, from As- and Sb-contaminated mining sites. Some other Sb(III) oxidizers have been identified as heterotrophs. For example, Nguyen and Lee (2015) isolated eight Sb(III) oxidizing bacteria from sediments in the vicinity of an Sb factory, and these Sb(III) oxidizing bacteria can only oxidize Sb(III) in the presence of organic nutrients. This observation indicates that heterotrophic Sb(III) oxidation may play more of a role in cellular detoxification (from more toxic Sb(III) to less toxic Sb(V)), rather than principally generating energy to support metabolic activity.

The Sb(III) oxidizers generally use  $\text{O}_2$  as their electron acceptor. Some of them (e.g., *Acinetobacter johnsonii* JH7, *Acinetobacter* sp. JL7, *Comamonas testosteroni* S44, *Stenotrophomonas* sp. JL9, *Variovorax* sp. JL23, *Hydrogenophaga*

**Table 9.2** Microorganisms involved in antimony metabolism

Organism	Source	Taxonomic affiliation	As metabolism	Reference
<b>Antimony-oxidizing microorganisms</b>				
<i>Acinetobacter johnsonii</i> JH7	Sb mine tailings, Nandan, China	Gammaproteobacteria	n.a.	Gu et al. (2019)
<i>Acinetobacter</i> sp. DS2, LH3, LH & DC2	Mining sites, China	Gammaproteobacteria	No	Shi et al. (2013)
<i>Acinetobacter</i> sp. JL7	Xikuangshan Sb mine, China	Gammaproteobacteria	n.a.	Li et al. (2013)
<i>Acinetobacter</i> sp. NL1 & NL12	Sediments in the vicinity of an Sb factory, Korea	Gammaproteobacteria	n.a.	Nguyen and Lee (2015)
<i>Agrobacterium tumefaciens</i> 5A	As-contaminated soil in the Madison River Valley, USA	Alphaproteobacteria	Yes	Lehr et al. (2007)
<i>Agrobacterium tumefaciens</i> GW4	As-contaminated aquifer sediments, China	Alphaproteobacteria	Yes	Li et al. (2015)
<i>Aminobacter</i> sp. LS5	Sandy loam/Sb soil, China	Alphaproteobacteria	No	Shi et al. (2013)
<i>Arthrobacter</i> sp. LH11	Sandy loam/Sb mine, China	Actinobacteria	No	Shi et al. (2013)
<i>Bacillus</i> sp. DF4	Sandy loam/Fe mine, China	Firmicutes	No	Shi et al. (2013)
<i>Bacillus</i> sp. S3	Xikuangshan Sb mine, China	Firmicutes	n.a.	Li et al. (2018)
<i>Bosea</i> sp. AS-1	Xikuangshan Sb mine, China	Alphaproteobacteria	Yes	Lu et al. (2018)
<i>Comamonas</i> sp. DF1, DF2, DS1, JC9, JC12 & JC13	Mining sites, China	Betaproteobacteria	No	Shi et al. (2013)
<i>Comamonas</i> sp. S44, JL25 & JL40	Xikuangshan Sb mine, China	Betaproteobacteria	n.a.	Li et al. (2013)
<i>Cupriavidus</i> sp. NL4 & NL11	Sediments in the vicinity of an Sb factory, Korea	Betaproteobacteria	n.a.	Nguyen and Lee (2015)
<i>Cupriavidus</i> sp. S1	Xikuangshan Sb mine, China	Betaproteobacteria	n.a.	Li et al. (2018)
<i>Ensifer</i> sp. NLS4	Sb-contaminated soil, Korea	Alphaproteobacteria	No	Choi et al. (2017)
<i>Flaviumibacter stibioxidans</i> YS-17	Lengshuijiang Sb mine, China	Bacteroidetes	n.a.	Han et al. (2016)
<i>Hydrogenophaga</i> sp. IDSBO-1	As- and Sb-contaminated Stibnite/Yellow	Betaproteobacteria	Yes	Terry et al. (2015)

(continued)

**Table 9.2** (continued)

Organism	Source	Taxonomic affiliation	As metabolism	Reference
	Pine mining area of Idaho, USA			
<i>Janibacter</i> sp. LH2	Sandy loam/Sb mine, China	Actinobacteria	No	Shi et al. (2013)
<i>Moraxella osloensis</i> S2	Xikuangshan Sb mine, China	Gammaproteobacteria	n.a.	Li et al. (2018)
<i>Paracoccus</i> sp. LH8 & JC6	Mining sites, China	Alphaproteobacteria	No	Shi et al. (2013)
<i>Paracoccus versutus</i> XT0.6	Xikuangshan Sb mine, China	Alphaproteobacteria	No	Loni et al. (2020)
<i>Pseudomonas</i> sp. DF12, DF3 & DF9	Sandy loam/Fe mine, China	Gammaproteobacteria	Yes	Shi et al. (2013)
<i>Pseudomonas</i> sp. DS7, DF5, FD7, DS4, DA5, DA2, DF11, DC5, DC8, JC11, TC13, DC7, DF8 & DA4	Mining sites, China	Gammaproteobacteria	No	Shi et al. (2013)
<i>Pseudomonas</i> sp. IK-S1	Former Sb mine, Japan	Gammaproteobacteria	No	Hamamura et al. (2013)
<i>Pseudomonas</i> sp. NL2, NL5, NL6 & NL10	Sediments in the vicinity of an Sb factory, Korea	Gammaproteobacteria	n.a.	Nguyen and Lee (2015)
<i>Pseudomonas</i> sp. TS44	As contaminated soil, China	Gammaproteobacteria	Yes	Wang et al. (2016)
<i>Pseudorhizobium banfieldiae</i> NT-26	Granites goldmine in Northern Territory, Australia	Alphaproteobacteria	Yes	Wang et al. (2015)
<i>Roseomonas rhizosphaerae</i> YW11	As and Sb contained soil in Yangzhou, China	Alphaproteobacteria	Yes	Sun et al. (2020)
<i>Shinella</i> sp. NLS1	Sb-contaminated soil, Korea	Alphaproteobacteria	Yes	Choi et al. (2017)
<i>Shinella</i> sp. VKA3 & VKA4	Activated sludge, Germany	Alphaproteobacteria	Yes	Nguyen et al. (2021)
<i>Sinorhizobium</i> sp. GW3	As contaminated groundwater sediments, China	Alphaproteobacteria	Yes	Li et al. (2019)
<i>Sphingopyxis</i> sp. DA6	Sandy/Gold mine, China	Alphaproteobacteria	Yes	Shi et al. (2013)
<i>Sphingopyxis</i> sp. DS8	Sandy/Cu-Fe mine, China	Alphaproteobacteria	No	Shi et al. (2013)
<i>Stenotrophomonas</i> sp. IK-S2	Former Sb mine, Japan	Gammaproteobacteria	No	Hamamura et al. (2013)
		Gammaproteobacteria	n.a.	

(continued)



**Table 9.2** (continued)

Organism	Source	Taxonomic affiliation	As metabolism	Reference
<i>Stenotrophomonas</i> sp. JL9	Xikuangshan Sb mine, China			Li et al. (2013)
<i>Stibiobacter senarmontii</i>	Antimony ore deposit in Yugoslavia	Unclassified bacteria	n.a.	Lialikova (1974)
<i>Thiobacillus ferrooxidans</i>	Acid mine waters in northern Quebec, Canada	Betaproteobacteria	n.a.	Torma and Gabra (1977)
<i>Variovorax</i> sp. IDSBO-4	As- and Sb-contaminated Stibnite/Yellow Pine mining area of Idaho, USA	Betaproteobacteria	Yes	Terry et al. (2015)
<i>Variovorax</i> sp. JL23	Xikuangshan Sb mine, China	Betaproteobacteria	n.a.	Li et al. (2013)
<i>Variovorax</i> sp. LS1	Xikuangshan Sb mine, China	Betaproteobacteria	No	Shi et al. (2013)
<b>Antimony-reducing microorganisms</b>				
<i>Cryptococcus humicolus</i> ATCC 26699	Raw sewage	Fungi	n.a.	Smith et al. (2002b)
<i>Dechloromonas</i> sp. AR-2 & AR-3	Sedimentation basin in an antimony wastewater treatment facility, Japan	Betaproteobacteria	n.a.	Yang et al. (2020)
<i>Desulfuribacillus stibiarsenatis</i> MLFW-2	Sediment from Navy Beach, California, USA	Firmicutes	Yes	Abin and Hollibaugh (2017)
<i>Geobacter</i> sp. SVR	Former Sb mine in Hyogo Prefecture, Japan	Deltaproteobacteria	No	Yamamura et al. (2021)
<i>Methanobacterium formicicum</i> DSMZ 1535	Anaerobic sewage sludge	Archaea	n.a.	Michalke et al. (2000)
<i>Pseudomonas fluorescens</i> K27	Kesterson Reservoir, USA	Gammaproteobacteria	n.a.	Gürleyük et al. (1997)
<i>Shewanella</i> sp. ANA-3	As-treated wooden pier in a brackish estuary, USA	Gammaproteobacteria	Yes	Saltikov et al. (2003)
<i>Shewanella</i> sp. CNZ-1	Marine sediment of the Bohai Strait, China	Gammaproteobacteria	n.a.	Zhang and Hu (2019)
<i>Sinorhizobium</i> sp. JUK-1		Alphaproteobacteria	n.a.	

(continued)

**Table 9.2** (continued)

Organism	Source	Taxonomic affiliation	As metabolism	Reference
	Sediments in the vicinity of an Sb factory, Korea			Nguyen and Lee (2014)
Undefined	Sediment from an antimony mine in Hangzhou, China	Dominated by <i>Rhizobium</i> (Alphaproteobacteria)	n.a.	Lai et al. (2016)
Undefined	Anaerobic membrane biofilm batch reactor	Dominated by <i>Methanosarcina</i> (Archaea)	n.a.	Lai et al. (2018a)
Undefined	Flooded gold and antimony mine near Yellow Pine, Idaho, USA	n.a.	Yes	Kulp et al. (2014)
Undefined	Soil from a military shooting range, Switzerland	n.a.	n.a.	Hockmann et al. (2014)
Undefined	Subsurface near an active Sb mine, China	Dominated by <i>Alkaliphilus</i> , <i>Clostridiaceae</i> , <i>Tissierella</i> and <i>Lysinibacillus</i>	n.a.	Wang et al. (2018)
Antimony-methylating microorganisms				
<i>Clostridium acetobutylicum</i> NCIMB 619	n.a.	Firmicutes	n.a.	Smith et al. (2002a)
<i>Clostridium butyricum</i> NCIMB 7423	n.a.	Firmicutes	n.a.	Smith et al. (2002a)
<i>Clostridium cochlearium</i> NCIMB 10629	n.a.	Firmicutes	n.a.	Smith et al. (2002a)
<i>Vanrija humicola</i> ATCC 26699	n.a.	Fungi	n.a.	Hartmann et al. (2003)
<i>Flavobacterium</i> sp. NCIMB 281	n.a.	Bacteroidetes	n.a.	Jenkins et al. (2002)
<i>Methanobacterium formicicum</i> DSMZ 1535	Domestic sewage sludge digester in Urbana, USA	Archaea	Yes	Michalke et al. (2000)
<i>Phaeolus schweinitzii</i> ATCC 10013	n.a.	Fungi	Yes	Andrewes et al. (2001)
<i>Scopulariopsis brevicaulis</i> 1524	n.a.	Fungi	Yes	Boriová et al. (2014)
	n.a.	Fungi	Yes	Andrewes et al. (2000)

(continued)

**Table 9.2** (continued)

Organism	Source	Taxonomic affiliation	As metabolism	Reference
<i>Scopulariopsis brevicaulis</i> ATCC 7903				
<i>Scopulariopsis brevicaulis</i> IMI 17297	n.a.	Fungi	Yes	Jenkins et al. (1998b)
<i>Clostridium</i> sp. ASI-1	Alluvial soil near river Ruhr at Essen-Werden, Germany	Firmicutes	Yes	Meyer et al. (2007)
<i>Cryptococcus humicolus</i> ATCC 26699	Raw sewage	Fungi	n.a.	Hartmann et al. (2003)
Undefined	Anaerobic soil enrichment cultures	Include nitrate-reducing, methane-producing or fermentative bacteria	n.a.	Jenkins et al. (1998a)
Undefined	Sewage sludge	Dominant by methanogenic Archaea community	n.a.	Wehmeier and Feldmann (2005)

Note: n.a. represent data are not available

sp. IDSBO-1, *Ensifer* sp. NLS4, and *Paracoccus versutus* XT0.6) have been shown capable of reducing Sb(III) under both oxic and anoxic conditions (Choi et al. 2017; Gu et al. 2019; Li et al. 2013; Loni et al. 2020; Terry et al. 2015). Nitrate can be an alternative electron acceptor in the anaerobic Sb(III) reduction process. The coupling of Sb(III) oxidation and nitrate reduction in a Sb-contaminated paddy soil was demonstrated by a culture-independent approach utilizing stable isotope probing (SIP) coupled with omics analyses (Zhang et al. 2021c). Putative Sb(III) oxidizers affiliated with genera *Azoarcus*, *Azospira* and *Chelativorans* contributed to the process.

The similar chemical properties of Sb and As suggest a connection between the biotransformation of these two metalloids. The oxidation of Sb(III) and As(III) is mediated by many of the same bacterial strains, such as *Hydrogenophaga* sp. IDSBO-1, *Variovorax* sp. IDSBO-4, *Shinella* sp. NLS1, *Agrobacterium tumefaciens* GW4, *Agrobacterium tumefaciens* 5A, and *Sinorhizobium* sp. GW3 (Choi et al. 2017; Terry et al. 2015). The oxidation rates of Sb(III) and As(III) by these versatile microorganisms were different, however. The oxidation rate of Sb(III) by *Roseomonas rhizosphaerae* YW11 was twice the rate of As(III) oxidation (Sun et al. 2020). Lu et al. (2018) found *Bosea* sp. AS-1 preferred to oxidize Sb(III) with lactate as the carbon substrate, while As(III) was favored with yeast extract. Besides, not all of the Sb(III) oxidizers are able to oxidize As(III) (Table 9.2). For instance, Shi et al. (2013) isolated 36 Sb(III) oxidizers from different mining soil samples,

among them only 4 isolates showed As(III) oxidation activity. These examples indicate the differences between Sb(III) and As(III) oxidizers as well as their metabolic diversity.

### 9.3.3 *Sb-Reducing Microorganisms*

Microbial reduction of Sb(V) to Sb(III) has been observed mainly in anoxic environments; microbial Sb(V) reduction can be irreversibly inhibited by O<sub>2</sub> (Lai et al. 2018b). More recently, Yang et al. (2021b) reported two isolates, *Dechloromonas* sp. AR-2 and *Propionivibrio* sp. AR-3, which could reduce Sb(V) under both anaerobic and microaerophilic conditions. Microorganisms are able to reduce Sb(V) through two metabolic pathways, i.e., respiratory and non-respiratory reductions. Sb(V)-respiring bacteria, such as *Shewanella* sp. ANA-3, *Sinorhizobium* sp. JUK-110 and *Desulfuribacillus stibiiarsenatis* MLFW-2, are capable of using Sb(V) as the electron acceptor to generate cellular energy for their growth (Abin and Hollibaugh 2014; Nguyen and Lee 2014; Wang et al. 2020). In the process of respiratory reduction, Sb(V) receives electrons mainly from the oxidation of organic compounds (e.g., acetate, lactate, citrate, pyruvate) but also from some inorganic compounds. Lai et al. (2016) showed that Sb(V) reduction could be coupled with H<sub>2</sub> oxidation, the electron utilization rate of H<sub>2</sub>-fed culture (98%) was significantly higher than that of the same culture fed lactate (12%). Kulp et al. (2014) observed that the Sb(V) reduction rate in microcosms inoculated with material from a stibnite mine was enhanced by amendment with either lactate or acetate, but not stimulated by H<sub>2</sub>. Moreover, Lai et al. (2018a) suggested Sb(V) reduction using CH<sub>4</sub> as the electron donor. These observations indicate that Sb(V) reducers have a special appetite toward different electron donors. However, these findings have only demonstrated the occurrence of Sb(V) reduction, specific microorganisms responsible for chemolithotrophic Sb(V) reduction utilizing H<sub>2</sub> or CH<sub>4</sub> have not been identified yet. Sb(V) reduction using glutathione or trypanothione as the reductant, catalyzed by cytoplasmic enzymes, has been identified in *Leishmania major* (Denton et al. 2004; Duval et al. 2008; Yan et al. 2003). These non-respiratory reductions of Sb(V) occur via energy conservation pathways such as detoxification.

The Sb(V) reduction products may accumulate in the forms of dissolved Sb(III) or precipitated Sb<sub>2</sub>O<sub>3</sub> (Lai et al. 2018a; Yamamura et al. 2021; Zhang and Hu 2019). Sb(V) can be enzymatically reduced by sulfate-reducing bacteria, and the reduced Sb immobilized via Sb<sub>2</sub>S<sub>3</sub> formation (Liu et al. 2018; Wang et al. 2018). In addition, sulfate-reducing bacteria are able to reduce Sb(V) via an indirect chemical reaction (Zhang et al. 2016). Instead of the enzymatically mediated Sb(V) reduction, sulfate is reduced to sulfide, which chemically reduces Sb(V) to Sb(III). Then, the reduction product Sb(III) reacts with excess sulfide, resulting in the formation of Sb<sub>2</sub>S<sub>3</sub>. The volatile Sb compounds stibine (SbH<sub>3</sub>) is another reduction product of Sb(V). Smith et al. (2002b) reported that SbH<sub>3</sub> was the major Sb species in the headspace gas of *Cryptococcus humicolus* (now named *Vanrija humicola*) cultures. SbH<sub>3</sub> formation

occurred from Sb(V) substrate but not Sb(III) substrate. Nevertheless, Meyer et al. (2007) found that  $\text{SbH}_3$  was produced by *Methanobacterium formicicum* cultures from Sb(III) substrate. The generation of  $\text{SbH}_3$  from Sb(III) has also been observed in *Scopulariopsis brevicaulis* cultures (Andrewes et al. 1998). In addition, another volatile Sb compounds trimethylstibine ( $(\text{CH}_3)_3\text{Sb}$ ) was formed in *Pseudomonas fluorescens* K27 from the synthesized trimethyldibromoantimony ( $(\text{CH}_3)_3\text{SbBr}_2$ ), which is the only report of microbial Sb reduction among methylated Sb species (Gürleyük et al. 1997).

Though Sb(V) and As(V) have similar chemical properties, some microorganisms show different metabolism of Sb(V) as compared to As(V). For example, *Desulfuribacillus stibiiarsenatis* MLFW-2 and *Shewanella* sp. ANA-3 were able to reduce both Sb(V) and As(V) (Abin and Hollibaugh 2019; Saltikov et al. 2003). However, the Sb(V)-reducing bacterium *Geobacter* sp. SVR was not able to use As(V) as the electron acceptor (Yamamura et al. 2021). These findings indicate that there are overlaps between Sb(V)- and As(V)-reducing microorganisms, but there is diversity rather than identity.

### 9.3.4 Sb-Methylating Microorganisms

Microbial Sb methylation has been recognized since the 1990s. Jenkins et al. (1998b) first reported the generation of methylated Sb by the fungus *Scopulariopsis brevicaulis* IMI 17297 growing in the presence of inorganic Sb(III). Further study indicated that *S. brevicaulis* could generate trimethyl-Sb, without any other volatile Sb species, in an aerobic environment (Craig et al. 1999). Different strains of *S. brevicaulis* showed different Sb methylation characteristics: strain ATCC 7903 could transform inorganic Sb(III) compounds to methylated Sb species and  $\text{SbH}_3$  only under aerobic conditions (Andrewes et al. 1998), while Sb methylation by strain ATCC 7903 was inactive in the presence of Sb(V) compounds, and strain 1524 transformed both Sb(III) and Sb(V) to volatilized species (Boriova et al. 2014).

Biomethylation of Sb can also occur in anoxic environments. Meyer et al. (2007) isolated a strictly anaerobic bacterium, *Clostridium* sp. ASI-1, from alluvial soil with metalloid contamination. TMSb was formed in the anaerobically incubated alluvial soil samples and pure cultures of strain ASI-1. *Methanobacterium formicicum* DSMZ 1535, an archaeon from anaerobic sewage sludge, was able to generate methylated Sb species (i.e., MMSb, DMSb, TMSb) and  $\text{SbH}_3$  from inorganic Sb(III) (Michalke et al. 2000). Sb methylation by enrichment cultures of anaerobic soils and activated sludge have been frequently observed, indicating the wide distribution of Sb-methylating microorganisms in these anoxic environments (Jenkins et al. 1998a; Wehmeier and Feldmann 2005).

Many Sb-methylating microorganisms (i.e., *M. formicicum*, *Phaeolus schweinitzii*, *S. brevicaulis*, *Clostridium* sp.) also show the capacity for As methylation, while for others As metabolic activity is yet not known. *Clostridium* sp. ASI-1 is of particular interest with the ability of generating volatile derivatives from various

metals and metalloids, such as antimony, arsenic, bismuth, selenium, tin, tellurium, lead and mercury (Meyer et al. 2007). These findings imply similarities in the biomethylation processes of different metalloids. However, the molecular mechanisms, including the functional genes and enzymes, of Sb biomethylation remain unknown.

### 9.3.5 Diversity of Sb-Transforming Microorganisms

The identified Sb-oxidizing microorganisms not only have diverse geographical origins (Table 9.2), but are also phylogenetically diverse (Fig. 9.2) with representatives from over 20 bacterial genera. Most of them fall within three subdivisions of the Proteobacteria, including Gammaproteobacteria (34 strains), Betaproteobacteria (17 strains) and Alphaproteobacteria (16 strains). Two Actinobacteria, *Arthrobacter* sp. LH11 and *Janibacter* sp. LH2, were isolated by from the same Sb mine (Shi et al. 2013). In the phylum Firmicutes, two *Bacillus* strains were identified as Sb-oxidizing bacteria (Li et al. 2018; Shi et al. 2013).

There are as yet only a few isolates confirmed as Sb-reducing microorganisms, and their membership includes not only bacteria, but also fungi and archaea. The Sb-reducing bacteria are mainly classified into Gammaproteobacteria (3 strains), Betaproteobacteria (1 strain), Alphaproteobacteria (1 strain), as well as a strain in the phylum Firmicutes. *Clostridium acetobutylicum* NCIMB 619 is a Sb-reducing bacterium isolated from raw sewage (Smith et al. 2002a). The archaeon *Methanobacterium formicicum* DSMZ 1535 isolated from anaerobic sewage sludge also showed the capacity for Sb reduction (Table 9.2). Moreover, Lai et al. (2018a) found that Sb was reduced in an anaerobic membrane biofilm batch reactor, in which *Methanosarcina* dominated. However, the responsible microorganisms were not conclusively identified.

The Sb-methylating microorganisms identified thus far are mostly affiliated with Firmicutes (4 strains) and fungi (6 strains) (Table 9.2). A Sb-methylating archaeon, *Methanobacterium formicicum* DSMZ 1535, was isolated from a domestic sewage sludge digester by Michalke et al. (2000). In addition, *Flavobacterium* sp. NCIMB 281 was identified as a Sb-methylating bacterium by Jenkins et al. (2002). No study has linked Proteobacteria with Sb methylation, which is different from the findings for Sb oxidation or reduction.

## 9.4 Biochemical Mechanisms of Sb Metabolism

### 9.4.1 Sb Oxidation

The molecular biological mechanisms of Sb(III) oxidation have been explored recently. Wang et al. (2015) provided the first evidence that the As(III) oxidase

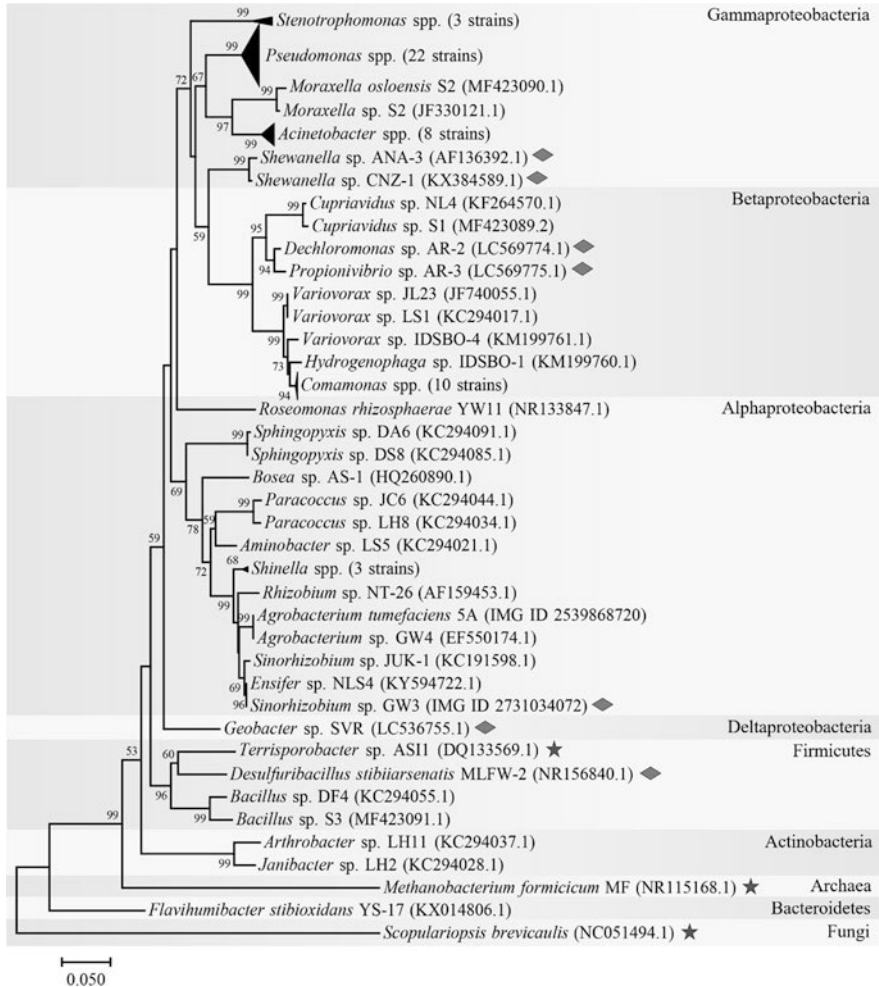


**Fig. 9.2** Phylogeny of known Sb-transforming microorganisms based on partial 16S rRNA gene sequences. The unmarked strains represent Sb-oxidizing microorganisms, the strains marked by rhombus and stars represent Sb-reducing and Sb-methylating microorganisms, respectively. The compressed *Stenotrophomonas* spp. includes 3 strains (JL9, 6B2-1 and IK-S2), the compressed *Pseudomonas* spp. includes 22 strains (DA2, DA4, DA5, DC5, DC7, DC8, DF3, DF5, DF7, DF8, DF9, DF11, DF12, DS4, DS7, JC11, NL2, NL5, NL6, NL10, IK-S1, TC13), the compressed *Acinetobacter* spp. includes strains 8 strains (DC2, DS2, JL7, JH7, LH3, LH4, NL1, NL12), the compressed *Comamonas* spp. includes 10 strains (DF1, DF2, DS1, JC9, JC12, JC13, JL25, JL40, NL11, S44), the compressed *Shinella* spp. includes 3 strains (NLS1, VKA3, VKA4). The tree was constructed using neighbor-joining (NJ) approach, based on Tamura-Nei model from a total of 1658 unambiguously aligned nucleotide positions in the final data set. Bootstrap values (expressed as percentages of 1000 replicates) of  $\geq 50\%$  are shown at branch points

AioA is also involved in Sb(III) oxidation. A mutation in *aioA* reduced Sb(III) oxidation by a third in the model organism *Agrobacterium tumefaciens* 5A (Lehr et al. 2007). In vitro experiments further confirmed the Sb(III) oxidation ability of AioA. Sun et al. (2020) observed that an *aioA* mutation in *R. rhizosphaerae* YW1 caused complete loss of Sb(III) oxidation capacity (Table 9.3). The *aioA* gene has been detected in many other Sb(III)-oxidizing microorganisms, such as *Variovorax paradoxus* IDSBO-1, IDSBO-4 and *Shinella* spp. (VKA3, VKA4, NLS1) (Choi et al. 2017; Nguyen et al. 2021; Terry et al. 2015). Zhang et al. (2021b) identified putative Sb(III)-oxidizing microorganisms (e.g., *Paracoccus*, *Rhizobium*, *Achromobacter* and *Hydrogenophaga*) by the combination of DNA-SIP, shotgun metagenomics and RT-qPCR analyses. All of the putative Sb(III)-oxidizing microorganisms contained *aioA* genes, and presence of *aioA* gene products increased along with Sb(V) generation, indicating that *aioA* was responsible for Sb oxidation.

The expression of *aioA* may be influenced by different regulators. The disruption of the *mcp* gene inhibited the expression of *aioBA*, and the transcriptional regulator *AioR* regulated the expression of both *aioBA* and *mcp* (Shi et al. 2017). Chen et al. (2015a) found that the two-component system PhoBR could regulate *aioBA* expression. These regulators posed an influence on not only *aioBA* gene repression, but also the As(III) oxidation performance, while the role of the regulators with respect to Sb(III) oxidation has yet to be confirmed.

Although AioA has been found to oxidize both Sb(III) and As(III), it exhibits different catalytic efficiency of Sb(III) and As(III) oxidation. An example of this difference is provided by the results from in vitro study of AioBA oxidase from *Pseudorhizobium banfieldiae* NT-26, which showed that  $V_{max}$  of As(III) oxidation was  $120 \text{ mol}^{-1} \text{ min}^{-1} \text{ mg}^{-1}$ , which was  $6.5 \times 10^3$  times faster than the  $V_{max}$  of Sb(III) oxidation (Wang et al. 2015). However, Sun et al. (2020) investigated the in vivo role of *aioA* in *R. rhizosphaerae* YW11, in which an *aioA* mutant lost Sb(III) and As(III) oxidation abilities. It was found that strain YW11 preferred to oxidize Sb(III), while the oxidation rate of As(III) was only 50%. Choi et al. (2017) reported that the Sb(III)-oxidizing bacteria, *Ensifer* sp. NLS4, does not possess As(III) oxidation ability. Furthermore, the *aioA* gene is not found in strain NLS4, which indicates that Sb(III) oxidation could be accomplished by other enzymatic pathways.

AnoA is another Sb(III) oxidase identified in the Sb(III)-oxidizing bacterium *A. tumefaciens* GW4 (Li et al. 2015). Proteomic analysis found that the *anoA* gene in strain GW4 was up-regulated in the presence of Sb(III). An *anoA* deletion in strain GW4 reduced Sb(III) oxidation, while *anoA* overexpression enhanced the Sb(III) oxidation rate of strain GW4. In vitro study confirmed that AnoA possesses the oxidation capacity of both Sb(III) ( $V_{max}$ :  $150 \text{ nmol}^{-1} \text{ min}^{-1} \text{ mg}^{-1}$ ) and As(III) ( $V_{max}$ :  $88 \text{ nmol}^{-1} \text{ min}^{-1} \text{ mg}^{-1}$ ) (Li et al. 2016). The *anoA* gene has also been observed in many other Sb(III)-oxidizing bacteria (e.g., *A. tumefaciens* 5A, *Sinorhizobium* sp. Sb3).

ArsV, an NADPH-dependent flavin monooxygenase, was identified as a Sb(III) oxidase in *Ensifer adhaerens* ST2 (Zhang et al. 2021a). The purified ArsV protein



**Table 9.3** Genes involved in antimony metabolism

Gene	Protein	Protein abbr.	Function	Host	Reference
<b>Sb(III) oxidation</b>					
<i>aiiA</i> and <i>aiiB</i>	As(III) oxidase	AioAB	Involved in Sb(III) and As(III) oxidation	<i>Roseomonas rhizosphaerae</i> YW11	Sun et al. (2020)
<i>mcp</i>	Chemoreceptor-encoding gene	Mcp	Involved in <i>aiiAB</i> expression	<i>Agrobacterium tumefaciens</i> GW4	Shi et al. (2017)
<i>aiiR</i>	Transcriptional regulator	AioR	Regulates the expression of <i>aiiAB</i> and <i>mcp</i>	<i>Agrobacterium tumefaciens</i> GW4	Shi et al. (2017)
<i>anoA</i>	Oxidoreductase	AnoA	Oxidizes Sb(III)	<i>Agrobacterium tumefaciens</i> GW4	Li et al. (2015)
<i>arsV</i>	Flavin-dependent monoxygenase	ArsV	Oxidizes Sb(III) and TMA <sub>s</sub> (III)	<i>Ensifer adhaerens</i> ST2	Zhang et al. (2021a)
<i>gshA</i>	Glutamate cysteine ligase	GshA	Indirect inhibition of Sb(III) oxidation by degrading H <sub>2</sub> O <sub>2</sub>	<i>Pseudomonas stutzeri</i> TS44	Wang et al. (2016)
<i>kata</i>	Catalase-peroxidase	KatA	Indirect inhibition of Sb(III) oxidation by degrading H <sub>2</sub> O <sub>2</sub>	<i>Agrobacterium tumefaciens</i> GW4	Li et al. (2017)
<i>phoB</i> and <i>phoR</i>	Phosphate regulon sensor protein	PhoBR	Regulates the expression of <i>aiiAB</i>	<i>Hatomonas</i> sp. HAL1	Chen et al. (2015a)
<b>Sb(V) reduction</b>					
<i>ACR1</i>	Transcriptional regulatory protein	ACR1	Regulates the expression of <i>ACR</i> gene	<i>Saccharomyces cerevisiae</i>	Bobrowicz et al. (1997)
<i>ACR2</i>	As(V) reductase	ACR2	Reduces Sb(V) and As(V)	<i>Leishmania major</i>	Zhou et al. (2004)
<i>arrA</i> and <i>arrB</i>	As(V) respiratory reductases	ArrAB	Reduces Sb(V) and As(V)	Shewanella sp. ANA-3	Wang et al. (2020)
<i>luxS</i>	S-ribose/homocysteine lyase	LuxS	Regulates the expression of ArrAB	Shewanella sp. ANA-3	Wang et al. (2020)

<i>TDR1</i>	Thiol-dependent reductase	TDR1	Reduces Sb(V)	<i>Leishmania major</i>	Denton et al. (2004)
Sb transport					
<i>ACR3</i>	As(III) efflux pump	Acr3	Mediates Sb(III) and As(III) efflux	<i>Saccharomyces cerevisiae</i>	Maciaszczyk-Dziubinska et al. (2010)
<i>antA</i>	Antimonite-specific efflux ATPase	AntA	Involved in Sb(III) efflux	<i>Comamonas testosteroni</i> JL40	An et al. (2021)
<i>Aqp1</i>	Aquaporin-1	AQP1	Sb(III) and As(III) uptake, form water-specific channel	<i>Leishmania</i> promastigotes	Gourbal et al. (2004)
<i>Aqp7</i>	Aquaporin-7	AQP7	Sb(III) and As(III) uptake, form channel that mediates water, glycerol, and urea channel	<i>Xenopus oocytes</i>	Liu et al. (2002)
<i>Aqp9</i>	Aquaporin-9	AQP9	Sb(III) and As(III) uptake, form water channel with a broad specificity	<i>Saccharomyces cerevisiae</i> , <i>Xenopus oocytes</i>	Liu et al. (2002)
<i>arsA</i>	Arsenical pump-driving ATPase	ArsA	Catalytic subunit of an anion-transporting ATPase	<i>Escherichia coli</i>	Bhattacharjee et al. (1995)
<i>arsB</i>	Arsenical pump membrane protein	ArsB	Forms the channel to extrude Sb(III) and As(III)	<i>Comamonas</i> sp. S44	Li et al. (2013)
<i>arsD</i>	Arsenic metallochaperone	ArsD	Increases <i>ars</i> transcription at high inducer level	<i>Escherichia coli</i>	Chen and Rosen (1997)
<i>arsK</i>	As(III) efflux MFS transporter	ArsK	Involved in Sb(III) and As(III) efflux	<i>Agrobacterium tumefaciens</i> GW4	Shi et al. (2018)
<i>arsR</i>	Arsenical resistance operon repressor	ArsR	Increases <i>ars</i> transcription at low inducer level	<i>Escherichia coli</i>	Chen and Rosen (1997)
<i>arsR2</i>	ArsR family transcription regulator	ArsR2	Regulates the expression of <i>arsK</i> gene	<i>Agrobacterium tumefaciens</i> GW4	Shi et al. (2018)
<i>FPS1</i>	Glycerol uptake/efflux facilitator protein	Fps1p	Sb(III) and As(III) uptake, yeast glycerol channel	<i>Saccharomyces cerevisiae</i>	Wysocki et al. (2001)
<i>glpF</i>		GlpF		<i>Escherichia coli</i>	Meng et al. (2004)

(continued)

**Table 9.3** (continued)

Gene	Protein	Protein abbr.	Function	Host	Reference
	Glycerol uptake facilitator protein		Sb(III) and As(III) uptake, transporter of glycerol across the cytoplasmic membrane		
<i>mrpA</i>	ABC transporter	MRPA	Involved in Sb(III) efflux	<i>Leishmania infantum</i>	Douanne et al. (2020)

showed capacity for oxidizing both Sb(III) and TMAs(III). Metagenomic analysis indicated that *arsV*-like genes are widely present in soil environments.

Hydrogen peroxide ( $H_2O_2$ ) as a reactive oxygen species (ROS) can be generated intracellularly under stress conditions (Ma et al. 1999).  $H_2O_2$  is an efficient oxidant of Sb(III) in aqueous solution (Leuz and Johnson 2005; Quentel et al. 2004). Thus, a non-enzymatically mediated process using intracellular  $H_2O_2$  as the oxidant could contribute to Sb(III) oxidation. KatA is a major catalase with the capacity of consuming  $H_2O_2$ . Li et al. (2017) found that Sb(III) induced the cellular generation of both  $H_2O_2$  and the *katA* gene product in *A. tumefaciens* GW4. A *katA* disruption in strain GW4 significantly increased the observed Sb(III) oxidation, while the disruption of either *anoA* or *aioA* genes reduced Sb(III) oxidation. Glutathione (GSH) is an essential intracellular antioxidant involved in scavenging ROS. The enzyme GshA is responsible for the biosynthesis of GSH (Janowiak and Griffith 2005). Disruption of the *gshA* gene in *P. stutzeri* TS44 has been found to reduce cellular GSH content, which further increased both the accumulation of  $H_2O_2$  and the Sb(III) oxidation efficiency (Wang et al. 2016). A positive linear correlation between  $H_2O_2$  content and Sb(III) oxidation rate was observed in strain TS44, suggesting that Sb(III) oxidation was closely related to the  $H_2O_2$  concentration. These studies demonstrated that the genes and enzymes involved in  $H_2O_2$  transformation could indirectly regulate Sb(III) oxidation.

### 9.4.2 Sb Reduction

Sb(III) reductase can reduce intracellular Sb(V) to Sb(III), which is then pumped out from the cell by a Sb(III) translocator. Similar to As, the reduction of Sb(V) is crucial to Sb detoxification and resistance. Early research on the mechanisms of Sb(V) reduction was carried out in the *Leishmania* parasite, which causes the disease leishmaniasis (Denton et al. 2004; Zhou et al. 2004). Sb(V)-containing drugs once were widely applied in the treatment of leishmaniasis (Haldar et al. 2011). The reduction of Sb(V) to the more toxic Sb(III) occurs in *Leishmania* (Sereno et al. 1998). The non-enzymatic reduction of Sb(V) by GSH was first revealed by Frézard et al. (2001), showing that Sb(V) could be sufficiently reduced to Sb(III) under the GSH: Sb(V) ratio of 5:1. Subsequently, Denton et al. (2004) reported that a thiol-dependent reductase TDR1 was able to catalyze the Sb(V) reduction with GSH as the reductant. Trypanothione is another reductant inside *Leishmania* that has been found capable of reducing Sb(V) (Yan et al. 2003). The As(V) reductase ACR2 has been observed in *Leishmania major*, and it was able to reduce Sb(V) both in vivo and in vitro (Zhou et al. 2004). Both the TDR1 and ACR2 systems only serve a detoxification function and are unable to produce energy during the reduction.

Recently, the mechanisms of respiratory Sb(V) reduction in prokaryotes have been investigated. By using as *Shewanella* sp. ANA-3 a model organism, Wang et al. (2020) observed that the As(V) reductase gene *arrAB* was highly expressed during respiratory Sb(V) reduction. Disruption of the *arrA* gene in strain ANA-3

inactivated Sb(V) reduction, while an *arrB* disruption decreased the Sb(V) reduction rate by 90%. In vitro study has further confirmed that ArrAB mediates Sb(V) reduction. In addition, the transcription and expression of ArrAB is regulated by quorum sensing through the *luxS* gene, and disruption of the *luxS* gene in strain ANA-3 decreases the Sb(V) reduction rate (Wang et al. 2020). The enrichment of *arrA* in Sb-contaminated anoxic soils has been observed by Kong et al. (2021), suggesting that *arrA* could play an important role in Sb(V) reduction in the environment.

Genes that may be involved in Sb(V) reduction have been revealed by omics approaches. Abin and Hollibaugh (2019) observed that the *anrA* gene was upregulated tenfold during growth of the Sb(V)-reducing bacterium *Desulfuribacillus stibiiarsenatis* MLFW-2 in Sb(V) medium. Furthermore, the *anrA* gene is associated with a respiratory reductase of the dimethyl sulfoxide reductase (DMSOR) family and has been speculated to encode the catalytic subunit of Sb(V) reductase (Abin and Hollibaugh 2019). The putative Sb(V) reductase AnrA was also observed in the meta-transcriptome of strain MLFW-2 (Shi et al. 2019). Furthermore, Yamamura et al. (2021) isolated a dissimilatory Sb(V)-reducing bacterium, *Geobacter* sp. SVR, which was unable to reduce As(V). The *anrA* gene was observed in the genome of strain SVR, while the Sb(V) reductase gene *arrA* was not found. In addition to AnrA, another putative Sb(V) reductase encoded by *SbrA* has been put forward based on the Sb(V) reduction study of a methane-fed bioreactor (Shi et al. 2019). Nevertheless, more evidence is needed before defining either AnrA or SbrA as being Sb(V) reductases.

### 9.4.3 Sb Transport

Sb metabolism is an interplay between oxidation, reduction, uptake, expulsion, and sequestration. The transport of Sb has been regarded as an important resistance mechanism and survival strategy of Sb-respiring microorganisms (Mittal et al. 2007; Rai et al. 2013). The glycerol facilitator GlpF was first identified to play a role in the entry of Sb(III) into *E. coli* (Sanders et al. 1997), in which Sb(III) was recognized as a polyol by the glycerol facilitator. Disruption of the *glpF* gene significantly reduced the uptake of both Sb(III) and As(III) (Meng et al. 2004). The GlpF homolog Fps1, an aquaglyceroporin (AQP) encoded by the *FPS1* gene, was shown to mediate the influx of both Sb(III) and As(III) in *Saccharomyces cerevisiae*. The disruption of *FPS1* has been reported to increase microbial resistance to both Sb(III) and As(III), while *glpF* disruption only increased the resistance to Sb(III) (Sanders et al. 1997; Wysocki et al. 2001). Subsequently, the mammalian AQP subfamilies AQP1, AQP7 and AQP9 were shown to be involved in the uptake of both Sb(III) and As(III) (Liu et al. 2002). The influence of *Aqp1* disruption in *Leishmania* has been tested, and the *Aqp1*-null mutant obtained a greater than tenfold increase in Sb(III) resistance as compared to the wildtype *Leishmania* (Gourbal et al. 2004).

The efflux of Sb is the most direct and effective approach for Sb detoxification. Maciaszczyk-Dziubinska et al. (2010) found that the Acr3 permease could be induced by both Sb(III) and As(III). Disruption of the *ACR3* gene in yeast cells has been found to significantly reduce Sb(III) and As(III) efflux rates, confirming the ability of Acr3 to extrude both Sb(III) and As(III) (Maciaszczyk-Dziubinska et al. 2010). Further study indicated that the maximum As(III) efflux efficiency of Acr3 was threefold higher than that of Sb(III) (Maciaszczyk-Dziubinska et al. 2011). The Acr3 homologs are widely observed in bacteria, archaea, fungi and plant cells, suggesting the significant role of Acr3 in metalloid resistance of organisms (Achour et al. 2007; Fu et al. 2009; Indriolo et al. 2010).

Another well-characterized efflux permease is ArsB, which exists in nearly every extant microorganism (Zhu et al. 2017). ArsB was initially known as an As(III) transporter (Kuroda et al. 1997). Meng et al. (2004) revealed the ability of ArsB to transport inorganic Sb(III) out of *E. coli*. The transport of Sb(III) by ArsB was inhibited by As(III), while Sb(III) increased the efficiency of ArsB-mediated As(III) transport. The *ars* operon also includes *arsA*, *arsC*, *arsD*, *arsJ*, *arsK*, *arsP* and *arsR*. ArsA is the catalytic subunit of As(III)/Sb(III)-transporting ATPase. Although ArsB is able to catalyze Sb(III) alone, the ArsA-ArsB complex has been found to accomplish a higher level of Sb(III) resistance (Meng et al. 2004). An in vivo transport study indicated that ArsB catalyzed electrochemical energy-driven transport, whereas the ArsA-ArsB complex catalysis was driven by chemical energy (Dey and Rosen 1995). In *A. tumefaciens* GW4 the *arsK* gene was found on an As gene island, with *arsK* induced in the presence of either As(III), As(V), or Sb(III) (Shi et al. 2018). The expression of *arsK* reduced the accumulation of As(III) and Sb(III) in *E. coli*, suggesting the ability of ArsK to expel metalloids. The function of *arsR2* gene, which is present upstream of *arsK*, has been investigated. *ArsR2* plays a negative role in regulating the expression of *arsK*. ArsJ was reported to extrude As(V) as the form of 1-arseno-3-phosphoglyceric acid, ArsP showed the capacity of extruding the methylated-As(III) but not inorganic As(III) (Chen et al. 2015b, 2016; Zhao 2016). Nevertheless, the function of ArsJ and ArsP in Sb transport has not been reported. In addition, although ArsC has been confirmed to be an As(V) reductase, its role in Sb transformation remains to be studied (Ben Fekih et al. 2018; Ji and Silver 1992). The *arsD* and *arsR* genes in the *ars* operon encode *trans*-acting regulatory proteins. ArsD and ArsR are able to regulate the *ars* expression at high and low levels of metalloids, respectively Chen and Rosen (1997). The metalloids Sb or As would cause dissociation of the two repressors, induce the expression of *ars* genes and increase the synthesis of the Ars efflux pump (Chen and Rosen 1997).

The ATP-binding cassette protein MRPA could combine with thiol-conjugated metals and subsequently extrude those metals out of the cell. The *mrpA* gene has been observed in many Sb-resistant microorganisms (Leprohon et al. 2009; Mukherjee et al. 2007). Recently, Douanne et al. (2020) found that the disruption of *mrpA* leads to Sb(III) accumulation in *Leishmania infantum*, suggesting that gene plays a role in Sb(III) efflux. An et al. (2021) reported a novel Sb(III) translocating ATPase AntA in *Comamonas testosteroni* JL40. The *ant* operon could be up-regulated by Sb(III), the expression of *antA* in *E. coli* reduced intracellular Sb

(III) accumulation but not As(III) accumulation, which is the first report of a microorganism to specifically extrude Sb(III).

## 9.5 Conclusions and Perspectives

The transformations of Sb are catalyzed by a series of enzymes in diverse environmental microorganisms. Many microorganisms and enzymes are active in both Sb and As metabolism, whereas unique Sb-respiring microorganisms and Sb metabolic pathways have also been discovered. Nevertheless, our knowledge of Sb biotransformation lags behind that of As. Although many Sb-oxidizing microorganisms have been characterized, our knowledge regarding Sb-reducing and Sb-methylating microorganisms is still limited. Only a few genes involved in Sb(III) oxidation and Sb(V) reduction have been identified, and the molecular mechanisms of Sb methylation and demethylation are still ambiguous. The development of omics approaches, SIP techniques and analytical chemistry will accelerate our understanding of the diversity of Sb-respiring microorganisms and functional genes in the natural environment. The biotransformation of Sb is often coupled to the cycling of other elements, such as carbon, nitrogen, sulfur, iron, and is influenced by environmental conditions, such as pH and redox potential. Biotransformation of Sb also is influenced by the microbiological community composition. It will be meaningful to investigate how microbial Sb transformations contribute to the geochemical cycling of Sb in complex environments. Systematic research of the interactions between processes of Sb metabolism and environment variables will provide guidance for the remediation of Sb-contaminated sites.

## References

- Abin CA, Hollibaugh JT (2014) Dissimilatory antimonate reduction and production of antimony trioxide microcrystals by a novel microorganism. *Environ Sci Technol* 48(1):681–688
- Abin CA, Hollibaugh JT (2017) *Desulfuribacillus stibiiarsenatis* sp. nov., an obligately anaerobic, dissimilatory antimonate- and arsenate-reducing bacterium isolated from anoxic sediments, and emended description of the genus *Desulfuribacillus*. *Int J Syst Evol Microbiol* 67(4):1011–1017
- Abin CA, Hollibaugh JT (2019) Transcriptional response of the obligate anaerobe *Desulfuribacillus stibiiarsenatis* MLFW-2T to growth on antimonate and other terminal electron acceptors. *Environ Microbiol* 21(2):618–630
- Achour AR, Bauda P, Billard P (2007) Diversity of arsenite transporter genes from arsenic-resistant soil bacteria. *Res Microbiol* 158(2):128–137
- Álvarez-Ayuso E, Otones V, Murciego A, García-Sánchez A, Santa Regina I (2012) Antimony, arsenic and lead distribution in soils and plants of an agricultural area impacted by former mining activities. *Sci Total Environ* 439:35–43
- An YJ, Kim M (2009) Effect of antimony on the microbial growth and the activities of soil enzymes. *Chemosphere* 74(5):654–659

- An L, Luo X, Wu M, Feng L, Shi K, Wang G, Rosen BP, Li M (2021) *Comamonas testosteroni antA* encodes an antimonite-translocating P-type ATPase. *Sci Total Environ* 754:142393
- Andreae MO, Froelich PN Jr (1984) Arsenic, antimony, and germanium biogeochemistry in the Baltic Sea. *Tellus B Chem Phys Meteorol* 36(2):101–117
- Andrewes P, Cullen WR, Feldmann J, Koch I, Polishchuk E, Reimer KJ (1998) The production of methylated organoantimony compounds by *Scopulariopsis brevicaulis*. *Appl Organomet Chem* 12(12):827–842
- Andrewes P, Cullen WR, Polishchuk E (2000) Arsenic and antimony biomethylation by *Scopulariopsis brevicaulis*: interaction of arsenic and antimony compounds. *Environ Sci Technol* 34(11):2249–2253
- Andrewes P, Cullen WR, Polishchuk E, Reimer KJ (2001) Antimony biomethylation by the wood rotting fungus *Phaeolus schweinitzii*. *Appl Organomet Chem* 15(6):473–480
- Ashley P, Lottermoser B (1999) Arsenic contamination at the mole river mine, northern New South Wales. *Aust J Earth Sci* 46(6):861–874
- Ashley P, Graham B, Tighe M, Wolfenden BJ (2007) Antimony and arsenic dispersion in the Macleay River catchment, New South Wales: a study of the environmental geochemical consequences. *Aust J Earth Sci* 54(1):83–103
- Baeza M, Ren J, Krishnamurthy S, Vaughan TC (2010) Spatial distribution of antimony and arsenic levels in Manadas Creek, an urban tributary of the Rio Grande in Laredo, Texas. *Arch Environ Contam Toxicol* 58(2):299–314
- Beauchemin S, Kwong YJ, Desbarats AJ, MacKinnon T, Percival JB, Parsons MB, Pandya K (2012) Downstream changes in antimony and arsenic speciation in sediments at a mesothermal gold deposit in British Columbia, Canada. *Appl Geochem* 27(10):1953–1965
- Ben Fekih I, Zhang C, Li YP, Zhao Y, Alwathnani HA, Saquib Q, Rensing C, Cervantes C (2018) Distribution of arsenic resistance genes in prokaryotes. *Front Microbiol* 9:2473
- Bentley R, Chasteen TG (2002) Microbial methylation of metalloids: arsenic, antimony, and bismuth. *Microbiol Mol Biol Rev* 66(2):250–271
- Bhattacharjee H, Li J, Ksenzenko MY, Rosen BP (1995) Role of cysteinyl residues in metalloactivation of the oxyanion-translocating ArsA ATPase. *J Biol Chem* 270(19):11245–11250
- Bobrowicz P, Wysocki R, Owsianik G, Goffeau A, Ułaszewski S (1997) Isolation of three contiguous genes, ACR1, ACR2 and ACR3, involved in resistance to arsenic compounds in the yeast *Saccharomyces cerevisiae*. *Yeast* 13(9):819–828
- Boriová K, Čerňanský S, Matúš P, Bujdoš M, Šimonovičová A (2014) Bioaccumulation and biovolatilization of various elements using filamentous fungus *Scopulariopsis brevicaulis*. *Lett Appl Microbiol* 59(2):217–223
- Casiot C, Ujevic M, Munoz M, Seidel J, Elbaz-Poulichet F (2007) Antimony and arsenic mobility in a creek draining an antimony mine abandoned 85 years ago (upper Orb basin, France). *Appl Geochem* 22(4):788–798
- Chen Y, Rosen BP (1997) Metalloregulatory properties of the ArsD repressor. *J Biol Chem* 272(22):14257–14262
- Chen F, Cao Y, Wei S, Li Y, Li X, Wang Q, Wang G (2015a) Regulation of arsenite oxidation by the phosphate two-component system PhoBR in *Halomonas* sp. HAL1. *Front Microbiol* 6:923
- Chen J, Madegowda M, Bhattacharjee H, Rosen BP (2015b) ArsP: a methylarsenite efflux permease. *Mol Microbiol* 98(4):625–635
- Chen J, Yoshinaga M, Garbinski LD, Rosen BP (2016) Synergistic interaction of glyceraldehyde-3-phosphate dehydrogenase and ArsJ, a novel organoarsenical efflux permease, confers arsenate resistance. *Mol Microbiol* 100(6):945–953
- Choi W, Yu J, Lee T (2017) Microbial oxidation of antimonite and arsenite by bacteria isolated from antimony-contaminated soils. *Int J Hydrog Energy* 42(45):27832–27842
- Cidu R, Dore E, Biddau R, Nordstrom DK (2018) Fate of antimony and arsenic in contaminated waters at the abandoned Su Suergiu mine (Sardinia, Italy). *Mine Water Environ* 37(1):151–165



- Craig P, Jenkins R, Dewick R, Miller D (1999) Trimethylantimony generation by *Scopulariopsis brevicaulis* during aerobic growth. *Sci Total Environ* 229(1–2):83–88
- Culioli JL, Fouquoire A, Calendini S, Mori C, Orsini A (2009) Trophic transfer of arsenic and antimony in a freshwater ecosystem: a field study. *Aquat Toxicol* 94(4):286–293
- Denton H, McGregor JC, Coombs GH (2004) Reduction of anti-leishmanial pentavalent antimonial drugs by a parasite-specific thiol-dependent reductase, TDR1. *Biochem J* 381(2):405–412
- Dey S, Rosen BP (1995) Dual mode of energy coupling by the oxyanion-translocating ArsB protein. *J Bacteriol* 177(2):385–389
- Douanne N, Wagner V, Roy G, Leprohon P, Ouellette M, Fernandez-Prada C (2020) MRPA-independent mechanisms of antimony resistance in *Leishmania infantum*. *Int J Parasitol Drugs Drug Resist* 13:28–37
- Douay F, Pruvot C, Roussel H, Ciesielski H, Fourier H, Proix N, Waterlot C (2008) Contamination of urban soils in an area of Northern France polluted by dust emissions of two smelters. *Water Air Soil Pollut* 188(1):247–260
- Dupont D, Arnout S, Jones PT, Binnemans K (2016) Antimony recovery from end-of-life products and industrial process residues: a critical review. *J Sustain Metall* 2(1):79–103
- Duval S, Ducluzeau AL, Nitschke W, Schoepp-Cothenet B (2008) Enzyme phylogenies as markers for the oxidation state of the environment: the case of respiratory arsenate reductase and related enzymes. *BMC Evol Biol* 8(1):1–13
- Filella M (2010) Alkyl derivatives of antimony in the environment. In: Sigel A, Sigel H, Sigel RKO (eds) *Organometallics in environment and toxicology*. Royal Society of Chemistry, pp 267–301
- Filella M, Belzile N, Chen YW (2002) Antimony in the environment: a review focused on natural waters: I. Occurrence. *Earth Sci Rev* 57(1–2):125–176
- Flynn HC, Meharg AA, Bowyer PK, Paton GI (2003) Antimony bioavailability in mine soils. *Environ Pollut* 124(1):93–100
- Frézard F, Demicheli C, Ferreira CS, Costa MA (2001) Glutathione-induced conversion of pentavalent antimony to trivalent antimony in meglumine antimoniate. *Antimicrob Agents Chemother* 45(3):913–916
- Fu HL, Meng Y, Ordóñez E, Villadangos AF, Bhattacharjee H, Gil JA, Mateos LM, Rosen BP (2009) Properties of arsenite efflux permeases (Acr3) from *Alkaliphilus metalliredigens* and *Corynebacterium glutamicum*. *J Biol Chem* 284(30):19887–19895
- Gourbal B, Sonuc N, Bhattacharjee H, Legare D, Sundar S, Ouellette M, Rosen BP, Mukhopadhyay R (2004) Drug uptake and modulation of drug resistance in *Leishmania* by an aquaglyceroporin. *J Biol Chem* 279(30):31010–31017
- Gu J, Sunahara G, Duran R, Yao J, Cui Y, Tang C, Li H, Mihucz VG (2019) Sb(III)-resistance mechanisms of a novel bacterium from non-ferrous metal tailings. *Ecotoxicol Environ Saf* 186: 109773
- Guillamot F, Calvert V, Millot MV, Criquet S (2014) Does antimony affect microbial respiration in Mediterranean soils? A microcosm experiment. *Pedobiologia* 57(2):119–121
- Gürleyük H, Van Fleet-Stalder V, Chasteen TG (1997) Confirmation of the biomethylation of antimony compounds. *Appl Organomet Chem* 11(6):471–483
- Haldar AK, Sen P, Roy S (2011) Use of antimony in the treatment of leishmaniasis: current status and future directions. *Mol Biol Int*. <https://doi.org/10.4061/2011/571242>
- Hamamura N, Fukushima K, Itai T (2013) Identification of antimony- and arsenic-oxidizing bacteria associated with antimony mine tailing. *Microbes Environ* 28:257–263
- Han Y, Zhang F, Wang Q, Zheng S, Guo W, Feng L, Wang G (2016) *Flavihumibacter stibioxidans* sp. nov., an antimony-oxidizing bacterium isolated from antimony mine soil. *Int J Syst Evol Microbiol* 66(11):4676–4680
- Hartmann LM, Craig PJ, Jenkins RO (2003) Influence of arsenic on antimony methylation by the aerobic yeast *Cryptococcus humicola*. *Arch Microbiol* 180(5):347–352
- He M, Yang J (1999) Effects of different forms of antimony on rice during the period of germination and growth and antimony concentration in rice tissue. *Sci Total Environ* 243:149–155

- He M, Wang N, Long X, Zhang C, Ma C, Zhong Q, Wang A, Wang Y, Pervaiz A, Shan J (2019) Antimony speciation in the environment: recent advances in understanding the biogeochemical processes and ecological effects. *J Environ Sci* 75:14–39
- Herath I, Vithanage M, Bundschuh J (2017) Antimony as a global dilemma: geochemistry, mobility, fate and transport. *Environ Pollut* 223:545–559
- Hiller E, Lalinská B, Chovan M, Jurkovič E, Klimko T, Jankulár M, Hovorič R, Šottník P, Flaková R, Ženišová Z (2012) Arsenic and antimony contamination of waters, stream sediments and soils in the vicinity of abandoned antimony mines in the Western Carpathians, Slovakia. *Appl Geochem* 27(3):598–614
- Hockmann K, Lenz M, Tandy S, Nachtegaal M, Janousch M, Schulin R (2014) Release of antimony from contaminated soil induced by redox changes. *J Hazard Mater* 275:215–221
- Hoffman LE, Hendrix JL (1976) Inhibition of *Thiobacillus ferrooxidans* by soluble silver. *Biotechnol Bioeng* 18(8):1161–1165
- Indriolo E, Na G, Ellis D, Salt DE, Banks JA (2010) A vacuolar arsenite transporter necessary for arsenic tolerance in the arsenic hyperaccumulating fern *Pteris vittata* is missing in flowering plants. *Plant Cell* 22(6):2045–2057
- Janowiak BE, Griffith OW (2005) Glutathione synthesis in *Streptococcus agalactiae*: one protein accounts for  $\gamma$ -glutamylcysteine synthetase and glutathione synthetase activities. *J Biol Chem* 280(12):11829–11839
- Jenkins R, Craig P, Miller D, Stoop L, Ostah N, Morris TA (1998a) Antimony biomethylation by mixed cultures of micro-organisms under anaerobic conditions. *Appl Organomet Chem* 12(6):449–455
- Jenkins RO, Craig PJ, Goessler W, Miller D, Ostah N, Irgolic KJ (1998b) Biomethylation of inorganic antimony compounds by an aerobic fungus: *Scopulariopsis brevicaulis*. *Environ Sci Technol* 32(7):882–885
- Jenkins RO, Forster SN, Craig PJ (2002) Formation of methylantimony species by an aerobic prokaryote: *Flavobacterium* sp. *Arch Microbiol* 178(4):274–278
- Ji G, Silver S (1992) Reduction of arsenate to arsenite by the ArsC protein of the arsenic resistance operon of *Staphylococcus aureus* plasmid pI258. *Proc Natl Acad Sci U S A* 89(20):9474–9478
- Johnson CA, Moench H, Wersin P, Kugler P, Wenger C (2005) Solubility of antimony and other elements in samples taken from shooting ranges. *J Environ Qual* 34(1):248–254
- Kong T, Lin H, Xiao E, Xiao T, Gao P, Li B, Xu F, Qiu L, Wang X, Sun X (2021) Investigation of the antimony fractions and indigenous microbiota in aerobic and anaerobic rice paddies. *Sci Total Environ* 771:145408
- Krenev V, Dergacheva N, Fomichev S (2015) Antimony: resources, application fields, and world market. *Theor Found Chem Eng* 49(5)
- Kulp TR, Miller LG, Braiotta F, Webb SM, Kocar BD, Blum JS, Oremland RS (2014) Microbiological reduction of Sb (V) in anoxic freshwater sediments. *Environ Sci Technol* 48(1):218–226
- Kuroda M, Dey S, Sanders OI, Rosen BP (1997) Alternate energy coupling of ArsB, the membrane subunit of the Ars anion-translocating ATPase. *J Biol Chem* 272(1):326–331
- Lai CY, Wen LL, Zhang Y, Luo SS, Wang QY, Luo YH, Chen R, Yang X, Rittmann BE, Zhao HP (2016) Autotrophic antimonate bio-reduction using hydrogen as the electron donor. *Water Res* 88:467–474
- Lai CY, Dong QY, Rittmann BE, Zhao HP (2018a) Bioreduction of antimonate by anaerobic methane oxidation in a membrane biofilm batch reactor. *Environ Sci Technol* 52(15):8693–8700
- Lai CY, Dong QY, Zhao HP (2018b) Oxygen exposure deprives antimonate-reducing capability of a methane fed biofilm. *Sci Total Environ* 644:1152–1159
- Lehr CR, Kashyap DR, McDermott TR (2007) New insights into microbial oxidation of antimony and arsenic. *Appl Environ Microbiol* 73(7):2386–2389
- LePan N (2020) All the world's metals and minerals in one visualization. *Visual Capitalist*, Vancouver

- Leprohon P, Legare D, Raymond F, Madore E, Hardiman G, Corbeil J, Ouellette M (2009) Gene expression modulation is associated with gene amplification, supernumerary chromosomes and chromosome loss in antimony-resistant *Leishmania infantum*. *Nucleic Acids Res* 37(5): 1387–1399
- Leuz AK, Johnson CA (2005) Oxidation of Sb (III) to Sb (V) by O<sub>2</sub> and H<sub>2</sub>O<sub>2</sub> in aqueous solutions. *Geochim Cosmochim Acta* 69(5):1165–1172
- Leuz AK, Hug SJ, Wehrli B, Johnson CA (2006) Iron-mediated oxidation of antimony (III) by oxygen and hydrogen peroxide compared to arsenic (III) oxidation. *Environ Sci Technol* 40(8): 2565–2571
- Li J, Wang Q, Zhang S, Qin D, Wang G (2013) Phylogenetic and genome analyses of antimony-oxidizing bacteria isolated from antimony mined soil. *Int Biodeterior Biodegradation* 76:76–80
- Li J, Wang Q, Li M, Yang B, Shi M, Guo W, McDermott TR, Rensing C, Wang G (2015) Proteomics and genetics for identification of a bacterial antimonite oxidase in *Agrobacterium tumefaciens*. *Environ Sci Technol* 49(10):5980–5989
- Li J, Wang Q, Oremland RS, Kulp TR, Rensing C, Wang G (2016) Microbial antimony biogeochemistry: enzymes, regulation, and related metabolic pathways. *Appl Environ Microbiol* 82(18):5482–5495
- Li J, Yang B, Shi M, Yuan K, Guo W, Wang Q, Wang G (2017) Abiotic and biotic factors responsible for antimonite oxidation in *Agrobacterium tumefaciens* GW4. *Sci Rep* 7(1):43225
- Li J, Yu H, Wu X, Shen L, Liu Y, Qiu G, Zeng W, Yu R (2018) Novel hyper antimony-oxidizing bacteria isolated from contaminated mine soils in China. *Geomicrobiol J* 35(8):713–720
- Li J, Zhang Y, Zheng S, Liu F, Wang G (2019) Anaerobic bacterial immobilization and removal of toxic Sb (III) coupled with Fe(II)/Sb(III) oxidation and denitrification. *Front Microbiol* 10:360
- Li Y, Zhang M, Xu R, Lin H, Sun X, Xu F, Gao P, Kong T, Xiao E, Yang N, Sun W (2021) Arsenic and antimony co-contamination influences on soil microbial community composition and functions: relevance to arsenic resistance and carbon, nitrogen, and sulfur cycling. *Environ Int* 153:106522
- Lialikova N (1967) Antimonite oxidation by a new culture of *Thiobacteria*. *Dokl Akad Nauk SSSR* 176(6):1432–1434
- Lialikova N (1974) *Stibiobacter senarmontii* - a new microorganism oxidizing antimony. *Mikrobiologiya* 43(6):941–948
- Liu Z, Shen J, Carbrejy JM, Mukhopadhyay R, Agre P, Rosen BP (2002) Arsenite transport by mammalian aquaglyceroporins AQP7 and AQP9. *Proc Natl Acad Sci* 99(9):6053–6058
- Liu F, Zhang G, Liu S, Fu Z, Chen J, Ma C (2018) Bioremoval of arsenic and antimony from wastewater by a mixed culture of sulfate-reducing bacteria using lactate and ethanol as carbon sources. *Int Biodeterior Biodegradation* 126:152–159
- Long X, Wang X, Guo X, He M (2020) A review of removal technology for antimony in aqueous solution. *J Environ Sci* 90:189–204
- Loni PC, Wu M, Wang W, Wang H, Ma L, Liu C, Song Y, Tuovinen OH (2020) Mechanism of microbial dissolution and oxidation of antimony in stibnite under ambient conditions. *J Hazard Mater* 385:121561
- Lu X, Zhang Y, Liu C, Wu M, Wang H (2018) Characterization of the antimonite-and arsenite-oxidizing bacterium *Bosea* sp. AS-1 and its potential application in arsenic removal. *J Hazard Mater* 359:527–534
- Luo J, Bai Y, Liang J, Qu J (2014) Metagenomic approach reveals variation of microbes with arsenic and antimony metabolism genes from highly contaminated soil. *PLoS One* 9(10): e108185
- Ma JF, Ochsner UA, Klotz MG, Nanayakkara VK, Howell ML, Johnson Z, Posey JE, Vasil ML, Monaco JJ, Hassett DJ (1999) Bacterioferritin A modulates catalase A (KatA) activity and resistance to hydrogen peroxide in *Pseudomonas aeruginosa*. *J Bacteriol* 181(12):3730–3742
- Macgregor K, MacKinnon G, Farmer JG, Graham MC (2015) Mobility of antimony, arsenic and lead at a former antimony mine, Glendinning, Scotland. *Sci Total Environ* 529:213–222

- Maciaszczyk-Dziubinska E, Wawrzycka D, Sloma E, Migocka M, Wysocki R (2010) The yeast permease Acr3p is a dual arsenite and antimonite plasma membrane transporter. *Biochim Biophys Acta* 1798(11):2170–2175
- Maciaszczyk-Dziubinska E, Migocka M, Wysocki R (2011) Acr3p is a plasma membrane antiporter that catalyzes As (III)/H<sup>+</sup> and Sb (III)/H<sup>+</sup> exchange in *Saccharomyces cerevisiae*. *Biochim Biophys Acta* 1808(7):1855–1859
- Meng YL, Liu Z, Rosen BP (2004) As (III) and Sb (III) uptake by GlpF and efflux by ArsB in *Escherichia coli*. *J Biol Chem* 279(18):18334–18341
- Meyer J, Schmidt A, Michalke K, Hensel R (2007) Volatilisation of metals and metalloids by the microbial population of an alluvial soil. *Syst Appl Microbiol* 30(3):229–238
- Michalke K, Wickenheiser E, Mehring M, Hirner A, Hensel R (2000) Production of volatile derivatives of metal(loid)s by microflora involved in anaerobic digestion of sewage sludge. *Appl Environ Microbiol* 66(7):2791–2796
- Michalski R, Jabłońska-Czapla M, Szopa S, Łyko A, Grygoyć K (2016) Variability in different antimony, arsenic and chromium species in waters and bottom sediments of three water reservoirs in Upper Silesia (Poland): a comparative study. *Int J Environ Anal Chem* 96(7): 682–693
- Mittal MK, Rai S, Gupta S, Sundar S, Goyal N (2007) Characterization of natural antimony resistance in *Leishmania donovani* isolates. *Am J Trop Med Hyg* 76(4):681–688
- Mukherjee A, Padmanabhan PK, Singh S, Roy G, Girard I, Chatterjee M, Ouellette M, Madhubala R (2007) Role of ABC transporter MRPA,  $\gamma$ -glutamylcysteine synthetase and ornithine decarboxylase in natural antimony-resistant isolates of *Leishmania donovani*. *J Antimicrob Chemother* 59(2):204–211
- Multani RS, Feldmann T, Demopoulos GP (2016) Antimony in the metallurgical industry: a review of its chemistry and environmental stabilization options. *Hydrometallurgy* 164:141–153
- Nguyen VK, Lee JU (2014) Isolation and characterization of antimony-reducing bacteria from sediments collected in the vicinity of an antimony factory. *Geomicrobiol J* 31(10):855–861
- Nguyen VK, Lee JU (2015) Antimony-oxidizing bacteria isolated from antimony-contaminated sediment—a phylogenetic study. *Geomicrobiol J* 32(1):50–58
- Nguyen DD, Ha M-G, Kang HY (2021) Potential of versatile bacteria isolated from activated sludge for the bioremediation of arsenic and antimony. *J Water Process Eng* 39:101890
- Obiakor MO, Wilson SC, Tighe M, Pereg L (2019) Antimony causes mortality and induces mutagenesis in the soil functional bacterium *Azospirillum brasilense* Sp7. *Water Air Soil Pollut* 230(8):183
- Oorts K, Smolders E, Degryse F, Buekers J, Gascó G, Cornelis G, Mertens J (2008) Solubility and toxicity of antimony trioxide (Sb<sub>2</sub>O<sub>3</sub>) in soil. *Environ Sci Technol* 42(12):4378–4383
- Park SC, Boyanov MI, Kemner KM, O’Loughlin EJ, Kwon MJ (2021) Distribution and speciation of Sb and toxic metal (loid) s near an antimony refinery and their effects on indigenous microorganisms. *J Hazard Mater* 403:123625
- Pierart A, Shahid M, Séjalon-Delmas N, Dumat C (2015) Antimony bioavailability: knowledge and research perspectives for sustainable agricultures. *J Hazard Mater* 289:219–234
- Pratas J, Prasad M, Freitas H, Conde L (2005) Plants growing in abandoned mines of Portugal are useful for biogeochemical exploration of arsenic, antimony, tungsten and mine reclamation. *J Geochem Explor* 85(3):99–107
- Quentel F, Filella M, Elleouet C, Madec CL (2004) Kinetic studies on Sb (III) oxidation by hydrogen peroxide in aqueous solution. *Environ Sci Technol* 38(10):2843–2848
- Rai S, Goel SK, Dwivedi UN, Sundar S, Goyal N (2013) Role of efflux pumps and intracellular thiols in natural antimony resistant isolates of *Leishmania donovani*. *PLoS One* 8(9):e74862
- Rapant S, Dietzová Z, Cicmanová S (2006) Environmental and health risk assessment in abandoned mining area, Zlata Idka, Slovakia. *Environ Geol* 51(3):387–397
- Ritchie VJ, Ilgen AG, Mueller SH, Trainor TP, Goldfarb RJ (2013) Mobility and chemical fate of antimony and arsenic in historic mining environments of the Kantishna Hills district, Denali National Park and Preserve, Alaska. *Chem Geol* 335:172–188

- Rouvray DH (2004) Elements in the history of the Periodic Table. *Endeavour* 28(2):69–74
- Saltikov CW, Cifuentes A, Venkateswaran K, Newman DK (2003) The ars detoxification system is advantageous but not required for As (V) respiration by the genetically tractable *Shewanella* species strain ANA-3. *Appl Environ Microbiol* 69(5):2800–2809
- Sanders OI, Rensing C, Kuroda M, Mitra B, Rosen BP (1997) Antimonite is accumulated by the glycerol facilitator GlpF in *Escherichia coli*. *J Bacteriol* 179(10):3365–3367
- Sereno D, Cavaleyra M, Zemzoumi K, Maquaire S, Ouaiissi A, Lemesre J (1998) Axenically grown amastigotes of *Leishmania infantum* used as an in vitro model to investigate the pentavalent antimony mode of action. *Antimicrob Agents Chemother* 42(12):3097–3102
- Serfor-Armah Y, Nyarko B, Dampare S, Adomako D (2006) Levels of arsenic and antimony in water and sediment from Prestea, a gold mining town in Ghana and its environs. *Water Air Soil Pollut* 175(1):181–192
- Shi Z, Cao Z, Qin D, Zhu W, Wang Q, Li M, Wang G (2013) Correlation models between environmental factors and bacterial resistance to antimony and copper. *PLoS One* 8(10):e78533
- Shi K, Fan X, Qiao Z, Han Y, McDermott TR, Wang Q, Wang G (2017) Arsenite oxidation regulator AioR regulates bacterial chemotaxis towards arsenite in *Agrobacterium tumefaciens* GW4. *Sci Rep* 7(1):43252
- Shi K, Li C, Rensing C, Dai X, Fan X, Wang G (2018) Efflux transporter ArsK is responsible for bacterial resistance to arsenite, antimonite, trivalent roxarsone, and methylarsenite. *Appl Environ Microbiol* 84(24):e01842–e01818
- Shi LD, Wang M, Han YL, Lai CY, Shapleigh JP, Zhao HP (2019) Multi-omics reveal various potential antimonate reductases from phylogenetically diverse microorganisms. *Appl Microbiol Biotechnol* 103(21):9119–9129
- Silver M, Torma AE (1974) Oxidation of metal sulfides by *Thiobacillus ferrooxidans* grown on different substrates. *Can J Microbiol* 20(2):141–147
- Smith L, Craig P, Jenkins R (2002a) Formation of involatile methylantimony species by *Clostridium* spp. *Chemosphere* 47(4):401–407
- Smith L, Maher W, Craig P, Jenkins R (2002b) Speciation of volatile antimony compounds in culture headspace gases of *Cryptococcus humicolus* using solid phase microextraction and gas chromatography-mass spectrometry. *Appl Organomet Chem* 16(6):287–293
- Stauffer RE, Thompson JM (1984) Arsenic and antimony in geothermal waters of Yellowstone National Park, Wyoming, USA. *Geochim Cosmochim Acta* 48(12):2547–2561
- Sun W, Xiao E, Dong Y, Tang S, Krumins V, Ning Z, Sun M, Zhao Y, Wu S, Xiao T (2016) Profiling microbial community in a watershed heavily contaminated by an active antimony (Sb) mine in Southwest China. *Sci Total Environ* 550:297–308
- Sun W, Xiao E, Xiao T, Krumins V, Wang Q, Häggblom M, Dong Y, Tang S, Hu M, Li B (2017) Response of soil microbial communities to elevated antimony and arsenic contamination indicates the relationship between the innate microbiota and contaminant fractions. *Environ Sci Technol* 51(16):9165–9175
- Sun Q, Cui PX, Liu C, Peng SM, Alves ME, Zhou DM, Shi ZQ, Wang YJ (2019a) Antimony oxidation and sorption behavior on birnessites with different properties ( $\delta$ -MnO<sub>2</sub> and triclinic birnessite). *Environ Pollut* 246:990–998
- Sun W, Sun X, Li B, Häggblom MM, Han F, Xiao E, Zhang M, Wang Q, Li F (2019b) Bacterial response to antimony and arsenic contamination in rice paddies during different flooding conditions. *Sci Total Environ* 675:273–285
- Sun X, Li B, Han F, Xiao E, Xiao T, Sun W (2019c) Impacts of arsenic and antimony co-contamination on sedimentary microbial communities in rivers with different pollution gradients. *Microb Ecol* 78(3):589–602
- Sun LN, Guo B, Lyu WG, Tang XJ (2020) Genomic and physiological characterization of an antimony and arsenite-oxidizing bacterium *Roseomonas rhizosphaerae*. *Environ Res* 191:110136

- Telford K, Maher W, Krikowa F, Foster S, Ellwood MJ, Ashley PM, Lockwood PV, Wilson SC (2009) Bioaccumulation of antimony and arsenic in a highly contaminated stream adjacent to the Hillgrove Mine, NSW, Australia. *Environ Chem* 6(2):133–143
- Terry LR, Kulp TR, Wiatrowski H, Miller LG, Oremland RS (2015) Microbiological oxidation of antimony (III) with oxygen or nitrate by bacteria isolated from contaminated mine sediments. *Appl Environ Microbiol* 81(24):8478–8488
- Tighe M, Ashley P, Lockwood P, Wilson S (2005) Soil, water, and pasture enrichment of antimony and arsenic within a coastal floodplain system. *Sci Total Environ* 347(1–3):175–186
- Torma A, Gabra G (1977) Oxidation of stibnite by *Thiobacillus ferrooxidans*. *Antonie Van Leeuwenhoek* 43(1):1–6
- Tschan M, Robinson BH, Schulin R (2009) Antimony in the soil-plant system - a review. *Environ Chem* 6(2):106–115
- Wang Q, He M, Wang Y (2011) Influence of combined pollution of antimony and arsenic on culturable soil microbial populations and enzyme activities. *Ecotoxicology* 20(1):9–19
- Wang X, He M, Lin C, Gao Y, Zheng L (2012) Antimony (III) oxidation and antimony (V) adsorption reactions on synthetic manganite. *Geochemistry* 72:41–47
- Wang Q, Warelow TP, Kang Y-S, Romano C, Osborne TH, Lehr CR, Bothner B, McDermott TR, Santini JM, Wang G (2015) Arsenite oxidase also functions as an antimonite oxidase. *Appl Environ Microbiol* 81(6):1959–1965
- Wang D, Zhu F, Wang Q, Rensing C, Yu P, Gong J, Wang G (2016) Disrupting ROS-protection mechanism allows hydrogen peroxide to accumulate and oxidize Sb (III) to Sb (V) in *Pseudomonas stutzeri* TS44. *BMC Microbiol* 16(1):1–11
- Wang L, Ye L, Yu Y, Jing C (2018) Antimony redox biotransformation in the subsurface: effect of indigenous Sb (V) respiring microbiota. *Environ Sci Technol* 52(3):1200–1207
- Wang L, Ye L, Jing C (2020) Genetic identification of antimonate respiratory reductase in *Shewanella* sp. ANA-3. *Environ Sci Technol* 54(21):14107–14113
- Warnken J, Ohlsson R, Welsh DT, Teasdale PR, Chelsky A, Bennett WW (2017) Antimony and arsenic exhibit contrasting spatial distributions in the sediment and vegetation of a contaminated wetland. *Chemosphere* 180:388–395
- Wehmeier S, Feldmann J (2005) Investigation into antimony mobility in sewage sludge fermentation. *J Environ Monit* 7(12):1194–1199
- Wei C, Ge Z, Chu W, Feng R (2015) Speciation of antimony and arsenic in the soils and plants in an old antimony mine. *Environ Exp Bot* 109:31–39
- Wilson N, Craw D, Hunter K (2004) Antimony distribution and environmental mobility at an historic antimony smelter site, New Zealand. *Environ Pollut* 129(2):257–266
- Wilson SC, Lockwood PV, Ashley PM, Tighe M (2010) The chemistry and behaviour of antimony in the soil environment with comparisons to arsenic: a critical review. *Environ Pollut* 158(5):1169–1181
- Wysocki R, Chéry CC, Wawrzycka D, Van Hulle M, Cornelis R, Thevelein JM, Tamás MJ (2001) The glycerol channel Fps1p mediates the uptake of arsenite and antimonite in *Saccharomyces cerevisiae*. *Mol Microbiol* 40(6):1391–1401
- Yamamura S, Iida C, Kobayashi Y, Watanabe M, Amachi S (2021) Production of two morphologically different antimony trioxides by a novel antimonate-reducing bacterium, *Geobacter* sp. SVR. *J Hazard Mater* 411:125100
- Yan S, Li F, Ding K, Sun H (2003) Reduction of pentavalent antimony by trypanothione and formation of a binary and ternary complex of antimony (III) and trypanothione. *J Biol Inorg Chem* 8(6):689–697
- Yang Z, Hosokawa H, Sadakane T, Kuroda M, Inoue D, Nishikawa H, Ike M (2020) Isolation and characterization of facultative-anaerobic antimonate-reducing bacteria. *Microorganisms* 8(9):1435
- Yang Z, Hosokawa H, Kuroda M, Inoue D, Ike M (2021a) Microbial antimonate reduction and removal potentials in river sediments. *Chemosphere* 266:129192

- Yang Z, Sadakane T, Hosokawa H, Kuroda M, Inoue D, Ike M (2021b) Factors affecting antimonate bioreduction by *Dechloromonas* sp. AR-2 and *Propionivibrio* sp. AR-3. *3 Biotech* 11(4):163
- Yu H, Zheng X, Weng W, Yan X, Chen P, Liu X, Peng T, Zhong Q, Xu K, Wang C (2021) Synergistic effects of antimony and arsenic contaminations on bacterial, archaeal and fungal communities in the rhizosphere of *Miscanthus sinensis*: insights for nitrification and carbon mineralization. *J Hazard Mater* 411:125094
- Zhang H, Hu X (2019) Bioadsorption and microbe-mediated reduction of Sb (V) by a marine bacterium in the presence of sulfite/thiosulfate and the mechanism study. *Chem Eng J* 359:755–764
- Zhang G, Liu CQ, Liu H, Hu J, Han G, Li L (2009) Mobilisation and transport of arsenic and antimony in the adjacent environment of Yata gold mine, Guizhou province, China. *J Environ Monit* 11(9):1570–1578
- Zhang G, Ouyang X, Li H, Fu Z, Chen J (2016) Bioremoval of antimony from contaminated waters by a mixed batch culture of sulfate-reducing bacteria. *Int Biodeterior Biodegradation* 115:148–155
- Zhang J, Chen J, Wu Y, Wang Z, Qiu J, Li X, Cai F, Xiao K, Sun X, Rosen B, Zhao F (2021a) Oxidation of organoarsenicals and antimonite by a novel flavin monooxygenase widely present in soil bacteria. *Environ Microbiol.* <https://doi.org/10.1111/1462-2920.15488>
- Zhang M, Kolton M, Li Z, Lin H, Li F, Lu G, Gao P, Sun X, Xu R, Xu F, Sun W (2021b) Bacteria responsible for antimonite oxidation in antimony-contaminated soil revealed by DNA-SIP coupled to metagenomics. *FEMS Microbiol Ecol* 97(5):fiab057
- Zhang M, Li Z, Häggblom MM, Young L, Li F, He Z, Lu G, Xu R, Sun X, Qiu L (2021c) Bacteria responsible for nitrate-dependent antimonite oxidation in antimony-contaminated paddy soil revealed by the combination of DNA-SIP and metagenomics. *Soil Biol Biochem* 156:108194
- Zhao FJ (2016) A novel pathway of arsenate detoxification. *Mol Microbiol* 100(6):928–930
- Zhou Y, Messier N, Ouellette M, Rosen BP, Mukhopadhyay R (2004) *Leishmania major* LmACR2 is a pentavalent antimony reductase that confers sensitivity to the drug pentostam. *J Biol Chem* 279(36):37445–37451
- Zhou J, Nyirenda MT, Xie L, Li Y, Zhou B, Zhu Y, Liu H (2017) Mine waste acidic potential and distribution of antimony and arsenic in waters of the Xikuangshan mine, China. *Appl Geochem* 77:52–61
- Zhu YG, Xue XM, Kappler A, Rosen BP, Meharg AA (2017) Linking genes to microbial biogeochemical cycling: lessons from arsenic. *Environ Sci Technol* 51(13):7326–7339

# Chapter 10

## Microbial Remediation of Chromium



**M. Gomathy, K. G. Sabarinathan, K. S. Subramaian, T. Sivashankari Devi, K. Ananthi, P. Kalaiselvi, and M. Jeysree**

**Abstract** Chromium is considered to be an environmental pollutant and a threatening agent to human health. Due to the industrial applications of this particular metal, usage presently is unavoidable and hence requires remediation technologies. There are several technologies employed for remediation of chromium, among them bioremediation finds a first and foremost place as it is cheap and environmentally friendly. Availability and toxicity of chromium depend on its speciation where Cr (VI) is highly toxic and Cr (III) is less toxic. Plants lack specific transport mechanisms for chromium and it invades the plants with other essential ions such as sulfates and iron. Microorganisms are employed for remediation of chromium affected soils which not only removes the pollutants from the soil but also helps to grow crops in those contaminated sites. Among the microbes, AM fungi have proven to be a good candidate to remove the contaminant through a process called rhizofiltration, where the chromium remains in the roots without being translocated to the vegetative and reproductive parts of the plants. Microorganisms have adapted several mechanisms to overcome chromium toxicity, including biosorption, solubilization, complexation, precipitation, binding, and dilution. In recent years, the popularity of using bioremediation techniques for decontaminating polluted sites is increasing and researchers are concentrating efforts on using microbial remediation to overcome chromium contamination. This chapter gives an overview of the above-discussed points and gives additional insight into microbial remediation of chromium.

---

M. Gomathy (✉) · K. G. Sabarinathan · K. S. Subramaian · T. Sivashankari Devi · K. Ananthi · P. Kalaiselvi · M. Jeysree  
Tamil Nadu Agricultural University, Coimbatore, Tamil Nadu, India



## 10.1 Understanding Environmental Contamination by Heavy Metals

Heavy metals are creating problems for humankind due to the overutilization of resources and industrial establishments to meet the needs of our growing population (Medfu et al. 2020). Nowadays, heavy metal contamination has become a significant environmental issue that needs an immediate solution (Igiri et al. 2018; Siddiquee et al. 2015) as it leads to serious threats to the ecosystem and its living creatures (Okolo et al. 2016). According to a report by the Environmental Protection Agency (EPA) 2010, microbial processes are much needed to degrade and transform the hazardous contaminants into less or nontoxic forms which ultimately remediate the environment or soil. Microbes have the ability to use the chemical pollutants for their energy and degrade them through their metabolic processes. However, an overload of inorganic nutrients in soil can inhibit the necessary microbial populations (Ahirwar et al. 2015).

These heavy metals can be defined on the basis of density, atomic number, and chemical properties. Bioavailability of heavy metals depends on the absorbed dose (Okolo et al. 2016). Most agrochemicals, especially pesticides, are both organic and inorganic in nature and even sometimes contain Hg, As, Cu, Zn, and other heavy metals (Arao et al. 2010). These agrochemicals tend to contaminate soil and water bodies. One important point to be noted is the fate of these heavy metal pollutants as they remain in the environment for an indefinite period of time and many organo-metallic compounds will not degrade easily (Ferraz et al. 2012). We need to give attention and help develop specific mechanisms to break or degrade them in environments where they are creating a problem.

Concentration and type of heavy metals in the environment vary with respect to ecosystem and influence human health. Higher concentrations of heavy metals cause severe diseases (Poli et al. 2009) and accumulate in the body systems (Hussain et al. 2013). They exist as such inside the tissues where they can have a longer biological half-life and also easily bind with various biomolecules viz., proteins, nucleic acids, and metabolites (Yu 2001). Heavy metals, especially Cr, that emerge from tanneries caused serious soil degradation besides causing extensive damage to human health (Suganya 2004).

### 10.1.1 Industrial Uses of Chromium

Chromium, has several applications in many industries viz., steel industries for manufacturing of stainless steel, where Cr is used to harden the steel, to polishing mirrors. Cr compounds are also used as industrial catalysts and in the manufacturing of pigments. Rubies are brightened to red color using Cr, and also Cr treated glass will have an emerald, green color. Potassium dichromate ( $K_2Cr_2O_7$ ) is used in breath analyzers to assess blood alcohol content (BAC). Cr is also used in the production of

pigments and dyes where the pigments are produced by mixing solutions of Pb (NO<sub>3</sub>)<sub>2</sub>, and K<sub>2</sub>CrO<sub>4</sub>. Cr (VI) salts are used as a wood preservative, due to their highly toxic nature. For example, “Chromated Copper Arsenate” (CCA) is used to control wood decaying fungi (Hans 2015).

### ***10.1.2 Tanning Industry as a Source of Contaminating Metals***

Heavy metals enters the soil through agricultural, industrial, and inland effluents. The tanning industry is one of the more economically important contaminating industries in that it significantly contributes to foreign exchange and provides employment opportunities to more than three million people (Gomathy 2008). The tanning process includes dehairing, removal of flesh, fat, and treatment with chemicals to form a stable, durable material. Leather manufacturers use a series of chemical processes and physical operations to attain the desired end product of leather and they use a 90% Cr-based tanning agent for converting raw skin into leather. In the leather industry, Cr (III) is used for stabilizing the leather by cross-linking collagen fibers. As a final product, Cr tanned leather contains 4 to 5% of Cr, which is tightly bound to the proteins (Morera et al. 2011). Other metals such as titanium, aluminum, iron, and zirconium are also used in a stepwise process for leather product manufacturing (Jayakumar et al. 2016).

The major leather producing states in India are Tamil Nadu, Andhra Pradesh, Karnataka, Punjab, Delhi, West Bengal, Uttar Pradesh, and Maharashtra. Though the tanning industry is one of the forerunners in providing employment to people, it causes several impacts on the environment by discharging effluents containing a heavy load of pollutants. Tannery waste devastates both vegetation and also the associated microbial communities in and around the industrial locations. In chrome tanning, 276 chemicals and 14 heavy metals are used and 32,000 t of basic Cr sulfate salts are used annually in Indian tanneries which amounts to an annual discharge of nearly 2000–3200 t of Cr (Ramamathy and Naidu 2000).

## **10.2 An Introduction to Chromium**

Chromium (Cr) is a silver colored hard metal. The agency for toxic substances and disease registry has ranked Cr as the 17th most abundant element among the hazardous substances (CERCLA 2017). Chromium was first discovered in Siberian red lead ore (1798) by the French chemist Vauquelin (Avudainayagam et al. 2003). It is a transition element located in the group VI-B of the periodic table with a ground-state electronic configuration of Ar 3d<sup>5</sup>4s<sup>1</sup>. The stable forms of Cr are the

trivalent Cr (III) and the hexavalent Cr (VI) species. Other valence states are unstable and short lived in biological systems. Cr (VI) is considered the most toxic form of Cr, which associates with oxygen as either chromate ( $\text{CrO}_4^{2-}$ ) or dichromate ( $\text{Cr}_2\text{O}_7^{2-}$ ) oxyanions. Cr (III) is less mobile, less toxic, and is mainly bound to organic matter in soil and aquatic environments (Becquer et al. 2003). Cr (VI) is a strong oxidant with a high redox potential in the range of 1.33–1.38 eV accounting for a rapid and high generation of reactive oxygen species and it has resultant toxicity (Shanker et al. 2009). Cr has been reported to be a number one carcinogen according to the International Agency for Research on Cancer (1987). Hence its presence in the environment needs attention and understanding of the metals uptake, transport, and bioaccumulation within plants and also its persistence in the soil–plant system (Sharma et al. 2020).

Cr is present in all kinds of environments. That assessment includes water, air, and soil, at levels that range from 10 to 50 ppm as decided by the parent material (Nriagu 1988). In natural conditions, the concentration of Cr in soil can range between 10 and 50 mg kg<sup>-1</sup> and in agricultural soils it may go beyond 350 mg kg<sup>-1</sup> (Ertani et al. 2017). The oxidation state of Cr in these environments shifts between “hexavalent” Cr (VI) and “trivalent” Cr (III) depending upon redox potential and chemistry. The transition state affects both chromium bioavailability in soil and translocation.

## 10.3 The Effect of Chromium Upon Plants

### 10.3.1 Chromium Uptake, Translocation, and Accumulation by Plants

Heavy metals interact with the signal transduction pathways of plants and influence their metabolic processes including plant growth (Shanker et al. 2009). Cr is a nonessential element and is a toxic heavy metal that lacks a specific uptake mechanism, thus its toxic effects mainly are based on the speciation and translocation of the metal, which together affect its accumulation. Pathways of Cr (VI) involve carriers such as Fe, S, and P that compete with each other for binding (Wallace et al. 1976). Uptake of Cr (VI) has been found to be inhibited by metabolic inhibitors and thus it depends on metabolic energy, but a study of Cr (III) determined that its uptake did not get disturbed by metabolic inhibitors, and also it has been noted that the movement of Cr (III) can be observed in xylem (Skeffington et al. 1976). Accumulation of Chromium was more in the form of Cr (VI) than Cr (III) (Zayed et al. 1998). Distribution of Cr in crops does not depend on soil properties and concentration (Golovatyj et al. 1999) and this contaminant has been found to be higher in roots rather than in shoots and reproductive organs. In bean plants, 0.1% of soil chromium was translocated into seeds against 98% remaining in the roots that

might be due to the relative movement of Cr (VI) and Cr (III) across the endodermis via symplast (Huffman and Allaway 1973). The retention of Cr in roots was more in the form of Cr (III) than Cr (VI) (Shanker et al. 2009). Even after the entry of Cr (VI) into plant cells it reduced to Cr (V), Cr (IV), and Cr (III) (Stambulska et al. 2018). Accumulation of Cr in the vacuoles of roots seems to represent a sequestration process that serves as a protective mechanism for the plant (Mangabeira et al. 2011).

Uptake and accumulation of Cr in plants reduce growth, induces chlorosis, alters enzyme production, reduces pigment production, damages the root cells, causes ultrastructural modifications of the chloroplast, increases the transpiration, etc. (Panda 2003). Several reports have stated that Cr did not have any beneficial biological role in physiology of plants (Reale et al. 2016). But high and excessive levels of Cr in tissues of plants may lead to morphological and physiological changes (Kamran et al. 2017). Toxic effects of Cr mainly are due to the higher production of reactive oxygen species (ROS) that disrupt the redox balance in plants (Anjum et al. 2017).

Plant roots and the microbes associated with the rhizosphere secrete root exudates that contain a lot of organic acids such as malic, oleic, fumaric, butyric, and succinic acids (Renuga Devi et al. 2020). These organic acids play a major role in solubilizing the metals apart from provisioning the plant with relatively insoluble nutrients (Kaur et al. 2018). Increased accumulation of Cr in tomato plants were noted by the presence of citrate, aspartate, and oxalate exuded as root exudates (Srivastava et al. 1998).

## 10.3.2 Phytotoxicity of Chromium

### 10.3.2.1 Photosynthesis

Stress related to Cr is an important factor that affects photosynthesis, CO<sub>2</sub> fixation, electron transport, photophosphorylation, etc. (Clijsters and Van Assche 1985). In peas Cr (VI) has a pronounced effect on Photosystem I (plastocyanin–ferredoxin oxidoreductase) that affects photosynthesis (Bishnoi et al. 1993). Similarly, Cr has been observed to inhibit both light and dark reactions in mung beans that reduced the chlorophyll a, chlorophyll b, and total chlorophyll (Krupa and Baszynski 1995). In *Triticum aestivum* chlorophyll content has been noticed to decrease at 200 ppm of Cr (Sharma and Sharma 1993). Cr (III) and Cr (VI) have been found to cause ultrastructural changes in chloroplasts and inhibit both photosynthesis and growth (Panda and Patra 2000). Significant chromium toxicity, as noted by reduction in chlorophyll and carotenoid, has been observed in *Salvinia minima*.

### 10.3.2.2 Antioxidant Enzymes

Under stress conditions, reactive oxygen species (ROS) are produced and these need to be quenched to protect the cells from oxidative damage. Cr exposure decreased catalase activity in ten days old seedlings of wheat (Panda and Patra 2000). Cr (VI) addition generated more singlet oxygen than Cr (III) in *L. leucocephala*. The increase in antioxidant enzymes activity due to exposure to Cr might be due to the generation of superoxide radical by Cr that induced blockage of the electron transport chain in the mitochondria (Shanker et al. 2009).

### 10.3.2.3 Seed Germination

Cr toxicity has a severe impact on seed germination and radicle growth of the emerging seedlings (Panda 2002). In sugarcane, bud germination was severely affected and reduced to 57% with the exposure of 80 ppm of Cr (Jain et al. 2000). Reduction in germination and vigor was noticed in soybean when treated with varying levels of Cr (5–200 mg l<sup>-1</sup>). Seedling vigor was reduced in *Vigna radiata* when treated with 100 ppm of Cr (Shafiq et al. 2018).

### 10.3.2.4 Root and Shoot Growth

Plant growth has been much affected by Cr and caused the roots to wilt (Bassi et al. 1990). Root length of wheat plants was increased with 1 μM of Cr in the soil and decreased with higher concentration of Cr (Panda and Patra 2000). In *Caesalpinia pulcherrima* 100 ppm of Cr inhibited the root length and root weight (Iqbal et al. 2001). In wheat 20 ppm concentration of Cr in soil reduced the root length (Chen et al. 2001). In the plant *Acacia nilotica*, length of root was much affected by Cr than by any other heavy metals (Prasad et al. 2001) and adverse effects were also obvious in shoot growth (Rout et al. 1997).

Shoot growth was inhibited by the addition of Cr (III) in lucerne crop (Barton et al. 2000). The reduction in plant height might be mainly due to the reduced root growth and lesser absorption of nutrients to the above parts of the plant. Cr transport to the aerial parts of plants ultimately reduces the plants' growth. Cr toxicity severely affects plant development and plant establishment as it induces oxidative stress which in turn induces lipid peroxidation in plants (Kumar et al. 2016).

### 10.3.2.5 Dry Matter Production

Dry matter production is one of the important aspects that decide the yield of a crop. Higher rates of photosynthetic processing need to be carried out for higher dry matter

production (Kumar et al. 2016). Plants such as *Phaseolus vulgaris* and maize exposed to 1  $\mu\text{M}$  of Cr (III) in the soil accumulated higher root and leaf dry weight than did plants grown under control conditions (Barcelo et al. 1993). Application of Cr has the effect on quality and quantity of biomass in sunflower, maize, *Vicia faba* and the dry matter production was not significantly influenced by Cr (VI) (Kocik and Ilavsky 1994). Cauliflower cultivated at 0.5 mM Cr (VI) had lesser dry biomass compared to control (Chatterjee and Chatterjee 2000). Combined influence of salinity and Cr (VI) (500 ppm) significantly decreased the dry biomass accumulation in *Portulaca oleracea* (Zurayk et al. 2001).

### 10.3.2.6 Yield

Chromium affects plant growth and development starting from seed germination through a possible reduction in yield and these consequences have been observed due to poor translocation and partitioning of assimilates to the economically important parts of the plant (Shanker et al. 2009). Higher accumulation of Cr in plants reduced the growth rate and yield of wheat plants (Dotaniya et al. 2014). In *Chenopodium album*, plant growth, pod number, grain yield and protein content of the grain was significantly reduced (Singh et al. 2020). Yield reduction due to Cr in *Brassica campestris* was mainly because of the unavailability of essential nutrients (Na, Cu, Zn, Mn, Fe, etc.) that affected the metabolic processes of the plants (Zhao et al. 2019).

## 10.4 Transformation of Chromium in Soils

Both in soil and water Cr typically exists as Cr (III) and Cr (VI) (Kabata-Pendias et al. 2000), which are these elements most environmentally stable forms. The availability of manganese oxides in soils determines the form of Cr because Cr (III) is oxidized into Cr (VI) by manganese oxides in soils (Kim et al. 2002). Between these two, Cr (III) is a more stable form and a less soluble cation in soils. Cr (III) is essential to human health but, Cr (VI) is a class A human carcinogen. In some plants, Cr has been found as Cr (V) which is an intermediate product of Cr (VI) reduction.

The presence of oxidants and reductants determines the transformation of Cr between Cr (III) and Cr (VI) in soils and water. Cr (III) is first oxidized into Cr (VI) by moist soil and then reduced again (Bartlett and James 1988). The overall mobility of Cr in soils and groundwater is controlled by the distribution between Cr (III) and Cr (VI) and among various solid phase components. It was also described that Cr (III) is primarily present in the organic matter bound fraction in arid zone soils under saturated, field capacity, and wetting drying cycle moisture regimes (Han et al. 2001). Organic matter amended soils removed higher amounts of Cr (VI) from

irrigated water (Losi et al. 1994). Solid phase distribution, transformation, and bioavailability of Cr in Cr (III) and Cr (VI) was analyzed in the contaminated soils (Han et al. 2004).

## 10.5 Bioremediation of Chromium by Microorganisms

Traditional approaches aimed to remove the heavy metals from soil and water, i.e., from the environment, include chemical precipitation, oxidation/reduction, ion exchange, filtration, use of membranes, evaporation and adsorption on activated coal, alum, kaolinite, and ash (Barceloux 1999). However, these methods often require high energy and large quantities of chemical reagents. The above said methods also produce secondary pollutants that again create the problem of pollution (Jeyasingh and Ligy 2005). Removing low concentrations of Cr (VI) from the environment by traditional methods will be non-economical (Kratochvil et al. 1998). Hence, alternate strategies need to be considered. Bioremediation has been found to be an innovative technology, in which the metabolic potential of microorganisms may be used to remove the toxic metals from contaminated sites. Microbial bioremediation can be classified as either in situ, where the microorganism itself is used in the polluted sites, or ex situ, where a portion of environmental samples such as water, sediment, or soil will be taken to a treatment plant where microorganisms will be used for removing the contaminants from the environmental materials (Kratochvil et al. 1998).

The environmental stability of Cr (III) facilitates its precipitation and removal and the biotransformation of Cr (VI) to Cr (III) has been considered as an alternative process for treating Cr (VI) contaminated wastes (Cervantes et al. 2001). Reduction of Cr (VI) to Cr (III) is a very important process for recovery of sites contaminated by Cr (VI) (Polti et al. 2010) and Cr (VI)-resistant microorganisms represent an important group because of their potential to allow safe, economical, and environmentally friendly methods for reducing Cr (VI) to Cr (III) (Raspor et al. 2000). Removal of Cr (VI) using microorganisms is considered to be an effective method and receiving great attention for potential application in bioremediation (Ganguli and Tripathi 2002). Among the biotechnological approaches, microbial reduction of Cr (VI) is cost-effective and ecofriendly and can offer a viable alternative (Xu et al. 2011).

### 10.5.1 Bacterial Remediation of Chromium

Heavy metals show a lethal effect on soil biota. They can affect the crucial microbial process and reduce the number and activity of soil microorganisms (Obbard 2001). Metal contaminants usually are found in soils, sediments, and water. Interestingly, microorganisms can reduce the mobility and toxicity of metals, and those are termed

“microbial affects,” which helpfully reduce the potential extensiveness of contamination. So far, microbial tolerance mechanisms for metals such as copper, zinc, arsenic, Cr, cadmium, and nickel have been studied in detail.

Bacteria are ubiquitous in nature and importantly this group of microorganisms often has been used for treating heavy metal contamination. In an anaerobic condition, *Pseudomonas* species could reduce Cr (VI) (Romanenko and Koren'kov 1977). Among the microbes, bacteria has the ability to fight with the heavy metal (Kaur and Kumar 2014). This capability is composed of several processes such as adsorption, absorption, accumulation, and transformation inside its cell (Zahoor and Rehman 2009). Biosorption is perhaps the most significant capability of bacteria for reducing the amount of pollutants from the contaminated environment (Oves et al. 2013).

The same metal-binding capabilities that exist in environmental microorganisms can be evidenced in human gastrointestinal bacteria. Bacterial species belonging to the genus *Lactobacillus*, present in human body and in fermented foods, have the ability to bind metals, including Cr (VI) and detoxify it (Monachese et al. 2012). *Arthrobacter* sp. and *Bacillus* sp., isolated from tannery wastewater proved to have the ability to reduce the toxic Cr (VI) to less toxic Cr (III), a detoxification process in cell suspensions and cell extracts (Megharaj et al. 2003).

Bacterial chromate reductase is an enzyme that can convert soluble and particulate forms of metals, especially notable for converting toxic chromate Cr (VI) to insoluble and less toxic Cr (III). Bioremediation can be effective in removing Cr (VI) more toxic form from the environment, especially if the bacterial ability for such elimination is improved by biochemical and molecular engineering. A Gram-positive, Cr-resistant bacterial strain (ATCC 700729) was isolated from tannery effluent, was able to grow in media with potassium dichromate up to 80 mg/ml (Thacker and Datta 2006). Cr-resistant bacterial strain *Bacillus cereus* S6 was isolated from tannery effluent and was used for the reduction of toxic hexavalent Cr [Cr (VI)] into less toxic trivalent Cr (III) (Megharaj et al. 2003).

Many genera of microbes like *Bacillus*, *Enterobacter*, *Escherichia*, *Pseudomonas*, and also some yeasts and other fungi help in bioremediation of heavy metals and Cr contaminated soil and water by bioabsorption and bioaccumulation of Cr in the cell (Bento and Okeke 2003).

When looking at the microbial communities of metal contaminated sites, it has been found that among the bacteria present, there is supplementary potential for unique forms of respiration. Also, since the oxidation state of a metal ion may govern its solubility, many scientists have been trying to use microbes that are able to oxidize or reduce heavy metals in order to remediate metal contaminated sites. Another inference of heavy metal tolerance in the environment is that it may contribute to the maintenance of antibiotic resistance genes in the organisms.

Bacterial genera such as *Azotobacter* S8, *Bacillus subtilis*, and *Pseudomonas putida* have demonstrated resistance and are able to reduce heavy metal contaminants (Purwanti et al. 2017). *Azotobacter* S8 has an ability to resist Cr (VI) up to 300 mg/L (Pavel et al. 2012) whereas *Pseudomonas* is able to resist Cr (III) up to



400 µg/mL (Bahig et al. 2008). *Bacillus subtilis*, a Gram-positive bacteria, was known to survive in a medium containing Cr(III) up to 400 µg/mL (Bahig et al. 2008). Hexavalent Cr can be removed by *Klebsiella* sp. cells both from tannery effluents and from pond water. Biosorption of Cr(VI) was effectively achieved by dried *Klebsiella* sp. (Hossan et al. 2020). The isolates from heavy metal contaminated sites, viz., *Pseudomonas fluorescence*, *Bacillus cereus*, and *Alkalihalobacillus decolorationis*, were able to show intrinsic resistance to Cr and support the plant growth to have enhanced germination percentage and seedling growth in contaminated areas (Ahirwar et al. 2015). The immobilized bacterial cells activity was superior to live bacterial cells as the immobilized cells are stable, easier to reuse can withstand sudden fluctuations, etc. (Rawat et al. 2013).

### 10.5.2 Fungal Remediation of Chromium

Rhizosphere is the region where diversity of microbes exists that form symbiotic associations with the roots and these microbes can be helpful to remediate the soil from external contaminants (Gomathy et al. 2018). Using microbial cultures to reclaim these environments and to exploit these beneficial microbes to enhance the nutrient content of soil needs to be encouraged greatly (Khan 2002).

In a contaminated ecosystem, microbes are doing their level best to decontaminate the area by using their own resistance and adaptive mechanisms (García-Hernandez et al. 2017). Fungi are unique and versatile microbes as they can grow even under extreme environmental conditions. Several mechanisms have been adapted by fungi to survive under hostile environments of high metal concentrations. Those fungal mechanisms used to clean up polluted environments will vary depending upon the genetics of the fungi, and the type of metal, along with other influential factors. Perhaps the main point to applying fungal inoculants in metal contaminated environments (Gomathy et al. 2018) is that even in the harshness of metal polluted sites these fungi flexibly adapt themselves through interaction between metals and the microbial cell wall, periplasm, membranes, and cytoplasm, with all of those cellular components playing their own key role in the organisms adaptation techniques (Cervantes et al. 2006).

Filamentous fungi have the ability to tolerate Cr (VI) and can colonize polluted sites efficiently and sequester those metals. Cr (VI) was efficiently reduced through the enzymes produced by *A. niger*. The fungal cell wall has excellent metal binding properties and can tolerate toxic substances (Pradhan et al. 2017). Particular fungi produce enzymes that mediate the bioremediation process and treat the tannery effluents throughout the growth cycle of fungi (Sharma and Malaviya 2016). Cr (VI) was efficiently detoxified by *Aspergillus flavus* and extracellular enzyme reduction and intracellular biosorption was observed in *Paecilomyces* sp. Biotransformation of Cr (VI) to Cr (III) was noticed in *Fusarium* sp. (Xu et al. 2017). When compared to other microorganisms, the biomass of the fungi can be

huge and has the ability to remove a lot of heavy metals such as copper, cadmium, and Cr (VI) up to the tune of 300 mg/L Cr(VI) through oxidoreduction reactions (Sharma and Malaviya 2016). The mechanism adapted by various fungi might be biosorption, bioaccumulation, biotransformation, biomineralization, extracellular precipitation, etc. (Jobby et al. 2018).

Filamentous fungi such as *Aspergillus fumigatus* and *Cladosporium* sp. have been found to be potential candidates for removal of heavy metals from effluents (Tatiani et al. 2020). Among the different *Aspergillus* species (*A. niger*, *A. flavus*, *A. fumigatus*, *A. nidulans*, *A. heteromorphus*, *A. foetidus*, and *A. viridinutans*) *A. niger* performed well to remediate tannery effluent (Sivakumar 2016). Fungal isolates (*Fusarium chlamydosporum*, *Aspergillus* sp., *Purpureocillium lilacinum*, *Cladosporium perangustum*, *Penicillium commune*, and *Fusarium equiseti*) obtained from tannery industries have a track record for complete removal of Cr (VI) from tannery effluents even at higher concentrations. *Glomus versicolor* tolerated 1000 ppm and *F. solani* tolerated up to 5000 ppm of Cr (VI).

The Cr (VI) tolerance of *A. niger* was found to be 500 ppm. The Cr tolerance limit of *Penicillium* sp. and *A. niger* was 800 and 512 ppm, respectively. Fungal biomass of *Mucor hiemalis* have the ability to tolerate 100 ppm of Cr (VI) (Tewari et al. 2005).

### **10.5.3 Arbuscular Mycorrhizal Fungi (AM Fungi) and Chromium Remediation**

Among the fungi, those defined as Arbuscular Mycorrhizal fungi (AM fungi) are very particular and represent a direct link between soil and the roots of crop plants. The region in and around the root is called Rhizosphere region and it is highly influenced by flow of nutrients and energy (Wright and Miller 1994). Many of the mechanisms adapted by AM fungi to overcome Cr stress have been described by researchers (Smith and Read 1997; Khan et al. 2000). Apart from the roles played by the AM fungi such as mineral and nutrient transfer to plants, these fungi also participate in drought tolerance, carbon sequestration, reclamation of soils, etc. (Gomathy et al. 2018). Using AM fungi for reclamation or amelioration of soil contamination is called mycoremediation. This can be achieved by AM fungi linking the soil and the plants with their fungal hyphae. These hyphae form a network that may extend beyond several kilometers and potentially could explore a large volume of soil, enhancing their efficiency to reclaim polluted sites. This fungal activity helps the soil to remain at a minimum level of metal concentration by hyperaccumulating the heavy metals in its biomass. Rhizofiltration is a similar process which uses the roots of hydroponically cultivated plants for removing metals from groundwater (Gonzalez-Chavez et al. 2002; Subramanian et al. 2008; Gomathy et al. 2011). Uptake of heavy metals depends on the species of AM fungi,

concentration of metal, soil fertility, pH, etc. (Gonzalez-Chavez et al. 2002). Mycorrhizae-treated plants have been found to accumulate greater quantities of metals than did control plants (Joner and Leyval 1997). They store the heavy metals in their fungal tissues and spores (Chen et al. 2001). Heavy metal contaminated sites have been found to abundantly contain many mycorrhizal species such as *Glomus*, *Gigaspora*, *Acaulospora*, and *Sclerocystis*. Presence of different species of AM fungi varies based on different locations, different soils, prevailing environment, presence of crop, etc.

### 10.5.4 Algal and Cyanobacterial Remediation of Chromium

Algae and cyanobacteria are common microbes found in almost every environment including those considered of extreme aquatic or terrestrial nature (Panosyan 2015). Among these are several groups of algae and also groups of cyanobacteria that can be used for the removal of heavy metals from the environment. Algae are photosynthetic organisms and hence require lower quantities of nutrients. When compared to other microbial biosorbents algae produce an enormous amount of biomass that is an added advantage for the removal of Cr from the polluted site. Mutant, wildtype, or genetically modified cyanobacteria also can be used for bioremediation of heavy metals (Ananya and Ahmad 2014). These organisms act as biosorbents, and are used to detoxify the metal contaminated environments (Abbas et al. 2014). Algal biomass is used for attenuation of heavy metal effluent via adsorption or by integration into cells.

Phycoremediation can be defined as the use of algae and cyanobacteria to detoxify heavy metals by either removal or degradation of toxicants (Chabukdhara et al. 2017). Algae have various chemical moieties on their surface which act as metal binding sites such as amide, carboxyl, hydroxyl, and phosphate groups (Abbas et al. 2014). Among the microbes, algae are able to take up, accumulate and concentrate heavy metals in significant amounts from the aqueous solution. Because of easy handling, cheap availability, relatively high surface area, and high binding affinity, algae are considered to be potentially very effective biosorbents (Dominic et al. 2009, Doshi et al. 2008 and Ahluwalia and Goyal 2007).

For the bioreduction of Cr (VI), variables like agitation, initial Cr (VI) concentration, temperature, nutrient supplements, pH, cell immobilizers, and reactor design have been proven as influential factors (Dhal et al. 2013). Photosynthetic microalgae absorb metal ions dissolved in water during their autotrophic primary production (Salt et al. 1997). Microalgae detoxify metal ions present in the water in different ways, either by changing the metal ions' thermodynamic stability in water or by complexation (Duarte et al. 2007). *Chlorella vulgaris* used for the reduction of Cr (VI) by a photochemical process (Deng et al. 2006). During the photochemical reduction, different parameter values were observed such that Cr (VI) was

increasingly reduced by the *C. vulgaris* with increase of exposure time, algal concentration and decrease of pH. The microalgae *Chlamydomonas reinhardtii* was used for biosorption of Cr (VI) ions (Arica and Bayramoğlu 2005). Cr (VI) was biosorped from aqueous solution of waste cyanobacterial biomass of *Nostoc linckia* (Sharma et al. 2011). The use of cyanobacterial mat was used to remove hexavalent Cr (Shukla et al. 2012). A macro alga *Sargassum cymosum* was used for Cr (VI) removal, which was followed by both reduction and adsorption processes (De Souza et al. 2016). There is a mechanism of hexavalent Cr reduction due to organelles of *Chlorella vulgaris* (Chen et al. 2016).

Maximum removal and sorption of Cr (VI) ions were done by *Spirogyra species* (Gupta et al. 2001). The blue-green alga *Phormidium* sp. could bioaccumulate both Cr (VI) ions and reactive dyes (Sadettin and Dönmez 2007). Cyanobacterial biomass of *Desmonostoc muscorum* could be used as a biosorbent for the removal of Cr(VI) from wastewater (Gupta and Rastogi 2008). Using the biomass of microalgae *Scenedesmus* sp Cr (VI) was removed from the solution (Pradhan et al. 2019). From estuaries polluted with tannery effluents microalgal species, namely *Spirogyra* and the cyanobacterial species *Anabaena*, *Oscillatoria*, *Phormidium*, were examined for Cr (VI) biosorption potential and found to be efficient species that could be employed for effective removal of Cr(VI) (Balaji et al. 2016).

## 10.6 Mechanisms of Heavy metal Tolerance

The contaminated sites have an abundant and diversified population of microorganisms, and the microbial species present in those environments have their own selective mechanisms to overcome or withstand the pollutants (Meharg 2003; Subramanian et al. 2008). Microbial cells interact with Cr both externally and internally viz., processes associated with the cell wall, periplasm, cytoplasmic membrane, cytoplasm, etc. External mechanisms adapted by the microbial cell mainly focus upon preventing the entry of Cr to the inside the cell, and this blockage is achieved through chelation, adsorption, ion exchange, etc. The internal mechanisms often aim to reduce chromate availability by processes such as compartmentalization, precipitation, and chelation. In the process of microbial remediation, various additional mechanisms are employed viz., redox process, complexation, and electrostatic attraction.

### 10.6.1 Biosorption

Microbes are good agents to detoxify or remove contaminating chromium from polluted sites through the mechanisms of either biosorption or bioaccumulation. Biosorption is the mechanism by which the pollutant can be adsorbed, accumulated, and transformed inside the microbial cell (Deepali 2011). Biosorption is a kind of

bioaccumulation where the hexavalent Cr gets entrapped in cellular structures. Sequestration of Cr (VI) by microbes is mainly related to the polysaccharides and proteins present over the cell wall. The process of biosorption by fungi involves two components, one of those being cell wall proteins and the other is represented by functional groups (Ismail and Mustafa 2016). The Chitin, proteins, glucans, and lipids, found in fungal cell wall components are biosorbents. Those have functional groups such as carboxyl ( $-\text{COOH}$ ), phosphate ( $\text{PO}_4^{3-}$ ), amine ( $-\text{NH}_2$ ), thiol ( $-\text{SH}$ ), hydroxyl, and hydroxide ( $-\text{OH}$ ) moieties. The functional groups may involve in adsorbing Cr (III) on the surface of *P. putida*. Some of the bacterial genera that follow the biosorption mechanism for Cr bioremediation are species of *Bacillus* (Samarth et al. 2012; Zouboulis et al. 2004), *Pseudomonas* (Lopez et al. 2000), *Desulfovibrio* (Kim et al. 2015), and *Geobacter* (He et al. 2019).

Actually, several researchers have noted that either living or dead microbial cells could be involved in the removal of Cr (VI) from wastewater through the biosorption process (Anjana et al. 2007). The dead biomass of fungal cells also has been used for adsorption of Cr. In algal cells, Cr (VI) biosorption has been observed to take place rapidly, independent of metabolism (Joutey et al. 2015). In *Chlorella miniata* and *Cladophora albida* Cr (VI) was biosorbed first and then it was reduced to Cr (III).

In AM fungi, the fungal mycelia have high metal adsorbing capacity when compared to other ions and the metal concentration in soil was observed to be lower in the vicinity of hyphal mats. Not only the AM fungal hyphae, but also the AM cell walls by themselves have high adsorption of Cr. The mycorrhizal cell wall is loaded with negatively charged ligands such as phosphoryl, carboxyl, hydroxyl, and phenolic groups that ultimately attract the metal ligand. When compared to other fungal genera, AM fungal hyphae have more surface area that can serve as a good adsorptive site for accumulation of toxic metals (Joner et al. 2000). The mycelia of *G. mosseae* adsorbs more metals.

### 10.6.2 Ion Exchange

The metal ions in contaminated soil exchange with the bivalent metal ions and polysaccharides present in the cell walls of AM fungi. The binding that exists between the metal ions and the fungal hyphal sites is metabolic binding as compared with non-metabolic binding. Fungal cell walls have negatively charged groups and this determines the cation exchange capacity (CEC). This CEC differs between AM fungal species and fluctuates based on the pH. If the pH increases, then it might also increase cation sorption in the cell wall of AM fungi.

### 10.6.3 Complexation

Rhizosphere contribute more for the detoxification of metal ligands as they are responsible for exudation of higher quantities of root exudates that contain organic acids, amino acids, sugars etc. which complex the metals and keeps the rhizospheric region free from metal contaminants (Gomathy et al. 2011). The cystine ligands present on AM fungal hyphae complexed those metals present in the surrounding region. The metallo-organic complexes are important components in the reduction of metal concentrations in the root zone (Shanker et al. 2009).

Both intracellular and extracellular sequestrations complex the heavy metals and contribute to providing an environment that contains less free metal. Extracellular sequestration complexation occurs in periplasm whereas intracellular sequestration happens within the microbial cell and this is predominantly utilized for the treatment of effluents (Bernard et al. 2018).

### 10.6.4 Precipitation

Precipitation is another mechanism that occurs through extracellular sequestration. This mechanism is employed by *Geobacter* species such as *G. sulfurreducens* and *G. metallireducens* that change Cr (VI) to less toxic Cr (III) (Bruschi and Florence 2006). In sulfate-reducing bacteria, higher quantities of hydrogen sulfide precipitate metal cations (Luptakova and Kusnierova 2005).

AM fungi also follow this mechanism to reclaim the soil from tannery effluents that contain Cr (Gomathy et al. 2018). AM fungi intracellularly precipitated the metallic cations in their hyphae. Moreover, AM fungi produce copious amounts of a protein called glomalin from their extraradical hyphae, and that protein is responsible for the precipitation of heavy metals (Wright and Upadhyaya 1998). The higher precipitation of metals occurred in fungal structures such as vesicles and intracellular spaces.

### 10.6.5 Solubilization

In metalliferous soils, metals strongly bind with the soil particles and certain measures are needed to extract them out of the soil particles. Here comes the role of solubilization, and it occurs with the help of the production of organic acids which acidify the rhizosphere.

The solubility level of heavy metals varies and elements such as Zn, Ni, and Cu are easily dissolved, whereas  $Pb^{2+}$  and Cr are less soluble (Kapoor and Viraraghavan 1997). Many of the bacterial genera secrete organic acids that solubilize relatively insoluble metal ligands. One of the important groups of bacteria active in this

process are phosphobacteria, said to be promising agents that solubilize unavailable forms of phosphorous and also metals by the production of organic acids. The bioavailability of metals can further be increased by inoculating biosurfactant-producing phosphorus solubilizing bacteria that further releases metals from the soil particles. The hyphae of AM fungi produce organic acids and solubilize not only the minerals but also their metal ligands. The mycorrhizal fungi solubilized and accumulated a greater quantity of metals that remained in the soil solution.

### ***10.6.6 Compartmentalization Strategies***

In compartmentalization processes, the toxic metal is compartmentalized in specific organs either in plants or in specific structures in the microbial cell. In these compartments, the adverse effects of metals upon biologically important metabolic functions may be less active and the metals may be changed to become non-toxic. The compartmental organs involved in these processes might be vacuoles or other subcellular compartments. In plastids, the compartmentalization of metals occurred. Protein metal ligands transfer toxic metals into the vacuoles.

AM fungal inoculated plants have luxurious production of roots and also have external mycelium, which can help the plants to absorb, translocate and transfer Cr, and other heavy metals from the surrounding soil. Amelioration of heavy metals has been observed to occur by accumulating them in mycelium and vesicles thereby preventing mobilization of the metals to aerial parts of the plants (Dhalaria et al. 2020).

### ***10.6.7 Dilution***

Biofertilizers can serve to inoculate plants, and the plants that harbor huge amounts of beneficial microorganisms have luxurious growth of roots and shoots compared to uninoculated plants (Gomathy et al. 2018). This leads to the dilution mechanism in which the metals get diluted in the vegetative portion and effectively remediates heavy metals from the soil. In the case of AM fungi, the external mycelium explore a larger volume of soil than do the roots, which results in higher uptake of minerals as well metals both in the mycelium and in a higher number of lateral roots hairs.

### ***10.6.8 Binding***

In soil, the bioavailability of heavy metals is based on metal speciation and other environmental factors. The cell wall of AM fungi has many functional groups that bind with toxic metals like Cu, Pb, Cd, and Cr (Kapoor and Viraraghavan 1997).

Glomalin is a glycoprotein produced from external mycelium, and spores of AM fungi have ability to sequester metals and remediate the soil (Wright and Upadhyaya 1996; Gonzalez-Chavez et al. 2004). Glomalin plays the major role in sequestering metals in the rhizosphere of citrus (Wang et al. 2017).

## 10.7 Conclusion

Cr is extensively used for various industrial processes and these industries discharge this contaminant through their outlets to the environment, and thus pollution due to these contaminants is continuously occurring. This causes a serious threat not only to the environment but also to human health as the contamination is toxic and persistently prevails in the ecosystem. The prevalent forms of Cr viz., Cr (III) and Cr (VI) have their own biological effects, plus they have been found to be carcinogenic and mutagenic. Several chemical methods are available to remove this contaminant from the environment but they are not safe and they further contribute to pollution of the environment. The important aspect of using beneficial microbes for the remediation of Cr includes that the methods are cheap, ecofriendly, nonhazardous, and do not require high energy resources. However, some uncertainty remains regarding the efficiency of microbes and the ways in which environmental factors influence the growth and development of these microbes. The mechanisms by which microbes remediate the pollutant vary accordingly, with some detoxifying intracellularly and others are doing so extracellularly. The process of microbial remediation of Cr seems to be effective as it is steady and stable. Choosing the right microbe, plus understanding its mechanisms for remediating Cr contaminants, are the keys that will allow us to move forward along the road of success to green the Cr polluted gray areas.

## References

- Abbas SH, Ismail IM, Mostafa TM, Sulaymon AH (2014) Biosorption of heavy metals: a review. *J Chem Sci Technol* 3(4):74–102
- Ahirwar NK, Gupta G, Singh V (2015) Biodegradation of chromium contaminated soil by some bacterial species. *Int J Sci Res* 4(4):1024–1029
- Ahluwalia SS, Goyal D (2007) Microbial and plant derived biomass for removal of heavy metals from wastewater. *Bioresour Technol* 98(12):2243–2257
- Ananya AK, Ahmad IZ (2014) Cyanobacteria “the blue green algae” and its novel applications: A brief review. *Int J Innov Appl Stud* 7(1):251
- Anjana K, Kaushik A, Kiran B, Nisha R (2007) Biosorption of Cr(VI) by immobilized biomass of two indigenous strains of cyanobacteria isolated from metal contaminated soil. *J Hazard Mater* 148:383–386
- Anjum SA, Ashraf U, Khan I, Tanveer M, Shahid M, Shakoore A, Wang L (2017) Phyto-toxicity of chromium in maize: oxidative damage, osmolyte accumulation, anti-oxidative defense and chromium uptake. *Pedosphere* 27:262–273



- Arao T, Ishikawa S, Murakami IM, Abe K, Maejima Y, Makino T (2010) Heavy metal contamination of agricultural soil and counter measures in Japan. *Paddy Water Environ* 8(3):247–257
- Arıca MY, Bayramoğlu G (2005) Cr (VI) biosorption from aqueous solutions using free and immobilized biomass of *Lentinus sajor-caju*: preparation and kinetic characterization. *Colloids Surf A Physicochem Eng Asp* 253(1–3):203–211
- Avudainayagam S, Megharaj M, Owens G, Kookana RS, Chittleborough D, Naidu R (2003) Chemistry of chromium in soils with particular emphasis on tannery waste contaminated sites. *Rev Environ Contamin Toxicol* 178:223–225
- Bahig AE, Aly EA, Khaled AA, Amel KA (2008) Isolation, characterization and application of bacterial population from agricultural soil at Sohag Province, Egypt. *Malays J Microbiol* 4(2): 42–50
- Balaji S, Kalaivani T, Shalini M, Gopalakrishnan M, Rashith Muhammad MA, Rajasekaran C (2016) Sorption sites of microalgae possess metal binding ability towards Cr (VI) from tannery effluents—a kinetic and characterization study. *Desalin Water Treat* 57(31):14518–14529
- Barcelo J, Poschenrieder C, Vazquez MD, Gunse B, Vernet JP (1993) Beneficial and toxic effects of chromium in plants: solution culture, pot and field studies. In: *Studies in environmental science* No. 55. Paper presented at the 5th international conference on environmental contamination, Morges, Switzerland
- Barceloux DG (1999) Chromium. *Clin Toxicol* 37:173–194
- Bartlett RJ, James BR (1988) Mobility and bioavailability of chromium in soils. In: Nriagu JO, Nieboer E (eds) *Chromium in nature and human environments*. Wiley, New York
- Bartson LL, Johnson GV, Nan AGO, Wagener BM (2000) Inhibition of ferric chelate reductase in alfalfa roots by cobalt, nickel, chromium, and copper. *J Plant Nutr* 23:1833–1845
- Bassi M, Corradi MG, Realini M (1990) Effects of chromium (VI) on two freshwater plants, *Lemna minor* and *Pistia stratiotes* morphological observations. *Cytobios* 62:27–38
- Becquer T, Quantin C, Sicot M, Boudot JP (2003) Chromium availability in ultramafic soils from New Caledonia. *Sci Total Environ* 301:251–261
- Bento H, Okeke O (2003) Chromate reduction by chromium resistant bacteria isolated from soils contaminated with dichromate. *J Environ Qual* 32:1228–1233
- Bernard EI, Okoduwa SIR, Idoko GO, Akabuogu EP, Adeyi AO, Ejiogu IK (2018) Toxicity and bioremediation of Heavy metals contaminated ecosystem from tannery wastewater: a review. *J Toxicol* 2018:2568038
- Bishnoi NR, Anita D, Gupta VK, Shawaney SK (1993) Effect of chromium on seed germination seedling growth and yield of peas. *Agric Ecol Ecosyst* 47:47–57
- Bruschi M, Florence G (2006) New bioremediation technologies to remove heavy metals and radionuclides using Fe(III)-, sulfate- and sulfur-reducing bacteria. In: Singh SN, Tripathi RD (eds) *Environmental Bioremediation Technologies*. Springer, Heidelberg, pp 35–55
- CERCLA Priority List of hazardous substances. Agency for Toxic Substances and Disease Registry, USA (2017)
- Cervantes C, García CJ, Devars S, Corona GF, Tavera LH, Guzmán TJC, Sánchez MR (2001) Interactions of chromium with microorganisms and plants. *FEMS Microbiol Rev* 25:335–347
- Cervantes C, Espino SAE, Acevedo AF, Leon RIL, Rivera CME, Avila RM, Wrobel KK, Wrobel ZK, Gutierrez CJF, Rodriguez ZJS, Moreno SR (2006) Interacciones microbianas con metales pesados. *Rev Latinoam Microbiol* 48:203–210
- Chabukdhara M, Gupta SK, Gogoi M (2017) Phycoremediation of heavy metals coupled with generation of bioenergy. In: *Algal biofuels*. Springer, Cham, pp 163–188
- Chatterjee J, Chatterjee C (2000) Phytotoxicity of cobalt, chromium and copper in cauliflower. *Environ Pollut* 109:69–74
- Chen B, Christie P, Li L (2001) A modified glass bead compartment cultivation system for studies on nutrient and trace metal uptake by arbuscular mycorrhiza. *Chemosphere* 42:185–192
- Chen Z, Song S, Wen Y (2016) Reduction of Cr (VI) into Cr (III) by organelles of *Chlorella vulgaris* in aqueous solution: an organelle-level attempt. *Sci Total Environ* 572:361–368

- Clijsters H, Van Assche F (1985) Inhibition of photosynthesis by heavy metals. *Photosynth Res* 7:31–40
- De Souza FB, de Lima Brandão H, Hackbarth FV, de Souza AAU, Boaventura RA, de Souza SMGU, Vilar VJ (2016) Marine macro-alga *Sargassum cymosum* as electron donor for hexavalent chromium reduction to trivalent state in aqueous solutions. *Chem Eng J* 283:903–910
- Deepali (2011) Bioremediation of chromium (VI) from textile Industry's effluent and contaminated soil using *Pseudomonas putida*. *J Energy Environ* 2(1):24–31
- Deng L, Wang H, Deng N (2006) Photoreduction of chromium (VI) in the presence of algae, *Chlorella vulgaris*. *J Hazard Mater* 138(2):288–292
- Dhal B, Thatoi HN, Das NN, Pandey BD (2013) Chemical and microbial remediation of hexavalent chromium from contaminated soil and mining/metallurgical solid waste: a review. *J Hazard Mater* 250:272–291
- Dhalaria R, Kumar D, Kumar H, Nepovimova E, Kuca K, Islam MT, Verma R (2020) Arbuscular Mycorrhizal Fungi as Potential Agents in Ameliorating Heavy Metal Stress in Plants. *Agronomy* 10:815
- Dominic VJ, Murali S, Nisha MC (2009) Phycoremediation efficiency of three micro algae *Chlorella vulgaris*, *Synechocystis Salina* and *Gloeocapsa gelatinosa*. *SB Acad Rev* 16(1):138–146
- Doshi H, Seth C, Ray A, Kothari IL (2008) Bioaccumulation of heavy metals by green algae. *Curr Microbiol* 56(3):246–255
- Dotaniya ML, Das H, Meena VD (2014) Assessment of chromium efficacy on germination, root elongation, and coleoptile growth of wheat (*Triticum aestivum* L.) at different growth periods. *Environ Monit Assess* 186(5):2957–2963
- Duarte B, Delgado M, Caçador I (2007) The role of citric acid in cadmium and nickel uptake and translocation in *Halimione portulacoides*. *Chemosphere* 69(5):836–840
- Environmental Protection Agency (EPA) (2010) Assessment and remediation of contaminated sediments (ARCS) program, final summary report (EPA905-S-94-001). EPA, Chicago, IL
- Ertani A, Mietto A, Borin M, Nardi S (2017) Chromium in agricultural soils and crops: a review. *Water Air Soil Pollut* 228:1–12
- Ferraz P, Fidalgo F, Almeida A, Teixeira J (2012) Phytostabilization of nickel by the zinc and cadmium hyperaccumulator *Solanum nigrum* L. are metallothioneins involved? *Plant Physiol Biochem* 57:254–260
- Ganguli A, Tripathi AK (2002) Bioremediation of toxic chromium from electroplating effluent by chromate-reducing *Pseudomonas aeruginosa* A2Chr in two bioreactors. *Appl Microbiol Biotechnol* 58:416–420
- Garcia-Hernandez MA, Villareal-Chiu JF, Garza-Gonzalez MT (2017) Metallophilic fungi research: an alternative for its use in the bioremediation of hexavalent chromium. *Int J Environ Sci Technol* 2017(14):2023–2038
- Golovatyj SE, Bogatyreva EN, Golovaty SE (1999) Effect of levels of chromium content in a soil on its distribution in organs of corn plants. *Soil Res Fert* 19:197–204
- Gomathy M (2008) Role of mycorrhizal symbiosis in alleviation of chromium in the maize rhizosphere, Ph D., Thesis Tamil Nadu Agricultural University, Coimbatore
- Gomathy M, Sabarinathan KG, Thangaraju M, Subramanian KS, Sivashankari Devi T, Ananthi K (2011) The effect of mycorrhizae inoculated maize root exudates in alleviation of chromium toxicity in chromium polluted environments. *Insight Micro* 1(2):20–30
- Gomathy M, Sabarinathan KG, Sivasankari Devi T, Pandiyarajan P (2018) Arbuscular mycorrhizal fungi and glomalin super glue. *Int J Curr Microbiol Appl Sci* 7(7):2853–2857
- Gonzalez Chavez C, Haen JD, Van Angronsveld J, Dodd JC (2002) Copper sorption and accumulation by the extra radical mycelium of different *Glomus* sp isolated from the same polluted soil. *Plant Soil* 240:287–297
- Gonzalez-Chavez MC, Gonzalez RC, Wright SF, Nichols KA (2004) The role of glomalin, a protein produced by Arbuscular mycorrhizal fungi, in sequestering potentially toxic elements. *Environ Pollution* 130(3):317–323

- Gupta VK, Rastogi A (2008) Sorption and desorption studies of chromium (VI) from nonviable cyanobacterium *Nostoc muscorum* biomass. *J Hazard Mater* 154(1–3):347–354
- Gupta VK, Shrivastava AK, Jain N (2001) Biosorption of chromium (VI) from aqueous solutions by green algae *Spirogyra* species. *Water Res* 35(17):4079–4085
- Han FX, Banin A, Triplett GB (2001) Redistribution of heavy metals in arid-zone soils under a wetting-drying soil moisture regime. *Soil Sci* 166:18–28
- Han FX, Yi S, Sridhar BBM, Monts DL (2004) Distribution, transformation and bioavailability of trivalent and hexavalent chromium in contaminated soil. *Plant Soil* 265(243–252):2004
- Hans JL (2015) Discovery, properties and applications of chromium and its compounds. *Chem Text* 1:6
- He Y, Gong Y, Su Y, Zhang Y, Zhou X (2019) Bioremediation of Cr (VI) contaminated ground-water by *Geobacter sulfurreducens*: environmental factors and electron transfer flow studies. *Chemosphere* 221:793–801
- Hossain S, Hossain S, Islam RF, Kabir MH, Ali S, Islam MDS, Imran KM, Moniruzzaman M, Mou TJ, Parvez AK, Mahmud ZH (2020) Bioremediation of hexavalent chromium by chromium resistant bacteria reduces Phytotoxicity. *Int J Environ Res Public Health* 17(6013):1–19
- Huffman EWD Jr, Allaway WH (1973) Growth of plants in solution culture containing low levels of chromium. *Plant Physiol* 52:72–75
- Hussain A, Alamzeb S, Begum S (2013) Accumulation of heavy metals in edible parts of vegetables irrigated with waste water and their daily intake to adults and children, District Mardan. *Pakistan Food Chem* 136(3–4):1515–1523
- Igiri BE, Okoduwa SI, Idoko GO, Akabuogu EP, Adeyi AO, Ejiogu IK (2018) Toxicity and bioremediation of heavy metals contaminated ecosystem from tannery wastewater: A review. *J Toxicol* 2018:1–16
- Iqbal MZ, Saeeda S, Muhammad S (2001) Effects of chromium on an important arid tree (*Caesalpinia pulcherrima*) of Karachi city. *Pak Ecol Bratislava* 20:414–422
- International Agency for Research on Cancer (1987) Overall evaluations of carcinogenicity: And updating of IARC monographs, vol. 1 to 42. IARC monographs on the evaluation of the carcinogenic risk of chemicals to humans: Suppl 7. IARC 1987, 7, 1–440
- Ismail IM, Moustafa TM (2016) Biosorption of heavy metals. In: Pathania D (ed) *Heavy metals: sources, toxicity and remediation techniques*. Nova Science Publishers, Hauppauge, NY. Chapter 5
- Jain R, Srivastava S, Madan VK (2000) Influence of chromium on growth and cell division of sugarcane. *Indian J Plant Physiol* 5:228–231
- Jayakumar GC, Kumar G, Tesema AF, Thi NBD, Kobayashi T, Kaiqin X (2016) Bioremediation for tanning industry: a future perspective for zero emission. In: Saleh HE-DM, Abdel Rahman RO (eds) *Management of hazardous wastes*. IntechOpen. <https://doi.org/10.5772/63809>
- Jeyasingh J, Ligy P (2005) Bioremediation of chromium contaminated soil: optimization of operating parameters under laboratory conditions. *J Hazard Mater* 118:113–120
- Jobby R, Jha P, Yadav AK, Desai N (2018) Biosorption and biotransformation of hexavalent chromium [Cr(VI)]: A comprehensive review. *Chemosphere* 207:255–266
- Joner EF, Leyval C (1997) Uptake of <sup>109</sup>Cd by roots and hyphae of a *G.mosseae*, *Trifolium subterraneum mycorrhiza* from soil amended with high and low concentrations of cadmium. *New Phytol* 135:353–360
- Joner EJ, Leyval C, Briones R (2000) Metal binding capacity of arbuscular mycorrhizal mycelium. *Plant Soil* 226:227–234
- Joutey NT, Sayel H, Bahafid W, El Ghachtouli N (2015) Mechanisms of hexavalent chromium resistance and removal by microorganisms. In: Whitacre DM (ed) *Reviews of environmental contamination and toxicology*. Springer, Cham, p 233
- Kabata-Pendias A, Pendias H, Kabata-Pendias A (2000) *Trace elements in soils and plants*, 3th edn. CRC Press, Boca Raton, FL

- Kamran M, Eqani S, Katsoyiannis A, Xu R, Bibi S, Benizri E, Chaudhary H (2017) Phytoextraction of chromium (Cr) and influence of *Pseudomonas putida* on *Eruca sativa* growth. *J Geochem Explor* 182:269–274
- Kapoor A, Viraraghavan T (1997) Heavy metal biosorption sites in *Aspergillus niger*. *Bioresour Technol* 61:221–227
- Kaur H, Kumar A (2014) Bioremediation of hexavalent chromium in wastewater effluent by *Pseudomonas putida* (MTCC 102). *J Res Earth Environ Sci* 1(4):18–24
- Kaur R, Yadav P, Thukral AK, Sharma A, Bhardwaj R, Alyemeni MN, Wijaya L, Ahmad P (2018) Castasterone and citric acid supplementation alleviates cadmium toxicity by modifying antioxidants and organic acids in *Brassica juncea*. *J Plant Growth Regul* 37:286–299
- Khan E, Kuek C, Chaudhry TM, Khoo CS, Hayes WJ (2000) Role of plants, mycorrhizae and phytochelators in heavy metal contaminated land remediation. *Chemosphere* 41:197–207
- Khan AG (2002) The significance of microbes. In: Wong MH, Bradshaw AD (eds) *The restoration and management of derelict land: modern approaches*. World Scientific Publishing, Singapore, pp 80–92
- Kim JG, Dixon JB, Chusuei CC, Deng Y (2002) Oxidation of chromium (III) to (VI) by manganese oxides. *Soil Sci Soc Am J* 66:306–315
- Kim IH, Choi JH, Joo JO, Kim YK, Choi JW, Oh BK (2015) Development of a microbe-zeolite carrier for the effective elimination of heavy metals from seawater. *J Microbiol Biotechnol* 25(9):1542–1546
- Kocik K, Ilavsky J (1994) Effect of Sr and Cr on the quantity and quality of the biomass of field crops In: *Proceedings of a seminar on Production and utilization of agricultural and forest biomass for energy held at Zvolen Slovakia*, pp 168–178
- Kratochvil D, Pimentel P, Volesky B (1998) Removal of trivalent and hexavalent chromium by seaweed biosorbent. *Environ Sci Technol* 32:2693–2698
- Krupa Z, Baszynski T (1995) Some aspect of heavy metal toxicity towards photosynthetic apparatus direct and indirect effect of light and dark reactions. *Acta Physiol Plant* 17:177–190
- Kumar V, Suryakant SPK, Kumar S, Kumar N (2016) Effect of chromium toxicity on plants: A review. *Agriways* 4(1):107–120
- Lopez A, Lazaro N, Priego J, Marques A (2000) Effect of pH on the biosorption of nickel and other heavy metals by *Pseudomonas fluorescens* 4F39. *J Ind Microbiol Biotechnol* 24(2):146–151
- Losi ME, Amrhein C, Frankenberger WT (1994) Factors affecting chemical and biological reduction of Cr(VI) in soil. *Environ Toxicol Chem* 13:1727–1735
- Luptakova A, Kusnierova M (2005) Bioremediation of acid mine drainage contaminated by SRB. *Hydrometallurgy* 77(1–2):97–102
- Mangabeira PA, Ferreira AS, de Almeida A-AF, Fernandes VF, Lucena E, Souza VL, dos Santos Júnior AJ, Oliveira AH, Grenier-Loustalot MF, Barbier F (2011) Compartmentalization and ultrastructural alterations induced by chromium in aquatic macrophytes. *Biometals* 24:1017–1026
- Medfu TM, Salilih FZ, Ishetu AI (2020) Microbes used as a tool for bioremediation of heavy metal from the environment. *Cogent Food Agric* 6(1):1783174
- Megharaj M, Avudainayagam S, Naidu R (2003) Toxicity of hexavalent chromium and its reduction by bacteria isolated from soil contaminated with tannery waste. *Curr Microbiol* 47: 51–54
- Meharg A (2003) The mechanistic basis of interactions between mycorrhizal associations and toxic metal cations. *Mycol Res* 107:1253–1265
- Monachese M, Burton JP, Reid G (2012) Bioremediation and tolerance of humans to heavy metals through microbial processes: a potential role for probiotics? *Appl Environ Microbiol* 78:6397–6404
- Moreira JM, Bartoli E, Chico R, Sole C, Cabeza LF (2011) Online. *Vers J Clean Prod* 19:2128–2132
- Nriagu JO (1988) Production and uses of chromium. In: *Chromium in natural and human environment*. Wiley, New York, pp 81–105

- Obbard P (2001) Ecotoxicological assessment of heavy metals in sewage sludge amended soils. *J Appl Geochem* 16:1405–1411
- Okolo NV, Olowolafe EA, Akawu I, Okoduwa SIR (2016) Effects of industrial effluents on soil resources in Challawa industrial area, Kano, Nigeria. *J Glob Ecol Conserv* 5:1–10
- Oves M, Khan MS, Zaidi A (2013) Chromium reducing and plant growth promoting novel strain *Pseudomonas aeruginosa* OSG41 enhance chickpea growth in chromium amended soils. *Eur J Soil Biol* 56(1):72–83
- Panda SK, Patra HK (2000) Nitrate and ammonium ions effect on the chromium toxicity in developing wheat seedlings. *P Natl Acad Sci India B* 70:75–80
- Panda SK (2002) The biology of oxidative stress in green cells a review. In: Panda SK (ed) *Advances in stress physiology of plants*. Scientific Publishers, Jhodsipur, pp 1–3
- Panda SK (2003) Heavy metal phytotoxicity induces oxidative stress in *Taxithelium* sp. *Curr Sci* 84:631–633
- Panosyan H (2015) Thermophilic and halophilic prokaryotes isolated from extreme environments of Armenia and their biotechnological potential. In: Singh RP, Manchanda G, Maurya IK, Wei Y (eds) *Microbial versatility in varied environments*. Springer, Singapore, pp 13–34
- Pavel VL, Diaconu M, Gavrilescu M (2012). Studies of toxicity of Chromium(VI) and Cadmium (II) on some microbial species. International symposium on biosorption and bioremediation. Romania.
- Poli A, Salerno A, Laezza G, Di Donato P, Dumontet S, Nicolaus B (2009) Heavy metal resistance of some thermophiles: Potential use of  $\alpha$ -amylase from *Anoxybacillus amylolyticus* as a microbial enzymatic bioassay. *Res Microbiol* 160(2):99–106
- Polti MA, Amoroso MJ, Abate CM (2010) Chromate reductase activity in *Streptomyces* sp. MC1. *J Gen Appl Microbiol* 56:11
- Pradhan D, Sukla LB, Sawyer M, Rahman PKSM (2017) Recent bioreduction of hexavalent chromium in wastewater treatment: a review. *J Ind Eng Chem* 55:1–20
- Pradhan D, Sukla LB, Mishra BB, Devi N (2019) Biosorption for removal of hexavalent chromium using microalgae *Scenedesmus* sp. *J Clean Prod* 209:617–629
- Prasad MNV, Greger M, Landberg T (2001) *Acacia nilotica* L bark removes toxic elements from solution: corroboration from toxicity bioassay using *Salix viminalis* L in hydroponic system. *Int J Phytoremed* 3:289–300
- Purwanti IF, Kurniawan SB, Tangahu BV, Rahayu NM (2017) Bioremediation of Trivalent Chromium in Soil Using Bacteria. *Int J Appl Res* 12(20):9346–9350
- Ramasamy K, Naidu R (2000) Status of tanning industries in India. In: Naidu R et al (eds) *Towards better management of soils contaminated with tannery wastes*. ACIAR Publication No 88, pp 13–21
- Raspor P, Batic M, Jamnik P, Josic D, Milacic R, Pas M, Recek M, Rezic-Dereani V, Skrt M (2000) The influence of chromium compounds on yeast physiology. *Acta Microbiol Immunol Hung* 47: 143–173
- Rawat M, Rawat AP, Giri K, Rai JPN (2013) Cr(VI) sorption by free and immobilised chromate-reducing bacterial cells in PVA–alginate matrix equilibrium isotherms and kinetic studies. *Environ Sci Pollut Res* 20:5198–5211
- Reale L, Ferranti F, Mantilacci S, Corboli M, Aversa S, Landucci F, Baldisserotto C, Ferroni L, Pancaldi S, Venanzoni R (2016) Cyto-histological and morpho-physiological responses of common duckweed (*Lemna minor* L.) to chromium. *Chemosphere* 145:98–105
- Renuga Devi V, Gomathy M, Sabarinathan KG, Jeysree M, Kalaiyarasi V (2020) Assessing the plant growth promoting activity of phylloplane associated plant bacteria of rice. *Int J Curr Microbiol App Sci* 9(7):384–391
- Romanenko VI, Koren'kov VN (1977) Pure culture of bacteria using chromates and bichromates as hydrogen acceptors during development under anaerobic conditions. *Mikrobiologiya* 46(3): 414–417
- Rout GR, Samantaray S, Das P (1997) Differential chromium tolerance among eight mung bean cultivars grown in nutrient culture. *J Plant Nutr* 20:473

- Sadettin S, Dönmez G (2007) Simultaneous bioaccumulation of reactive dye and chromium (VI) by using thermophil *Phormidium* sp. *Enzym Microb Technol* 41(1–2):175–180
- Salt DE, Pickering IJ, Prince RC, Gleba D, Dushenkov S, Smith RD, Raskin I (1997) Metal accumulation by aquacultured seedlings of Indian mustard. *Environ Sci Technol* 31(6):1636–1644
- Samarth DP, Chandekar CJ, Bhadekar RK (2012) Biosorption of heavy metals from aqueous solution using *Bacillus licheniformis*. *Int J Pure Appl Sci Technol* 10(2):12–19
- Shafiq M, Farooqi Z, Kabir M, Murtaza S (2018) Effects of chromium on seed germination and seedling growth of mung bean (*Vigna radiata* L.). *RJLBPS* 25:2–10
- Shanker AK, Djanaguiraman M, Venkateswarlu B (2009) Chromium interactions in plants: current status and future strategies. *Metallomics* 1:375–383
- Sharma S, Malaviya P (2016) Bioremediation of tannery wastewater by chromium resistant novel fungal consortium. *Ecol Eng* 91:419–425
- Sharma DC, Sharma CP (1993) Chromium uptake and its effects on growth and biological yield of wheat. *Cereal Res Commun* 21:317–321
- Sharma M, Kaushik A, Kaushik CP (2011) *Int Biodeterior Biodegradation* 65(4):656–663
- Sharma A, Kapoor D, Wang J, Shahzad B, Kumar V, Bali AS, Jasrotia S, Zheng B, Yuan H, Yan D (2020) Chromium bioaccumulation and its impacts on plants: an overview. *Plan Theory* 9:100
- Shukla D, Vankar PS, Srivastava SK (2012) Bioremediation of hexavalent chromium by a cyanobacterial mat. *Appl Water Sci* 2(4):245–251
- Siddiquee S, Rovina K, Azad SA, Naher L, Suryani S, Chaikaew P (2015) Heavy metal contaminants removal from wastewater using the potential filamentous fungi biomass: a review. *J Microb Biochem Technol* 7(6):384–395
- Singh D, Sharma NL, Singh CK, Sarkar SK, Singh I, Dotaniya ML (2020) Effect of chromium (VI) toxicity on morpho-physiological characteristics, yield, and yield components of two chickpea (*Cicer arietinum* L.) varieties. *PLoS One* 15(12):e0243032
- Sivakumar D (2016) Biosorption of hexavalent chromium in a tannery industry wastewater using fungi species. *Glob J Environ Sci Manag* 2(2):105–124
- Skeffington RA, Shewry PR, Petersen PJ (1976) Chromium uptake and transport in barley seedlings *Hordeum vulgare*. *Planta* 132:209–214
- Smith SE, Read DJ (1997) In: *Mycorrhizal Symbiosis*, 2nd edn. Academic press, London, p 589
- Srivastava S, Nigam R, Prakash S, Srivastava MM (1998) Mobilization of trivalent chromium in presence of organic acids: a hydroponic study of wheat plant (*Triticum vulgare*). *Bull Environ Contam Toxicology* 63:524–530
- Stambulska UY, Bayliak MM, Lushchak VI (2018) Chromium (VI) toxicity in legume plants: modulation effects of rhizobial symbiosis. *Biomed Res Int*:1–13
- Subramanian KS, Thangaraju M, Jegan RA (2008) Mechanisms involved in tolerance of mycorrhizal plants to heavy metals. In: Saikia R, Bezbaruah R, Bora T (eds) *Microbial biotechnology*. New India Publishing Agency, New Delhi, pp 299–317
- Suganya K (2004) Fate of added chromium, its uptake and translocation as influenced by amendments under selected soils and crops, M Sc Thesis Tamil Nadu Agricultural University, Coimbatore
- Tatiani AM, Scapini T, Dalastra C, Kubeneck S, Camargo AF, Bordin ER, Venturin B, Jacques RJS, de Andrade N, Belle C, Haminiuk CWI, Fongaro G, Treichel H (2020) Hexavalent Chromium Removal Using Filamentous Fungi: Sustainable Biotechnology. *Mary Ann Liebert Inc* 16:2
- Tewari N, Vasudevan P, Guha BK (2005) Study on biosorption of Cr(VI) by *Mucor hiemalis*. *Biochem Eng J* 23:185–192
- Thacker U, Datta M (2006) Reduction of toxic chromium and partial localization of chromium reductase activity in bacterial isolate DM1. *World J Microbiol Biotechnol* 21:891–899
- Wallace A, Soufi SM, Cha JW, Romney EM (1976) Some effects of chromium toxicity on bush bean plants grown in soil. *Plant Soil* 44:471–473

- Wang M, Liu J, Lai W (2017) Seasonal and spatial distribution of glomalin-related soil protein and sequestered metals affected by AM fungi in the citrus rhizosphere. *Adv Plants Agric Res* 6(6): 182–186
- Wright SF, Miller PD (1994) Dynamic processes of vesicular-arbuscular mycorrhizae: a mycorrhizosystem within the agroecosystem. In: Hatfeld JL, Stewart BA (eds) *Advances in soil science. Soil biology: effects on soil quality*. Lewis Publishers, Boca Raton, pp 29–59
- Wright SF, Upadhyaya A (1996) Extraction of an abundant and unusual protein from soil and comparison with hyphal protein of arbuscular mycorrhizal fungi. *Soil Sci* 161:575–586
- Wright SF, Upadhyaya A (1998) A survey of soils for aggregate stability and glomalin, a glycoprotein produced by hyphae of arbuscular mycorrhizal fungi. *Plant Soil* 198:97–107
- Xu L, Luo M, Li W, Wei X, Xie K, Liu L, Jiang C, Liu H (2011) Reduction of hexavalent chromium by *Pannonibacter phragmitetus* LSSE-09 stimulated with external electron donors under alkaline conditions. *J Hazard Mater* 185:1169–1176
- Xu X, Xia L, Chen W, Huang Q (2017) Detoxification of hexavalent chromate by growing *Paecilomyces lilacinus* XLA. *Environ Pollut* 225:47–54
- Yu MH (2001) *Impacts of environmental toxicants on living systems*. Environmental toxicology. CRC Press LLC
- Zahoor A, Rehman A (2009) Isolation of Cr(VI) reducing bacteria from industrial effluents and their potential use in bioremediation of chromium containing wastewater. *J Environ Sci* 21(6): 814–820
- Zayed A, Lytle CM, Jin-Hong Q, Terry N, Qian JH (1998) Chromium accumulation, translocation and chemical speciation in vegetable crops. *Planta* 206:293–299
- Zhao Y, Hu C, Wang X, Qing X, Wang P, Zhang Y (2019) Selenium alleviated chromium stress in Chinese cabbage (*Brassica campestris* L. ssp. *Pekinensis*) by regulating root morphology and metal element uptake. *Ecotox Environ Safe* 173:314–321
- Zouboulis AI, Loukidou MX, Matis KA (2004) Biosorption of toxic metals from aqueous solutions by bacteria strains isolated from metal-polluted soils. *Process Biochem* 39(8):909–916
- Zurayk R, Sukkariyah B, Baalbaki R (2001) Common hydrophytes as bioindicators of nickel, chromium and cadmium pollution. *Water Air Soil Pollut* 127:373–388

# Chapter 11

## Microbial Interactions with Gold and Uranium



Sadia Ilyas, Hyunjung Kim, and Rajiv Ranjan Srivastava

**Abstract** The involvement of metals (both directly and indirectly) in microorganisms' growth, metabolism, and differentiation are interdependent to the metal species and microbial environment as well. A variety of properties that exhibit the changes in metal species and mobility through the metal-to-microbe interaction, mineral transformation, and deterioration often follow certain mechanisms that are important to natural bio-geo-chemical cycles of metal-bearing resources like auriferous and radionuclide ores. This chapter is, therefore, devoted to the investigations of microbial interactions with gold and uranium in solid and aqueous systems. Microbes mediate gold and uranium solubilization from solid systems via excretion of various metabolites such as amino acids, cyanide, thiosulfate, and by redox transformations which this chapter explains in detail. Additionally, microbial capability to precipitate metal ions intra-/extracellular products is also discussed. Furthermore, the microbial genomic and biochemical responses addressing the toxic metal complexes from surrounding aquatic environment are also discussed.

### 11.1 Microbial Interaction with Metals

Metals, metalloids, and minerals are essential to human existence. They are ubiquitous in the biosphere with a key role in infrastructure, transportation, and consumer goods to ensure the sustainable development goals (SDGs). In addition, metals are allocated in terrestrial and aquatic habitats because of the industrial revolution and landfill disposal of end-of-life (EoL) products (Srivastava et al. 2020). A direct/indirect involvement of metals in every aspect of microbial growth, its metabolism, and differentiation through surface interaction in a natural and synthetic environment

---

S. Ilyas (✉) · H. Kim

Department of Earth Resources and Environmental Engineering, Hanyang University, Seoul, Republic of Korea

R. R. Srivastava

Center for Advanced Chemistry, Institute of Research and Development, Duy Tan University, Da Nang, Vietnam



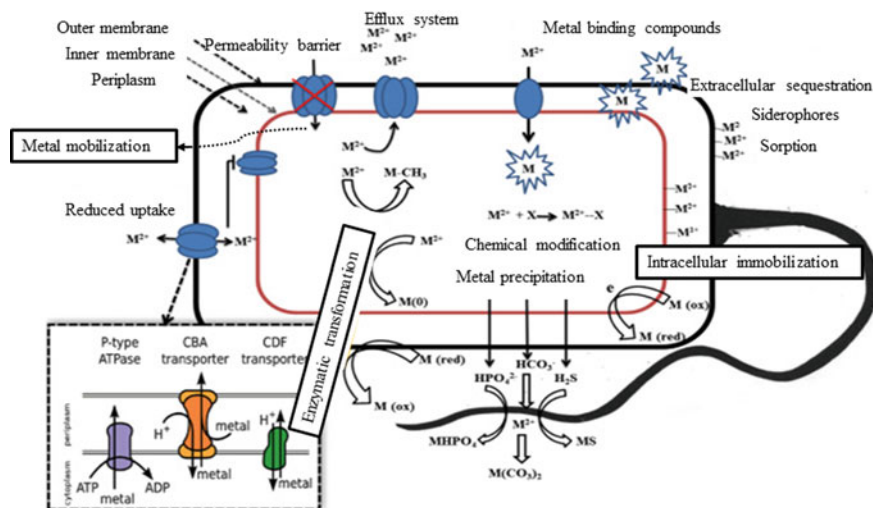


Fig. 11.1 Various microbial-metal interactions (adapted from Etesami 2018 after permission)

can significantly alter their physiochemical states (Gadd 2010). Microorganisms are usually intimately associated with metals, and associated elements, wherein the activities can result in mobilization and/or, immobilization of metal ions depending upon the mechanism pathways and the microenvironment where the organism(s) are located (Gadd 2002). Some of the typical metal-to-microbe interactions are shown in Fig. 11.1. A variety of properties that exhibit the changes in metal species and mobility through the metal-to-microbe interaction, mineral transformation, and deterioration often follow certain mechanisms that are important to natural bio-geo-chemical cycles of metal-bearing resources like auriferous and radionuclide ores.

## 11.2 Microbial Interactions with Gold

Gold is precious and among one of the ten rarest elements of this planet. On average, 0.005 parts per million (ppm) of gold content in the solid material of Earth's crust and a concentration range of 0.02 ~ 0.2 parts per billion (ppb) gold in natural waters has been identified. However, the nonuniform distribution of gold which often gets enriched in a mineralized zone to potentially form the economically viable deposits in terms of primary reserves, e.g., skarn type-, vein type-, and disseminated deposits (Boyle 1979). This deposition in primary minerals commonly takes place through the metal-rich hydrothermal fluids, which circulate in open pores of rock-veins and gets deposited in resultant of the consecutive cooling and/or heating effects. Microbes interact with gold from solid and aqueous systems in the following ways:

- (i) Microbes mediate gold solubilization from solid systems and via excretion of a number of metabolites which can affect the solubilization and deposition of gold (e.g., amino acids, thiosulfate, and cyanide).
- (ii) Direct genomic and biochemical responses that deal the gold complexes from the surrounding aquatic environment.
- (iii) Precipitating gold's intra-/extracellular products (e.g., EPS and sulfide minerals).

### ***11.2.1 Microbial Interaction with Gold in Solid Systems***

After interacting with metal-constituent bodies in the environment, microbes can act to: (i) binding the metal species which influences the cell surface; (ii) carrying microbes into the cell for producing various intercellular functions; and (iii) forming various metabolic products which can be used for chelating the metal ions. Furthermore, the oxidation of refractory gold-containing ores and removal of disrupting ore constituents is an act following either direct (physical) or indirect (metabolic) mechanisms or, a combination of both as well. The pre-treatment mechanism of microbial activities associated with gold bio-oxidation has been further clarified by as follows:

- (i) The attached microbes onto mineral surface can oxidize the mineral bodies (usually sulfides) by releasing  $\text{H}_2\text{SO}_4$ .
- (ii) The attached microbes oxidize  $\text{Fe}^{2+}$  ions to  $\text{Fe}^{3+}$  ions in order to mediate the liberation of metal from sulfide minerals.
- (iii) The transfer of oxidized  $\text{Fe}^{3+}$  ions into bulk mediates the bio-oxidation reaction onto mineral surface in terms of iron liberation and simultaneously gold enrichment in the mineral particles.

There are microbially associated direct mechanisms that are enzyme mediated (oxidases and reductases), whereas indirect mechanisms often are associated with the metabolites (for example, carboxyl-based organic acids or, mineral (inorganic) acids) of the microorganisms (Dew et al. 1999). However, no strong evidence persists for a direct breaking of sulfides by microbial activities (Sand et al. 1995; Tributsch 2001; Watling 2006). The widely accepted mechanism can be understood by the thiosulfate or polysulfate pathways (Rawlings 2005; Srivastava et al. 2020).

After a microbial pre-treatment (usually termed as the bio-oxidation) step, gold leaching in a suitable lixiviant solution can be performed by either using chemical reagents or metabolic products. Figure 11.2 indicated various mechanisms of microbial metal interaction and biogenic lixiviant production.

Microbial mechanisms to solubilize gold from the auriferous material include oxidation followed by gold cyanidation with biogenic cyanide excreted by the HCN synthesis using cyanogenic microorganisms or synthesized by oxidative decarboxylation of glycine. The process leads to form dicyanoaurate complexes, i.e.,  $\text{Au}(\text{CN})_2^-$

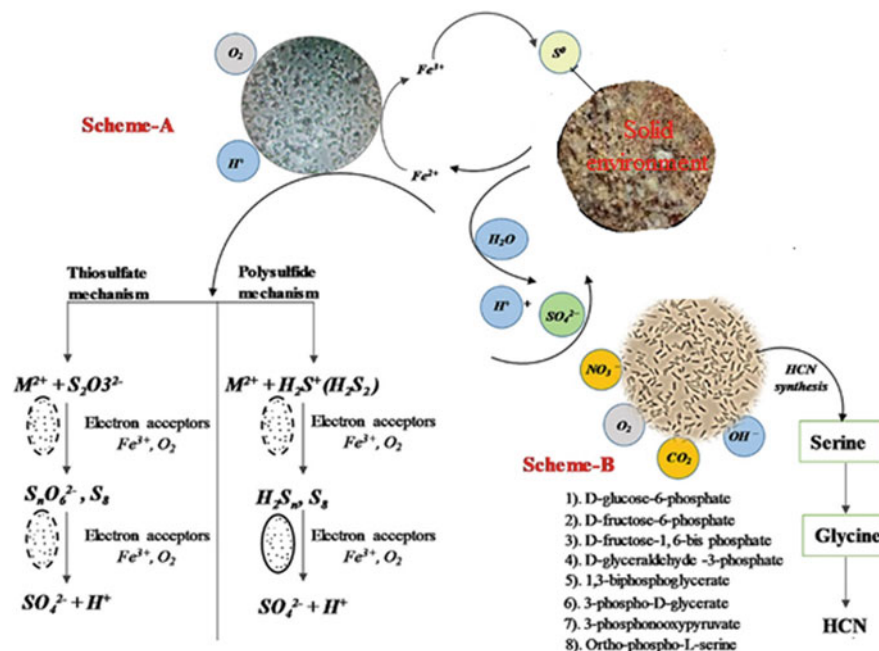


**Fig. 11.2** Thiosulfate and polysulfide mechanisms of microbial–metal oxidation and biogenic lixiviant production for gold complexation (modified from Srivastava et al. 2020 after permission)

$(CN)_2^-$  (Rodgers and Knowles 1978; Faramarzi et al. 2004; Faramarzi and Brandl 2006; Habashi 1970) by following the reaction as below:

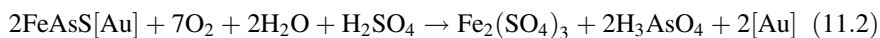


At a physiological (mild acidic to neutral range of) pH, the cyanide mainly remains in the gaseous form of HCN (pKa, 9.3), which is a highly toxic volatile substance (Faramarzi and Brandl 2006). But in alkaline pH range of more than 10.5, the cyanide remains dissociated as  $CN^-$  ions in solubilized form. Therefore, the biogenic cyanide captured in a higher alkaline solution can improve gold solubilization by forming the  $[Au(CN)_2^-]$  complex (Faramarzi and Brandl 2006). An in vitro study conducted by Campbell et al. (2001) using the cyanide producing microorganism, *Chromobacterium violaceum* showed that the biofilm developed onto gold surface could solubilize all gold within 17 days of duration. A final concentration of 35 ppm gold and 14.4 ppm free cyanide was obtained in the leached solution. In another study performed using *Pseudomonas plecoglossicida*, Faramarzi and Brandl (2006) showed 69% Au leaching from the shredded sample of waste printed circuit boards, which took ~80 h of incubation to produce ~500 ppm Au  $(CN)_2^-$  complex.

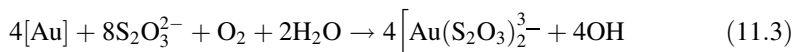
Bio-cyanide synthesis and its excretion in soil are commonly observed through the microbial activities exhibited by the bacterium viz. *Pseudomonas fluorescens*, *Chromobacterium violaceum*, *Pseudomonas chlororaphis* subsp. *aureofaciens*, *Pseudomonas plecoglossicida*, *Pseudomonas aeruginosa*, *Pseudomonas syringae*, *Pseudomonas putida*, *Priestia megaterium*, archaea species such as *Ferroplasma acidiphilum*, and *Ferroplasma acidarmanus* that produce cyanide via the membrane-bound enzyme complex and HCN syntheses (Faramarzi and Brandl 2006). Notably, metabolic cyanide production is possible only for a shorter duration (of 2 ~ 4 days of early stationary phase) in the presence of glycine (Castric 1981; Kita et al. 2006) as a secondary metabolite independent from the growth phase (Castric 1975). Glycine (NH<sub>2</sub>CH<sub>2</sub>COOH) preliminary acts to be a precursor through an oxidative decarboxylation via the enzymatic synthesis of HCN, and remains associated with the cell membrane that represents the cyanogenic group. Further, the oxidative product of glycine forming imino acetic acid (H–C(NH)–COOH) followed by C–C bond splitting with an attendant second dehydrogenase reaction producing metabolic HCN and CO<sub>2</sub> as depicted in Fig. 11.5 (Laville et al. 1998). To trap this volatile HCN, an alkaline trap is required to simultaneously build up the cyanide concentration therein the solution.

In this manner, glycine has been found to be a common metabolic precursor to progress the microbial cyanidation process (Knowles 1976; Rodgers and Knowles 1978). After 20 days of incubation duration, the highest glycine concentration in Tomakin Park Gold Mine soil microcosms has been detected (soil incubation; oxic or anoxic, unamend or amend with Au pellet- or cycloheximide in a 1:4 (w:v) aqueous slurry at 25 °C in the dark) (Reith and McPhail 2006). All these findings suggest that gold forming dicyanoaurate complex takes place through the solubilization of gold with amino acids.

In surficial and arid environments (at below 500 m of land surface), iron- and sulfur-oxidizing chemolithoautotrophic bacteria like *Acidithiobacillus thiooxidans* and *Acidithiobacillus ferrooxidans* and archaea. They can form biofilms on the surfaces of metal sulfides and obtain the required energy source by oxidizing the mineral through a number of metabolic pathways. For example, the sulfur oxidase pathway (*Sox*) and the reverse *Dsr* pathways are good examples (Nordstrom and Southam 1997; Friedrich et al. 2005; Southam and Saunders 2005). The biofilms altogether provide the reaction spaces for sulfide oxidation at interface, biogenic sulfuric acid for hydrolysis of proton ions and keep Fe<sup>3+</sup> in its oxidized form and reactive state as well (Sand et al. 1995; Rawlings 2005; Mielke et al. 2003). Subsequently, a higher ferric and proton ions' concentration actively attacks the valence bonds of sulfides to degrade through an intermediate product forming thiosulfate (Sand et al. 1995). Similarly, the oxidation of sulfidic minerals can also release the companion metals into the solution (Southam and Saunders 2005):



During that course, a few sulfur and iron oxidizers as *Thiobacillus thiooparus* and *A. ferrooxidans* also excrete thiosulfate. Further, in the presence of oxygen, the oxidation of gold through complexation with thiosulfate takes place as follows (Aylmore and Muir 2001):



The metabolic production of thiosulfate can also be performed by some alternative procedures that involve different microbial groups which can stimulate gold dissolution. Sulfate reducing bacteria, commonly found in acid sulfate soils (in anoxic, metal-rich, sulfate-containing sites) can produce thiosulfate while sulfite is reduced by  $\text{H}_2$  and formate (Fitz and Cypionka 1990). The gold dissolution mechanism involving heterotrophic microorganisms (i.e., *Pseudomonas fluorescens*, *Bacillus subtilis*, *Paenibacillus alvei*, *Serratia liquefaciens*, and *Brevibacillus nitrificans*) have been underpinned by previous studies, where under an in vitro condition, approximately 35 ppm of gold was solubilized by forming the complexes with metabolic amino acid (Lyalikova and Mockeicheva 1969; Korobushkina et al. 1974, 1976; Boyle 1979; Korobushkina et al. 1983). An assessment of DNA fingerprinting and metabolic function of the microorganism community (during the incubation period) along with gold and amino acid analyses, a change in bacterial community has been observed by Reith and McPhail (2006). Some of the bacteria such as *Streptomyces fradiae* can produce thiosulfate in resultant to sulfur metabolization from cysteine and further assist to gold solubilization (Kunert and Stransky 1988).

### 11.2.2 Microbial Interaction with Gold in Aqueous Systems

The presence of gold in microbial system is very toxic to the microorganisms even at a lower concentration of gold. For example, the minimal inhibitory concentration (MIC) in *Escherichia coli* has been observed to be 20  $\mu\text{M}$  gold (i.e., about 4.0 ppm). Notably, it is also analyzed that the adverse toxicity toward microbial growth starts at about 1/1000 of MIC (Nies 1999). This produces acute toxicity to the microorganism when the concentration of gold from auriferous soil leaching can be up to 100 ppb (Reith and McPhail 2006), which can be much higher in the leach solutions obtained by dissolution of gold nuggets. Hence, the bacterial community developed in these zones is supposed to adapt to the detoxification of cell environment. In this context, many microbes have grown with a direct genomic and biochemical responses that deal the gold toxicity from various aquatic environments.

In scenarios of genomic and biochemical responses of bacterial species, it was observed that cytoplasmic transcriptional regulators (metal ion responsive) were playing an important role to regulate genes' expression involved in homeostasis and efflux systems of metal ions (Silver 1996; Nies 1999; Hobman 2007). The *MerR*

family of transcriptional activators (which is a kind of metal-sensing regulators) were observed in several bacterial communities and found to recognize and respond to a variety of metal ions in various aqueous environments (Silver 1996; Nies 1999; Hobman 2007). The specific regulation of transcription exhibited by gold complexes with *E. coli*. Was demonstrated by Stoyanov and Brown (2003). Wherein, the *MerR*-like transcriptional activator (i.e., *CueR* usually responds to  $\text{Cu}^+$ ) was observed to be activated by gold complexes which were promoted by the specific binding of gold to the cysteine residues 112 and 120 (Cys 112 and 120). On the other hand, a newly characterized transcriptional regulator (i.e., *GolS*) in a bacterium *Salmonella enterica* was found to share Cys 112 and 120 with other *MerR* family regulators but retained exclusive specificity to gold chloride,  $\text{AuCl}_4^-$  (Checa et al. 2007). The occurrence of a minimum two open reading frames whose expression was activated by *GolS* was disclosed. Wherein, (i) predicted transmembrane efflux ATPase (*GolT*) and (ii) predicted metallochaperone (*GolB*) suggested the resistant mechanism to gold complexes along with the organization of other metal resistances. It was also observed that an *MerR* regulator not only controls the production of itself but also the production of a P-type ATPase and a chaperone protein as well (Checa et al. 2007; Hobman 2007).

In the case of using *A. thiooxidans*, gold accumulation inside cells as the fine-grained colloids (of size 5 to 10 nm in diameter) and in the aqueous solution as crystalline gold (of several micrometers) can be achieved (Lengke and Southam 2005). Gold deposition on cells occurs through the concentration build-up along the cytoplasmic membrane, indicating that gold precipitation improves via electron transportation in association with energy generation. When gold thiosulfate complex ( $\text{Au}^+$ ) enters into cells, thiosulfate is consumed in metabolic process within the periplasmic space while gold is transported into cytoplasmic membrane via the chemiosmotic gradient in association with ATP hydrolysis. As gold is nondegradable,  $\text{Au}^+$  presumably forms either a new complex or gets reduced to zero-valance gold ( $\text{Au}^0$ ). However,  $\text{Au}^0$  can further re-oxidized to form a new complex that can be transported outside the cytoplasm. On the other side, in the presence of  $[\text{Au}(\text{S}_2\text{O}_3)_2]^{3-}$  as sole energy source, the exchange between sulfur species and gold is allowed through an outer membrane pore. In this case, the reactions of sulfur occur in the periplasmic space instead of the cytoplasmic membrane wherein gold gets reduced. Thereafter, both (reduced gold and oxidized sulfur) are released through the outer membrane pores (Lengke and Southam 2005). The entire schematic for gold thiosulfate complex mechanism exhibited by *A. thiooxidans* is depicted in Fig. 11.3.

Similarly, many bacterial species were observed to precipitate gold intra-/extra-cellularly, and in their metabolic products. Lengke et al. (2006) demonstrated that *Leptolyngbya boryana* cells release membrane vesicles after interacting with a higher  $[\text{Au}(\text{S}_2\text{O}_3)_2]^{3-}$  concentration. These vesicles connected with cell envelopes prevent the uptake of  $[\text{Au}(\text{S}_2\text{O}_3)_2]^{3-}$  and keep away from sensitive cellular components. Further, such an interaction between  $[\text{Au}(\text{S}_2\text{O}_3)_2]^{3-}$  complex and the vesicle components resulting to precipitate gold in its elemental form, most probably via the interactions with phosphorus, sulfur, or nitrogen ligands of vesicle components

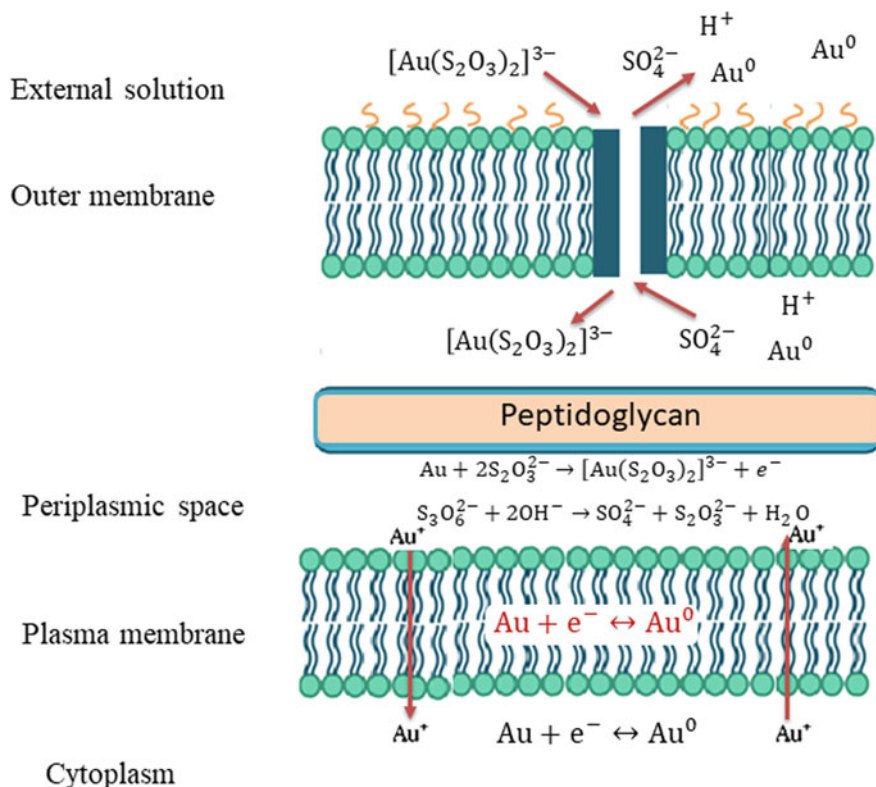


**Fig. 11.3** Gold thiosulfate complex utilization and gold precipitation by *A. thiooxidans* (adapted from Lengke and Southam 2005 after modifications)

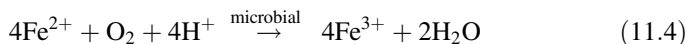
(Lengke et al. 2006). Thus, the compatible microorganism (viz. *S. enterica*, *Cupriavidus metallidurans*, and *Leptolyngbya boryana*) evolves effective mechanisms to detect gold toxicity and detoxification as well, allowing microbes to thrive in gold-rich surroundings.

It is also believed that bioaccumulation of gold by diverse microbial communities may also lead to biomineralization of secondary gold grains of different shapes. Southam and Beveridge (1994) showed the formation of octahedral gold (as  $Au^0$ ) using biogenic organic phosphate and sulfur compounds at a pH value of about 2.6. The potential of *C. metallidurans* to accumulate gold from an aquatic environment revealed through molecular profiling was indicated by Reith et al. Lengke and Southam (2005) observed the formation of octahedral gold by *Leptolyngbya boryana* at pH 1.9–2.2. The cyanobacteria, which are killed during the process, could potentially immobilize (intracellularly)  $> 100 \mu\text{g mg}^{-1}$  gold grains. The ability of sulfur redox bacteria in transformation of gold complexes to octahedral elemental gold indicates the formation of gold platelets due to the bacterial contribution in the supergene environment.

### 11.3 Microbial Interactions with Uranium

#### 11.3.1 Microbial Interaction with Uranium in Solid Systems

Uranium exists as an admixture of  $U^{6+}$  and  $U^{4+}$  states in various natural uranium ores and mill tailings.  $U^{4+}$  is insoluble in sulfate-rich acidic solutions and usually requires to be oxidized to  $U^{6+}$  state to readily solubilize as uranyl ion ( $UO_2^{2+}$ ), commonly in a diluted solution of  $H_2SO_4$ . The dominant microbes commonly represented in these processes are *Acidithiobacillus*, *Leptospirillum*, *Sulfobacillus*, *Alicyclobacillus*, and *Ferroplasma*. *Alicyclobacillus* and *Sulfobacillus* spp. are observed in column leaching of the weathered low-grade uranium ore (Habashi 2020; Kaksonen et al. 2020). Mostly, microbes mobilize uranium either directly or indirectly depending on the valence of uranium, biogenic lixiviant, matrix composition, and contaminant solubility. The role of the microorganisms in terms of involving indirect mobilization is to oxidize zero-valance sulfur ( $S^0$ ) to sulfuric acid ( $H_2SO_4$ ) and subsequently oxidize ferrous iron ( $Fe^{2+}$ ) to ferric species ( $Fe^{3+}$ ) after taking electrons (refer Eq. 11.2) as indicated in Fig. 11.4.



Biogenic ferric iron and sulfuric acid mobilize uranium as shown in Eqs. (11.6) and (11.7), respectively. These uranyl ions further interact with biogenic sulfate ions and form sulfate complexes.

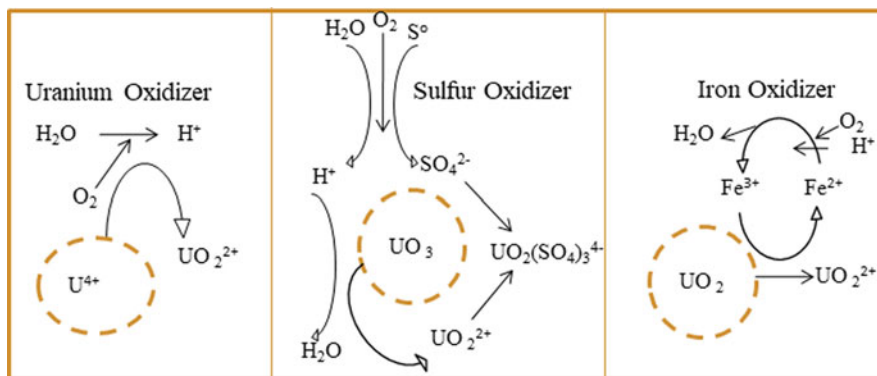
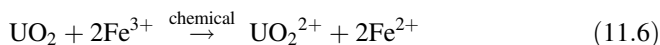
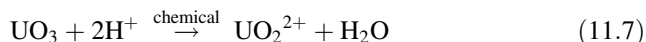
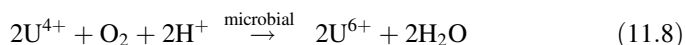


**Fig. 11.4** Integration of iron, sulfur, and uranium oxidizing bacteria with uranium containing solid system (modified from Kaksonen et al. 2020 and DiSpirito and Tuovinen 1982)

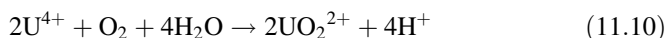
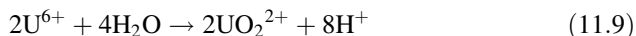




This indicates a combined redoxolysis and acidolysis mechanism for metal mobilization. The bio-mobilization rate is majorly dependent on the initial conditions of solution pH,  $\text{Fe}^{2+}$  ions concentration, and its oxidation rate to forming  $\text{Fe}^{3+}$ . For microbes, the bio-oxidation of ferrous iron ( $\text{Fe}^{2+}$ ) and regeneration of ferric iron ( $\text{Fe}^{3+}$ ) needs a sufficient availability of dissolved  $\text{O}_2$  and  $\text{CO}_2$ . In addition to the ferric iron-mediated mobilization, direct oxidation of  $\text{U}^{4+}$  to  $\text{U}^{6+}$  by *Acidithiobacillus ferrooxidans* was also investigated by some researchers (DiSpirito et al. 1983) as shown in Eq. 11.8.



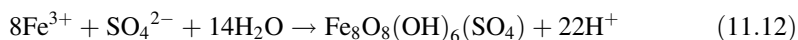
Further, the hexavalent uranium species as uranyl ions dominate at a solution pH of 2.5 (refer Eq. 11.9); hence, the net oxidation reaction can be written as Eq. 11.10.



On the other side, the secondary mineral phase (like jarosite,  $\text{MFe}_3(\text{SO}_4)_2(\text{OH})_6$ ) by precipitation of iron and sulfur species is inevitable. Wherein, a structural monovalent cation (usually  $\text{Na}^+$ ,  $\text{K}^+$ ,  $\text{NH}_4^+$ ,  $\text{H}_3\text{O}^+$ ) or a 0.5 equivalent of a divalent metal cation at ambient temperature and at a pH value below 3.5 reacts as Eq. (11.11).



Depending on the composition of monovalent cations in systems and concentration and in the absence of hydroxyl ions, the hydrolysis of  $\text{Fe}^{3+}$  ions at ambient temperature also leads to form ferric hydroxysulfate complexes, of which poorly crystallized schwertmannite is predominantly formed in a pH ranging between 2.0 and 3.5 (Bigham and Nordstrom 2000).



### 11.3.2 Microbial Interaction with Uranium in Aqueous Systems

Several key interactions of microbes-to-uranium ions that occur at low to neutral pH range facilitate metal binding with biogenic ligands onto the cell surfaces (Fowle

et al. 2000; Fein et al. 1997), interaction with intracellular polyphosphates, chelation by extracellular polysaccharides (Merroun et al. 2006; Suzuki and Banfield 2004), binding to siderophores, and S-layer proteins (Merroun et al. 2005), precipitation of mineral phases (Jeong et al. 1997; Martinez et al. 2007) or, reduction to form insoluble tetra-valence  $U^{4+}$  (Lovley et al. 1991). A study performed by Cologgi et al. (2011) recently revealed that the conductive pili (anchored to cell envelope) of *Geobacter sulfurreducens* get involved to catalyze the extracellular reduction of  $U^{6+}$  to  $U^{4+}$ . The expression of those pili improved the immobilization rate of uranium, preventing uranium permeation inside the periplasm, and also preserving the important functions of cell envelope and cell viability.

### 11.3.2.1 Microbial Interaction with Uranium by Redox Transformation; Bio-Reduction

Many physiologically active bacterial species can actively reduce soluble  $U^{6+}$  to insoluble  $U^{4+}$  to conserve energy for cellular growth or without any energy gain (Lovley and Phillips 1992; Lloyd and Renshaw 2005). In all these processes, the  $U^{6+}$  reduction was stimulated by injection of physiological electron donors such as acetate, lactate, or ethanol (Anderson et al. 2003; Haas et al. 2001; Volesky and Holan 1995).

The sulfate and iron-reducing bacterial species (Coates et al. 2001; Lloyd et al. 2005; Lovley and Phillips 1992; Suzuki et al. 2003), hyperthermophilic archaea (Kashefi and Lovley 2000), thermophiles (Kieft et al. 1999), fermentative bacteria (Francis et al. 1994; Suzuki and Suko 2006), acid-tolerant bacteria (Shelobolina et al. 2004), and myxobacteria (Wu et al. 2006) are well-known microorganisms applied to bio-reduction of uranium. In particular, *Desulfovibrio* spp., *Geobacter* spp., *Shewanella* spp., and *Clostridium* spp. are important microorganisms. Moreover, the responsible enzyme (tetraheme cytochrome  $c_3$ ) to bio-reduction of  $U^{6+}$  characterized in *Desulfovibrio vulgaris* exhibited in vitro  $U^{6+}$  reductase in combination with hydrogenase which served as its physiological electron donor (Payne et al. 2002). Similarly in another homologous system (triheme periplasmic cytochrome  $c_7$ ) of iron-reducing bacterium (*G. sulfurreducens*) eventually plays an important role in the reduction of  $U^{6+}$  to  $U^{4+}$  (Lloyd et al. 2003).

### 11.3.2.2 Microbial Interaction with Uranium by Redox Transformation; Bio-Oxidation

Microbially mediated bio-reduced  $U^{4+}$  can have probability of re-oxidation to  $U^{6+}$  by biotic or abiotic activities. Beller (2005) demonstrated the nitrate-dependent and anaerobic  $U^{4+}$  oxidation at neutral conditions by *Thiobacillus denitrificans* (the obligate chemolithoautotrophic bacterium). Senko et al. (2005) reported enzymatic oxidation of  $U^{4+}$  by nitrate-reducing *Klebsiella* sp. This enzymatic oxidation of  $U^{4+}$  was not linked to energy conservation which was imperative to the cell growth

(Finneran et al. 2002; Beller 2005; Senko et al. 2002) albeit coupled with nitrate reduction which is a commonly existing contaminant at uranium sites (Riley et al. 1992). Similar was also observed by Finneran et al. (2002) with nitrate grown pure cultures of *Geobacter metallireducens*.

Furthermore, the presence of siderophores, humic substances, and biogenic (bi)-carbonates are suggested to stimulate uraninite oxidation by the formation of highly stable  $U^{4+}$  complexes (Frazier et al. 2005; Gorman-Lewis et al. 2005). Wan et al. (2005) reported that even under reducing conditions, the reduced uranium can be re-oxidized from  $U^{4+}$  to  $U^{6+}$  that too in the presence of microorganisms that can effectively reduce the uranium. They observed that the carbonate accumulations due to microbial respiration lead to stabilizing the carbonato- $U^{6+}$  species, thus, increasing the thermodynamic feasibility of  $U^{4+}$  oxidation. The residual  $Fe^{3+}$  and possibly  $Mn^{4+}$ , as co-existing species, act like terminal electron acceptors to re-oxidation of  $U^{4+}$ .

### 11.3.2.3 Microbial Interaction with Uranium by Complexation; Biosorption

The metabolism independent sorption is termed biosorption that encompasses both adsorption and absorption. Most of the studies on this subject have indicated that uranium biosorption is species specific and is adversely affected by physiological condition of microbial cell, solution pH, nature of liquid media, other dissolved or coexisting species, and charged groups on the cell surface (Lloyd and Macaskie 2002). It is considered that microbial cell surface is a highly dynamic interface. On that cell surface, the new cell wall material and extracellular layers are added, signals are transduced, proteins are inserted, adherence to solid substrata occurs, nutrients and metabolites are exchanged and flocculation or mobility are controlled (Lalonde et al. 2008).

Since microbial cell surface along with cell wall remains in direct contact with a uranium-containing aqueous system, the charged functional groups within the surface layers can interact with charged molecules or ions present in the external milieu. Consequently, the metal cations become charged to bound with cell surfaces. The structural differences between cell walls of two microbial groups namely the Gram-positive and Gram-negative bacteria (as per their color behavior with Gram stain) exhibit a large potential to bind the cationic and anionic species as well (Frankel and Bazylinski 2003). The cell surface of both bacterial groups is shown in Fig. 11.5.

For a Gram-positive bacterium, the cell wall consists of highly cross-linked polymer that forms a peptidoglycan layer (or say, murein sacculus) of 25 nm thickness with enriched carboxylic groups. The secondary polymeric chains (like teichoic acid) of 8–50 glycerol/ribitol molecules that are closely etherified by phosphate bridges, or teichuronic acid, extend the arsenal of negatively charged compounds like the  $PO_4^{3-}$  and  $RCOO^-$  groups (Frankel and Bazylinski 2003). Kelly et al. (2002) further showed that these two metal-binding groups are implicated in radionuclide coordination. On the other side, the Gram-negative bacterium

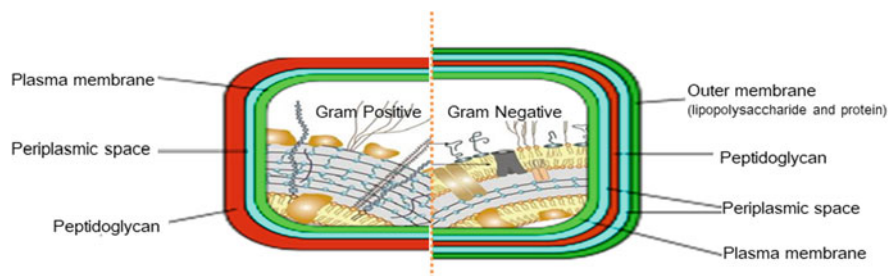


**Fig. 11.5** Cell wall of Gram-negative and Gram-positive bacteria

cell wall consists of a thin peptidoglycan layer (of thickness 4 nm) that remains isolated from the external environment by the bi-layeric lipoprotein of the outer membrane. The outward extended lipopolysaccharides are holding in place to the outer membrane with lipophilic ends with the preferred centers to bind cationic species with the counter anionic groups of  $\text{PO}_4^{3-}$  and  $\text{RCOO}^-$  (Beveridge and Koval 1981). Ferris and Beveridge reported that in *Escherichia coli* K-12 the residual phosphoryl of the polar head of phospholipids and lipopolysaccharides in the outer membrane exhibited the most possible binding sites for the cationic metal species. Further investigations indicated that the phosphoryl groups in the core-lipid A region of the lipopolysaccharides are primarily involved in metal binding in *Pseudomonas aeruginosa*. The studies conducted by Haas et al. (2001) and Fein et al. (1997) revealed that the uranyl ion sorption is progressed through two separate adsorptions to form the surface adsorbed complexes as  $> \text{COO}-\text{UO}_2^+$  and  $> \text{PO}_4\text{H}-\text{UO}_2(\text{OH})_2$ . Therefore, the  $\text{PO}_4^{3-}$  containing surface sites ( $\text{pK}_a \approx 7.0$ ),  $\text{RCOO}^-$  containing surface sites ( $\text{pK}_a < 4.27-4.37$ ),  $\text{OH}^-$  containing surface sites, and amine groups ( $\text{pK}_a > 8$ ) are supposed to do binding of radionuclide metal species.

Various surface structures of cell wall interact with metal cations. Their composition is majorly proteinaceous layers (e.g., S-layers) or polymeric carbohydrate (e.g., capsules) (Douglas and Beveridge 1998). The crystalline S-layer belongs to the outermost cell envelope components of numerous bacteria and archaea (Sára and Sleytr 2000). Mostly, their thickness of 5–15 nm is comprised of protein (or glycoprotein subunits) and their ability to provide a complete cover cell surface, during all stages of bacterial multiplication has been identified. S-layers may also possess pores of identical morphology and size ranging between 2 and 6 nm (Beveridge 1994). These proteins may act like molecular sieving to trap ions or protect the cells against environmental adversities of metal toxicity of radionuclides metal (Sleytr et al. 1996; Sleytr 1997). Saturation of the S-layer with radionuclides like uranium or toxic metals may lead to denaturation of its surface lattice by replacing it with the freshly synthesized proteins (Merroun et al. 2005). These proteins possess a large number of carboxyl and phosphate groups, which can be involved in uranium complexation (Merroun et al. 2005; Sleytr 1997; Pietzsch et al. 1999).

Microbial cells able to generate macromolecules that become positioned outside the cell walls are known as extracellular polymeric substances (EPS). An EPS is a metabolic product albeit it may be a resultant from organic matter of the effluents by hydrolysis or other cell activities (Wingender et al. 1999) that actively serves to protect the cells from the external adversities (Comte et al. 2008). Although they have complex composition but majorly consist of polysaccharides, humic substances, proteins, nucleic acids, uronic acids, and lipids containing ionizable functional groups like  $\text{PO}_4^{3-}$ ,  $\text{RCOO}^-$ , and  $\text{OH}^-$  to provide the potential binding sites for metals' sequestration (Wingender et al. 1999; Lawson et al. 1984).

The EPS of some isolated microbial species of diverse streams (like uranium mill tailings, uranium mining wastes, and groundwater repositories), exhibited high ability for uranium accumulation. The structural observations of uranium-complexed bacterial EPS exhibited similarity with U/fructose phosphate complexes (Koban et al. 2004) indicating the importance of organic phosphate present in EPS to coordination with metal species.

#### 11.3.2.4 Microbial Interaction with Uranium by Complexation; Precipitation

The microbial activities can potentially lead to precipitation of metal ions including the radionuclides as their salts in carbonate, phosphate, and hydroxide form at different pH of solutions (Van Roy et al. 1997). Additionally, metals can be precipitated by contacting with biogenic ligands like phosphate, sulfide, and oxalate (Lovley et al. 1991, Xu et al. 1999). Microbial catalyzed biomineralization process forming the rock-carbonates is an important one particular to capture the atmospheric  $\text{CO}_2$  (Braissant et al. 2002; Ehrlich 2002; Riding 2000). The processes have further a vital role in ornamental stone conservation (Rodriguez-Navarro et al. 2003), bio-geo-chemical cycling of elements (Banfield 1997, Ehrlich 2002), and metal-contaminated groundwater bioremediation (Mitchell and Ferris 2005).

The microbial-induced precipitation of uranium as phosphate salt forming the mineral phases of H-autunite and autunite/meta-autunite at the pH range between 4.5 and 7.0 is reported. The process exhibits passive adsorption of uranium cations by the negatively charged extracellular polymeric substances of the cell walls and active secretion of  $\text{PO}_4^{3-}$  groups through the phosphatase process (Renninger et al. 2004; Macaskie et al. 2000). Notably, the biomineralization process of uranium has been found to be independent of any geographic origin of the microorganisms rather strongly dependent on cell wall structure (i.e., Gram-positive and Gram-negative bacteria) at acidic and neutral conditions (Nedelkova et al. 2005; Jeong et al. 1997; Merroun et al. 2006). At physiological conditions of a pH value 6.9,  $\text{H}_2\text{UO}_2\text{PO}_4$  and  $\text{NaUO}_2\text{PO}_4$  phases are precipitated surrounding the cells of *Citrobacter* sp. (Lovley et al. 1991, Macaskie et al. 2000). At acidic conditions of pH 4 ~ 5, enzymatically assisted uranium precipitation by strains belonging to genera *Bacillus* and *Rahnella* are also revealed by Martinez et al. (2007) and Beazley et al. (2007). These bacteria precipitate uranium at a pH of about 4.5 by forming phosphate mineral phase of

meta-autunite group. At a pH value of 2.0, adsorption of uranium on cell surface organic phosphate occurs instead of exhibiting the precipitation phenomenon. A similar pH-dependent speciation has been observed in bacterial strains of *B. sphaericus* JG-7B, *Sphingomonas* sp. SW366–3, etc.

### 11.3.2.5 Microbial Interaction with Uranium by Complexation; Intracellular Accumulation

Uranium does not exhibit essential biological functions. Hence, its transportation to microbial cells also differing the metabolism mainly because of an increased membrane permeability due to uranium toxicity (Suzuki and Banfield 2004). The microbial cells have numerous mechanistic routes to immobilize uranium after its intracellular accumulation (e.g., uranium chelation by polyphosphate bodies). Polyphosphate's role in ATP substitution for sugar and adenylate kinases (as source energy) and metal chelation are established. TEM analysis indicated uranium accumulated in the cytoplasm that remains closer to the plasma membrane in *Pseudomonas migulae* CIP 105470. This uptake of uranium indicated the properties of bacterial outer cell membrane that allowed an inner cell diffusion of metal and their immobilization through the localized polyphosphate (Merroun and Selenska-Pobell 2008). Additionally, the U/polyphosphate accumulation in the form of needle-shape fibrils of various sizes alike the cytoplasm of natural isolates of *Arthrobacter* sp., *Sphingomonas* sp. S15–S1, and others are observed by Merroun et al. (2006). In the cells of *Stenotrophomonas maltophilia* JG-2, a strain isolated from mining waste, intracellular accumulated uranium, and its transport from the cell membranes to the cytoplasm was observed albeit the mechanistic route is yet to be disclosed.

**Acknowledgments** This work was supported by the Brain Pool Program through the National Research Foundation of Korea (NRF) funded by the Ministry of Science and ICT (Grant No. 2021H1D3A2A01100016) and the Basic Science Research Program through the National Research Foundation of Korea (NRF) funded by the Ministry of Education (Project No. 2020R111A1A01074249). The author, S. Ilyas would like to convey thanks to Prof. Christon J. Hurst for his valuable suggestions to shape this chapter.

## References

- Anderson RT, Vronis HA, Ortiz-Bernad I, Resch CT, Long PE, Dayvault R, Lovley DR (2003) Stimulating the in situ activity of Geobacter species to remove uranium from the groundwater of a uranium-contaminated aquifer. *Appl Environ Microbiol* 69(10):5884–5891
- Aylmore MG, Muir DM (2001) Thiosulfate leaching of gold—a review. *Miner Eng* 14:135–174
- Banfield JF (1997) Geomicrobiology: interactions between microbes and minerals. *Rev Mineral* 35: 448

- Beazley MJ, Martinez RJ, Sobecky PA, Webb SM, Taillefert M (2007) Uranium biomineralization as a result of bacterial phosphatase activity: insights from bacterial isolates from a contaminated subsurface. *Environ Sci Technol* 41(16):5701–5707
- Beller HR (2005) Anaerobic, nitrate-dependent oxidation of U (IV) oxide minerals by the chemolithoautotrophic bacterium *Thiobacillus denitrificans*. *Appl Environ Microbiol* 71(4): 2170–2174
- Beveridge TJ (1994) Bacterial S-layers. *Curr Opin Struct Biol* 4(2):204–212
- Beveridge TJ, Koval SF (1981) Binding of metals to cell envelopes of *Escherichia coli* K-12. *Appl Environ Microbiol* 42(2):325–335
- Bigham JM, Nordstrom DK (2000) Iron and aluminum hydroxysulfates from acid sulfate waters. *Rev Mineral Geochem* 40:351–403
- Boyle RW (1979) The geochemistry of gold and its deposits. *Geol Surv Can Bull* 280:583
- Braissant O, Verrecchia EP, Aragno M (2002) Is the contribution of bacteria to terrestrial carbon budget greatly underestimated? *Naturwissenschaften* 89(8):366–370
- Campbell SC, Olson GJ, Clark TR, McFeters G (2001) Biogenic production of cyanide and its application to gold recovery. *J Ind Microbiol Biotechnol* 26:134–139
- Castric PA (1975) Hydrogen cyanide, a secondary metabolite of *Pseudomonas aeruginosa*. *Can J Microbiol* 21:613–618
- Castric PA (1981) The metabolism of hydrogen cyanide by bacteria. In: Vennesland B, Conn EE, Knowles CJ, Westley J, Wissing F (eds) *Cyanide in biology*. Academic, London, pp 233–261
- Checa SK, Espariz M, Pérez Audero ME, Botta PE, Spinelli SV, Soncini FC (2007) Bacterial sensing of and resistance to gold salts. *Mol Microbiol* 63:1307–1318
- Coates JD, Bhupathiraju VK, Achenbach LA, McInerney MJ, Lovley DR (2001) *Geobacter hydrogenophilus*, *Geobacter chapellei* and *Geobacter grbiciae*, three new, strictly anaerobic, dissimilatory Fe (III)-reducers. *Int J Syst Evol Microbiol* 51(2):581–588
- Cologgi DL, Lampa-Pastirk S, Speers AM, Kelly SD, Reguera G (2011) Extracellular reduction of uranium via *Geobacter* conductive pili as a protective cellular mechanism. *Proc Natl Acad Sci U S A* 108:15248–15252
- Comte S, Guibaud G, Baudu M (2008) Biosorption properties of extracellular polymeric substances (EPS) towards Cd, Cu and Pb for different pH values. *J Hazard Mater* 151(1):185–193
- Dew DW, Van Buren C, McEwan K, Bowker C (1999) Bioleaching base metal sulfide concentrates: a comparison of mesophile and thermophile bacterial cultures. In: Amils R, Ballester A (eds) *Biohydrometallurgy and the environment. Toward the mining of the 21st century*, Part A. Elsevier, Amsterdam, pp 229–238
- DiSpirito AA, Tuovinen OH (1982) Uranous ion oxidation and carbon dioxide fixation by *Thiobacillus ferrooxidans*. *Arch Microbiol* 133(1):28–32
- DiSpirito AA, Talnagi JW, Tuovinen OH (1983) Accumulation and cellular distribution of uranium in *Thiobacillus ferrooxidans*. *Arch Microbiol* 135(4):250–253
- Douglas S, Beveridge TJ (1998) Mineral formation by bacteria in natural microbial communities. *FEMS Microbiol Rev* 26(2):79–88
- Ehrlich HL (2002) *Geomicrobiology of sulfur*, Geomicrobiology, 4th (ed) edn. Marcel Dekker Incorporated, New York
- Etesami H (2018) Bacterial mediated alleviation of heavy metal stress and decreased accumulation of metals in plant tissues: mechanisms and future prospects. *Ecotoxicol Environ Saf* 147:175–191
- Faramarzi MA, Brandl H (2006) Formation of water-soluble metal cyanide complexes from solid minerals by *Pseudomonas plecoglossicida*. *FEMS Microbiol Lett* 259:47–52
- Faramarzi MA, Stagars M, Pensini E, Krebs W, Brandl H (2004) Metal solubilization from metal-containing solid materials by cyanogenic *Chromobacterium violaceum*. *J Biotechnol* 113:321–326
- Fein JB, Daughney CJ, Yee N, Davis TA (1997) A chemical equilibrium model for metal adsorption onto bacterial surfaces. *Geochim Cosmochim Acta* 61(16):3319–3328

- Finneran KT, Housewright ME, Lovley DR (2002) Multiple influences of nitrate on uranium solubility during bioremediation of uranium-contaminated subsurface sediments. *Environ Microbiol* 4(9):510–516
- Fitz RM, Cypionka H (1990) Formation of thiosulfate and trithionate during sulfite reduction by washed cells of *Desulfovibrio desulfuricans*. *Arch Microbiol* 154:400–406
- Fowle DA, Fein JB, Martin AM (2000) Experimental study of uranyl adsorption onto *Bacillus subtilis*. *Environ Sci Technol* 34(17):3737–3741
- Francis AJ, Dodge CJ, Lu F, Halada GP, Clayton CR (1994) XPS and XANES studies of uranium reduction by *Clostridium* sp. *Environ Sci Technol* 28(4):636–639
- Frankel RB, Bazylinski DA (2003) Biologically induced mineralization by bacteria. *Rev Mineral Geochem* 54(1):95–114
- Frazier SW, Kretzschmar R, Kraemer SM (2005) Bacterial siderophores promote dissolution of  $UO_2$  under reducing conditions. *Environ Sci Technol* 39(15):5709–5715
- Friedrich CG, Bardischewsky F, Rother D, Quentmeier A, Fischer J (2005) Prokaryotic sulfur oxidation. *Curr Opin Microbiol* 8:1–7
- Gadd GM (2002) Interactions between microorganisms and metals/radionuclides: the basis of bioremediation. In: Keith-Roach MJ, Livens FR (eds) *Interactions of microorganisms with radionuclides*. Elsevier, Amsterdam, pp 179–203
- Gadd GM (2010) Metals, minerals and microbes: geomicrobiology and bioremediation. *Microbiol* 156(3):609–643. <https://doi.org/10.1099/mic.0.037143-0>
- Gorman-Lewis D, Elias PE, Fein JB (2005) Adsorption of aqueous uranyl complexes onto *Bacillus subtilis* cells. *Environ Sci Technol* 39(13):4906–4912
- Haas JR, Dichristina TJ, Wade R Jr (2001) Thermodynamics of U (VI) sorption onto *Shewanella putrefaciens*. *Chem Geol* 180(1–4):33–54
- Habashi F (1970) *Principles of extractive metallurgy*. Hydrometallurgy, 1st edn. Gordon & Breach, New York. 978-0677017808
- Habashi F (2020) Dissolution of uraninite. *Hydrometallurgy* 194:105329
- Hobman JL (2007) MerR family transcription activators: similar designs different specificities. *Mol Microbiol* 65:1275–1278
- Jeong BC, Hawes C, Bonthron KM, Macaskie LE (1997) Localization of enzymically enhanced heavy metal accumulation by *Citrobacter* sp. and metal accumulation in vitro by liposomes containing entrapped enzyme. *Microbiology* 143(7):2497–2507
- Kaksonen AH, Maija Lakaniemi A, Olli A, Tuovinen H (2020) Acid and ferric sulfate bioleaching of uranium ores: a review. *J Clean Prod* 264:121586
- Kashefi K, Lovley DR (2000) Reduction of Fe (III), Mn (IV), and toxic metals at 100 C by *Pyrobaculum islandicum*. *Appl Environ Microbiol* 66(3):1050–1056
- Kelly SD, Kemner KM, Fein JB, Fowle DA, Boyanov MI, Bunker BA, Yee N (2002) X-ray absorption fine structure determination of pH-dependent U-bacterial cell wall interactions. *Geochim Cosmochim Acta* 66(22):3855–3871
- Kieft TL, Fredrickson JK, Onstott TC, Gorby YA, Kostandarithes HM, Bailey TJ, Gray MS (1999) Dissimilatory reduction of Fe (III) and other electron acceptors by a *Thermus* isolate. *Appl Environ Microbiol* 65(3):1214–1221
- Kita Y, Nishikawa H, Takemoto T (2006) Effects of cyanide and dissolved oxygen concentration on biological Au recovery. *J Biotechnol* 124:545–551
- Knowles CJ (1976) Microorganisms and cyanide. *Bacteriol Rev* 40(3):652
- Koban A, Geipel G, Rossberg A, Bernhard G (2004) Uranium (VI) complexes with sugar phosphates in aqueous solution. *Radiochim Acta* 92(12):903–908
- Korobushkina ED, Chernyak AS, Mineyev GG (1974) Dissolution of gold by microorganisms and products of their metabolism. *Mikrobiologiya* 43:9–54
- Korobushkina ED, Mineyev GG, Praded GP (1976) Mechanism of the microbiological process of dissolution of gold. *Mikrobiologiya* 45:535–538
- Korobushkina ED, Karavaiko GI, Korobushkin IM (1983) Biochemistry of gold. In: Hallberg R (ed) *Environmental biogeochemistry*, vol 35. FRN, Stockholm, pp 325–333



- Kunert J, Stransky Z (1988) Thiosulfate production from cystine by the keratinolytic prokaryote *Streptomyces fradiae*. *Arch Microbiol* 150:600–601
- Lalonde SV, Smith DS, Owttrim GW, Konhauser KO (2008) Acid–base properties of cyanobacterial surfaces I: influences of growth phase and nitrogen metabolism on cell surface reactivity. *Geochim Cosmochim Acta* 72(5):1257–1268
- Laville J, Blumer C, Schroetter VC, Gaia V, Défago G, Keel C, Haas D (1998) Characterization of the hcnABC gene cluster encoding hydrogen cyanide synthase and anaerobic regulation by ANR in the strictly aerobic biocontrol agent *Pseudomonas fluorescens* CHA0. *J Bacteriol* 180: 3187–3196
- Lawson PS, Sterritt RM, Lester JN (1984) Factors affecting the removal of metals during activated sludge wastewater treatment II. The role of mixed liquor biomass. *Arch Environ Contam Toxicol* 13(4):391–402
- Lengke MF, Southam G (2005) The effect of thiosulfate-oxidizing bacteria on the stability of the gold-thiosulfate complex. *Geochim Cosmochim Acta* 69:3759–3772
- Lengke MF, Fleet ME, Southam G (2006) Morphology of gold nanoparticles synthesized by filamentous cyanobacteria from gold(I)-thiosulfate and gold(III)-chloride complexes. *Langmuir* 22:2780–2787
- Lloyd JR, Macaskie LE (2002) Biochemical basis of microbe-radionuclide interactions. In: Keith-Roach M, Livens F (eds) *Interactions of microorganisms with radionuclides*. Elsevier Sciences, Oxford, p 313
- Lloyd JR, Renshaw JC (2005) Microbial transformations of radionuclides: fundamental mechanisms and biogeochemical implications. *Met Ions Biol Syst* 44:205
- Lloyd JR, Leang C, Myerson ALH, Coppi MV, Cuifo S, Methe B, Lovley DR (2003) Biochemical and genetic characterization of PpcA, a periplasmic c-type cytochrome in *Geobacter sulfurreducens*. *Biochem J* 369(1):153–161
- Lloyd JR, Renshaw JC, May I, Livens FR, Burke IT, Mortimerc RJ, Morris K (2005) Biotransformation of radioactive waste microbial reduction of actinides and fission products. *J Nucl Radiochem Sci* 6(1):17–20
- Lovley DR, Phillips EJ (1992) Reduction of uranium by *Desulfovibrio desulfuricans*. *Appl Environ Microbiol* 58(3):850–856
- Lovley DR, Phillips EJ, Gorby YA, Landa ER (1991) Microbial reduction of uranium. *Nature* 350(6317):413–416
- Lyalikova NN, Mocheicheva LY (1969) The role of bacteria in gold migration in deposits. *Microbiol* 38:682–686
- Macaskie LE, Bonthron KM, Yong P, Goddard DT (2000) Enzymically mediated bioprecipitation of uranium by a *Citrobacter* sp.: a concerted role for exocellular lipopolysaccharide and associated phosphatase in biomineral formation. *Microbiol* 146(8):1855–1867
- Martinez RJ, Beazley MJ, Taillefert M, Arakaki AK, Skolnick J, Sobecky PA (2007) Aerobic uranium (VI) bioprecipitation by metal-resistant bacteria isolated from radionuclide-and metal-contaminated subsurface soils. *Environ Microbiol* 9(12):3122–3133
- Merroun ML, Selenska-Pobell S (2008) Bacterial interactions with uranium: an environmental perspective. *J Contam Hydrol* 102(3–4):285–295. <https://doi.org/10.1016/j.jconhyd.2008.09.019>
- Merroun ML, Raff J, Rossberg A, Hennig C, Reich T, Selenska-Pobell S (2005) Complexation of uranium by cells and S-layer sheets of *Bacillus sphaericus* JG-A12. *Appl Environ Microbiol* 71(9):5532–5543
- Merroun ML, Nedelkova M, Rossberg A, Hennig C, Selenska-Pobell S (2006) Interaction mechanisms of bacterial strains isolated from extreme habitats with uranium. *Radiochim Acta* 94(9–11):723–729
- Mielke RE, Pace DL, Porter T, Southam G (2003) A critical stage in the formation of acid mine drainage: colonization of pyrite by *Acidithiobacillus ferrooxidans* under pH neutral conditions. *Geobiology* 1:81–90

- Mitchell AC, Ferris FG (2005) The coprecipitation of Sr into calcite precipitates induced by bacterial ureolysis in artificial groundwater: temperature and kinetic dependence. *Geochim Cosmochim Acta* 69(17):4199–4210
- Nedelkova M, Radeva G, Selenska-Pobell S (2005) Molecular bacterial diversity in water at the deep-well monitoring site at Tomsk-7. In: Tsang CF, Apps J (eds) *Developments in water science, Underground injection science and technology*, vol 52. Elsevier BV, Amsterdam, p 521
- Nies DH (1999) Microbial heavy metal resistance. *Appl Microbiol Biotechnol* 51:730–750
- Nordstrom DK, Southam G (1997) Geomicrobiology of sulfide metal oxidation. *Rev Mineral* 35: 361–390
- Payne RB, Gentry DM, Rapp-Giles BJ, Casalot L, Wall JD (2002) Uranium reduction by *Desulfovibrio desulfuricans* strain G20 and a cytochrome c3 mutant. *Appl Environ Microbiol* 68(6):3129–3132
- Pietzsch K, Hard BC, Babel W (1999) A *Desulfovibrio* sp. capable of growing by reducing U (VI). *J Basic Microbiol* 39(5–6):365–372
- Rawlings DE (2005) Characteristics and adaptability of iron- and sulfur-oxidizing microorganisms used for the recovery of metals from minerals and their concentrates. *Microb Cell Factories* 4: 13–16
- Reith F, McPhail DC (2006) Effect of resident microbiota on the solubilization of gold in soils from the Tomakin Park Gold Mine, New South Wales, Australia. *Geochim Cosmochim Acta* 70: 1421–1438
- Renninger N, Knopp R, Nitsche H, Clark DS, Keasling JD (2004) Uranyl precipitation by *Pseudomonas aeruginosa* via controlled polyphosphate metabolism. *Appl Environ Microbiol* 70(12):7404–7412
- Riding R (2000) Microbial carbonates: the geological record of calcified bacterial–algal mats and biofilms. *Sedimentology* 47:179–214
- Riley RG, Zachara JM, Wobber FJ (1992) Chemical contaminants on DOE lands and selection of contaminated mixtures for subsurface science research. US-DOE Off. Energy Res Subsur Sci Prog, Washington DC
- Rodgers PB, Knowles CJ (1978) Cyanide production and degradation during growth of *Chromobacterium violaceum*. *J Gen Microbiol* 108:261–267
- Rodriguez-Navarro C, Rodriguez-Gallego M, Chekroun KB, Gonzalez-Munoz MT (2003) Conservation of ornamental stone by *Myxococcus xanthus*-induced carbonate biomineralization. *Appl Environ Microbiol* 69(4):2182–2193
- Sand W, Gehrke T, Hallmann R (1995) Sulfur chemistry, biofilm, and the (in) direct attack mechanism a critical evaluation of bacterial leaching. *Appl Microbiol Biotechnol* 43:961–966
- Sára M, Sleytr UB (2000) S-layer proteins. *J Bacteriol* 182(4):859–868
- Senko JM, Istok JD, Suflita JM, Krumholz LR (2002) In-situ evidence for uranium immobilization and remobilization. *Environ Sci Technol* 36(7):1491–1496
- Senko JM, Mohamed Y, Dewers TA, Krumholz LR (2005) Role for Fe (III) minerals in nitrate-dependent microbial U (IV) oxidation. *Environ Sci Technol* 39(8):2529–2536
- Shelobolina ES, Sullivan SA, O'Neill KR, Nevin KP, Lovley DR (2004) Isolation, characterization, and U (VI)-reducing potential of a facultatively anaerobic, acid-resistant bacterium from low-pH, nitrate-and U (VI)-contaminated subsurface sediment and description of *Salmonella subterranea* sp. *Appl Environ Microbiol* 70(5):2959–2965
- Silver S (1996) Bacterial resistances to toxic metal ions—a review. *Gene* 179:9–19
- Sleytr UB (1997) Basic and applied S-layer research: an overview. *FEMS Microbiol Rev* 20(1–2): 5–12
- Sleytr UB, Messner P, Pum D, Sara M (1996) *Crystalline bacterial cell surface proteins*. RG Landes Company, Academic Press, London
- Southam G, Saunders JA (2005) The geomicrobiology of ore deposits. *Econ Geol* 100:1067–1084
- Srivastava RR, Ilyas S, Kim HJ, Sowon C, Trinh HB, Ghauri MA, Ilyas N (2020) Biotechnological recycling of critical metals from waste printed circuit boards. *J Chem Technol Biotechnol* 95(11):2796–2810

- Stoyanov JV, Brown NL (2003) The *Escherichia coli* copper-responsive *copA* promoter is activated by gold. *J Biol Chem* 278:1407–1410
- Suzuki Y, Banfield JF (2004) Resistance to, and accumulation of, uranium by bacteria from a uranium-contaminated site. *Geomicrobiol J* 21(2):113–121
- Suzuki Y, Suko T (2006) Geomicrobiological factors that control uranium mobility in the environment: update on recent advances in the bioremediation of uranium-contaminated sites. *J Mineral Petrol Sci* 101:299–307
- Suzuki Y, Kelly SD, Kemner KM, Banfield JF (2003) Microbial populations stimulated for hexavalent uranium reduction in uranium mine sediment. *Appl Environ Microbiol* 69(3):1337–1346
- Tributsch H (2001) Direct versus indirect bioleaching. *Hydrometallurgy* 59:177–185
- Van Roy S, Peys K, Dresselaers T, Diels L (1997) The use of an *Alcaligenes eutrophus* biofilm in a membrane bioreactor for heavy metal recovery. *Res Microbiol* 148(6):526–528
- Volesky B, Holan ZR (1995) Biosorption of heavy metals. *Biotechnol Prog* 11(3):235–250
- Wan J, Tokunaga TK, Brodie E, Wang Z, Zheng Z, Herman D, Sutton SR (2005) Reoxidation of bio-reduced uranium under reducing conditions. *Environ Sci Technol* 39(16):6162–6169
- Watling HR (2006) The bioleaching of sulfide minerals with emphasis on copper sulfides – a review. *Hydrometallurgy* 84:81–108
- Wingender J, Neu TR, Flemming HC (1999) Microbial extracellular polymeric substances: characterization, structure and function. Springer, Berlin, p 123
- Wu Q, Sanford RA, Löffler FE (2006) Uranium (VI) reduction by *Anaeromyxobacter dehalogenans* strain 2CP-C. *Appl Environ Microbiol* 72(5):3608–3614
- Xu H, Barton LL, Zhang P, Wang Y (1999) TEM investigation of  $U^{6+}$  and  $Re^{7+}$  reduction by *Desulfovibrio desulfuricans*, a sulfate-reducing bacterium. *Mater Res Soc Symp Proc* 608:299–304

# Chapter 12

## Prokaryotic Ferrous Iron Transport: Exploiting Pools of Reduced Iron Across Multiple Microbial Environments



Alex E. Sestok, Mark A. Lee, and Aaron T. Smith

**Abstract** Iron is essential to nearly all forms of life, but the redox activity of this element necessitates its cellular regulation. All iron-utilizing organisms require this nutrient to be tightly managed, which is accomplished by a suite of proteins and nucleic acids involved in the acquisition, the delivery, the storage, the regulation, and the export of this essential element. For infectious organisms, iron acquisition systems are commonly associated with intracellular growth, survival, and virulence of pathogens, which are dynamically able to modify their iron uptake strategies in response to changing host environments. The past few decades have been marked with an increased understanding of pathogenic ferric iron ( $\text{Fe}^{3+}$ ) and heme acquisition. In contrast, though the necessity of ferrous iron ( $\text{Fe}^{2+}$ ) transport for pathogenesis has been established, the precise details of this process remain enigmatic, and  $\text{Fe}^{2+}$  transporters remain unexploited as drug targets to combat drug-resistant organisms. This chapter will overview a current understanding of  $\text{Fe}^{2+}$  transport in microbes and highlight gaps in our knowledge that must be closed in order to establish a comprehensive understanding of unicellular  $\text{Fe}^{2+}$  metabolism.

### 12.1 Introduction

Throughout evolution, iron has emerged to become one of the most vital elements to virtually every living organism. In the modern era, biological systems that accomplish a suite of cellular processes, from aerobic cellular respiration,  $\text{N}_2$  fixation, gene regulation, to even DNA biosynthesis make use of iron in all of its different forms (Sestok et al. 2018; Andrews et al. 2003; Lau et al. 2016). Iron has a diverse functionality and may be utilized as an ionic cofactor and bound by biological macromolecules, complexed within iron-sulfur clusters, or even chelated by organic molecules such as protoporphyrin-IX (heme) (Andrews et al. 2003; Sestok et al.

---

A. E. Sestok · M. A. Lee · A. T. Smith (✉)

Department of Chemistry and Biochemistry, University of Maryland, Baltimore County,  
Baltimore, MD, USA

e-mail: [smitha@umbc.edu](mailto:smitha@umbc.edu)

© Springer Nature Switzerland AG 2022

C. J. Hurst (ed.), *Microbial Metabolism of Metals and Metalloids*, Advances in  
Environmental Microbiology 10, [https://doi.org/10.1007/978-3-030-97185-4\\_12](https://doi.org/10.1007/978-3-030-97185-4_12)

299



**Fig. 12.1** The Fenton reaction. In the presence of hydrogen peroxide, ferrous iron ( $\text{Fe}^{2+}$ ) is readily oxidized into ferric iron ( $\text{Fe}^{3+}$ ), forming both a hydroxyl radical and a hydroxide ion in the process. Hydroxyl radicals can lead to harmful and deleterious oxidation of biomolecules if uncontrolled

2018). Biology is replete with essential proteins and enzymes that use some or even all forms of this element. For example, iron-dependent ribonucleotide reductases reduce ribonucleotides to deoxyribonucleotides by making use of a diiron center that shuttles electrons for nucleotide reduction (Torrents 2014). Nitrogenase enzymes, which allow bacteria to fix  $\text{N}_2$ , utilize multiple iron-sulfur clusters ([4Fe-4S], [8Fe-7S], and [7Fe-Mo-9S]) throughout the fixation cycle (Hu and Ribbe 2015). Hemoglobin (Wittenberg et al. 2002) and myoglobin (Brunori 2010) both require a heme *b* cofactor for  $\text{O}_2$  transport. This large assortment of iron-containing proteins clearly demonstrates the dependence on iron for the survival of organisms found across every kingdom life.

Iron is capable of fulfilling such a dynamic role in life because of its abundance on earth and its versatility as an element, if it can be acquired. For example, iron is the most abundant transition metal on earth's crust, comprising up to ca. 5% of the outermost layer of the planet. However, unlike oxygen, silicon, and aluminum, which make up significantly more of the outer layer of Earth, the chemistry of iron is much more diverse. Iron can sample multiple oxidation and spin states, and its electronic reactivity can be modulated by the ligands responsible for binding the metal in biological macromolecules. This tunability controls the redox potential of iron, which can span from ca.  $-300$  mV to  $+700$  mV (i.e., a 1 V range), affording organisms the potent oxidizing and reducing iron-based cofactors necessary to accomplish a wide swath of complex chemical transformations (Andrews et al. 2003). However, despite its abundance, acquisition of this essential element is no small feat. While  $\text{Fe}^{3+}$  (ferric iron) predominates in oxic environments, it is highly insoluble (ca.  $10^{-18}$  M at pH 7.0) and easily forms recalcitrant ferric oxides and hydroxides, whereas  $\text{Fe}^{2+}$  (ferrous iron) is more soluble (as high as 0.1 M at pH 7.0) but is present under anoxic and reducing conditions and is susceptible to rapid oxidation (Fig. 12.1) (Andrews et al. 2003; Krewulak and Vogel 2008; Winterbourn 1995), presenting a conundrum to many organisms. Given the critical importance of iron to life, decades of research have focused on the mechanisms of iron transport, utilization, and even regulation. Much of this research has centered around bacterial iron homeostasis due to its simpler mode of study and spurred by the strong relationship between iron availability and bacterial pathogenesis.

In order to utilize iron, this nutrient must first be obtained from the environment and subsequently transported to the necessary locations within the cell where the metal is needed. This process requires organisms to employ diverse iron sequestration systems capable of functioning under a variety of different physiological niches and in different environments to exploit whatever pools of iron may be available (Andrews et al. 2003; Sestok et al. 2018). In Gram-negative bacteria,  $\text{Fe}^{3+}$  can be scavenged by siderophores, low molecular weight molecules with a high affinity for

$\text{Fe}^{3+}$  ( $K_{\text{aff}} > 10^{30} \text{ M}^{-1}$ ) that are secreted into the extracellular space. Siderophores compete for  $\text{Fe}^{3+}$  already bound to host proteins and help to keep  $\text{Fe}^{3+}$  soluble during the transport process. Uptake of the  $\text{Fe}^{3+}$ -siderophore complex from the extracellular space into the periplasm typically occurs via a TonB-dependent outer membrane receptor coupled to the proton motive force (PMF) and often specific to the siderophore (Andrews et al. 2003; Sestok et al. 2018; Krewulak and Vogel 2008; Chu et al. 2010; Ellermann and Arthur 2017). Periplasmic binding proteins then chaperone the complex to a dedicated inner membrane protein, typically an ATP-binding cassette (ABC) transporter. Once in the cytoplasm,  $\text{Fe}^{3+}$  can be reduced to  $\text{Fe}^{2+}$  or the siderophore can be degraded to release the iron (Cain and Smith 2021). Uptake of siderophores is similar in Gram-positive bacteria, except that the  $\text{Fe}^{3+}$ -siderophore complex binds to a membrane anchored lipoprotein before being handed off to the ABC transporter (Andrews et al. 2003; Sestok et al. 2018; Krewulak and Vogel 2008; Chu et al. 2010; Ellermann and Arthur 2017). Heme sequestered from host proteins also serves as a form of iron to bacteria; however, because of its dramatically different composition from that of free iron, dedicated heme acquisition and transport systems are necessary. Pathogenic bacteria can employ hemolysins and proteases to release heme from red blood cells. Bacteria can then bind heme by using dedicated hemophores or by utilizing outer membrane receptors to transport host heme-binding proteins into the cell (Andrews et al. 2003; Sestok et al. 2018; Krewulak and Vogel 2008; Huang and Wilks 2017; Richard et al. 2019). The heme-hemophore complex is transported across the outer membrane in a TonB-dependent manner, similar to siderophore uptake. ABC transporters may also shuttle hemophores across the cytoplasmic membrane where the heme is degraded by heme oxygenase (HO), releasing iron and protoporphyrin catabolites (Andrews et al. 2003; Sestok et al. 2018; Krewulak and Vogel 2008; Huang and Wilks 2017; Richard et al. 2019). Both ferric iron and heme serve as indispensable iron sources for bacteria and have been well studied.

Recently, it has become apparent that  $\text{Fe}^{2+}$  acquisition and utilization are both necessary for bacterial growth, survival, and in some cases, for pathogenesis (Sestok et al. 2018; Andrews et al. 2003). However, bacterial ferrous iron uptake is not as well characterized as that of ferric iron and heme uptake. Ferrous iron is likely to be the dominant iron source for bacteria that thrive in microaerophilic or anoxic environments, such as those living within biofilms, and those living in acidified, reducing environments like the stomach. Additionally, there is evidence that  $\text{Fe}^{3+}$  utilization is linked to  $\text{Fe}^{2+}$  transport, especially in cases where organisms utilize non-native siderophores known as xenosiderophores (Cain and Smith 2021; Schröder et al. 2003). These molecules can be transported across the outer membrane through TonB-dependent receptors specific for the xenosiderophores or through outer membrane receptors with broad specificity for several siderophores (Cornelis 2010; Sheldon and Heinrichs 2015). However, since organisms that can utilize xenosiderophores often lack siderophore-specific, inner membrane transporters, they must therefore either reduce  $\text{Fe}^{3+}$  to  $\text{Fe}^{2+}$ , through the use of a ferric iron reductase (Cain and Smith 2021), or degrade the xenosiderophore within the periplasm. In either scenario, transport of  $\text{Fe}^{2+}$  into the cytoplasm requires dedicated

and selective  $\text{Fe}^{2+}$  transporters. Ferric iron reductases can also function extracellularly and exhibit broad substrate specificity for different  $\text{Fe}^{3+}$ -chelates, necessitating  $\text{Fe}^{2+}$  transport across the outer membrane. The process of  $\text{Fe}^{3+}$  reduction may involve a flavin cofactor (soluble ferric reductases) or heme *b* (membrane ferric reductases) to transport electrons for iron reduction (Cain and Smith 2021). Thus ferric iron reductases allow for organisms to generate and to utilize  $\text{Fe}^{2+}$  even in oxic environments (Schröder et al. 2003). Ferrous iron transporters have been discovered in many kingdoms of life, but most remain under- or poorly-studied. This chapter focuses on how microbes specifically exploit the presence of pools of reduced, ferrous iron in the environment to fulfill metabolic needs and to establish infection within host niches. Importantly, while reduced iron availability has changed throughout Earth's evolution, microbes have adapted and maintained the ability to acquire this necessary nutrient through conserved mechanisms across multiple microbial environments.

## 12.2 Iron and Bacteria on Early Earth

Bacteria first appeared on Earth approximately 4 billion years ago and thrived in an environment remarkably different from that of today's (DeLong and Pace 2001). The presence of *banded iron formations* (BIFs) have shown that Earth's first oceans were ferruginous (rich in iron), and these mineral "snapshots" offer insight into how the composition of Earth's oceans have changed throughout Earth's evolution (Li et al. 2018; Schad et al. 2019; Konhauser et al. 2017). While there are multiple mechanisms by which iron oxidation to promote BIFs could have transpired, one prevailing hypothesis suggests formation occurred through oxidation of iron by bacteria, such as *Gallionella ferruginea*, as fossilized bacteria have been discovered co-deposited within BIFs (Konhauser et al. 2017). These ancient bacteria were micro-aerophilic, being either (or both) nitrate-reducing, phototrophic ferrous iron ( $\text{Fe}^{2+}$ )-oxidizers or ferric iron ( $\text{Fe}^{3+}$ )-reducers (Schad et al. 2019). Studies have shown that bacteria inhabiting the surface of the early oceans likely utilized  $\text{Fe}^{2+}$  oxidation to produce  $\text{Fe}^{3+}$ -containing minerals as protective mechanisms against harmful UV-radiation prior to the more modern development of the ozone layer (Gauger et al. 2015, 2016).  $\text{Fe}^{2+}$  was also proposed to be involved in the photosynthetic process known as photoferrotrophy, whereby UV-radiation facilitated oxidation of dissolved  $\text{Fe}^{2+}$  species that was subsequently coupled to several essential assimilatory processes, such as reduced carbon fixation,  $\text{CO}_2$  fixation, and even  $\text{N}_2$  fixation (Konhauser et al. 2017; Schad et al. 2019). However, changes in Earth's atmospheric composition quickly altered metal speciation on the surface and within the oceans.

The presence of significant levels of atmospheric  $\text{O}_2$  during the *Great Oxygenation Event* (GOE) was thought to have appeared around 2.4 billion years ago, though this estimation is complicated by the lack of consensus as to exactly when and where cyanobacterial photosynthesis began (either in the early Archean Eon or

the late Paleoproterozoic Eon) (Schad et al. 2019; Glass 2015; Shih 2019). Regardless of the precise date, the emergence of photosynthetic cyanobacteria resulted in the release of substantive amounts of  $O_2$  into the atmosphere and dissolved within the oceans. This increase in  $O_2$  caused dramatic changes in early microbial environments, leading to pressures on anaerobic metabolizers and the alteration of metal bioavailability, chiefly due to  $O_2$ 's effects on oxidation state speciation of multiple essential transition metals.

Notably and especially affected was iron, as the GOE heavily altered the iron biogeochemical cycle (Glass 2015; Schad et al. 2019; Shih 2019). As the distribution of iron shifted from the soluble  $Fe^{2+}$  form to the insoluble  $Fe^{3+}$  form, microbes were pressured to adapt to fulfill their metabolic needs or perish. As fossil records do not indicate a mass bacterial extinction event, it is clear that microbes overcame this challenge through evolved mechanisms of metal scavenging, metal storage, metal substitution, and a metabolic shift towards different metal speciation (Glass 2015). However, not every planetary niche was transformed by the GOE. Studies suggest that some ferruginous environments were preserved, and microbes in those environments likely maintained a necessity for  $Fe^{2+}$ , which was still present in relatively high concentrations in these locations (Derry 2015; Konhauser et al. 2017).

Despite its difficulty to obtain from the environment, iron still serves as an indispensable metal cofactor for many enzymes (Glass 2015); however, before iron may be incorporated into proteins and enzymes and used in cofactor biosynthesis, iron must first be solubilized and transported into the cell. As microbes may encounter multiple forms of environmental iron, it is unsurprising that this process is accomplished by a variety of iron acquisition systems. A large number of microbial iron uptake mechanisms have been discovered and characterized extensively. Consistent with the essential nature of iron as a micronutrient, these acquisition systems have been determined to be essential for microbial growth, survival, and even virulence. However, most studies have focused on mechanisms of  $Fe^{3+}$  acquisition, such as  $Fe^{3+}$ -siderophore transport, heme transport, and even the acquisition of host  $Fe^{3+}$ -binding proteins from the extracellular space. In stark contrast, much less is known about  $Fe^{2+}$  uptake despite the importance of  $Fe^{2+}$  for the survival of both the first organisms that inhabited the planet and numerous bacteria located in modern-day ferruginous environments.

### 12.3 $Fe^{2+}$ Acquisition Systems

Several  $Fe^{2+}$  uptake systems have been identified in bacteria, and it is likely that more exist that have not yet been characterized (Fig. 12.2). Furthermore, while some transport systems are specific to  $Fe^{2+}$  transport (such as the Feo and Efe systems), other systems mediate the transport of multiple divalent metal ions such as  $Mn^{2+}$ ,  $Cu^{2+}$ ,  $Zn^{2+}$ ,  $Ni^{2+}$ , and  $Co^{2+}$ . Given the different coordination properties of  $Fe^{2+}$  and  $Fe^{3+}$ , and the different environments in which these two ions are obtained, different machinery is required for the transport of  $Fe^{2+}$  and  $Fe^{3+}$ . For instance, siderophores



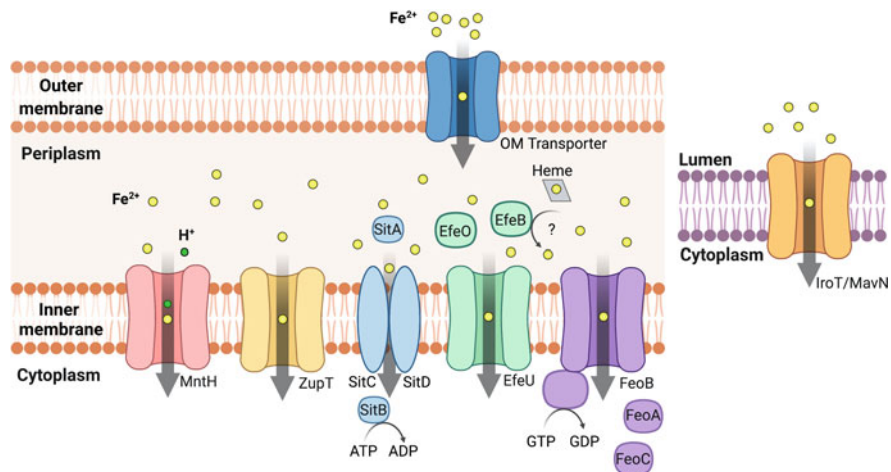


**Fig. 12.2** A cartoon of the currently known bacterial ferrous iron uptake systems, depicted here for a Gram-negative bacterium.  $\text{Fe}^{2+}$  is transported into the periplasm via an unidentified outer membrane transporter where it is then taken up by one or multiple inner membrane  $\text{Fe}^{2+}$  transport systems. MntH, ZupT, and SitABCD transport multiple divalent metal ions in addition to  $\text{H}^+$ , while EfeUOB is specific for  $\text{Fe}^{2+}$ , but is only functional in pathogenic bacteria. IroT/MavN has been identified in *Legionella* species and functions at the LCV membrane. In contrast, Feo is the most widespread, dedicated  $\text{Fe}^{2+}$  transport system in bacteria. Figure created with BioRender

typically coordinate  $\text{Fe}^{3+}$  in an octahedral geometry with hexadentate ligands and are highly specific for hard Lewis acids (Andrews et al. 2003; Krewulak and Vogel 2008). Such a molecule does not coordinate the softer Lewis acid  $\text{Fe}^{2+}$  with the same affinity or even the same geometry in many cases. Additionally, because  $\text{Fe}^{2+}$  is much more soluble than  $\text{Fe}^{3+}$ , it is unnecessary for the ion to be bound to large chelates during the transport process but may instead be transported as an ion via  $\text{Fe}^{2+}$ -specific transporters. Though not an exhaustive list, some of the best characterized  $\text{Fe}^{2+}$  transporters are described below.

### 12.3.1 *Natural Resistance-Associated Macrophage Proteins (NRAMPs) and Divalent Metal Transporters (DMTs)*

Natural resistance-associated macrophage proteins (NRAMPs) are a family of divalent metal transporters (DMTs), also known as solute carriers (SLCs), involved in both eukaryotic and prokaryotic iron homeostasis. Eukaryotes express two separate NRAMPs, NRAMP1 (or SLC11A1) and NRAMP2 (or SLC11A2/DMT1). NRAMP1 is phagosomally-expressed and aids in the fight against pathogens by sequestering iron (among other transition metals) from the invading bacterium during phagocytosis by macrophages, whereas NRAMP2 facilitates the absorption of dietary iron and is critical in maintaining iron homeostasis (Ehrnstorfer et al.

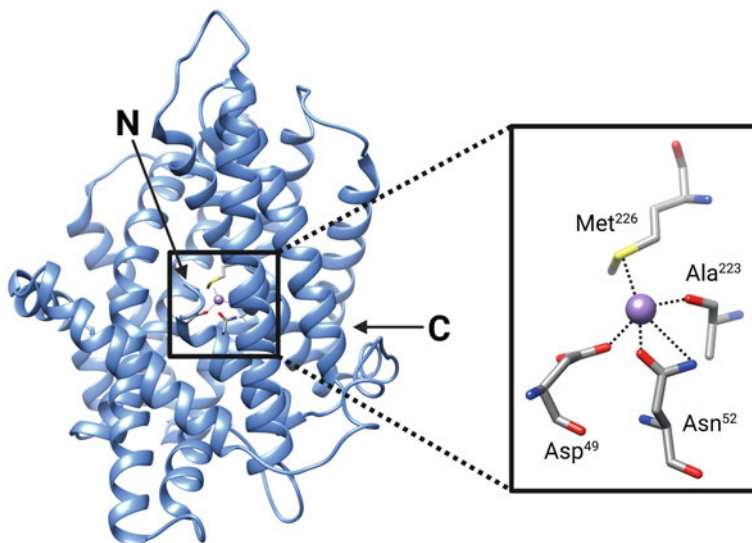


**Fig. 12.3** X-ray crystal structure of *ScaDMT* bound to  $Mn^{2+}$  (PDB ID: 4WGW).  $Mn^{2+}$  (purple sphere) is coordinated by side chains from Met, Asp, and Asn residues, and a peptidyl oxygen from Ala (expanded region). ‘N’ and ‘C’ represent the N- and C-termini respectively. Figure created with BioRender

2014; Bozzi et al. 2016). Bacterial NRAMP homologues constitute three “clades” (A, B, C) and display a high degree of sequence conservation to their eukaryotic counterparts, suggesting that their metal specificity and transport mechanisms may be similar to those exhibited in eukaryotes (Ehrnstorfer et al. 2014; Bozzi et al. 2016).

Recent studies have sought to understand the mechanism of NRAMP-mediated divalent metal ion transport through a combination of structural and biochemical techniques. In an X-ray crystal structure of a truncated *Staphylococcus capitis* DMT (*ScaDMT*) (belonging to clade C but lacking 41 N-terminal residues) the transmembrane (TM) I region contains an inverted repeat of the first five TM helices (known as a LeuT fold) and an unstructured region in the first helix in the inverted repeat (between helix 1 and helix 6), providing the coordinating ligands for metal substrates (Ehrnstorfer et al. 2014). The metal-coordinating residues of a metal-bound state were initially determined by solving the X-ray crystal structure of  $Mn^{2+}$ -bound *ScaDMT* (PDB ID: 4WGW), which revealed the side chains of Met, Asp, and Asn (conserved residues in human DMT1) as well as the peptidyl carbonyl oxygen all bound to  $Mn^{2+}$  (Fig. 12.3) (Ehrnstorfer et al. 2014). Further structural and functional characterization of *ScaDMT* demonstrated binding of  $Fe^{2+}$ ,  $Co^{2+}$ ,  $Ni^{2+}$ ,  $Cd^{2+}$ ,  $Pb^{2+}$ , and  $Cu^{2+}$  (albeit in a slightly shifted position).  $Mn^{2+}$ ,  $Co^{2+}$ ,  $Ni^{2+}$ , and  $Cd^{2+}$  could be transported into *ScaDMT*-containing liposomes, although  $Fe^{2+}$  transport was not confirmed in this study (Ehrnstorfer et al. 2014). Intriguing follow-up studies demonstrated that the coordinating Met lends itself importantly to specificity by

discriminating against alkali earth metals (Bozzi et al. 2016), which could be a common theme amongst  $\text{Fe}^{2+}$  transporters.

An X-ray crystal structure of *Deinococcus radiodurans* NRAMP (*DraNRAMP*), a member of prokaryotic clade A NRAMPS, similarly displayed a LeuT fold in an inward-facing conformation but included the missing N-terminal residues from the *ScaDMT* structure. The position of TM helix 1a to that of 1b is striking as the angle between the two helices is  $103^\circ$ . This bent conformation is believed to create an “aqueous vestibule” that may allow for a water molecule to coordinate metal bound between helices 1 and 6 (Bozzi et al. 2016). Furthermore, molecular snapshots obtained from cysteine accessibility scanning suggest that *DraNRAMP* undergoes a series of conformational changes to facilitate the transport of divalent metal ions through an extracellular metal-permeation pathway before reaching the metal-binding site, which could be a common mechanism among NRAMPs (Bozzi et al. 2016). While more structural information will be necessary to elucidate the full mechanism of divalent metal transport in these proteins and to characterize mutations resulting in disease states, the current structures and functional analyses have contributed to understanding how a broad range of metal substrates can be recognized, demonstrating the high flexibility and substrate promiscuity of some transporters. These models could prove useful for other uncharacterized transporters.

The  $\text{H}^+$ -dependent manganese transport system (MntH) (Fig. 12.2, pink) is a NRAMP homolog first identified in *E. coli* in 1969 (Silver and Kralovic 1969; Silver et al. 1970; Bhattacharyya 1970; Makui et al. 2000). Though MntH has a preference for  $\text{Mn}^{2+}$ , it has also been linked to the transport of  $\text{Fe}^{2+}$ , and cells overexpressing MntH accumulate  $\text{Fe}^{2+}$  via active transport, as observed by in vivo  $^{55}\text{Fe}^{2+}$  uptake experiments. In this study,  $^{55}\text{Fe}^{2+}$  uptake could also be inhibited by  $\text{Mn}^{2+}$  and  $\text{Zn}^{2+}$  when supplied at a 100-fold molar excess or by the addition of protonophores (Makui et al. 2000). Similar experiments performed to monitor in vivo  $^{54}\text{Mn}^{2+}$  uptake reveal the same proton-dependent uptake as  $^{55}\text{Fe}^{2+}$ . However,  $^{54}\text{Mn}^{2+}$  accumulated to approximately ten-fold higher concentration over  $^{55}\text{Fe}^{2+}$ , demonstrating MntH's specificity for  $\text{Mn}^{2+}$  (Makui et al. 2000). In addition, the overexpression of MntH allowed cells to accumulate  $\text{Cd}^{2+}$ ,  $\text{Zn}^{2+}$ , and  $\text{Co}^{2+}$  as well as  $\text{Ni}^{2+}$  and  $\text{Cu}^{2+}$ , but to a lesser extent, suggesting that  $\text{Ni}^{2+}$  and  $\text{Cu}^{2+}$  represent poor MntH substrates (Makui et al. 2000).

Another study measured the apparent  $K_M$  of  $\text{Mn}^{2+}$  uptake to be  $1\ \mu\text{M}$  in *E. coli* and  $100\ \text{nM}$  in *Salmonella typhimurium*. In *S. typhimurium*, transport of  $\text{Mn}^{2+}$  was not inhibited by  $\text{Na}^+$ ,  $\text{K}^+$ ,  $\text{Mg}^{2+}$ , or  $\text{Ca}^{2+}$ . Contrary to the results described above,  $\text{Ni}^{2+}$ ,  $\text{Cu}^{2+}$ , and  $\text{Zn}^{2+}$  required a 1000-fold excess to inhibit  $\text{Mn}^{2+}$  uptake, suggesting they are not potential substrates of MntH. However,  $\text{Cd}^{2+}$  greatly inhibited  $\text{Mn}^{2+}$  transport (Kehres et al. 2000). Similar observations were seen for *EcMntH*. Unsurprisingly, though  $\text{Fe}^{2+}$  could be accumulated by both *Ec*- and *StMntH*, transport of  $\text{Fe}^{2+}$  was significantly inhibited by  $\text{Mn}^{2+}$ . These results corroborate MntH's preference for  $\text{Mn}^{2+}$  even though it is capable of transporting other divalent metal ions (Kehres et al. 2000). Consistent with this specificity, regulation of *EcMntH* is accomplished via the  $\text{Mn}^{2+}$ -responsive transcriptional regulator, MntR, which belongs to the DtxR family, although partial repression by  $\text{Fe}^{2+}$ -Fur was also

observed, indicating cross-talk between Mn and Fe homeostasis in this organism (Patzer and Hantke 2001).

The ZupT divalent metal transporter (Fig. 12.2, yellow) from *E. coli* is also believed to transport  $\text{Fe}^{2+}$  in addition to  $\text{Zn}^{2+}$  and other metals (Grass et al. 2002, 2005a). This protein belongs to the zinc-regulated transporter (ZRT), iron-regulated transporter (IRT)-like proteins known as the ZIP family. This family has been identified in animals, plants, protists, and fungi, and these transporters are known to mobilize  $\text{Fe}^{2+}$ ,  $\text{Zn}^{2+}$ ,  $\text{Mn}^{2+}$ , and  $\text{Cd}^{2+}$  (Guerinot 2000). ZupT is the first member of this family to be found in the bacterial kingdom (Guerinot 2000; Grass et al. 2002, 2005a). Strains of *E. coli* defective for all other iron transport systems except for ZupT were able to grow in the absence of metals and in the presence of  $\text{Mg}^{2+}$ ,  $\text{Zn}^{2+}$ ,  $\text{Mn}^{2+}$ , and  $\text{Fe}^{3+}$ .  $^{55}\text{Fe}$  uptake assays demonstrated that *E. coli* strains defective for iron transport but harboring an inducible plasmid for ZupT demonstrated the ability to import  $\text{Fe}^{2+}$  (Grass et al. 2005a). ZupT was also able to transport  $\text{Co}^{2+}$  in a strain carrying an additional deletion for CorA, a  $\text{Co}^{2+}$  transporter. Further demonstrating its substrate promiscuity, ZupT is also believed to transport  $\text{Mn}^{2+}$ , but at a much lower affinity (Grass et al. 2005a). When compared to MntH and Feo (vide infra), the ZupT protein was not as efficient for  $\text{Fe}^{2+}$  transport, suggesting that ZupT could be a secondary  $\text{Fe}^{2+}$  transporter in *E. coli* (Grass et al. 2005a). Despite evidence of broad divalent metal ion substrate specificity by ZupT, this protein remains largely uncharacterized, and more work is needed to understand the molecular details of the metal binding and transport process to determine how ZupT contributes to  $\text{Fe}^{2+}$  uptake in *E. coli*.

### 12.3.2 ATP-Binding Cassette (ABC) Transporters

The *Salmonella* iron transporter (*sit*) operon in *Salmonella typhimurium* was first identified in 1999 in the centisome 63 pathogenicity island and has high homology to the *yfe* system (Bearden et al. 1998) from *Y. pestis*. The *sit* operon encodes for four proteins: SitA, a putative periplasmic binding protein with homology to YfeA; SitB, the ABC transporter; and SitC and SitD, putative integral membrane permeases with homology to YfeC and YfeD (Fig. 12.2, blue) (Zhou et al. 1999). To test the role of the Sit system in  $\text{Fe}^{2+}$  transport, *SitABCD* was introduced into an enterobactin-deficient strain of *E. coli*. Expression of the *sit* operon rescued a growth defect of the *E. coli* strain in iron-limited media (Zhou et al. 1999). A  $\Delta\textit{sitBCD}$  deletion strain was tested in vivo to determine the effect of the Sit system on *S. typhimurium* virulence; however, no difference in the virulence of the  $\Delta\textit{sitBCD}$  deletion strain was detected, which is likely the result of redundant iron transport systems present in *S. typhimurium* (Zhou et al. 1999). A different study demonstrated that *sitABCD* is induced in mouse liver when infected intraperitoneally, but induction of *sitABCD* was much lower in other organs when mice were infected orally. These results suggest that *sitABCD* is expressed during late-stage infection, after invasion of the intestines (Janakiraman and Slauch 2000). In contrast to previous results,

*S. typhimurium* strains bearing a *sitA* mutation, which was polar on downstream *sit* genes, exhibited growth and survival defects in mice (Janakiraman and Slauch 2000). Additionally, the *sit* operon was found to be controlled by  $\text{Fe}^{2+}$  and Fur, though another study determined MntR and  $\text{Mn}^{2+}$  also regulated the *sit* operon (Zhou et al. 1999; Janakiraman and Slauch 2000; Ikeda et al. 2005). Similar regulation is also observed for the Yfe system of *Y. pestis* (Bearden et al. 1998; Perry et al. 2012).

Though the Sit system was first identified as an ATP-dependent  $\text{Fe}^{2+}$  uptake system, it is also able to transport  $\text{Mn}^{2+}$  with a higher affinity than that of  $\text{Fe}^{2+}$ . Similar to MntH, the apparent affinity of  $^{54}\text{Mn}^{2+}$  transport by *S. typhimurium* SitABCD was 0.1  $\mu\text{M}$  and was not affected by pH. In contrast to the association constant, maximal  $\text{Mn}^{2+}$  transport was pH-dependent and increased at alkaline pH (Kehres et al. 2002), and  $\text{Fe}^{2+}$  inhibition of  $\text{Mn}^{2+}$  transport was also observed. Somewhat similarly, transport of  $^{55}\text{Fe}^{2+}$  by SitABCD occurred in a pH-dependent manner and was inhibited by  $\text{Mn}^{2+}$  though inhibition was not pH-dependent (Kehres et al. 2002).  $\text{Cd}^{2+}$ ,  $\text{Zn}^{2+}$ ,  $\text{Co}^{2+}$ ,  $\text{Cu}^{2+}$ ,  $\text{Ni}^{2+}$  and  $\text{Fe}^{3+}$  were also tested for their ability to inhibit  $\text{Mn}^{2+}$  transport with  $\text{Cd}^{2+}$  and  $\text{Zn}^{2+}$  being the most potent inhibitors (Kehres et al. 2002). Whether  $\text{Fe}^{2+}$  is a natural substrate of the Sit system remains debated and may be dependent upon the conditions under which the Sit system is expressed.

### 12.3.3 Oxidase-Dependent $\text{Fe}^{2+}$ Transporters (OFeTs)

The elemental ferrous iron uptake (EfeU) protein (also known as YcdN) is a unique  $\text{Fe}^{2+}$  transporter that has been well characterized but is operative only in select pathogenic species (Fig. 12.2, green). Belonging to the *ycdNOB* operon, EfeU is homologous to the yeast high-affinity ferric iron permease protein Ftr1p that belongs to the oxidase-dependent iron transporters (OFeTs) (Grosse et al. 2006). These transporters are part of a larger family of proteins known as the iron/lead transporter (ILT) superfamily that transports  $\text{Fe}^{2+/3+}$  and  $\text{Pb}^{2+}$  (Saier et al. 2006, 2021). Yeast Ftr1p contains an REXXE iron-binding motif, similar to other metal transporters (Stearman et al. 1996; Severance et al. 2004; Grosse et al. 2006), and yeast Ftr1p functions in tandem with a multicopper ferroxidase, Fet3p, and an extracellular reductase, Fre, to transport iron. Fre must first reduce  $\text{Fe}^{3+}$  to  $\text{Fe}^{2+}$ , at which point Fet3p binds the metal and oxidizes the ion back to  $\text{Fe}^{3+}$ . A hand-off of the metal occurs between Fet3p and Ftr1p (Askwith et al. 1994; Askwith and Kaplan 1997). By comparison, in *E. coli*, the *eFeUOB* operon (also termed the *ycdNOB* operon) is polycistronic and is expressed under iron-deplete conditions. Expression of *eFeUOB* is controlled by FUR and is not regulated in response to  $\text{O}_2$  (Grosse et al. 2006; Cao et al. 2007). When pH-dependent expression of *eFeU* was determined, *eFeU* displayed higher expression at lower pH (pH = 5.0), under which  $\text{Fe}^{2+}$  would be stabilized, than at higher pH (pH = 8.0) for both iron-deplete and iron-replete conditions. This pH-dependent regulation is accomplished by *cpxAR*, a

two-component sensor regulator, where CpxA is a histidine kinase localized to the inner membrane and CpxR is an OmpR-like response regulator (Cao et al. 2007). Given EfeU's homology to yeast Ftr1p, these results could provide insight into the mechanism of iron uptake by EfeU.

EfeU is a 276 amino acid protein predicted to have seven TM helices with a periplasmic N-terminal domain and a cytoplasmic C-terminal domain. REXXE iron binding motifs are located in TM helix 1 and TM helix 4. Additionally, an  $\approx 40$  amino acid periplasmic extension is one of two glutamate-rich periplasmic regions located between TM helix 6 and TM helix 7. The TM region is devoid of both negatively charged residues and His residues and, with the exception of the REXXE motifs and some Met residues, appears to be lacking in other metal-binding amino acids (Grosse et al. 2006). To test the importance of the REXXE motifs in EfeU, each motif was individually mutated. Regardless of which motif harbored the mutation, an iron uptake deficient strain of *E. coli* was unable to grow. These results suggest that mutation of the REXXE motifs rendered the organism incapable of binding and transporting iron for growth under experimental conditions. EfeU is also believed to be highly-specific for iron, as EfeU was found to not be involved in the transport of  $\text{Zn}^{2+}$ ,  $\text{Pb}^{2+}$ , or  $\text{Cu}^{2+}$  (Grosse et al. 2006), and a preference for  $\text{Fe}^{2+}$  over  $\text{Fe}^{3+}$  was also observed, indicating high specificity of EfeU (Cao et al. 2007). EfeU was also tested for in vitro metal transport into proteoliposomes to verify which oxidation state of iron is transported by the protein. Using Phen Green SK as a fluorescence reporter for metal transport into the proteoliposomes, only  $\text{Fe}^{2+}$  translocation was observed. This transport process is believed to occur via facilitated diffusion, though the energy coupling process has not been fully elucidated (Grosse et al. 2006). It is also possible that additional factors may contribute to  $\text{Fe}^{2+}$  binding and transport of EfeU, such as the proteins EfeB and EfeO.

EfeB is believed to be a periplasmic paralog of the dye-decolorizing peroxidases. In *E. coli*, the EfeB protein contains a twin-arginine signal sequence suggesting the protein is translocated across the cytoplasmic membrane to the periplasm via the twin-arginine-translocation (Tat) system. However, some EfeB has also been detected in the cytoplasm. EfeB is known to be a heme *b* containing-protein regardless of compartmental localization (Sturm et al. 2006). EfeB was confirmed to have peroxidase activity by monitoring  $\text{H}_2\text{O}_2$ -dependent oxidation of guaiacol, a naturally-occurring organic compound; however, no specific substrate of EfeB was identified (Sturm et al. 2006). A later study evaluated the ability of EfeB to degrade heme for iron utilization in *E. coli*. Soluble fractions of cell lysates containing overexpressed EfeB were able to extract iron from heme (Létoffé et al. 2009). As no other protoporphyrin metabolites were identified upon iron release from heme by YfeX or EfeB, it was suggested that both proteins have deferrochelation activity and thus leave the protoporphyrin ring intact. It is possible that, in the context of the Efe system, EfeB serves to demetallate heme to provide iron, likely  $\text{Fe}^{2+}$ , to EfeU for transport into the cytoplasm (Létoffé et al. 2009). Both EfeB and its paralog YfeX were subsequently found to be essential for exogenous heme iron acquisition in vivo and strains lacking either *yfeX* or *efeB* or both could utilize exogenous heme when complemented with *pigA*, a heme oxygenase from *Pseudomonas aeruginosa*,

suggesting their functions are related to the release of iron from heme (Létoffé et al. 2009). In the absence of functional heme-uptake systems, overexpression of a functional *efeUOB* operon allowed for heme acquisition in *E. coli*.

To further investigate the function of EfeB, the protein was crystallized in complex with heme and the structure was determined to 1.95 Å resolution (PDB ID: 2Y4E). The asymmetric unit consisted of homodimeric EfeB (residues 48–422) in which both molecules were bound to heme (Liu et al. 2011). The crystal structure revealed that EfeB is structurally similar to the de-colorizing peroxidase enzymes and adopts a ferredoxin-like fold. The N-terminal and C-terminal domains of EfeB are connected via a 22-amino acid loop termed the switch loop. This loop helps to stabilize the heme-EfeB interaction solely by interaction with the heme cofactor, potentially to mediate demetallation of the heme cofactor (Liu et al. 2011). While EfeB removes iron from heme in vivo, resulting in the accumulation of protoporphyrin-IX, purified EfeB does not display this enzymatic activity, likely due to the absence of an additional cofactor or cosubstrate. Though EfeB is undeniably involved in the iron transport process, the mechanism of demetallation, and what additional factors may be involved in this process (such as peroxidase activity), remain unknown. Given the role of iron in bacterial pathogenesis, EfeB could serve as an antibacterial target, an endeavor that would be facilitated by further characterization of EfeB and its homologs.

EfeO (YcdO) is a predicted periplasmic protein that has also been found to be similar to dye-decolorizing peroxidases. Similar to EfeB, *E. coli* EfeO was also predicted to be a Tat-substrate; however, its twin-arginine signal sequence is not conserved amongst other EfeO homologs (Sturm et al. 2006). Though EfeO is not well characterized, EfeO proteins have been grouped into five classes based on their domain architectures: class I, comprising a N-terminal cupredoxin-containing domain (Cup domain) and a C-terminal peptidase-M75 or imelysin-like domain; class II, comprising only a M75 domain (termed EfeM); class III, comprising an unidentified N-terminal domain and a M75 domain; class IV, comprising a class I EfeO fused to EfeU; and class V, comprising only a Cup domain (Rajasekaran et al. 2010). The Cup domain is posited to be involved in electron transfer and also has potential metal binding sites for  $\text{Cu}^{2+}$  and  $\text{Fe}^{3+}$ . Within the M75 domain is a conserved HXXE motif, a putative metal binding site through which iron could be transferred to EfeU (Rajasekaran et al. 2010), but the validity of this hypothesis remains unclear. More work will be necessary to understand the structure, function, and metal binding properties of EfeO to determine its role in the iron transport process.

### 12.3.4 Iron Transporter/More Regions Allowing Vacuolar Colocalization N Protein (*IroT/MavN*)

*Legionella pneumophila* is the causative agent of Legionnaires' disease, and when *L. pneumophila* infects host cells, it establishes a *Legionella*-containing vacuole (LCV) associated with the endoplasmic reticulum. Iron is required for the survival and virulence of intravacuolar pathogens, and *IroT/MavN* is a key transporter that functions at this location (Fig. 12.2, orange) (Portier et al. 2015; Isaac et al. 2015). A substrate of the intracellular multiplication/defect in organelle trafficking (*Icm/Dot*) type IV secretion system of the LCV, *mavN* is an iron-regulated gene encoding a 660 amino acid, 75 kDa protein that contributes to *Legionella* growth and iron transport in both amoeba and macrophages (Isaac et al. 2015; Portier et al. 2015; Christenson et al. 2019). Additionally, *L. pneumophila* bearing a non-functional *MavN* exhibited growth defects on iron-restricted agar and acquired  $\text{Fe}^{2+}$  at levels lower than wild type (WT) strains (Portier et al. 2015). These results indicate that *MavN* is important for iron acquisition to support the growth and the survival of this pathogen living within a variety of different environments.

Topologically, *MavN* is predicted to have 8 TM helices with both the N- and C-termini located in the cytoplasm. *MavN* also contains four predicted cytoplasmic loops and three predicted loops in the LCV lumen. This topology was verified by the transmembrane-substituted cysteine accessibility method (Christenson et al. 2019; Isaac et al. 2015). Like other iron-binding proteins, *MavN* also contains EXXE motifs and nine of these motifs can be found within the protein. An EXXE motif in a 70-amino acid loop (denoted as loop 7) mapped to the LCV lumen and conserved amongst all *Legionellaceae* species was the only one of these motifs determined to be wholly essential for *L. pneumophila* growth, as a plasmid carrying this mutation could not complement a  $\Delta\text{mavN}$  growth defect (Isaac et al. 2015; Christenson et al. 2019). This loop also contains eight His residues, three of which were found to be important for *MavN* function in a triple mutant (Isaac et al. 2015). Only one His residue is predicted to be localized to the TM region along TM helix 6, and mutation of this residue exhibits a growth defect. Additionally, of the four Met residues in *MavN*, only one (along TM helix 3) led to a growth defect in vivo (Christenson et al. 2019). These in vivo results were subsequently used to test an in vitro transport model of *MavN*.

For in vitro analysis of *MavN*, the protein was heterologously expressed and purified from the methylotrophic yeast *Pichia pastoris*. Solubilization and purification in detergents  $\text{C}_{12}\text{E}_6$  and  $\text{C}_{12}\text{E}_8$  and yielded predominately dimeric protein (Christenson et al. 2019). To test substrate binding,  $\text{Co}^{2+}$  and  $\text{Ni}^{2+}$  were tested for their ability to bind to *MavN* as surrogates for  $\text{Fe}^{2+}$  under oxic conditions, and both substrates bound with modest affinity ( $K_d$  ca.  $\mu\text{M}$ ) (Christenson et al. 2019). *MavN* was then reconstituted into a liposome to test for metal ion transport using calcein, a dye whose fluorescence is quenched by metal binding. Transport of several metal ions into proteoliposomes were tested and a  $K_M$  for  $\text{Fe}^{2+}$  transport was measured to be  $16 \mu\text{M}$ . Though transport of  $\text{Mn}^{2+}$ ,  $\text{Co}^{2+}$ , and  $\text{Zn}^{2+}$  into the proteoliposomes was



also observed, transport of  $\text{Cu}^+$ ,  $\text{Cu}^{2+}$ , and  $\text{Ni}^{2+}$  was not (Christenson et al. 2019). To determine whether  $\text{Mn}^{2+}$  and  $\text{Zn}^{2+}$  could serve as substrates for MavN, these metals were provided in excess to a  $\Delta\text{mavN}$  strain growing in bone marrow deficient macrophages, in addition to  $\text{Fe}^{2+}$ . In these experiments, both  $\text{Mn}^{2+}$  and  $\text{Zn}^{2+}$  stimulated growth of the  $\Delta\text{mavN}$  strain, suggesting substrates other than  $\text{Fe}^{2+}$  could be translocated by MavN in vivo (Christenson et al. 2019). In vitro studies of  $\text{Fe}^{2+}$  transport into proteoliposomes with variant MavNs showed an importance for His and Met residues in  $\text{Fe}^{2+}$  translocation, while Cys variants only had modest effect on  $\text{Fe}^{2+}$  transport (Christenson et al. 2019).

Another study published shortly after also reconstituted MavN into liposomes for metal transport studies. In this study, MavN was heterologously expressed in *E. coli*, extracted from membranes with *n*-tetradecylphosphocholine (Fos-choline-14) and then purified in 7-cyclohexyl-1-heptyl- $\beta$ -D-maltoside (Cymal-7), which resulted in chiefly monomeric protein (Abeyrathna et al. 2019). MavN was then incorporated into liposomes containing FluoZin-3, a turn-on fluorescent probe, to monitor transport activity. Transport of  $\text{Fe}^{2+}$  was monitored in an anoxic environment and similar  $K_d$  values ( $\mu\text{M}$ ) were observed (Abeyrathna et al. 2019). However, contrary to the previous study, transport of  $\text{Fe}^{2+}$  was highly specific, and  $\text{Co}^{2+}$ ,  $\text{Ni}^{2+}$ , and  $\text{Zn}^{2+}$  provided  $<5\%$  of the  $\text{Fe}^{2+}$  response. As a control,  $\text{Fe}^{3+}$  was also tested for transport, and was not taken up by MavN. These results suggest that MavN could be highly specific for  $\text{Fe}^{2+}$  (Abeyrathna et al. 2019). Because of the acidic pH of the LCV, it was suggested that  $\text{Fe}^{2+}$  transport could be coupled to proton counter-transport. To test this, a pH indicator, pyranine, was incorporated into the proteoliposomes. Subsequently, as  $\text{Fe}^{2+}$  uptake occurred, the pH inside the vesicles increased, suggesting that MavN could function as an  $\text{Fe}^{2+}/\text{H}^+$  antiporter or as a secondary active transporter (Abeyrathna et al. 2019). To determine which residues may contribute to  $\text{Fe}^{2+}$  uptake, a series of variant proteins were constructed and incorporated into liposomes. A variant protein containing mutations to Glu and His residues in TM helices 2 and 3 and Asp and Cys residues in TM helix 8 was constructed and tested for transport. This variant maintained the same  $V_{\text{max}}$  as the WT protein; however,  $K_M$  was higher ( $>25 \mu\text{M}$ ) (Abeyrathna et al. 2019). A different variant of Glu, Cys, and His residues at the TM-LCV interface abolished  $\text{Fe}^{2+}$  uptake, indicating that these residues could serve to release  $\text{Fe}^{2+}$  into the vacuole (Abeyrathna et al. 2019). Taken together, these in vitro assays to assess metal transport will be useful models for determining real-time metal transport of other transporters, especially for determining residues involved in the transport process. If used in conjunction with other biochemical and biophysical techniques, transport mechanisms could be determined, which could aid in the design of molecules that inhibit the transport process.

While the systems described above are known or are purported to be  $\text{Fe}^{2+}$  transport systems, they remain largely uncharacterized at both the cellular and the atomic levels. Furthermore, some of these transporters display a broad substrate specificity and they may have a relatively weak affinity for  $\text{Fe}^{2+}$ , at least under the tested experimental conditions. Additionally, some transporters such as ZupT do not appear to be broadly distributed amongst bacteria, though it is possible that

homologs have yet to be identified. The Efe system, though specific for  $\text{Fe}^{2+}$ , is only distributed in some pathogenic bacteria. To our knowledge, the only widespread, prokaryotic,  $\text{Fe}^{2+}$ -specific transport system to be identified and characterized in several organisms is the ferrous iron transport (Feo) system, which is described in detail below.

### 12.3.5 Ferrous Iron Transport by the Feo System

The Feo system is the predominant prokaryotic  $\text{Fe}^{2+}$  transport system (Fig. 12.2, purple). The *feo* operon, encoding for the Feo system, was first discovered in 1987 by isolating an *E. coli* strain defective for  $\text{Fe}^{2+}$  uptake (Hantke 1987). At that time, five *E. coli*  $\text{Fe}^{3+}$  transport systems for ferric siderophores had been identified, but no system had been identified for  $\text{Fe}^{2+}$  transport. The locus responsible for  $\text{Fe}^{2+}$  transport was then termed *feo*, but its position within the *E. coli* genome remained unknown at the time. Feo was subsequently identified to be a high affinity transporter, as cellular uptake studies revealed an apparent  $K_M$  of  $\text{Fe}^{2+}$  to be  $\approx 0.5 \mu\text{M}$ , and in 1993, the *feoA* and *feoB* genes were cloned and their sequences were published (Kammler et al. 1993). The Feo system also appears to be under regulation by the fumarate and nitrate reduction regulator (FNR) as FNR binding sites were found near the genes encoding for FeoA and FeoB (Fig. 12.4). FNR is a cAMP-like

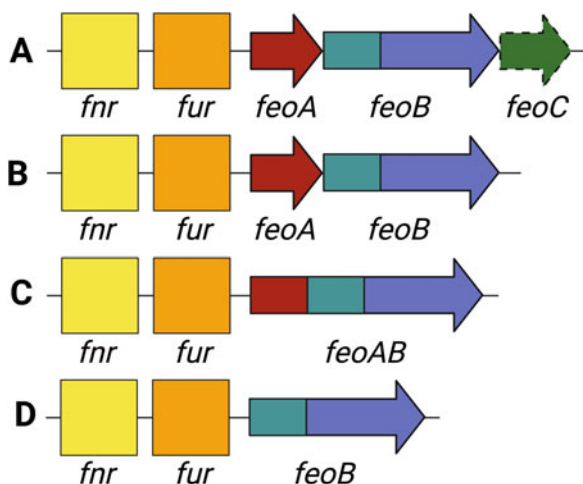


**Fig. 12.4** The most common arrangements of the *feo* operon. (a) The operon encoding for FeoA, FeoB, and FeoC was first discovered in *E. coli* in 1987. However, the FeoC protein is poorly conserved (found in  $\approx 13\%$  of bacteria), which is denoted by a dashed line. These genes are downstream of the binding sites for the FNR and FUR regulators. (b) The most common operon arrangement encodes for only FeoA and FeoB. (c) Though rare, some *feo* operons encode for an FeoA-FeoB fusion, such as in *Bacteroides fragilis*. (d) Some *feo* operons encode for FeoB alone, demonstrating the essential nature of this gene. Figure created with BioRender

transcriptional regulator that senses oxygen using a [4Fe-4S] cluster and binds to DNA using a helix-turn-helix domain. The [4Fe-4S] cluster is degraded in the presence of oxygen, and this cluster change controls DNA binding and alters a metabolic “switch” that converts bacterial metabolism from anaerobic to aerobic respiration (Spiro and Guest 1990; Uden et al. 2002; Crack et al. 2008). Additionally, a FUR binding site (*ferric uptake regulator*, one of the master regulators of general prokaryotic iron metabolism) was also discovered downstream from the FNR binding site (Fig. 12.4) (Kammler et al. 1993). When cellular iron is low, the  $\text{Fe}^{2+}$ -FUR complex dissociates and allows for transcription of iron-responsive genes (Escobar et al. 1999; Troxell and Hassan 2013; Fillat 2014). Unsurprisingly, a *fur* mutant was observed to accumulate  $\text{Fe}^{2+}$  more rapidly than WT, indicating *feo* to be under FUR regulation. Thus, Feo-mediated  $\text{Fe}^{2+}$  transport is highly regulated, but whether additional levels of regulation exist for this system remains unclear.

As more genomic data have become available, it has been proposed that Feo represents an ancient  $\text{Fe}^{2+}$  transport system (Hantke 2003), which is supported by several lines of evidence. First, as previously described, it is clear that  $\text{Fe}^{2+}$  was the predominant species of iron present on Earth as bacteria first evolved, undoubtedly necessitating an  $\text{Fe}^{2+}$  uptake system. Second, several cyanobacterial descendants (among the first unicellular organisms to exist on the planet) retain an FeoB protein within their genomes, suggesting that this system has played a major role during their evolution to necessitate such prolonged genetic retention. In fact, this conservation suggests that despite the switch from an anoxic to a more oxygen-rich atmosphere,  $\text{Fe}^{2+}$  transport was still necessary for the survival of many organisms. FeoB may have co-evolved alongside organisms to supply metabolic feedstocks of  $\text{Fe}^{2+}$ , a strategy that is undoubtedly still operative on modern Earth. Underscoring this point is the major conservation and distribution of the *feo* operon across present-day bacterial species. As of 2003, it was estimated that  $\approx 50\%$  of all bacterial genomes that had been sequenced at that time contained an *feoB*-like gene (Hantke 2003), emphasizing the dominance of Feo in prokaryotic  $\text{Fe}^{2+}$  acquisition.

The organization of the tripartite *feoA/feoB/feoC* operon found in *E. coli* is considered to be canonical, as it was the first to be discovered (Fig. 12.4a) (Hantke 2003, 1987; Kammler et al. 1993). However, there are several other arrangements of the *feo* operon, and it is now clear that a tripartite system is unlikely to be the dominant arrangement in most sequenced prokaryotic genomes. The tripartite operon arrangement is predominantly found in the  $\gamma$ -proteobacteria class but can also be found in terrabacteria (Cartron et al. 2006; Lau et al. 2016; Sestok et al. 2018, 2021). The FeoA protein is most commonly found alongside FeoB and some operons are predicted to encode for multiple FeoA proteins (Fig. 12.4b) (Lau et al. 2016; Cartron et al. 2006; Sestok et al. 2018). A recent search of the FeoA protein (IPR007167) using the InterPro Database (accessed February 2021) revealed that  $\approx 3\%$  of all FeoA proteins exist as fusions of either two or three FeoA proteins (Sestok et al. 2021). FeoA can also exist as a naturally-occurring fusion to the N-terminal domain of FeoB (Fig. 12.4c) (Sestok et al. 2018; Lau et al. 2016; Veeranagouda et al. 2014; Rocha et al. 2019; Dashper et al. 2005); these fusions are rare, found predominantly in the *Bacteroidia* and *Clostridia* classes, and account

for only  $\approx 8\%$  of all FeoA-domain containing proteins in the InterPro Database (Sestok et al. 2021). Finally, some bacterial genomes encode for only FeoB (Fig. 12.4d).

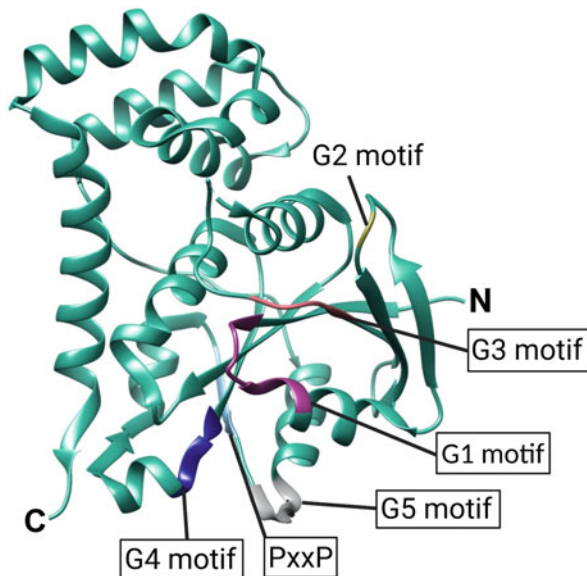
Regardless of the arrangement of the organism's operon, it is clear that FeoB is the chief component of the Feo system based on its conservation (Fig. 12.4). FeoB is a complex, polytopic membrane protein thought to resemble a covalent fusion of a G-protein to that of a *G-protein-coupled receptor* (GPCR). Guanine nucleotide-binding proteins, termed G-proteins, are a family of intracellular proteins and are associated with transmitting signals from external stimuli to the cell's interior. Each protein has two states, termed active and inactive, and for this reason G-proteins have been likened to molecular versions of switches. Consistent with this description, FeoB is typically composed of three main domains with their residues numbered relative to *E. coli* K-12 FeoB (Uniprot ID P33650): the G-protein domain that binds and hydrolyzes GTP (residues 1–170), the guanine dissociation inhibitor (GDI) domain (residues 171–276) that increases GDP affinity, and the TM region (residues 277–773) that has an ill-defined function. The G-protein domain and the GDI domain comprise the full N-terminal soluble domain of FeoB, which is termed NFeoB. To date, the majority of published literature on the Feo system has focused solely on NFeoB (vide infra), likely due to its more tractable, soluble form and its intriguing similarity to well-characterized G-proteins.

G-proteins play important roles in signal transduction in eukaryotic cells, but their roles in bacterial physiology are not well understood. In eukaryotes, G-proteins are numerous and as such are responsible for an array of cellular processes such as nuclear import and export, vesicle formation, exocytosis, regulation of the cytoskeleton, and cellular differentiation (Bos et al. 2007). In contrast, bacterial G-proteins may be involved in ribosome biogenesis, tRNA modification, cell cycle progression, or DNA replication. G-proteins cycle between on and off states, dependent on the identity of the nucleotide bound to the protein to carry out their molecular functions (Vetter and Wittinghofer 2001). GDP dissociation from a G-protein results in activation, which is followed by GTP binding and hydrolysis, returning the protein to its inactive form (Vetter and Wittinghofer 2001). Interestingly, bacterial G-proteins are structurally similar to eukaryotic G-proteins, but their nucleotide binding affinities are several orders of magnitude lower. Because eukaryotic GTPases display high nucleotide binding affinities and intrinsically slow GTP hydrolysis and GDP dissociation, *G-activating proteins* (GAPs) or guanine exchange factors (GEFs) are needed either to increase the rate of GTP hydrolysis or to facilitate the release of GDP (Vetter and Wittinghofer 2001). Regions within the G-protein domain are also important for how guanine nucleotides are recognized, and how these proteins interact with downstream effectors. Conformational changes are observed in these regions (termed switch I and switch II), dependent upon the nucleotide-state of the G-protein (Bos et al. 2007; Vetter and Wittinghofer 2001). Many of these aspects have been explored with regards to NFeoB function, and an abbreviated synopsis is presented below.

**Table 12.1** Consensus sequences for G-protein motifs in NFeoB. The G1–G4 motifs are conserved across bacterial taxonomic groups and were initially identified through multiple sequence alignments. The G5 motif was identified through structural alignments. All amino acid numberings are based on *EcFeoB*

Motif	Position	Sequence	Role
G1	10–17	GXXXXGK(S/T)	Binds to $\alpha$ - and $\beta$ -phosphate of GTP
G2	37	T	Binds to $\gamma$ -phosphate of GTP and $Mg^{2+}$
G3	56–59	DXXG	Binds to $\gamma$ -phosphate of GTP and $Mg^{2+}$
G4	120–123	NXXD	H-bonding to guanine nucleotide
G5	150–155	STRGRG	H-bonding to guanine nucleotide

**Fig. 12.5** X-ray crystal structure of *E. coli* NFeoB (PDB ID: 3I8S), comprising the GDI and G-protein domains. Five G-protein motifs are found in NFeoB and are responsible for the recognition and the binding of guanine nucleotides. The Pro-rich hydrophobic sequence in NFeoB is located along a  $\beta$  strand adjacent to the G5 motif and is believed to be the site of FeoA-FeoB interactions. ‘N’ and ‘C’ represent the N- and C-termini respectively. Figure created with BioRender



### 12.3.5.1 Composition and Structure of NFeoB

*E. coli* FeoB (*EcFeoB*) was demonstrated to contain a G-protein domain in 2002, representing the first example of a G protein tethered to a prokaryotic membrane protein (Marlovits et al. 2002). At that time, >95 species containing FeoB homologs had been identified. There was (and still is) no predicted homology between the TM domain of FeoB and that of other transmembrane proteins (Marlovits et al. 2002). Using multiple sequence alignments, four of the five G-protein motifs were identified in *EcFeoB* that are responsible for binding and hydrolyzing GTP (Table 12.1 and Fig. 12.5) (residues numbered based on *E. coli* K-12 FeoB; Uniprot ID P33650): G1 (residues 10–17; Fig. 12.5, purple), G2 (residue 37; Fig. 12.5, yellow), G3 (residues 56–59; Fig. 12.5, salmon) and G4 (residues 120–123; Fig. 12.5 blue). At

the time, the G5 motif (Fig. 12.5, gray) could not initially be identified because of poor sequence conservation (Marlovits et al. 2002).

In 2008, the linker region between the G-protein domain and the TM region in FeoB was identified as a GDI domain. Initially, a weakly-conserved LXXXE motif in the TM linker region identified by sequence alignments was believed to resemble a binding site for a GEF. An E210A variant was generated in both *EcNFeoB* and full-length *EcFeoB*. The *EcNFeoB*<sup>E210A</sup> variant exhibited a decreased 3'-*O*-(*N*-Methyl-anthraniloyl)-GTP (mant-GTP) affinity by approximately two-fold, but the mant-GDP affinity decreased by approximately four-fold. The authors attributed the function of the linker region between the G-protein domain and the TM region to that of a GDI domain instead of a GEF. The *EcFeoB*<sup>E210A</sup> variant was not functional in vivo, suggesting the GDI domain could play an important role in FeoB function (Eng et al. 2008). Subsequently, each domain was tested for the ability to affect nucleotide binding affinities. The presence of the GDI domain increased the affinity of mant-GDP by 13-fold, and the presence of the TM region further increased the affinity for mant-GDP by 400-fold. The binding affinity for mant-GTP by the G-protein domain and NFeoB were similar; however, the full-length *EcFeoB* exhibited much stronger binding of mant-GTP, further demonstrating that this region functions as a GDI domain (Eng et al. 2008). Interestingly, multiple sequence alignments of the NFeoB domains from *E. coli*, *Salmonella typhimurium*, *Vibrio cholerae*, and *Helicobacter pylori* showed that the linker region varies in sequence and length, which could be a functional variation among species for this domain. Subsequent structural analyses then provided further insight into this intriguing domain.

Some of the first structures of the G-protein domain of FeoB (residues 1–184) were determined in 2009 from the archaeon *Methanococcus jannaschii* in the apo (PDB ID: 2WJH), GDP-bound (PDB ID: 2WJG), and GMP-PNP bound (PDB ID: 2WJI) forms (Koster et al. 2009a, b). *M. jannaschii* NFeoB (*MjNFeoB*) crystallized as a homodimer in the presence and absence of nucleotides, in which the nucleotide binding pockets form the dimeric interface. The overall structure of *MjNFeoB* revealed six  $\alpha$ -helices and a core  $\beta$ -sheet composed of seven  $\beta$ -strands. However, major structural differences exist in the G-domain dependent upon the nucleotide state of the protein. In the GTP-bound form, the Switch I loop points away from the nucleotide binding site and the  $\beta$ -sheet in the GTP-bound form lacks one  $\beta$ -strand (residues 32–36), which could not be seen in the electron density. This suggests that the Switch I loop, located between the G1 and G2 motif, may be more flexible in the GTP-bound form. Additionally, structural alignments of *MjNFeoB* with eukaryotic GTPases revealed the G5 motif, not previously identified through sequence alignments, to be located at position 145–148 (SAAK) (Koster et al. 2009b).

The *Streptococcus thermophilus* NFeoB was crystallized in the presence of GDP·AlF<sub>4</sub><sup>-</sup>, a transition-state analog that locks the G-protein in its active state, providing insight into how GTP hydrolysis is initiated (Ash et al. 2011). *StNFeoB* was co-crystallized with GDP·AlF<sub>4</sub><sup>-</sup>, one K<sup>+</sup> ion, and one Mg<sup>2+</sup> ion (PDB ID: 3SS8) (Ash et al. 2011). This transition-state structure of *StNFeoB* captured the Switch II region pointing away from the nucleotide binding site, in contrast with the Switch I

region that caps the nucleotide binding site, as observed in the previous mant-GMP-PNP bound structures (Ash et al. 2011). The  $K^+$  ion is bound in the nucleotide binding site with coordination by Gly29, Trp31, and Asn11, similar to its position in 3LX5, while the  $Mg^{2+}$  ion,  $\approx 5$  Å away from the  $K^+$ , contacts the planar  $AlF_4^-$  molecule that mimics the  $\gamma$ -phosphate of the nucleotide. Additional  $AlF_4^-$  interactions include an oxygen atom from the  $\beta$ -phosphate, backbone amides from Gly33, Val34, and Thr35 in the Switch I region, and a water molecule that performs nucleophilic attack (Ash et al. 2011). Importantly, the attacking water appears to be solvent exposed in this structure, which could allow the positioning of another catalytic residue, possibly from a different domain in FeoB or another partner protein (Ash et al. 2011).

In 2013, the X-ray crystal structure of NFeoB from *Gallionella capsiferiformans* was published in both the apo and the GDP-bound states. *G. capsiferiformans* provides a unique look into the structure of the cytoplasmic domain of FeoB, as *GcFeoB* lacks a GDI domain while the G-protein domain is structurally analogous to that of *EcNFeoB* (PDB ID: 3HYT) (Deshpande et al. 2013). While *GcNFeoB* was chiefly monomeric in solution, the protein crystallized as a domain-swapped dimer (Deshpande et al. 2013). *GcNFeoB* also contained the five G-protein motifs but exhibited a highly disordered G5 motif in both the apo structure and the GDP-bound structure (Deshpande et al. 2013). In agreement with the crystal structure of *S. thermophilus* NFeoB, the Switch I region was oriented away from the GDP binding pocket, supporting the hypothesis that the Switch I region is necessary for nucleotide binding and release (Deshpande et al. 2013).

Another crystal structure of NFeoB from *E. coli* BL21 was solved in 2016 (Hagelueken et al. 2016). After removal of the nucleotide, which typically co-purified with the protein, *EcNFeoB* crystallized as a trimer. This structure was similar to other apo NFeoB structures with the switch I region pointing away from the nucleotide binding site (suggested to be in the “open” conformation) (Hagelueken et al. 2016).

Numerous X-ray crystal structures of variant NFeoBs from several organisms have since been solved. However, these structures have failed to answer questions about how the Switch I and Switch II regions may be involved in regulating nucleotide binding and release,  $Fe^{2+}$  transport, and potential protein-protein interactions. Likewise, structural changes that might occur in the GDI domain upon metal binding and release have not been determined because FeoB lacks the TM region, further underscoring the importance of undertaking structural studies of full-length FeoB.

### 12.3.5.2 NFeoB Function and GTPase/NTPase Activity

Early seminal results revealed the ability of NFeoB to bind guanine nucleotides, and experiments have importantly linked the activity of the G-protein domain to  $Fe^{2+}$  uptake. Stopped-flow studies of *EcNFeoB* with non-hydrolyzable guanine and adenine nucleotide analogs, mant-5'-Guanylyl-imidodiphosphate (mant-GMP-

PNP) and mant-5'-Adenylyl-imidodiphosphate (mant-AMP-PNP), revealed specificity towards guanine nucleotides (Marlovits et al. 2002). At 20 °C, the  $K_d$  of affinity-tagged *EcNFeoB* for mant-GMP-PNP was determined to be  $\approx 4 \mu\text{M}$  (based on slow association but fast release kinetics), similar to Era but three orders of magnitude lower than p-21 Ras (Marlovits et al. 2002). However, a follow-up study of *EcNFeoB* measured a  $K_d$  for mant-GTP to be 12  $\mu\text{M}$ , a threefold increase over what was previously observed for mant-GMP-PNP, suggesting the non-hydrolyzable analog may not be a good proxy for GTP binding (Eng et al. 2008). GTP hydrolysis of *EcNFeoB* was markedly slow at  $\approx 0.0015 \text{ s}^{-1}$  and hydrolysis of ATP was not observed (Marlovits et al. 2002). Initially, two potential sites existed for the G4 motif, residues 91–94 or residues 120–123. To determine which site contained the G4 motif, two variants (D94N and D123N) were tested for their ability to bind mant-GMP-PNP in stopped-flow experiments and only the D94N variant could bind mant-GMP-PNP, confirming the G4 motif is located at positions 120–123 (Marlovits et al. 2002). Because the D123N variant failed to recognize mant-GMP-PNP, it was suggested that D123 could impact  $\text{Fe}^{2+}$  transport in the full-length protein. In an *feoB* deletion strain deficient for  $\text{Fe}^{2+}$  uptake, full-length FeoB was able to rescue  $\text{Fe}^{2+}$  uptake whereas a plasmid carrying a D123N variant was not. These results thus demonstrated a link between GTP binding, GTP hydrolysis, and  $\text{Fe}^{2+}$  transport (Marlovits et al. 2002).

Following these results, biochemical and structural experiments have revealed the contributions of some G motifs (and G5 in particular) to NFeoB-catalyzed GTP hydrolysis. Eight *EcNFeoB* variants located in the G motifs and switch regions, were examined for their effects on nucleotide binding and *feoB* function in vivo. All variants exhibited at least a two-fold decrease in GDP affinity, while only a T37A variant drastically decreased GTP affinity and could not restore  $\text{Fe}^{2+}$  uptake in a *feoB*-deficient strain (Eng et al. 2008). The N32A and D73A variants were able to hydrolyze GTP, but could not restore  $\text{Fe}^{2+}$  transport in a *feoB*-deficient strain (Eng et al. 2008). Additionally, the P12G, T60Q, and Y61A variants restored in vivo function of FeoB while the Y61E and P58A variants did not (Eng et al. 2008). Another study on *EcNFeoB* investigated changes in GDP release as a result of differences in sequence composition in the G5 motif (Álvarez-Fraga et al. 2018). Structural changes in the G5 motif are common in GTPases, but the NFeoB G5 motif seems to have poor sequence conservation and consists of six amino acids (V149–G154). In several structures of NFeoB, the loop formed by the G5 motif interacts with nucleotides through a mixture of H-bonding and hydrophobic interactions between the polypeptide and the nucleotide base (Álvarez-Fraga et al. 2018). This interaction must be important, as this structural motif is conserved despite low sequence conservation. An alanine in the second position in the G5 motif is typically the most conserved residue, and mutation of this analogous residue in eukaryotic GTPases results in severe health complications (GDP is released so fast the protein is always “on”) (Álvarez-Fraga et al. 2018). Interestingly, *E. coli* FeoB does not conserve an alanine residue, but rather a serine residue in this position. For WT *EcNFeoB*, GTPase activity was measured at  $0.40 \text{ min}^{-1}$  in the presence of  $\text{K}^+$ , a sevenfold increase than in the presence of  $\text{Na}^+$  (Álvarez-Fraga et al. 2018).



Subsequently, each residue was separately mutated to an alanine. All variants, with the exception of a S150A variant, displayed lower GTPase activity. The S150A variant's GTPase activity was 1.5-fold faster than the WT protein and exhibited a seven-fold slower release rate of mant-GDP (Guilfoyle et al. 2014). Using ITC, the S150A variant bound GDP five-fold higher than the WT, which correlates well with an observed slower GDP release (Álvarez-Fraga et al. 2018). Interestingly, differences in nucleotide binding and release are attributed to alterations in the hydrogen bonding network to the nucleotide base when serine is present versus alanine, destabilizing the nucleotide base. While the sequence composition of the G5 loop is clearly important for nucleotide binding and release, it remains unknown whether GDP release is a result of loop movement or if loop movement is a result of GDP release (Álvarez-Fraga et al. 2018).

Despite structural homology to eukaryotic G-proteins, recent publications have suggested that some FeoB proteins may be NTPases rather than strict GTPases. The first study to explore this idea found that *VcNFeoB* could hydrolyze both GTP and ATP, with a preference for GTP over ATP. Interestingly, *VcNFeoB* was also able to hydrolyze inosine triphosphate (ITP), but saturating conditions were never achieved. In contrast, *EcNFeoB* hydrolyzed GTP and ITP but did not hydrolyze ATP (Shin et al. 2019). Two variants in the G5 motif (S148T and N150T), which are responsible for interactions with the nucleotide base, displayed decreased ATPase activity but were able to transport  $\text{Fe}^{2+}$  in vivo, suggesting the variant *VcNFeoBs* were functional GTPases but not functional NTPases (Shin et al. 2019). *Helicobacter pylori* NFeoB was also tested for NTPase activity in this study and was able to hydrolyze GTP, ITP, and ATP, thus leading to the classification of *HpNFeoB* as an NTPase (Shin et al. 2019). *VcFeoA* and *VcFeoC* were also tested for their effects on GTPase and ATPase activity of *VcNFeoB*. When *VcFeoA* and *VcNFeoB* were mixed at a 1:1 ratio in the presence of 650  $\mu\text{M}$  ATP, ATP hydrolysis was reduced by  $\approx 60\%$ , and the addition of *VcFeoC* at a 2:1:2 ratio did not have any further effect on ATPase activity. Conversely, *VcFeoA* and *VcFeoC* stimulated GTPase activity of *VcNFeoB* at a 2:1:2 ratio. These results suggest that, at least in *V. cholerae*, FeoA and FeoC could function to regulate nucleotide hydrolysis activity (Shin et al. 2019). These observations raise interesting questions about the roles of FeoA and FeoC and whether their functions differ depending on whether their cognate FeoBs are strict GTPases or promiscuous NTPases.

A follow-up study further characterized NFeoB proteins from different organisms and suggested a sequence dependence on GTPase/NTPase classification (Shin et al. 2020). The authors found that NFeoBs from *E. coli*, *Salmonella enterica* serovar Typhimurium, and *Pseudomonas aeruginosa* (all Gram-negative pathogens) were only capable of hydrolyzing GTP, whereas NFeoBs from *Streptococcus mutans*, *Staphylococcus aureus*, and *Bacillus cereus* (all Gram-positive pathogens) were able to utilize both GTP and ATP (Shin et al. 2020). Through the use of multiple sequence alignments, the presence of a serine or alanine at position 150 (in *EcNFeoB*) was used to predict whether a NFeoB protein would be a GTPase or an NTPase, respectively. Phylogenetic analysis showed that NFeoB proteins with GTPase activity and the conserved Ser appear to be clustered together and

predominantly present in  $\gamma$ -proteobacteria, with the exception of *V. cholerae* and *H. pylori*, while those with NTPase activity and the conserved Ala are broadly distributed in different phyla (Shin et al. 2020). All WT NFeoBs displayed increased GTP and ATP hydrolysis with increasing temperature. Interestingly, *Bc*NFeoB displayed a preference for ATP at lower temperatures and GTP at higher temperatures (Shin et al. 2020). Why some FeoB proteins would potentially favor dual nucleotide specificity and some would favor GTP as a substrate remains unknown, and further studies investigating nucleotide binding and hydrolysis in full-length FeoBs will be necessary to determine dual nucleotide specificity.

While several NFeoBs have been structurally characterized throughout the GTP-hydrolysis cycle, there has been much debate regarding the functional oligomeric state of NFeoB (and thus full-length FeoB) in vivo. Q-band pulsed electron-electron double resonance (PELDOR) spectroscopy was used to characterize conformational, dynamical, and oligomeric changes in *Ec*NFeoB in the presence and absence of GTP. These data demonstrated that the largest structural changes in NFeoB during GTP binding occur in the switch I region (Hagelueken et al. 2016). A doubly MTSSL spin labelled but apo (nucleotide-free) *Ec*NFeoB was found to adopt an “open” conformation in solution ( $\approx 40$  Å label distance), similar to that seen in the crystal structure of *Ec*NFeoB. The addition of a 20-fold molar excess of GTP or GDP decreased the distance distribution of the spin labels on the protein to  $\approx 20$  Å, which was attributed to the “closed” state of the protein in which the switch I region moves to cover the GTP binding pocket, similar to the PELDOR observations (Hagelueken et al. 2016). This experiment was repeated with a 100-fold molar excess of GMP-PNP, which induced a conformational change from the “open” state to the “closed” states; however, this shift only corresponded to  $\approx 5\%$  of *Ec*NFeoB molecules in the “closed” state (Hagelueken et al. 2016). While the presence of  $K^+$  did stimulate GTP hydrolysis activity of *Ec*NFeoB, the presence of  $K^+$  did not affect the conformation of the switch I region (Hagelueken et al. 2016). A K1 spin label was then incorporated into *Ec*NFeoB to investigate oligomeric states present in solution. At low concentrations (25  $\mu$ M), *Ec*NFeoB was found to be monomeric in solution, but  $\approx 5\%$  of *Ec*NFeoB molecules formed higher-order oligomers at much higher protein concentrations ( $\approx 500$   $\mu$ M). While the data suggest *Ec*NFeoB monomers could interact at high concentrations, the authors noted that these interactions do not appear to be specific as the distance distribution observed was broad (Hagelueken et al. 2016). Thus, the exact oligomerization of the soluble NFeoB domain remains an open debate.

### 12.3.5.3 Full-Length FeoB

An intellectually curious aspect of FeoB is its unique combination of a G-protein covalently attached to a large TM region, resembling a hybrid of strategies commonplace in nature. Typically, small G-proteins cycle between active (GTP-bound) and inactive (GDP-bound) conformations depending on the nucleotide status of the protein and the cell (Bos et al. 2007). To assist localization of G-proteins to the

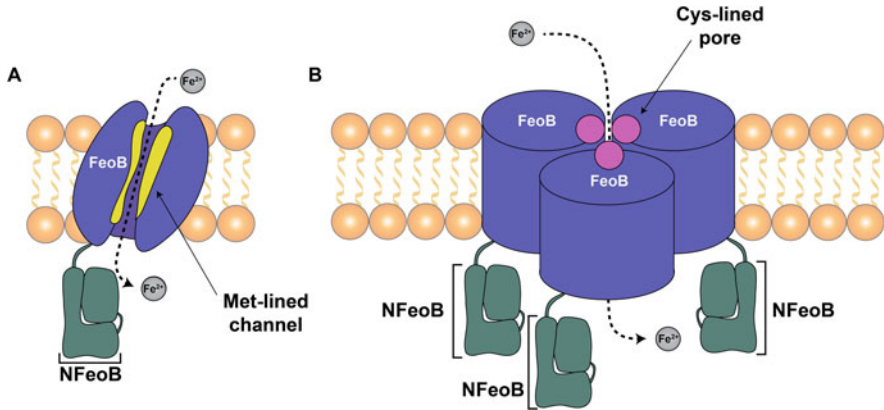


**Fig. 12.6** Models of FeoB-mediated  $\text{Fe}^{2+}$  transport. (a) Our laboratory has proposed that FeoB utilizes a Met-lined channel (yellow) to bind and to transport ferrous iron across the bacterial membrane (Sestok et al. 2018) based on a de novo calculated model of *Ec*FeoB (Ovchinnikov et al. 2017). (b) Others have proposed that FeoB utilizes an oligomerically-induced Cys-lined pore (pink) to bind and to transport  $\text{Fe}^{2+}$  across the bacterial membrane based on a model of *Pa*FeoB that has modest sequence homology to several functionally different bacterial transporters (Seyedmohammad et al. 2016)

membrane, their C- and/or N-termini may be prenylated, myristoylated, or acetylated (Bos et al. 2007). GDI domain-lipid tail interactions allow for G-proteins to be removed from the membrane and provide another level of control over G-proteins, in addition to GAPs and GEFs. GDI domain regulation in G-proteins is common in Rho and Rab GTPases (Bos et al. 2007). In the case of FeoB, the G-protein domain is uniquely tethered to its TM region by a GDI domain. It could be possible that interactions between the GDI domain and the TM region provide control over nucleotide binding at the G-protein domain, nucleotide hydrolysis, and even  $\text{Fe}^{2+}$  transport. However, structural and functional studies on FeoB are scarce, representing a major hole in our understanding of this component of the Feo system.

While no structure of an intact FeoB exists, the first model to appear was that of *Pseudomonas aeruginosa* FeoB (*Pa*FeoB) (Fig. 12.6). In this model, the predicted structure of the N-terminal domain was based on homology to the crystal structure of *Ec*NFeoB (crystallized as a trimer in the presence of mant-GTP; PDB ID: 3HYT) (Seyedmohammad et al. 2016). The TM region of FeoB was then modelled based on sequence similarity to an archaeal glutamate transporter (crystallized as a trimer; PDB ID: 1XFH). The linker region responsible for joining the soluble *Pa*NFeoB domain with the TM region was modelled based on sequence identity to the EDH2 ATPase (crystallized as a dimer; PDB ID: 2QPT), and the C-terminal domain of *Pa*FeoB was modelled based on sequence identity to dihydrodipicolinate reductase (crystallized as a tetramer; PDB ID: 1DIH) (Seyedmohammad et al. 2016). Despite these oligomeric discrepancies, the entirety of the *Pa*FeoB polypeptide was modelled as a homotrimer, and two conserved cysteine residues in *Pa*FeoB were suggested to be involved in the binding and transport of  $\text{Fe}^{2+}$  (Fig. 12.6). Blue native

PAGE and atomic force microscopy of purified *PaFeoB* in  $C_{12}E_8$  revealed three oligomeric states to be present: monomer, trimer, and hexamer. Based on the available data, monomeric *PaFeoB* seems to be the predominant oligomeric state followed by trimeric *PaFeoB*, with hexameric *PaFeoB* being the least prevalent (Seyedmohammad et al. 2016). A putative metal-binding residue Cys<sup>429</sup>, topographically modeled to be in TM helix 4, is predicted to form a ring within the homotrimer model. With an estimated diameter of  $\approx 5$  Å, this pore is hypothesized to be in the “open” state of the protein, which would be capable of transporting  $Fe^{2+}$  (Seyedmohammad et al. 2016). To probe this hypothesis further, GTPase activity of WT and variant *PaFeoBs* was measured and tested for stimulation by  $Fe^{2+}$ . Maximal stimulation of GTPase activity occurred in the presence of 1–1.5 mM  $Fe^{2+}$ . Furthermore, a C429S variant had no effect on GTPase activity while a C675S variant, topographically modeled to be in TM helix 7 and predicted to be exposed to the periplasmic space, significantly reduced GTPase activity. The authors thus rationalized that Cys<sup>675</sup> could serve as an  $Fe^{2+}$  sensor (Seyedmohammad et al. 2016). While this model provides one starting place for biochemical experiments to probe the mechanism of FeoB-mediated  $Fe^{2+}$  transport, another model exists that suggests a different transport mechanism could be possible.

A second model, this time of *E. coli* FeoB, was published in 2017 (Fig. 12.6) (Ovchinnikov et al. 2017). There are no true homologs of full-length FeoB and, because of its large size, accurate de novo models have been difficult to generate. Unlike the *PaFeoB* model, which was created by using proteins with modest sequence similarity to *PaFeoB*, the *EcFeoB* model was generated by determining residue-residue contacts with metagenome sequence data. This combination of evolutionary data and structural prediction has resulted in the generation of hundreds of structures of proteins from families without previously known structures (Ovchinnikov et al. 2017). Analysis of the de novo *EcFeoB*, a monomeric structure, reveals within FeoB the presence of a Met-lined channel that could serve as a translocation pathway for  $Fe^{2+}$  (Fig. 12.6) (Sestok et al. 2018). Additionally, the Cys residue predicted to be located at the periplasmic face and involved in the formation of a Cys-lined pore in the *PaFeoB* model (Cys<sup>675</sup>) is located within the TM region in the *EcFeoB* model (Cys<sup>677</sup>) (Sestok et al. 2018). However, despite the presence of two FeoB models, neither has been validated, and a full-length structure of FeoB is still unrealized, likely due to the difficulty of working with the intact membrane protein.

Despite the lack of atomic-level details of FeoB, at least a few publications have aimed to broaden our understanding of FeoB by addressing the challenge of large-scale expression and purification of the intact protein. In 2014, full-length *PaFeoB* and a D123N variant were the first particulate FeoB constructs to be solubilized in *n*-dodecyl- $\beta$ -D-maltoside (DDM) micelles, to be purified, and to be characterized functionally in vitro. Unstimulated GTP hydrolysis was slow ( $\approx 0.0035$  s<sup>-1</sup>), in agreement with the slow hydrolysis rates measured for soluble NFeoB. GTP hydrolysis by the D123N variant (a key G4 motif) was modestly altered to  $\approx 0.0012$  s<sup>-1</sup>, demonstrating the importance of this residue in the full-length protein (Seyedmohammad et al. 2014). Functional reconstitution of *PaFeoB* into

inside-out vesicles was also performed, and the GTP hydrolysis was modestly increased to  $\approx 0.0046 \text{ s}^{-1}$  in the absence of any metal or additional proteins (Seyedmohammad et al. 2014). In 2015, full-length *EcFeoB* and N-terminal *EcNFeoB* were both expressed and purified for spin-labelling EPR studies. An unnatural amino acid, *para*-acetylphenylalanine (pAcF), was incorporated into full-length *EcFeoB* at Lys<sup>127</sup> for this purpose (Hagelueken et al. 2015). Labeled *EcFeoB* was subsequently solubilized and purified in DDM. The dominant sizing profile of purified *EcFeoB* corresponded to a molecular weight of  $\approx 480 \text{ kDa}$ , while EPR experiments used rotational constants of the spin label to estimate the size of *EcFeoB* at  $\approx 300 \text{ kDa}$ . The results suggest that *EcFeoB* can form higher-order oligomers under these conditions (Hagelueken et al. 2015). However, spin labelled, full-length *EcFeoB* solubilized in DDM or incorporated into 3-([3-Cholamidopropyl]dimethylammonio)-2-hydroxy-1-propanesulfonate/dipalmitoylphosphatidylcholine (CHAPSO/DMPC) bicelles did not appear to form higher order oligomers based on PELDOR experiments. These results were confirmed by mass spectrometry and negative-stain electron microscopy (Hagelueken et al. 2016). Thus, the *in vitro* oligomerization of *EcFeoB* remains an open debate.

In 2018, expression, solubilization, and purification of full-length *Klebsiella pneumoniae* FeoB in DDM and C<sub>12</sub>E<sub>8</sub> was the first *in vitro* study of this construct. In contrast to previous studies that measured the GTP hydrolysis rates of *KpNFeoB* alone, GTP hydrolysis of full-length *KpFeoB* was determined to be orders of magnitude higher at  $\approx 0.09 \text{ s}^{-1}$  for the DDM-solubilized protein and  $\approx 0.03 \text{ s}^{-1}$  for the C<sub>12</sub>E<sub>8</sub>-solubilized protein (Smith and Sestok 2018). The stimulation of GTP hydrolysis by exogenous potassium was not observed, in contrast to *KpNFeoB*. Intriguingly, given the rapid rate of basal GTP hydrolysis, these observations suggest that the TM region of FeoB is able to significantly increase GTP hydrolysis levels, which could be operative for active transport. Whether FeoB transports Fe<sup>2+</sup> in a facilitated or active manner remains an open debate. Additional factors that could stimulate GTP hydrolysis further, such as protein-membrane or protein-protein interactions, have yet to be identified (Smith and Sestok 2018). This paucity of information on the intact, full-length protein further emphasizes the need for additional biophysical and biochemical studies of intact FeoB.

#### 12.3.5.4 FeoA

Within the *feo* operon, *feoA* is the most common gene appearing alongside *feoB* (Lau et al. 2013), suggesting FeoA plays an important role in Fe<sup>2+</sup> uptake. FeoA is a small, cytoplasmic,  $\beta$ -barrel protein (Fig. 12.7) of approximately 8 kDa chiefly composed of a Src Homology 3-Like (SH3) domain. SH3 proteins fold to form a hydrophobic core, with the  $\beta$ -sandwich held together by three loops termed the RT-Src loop, the N-Src loop, and the distal loop. The RT-Src loop and the N-Src loop contribute to peptide binding while the distal loop contributes to ligand binding (D'Aquino and Ringe 2003; Li 2005). In eukaryotes, SH3 domains have been implicated in a suite of signal transduction mechanisms, facilitating protein-protein

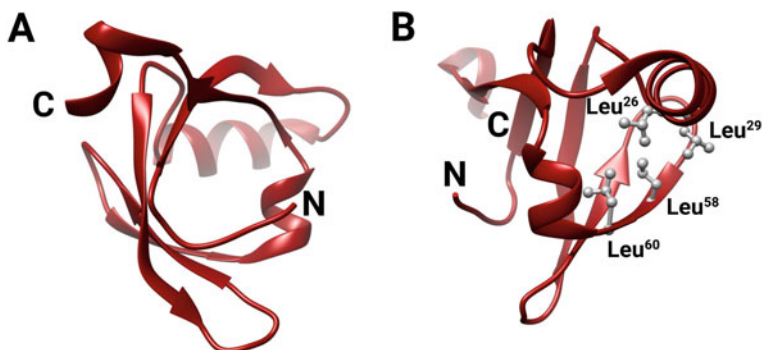


**Fig. 12.7** X-ray crystal structure of *KpFeoA* (PDB ID: 6E55). (a) FeoA is a  $\beta$ -barrel protein composed of an SH3-like domain. (b) FeoA contains a hydrophobic clamp with Leu residues (displayed in gray) postulated to be involved in protein-protein interactions with the N-terminal domain of FeoB. Panel b is displayed as a 90° vertical rotation relative to Panel a. ‘N’ and ‘C’ represent the N- and C-termini respectively. Figure created with BioRender

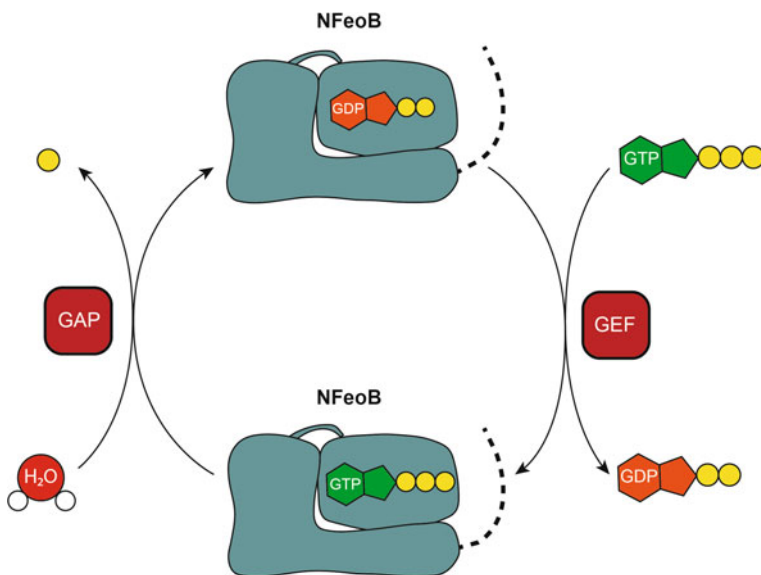


**Fig. 12.8** Cartoon representing two possible functions of FeoA (red polygon) with respect to NFeoB (teal polygon). FeoA has been speculated to act as either a GTPase activating protein (GAP), which facilitates GTP hydrolysis to GDP in order to turn “off” function, or as a guanine exchange factor (GEF), which facilitates exchange of bound GDP for GTP in order to turn “on” function

interactions by interacting with their binding partners through a Pro-rich region that typically folds into a left-handed helical conformation (D’Aquino and Ringe 2003; Li 2005). SH3 proteins were initially believed to be absent from prokaryotes, but

have since been discovered while remaining widely uncharacterized (D'Aquino and Ringe 2003). Structures of FeoA from different organisms have been determined, yet the function of FeoA still remains unknown. Two plausible roles for FeoA include functioning as either a GEF or as a GAP (Fig. 12.8). In eukaryotes, GEFs and GAPs are crucial regulatory proteins that participate in the nucleotide cycling of G-proteins and provide signaling specificity (Bos et al. 2007; Vetter and Wittinghofer 2001). GEFs function by physically removing GDP bound to G-proteins via protein-protein interactions, allowing for GTP subsequently to bind to the apo G-protein (turning the signal from “off” to “on”). Conversely, GAPs function by catalyzing the hydrolysis of GTP to GDP, most commonly by intercalating a positively-charged residue on the GAP (such as Arg and Lys) into the GTP-binding site on the G-protein, increasing the polarization rate of the GTP phosphoester bond (turning the signal from “on” to “off”) (Fig. 12.8) (Bos et al. 2007; Vetter and Wittinghofer 2001). Whether FeoA functions as a GEF or GAP remains to be seen, but the structure of FeoA strongly suggests its involvement in protein-protein interactions.

While several unpublished NMR structures of the FeoA SH3-like domain appeared in the PDB (*Protein Data Bank*) in the early 2000s (*P. aeruginosa* FeoA PDB ID: 2H3J; *K. pneumoniae* FeoA PDB ID: 2GCX; and *Clostridium thermocellum* FeoA PDB ID: 2K5L) the first published X-ray structure of FeoA appeared in 2010 from *Stenotrophomonas maltophilia* (PDB ID: 3MXH) (Su et al. 2010). The structure was determined to 1.7 Å resolution and contained two molecules in the asymmetric unit. Both molecules of FeoA adopted a SH3-like fold, as seen in the previous, unpublished NMR structures (Su et al. 2010). The SH3-like fold in FeoA is chiefly composed of 5 β-strands linked together through the RT-loop, the N-Src-loop, and α-helices (Fig. 12.7). One intriguing aspect of the *Sm*FeoA structure is the presence of two zinc ions and six chloride ions, which the authors attribute to the facilitation of *Sm*FeoA oligomerization (Su et al. 2010). The second published structure of FeoA was an NMR structure of *Ec*FeoA (Lau et al. 2013). Similar to *Sm*FeoA, *Ec*FeoA comprises two antiparallel β-sheets that form the β-barrel, and unstructured loop regions. However, *Sm*FeoA contains three α-helices whereas *Ec*FeoA only contains 2 α-helices (Lau et al. 2013; Su et al. 2010). These small, structural differences could be the result of low sequence conservation between *Sm*FeoA and *Ec*FeoA, while *Ec*FeoA and *Kp*FeoA have high sequence identity (90%) and are more structurally similar (Lau et al. 2013; Su et al. 2010). Finally, a recent X-ray crystal structure of *Kp*FeoA (PDB ID: 6E55) was determined to 1.5 Å resolution. Noteworthy was the observation of FeoA-FeoA interactions, which were speculated to be the location for FeoA-NFeoB interactions. Two sets of *Kp*FeoA dimers were present in the asymmetric unit and participate in unique FeoA-FeoA interactions at the dimer interface via intercalation of hydrophobic Leu residues (Fig. 12.7b) from one *Kp*FeoA molecule with Ala residues on the second *Kp*FeoA molecule (Linkous et al. 2019). When compared to an unpublished NMR structure of *Kp*FeoA (PDB ID: 2GCX), there is an ≈4 Å closure in the clamp. This crystallographic *Kp*FeoA is believed to represent the “closed” state while the FeoA present in the NMR structure is believed to represent the “open” state. In silico docking experiments using a 10 amino acid sequence from *Kp*FeoB containing the

PXXP motif revealed that the 10-mer could bind in the “open” *KpFeoA* model. Strikingly, the 10-mer was predicted to bind within the “C-shaped” clamp (Fig. 12.7b), similar to where the FeoA-FeoA interactions occur, but only in the “open” form of the model. It is thus possible that FeoA interacts with FeoB at the PXXP site via the hydrophobic residues in the clamp region and could alter the nucleotide status of the G-protein domain by increasing GTP hydrolysis or facilitating GDP release thus regulating Fe<sup>2+</sup> uptake via FeoB (Linkous et al. 2019). However, these structures alone are insufficient to determine the function of FeoA and more research will be necessary to determine the nature of the interaction between FeoA and FeoB and whether these hydrophobic residues are necessary to mediate the interaction.

Despite the availability of several FeoA structures revealing an SH3-like fold, the function of FeoA remains unknown and is of debate. Unlike eukaryotic SH3 domains, prokaryotic SH3 domains are not as well characterized. The presence of the SH3-like domain suggests that FeoA could be involved in protein-protein interactions, likely with FeoB as suggested by the *KpFeoA* structure. However, while some studies have tried to establish the function of FeoA little information exists about FeoA-FeoB interactions at the protein level. One study explored the effect of *EcFeoA* on the GTP hydrolysis activity of *EcNFeoB* by using NMR to monitor <sup>31</sup>P signals indicative of GTP hydrolysis (Lau et al. 2013). In the presence of equimolar amounts of *EcFeoA*, *EcNFeoB* did not exhibit any obvious changes in GTPase activity, leading to the conclusion that FeoA does not act as a GAP on NFeoB alone (Lau et al. 2013). However, the effect of FeoA on intact FeoB is still unknown and higher stoichiometric ratios of FeoA:FeoB may be necessary for activity. More studies will ultimately be necessary to determine if FeoA has any effect on GTP hydrolysis, GDP release, and/or Fe<sup>2+</sup> transport.

### 12.3.5.5 FeoAB Fusions

Some *feo* operons encode for a single polypeptide in which FeoA is naturally fused to the N-terminal soluble domain of FeoB. While these fusions are rare in genomic distribution, these observations further support the hypothesis that FeoA and FeoB are meant to interact physically to affect function. While these fusions are not well studied, they appear in the genomes of some very common human pathogens, such as *Porphyromonas gingivalis* and *Bacteroides fragilis*. Work on these fusions has chiefly been done at the cellular level (vide infra); unfortunately, no work at the protein level has examined these proteins.

### 12.3.5.6 FeoC

FeoC is a small protein of unknown function encoded along the *feoC* portion of the *feo* operon (Fig. 12.9). Unlike the strongly conserved *feoA* gene, *feoC* is thought to be present in only ≈13% of *feo* operons, predominantly in  $\gamma$ -proteobacteria (Lau



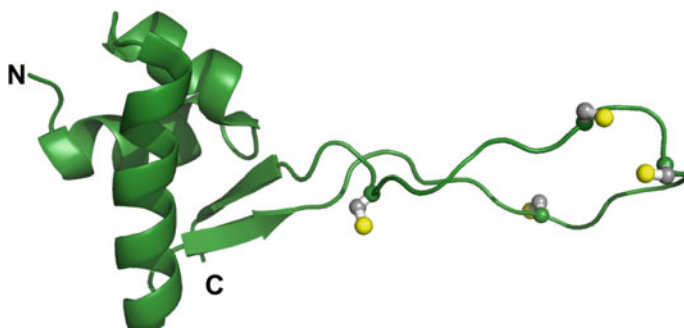


**Fig. 12.9** Lowest-energy NMR conformer of *E. coli* FeoC (PDB ID: 1XN7). Displayed in gray and yellow are the highly-conserved Cys residue sidechains that are involved in coordination of the [Fe-S] cluster. Labels ‘N’ and ‘C’ represent the N- and C-termini, respectively

et al. 2013). The solution NMR structure of monomeric *Kp*FeoC (PDB ID: 2K02) was the first to be described and demonstrated that FeoC contains an N-terminal helical domain and a C-terminal unstructured loop, which combined are reminiscent of a winged-helix domain (Fig. 12.9) (Hung et al. 2012a). It has therefore been suggested that FeoC could serve as a transcriptional regulator (Cartron et al. 2006). However, upon comparison of the protein electrostatics of *Kp*FeoC to that of other DNA binding proteins, such as DtxR and the DNA binding domain of BlaI, it has been noted that the corresponding helix in *Kp*FeoC is very negatively charged and therefore would not favor an interaction with DNA based on electrostatics. Supporting this statement, the authors failed to detect DNA binding to *Kp*FeoC (Hung et al. 2012a). Furthermore, the authors also observed  $Zn^{2+}$  binding (but surprisingly not  $Fe^{2+}$  binding) in the winged region of *Kp*FeoC, although this failed to promote DNA binding (Hung et al. 2012a). While *Kp*FeoC did not bind  $Fe^{2+}$ , the presence of four conserved Cys residues in the wing region (including a CXXC motif) suggested the possibility of iron-sulfur cluster binding (Fig. 12.9). As such, cellular and biochemical studies have sought to understand the identity and the role of iron-sulfur cluster binding to FeoC.

The determination of the exact nature of the FeoC [Fe-S] cluster was difficult due to its redox- and oxygen-sensitivity. The first biochemical study to investigate the ability of *Kp*FeoC to bind an [Fe-S] cluster was published in 2013. The presence of a paramagnetic center in *Kp*FeoC was first indicated by strong paramagnetic shifts in  $^1H$  NMR experiments. Further biophysical characterization of reconstituted *Kp*FeoC (exhibiting only 10% incorporation) under oxic conditions using electronic absorption spectroscopy suggested that the identity of the cluster was either that of a [2Fe-2S] cluster or a [4Fe-4S] cluster (Hsueh et al. 2013). When reconstituted *Kp*FeoC was analyzed by electron paramagnetic resonance (EPR) spectroscopy, experimental  $g$  values were attributed to the presence of an unusual *high-potential* iron sulfur protein (HiPIP) cluster (Hsueh et al. 2013). Lastly, X-ray absorption spectroscopy (XAS) confirmed the cluster in *Kp*FeoC to be ligated by four cysteine residues (Hsueh et al. 2013). The role of the cysteine residues in *Kp*FeoC were

evaluated by testing the ability of cysteine to serine variants to bind an iron-sulfur cluster. Three of four of the cysteine residues (Cys<sup>56</sup>, Cys<sup>64</sup>, and Cys<sup>71</sup>) were essential for cluster binding whereas Cys<sup>61</sup> was not essential (Hsueh et al. 2013). Very surprisingly, the [4Fe-4S] cluster present in *KpFeoC* had an unusually long average half-life of 17 h upon exposure to oxygen (Hsueh et al. 2013).

The most recent publication that characterized the iron-sulfur cluster in the FeoC protein was published in 2019. In this study, the cluster was reconstituted under strictly anoxic conditions and subsequently characterized by electronic absorption spectroscopy, EPR, XAS, and dynamic light scattering (DLS) (Smith et al. 2019). Reconstituted under anoxic conditions, the cluster of *EcFeoC* was assigned to the more common redox active [4Fe-4S]<sup>2+/+</sup> species (Smith et al. 2019). Electronic absorption spectra of the cluster-bound *EcFeoC* revealed that the [4Fe-4S]<sup>2+</sup> cluster is O<sub>2</sub>-sensitive and rapidly degrades to a [2Fe-2S]<sup>2+</sup> cluster in ≈5 min ( $k_{obs} \approx 0.04 \text{ s}^{-1}$ ) in O<sub>2</sub>-replete conditions (Smith et al. 2019). When these experiments were repeated for *KpFeoC*, nearly identical electronic absorption features, XAS spectra, and EPR signals were observed confirming that *KpFeoC* also binds a redox active, O<sub>2</sub>-sensitive [4Fe-4S]<sup>2+/+</sup> cluster (Smith et al. 2019). Lastly, anoxic DLS measurements demonstrated that cluster binding to both *EcFeoC* and *KpFeoC* resulted in a compaction of the protein conformation, but cluster binding did not promote oligomerization. Though the exact role of FeoC remains unknown, these data support that FeoC may function as a redox-active iron sensor, similar to that of FNR (Smith et al. 2019). However, some bacteria, such as *V. cholerae* lack the necessary Cys residues that are required to bind an [Fe-S] cluster. Whether these proteins function similarly to cluster-binding FeoCs has yet to be determined.

### 12.3.5.7 FeoA/B/C Interaction Studies

Despite in vitro studies of small soluble proteins of the Feo system (FeoA and FeoC) and single isolated domains (NFeoB), few studies have investigated how FeoA, FeoB, and/or FeoC may function in concert to transport Fe<sup>2+</sup> iron across a bacterial membrane. In 2012, the ability of FeoA and FeoB to interact was explored in *Salmonella enterica* using a bacterial two hybrid (BACTH) assay. When *feoB* was deleted from strain JH380 ( $\Delta mntH$ ,  $\Delta sitABCD$  background), Fe<sup>2+</sup> uptake was threefold lower than in the WT, and these results were recapitulated with an *feoA* deletion. Reintroduction of *feoA* was able to rescue the phenotype. In other words, the loss of *feoA* was as detrimental to ferrous iron uptake in *S. enterica* as the loss of *feoB* (Kim et al. 2012). An *feoAB* deletion strain was then created to test whether FeoA function would be dependent on FeoB. Complementation with only *feoB* resulted in Fe<sup>2+</sup> uptake approximately three-fold lower than JH380, whereas complementation with only *feoA* resulted in no rescue of Fe<sup>2+</sup> uptake; complementation of both *feoA* and *feoB* restored Fe<sup>2+</sup> uptake. These results suggest that FeoA is necessary for FeoB to transport ferrous iron in vivo (Kim et al. 2012).

As FeoA-based dependence might be the result of protein-protein interactions between FeoA and FeoB, this hypothesis was further probed in vivo. A BACTH

assay in *S. enterica* where FeoA was fused to T18 and FeoB was fused to T25 was initially constructed, and  $\beta$ -galactosidase activity indicated an interaction between FeoA and FeoB in vivo (Kim et al. 2012). FeoA variants (P20A/L26Q and W9G/L26Q) demonstrated  $\approx 28$ -fold lower  $\beta$ -galactosidase activity compared to the WT. Single variant studies suggested that L26 may be an essential residue for FeoA-FeoB interactions (Kim et al. 2012). These cellular results support the hypothesis that FeoA is important for FeoB-mediated ferrous iron transport in *S. enterica* (Kim et al. 2012), but the exact mechanism is unknown.

The presence of the FeoC HTH motif suggests that the protein could serve as a transcriptional regulator of the Feo system, which could be linked to the protein's cluster composition. As such, studies have examined how FeoC affects the expression levels of the *feoB* gene in *S. enterica* (Kim et al. 2013). Maximal expression of *feoB* occurs under both low iron and low O<sub>2</sub> conditions, which could be further enhanced in the absence of a functional *fur* gene or impaired in the absence of a functional *ftr* gene (Kim et al. 2013). A *feoC* deletion strain exhibited low levels of *feoB* expression, which could be restored by complementation with an *feoC*-containing plasmid. Interestingly, levels of *feoB* mRNA were higher in this strain than in the WT suggesting that *feoC* does not act at the point of transcription, but rather post-transcriptionally (Kim et al. 2013). BACTH experiments demonstrated that FeoB and FeoC interact, and these results were confirmed using pulldown experiments with NFeoB and His<sub>6</sub>-FeoC, although the oxidation state and metal-bound form of FeoC was not controlled. *S. enterica* harboring both a *feoC* and a *ftsH* deletion resulted in lower levels of FeoB suggesting that FeoC may protect FeoB from proteolysis by FtsH. Additionally, a  $\Delta$ *feoC* strain of *S. enterica* accumulated 4.5-fold less Fe<sup>2+</sup> than the WT strain indicating that the FeoC protein is important for Fe<sup>2+</sup> uptake in vivo (Kim et al. 2013). A follow-up study investigated Lon-mediated proteolysis of FeoC in *S. enterica* (Kim et al. 2015). FeoC expression from an IPTG-inducible plasmid in *S. enterica* was only detectable under low-oxygen conditions and did not appear to be affected by low- or high-iron concentrations. Interestingly, the FeoC protein was rapidly degraded when expressed in cells growing in a high-oxygen and high-iron environment ( $t_{1/2}$  ca. 5 min), similar to the rate of the O<sub>2</sub>-mediated cluster decomposition. A switch to anoxic conditions increased FeoC stability ( $t_{1/2}$  ca. 50 min) and was unaffected by the presence or absence of iron (Kim et al. 2015). Mutation of all four Cys residues in the wing of FeoC, the likely sites for binding of an iron-sulfur cluster as shown in *K. pneumoniae* and *E. coli*, further increased FeoC stability. Additionally, FeoC stability appears to affect the accumulation of FeoB. In the absence of the Lon-protease, FeoC can accumulate under both high- and low-oxygen conditions which promotes the accumulation of FeoB (Kim et al. 2015). The authors suggest that this could be a method by which *S. enterica* regulates Feo-mediated Fe<sup>2+</sup> uptake under anoxic and iron-limiting conditions, when regulation by FUR and FNR would be negligible (Kim et al. 2015). Binding of an iron-sulfur cluster to FeoC could serve to control the oxygen-sensitivity of FeoC; however, no studies have examined how cluster binding affects FeoC stability and degradation.

In *Vibrio cholerae*, the causative agent of the disease cholera, the Feo system is composed of FeoA, FeoB, and FeoC, which may interact to regulate Feo-mediated  $\text{Fe}^{2+}$  transport (Weaver et al. 2013). A BACTH assay was performed to assess interactions between and among the Feo proteins. No interactions were detected between FeoA-FeoB or FeoA-FeoC. In contrast, this method did reveal an interaction between FeoB and FeoC, which was mapped to the N-terminal domain of FeoB. E29G and M35A variants of FeoC abolished the FeoB-FeoC interaction, but conservation of these residues is poor among  $\gamma$ -proteobacteria (Weaver et al. 2013). In contrast to these first studies, later work on the *V. cholerae* Feo system suggested that FeoA, FeoB, and FeoC all interact to form a large complex. In 2016, in vivo formaldehyde cross-linking was used to probe which Feo complexes might be present or active in vivo. Several higher-order complexes of FeoA, FeoB, and FeoC were observed localized to the inner membrane based on SDS- and blue native-PAGE. The complexes were estimated to be  $\approx 250$  kDa,  $\approx 500$  kDa, and  $\approx 720$  kDa. Immunoprecipitation and LC-MS/MS demonstrated that FeoA and FeoB could be detected in the complex at  $\approx 720$  kDa, but not FeoC. However, when the V5 tag for immunoprecipitation was placed on FeoC instead of FeoB, then FeoC could be detected in the largest complex suggesting that the tag may hinder FeoB-FeoC interaction (Stevenson et al. 2016). The exact stoichiometry of the large complex ( $\approx 720$  kDa) could not be determined, but it was suggested that a trimer of FeoB trimers may interact with one or more FeoA or FeoC proteins to transport ferrous iron (Stevenson et al. 2016). Some additional complexes were found to contain only FeoB, while a complex at  $\approx 100$  kDa was found to contain FeoA, FeoB, and FeoC. Smaller complexes were proposed to be intermediates or possibly products from the disassembly and the breakdown of a larger Feo complex. Additionally, when FeoA was tagged with the V5 epitope for immunoprecipitation, the protein could not be detected in any complexes (Stevenson et al. 2016). It could not be determined which, if any, of these complexes are dominant within the cell, but these results do suggest that all three of the Feo proteins may interact at some point within the cellular context.

Mutational analyses have given some insight into how a larger Feo complex may form in *V. cholerae*. For example, an FeoB K15D variant in the G1 motif abolished Feo function and resulted in no detectable complex formation, indicating that nucleotide binding may be important for protein-protein interactions. An FeoB variant of the switch II region, D72A, resulted in the loss of function and the inability to form a larger complex (Stevenson et al. 2016). In an FeoC deletion strain, FeoB was found expressed at lower levels in the inner membrane, yet an FeoA-FeoB complex was still observed, suggesting that FeoC plays a role in FeoB expression but is not required for complex formation. In contrast, plasmid-driven expression of FeoB in tandem with any of four FeoA variants (G32K, A45D, P50R, and V72K) failed to display complex formation, suggesting that intact FeoA is a pre-requisite for Feo interactions (Stevenson et al. 2016). Further structural studies on Feo protein complexes would be useful in clarifying why and how these variants lead to disruption in complex formation.

Finally, structural and biophysical measurements have shown an interaction between *Klebsiella pneumoniae* NFeoB and its cognate FeoC. ITC experiments of nucleotide-free *Kp*NFeoB and apo *Kp*FeoC titrations demonstrated a 1:1 molar interaction with a  $K_d$  of  $\approx 0.5$   $\mu\text{M}$ , and SEC experiments revealed co-migration of monomeric, nucleotide-free *Kp*NFeoB with apo, monomeric *Kp*FeoC (Hung et al. 2012b). These observations were supported by an X-ray crystal structure of nucleotide-free *Kp*NFeoB co-crystallized with apo *Kp*FeoC. Each asymmetric unit contained one nucleotide-free *Kp*NFeoB and one apo *Kp*FeoC in which the N-terminus of FeoC interacted with the GDI domain of NFeoB (Hung et al. 2012b). Unfortunately, the wing region of FeoC was not present in electron density, likely a result of the flexibility of the wing region (Hung et al. 2012b). Additionally, this dynamic region of *Kp*FeoC is known to interact with an [Fe-S] cluster, which was not probed. Thus, it is unclear whether either [Fe-S] cluster binding or possibly nucleotide binding would affect this NFeoB-FeoC interaction and how.

## 12.4 Metal-Rich, Anoxic, and Acidic Environments

Iron-oxidizing bacteria (FeOB) utilize the oxidation of  $\text{Fe}^{2+}$  to  $\text{Fe}^{3+}$  as a means to generate energy for growth. These organisms obtain the iron necessary for essential metabolic processes from their native environment and play an important role in the iron biogeochemical cycle (Emerson et al. 2010). Given the insolubility of  $\text{Fe}^{3+}$ , and the production of ROS upon spurious  $\text{Fe}^{2+}$  oxidation, iron-dependent survival presents a unique challenge to FeOB. Furthermore, the energy derived from abiotic  $\text{Fe}^{2+}$  oxidation is low ( $\approx 29$   $\text{kJ mol}^{-1}$ ) near neutral pH, and the half-life of  $\text{Fe}^{2+}$  under oxic conditions is  $< 1$  min (Emerson et al. 2010; Roden et al. 2004). FeOB living under these conditions would therefore produce iron oxyhydroxides, which would be detrimental to the organism. As a result, FeOB must grow under microaerophilic conditions that stabilize  $\text{Fe}^{2+}$  over  $\text{Fe}^{3+}$  (Emerson et al. 2010; Roden et al. 2004). FeOB inhabit a variety of ecological niches including the soil, freshwater and marine environments, waste and bioreactor sites, and hydrothermal vents (Emerson et al. 2010). A greater understanding how FeOB transport  $\text{Fe}^{2+}$  would thus improve our understanding of their contribution to the iron biogeochemical cycle and would shed light on this ancient form of metabolism.

In contrast to FeOB, iron-reducing bacteria (FeRB or IRB) generate energy by reducing  $\text{Fe}^{3+}$ , typically from insoluble iron oxides, to  $\text{Fe}^{2+}$ . Bacteria that couple this process to the oxidation of organic molecules, such as sugars and amino acids, aromatic compounds, long chain fatty acids, and butyrate, propionate, and acetate or  $\text{H}_2$  are termed dissimilatory iron reducing bacteria (Esther et al. 2015; Lovley 1997; Richter et al. 2012; Weber et al. 2006). These organisms can often be found cohabitating with FeOB because the  $\text{Fe}^{3+}$  produced may function as an FeRB feedstock. FeRB play a role in mineral formation, such as when reduced iron is exposed to oxygen, and iron cycling (Lovley 1997; Esther et al. 2015; Richter et al. 2012; Weber et al. 2006). Reduction of  $\text{Fe}^{3+}$ -rich surfaces can be accomplished via

several routes. One of these routes is by direct contact of a bacterial biofilm with an  $\text{Fe}^{3+}$ -rich surface, as the biofilm may help mediate electron transfer.  $\text{Fe}^{3+}$  reduction can also be facilitated by chelators or siderophores that solubilize  $\text{Fe}^{3+}$  and increase its bioavailability (Esther et al. 2015; Lovley 1997; Thormann et al. 2004; Richter et al. 2012; Weber et al. 2006). Additionally, FeRB can cycle electron shuttles to reduce  $\text{Fe}^{3+}$ -rich surfaces. Somewhat similar to biofilm contact, pili, or protein nanowires, can also mediate contact with  $\text{Fe}^{3+}$ -rich surfaces for reduction (Esther et al. 2015; Richter et al. 2012; Brutinel and Gralnick 2012; Weber et al. 2006). Unfortunately, the iron transport mechanisms in these bacteria remain largely uncharacterized, but a synopsis of what is currently known in the literature is presented below.

### 12.4.1 Magnetotactic Bacteria

Magnetotactic bacteria (MB), microorganisms that orient themselves and move along Earth's magnetic field through a process known as magnetotaxis, were first discovered in 1975 (Blakemore 1975). MB were isolated from samples taken from surface sediments of salt marshes and surface layers of sedimentary cores in Massachusetts (Blakemore 1975). Using transmission electron microscopy (TEM), crystal-like particles that are now termed magnetosomes were initially discovered. At that time, it was posited that these intracellular compartments might be magnetic, formed from a mineral such as magnetite. Supporting this presumption, energy dispersive X-ray microanalysis subsequently revealed these particles to be composed predominantly of iron. Concurrently, different species of morphologically distinct MB were also identified in several other marsh muds (Blakemore 1975). In 1988, MB isolated from an estuarine salt marsh were analyzed for elemental content of the magnetic particles, which were determined to be composed of iron and oxygen in the form of magnetite ( $\text{Fe}_3\text{O}_4$ ) constituting ca. 1.6% of the dry weight of the organism (Bazylinski et al. 1988). Variations in particle composition, comprising iron and sulfur in the form of greigite ( $\text{Fe}_3\text{S}_4$ ) and pyrite ( $\text{FeS}_2$ ), were then found (Mann et al. 1990) and can be correlated to distinct growth environments.

MB are diverse microorganisms that grow optimally within anoxic and microaerophilic environments, but they can also be isolated from deep sea sediments. In the deep oceans, MB are proposed to play an important role in marine iron and sulfur cycling as accumulated, intracellular iron and sulfur can be released into the environment upon cell death and lysis thus promoting additional microbial activity (Simmons et al. 2004). High concentrations of particulate iron support a high abundance of MB, and this environment occurs at the oxycline, the point in the aquatic environment where the concentration of oxygen changes steeply and beyond which sulfur concentrations begin to peak (Simmons et al. 2004). MB appear to be widely distributed among the bacterial kingdom, including the classes  $\alpha$ - through  $\epsilon$ -proteobacteria, *Chlorobiales*, and Cyanobacteria, among others (Simmons et al. 2004). Due to their high iron requirements and their anoxic and microaerophilic

growth environments, it is likely that the iron acquisition systems present in MB mimic those present on early Earth, providing a glimpse of life prior to the GOE.

Consistent with their high demand for iron, MB must utilize a combination of tactics to accumulate this essential element. One major strategy is the use of siderophores. Like MB, many (but not all) prokaryotes engage in the metabolically-demanding biosynthesis and secretion of siderophores to scavenge for ferric iron. Retrieved ferric iron trapped in these siderophores can be released by either destruction of the siderophore itself via bond cleavage, or through a ferric reductase-mediated iron reduction and release mechanism (Cain and Smith 2021). Importantly, as MB are found in a number of anoxic niches, ferrous iron acquisition also represents a major acquisition route of reduced environmental iron.

*Magnetospirillum magneticum* strain AMB-1 relies on catechol and hydroxamate siderophores as well as ferrous iron transport as its primary means of iron uptake (Calugay et al. 2003). A global expression analysis of the *M. magneticum* strain AMB-1 genome has revealed multiple iron-regulated genes in this organism. In magnetosome-forming cultures, approximately 70% of extracellular iron was rapidly assimilated within 1 h (Suzuki et al. 2006). Under these conditions  $\text{Fe}^{2+}$  transport genes (*ftr1*, *tpd*, *feoA*, and *feoB*) were upregulated whereas in non-magnetosome-forming conditions ferric iron uptake genes (such as *tonB*, *fepA*, and *napABC*) were down-regulated (Suzuki et al. 2006). In contrast to the down-regulated ferric iron uptake genes, *cirA* and *fepC* were upregulated in iron-replete conditions and encode a ferric-siderophore outer membrane receptor and an inner membrane ferric-siderophore transporter, respectively (Suzuki et al. 2006). *M. magneticum* strain AMB-1 is capable of growing under oxic conditions (Matsunaga et al. 1991), and at least one catechol siderophore has been identified to be 3,4-dihydroxybenzoic acid (Calugay et al. 2006). Siderophore-mediated ferric iron uptake was significant when concentrations of ferric iron in the medium were 40–80  $\mu\text{M}$  (Calugay et al. 2003), but this condition is not conducive to magnetosome formation.

When taken together, these results indicate that  $\text{Fe}^{2+}$  uptake is likely the predominant source of iron under magnetosome-forming conditions (Suzuki et al. 2006), and there seems to be more than one route for ferrous iron assimilation. *Ftr1* is uncharacterized but annotated as a  $\text{Fe}^{2+}/\text{Pb}^{2+}$  permease, *Tpd* is uncharacterized but annotated to be involved in high-affinity  $\text{Fe}^{2+}$  uptake, and *Amb3335* is predicted to be a ferric iron reductase, which is also upregulated in iron-replete conditions (Suzuki et al. 2006). In a nonmagnetic mutant of *M. magneticum* strain AMB-1 deficient for siderophore uptake (denoted strain NMA61), a cytoplasmic ATPase that contributes to  $\text{Fe}^{2+}$  uptake was also identified (Suzuki et al. 2007). This ATPase bears homology to *ArgK*, a protein kinase (Suzuki et al. 2007). Previous reports speculate that the ATPase may provide energy for a  $\text{Fe}^{2+}$  transporter such as *Feo*, *Tpd*, and *Frt1*, thus supplying ferrous iron to magnetosome formation (Suzuki et al. 2007). In 2008, iron transporters expressed in *M. magneticum* strain MS-1 were identified using 2-D electrophoresis by comparing proteins expressed during growth in  $\text{Fe}^{2+}$ - and  $\text{Fe}^{3+}$ -rich media (Taoka et al. 2009). Two of the proteins expressed under  $\text{Fe}^{2+}$ -rich conditions were 76 kDa and 70 kDa in size and with homology to TonB-dependent outer membrane ferric-siderophore receptors in *Beijerinckia indica*

and *Rhodospseudomonas palustris*, respectively (Taoka et al. 2009). Two sets of the *feoA* and *feoB* genes were also identified in this study. Expression of FeoB was confirmed by utilizing polyclonal antibodies generated from recombinant NFeoB1. In these studies, FeoB appears as a band at  $\approx 75$  kDa localized to the cytoplasmic membrane, consistent with predictions of FeoB's location (Taoka et al. 2009). Further functional studies have yet to be reported.

*M. gryphiswaldense* MSR-1 does not secrete siderophores but does utilize  $\text{Fe}^{3+}$  through extensive ferric reductase activity and subsequent  $\text{Fe}^{2+}$  uptake. Ferric reductase activity in whole cells, the cytoplasm, and membrane fractions (but not the periplasm) of *M. gryphiswaldense* was first demonstrated in 2007 (Xia et al. 2007). Native PAGE coupled with ferric reductase active staining afforded the identification of six bands in the cytoplasmic fraction and three bands in the membrane fraction of cells corresponding to ferric reductase isozymes. These ferric reductases were named FeR-1 to FeR-6. FeR-6 was subsequently purified as it had the greatest activity among all of the reductases. FeR-6 is  $\approx 16$  kDa and does not appear to have sequence homology to other proteins (Xia et al. 2007). Ferric citrate, reduced nicotinamide adenine dinucleotide (NADH), and oxidized flavin mononucleotide (FMN) were used in ferric reductase assays to determine the reductase activity of FeR-6. The protein had a modest  $K_M$  for ferric citrate of  $\approx 45$   $\mu\text{M}$  and a  $V_{\text{max}}$  of  $\approx 1.2$   $\mu\text{M}/\text{min}$ . Interestingly, ferric reductase activity was strongly inhibited by  $\text{Ag}^+$  and divalent metal ions such as  $\text{Zn}^{2+}$ ,  $\text{Mn}^{2+}$ ,  $\text{Cu}^{2+}$ , and  $\text{Co}^{2+}$  (Xia et al. 2007). In a follow-up study, FeR-5 and FeR-6 were identified as bifunctional enzymes with thioredoxin reductase activity and flavin reductase activity, respectively, and deletion of both genes inhibited magnetosome formation (Zhang et al. 2013). Although FeR-6 could reduce  $\text{Fe}^{3+}$  without the FMN cofactor,  $\text{Fe}^{3+}$  reductase activity was 20-fold higher with FMN (Zhang et al. 2013), emphasizing the importance of the flavin cofactor. The remaining four isozymes have not yet been characterized.

As the ferric reductases are located in the cell membrane, they are speculated to provide reduced iron for transport via a membrane  $\text{Fe}^{2+}$  transporter (Zhang et al. 2013). Early studies examining the growth and magnetosome formation of *M. gryphiswaldense* MSR-1 indicate that magnetite formation can only occur under microaerophilic conditions and is tightly coupled to iron uptake (Schüler and Baeuerlein 1998). Under these conditions, recent experiments suggest that ferric reductase activity could supply the inner membrane transporter FeoB with  $\text{Fe}^{2+}$ , which is then transported into the cell for magnetosome incorporation. In 2008, two *feoB* genes in *M. gryphiswaldense* strain MSR-1 were identified and characterized (Rong et al. 2008). The predicted FeoB1 protein encoded by the *feoB1* gene (704 amino acids) has high sequence identity to FeoBs from other magnetotactic bacteria but only 35% identity (53% similarity) to FeoB2, encoded by *feoB2*. A putative *feoA* gene was found within the region of *feoB1* and named *feoA1*. FeoB1 contains conserved G-protein motifs in the N-terminal region, and the C-terminal domain was predicted to be imbedded in the cytoplasmic membrane by 9 TM helices (Rong et al. 2008). TEM was used to monitor magnetosome formation of a  $\Delta\text{feoB1}$  strain, which produced lower amounts of magnetosomes, smaller magnetosomes, and lower iron content compared to the WT strain. These defects could be rescued by



complementation with *feoB1*. Similar results were observed for cells grown in the presence of either  $\text{Fe}^{2+}$ - or  $\text{Fe}^{3+}$ -citrate (Rong et al. 2008). The *feoA1* and *feoB1* genes were also found to be downregulated under iron-rich conditions. A later study investigated the role of *feoB2* in *M. gryphiswaldense* MSR-1 (Rong et al. 2012). Interestingly, when a  $\Delta\text{feoB2}$  strain was analyzed for magnetosome formation, the size and number of the magnetosomes were similar to the WT strain suggesting that FeoB2 does not contribute to magnetosome formation when FeoB1 is present. Surprisingly, in cells lacking both a functional FeoB1 and FeoB2, magnetosome formation and size was similar to that of WT; however, the number of magnetosomes per cell were lower in the double mutant than in the *feoB1* deletion strain. Additionally, when cells were grown in the presence of ferric citrate, the  $\Delta\text{feoB2}$  strain had significantly lower levels of cellular iron content than that of the  $\Delta\text{feoB1}$  strain (Rong et al. 2012). For all deletion strains, the cellular metal content of Mn, Zn, Cu, and Mg was similar to WT confirming that both FeoBs are dedicated to iron uptake (Rong et al. 2012). The deletion strains were also tested for their ability to respond to oxidative stress. Deletion strains demonstrated sensitivity when grown in 500  $\mu\text{M}$   $\text{H}_2\text{O}_2$ , and all had significantly lower superoxide dismutase and catalase activities when compared to the WT strain (Rong et al. 2012), suggesting that some of the acquired ferrous iron is necessary for assimilation into these two essential enzymes that combat oxidative stress.

### 12.4.2 *Gallionella and Geobacter*

*Gallionella ferruginea*, a microaerophilic bacterium with a growth requirement for  $\text{Fe}^{2+}$ , was first described in 1837 and is the first known FeOB to be identified. *G. ferruginea* has an intriguing ability to form an Fe-oxyhydroxide-encrusted stalk during growth (Emerson et al. 2010). *G. ferruginea* is able to grow at the end of the stalk, which can form at a rate of 80–90  $\mu\text{m}/\text{h}$  in microcultures. These stalks are likely used as a positioning mechanism to find the appropriate iron/oxygen gradients needed for *G. ferruginea* growth, but they may also function as a sink to deposit precipitated iron oxyhydroxides that would otherwise result in the death of the organism (Hanert 1974; Emerson et al. 2010). Questions remain regarding the composition of the stalks and the mechanism by which the precipitated iron is excreted.

While  $\text{Fe}^{2+}$  transport mechanisms have not been well-characterized in *Gallionella*, this transport process undoubtedly contributes to the ability of this organism to cycle iron in different and often harsh iron-rich environments. Acid mine drainage (AMD) sites are low-pH, anoxic springs containing high levels of iron as a result of mining (Jones et al. 2015). The Upper and Lower Red Eyes in Pennsylvania constitute an AMD with pH ranging from 4.0–4.5 and  $\text{Fe}^{2+}$  concentrations  $>6.5$  mM. FeOB, such as *Gallionella*, offer the possibility to bioremediate such sites using biological iron oxidation (Jones et al. 2015). An analysis of free-living bacteria at this site showed that the *Gallionellaceae* family composed 42% of

all bacterial species identified. Bacteria from the orders of *Rhodospirillales*, *Acidimicrobiales*, *Xanthomonadales*, *Acidobacteriales*, and *Nitrospira* were also present, but their distribution was dependent on both pH and  $[\text{Fe}^{2+}]$ . For instance, *Gallionellaceae* were more abundant at high  $\text{Fe}^{2+}$  concentrations while *Acidithiobacillus* spp. were more abundant at lower  $\text{Fe}^{2+}$  concentrations (Jones et al. 2015). Though not as well characterized, the Arctic tundra also contains regions where FeOB inhabit acidic soils, sediment surfaces, and water sources. *Gallionella* spp. have been identified in all of these environments (Emerson et al. 2015). Thus, it is clear that adaptation to high acidic environments that may be rich in  $\text{Fe}^{2+}$  is necessary to support the survival of *Gallionella* and related species.

Similarly adapted is *Geobacter sulfurreducens*, a hydrogen- and acetate-oxidizing, dissimilatory metal- and sulfur-reducing bacterium that can be found in soils, aquatic sediments, and subsurface environments. Reduction of insoluble minerals such as  $\text{Fe}^{3+}$  oxides is facilitated by electron transport through pili rich in *c*-type cytochromes, which are localized to the periplasm and often excreted into the extracellular space (Caccavo et al. 1994; Lovley and Walker 2019; Weber et al. 2006; Smith et al. 2013; Seeliger et al. 1998). Though iron transport has not been extensively studied in *Geobacter*, one study analyzed the *Geobacter* iron stimulon by determining differences in gene expression for cells growing in iron-replete, iron-sufficient, and iron-deficient conditions. Genes differentially expressed in *Geobacter* encoded for *c*-type cytochromes and other proteins containing heme or iron-sulfur clusters, and  $\text{Fe}^{3+}$  reductases such as the OmcZ cytochrome (Embree et al. 2014). Both FeoA and FeoB were the most downregulated during  $\text{Fe}^{3+}$  reduction, suggesting that  $\text{Fe}^{2+}$  generated from reduction is not used as a substrate for the Feo system. Eleven efflux pumps/subunits and one ferritin-like protein domain were also downregulated, while another ferritin-like protein domain was upregulated (Embree et al. 2014). The Fur and IdeR proteins were more highly expressed under iron-sufficient conditions and exhibited repression as extracellular  $\text{Fe}^{2+}$  concentrations increased. These results suggest that iron homeostasis is tightly regulated in *Geobacter* in response to the large amounts of  $\text{Fe}^{2+}$  produced from metabolic processes and to maintain intracellular iron stores (Embree et al. 2014). Future characterization of *Gallionella* and *Geobacter* could lead to the ability to tailor these metal-tolerant bacteria for bioremediation purposes.

### 12.4.3 *Shewanella*

*Shewanella oneidensis* MSR-1 is both a facultative anaerobe and a dissimilatory metal-reducing bacterium that inhabits aquatic environments and iron rich-sediments, and can use oxidized iron as a terminal electron acceptor (Bennett et al. 2015). As respiration occurs, Feo-transported  $\text{Fe}^{2+}$  accumulates inside of the bacterium and becomes incorporated into iron-utilizing proteins and solid-phase minerals (Bennett et al. 2015). In addition to Feo, *Shewanella* may possess another uncommon  $\text{Fe}^{2+}$  import system. The MgtE protein is a  $\text{Mg}^{2+}/\text{Co}^{2+}$  transporter first

identified in *Bacillus firmus* (Smith et al. 1995) but present in *S. oneidensis* MR-1, which contains three *mgtE* homologs. One of these homologs (*SO\_3966*) is found in 26 of 36 *Shewanella* genomes and has been named the ferrous iron and cobalt importer (FicI) (Bennett et al. 2018). A role in  $\text{Fe}^{2+}$  uptake was proposed upon observations that a  $\Delta\text{ficI}$  strain of *Shewanella* conferred resistance to  $\text{Fe}^{2+}$ . This hypothesis was confirmed by measuring  $\text{Fe}^{2+}$  uptake in a  $\Delta\text{ficI}$  strain which was  $\approx 90\%$  lower than that of the WT strain and also displayed  $\text{Co}^{2+}$  and  $\text{Mg}^{2+}$  sensitivity (Bennett et al. 2018). However, it seems that the FicI system is less important than the Feo system when iron is scarce, as the  $\Delta\text{feoB}$  strain was unable to grow under iron-limiting conditions unlike the  $\Delta\text{ficI}$  strain. It is suggested that FeoB serves as the primary  $\text{Fe}^{2+}$  transporter for *Shewanella* while FicI serves as a secondary  $\text{Fe}^{2+}$  transporter.

Due to its high rate of  $\text{Fe}^{2+}$  acquisition, *Shewanella* has had to adapt mechanisms to prevent iron overload (Bennett et al. 2015; Carlson et al. 2012; Dunning et al. 1998). One such mechanism is through the use of a ferrous iron exporter encoded by the gene locus *SO\_4475* and named FeoE (herein referred to as *SoFeoE*), although it is not associated with the *feo* operon. FeoE is predicted to be a member of the cation diffusion facilitator (CDF) family, which is a family of inner membrane proteins that efflux divalent metal ions using the proton motive force (Bennett et al. 2015; Nies and Silver 1995; Paulsen and Saier 1997). *SoFeoE* shares sequence similarity and identity ( $\approx 60\%$  and  $\approx 48\%$ , respectively) with the YiiP (FieF) protein from *E. coli*, which has been shown to export  $\text{Zn}^{2+}$ ,  $\text{Cd}^{2+}$  and  $\text{Fe}^{2+}$  (Chao and Fu 2004; Wei and Fu 2005; Grass et al. 2005b). *SoFeoE* was also previously shown to export  $\text{Zn}^{2+}$  and  $\text{Cd}^{2+}$ , but had not been tested for its ability to export  $\text{Fe}^{2+}$ , either in vitro or in vivo (Coudray et al. 2013). One study examined the ability of *SoFeoE* to protect *S. oneidensis* MSR-1 against  $\text{Fe}^{2+}$  toxicity when utilizing ferric citrate for anaerobic respiration by examining the survivability of  $\Delta\text{feoE}$  strains. *S. oneidensis* deficient for *feoE* exhibited a growth defect compared to the WT strain but could be rescued with complementation by *feoE* (Bennett et al. 2015). Ferrozine assays measuring  $\text{Fe}^{2+}$  directly resulting from ferric citrate respiration were similar for both deletion and WT strains, supporting the hypothesis that respiration on ferric citrate is not impaired in the  $\Delta\text{feoE}$  strain, but functions to prevent  $\text{Fe}^{2+}$  toxicity (Bennett et al. 2015). This assertion was further supported by lower growth rates of the  $\Delta\text{feoE}$  strain when grown in the presence of 1 mM  $\text{FeCl}_2$ , and by iron retention assays demonstrating that *feoE* deficient *S. oneidensis* retain significantly more iron than the WT *S. oneidensis* (Bennett et al. 2015). Sensitivity of the  $\Delta\text{feoE}$  strain was tested against a range of divalent metal ions and *feoE* was found to be specific for  $\text{Fe}^{2+}$ , in contrast with the previous suggestion of metal promiscuity (Bennett et al. 2015). Furthermore, the FeoE protein is conserved amongst *Shewanella* spp. suggesting that it is a common mechanism to protect against  $\text{Fe}^{2+}$  toxicity. Homologs of FeoE may also be present in *Geobacter metallireducens* and *Geobacter sulfurreducens*, but share a much lower sequence similarity (Bennett et al. 2015).

Ferrous iron uptake likely accounts for one of the dominant iron sources in this bacterial family, as *Shewanella* encode for just one natural siderophore, putrebactin (Pub), synthesized by the *pubABC* operon using putrescine as a precursor. The

TonB-specific ferric siderophore receptor is encoded by *putA* and the Pub reductase is encoded by *putB* (Ledyard and Butler 1997; Kadi et al. 2008; Soe and Codd 2014; Liu et al. 2018). A spontaneous mutant of *S. oneidensis*, SO-X2, was identified and believed to be deficient for cytochrome *c* production as colonies of *S. oneidensis* appeared white instead of red (Dong et al. 2017). However, this was not the result of a mutation within the cytochrome *c* biosynthesis genes, but rather due to a mutation in the *putA* gene (Dong et al. 2017). The deletion of *putA* resulted in an  $\approx 50\%$  decrease in intracellular iron concentration when compared to the WT and also resulted in colorless colonies as the inability of the  $\Delta putA$  strain to deliver iron to the cytosol has downstream effects on *Shewanella*'s ability to produce both cytochrome *c* and heme (Dong et al. 2017; Liu et al. 2018). Correlating with these results was the observation that the  $\Delta putA$  strain also produced Pub at a significantly higher level under iron-limiting conditions compared to the WT (Dong et al. 2017). Knockouts of the *pub* operon and *putB* were also tested for their effects on iron uptake in *Shewanella*. Both  $\Delta pub$  and  $\Delta putB$  strains exhibited normal levels of intracellular iron, though the  $\Delta pub$  strain was incapable of producing Pub. This result indicates the presence of a primary functional iron uptake system, such as Feo, that is capable of circumventing this loss (Liu et al. 2018). In this study, a  $\Delta feo$  deletion strain had a lower total iron concentration than the WT, but also had significantly more total iron than the  $\Delta putA$  strain. However, loss of *feo* appeared to be more detrimental to *Shewanella* growth when compared to the growth of the  $\Delta putA$  strain. A double deletion strain grew poorly under iron depleted conditions, but could grow at  $Fe^{2+}$  concentrations of 0.5 mM and higher, likely using FicI as a secondary  $Fe^{2+}$  transporter (Liu et al. 2018). Thus, it is clear that ferrous iron uptake contributes strongly to iron homeostasis in *Shewanella*, and it is likely that similar mechanisms may be operative in other FeOB and FeRB, although more characterization is warranted.

## 12.5 The Host-Pathogen Interface

Among other functions, humans depend on mononuclear and dinuclear iron proteins for carnitine biosynthesis, hypoxic sensing, DNA biosynthesis, and functionalization of unsaturated lipids. Additionally, cellular iron is also incorporated into [Fe-S] clusters and utilized in heme biosynthesis, both of which serve as cofactors for enzymes involved in gene regulation, oxygen transport, and even drug metabolism (Hider and Kong 2013; Ganz 2008). The labile iron pool is composed mostly (>80%) of  $Fe^{2+}$ , with iron concentrations estimated to be between ca.  $10^{-7}$  M and ca.  $10^{-6}$  M in either erythroid cells or hepatocytes (Hider and Kong 2013). By way of comparison, one estimate places free iron concentrations in human serum at  $\approx 10^{-24}$  M (Fischbach et al. 2006). Because ferrous iron is significantly more soluble and more kinetically labile compared to ferric iron at physiological pH ( $\approx 7.4$ ), ferrous iron is typically the species that is transported into cells, translocated within cells, and even incorporated into iron-dependent enzymes and proteins (Hider and Kong 2013). Thus, the prevalence of  $Fe^{2+}$  in human enzymes

and within the labile iron pool suggests that invading microbes might encounter a significant amount of  $\text{Fe}^{2+}$  within their colonization niches.

The concentration of iron in the labile  $\text{Fe}^{2+}$  pool is governed by several factors. The amount of iron required for normal physiology may differ among both organisms and cells (e.g., mitochondria have a higher iron requirement since that is where heme and iron-sulfur cluster biosyntheses take place). One mechanism for regulating the intracellular labile iron pool is to control the rate of iron transport into cells by divalent metal ion transporters (Hider and Kong 2013). Iron within the labile iron pool can be temporarily depleted by oxidation of iron and storage within ferritins. Finally, iron efflux via ferroportin can also control the concentration of the labile iron pool, preventing iron overload and potential redox stress within the cell (Hider and Kong 2013). Together, these mechanisms maintain iron homeostasis in humans, and these systems are tightly regulated to control iron availability during times of infection.

Iron homeostasis in humans and animals is heavily altered during microbial infection. One of the host's first defense mechanisms against invading pathogens is to reduce the absorption of dietary iron. The host also sequesters iron already present in the extracellular space to further limit the availability of this essential nutrient to pathogens. These processes combined are often termed "iron withholding" and constitute a part of the host defense mechanism known as nutritional immunity (Ganz 2008; Abu Kwaik and Bumann 2013; Skaar 2010). Bacteria are estimated to require cytoplasmic iron pools at a concentration of  $\approx 10^{-6}$  M, and the host can significantly limit the amount of iron available to microbes depending on the niche in which they colonize. In response, bacteria must overcome these limiting conditions in order to survive (Fischbach et al. 2006). Some pathogens have adapted to live within the cytosol of eukaryotic cells where essential nutrients, including iron, are plentiful. Bacteria may also secrete proteases that degrade host proteins and enzymes, releasing essential nutrients that may be acquired by pathogens (Parrow et al. 2013). One important mechanism utilized by bacteria to establish infection is  $\text{Fe}^{2+}$  uptake driven predominantly by the Feo system. This section summarizes our knowledge of ferrous iron acquisition during infection of unicellular pathogens, which is strongly linked to the Feo system.

### ***12.5.1 Cellular Studies of Ferrous Iron Acquisition at the Host-Pathogen Interface***

*Helicobacter pylori* is the causative agent of chronic gastritis and though several virulence factors had been identified in *H. pylori*, its mechanisms of iron transport and homeostasis are not well understood. *H. pylori* does not appear to produce siderophores but relies on both  $\text{Fe}^{2+}$  and heme uptake as well as iron sequestered from human lactoferrin. *H. pylori* also possesses ferric reductase activity, which likely facilitates  $\text{Fe}^{2+}$  transport via the Feo system (Velayudhan et al. 2000).

Inactivation of *feoB* in *H. pylori* significantly reduced the rate of  $^{55}\text{Fe}$  uptake regardless of oxidation state, and this phenotype could be restored by complementation with *feoB*.  $\text{Fe}^{2+}$  uptake kinetics have revealed that FeoB constitutes a high affinity  $\text{Fe}^{2+}$  transporter (apparent Michaelis constant of ca. 0.5  $\mu\text{M}$ ), and the presence of a second, unidentified, low affinity  $\text{Fe}^{2+}$  transporter was also suggested. Though FeoB is considered to be specific for  $\text{Fe}^{2+}$  transport, the presence of  $\text{Cu}^{2+}$  in a 100-fold excess of  $\text{Fe}^{2+}$  inhibited  $\text{Fe}^{2+}$  uptake by 74%, while  $\text{Co}^{2+}$ ,  $\text{Mn}^{2+}$ ,  $\text{Ni}^{2+}$ , and  $\text{Zn}^{2+}$  had no inhibitory effect on  $\text{Fe}^{2+}$  transport (Velayudhan et al. 2000). Intriguingly, the ATP synthesis inhibitor, DCCD, strongly inhibited  $\text{Fe}^{2+}$  transport, perhaps due to NTP promiscuity of this organism's FeoB. Inhibition also occurred in the presence of orthovanadate, a molecule that inhibits ATP hydrolysis. These results suggested that FeoB-mediated  $\text{Fe}^{2+}$  transport could utilize active ATP hydrolysis as an energy source for the transport process (Velayudhan et al. 2000).

*Legionella pneumophila* colonizes human macrophages and freshwater amoebae within a parasitic vacuole, where  $\text{Fe}^{2+}$  likely dominates (Robey and Cianciotto 2002). An *feoB* mutant transported virtually no radiolabeled  $\text{Fe}^{2+}$  but did not exhibit complete attenuation for extracellular growth in iron-limited media. However, the *feoB* mutant also confers increased resistance to the antibiotic streptonigrin, a direct result of decreased iron pools in the mutant as streptonigrin toxicity is iron-dependent (Robey and Cianciotto 2002). Upon co-culturing the *feoB* mutant with the amoeba *Hartmannella vermiformis* under iron-limiting conditions, the mutant strain was detected at a significantly diminished concentration, indicating that FeoB is necessary for growth and survival in *L. pneumophila* (Robey and Cianciotto 2002). The role of FeoB for intracellular colonization and survival was confirmed in a human macrophage model where the mutant *L. pneumophila* was attenuated in its ability to kill macrophages. Furthermore, a mouse model of infection demonstrated that the lungs of the mice contained lower concentrations of the *feoB* mutant compared to the WT, confirming the importance of *feoB* to *L. pneumophila* virulence (Robey and Cianciotto 2002).

*Campylobacter jejuni* is a causative agent of foodborne gastroenteritis, and the connection between FeoB and *C. jejuni* pathogenesis was first investigated in 2003 (Raphael and Joens 2003). Iron uptake and growth of different *C. jejuni* strains were compared to that of *E. coli* W3110. The acquisition of  $^{55}\text{Fe}^{2+}$  in *C. jejuni* was generally lower than that of *E. coli* W3110 (Raphael and Joens 2003). An insertion mutation of *feoB* in *C. jejuni* was then analyzed for  $^{55}\text{Fe}^{2+}$  uptake and rates were similar to those observed in the WT strains. The experiments were repeated with a *feoB* mutation strain generated through allelic exchange, but no difference in  $^{55}\text{Fe}^{2+}$  uptake was observed, suggesting  $^{55}\text{Fe}^{2+}$  uptake was not mediated by FeoB and that FeoB was not be required for  $\text{Fe}^{2+}$  uptake in *C. jejuni* (Raphael and Joens 2003). However, a later study reinvestigated the role of FeoB in *C. jejuni* as the genomes for the strains previously investigated had not been sequenced, and the presence of an additional FeoB homolog could not be precluded (Naikare et al. 2006). In *C. jejuni* NCTC 11168, *feoA* and *feoB* were found to be cotranscribed and thus constituted an operon. Interestingly, *feoA* expression was elevated six to eight-fold over that of the WT strain in *feoB* mutants (Naikare et al. 2006). Furthermore, the *feoB* mutant

acquired  $\text{Fe}^{2+}$  at ten-fold less compared to the WT strain. Isolation of spheroplasts from the WT and  $\Delta feoB$  strain showed that 90% of the transported iron was contained within the cytosol, suggesting that *C. jejuni* can also transport  $\text{Fe}^{2+}$  via a different transporter (Naikare et al. 2006). FeoB also promoted the growth of *C. jejuni* in iron limited media compared to the  $\Delta feoB$  strain. Analysis of iron content during these experiments revealed that a majority of accumulated  $^{55}\text{Fe}^{2+}$  in the  $\Delta feoB$  strain was localized in the periplasm suggesting the lack of a functional inner membrane transporter (Naikare et al. 2006). *C. jejuni* 81-176 and a *feoB* mutant were then tested for their ability to invade human INT-407 embryonic intestinal cells and porcine IPEC-1 small intestinal epithelial cells. Both strains were equally able to invade both types of cells and survive for up to 48 h. However, after 48 h the *feoB* mutant exhibited a decreased ability to survive in the eukaryotic cells indicating that *feoB* contributes to intracellular survival in *C. jejuni* (Naikare et al. 2006). The *feoB* mutants examined in this study also exhibited a decreased ability to colonize in a chick cecum model and in a rabbit ileal loop model demonstrating that FeoB is important for colonization within the host (Naikare et al. 2006). Lastly, *C. jejuni* WT strains and *feoB* mutants were examined for their ability to colonize in a piglet intestine to simulate infection and colonization in a human host. Three days post-infection, different parts of the gastrointestinal tract of the piglets were harvested and through competition assays it was determined that *feoB* mutants were unable to colonize in the intestinal tract of the piglets (Naikare et al. 2006).

*Francisella tularensis* is responsible for zoonotic tularemia infections, is highly infectious, and has a high mortality rate, which can be linked in part to Feo utilization (Thomas-Charles et al. 2013). *F. tularensis*  $\Delta feoB$  strains exhibit reduced colony size as a result of inefficient  $\text{Fe}^{2+}$  uptake, and this strain exhibited significantly slower growth in iron-restricted medium compared to the WT strain. The loss of FeoB also results in increased secretion of the rhizoferrin-like siderophore encoded by the *fsl* operon suggesting that *F. tularensis* attempts to overcome the loss of FeoB through an alternative iron uptake system (Thomas-Charles et al. 2013). The  $\Delta feoB$  strain also contained significantly reduced cellular iron content, which could be restored with complementation. Unsurprisingly, the strain displayed significantly reduced replication in human lung epithelial cells and macrophages. However, despite the lack of a functional *feoB*, the deletion strain still caused 100% mortality rate in infected mice; however, at 3 days post-infection, the lungs, livers and spleens were collected to analyze the presence of each strain and it was determined that the  $\Delta feoB$  strain was present in reduced quantities (Thomas-Charles et al. 2013). Another study of *F. tularensis* Schu4 demonstrated that FeoB was similarly necessary for bacterial growth,  $\text{Fe}^{2+}$  uptake under both iron-replete and iron-deplete conditions, and that in a  $\Delta feoB'$  (encoding FeoB without the C-terminus) strain the *fsl* operon displayed increased expression (Pérez et al. 2016). The  $\Delta feoB'$  strain could replicate within murine macrophages but showed reduced replication in human liver carcinoma cells. A double deletion strain also lacking the *fslA* gene could not replicate within the murine macrophages or the human liver carcinoma cells. A murine model demonstrated that the  $\Delta feoB'$  strain could kill infected mice within 5–7 days, similar to the WT *F. tularensis* Schu4, while mice infected with the

double deletion strain lived for at least 21 days post-infection, demonstrating the importance of FeoB coupled to other iron acquisition systems for full bacterial virulence (Pérez et al. 2016).

In a similar manner, the Feo system of the avian pathogen *E. coli* O78 (APEC) is connected to other metal uptake routes for maximum virulence (Sabri et al. 2008). In APEC, SitABCD contributes to virulence in chickens, and strains lacking this system exhibited significantly reduced colonization. However, in the presence of a functional SitABCD system, strains carrying either a  $\Delta feoB$  or a  $\Delta mntH$  behaved similar to WT APEC and persisted in the chicken model, suggesting Feo and MntH are less important for APEC virulence compared to SitABCD (Sabri et al. 2008). Double deletion strains were tested for their effects on APEC virulence as well. Both a  $\Delta sitABCD\Delta mntH$  strain and a  $\Delta sitABCD\Delta feoB$  strain were just as attenuated for virulence as the  $\Delta sitABCD$  strain, confirming the previous result that *feoB* and *mntH* do not contribute to APEC virulence as much as *sitABCD* (Sabri et al. 2008). Interestingly, the  $\Delta sitABCD\Delta feoB$  strain was found at lower levels in the blood, lungs, and spleen of the chicken model but was present in higher levels in the liver. These results suggest that each metal transport system may be important for colonization in certain niches within the host (Sabri et al. 2008).

*Shigella flexneri* infections cause dysentery in humans, and this pathogen also utilizes multiple divalent metal ion uptake systems including Feo to maintain proper metal homeostasis. Akin to APEC, a *feoB* mutant strain was modestly attenuated for growth, similar to an *iucD* mutant, which is a component of the aerobactin siderophore synthesis system. Interestingly, a double mutant of *feoB* and *iucD* grew poorly, though it is not understood why (Runyen-Janecky et al. 2003). Henle cells were utilized to determine whether the mutant *S. flexneri* could form plaques. Single mutants of *sitA*, *feoB*, and *iucD* all formed plaques comparable to WT *S. flexneri*. However, the loss of any two of the three genes resulted in reduced plaque formation and size, suggesting a link between  $Fe^{2+}$  uptake and plaque formation. Lastly, a triple mutant deficient for all three genes was fully attenuated for plaque formation (Runyen-Janecky et al. 2003). These data suggest that each  $Fe^{2+}$  transport system may be important for growth, virulence, and/or survival of *S. flexneri*.

*Yersinia pestis*, the pathogen responsible for bubonic, septicemic, and pneumonic plagues in humans and animals, also utilizes the Feo system for virulence. *Y. pestis* is strongly adapted to scavenge iron from its environment as it encodes up to 12 putative iron transport systems, including Feo. The Yfe system, homologous to the Sit system, transports  $Mn^{2+}$  and  $Fe^{2+}$  and has been shown to be important for pathogenesis in mice (Perry et al. 2007). *Y. pestis* encodes for its own siderophore, Yersiniabactin ( $Fe^{3+}$ -utilizing), which was previously shown to be an essential virulence factor during the early stages of infection, whereas the Yfe system ( $Fe^{2+}$ -utilizing) was indispensable for late stage infection, delineating a clear role for  $Fe^{3+}$  and  $Fe^{2+}$  at different stages of infection (Perry et al. 2007). Under microaerophilic conditions, a *Y. pestis*  $\Delta feoB$  strain was attenuated for growth by  $\approx 50\%$ , nearly to the same extent as a  $\Delta yfe$  strain. The loss of both  $Fe^{2+}$  transport systems attenuated growth further. These effects were not observed in the deletion strains growing under



oxic conditions (Perry et al. 2007). Interestingly, the FeoC protein does not appear to be essential for *Y. pestis* growth, while the loss of a functional FeoA attenuated growth to the same extent as the  $\Delta feoB$  strain. The *Y. pestis*  $\Delta feoB$  strain and the *Y. pestis*  $\Delta yfe$  strain were still able to replicate intracellularly in murine macrophages, whereas a strain lacking both *feoB* and *yfe* could not replicate in the murine macrophages, indicating that one system can compensate for the loss of the other during infection (Perry et al. 2007).

A 2009 study demonstrated the importance of FeoB to the virulence of *Streptococcus suis*, a pathogen that infects swine and is responsible for septicemia and meningitis. In silico analysis of *S. suis* led to the discovery of an *feoA* gene in *S. suis* predicted to encode a larger than usual 156 amino acid protein and *feoB* was identified and predicted to encode a 714 amino acid protein. No *feoC* gene was identified (Aranda et al. 2009). Using electrophoretic mobility shift assays (EMSAs), the *S. suis* Fur protein was found to bind specifically to the *feo* operon's promoter, and derepression of *feoA* and *feoB* expression was observed in a *fur* mutant. A murine infection model was then used to establish the contribution of *feo* to virulence. In a *feoB* mutant strain, in vitro growth of the mutant was lower in iron-depleted conditions, and virulence in mice was significantly attenuated, linking *feoB* to full virulence of *S. suis* in murine models (Aranda et al. 2009).

*P. aeruginosa* is an opportunistic pathogen reliant on host iron that is obtained via multiple acquisition systems, and this pathogen is the dominant infectious agent of late-stage cystic fibrosis (CF) patients. *P. aeruginosa*'s reliance on host iron is evident, as transcripts of *feoA*, *feoB*, *bqsR/S* (a two-component  $Fe^{2+}$  sensing system), *pvdA* (the pyoverdine biosynthetic protein), *fptA* (the ferripyochelin receptor), and *hasAp* (the heme uptake protein) have all been detected at various levels in the sputum. As CF progresses and becomes more severe,  $O_2$  permeability of lung tissue generally decreases, and the concentration of  $Fe^{2+}$  in lung sputum increases and is correlated with declining lung function (Hunter et al. 2013). One possible source of reduced iron could come from reaction with excreted reducing agents, such as phenazines, which are redox-active compounds that can reduce  $Fe^{3+}$  to  $Fe^{2+}$ . Intriguingly, the phenazines pyocyanin and phenazine-1-carboxylic acid are present in ca. 80% of sputum samples; however, phenazine levels do not appear to correlate with increased  $Fe^{2+}$  concentrations (Hunter et al. 2013), making the source of  $Fe^{2+}$  in the CF lung unclear. Nevertheless, it has been suggested that iron in CF lungs exists in mixed oxidation states at various stages of disease progression, and that the iron composition changes over time (Hunter et al. 2013), likely an important factor for biofilms. There is also evidence that FeoB is necessary for *P. aeruginosa* to utilize  $Fe^{3+}$  derived from citrate transport across the outer membrane receptor FecA (Marshall et al. 2009). Thus Feo appears to play an important role in oxic iron transport, in addition to anoxic iron transport within *P. aeruginosa*.

CF disease progression is correlated with increased biofilm formation by *P. aeruginosa*, and iron availability is an important factor for biofilm formation. A biofilm assay under hypoxic conditions demonstrated that an  $Fe^{3+}$  chelator, conalbumin, and a  $Fe^{2+}$  chelator, ferrozine, could inhibit biofilm formation by >50%. Biofilm formation could be restored by the addition of excess iron, suggesting that

iron bioavailability is important for biofilm formation in cystic fibrosis lungs (Hunter et al. 2013). Both chelators were then tested for their ability to dissolve preformed biofilms under oxic and anoxic conditions. Significant biofilm dissolution was observed when both chelators were present. Under anoxic conditions, ferrozine alone could dissolve preformed biofilms by 20%. Biofilms reformed with the addition of iron, suggesting biofilm formation is iron-mediated (Hunter et al. 2013). This interesting corollary between biofilms and iron availability could be a future direction of exploration into the progression of CF disease.

*Acinetobacter baumannii* has recently been listed as one of the most dangerous opportunistic pathogens by the World Health Organization, and Feo is one of the contributing factors to this organism's virulence (Álvarez-Fraga et al. 2018). 50 clinical strains of *A. baumannii* containing the Feo operon (*feoA* and *feoB*) were previously identified, and it was found that overexpression of *feoA* occurred during infection of *A. baumannii* within the lung. A clinically-relevant strain lacking the *feoA* gene was constructed and growth of this strain was tested under both iron-sufficient and iron-limited conditions. In iron-replete media, both the  $\Delta$ *feoA* and WT strains showed no differences in growth; however, the generation time of the  $\Delta$ *feoA* strain was significantly higher in iron-limited media compared to the WT strain, indicating that *feoA* is important for the fitness of *A. baumannii* (Álvarez-Fraga et al. 2018). In experiments assessing biofilm formation and cellular adhesion, the inactivation of *feoA* detrimentally affected both markers of *A. baumannii* virulence. When the  $\Delta$ *feoA* strain was complemented with a plasmid encoding for *feoA*, both abilities were only partially restored. Cells lacking *feoA* were also more susceptible to oxidative stress as opposed to the WT strain (Álvarez-Fraga et al. 2018). A *Galleria mellonella* (moth) infection model and a murine pneumonia model have both been used to study how *feoA* affects the virulence of this pathogen. *A. baumannii*  $\Delta$ *feoA* strains were unable to infect and kill *G. mellonella*. Similarly, mice that were intratracheally infected with the  $\Delta$ *feoA* strain had significantly decreased mortality rates, and the occurrence of positive sterling blood cultures for mice infected with the  $\Delta$ *feoA* strain increased by 75% compared to the WT, demonstrating that *feoA* is necessary for *A. baumannii* virulence (Álvarez-Fraga et al. 2018). Thus, these results suggest that FeoA could serve as a novel therapeutic target given its strong contribution to *A. baumannii* virulence.

*P. gingivalis* is an oral pathogen and the causative agent of gingivitis, one of the most common human infections worldwide, and its genome contains an *feoA-feoB* fusion. *P. gingivalis* has a growth requirement for iron, but it cannot synthesize heme, does not produce siderophores, and lacks ferric iron reductase activity, necessitating  $\text{Fe}^{2+}$  uptake as one of its major routes of iron acquisition (Dashper et al. 2005). At first glance, two genes annotated as *feoB* are present in the organism (*feoB1* and *feoB2*). The *feoB1* gene was demonstrated to encode a ferrous iron transporter necessary for pathogenesis (lesion formation) in murine models, while *feoB2* was demonstrated to encode a functional manganese transporter. Interestingly, in the absence of the functional ferrous iron transporter (*feoB1*), the functional manganese transporter (*feoB2*) may be upregulated to support growth and survival, but this gene product does not support infection. This is the first example of an

FeoB-like protein transporting a metal other than ferrous iron (Dashper et al. 2005), but it remains unclear whether *feoB2* is a bona fide FeoB protein. In contrast, it is clear that the *feoB1* gene encodes for a naturally-tethered FeoA-FeoB polypeptide based on sequence conservation. Beyond this information, no work at the protein level has detailed the function of this novel fusion.

*B. fragilis* is a commensal bacterium that can become opportunistic when and if it enters environments outside of the gut, is becoming increasingly resistant to metronidazole (the most widely used treatment for *B. fragilis* infections), and its genome also contains an *feoA-feoB* fusion (Veeranagouda et al. 2014; Rocha et al. 2019). Intriguingly, the absence of the *feoAB* gene conferred metronidazole resistance to *B. fragilis* in one study, despite exhibiting slower growth kinetics. However, the reason for increased resistance to metronidazole in *feoAB* mutants and the effect of iron on resistance remains unknown (Rocha et al. 2019). Additionally, both heme and non-heme iron are necessary for the survival of *B. fragilis* during infection (Rocha et al. 2019). *B. fragilis* cannot synthesize heme de novo, but it has an ability to remove metal from nonferrous metallated porphyrins (dechelatase activity) and to then insert ferrous iron into the apo porphyrins (ferrochelataase activity) (Rocha et al. 2019). The acquisition of ferrous iron is thus important to heme metabolism in *B. fragilis*, and a  $\Delta$ *feoAB* strain was unable to grow in the presence of heme, suggesting that iron derived from heme is necessary for growth (Rocha et al. 2019). Consistent with this hypothesis, when supplemented with 100  $\mu$ M FeSO<sub>4</sub> growth of the deletion strain was rescued. It is suggested that iron is removed from heme in the periplasm and transported via FeoAB to support growth, thus linking heme metabolism and Feo-mediated Fe<sup>2+</sup> uptake in this organism (Rocha et al. 2019). However, like *P. gingivalis*, work at the protein level on the *B. fragilis* FeoA-FeoB fusion is unrealized.

Finally, pathogens utilizing the Feo system also infect plants, although this host-pathogen interface is not well-studied. *Xanthomonas* is a genus of Gram-negative bacteria responsible for causing approximately 400 different diseases in plants, including bacterial blight disease in rice (Pandey and Sonti 2010). *Xanthomonas oryzae* pv. *oryzae* causes disease in the xylem vessels of rice leaves, and this pathogen encodes for a tripartite FeoA, FeoB, and FeoC system. These genes are cotranscribed when iron is both replete and limiting (Pandey and Sonti 2010). In *X. oryzae*, an *feoB* mutant was defective for growth and overproduced siderophores, while the WT strain did not, suggesting that the pathogen was trying to overcome the loss of an essential iron transport system (Pandey and Sonti 2010). Rice inoculated with the *Xanthomonas feoB* mutant produced fewer lesions than those inoculated with WT, whereas bacteria deficient for siderophore production were as virulent as WT, suggesting that the Feo system is an essential component of *in planta* virulence (Pandey and Sonti 2010).

## 12.6 Conclusions and Outlook

From early to present-day Earth, multiple pools of ferrous iron are important for microorganisms to meet their metabolic needs. This principle is especially true in the anoxic and acidic environments that bacteria encounter within a host or in soils, aquatic environments, or waste sites, to name a few. Given the drastic changes in environments that microbes encounter, from iron-replete to iron-depleted conditions, it is absolutely essential for iron uptake and storage to be regulated in a manner that maintains intracellular iron stores at appropriate levels and fulfills the varying metabolic needs of each organism.

Several  $\text{Fe}^{2+}$  uptake systems have been identified in bacteria, though many are not specific for  $\text{Fe}^{2+}$  and have not been well-characterized either at the cellular level or at the protein level, and thus their contribution to bacterial virulence remains unknown. In contrast, cellular studies have established the role of Feo (and in particular FeoB), the dominant prokaryotic  $\text{Fe}^{2+}$  transport system, for bacterial survival and virulence. Despite this importance, several gaps in our knowledge still remain regarding the structure of full-length FeoB and how FeoB facilitates transport of  $\text{Fe}^{2+}$  across the cytoplasmic membrane. It is unclear if a periplasmic binding protein or another chelator facilitates transfer of  $\text{Fe}^{2+}$  to FeoB, potentially through the periplasmic loop, which resides in the TM region binding and translocating  $\text{Fe}^{2+}$  across the membrane, and what happens to  $\text{Fe}^{2+}$  once it reaches the cytosol. Additional questions remain regarding the GTPase/NTPase activity of the G-protein domain of NFeoB and how nucleotide hydrolysis is linked to  $\text{Fe}^{2+}$  transport. FeoA and FeoC, both small cytosolic proteins, have been subjected to numerous studies though their functions remain undetermined. Given that FeoA can be found fused to NFeoB through a linker region to the G-protein domain, it is likely that FeoA and NFeoB interact. However, the exact site of this potential interaction and the functional implications have not been elucidated. Lastly, FeoC has been shown to bind a redox active [4Fe-4S] cluster, implying that FeoC could add an additional layer of regulation to the Feo system. However, FeoC is poorly conserved and some FeoC proteins, such as from *Vibrio* species, do not contain the conserved Cys residues required for iron-sulfur cluster binding. Undoubtedly, more experiments aimed at elucidating these details and more functional models of FeoB will be necessary to gain a better understanding of this broadly distributed  $\text{Fe}^{2+}$  transport pathway.

Despite this lack in knowledge, it is clear that ferrous iron acquisition, linked in particular to the Feo system, is important for the survival of bacterial species across multiple environments, and this point is especially true of pathogenic bacteria that are becoming alarmingly problematic. Antibiotic resistance has become one of the world's greatest public health challenges. Both the challenges and breakthroughs associated with antibiotic resistance continue to change as resistant pathogens evolve. According to a 2019 report from the Centers for Disease Control and Prevention (CDC), there are 2.8 million antibiotic-resistant infections in the United States every year which results in more than 35,000 deaths (Antibiotic resistance threats in the United States 2019). In fact, in the United States it is estimated that

deaths associated with resistant infections will outpace those associated with cancer by the year 2050. As iron acquisition is linked to pathogenesis, and bacteria lacking functional ferrous iron transport systems (such as Feo) have been shown to be avirulent or unable to colonize in a host-associated environment, a greater understanding of the mechanisms underlying ferrous iron acquisition could be leveraged for the development of new therapeutics that could help to combat the growing global emergency of antibiotic resistance.

**Acknowledgements** This work was supported by NIH R21 DE027803 (A. T. S.), NIH R35 GM133497 (A. T. S.), and in part by NIH T32 GM066706 (A. E. S.).

## References

- Abeyrathna SS, Abeyrathna NS, Thai NK, Sarkar P, D'Arcy S, Meloni G (2019) IroT/MavN is a *Legionella* transmembrane Fe(II) transporter: metal selectivity and translocation kinetics revealed by *in vitro* real-time transport. *Biochemistry* 58(43):4337–4342. <https://doi.org/10.1021/acs.biochem.9b00658>
- Abu Kwaik Y, Bumann D (2013) Microbial quest for food *in vivo*: ‘nutritional virulence’ as an emerging paradigm. *Cell Microbiol* 15(6):882–890. <https://doi.org/10.1111/cmi.12138>
- Álvarez-Fraga L, Vázquez-Ucha JC, Martínez-Gutián M, Vallejo JA, Bou G, Beceiro A, Poza M (2018) Pneumonia infection in mice reveals the involvement of the feoA gene in the pathogenesis of *Acinetobacter baumannii*. *Virulence* 9(1):496–509. <https://doi.org/10.1080/21505594.2017.1420451>
- Andrews SC, Robinson AK, Rodríguez-Quñones F (2003) Bacterial iron homeostasis. *FEMS Microbiol Rev* 27(2-3):215–237
- Antibiotic resistance threats in the United States (2019)
- Aranda J, Cortés P, Garrido ME, Fittipaldi N, Llagostera M, Gottschalk M, Barbé J (2009) Contribution of the FeoB transporter to *Streptococcus suis* virulence. *Int Microbiol* 12(2): 137–143
- Ash MR, Maher MJ, Guss JM, Jormakka M (2011) The initiation of GTP hydrolysis by the G-domain of FeoB: insights from a transition-state complex structure. *PLoS One* 6(8):e23355. <https://doi.org/10.1371/journal.pone.0023355>
- Askwith C, Kaplan J (1997) An oxidase-permease-based iron transport system in *Schizosaccharomyces pombe* and its expression in *Saccharomyces cerevisiae*. *J Biol Chem* 272(1):401–405. <https://doi.org/10.1074/jbc.272.1.401>
- Askwith C, Eide D, Van Ho A, Bernard PS, Li L, Davis-Kaplan S, Sipe DM, Kaplan J (1994) The FET3 gene of *S. cerevisiae* encodes a multicopper oxidase required for ferrous iron uptake. *Cell* 76(2):403–410. [https://doi.org/10.1016/0092-8674\(94\)90346-8](https://doi.org/10.1016/0092-8674(94)90346-8)
- Bazylinski DA, Frankel RB, Jannasch HW (1988) Anaerobic magnetite production by a marine, magnetotactic bacterium. *Nature* 334(6182):518–519. <https://doi.org/10.1038/334518a0>
- Bearden SW, Staggs TM, Perry RD (1998) An ABC transporter system of *Yersinia pestis* allows utilization of chelated iron by *Escherichia coli* SAB11. *J Bacteriol* 180(5):1135–1147
- Bennett BD, Brutinel ED, Gralnick JA (2015) A ferrous iron exporter mediates iron resistance in *Shewanella oneidensis* MR-1. *Appl Environ Microbiol* 81(22):7938–7944. <https://doi.org/10.1128/AEM.02835-15>
- Bennett BD, Redford KE, Gralnick JA (2018) MgtE homolog FicI acts as a secondary ferrous iron importer in *Shewanella oneidensis* strain MR-1. *Appl Environ Microbiol* 84(6). <https://doi.org/10.1128/AEM.01245-17>

- Bhattacharyya P (1970) Active transport of manganese in isolated membranes of *Escherichia coli*. *J Bacteriol* 104(3):1307–1311. <https://doi.org/10.1128/JB.104.3.1307-1311.1970>
- Blakemore R (1975) Magnetotactic bacteria. *Science* 190(4212):377–379. <https://doi.org/10.1126/science.170679>
- Bos JL, Rehmann H, Wittinghofer A (2007) GEFs and GAPs: critical elements in the control of small G proteins. *Cell* 129(5):865–877. <https://doi.org/10.1016/j.cell.2007.05.018>
- Bozzi AT, Bane LB, Weihofen WA, Singharoy A, Guillen ER, Ploegh HL, Schulten K, Gaudet R (2016) Crystal structure and conformational change mechanism of a bacterial Nramp-family divalent metal transporter. *Structure* 24(12):2102–2114. <https://doi.org/10.1016/j.str.2016.09.017>
- Brunori M (2010) Myoglobin strikes back. *Protein Sci* 19(2):195–201. <https://doi.org/10.1002/pro.300>
- Brutinel ED, Gralnick JA (2012) Shuttling happens: soluble flavin mediators of extracellular electron transfer in *Shewanella*. *Appl Microbiol Biotechnol* 93(1):41–48. <https://doi.org/10.1007/s00253-011-3653-0>
- Caccavo F, Lonergan DJ, Lovley DR, Davis M, Stolz JF, McInerney MJ (1994) *Geobacter sulfurreducens* sp. nov., a hydrogen- and acetate-oxidizing dissimilatory metal-reducing microorganism. *Appl Environ Microbiol* 60(10):3752–3759. <https://doi.org/10.1128/AEM.60.10.3752-3759.1994>
- Cain TJ, Smith AT (2021) Ferric iron reductases and their contribution to unicellular ferrous iron uptake. *J Inorg Biochem* 218:111407. <https://doi.org/10.1016/j.jinorgbio.2021.11.1407>
- Calugay RJ, Miyashita H, Okamura Y, Matsunaga T (2003) Siderophore production by the magnetic bacterium *Magnetospirillum magneticum* AMB-1. *FEMS Microbiol Lett* 218(2): 371–375. [https://doi.org/10.1016/S0378-1097\(02\)01188-6](https://doi.org/10.1016/S0378-1097(02)01188-6)
- Calugay RJ, Takeyama H, Mukoyama D, Fukuda Y, Suzuki T, Kanoh K, Matsunaga T (2006) Catechol siderophore excretion by magnetotactic bacterium *Magnetospirillum magneticum* AMB-1. *J Biosci Bioeng* 101(5):445–447. <https://doi.org/10.1263/jbb.101.445>
- Cao J, Woodhall MR, Alvarez J, Cartron ML, Andrews SC (2007) EfeUOB (YcdNOB) is a tripartite, acid-induced and CpxAR-regulated, low-pH Fe<sub>2+</sub> transporter that is cryptic in *Escherichia coli* K-12 but functional in *E. coli* O157:H7. *Mol Microbiol* 65(4):857–875. <https://doi.org/10.1111/j.1365-2958.2007.05802.x>
- Carlson HK, Clark IC, Melnyk RA, Coates JD (2012) Toward a mechanistic understanding of anaerobic nitrate-dependent iron oxidation: balancing electron uptake and detoxification. *Front Microbiol* 3:57. <https://doi.org/10.3389/fmicb.2012.00057>
- Cartron ML, Maddocks S, Gillingham P, Craven CJ, Andrews SC (2006) Feo-transport of ferrous iron into bacteria. *Biometals* 19(2):143–157. <https://doi.org/10.1007/s10534-006-0003-2>
- Chao Y, Fu D (2004) Thermodynamic studies of the mechanism of metal binding to the *Escherichia coli* zinc transporter YiiP. *J Biol Chem* 279(17):17173–17180. <https://doi.org/10.1074/jbc.M400208200>
- Christenson ET, Isaac DT, Yoshida K, Lipo E, Kim JS, Ghirlando R, Isberg RR, Banerjee A (2019) The iron-regulated vacuolar. *Proc Natl Acad Sci U S A* 116(36):17775–17785. <https://doi.org/10.1073/pnas.1902806116>
- Chu BC, Garcia-Herrero A, Johanson TH, Krewulak KD, Lau CK, Peacock RS, Slavinskaya Z, Vogel HJ (2010) Siderophore uptake in bacteria and the battle for iron with the host; a bird's eye view. *Biometals* 23(4):601–611. <https://doi.org/10.1007/s10534-010-9361-x>
- Cornelis P (2010) Iron uptake and metabolism in pseudomonads. *Appl Microbiol Biotechnol* 86(6): 1637–1645. <https://doi.org/10.1007/s00253-010-2550-2>
- Coudray N, Valvo S, Hu M, Lasala R, Kim C, Vink M, Zhou M, Provasi D, Filizola M, Tao J, Fang J, Penczek PA, Ubarretxena-Belandia I, Stokes DL (2013) Inward-facing conformation of the zinc transporter YiiP revealed by cryoelectron microscopy. *Proc Natl Acad Sci U S A* 110(6):2140–2145. <https://doi.org/10.1073/pnas.1215455110>
- Crack JC, Le Brun NE, Thomson AJ, Green J, Jervis AJ (2008) Reactions of nitric oxide and oxygen with the regulator of fumarate and nitrate reduction, a global transcriptional regulator,

- during anaerobic growth of *Escherichia coli*. *Methods Enzymol* 437:191–209. [https://doi.org/10.1016/S0076-6879\(07\)37011-0](https://doi.org/10.1016/S0076-6879(07)37011-0)
- D'Aquino JA, Ringe D (2003) Determinants of the SRC homology domain 3-like fold. *J Bacteriol* 185(14):4081–4086. <https://doi.org/10.1128/jb.185.14.4081-4086.2003>
- Dashper SG, Butler CA, Lissel JP, Paolini RA, Hoffmann B, Veith PD, O'Brien-Simpson NM, Snelgrove SL, Tsiros JT, Reynolds EC (2005) A novel *Porphyromonas gingivalis* FeoB plays a role in manganese accumulation. *J Biol Chem* 280(30):28095–28102. <https://doi.org/10.1074/jbc.M503896200>
- DeLong EF, Pace NR (2001) Environmental diversity of bacteria and archaea. *Syst Biol* 50(4):470–478
- Derry LA (2015) Causes and consequences of mid-Proterozoic anoxia. *Geophys Res Lett* 42(20):8538–8546. <https://doi.org/10.1002/2015GL065333>
- Deshpande CN, McGrath AP, Font J, Guilfoyle AP, Maher MJ, Jormakka M (2013) Structure of an atypical FeoB G-domain reveals a putative domain-swapped dimer. *Acta Crystallogr Sect F Struct Biol Cryst Commun* 69(4):399–404. <https://doi.org/10.1107/S1744309113005939>
- Dong Z, Guo S, Fu H, Gao H (2017) Investigation of a spontaneous mutant reveals novel features of iron uptake in *Shewanella oneidensis*. *Sci Rep* 7(1):11788. <https://doi.org/10.1038/s41598-017-11987-3>
- Dunning JC, Ma Y, Marquis RE (1998) Anaerobic killing of oral streptococci by reduced, transition metal cations. *Appl Environ Microbiol* 64(1):27–33. <https://doi.org/10.1128/AEM.64.1.27-33.1998>
- Ehrnstorfer IA, Geertsma ER, Pardon E, Steyaert J, Dutzler R (2014) Crystal structure of a SLC11 (NRAMP) transporter reveals the basis for transition-metal ion transport. *Nat Struct Mol Biol* 21(11):990–996. <https://doi.org/10.1038/nsmb.2904>
- Ellermann M, Arthur JC (2017) Siderophore-mediated iron acquisition and modulation of host-bacterial interactions. *Free Radic Biol Med* 105:68–78. <https://doi.org/10.1016/j.freeradbiomed.2016.10.489>
- Embree M, Qiu Y, Shieu W, Nagarajan H, O'Neil R, Lovley D, Zengler K (2014) The iron stimulon and fur regulon of *Geobacter sulfurreducens* and their role in energy metabolism. *Appl Environ Microbiol* 80(9):2918–2927. <https://doi.org/10.1128/AEM.03916-13>
- Emerson D, Fleming EJ, McBeth JM (2010) Iron-oxidizing bacteria: an environmental and genomic perspective. *Annu Rev Microbiol* 64:561–583. <https://doi.org/10.1146/annurev.micro.112408.134208>
- Emerson D, Scott JJ, Benes J, Bowden WB (2015) Microbial iron oxidation in the Arctic tundra and its implications for biogeochemical cycling. *Appl Environ Microbiol* 81(23):8066–8075. <https://doi.org/10.1128/AEM.02832-15>
- Eng ET, Jalilian AR, Spasov KA, Unger VM (2008) Characterization of a novel prokaryotic GDP dissociation inhibitor domain from the G protein coupled membrane protein FeoB. *J Mol Biol* 375(4):1086–1097. <https://doi.org/10.1016/j.jmb.2007.11.027>
- Escolar L, Pérez-Martín J, de Lorenzo V (1999) Opening the iron box: transcriptional metalloregulation by the Fur protein. *J Bacteriol* 181(20):6223–6229
- Esther J, Sukla LB, Pradhan N, Panda S (2015) Fe (III) reduction strategies of dissimilatory iron reducing bacteria. *Korean J Chem Eng* 32(1):1–14. <https://doi.org/10.1007/s11814-014-0286-x>
- Fillat MF (2014) The FUR (ferric uptake regulator) superfamily: diversity and versatility of key transcriptional regulators. *Arch Biochem Biophys* 546:41–52. <https://doi.org/10.1016/j.abb.2014.01.029>
- Fischbach MA, Lin H, Liu DR, Walsh CT (2006) How pathogenic bacteria evade mammalian sabotage in the battle for iron. *Nat Chem Biol* 2(3):132–138. <https://doi.org/10.1038/nchembio771>
- Ganz T (2008) Iron homeostasis: fitting the puzzle pieces together. *Cell Metab* 7(4):288–290. <https://doi.org/10.1016/j.cmet.2008.03.008>

- Gauger T, Konhauser K, Kappler A (2015) Protection of phototrophic iron(II)-oxidizing bacteria from UV irradiation by biogenic iron(III) minerals: implications for early Archean banded iron formation. *Geology* 43(12):1067–1070. <https://doi.org/10.1130/G37095.1>
- Gauger T, Konhauser K, Kappler A (2016) Protection of nitrate-reducing Fe(II)-oxidizing bacteria from UV radiation by biogenic Fe(III) minerals. *Astrobiology* 16(4):301–310. <https://doi.org/10.1089/ast.2015.1365>
- Glass J (2015) Microbes that meddle with metals: microorganisms depend on numerous metal cofactors; these requirements in turn depend on microbial species, type of metabolism, and environmental conditions. *Microbe* 10:197–202. <https://doi.org/10.1128/microbe.10.197.1>
- Grass G, Wong MD, Rosen BP, Smith RL, Rensing C (2002) ZupT is a Zn(II) uptake system in *Escherichia coli*. *J Bacteriol* 184(3):864–866. <https://doi.org/10.1128/jb.184.3.864-866.2002>
- Grass G, Franke S, Taudte N, Nies DH, Kucharski LM, Maguire ME, Rensing C (2005a) The metal permease ZupT from *Escherichia coli* is a transporter with a broad substrate spectrum. *J Bacteriol* 187(5):1604–1611. <https://doi.org/10.1128/JB.187.5.1604-1611.2005>
- Grass G, Otto M, Fricke B, Haney CJ, Rensing C, Nies DH, Munkelt D (2005b) FieF (YiiP) from *Escherichia coli* mediates decreased cellular accumulation of iron and relieves iron stress. *Arch Microbiol* 183(1):9–18. <https://doi.org/10.1007/s00203-004-0739-4>
- Grosse C, Scherer J, Koch D, Otto M, Taudte N, Grass G (2006) A new ferrous iron-uptake transporter, EfeU (YcdN), from *Escherichia coli*. *Mol Microbiol* 62(1):120–131. <https://doi.org/10.1111/j.1365-2958.2006.05326.x>
- Guerinot ML (2000) The ZIP family of metal transporters. *Biochim Biophys Acta* 1465(1-2):190–198. [https://doi.org/10.1016/s0005-2736\(00\)00138-3](https://doi.org/10.1016/s0005-2736(00)00138-3)
- Guilfoyle AP, Deshpande CN, Schenk G, Maher MJ, Jormakka M (2014) Exploring the correlation between the sequence composition of the nucleotide binding G5 loop of the FeoB GTPase domain (NFeoB) and intrinsic rate of GDP release. *Biosci Rep* 34(6):e00158. <https://doi.org/10.1042/BSR20140152>
- Hagelueken G, Duthie FG, Florin N, Schubert E, Schiemann O (2015) Expression, purification and spin labelling of the ferrous iron transporter FeoB from *Escherichia coli* BL21 for EPR studies. *Protein Expr Purif* 114:30–36. <https://doi.org/10.1016/j.pep.2015.05.014>
- Hagelueken G, Hoffmann J, Schubert E, Duthie FG, Florin N, Konrad L, Imhof D, Behrmann E, Morgner N, Schiemann O (2016) Studies on the X-ray and solution structure of FeoB from *Escherichia coli* BL21. *Biophys J* 110(12):2642–2650. <https://doi.org/10.1016/j.bpj.2016.05.018>
- Hanert H (1974) In vivo kinetics of individual development of *Gallionella ferruginea* in batch microculture. *Arch Microbiol* 96(1):59–74. <https://doi.org/10.1007/BF00590163>
- Hantke K (1987) Ferrous iron transport mutants in *Escherichia coli* K12. *FEMS Microbiol Lett* 44(1):53–57. <https://doi.org/10.1111/j.1574-6968.1987.tb02241.x>
- Hantke K (2003) Is the bacterial ferrous iron transporter FeoB a living fossil? *Trends Microbiol* 11(5):192–195
- Hider RC, Kong X (2013) Iron speciation in the cytosol: an overview. *Dalton Trans* 42(9):3220–3229. <https://doi.org/10.1039/c2dt32149a>
- Hsueh KL, Yu LK, Chen YH, Cheng YH, Hsieh YC, Ke SC, Hung KW, Chen CJ, Huang TH (2013) FeoC from *Klebsiella pneumoniae* contains a [4Fe-4S] cluster. *J Bacteriol* 195(20):4726–4734. <https://doi.org/10.1128/jb.00687-13>
- Hu Y, Ribbe MW (2015) Nitrogenase and homologs. *J Biol Inorg Chem* 20(2):435–445. <https://doi.org/10.1007/s00775-014-1225-3>
- Huang W, Wilks A (2017) Extracellular heme uptake and the challenge of bacterial cell membranes. *Annu Rev Biochem* 86:799–823. <https://doi.org/10.1146/annurev-biochem-060815-014214>
- Hung KW, Juan TH, Hsu YL, Huang TH (2012a) NMR structure note: the ferrous iron transport protein C (FeoC) from *Klebsiella pneumoniae*. *J Biomol NMR* 53(2):161–165. <https://doi.org/10.1007/s10858-012-9633-6>
- Hung KW, Tsai JY, Juan TH, Hsu YL, Hsiao CD, Huang TH (2012b) Crystal structure of the *Klebsiella pneumoniae* NFeoB/FeoC complex and roles of FeoC in regulation of Fe<sup>2+</sup> transport



- by the bacterial Feo system. *J Bacteriol* 194(23):6518–6526. <https://doi.org/10.1128/JB.01228-12>
- Hunter RC, Asfour F, Dingemans J, Osuna BL, Samad T, Malfroot A, Cornelis P, Newman DK (2013) Ferrous iron is a significant component of bioavailable iron in cystic fibrosis airways. *mBio* 4(4). <https://doi.org/10.1128/mBio.00557-13>
- Ikeda JS, Janakiraman A, Kehres DG, Maguire ME, Slauch JM (2005) Transcriptional regulation of sitABCD of *Salmonella enterica* serovar typhimurium by MntR and Fur. *J Bacteriol* 187(3): 912–922. <https://doi.org/10.1128/JB.187.3.912-922.2005>
- Isaac DT, Laguna RK, Valtz N, Isberg RR (2015) MavN is a *Legionella pneumophila* vacuole-associated protein required for efficient iron acquisition during intracellular growth. *Proc Natl Acad Sci U S A* 112(37):E5208–E5217. <https://doi.org/10.1073/pnas.1511389112>
- Janakiraman A, Slauch JM (2000) The putative iron transport system SitABCD encoded on SPI1 is required for full virulence of *Salmonella typhimurium*. *Mol Microbiol* 35(5):1146–1155. <https://doi.org/10.1046/j.1365-2958.2000.01783.x>
- Jones DS, Kohl C, Grettenberger C, Larson LN, Burgos WD, Macaladya JL (2015) Geochemical niches of iron-oxidizing acidophiles in acidic coal mine drainage. *Appl Environ Microbiol* 81(4):1242–1250. <https://doi.org/10.1128/AEM.02919-14>
- Kadi N, Arbache S, Song L, Oves-Costales D, Challis GL (2008) Identification of a gene cluster that directs putrebaectin biosynthesis in *Shewanella* species: PubC catalyzes cyclodimerization of N-hydroxy-N-succinylputrescine. *J Am Chem Soc* 130(32):10458–10459. <https://doi.org/10.1021/ja8027263>
- Kammler M, Schön C, Hantke K (1993) Characterization of the ferrous iron uptake system of *Escherichia coli*. *J Bacteriol* 175(19):6212–6219. <https://doi.org/10.1128/jb.175.19.6212-6219.1993>
- Kehres DG, Zaharik ML, Finlay BB, Maguire ME (2000) The NRAMP proteins of *Salmonella typhimurium* and *Escherichia coli* are selective manganese transporters involved in the response to reactive oxygen. *Mol Microbiol* 36(5):1085–1100. <https://doi.org/10.1046/j.1365-2958.2000.01922.x>
- Kehres DG, Janakiraman A, Slauch JM, Maguire ME (2002) SitABCD is the alkaline Mn<sup>2+</sup> transporter of *Salmonella enterica* serovar typhimurium. *J Bacteriol* 184(12):3159. <https://doi.org/10.1128/JB.184.12.3159-3166.2002>
- Kim H, Lee H, Shin D (2012) The FeoA protein is necessary for the FeoB transporter to import ferrous iron. *Biochem Biophys Res Commun* 423(4):733–738. <https://doi.org/10.1016/j.bbrc.2012.06.027>
- Kim H, Lee H, Shin D (2013) The FeoC protein leads to high cellular levels of the Fe(II) transporter FeoB by preventing FtsH protease regulation of FeoB in *Salmonella enterica*. *J Bacteriol* 195(15):3364–3370. <https://doi.org/10.1128/jb.00343-13>
- Kim H, Lee H, Shin D (2015) Lon-mediated proteolysis of the FeoC protein prevents *Salmonella enterica* from accumulating the Fe(II) transporter FeoB under high-oxygen conditions. *J Bacteriol* 197(1):92–98. <https://doi.org/10.1128/jb.01826-14>
- Konhauser KO, Planavsky NJ, Hardisty DS, Robbins LJ, Warchola TJ, Haugaard R, Lalonde SV, Partin CA, Onk PBH, Tsikos H, Lyons TW, Bekker A, Johnson CM (2017) Iron formations: a global record of neoarchaeal to palaeoproterozoic environmental history. *Earth-Sci Rev* 172: 140–177. <https://doi.org/10.1016/j.earscirev.2017.06.012>
- Koster S, Kuhlbrandt W, Yildiz O (2009a) Purification, crystallization and preliminary X-ray diffraction analysis of the FeoB G domain from *Methanococcus jannaschii*. *Acta Crystallogr Sect F Struct Biol Cryst Commun* 65(Pt 7):684–687. <https://doi.org/10.1107/s1744309109019216>
- Koster S, Wehner M, Herrmann C, Kuhlbrandt W, Yildiz O (2009b) Structure and function of the FeoB G-domain from *Methanococcus jannaschii*. *J Mol Biol* 392(2):405–419. <https://doi.org/10.1016/j.jmb.2009.07.020>
- Krewulak KD, Vogel HJ (2008) Structural biology of bacterial iron uptake. *Biochim Biophys Acta* 1778(9):1781–1804. <https://doi.org/10.1016/j.bbamem.2007.07.026>

- Lau CK, Ishida H, Liu Z, Vogel HJ (2013) Solution structure of *Escherichia coli* FeoA and its potential role in bacterial ferrous iron transport. *J Bacteriol* 195(1):46–55. <https://doi.org/10.1128/jb.01121-12>
- Lau CK, Krewulak KD, Vogel HJ (2016) Bacterial ferrous iron transport: the Feo system. *FEMS Microbiol Rev* 40(2):273–298. <https://doi.org/10.1093/femsre/fuv049>
- Ledyard KM, Butler A (1997) Structure of putrebactin, a new dihydroxamate siderophore produced by *Shewanella putrefaciens*. *J Biol Inorg Chem* 2(1):93–97. <https://doi.org/10.1007/s007750050110>
- Létouffé S, Heuck G, Delepelaire P, Lange N, Wandersman C (2009) Bacteria capture iron from heme by keeping tetrapyrrole skeleton intact. *Proc Natl Acad Sci U S A* 106(28):11719–11724. <https://doi.org/10.1073/pnas.0903842106>
- Li SS (2005) Specificity and versatility of SH3 and other proline-recognition domains: structural basis and implications for cellular signal transduction. *Biochem J* 390(Pt 3):641–653. <https://doi.org/10.1042/bj20050411>
- Li ZQ, Zhang LC, Xue CJ, Zheng MT, Zhu MT, Robbins LJ, Slack JF, Planavsky NJ, Konhauser KO (2018) Earth's youngest banded iron formation implies ferruginous conditions in the early Cambrian Ocean. *Sci Rep* 8(1):9970. <https://doi.org/10.1038/s41598-018-28187-2>
- Linkous RO, Sestok AE, Smith AT (2019) The crystal structure of *Klebsiella pneumoniae* FeoA reveals a site for protein-protein interactions. *Proteins* 87(11):897–903. <https://doi.org/10.1002/prot.25755>
- Liu X, Du Q, Wang Z, Zhu D, Huang Y, Li N, Wei T, Xu S, Gu L (2011) Crystal structure and biochemical features of EfeB/YcdB from *Escherichia coli* O157: ASP235 plays divergent roles in different enzyme-catalyzed processes. *J Biol Chem* 286(17):14922–14931. <https://doi.org/10.1074/jbc.M110.197780>
- Liu L, Li S, Wang S, Dong Z, Gao H (2018) Complex iron uptake by the Putrebactin-mediated and Feo systems in *Shewanella oneidensis*. *Appl Environ Microbiol* 84(20). <https://doi.org/10.1128/AEM.01752-18>
- Lovley DR (1997) Microbial Fe(III) reduction in subsurface environments. *FEMS Microbiol Rev* 20(3-4):305–313. <https://doi.org/10.1111/j.1574-6976.1997.tb00316.x>
- Lovley DR, Walker DJF (2019) Protein Nanowires. *Front Microbiol* 10:2078. <https://doi.org/10.3389/fmicb.2019.02078>
- Makui H, Roig E, Cole ST, Helmann JD, Gros P, Cellier MF (2000) Identification of the *Escherichia coli* K-12 Nramp orthologue (MntH) as a selective divalent metal ion transporter. *Mol Microbiol* 35(5):1065–1078. <https://doi.org/10.1046/j.1365-2958.2000.01774.x>
- Mann S, Sparks N, Frankel R, Bazylinski D, Jannasch H (1990) Biomineralization of ferrimagnetic greigite (Fe<sub>3</sub>S<sub>4</sub>) and iron pyrite (FeS<sub>2</sub>) in a magnetotactic bacterium. *Nature* 343. <https://doi.org/10.1038/343258a0>
- Marlovits TC, Haase W, Herrmann C, Aller SG, Unger VM (2002) The membrane protein FeoB contains an intramolecular G protein essential for Fe(II) uptake in bacteria. *Proc Natl Acad Sci U S A* 99(25):16243–16248. <https://doi.org/10.1073/pnas.242338299>
- Marshall B, Stintzi A, Gilmour C, Meyer JM, Poole K (2009) Citrate-mediated iron uptake in *Pseudomonas aeruginosa*: involvement of the citrate-inducible FecA receptor and the FeoB ferrous iron transporter. *Microbiology* 155(Pt 1):305–315. <https://doi.org/10.1099/mic.0.023531-0>
- Matsunaga T, Sakaguchi T, Tadakoro F (1991) Magnetite formation by a magnetic bacterium capable of growing aerobically. *Appl Microbiol Biotechnol* 35(5):651–655. <https://doi.org/10.1007/BF00169632>
- Naikare H, Palyada K, Panciera R, Marlow D, Stintzi A (2006) Major role for FeoB in *Campylobacter jejuni* ferrous iron acquisition, gut colonization, and intracellular survival. *Infect Immun* 74(10):5433–5444. <https://doi.org/10.1128/iai.00052-06>
- Nies DH, Silver S (1995) Ion efflux systems involved in bacterial metal resistances. *J Ind Microbiol* 14(2):186–199. <https://doi.org/10.1007/BF01569902>

- Ovchinnikov S, Park H, Varghese N, Huang PS, Pavlopoulos GA, Kim DE, Kamisetty H, Kyrpidis NC, Baker D (2017) Protein structure determination using metagenome sequence data. *Science* (New York, NY) 355(6322):294–298. <https://doi.org/10.1126/science.aah4043>
- Pandey A, Sonti RV (2010) Role of the FeoB protein and siderophore in promoting virulence of *Xanthomonas oryzae* pv. *oryzae* on rice. *J Bacteriol* 192(12):3187–3203. <https://doi.org/10.1128/jb.01558-09>
- Parrow NL, Fleming RE, Minnick MF (2013) Sequestration and scavenging of iron in infection. *Infect Immun* 81(10):3503–3514
- Patzter SI, Hantke K (2001) Dual repression by Fe<sup>2+</sup>-Fur and Mn<sup>2+</sup>-MntR of the *mntH* gene, encoding an NRAMP-like Mn<sup>2+</sup> transporter in *Escherichia coli*. *J Bacteriol* 183(16):4806–4813. <https://doi.org/10.1128/JB.183.16.4806-4813.2001>
- Paulsen IT, Saier MH (1997) A novel family of ubiquitous heavy metal ion transport proteins. *J Membr Biol* 156(2):99–103. <https://doi.org/10.1007/s002329900192>
- Pérez N, Johnson R, Sen B, Ramakrishnan G (2016) Two parallel pathways for ferric and ferrous iron acquisition support growth and virulence of the intracellular pathogen *Francisella tularensis* Schu S4. *MicrobiologyOpen* 5(3):453–468. <https://doi.org/10.1002/mbo3.342>
- Perry RD, Mier I Jr, Fetherston JD (2007) Roles of the Yfe and Feo transporters of *Yersinia pestis* in iron uptake and intracellular growth. *Biomaterials* 20(3-4):699–703. <https://doi.org/10.1007/s10534-006-9051-x>
- Perry RD, Craig SK, Abney J, Bobrov AG, Kirillina O, Mier I, Truszczynska H, Fetherston JD (2012) Manganese transporters Yfe and MntH are Fur-regulated and important for the virulence of *Yersinia pestis*. *Microbiology* 158(Pt 3):804–815. <https://doi.org/10.1099/mic.0.053710-0>
- Portier E, Zheng H, Sahr T, Burnside DM, Mallama C, Buchrieser C, Cianciotto NP, Hécharde Y (2015) IroT/mavN, a new iron-regulated gene involved in *Legionella pneumophila* virulence against amoebae and macrophages. *Environ Microbiol* 17(4):1338–1350. <https://doi.org/10.1111/1462-2920.12604>
- Rajasekaran MB, Nilapwar S, Andrews SC, Watson KA (2010) EfeO-cupredoxins: major new members of the cupredoxin superfamily with roles in bacterial iron transport. *Biomaterials* 23(1):1–17. <https://doi.org/10.1007/s10534-009-9262-z>
- Raphael BH, Joens LA (2003) FeoB is not required for ferrous iron uptake in *Campylobacter jejuni*. *Can J Microbiol* 49(11):727–731. <https://doi.org/10.1139/w03-086>
- Richard KL, Kelley BR, Johnson JG (2019) Heme uptake and utilization by gram-negative bacterial pathogens. *Front Cell Infect Microbiol* 9:81. <https://doi.org/10.3389/fcimb.2019.00081>
- Richter K, Schicklberger M, Gescher J (2012) Dissimilatory reduction of extracellular electron acceptors in anaerobic respiration. *Appl Environ Microbiol* 78(4):913–921. <https://doi.org/10.1128/AEM.06803-11>
- Robey M, Cianciotto NP (2002) *Legionella pneumophila* feoAB promotes ferrous iron uptake and intracellular infection. *Infect Immun* 70(10):5659–5669
- Rocha ER, Bergonia HA, Gerdes S, Jeffrey Smith C (2019) *Bacteroides fragilis* requires the ferrous-iron transporter FeoAB and the CobN-like proteins BtuS1 and BtuS2 for assimilation of iron released from heme. *MicrobiologyOpen* 8(4):e00669. <https://doi.org/10.1002/mbo3.669>
- Roden EE, Sobolev D, Glazer B, Luther GW (2004) Potential for microscale bacterial Fe redox cycling at the aerobic-anaerobic interface. *Geomicrobiol J* 21(6):379–391. <https://doi.org/10.1080/01490450490485872>
- Rong C, Huang Y, Zhang W, Jiang W, Li Y, Li J (2008) Ferrous iron transport protein B gene (*feoB1*) plays an accessory role in magnetosome formation in *Magnetospirillum gryphiswaldense* strain MSR-1. *Res Microbiol* 159(7):530–536. <https://doi.org/10.1016/j.resmic.2008.06.005>
- Rong C, Zhang C, Zhang Y, Qi L, Yang J, Guan G, Li Y, Li J (2012) FeoB2 functions in magnetosome formation and oxidative stress protection in *Magnetospirillum gryphiswaldense* strain MSR-1. *J Bacteriol* 194(15):3972–3976. <https://doi.org/10.1128/JB.00382-12>

- Runyen-Janecky LJ, Reeves SA, Gonzales EG, Payne SM (2003) Contribution of the *Shigella flexneri* Sit, Iuc, and Feo iron acquisition systems to iron acquisition in vitro and in cultured cells. *Infect Immun* 71(4):1919–1928
- Sabri M, Caza M, Proulx J, Lymberopoulos MH, Brée A, Moulin-Schouleur M, Curtiss R 3rd, Dozois CM (2008) Contribution of the SitABCD, MntH, and FeoB metal transporters to the virulence of avian pathogenic *Escherichia coli* O78 strain chi7122. *Infect Immun* 76(2): 601–611. <https://doi.org/10.1128/iai.00789-07>
- Saier MH, Tran CV, Barabote RD (2006) TCDB: the transporter classification database for membrane transport protein analyses and information. *Nucleic Acids Res* 34(Database issue): D181–D186. <https://doi.org/10.1093/nar/gkj001>
- Saier MH, Reddy VS, Moreno-Hagelsieb G, Hendargo KJ, Zhang Y, Iddamsetty V, Lam KJK, Tian N, Russum S, Wang J, Medrano-Soto A (2021) The transporter classification database (TCDB): 2021 update. *Nucleic Acids Res* 49(D1):D461–D467. <https://doi.org/10.1093/nar/gkaa1004>
- Schad M, Konhauser KO, Sánchez-Baracaldo P, Kappler A, Bryce C (2019) How did the evolution of oxygenic photosynthesis influence the temporal and spatial development of the microbial iron cycle on ancient earth? *Free Radic Biol Med* 140:154–166. <https://doi.org/10.1016/j.freeradbiomed.2019.07.014>
- Schröder I, Johnson E, de Vries S (2003) Microbial ferric iron reductases. *FEMS Microbiol Rev* 27(2-3):427–447. [https://doi.org/10.1016/S0168-6445\(03\)00043-3](https://doi.org/10.1016/S0168-6445(03)00043-3)
- Schüler D, Baeuerlein E (1998) Dynamics of iron uptake and Fe3O4 biomineralization during aerobic and microaerobic growth of *Magnetospirillum gryphiswaldense*. *J Bacteriol* 180(1): 159–162
- Seeliger S, Cord-Ruwisch R, Schink B (1998) A periplasmic and extracellular c-type cytochrome of *Geobacter sulfurreducens* acts as a ferric iron reductase and as an electron carrier to other acceptors or to partner bacteria. *J Bacteriol* 180(14):3686–3691. <https://doi.org/10.1128/JB.180.14.3686-3691.1998>
- Sestok AE, Linkous RO, Smith AT (2018) Toward a mechanistic understanding of Feo-mediated ferrous iron uptake. *Metallomics* 10(7):887–898. <https://doi.org/10.1039/c8mt00097b>
- Sestok AE, Lee MA, Smith AT (2021) Unpublished results
- Severance S, Chakraborty S, Kosman DJ (2004) The Ftr1p iron permease in the yeast plasma membrane: orientation, topology and structure-function relationships. *Biochem J* 380(Pt 2): 487–496. <https://doi.org/10.1042/BJ20031921>
- Seyedmohammad S, Born D, Venter H (2014) Expression, purification and functional reconstitution of FeoB, the ferrous iron transporter from *Pseudomonas aeruginosa*. *Protein Expr Purif* 101:138–145. <https://doi.org/10.1016/j.pep.2014.06.012>
- Seyedmohammad S, Fuentealba NA, Marriott RA, Goetze TA, Edwardson JM, Barrera NP, Venter H (2016) Structural model of FeoB, the iron transporter from *Pseudomonas aeruginosa*, predicts a cysteine lined, GTP-gated pore. *Biosci Rep* 36(2). <https://doi.org/10.1042/bsr20160046>
- Sheldon JR, Heinrichs DE (2015) Recent developments in understanding the iron acquisition strategies of gram positive pathogens. *FEMS Microbiol Rev* 39(4):592–630. <https://doi.org/10.1093/femsre/fuv009>
- Shih PM (2019) Early cyanobacteria and the innovation of microbial screens. *mBio* 10(3). <https://doi.org/10.1128/mBio.01262-19>
- Shin M, Mey AR, Payne SM (2019) FeoB contains a dual nucleotide-specific NTPase domain essential for ferrous iron uptake. *Proc Natl Acad Sci U S A* 116(10):4599–4604. <https://doi.org/10.1073/pnas.1817964116>
- Shin M, Park J, Jin Y, Kim IJ, Payne SM, Kim KH (2020) Biochemical characterization of bacterial FeoBs: a perspective on nucleotide specificity. *Arch Biochem Biophys* 685:108350. <https://doi.org/10.1016/j.abb.2020.108350>
- Silver S, Kralovic ML (1969) Manganese accumulation by *Escherichia coli*: evidence for a specific transport system. *Biochem Biophys Res Commun* 34(5):640–645. [https://doi.org/10.1016/0006-291x\(69\)90786-4](https://doi.org/10.1016/0006-291x(69)90786-4)

- Silver S, Johnseine P, King K (1970) Manganese active transport in *Escherichia coli*. J Bacteriol 104(3):1299–1306. <https://doi.org/10.1128/JB.104.3.1299-1306.1970>
- Simmons SL, Sievert SM, Frankel RB, Bazylnski DA, Edwards KJ (2004) Spatiotemporal distribution of marine magnetotactic bacteria in a seasonally stratified coastal salt pond. Appl Environ Microbiol 70(10):6230–6239. <https://doi.org/10.1128/AEM.70.10.6230-6239.2004>
- Skaar EP (2010) The battle for iron between bacterial pathogens and their vertebrate hosts. PLoS Pathog 6(8):e1000949. <https://doi.org/10.1371/journal.ppat.1000949>
- Smith AT, Sestok AE (2018) Expression and purification of functionally active ferrous iron transporter FeoB from *Klebsiella pneumoniae*. Protein Expr Purif 142:1–7. <https://doi.org/10.1016/j.pep.2017.09.007>
- Smith RL, Thompson LJ, Maguire ME (1995) Cloning and characterization of MgtE, a putative new class of Mg<sup>2+</sup> transporter from *Bacillus firmus* OF4. J Bacteriol 177(5):1233–1238. <https://doi.org/10.1128/jb.177.5.1233-1238.1995>
- Smith JA, Lovley DR, Tremblay PL (2013) Outer cell surface components essential for Fe(III) oxide reduction by *Geobacter metallireducens*. Appl Environ Microbiol 79(3):901–907. <https://doi.org/10.1128/AEM.02954-12>
- Smith AT, Linkous RO, Max NJ, Sestok AE, Szalai VA, Chacón KN (2019) The FeoC [4Fe–4S] cluster is redox-active and rapidly oxygen-sensitive. Biochemistry 58(49):4935–4949. <https://doi.org/10.1021/acs.biochem.9b00745>
- Soe CZ, Codd R (2014) Unsaturated macrocyclic dihydroxamic acid siderophores produced by *Shewanella putrefaciens* using precursor-directed biosynthesis. ACS Chem Biol 9(4):945–956. <https://doi.org/10.1021/cb400901j>
- Spiro S, Guest JR (1990) FNR and its role in oxygen-regulated gene expression in *Escherichia coli*. FEMS Microbiol Rev 6(4):399–428
- Stearman R, Yuan DS, Yamaguchi-Iwai Y, Klausner RD, Dancis A (1996) A permease-oxidase complex involved in high-affinity iron uptake in yeast. Science 271(5255):1552–1557. <https://doi.org/10.1126/science.271.5255.1552>
- Stevenson B, Wyckoff EE, Payne SM (2016) *Vibrio cholerae* FeoA, FeoB, and FeoC interact to form a complex. J Bacteriol 198(7):1160–1170. <https://doi.org/10.1128/jb.00930-15>
- Sturm A, Schierhorn A, Lindenstrauss U, Lilie H, Brüser T (2006) YcdB from *Escherichia coli* reveals a novel class of Tat-dependently translocated hemoproteins. J Biol Chem 281(20):13972–13978. <https://doi.org/10.1074/jbc.M511891200>
- Su YC, Chin KH, Hung HC, Shen GH, Wang AH, Chou SH (2010) Structure of *Stenotrophomonas maltophilia* FeoA complexed with zinc: a unique prokaryotic SH3-domain protein that possibly acts as a bacterial ferrous iron-transport activating factor. Acta Crystallogr Sect F Struct Biol Cryst Commun 66(Pt 6):636–642. <https://doi.org/10.1107/s1744309110013941>
- Suzuki T, Okamura Y, Calugay RJ, Takeyama H, Matsunaga T (2006) Global gene expression analysis of iron-inducible genes in *Magnetospirillum magneticum* AMB-1. J Bacteriol 188(6):2275–2279. <https://doi.org/10.1128/JB.188.6.2275-2279.2006>
- Suzuki T, Okamura Y, Arakaki A, Takeyama H, Matsunaga T (2007) Cytoplasmic ATPase involved in ferrous ion uptake from magnetotactic bacterium *Magnetospirillum magneticum* AMB-1. FEBS Lett 581(18):3443–3448. <https://doi.org/10.1016/j.febslet.2007.06.047>
- Taoka A, Umeyama C, Fukumori Y (2009) Identification of iron transporters expressed in the magnetotactic bacterium *Magnetospirillum magnetotacticum*. Curr Microbiol 58(2):177–181. <https://doi.org/10.1007/s00284-008-9305-7>
- Thomas-Charles CA, Zheng H, Palmer LE, Mena P, Thanassi DG, Furie MB (2013) FeoB-mediated uptake of iron by *Francisella tularensis*. Infect Immun 81(8):2828–2837. <https://doi.org/10.1128/iai.00170-13>
- Thormann KM, Saville RM, Shukla S, Pelletier DA, Spormann AM (2004) Initial phases of biofilm formation in *Shewanella oneidensis* MR-1. J Bacteriol 186(23):8096–8104. <https://doi.org/10.1128/JB.186.23.8096-8104.2004>
- Torrents E (2014) Ribonucleotide reductases: essential enzymes for bacterial life. Front Cell Infect Microbiol 4:52. <https://doi.org/10.3389/fcimb.2014.00052>

- Troxell B, Hassan HM (2013) Transcriptional regulation by ferric uptake regulator (Fur) in pathogenic bacteria. *Front Cell Infect Microbiol* 3:59. <https://doi.org/10.3389/fcimb.2013.00059>
- Uden G, Achebach S, Holighaus G, Tran HG, Wackwitz B, Zeuner Y (2002) Control of FNR function of *Escherichia coli* by O<sub>2</sub> and reducing conditions. *J Mol Microbiol Biotechnol* 4(3): 263–268
- Veeranagouda Y, Husain F, Boente R, Moore J, Smith CJ, Rocha ER, Patrick S, Wexler HM (2014) Deficiency of the ferrous iron transporter FeoAB is linked with metronidazole resistance in *Bacteroides fragilis*. *J Antimicrob Chemother* 69(10):2634–2643. <https://doi.org/10.1093/jac/dku219>
- Velayudhan J, Hughes NJ, McColm AA, Bagshaw J, Clayton CL, Andrews SC, Kelly DJ (2000) Iron acquisition and virulence in *Helicobacter pylori*: a major role for FeoB, a high-affinity ferrous iron transporter. *Mol Microbiol* 37(2):274–286
- Vetter IR, Wittinghofer A (2001) The guanine nucleotide-binding switch in three dimensions. *Science* 294(5545):1299–1304. <https://doi.org/10.1126/science.1062023>
- Weaver EA, Wyckoff EE, Mey AR, Morrison R, Payne SM (2013) FeoA and FeoC are essential components of the *Vibrio cholerae* ferrous iron uptake system, and FeoC interacts with FeoB. *J Bacteriol* 195(21):4826–4835. <https://doi.org/10.1128/jb.00738-13>
- Weber KA, Achenbach LA, Coates JD (2006) Microorganisms pumping iron: anaerobic microbial iron oxidation and reduction. *Nat Rev Microbiol* 4(10):752–764. <https://doi.org/10.1038/nrmicro1490>
- Wei Y, Fu D (2005) Selective metal binding to a membrane-embedded aspartate in the *Escherichia coli* metal transporter YiiP (FieF). *J Biol Chem* 280(40):33716–33724. <https://doi.org/10.1074/jbc.M506107200>
- Winterbourn CC (1995) Toxicity of iron and hydrogen peroxide: the Fenton reaction. *Toxicol Lett* 82-83:969–974
- Wittenberg JB, Bolognesi M, Wittenberg BA, Guertin M (2002) Truncated hemoglobins: a new family of hemoglobins widely distributed in bacteria, unicellular eukaryotes, and plants. *J Biol Chem* 277(2):871–874. <https://doi.org/10.1074/jbc.R100058200>
- Xia M, Wei J, Lei Y, Ying L (2007) A novel ferric reductase purified from *Magnetospirillum gryphiswaldense* MSR-1. *Curr Microbiol* 55(1):71–75. <https://doi.org/10.1007/s00284-007-0023-3>
- Zhang C, Meng X, Li N, Wang W, Sun Y, Jiang W, Guan G, Li Y (2013) Two bifunctional enzymes with ferric reduction ability play complementary roles during magnetosome synthesis in *Magnetospirillum gryphiswaldense* MSR-1. *J Bacteriol* 195(4):876–885. <https://doi.org/10.1128/JB.01750-12>
- Zhou D, Hardt WD, Galán JE (1999) *Salmonella typhimurium* encodes a putative iron transport system within the centisome 63 pathogenicity island. *Infect Immun* 67(4):1974–1981

# Chapter 13

## Pterin-Containing Microbial Molybdenum Enzymes



Mikayla C. Metzger and Partha Basu

**Abstract** In this chapter, several facets of microbial molybdenum enzymes are discussed. First, the sources and uptake of molybdenum into cells, as well as cofactor synthesis, are reviewed. Genes involved in cofactor synthesis are mentioned along with whether or not they have a well-defined function. The biogeochemical importance as well as evolutionary origin of the cofactor and relationship to phylogenetic classification are examined. Representative structures of microbial molybdenum enzymes from the three main families (xanthine oxidase, sulfite oxidase, and dimethyl sulfoxide (DMSO) reductase) are also included. The functions of these enzyme families have been well accepted. This chapter also highlights select general mechanisms that are still under discussion, such as oxygen atom transfer (OAT) and hydroxylation, as well as catalytic cycles of specific enzymes. The chapter also includes sections on amino acids near the metal center and other amino acids that influence either substrate specificity or mechanistic properties.

### 13.1 Introduction

Molybdenum is a 4d transition metal that is required for all forms of life, including microbial life. Naturally abundant molybdenum does not come in the metallic form; rather, it comes in the form of complex ores. In chemical compounds, molybdenum can be found in oxidation states from  $-2$  to  $+6$ . Higher oxidation states are pertinent to its biological roles and terrestrial occurrence. The very low oxidation states are typically found in organometallic compounds, and the remainder oxidation states are found in metal clusters. In the context of the enzyme function, this account will focus mostly on the higher oxidation states. There are more than 50 molybdenum enzymes known. They are broadly classified into two categories: one where molybdenum is in a multinuclear cluster and the other consists of mononuclear centers. The latter class

---

M. C. Metzger · P. Basu (✉)

Department of Chemistry & Chemical Biology, Indiana University - Purdue University  
Indianapolis, Indianapolis, IN, USA

e-mail: [basup@iupui.edu](mailto:basup@iupui.edu)

of enzymes also has a modified pterin cofactor that binds the molybdenum. This account focuses on the pterin-containing molybdenum enzymes and specifically emphasizes those that are from microbial sources. In the text, the pterin-containing molybdenum enzymes are referred to simply as molybdenum enzymes. This chapter focuses on the most pertinent reports on structure and reactivity of the pterin-containing molybdenum enzymes of three families, and the biosynthesis of the cofactor and throughout the chapter, relevant references have been made to related eukaryotic partners.

## 13.2 The Molybdenum Cofactors

The molybdenum cofactor comes in many flavors with different nucleotides or no nucleotides, as discussed below; therefore, they should be called molybdenum cofactors, like hemes. This section discusses different aspects of molybdenum cofactors.

### 13.2.1 Source of Molybdenum

Molybdenum-containing minerals have been known for a long time. It was first discovered as a new material by Carl Wilhelm Scheele (Lundgren 2021) and was first isolated from molybdenite by Peter Jacob Hjelm (Britannica 2020). Molybdenum can exist in many different forms with varying redox states, but molybdate is the most oxidized form where Mo exists in the +6 oxidation state.

Molybdate is water-soluble and is known to be nearly uniformly distributed in oceanic water columns and the predominant species is  $[\text{MoO}_4]^{2-}$  in a wide pH range and oxygen fugacity (Fig. 13.1) (Smedley and Kinniburgh 2017). The high water solubility of molybdate leads to its near-universal distribution in biology. The first implication that molybdenum may be important in biology was proposed by Bortels, who demonstrated its catalytic function in fixing nitrogen by *Azotobacter chroococcum*, a free-living bacterium (Bortels 1930). Today, molybdenum is considered to be an essential transition metal and is known to be present in all phyla of life, and molybdenum-containing enzymes are considered to provide vitality in diverse microbial lives (Coughlan 1983; Hille 1996). While the first molybdenum enzyme was reported nearly a century ago, in the past four decades the field has matured, in part, due to the crystallographic characterization of many molybdenum enzymes. More than 50 molybdenum enzymes have been biochemically characterized, and genomic and bioinformatic information suggests many more to be characterized (Hille et al. 2014). This is especially exciting as more microbes are being discovered and sequenced, which promises continuous growth of the field (Zhang and Zheng 2020). These enzymes catalyze numerous reactions that are important to



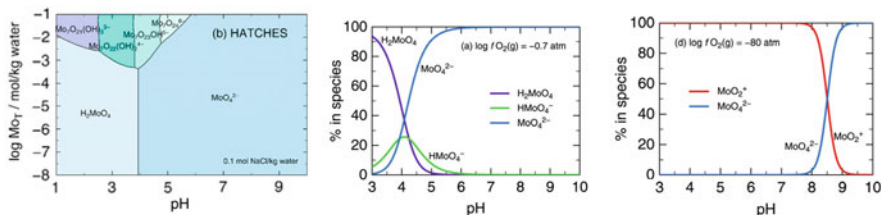


**Fig. 13.1** Left panel: predominance diagram showing the dominant species in the Mo-H<sub>2</sub>O system calculated using HATCHES thermodynamic databases; middle and right panels: calculated variation in the aqueous speciation of molybdenum based on data from the HATCHES database showing the redox status is controlled by equilibration with an atmosphere as a function of oxygen fugacity: -0.7 atm (near atmospheric) and -80 atm (strongly anoxic). The total Mo concentration is 10<sup>-4</sup> mol/kg water in all cases and the background solution contained 0.01 mol NaCl/kg water. As one can see, under biological conditions, the most prevalent species is the MoO<sub>4</sub><sup>2-</sup>. Taken from Smedley and Kinniburgh (2017)

the microbial life processes. This chapter focuses on pterin-containing molybdenum enzymes.

### 13.2.2 Transport of Molybdenum

Comparative genomic analyses have revealed a widespread utilization of Mo in all three domains of life. In the environment, the source of molybdenum for cells is molybdate. Even though molybdenum is transported into the cell in the molybdate +6 oxidation state, it can be reduced, and in most molybdenum enzymes under physiological conditions the molybdenum can shuttle between the oxidation states of +4 and +6. The molybdate ions are transported into the cell via a high-affinity ATP binding cassette (ABC) transporter, ModABC system (Hollenstein et al. 2007). In *Escherichia coli*, the system consists of a periplasmic molybdate binding protein ModA, two integral membrane proteins of the ModB family, and hydrophilic membrane ModC ATPase proteins (Rech et al. 1996). Interestingly, a separate system (TupABC) exists for tungstate transport even though the sizes of these two tetrahedral dianionic oxyanions are very similar (Aguilar-Barajas et al. 2011; Makdessi et al. 2001). In addition, there is another transport system, i.e., WtpABC, can bind both molybdate and tungstate (Hagen 2011). Site-directed mutagenesis studies have shown that in WtpA, an aspartate residue may confer the substrate (tungstate) selectivity. In organisms that lack the *modABC* genes, molybdenum can be taken up by nonspecific transporters such as sulfate transporters or by lower affinity Mo uptake systems, e.g., the MolBCA transporter system found in certain strains of *Haemophilus influenzae* (Tirado-Lee et al. 2011; Rice et al. 2014; Zhong et al. 2020). A defect in the Mo uptake system is likely to lower the availability of molybdenum for cellular incorporation into the Mo enzymes and may result in a partial or complete loss of functions relating to Mo enzymes. For example, *E.coli*

BL21 (DE3) strain does not possess the genes required for the molybdate transport system (*mod* operon) or the molybdenum-responsive transcriptional regulator (ModE) and is naturally devoid of molybdenum-dependent formate dehydrogenase (Fdh) and nitrate reductase activity (Pinske et al. 2011). Such a defect reduces mature molybdopterin enzyme production; however, supplementation of growth media with excess molybdate permits the production of molybdopterin enzymes with limited cofactor incorporation. The addition of a plasmid containing the fumarate nitrate reductase regulator (*fnr*) gene and media supplementation with molybdate, allowed formate-dependent hydrogen production, and nitrate reductase activity could be restored, albeit to 25–30% of an *E. coli* K12 strain. The observed formate dehydrogenase activity was due to the Fdh-H homolog, while activity for the Fdh-N homolog could not be restored. The addition of ModE could only partially restore the activities of both Fdh enzymes. In pathogenic bacteria, a high-affinity uptake of molybdate is important, as they may be competing with the host for molybdate. Molybdate concentrations are known to be <1 µg of molybdenum per 1 g of wet organ/ash in body places affected by pathogenic bacteria, e.g., the GI tract, lung, bladder, and uterus (Schroeder et al. 1970).

### 13.2.3 Molybdenum Cofactor (Moco) Biosynthesis

The chemical nature of the molybdenum cofactor (Moco) was first proposed by Rajagopalan and coworkers, where a unique 1,2-ene-dithiolate moiety, appended to a pterin functionality, was proposed to bind the molybdenum atom (Rajagopalan and Johnson 1992; Johnson et al. 1980). Later, crystallographic studies confirmed the binding of the molybdenum atom by the 1,2-ene-dithiolate moiety. In addition, the crystallographic studies revealed a third ring, i.e., the pyran ring, of the pterin cofactor. Thus, in Moco, there are four rings, including the chelate ring where Mo is bound. In bacterial enzymes, this basic structure is modified with the addition of nucleotides to the phosphate group of the Moco forming molybdopterin guanine dinucleotide (MGD) or molybdopterin cytosine dinucleotide (MCD) (Fischer et al. 1998). The cofactor with the basic phosphate without any nucleotide is called molybdopterin (MPT), and because it exists in form with a pyran ring fused with the pterin at the 6,7-position, it is also referred to as pyranopterin. In general, the enzymes of the xanthine oxidase (XO) family harbor either MPT or MCD as a cofactor. Enzymes of the sulfite oxidase (SO) family contain the MPT form while enzymes of the DMSO reductase family exclusively contain the MGD cofactor (Grimaldi et al. 2013).

The biosynthesis of Moco is a complex, coordinated, and conserved process that was unraveled by purifying and conducting enzymatic processes of the respective enzymes. In *E. coli*, several gene products (MoaA, MoaC, MobA, MocA, MoaD, MoaE, MoeA, MoeB, and MogA), organized in distinct loci, are involved in the biosynthesis of Moco (Fig. 13.2). The biosynthesis of the basic Moco involves three steps: (13.1) cyclization of 5'-GTP to form a 6-alkyl pterin with a cyclic phosphate

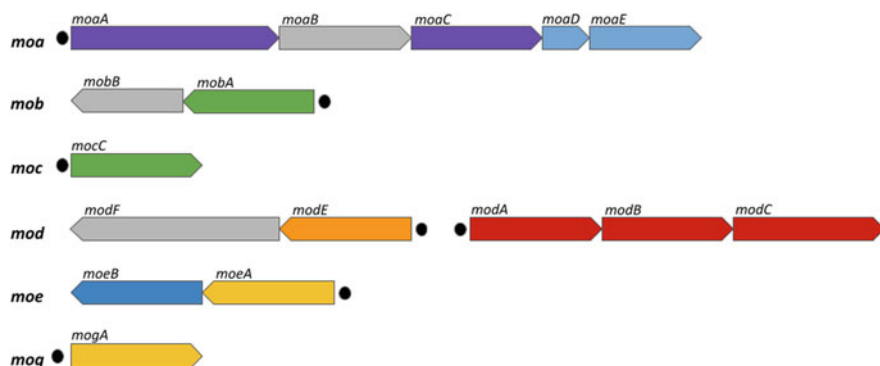


**Fig. 13.2** Genes involved in Moco biosynthesis in *E. coli*. There are 16 genes grouped into six loci. The loci are labeled on the left side: *moa*, *mob*, *moc*, *mod*, *moe*, and *mog*. The genes are colored based upon their function: red is Mo transport; purple is cPMP biosynthesis; blue is MPT synthesis; gold is molybdenum ligation; green is nucleotide addition; orange is a transcriptional regulator. The functions of genes with gray color are yet to be well defined. The genes are drawn approximately to scale. The black dots represent the promoter regions

group at the C2' and C4' atoms (cPMP) intermediate, also referred to as Precursor Z; (2) sulfuration of cPMP to give the mature MPT; and (3) coordination of molybdate to the ene-dithiolate (Iobbi-Nivol and Leimkühler 2013; Leimkühler and Iobbi-Nivol 2015; Leimkühler 2020).

In bacterial systems, the first step is catalyzed by two proteins, MoaA and MoaC. MoaA belongs to the superfamily of S-adenosylmethionine (SAM) dependent radical enzymes, and X-ray structures of this enzyme from several sources have been reported, which harbors two [4Fe-4S] clusters, both coordinated by three cysteine residues. The fourth position in the N-terminal cluster is occupied by the aminoacyl end of SAM, bound in a bidentate fashion, while that of the C-terminal cluster is occupied by the exocyclic amino group of GTP. MoaA catalyzes the H-atom abstraction and reductive cleavage, generating 5-deoxyadenosyl radical and a radical migration results in (8*S*)-3',8-cyclo-7,8-dihydroguanosine 5'-triphosphate (3',8- $\text{cH}_2\text{GTP}$ ). The crystal structures of MoaC from different organisms have been reported. The basic structure is an  $\alpha_2$  dimer. MoaC converts 3',8- $\text{cH}_2\text{GTP}$  to cPMP through cleavage of pyrophosphate resulting in the cyclic phosphate in cPMP.

The second step in the biosynthesis is the conversion of cPMP to MPT by inserting two sulfur atoms at the C1' and C2' positions that results in the formation of an ene-dithiolate functionality. In bacteria, this reaction is catalyzed by MPT synthase, an  $(\alpha\beta)_2$  heterotetramer consisting of two equivalents each of the MoaD and MoaE subunits. The required sulfur atoms are provided by a thiocarboxylate group present at the C terminus of MoaD. Two MoaD molecules are required for the sulfur insertion, and the insertion occurs on cPMP bound to MoaE; each MoaE subunit acts independently, allowing the interaction of two MoaD molecules. The sulfur insertions occur in a stepwise fashion, with the first sulfur atom inserted into the C2' position followed by the C1' position of the cPMP. This reaction occurs

together with the hydrolysis of cPMP. After the insertion of the second sulfur atom, MoaD is released.

For catalysis to continue, thiocarboxylate group in MoaD is regenerated. This is catalyzed by MoeB by forming a MoaD•MoeB complex followed by  $Mg^{2+}$ -ATP-dependent adenylation of the C-terminus of MoaD. It is this acyl adenylate form of MoaD, still in complex with MoeB, that reacts with the sulfur donor, such as the cysteine desulfurase (IscS) in *E. coli*. It is notable that IscS is a pyridoxal phosphate-dependent cysteine desulfurase that transfers the sulfur from a substrate, cysteine, to an active site cysteine residue of the enzyme forming a persulfide, releasing the remainder of the substrate cysteine as alanine. This persulfide attacks the adenylated MoaD C-terminus, releasing AMP and creating a transient perthiocarboxylate linkage between IscS and MoaD. This perthiocarboxylate molecule is reductively cleaved, releasing MoaD-SH.

The insertion of molybdenum serves as the third step in the biosynthesis of the molybdenum cofactor in the basic form. In *E. coli*, the gene products MogA and MoeA add the molybdenum into the pterin cofactor. In the process, MogA forms an adenylated MPT intermediate prior to insertion of the metal. Crystal structures of the *E. coli* MogA enzyme show that it forms a trimeric structure (Liu et al. 2000). In any event, the intermediate is transferred to MoeA where molybdenum is inserted from  $MoO_4^{2-}$  under low concentrations. The molybdenum is coordinated by the dithiolene moiety of the cofactor and is present in a trioxo-Mo moiety. In the enzymes, where only one pterin cofactor is present, this newly formed cofactor can be modified either through the addition of a nucleotide or coordination to molybdenum by an amino acid residue. The trioxo-Mo center is reduced to its dioxo-Mo form in enzymes of the sulfite oxidase family (vide infra).

Some bacterial XO family enzymes, however, contain the MCD form of the cofactor. The formation of the MCD cofactor is catalyzed by MocA, a protein similar in sequence to MobA. MocA acts like a CTP transferase where the MPT is linked with CMP. In this case, the end product is the MCD cofactor, not bis-Mo-MCD. In addition, members of the XO family have one terminal sulfido group, which is installed after formation of the MCD/MGD cofactor.

In bacterial enzymes, the terminal phosphate group is connected to a nucleotide such as GMP or CMP, and the members of the DMSO reductase family have two equivalents of the pterin cofactor per molybdenum. The  $Mo(MPT)_2$  complex is formed first from the basic molybdenum cofactor, and the cofactor is modified to incorporate GMP, and GMP incorporation is catalyzed by MobA. For this reaction to proceed, formation of the basic cofactor with molybdenum is essential. After the addition of the nucleotide, the mature  $Mo(MGD)_2$  cofactor is released from MobA. Because molybdenum cofactors are inherently unstable, molybdenum binding chaperones bind the cofactor and transport it to the enzyme site where they are incorporated.

In molybdenum enzymes, the incorporation of the cofactor is the last step for the biosynthesis of the target enzymes. In many bacterial enzymes, other prosthetic groups such as heme, FeS cluster, or flavin are present; and these prosthetic groups are inserted prior to the insertion of the molybdenum cofactor (Moco) (Mendel and

Leimkuhler 2015). Once the Moco is inserted, the protein folds properly, resulting in the active enzyme.

### 13.2.4 Moco Insertion and Holo Enzyme Formation

The Moco insertion step is catalyzed by variant-specific Moco-binding chaperone (Leimkuhler 2020). The studies on *E.coli* TMAO reductase TorD/TorA system are revealing (Pommier et al. 1998; Jack et al. 2004), which were subsequently also investigated in *Shewanella* (Dos Santos et al. 1998). Here, TorD plays a direct role in the insertion of Moco in apo TorA (Giudici-Ortoni et al. 2003). In *E.coli* respiratory nitrate reductase, NarJ serves as the chaperone of NarGHI; NarW is the chaperone of NarZYV; DmsD is the chaperone in DmsABC and YnfE/F; NapD is the chaperone for NapA; and in FDH, FdFD serves as the chaperone for FdhF. Crystal structures of TorD, DmsD, NarJ, and NapD have been reported. Interestingly, these chaperones are also called redox enzyme maturation proteins (REMP) (Mintmier et al. 2020).

Molecular chaperones have been identified in the XO family. For example, in *Rhodobacter capsulatus* XDH has XdhC as the molecular chaperon. Thus far, no molecular chaperone has been identified in the SO family, where the structure of the basic cofactor is not significantly modified. In this case, the MPT cofactor may be directly given to the enzyme in question and MoeA protein may catalyze this reaction.

In general, mutations in any of the genes in the Moco biosynthesis pathway completely abolish the formation of a functional cofactor, leading to a loss of activity for all Mo enzymes and results in a pleiotropic phenotype. This has been demonstrated in *Mycobacterium tuberculosis* and pathogenic Enterobacteriaceae, where regardless of which Moco biosynthetic enzyme was lost, the mutant strains displayed significantly reduced fitness and virulence in host–pathogen interactions (Contreras et al. 1997; Levillain et al. 2017; Hughes et al. 2017). In humans, such a defect causes severe physiological disorder (Schwarz et al. 2009).

## 13.3 Families of Molybdenum Enzymes and Their Roles

### 13.3.1 Classification

As mentioned earlier, molybdenum enzymes come in two flavors: one in which molybdenum is incorporated into a [MoFe<sub>7</sub>S<sub>9</sub>] cluster as in the active site of nitrogenase, and in the other, molybdenum is coordinated by a complex pterin containing cofactor called pyranopterin, also known as molybdopterin (Schwarz et al. 2009). The molybdenum-bound form of the pterin cofactor is called molybdopterin (Moco), and this chapter focuses on the Moco-containing enzymes.

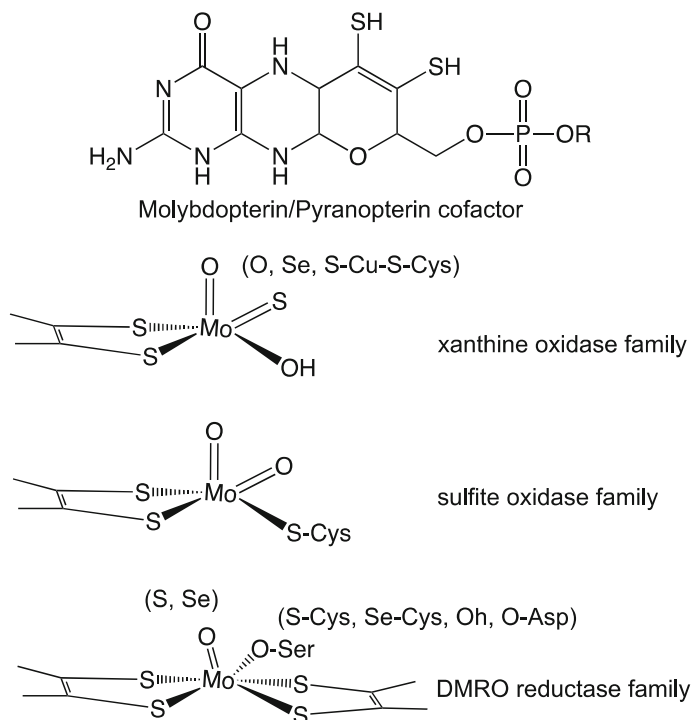


**Fig. 13.3** Structure of the molybdopterin/pyranopterin and the structures of molybdenum centers found in the Moco-containing enzymes

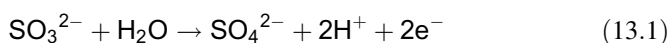
The Moco enzymes fall into three large families that are mutually exclusive. These are the xanthine oxidase (XO) family, the sulfite oxidase (SO) family, and the DMSO reductase (DMSOR) family, named after their prototype members, and each family can be further subdivided based on function (Hille 1996). More recently, a novel molybdenum enzyme family has been found in bacteria (YcbX and YiiM) (Kozmin et al. 2008). Members of that family are similar to the eukaryotic analog mitochondrial amidoxime reducing component, mARC) (Sparacino-Watkins et al. 2014b; Havemeyer et al. 2006). These enzymes exhibit Moco-dependent catalytic activity and exhibit a high degree of sequence similarities to the C-terminus of the Moco-binding domain of eukaryotic Moco sulfurase. All three families have been found in bacteria. The molybdenum centers in these families are represented in Fig. 13.3.

**The Xanthine Oxidase (XO) Family** Historically, the members of this family, i.e., xanthine oxidase (XO) and aldehyde oxidase (AO), were studied from mammalian sources, although similar microbial enzymes have been investigated. Enzymes of this family generally catalyze hydroxylation reactions, carried out at the Moco center, and are inhibited by cyanide. Enzymes of this family generally have a FAD, and [Fe-S] clusters in addition to the Moco center. One of the essential features

of this family of enzymes is the presence of a terminal sulfido group at the equatorial position. While the majority of the enzymes have a terminal sulfido group, nicotinate dehydrogenase has a terminal selenido group. Another interesting feature in this family is the absence of any protein-derived ligation to molybdenum. Although there is no protein-derived ligand to Mo, several residues near the catalytic center are thought to be involved in the proton transfer pathway. In addition, members of the family have the phosphate group of the cofactor modified with CMP nucleotide, forming molybdopterin cytosine dinucleotide (MCD).

Among the well-characterized enzymes of this family are xanthine dehydrogenase from *Rhodobacter capsulatus* (Truglio et al. 2002), aldehyde oxidoreductase from *Desulfovibrio gigas* (Romao et al. 1995), quinoline 2- oxidoreductase from *Pseudomonas putida* (Bonin et al. 2004), nicotinate dehydrogenase from *Eubacterium barkeri* (Wagener et al. 2009), CO dehydrogenase (CODH) from *Afpia carboxidovorans* (previously known as *Oligotropha carboxidovorans*) (Dobbek et al. 2002), and 4-hydroxy benzoyl CoA reductase from *Thauera aromatica* (Unciuleac et al. 2004). CODH from *A. carboxidovorans* and *Hydrogenophaga pseudoflava* have been characterized in detail (Meyer et al. 1986). These aerobic organisms can grow on CO as their sole source of carbon as well as energy. CODH catalyzes the transformation of CO to CO<sub>2</sub> with the release of two protons and two electrons. The produced CO<sub>2</sub> can be fixed via the reductive pentose pathway, a process that has significant environmental consequences (King and Weber 2007).

**The Sulfite Oxidase (SO) Family** Since the original classification of the sulfite oxidase (SO) enzyme family, more enzymes of the same class have been reported, and this family has also been called the sulfite-oxidizing family. Members of this family often contain b-type heme groups that act as additional redox centers. Based on their ability to transfer electrons to molecular oxygen, two types of molybdenum-containing SO enzymes are usually distinguished: sulfite oxidases which use molecular oxygen as an electron acceptor, and sulfite dehydrogenases which use other electron acceptors such as cytochrome c. The general reaction catalyzed by these enzymes is shown in Eq. 13.1. In systems where oxygen serves as the electron acceptor, hydrogen peroxide is produced, while in sulfite dehydrogenases, cytochrome c is the electron acceptor (Kappler 2011).



An important process for living organisms is the repair of oxidative damage to proteins associated with the formation of methionine sulfoxide. This reparation is possible due to the presence of the ubiquitous methionine sulfoxide reductase enzymes (Msr), which catalyze the reduction of methionine sulfoxide into methionine. A newly discovered type of Msr in Gram-negative bacteria appears to be involved in the repair of periplasmic proteins that have been oxidized by hypochlorous acid (HClO). HClO is generated within phagocytic cells of the mammalian innate immune system to kill pathogens that have been internalized. Hypochlorous acid is a powerful antimicrobial agent and has the capability to

oxidize methionine residues into methionine sulfoxide, leading to protein misfolding, loss of cellular function, and aggregation (Juillan-Binard et al. 2017).

This newfound methionine sulfoxide reductase system, named MsrPQ, involves two proteins that are encoded in the same operon. The first protein, MsrP, carries out the Msr activity and is a periplasmic soluble protein with a Moco active site. It was previously named YedY until its Msr activity was discovered (Juillan-Binard et al. 2017). In order for MsrP to be functional *in vivo*, it has to be specifically associated with MsrQ. This second protein MsrQ was previously named YedZ, and it is an integral b-type heme-containing membrane-spanning protein. MsrQ was proposed to be the specific electron donor for MsrP, allowing catalysis of methionine sulfoxide reduction. MsrQ has been characterized by bioinformatics and classified as a member of the ferric reductase domain (FRD) superfamily of heme-containing membrane proteins.

**The Dimethyl Sulfoxide Reductase (DMSOR) Family** Members of the DMSO reductase family typically catalyze a proper oxygen atom transfer reaction to or from an available substrate. In this way, they are similar to enzymes from the sulfite oxidase family. This family is the most diverse in terms of their active site structure and the reactions that they catalyze. The DMSO reductase family comprises enzymes from bacteria and archaea like dimethyl sulfoxide reductase (DMSOR), trimethylamine oxidoreductase (TMAOR), dissimilatory nitrate reductase (Nar), formate dehydrogenase (Fdh), polysulfide reductases, arsenite oxidases, and formylmethanofuran dehydrogenase. Prosthetic groups found in members of the enzyme family are, in addition to the Mo(MGD)<sub>2</sub> moiety at the active site, [2Fe-2S], [3Fe-4S], and [4Fe-4S] clusters, b-type heme groups, or flavin groups (Sigel and Sigel 2002).

Because many of these enzymes also contain an iron–sulfur cluster, they are also called the complex iron–sulfur molybdoenzyme (CISM) family (Rothery et al. 2008). This family of enzymes is comprised of: (i) a molybdenum cofactor (Moco)-containing a catalytic subunit that also contains a [4Fe-4S] cluster (FS0); (ii) a four-cluster protein (FCP) subunit that contains four [Fe-S] clusters (FS1 to FS4); and (iii) a membrane anchor protein (MAP) subunit which anchors the catalytic and FCP subunits to the membrane.

The catalytic subunit provides three functionalities: (i) a molecular scaffold for the complex and highly labile Moco; (ii) a substrate-binding channel allowing facile substrate entry and egress to and from the site of catalysis at the Mo center; and (iii) the segment of the electron transfer relay that incorporates the FS0 cluster leading to or from the [Fe-S] clusters of the FCP. In some members of the CISM family, the catalytic subunit is located in the periplasm, while in others, it is targeted to the inner surface of the cytoplasmic membrane. The core structure of the catalytic subunit of a CISM is that of the DMSO reductase (DMSOR) from *Rhodobacter capsulatus* (*Rc*) and *Cereibacter sphaeroides* (*Rs*) (previously known as *Rhodobacter sphaeroides*). This basic structure is modified by the inclusion of a Fe-S cluster, and as the size of the protein increases, additional domains are added. The CISM family includes numerous enzymes of different sizes and complexities. While several enzymes of



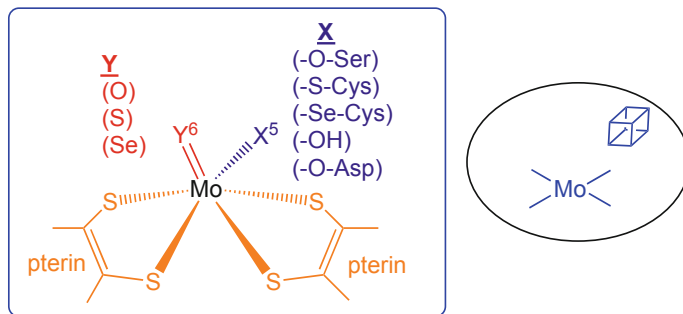


**Fig. 13.4** Schematic representation of the Mo coordination sites in the DMSOR family of enzymes (left) and the most common arrangement of prosthetic groups (right). The cube represents a [4Fe-4S] cluster

this family have been characterized, many more are yet to be isolated (Peng et al. 2018).

Several members of this family have been crystallographically characterized, and that has provided clarity of the active site structure. The trigonal prismatic Mo-center is coordinated by four sulfur donors from two molybdopterin (MPT) cofactors, and the 5th and 6th positions vary depending on the enzyme (Fig. 13.4). The 5th position (X in Fig. 13.4) is occupied by a coordinated amino acid residue, and the 6th position is defined as the terminal position (Y in Fig. 13.4). Thus, there is considerable diversity among members of the DMSOR with respect to the identity of the amino acid residue coordinating the Mo-center and the nature of the Mo = Y ligand in the oxidized form of the enzyme (Y = O, S, Se). It has been proposed that many enzymes in the DMSOR family use oxygen atom transfer (OAT) reactions for substrate transformation (*vide infra*).

### 13.3.2 Role of Molybdenum Enzymes in Biogeochemistry

Molybdenum enzymes play important roles in the biogeochemical cycling of several elements, and perhaps the most significant one is in the biogeochemical cycle of nitrogen (Stiefel 1993). The reservoirs of nitrogen are soil, where nitrogen is present mostly as organic material, water where nitrogen is present as nitrate and nitrite, and air where nitrogen mostly is in its elemental form also termed dinitrogen. In order for nitrogen to be assimilated into cellular mass, it must be in the reduced form as in ammonia. The reduced states are formed from the decomposition of organonitrogen materials, reduction of aqueous nitrate and reduction of atmosphere dinitrogen. In each of these processes, molybdenum enzymes are involved.

Organonitrogen compounds are decomposed via their hydroxylation reactions catalyzed by Mo enzymes, represented by xanthine oxidase, aldehyde oxidase, quinoline oxidase, and picolinic acid dehydrogenase. The hydroxylated species

subsequently undergo hydrolytic or oxidative deconstruction leading to reduced nitrogen species. Inorganic nitrogen species such as nitrate is reduced by nitrate reductases, again molybdenum enzymes, to nitrite, which subsequently either generates dinitrogen in a dissimilatory process or is reduced to ammonia via assimilatory or dissimilatory processes. Organic nitrogen oxides such as trimethylamine oxide (TMAO), which is reduced by TMAO reductase to trimethyl amine (TMA). The dinitrogen molecules are reduced to ammonia by nitrogenase enzymes. Regardless of the process, microbial Mo enzymes are involved, thus providing biogeochemical vitality.

In the sulfur cycle, molybdenum enzymes are involved in the redox transformation of organosulfur compounds (Stiefel 1993). For example, DMSO reductase is involved in the reduction of DMSO to DMS. The oxidation of volatile DMS can lead to methylsulfonic acid, a compound implicated in cloud nucleation, especially over oceans. This creation of methylsulfonic acid is considered to be a key part of temperature control in the Gaia hypothesis. Other organic sulfur oxides such as methionine sulfoxide are reduced to methionine by methionine sulfoxide reductase (MSOR), and biotin sulfoxide is reduced by biotin sulfoxide reductase (BSOR). Inorganic sulfur oxides exist, such as tetrathionate that is reduced to thiosulfate by tetrathionate reductase. Similarly, polysulfide reductase reduces polysulfide to hydrogen sulfide. Sulfite oxidase is involved in oxidizing sulfite to sulfate, although the effect of sulfite oxidase in the geochemical cycling of sulfur is less studied (Bilen and Dick 2011). Thus, these microbial Mo enzymes play a crucial role in the biogeochemical cycling of sulfur.

In the carbon cycle, CO<sub>2</sub> is fixed through processes that include conversion of methylfuran to formylmethylfuran by formylmethanofuran dehydrogenase. This same enzyme is important to methanogenic microbial process that can be used for fixing CO<sub>2</sub>. Other Mo enzymes such as arsenate reductase reduce arsenate to arsenite, and arsenite oxidase oxidizes arsenite to arsenate. Both of these processes are important in the cycling of arsenic biogeochemically. These enzymes have been isolated from organisms that grow in arsenic-rich environments (Oremland and Stolz 2003). Several of them have been biochemically (Afkar et al. 2003; Krafft and Macy 1998) and structurally characterized (Warelow et al. 2013; Ellis et al. 2001; Glasser et al. 2018). Similarly, chlorate and perchlorate reductase reduce chlorate and perchlorate, respectively. These enzymes have not been studied as extensively (Youngblut et al. 2016); however, they too may play a role in the biogeochemistry of the chlorine cycle. Finally, while some molybdenum enzymes have selenium in their active site either in the form of selenocysteine or a terminal selenido, molybdenum enzymes can also transform selenite to elemental selenium (Wells et al. 2019). This is a new development, and more information is to come in the future (Wells et al. 2021).

### 13.3.3 *Origin of Molybdenum Enzymes*

As expected, analysis of prokaryotic genomes has revealed a wide distribution of genes encoding Moco biosynthesis and Mo-containing proteins. In nearly all organisms, both Moco biosynthesis proteins and known molybdoenzymes are found together (Zhang and Gladyshev 2008). The joint absence of them suggests a correspondence between the occurrence of the Moco biosynthesis trait and Moco-dependent enzymes. In bacteria, with the exception of the XO family, other Moco-containing enzymes are widespread. Among these, the DMSO reductase family is most widespread and is largely represented by nitrate reductase and formate dehydrogenase. Many organisms possessed two or three Moco-containing protein families and there are several subfamilies within these families. However, the low occurrence or absence of SO and XO families in some phyla (e.g., SO in Firmicutes/Clostridia, Bacteroidetes, Chlorobi, XO in Chlorobi, Cyanobacteria, Epsilonproteobacteria, and several Gammaproteobacteria clades), most of which possess the DMSOR family, suggested an independent relationship among molybdoenzymes.

Several researchers have used the catalytic subunit, particularly those of the DMSO reductase family, for phylogenetic analysis to understand the branching points in the evolution of these enzymes (Rothery et al. 2008; Schoepp-Cothenet et al. 2012). Interest in phylogenetic analysis of the DMSO reductase family stems from their prevalence in archaea and bacteria, and they are believed to be the core components of the first anaerobic respiratory chains and thus present at life's origins (Schoepp-Cothenet et al. 2013; Schoepp-Cothenet et al. 2012; Sousa et al. 2013). As mentioned, reactions catalyzed by these enzymes are integral components of the carbon, nitrogen, and sulfur biogeochemical cycles, as well as the biogeochemical cycles of arsenic and selenium (Stolz et al. 2002; Stolz et al. 2006). Of these, arsenic metabolism has been considered to be an important marker in evolution as it has previously been documented in 2.72 billion year old stromatolites. This provides convincing evidence that arsenic cycling was, in fact, an active feature of Neoproterozoic environments (Sforna et al. 2014). During aerobic (Stolz et al. 2006) and anaerobic (Zargar et al. 2012; Zargar et al. 2010) respiration, arsenite can serve as an electron donor to stimulate chemolithoautotrophic growth as well as being utilized as an electron donor for photolithoautotrophic growth during anoxygenic photosynthesis (Kulp et al. 2008). The ability to use arsenate as a terminal electron acceptor during anaerobic respiration is a trait found among phylogenetically diverse *Bacteria* and *Archaea* (Oremland et al. 2009).

Of the three (i.e., XO, SO, and DMSOR) molybdoenzyme families, SO and XO span all three domains of life. It has been suggested that if a protein family has representatives in all domains of life, then that protein may have been present in the last universal common ancestor (LUCA) (Doolittle 2000). Therefore, it has been suggested that the SO and XO families had an evolved form in the common ancestor. Indeed, phylogenetic analysis of the molybdenum enzyme families suggests that several members had been present before the divergence between archaea and

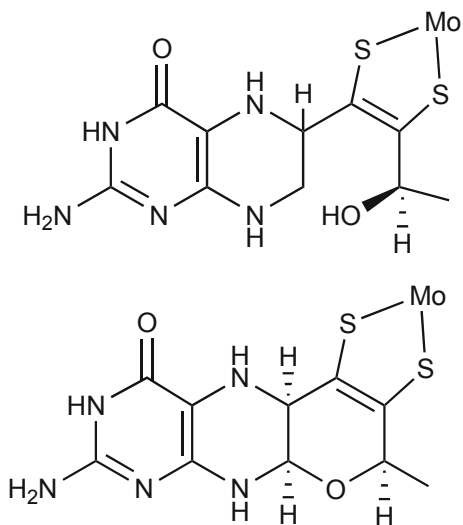
bacteria, i.e., in the LUCA. In contrast, the DMSOR families show a more limited occurrence and are detected only in prokaryotes (Zhang and Gladyshev 2008).

Rigorous phylogenetic analyses of the DMSOR members and their closely related lineages has revealed several novel insights into the evolution of DMSO reductases (Wells et al. 2020). That analysis supports a hydrogenotrophic methanogenic origin for this family, with formylmethanofuran dehydrogenase subunit B (FwdB/FmdB) constituting the most deeply branching lineage. It also shows that the 21st amino acid selenocysteine (Sec) is likely the ancestral ligand for the Mo/W atom of the Mo/W(MGD)<sub>2</sub> cofactor. In addition, it demonstrates that the arsenate reductase (ArxA/ArrA) lineage is more deeply rooted in the tree topology than is arsenite oxidase (AioA). Moreover, it reveals that the AioA diversified from the assimilatory nitrate reductase lineage rather than constituting a primordial enzyme present in LUCA.

### 13.4 Structures of Molybdenum Enzymes

In the past three decades, crystal structures of several molybdenum enzymes have been determined. In the majority of these cases, the molybdopterin cofactor is found to be tricyclic in nature with the pyran ring intact; however, in respiratory nitrate reductase and in ethylbenzene dehydrogenase, the pyran ring was found to be open (Fig. 13.5). Pterins are redox active molecules, and the redox states are defined by the number of hydrogen atoms in the pyrazine ring, such as the dihydro and tetrahydro pterins (Basu and Burgmayer 2011). In all cases, the pterin ring was found to be distorted, and the extent of distortion can be indicative of the redox state of the pterin. For the members of the DMSOR family, the pterin that is closer to the

**Fig. 13.5** Schematic representation of the molybdenum cofactor in pyran ring open form (top) and pyran ring close form (bottom)



[4Fe-4S] cluster is termed as the proximal (P) pterin, and the other pterin is designated as the distal (D) pterin. This designation is not to be confused with the crystallographic description of P and Q pterins. A detailed analysis showed that the two pyranopterins of the DMSOR family members exhibit distinct conformations. The P-pterins are similar to a tetrahydro form while the D-pterins exhibit a dihydro pterin conformation. Enzymes with a single pyranopterin, i.e., the members of the XDH or SO families, exhibit pyranopterin conformations similar to those of tetrahydro and dihydro forms, respectively (Rothery et al. 2012). Additionally, the Mo centers are placed  $\sim 15$  Å from the surface, which also influences the redox potentials (Basu et al. 2003). Moreover, crystal structures are often determined with highly intense X-ray radiation from synchrotron facilities, which causes photoreduction of the metal center. George argued that most of the crystal structures of molybdenum enzymes are thus in the reduced form and the data are to be interpreted with caution (George et al. 2012; Pushie and George 2011).

### 13.4.1 Microbial Xanthine Oxidase

The crystal structures of several molybdenum hydroxylases are known, e.g., aldehyde oxidoreductase (AOR) from *Desulfovibrio gigas* (Romao et al. 1995) and xanthine dehydrogenase (XDH) from *Rhodobacter capsulatus* (Truglio et al. 2002). In addition, the structure of carbon monoxide dehydrogenase from *A. carboxidovorans*, an enzyme that catalyzes CO oxidation to CO<sub>2</sub> without cleavage of a C–H bond and bears strong structural homology to the proper molybdenum hydroxylases, has been reported. These enzymes possess the same overall architecture, with a pair of [2Fe–2S] clusters in separate domains at the N-terminus, FAD in a third domain (absent in the *D. gigas* enzyme), and the molybdenum-binding portion of the protein is at the C-terminus, with the molybdenum center at the interface of two elongated domains that lie across one another at an angle of approximately 90°. The overall structure is shown in Fig. 13.6.

The substrate binding sites of the xanthine oxidizing enzymes consist of several highly conserved amino acid residues: Phe 914, Phe 1009, Glu 802, Glu 1261, and Arg 880 (following the numbering in *B. taurus* XDH) (Enroth et al. 2000a). On the basis of the crystal structures of the *R. capsulatus* XDH and bovine XDH, it has been demonstrated that substrate intercalates between the phenylalanine residues in binding to the enzyme (Truglio et al. 2002). The two glutamate residues lie on opposite sides of the substrate-binding cleft defined by the phenylalanine residues. Glutamate 802 is within the hydrogen-bonding distance of the heterocyclic substrate and Glu 1261 within a similar distance to the molybdenum center. Arginine 880 lies on the same side of the substrate-binding pocket as Glu 1261, not as near to the molybdenum center, but appears positioned to interact with the substrate (Truglio et al. 2002).

The molybdenum center of XOs consists of the metal in a distorted square pyramidal coordination geometry. The apical position is occupied by a Mo = O group, and the four equatorial ligands are a terminal Mo = S group, two sulfurs from

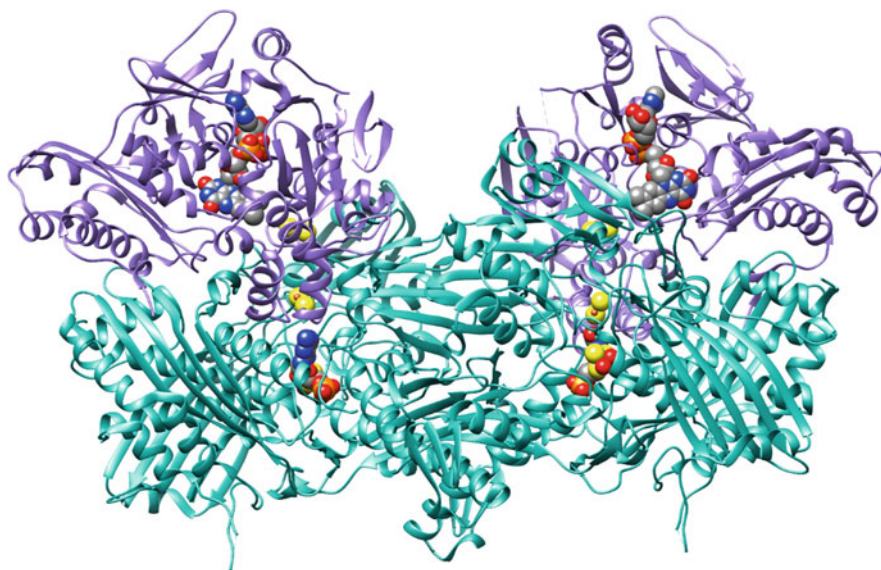


**Fig. 13.6** Crystal structure of *R. capsulatus* XDH (PDB Code 1JRO). The overall architecture is a heterotetramer composed of two functionally independent  $\alpha\beta$  heterodimers related by a twofold axis of symmetry. Each  $\alpha$  subunit is shown in purple, each  $\beta$  subunit is shown in teal, and the cofactors are shown in space fill model

a pterin cofactor, and a ligand that was determined to be water on the basis of crystallography.

Molybdenum-containing carbon monoxide dehydrogenase (CODH) enzymes from aerobic carboxydophilic bacteria such as *A. carboxidovorans* (Dobbek et al. 1999) or *Hydrogenophaga pseudoflava* (Dobbek et al. 2002) have been crystallographically characterized. Carboxydotrophs like *A. carboxidovorans* are able to grow with CO as their sole source of both carbon and energy. CODH from both *O. carboxidovorans* and *H. pseudoflava* have solved crystal structures; however, the former has been studied in greater detail (Dobbek et al. 1999; Hänzelmann et al. 2000). Overall, *A. carboxidovorans* CODH has a molecular weight of 277 kDa. The enzyme is a Mo- and Cu-containing iron-sulfur flavoprotein. The general architecture is a dimer of CoxLMS heterotrimers (Dobbek et al. 2002). Each heterotrimer is composed of a small 18 kDa subunit (CoxS) containing two [2Fe-2S] iron-sulfur clusters, a medium 30 kDa subunit (CoxM) containing FAD, and a large 89 kDa subunit (CoxL) containing the binuclear active site (Hille et al. 2015). Each subunit is sequentially and structurally similar to the homologous subunits of bovine xanthine oxidoreductase (Enroth et al. 2000b), and therefore considered a member of the xanthine oxidase family. The coordination geometry of the binuclear center of CO dehydrogenase in its oxidized Mo<sup>VI</sup> form is distorted square-pyramidal with an apical Mo = O and an equatorial plane consisting of a second Mo = O group, rather than the catalytically labile Mo-OH seen in other xanthine oxidases, and two sulfurs

from a pyranopterin cofactor (Hille et al. 2015). The fourth ligand of the equatorial plane is a  $\mu$ -sulfido bridge to the  $\text{Cu}^{\text{I}}$ , where  $\text{Mo} = \text{S}$  is typically found in xanthine oxidases. Cys 388 contributes a second thiolate ligand to the  $\text{Cu}^{\text{I}}$  ion and is also coordinated by a water molecule. Additionally, the active site residue Glu 763 (homologous to Glu 1261 in bovine xanthine oxidoreductase) is conserved in CODH. The binuclear center of CODH is deeply buried in the structure and access is sterically controlled. A phenylalanine residue (Phe 390) is displaced in order to accommodate Cu and Cys 388 for coordination. This interaction moves phenylalanine into the solvent access channel, obstructing it.

### 13.4.2 Microbial Sulfite Oxidase

The crystal structure of MsrP from *E. coli* has firmly placed the protein within the sulfite oxidase family based on its active site structure. Its molybdenum-binding domain closely resembles those of chicken liver sulfite oxidase (Kisker et al. 1997a) and *Arabidopsis thaliana* sulfite oxidase (Schrader et al. 2003) with regard to the square-pyramidal coordination geometry of the Mo center as well as the homologous cysteine residue that coordinates to molybdenum. The Mo center of MsrP uses a less-reduced dihydro form of the pyranopterin similar to SO. Although there are significant similarities, there are also several differences that distinguish MsrP from sulfite oxidase. First, the as-isolated MsrP exists in the  $\text{Mo}^{\text{V}}$  oxidation state as opposed to the  $\text{Mo}^{\text{VI}}$  oxidation state that is more commonly assumed in sulfite oxidases. Second, XAS analysis of MsrP suggests that the Mo center consists of one oxo and one hydroxo coordination instead of the two terminal oxo ligands that are most commonly found in members of the SO family (Havelius et al. 2011). It has also been suggested that a long oxygen or nitrogen coordination from either asparagine or glutamate to Mo might be present in this  $\text{Mo}^{\text{V}}$  state (Lee et al. 2016).

MsrP (YedY) has been structurally well characterized, showing similarities with the members of the SO family (Fig. 13.7); however, biochemical studies on MsrQ (YedZ) are less abundant. Before the physiological function of MsrQ was known, bioinformatic studies recognized it as an archetypal domain present in a superfamily of heme-containing membrane proteins, and originally termed the YedZ family. More recently, this domain has been renamed as the ferric reductase domain (FRD) (Zhang et al. 2013). This nomenclature was based on its identification within the six-transmembrane epithelial antigen of the prostate (STEAP) and also yeast ferric reductases (FRE), both of which are proteins involved in iron metabolism. The FRD domain is also present within the NADPH oxidase (NOX/DUOX) family of transmembrane enzymes involved in the production of reactive oxygen species.

The archetype of this FRD membrane domain is structurally similar to cytochrome b of the mitochondrial  $\text{bc}_1$  complex. This domain consists of six transmembrane segments (TM), including two transmembrane segments (TM3 and TM5) with bis-histidyl motifs, in allowing the chelation of two b-type hemes. Phylogenetic analyses suggest that among the FRD family, MsrQ proteins form a specific clade

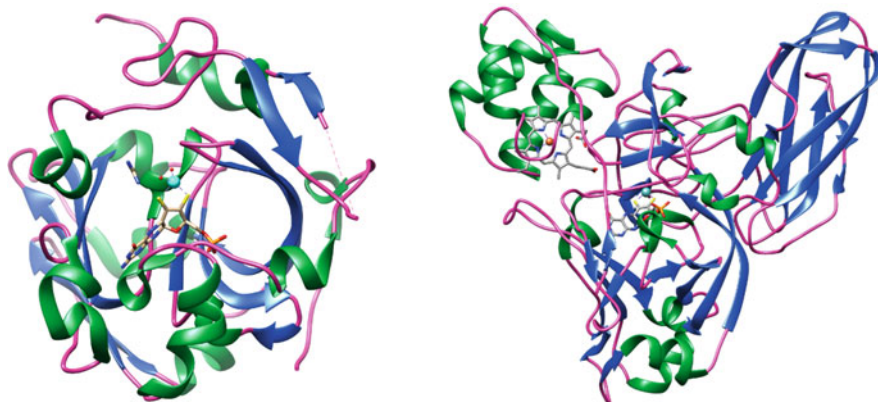


**Fig. 13.7** Unique structures sharing the SO fold: left: *E. coli* MsrP/YedY (PDB code, 1XDQ); right: *Starkeya novella* SDH (PDB code, 2BLF)

together with the eukaryotic ferric reductases of the STEAP family on one side and the FRE and NOX families on the other (Sanchez-Pulido et al. 2004). A difference within the NOX and FRE family is the number of predicted histidine residues involved in heme binding. In the MsrQ and STEAP families, one of these histidines is replaced by an arginine residue. The STEAP proteins possess two histidyl residues, where MsrQ possesses three histidines among the four amino acids. These evidences suggest that the STEAP and MsrQ proteins may lack one of the two b-type hemes that are present in the NOX and flavin reductase (FRE) enzymes. MsrQ has only the transmembrane domain without any additional cytosolic domains, in contrast to the NOX, FRE, or STEAP proteins that contain one or more additional cytosolic dehydrogenase domains. These domains allow NADPH and flavin binding, permitting electron transfer from NADPH to the membrane b-type hemes. For MsrQ, the membrane reduced quinone pool was proposed to be the source of electrons for its heme reduction. Soluble cytosolic dehydrogenase protein has also been proposed to function as an electron donor to heme moieties of the MsrQ (Gennaris et al. 2015). In the case of MsrQ, the dehydrogenase is not associated with the cytosolic domain, but has a separate soluble partner (Juillan-Binard et al. 2017). Thus, MsrQ seems to be well designed to receive electrons from redox-soluble cytosolic component(s) and transfer them across the membrane to the molybdenum cofactor of MsrP located in the periplasmic space. MsrQ has been efficiently reduced by FRE in the presence of free FMN and NADPH, and the rate of reduction is identical to that of FMN reduction by FRE in the presence of NADPH. The oxidation of one molecule of NADPH involves two electrons and the reduction of MsrQ also involves two electrons. There are data suggesting that all of the FMN molecules reduced by FRE are fully oxidized by MsrQ (Juillan-Binard et al. 2017). Therefore, FRE could serve as an alternate electron source instead of the membrane-bound quinones for MsrQ. It is hypothesized that the FRE MsrQ-reductase activity might play an essential role under conditions where formation of the reduced



quinone pool is deficient (Juillan-Binard et al. 2017). Further studies are required to better specify the physiological role of FRE for the reduction of methionine sulfoxide associated with hypochlorite damage.

An MsrQ-GFP fusion strategy has allowed for biochemical characterizations and shows the presence of two b-type hemes per MsrQ polypeptide (Juillan-Binard et al. 2017). This result differs from previous studies, which have reported the presence of only one heme per MsrQ (YedZ) protein. This discrepancy regarding heme to protein ratio was proposed to be heme depletion during purification, and it was observed that in the last purification step of MsrQ, some fractions of MsrQ were in apo-forms. The results suggest that His 91 and His 164 are directly involved in the coordination of the first heme-b, whereas His 151 is involved in the coordination of the second heme-b. A second histidyl ligand associated with His 151 for coordination of this heme is missing and replaced by a well conserved arginine residue (Arg 77). It has been postulated that this arginine residue may bind to the heme iron (Juillan-Binard et al. 2017).

The first heme of MsrQ, with its canonical heme-binding histidines (His 91 and His 164), is expected to face the periplasmic compartment, whereas the second heme, with the atypical coordination, would be located on the cytosolic side. The data provide a new perspective on the phylogenetic relationship between MsrQ, STEAP, and NOX/FRE proteins (Juillan-Binard et al. 2017). When STEAP and NOX are compared with MsrQ, both membrane-bound protein families display a soluble dehydrogenase domain on their cytosolic side, fused to their N or C terminus, respectively. The identification of FRE as a potential dehydrogenase partner for MsrQ suggests the existence of a two-component system homologous to the NOX/FRE. Identification of these systems supports Sumimoto's hypothesis (Sumimoto 2008) of a prokaryotic origin for the eukaryotic NOX enzyme, resulting from the fusion of a membrane cytochrome b and an FNR-like dehydrogenase domain. The MsrQ/Fre two-component system then may be viewed as a prokaryotic intermediate preceding the fused NOX enzymes.

### 13.4.3 Microbial Dimethyl Sulfoxide (DMSO) Reductase

Several members of the DMSOR family have been structurally characterized by X-ray crystallography, including DMSOR of *R. capsulatus* (McAlpine et al. 1998) and of *C. sphaeroides* (Li et al. 2000), FDH-H of *E. coli* (Raaijmakers et al. 2002; Boyington et al. 1997), NarG of *E. coli* (Jormakka et al. 2004; Bertero et al. 2003); NapA of *D. desulfuricans* (Dias et al. 1999); TMAOR of *Shewanella massilia* (Buc et al. 1999), and Aio of *A. faecalis* (Ellis et al. 2001).

**DMSO Reductase/TMAO Reductase** DMSO reductase serves as a terminal electron acceptor during anaerobic growth in the presence of DMSO. The DMSOR enzymes from *C. sphaeroides* and *R. capsulatus* are monomeric and composed of a single subunit and no additional cofactors except Moco. The monomer contains four

domains that are grouped around the cofactor. The two pterin cofactors, P- and D-MGDs form an elongated structure that can extend to  $\sim 35$  Å between the two nitrogen atoms of the two guanine moieties. The active site is located at the bottom of a deep indentation in the protein surface, and the hydroxyl group of Ser 147 provides the protein ligand at the molybdenum center. DMSOR structures all share a similar fold, although different Mo environments have been described (Sigel and Sigel 2002). However, later studies revealed a heterogeneity in the samples that may have contributed to the reportedly different geometries (Li et al. 2000). The Mo center is coordinated by dithiolene sulfurs of the two MGD cofactors, the side chain of Ser 147, and a terminal oxo group in the oxidized state. The overall geometry is trigonal prismatic, which differs from model compounds suggesting that the protein environment may have played a role in stabilizing such a geometry. This geometric organization stabilizes an entatic state facilitating the catalysis (Ha et al. 2014).

The DMSO reductases cycle between mono-oxo-Mo<sup>VI</sup> and des-oxo-Mo<sup>IV</sup> states, as mentioned, their Mo center is coordinated by four sulfur atoms, and the oxygen atom from the serine ligation remains coordinated during catalysis. The terminal oxo group is present in the oxidized state but not in the reduced des-oxo state. The labile nature of the terminal oxo group has been demonstrated by soaking oxidized DMSOR in DMS, after which a crystal structure analysis revealed the formation of DMSO replacing the terminal the oxo ligand (McAlpine et al. 1998).

The crystal structure of *S. massilia* TMAOR is very similar to that of *C. sphaeroides* DMSOR and *R. capsulatus* DMSOR (Czjzek et al. 1998). The most significant differences appear to be in regions far from the active site. The global arrangements of the two MGD cofactors are very similar, although the resolution of the crystal structure has not been high enough to clearly determine the Mo coordination sphere. A mobile loop region that includes residues 380–394 in DMSOR and residues 384–398 in TMAOR has been shown to exhibit several conformations. In the structure for *S. massilia* TMAOR, this loop is located on the exterior top surface of the active-site funnel. The crystal structure of *R. capsulatus* DMSOR showed that loop acting as a lid over the active site funnel with the sidechain of Trp 388 packed against a bound DMS molecule (McAlpine et al. 1998).

**Formate Dehydrogenase** The oxidized (by oxygen) and formate-oxidized (H<sup>+</sup> translocation by formate) crystal structures of *E. coli* Fdh-H, a component of the anaerobic formate hydrogen lyase complex, have been solved and later revised (Boyington et al. 1997; Raaijmakers and Romao 2006). The active subunit contains an [4Fe-4S] cluster, a Mo atom that is coordinated by two MGD cofactors, and a selenocysteine residue (Axley et al. 1990). During substrate transformation, Fdh-H oxidizes formate to carbon dioxide with the release of a proton and two electrons. The reaction mechanism has been under intense scrutiny, and the structure-based mechanism has been revised (Hille et al. 2020).

*E. coli* Fdh-H is an 80-kD protein that consists of four  $\alpha\beta$  domains. Domain I consists of two small antiparallel  $\beta$  sheets and four helices and coordinates the [4Fe-4S] cluster. Domains II and III are MGD-binding domains and are both  $\alpha\beta\alpha$  sandwiches. The N-terminus of domain III is also the location of Sec 140, an

essential ligand to Mo. The molybdenum atom of the active site is coordinated by two MGD cofactors, where domain IV forms a cap over the pterins. In both the reduced Mo<sup>IV</sup> and oxidized Mo<sup>VI</sup> structures, Mo is ligated to the four cis-dithiolene sulfurs of the MGD cofactors and the selenium of Sec 140 (Boyington et al. 1997). The coordination geometry of the formate-reduced form is square pyramidal, in which the four sulfur atoms occupy the equatorial positions and the selenium is positioned axially.

The reevaluation of the original *E. coli* Fdh-H crystallographic data has shown structural differences for the formate-reduced form, which also influences the previously proposed reaction mechanism. It has been reported that a loop close to the molybdenum active site was mistraced, implying that some of the reported positions for catalytically relevant residues were incorrect (Raaijmakers and Romao 2006). The loop near the active site contains residues Sec 140 and His 141, which are involved in catalysis. The essential Sec 140 is no longer bound to the metal after reduction of the enzyme with formate (Raaijmakers and Romao 2006). Aside from the mistraced loop in the reduced form, both forms of the enzyme adopt remarkably similar structures.

The *R. capsulatus* operon *fdsGBACD* has been homologously expressed, yielding the Fds protein which has been purified (Radon et al. 2020). The purified complex consists of four subunits, FdsA, FdsB, FdsG, and FdsD. The ‘as isolated’ protein has been investigated by cryo-electron microscopy. The *R. capsulatus* FDH complex forms a 360-kDa dimer of FdsABGD heterotetramers and adopts an elongated structure, as shown in Fig. 13.8. The dimer is formed by the two FdsA (105 kDa, 958 amino acids) subunits, FdsB attaches to the N-terminus of FdsA, and FdsD is near the C-terminus of FdsA. FdsB and FdsG are a diaphorase unit, and the FdsA subunit binds the Mo(MGD)<sub>2</sub> cofactor, which coordinates the molybdenum atom in the active site along with the conserved Cys 386 residue. FdsA contains four [4Fe-4S] clusters and one [2Fe-2S] cluster, where three [4Fe-4S] clusters and the [2Fe-2S] cluster are located in the N-terminal 250 amino acid FdsA peptide.

FdsB can be organized into two domains. The first domain consists of the 100 N-terminal amino acids that form a ferredoxin-like domain. However, it lacks the ability to bind a [2Fe-2S] cluster. The second domain contains the conserved binding site for NAD<sup>+</sup>, the flavin mononucleotide (FMN) cofactor, and one [4Fe-4S] cluster. The FdsG subunit binds one [2Fe-2S] cluster and is suggested to minimize reactive oxygen species production due to formation of flavin semiquinone radicals in the presence of oxygen. It does this either by temporarily storing electrons, inducing structural rearrangements that stabilize NAD<sup>+</sup> binding upon reduction, or increasing overall enzyme stability (Gnandt et al. 2017).

FdsD is predicted to influence the insertion of Mo(MGD)<sub>2</sub> into *R. capsulatus* Fdh by either functioning as a chaperone for Mo(MGD)<sub>2</sub> or by stabilizing the quaternary structure of FdsA. Cryo-EM has revealed that FdsD folds into a four-helix bundle and interfaces 23 out of its 69 amino acids with both MGD-coordinating domains of FdsA and with a loop that extends from the C-terminal cap domain shielding the Mo (MGD)<sub>2</sub> cofactor. A handful of hydrogen bonds, three salt bridges, plus an aromatic

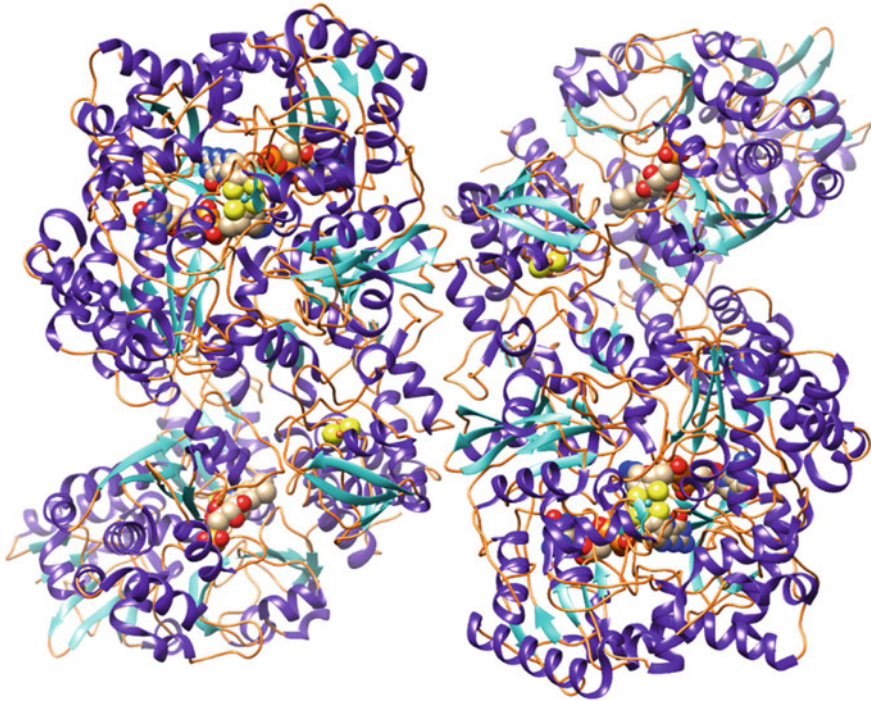


**Fig. 13.8** Cryo-EM structure of *R. capsulatus* Fds (PDB code, 6TGA). The complex is a dimer of heterotetramers;  $\alpha$  helices colored purple,  $\beta$  sheets colored cyan, coils colored orange, and the cofactors are shown in space fill model

stacking between Trp 917 in FdsA and phenylalanines 16 and 17 in FdsD mediate the interaction between FdsD and FdsA. Trp 917 is located at the tip of the cap loop of FdsA and is highly conserved in all Fdh complexes predicted to contain FdsD. Both ends of the loop contain conserved aromatic and charged residues that interact with both MGD cofactors of FdsA. The cap loop is thought to function as a sensor for Mo(MGD)<sub>2</sub> insertion during FDH assembly. FdsD binding to FdsA would lock the cap domain of FdsA in place, and this would prevent damage or loss of the cofactors (Radon et al. 2020).

The Mo(MGD)<sub>2</sub> containing the active site of *R. capsulatus* Fdh (FdsA) has been structurally characterized (Radon et al. 2020). The EM map around molybdenum indicates six ligands coordinated in a trigonal prismatic geometry. Two dithiolene groups of Mo(MGD)<sub>2</sub> coordinating molybdenum from one side form the base of the prism. Cys 386 sulfur and a small ligand, likely a terminal sulfido, oriented toward Val 592 occupy the other two coordination sites. The active site residue Arg 587 is proposed to orient formate for C–H bond cleavage and the His 387 is proposed to elevate the pK<sub>a</sub> of the cysteine ligand. Two tunnels have been identified in *R. capsulatus* Fdh, both beginning at the molybdenum then separating at active site residue Arg 587. The pore of the shorter tunnel is mainly formed by polar and

charged residues, inferring it may channel hydrophilic substrate to the active site. The second tunnel mostly contains hydrophobic residues suggesting it may transport gas to or from the active site. The direct electron transfer chain between Mo(MGD)<sub>2</sub> and FMN of the heterotetramer measures 76 Å and consists of five Fe–S clusters, as well as two additional clusters outside of the electron transfer pathway from Mo(MGD)<sub>2</sub> to FMN.

**Perchlorate Reductase** Significant information on perchlorate and its environmental prevalence has been reported recently, whereas previously, it was mostly known as a groundwater contaminant due to Cold War munition manufacturing (Coates and Achenbach 2004). Perchlorate has been found in both terrestrial and extraterrestrial planetary and non-planetary samples, indicating it is likely found all throughout the solar system. Perchlorate's abundance is quite widespread; it has been identified on Mars, Earth's moon, in meteorites, as well as recently being determined to have a natural atmospheric source. It has been found that microbial respiration leads to terrestrial perchlorate diagenesis (Jackson et al. 2015).

Perchlorate or chlorate (collectively (per)chlorate) can be the terminal electron acceptor during anaerobic respiration for (per)chlorate-reducing bacteria. (Per)chlorate reduction is a highly conserved process among phylogenetically related species. Perchlorate is sequentially reduced to chlorite by the perchlorate reductase (PcrAB), and further dismutated into chloride and oxygen by chlorite dismutase (Cld). The same microorganism that produced this oxygen can then respire it, posing a unique relation between aerobic and anaerobic metabolisms. Relatively little has been known about the PcrAB, until recently (Youngblut et al. 2016). It has been shown that the PcrAB is an oxygen-sensitive heterodimeric periplasmic enzyme that catalyzes a 2e<sup>-</sup> reduction of perchlorate to chlorate. PcrA is the catalytic subunit and phylogenetically closely related to NarG of nitrate reductase, and both proteins are part of the DMSO reductase superfamily and strongly associated with intermediate electron-shuttling protein subunits (Youngblut et al. 2016).

Crystal structures of PcrAB have revealed all metal ion cofactors along with a novel gating mechanism at the active site that grants the enzyme some distinctive biophysical characteristics. PcrAB was found to be more efficient at low perchlorate concentration, so to explore this phenomenon the anaerobically purified enzyme was crystallized. The crystal structure of oxidized PcrAB formed a trimer of heterodimers (Fig. 13.9). The oxidized PcrA structure, where the oxidation state of molybdenum is most likely Mo<sup>V</sup> or Mo<sup>VI</sup>, resembles other enzymes of the DMSOR family. PcrA is composed of one Mo(MGD)<sub>2</sub> cofactor and one [4Fe-4S] cluster (FS0), and PcrB is composed of three [4Fe-4S] clusters (FS1–3) and one [3Fe-4S] cluster (FS4). All [Fe-S] clusters coordinate with cysteine residues except the FS0 cluster, which coordinates with one iron atom by the His 32 residue. The molybdenum atom is coordinated in trigonal prismatic geometry with four proximal thiolates of Mo(MGD)<sub>2</sub> cofactor (average Mo–S bond distance of 2.4 Å) along with an Asp 170 residue and an additional oxygen atom (either an oxo, hydroxyl, or associated water molecule) in the two distal positions. Mo–O bond distances were about

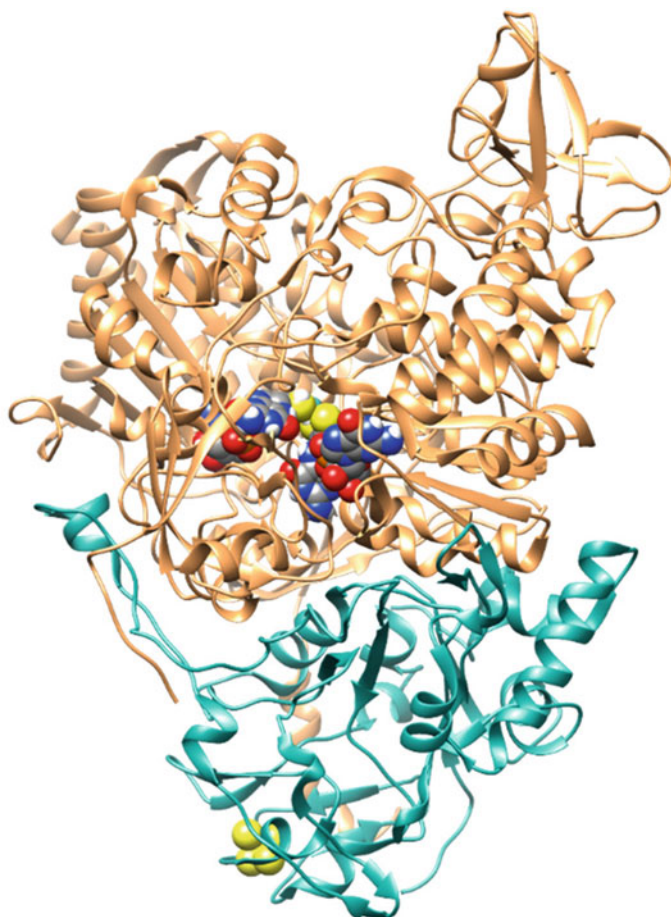


**Fig. 13.9** Crystal structure of *Azospira oryzae* (previously known as *Azospira suillum*) perchlorate reductase heterodimer (PcrAB) (PDB code, 4YDD). PcrA subunit in tan, Pcr B subunit in teal, and cofactors are shown in space fill model

2.0–2.1 and 2.4–3.1 Å for Asp 170 and the additional oxygen atom, respectively, in the three PcrA molecules in the asymmetric unit.

Based on the structure, one can suggest that the substrate travels to the active site via a funnel-shaped access tunnel. Residue Phe 164 in the tunnel near the active site gate may influence substrate access, while two aromatic residues (Tyr 165 and Trp 461) adjacent to Phe 164 form a hydrophobic gate that controls active site access. The substrate access tunnel of PcrA has predominantly positive charges, which creates a relatively high affinity for oxyanions. The corresponding gate residues in *E. coli* NarG overlay well with both the PcrA structure and with phylogenetic analysis. Focusing on the gate and active site residues mentioned above has been done to compare closely related members of the DMSOR family of enzymes. These

analyses indicate that there is a monophyletic clade for PcrA closely related to the NarG. The NarG-containing enzymes face the cytoplasm (cNarG) or periplasm (pNarG), differentiated by the presence of twin-arginine translocation sequences that target pNarG to the periplasm. Twin arginine translocation sequences have been reported on all perchlorate reductases (that have been sequenced). Sequence alignments of PcrA, pNarG, and cNarG display that they share several conserved regions as well as a signature aspartate residue at their active site, which coordinates the molybdenum atom from a Mo(MGD)<sub>2</sub>. The sequences of these three enzymes also contain several conserved residues in the N-terminal portion of the molybdopterin-binding domain. Crystal structure of PcrAB also reveals that the gate residues, Phe 164 and Tyr 165, are conserved in NarG, and Trp 461 is glutamate in NarG (Youngblut et al. 2016).

**Arsenate Reductase/Arsenite Oxidase** Gram-negative and Gram-positive bacteria, as well as other phylogenetically diverse species, encode for arsenate respiratory reductase (Arr), which allows for arsenate respiration (Stolz et al. 2006; Afkar et al. 2003; Richey et al. 2009). The Arr complex, comprising a large subunit ArrA and a small subunit ArrB, is a member of the DMSO reductase family. The ArrA subunit is predicted to contain a Mo atom coordinated by a pyranopterin guanine dinucleotide cofactor (Mo(MGD)<sub>2</sub>), as well as a single [4Fe–4S] cluster. The ArrA subunit has an N-terminal twin-arginine translocation (TAT) signal, which suggests the assembled ArrAB complex is transferred across the cytoplasmic membrane post-translationally. It has also been confirmed that ArrAB is located in the periplasmic space in Gram-negative bacteria. In some organisms, ArrAB may associate with a third subunit ArrC, a heme-containing quinol oxidase that is likely to be the electron donor for the complex. In species that are lacking the ArrC subunit, electrons are donated from the tetraheme cytochrome CymA (Glasser et al. 2018).

The ArrAB complex structure and arrangement is similar to other Mo(MGD)<sub>2</sub> protein complexes such as NarGH, FdnGHI, and PcrAB (Glasser et al. 2018). All five proteins have iron–sulfur clusters [4Fe–4S] with each iron atom coordinated by a cysteine side chain.

The ArrA subunit contains a four-domain structure much like other Mo(MGD)<sub>2</sub> proteins and a substrate funnel that is lined mostly with basic and aromatic residues. The molybdenum atom coordination geometry is distorted octahedral with Cys 193 in the apical position and the dithiolenes of both MGD cofactors (Fig. 13.10). The [4Fe–4S] cluster in ArrA (FS0) is coordinated by cysteines 61, 64, 68, and 96. An oxygen atom is suggested to complete the coordination geometry in the equatorial plane, based on electron density map findings.

The structure of the arsenate bound form has also been determined (Glasser et al. 2018). In the conformation where arsenate is closest to the molybdenum, the substrate forms hydrogen bonds with Arg 165, His 189, Tyr 166, Tyr 210, as well as several water molecules. In the second conformation, arsenate hydrogen bonds with Tyr 166, Ser 190, Lys 198, and multiple water molecules, but two water molecules are substituted for arsenate oxygen atoms from the first conformation. Structures bound to arsenite, the product of the arsenate respiration, have also been

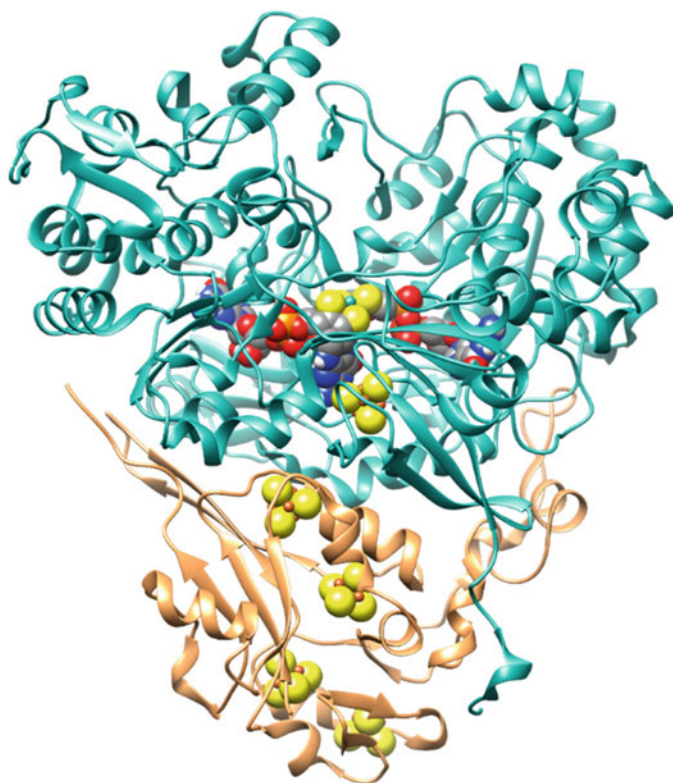


**Fig. 13.10** *Shewanella* sp. ANA-3 arsenite reductase heterodimer (ArrAB). Subunit A in teal, subunit B in tan, and the cofactors are shown in space fill model

recorded. The first conformation closely resembles the one mentioned above; arsenite is coordinated by the same residues but is shifted a bit closer to the Mo atom and forms a Mo–O bond while in this position. The distance of arsenite to the coordinating cysteine is similar to others observed, but the crystallographic Cys–S–As distance is too long to represent a covalent bond (Oden et al. 1994). This form may be depicting arsenite-binding Mo<sup>IV</sup> or Mo<sup>V</sup> instead of Mo<sup>VI</sup> that would be predicted in the reaction cycle, and it may be inferred that this a non-physiological form (Glasser et al. 2018).

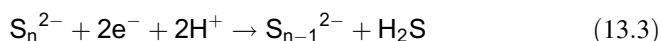
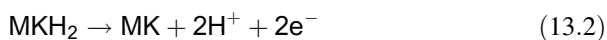
The crystal structure of arsenite oxidase (Aio) of the Gram-negative bacteria *Alcaligenes faecalis* has been solved. Aio is a 100-kDa molybdenum- and iron-sulfur-containing protein located on the outer surface of the inner membrane of the bacterium (Ellis et al. 2001). Arsenite oxidase contains two equivalents of pterin cofactor and is considered part of the DMSOR family, although it does not have a protein-based ligation to Mo. The overall architecture of *A. faecalis* arsenite oxidase is heterodimeric with a large subunit of 825 residues, which holds the molybdenum center and an [3Fe-4S] cluster, and a small subunit of 134 residues that harbors a



Rieske-type [2Fe-2S] cluster (Anderson et al. 1992). The two subunits are associated with hydrogen bonding. The large subunit is divided into four domains, where domain I harbors the [3Fe-4S] cluster and the Rieske subunit and domains II–IV bind the molybdenum center. Domain I is composed of three antiparallel  $\beta$  sheets and six helices. Domain II is an  $\alpha\beta\alpha$  sandwich consisting of a seven-stranded parallel  $\beta$  sheet with five helices on one side and seven helices and a small two-stranded antiparallel  $\beta$  sheet on the other. Domain III is also an  $\alpha\beta\alpha$  sandwich consisting of a parallel five-stranded  $\beta$  sheet with six helices on one side and nine helices and a small two-stranded parallel  $\beta$  sheet on the other. Domain IV is a six-stranded  $\beta$  barrel surrounded by helices capping each end and one side, and three more helices on the other side. The [3Fe-4S] cluster is coordinated near domains III and IV (Ellis et al. 2001). The molybdenum center is located deep in a funnel shaped depression formed by domains I, II, and III. The Mo atom is symmetrically coordinated to the four cis-dithiolene sulfur atoms of two MGD cofactors. The P-MGD cofactor lies between domains II and IV, and the D-MGD (previously noted as Q-MGD) cofactor lies between domains III and IV. Both domains II and III display a pseudosymmetry relative to each other, much like the pseudosymmetry of the molybdenum cofactor (Anderson et al. 1992).

**Polysulfide Reductase** Polysulfide Reductase (Psr) is an enzyme that carries out quinone-coupled reduction of polysulfides. Polysulfides are a class of compounds constituted of chains of sulfur atoms wherein their simplest form exists as an anion ( $S_n^{2-}$ ). Extreme environments in nature, such as deep-sea vents and hot springs, are where polysulfides are found in particularly high concentrations. In these environments, the reduction and oxidation of polysulfides are vital processes for many bacteria, as well as essential steps in the global sulfur cycle. Interestingly, the reduction of polysulfide to hydrogen sulfide is often linked to energy-generating respiratory processes that support the growth of many microorganisms such as hyperthermophiles.

Psr is a membrane-bound enzyme that belongs to the  $Mo(MGD)_2$  oxidoreductases.  $Mo(MGD)_2$  enzymes typically consist of two membrane associated subunits and one integral membrane subunit with five to nine transmembrane spanning helices (TMs). Psr has an integral membrane subunit that is predicted to have eight TMs, and does not contain any redox centers, such as a b-type heme. Two electrons and two protons are released from the bound substrate, menaquinone-7 (MK-7), in the Psr catalytic cycle. The electrons are then transferred by five [4Fe-4S] iron–sulfur clusters to the  $Mo(MGD)_2$  cofactor to reduce polysulfide. The following reactions in the membrane and in the periplasm are catalyzed by Psr (eqs. 13.2 and 13.3).



Crystal structures of the native *Thermus thermophilus* Psr as well as complexes of Psr with three quinone analogs have been recorded. The structure reveals a

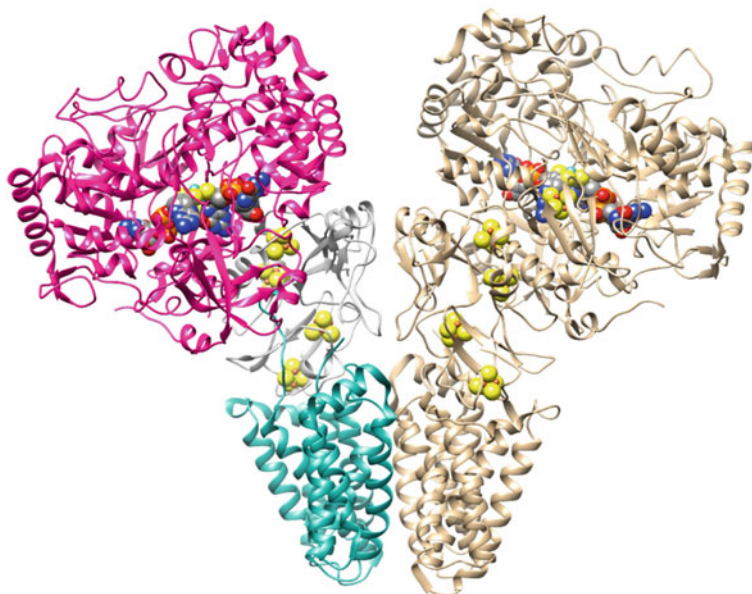


**Fig. 13.11** Crystal structure of *T. thermophilus* polysulfide reductase heterotrimeric dimer (PsrABC) (PDB code, 2VPZ). Top heterotrimer: PsrA colored in fuschia, PsrB colored in gray, PsrC colored in cyan. Bottom heterotrimer: PsrA, PsrB, PsrC in tan, the cofactors are shown in space fill model

heterotrimeric dimer configuration, with a total molecular weight of approximately 260 kDa (Fig. 13.11). The dimer is presumably physiological, as evidenced by a sizable interface between the two heterotrimeric monomers as well as a complex hydrogen bond network between the PsrB subunits. This dimeric structure is physiological for nitrate reductase (NarGHI), which may further support this probability for Psr. The comprehensive structure of Psr, consisting of two membrane associated subunits (PsrA and PsrB) and one integral membrane subunit (PsrC), resembles NarGHI; as mentioned, as well as FdnGHI (Jormakka et al. 2008).

The PsrA and PsrB subunits sit on the same side of the inner membrane as the N- and C-terminus of the PsrC subunit, which is evidenced to be found in the periplasm. The PsrA N-terminus contains a TAT motif. The TAT signal sequence is absent, however, in the N-terminal sequencing and the structure of the PsrA subunit, suggesting that this signal was processed and the PsrAB dimer is situated in the periplasmic space.

The PsrA subunit is composed of 733 amino acid residues and contains two Mo (MGD)<sub>2</sub> cofactors, designated P and D, and a cubane-type [4Fe-4S] cluster. The subunit has four distinct domains that are related by an internal pseudo twofold symmetry. Domain I includes four cysteine residues that coordinate the [4Fe-4S] cluster. Domains II and III anchor the Mo(MGD)<sub>2</sub> cofactor through multiple hydrogen bonding interactions associated with their  $\alpha/\beta$  sandwich conformation. Domain

IV is a  $\beta$ -barrel and is also involved in the  $\text{Mo}(\text{MGD})_2$  coordination. The structure of the four domains is similar to the domains of FdnG, with the major differences being located in the channel that goes from the periplasm to the active site. The channel is formed by the  $\alpha/\beta$  sandwiches of Domains II and III and shaped like a funnel, with the active site found at the bottom. The opening of the funnel is narrow, primarily having basic residues at the entrance, which may function in substrate selectivity. The crystal structure of the native Psr enzyme was obtained under aerobic conditions, so Mo likely was in the  $\text{Mo}^{\text{VI}}$  state. The crystal structure shows the Mo coordinated with the sulfur group of CysA 173, a water molecule, and the four sulfurs of the  $\text{Mo}(\text{MGD})_2$  cis-thiolate groups. The Mo atom coordination geometry is a trigonal prismatic configuration, where the distance between the coordinating water and Mo indicates that this is an oxo group rather than a hydroxide group. An additional water molecule is situated 2.52 Å from the coordinating water molecule, and hydrogen bonds are provided to the waters by Arg 332. The coordination of arginine to two water molecules is a common feature among peroxidase enzymes but interestingly has not been previously observed in  $\text{Mo}(\text{MGD})_2$  enzymes. An arginine residue binds to two water molecules in peroxidases because those water molecules are generated through the reduction of hydrogen peroxide. By structural analogy, it may be proposed that the two water molecules of polysulfide reductase represent the positions of two sulfur atoms in the polysulfide substrate, where Arg 332 is key to coordination of the substrate at the active site. Additionally, several key residues in catalysis have been identified; His 145 lies in close proximity to the second water molecule and could be involved during substrate turnover; Phe 48, Arg 50, Ser 169, Thr 174, and His 215 are near the active site and may be involved either in substrate specificity or in the catalytic cycle. Additionally, His 215 may be involved in proton delivery to the active site, this premise is supported by the observation of a highly structured solvent chain connecting the His 215 residue to the protein's exterior.

Typically,  $\text{Mo}(\text{MGD})_2$  enzymes carry out catalytic reactions that involve oxygen atom transfer, where the tetrathionate, thiosulfate, and polysulfide reductases catalyze reactions that involve either sulfur transfer or reductive cleavage of a sulfur-sulfur bond. It has been suggested that in these reactions, the substrate remains directly ligated to the Mo center during the catalytic cycle. If, as mentioned above, the sulfur atoms replace the two water molecules, then perhaps the molybdenum is hexa-coordinated by sulfur atoms during the catalytic cycle, and Arg 332 acts directly as a ligand to the substrate. If this is, in fact, the case, then binding of the substrate would cleave the polysulfide, releasing  $\text{S}_{(n-1)}^{2-}$  and leaving a  $\text{Mo}^{\text{VI}}$  core. Once electrons and protons are delivered,  $\text{H}_2\text{S}$  would be produced, and Mo would be in the  $\text{Mo}^{\text{V}}$  state (Jormakka et al. 2008).

The PsrB subunit is an [4Fe-4S] electron transfer subunit and is composed of 194 residues. The four FeS clusters in PsrB and the coordinating [4Fe-4S] cluster in PsrA are aligned in a single chain, with the adjacent redox centers within the presumed limits of physiological electron transfer capability. Redox potentials are not yet known for the Psr clusters but are hypothesized to be akin to those of *E. coli*

DMSOR and Nar, in which these enzymes share a similar distribution of redox potentials (Jormakka et al. 2008).

**Nitrate Reductase** Three different types of bacterial nitrate reductases have been identified: membrane bound respiratory nitrate reductase (Nar), periplasmic nitrate reductase (Nap), and cytosolic assimilatory nitrate reductase (Nas) (Stolz and Basu 2002). Of these Nar and Nap function as dissimilatory nitrate reductases, although they carry out other functions. Nap is considered a dissimilatory enzyme because quinol oxidation by Nap is not directly coupled to the generation of a proton motive force, as well as being independent of the cytochrome  $bc_1$  complex. However, Nap may also function to poise cellular redox by consuming extra redox equivalents. Thus, nitrate reductases can have different functions depending on the conditions, and they are generally classified on the fate of the product, nitrite. *E. coli* can assimilate nitrite generated by anaerobic nitrate respiration, and other denitrifiers may use the nitrite formed by Nap to perform anaerobic nitrite respiration or aerobic denitrification (Moreno-Vivián et al. 1999).

Nap and Nar are also catalytically distinct. Nap is less sensitive to inhibition by cyanide, does not use chlorate as a substrate, and is slightly stimulated by thiocyanate and azide. In *C. sphaeroides*, Nap activity is competitively inhibited by chlorate. Both nitrate and chlorate stimulate phototrophic growth in the wild-type strain of *C. sphaeroides*. Nap-dependent chlorate or nitrate stimulation of bacterial growth has been explained as the dissipation of excess photosynthetic reducing power, allowing optimal growth in terms of redox balancing (Moreno-Vivián et al. 1999).

**Respiratory Nitrate Reductase** *E. coli* has at least two distinct types of Nitrate Reductase (Nar) encoded by different operons: *narKGHJI* and *narUZYWV*, respectively, generating NarGHI and NarZYW as their gene products. These two similar enzymes have distinct physiological roles, and their regulation has been investigated (Constantinidou et al. 2006; Huynh et al. 2010). The NarX-NarL and NarP-NarQ partner systems, which are nitrate-specific regulators, acting along with FNR (fumarate nitrate reductase regulator) control the expression of NarGHI. FNR directly activates *narKGHJI* but not *narUZYWV*. The *narUZYWV* is expressed under aerobic conditions in the presence of nitrate. The *Shewanella oneidensis* genome interestingly encodes for one NarQ/NarX homolog and two NarP/NarL homologs, and only the NarP/NarL is actively transcribed (Dong et al. 2012).

NarGHI is heterotrimeric and contains the Mo(MGD)<sub>2</sub> subunit (NarG), an [Fe-S] cluster-containing electron transfer subunit (NarH), and a heme-containing membrane anchor subunit (NarI). It is likely there are two hemes in NarI, four [Fe-S] clusters found in NarH, and one Mo(MGD)<sub>2</sub> cofactor in NarG. These groups delineate an electron transfer chain linking a quinol oxidation site in the periplasm to a nitrate reduction site in the cytoplasm. Formate dehydrogenase-N (FdnGHI) and NarGHI construct a respiratory chain that carries out electron transfer from formate to nitrate by coupling to the generation of a PMF (proton motive force) across the cytoplasmic membrane (Bertero et al. 2003).

The structure of *E. coli* NarGHI has been determined by multiwavelength anomalous diffraction (MAD) and multiple isomorphous replacements and anomalous scattering (MIRAS). The NarGHI heterotrimer structure is flower-shaped with dimensions of  $90 \times 128 \times 70$  Å. The cytoplasmic subunits NarG and NarH interact through a large interface while NarI, the membrane-intrinsic subunit, anchors NarGH to the membrane through an interface that is mostly hydrophobic. The interactions between these subunits make for a very stable heterotrimer. The N-terminal tail of NarG, containing two  $\alpha$ -helices separated by an extended  $\beta$ -hairpin, harbors a significant amount of these subunit interactions. The longer of the two helices, spanning from Asn 28 to Gln 40, is completely buried in NarH, where one face of the helix provides electrostatic side chain interactions and the other face provides a series of hydrophobic and stacking interactions, mainly with aromatic residues. The  $\beta$ -hairpin in NarG hydrogen bonds with the C-terminal  $\beta$ -strand of NarI as well as a  $\beta$ -hairpin from NarH to altogether form a twisted  $\beta$ -sheet. The N-terminal helix of NarG sits adjacent to NarI and a helix from NarH, where the amphipathic properties of the NarG and NarH helices support their role in membrane association. A phosphatidylglycerol molecule that is bound in a pocket formed by the three subunits also aids in the stabilization of the heterotrimer. The positions of the subunits of NarGHI in the membrane are defined by the interaction of the NarGH with positively charged stop-transfer sequences of NarI, which infers that NarGH is localized on the cytosolic side of the membrane. Based on the electron density, it is found that there are eight redox centers aligned on a single chain that runs in a broad arc through the center of NarGHI. The redox centers are as follows: heme b-D (distal), heme b-P (proximal), an [3Fe-4S] cluster (named FS4), four [4Fe-4S] clusters (named FS3, FS2, FS1, FS0), and the Mo(MGD)<sub>2</sub> cofactor. The pathway connects energetic processes such that electron transfer can occur from the menaquinol (MQH<sub>2</sub>) binding site in NarI to the Mo-bisMGD active site in NarG, where nitrate is reduced to nitrite (Bertero et al. 2003).

NarG is a member of the well-defined DMSOR family that contains Mo(MGD)<sub>2</sub> as a cofactor which enables catalytic activity. NarG, containing 1246 residues, is the largest of the Mo(MGD)<sub>2</sub> enzymes whose crystal structures are known. The NarG structure is composed of four conserved  $\alpha$ - $\beta$  domains surrounding the cofactor. There are also several distinct motifs in the NarG structure that are exclusively located at the cytoplasmically exposed surface of the enzyme, with the exception of the N-terminal motif. These motifs possibly serve as interaction sites with other regulatory and accessory proteins involved in NarGH assembly as well as its delivery to the NarI subunit. NarJ may be a protein that binds NarG, as it is proposed to act as a chaperone for obtaining the Mo(MGD)<sub>2</sub> before NarGH is bound to NarI. The four domains of NarG surround the catalytic center, as mentioned. Domain I is composed of two mixed  $\beta$ -sheets, three helices, the N-terminal tail, and a [4Fe-4S] cluster (FS0). The coordination arrangement of FS0 is an uncommon one, with one histidine (His 50) and three cysteines (Cys 54, Cys 58, Cys 93). FS0 is positioned between the Mo(MGD)<sub>2</sub> and the FS1 cluster in NarH, likely having a direct role in the electron transfer mechanism. Arg 94 is close to one of the pterin centers of Mo(MGD)<sub>2</sub> and forms a hydrogen bond with the Cys 92 ligand of FS0, providing a path

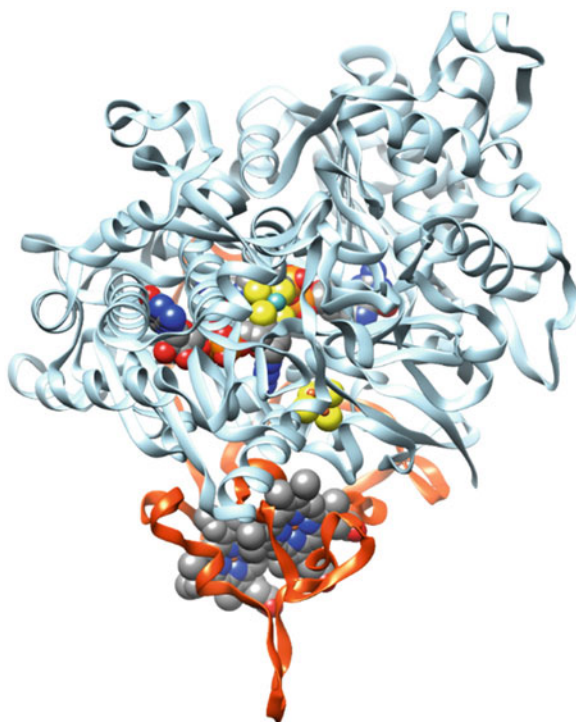
for electron transfer from FSO to the molybdenum atom in the active site. FSO is also shielded from solvent access by a cluster of aromatic residues. The mixed  $\alpha - \beta$  domains II and III have an elongated structure with a covalently linked MGD-P moiety that is coordinated by domain II, and D-MGD that is coordinated by domain III, both stabilized by a network of hydrogen bonds. Due to purification and crystallization performed in aerobic conditions, the molybdenum center is likely to be in oxidized Mo<sup>VI</sup> state. The molybdenum of the NarG nitrate-reducing active site is coordinated by six ligands with a geometry best described as a distorted trigonal prism. The ligands are four cis-dithiolene sulfur atoms of the Mo(MGD)<sub>2</sub> and a bidentate interaction from both side chain oxygen atoms in the Asp 222 carboxylate group. Asp 222 is a highly conserved residue in the NarG subunits of Gram-negative and -positive bacteria. This Asp-Mo coordination is novel in the Mo(MGD)<sub>2</sub> enzyme family. Asp 222 is buried in the active site, with one face of the side chain carboxylate exposed to a relatively hydrophobic environment and the negative charge from the carboxylate ligand interacting with molybdenum. This environment surrounding the coordinating aspartate residue is also unusually lacking hydrogen bonds to other protein atoms. Electron density analysis reveals that D-MGD possesses a novel bicyclic dihydropterin structure, whereas tricyclic pyranopterin structures typically are observed for the P-MGD moiety. The observation of a bicyclic dihydropterin in NarG suggests that NarGHI is able to bind both bi-/tri-cyclic forms of the cofactor Mo(MGD)<sub>2</sub> cofactor also may be directly involved in the catalytic mechanism for substrate transformation. If this is the case, then scission and condensation reactions of the pyran ring may be part of the process that is associated with maneuvering those protons needed for nitrate reduction. A proposed proton diffusion route may be through D-MGD itself, with the guanine component close to the protein surface. The guanine amide moiety would form hydrogen bond to Asp 822 and to Lys 794, which would also be hydrogen bonded to a water molecule at the protein surface (Bertero et al. 2003).

**Periplasmic Nitrate Reductase (Nap)** Periplasmic nitrate reductases were first found in phototrophic and denitrifying bacteria, but their existence is now known to be widespread among Gram-negative bacteria. Nap systems have been studied at the biochemical or genetic level in *Cupriavidus necator* (previously known as *Ralstonia eutropha*), *Paracoccus denitrificans*, *E. coli*, and *Rhodobacter* species (Sparacino-Watkins et al. 2014a). The first crystal structure of a periplasmic nitrate reductase was solved for *Desulfovibrio desulfuricans* NapA, which is a monomeric protein (Dias et al. 1999). However, in many cases Nap is found to be a heterodimer consisting of a ~ 90–110 kDa catalytic subunit, NapA, and a 15-kDa diheme c cytochrome, NapB. NapA contains an MGD cofactor and an N-terminal [4Fe-4S] center, and NapB receives electrons from NapC, a membrane-bound tetraheme cytochrome c of 25 kDa. Known NapC homologues are involved in electron transfer between the membrane quinol pool and several soluble periplasmic reductases, giving evidence to NapC having a role in electron transfer. Electron transfer by the NapC family is proposed to be independent of cytochrome bc1 and not coupled to proton translocation.

The Nap protein is folded into four domains, all of which are involved in MGD cofactor binding. A single molybdenum atom is found in the active site and is coordinated to two MGD cofactors, a cysteine residue, a hydroxo ligand, as well as an electron transfer pathway whose bonds connect the molybdenum and the [4Fe-4S] center. In the oxidized state, the 6th coordination site is occupied by a hydroxide group. Based on this structure, a catalytic cycle involving a mono-oxo and a desoxo state has been proposed. However, based on subsequent crystal structures a revised the active site structure of NapA, where the terminal oxo group was replaced by a terminal sulfido group (Cerqueira et al. 2015). This structural variation has significant mechanistic consequences.

It is imperative to discuss the structure of NapA in comparison with the structures of other proteins that are similar to NapA. Several crystal structure studies (Cerqueira et al. 2009; Cerqueira et al. 2015; Najmudin et al. 2008) have raised questions regarding the identity of the ligand in the 6th coordination site, which has a significant impact on the reaction mechanism for these enzymes. In the fully oxidized state, the sixth coordination site is generally occupied by a terminal group (e.g., oxo and sulfido). A structural study on *E. coli* Fdh-H indicated that the terminal group is a sulfido rather than the originally suggested Mo—OH (Raaijmakers and Romao 2006). While the 2.3 Å structural resolution is not definitive, support of this idea came from biochemical studies (Thome et al. 2012). The FdhD gene product (*fdhD* is present in the *fdh* operon) is a sulfur transferase that inserts a cyanolyzable sulfur into the Mo-center in FdhF, the catalytic subunit of Fdh. Because FdhD is required for the proper maturation of all *E. coli* Fdh, it suggests that FdhF has a sulfido group as the sixth ligand forming Mo<sup>VI</sup>=S moiety rather than Mo = O or Mo – OH. When a sulfido group is present, it is thought to form a partial S---S or S---Se bond with the coordinating amino acid residue, cysteine, and selenocysteine, respectively. The description of the Mo center in NapA has also been revised similarly. The first crystal structure of the monomeric *D. desulfuricans* NapA (1.9 Å resolution) (Dias et al. 1999) demonstrated the presence of two prosthetic groups—FS0 and Moco, and a cysteine sulfur coordinating the Mo center. Based on electron density determinations, the 6th coordination position was assigned as being a terminal oxo group and later revised to include a terminal sulfido ligand instead (Najmudin et al. 2008). The structures of dimeric NapAB from *Cupriavidus necator* (resolution: oxidized, 1.6 Å; reduced, 1.72 Å) emphasized a Mo = S moiety in the active site (Coelho et al. 2011). The structures in the oxidized state as compared to those of the reduced state exhibit minimal perturbation with regard to the terminal ligand (Fourmond et al. 2008). Both the (Mo)S---S(cys) and Mo = S distances, 2.7 Å and 2.4 Å, respectively, are longer than typical distances found in small molecules (from a CCDC search, mean d(S---S) = 2.05 ± 0.06 Å, and mean d(Mo = S) = 2.15 ± 0.04 Å). Interestingly, there is no *fdhD* homolog in the *nap* operon, so the sulfido group is likely to be inserted using a protein not present in the *nap* operon. Arsenate reductase (ArrA), another member of the CISM family, shares a high degree of structural similarity with NapA. Recently, the crystal structure (1.8 Å resolution) of ArrAB from *Shewanella* sp. ANA-3 revealed the Mo center is coordinated by a cysteine sulfur and the 6th position is occupied by a

**Fig. 13.12** Crystal structure for NapAB heterodimer (PDB code 1OGY). NapA colored in blue, NapB in orange and the cofactors are shown in space fill model



terminal oxo group (Glasser et al. 2018). Like *nap*, the *arr* operon does not have an *fdhD* homolog. Whether the terminal ligand is an oxo- or sulfido has a profound implication on the reaction mechanism.

In addition, the crystal structure of *C. sphaeroides* NapAB complex has been determined (Fig. 13.12) to exhibit an electron transfer path from the heme centers in NapB to the Mo center through an intervening [4Fe-4S] cluster (Arnoux et al. 2003). The catalytic subunit, NapA, is composed of four domains. Domain I contains the cysteine residues that hold the [4Fe-4S] cluster in proximity to the D-MGD cofactor. Domains II and III have a mixed  $\alpha/\beta$  fold and are responsible for binding the P- and D-MGD molecules. Domain IV has an extending N-terminus that spans domains II and III ending in a  $\beta$ -barrel that sits above both MGD molecules. The overall architecture of NapB is pyramidal with a triangular base that docks onto NapA. The interaction between the two subunits is maintained by several hydrogen bonds as well as a salt bridge.

*Ethylbenzene dehydrogenase (EbdH)*. Ethylbenzene dehydrogenase produces chiral alcohols by irreversible, catalytic hydroxylation of hydrocarbons. Ethylbenzene dehydrogenase (EbdH) is a promiscuous enzyme that is able to catalyze the chiral hydroxylation of many alkylaromatic and alkylheterocyclic compounds into secondary alcohols. EbdH is another molybdoenzyme that belongs to the DMSOR family, and is able to catalyze the oxygen-independent, stereospecific hydroxylation



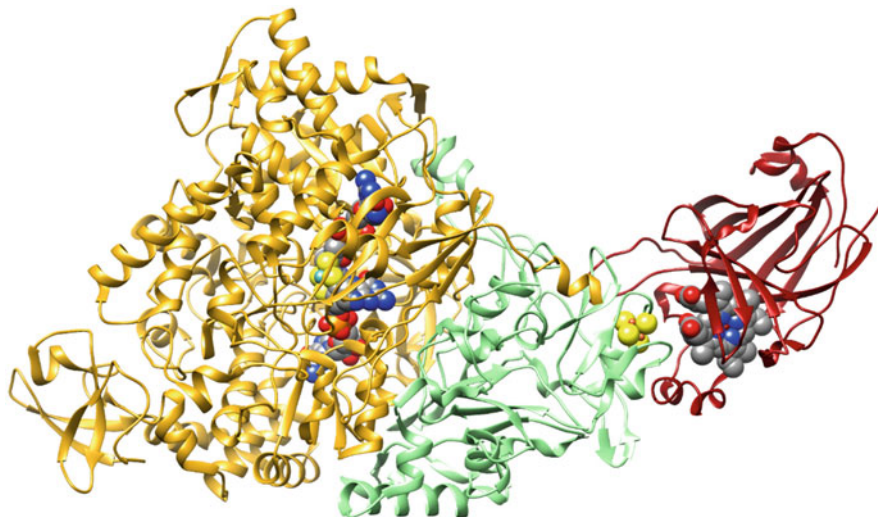


**Fig. 13.13** Crystal structure of *A. aromaticum* EbDH (PDB code, 2IVF). The protein is an  $\alpha\beta\gamma$  heterotrimer. The  $\alpha$  subunit is colored gold, the  $\beta$  subunit colored green, and the  $\gamma$  subunit colored cyan. The cofactors are shown in space fill model

of ethylbenzene to (S)-1-phenylethanol. EbDH is the first known enzyme to be capable of the direct anaerobic hydroxylation of nonactivated hydrocarbons, and in *Aromatoleum aromaticum*, a denitrifying betaproteobacterium, this enzyme is involved with the mineralization of ethylbenzene. EbDH is an  $\alpha\beta\gamma$  heterotrimer with subunits of molecular weights 96, 43, and 23 kDa (Fig. 13.13). It contains a molybdenum cofactor as well as a heme b559 cofactor that is linked by five iron–sulfur clusters a row. The active site is buried in the bottom of the  $\alpha$  subunit composed of Moco, and Asp 223 and His 192 side chains, which are thought to be involved in the catalytic process. Based upon other analogous molybdenum enzymes in the DMSO reductase family that catalyze oxygen atom transfer (OAT) reactions, it is proposed that an oxo ligand is coordinated to Mo in the oxidized form of the catalytically active enzyme (Szaleniec et al. 2014).

### 13.5 Mechanism of Action

The reactions of the pterin-containing molybdenum enzymes can broadly be divided into two categories: hydroxylation reactions and oxygen atom transfer (OAT) reactions. Both types of reactions result in a net change in one oxygen atom in the substrate. Significant research has been conducted toward the goal of understanding the reactivity of these enzymes, and several synthetic models have been developed. These two types of enzymatic reactions are summarized below.

### 13.5.1 Hydroxylation

**Xanthine Oxidase** The molybdenum hydroxylase enzymes, represented by the members of the xanthine oxidase (XO) family, contain an active site with a MoOS moiety. Xanthine oxidase itself can exist in two forms. The oxidized form is mostly seen in those mammalian enzymes where thiols are oxidized to disulfides. The reduced dehydrogenase form and the bacterial enzymes are generally stable in their dehydrogenase form. Xanthine dehydrogenase (XDH) catalyzes the oxidation of hypoxanthine to xanthine followed by oxidation of xanthine to uric acid with concomitant reduction of  $\text{NAD}^+$  (Fig. 13.14). All members of the XO family have at least another prosthetic group, in addition to the Moco, that serves as a partner electron transfer unit. This family of enzymes catalyzes hydroxylation reactions on a variety of aldehydes and aromatic heterocycles. During catalysis of the substrate, oxygen from water is incorporated into the enzymatic product and reducing equivalents are produced, rather than consumed as typically would occur in reactions of many monooxygenase systems (Hille 2005). The catalytic sites of several molybdenum hydroxylases are well studied and share many structural similarities, and the reaction mechanism is now understood in terms of the molecular structure.

The previously discussed Mo-OH group has been found to be the catalytically labile site for xanthine oxidase. This group is the donor of the oxygen atom that is incorporated into the product. This site is then regenerated with oxygen from the solvent with each catalytic cycle (Hille 2005). While the exact mechanism has been debated for years, now it is generally coalescing into the steps outlined in Fig. 13.15. The Mo-OH proton is abstracted by the conserved glutamate residue, there then occurs a nucleophilic attack on a carbon atom of the substrate to be hydroxylated. Because the Mo-O<sup>-</sup> moiety is a stronger electrophile than Mo-OH, it is expected that the active unit is Mo-OH rather than Mo-OH<sub>2</sub>.

Kinetic data of product formation by this enzyme complex can be plotted to yield a pK<sub>a</sub> curve of the ionization of the substrate, xanthine (Hille 2005). The pK<sub>a</sub> range was 6.6–7.4, where the pK<sub>a</sub> of 6.6 is attributed to Glu 1261 in the active site, which is also a universally conserved residue amongst the molybdenum hydroxylases. The pK<sub>a</sub> of 6.6 indicates that Glu 1261 acts as a general base catalyst to initiate the hydrolysis reaction (Hille 2005). The mechanism has also been investigated via computational analysis. The model for the active site, (ethylenedithiol)MoOS(OH), has been analyzed with a variety of substrates. The reaction with formamide gave a

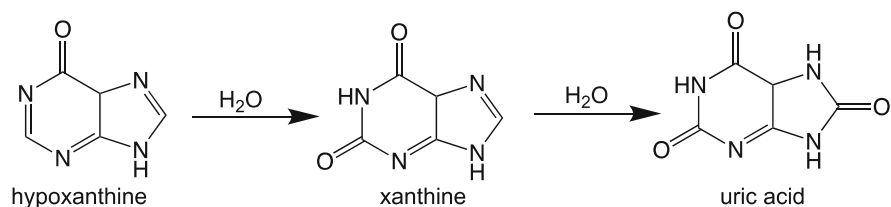


**Fig. 13.14** Conversion of hypoxanthine to xanthine to uric acid

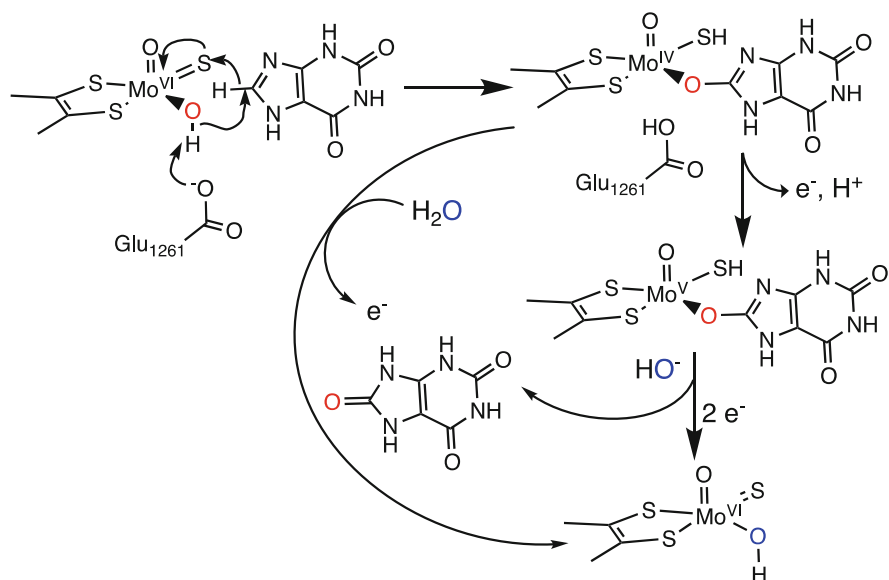


**Fig. 13.15** Hydroxylation mechanism displaying the role of conserved amino acid residue, Glu 1261

reduced model complex containing carbamate, the hydroxylated product of formamide (Hille 2005). Disposition of the partial bonds surrounding the carbon being hydroxylated causes a partial negative charge to accumulate on the hydrogen that is transferred to the  $\text{Mo}=\text{S}$  group (Hille 2005). This evidence is also consistent with the nucleophilic attack mechanism.

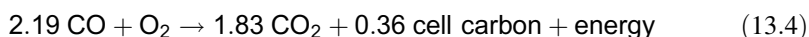
At the same time, a hydride transfer takes place to the  $\text{Mo}=\text{S}$  moiety resulting in  $\text{MoO}(\text{SH})$ . The product is dissociated from the Mo coordination sphere with a concerted electron–proton transfer regenerating the active  $\text{Mo}-\text{OH}$  moiety and the terminal  $\text{Mo}=\text{S}$  group. In this step, a base (solvent, i.e., water) regenerates the coordinated hydroxyl group. The exact sequence of events depends on the substrate and the reaction condition. In most cases, it is thought that the product dissociates before the electron transfer step. When the electron transfer precedes the displacement of the coordinated product, it generates the so-called ‘very rapid’ EPR signal. Several lines of experimental data support such a mechanism. The  $k_{\text{cat}}/K_{\text{m}}$  and  $k_{\text{red}}/K_{\text{m}}$  follow similar pH dependency (Albert and Brown 1954). The proton source for this  $\text{Mo}-\text{SH}$  moiety is the substrate as opposed to the solvent (Gutteridge et al. 1978). The slow turnover of 2-hydroxy-6-methyl purine (Tanner et al. 1978) gives rise to the very rapid signal, and the species giving rise to this very rapid signal has been spectroscopically characterized (Lorigan et al. 1994) (Howes et al. 1996; Manikandan et al. 2001).

Aldehyde oxidases presumably follow a similar mechanism as they have very similar structural attributes, including their active site structure, i.e., an equatorial sulfido group and an active  $\text{Mo}-\text{OH}$  moiety rather than a  $\text{Mo}-\text{OH}_2$  unit. It should be

noted, though, that aldehydes are generally more susceptible to nucleophilic attack than are heterocycles. Detailed mechanistic analyses of any bacterial aldehyde oxidase are yet to emerge. However, the *D. gigas* enzyme was the first crystallographically characterized aldehyde oxidase (Santos-Silva et al. 2009). A crystal structure of this arsenite-inhibited enzyme has been reported, which shows arsenite is bonded in the equatorial position suggesting the catalytically active Mo-OH moiety lies in the equatorial position (Boer et al. 2004).

A second xanthine dehydrogenase, *yagTSRQ*, has been identified in *E. coli* that encodes for YagTSR, later on called as PaoABC. It is a trimeric  $\alpha\beta\gamma$  protein as opposed to a more common  $(\alpha\beta\gamma)_2$  hexamer; it has a FAD as well as two [2Fe2S] clusters and is periplasmically located. PaoABC is very effective in catalyzing the oxidation of aromatic aldehydes (e.g., benzaldehyde and vanillin) with an enzymatic efficiency ( $k_{\text{cat}}/K_m$ ) of  $10^6$  and thus may be useful in detection (Badalyan et al. 2013) or detoxification of toxic chemicals (Neumann et al. 2009).

**CO Dehydrogenase** The overall reaction for CODH is shown in Eq. 13.4 (Hille et al. 2015):



In this process, oxidation of approximately six equivalents of CO to CO<sub>2</sub> provides the energy required to reductively fix one of the six equivalents of CO<sub>2</sub> formed via the pentose phosphate pathway (Jacobitz and Meyer 1989). This reaction has been examined computationally by two groups (Siegbahn and Shestakov 2005; Hofmann et al. 2005), where both mechanisms begin with CO coordination to the copper, then the activated CO undergoes nucleophilic attack by the equatorial Mo = O to yield the initial intermediate (Fig. 13.16). In one study, it was proposed that a thiocarbamate intermediate is very stable but can be forced to release CO<sub>2</sub> by either water or hydroxide displacement of the thiocarbamate from the Mo (Siegbahn and Shestakov 2005). Another study has stated that the previously mentioned thiocarbamate intermediate was not likely to form during the course of catalysis and proposed the reaction to proceed through the series of intermediates that ultimately release CO<sub>2</sub> (Hofmann et al. 2005). This proposed series of intermediates involves the CO carbon bonded to each of the Mo,  $\mu\text{S}$ , and Cu atoms. It has been suggested that these intermediates either may represent alternate resonances of a single structure or that the intermediates interconvert during catalysis (Shanmugam et al. 2013). Another possibility regarding the mechanism involving solvent water as nucleophile rather than the equatorial Mo = O has been considered, albeit considered less likely (Pelzmann et al. 2009). In that proposal, the active site Glu 763 acts as a base catalyst in deprotonating the water rather than having a direct attack by the Mo = O.

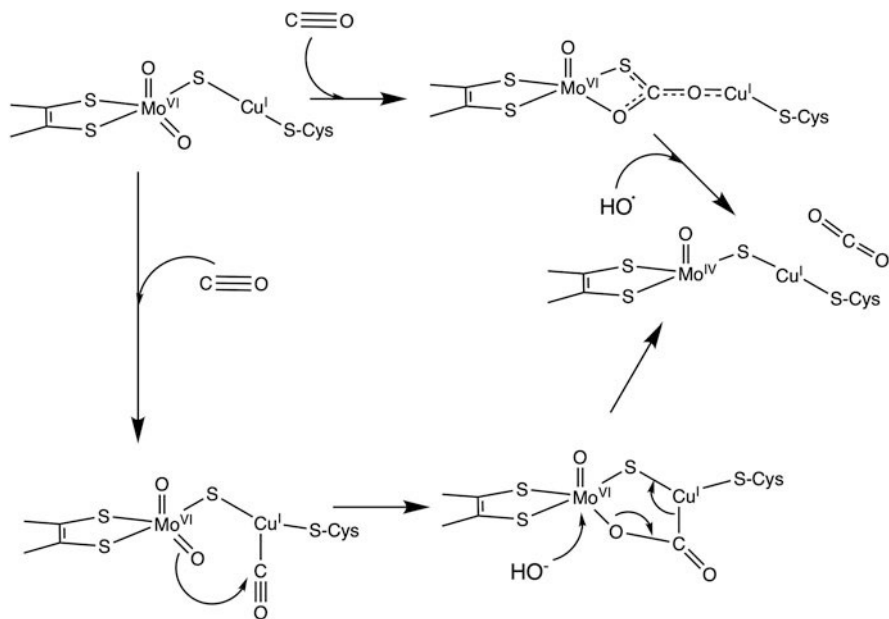


**Fig. 13.16** Two proposed reaction mechanisms for CO dehydrogenase: top, based on the crystal structure and bottom, based on a model isonitrile complex

### 13.5.2 Oxygen Atom Transfer

The members of the DMSO reductase and SO family carry out a direct oxygen atom transfer between their substrate and their product. Because oxo transferases transform their substrates into either reduced or oxidized forms by adding or removing an oxygen atom, the DMSOR and SO family members are called oxotransferases. The source, or sink, of the transferred oxygen atom is water as used by the XO family. These enzymes are also more diverse compared to other molybdenum enzymes in terms of their active site structure. They either possess a Mo-O(Ser), Mo-S(Cys), or Mo-Se(Sec) group that is contributed by the polypeptide in place of a labile Mo-OH group, and many do as well have a Mo = S group in place of the apical Mo = O.

The DMSO reductase reaction can be viewed as a combination of two half-cycles: the reductive half-cycle with oxidized mono oxo-Mo<sup>VI</sup> species and the oxidative half-cycle with reduced *des* oxo-Mo<sup>IV</sup> species. In the oxidative half-cycle, the reduced Mo<sup>IV</sup> form of the enzyme binds the substrate. Two electrons are then transferred from molybdenum to the substrate, yielding the reaction product DMS and the oxygen atom of the substrate is bound to the metal as an oxo-ligand (Kisker et al. 1997b). In the reductive half-cycle, two protons and two electrons are transferred to the molybdenum center via two proton coupled electron transfer (PCET) steps, yielding water and regenerating the Mo<sup>IV</sup> state. The mechanism used by

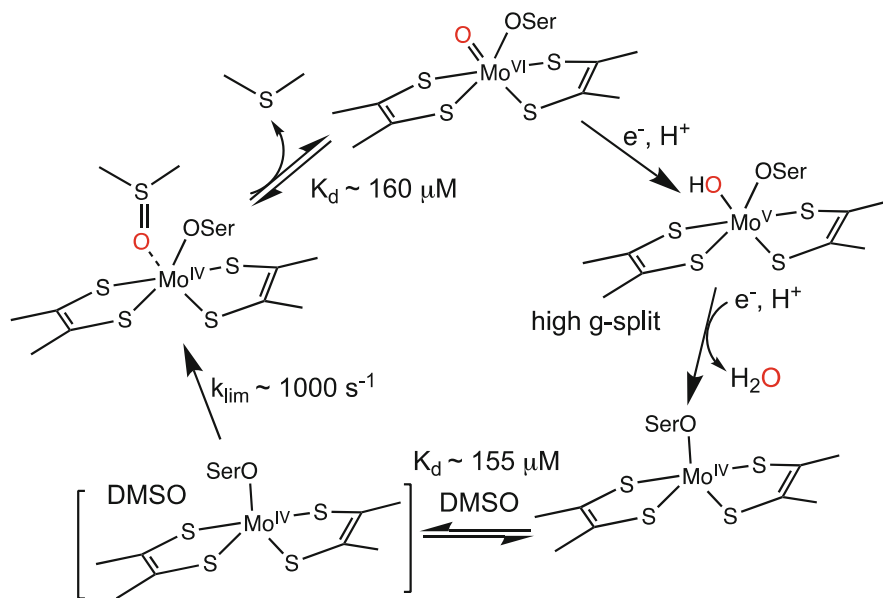


**Fig. 13.17** Catalytic cycle of DMSOR (adopted from Hille et al. (2014))

*C. sphaeroides* DMSOR has been studied under high enzyme concentrations by monitoring optical signals of the enzyme itself. Multiple component analysis of the optical and EPR spectra collected under steady-state conditions have revealed four different species: the reduced enzyme, the reduced enzyme complexed with DMSO, the oxidized enzyme, and the EPR active  $\text{Mo}^{\text{V}}$  high- $g$  split form that has been detected during rereduction of the enzyme. Of these, the  $\text{E}_{\text{red}} \cdot \text{DMSO}$  complex accumulates with reduced catalytic output (Cobb et al. 2005). The presence of the  $\text{E}_{\text{red}} \cdot \text{DMSO}$  complex has been corroborated by spectroscopic and crystallographic investigations.

Since DMSO reductase does not contain a second cofactor that could transfer electrons to Moco, an external electron donor, such as cytochrome, is required for this step. Direct binding of DMSO to Mo through the oxygen atom is possible because of the decreased number of metal ligands and the sidechain of Ser 147 in the reduced form (Kisker et al. 1997b). The binding of the substrate leads to this coordinated process of electron transfer, where the lengthening of the S–O bond stabilizes the S–O  $\pi$  orbital. This acts to facilitate electron transfer from the molybdenum concomitantly with electron transfer from the oxygen to sulfur. The dithiolate ligands act to stabilize the ground state in the reduced complex, facilitating the overall reaction. After the reaction product is liberated, molybdenum would be oxidized to the  $\text{Mo}^{\text{VI}}$  state, binding to the oxo ligand, which completes the oxidative half-cycle of the reaction (Kisker et al. 1997b). The axial terminal oxygen as  $\text{Mo}=\text{O}$  allows for regeneration of the reduced enzyme following oxygen transfer. In each

cycle, a single electron is transferred to the active site, which restores the Mo<sup>IV</sup> state of the enzyme (Fig. 13.17).

Two mechanisms by which the electron-donating cytochrome binds to the enzyme have been suggested. One mechanism proposes that cytochrome binds into the large depression above the active site and electron transfer to the molybdenum center is mediated by the side chain of Trp 388 (Schindelin et al. 1996). After the formation of the Mo<sup>IV</sup> state, a conformational change of this residue could allow entry of DMSO to the active site. The second mechanism proposes cytochrome binding to the surface nearest the pterin, where it could transfer electrons via this pterin to the molybdenum (Schneider et al. 1996). This part of the surface is covered by the conserved residues 643–650, which mediate numerous protein-cofactor interactions. In this proposed mechanism, an oxygen atom would ultimately be transferred from the substrate, generating water. The sidechain of Tyr114, which is hydrogen-bonded to the oxo ligand, has been hypothesized to accompany this proton transfer. However, this residue is not conserved among other oxo transferases and may indicate that the proton donor can vary throughout members of this family (Kisker et al. 1997b). Steady state kinetic assays of the DMSOR Y114F variant show three times higher  $k_{\text{cat}}$  than the wild-type variant and a much higher  $K_m$ . The breakdown of the  $E_{\text{red}} \cdot \text{DMSO}$  complex is faster in the variant than in the wild-type enzymes and rebinding of DMS to the oxidized enzyme occurs to a lesser extent in the variant. This variant also exhibits the high-g split EPR signal (Johnson and Rajagopalan 2001). Thus, suggesting the tyrosine does not interact with the Mo center and this is consistent with a proposal of the tyrosine interacting with the substrate. Interestingly, in related TMAO reductases, the tyrosine is replaced with valine and the behavior of the TMAO reductase is similar to that of the DMSOR Y114F variant.

Direct atom transfer between DMSO and the Mo center of DMSO reductase has been probed in the *C. sphaeroides* enzyme by using <sup>18</sup>O labeled DMSO (Schultz et al. 2002). Under the single turnover condition, the labeled oxygen is transferred to the Mo center, which can then be extracted with oxygen abstracting water-soluble phosphine. The labeled phosphine has been probed by mass spectrometry. This unequivocally proves the direct oxygen atom transfer between the substrate and the Mo center in DMSO reductase.

The reaction mechanism of the chicken liver and human sulfite oxidase has been investigated in detail (Astashkin et al. 2007; Johnson-Winters et al. 2010) while the corresponding bacterial analogs, i.e., sulfite dehydrogenase, have not been investigated to that same extent. It is, however, expected that the active center of the enzyme is composed of a dioxo-Mo<sup>VI</sup> center that transfers its equatorial oxo- group to the substrate sulfite. Dioxo-Mo centers are well known oxo-donors, and important small molecule models have been developed in an effort to understand the reaction mechanism of this oxygen atom chemistry (Basu et al. 2010; Kail et al. 2006; Basu et al. 2009).

### 13.5.3 *Effects of the Coordinating Amino Acids: Spectator and Actor*

The coordinating residues of molybdenum enzymes are critical for their physiological function. Among three families of molybdenum enzymes; DMSO reductases, sulfite oxidases, and xanthine oxidases, only members of the xanthine oxidase family do not have any coordinated amino acid residue. Members of the sulfite oxidase family, on the other hand, have a coordinated amino acid residue, namely cysteine, that remains coordinated during the course of the catalysis. The members of the DMSO reductase family have a more diverse protein-based coordination to the molybdenum site and a relevant question is how does the coordinated amino acid residue impact the mechanism.

The coordinating residues for the DMSO reductase family have been hypothesized to influence substrate preference by adjusting the physical properties of the molybdenum center (Boyington et al. 1997). It is generally believed that the coordinating amino acid residue can modulate the redox potential of the metal center and, in some cases, the coordinated amino acid may also serve as a conduit for the proton shuttle.

The main function of sulfite oxidase is to oxidize sulfite to sulfate, which takes two electrons, and the catalytic center is regenerated by external electron acceptors such as either cytochrome C or O<sub>2</sub>. These two half-reactions constitute the catalytic cycle in sulfite oxidase, and in both half reactions, the coordinated amino acid residue remains coordinated at the equatorial position. Glasser et al. proposed a direct oxygen atom transfer reaction for the transformation of arsenate to arsenite by arsenate reductase (Glasser et al. 2018). In this mechanism, the ligating cysteine residue remains coordinated to Mo during catalysis (Fig. 13.16). Thus, in these cases, the coordinated amino acid residue plays a “spectator” role. However, in some other cases, the coordinated amino acid residue may not remain coordinated in the same fashion and thus plays an “actor” role.

The reaction mechanism of arsenite oxidase is likely to involve oxygen atom transfer, similar to that of DMSO reductase and nitrate reductase. The oxygen atom is proposed to be transferred from molybdenum to arsenite followed by two one-electron oxidations of the Mo center.

Formate dehydrogenases are structurally diverse enzymes with a conserved active site. In the oxidized state, the Mo center is coordinated by four sulfur atoms from the pterin cofactor and a protein-based ligand (cysteine or selenocysteine) and a terminal sulfido group in a trigonal prismatic geometry (Boyington et al. 1997). The structure of the reduced site is less clear in *E.coli* Fdh-H. The molybdenum center is square pyramidal with four sulfurs occupying the equatorial positions and the Se atom is the apical position. A reinterpretation of the structure shows that the Se atom is actually dissociated from the Mo atom, and the 5th position is occupied by a sulfido group (Raaijmakers and Romao 2006). However, X-ray absorption studies showed that the Sec/Cys is in the bonding distance of Mo and there is a short Se—S distance. The structural features led to a mechanistic proposal called the “S-shift” mechanism.



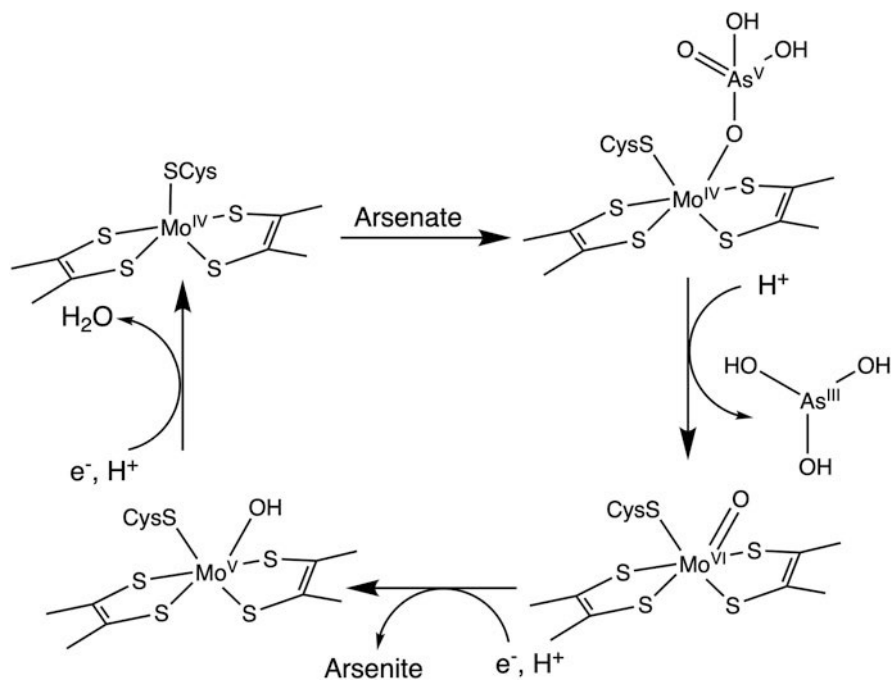


**Fig. 13.18** Arsenate reductase molybdenum center architecture and substrate transformation adopted from Glasser et al. (2018)

In the S-shift mechanism, the coordinated amino acid residue shifts to form a disulfide/sulfide-selenide bond, thus opening the coordination site for the substrate to bind. This shift presumably provides energetically favorable pathways for substrate transformation. Computational studies have provided support for such structural change that happens only in the presence of the substrate. Thus, when there is no substrate present, the Mo-center remains hexa coordinated. The same mechanism has been proposed for the periplasmic nitrate reductase with a terminal sulfido group as opposed to a terminal oxo group.

The initially proposed catalytic mechanism for NapA was based on the structure of *D. desulfuricans* NapA, where  $\text{NO}_3^-$  binds to the five-coordinate Mo<sup>IV</sup>-center via one O-atom to give a six-coordinate center (Dias et al. 1999). The  $\text{NO}_3^-$  is reduced to  $\text{NO}_2^-$  and the bridging oxygen is transferred to Mo, becoming a terminal oxo group of the now oxidized Mo<sup>VI</sup> center. Reduction and protonation of the Mo<sup>VI</sup>-center results in conversion of the Mo = O unit to a Mo<sup>IV</sup>—(OH<sub>2</sub>) moiety, leading to regeneration of the active center. This mechanism is consistent with the OAT reaction proposed for DMSOR and ArrAB (Figs. 13.17 and 13.18). The conclusion that the terminal ligand to Mo in oxidized NapA of both *D. desulfuricans* and *C. necator* is a sulfido rather than oxo group has led to a revision of the mechanism (Najmudin et al. 2008; Coelho et al. 2011). Specifically, a disulfide bond between the

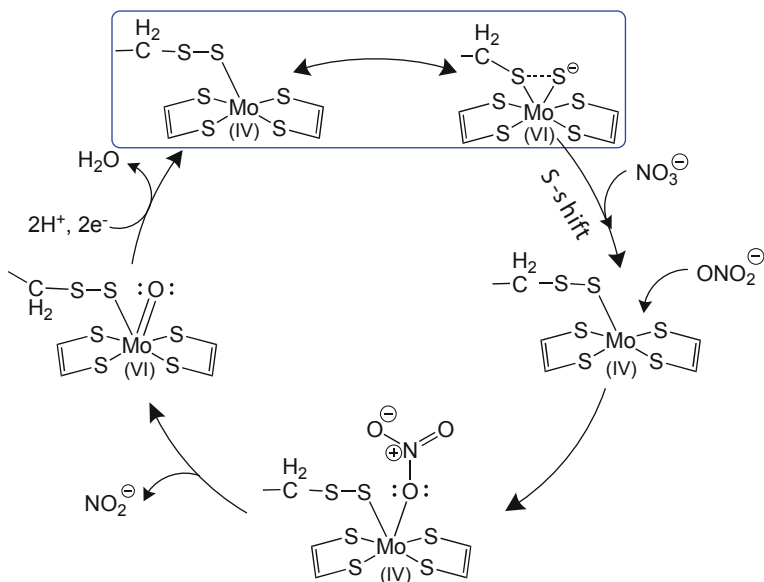


**Fig. 13.19** Catalytic cycle of NapA showing the S-shift mechanism

terminal sulfido and ligating cysteine sulfur has been proposed to form in the presence of substrate, with decoordination of the cysteine S from Mo. Nitrate binds to the vacant site, transfers an oxygen atom to the Mo-center, and nitrite is released. The change in the coordination of cysteine S is termed as an ‘S-shift’ event (Fig. 13.19). An updated S-shift mechanism proposes the initial state of the enzyme to have a  $\text{Mo}-\text{S}^-$  as opposed to the  $\text{Mo}=\text{S}$  moiety in the catalytic cycle and no state had a discrete  $\text{Mo}=\text{S}$  bond (Cerqueira et al. 2015). Support for this mechanism came from density functional theory (DFT) calculations (Cerqueira et al. 2009; Hofmann 2009). Later, DFT calculations of EPR parameters indicated the presence of a putative  $\text{MoS}_6$  species with a terminal sulfido group (Biaso et al. 2012). A terminal sulfido group can undergo internal redox with the cysteine sulfur forming a disulfide bond, as shown in Fig. 13.17 (Sparacino-Watkins et al. 2014a).

It is generally believed that the catalytic mechanism of TMAO reductase follows that of DMSO reductase following a direct oxygen atom transfer reaction. However, the direct OAT mechanism for *E. coli* TMAOR has been updated (Kaufmann et al. 2018). Cells grown under anaerobic conditions show a terminal sulfido group, whereas cells grown under aerobic conditions show an oxo group. Both forms exhibit TMAOR activity, and the sulfurated form exhibits a higher specific activity compared to the oxo form. Since TMAO cannot bind to the coordinatively saturated Mo through its oxygen atom, it was suggested that the coordinated serine residue dissociates from the Mo-center, generating a vacant site for substrate binding. An OAT from TMAO to Mo would result in an oxo-sulfido- $\text{Mo}^{\text{VI}}$  center, and the terminal sulfido group remains intact throughout the catalytic turnover (Fig. 13.20).

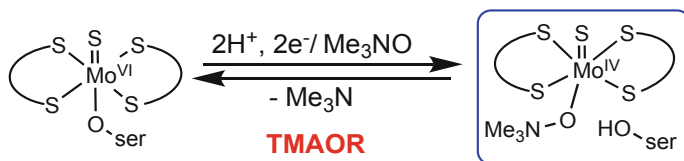
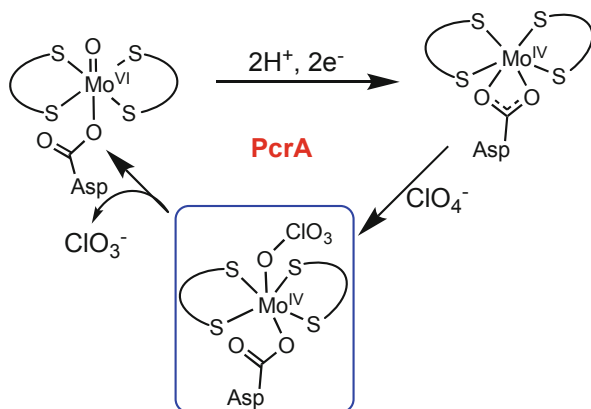


**Fig. 13.20** Proposed dissociation of the coordinated serine from Mo-center during catalysis of TMAO reductase

**Fig. 13.21** Proposed catalytic cycle of PcrA showing a shift in the coordination mode during catalysis



The structure of perchlorate reductase (PcrAB) reported by Youngblut et al. (Youngblut et al. 2016) suggests that the reduction of perchlorate occurs via an OAT reaction (Fig. 13.21). In the absence of substrate, the coordinating aspartate binds the Mo<sup>IV</sup> center in a bidentate fashion. In the presence of ClO<sub>4</sub><sup>-</sup> the Asp residue shifts to a monodentate coordination mode for ClO<sub>4</sub><sup>-</sup> to bind the Mo-center allowing the OAT reaction to occur, resulting in ClO<sub>3</sub><sup>-</sup> and an oxo-Mo<sup>VI</sup> center. Upon 2e<sup>-</sup> reduction of this Mo<sup>VI</sup> center coupled with proton transfer, the Asp residue shifts to a bidentate mode of coordination to the Mo<sup>IV</sup> center. Thus, in perchlorate reductase, the coordinated amino acid residue plays a gating role as an active participant in catalysis. The overall folds and active site of PcrA are very close to that of NarG. Thus, NarG may also function similarly where the coordinating carboxylate residue switches its binding modes.

While major structural changes can be visualized from crystallography, the subtle influence of amino acid residues is not always easily detected. Even more subtle is the impact of coordinated amino acid residues on the energy landscape of catalysis. A comprehensive investigation where systematic change, through site-directed mutagenesis, has been reported and allowed estimating the energy profile of periplasmic nitrate reductase (NapA) from *Campylobacter jejuni* (Mintmier et al. 2021). The coordinating amino acid in *C. jejuni* NapA is Cys 176, and that gene has been mutated to generate three variants, C176S, C176D, and C176A, and the kinetic parameters of those variants have been tested using various substrates (Mintmier et al. 2021; Mintmier et al. 2018). The kinetic findings were used to calculate ES and

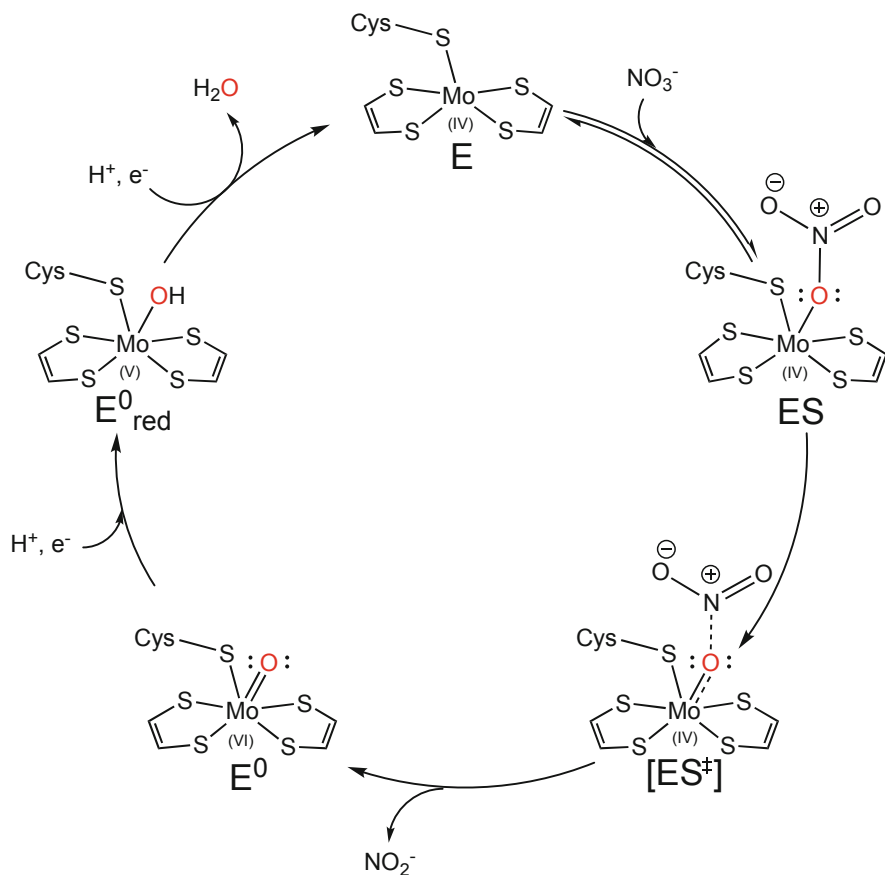


**Fig. 13.22** Proposed catalytic cycle for the periplasmic nitrate reductase (Nap) adopted from Mintmier et al. (2021)

[ES<sup>‡</sup>] energy states of the native and variant enzymes (Mintmier et al. 2021), where ES is the enzyme–substrate complex, and [ES<sup>‡</sup>] is the enzyme bound to the substrate in the transition state (Fig. 13.22).

The activation energy is lower for nitrate reduction in native NapA and higher in the serine and aspartate variants. The coordinating cysteine residue in the native enzyme was found to be involved in stabilizing ES and greatly stabilizing [ES<sup>‡</sup>] states during catalysis of nitrate (Mintmier et al. 2021). Reduction of non-native substrate TMAO by native NapA had a higher activation energy barrier than that of nitrate reduction (Mintmier et al. 2021). In the C176S variant, the coordinating serine impacted the binding energy by stabilizing the ES state in TMAO reduction. This increased  $K_M$  and  $k_{cat}$  compared to native NapA, while C176D and C176A variants were completely inactive toward TMAO. The increase in the C176S enzyme's reductive activity was attributed to lowering ES binding energy and

lowering  $K_M$  in the native enzyme. The serine ligand destabilizes the ES and  $[ES^\ddagger]$  states, which lowers the activation energy when nitrate is used as the substrate, whereas it stabilizes in the reaction with TMAO. This evidence shows the serine residue tunes substrate selectivity. The C176D variant mostly impacted ES, impacting  $[ES^\ddagger]$  a little bit and stabilized binding to non-native substrate DMSO, while other variants did not. The aspartate variant was interestingly able to catalyze the DMSO reduction when neither native NapA nor other variants could. Overall, this investigation provided insight into the coordinating amino acid's role in catalysis, substrate affinity, and stabilization. The coordinating residue is a crucial component in this molybdenum enzyme's substrate selectivity and its ability to then turn the substrate over. The coordinating residue achieve this goal by physically adjusting the properties of the molybdenum center.

### 13.5.4 Effects of Amino Acids Near the Metal Center

Within the molybdenum enzymes, there are a slew of critical and influential amino acids other than the coordinating one. Often, these amino acid residues are crucial in substrate binding that allows the proper orientation of the substrate for catalysis. In addition, there are amino acid residues that stabilize the molybdenum cofactor, perhaps poising it to optimal redox potentials through opening or closing of the pyran ring. Often these effects are very specific to the enzyme in question, and they can be observed from the structure. For example, the polypeptide chain of DMSO reductase folds into four domains: I, II, III, and IV, which form a slightly elongated molecule, as mentioned previously (Kisker et al. 1997b). The amino acids in these domains provide numerous interactions between the protein and cofactor, including about 45 direct hydrogen bonds. Domains II and III interact primarily with each of the guanosines and share similar structural attributes. The polypeptide loop in domain IV contains a large number of highly conserved residues and is crucial for binding the two pterin moieties of the cofactor (Kisker et al. 1997b). Residues 381–393 of *C. sphaeroides* DMSO reductase were found to be disordered in the crystal structure. Residual density near the active site was assigned to the sidechain that contains Trp 388, where it takes two alternate conformations. In the first conformation, Trp 388 blocks access to the active site by insertion of its sidechain between the aromatic ring systems of Tyr 165 and Trp 196, leading to stacking interactions. In the second conformation, the sidechain is displaced and perpendicular to that of Trp 196, which may suggest that Trp 388 might serve as a lid that can shield the active site when necessary (Kisker et al. 1997b).

In the case of xanthine oxidase, as discussed earlier, the sidechain of Glu 869 acts as a nucleophile to abstract the proton from the hydroxide group. This side chain is thought to cause a slight rotation that allows substrate to bind to the active center (Kisker et al. 1997b).

These are just a few examples of the effects of amino acids near the molybdenum center but give an insight into their functions. Several domains of an enzyme play

important coordinated roles in catalysis despite all not being directly present in the active site. The residues within these domains may interact with others for stabilization or may fold in certain ways to physically aid in substrate funneling to the active site. The influence of some of these amino acid residues has been discussed in the above, in the structures section (Sect. 13.4) of this chapter.

## 13.6 Concluding Remarks

It should be evident from this account that pterin-containing microbial molybdenum enzymes are important in essential life processes. These enzymes have contributed to the enormous diversity of the microbial world. The advent of genomics and proteomics significantly enhanced both our appreciation and our understanding of this family of enzymes. The presence of Moco in LUCA has firmly placed molybdenum enzymes in the context of evolution, and a detailed analysis of ~1600 sequences from a wide variety of species revealed that arsenate reductase is the ancient molybdenum enzyme. We now understand important processes such as the transport of molybdenum into a cell, and biosynthesis of the cofactors, although more remains to be learned about the functional roles of some proteins such as ModF and MoaB. The importance of radical SAM enzymes in the biosynthesis of molybdenum cofactors indicates the pterin molybdenum enzymes are reliant on the radical SAM superfamily of metalloenzymes. With crystal structures of several molybdoenzymes having been determined, it is now possible to interrogate the mechanism of action at an atomic level. Over the years, there has been significant progress in this area. The mechanism of sulfite oxidase is well defined. However, the mode of action in a more complex family, i.e., DMSOR family is not completely understood. For example, we still need to know how the S-shift mechanism works in NapA. The future of research in this field of science promises to be exciting as surely more will be learned. At this point, there is limited knowledge about the processing of enzyme degradation, and it is expected that this area will be developed in the future. Very importantly, technological application of these diverse and rich enzymes is likely to come. For example, we might ask if these enzymes can be used as sensors for the detection of toxic materials such as arsenic in the field, and can the enzymes be modified for biotechnological application in remediating the toxic materials. Substantial progress has been made in the area of expression, purification and characterization of this important class of enzymes. The advances made in this area of science are going to be even more important for understanding the chemistry of enzymes that are identified by genomics in difficult to culture organisms. The field itself has attracted scientists from different subdisciplines from microbiology, genomics, geology, biochemistry, synthetic chemistry, to molecular spectroscopy, and it is likely to grow. This account details much have been learned, and it also promises more to come.

**Acknowledgments** We thank our past and present coworkers and collaborators who have inspired us with stimulating discussions. We are grateful for financial support from the National Institutes of Health and National Science Foundation for support of our work on microbial molybdenum enzymes.

## References

- Afkar E, Lisak J, Saltikov C, Basu P, Oremland RS, Stolz JF (2003) The respiratory arsenate reductase from *Bacillus selenitireducens* strain MLS10. *FEMS Microbiol Lett* 226:107–112
- Aguilar-Barajas E, Díaz-Pérez C, Ramírez-Díaz MI, Riveros-Rosas H, Cervantes C (2011) Bacterial transport of sulfate, molybdate, and related oxyanions. *Biometals* 24:687–707. <https://doi.org/10.1007/s10534-011-9421-x>
- Albert A, Brown D (1954) Purine studies. Part I. Stability to acid and alkali. Solubility. Ionization. Comparison with pteridines. *J Chem Soc* 1954:2060–2071
- Anderson GL, Williams J, Hille R (1992) The purification and characterization of Arsenite oxidase from *Alcaligenes faecalis*, a molybdenum-containing hydroxylase. *J Biol Chem* 267:23674–23682
- Arnoux P, Sabaty M, Alric J, Frangioni B, Guigliarelli B, Adriano J-M et al (2003) Structural and redox plasticity in the heterodimeric periplasmic nitrate reductase. *Nat Struct Biol* 10:928–934. <https://doi.org/10.1038/nsb994>
- Astashkin AV, Johnson-Winters K, Klein EL, Byrne RS, Hille R, Raitsimring AM et al (2007) Direct demonstration of the presence of coordinated sulfate in the reaction pathway of *Arabidopsis thaliana* sulfite oxidase using <sup>33</sup>S labeling and ESEEM spectroscopy. *J Am Chem Soc* 129:14800–14810
- Axley M, Grahame DA, Stadtman TC (1990) *Escherichia coli* formate-hydrogen lyase. Purification and properties of the selenium-dependent formate dehydrogenase component. *J Biol Chem* 265:18213–18218
- Badalyan A, Neumann-Schaal M, Leimkühler S, Wollenberger U (2013) A biosensor for aromatic aldehydes comprising the mediator dependent PaoABC-aldehyde oxidoreductase. *Electroanalysis* 25:101–108
- Basu P, Burgmayer SJN (2011) Pterin chemistry and its relationship to the molybdenum cofactor. *Coord Chem Rev* 255:1016–1038. <https://doi.org/10.1016/j.ccr.2011.02.010>
- Basu P, Kail BW, Young CG (2010) Influence of the oxygen atom acceptor on the reaction coordinate and mechanism of oxygen atom transfer from the Dioxo-Mo(VI) complex, TpiPrMoO<sub>2</sub>(OPh), to tertiary phosphines. *Inorg Chem* 49:4895–4900
- Basu P, Nemykin VN, Sengar RS (2003) Syntheses, spectroscopy, and redox chemistry of encapsulated Oxo-Mo(V) centers: implications for Pyranopterin-containing molybdoenzymes. *Inorg Chem* 42:7489–7501
- Basu P, Nemykin VN, Sengar RS (2009) Substituent effect on oxygen atom transfer reactivity from oxomolybdenum centers: synthesis, structure, electrochemistry, and mechanism. *Inorg Chem* 48:6303–6313
- Bertero M, Rothery R, Palak M, Hou C, Lim D, Blasco F et al (2003) Insights into the respiratory electron transfer pathway from the structure of nitrate reductase A. *Nature Struct Biol* 10:681–687. <https://doi.org/10.1038/nsb969>
- Biaso F, Burlat B, Guigliarelli B (2012) DFT investigation of the molybdenum cofactor in periplasmic nitrate reductases: structure of the Mo(V) EPR-active species. *Inorg Chem* 51:3409–3419. <https://doi.org/10.1021/ic201533p>
- Bilen S, Dick WA (2011) Sulfite oxidase enzyme activity in soil. *Biol Fertil Soils* 47:647–654

- Boer DR, Thapper A, Brondino CD, Romão MJ, Moura JJ (2004) X-ray crystal structure and EPR spectra of "Arsenite-inhibited" *Desulfovibrio gigas* aldehyde dehydrogenase: A member of the xanthine oxidase family. *J Am Chem Soc* 126:8614–8615
- Bonin I, Martins BM, Purvanov V, Fetzner S, Huber R, Dobbek H (2004) Active site geometry and substrate recognition of the molybdenum hydroxylase quinoline 2-oxidoreductase. *Structure* 12: 1425–1435
- Bortels H (1930) Molybdenum as a catalyzer in biological nitrogen-fixation. *Arch Mikrobiol* 1: 333–342
- Boyington JC, Gladyshev VN, Khangulov SV, Stadtman TC, Sun PD (1997) Crystal structure of formate dehydrogenase H: catalysis involving Mo, molybdopterin, selenocysteine, and an Fe<sub>4</sub>S<sub>4</sub> cluster. *Science* 275:1305–1308
- Britannica T Editors of Encyclopaedia (2020) Peter Jacob Hjelm. Accessed <https://www.britannica.com/biography/Peter-Jacob-Hjelm>
- Buc J, Santini CL, Giordani R, Czjzek M, Wu LF, Giordano G (1999) Enzymatic and physiological properties of the tungsten-substituted molybdenum TMAO reductase from *Escherichia coli*. *Mol Microbiol* 32:159–168
- Carqueira NMFSA, Gonzalez PJ, Brondino CD, Romao MJ, Romao CC, Moura I et al (2009) The effect of the sixth sulfur ligand in the catalytic mechanism of periplasmic nitrate reductase. *J Comput Chem* 30:2466–2484. <https://doi.org/10.1002/jcc.21280>
- Carqueira NMFSA, Gonzalez PJ, Fernandes PA, Moura JGG, Ramos MJ (2015) Periplasmic nitrate reductase and Formate dehydrogenase: similar molecular architectures with very different enzymatic activities. *Acc Chem Res* 48:2875–2884. <https://doi.org/10.1021/acs.accounts.5b00333>
- Coates JD, Achenbach LA (2004) Microbial perchlorate reduction: rocket-fuelled metabolism. *Nature Rev Microbiol* 2:569–580
- Cobb N, Conrads T, Hille R (2005) Mechanistic studies of *Rhodobacter sphaeroides* Me2SO reductase. *J Biol Chem* 280:11007–11017
- Coelho C, Gonzalez PJ, Moura JG, Moura I, Trincao J, Romao MJ (2011) The crystal structure of *Cupriavidus necator* nitrate reductase in oxidized and partially reduced states. *J Mol Biol* 408: 932–948. <https://doi.org/10.1016/j.jmb.2011.03.016>
- Constantinidou C, Hobman JL, Griffiths L, Patel MD, Penn CW, Cole JA et al (2006) A reassessment of the FNR regulon and transcriptomic analysis of the effects of nitrate, nitrite, NarXL, and NarQP as *Escherichia coli* K12 adapts from aerobic to anaerobic growth. *J Biol Chem* 281:4802–4815
- Contreras I, Toro CS, Troncoso G, Mora GC (1997) *Salmonella typhi* mutants defective in anaerobic respiration are impaired in their ability to replicate within epithelial cells. *Microbiology* 143(Pt 8):2665–2672. <https://doi.org/10.1099/00221287-143-8-2665>
- Coughlan M (1983) The role of molybdenum in human biology. *J Inher Metabol Dis* 6:70–77
- Czjzek M, Dos Santos J-P, Pommier J, Giordano G, Méjean V, Haser R (1998) Crystal structure of oxidized trimethylamine N-oxide reductase from *Shewanella massilia* at 2.5 Å resolution. *J Mol Biol* 284:435–447
- Dias J, Than M, Humm A, Bourenkov GP, Bartunik HD, Bursakov S et al (1999) Crystal structure of the first dissimilatory nitrate reductase at 1.9 Å solved by MAD methods. *Structure* 7:65–79. [https://doi.org/10.1016/s0969-2126\(99\)80010-0](https://doi.org/10.1016/s0969-2126(99)80010-0)
- Dobbek H, Gremer L, Kiefersauer R, Huber R, Meyer O (2002) Catalysis at a dinuclear [CuSMo(O)OH] cluster in a CO dehydrogenase resolved at 1.1-Å resolution. *Proc Natl Acad Sci U S A* 99:15971–15976
- Dobbek H, Gremer L, Meyer O, Huber R (1999) Crystal structure and mechanism of CO dehydrogenase, a molybdo iron-sulfur flavoprotein containing S-selenylcysteine. *Proc Natl Acad Sci U S A* 96:8884–8889
- Dong Y, Wang J, Fu H, Zhou G, Shi M, Gao H (2012) A Crp-dependent two-component system regulates nitrate and nitrite respiration in *Shewanella oneidensis*. *PLoS One* 7:e51643



- Doolittle WF (2000) The nature of the universal ancestor and the evolution of the proteome. *Curr Opin Struct Biol* 10:355–358. [https://doi.org/10.1016/S0959-440X\(00\)00096-8](https://doi.org/10.1016/S0959-440X(00)00096-8)
- Dos Santos J-P, Iobbi-Nivol C, Couillaud C, Giordano G, Méjean V (1998) Molecular analysis of the trimethylamine N-oxide (TMAO) reductase respiratory system from a *Shewanella* species. *J Mol Biol* 284:421–433
- Ellis PJ, Conrads T, Hille R, Kuhn P (2001) Crystal structure of the 100 kDa arsenite oxidase from *Alcaligenes faecalis* in two crystal forms at 1.64 Å and 2.03 Å. *Structure* 9:125–132
- Enroth C, Eger BT, Okamoto K, Nishino T, Nishino T, Pai EF (2000a) Crystal structures of bovine milk xanthine dehydrogenase and xanthine oxidase: structure-based mechanism of conversion. *Proc Natl Acad Sci U S A* 97:10723–10728
- Enroth C, Eger BT, Okamoto K, Nishino T, Nishino T, Pai EF (2000b) Crystal structures of bovine milk xanthine dehydrogenase and xanthine oxidase: structure-based mechanism of conversion. *Proc Natl Acad Sci* 97:10723–10728
- Fischer B, Enemark JH, Basu P (1998) A chemical approach to systematically designate the pyranopterin centers of molybdenum and tungsten enzymes and synthetic models. *J Inorg Biochem* 72:13–21
- Fourmond V, Burlat B, Dementin S, Arnoux P, Sabaty M, Boiry S et al (2008) Major Mo(V) EPR signature of *Rhodobacter sphaeroides* periplasmic nitrate reductase arising from a dead-end species that activates upon reduction. Relation to other Molybdoenzymes from the DMSO reductase family. *J Phys Chem B* 112:15478–15486. <https://doi.org/10.1021/jp807092y>
- Gennaris A, Ezraty B, Henry C, Agrebi R, Vergnes A, Oheix E et al (2015) Repairing oxidized proteins in the bacterial envelope using respiratory chain electrons. *Nature* 528:409–412
- George GN, Pickering IJ, Pushie MJ, Nienaber K, Hackett MJ, Ascone I et al (2012) X-ray-induced photo-chemistry and X-ray absorption spectroscopy of biological samples. *J Synchro Rad* 19: 875–886
- Giudici-Orticoni M-T, Samama J-P, Ilbert M, Méjean V, Iobbi-Nivol C (2003) Involvement of a mate chaperone (TorD) in the maturation pathway of molybdoenzyme TorA. *J Biol Chem* 278: 28787–28792
- Glasser NR, Oyala PH, Osborne TH, Santini JM, Newman DK (2018) Structural and mechanistic analysis of the arsenate respiratory reductase provides insight into environmental arsenic transformations. *Proc Natl Acad Sci* 115:E8614–E8623
- Gnandt E, Schimpf J, Harter C, Hoerer J, Friedrich T (2017) Reduction of the off-pathway iron-sulphur cluster N1a of *Escherichia coli* respiratory complex I restrains NAD<sup>+</sup> dissociation. *Sci Rep* 7:1–10
- Grimaldi S, Schoepp-Cothenet B, Ceccaldi P, Guigliarelli B, Magalon A (2013) The prokaryotic Mo/W-bisPGD enzymes family: a catalytic workhorse in bioenergetic. *Biochimica et Biophysica Acta (BBA)-Bioenergetics* 1827:1048–1085
- Gutteridge S, Tanner S, Bray R (1978) The molybdenum centre of native xanthine oxidase. Evidence for proton transfer from substrates to the centre and for existence of an anion-binding site. *Biochem J* 175:869–878
- Ha Y, Tenderholt AL, Holm RH, Hedman B, Hodgson KO, Solomon EI (2014) Sulfur K-edge X-ray absorption spectroscopy and density functional theory calculations on Monooxo MoIV and Bisoxo MoVI Bis-dithiolenes: insights into the mechanism of Oxo transfer in sulfite oxidase and its relation to the mechanism of DMSO reductase. *J Am Chem Soc* 136:9094–9105
- Hagen WR (2011) Cellular uptake of molybdenum and tungsten. *Coord Chem Rev* 255:1117–1128
- Hänzelmann P, Dobbek H, Gremer L, Huber R, Meyer O (2000) The effect of intracellular molybdenum in *Hydrogenophaga pseudoflava* on the crystallographic structure of the selenomolybdo-iron-sulfur flavoenzyme carbon monoxide dehydrogenase. *J Mol Biol* 301:1221–1235
- Havelius KG, Reschke S, Horn S, Döring A, Nicks D, Hille R et al (2011) Structure of the molybdenum site in YedY, a sulfite oxidase homologue from *Escherichia coli*. *Inorg Chem* 50:741–748

- Havemeyer A, Bittner F, Wollers S, Mendel R, Kunze T, Clement B (2006) Identification of the missing component in the mitochondrial benzamidoxime prodrug-converting system as a novel molybdenum enzyme. *J Biol Chem* 281:34796–34802
- Hille R (1996) The mononuclear molybdenum enzymes. *Chem Rev* 96:2757–2816
- Hille R (2005) Molybdenum-containing hydroxylases. *Arch Biochem Biophys* 433:107–116. <https://doi.org/10.1016/j.abb.2004.08.012>
- Hille R, Dingwall S, Wilcoxon J (2015) The aerobic CO dehydrogenase from *Oligotropha carboxidovorans*. *J Biol Inorg Chem* 20:243–251
- Hille R, Hall J, Basu P (2014) The mononuclear molybdenum enzymes. *Chem Rev* 114:3963–4038. <https://doi.org/10.1021/cr400443z>
- Hille R, Young T, Niks D, Hakopian S, Tam TK, Yu X et al (2020) Structure: function studies of the cytosolic, Mo- and NAD<sup>+</sup>-dependent formate dehydrogenase from *Cupriavidus necator*. *Inorganics* 8:41
- Hofmann M (2009) Density functional theory study of model complexes for the revised nitrate reductase active site in *Desulfovibrio desulfuricans* NapA. *J Biol Inorg Chem* 14:1023–1035. <https://doi.org/10.1007/s00775-009-0545-1>
- Hofmann M, Kassube JK, Graf T (2005) The mechanism of Mo-/Cu-dependent CO dehydrogenase. *J Biol Inorg Chem* 10:490–495
- Hollenstein K, Frei DC, Locher KP (2007) Structure of an ABC transporter in complex with its binding protein. *Nature* 446:213–216. <https://doi.org/10.1038/nature05626>
- Howes BD, Bray RC, Richards RL, Turner NA, Bennett B, Lowe DJ (1996) Evidence favoring molybdenum– carbon bond formation in xanthine oxidase action: 17O- and 13C-ENDOR and kinetic studies. *Biochemistry* 35:1432–1443
- Hughes ER, Winter MG, Duerkop BA, Spiga L, Furtado de Carvalho T, Zhu W et al (2017) Microbial respiration and Formate oxidation as metabolic signatures of inflammation-associated dysbiosis. *Cell Host Microbe* 21:208–219. <https://doi.org/10.1016/j.chom.2017.01.005>
- Huynh TN, Noriega CE, Stewart V (2010) Conserved mechanism for sensor phosphatase control of two-component signaling revealed in the nitrate sensor NarX. *Proc Natl Acad Sci* 107:21140–21145
- Iobbi-Nivol C, Leimkühler S (2013) Molybdenum enzymes, their maturation and molybdenum cofactor biosynthesis in *Escherichia coli*. *Biochim Biophys Acta* 1827:1086–1101. <https://doi.org/10.1016/j.bbabi.2012.11.007>
- Jack RL, Buchanan G, Dubini A, Hatzixanthis K, Palmer T, Sargent F (2004) Coordinating assembly and export of complex bacterial proteins. *EMBO J* 23:3962–3972
- Jackson WA, Böhlke JK, Andraski BJ, Fahlquist L, Bexfield L, Eckardt FD et al (2015) Global patterns and environmental controls of perchlorate and nitrate co-occurrence in arid and semi-arid environments. *Geochim Cosmochim Acta* 164:502–522
- Jacobitz S, Meyer O (1989) Removal of CO dehydrogenase from *Pseudomonas carboxydovorans* cytoplasmic membranes, rebinding of CO dehydrogenase to depleted membranes, and restoration of respiratory activities. *J Bacteriol* 171:6294–6299
- Johnson JL, Hainline BE, Rajagopalan KV (1980) Characterization of the molybdenum cofactor of sulfite oxidase, xanthine oxidase, and nitrate reductase. Identification of a pteridine as a structural component. *J Biol Chem* 255:1783–1786
- Johnson KE, Rajagopalan KV (2001) An active site tyrosine influences the ability of the dimethyl sulfoxide reductase family of molybdopterin enzymes to reduce S-oxides. *J Biol Chem* 276:13178–13185
- Johnson-Winters K, Tollin G, Enemark JH (2010) Elucidating the catalytic mechanism of sulfite oxidizing enzymes using structural, spectroscopic, and kinetic analyses. *Biochemistry* 49:7242–7254. <https://doi.org/10.1021/bi1008485>
- Jormakka M, Richardson D, Byrne B, Iwata S (2004) Architecture of NarGH reveals a structural classification of Mo-bisMGD enzymes. *Structure* 12:95–104

- Jormakka M, Yokoyama K, Yano T, Tamakoshi M, Akimoto S, Shimamura T et al (2008) Molecular mechanism of energy conservation in polysulfide respiration. *Nat Struct Mol Biol* 15:730–737. <https://doi.org/10.1038/nsmb.1434>
- Juillan-Binard C, Picciocchi A, Andrieu J-P, Dupuy J, Petit-Hartlein I, Caux-Thang C et al (2017) A two-component NADPH oxidase (NOX)-like system in bacteria is involved in the electron transfer chain to the methionine sulfoxide reductase MsrP. *J Biol Chem* 292:2485–2494. <https://doi.org/10.1074/jbc.M116.752014>
- Kail BW, Perez LM, Zaric SD, Millar AJ, Young CG, Hall MB et al (2006) Mechanistic investigation of the oxygen-atom-transfer reactivity of dioxo-molybdenum(VI) complexes. *Chem Eur J* 12:7501–7509
- Kappler U (2011) Bacterial sulfite-oxidizing enzymes. *Biochim Biophys Acta* 1807:1–10. <https://doi.org/10.1016/j.bbabi.2010.09.004>
- Kaufmann P, Duffus BR, Mitrova B, Iobbi-Nivol C, Teutloff C, Nimtz M et al (2018) Modulating the molybdenum coordination sphere of *Escherichia coli* trimethylamine N-oxide reductase. *Biochemistry* 57:1130–1143. <https://doi.org/10.1021/acs.biochem.7b01108>
- King GM, Weber CF (2007) Distribution, diversity and ecology of aerobic CO-oxidizing bacteria. *Nature Rev Microbiol* 5:107–118
- Kisker C, Schindelin H, Pacheco A, Wehbi WA, Garrett RM, Rajagopalan K et al (1997a) Molecular basis of sulfite oxidase deficiency from the structure of sulfite oxidase. *Cell* 91:973–983
- Kisker C, Schindelin H, Rees D (1997b) Molybdenum-cofactor-containing enzymes: structure and mechanism. *Annu Rev Biochem* 66:233–267. <https://doi.org/10.1146/annurev.biochem.66.1.233>
- Kozmin SG, Leroy P, Pavlov YI, Schaaper RM (2008) YcbX and yiiM, two novel determinants for resistance of *Escherichia coli* to N-hydroxylated base analogues. *Mol Microbiol* 68:51–65. <https://doi.org/10.1111/j.1365-2958.2008.06128.x>
- Krafft T, Macy JM (1998) Purification and characterization of the respiratory arsenate reductase of *Chrysiogenes arsenatis*. *Eur J Biochem* 255:647–653
- Kulp T, Hoelt S, Asao M, Madigan M, Hollibaugh J, Fisher J et al (2008) Arsenic (III) fuels anoxygenic photosynthesis in hot spring biofilms from Mono Lake, California. *Science* 321:967–970
- Lee CC, Sickerman NS, Hu Y, Ribbe MW (2016) YedY: A mononuclear molybdenum enzyme with a redox-active ligand? *Chembiochem* 17:453–455. <https://doi.org/10.1002/cbic.201600004>
- Leimkühler S (2020) The biosynthesis of the molybdenum cofactors in *Escherichia coli*. *Environ Microbiol* 22:2007–2026. <https://doi.org/10.1111/1462-2920.15003>
- Leimkühler S, Iobbi-Nivol C (2015) Bacterial molybdoenzymes: old enzymes for new purposes. *FEMS Microbiol Rev* 40:1–18. <https://doi.org/10.1093/femsre/fuv043>
- Levillain F, Poquet Y, Mallet L, Mazères S, Marceau M, Brosch R et al (2017) Horizontal acquisition of a hypoxia-responsive molybdenum cofactor biosynthesis pathway contributed to *Mycobacterium tuberculosis* pathoadaptation. *PLoS Pathog* 13:e1006752. <https://doi.org/10.1371/journal.ppat.1006752>
- Li H-K, Temple C, Rajagopalan K, Schindelin H (2000) The 1.3 Å crystal structure of *Rhodospirillum rubrum* dimethyl sulfoxide reductase reveals two distinct molybdenum coordination environments. *J Am Chem Soc* 122:7673–7680
- Liu MT, Wuebbens MM, Rajagopalan K, Schindelin H (2000) Crystal structure of the gephyrin-related molybdenum cofactor biosynthesis protein MogA from *Escherichia coli*. *J Biol Chem* 275:1814–1822
- Lorigan GA, Britt RD, Kim JH, Hille R (1994) Electron spin echo envelope modulation spectroscopy of the molybdenum center of xanthine oxidase. *Biochimica et Biophysica Acta (BBA)-Bioenergetics* 1185:284–294
- Lundgren A (2021) Carl Wilhelm Scheele. *Encyclopedia Britannica*. <https://www.britannica.com/biography/Carl-Wilhelm-Scheele>. Accessed 10 July 2021

- Makdessi K, Andreesen JR, Pich A (2001) Tungstate uptake by a highly specific ABC transporter in *Eubacterium acidaminophilum*. *J Biol Chem* 276:24557–24564. <https://doi.org/10.1074/jbc.M101293200>
- Manikandan P, Choi E-Y, Hille R, Hoffman BM (2001) 35 GHz ENDOR characterization of the “very rapid” signal of xanthine oxidase reacted with 2-Hydroxy-6-methylpurine (13C8): evidence against direct Mo–C8 interaction. *J Am Chem Soc* 123:2658–2663
- McAlpine A, McEwan A, Bailey S (1998) The high resolution crystal structure of DMSO reductase in complex with DMSO. *J Mol Biol* 275:613–623
- Mendel RR, Leimkuhler S (2015) The biosynthesis of the molybdenum cofactors. *J Biol Inorg Chem* 20:337–347
- Meyer O, Jacobitz S, Krüger B (1986) Biochemistry and physiology of aerobic carbon monoxide-utilizing bacteria. *FEMS Microbiol Rev* 2:161–179
- Mintmier B, McGarry JM, Bain DJ, Basu P (2021) Kinetic consequences of the endogenous ligand to molybdenum in the DMSO reductase family: a case study with periplasmic nitrate reductase. *JBIC. J Biol Inorg Chem* 26:13–28. <https://doi.org/10.1007/s00775-020-01833-9>
- Mintmier B, McGarry JM, Sparacino-Watkins CE, Sallmen J, Fischer-Schrader K, Magalon A et al (2018) Molecular cloning, expression and biochemical characterization of periplasmic nitrate reductase from *Campylobacter jejuni*. *FEMS Microbiol Lett* 365:fny151. <https://doi.org/10.1093/femsle/fny151>
- Mintmier B, Nassif S, Stolz JF, Basu P (2020) Functional mononuclear molybdenum enzymes: challenges and triumphs in molecular cloning, expression, and isolation. *JBIC. J Biol Inorg Chem* 25:547–569
- Moreno-Vivián C, Cabello P, Martínez-Luque M, Blasco R, Castillo F (1999) Prokaryotic nitrate reduction: molecular properties and functional distinction among bacterial nitrate reductases. *J Bacteriol* 181:6573–6584
- Najmudin S, Gonzalez PJ, Trincão J, Coelho C, Mukhopadhyay A, Cerqueira NMFSA et al (2008) Periplasmic nitrate reductase revisited: a sulfur atom completes the sixth coordination of the catalytic molybdenum. *J Biol Inorg Chem* 13:737–753. <https://doi.org/10.1007/s00775-008-0359-6>
- Neumann M, Mittelstädt G, Iobbi-Nivol C, Saggiu M, Lenzian F, Hildebrandt P et al (2009) A periplasmic aldehyde oxidoreductase represents the first molybdopterin cytosine dinucleotide cofactor containing molybdo-flavoenzyme from *Escherichia coli*. *FEBS J* 276:2762–2774
- Oden KL, Gladysheva TB, Rosen BP (1994) Arsenate reduction mediated by the plasmid-encoded ArsC protein is coupled to glutathione. *Mol Microbiol* 12:301–306
- Oremland RS, Saltikov CW, Wolfe-Simon F, Stolz JF (2009) Arsenic in the evolution of earth and extraterrestrial ecosystems. *Geomicrobiol J* 26:522–536
- Oremland RS, Stolz JF (2003) The ecology of arsenic. *Science* 300:939–944
- Pelzmann A, Ferner M, Gnida M, Meyer-Klaucke W, Maisel T, Meyer O (2009) The CoxD protein of *Oligotropha carboxidovorans* is a predicted AAA+ ATPase chaperone involved in the biogenesis of the CO dehydrogenase [CuSMoO<sub>2</sub>] cluster. *J Biol Chem* 284:9578–9586
- Peng T, Xu Y, Zhang Y, Peng T, Xu Y (2018) Comparative genomics of molybdenum utilization in prokaryotes and eukaryotes. *BMC Genomics* 19:691
- Pinske C, Bönn M, Krüger S, Lindenstrauß U, Sawers RG (2011) Metabolic deficiencies revealed in the biotechnologically important model bacterium *Escherichia coli* BL21 (DE3). *PLoS One* 6:e22830
- Pommier J, Méjean V, Giordano G, Iobbi-Nivol C (1998) TorD, a cytoplasmic chaperone that interacts with the unfolded trimethylamine N-oxide reductase enzyme (TorA) in *Escherichia coli*. *J Biol Chem* 273:16615–16620
- Pushie MJ, George GN (2011) Spectroscopic studies of molybdenum and tungsten enzymes. *Coord Chem Rev* 255:1055–1084
- Raaijmakers H, Macieira S, Dias JM, Teixeira S, Bursakov S, Huber R et al (2002) Gene sequence and the 1.8 Å crystal structure of the tungsten-containing formate dehydrogenase from *Desulfovibrio gigas*. *Structure* 10:1261–1272

- Raaijmakers HC, Romao MJ (2006) Formate-reduced *E. coli* formate dehydrogenase H: the reinterpretation of the crystal structure suggests a new reaction mechanism. *JBIC. J Biol Inorg Chem* 11:849–854
- Radon C, Mittelstädt G, Duffus BR, Bürger J, Hartmann T, Mielke T et al (2020) Cryo-EM structures reveal intricate Fe-S cluster arrangement and charging in *Rhodobacter capsulatus* formate dehydrogenase. *Nat Commun* 11:1–9. <https://doi.org/10.1038/s41467-020-15614-0>
- Rajagopalan KV, Johnson JL (1992) The pterin molybdenum cofactors. *J Biol Chem* 267:10199–10202
- Rech S, Wolin C, Gunsalus RP (1996) Properties of the periplasmic ModA molybdate-binding protein of *Escherichia coli*. *J Biol Chem* 271:2557–2562. <https://doi.org/10.1074/jbc.271.5.2557>
- Rice AJ, Harrison A, Alvarez FJ, Davidson AL, Pinkett HW (2014) Small substrate transport and mechanism of a molybdate ATP binding cassette transporter in a lipid environment. *J Biol Chem* 289:15005–15013. <https://doi.org/10.1074/jbc.M114.563783>
- Richey C, Chovanec P, Hoefl SE, Oremland RS, Basu P, Stolz JF (2009) Respiratory arsenate reductase as a bidirectional enzyme. *Biochem Biophys Res Commun* 382:298–302
- Romao MJ, Archer M, Moura I, Moura JJ, LeGall J, Engh R et al (1995) Crystal structure of the xanthine oxidase-related aldehyde oxido-reductase from *D. gigas*. *Science* 270:1170–1176
- Rothery RA, Stein B, Solomonson M, Kirk ML, Weiner JH (2012) Pyranopterin conformation defines the function of molybdenum and tungsten enzymes. *Proc Natl Acad Sci* 109:14773–14778
- Rothery RA, Workun GJ, Weiner JH (2008) The prokaryotic complex iron–sulfur molybdoenzyme family. *Biochim Biophys Acta* 1778:1897–1929. <https://doi.org/10.1016/j.bbamem.2007.09.002>
- Sanchez-Pulido L, Rojas AM, Valencia A, Martinez-A C, Andrade MA (2004) ACRATA: a novel electron transfer domain associated to apoptosis and cancer. *BMC Cancer* 4:1–6
- Santos-Silva T, Ferroni F, Thapper A, Marangon J, Gonzalez PJ, Rizzi AC et al (2009) Kinetic, structural, and EPR studies reveal that aldehyde oxidoreductase from *Desulfovibrio gigas* does not need a Sulfido ligand for catalysis and give evidence for a direct Mo-C interaction in a biological system. *J Am Chem Soc* 131:7990–7998
- Schindelin H, Kisker C, Hilton J, Rajagopalan K, Rees DC (1996) Crystal structure of DMSO reductase: redox-linked changes in molybdopterin coordination. *Science* 272:1615–1621
- Schneider F, Löwe J, Huber R, Schindelin H, Kiser C, Knäblein J (1996) Crystal structure of dimethyl sulfoxide reductase *Rhodobacter capsulatus* at 1.88 Å resolution. *J Mol Biol* 263:53–69
- Schoepp-Cothenet B, van Lis R, Atteia A, Baymann F, Capowicz L, Ducluzeau A-L et al (2013) On the universal core of bioenergetics. *Biochimica et Biophysica Acta (BBA)-Bioenergetics* 1827: 79–93
- Schoepp-Cothenet B, van Lis R, Philippot P, Magalon A, Russell MJ, Nitschke W (2012) The ineluctable requirement for the trans-iron elements molybdenum and/or tungsten in the origin of life. *Sci Rep* 2:263. <https://doi.org/10.1038/srep00263>
- Schrader N, Fischer K, Theis K, Mendel RR, Schwarz G, Kisker C (2003) The crystal structure of plant sulfite oxidase provides insights into sulfite oxidation in plants and animals. *Structure* 11: 1251–1263
- Schroeder HA, Balassa JJ, Tipton IH (1970) Essential trace metals in man: molybdenum. *J Chronic Dis* 23:481–499. [https://doi.org/10.1016/0021-9681\(70\)90056-1](https://doi.org/10.1016/0021-9681(70)90056-1)
- Schultz BE, Hille R, Holm RH (2002) Direct oxygen atom transfer in the mechanism of action of *Rhodobacter sphaeroides* dimethyl sulfoxide reductase. *J Am Chem Soc* 117:827–828. <https://doi.org/10.1021/ja00107a031>
- Schwarz G, Mendel RR, Ribbe MW (2009) Molybdenum cofactors, enzymes and pathways. *Nature* 460:839–847

- Sforna MC, Philippet P, Somogyi A, Van Zuilen MA, Medjoubi K, Schoepp-Cothenet B et al (2014) Evidence for arsenic metabolism and cycling by microorganisms 2.7 billion years ago. *Nat Geosci* 7:811–815
- Shanmugam M, Wilcoxon J, Habel-Rodriguez D, Cutsail GE III, Kirk ML, Hoffman BM et al (2013)  $^{13}\text{C}$  and  $^{63}\text{Cu}$  ENDOR studies of CO dehydrogenase from *Oligotropha carboxidovorans*. Experimental evidence in support of a copper–carbonyl intermediate. *J Am Chem Soc* 135:17775–17782
- Siegbahn PE, Shestakov AF (2005) Quantum chemical modeling of CO oxidation by the active site of molybdenum CO dehydrogenase. *J Comput Chem* 26:888–898
- Sigel A, Sigel H (2002) Metals Ions in biological system: Volume 39: Molybdenum and Tungsten: their roles in biological processes. CRC Press, New York
- Smedley PL, Kinniburgh DG (2017) Molybdenum in natural waters: A review of occurrence, distributions and controls. *Appl Geochem* 84:387–432. <https://doi.org/10.1016/j.apgeochem.2017.05.008>
- Sousa FL, Thiergart T, Landan G, Nelson-Sathi S, Pereira IA, Allen JF et al (2013) Early bioenergetic evolution. *Philosophical Transactions of the Royal Society B: Biological Sciences* 368:20130088
- Sparacino-Watkins C, Stolz JF, Basu P (2014a) Nitrate and periplasmic nitrate reductases. *Chem Soc Rev* 43:676–706. <https://doi.org/10.1039/c3cs60249d>
- Sparacino-Watkins CE, Tejero J, Sun B, Gauthier MC, Thomas J, Ragireddy V et al (2014b) Nitrite reductase and nitric-oxide synthase activity of the mitochondrial molybdopterin enzymes mARC1 and mARC2. *J Biol Chem* 289:10345–10358
- Stiefel EI (1993) Molybdenum enzymes, cofactors, and chemistry: an introductory survey. American Chemical Society, Washington, DC
- Stolz JF, Basu P (2002) Evolution of nitrate reductase: molecular and structural variations on a common function. *Chembiochem* 3:198–206
- Stolz JF, Basu P, Oremland RS (2002) Microbial transformation of elements: the case of arsenic and selenium. *Int Microbiol* 5:201–207. <http://link.springer.com/article/10.1007%2Fs10123-002-0091-y>
- Stolz JF, Basu P, Santini JM, Oremland RS (2006) Arsenic and selenium in microbial metabolism. *Annu Rev Microbiol* 60:107–130
- Sumimoto H (2008) Structure, regulation and evolution of Nox-family NADPH oxidases that produce reactive oxygen species. *FEBS J* 275:3249–3277
- Szaleniec M, Dudzik A, Kozik B, Borowski T, Heider J, Witko M (2014) Mechanistic basis for the enantioselectivity of the anaerobic hydroxylation of alkylaromatic compounds by ethylbenzene dehydrogenase. *J Inorg Biochem* 139:9–20. <https://doi.org/10.1016/j.jinorgbio.2014.05.006>
- Tanner SJ, Bray RC, Bergmann F (1978)  $^{13}\text{C}$  hyperfine splitting of some molybdenum electron-paramagnetic-resonance signals from xanthine oxidase. Portland Press Ltd
- Thome R, Gust A, Toci R, Mendel R, Bittner F, Magalon A et al (2012) A Sulfurtransferase is essential for activity of Formate dehydrogenases in *Escherichia coli*. *J Biol Chem* 287:4671–4678. <https://doi.org/10.1074/jbc.M111.327122>
- Tirado-Lee L, Lee A, Rees DC, Pinkett HW (2011) Classification of a Haemophilus influenzae ABC transporter HI1470/71 through its cognate molybdate periplasmic binding protein, MoIA. *Structure* 19:1701–1710. <https://doi.org/10.1016/j.str.2011.10.004>
- Truglio JJ, Theis K, Leimkühler S, Rappa R, Rajagopalan KV, Kisker C (2002) Crystal structures of the active and Alloxanthine-inhibited forms of xanthine dehydrogenase from *Rhodobacter capsulatus*. *Structure* 10:115–125. [https://doi.org/10.1016/S0969-2126\(01\)00697-9](https://doi.org/10.1016/S0969-2126(01)00697-9)
- Unciuleac M, Warkentin E, Page CC, Boll M, Ermiler U (2004) Structure of a xanthine oxidase-related 4-hydroxybenzoyl-CoA reductase with an additional [4Fe-4S] cluster and an inverted electron flow. *Structure* 12:2249–2256
- Wagener N, Pierik AJ, Ibdah A, Hille R, Dobbek H (2009) The Mo-Se active site of nicotinate dehydrogenase. *Proc Natl Acad Sci* 106:11055–11060

- Warelow TP, Oke M, Schoepp-Cothenet B, Dahl JU, Bruselat N, Sivalingam GN et al (2013) The respiratory arsenite oxidase: structure and the role of residues surrounding the rieske cluster. *PLoS One* 8:e72535
- Wells M, Basu P, Stolz JF (2021) The physiology and evolution of microbial selenium metabolism. *Metallomics* 13:mfab024
- Wells M, Kanmanii NJ, Janecka JE, Basu P, Oremland RS, Stolz JF (2020) Methane, arsenic, selenium and the origins of the DMSO reductase family. *Sci Rep* 10:1–14
- Wells M, McGarry J, Gaye MM, Basu P, Oremland RS, Stolz JF (2019) Respiratory selenite reductase from bacillus selenitireducens strain MLS10. *J Bacteriol* 201:e00614–e00618
- Youngblut MD, Tsai C-L, Clark IC, Carlson HK, Maglaqui AP, Gau-Pan PS et al (2016) Perchlorate reductase is distinguished by active site aromatic gate residues\*. *J Biol Chem* 291:9190–9202. <https://doi.org/10.1074/jbc.M116.714618>
- Zargar K, Conrad A, Bernick DL, Lowe TM, Stolc V, Hoelt S et al (2012) ArxA, a new clade of arsenite oxidase within the DMSO reductase family of molybdenum oxidoreductases. *Environ Microbiol* 14:1635–1645
- Zargar K, Hoelt S, Oremland R, Saltikov CW (2010) Identification of a novel arsenite oxidase gene, arxA, in the haloalkaliphilic, arsenite-oxidizing bacterium *Alkalilimnicola ehrlichii* strain MLHE-1. *J Bacteriol* 192:3755–3762
- Zhang X, Krause KH, Xenarios I, Soldati T, Boeckmann B (2013) Evolution of the ferric reductase domain (FRD) superfamily: modularity, functional diversification, and signature motifs. *PLoS One* 8:e58126. <https://doi.org/10.1371/journal.pone.0058126>
- Zhang Y, Gladyshev VN (2008) Molybdoproteomes and evolution of molybdenum utilization. *J Mol Biol* 379:881–899. <https://doi.org/10.1016/j.jmb.2008.03.051>
- Zhang Y, Zheng J (2020) Bioinformatics of metalloproteins and metalloproteomes. *Molecules* 25:3366
- Zhong Q, Kobe B, Kappler U (2020) Molybdenum enzymes and how they support virulence in pathogenic bacteria (review). *Front Microbiol* 11:615860. <https://doi.org/10.3389/fmicb.2020.615860>

# Chapter 14

## Microbial Metabolism of Nickel



Robert P. Hausinger

**Abstract** This chapter summarizes the multiple processes that microorganisms use to metabolize nickel ions and describes nickel-dependent enzymatic transformations. A wide variety of microbial species sense and respond to nickel ion concentrations by synthesizing nickel-specific transcription factors, and a few possess nickel-responsive riboswitches. During nickel deficiency, some microbes are capable of taking up this micronutrient using influx systems that include ATP binding cassette transporters and secondary transporters such as permeases. Certain microorganisms eliminate excess concentrations of internal nickel ions by using nickel-specific cation diffusion facilitators, major facilitator protein superfamily members, P-type ATPases, and other efflux systems. The basis of nickel toxicity and several mechanisms of nickel resistance also are described in this chapter. Many microorganisms utilize nickel, variously incorporating it into glyoxalase I, acireductone dioxygenase, quercetin 2,4-dioxygenase, superoxide dismutase, urease, [NiFe] hydrogenase, carbon monoxide dehydrogenase, the acetyl-coenzyme A synthase/decarbonylase complex, 2-hydroxyacid racemases and epimerases, and methyl-S-coenzyme M reductase. Auxiliary proteins often function during the biosynthesis of nickel enzymes by delivering the nickel ion, synthesizing a nickel-containing organometallic cofactor, coupling the energy of nucleotide hydrolysis to the metal incorporation, or acting in other ways. Nickel storage proteins are present in some microorganisms. In sum, the microbial metabolism of nickel involves a rich landscape of biological processes.

---

R. P. Hausinger (✉)

Microbiology and Molecular Genetics, Biomedical Physical Sciences, Michigan State University, East Lansing, MI, USA

e-mail: [hausinge@msu.edu](mailto:hausinge@msu.edu)



## 14.1 Introduction: Nickel in the Environment

Nickel is the fifth most abundant element on earth, although much of it is concentrated in the earth's core where it is second most in abundance at 8.5% (Zamble et al. 2017). The earth's crust contains 0.009% nickel, placing it among the top 25 most prevalent elements. The nickel content of soils ranges from 3 to over 1000 ppm ( $\mu\text{g/g}$ ) depending on the origin of the parent rock, with an average of  $\sim 16$  ppm (Iyaka 2011). In an extreme natural case, nickel is present at  $>1$  mg/g in serpentine soils. The nickel content of lakes and rivers averages about 1 ppm, but varies widely depending on the type of soil associated with the watershed of interest (Nriagu 1980). In the ocean, the nickel concentration is quite uniform at the surface (2–4 nM), increasing at greater depth to 10 nM in the Pacific and 6 nM in Atlantic (Glass and Dupont 2017). Anthropogenic sources of nickel include mining of nickel ores and certain industrial processes that can lead to local areas of very high nickel concentrations. Regardless of the source of nickel or the properties of diverse environments, the biologically relevant form of the metal typically occurs as the dication ( $\text{Ni}^{2+}$ ).

Nickel may have beneficial or toxic effects depending on the microbial species and the metal ion concentration. Importantly, the availability of nickel depends on factors other than just its concentration: this metal ion forms complexes with inorganic matrices such as sulfides and iron oxyhydroxides or with organic compounds such as humic and fulvic acids. These anionic substances reduce the effective nickel concentration by sequestration. A growth requirement for nickel was first reported in 1965 for two strains of hydrogen-oxidizing bacteria (Bartha and Ordal 1965) and this metal ion has since been shown to be essential for multiple microorganisms. Negative effects of nickel on microorganisms also have long been established (Babich and Stotzky 1983).

This chapter surveys the metabolism of nickel by microorganisms. It starts by describing homeostasis mechanisms by which microbes sense the intracellular (or periplasmic) concentration of this metal and use various mechanisms to facilitate either its import or efflux, depending on whether the available levels of this nutrient are inadequate or if in excess as a toxicant. The chapter then explains the basis for nickel toxicity and describes how microorganisms circumvent this damage. Next, the nickel-containing enzymes are highlighted including their biosynthetic pathways that sometimes use nickel storage and delivery proteins, nucleotide hydrolyzing enzymes, and other components.

## 14.2 Nickel Homeostasis

Many microorganisms contain elaborate systems to sense the cytoplasmic (or periplasmic) concentration of nickel, turn on nickel-specific uptake transporters when the metal ion is limiting, and increase levels of nickel-specific efflux systems

**Table 14.1** Summary of selected nickel-dependent transcriptional regulators (sensors) and their associated nickel transport systems.

Microorganism	Sensor	Transporter (type) <sup>a</sup>	References
<i>Agrobacterium tumefaciens</i>	DmeR	DmeF (CDF exporter)	Dokpikul et al. (2016)
<i>Brucella abortus</i>	NikR	NikABCDE (ABC-type importer)	Budnick et al. (2018)
<i>Escherichia coli</i>	NikR	NikABCDE (ABC-type importer)	de Pina et al. (1999) and Navarro et al. (1993)
	RcnR	RcnA (efflux pump)	Koch et al. (2007)
<i>Cupriavidus metallidurans</i> CH34	CnrYXH	CnrCBA (RND efflux pump)	Grass et al. (2000) and Tibazarwa et al. (2000)
<i>Geobacter uraniireducens</i>	NikR	Nik(MN)1 and Nik(MN)2-NikQO (ECF-type importer components)	Benanti and Chivers (2010)
<i>Haemophilus influenzae</i>	NimR	NikKLMQO (ECF-type ABC importer)	Kidd et al. (2011)
<i>Helicobacter hepaticus</i>	NikR	NikABDE (ABC-type importer) and HH0418 (OM transporter)	Benoit et al. (2013)
<i>Helicobacter pylori</i>	NikR	NixA (uptake permease), HP1515 (OM importer), TonB-ExbB-ExbD (OM energizer), NiuBDE (ABC-type transporter), and CeuE (another periplasmic Ni-binding protein)	Contreras et al. (2003), Davis et al. (2006), Ernst et al. (2005), Ernst et al. (2006), Fischer et al. (2016), Jones et al. (2015), and Wolfram et al. (2006)
<i>Leptospirillum ferriphilum</i>	NcrB	NcrAC (efflux pump)	Tian et al. (2007) and Zhu et al. (2011)
<i>Mycobacterium tuberculosis</i>	NmtR	NmtA (P-type ATPase)	Cavet et al. (2002)
	KmtR	Rv2025c (CDF exporter)	Campbell et al. (2007)
<i>Rhizobium leguminosarum</i>	DmeR	DmeF (CDF exporter)	Rubio-Sanz et al. (2013)
<i>Streptomyces coelicolor</i>	Nur	NikABCDE and NikMNOQ (ABC-type uptake systems)	Ahn et al. (2006) and An et al. (2009)
	NmtR	NmtA (P-type ATPase for efflux)	Kim et al. (2015)
<i>Synechocystis</i> sp. PCC 6803	InrS	NrsD (efflux permease)	Foster et al. (2012)
	NrsRS	NrsBACD (RND exporter)	Garcia-Dominguez et al. (2000) and Lopez-Maury et al. (2002)

<sup>a</sup> The abbreviations are defined in the text sections related to each topic

when the metal is in excess (Table 14.1). Numerous excellent reviews covering these homeostatic process are available for those interested in more extensive treatment of this topic (Chivers 2017; Higgins 2019; Higgins et al. 2012a; Iwig and Chivers 2010;

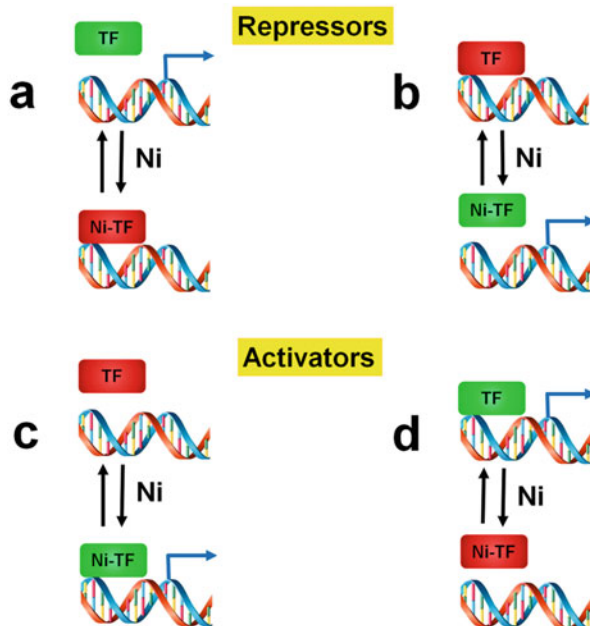
Li and Zamble 2009; Musiani et al. 2015; Rodrigue et al. 2017; Zeer-Wanklyn and Zamble 2017). The highlights of the better-studied systems are described here.

A few general comments about cellular nickel concentrations are worth mentioning. Unless located in a nickel-rich environment, microorganisms tend to concentrate the metal ion to levels exceeding that found in their external milieu. For example, *Escherichia coli* concentrates this metal ion from minimal or LB media (where nickel is present at  $\sim 10^{-8}$  M and  $\sim 10^{-7}$  M, respectively) to greater than  $10^{-6}$  M in the cell (Outten and O'Halloran 2001). One can calculate that a single atom of nickel in an *E. coli* cell ( $\sim 2$   $\mu\text{m}$  in length and  $\sim 0.5$   $\mu\text{m}$  in diameter or  $\sim 4 \times 10^{-16}$  L) yields a concentration of approximately 4 nM ( $4 \times 10^{-9}$  M). This value is of interest when considering the measured dissociation constants ( $K_d$ ) for nickel-binding sensors such as NikR of *E. coli* (described in greater detail below) with a value of less than 1 pM ( $10^{-12}$  M)—nearly three orders of magnitude less than one per cell (Chivers and Sauer 2002; Wang et al. 2004). This apparent discrepancy arises because the measured concentration of nickel within cells does not equate to the level of free or available nickel ion—much of it is found dynamically associated with cytoplasmic components (thiols, polynucleotides, amino acids, etc.). The nickel sensors assure that an ideal regulatory balance of nickel import and export exists to provide optimal metal levels for cellular growth. Selected examples of nickel sensing transcriptional regulators are described in Sect. 14.2.1. That section is followed by discussions of the systems controlled by these sensors: nickel uptake (Sect. 14.2.2) and nickel efflux (Sect. 14.2.3).

### 14.2.1 Nickel-Sensing Transcription Factors

Metalloregulatory transcription factors undergo protein conformational changes upon binding their cognate metal ions, with consequent modification of their transcriptional regulatory properties. Figure 14.1 depicts four highly simplified mechanisms for transcription factor regulation by metal ions, but it is important to note that many other options exist. In the first case, a metal-repressor complex (co-repressor) binds to the operator region of a gene to prevent transcription, whereas the apoprotein form of the transcription factor is non-functional as a repressor. The opposite situation occurs when the apoprotein of the transcription factor directly represses transcription, with metal binding leading to de-repression that allows the gene to be transcribed. The third option parallels the first in that only the metal-bound transcription factor binds to DNA, but in this case the complex (co-activator) interacts with RNA polymerase to enhance gene expression. A final option occurs when the apoprotein of the transcription factor functions as the activator, with metal binding leading to loss of activation capability. As described below, all of these mechanisms, at least in modified forms, apply to nickel-sensing transcription factors.

**Fig. 14.1** Four potential roles for nickel-dependent transcriptional regulatory factors. (a) Co-repression of a gene by the complex of nickel bound to the transcription factor (Ni-TF). (b) Loss of repressor function induced by the binding of nickel. (c) Co-activation of a gene by the nickel-transcription factor complex. (d) Loss of activator function caused by the binding of nickel



### 14.2.1.1 NikR

*E. coli* NikR nicely illustrates the metalloregulatory mechanism shown in Fig. 14.1a. When nickel binds to this protein (subunit size of 15-kDa) it functions as a repressor of the *nikABCDE* operon encoding an ATP-binding cassette (ABC) nickel-uptake system located in the cytoplasmic membrane (de Pina et al. 1999). Mutants affecting *nikR* lead to constitutive expression of the *nik* operon. The nickel-bound repressor binds to an operator site consisting of dyad-symmetric 6-base pair recognition sequences (GTATGA) separated by 16 base pairs (Chivers and Sauer 2000). A high affinity nickel-binding site ( $K_d$  measured in the pM range except for one report of a sub- $\mu$ M value) must be occupied for NikR to bind DNA, but tighter interaction with DNA ( $K_d \sim 20$  pM) occurs when additional nickel is bound to a poorly characterized lower affinity site on NikR ( $K_d$  ranging from 30 nM to 30  $\mu$ M) (Bloom and Zamble 2004; Chivers and Sauer 2002; Diederix et al. 2008; Wang et al. 2010a). Potassium also must bind to NikR for effective interaction with DNA (Wang et al. 2010b).

A series of crystal structures provides important insights into how *E. coli* NikR functions as a transcription factor. The tetrameric apoprotein possesses two dimeric ribbon-helix-helix DNA-binding regions separated by a nickel-binding regulatory domain (Schreiter et al. 2003). The structurally-characterized C-terminal domain is a tetramer that binds four nickel atoms at high-affinity square-planar sites using His87, His89, and Cys95 from one subunit along with His76' from another subunit

(Schreiter et al. 2003). The structure of the full-length NikR holoprotein reveals that nickel addition results in a protein conformational change affecting the relative orientations of the DNA-binding regions (Schreiter et al. 2006). A further change occurs when the nickel-NikR complex binds to operator DNA (Fig. 14.2a) (Schreiter et al. 2006). In particular, the DNA-binding regions rotate to allow both to bind to the DNA simultaneously, leading to a bend in the operator region. Co-repressor binding to this region prevents its interaction with RNA polymerase, thus leading to cessation of transcription. This structure also identifies how potassium is coordinated; i.e. via bidentate Glu30, bidentate Asp34, and backbone carbonyls of Ile116, Gln118, and Val121. Additional structural studies have probed the basis for the metal-binding specificity of *E. coli* NikR by identifying sites for binding other metals (Phillips et al. 2008) and analyzed low-affinity binding sites for nickel (Phillips et al. 2010). Despite its ability to bind other metals, the cellular response of NikR as a transcriptional regulator is specific to nickel.

NikR in *Helicobacter pylori* exhibits several intriguing differences from the protein described above. Like *E. coli* NikR, the nickel-bound *H. pylori* NikR functions as a co-repressor (Fig. 14.1a) of a cytoplasmic membrane-associated nickel import system; however, this NikR-dependent regulation primarily involves *nixA* encoding a single-component secondary or permease-type transporter (Contreras et al. 2003; Ernst et al. 2005; Wolfram et al. 2006). Another NikR target is *fecDE* (Jones et al. 2015), a cluster that was later expanded, renamed, and shown to encode the NiuBDE ABC-type nickel uptake system (Fischer et al. 2016). Various strains of *H. pylori* contain periplasmic components of the ABC-type uptake system (comparable to NikA) known as NiuB1, NiuB2, and CeuE, with the latter also regulated by NikR (Jones et al. 2015). Of further interest, *ceuE* and *fecDE* encode an ABC-type transporter in *Helicobacter mustelae* (Stoof et al. 2010a). NikR of *H. pylori* also regulates production of a system for nickel transport across the outer membrane (OM) involving the OM protein HP1512 and the ExbB-ExbD-TonB cross-periplasm energizer (Davis et al. 2006; Ernst et al. 2006). In addition, the nickel-bound form of *H. pylori* NikR functions as a co-activator (Fig. 14.1c) of the gene cluster encoding urease, a nickel-containing enzyme (van Vliet et al. 2002), and it modulates several other nickel-repressed or nickel-activated genes (Contreras et al. 2003; Ernst et al. 2006; Vannini et al. 2017). The operator region recognized by *H. pylori* NikR differs from that bound by the *E. coli* protein and has poorly conserved inverted repeats (Delany et al. 2005). Additional changes in regulatory properties relate to pH-dependent effects (Bury-Moné et al. 2004; Jones and Zamble 2018; van Vliet et al. 2004) and hierarchical effects that provide an order to gene regulation (Dosanjh et al. 2009; Muller et al. 2011). Nickel binding to the *H. pylori* tetrameric protein also differs from that for the *E. coli* protein; two nickel are bound with greater affinity ( $K_d \sim 10$  nM), two with less affinity ( $K_d \sim 100$  nM), and others with weak affinity ( $K_d \sim \mu\text{M}$ ) (Zambelli et al. 2007a). Crystal structures are reported for the *H. pylori* NikR apoprotein and several holoprotein forms (Benini et al. 2011; Dian et al. 2006; West et al. 2010). The overall structures closely resemble that of the *E. coli* protein with some differences noted for nickel sites in the holoproteins, but all

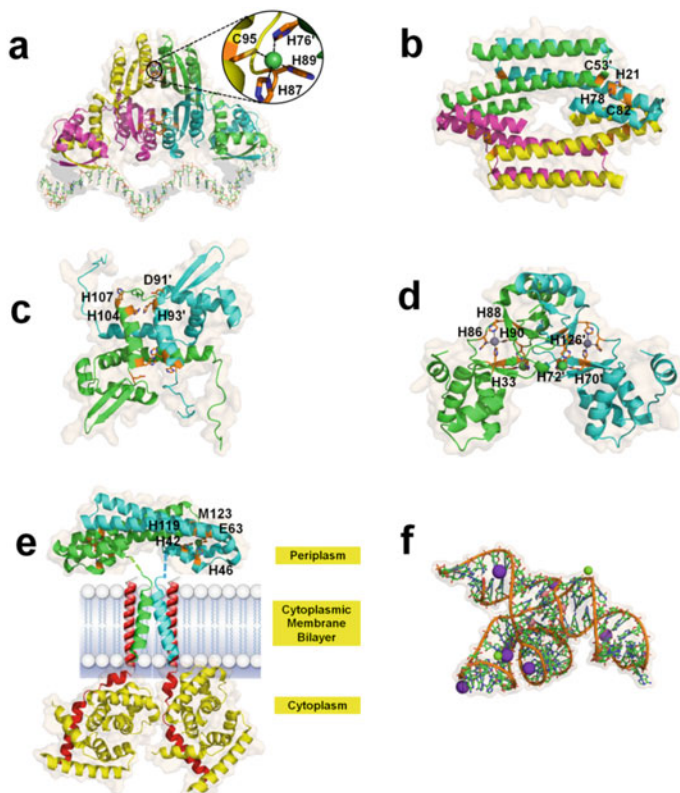


**Fig. 14.2** Selected structures of nickel-dependent transcription regulatory factors. (a) *Escherichia coli* NikR homotetramer in complex with nickel and bound to DNA (PDB ID 2hzv). The inset reveals one of the four nickel-binding sites with its ligands. (b) *Synechocystis* sp. PCC 6803 InrS homotetrameric transcription factor in its apoprotein form (PDB ID 5fnn) with the four residues likely to coordinate one of the four metal-binding sites indicated. (c) Homodimeric *Mycobacterium tuberculosis* NmtR transcription factor apoprotein (PDB ID 2lqp). Four likely coordinating residues, with two others not yet identified, are shown for one of the two sites. (d) Homodimeric *Streptomyces coelicolor* Nur transcription factor (PDB ID 3eyy). Two types of metal sites are shown (gray and green spheres). (e) *Cupriavidus metallidurans* CH34 CnrX-CnrY-CnrH tripartite nickel sensor with its periplasmic CnrX homodimer (cyan and green; residues 39–148 are from PDB ID 2y39 and the membrane-bound amino-terminal region is modeled) and a complex (PDB ID 4cxf) between the transmembrane CnrY (red; residues 2–30 are from the structure and a membrane-localized helix is modeled) and cytoplasmic CnrH (yellow). The metal sites in CnrX are indicated. Nickel binding to CnrX results in release of the sigma factor CnrH for interaction with RNA polymerase. (f) NiCo riboswitch from *Erysipelotrichaceae* bacterium. The riboswitch RNA structure (PDB ID 4rum) contains four cobalt (brown spheres, likely equivalent to the nickel-binding sites), two magnesium (green spheres), and seven potassium atoms (purple spheres). For all panels, the proteins are illustrated in cartoon mode with partially transparent surfaces, and individual subunits are in different colors. DNA and RNA are shown as sticks with RNA also depicted as wires. Residues of interest are shown in stick mode with orange carbon atoms. When bound, nickel is shown as green spheres

showing at least one of the familiar square-planar site (His99, His101, and Cys107 from one subunit with His88' from a second subunit).

Several other NikR proteins are characterized to various extents, with four examples cited here. In *Helicobacter hepaticus*, NikR-dependent regulation resembles features of the *H. pylori* and *E. coli* systems. This NikR controls the levels of a putative inner-membrane ABC-type nickel transporter (encoded by *nikABDE*) and a possible OM nickel transporter (using *hh0418*), along with affecting levels of nickel-dependent urease and [NiFe] hydrogenase activities (Benoit et al. 2013). The situation in *Brucella abortus* is comparable to that in *E. coli*, with NikR serving as a transcriptional regulator of *nikABCDE* (Budnick et al. 2018). NikR from *Geobacter uraniireducens* binds cooperatively to promoter regions of *nik(MN)1* and *nik(MN)2*, components of ABC-type transporters (Benanti and Chivers 2010). Finally, NikR from *Pyrococcus horikoshii*, for which the transcriptional target has not been reported, is notable because crystal structures were determined for its apoprotein and four nickel-bound conformations (Chivers and Tahirov 2005). The overall tetrameric structures closely resemble those cited above, with the DNA-binding domains undergoing bending and rotational changes in conformation. The high affinity nickel-binding site is square planar and utilizes His89, His91, and Cys97 from one subunit along with His78' from a second subunit, thus creating a situation essentially identical to the other NikR nickel sites.

#### 14.2.1.2 RcnR/InrS/DmeR/NcrB

The *E. coli* RcnR nickel and cobalt sensor operates by metal-dependent de-repression or release of the regulatory protein from the DNA (Fig. 14.1b), resulting in up-regulation of *rcnA* encoding a nickel/cobalt efflux system (Iwig et al. 2006; Koch et al. 2007). The designation *rcn* is named for *resistance to cobalt and nickel*, with increased sensitivity to these metals noted when *rcnA* is deleted (Rodrigue et al. 2005) and decreased metal sensitivity for the case of *rcnR* deletion (Koch et al. 2007). The 40-kDa homotetrameric RcnR sensor apoprotein binds to a TACT-G<sub>6</sub>-N-AGTA motif between the divergently transcribed *rcnR* and *rcnA* genes (Iwig et al. 2006; Iwig and Chivers 2009). Dissociation from the DNA occurs upon binding one cobalt or nickel ion per 89-residue subunit, with the metals exhibiting nM affinity (Iwig et al. 2008). X-ray absorption spectroscopy (XAS) provides evidence for partial thiolate ligation of the metals, which are 6-coordinate (Iwig et al. 2008). This technique was combined with mutagenesis methods and modeling studies (using the structure of the copper-sensor CsoR as a template) to propose the nickel is bound by the amino-terminal amine, Glu63, and His64 of one subunit along with Cys35' of another subunit (Carr et al. 2017b; Higgins et al. 2012b; Iwig et al. 2008; Musiani et al. 2015). Crystals of the RcnR-DNA complex were reported (Li et al. 2020), but no structure is yet available.

*Synechocystis* sp. PCC 6803 contains the nickel-responsive regulatory protein InrS (named for *internal nickel responsive sensor*) that belongs to the same protein family as RcnR and CsoR (Foster et al. 2012). The tetrameric cyanobacterial

protein is a repressor of *nrsD* (Fig. 14.1b), encoding a nickel efflux pump, and the repression is relieved by nickel binding (one metal ion per subunit) with an estimated  $K_d$  of  $2 \times 10^{-14}$  M (Foster et al. 2012). Mutagenesis studies indicate that nickel binds to the protein using Cys53, His78, and Cys82 ligands, perhaps also including His21 (Foster et al. 2014). A crystal structure of the InrS apoprotein (Fig. 14.2b) is consistent with this same set of coordinating residues, where Cys53 from one subunit partners with the other three residues from a second subunit (Foster et al. 2017). XAS analysis of nickel-bound InrS was consistent with a square-planar Ni (His)<sub>2</sub>(Cys)<sub>2</sub> site (Carr et al. 2017a). The protein can also bind copper or cobalt, but its physiological function is specific to nickel.

*Rhizobium leguminosarum* also possesses an RcnR-like protein that is denoted DmeR for *divalent metal efflux repressor* (Rubio-Sanz et al. 2013). The apoprotein form of DmeR represses *dmeF*, encoding a cation diffusion facilitator (CDF) efflux transporter, and repression is alleviated by nickel or cobalt (Fig. 14.1b). A similar *dmeRF* gene cluster is responsible for nickel (or cobalt)-dependent regulation and export in *Agrobacterium tumefaciens* (Dokpikul et al. 2016). Structural characterization has not been reported for any DmeR.

Another sequence-related family member is NcrB from *Leptospirillum ferriphilum* strain UBK03, an iron-oxidizing, metal-resistant bacterium containing the *ncrABC* gene cluster that confers resistance to nickel (Tian et al. 2007). NcrB is a histidine-rich, 89-residue protein that functions as a repressor of the gene cluster in its apoprotein form, but the regulation is derepressed by nickel binding to the protein (Fig. 14.1b) leading to synthesis of the NcrAC efflux pump (Zhu et al. 2011). The structure of NcrB has not been determined.

### 14.2.1.3 NmtR/KmtR

Examples of repressors that dissociate from the DNA upon binding nickel (Fig. 14.1b), yet are unrelated to those just described, include NmtR and KmtR from *Mycobacterium tuberculosis* (Campbell et al. 2007; Cavet et al. 2002). These proteins are members of the ArsR/SmtB family of transcriptional regulatory proteins (Busenlehner et al. 2003). The apoprotein forms of NmtR and KmtR bind to operator-promoter sites upstream of *nmtA* and *cdf*, encoding a P-type ATPase efflux pump and a CDF protein, respectively. Spectroscopic and mutagenesis studies suggest that nickel binds to NmtR in octahedral coordination, with the likely involvement of Asp91, His93, His104, and His107 along with residues near the amino-terminus (Cavet et al. 2002; Pennella et al. 2003; Reyes-Caballero et al. 2011). These residues are not conserved in KmtR and its higher affinity nickel binding site was suggested to involve His88, Glu101, His102, His110, and His111 (Campbell et al. 2007). The dimeric NmtR protein binds two nickel with  $K_d \sim 10^{-10}$  M (Reyes-Caballero et al. 2011). The solution structure for the NmtR apoprotein, determined by NMR methods (Lee et al. 2012), revealed the winged-helix appearance that is typical for this family of proteins (Fig. 14.2c).



Related nickel sensor proteins have been characterized in two other microorganisms. An NmtR sensor exists in *Streptomyces coelicolor* where it regulates production of a P-type ATPase efflux transporter (Kim et al. 2015). *Streptomyces griseus* contains another example of the ArsR/SmtB family named SrnR. This protein forms a complex with SrnQ that regulates *sodF*, encoding an iron-containing superoxide dismutase, by binding to the inverted repeat sequence TTGCA-N<sub>7</sub>-TGCAA. As originally proposed, neither protein binds to DNA in the absence of nickel whereas the nickel-bound hetero-octamer functions as a repressor (Fig. 14.1a) (Kim et al. 2003b). More recent efforts suggested that SrnR does bind DNA and activates transcription, whereas further binding of nickel-bound SrnQ leads to dissociation and reduced levels of transcription (Fig. 14.1d) (Beniamino et al. 2020). SrnR binds nickel with moderate affinity ( $K_d \sim 0.65 \mu\text{M}$ ) (Beniamino et al. 2020), but the primary nickel-binding regulatory site is associated with SrnQ (one nickel per protein subunit) (Kim et al. 2003b). The structure of SrnRQ and its nickel-binding site(s) are unknown.

#### 14.2.1.4 Nur

The *S. coelicolor* Nur (nickel uptake regulator) protein, a member of the Fur family of transcriptional regulators, binds nickel to form a complex that represses transcription of some genes (Fig. 14.1a) while activating transcription of another gene (Fig. 14.1c). Specifically, nickel is a co-repressor of the *nikABCDE* and *nikMNOQ* operons for nickel uptake and of *sodF* encoding an iron-dependent superoxide dismutase, while the metal is a co-activator of *sodN* coding for a nickel-dependent superoxide dismutase (Ahn et al. 2006; An et al. 2009). The nickel-Nur complex binds to the “Nur box” palindromic sequence tTGCAa-N5-ttGCAA. The structure of the 16-kDa Nur protein (Fig. 14.2d) reveals a homodimeric winged-helix motif that wraps around DNA and binds four metals per dimer (An et al. 2009). Two sites near the subunit interface coordinate nickel in octahedral geometry with three side chain residues (His70, His72, and His126) along with three oxygen atoms from buffer components. Two other sites, initially suggested to not be responsive to nickel, coordinate the metals in square-planar geometry using His33, His86, His88, and His90 side chains. More recent studies using a combination of mutagenesis, metal titration, and fluorescence anisotropy methods suggest that nickel binding to this site is the critical regulatory process used for protein binding to the DNA, with the other site having a fine-tuning role (Manley et al. 2020). Isothermal titration calorimetry (ITC) studies confirm the dimeric protein binds four nickel ions in pairs with  $K_d$  values of 10 nM and 280 nM (Musiani et al. 2015).

#### 14.2.1.5 CnrX

*Cupriavidus metallidurans* (formerly named *Ralstonia metallidurans*) CH34 contains a nickel sensor, CnrX, that operates by a very different process. This organism

tolerates high concentrations of several types of heavy metals by using a set of efflux pumps. In particular, this microorganism contains the *cnrYXH-cnrCBA* gene cluster (located on the pMOL28 plasmid) that is associated with, and named for, cobalt and nickel resistance (Grass et al. 2000; Tibazarwa et al. 2000). CnrCBA is the nickel exporter, CnrH is a sigma factor regulating both halves of the gene cluster, CnrY is a trans-membrane connector, and CnrX is a periplasmic nickel-sensing protein (Fig. 14.2e). The cytoplasmic face of CnrY binds CnrH while its periplasmic face binds CnrX. These three proteins work together in what is termed an extracellular function-type sigma factor; nickel coordination to CnrX ( $K_d \sim \text{pM}$ ) leads to a conformational change that propagates through CnrY causing the release of CnrH, which then binds to the appropriate DNA sequence to stimulate transcription by RNA polymerase. This mechanism is akin to, but more complicated than, the co-activator mechanism described earlier (Fig. 14.1c); in particular, the nickel sensor resides in the periplasm.

The X-ray crystal structure of dimeric CnrX is available for residues 31–148 of the apoprotein and the copper-bound forms (Pompidor et al. 2008). The copper is coordinated by His42, His46, Glu63, and His119, with Met123 (numbering based on the full-length protein) also being nearby. Follow-up studies reveal structures of the nickel- (Fig. 14.2e), cobalt-, and zinc-bound forms; the nickel and cobalt species exhibit octahedral coordination involving these same five residues with bidentate Glu63 accounting for the metal-specific conformational changes needed for signaling (Trepreau et al. 2011b). The structure of the nickel-bound species includes residues 39–148, and the amino terminal region is membrane embedded. A crystal structure of the complex between the cytosolic domain of CnrY (residues 2–30) and much of CnrH (residues 5–190 except for 92–122) is known (Maillard et al. 2014). The conformational changes associated with nickel binding to CnrX were explored in greater detail by metal titration analysis and high resolution (1.1 Å) structural studies of selected variant forms of the protein (Maillard et al. 2015). The spectroscopic properties of cobalt-bound CnrX are defined and two additional cobalt binding sites are demonstrated to exist at the amino terminus of the protein (Trepreau et al. 2011a). A structure also is available for the related NccX protein from strain 31A of the same species; significant structural differences are noted when comparing to the strain CH34-derived CnrX protein, but these variations are attributed to the redistribution of hydrophobic surfaces during solubilization of the protein by detergent (Ziani et al. 2014).

#### 14.2.1.6 NrsRS

A microorganism already mentioned, *Synechocystis* sp. PCC 6803, contains a second nickel sensor that operates by a very different mechanism from that detailed earlier (Sect. 14.2.1.2). According to the current model (Garcia-Dominguez et al. 2000; Lopez-Maury et al. 2002), NrsS has an amino-terminal domain localized in the periplasm, two transmembrane helices, and a carboxyl-terminal kinase domain. Nickel binding to the periplasmic region stimulates the kinase domain to transfer

phosphate to the cytoplasmic membrane-localized NrsR, which activates transcription by binding at up to four sites in the intergenic region of the divergent *nrsBACD* and *nrsRS* gene clusters. No structural studies have been described for the NrsRS system. The behavior of this two-component system is reminiscent of the co-activator mechanism detailed earlier (Fig. 14.1c). Note that the *nrsD* mentioned here is the same gene as that regulated more directly by InrS, which uses a promoter binding site that immediately precedes the gene.

#### 14.2.1.7 NimR

*Haemophilus influenzae* possesses a distinct nickel sensor belonging to the Mer family of transcriptional regulatory proteins, typically associated with regulatory responses to toxic metals such as mercury, cadmium, and lead. This protein, NimR, regulates the *nikKLMQO* operon encoding an ABC transporter for nickel uptake by a combination of two mechanisms shown in Fig. 14.1 (Kidd et al. 2011). Specifically, the NimR apoprotein binds to a site of dyad symmetry in the operator/promoter region of the nickel transport operon resulting in transcriptional activation (Fig. 14.1d); upon binding nickel, NimR ceases to activate and rather the complex functions as a co-repressor (Fig. 14.1b). The dimeric protein (15.6-kDa subunit) binds a single nickel at a site that has not been further characterized and the structure of the protein has not been reported.

#### 14.2.1.8 Other Nickel Sensors

Nickel-sensitive transcriptional regulatory proteins exist in many microorganisms beyond those mentioned above. These regulators often are related in sequence to the proteins already described, but novel types of sensor proteins also are known. Detailed structural studies and careful analyses of the corresponding nickel-binding sites generally are not available. When functionally characterized, these additional nickel-sensor proteins often have been found to control nickel-transport systems; however, other roles also are known such as regulating the production of nickel-containing enzymes. Such non-homeostatic regulatory functions of nickel sensors were noted earlier: the control of urease expression by NikR in *H. pylori* (van Vliet et al. 2002) and regulation of superoxide dismutases by Nur in *S. coelicolor* (Ahn et al. 2006) and SrnRQ in *S. griseus* (Beniamino et al. 2020; Kim et al. 2003b). Two additional examples of nickel sensors not involved in nickel transport are summarized below, followed by a brief discussion of a nickel-sensing RNA.

YqjI of *E. coli* is a nickel-binding regulatory protein that associates with inverted-repeat sequences in the region between the divergently transcribed *yqjH* and *yqjI* genes (Wang et al. 2011). The complex regulation pattern of this system requires that YqjI apoprotein bind to both promoter regions in a cooperative manner for full repression (Wang et al. 2014). Binding of nickel reduces the DNA-binding activity of the regulatory protein, allowing for *yqjH* expression (Wang et al. 2011). YqjH is a

flavin-containing enzyme that functions as an iron-siderophore reductase so it was renamed NfeF for *nickel-responsive Fe uptake flavoprotein*; consequently, YqjI was renamed NfeR for *nickel-response Fe-uptake regulator* (Blahut et al. 2018). In vivo transcriptional studies were used to assess mRNA levels of the wild-type protein and site-substituted variants, while purified YqjI/NfeR and several of its variants were analyzed by ITC, XAS, and other studies to better define the nickel-binding site. Although the metal exhibits 5-coordinate geometry with a sulfur ligand, none of the Cys-substituted variants affect nickel binding. Nevertheless, Cys42 and Cys43 are required for the in vivo response and these residues are suspected to form a vicinal disulfide (Blahut et al. 2018). Structural studies are needed to better define the NfeR nickel-binding site.

The *H. pylori* HP0868 gene product is a nickel-binding protein that affects the activity level of urease; thus, it was named Mua for *modulator of urease activity* (Benoit and Maier 2011). Dimeric Mua binds two nickel ions, and high nickel concentrations lead to repression of urease activity by this protein. Mua does not bind to the urease promoter region, or other DNA promoter sequences, and the mechanism of regulation is unknown. The nickel-coordinating residues are not identified and the structure of this nickel sensor has not been elucidated.

Comparative sequence analysis of genomes in the order Clostridiales reveals a novel class of structured RNA often residing upstream of *czcD* genes that encode CDF proteins (Furukawa et al. 2015). The corresponding RNA from *Clostridium botulinum* binds nickel and cobalt with a  $K_d$  of 12 and 6  $\mu\text{M}$ , respectively, leading to structural changes. The metal-bound form of the NiCo riboswitch is thought to prevent formation of a terminator loop in the RNA, thus allowing the *cdf* gene to be transcribed. Subsequent in vitro and in vivo studies demonstrated the riboswitch also responds to ferrous ion (Xu and Cotruvo Jr. 2020). The crystal structure is available for the cobalt-bound RNA from *Erysipelotrichaceae bacterium* (Fig. 14.2f), revealing two cobalt (and presumably nickel) sites, two magnesium atoms, and seven bound potassium ions (Furukawa et al. 2015).

## 14.2.2 Nickel Import Systems

Microorganisms possess nickel *uptake* systems to supply the requirements for nickel-containing enzymes and they use nickel *efflux* systems (Sect. 14.2.3) to limit the toxicity of this cation. Regulation of these transporters often is facilitated by using the nickel sensors described in Sect. 14.2.1. The following subsections describe mechanisms of nickel uptake that fall into two general classes: ABC transporters and permeases (or secondary transporters). The ABC transporter family is subdivided into those with a soluble substrate-binding protein or domain (Sect. 14.2.2.1) and those of the energy-coupling factor (ECF) subfamily (Sect. 14.2.2.2). The permease family (Sect. 14.2.2.3) includes the so-called NiCoT, UreH, and HupE/UreJ subfamilies (Chivers 2015; Eitinger and Mandrand-Berthelot 2000; Nies et al. 2017; Rodionov et al. 2006; Rodrigue et al. 2017). In addition to

describing each of these systems, this section summarizes the process used to facilitate import across the OM of Gram-negative cells (Sect. 14.2.2.4). The described examples are those with high specificity for nickel, although some other metals such as cobalt are often recognized. In addition to these nickel-targeted import processes, this metal also enters some cells via transporters that function in uptake of magnesium (Snavelly et al. 1991), other metals (Degen et al. 1999), metal-citrate complexes (Willecke et al. 1973), or other systems that are not detailed.

#### 14.2.2.1 Nickel Uptake by ABC Transporters Possessing a Substrate-Binding Protein/Domain

The most intensively studied ABC transporter system for nickel uptake is the NikABCDE system of *E. coli* (Navarro et al. 1993). NikA is a periplasmic substrate (nutrient)-binding protein, NikB and NikC are integral membrane proteins, and NikD and NikE are ATPases that drive the uptake process. Nickel binds to NikA with a  $K_d$  of less than  $0.1 \mu\text{M}$  (de Pina et al. 1995), but this value is shifted to  $\sim 75 \text{ nM}$  for the complex of metal bound to L-histidine (Chivers et al. 2012). Analysis of the structure of NikA provides a fascinating glimpse into the power and limitations of crystallography. The initial apoprotein and holoprotein structures revealed the same overall fold with two domains connected by a hinge used to enclose the substrate binding site; however, the bound pentahydrate nickel lacked any direct interaction with the protein (Hedde et al. 2003)—a coordination environment incompatible with earlier XAS analysis (Allan et al. 1998). A subsequent structure of NikA complexed with EDTA-bound iron implicated the binding of a metallophore, rather than the free metal ion (Cherrier et al. 2005). Another NikA structure was proposed to resolve the disparate findings; it used a variant protein and identified a second, distant nickel-binding site with His54 and His442 as coordinating ligands (Addy et al. 2007). The notion of NikA binding a metallophore was later supported by another structure in which NikA binds a complex of nickel and an endogenous ligand, tentatively identified as butane-1,2,4-tricarboxylate (Cherrier et al. 2008). Finally, after evidence had indicated NikA actually binds the Ni-(L-histidine)<sub>2</sub> complex (Chivers et al. 2012), the structure of this form of the protein was obtained and confirmed the metal coordination by His416 (Lebrette et al. 2013). In contrast to these extensive structural studies of NikA, no structure is reported for the other components of the Nik system. Because the NikBCDE components are likely to resemble other ABC-type metal transporters, Fig. 14.3a provides the structure of the transmembrane and ATPase components of a putative metal-chelate ABC transporter from *H. influenzae* (Pinkett et al. 2007) as a mimic of the nickel-specific proteins, along with that of the NikA-Ni-(L-His)<sub>2</sub> complex (Lebrette et al. 2013).

Many other microorganisms possess Nik-type ABC-transporters with a soluble periplasmic nickel-binding protein (or for Gram-positive bacteria, an attached extracellular domain), although in some cases different terminology is used for the components. Examples with experimental evidence for a nickel transport function include proteins encoded by *niuBDE* of *H. pylori* (Fischer et al. 2016), *nikABCDE* of

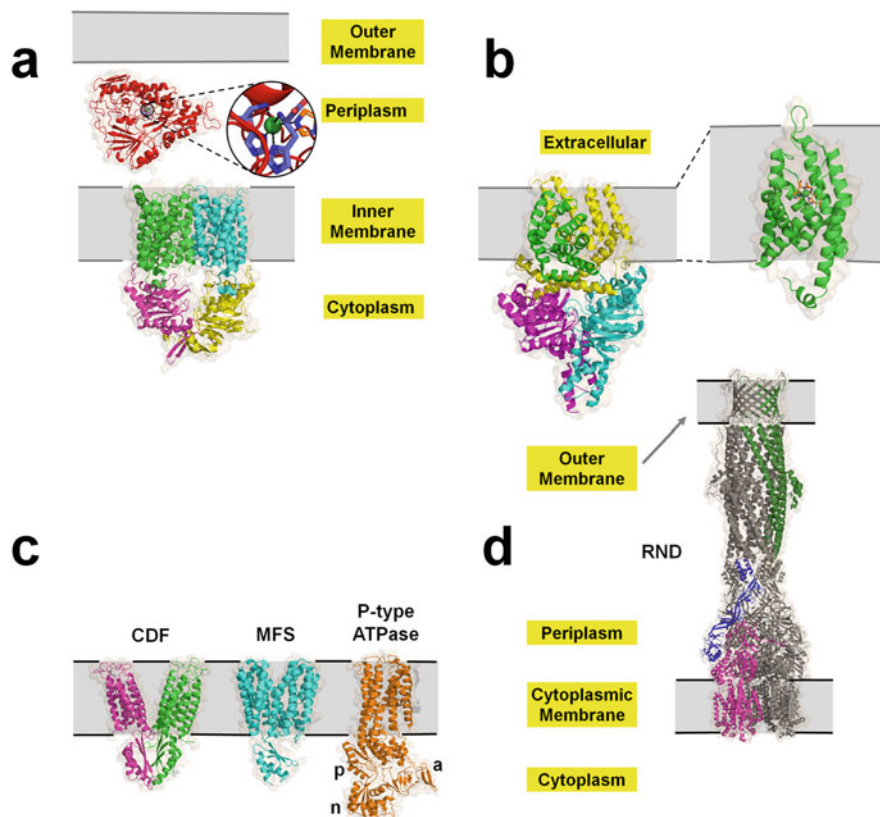


**Fig. 14.3** Structures of nickel transporters. (a) *Escherichia coli* NikA and a NikBCDE-like complex used for nickel import. The periplasmic NikA substrate-binding protein (red, PDB ID 4i8c) includes an inset illustrating the metal-binding site with His416 in orange sticks, two molecules of L-histidine in blue sticks, and nickel as a green sphere. The structure of NikBCDE is unknown, but likely resembles that depicted for the metal-chelate ABC transporter of *Haemophilus influenzae* (PDB ID 2nq2) with transmembrane (green/cyan) and ATPase (magenta/yellow) components. (b) *Thermoanaerobacter tengcongensis* NikM2 (green, PDB ID 4m58), the S component of a multi-component nickel ECF-type ABC importer, with the nickel-coordinating sidechains (Met1, His2, and His67) shown as orange sticks. The full importer structure is not established, but likely resembles the four-component folate transporter shown from *Lactobacillus brevis* (PDB ID 4huq; S in green, T in yellow, and A in magenta and cyan). (c) Structural mimics of CDF, MFS, and P-type ATPase nickel exporters are the homodimeric, zinc-specific, YiiP from *E. coli* (PDB ID 3h90, green and magenta), the monomeric, putative drug exporting, YajR from *E. coli* (PDB ID 3wdo, cyan), and the four-domain, single-component, copper-transporting, CopB from *Legionella pneumophila* (PDB ID 3rfu, orange). The latter includes a transmembrane region, actuator domain (a), phosphorylation domain (p), and nucleotide binding-domain (n). (d) A structural mimic of an RND export pump for nickel is CusABC that exports copper primarily from the periplasm of *E. coli* (PDB ID 3ne5 for CusAB and 3pik for CusC). The RND pump is gray, except for single subunits of CusA (red), CusB (blue), and CusC (dark green). All components are shown in cartoon mode with partially transparent surfaces

*Brucella suis* (Jubier-Maurin et al. 2001), *yntABCDE* of *Yersinia pseudotuberculosis* (Sebbane et al. 2002) and *Proteus mirabilis* (Brauer et al. 2020), *nikZYXWV* of *Campylobacter jejuni* (Howlett et al. 2012), and *cntABCDE* from *Staphylococcus aureus* (Remy et al. 2013). The latter Gram-positive microorganism lacks a periplasm so its NikA-like protein, CntA, is tethered to the membrane by an amino-terminal extension. Several NikA-related structures are known including CntA from *S. aureus* (Song et al. 2018), NikA from the same microorganism (Lebrette et al. 2015), CeuE from *H. pylori* (Shaik et al. 2014), NikA from *B. suis*, YntA from *Yersinia pestis*, NikZ from *C. jejuni* (Lebrette et al. 2014), and the analogous protein from *Sinorhizobium meliloti* (unpublished, PDB ID 4web). Although the overall structures of these nickel-binding proteins are related, the ligand binding sites are distinct. This finding is consistent with diversity in the substrate being transported (i.e., other than the Ni(L-His)<sub>2</sub> complex), as exemplified by CntA's interaction with the complex of nickel and staphylopin—a broad-spectrum nicotianamine-like metallophore (Ghssein et al. 2016; Song et al. 2018).

#### 14.2.2.2 Nickel Uptake by ECF-Type ABC Transporters

The second type of ABC transporter used for nickel uptake lacks a soluble periplasmic protein or extracellular domain for binding the metal ion or metallophore. Rather, CbiMNQO, NikMNQO, and related ECF-type importers possess a small (~20 kDa), integral-membrane protein for binding nickel, termed the S component, that interacts with another integral-membrane T component and two similar or identical cytosolic ATPases known as A components (Finkenwirth and Eitinger 2019; Rodionov et al. 2006; Slotboom 2014). Early examples of such systems are those reported in *Actinobacillus pleuropneumoniae* (Bossè et al. 2001) and *Streptococcus salivarius* 57.I (Chen and Burne 2003), where the nickel import genes are located adjacent to urease genes and shown to be important for nickel incorporation into this enzyme. Among other examples, nickel transport is demonstrated for the products of *nik(MN)QO* (where *nikM* and *nikN* are fused) of *Rhodopseudomonas capsulatus* (Rodionov et al. 2006), *nikLMNQO* of *H. influenzae* (Kidd et al. 2011), and *lar(MN)QO* (where *lar* indicates association with genes encoding the nickel-dependent lactate racemase) of *Lactobacillus plantarum* (Desguin et al. 2014). The structure of the S component for the nickel importer of *Thermoanaerobacter tengcongensis*, NikM, is shown in Fig. 14.3b (Yu et al. 2014). Nickel is 4-coordinated with the Met1 amine, His2 imidazole and amide, and His67 imidazole providing square-planar ligation. This figure also illustrates a four-component *Lactobacillus brevis* ECF-type transporter for folic acid as a mimic of the nickel ECF-type transporter.

### 14.2.2.3 Nickel Uptake by Permeases/Secondary Transporters

Many microorganisms possess single-protein nickel uptake systems that operate either by facilitated diffusion or are driven by the proton motive force (Eitinger and Mandrand-Berthelot 2000; Eitinger et al. 2005; Rodionov et al. 2006; Rodrigue et al. 2017). The nickel/cobalt transporter (NiCoT) subgroup of these proteins is probably the best characterized. The archetype member of this family is HoxN from *Cupriavidus necator* (formerly named *Alcaligenes eutrophus* and *Ralstonia eutropha*). Early studies identified the gene encoding this protein to be in the hydrogenase gene cluster (Eberz et al. 1989) and showed it participates in nickel transport (Eitinger and Friedrich 1991). A topological model indicated eight trans-membrane domains (Eitinger and Friedrich 1994) and the probable nickel-binding residues have been identified by mutagenesis studies (Eitinger et al. 1997). Another NiCoT family member used to import nickel for [NiFe] hydrogenase activation is HupN of *Bradyrhizobium japonicum* (Fu et al. 1994). By contrast, NixA of *H. pylori* is a NiCoT family member that was first identified by its relationship to synthesis of active urease (Mobley et al. 1995a). As in the case of HoxN, membrane topology and extensive mutagenesis studies defined the potential nickel-binding motifs (Fulkerson Jr. et al. 1998; Fulkerson Jr. and Mobley 2000). A second subgroup of nickel permeases with only six trans-membrane domains is named for the first representative identified: UreH encoded within the urease gene cluster of the thermophile *Bacillus* sp. TB-90 (Maeda et al. 1994). The corresponding family member in *Y. pseudotuberculosis* facilitates high-affinity, nickel-specific transport (Sebbane et al. 2002). HupE and UreJ are included in the third subgroup of nickel permeases (Eitinger et al. 2005). The *R. leguminosarum* HupE facilitator protein, encoded by a gene co-localizing with hydrogenase genes, was investigated by mutagenesis methods that identified critical residues for nickel uptake (Albareda et al. 2015; Brito et al. 2010). UreJ of *Bordetella bronchiseptica* possesses 37% identity with the *R. leguminosarum* protein, but is encoded within the urease gene cluster (McMillan et al. 1998). *Synechococcus* sp. strain WH8102 also contains a *hupE* gene; however, the function of the encoded protein is not defined and nickel transport in this organism is associated with a different permease named SodT (Dupont et al. 2012). Of further interest, a eukaryotic example of a nickel permease, Nic1p, occurs in *Schizosaccharomyces pombe* (Eitinger et al. 2000). Despite their importance for nickel transport in a wide range of microorganisms, no structures have been reported for any uptake nickel permease.

### 14.2.2.4 Nickel Uptake Through the OM

Although the OM of Gram-negative bacteria possesses porin proteins that allow passage across this barrier by small molecules (< ~600 Da), it is known that uptake of iron siderophores, heme, some sugars, and other compounds is promoted by making use of OM receptors that are energized by TonB, ExbB, and ExbD proteins,



with periplasmic substrate-binding components delivering the nutrient to inner membrane transporters (Braun and Hantke 2011). Evidence has accumulated that nickel is taken up in a similar way. For example, NikR and nickel regulate *H. pylori* genes (*hp1512*, *hp1339–1340*, and *hp1561*) thought to encode a receptor (FrpB4), energizer components (ExbB/ExbD), and a periplasmic protein (CeueE) (Contreras et al. 2003). Other groups confirmed the finding that FrpB4 is an outer membrane protein whose synthesis is regulated by NikR, and they identified the NikR-regulated FecA3 (encoded by *HP1400*) as a second likely OM receptor (Davis et al. 2006; Ernst et al. 2006). Mutagenesis studies demonstrated that *H. pylori* uses the TonB/ExbB/ExbD machinery to drive nickel uptake via FrpB4 (Schauer et al. 2007). *H. hepaticus* appears to have a similar system with NikR-regulated expression of a gene (*hh0418*) encoding an OM receptor (Benoit et al. 2013). Furthermore, *H. mustelae* possesses *nixA*, *fecDE*, *nikH*, and *ceueE* (encoding a permease, inner membrane ABC transporter, OM receptor, and periplasmic substrate-binding protein) involved in nickel transport, along with two *tonB* genes; TonB1 is needed for heme uptake and TonB2 is used for nickel uptake (Stoof et al. 2010a, b). Structural characterization of an outer membrane system for nickel uptake is lacking.

### 14.2.3 Nickel Export Systems

This section describes five systems by which microorganisms export nickel from the cell: RcnA and related proteins (Sect. 14.2.3.1), cation diffusion facilitators (CDFs, Sect. 14.2.3.2), the major facilitator protein superfamily (MFS, Sect. 14.2.3.3), P-type ATPases (Sect. 14.2.3.4), and resistance nodulation cell division (RND)-type efflux systems (Sect. 14.2.3.5). As in the case of the importer systems, these exporter systems often are not specific to nickel; however, each system emphasized here promotes nickel efflux.

#### 14.2.3.1 Nickel Export via RcnAB and Related Systems

The nickel efflux pump of *E. coli* is the inner membrane-bound protein RcnA as shown by the cellular decrease in nickel resistance when the corresponding gene is mutated (Rodrigue et al. 2005). An increase in cellular nickel concentration leads to dissociation of the RcnR regulatory protein from the DNA (Sect. 14.2.1.2), leading to enhanced *rcnA* transcription (Iwig et al. 2006). RcnA is distantly related to the NiCoT family (Sect. 14.2.2.3). RcnB, encoded by a gene located immediately downstream of *rcnA*, is a periplasmic, copper-binding protein that modulates the nickel export activity of RcnA by an unclear process (Blériot et al. 2011, 2015). Genes related to *rcnA*, sometimes paired with *rcnB*-like genes, have been identified in several other bacteria and typically have alternative names. A few examples for which an involvement in nickel resistance is demonstrated are *mrhH* in *Pseudomonas putida* KT2440 (Haritha et al. 2009), *nirC* of *Klebsiella oxytoca* (Park et al.

2008), and *nrcC* from three species: *Hafnia alvei* 5-5 (Park et al. 2004), *L. ferriphilum* (mentioned in Sect. 14.2.1.2 as being regulated by NcrB) (Tian et al. 2007), and *Serratia marscescens* (Marrero et al. 2007). No structure is available for any RcnA protein, but modeling studies suggest the presence of six trans-membrane regions (Rodrigue et al. 2017).

### 14.2.3.2 Export of Nickel by Cation Diffusion Facilitators (CDF)

Nickel export via proton antiporters is carried out by CDF family members. FieF and DmeF of *C. metallidurans* export nickel, although they are more effective at transporting other metals (Munkelt et al. 2004). DmeF proteins from *R. leguminosarum* and *A. tumefaciens* are efficient nickel exporters (Dokpikul et al. 2016; Rubio-Sanz et al. 2013). The nickel-efflux CDF protein of *M. tuberculosis* is called Rv2025c and regulated by KmtR (Campbell et al. 2007), as described in Sect. 14.2.1.3. *Rhizobium etli* possesses a CDF transporter of nickel termed NepA (Cubillas et al. 2013). Although no structure is reported for a nickel-specific CDF, the architecture of the zinc-specific CDF transporter YiiP from *E. coli* is available by crystallography (Lu et al. 2009). This protein (Fig. 14.3c, left) provides a reasonable facsimile of what one might expect for a nickel-transporting CDF. The homodimer is Y-shaped with each subunit having six transmembrane regions and a C-terminal cytoplasmic region.

### 14.2.3.3 Nickel Export Involving the Major Facilitator Protein Superfamily (MFS)

As expected for the term superfamily, MFS is a large group of membrane secondary transporters that act on a vast number of substances (Saier Jr. et al. 1999). The best example of a nickel-specific exporter is NreB from *Achromobacter xylooxidans* 31A, which confers nickel resistance in the native host or when synthesized in *E. coli* (Grass et al. 2001). NreB has a histidine-rich C-terminal region, but this sequence is not essential to its function. A related example, NrsD, exists in *Synechocystis* sp. strain PCC 6803 (Garcia-Dominguez et al. 2000). This protein was mentioned earlier (Sect. 14.2.1.2) because it is regulated by the nickel-sensor InrS. Although structures are not available for NreB or NrsD, several MFS transporters have been structurally characterized including the putative drug exporter YajR from *E. coli* (Jiang et al. 2013). The MRS proteins are thought to use a rocker-switch mechanism requiring conformational changes involving their 12 transmembrane helices. YajR, shown in its outward-facing conformation, exemplifies the likely structure of the nickel exporters (Fig. 14.3c, middle).

#### 14.2.3.4 P-Type ATPases Used for Nickel Efflux

ATP hydrolysis is used to drive the export of a wide range of substances via single-component P-type ATPases (Palmgren and Nissen 2011). NmtA from *M. tuberculosis* or *S. coelicolor*, mentioned earlier as being regulated by NmtR (Sect. 14.2.1.3), is likely to be such a protein (Cavet et al. 2002; Kim et al. 2015). CtpD of *Mycobacterium smegmatis* exports nickel, though it has a greater preference for cobalt, and deletion of the corresponding gene leads to accumulation and sensitivity to both metals (Raimunda et al. 2012). Another member of this family of proteins is *S. meliloti* Nia, named for being a nickel-iron ATPase (Zielazinski et al. 2013). Nia synthesis is induced by the presence of either metal and deletion of the corresponding gene leads to the accumulation of both cations. An extra domain near the C-terminus resembles hemerythrin and binds a dinuclear iron center, suggesting an additional role for this protein may exist. While none of these proteins have been structurally characterized, they are likely to exhibit extensive similarity to the copper-transporting P-type ATPase CopB from *Legionella pneumophila* (Gourdon et al. 2011). This protein, illustrated as a mimic for a nickel P-type ATPase (Fig. 14.3c, right), possesses a transmembrane portion, and the actuator (a), phosphorylation (p), and nucleotide binding (n) domains.

#### 14.2.3.5 RND Pumps for Export from the Periplasm

RND pumps are complicated systems for expelling a compound from the periplasm, although they are also capable of less efficient export from the cytoplasm. These systems are used as multidrug transporters and for transporting various other compounds. They consist of three parts: (1) the trimeric inner membrane RND pump that is driven by the proton motive force, (2) the periplasmic adaptor proteins that form a multimeric ring which spans between the inner and outer membranes, and (3) the trimeric OM factor (Symmonds et al. 2015). Nickel export via an RND pump was first described for *C. metallidurans* CH34 (Liesegang et al. 1993). The *cnrCBA* genes encoding this system are regulated by the products of *cnrYXH* (Sect. 14.2.1.5), where CnrX is a periplasmic nickel sensor protein (Maillard et al. 2015). Additional RND exporters of nickel include those encoded by *cznABC* of *H. pylori* (Stähler et al. 2006), *nrsAB* of *Synechocystis* (regulated by NrsRS, Sect. 14.2.1.6) (Garcia-Dominguez et al. 2000), and *cnrA* of *Bradyrhizobium* strains associated with a legume that grows in a high-nickel environment (Chaintreuil et al. 2007). No structure is available for any of these nickel export proteins, but the copper exporter CusABC (Fig. 14.3d) from *E. coli* provides a reasonable illustration of what one might expect. The CusA component of this RND pump forms a homotrimer in the cytoplasmic membrane, with each subunit possessing 12 transmembrane helices (Long et al. 2010). Six molecules of the CusB adaptor attach to the CusA homotrimer, forming a tunnel through part of the periplasm (Su et al. 2011). The distal end of this tunnel attaches to the trimeric OM component CusC that was

structurally characterized as an independent protein (Kulathila et al. 2011). This homotrimer completes the tunnel through the periplasm and forms a  $\beta$ -barrel in the OM that is anchored by a triacylated N-terminus.

### 14.3 Other Aspects of Nickel Toxicity and Resistance

Microorganisms have long been investigated with regard to nickel toxicity and nickel resistance. In 1967, for example, R factors were shown to mediate nickel tolerance of *E. coli* and *Salmonella* strains (Smith 1967). Early reviews of nickel toxicity documented the sensitivities of various microorganisms to this metal when growing under different conditions (Babich and Stotzky 1983; Gadd and Griffiths 1978), but in general the basis for the sensitivity to this metal ion remained enigmatic. This section begins by describing studies that define the primary site of nickel toxicity in *E. coli* (Sect. 14.3.1), then it briefly surveys other established mechanisms of nickel stress (Sect. 14.3.2). Following a similar sequence, initial microbial screening methods identified nickel-tolerant strains of microorganisms and by the mid-1980s genetic studies [e.g. (Mergeay et al. 1985; Siddiqui and Schlegel 1987)] began to identify some of the resistance determinants. More recent studies have identified nickel efflux, described in Sect. 14.2.3, as the most widely used system for allowing microorganisms to tolerate high concentrations of this metal ion. Aspects of these exporters will not be repeated here; rather, alternative resistance mechanisms will be summarized (Sect. 14.3.3).

#### 14.3.1 *The Primary Site of Nickel Toxicity in E. coli:* *Fructose-1,6-Bisphosphate Aldolase*

Growth of *E. coli* on glucose or fructose minimal medium is inhibited by the addition of 8  $\mu$ M nickel, but no growth inhibition was observed for this environmentally-relevant concentration of nickel when using succinate, lactate, or glycerol as carbon sources (Macomber et al. 2011). As expected, the inhibitory effect was exacerbated for *rcnA* mutant cells, which are inhibited by only 4  $\mu$ M of this metal ion. These results are consistent with a direct effect of nickel on fructose-1,6-bisphosphate aldolase (FbaA)—a critical enzyme for the metabolism of glucose and fructose, but not required for degradation of the other nutrients. The loss of cellular FbaA activity following nickel stress and the restoration of growth in the *rcnA* mutant cells by overexpression of *fbaA* confirmed this enzyme as the target of nickel toxicity. Prior structural studies had demonstrated that FbaA, a class II aldolase, possesses zinc at its active site (coordinated by His110, His226, and His264) with another zinc (coordinated by Asp144, Glu174, and Glu181) bound at a nearby non-catalytic metal-binding site (Hall et al. 1999). Nickel-treated FbaA lost approximately one

of these zinc atoms while binding about one nickel atom. Significantly, the D144A and E174A FbaA variants, affecting the non-catalytic site, are resistant to nickel inhibition. These studies provide clear evidence that the primary site of nickel toxicity for glucose- or fructose-grown *E. coli* is the non-catalytic zinc site of FbaA (Macomber et al. 2011). Cells grown on succinate, lactate, or glycerol are inhibited by high concentrations of nickel, but the target of toxicity under these conditions remains unknown.

### 14.3.2 Other Sites of Nickel Toxicity in Microorganisms

In contrast to the detailed mechanistic understanding of nickel toxicity for glucose- or fructose-grown *E. coli*, described above, few studies have investigated the basis of nickel's deleterious effects in other microorganisms (Macomber and Hausinger 2011). This section summarizes other potential sites of nickel toxicity in microbes (Fig. 14.4): oxidative stress effects, substitution of active site metal ions in important metalloenzymes (with redox-active or non-redox sites), and inhibitory binding to non-active sites of essential enzymes.

Proteomic studies of nickel-challenged *Burkholderia vietnamiensis* and *P. putida* UW4 showed increased production of proteins related to oxidative stress (Cheng et al. 2009; Van Nostrand et al. 2008), consistent with nickel increasing the cellular formation of reactive oxygen species (ROS). Furthermore, *E. coli* cells lacking both

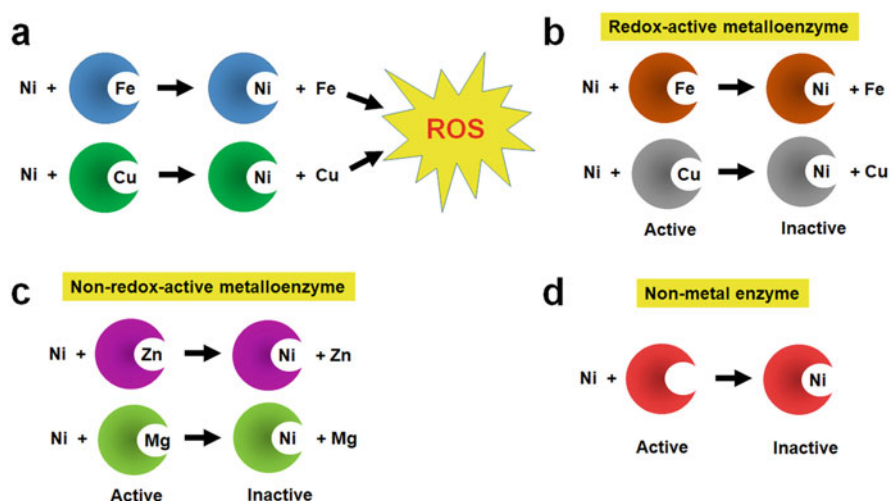


**Fig. 14.4** Mechanisms of nickel toxicity. (a) Substitution of nickel for a protein-bound redox-active metal ion with subsequent generation of ROS (reactive oxygen species). (b) Replacement of a redox-active metallocenter in an enzyme by nickel. (c) Substitution of a non-redox metal ion in an essential enzyme by nickel. (d) Other types of inactivation of an enzyme by nickel binding

its manganese- and iron-containing superoxide dismutases exhibited greater sensitivity towards nickel, consistent with formation of superoxide in nickel-stressed cells (Geslin et al. 2001). On the other hand, direct observations indicate that oxidative stress was not induced when treating cells with low concentrations of nickel that still inhibited growth (Kumar et al. 2017). Rather, these metal ions led to double-strand breaks in the DNA and blockage of the SOS repair pathways. These results are consistent with the known properties of free nickel ions that function poorly in generating reactive oxygen species compared to iron and copper (Valko et al. 2005). A plausible explanation for the connection between oxidative stress and nickel toxicosis is metal substitution, with the released iron and copper reacting with oxygen and leading to ROS with its consequent deleterious effects (Fig. 14.4a). Thus, nickel interaction with bacteria is unlike the situation with eukaryotes where the metal ion has been shown to directly cause oxidative stress with accompanying damage to DNA (Guo et al. 2019; Kasprzak and Salnikow 2007), alteration of the thiol/disulfide ratio (Randhawa et al. 2001), or enhanced lipid peroxidation (Niki et al. 2005; Paraszewicz et al. 2010).

Substitution of the relatively redox-stable nickel ion for a redox-active metal can inactivate a metalloenzyme, potentially leading to inhibition of cell metabolism (Fig. 14.4b). For example, nickel replaces the ferrous ion in taurine hydroxylase of *E. coli* by a slow-binding inhibition mechanism thus preventing its reactivity with oxygen (Kalliri et al. 2005); such inactivation of the enzyme would hinder growth of cells using taurine as the sole sulfur source. Similar inhibitory results are expected for other 2-oxoglutarate dependent oxygenases that play diverse roles in various bacteria (Herr and Hausinger 2018; Jia et al. 2017). Other examples of bacterial iron-containing enzymes inhibited by nickel include protocatechuate 3,4-dioxygenase and catechol 1,2-dioxygenase of *R. trifolii* (Chen et al. 1984, 1985), ATP:corrinoid adenosyltransferase of *Salmonella enterica* (Buan and Escalante-Semerena 2006), atrazine chlorohydrolase from a *Pseudomonas* species (Seffernick et al. 2002), and extracellular uricase from a strain of *Sphingobacterium thalophilum* (Ravichandran et al. 2015). Similarly, nickel inhibits some copper and cobalt enzymes such as nitrous oxide reductase of *Rhodobacter sphaeroides* (Sato et al. 1998) and cobaltochelataase of *Pseudomonas denitrificans* (Debussche et al. 1992). Depending on nutrient availability, the decreases in these enzyme activities could interfere with cell growth.

Nickel also can be a toxicant by substituting for a non-redox metal ion, such as zinc, magnesium, or calcium, in an essential enzyme (Fig. 14.4c). In these situations, the change in metal specificity may lead to subtle changes in protein structure or affect the coordination geometry of the metal. A structurally-characterized example of the latter situation was reported for glyoxalase I, which in some species is a zinc-dependent enzyme and in others requires nickel (Honek 2015). Whereas the native forms of the enzymes exhibit octahedral coordination of the appropriate metal using four protein ligands and two waters (replaced by substrate), an altered coordination geometry is observed for enzymes with the inactive metal bound (He et al. 2000). Partial or nearly complete inhibition was reported for a range of different non-redox metal enzymes such as the magnesium-dependent DNA polymerase I (Klenow

fragment) of *E. coli* (Snow et al. 1993), zinc- or calcium-dependent aminopeptidases from different species of *Streptomyces* (Arima et al. 2004), and a zinc-containing tripeptidase from *Pediococcus pentosaceus* (Simitsopoulou et al. 1997).

Finally, it is important to note that nickel can be inhibitory to non-metalloenzymes or by binding to sites distant from a metallocenter (Fig. 14.4d). A few such examples include cytosine 5-methyltransferase and uracil 5-methyltransferase of *E. coli* (Hurwitz et al. 1964), *N*-carbamoyl *D*-amino acid amidohydrolase of an *Agrobacterium* species (Louwrier and Knowles 1996), and mercuric ion reductase of *Azotobacter chroococcum* (Ghosh et al. 1999). The detailed inhibition mechanism generally has not been investigated, but the propensity of nickel to bind to histidine and cysteine side chains offers a reasonable hypothesis for enzyme inactivation. For example, *N*-carbamoyl *D*-amino acid amidohydrolase from *Agrobacterium radiobacter* contains a cluster of three histidine residues required for activity (Wang et al. 2001) and mercuric reductases possess a pair of cysteine residues that function in catalysis (Barkay et al. 2003); binding of nickel to these side chains could readily lead to loss of enzyme activity.

Although deleterious effects of nickel ions are proposed to include the production of reactive oxygen species and the inhibition of various types of microbial enzymes, the critical site of nickel toxicity in any particular microorganism is almost never known. Clearly, the basis of nickel stress in microbes requires further investigation.

### 14.3.3 Non-Efflux Mechanisms of Nickel Tolerance

Although nickel efflux is the most typical approach used by microorganisms for dealing with elevated concentrations of this metal ion, particular microbes handle nickel ion stress by avoidance, reduction, sequestration, compartmentalization, and several other mechanisms (Macomber and Hausinger 2011).

One straightforward technique to circumvent nickel stress is to simply avoid high concentrations of this toxic metal ion by responding to it as a chemotactic repellent, as demonstrated in *E. coli* (Englert et al. 2010). The mechanism of this response is not established, but it does not require nickel transport or the periplasmic NikA nickel-binding protein and it does utilize the Tar methyl-accepting chemotaxis protein.

When nickel ions cannot be avoided, some microbes minimize its toxicity by reducing the cation to the harmless elemental form. Precipitation of elemental nickel in the periplasm and on the cytoplasmic membrane was reported for *Pseudomonas aeruginosa* (Sar et al. 2001); the deposited metal was identified using energy-dispersive X-ray analysis. It is currently unclear whether this microorganism uses the reductive process as a means of nickel resistance. Reduction as a resistance mechanism was demonstrated for *Pseudomonas* sp. MBR that was grown aerobically with a wide range of electron donors (Zhan et al. 2012). Transmission electron microscopy identified nickel deposits in the periplasm and cytoplasmic membrane of this highly nickel-tolerant microorganism. Similarly, reduction of nickel ions to

elemental nickel in the cytoplasm was demonstrated using *Thiocapsa roseopersicina* and shown to be associated with nickel resistance (Zadvornyy et al. 2010). This microorganism produces dense nanoparticles of nickel metal in the cytoplasm when treated with nickel, but only in the presence of hydrogen gas. The purified *hyn*-encoded [NiFe] hydrogenase from these cells recapitulates the catalytic production of the reduced metal particles.

Another approach to overcome nickel stress is to reduce its concentration by sequestering it externally, in the periplasm, or within the cell. An external process is used by a nickel-resistant, sulfate-reducing strain of *Desulfotomaculum* that generates a soluble dark-brown nickel sulfide product (Fortin et al. 1994). External binding of nickel to anionic capsular polysaccharides is another way to potentially reduce the available concentration of this metal ion. The poly- $\gamma$ -glutamate capsule of *Bacillus licheniformis* and the cell wall of *Bacillus subtilis* are known to bind nickel; however, no studies have examined whether such binding confers nickel resistance to the cells (Beveridge and Murray 1976; McLean et al. 1990). Periplasmic sequestration of nickel is an option suggested for an isolate of *P. putida* S4 (Tripathi and Srivastava 2006). When these cells were exposed to nickel they produced an 18-kDa protein that may tightly bind the metal; however, detailed characterization of nickel binding by the peptide was not reported. Similarly, nickel sequestration in the periplasm was proposed for *Cupriavidus pauculus* KPS 201 that had been isolated from a nickel-rich ultramafic ecosystem; however, in this case two larger proteins of 74- and 66-kDa were suggested to be involved in binding the metal (Pal and Paul 2010). Again, no analysis of the proteins' interactions with nickel was reported. Cellular sequestration of nickel ions by an 82-residue peptide (SCO4226) in *S. coelicolor* was proposed (Lu et al. 2014), though clear evidence for participation in nickel resistance has not appeared. The structure of the holoprotein reveals a homodimer with ferredoxin-like folds containing four weakly bound ( $K_d$  of 10  $\mu$ M) nickel per dimer at distinct surface sites. Other cytoplasmic proteins used to sequester nickel are Hpn-1 and Hpn-2 (Sect. 14.4.12), which are abundant proteins of *H. pylori* and related microorganisms. These proteins are characterized for their nickel-binding abilities and are known to confer nickel resistance to these cells (Ge et al. 2006a; Seshadri et al. 2007; Vinella et al. 2015).

An alternative version of the sequestration mechanism is compartmentalization. An illustration of this approach involves nickel-resistant strains of *Saccharomyces cerevisiae* that place the metal into a vacuole as a complex with the amino acid histidine (Joho et al. 1990, 1992; Nishimura et al. 1998; Pearce and Sherman 1999). Such import of nickel into a subcellular organelle is not available to bacteria.

A poorly characterized system is operant in *B. vietnamiensis* PR1<sub>301</sub> that exhibits greater resistance to nickel when grown at pH 5 than at pH 7 (Van Nostrand et al. 2008). Two-dimensional gel electrophoresis coupled with mass spectrometric methods identified several proteins that are produced at greater abundance using the nickel-resistant conditions; surprisingly, these proteins are associated with cell shape and membrane composition. Fatty acid methyl ester analysis revealed a change in membrane structure for cells capable of growth at higher nickel



concentrations. The precise mechanism of resistance in this microorganism remains to be defined.

A genome-wide functional screening approach identified seven genes associated with nickel resistance in *Acidiphilium* sp. MP, a microbe isolated from the metal-contaminated Rio Tinto river in Spain (San Martin-Uriz et al. 2014). Two genes (*hslVU*) encode an ATP-dependent protease that, when heterologously expressed, confer nickel resistance to *E. coli* by an unknown mechanism. The other genes encode enzymes involved in lipopolysaccharide or branched chain amino acid biosynthesis; in these cases, it is unclear whether these molecules are directly involved in nickel resistance.

A proteomic analysis comparing the effects of 2 mM nickel treatment on *P. putida* UW4 revealed significant increases in 82 proteins and significant decreases of 81 proteins (Cheng et al. 2009). The proteins amplified during nickel stress include those for general stress adaptation, oxidative stress, and heavy metal efflux.

A role for superoxide dismutase in nickel resistance was suggested from studies using *E. coli* (Geslin et al. 2001). The nickel resistance of individual *sodA* or *sodB* mutants, encoding the manganese- or iron-dependent superoxide dismutase enzymes, was comparable to the wild type cells; however, the double mutant which lacked both activities exhibited increased sensitivity to this metal. These results suggest that excess levels of cellular nickel can promote the generation of ROS with deleterious consequences, and that superoxide dismutase alleviates these issues.

In summary, a wide range of mechanisms beyond the use of nickel efflux systems are likely to play a role in allowing microorganisms to tolerate this metal ion. Unfortunately, the relevance of many of these systems to nickel stress is not convincingly demonstrated and much work on alternative resistance mechanisms remains to be done.

## 14.4 Nickel Utilization by Microorganisms

In the past decade, nickel-containing enzymes have been the subject of several general review articles (Alfano and Cavazza 2020; Boer et al. 2014; Cheng et al. 2016; Kaluarachchi et al. 2010; Maroney and Ciurli 2014) and a book (Zamble et al. 2017). Here, the biochemical reactions of these enzymes are described (Fig. 14.5), their structures are highlighted (Fig. 14.6), and in many cases the pathways for biosynthesis of their metalcenters are summarized. The order of presentation is approximately in order of the complexity of their active site metalcenters, with glyoxalase I (Glo1), acireductone dioxygenase (ARD), quercetin 2,4-dioxygenase (QueD), and superoxide dismutase (SOD) each containing mononuclear nickel centers, urease using a dinuclear nickel site, [NiFe] hydrogenases possessing a heterodinuclear center along with auxiliary [FeS] clusters, carbon monoxide dehydrogenase (CODH) possessing an inorganic [Ni-4Fe-4S] complex plus other [FeS] clusters, acetyl-coenzyme A (CoA) synthase/decarbonylase (ACS)

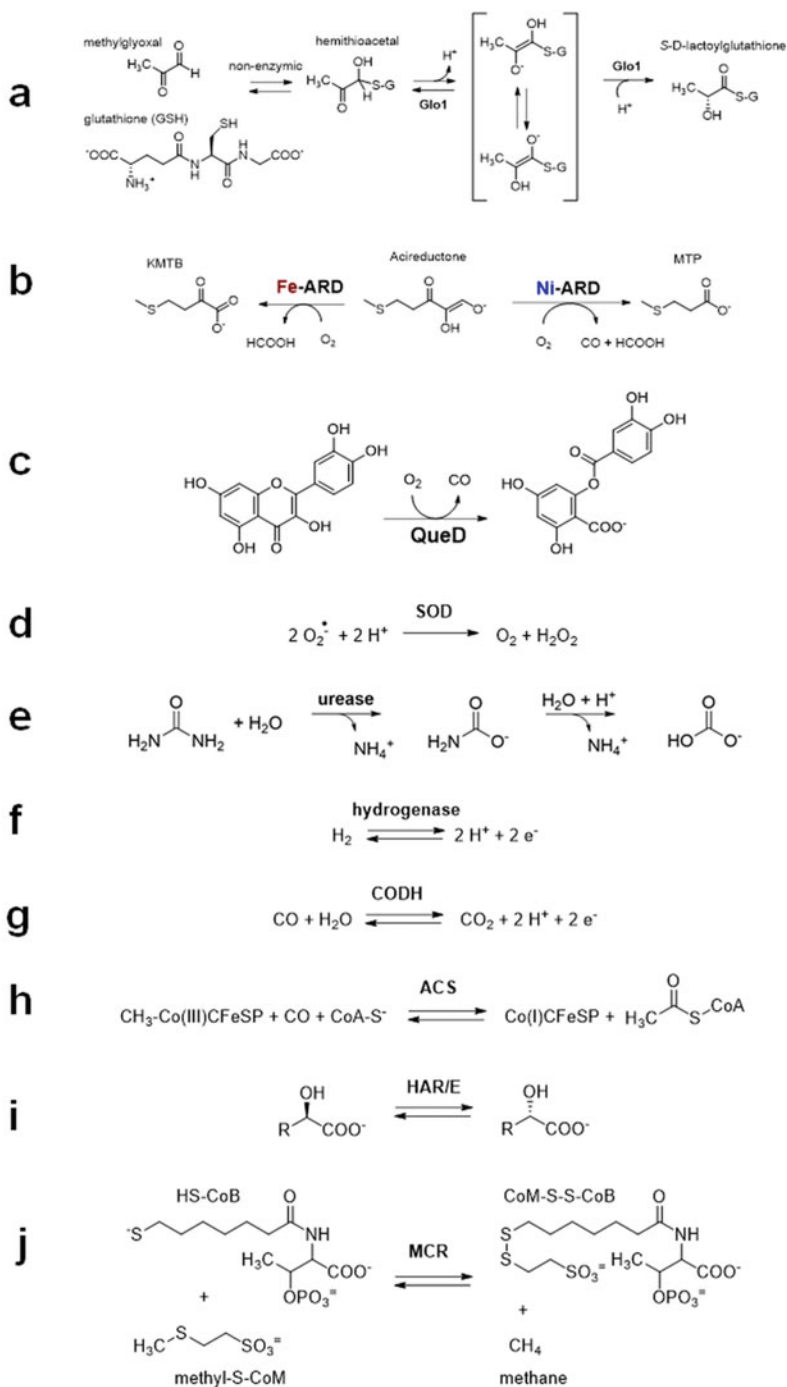


**Fig. 14.5** Reactions of nickel-dependent enzymes. (a) Glyoxalase (Glo1). (b) Two distinct acireductone dioxygenase (ARD) reactions depending on whether iron or nickel is bound. (c)

having both the CODH components and a [4Fe-4S]-Ni-Ni cluster, and finally 2-hydroxyacid racemases/epimerases (HAR/E) and methyl-*S*-coenzyme M reductase (MCR) possessing organometallic cofactors [the nickel-pincer nucleotide (NPN) and nickel-tetrapyrrole cofactor (F430), respectively] with nickel coordinated to an organic framework. In addition, other examples of possible nickel-containing enzymes are mentioned. Finally, cellular nickel storage is briefly addressed.

### 14.4.1 Glyoxalase I (*Glo1*)

Methylglyoxal and other 2-ketoaldehydes are naturally produced compounds, but they are toxic due to their electrophilic reactivity with biological molecules leading to advanced glycation end-products. The glyoxalase enzyme system converts these molecules into D-hydroxyacids in a three-step sequence: the substrate initially reacts reversibly and non-enzymatically with glutathione ( $\gamma$ -glutamyl-L-cysteinylglycine, GSH) or other intracellular thiol, glyoxalase I (abbreviated Glo1 here, but sometimes referred to as GlxI) isomerizes the hemithioacetal intermediate to form the corresponding thioester, such a *S*-D-lactoylglutathione, via a *cis*-enediolate intermediate (Fig. 14.5a), and glyoxalase II (*Glo2*) catalyzes its hydrolysis to obtain the product and regenerate the thiol (Honek 2015). Of interest for this chapter, Glo1 is a nickel-containing enzyme in some microorganisms (Honek 2017).

Glo1 from humans, yeast, and some bacteria is a zinc-dependent enzyme (Honek 2015, 2017), thus it came as a surprise to find the zinc-bound *E. coli* protein is inactive while the nickel-bound enzyme exhibits maximal activity (Clugston et al. 1998). Structural studies of *E. coli* Glo1 revealed a homodimer with its two active sites positioned at the interface of the subunits (Fig. 14.6a), closely resembling the structure of the human enzyme (He et al. 2000). Each nickel of *E. coli* Glo1 coordinates His5 and Glu56 from one subunit, His74' and Glu122' from the other subunit, and two water molecules, mimicking the octahedral zinc site of the human enzyme. The lack of activity for zinc-bound *E. coli* Glo1 arises from a switch to trigonal bipyramidal geometry for the metal, as shown by the crystal structure and XAS analysis (Davidson et al. 2000, 2001; He et al. 2000). These findings are consistent with the need for substrate to coordinate the metal binding site in a bidentate manner for the reaction to occur. Several other bacterial Glo1 enzymes utilize nickel including those from the important pathogens *Y. pestis*, *P. aeruginosa*, and *Neisseria meningitidis* (Sukdeo et al. 2004), the solvent-producing bacterium *Clostridium acetobutylicum* (Suttisansanee et al. 2011), and the soil-dwelling

---

**Fig. 14.5** (continued) Quercetin 2,4-dioxygenase (QueD). (d) Superoxide dismutase (SOD). (e) Urease. (f) Hydrogenase. (g) Carbon monoxide dehydrogenase (CODH). (h) Acetyl-CoA synthase/decarbonylase (ACS). (i) 2-Hydroxyacid racemase/epimerase (HAR/E). (j) Methyl coenzyme M reductase (MCR)

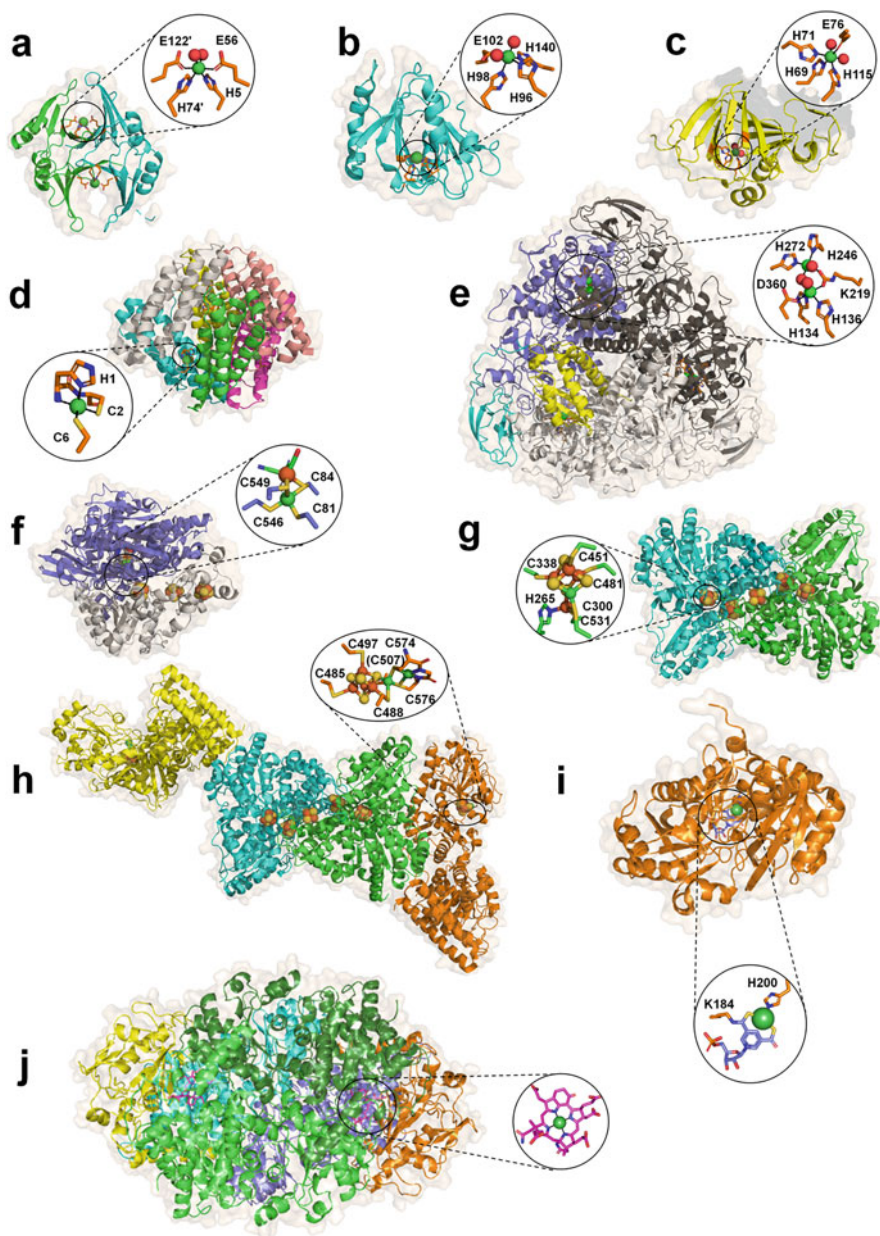


**Fig. 14.6** Structures of nickel-dependent enzymes and expanded views of their active sites. **(a)** *E. coli* glyoxalase homodimer (PDB ID 1f9z) showing a bridging nickel site bound to four side chains and two waters. **(b)** Acireductone dioxygenase of *K. oxytoca* monomer (PDB ID 1zrr) showing the nickel atom bound to four side chains and two waters. **(c)** Quercetin 2,4-dioxygenase from *Streptomyces* sp. strain FLA (PDB ID 5flh) with nickel bound to four side chains and two waters. **(d)** Homohexameric superoxide dismutase of *Streptomyces coelicolor* (PDB ID 1t6u) with nickel bound to the N-terminal amine, an amide, and three side chains. **(e)** Urease from *Klebsiella*

actinomycete *S. coelicolor* (Suttisansanee and Honek 2019). The structure of the *C. acetobutylicum* enzyme demonstrated the conformational flexibility of the enzyme, with domain swapping allowing for metal coordination by side chains that all derive from the same subunit (Suttisansanee et al. 2011). *S. coelicolor* Glo1 is of special interest because it uses mycothiol, 1-D-myo-inositol-2-(*N*-acetyl-L-cysteinyl)amido-2-deoxy- $\alpha$ -D-glucopyranoside, instead of glutathione in the reaction. An alternate thiol known as trypanothione, *N*<sup>1</sup>,*N*<sup>8</sup>-bis(L- $\gamma$ -glutamyl-L-hemicysteinyll-L-glycyl)spermidine, is used by the enzymes from the eukaryotic protozoa *Leishmania major*, *Leishmania donovani*, and *Trypanosoma cruzi*, which also depend on nickel for activity (Ariza et al. 2006; Greig et al. 2006; Padmanabhan et al. 2005; Vickers et al. 2004). The mechanism by which nickel is specifically incorporated into Glo1 is unknown, and no auxiliary proteins have been shown to facilitate its biosynthesis.

#### 14.4.2 Acireductone Dioxygenase (ARD)

ARD catalyzes a key step in the methionine salvage cycle by converting 1,2-dihydroxy-3-keto-5-(thiomethyl)pent-1-ene (acireductone) to formate and 2-keto-4-methylthiobutyrate (KMTB) (Fig. 14.5b). KMTB is subsequently transaminated to form methionine, an amino acid and a precursor of *S*-adenosylmethionine (AdoMet). Among several cellular metabolic transformations that utilize AdoMet, polyamine biosynthesis produces methylthioadenosine (MTA). MTA is transformed by a series of reactions to regenerate acireductone, thus conserving the valuable sulfur atom in these metabolites. In 1993, a bacterial enzyme was purified that uses acireductone as substrate, but rather than producing KMTB it generates carbon monoxide, formate, and 3-methylthiopropionate (MTP) (Wray and

---

**Fig. 14.6** (continued) aerogenes (PDB ID 1fwj) with one copy of each of three types of subunits colored and the other two copies shown in light and dark gray (see text for a description of non-(UreABC)<sub>3</sub> aggregation states) along with its dinuclear nickel site, coordinating residues, and three waters. (f) Heterodimeric [NiFe] hydrogenase from *Desulfovibrio vulgaris* Miyazaki F (PDB ID 4u9h) with its [NiFe] cluster in the H<sub>2</sub>-reduced state, four coordinating side chains, three diatomic iron ligands, and a bridging hydride atom. (g) *Rhodospirillum rubrum* carbon monoxide dehydrogenase homodimer (PDB ID 1jqk) containing an exposed [4Fe-4S] D-cluster bridging the subunits, a [4Fe-4S] B-cluster within each subunit, and the two [1Ni-4Fe-4S] C-clusters. (h) The  $\alpha_2\beta_2$  acetyl-CoA synthase/decarbonylase from *Clostridium autoethanogenum* (PDB ID 6ytt) with a central CODH component shown as in (g) and the terminal ACS components containing the [4Fe-4S]-Ni-Ni A-cluster. (i) Monomeric lactate racemase from *Lactobacillus plantarum* (PDB ID 5huq) as an example of a 2-hydroxyacid racemase/epimerase with its covalently tethered nickel-pincer nucleotide cofactor. (j) The ( $\alpha\beta\gamma$ )<sub>2</sub> methyl coenzyme M reductase from *Methanothermobacter marburgensis* (PDB ID 1mro) with its coenzyme F430 cofactor. For each protein, the different subunits are shown in cartoon view in different colors and with semi-transparent surfaces. Key residues and diatomic ligands are shown as sticks. Spheres are shown for nickel (green), water molecules (red), iron (brown), and inorganic sulfur (yellow)

Abeles 1993). Six years later this enzyme from *K. oxytoca* was shown to be a metal-substituted ARD (Dai et al. 1999). Thus, ARD catalyzes two distinct reactions depending on the identity of the metal that is bound: it produces KMTB when possessing iron and generates MTP when coordinating nickel. The purpose of the off-cycle pathway is unknown, but the observed partial nickel occupancy of the protein from wild-type cells suggests this reaction is physiologically relevant (Deshpande et al. 2017).

The nickel in *K. oxytoca* ARD, as probed by XAS analysis, is octahedral with O/N ligands that include 3–4 His residues (Al-Mjeni et al. 2002). The solution structure of nickel-ARD from this microorganism was obtained by NMR spectroscopy using special methods to overcome issues related to the metal ion paramagnetism (Pochapsky et al. 2002, 2008). Nickel coordinates His96, His98, Glu102, and His140, along with two water molecules (Fig. 14.6b). A crystal structure for cadmium-bound ARD from *Bacillus anthracis* indicated an essentially identical structure. NMR, XAS, and mutagenesis studies of *K. oxytoca* ARD revealed that iron binds to the same site of the protein as nickel (Chai et al. 2008; Ju et al. 2006), but ferrous ion resulted in subtle structural changes in the C-terminal region, a loop, and two helices so the two isoforms can be chromatographically separated. An extensive series of biomimetic studies have investigated the distinct chemistries in models of the active site with bound nickel versus iron [reviewed in (Deshpande et al. 2017)]. In all active forms, substrate displaces two waters from the six-coordinate metal and binds with bidentate coordination. Importantly, this binding likely results in a 6-membered ring for nickel and a 5-membered ring for iron. Subsequent reactions with oxygen generate distinct intermediates that decompose differentially to the observed products. Nothing is known about how the cell controls the metal specificity of the enzyme; e.g., no accessory proteins are known to be required for metal delivery.

### 14.4.3 Quercetin 2,4-Dioxygenase (QueD)

Many soil fungi and bacteria decompose flavonoid plant metabolites such as quercetin (3,5,7,3',4'-pentahydroxyflavone) via oxidative metabolism that initiates by the action of quercetin 2,4-dioxygenase or quercetinase, releasing carbon monoxide and forming 2-protocatechuoylphloroglucinolcarboxylic acid (Fig. 14.5c) (QueD). The fungal enzyme uses copper as a cofactor, whereas bacterial forms of the protein are more promiscuous in their metal ion requirements (Fetzner 2012). For example, *Bacillus subtilis* quercetinase purifies with stoichiometric manganese, but is also active with cobalt and copper (Schaab et al. 2006). Of particular interest here is QueD from *Streptomyces* sp. FLA. This dioxygenase contains nickel when isolated from the wild-type microorganism and is most active using this metal ion (Nianios et al. 2015). *Streptomyces* QueD is dimeric, with each subunit exhibiting the typical 6-stranded  $\beta$ -barrel cupin fold (Fig. 14.6c) (Jeoung et al. 2017). Nickel binds to three histidine and one glutamic acid, with additional coordination by two water

molecules. The C3 hydroxyl group of the substrate displaces one of the waters and binds to the metal ion. The second water molecule is lost upon binding of oxygen which exhibits side-on coordination (Jeoung et al. 2017). No information is available regarding how the protein specifically binds nickel.

#### 14.4.4 Superoxide Dismutase (SOD)

The superoxide anion,  $O_2^-$ , is both a reactive oxygen species and a cellular signaling compound (Wang et al. 2018). To limit the internal levels of this compound, cells utilize one or more superoxide dismutases (Fig. 14.5d) or a superoxide reductase (an enzyme that reduces this molecule to  $H_2O_2$  and is not discussed further) (Abreu and Cabelli 2010; Sheng et al. 2014). Biology has evolved three types of SODs with independent sequences, structures, and metalcenters; i.e., the copper/zinc SODs, the manganese- or iron-containing SODs, and the nickel-containing SODs. This section describes the discovery, properties, structure, and activation of the latter enzymes (Campeciño and Maroney 2017).

In 1996, the first examples of nickel-containing SODs were purified from *Streptomyces seoulensis* IMSNU-1 and *S. coelicolor* ATCC 10147 (Kim et al. 1996; Youn et al. 1996a). These enzymes possess near stoichiometric amounts of nickel (0.74 equivalents per 13.4-kDa subunit) and, unlike Glo1 or ARD, exhibit distinct spectral properties associated with their metalcenters. For example, the ultraviolet-visible (UV-vis) spectrum of nickel SOD possesses an absorption maximum near 380 nm, a broad peak near 530 nm, and the typical protein-derived electronic transitions. More remarkable, the nickel-containing SOD exhibits an electron paramagnetic resonance (EPR) spectrum with  $g$  values of 2.304, 2.248, and 2.012, where the latter component is split into a triplet (Youn et al. 1996a). This spectrum was attributed to a low spin ( $S = \frac{1}{2}$ )  $Ni^{3+}$  with an axial N-ligand leading to hyperfine splitting of the high-field feature. *S. griseus* possesses both a nickel-containing SOD, with properties essentially identical to that just described (0.89 Ni/13.0-kDa subunit, analogous UV-vis and EPR spectra), and an iron-containing SOD (Youn et al. 1996b). *S. coelicolor* also possesses both types of SOD, and their synthesis was found to be regulated by nickel (Kim et al. 1996). Analysis of a variety of *Streptomyces* isolates from clinical and soil samples demonstrates the universality of nickel-dependent SODs in this genus, with many strains also having iron-dependent activity (Leclere et al. 1999). Furthermore, a phylogenetic analysis demonstrates that *sodN*, the gene encoding these enzymes, is distributed widely in actinomycetes and cyanobacteria, along with being present in some gammaproteobacteria, bacteroidetes, planctomycetes, deltaproteobacteria, and even two marine eukaryotes (Dupont et al. 2008). Curiously, a *Mycobacterium* sp. has two copies of *sodN*, though it is unknown if either is functional.

Analysis of *S. coelicolor* *sodN* indicates ninefold enhanced transcription in the presence of nickel and shows that it encodes a 14-residue-extended precursor protein lacking activity (Kim et al. 1998b). Expression of *sodN* in *E. coli* provides only the

longer version of the protein with no activity, whereas expression of a truncated gene yields small levels of SOD activity (Kim et al. 1998b). Transcription of the gene encoding the iron-containing SOD, *sodF*, also is regulated at the transcriptional level by nickel, but in this case the transcript levels are reduced by the presence of this metal (Chung et al. 1999; Kim et al. 1998a). The repression of *sodF* in *S. griseus* is accomplished by a complex of SmR, a nickel sensor, and SmQ (Sect. 14.2.1.3) (Kim et al. 2003b). In addition, the nickel-bound sensor Nur acts as a repressor of *sodF* and an activator of *sodN* in *S. coelicolor* (Sect. 14.2.1.4) (Ahn et al. 2006; An et al. 2009).

Initial structural studies of the nickel-containing SOD focused on XAS of the *S. seoulensis* enzyme, revealing a five-coordinate metal site with about three sulfur donors, one nitrogen donor, and a nitrogen or oxygen donor (Choudhury et al. 1999). Reduction of nickel by dithionite results in loss of a nitrogen or oxygen donor, suggesting ligand dissociation. EPR spectra for the recombinant protein purified from *E. coli* with truncated *S. coelicolor* *sodN* has the same appearance as the wild-type enzyme, whereas the H1Q variant protein spectrum is altered; this result is consistent with His1 serving as a nickel ligand (Bryngelson et al. 2004). Studies comparing the XAS and magnetic circular dichroism spectra of the wild-type protein with variants involving Cys2 and Cys6 confirmed these residues also coordinate the metal (Johnson et al. 2010; Ryan et al. 2010). A detailed understanding of the nickel SOD metallocenter and the overall protein architecture is derived from crystal structures for the *S. seoulensis* (Wuerges et al. 2004) and *S. coelicolor* (Barondeau et al. 2004) enzymes (Fig. 14.6d). The proteins from both sources reveal nearly identical hexamers of 4-helix bundle monomers, as expected for the almost identical sequences. Nickel binds to what has been termed a “nickel-hook motif”, which requires protein truncation. Planar coordination of the metal is provided via the N-terminal amine, the backbone amide of the second residue, and the side chains of Cys2 and Cys6. This coordination environment is thought to lower the reduction potential of the metal by over 1 V, allowing it to be capable of catalyzing the dismutation reaction. The oxidized form of the protein also includes His1 as an axial ligand, but this ligand dissociates upon reduction (Barondeau et al. 2004; Wuerges et al. 2004). Several other nearby residues help to stabilize these interactions, including Pro5 that is present in *cis* configuration, but the region is unfolded in the absence of the metal.

Genomic sequence analyses were used to identify a gene adjacent to *sodN* in *Prochlorococcus marinus* MIT9313 that was hypothesized, then shown, to encode a protease specific for the N-terminus of SOD, as needed for enzyme activation (Eitinger 2004). The product of *sodX* is an SOD-specific peptidase that allows for generation of active SOD activity in *E. coli* cells co-expressing the *P. marinus* *sodN*. Bioinformatics studies have shown that most, but not all, *sodN* genes are adjacent to *sodX* (Dupont et al. 2008). Another protein, CbiXhp, had been proposed to function during activation of nickel-containing SOD in *S. seoulensis* (Kim et al. 2003a). This protein, named on the basis of its sequence similarity to cobaltochelatease (CbiX) of *Bacillus megaterium*, was purified by its ability to bind to nickel-nitritoltri-acetic acid resin using a histidine-rich sequence at its C-terminus. Co-expression of the



*S. seoulensis* genes encoding CbiXhp and SodN in *Streptococcus lividans* leads to greater levels of SOD activity than for expression of only *sodN*. It is possible this protein functions in nickel storage or as a nickel metallochaperone; however, no further analysis of *S. seoulensis* CbiXhp has been reported and homologs to this gene are not associated with *sodN* of other microorganisms. Thus, it is likely the enhanced SOD activity noted in those studies was fortuitous.

### 14.4.5 Urease

Urease and its substrate urea hold a special place in the history of science. The Dutch botanist Herman Boerhaave first isolated urea from urine in ~1727, although the French chemist Hilaire Marin Rouelle is often credited with the discovery of this substance in 1773 (Kurzer and Sanderson 1956). The name urea was coined by Antoine Francis comte de Fourcroy and Louis Vauquelin, who studied the compound in 1799 (Fourcroy and Vauguelin 1799). Urea is the first organic molecule ever synthesized from inorganic materials, an accomplishment of the German chemist Friedrich Wöhler in 1828 (Wöhler 1828). Others had shown that urea in urine transforms into carbonate and ammonia, but Louis Pasteur reported in 1860 that a living organism is responsible for this alkaline fermentation (Pasteur 1860). Shortly thereafter Philippe van Tieghem isolated a bacterium, later called *Micrococcus ureae*, that catalyzes this decomposition reaction (van Tieghem 1984), and in 1890 Pierre Miquel described several additional “ureolytic” microorganisms and termed the transforming agent “urease” (Miquel 1890). The next few decades included intense discussions of what physical components confer enzyme activities. Key to answering this question was the discovery by Takeuchi in 1909 that soybean, among other plants, possesses large amounts of urease activity (Takeuchi 1909). Working with seeds of the jack bean plant in 1929, James B. Sumner purified urease by crystallization, the first enzyme ever crystallized, hence demonstrating that enzymes are proteins (Sumner 1926). Nearly 50 years later, Bert Zerner and colleagues showed that jack bean urease contains nickel (Dixon et al. 1975), therefore becoming the first identified nickel-dependent enzyme. Bacterial ureases also contain nickel, as first demonstrated for the enzyme from *Arthrobacter oxydans* (Schneider and Kaltwasser 1984). The following paragraphs describe the reaction, distribution, structures, and biosynthesis of microbial ureases.

#### 14.4.5.1 Urease Functional Significance

Urea is an important metabolite in the global nitrogen cycle and its hydrolysis by urease (Fig. 14.5e) has far-reaching consequences. The substrate urea is produced industrially at a vast scale (>200 million metric tons per year) for use as a nitrogen-based fertilizer. When such fertilizers are released into the environment, urea hydrolysis by plant and microbial ureases produces ammonium ions for use by

crops and raises the pH due to consumption of protons. Rapid metabolism of fertilizer urea may damage agricultural crops due to ammonia toxicity or alkalinity, and these conditions volatilize the ammonia causing loss of this valuable nitrogen source (Mobley and Hausinger 1989). Several biological sources of urea exist, with the most prominent being the arginase-catalyzed hydrolysis of arginine. Arginase is found in many microorganisms and plays an essential role in mammals, where it functions to detoxify ammonia via the urea cycle that produces the urea found in urine. Urea metabolism by microorganisms can have detrimental medical consequences (Burne and Chen 2000; McLean et al. 1988; Mobley and Hausinger 1989; Mobley et al. 1995b). Ureolytic pathogens of the urinary tract are responsible for a substantial fraction (10–15%) of urinary stones due to high pH-induced precipitation of struvite and apatite salts (Flannigan et al. 2014; Griffith et al. 1976). The same process accounts for encrustation of catheters (Norsworthy and Pearson 2017). Infections of the urinary tract also can lead to pyelonephritis, the acute inflammation of the kidney and its pelvis (Nielubowicz and Mobley 2010). Peptic ulcers, gastritis, and even stomach cancers are associated with colonization of the stomach lining by *H. pylori*, a pathogen containing very high levels of urease (Atherton 2006; Covacci et al. 1999; Kusters et al. 2006; Wroblewski et al. 2010). Enzymatic metabolism of urea diffusing into the stomach from the bloodstream consumes protons immediately around the microorganism, thus acting as a buffer against the low pH environment (Sachs et al. 2002). Also of interest, high concentrations of ammonia produced by microbial metabolism of urea is implicated in cases of ammonia encephalopathy, hepatic encephalopathy, and hepatic coma (Mobley and Hausinger 1989; Mobley et al. 1995b; Rai et al. 2015).

Microbial urease activity is widespread in the environment, with the enzyme distributed in selected bacteria, archaea, yeasts, filamentous fungi, and algae (Mobley and Hausinger 1989). Its regulation varies with the source (Collins and D’Orazio 1993). For example, many microorganisms increase urease production during times of nitrogen starvation so as to utilize urea as a nitrogen source. Some strains that infect the urinary tract induce urease synthesis in the presence of elevated concentrations of urea. Furthermore, still other species exhibit generally constant levels of the enzyme. Urease typically is localized in the cytoplasm; however, this protein is quite stable and maintains its activity when released into the environment upon cell death, leading to the incorrect notion that urease is secreted by microbes (Marcus and Scott 2001).

#### 14.4.5.2 Urease Structure

The structure of urease exhibits one of four architectures, depending on the source. Most bacterial forms of the enzyme contain three types of subunits (UreA, UreB, and UreC), each present in three copies, i.e. (UreABC)<sub>3</sub>, with the entire structure containing three dinuclear nickel active sites as first elucidated for urease from *Klebsiella aerogenes* (Fig. 14.6e) (Jabri et al. 1995; Pearson et al. 1997). The extensively studied enzyme from *Sporosarcina* (formerly *Bacillus*) *pasteurii* has

an analogous structure (Benini et al. 1999). *Yersinia enterocolitica* urease also has three similar types of subunits, but structures obtained by crystallography (unpublished) and cryo-electron microscopy (Righetto et al. 2020) have shown these subunits assemble into a [(UreABC)<sub>3</sub>]<sub>4</sub> supermolecular spherical structure containing 12 active sites. Similarly, crystallography and cryo-electron microscopy studies indicate a dodecamer spherical structure is present in *H. pylori* and other *Helicobacter* species (Cunha et al. 2021; Ha et al. 2001); however, in these cases only two types of subunits are present with the smaller subunit (UreA) corresponding to a fusion of UreA plus UreB of most bacteria, and the larger subunit (UreB) corresponding to UreC in other genera. This [(UreAB)<sub>3</sub>]<sub>4</sub> situation also occurs for a dinuclear iron-containing urease from *Helicobacter mustelae* (Carter et al. 2011). In eukaryotes, a single type of subunit contains sequences homologous to each of the bacterial subunits. Three copies of this fused subunit assemble into a trimer, and two trimers stack together back-to-back forming a hexamer with six active dinuclear nickel active sites. Although no microbial example of such a structure has been reported, the architecture of fungal ureases probably resembles that of the jack bean enzyme (Balasubramanian and Ponnuraj 2010). The active sites of all ureases are identical, with their two nickel metal ions bridged by a carbamylated lysine residue, two histidine residues binding one of those nickel ions, and two histidine residues plus an aspartic acid residue coordinated to the second nickel ion. Each metal ion has a terminally-bound water and a third water bridges the two nickel ions, thus providing 5-coordinate and 6-coordinate geometries for the dinuclear site. The reaction mechanism of the enzyme metallocenter was recently reviewed (Mazzei et al. 2020).

### 14.4.5.3 Urease Maturation

The bacterial genes encoding the urease subunits typically are clustered with genes encoding accessory proteins that are required for urease activation (Mobley et al. 1995b). For example, *ureDABCEFG* of *K. aerogenes* encodes the three-subunit urease and four proteins (UreD, UreE, UreF, and UreG) needed to obtain a mature enzyme (Lee et al. 1992; Mulrooney and Hausinger 1990). Similarly, *ureABIEFGH* of *H. pylori* codes for the two-subunit enzyme, a proton-gated urea channel (UreI) (Weeks et al. 2000), and the same four maturation components (note: *Helicobacter* UreH is homologous to UreD of other bacteria) (Cussac et al. 1992; Labigne et al. 1991). In other microorganisms, the order of these genes may vary and additional genes may interrupt or flank the cluster such as those encoding ABC-type nickel transporters (Sect. 14.2.2.2) in *A. pleuropneumoniae* (Bossè et al. 2001) and *S. salivarius* 57.1 (Chen and Burne 2003) or encoding nickel permeases (Sect. 14.2.2.3) such as UreH and UreJ in *Bacillus* TB-90 (Maeda et al. 1994) and *B. bronchiseptica* (McMillan et al. 1998), respectively. In addition, the products of non-contiguous genes may facilitate urease activation in some species by assisting in nickel uptake, such as NixA in *H. pylori* (Wolfram and Bauerfeind 2002) (Sect. 14.2.2.3), or nickel delivery, such as HypA and HypB in the same organism (Olson

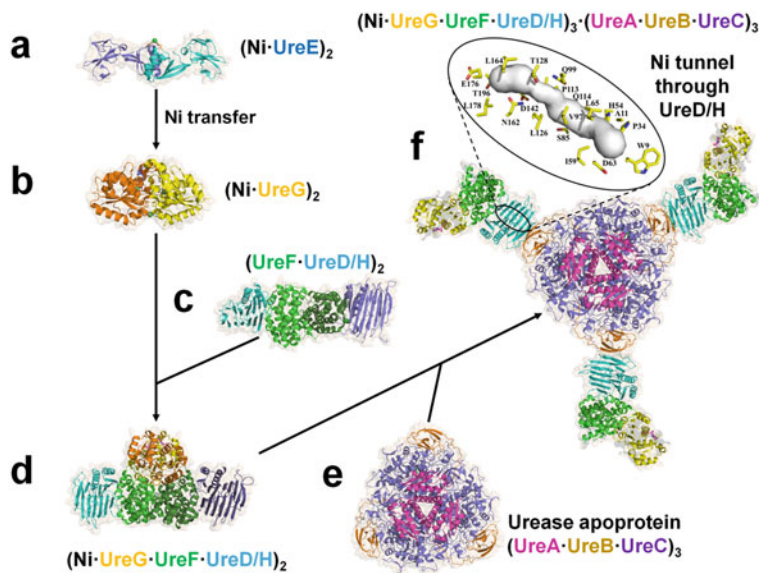


**Fig. 14.7** Urease maturation pathway. (a) UreE is a homodimeric nickel metallochaperone, as shown for the protein from *Sporosarcina pasteurii* (PDB ID 413k). (b) UreE forms complexes with and transfers nickel to its cognate UreG, as depicted for the homodimeric UreG from *Klebsiella pneumoniae* with bound nickel and GMPNP (PDB ID 5xkt). (c) UreG binds to a complex of UreF and UreD/H, as illustrated for the  $(\text{UreF}\cdot\text{UreD})_2$  complex of *Helicobacter pylori* (PDB ID 3sf5). (d) The resulting complex of three accessory proteins is illustrated by the GDP-bound  $(\text{UreG}\cdot\text{UreF}\cdot\text{UreD})_2$  from *H. pylori* (PDB ID 4hi0). (e) The accessory proteins bind to urease apoprotein, shown for  $(\text{UreA}\cdot\text{UreB}\cdot\text{UreC})_3$  of *Klebsiella aerogenes* (PDB ID 1kra). (f) A model of the resulting complex has  $(\text{UreG}\cdot\text{UreF}\cdot\text{UreD}/\text{H})$  bound via the UreD/H component to UreB of the urease apoprotein. GTP hydrolysis at UreG is coupled to release of nickel from that component, with the metal traversing a molecular tunnel through UreF and UreD (see inset) to be delivered to the nascent active site in UreC. Proteins are depicted in distinct colors using cartoon mode with semi-transparent surfaces, nickel atoms are shown as green spheres, and selected side chains along with nucleotides are indicated by sticks

et al. 2001). The biosynthesis of active urease almost universally requires the participation of UreD/H (two designations for the same protein), UreE, UreF, and UreG (Farrugia et al. 2013b; Nim and Wong 2019). One dramatic exception to this statement is urease of *B. subtilis* which possesses three types of subunits closely related to those of other bacterial ureases yet lacks genes related to the four urease maturation genes (Kim et al. 2005).

The urease maturation pathway (Fig. 14.7) begins with the metallochaperone or metal-delivery protein UreE. This protein from *Klebsiella aerogenes* possesses a carboxyl terminal His-rich sequence (10 of the last 15 residues) that binds multiple nickel ions (5–6 nickel per dimer,  $K_d \sim 10 \mu\text{M}$ ) (Grossoehme et al. 2007; Lee et al. 1993). By inserting a stop codon into the corresponding gene, one obtains a truncated protein that lacks the His-rich region yet it still functions in urease

activation and binds ~2 nickel ions per dimer (Colpas et al. 1998, 1999; Colpas and Hausinger 2000). The His-rich region is not a universal component of UreE as demonstrated by the *H. pylori* protein (Musiani et al. 2004). Crystal structures of UreE (Fig. 14.7a) are known for the proteins from *K. aerogenes* (Song et al. 2001), *S. pasteurii* (Remaut et al. 2001; Zambelli et al. 2013), and *H. pylori* (Banaszak et al. 2012; Shi et al. 2010). In all cases, the protein exists as a homodimer with each subunit possessing a metal-binding domain and a separate domain that is disposable for urease maturation (Mulrooney et al. 2005). The essential nickel-binding site is located at the interface of the UreE subunits (Colpas et al. 1999; Colpas and Hausinger 2000) where it is bound by complementary histidine residues and additional ligands in a disordered region near the carboxyl terminus (Banaszak et al. 2012; Zambelli et al. 2013). Secondary metal-binding sites may “feed” the metal into the essential UreE interfacial site for subsequent transfer to urease (Colpas et al. 1999; Grosseohme et al. 2007; Lee et al. 1993). In *H. pylori*, HypA·UreE is known from chemical cross-linking of the proteins (Benoit et al. 2007). This complex presumably reflects the previously mentioned *H. pylori*-specific enhancement of urease activity by HypA (Olson et al. 2001). Evidence indicates that nickel is transferred from HypA to UreE via a HypA·(UreE)<sub>2</sub> complex (Hu et al. 2018; Yang et al. 2014), with HypA and UreG competing for the UreE binding site (Benoit et al. 2012).

The second critical component in urease maturation is UreG. This protein, a nickel-binding GTPase, has been purified and characterized from a wide range of organisms, including the bacteria *K. aerogenes* (Boer et al. 2010; Martin-Diaconescu et al. 2017; Moncrief and Hausinger 1997), *Klebsiella pneumoniae* (Yuen et al. 2017), *S. pasteurii* (D’Urzo et al. 2014; Zambelli et al. 2005), *H. pylori* (Fong et al. 2013; Yang et al. 2015; Zambelli et al. 2009), *M. tuberculosis* (Zambelli et al. 2007b), and the archaea *Methanocaldococcus jannaschii* and *Metallosphaera sedula* (Miraula et al. 2015). Whereas some UreG proteins are monomeric in dilute solution (Boer et al. 2010; Moncrief and Hausinger 1997), others are dimers (Zambelli et al. 2005, 2007b), and still others exhibit a monomer-to-dimer equilibrium with the latter species stabilized by addition of zinc (D’Urzo et al. 2014; Miraula et al. 2015; Zambelli et al. 2009). All UreG species bind zinc or nickel, but the number of equivalents bound and the measured affinities differ for each protein [reviewed in Martin-Diaconescu et al. (2017)]. The structure of an N-terminally truncated UreG from *K. pneumoniae* in the presence of nickel and the GTP analogue GMPPNP reveals a dimer, with the critical nickel ion coordinated symmetrically by the conserved Cys-X-His motifs at the interface of the subunits (Fig. 14.7b) (Yuen et al. 2017). Additional nickel ions associate with each of the two GMPPNP molecules, corresponding to the more typical Mg·GTP interaction. Despite the ability of isolated *K. pneumoniae* UreG to crystallize into a distinct structure (Yuen et al. 2017) and the reported structure of a protein complex including *H. pylori* UreG (Fong et al. 2013), extensive evidence suggests that the *S. pasteurii* and archaeal proteins are intrinsically disordered (Miraula et al. 2015; Palombo et al. 2017; Zambelli et al. 2005, 2012). The significance of this finding is unclear.

Several studies have demonstrated an interaction between UreG and UreE, consistent with the two proteins transiently sharing coordination of the nickel. For example, nickel stimulates the interaction between the *K. aerogenes* proteins, forming a UreG·Ni·(UreE)<sub>2</sub> complex (Boer et al. 2010). In contrast, a (UreG)<sub>2</sub>·Ni·(UreE)<sub>2</sub> complex was identified for the *S. pasteurii* proteins (Merloni et al. 2014). Using the *H. pylori* components, (UreG)<sub>2</sub>·Zn·(UreE)<sub>2</sub> (Bellucci et al. 2009) along with UreG·Ni·(UreE)<sub>2</sub> and (UreG)<sub>2</sub>·Ni·(UreE)<sub>2</sub> were observed, with the latter found to predominate when Mg·GTP was present (Yang et al. 2015). No structure is available for any complex of UreE and UreG, but a model was proposed for the *H. pylori* species (Bellucci et al. 2009). A consensus hypothesis has emerged that nickel-loaded UreE transfers nickel to UreG by direct interaction of these protein components.

In the next step, UreG interacts with UreF and UreD/H to form a complex that has been characterized for components from *H. pylori* and *K. aerogenes*. Most notably, the crystal structure of *H. pylori* (UreG·UreF·UreD)<sub>2</sub> is available with GDP bound to UreG (Fig. 14.7d) (Fong et al. 2013), as well as structures of the precursors (UreF·UreD)<sub>2</sub> (Fig. 14.7c) (Fong et al. 2011) and (UreF)<sub>2</sub> (Lam et al. 2010). In addition, chemical cross-linking and ion mobility-mass spectrometric analysis of *K. aerogenes* proteins identified (UreG·UreF·UreD-MBP)<sub>2</sub>, where UreD-MBP is a fusion of UreD with the maltose-binding protein (MBP, used to enhance solubility) (Carter and Hausinger 2010). This *K. aerogenes* complex binds to the cognate urease apoprotein, (UreA·UreB·UreC)<sub>3</sub> (Fig. 14.7e), to form (UreG·UreF·UreD-MBP)<sub>3</sub>·(UreA·UreB·UreC)<sub>3</sub> (Fig. 14.7f) (Eschweiler et al. 2018; Farrugia et al. 2013a). The *K. aerogenes* apoprotein is identical in structure to the holoprotein, except for the absence of nickel and the lack of carbamylation at the active site lysine (Jabri and Karplus 1996). The connection between the accessory protein heterotrimer and urease occurs via UreD and UreB as shown by production and characterization of a (UreD)<sub>3</sub>·(UreA·UreB·UreC)<sub>3</sub> complex (Park et al. 1994). Similarly, co-expression of *ureF*, *ureD*, and *ureABC* allows for production of (UreF·UreD)<sub>3</sub>·(UreA·UreB·UreC)<sub>3</sub> (Moncrief and Hausinger 1996). Significantly, incubation of (UreF·UreD)<sub>3</sub>·(UreA·UreB·UreC)<sub>3</sub> with UreG, UreE, and nickel resulted in GTP-dependent generation of near fully active urease (Soriano and Hausinger 1999; Soriano et al. 2000). No structure is reported for any accessory protein bound to the urease apoprotein.

A current model for activation of bacterial urease (Fig. 14.7e) is derived by merging studies of the *K. aerogenes* and *H. pylori* urease systems. From ion mobility-mass spectrometry studies (Eschweiler et al. 2018; Farrugia et al. 2013a), it appears that the dimeric (UreG·UreF·UreD)<sub>2</sub> complex dissociates to monomeric UreG·UreF·UreD units when forming the (UreG·UreF·UreD)<sub>3</sub>·(UreA·UreB·UreC)<sub>3</sub> apoprotein complex. Chemical cross-linking studies indicate specific interactions between UreD and UreB, requiring the urease subunit to undergo a hinge-like motion that provides better access to the nascent active site, and small angle X-ray scattering studies are consistent with the overall structure of this species (Chang et al. 2004; Quiroz-Valenzuela et al. 2008). Computational studies using the *H. pylori* (UreH·UreF·UreG)<sub>2</sub> crystal structure (Fong et al. 2013) and a homology model for

*K. aerogenes* UreG·UreF·UreD (Farrugia et al. 2015) indicated the likely existence of a molecular channel for nickel transfer through UreF and UreH/D. Support for such a tunnel was obtained for the *K. aerogenes* components; UreD variants predicted to occlude the tunnel abolished the ability to activate the urease apoprotein (Farrugia et al. 2015). Although the role of GTP hydrolysis during activation remains unclear, a reasonable hypothesis is that nucleotide hydrolysis is coupled to the release of nickel into the tunnel. Diffusion of the metal ion through the molecular channel provides access to the nascent active site that otherwise is buried within UreC. Coordination of nickel to the active site residues leads to conformational changes resulting in release of the accessory proteins.

### 14.4.6 [NiFe] Hydrogenase

Hydrogenases catalyze the reversible oxidation of dihydrogen gas to form two protons and two electrons (Fig. 14.5f) (Adams et al. 1981; Peters et al. 2015; Vignais et al. 2001; Vignais and Billoud 2007). In some microorganisms, the electrons derived from hydrogen are used to reduce oxygen, sulfate, carbon dioxide, nitrate, or other electron acceptors, and this coupling serves as a means to provide energy to the cell. In particular microbes, the reverse reaction is used to eliminate excess cellular reducing potential derived by fermentation or photosynthesis. Thus, hydrogenases play central roles in the energy metabolism of many microorganisms. Three main enzyme classes are differentiated on the basis of their metalcenters: [NiFe] hydrogenases, [FeFe] hydrogenases, and iron-only hydrogenases. Only the [NiFe] hydrogenases are relevant to this chapter.

#### 14.4.6.1 Types and Structures of [NiFe] Hydrogenases

All of the [NiFe] hydrogenases possess at least two types of subunits: a large subunit (~60 kDa) containing nickel plus iron at a dinuclear [NiFe] active site cluster and a small subunit (~30 kDa) typically containing three iron-sulfur clusters that shuttle electrons between the [NiFe] active site and an external electron carrier. The names of the genes encoding the subunits are quite variable in different microorganisms with further nomenclature complications arising in microorganisms possessing multiple [NiFe] hydrogenases. Four distinct functional groupings and 22 subgroups of these enzymes have been identified on the basis of sequence analyses (Greening et al. 2016; Peters et al. 2015; Vignais and Billoud 2007).

Group 1 [NiFe] hydrogenases are periplasmic or membrane-associated and utilize H<sub>2</sub> for energy generation. Many periplasmic, heterodimeric enzymes have been characterized; e.g., the first [NiFe] hydrogenase to be structurally elucidated was the heterodimeric enzyme from *Desulfovibrio gigas* (Volbeda et al. 1995). The large subunit contains the deeply buried [NiFe] center (this site will be described separately, below), and the small subunit contains a linear arrangement of [4Fe-4S],

[3Fe-4S], and [4Fe-4S] clusters for electron transfer with a partner electron carrier located in the membrane. Similar heterodimeric structures are characterized for [NiFe] hydrogenases from other sulfate-reducing bacteria including *Desulfovibrio desulfuricans*, *Desulfovibrio vulgaris* Miyazaki F (Fig. 14.6f), *Desulfomicrobium norvegicum* (formerly *D. baculatum*), *D. vulgaris* Hildenborough, and *Desulfovibrio fructosovorans* (Garcin et al. 1999; Higuchi et al. 1997; Marques et al. 2010; Matias et al. 2001; Volbeda et al. 2005). Duplication of this architecture is seen in several non-sulfate-reducing bacteria such as *Hydrogenovibrio marinus*, the photosynthetic purple-sulfur bacterium *Allochromatium vinosum*, and an enzyme with very high affinity for H<sub>2</sub> from the actinobacterium *C. necator* (Ogata et al. 2010; Schäfer et al. 2016; Shomura et al. 2011). Additional enzymes that operate using low concentrations of H<sub>2</sub> are found in soil bacteria such as *Streptomyces* (Constant et al. 2010, 2011) and may have similar structures.

Additional subunits beyond the dimeric enzyme are present in many other group 1 cases. For example, *E. coli* uses a membrane-bound cytochrome *b* to shuttle electrons from hydrogenase-1 into the quinone pool, which then transfers electrons to an external electron acceptor. This enzyme is encoded by *hyaAB* and the cytochrome *b* is encoded by *hyaC*, all found in the *hyaABCDEF* operon (Sargent 2016). The structure of *E. coli* hydrogenase-1 contains two copies of each hydrogenase subunit (Volbeda et al. 2012) and this (HyaAB)<sub>2</sub> unit forms a complex with a single copy of HyaC (Volbeda et al. 2013). The C-termini of each small subunit have helical extensions that interact with a four-helix bundle of the membrane-bound cytochrome *b*. The three [FeS] clusters in each small subunit [including one with an extra cysteine residue replacing an inorganic sulfide (Volbeda et al. 2012)] aligns with the heme of HyaC to facilitate electron transfer. A second group 1 [NiFe] hydrogenase in *E. coli*, hydrogenase-2, has two standard subunits encoded by *hybO* and *hybC* plus an [FeS]-containing protein in the periplasm and a membrane-associated protein, encoded by *hybA* and *hybB* respectively, all associated with the *hybOABCDEFG* operon (Sargent 2016). The structure of (HybCO)<sub>2</sub> is known and closely resembles that of (HyaAB)<sub>2</sub>, but only a predicted structure is available for the (HybCOAB)<sub>2</sub> complex (Beaton et al. 2018).

Group 2 [NiFe] hydrogenases are cytoplasmic proteins that catalyze H<sub>2</sub> uptake. Four subgroupings are found, but only two are briefly mentioned here. First, the cyanobacterial enzymes (with subunits often designated HupSL) recapture the H<sub>2</sub> that is produced as a requisite side reaction of nitrogenase during its reduction of N<sub>2</sub> (Tamagnini et al. 2007). Second, H<sub>2</sub>-sensing enzymes (commonly designated HupUV or HoxBC) participate in the transcriptional regulation of other hydrogenases. *C. necator* provides a paradigm for this type of [NiFe] hydrogenase system; its group 2 cytoplasmic H<sub>2</sub>-sensor HoxBC is used to regulate production of the NAD-dependent, membrane-bound, HoxFUYH group 3 enzyme (see below) (Lenz and Friedrich 1998). No group 2 [NiFe] hydrogenase is structurally characterized at this time.

The group 3 [NiFe] hydrogenases typically function as bidirectional cytoplasmic enzymes that possess more than the two standard subunits. These additional components bind and transfer electrons to cytoplasmic electron carriers such as NAD<sup>+</sup>,



NADP<sup>+</sup>, or 8-hydroxy-5-deazaflavin (coenzyme F<sub>420</sub>, a cofactor found primarily found in methanogenic archaea). The structure of the F<sub>420</sub>-reducing [NiFe] hydrogenase from *Methanothermobacter marburgensis* is known from cryo-electron microscopy studies (Vitt et al. 2014). The large and small hydrogenase subunits, FrhA and FrhG, are relatively standard (except the first [4Fe-4S] is coordinated by Asp and three Cys instead of the usual four Cys). Also present is the F<sub>420</sub>-binding component, FrhB, that contains another [4Fe-4S] (aligned with the three clusters in FrhG) and FAD that interacts with the coenzyme F<sub>420</sub>. These three components form a spherical (FrhABG)<sub>12</sub> complex; i.e., a dodecamer of the heterotrimer. Such a large assemblage is not found in all group 3 members. For example, a cytoplasmic, NAD<sup>+</sup>-reducing [NiFe] hydrogenase from *Hydrogenophilus thermoluteolus* Th-1 is a heterotetramer (Shomura et al. 2017). This protein complex includes the large subunit HoxH (with an extra glutamate ligand of nickel compared to the typical situation, see below), the small subunit HoxU (with a non-typical and non-linear [4Fe-4S], [4Fe-4S], [2Fe-2S] arrangement), HoxY (containing a [4Fe-4S] between the [NiFe] site and first [4Fe-4S] of the small subunit), and HoxF (possessing a [4Fe-4S] in line with two clusters in the small subunit and an FMN at the NAD<sup>+</sup>-binding site). Of further interest, some enzymes in this group act in electron bifurcation reactions, such as a methanogen MvhAGD enzyme that uses H<sub>2</sub> ( $E'_{\circ} = -414$  mV) to simultaneously carry out an energetically downhill reaction (the reduction of a heterodisulfide,  $E'_{\circ} = -140$  mV) and an energetically uphill reaction (the reduction of a ferredoxin,  $E'_{\circ} = -500$  mV) (Thauer et al. 2010).

Group 4 [NiFe] hydrogenases are complex membrane-bound enzymes, typically containing at least six types of subunits, that evolve hydrogen from cells using low potential reductants, such as carbon monoxide or formate, and often use ferredoxin as an electron carrier. The classic example of this type of enzyme is *E. coli* hydrogenase-3, encoded by *hycBCDEFGHI* where *hycEG* corresponds to the standard subunit-encoding genes. This enzyme functions as a formate hydrogenlyase to metabolize formate to H<sub>2</sub> and CO<sub>2</sub> (Sargent 2016). Closely resembling the operon sequence for hydrogenase-3 is *hyfABCGHIJ* of *E. coli*, encoding hydrogenase-4 that may also function in formate metabolism; however, hydrogenase-4 activity has not been established. Also noteworthy are group 4 enzymes that function as energy-converting hydrogenases (ECHs) that couple electron transfer to ion translocation. One example of this type of enzyme is EchABCDEF of *Methanosarcina barkeri* that utilizes the proton motive force to facilitate the thermodynamically unfavorable reduction of ferredoxin by H<sub>2</sub> (Meuer et al. 1999). Sequence analyses indicate the small subunits of these enzymes contain a single [4Fe-4S] cluster (Greening et al. 2016) although other components may provide further electron transfer sites. No structures of group 4 enzymes are available.

The active sites of all four groups of [NiFe] hydrogenases possess a [NiFe] dinuclear cluster. The structure of the heterodimeric, periplasmic enzyme from *D. gigas* first revealed this site as nickel with another metal (tentatively assigned to iron) that binds three non-protein ligands depicted at the time as water molecules (Volbeda et al. 1995). Four cysteine residues bind the nickel and two of these ligands bridge to the second metal. Follow-up studies with this protein confirmed the

identity of iron and suggested the three non-protein ligands are diatomic molecules (Volbeda et al. 1996). The nature of the iron-coordinating ligands was established from studies in which *Chromatium vinosum* [NiFe] hydrogenase was purified from cells grown on medium containing  $^{13}\text{C}$  and  $^{15}\text{N}$ , then subjected to infrared spectroscopy (Happe et al. 1997; Pierik et al. 1999). Intense features in the 2150 to 1850  $\text{cm}^{-1}$  region demonstrate the presence of one carbon monoxide and two cyanide ligands. Subsequent studies (Ash et al. 2019; Fontecilla-Camps et al. 2007; Lubitz et al. 2014; Ogata et al. 2016; Shafaat et al. 2013; Volbeda and Fontecilla-Camps 2017), clarified the structures and properties of the [NiFe] site in enzymes from different species and in different states. Of particular interest is the active site structure of the  $\text{H}_2$ -reduced protein from *D. vulgaris* Miyazaki F at the remarkable resolution of 0.89 Å (Fig. 14.6f) revealing a hydride bridging the two metal ions (Ogata et al. 2015). In contrast to the typical four cysteines binding the dinuclear site, the *D. norvegicum* and *D. vulgaris* Hildenborough enzymes have a selenocysteine substituting for the C-terminal cysteine residue (Garcin et al. 1999; Marques et al. 2010). Another interesting structural variation is a [NiFe] hydrogenase from *C. necator* that binds four cyanide ligands (Van der Linden et al. 2004). The biosynthesis of the extraordinary [NiFe] site is an amazingly complicated process as described in the following paragraphs.

#### 14.4.6.2 [NiFe] Hydrogenase Maturation

Our understanding of [NiFe] hydrogenase maturation is highly dependent on genetic and biochemical studies performed in *E. coli* where investigators have shown the *hypABCDE* operon is needed for activation of hydrogenases-1, -2, and -3 (Jacobi et al. 1992; Lutz et al. 1991). The HybA-HypE proteins encoded by this operon, the non-subunit gene products encoded by the *hya*, *hyb*, and *hyc* operons, and other *E. coli* proteins all work in concert to generate active forms of the organism's three enzymes. A detailed description of these extensive studies for *E. coli*, and analogous biochemical and genetic work carried out with other microorganisms, is beyond the scope of this chapter, so the reader is referred to review articles describing the multiple insights generated by the laboratories of August Böck (Böck et al. 2006), Deborah Zamble (Lacasse and Zamble 2016; Leach and Zamble 2007), Gary Sawers (Forzi and Sawers 2007; Sawers and Pinske 2017), and others (Cheng et al. 2016; Peters et al. 2015; Sargent 2016; Senger et al. 2017). Here, I focus on a structural description of the elaborate [NiFe] hydrogenase activation process (Fig. 14.8), where much of this remarkable set of work was carried out using *Thermococcus kodakarensis* KOD1 components in the laboratory of Kunio Miki (Miki et al. 2020).

The cyanide ligands of the metalcenter are generated by a multi-step reaction sequence involving HypE and HypF. Structures are known for dimeric HypE from *T. kodakarensis* (Watanabe et al. 2007) as well as monomeric HypF proteins from this organism (Tominaga et al. 2012), *Caldanaerobacter subterraneus* (Shomura and Higuchi 2012), and (in truncated form) *E. coli* (Petkun et al. 2011). In addition, the structure is known for the transient heterotetramer (HypE-HypF)<sub>2</sub> from

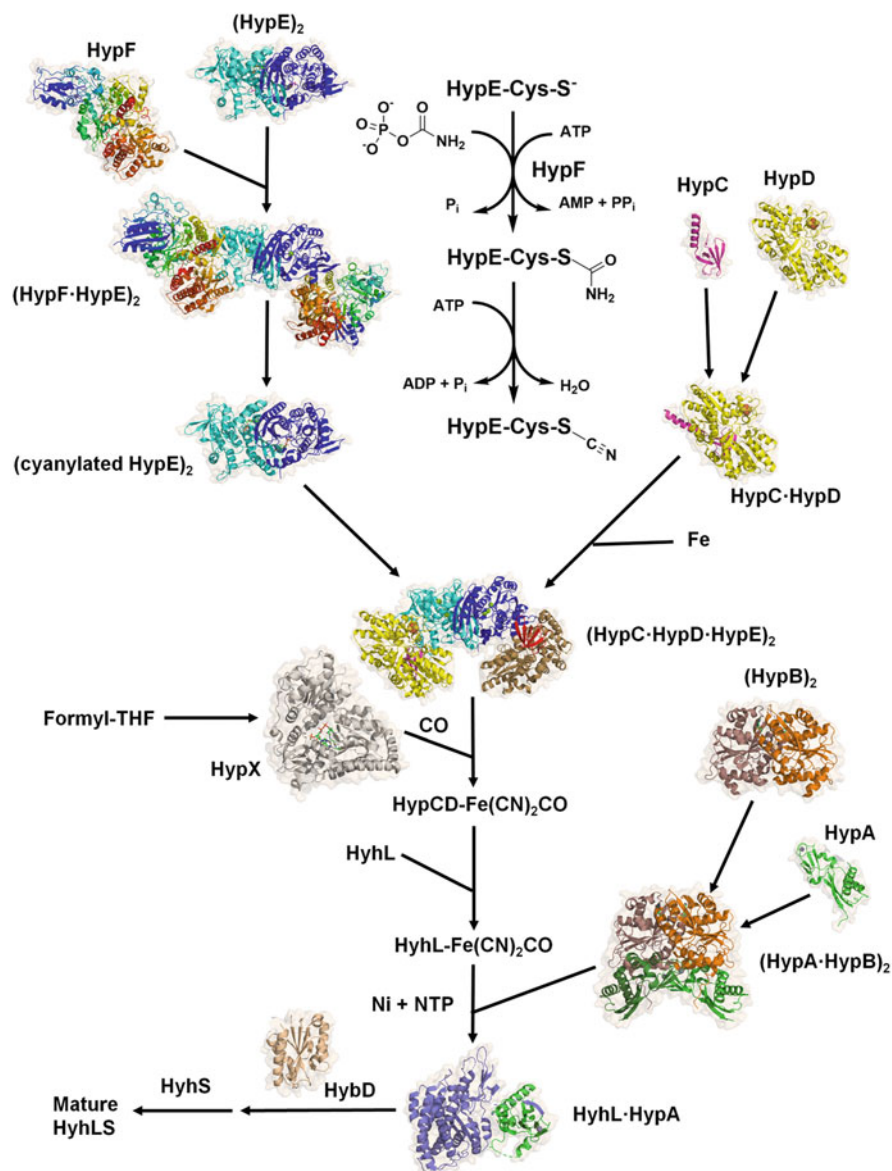


**Fig. 14.8** Hydrogenase maturation pathway. All structures are from *Thermococcus kodakarensis* except where indicated. (Upper left) The HypE homodimer (PDB ID 3wjv, cyan and dark blue) binds to monomeric HypF (PDB ID 4g9i, red to blue rainbow color to illustrate its four domains) forming the heterotetramer (HypF-HypE)<sub>2</sub> (PDB ID 3vti, from *Caldanaerobacter subterraneus* subspecies *tengcongensis* MB4). (Upper middle) HypF hydrolyzes carbamoylphosphate, adenylylates the resulting carbamate, and converts the carboxyl terminal cysteine of HypE to the carbamoylated residue (PDB ID 3wjj). HypE dehydrates this modification to generate a thiocyanated cysteine (PDB ID 3wjq). (Upper right) Monomeric HypC (PDB ID 2z1c, maroon) and monomeric HypD (PDB ID 2z1d, yellow) generate a heterodimer (PDB ID 3vyr). Two

*C. subterraneus* (Shomura and Higuchi 2012). The four-domain HypF hydrolyzes carbamoylphosphate to form carbamate that reacts with ATP to generate carbamoyladenylate, which is used to generate a thiocarboxamide at the C-terminal cysteine residue of HypE (Reissmann et al. 2003). HypE then catalyzes an ATP-dependent dehydration reaction to yield the thiocyanate derivative of this cysteine. In addition to the non-modified HypE species, structures of the thiocarboxamide and thiocyanate forms are reported (Tominaga et al. 2013).

HypC and HypD function as the scaffold for the iron atom of the [NiFe] site. Structures are known for the individual proteins and for HypC·HypD from *T. kodakarensis* (Watanabe et al. 2007, 2012). HypC has a  $\beta$ -barrel domain containing the essential Cys2 residue and an  $\alpha$ -helix extension at its C-terminus. HypD is a larger protein containing a [4Fe-4S] bound by four cysteine residues, four other redox-active cysteine residues located immediately adjacent to the cluster, and the essential Cys38 residue. The HypC·HypD heterodimer is hypothesized to bind iron (from a still unidentified source) using HypC Cys2 and HypD Cys38. Two molecules of HypC·HypD bind to the HypE homodimer, and the (HypC·HypD·HypE)<sub>2</sub> structure is known. The cyanide adduct of the HypE C-terminal cysteine is transferred onto the HypC·HypD-bound iron atom, presumably making use of reductive chemistry involving the [4Fe-4S] and the cysteine tetrad electron transfer components of HypD. This process is repeated twice to provide two cyanide ligands on the iron. The CO ligand is derived from formyl-tetrahydrofolate (THF) using formyl-THF decarbonylase, or HypX (Schulz et al. 2020), which was structurally defined for the protein from *Aquifex aeolicus* (Muraki et al. 2019). Studies with the *C. necator* enzyme show the formyl group is first transferred onto a tightly bound CoA molecule, with decarbonylation leading to release of CO and reformation of CoA (Schulz et al. 2020). The HypC·HypD-bound iron-(CN)<sub>2</sub>CO complex is subsequently transferred into the hydrogenase large subunit HyhL by a process that remains obscure.



**Fig. 14.8** (continued) molecules of this heterodimer bind iron and form a complex with the cyanylated HypE dimer, yielding the dimer of HypC·HypD·HypE (PDB ID 3vys). (Middle left) Monomeric HypX (PDB ID 6j0p, white, from *Aquifex aeolicus*) is a formyl-THF decarbonylase. Carbon monoxide derived from this reaction and two cyanide from cyanylated HypE become ligands to iron bound to HypC·HypD. The iron and its diatomic ligands are transferred into the hydrogenase large subunit, HyhL. (Bottom right) Dimeric HypB (PDB ID 3vx3, orange and brown) binds two molecules of monomeric HypA (PDB ID 3a43, green) to form a complex (PDB ID 5aun) with multiple nickel-binding sites. Nucleotide hydrolysis (ATP or GTP depending on the species) by this complex is coupled to nickel insertion into HyhL (slate blue) via HyhL·HypA (PDB ID 5yy0). (Bottom left) The HybD endoprotease (PDB ID 5ija, wheat) cleaves near the carboxyl terminus of HyhL causing the [NiFe] cluster to become buried in the protein and allowing for complex formation with the small subunit HyhS. Proteins are shown in cartoon depictions with semi-transparent surfaces. Metal and inorganic sulfur atoms are shown as spheres (nickel in green, zinc in grey, iron as brown, and sulfide as yellow). Selected side chains and nucleotides are illustrated in stick mode

Nickel is provided to HyhL by the metallochaperones HypA and HypB that are universally required for [NiFe] hydrogenase activation (Böck et al. 2006; Lacasse and Zamble 2016; Miki et al. 2020). Extensive efforts have characterized the nickel-binding properties and other features of these proteins from various organisms, and the structures of dimeric HypB and monomeric HypA from *T. kodakarensis* are known (Sasaki et al. 2013; Watanabe et al. 2009) as is that of their complex in the presence of ATP $\gamma$ S (Watanabe et al. 2015). In this microorganism, HypB does not bind nickel so it cannot deliver the metal to HypA as described for the *E. coli* proteins. Rather, the binding of HypB to HypA increases the affinity for nickel at the HypA site from a  $K_d$  of 4.1  $\mu$ M for the free protein to 7.3 nM for HypA·HypB. Nucleotide hydrolysis (typically using GTP, but the *T. kodakarensis* HypB protein uses ATP) is coupled to nickel insertion into HyhL via HyhL·HypA, for which the structure is established (Kwon et al. 2018). In *E. coli*, HypA is used only to activate hydrogenase-3 whereas a second version named HybF activates hydrogenase-1 and hydrogenase-2 (Blokesch et al. 2004). In *B. japonicum*, HypB binds ~9 nickel ions per monomer (predominantly using a His-rich region at the amino terminus) and was suggested to be, but not established as, a nickel storage protein named nickelin (akin to the term ferritin used for iron storage proteins) (Olson and Maier 2000). HypB of this microorganism is critical for activation of its [NiFe] hydrogenase, and its GTPase activity promotes nickel insertion into the protein (Fu et al. 1995). In *E. coli*, SlyD participates in nickel delivery to [NiFe] hydrogenases and perhaps also in nickel storage (Kaluarachchi et al. 2011; Zhang et al. 2005). This protein is one of several host factors required for lysis by a bacteriophage (hence, giving rise to the sensitive to lysis *D* or *slyD* name) (Maratea et al. 1985) and it is a common contaminant of poly-histidine-tagged proteins purified by immobilized metal affinity chromatograph (Wülfling et al. 1994). SlyD contains a histidine-rich region near its carboxyl terminus and a domain with peptidyl-prolyl *cis-trans* isomerase activity. Deletion of the corresponding gene results in large reductions of cellular nickel content and hydrogenase activity (Leach et al. 2007; Pinske et al. 2015; Zhang et al. 2005). Of additional interest, SlyD of *H. pylori* interacts with the NiuD permease (Denic et al. 2021), hinting at a possible handoff of metal from a nickel uptake protein to a nickel delivery protein.

Upon nickel binding, a conformational change occurs in HyhL to bury the metalcenter and expose the histidine cleavage site to the endopeptidase HybD with a known structure (Kwon et al. 2016). Structures are also known for *E. coli* HybD and HycI, analogous proteases used for maturation of hydrogenase-2 and hydrogenase-3 (Fritsche et al. 1999; Yang et al. 2006). After HyhL cleavage and release of HypA, the small subunit of hydrogenase, HyhS, binds to form the mature, active [NiFe] hydrogenase.

#### **14.4.7 Carbon Monoxide Dehydrogenase (CODH)**

A critical reaction for many microorganisms is the reversible interconversion between carbon monoxide (CO) and carbon dioxide (Fig. 14.5g). In aerobic

organisms, this reaction is carried out by using a copper-molybdopterin-[FeS] cluster-containing enzyme (King and Weber 2007). In contrast, anaerobes use an oxygen-labile nickel-dependent carbon monoxide dehydrogenase (CODH) of interest here (Can et al. 2014; Kung and Drennan 2017). CODHs are widely distributed in microorganisms, with one report indicating that over 6% of bacterial and archaeal genomes possess such genes that were resolved into six distinct clades (Techtmann et al. 2012). A more recent bioinformatics study identified 1942 non-redundant CODH genes in 1375 genomes covering 36 phyla and divided them into seven clades with 24 structural groups (Inoue et al. 2019). This section summarizes the properties of CODHs from carboxydrotrophs that utilize the low potential electrons derived from CO ( $E^{\circ\prime} -524$  mV) for energy metabolism, such as that resulting in hydrogen production, or for autotrophic growth. Described separately (Sect. 14.4.8) are CODHs present in larger protein assemblages containing acetyl-CoA synthase/decarbonylase (ACS) activities that are used for CO<sub>2</sub> fixation and for aceticlastic growth of methanogens.

Particularly well-characterized sources of homodimeric CODHs are *C. hydrogenoformans* and *Rhodospirillum rubrum*, microbes in which CO oxidation is coupled to the production of hydrogen gas, along with *D. vulgaris*, which does not utilize CO as an energy source (Hadj-Saïd et al. 2015; Voordouw 2002). Notably, the *C. hydrogenoformans* genome encodes five CODHs (Wu et al. 2005), and each of the corresponding enzymes has been characterized [e.g., (Domnik et al. 2017)]. The *R. rubrum* enzyme was the first CODH purified and shown to possess a metallocenter containing nickel, iron, and inorganic sulfide (Bonam and Ludden 1987). The nickel-free forms of the *R. rubrum* and *D. vulgaris* proteins were obtained by growing cells in medium lacking this metal ion or by growing in the absence of the CooC accessory protein (see below), allowing for studies involving nickel-dependent activation (Bonam et al. 1988; Ensign et al. 1990; Hadj-Saïd et al. 2015). An extensive array of spectroscopic and mechanistic studies have been summarized for the *R. rubrum* CODH (Can et al. 2014; Kung and Drennan 2017) and will not be repeated here. Rather, I focus below on the structures of these proteins.

#### 14.4.7.1 CODH Structure

The crystal structures of homodimeric CODHs from *C. hydrogenoformans* and *R. rubrum* were first reported in 2001 (Dobbek et al. 2001; Drennan et al. 2001) and shown to possess a [4Fe-4S] D-cluster that bridges the subunits, two additional [4Fe4S] B-clusters, and the deeply buried unique nickel-iron-sulfur C-clusters (Fig. 14.6g). The initial reports identified the *R. rubrum* CODH C-cluster as a [1Ni-3Fe-4S] cubane connected by one sulfide to a mononuclear Fe site, whereas the *C. hydrogenoformans* enzyme had an additional sulfide between the nickel and the non-core Fe (Dobbek et al. 2001; Drennan et al. 2001). Subsequent studies indicated the additional sulfide is not present in the catalytically active state of the enzyme (Kung and Drennan 2017). An essentially identical crystal structure was

obtained for a nickel-depleted form of one CODH from *Thermococcus* sp. AM4 (two such enzymes are present in that microorganism) (Benvenuti et al. 2020). The CODH structure from *D. vulgaris* is of special interest. This enzyme exhibits redox-dependent changes in its C cluster such that the Ni and mononuclear Fe alter their positions (Wittenborn et al. 2018). In addition, this protein tolerates short-term exposure to small concentrations of oxygen because the exposed D-cluster has a more stable [2Fe-2S] cluster rather than a [4Fe-4S] cluster (Wittenborn et al. 2020). External electron transfer proteins deliver reducing equivalents to or remove electrons from the D-cluster that connects, via the B-clusters, to the active site C-clusters, which interconverts CO and CO<sub>2</sub>.

#### 14.4.7.2 CODH Maturation

CODH of *R. rubrum* is encoded by *cooS* that is immediately followed by *cooC*, *cooT*, and *cooJ*. Deletion analysis demonstrated that *cooC* is required for biosynthesis of the [1Ni-4Fe-4S] metallocenter in CODH unless high concentrations of nickel are provided in the medium, whereas deletions in the adjacent *cooT* and *cooJ* genes have less marked effects (Kerby et al. 1997). In *C. hydrogenoformans*, *cooS-1* is located near *cooC1*, *cooS-2* is adjacent to *cooF*, and two other *cooC* copies along with a *cooT* are found elsewhere in the genome (Merrouch et al. 2018). Both *cooS* copies in *Thermococcus* are located near *cooC* genes, a third *cooC* has no clear function, and no *cooT* or *cooJ* is reported in this genome (Benvenuti et al. 2020). In *D. vulgaris*, *cooS* is immediately adjacent to *cooC*, but no *cooT* or *cooJ* has been described (Hadj-Saïd et al. 2015). A bioinformatics analysis of microorganisms possessing CODH reveals the genes encoding CooT and CooJ often are missing and that some microbes also lack CooC; thus, these proteins are not strictly needed for CODH enzyme activation in all microbes (Merrouch et al. 2018). The following paragraphs briefly highlight these proteins.

CooC is an ATPase or GTPase with sequence similarities to the HypB and UreG proteins involved in activation of hydrogenases and ureases (Jeon et al. 2001). The structurally-characterized CooC from *C. hydrogenoformans* is a nickel-binding protein with the metal bound to four cysteine residues located at the interface of the subunits (Fig. 14.9a) (Jeoung et al. 2009, 2010). Deletion of *cooC* in *D. vulgaris* leads to the synthesis of a nickel-free CODH whose structure was determined (Wittenborn et al. 2019).

CooT from *R. rubrum* and *C. hydrogenoformans* are nickel-binding proteins with known structures (Alfano et al. 2018; Timm et al. 2017). NMR, XAS, and modeling analyses of nickel-bound *R. rubrum* CooT suggested the presence of a unique square-planar nickel site at the subunit interface, with coordination by the side chains and amide groups of two Cys2 residues (note: the amino terminal Met1 residue was removed) (Fig. 14.9b, left) (Alfano et al. 2019c). *C. hydrogenoformans* CooT has a similar overall structure (Fig. 14.9b, right) despite being only 19% identical in sequence to that from *R. rubrum*; however, the presumed nickel site is modified and thought to involve coordination by the Cys2 and His55 side chains in

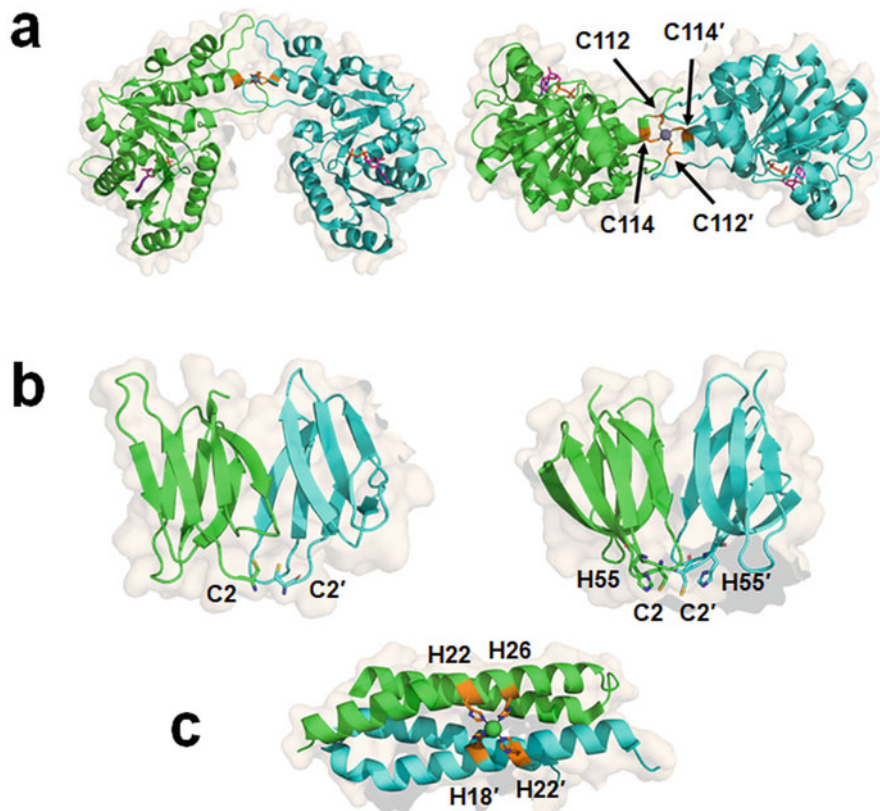


**Fig. 14.9** Structures of CODH maturation proteins. (a) Two views of CooC1 from *Carboxydotherrnus hydrogenoformans* (PDB ID 3kji) with bound ADP and zinc at the presumed nickel site. (b) CooT apoproteins from (left) *R. rubrum* and (right) *C. hydrogenoformans* (PDB ID 5n76 and 6fan) with their distinct nickel-binding sites. (c) Truncated CooJ from *R. rubrum* (PDB ID 6hk5) missing residues Asp69-Pro115 (the carboxyl terminal His-rich region) and highlighting the remaining nickel-binding site. Glu29'', not shown, from an adjacent dimer in the crystal coordinates as a bidentate ligand to the metal and completes its octahedral coordination sphere. The homodimeric proteins are shown in cartoon mode (green and cyan) with semi-transparent surfaces. Metals are shown as spheres and selected residues are depicted as sticks

each subunit (Alfano et al. 2018). Sequence comparisons show the two distinct nickel-binding motifs exist in other bacterial and archaeal CooT sequences (Alfano et al. 2019c).

CooJ from *R. rubrum* may assist in CODH maturation and is a potential nickel storage protein due to its His-rich carboxyl terminus (16 histidine residues in the last 34 amino acids) (Watt and Ludden 1998). The protein binds five nickel per dimer (four with a  $K_d \sim 1.6 \mu\text{M}$  and one with a  $K_d$  of 380 nM) (Alfano et al. 2019a). The structure of CooJ (truncated at the carboxyl region to remove the His-rich region) reveals nickel coordination by His22 and His26 from one subunit along with His18



and His22 of the second subunit, plus bidentate binding by Glu29 from another dimer (PDB ID 6hk5, Fig. 14.9c). The interaction with a neighboring dimer is consistent with the known ability of the protein to form higher-order oligomers in the presence of nickel (Alfano et al. 2019b). Direct evidence that the unique nickel-binding site is critical to CooJ function is lacking.

### 14.4.8 Acetyl-CoA Synthase/Decarboxylase (ACS)

In many microorganisms, CODH is a component of a larger protein complex known as acetyl-CoA synthase/decarboxylase (ACS) that includes a second nickel-containing metallocenter referred to as the A-cluster (Can et al. 2014; Kung and Drennan 2017). Versions of this enzyme are found in autotrophic anaerobes that use the Wood-Ljungdahl pathway for CO<sub>2</sub> fixation, such as many acetogens, methanogens, and sulfate-reducing bacteria, and in aceticlastic methanogens that grow anaerobically on acetate using a version of the enzyme that operates in the reverse direction. In the Wood-Ljungdahl pathway, one CO<sub>2</sub> undergoes three sequential two-electron reductions to generate a methyl group that is bound to tetrahydrofolate. The methyl group is then donated to a corrinoid-iron-sulfur protein (CFeSP), forming a methyl-Co bond. Meanwhile, the CODH component of ACS reduces one CO<sub>2</sub> to CO. In a remarkable reaction, the A cluster of ACS condenses the CFeSP-bound methyl group, the CO, and CoA to generate acetyl-CoA (Fig. 14.5h), used to synthesize all cellular carbon compounds. By contrast, the A-cluster of ACS in aceticlastic methanogens splits acetyl-CoA into CoA, CO, and a methyl group that becomes bound to a CFeSP. Subsequently, the methyl group is transferred to tetrahydromethanopterin, then to 2-thioethanesulfonate (CoM), the product of which is reduced by methyl-S-coenzyme M reductase (MCR) to generate methane (see Sect. 14.4.10). The electrons required for this last reduction step are derived from the oxidation of CO to form CO<sub>2</sub> by the CODH component of the protein.

#### 14.4.8.1 Structure of ACS

Structures are available for the native ACS from *Moorella thermoacetica* (formerly *Clostridium thermoaceticum*) (Darnault et al. 2003; Doukov et al. 2002) and *Clostridium autoethanogenum* (Lemaire and Wagner 2020). In addition, both the CODH component of ACS from *M. barkeri* (Gong et al. 2008) and the CODH-free ACS component from *C. hydrogenoformans* (Svetlitchnyi et al. 2004) have been structurally defined. The native  $\alpha_2\beta_2$  proteins from *M. thermoacetica* and *C. autoethanogenum* (Fig. 14.6h) contain the central core, equivalent to the homodimeric CODH enzyme, with two active site [1Ni-4Fe-4S] C-clusters, two [4Fe-4S] B-clusters for internal electron transfer, and the single [4Fe-4S] D-cluster for electron exchange with an external electron carrier. Flanking the CODH

component are subunits that contain the A-cluster as well as acetyl-CoA and CFeSP-binding sites. The highly dynamic nature of this subunit is shown by its two distinct conformations in crystallized *M. thermoacetica* and *C. autoethanogenum* enzymes and by the multiple structural arrangements found in *C. thermoacetica* ACS when examined by negative-stain electron microscopy (Cohen et al. 2020). The A-cluster is a novel [4Fe-4S]-Ni-Ni metallocenter that has a standard cubane cluster with one cysteine ligand bridging to a proximal nickel site ( $\text{Ni}_p$ ). Two additional cysteines connect  $\text{Ni}_p$  and a distal nickel atom ( $\text{Ni}_d$ ). The planar, 4-coordinate geometry of  $\text{Ni}_d$  is completed by two backbone amides. The tri-cysteine bound  $\text{Ni}_p$  is highly labile, with early structures depicting an enzyme lacking this metal, containing copper (Doukov et al. 2002), or with zinc (Darnault et al. 2003) at this position. The monomeric, CODH-free form of ACS from *C. hydrogenoformans* possesses the same [4Fe-4S]-Ni-Ni site (Svetlitchnyi et al. 2004). The structure of native ACS from *M. thermoacetica* revealed the existence of a 140 Å long molecular tunnel connecting the two C clusters in the CODH component and extending to  $\text{Ni}_p$  in each of the two A clusters. Direct evidence for this tunnel was obtained by showing that exogenous CO does not compete with CO produced at the C cluster for incorporation into acetyl-CoA at the A cluster and by demonstrating that addition of a CO-binding protein like myoglobin or hemoglobin has no effect on acetyl-CoA synthesis from  $\text{CO}_2$ , methyl-CFeSP, and CoA (Maynard and Lindahl 1999; Seravalli and Ragsdale 2000). Notably, crystals treated with pressurized xenon gas confirms the presence of a channel by showing these electron dense atoms within the protein (Darnault et al. 2003; Doukov et al. 2008).

The methanogen versions of ACS that operate in the direction of acetyl-CoA decomposition are best characterized for the proteins from *M. barkeri* and *Methanosarcina thermophila* (Grahame 1991; Terlesky et al. 1986). These corrinoid, nickel, iron, and sulfide-containing proteins each possess five types of subunits that aggregate into 2.4-MDa complexes with eight copies of each peptide. The structure of the intact complex is not known, but that for the  $\alpha_2\epsilon_2$  component exhibiting CODH activity is determined (Gong et al. 2008). The  $\alpha_2$  portion of this complex closely resembles the CODH structures described above, but it contains five metalloclusters; i.e., the typical [4Fe-4S] D-cluster bridging the subunits, two [4Fe-4S] B-clusters, and two [1Ni-4Fe-4S] C-clusters, along with two [4Fe-4S] E-clusters and two [4Fe-4S] F-clusters. The functions of the E- and F-clusters and that of the  $\epsilon$  subunits, not present in the previously described CODH and ACS structures, remain unknown.

#### 14.4.8.2 ACS Maturation

The remarkable complexity of the ACS metallocenters might lead one to suspect that multiple accessory proteins are required for their biosynthesis; however, that is not the case. Surprisingly, heterologous expression in *E. coli* of *acsA* and *acsB* (encoding the CODH component and the A cluster-containing protein) from *M. thermoacetica* provides a form of ACS that is indistinguishable from the native

enzyme missing Ni<sub>p</sub>; subsequent incubation with nickel yields active enzyme (Loke et al. 2000). Somewhat similarly, heterologous expression in *E. coli* of the gene encoding only the  $\beta$  subunit (i.e. the site of the A cluster) of *M. thermophila* ACS yields a nickel-free inactive protein that develops ACS activity after incubation with nickel (Gencic and Grahame 2003). These results suggest no accessory genes are needed for ACS maturation, but other studies provide evidence counter to this conclusion. Located in the same *M. thermoacetica* gene cluster as *acsAB* are *cooCI* and *acsF*, homologues of *R. rubrum* *cooC* encoding a protein with a nickel insertion auxiliary role. *M. thermoacetica* *CooC* has not been studied, whereas *AcsF* was found to exhibit ATPase activity, but no involvement in ACS activation was identified (Loke and Lindahl 2003). By contrast, *cooC2* in the ACS gene cluster of *C. hydrogenoformans* encodes an *AcsF* that clearly functions as an ACS maturation factor (Gregg et al. 2016). Two molecules of *AcsF* bind to inactive, monomeric ACS that lacks CODH (Svetlitchnyi et al. 2004), and the complex coordinates two atoms of nickel. Subsequent ATP hydrolysis is coupled to A cluster activation (Gregg et al. 2016). The authors concluded that *AcsF* installs the two nickel atoms of the A cluster.

#### 14.4.9 2-Hydroxyacid Racemase/Epimerase (HARE) Containing NPN

The ability of microorganisms to interconvert D- and L-lactic acid was first described for *Clostridium acetobutylicum* and *Clostridium beijerinckii* (formerly *C. butylicum*) in 1936 (Tatum et al. 1936). This activity provides a means for some lactic acid bacteria to obtain D-lactate for incorporation into their cell walls (Chapot-Chartier and Kulakauskas 2014), for other microbes to obtain L-lactate for synthesis of odd-numbered fatty acids (Weimer and Moen 2013), and for lactate degraders to utilize both enantiomers. Extensive studies of lactate racemase were carried out in the 1960s (Desguin et al. 2017), but only since 2015 has a detailed understanding of this enzyme and identification of other nickel-pincer nucleotide (NPN)-containing racemases/epimerases (Fig. 14.5i) been accomplished.

##### 14.4.9.1 Structure of Lactate Racemase and Discovery of the NPN Cofactor

The gene encoding lactate racemase (*larA*) was first identified in *L. plantarum* and shown to be located in the *larABCDE* gene cluster, adjacent to and transcribed opposite *larRMNQO* (Desguin et al. 2014). These operons are regulated by LarR, a lactic acid-dependent transcription factor (Desguin et al. 2015a). LarD is a lactate permease that allows for cellular entry/egress of both enantiomers (Bienert et al. 2013). The sequences of LarMN, LarQ, and LarO resemble those of ABC-type

nickel transporters (Sect. 14.2.2.2), leading to studies demonstrating that lactate racemase is a nickel-dependent enzyme requiring LarB, LarC, and LarE for activation (Desguin et al. 2014). The structure of LarA (Fig. 14.6i) reveals the presence of a covalently tethered cofactor, pyridinium-3-thioamide-5-thiocarboxylic acid mononucleotide (Desguin et al. 2015b). Because this cofactor is a nickel-containing pincer nucleotide complex (Nevarez et al. 2020), it is abbreviated NPN. Notably, the nickel in this coenzyme exhibits square-planar geometry with coordination by the pyridinium C4 carbon, the two sulfur atoms of NPN, and a histidine side chain. This cofactor participates in catalysis by a proton-coupled hydride transfer mechanism as shown by kinetic isotope studies demonstrating cleavage/reformation of the substrate C2-H bond, trapping of the pyruvate intermediate by two different methods, substrate-dependent perturbation of the NPN spectrum consistent with its reduction, and structural studies (Rankin et al. 2018). The presence of the novel NPN cofactor in LarA provides an explanation for why LarB, LarC, and LarE are required for racemase activity; they synthesize the coenzyme.

#### 14.4.9.2 NPN Cofactor Biosynthesis

Biosynthesis of the NPN cofactor (Fig. 14.10) initiates by LarB catalyzing dual activities with its substrate, nicotinic acid adenine dinucleotide (NaAD): carboxylation at C5 of the pyridinium ring and hydrolysis of the phosphoanhydride to produce pyridinium 3,5-dicarboxylic acid mononucleotide (P2CMN) while releasing AMP (Desguin et al. 2016). The structurally-characterized LarE then catalyzes a three-step sequence involving P2CMN carboxylate activation by adenylation (using ATP and releasing pyrophosphate), formation of a covalent bond between the mononucleotide and a cysteine side chain (while releasing AMP), and sacrificial loss of the cysteine sulfur atom (leaving the protein with dehydroalanine at this position) to generate the thioacid product. These steps are repeated for the second substrate carboxyl group using another LarE subunit, thus generating pyridinium 3,5-dithiocarboxylic acid mononucleotide (P2TMN) (Desguin et al. 2016; Fellner et al. 2017). LarC inserts nickel into this precursor via a stoichiometric cyclometallase reaction in a manganese- and CTP-dependent process (releasing CMP and pyrophosphate) (Desguin et al. 2018). LarC binds multiple atoms of nickel (Desguin et al. 2014), presumably using a histidine-rich sequence in its amino terminal domain, and may function as a metallochaperone. Efforts to crystallize LarC led to protein cleavage—perhaps involving trace amounts of protease acting on a highly susceptible sequence—to release the carboxyl-terminal domain (starting at residue 272) from the rest of the 420 residue full-length protein. The crystal structure was obtained for a hexamer of the smaller fragment, which lacks the nickel-binding region and the P2CMN-binding site; however, this domain binds  $Mn_2$ -CTP in a new nucleotide-binding configuration (Desguin et al. 2018).

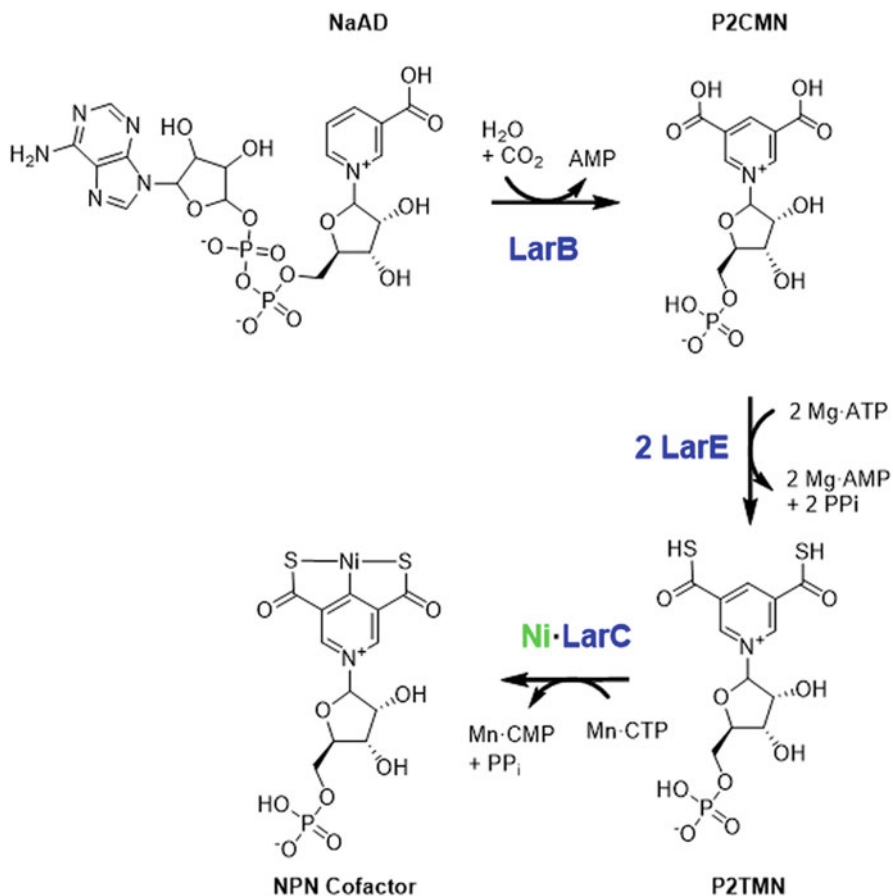


**Fig. 14.10** Biosynthesis of the nickel-pincer nucleotide (NPN) cofactor. LarB carboxylates C5 of the pyridinium ring and hydrolyzes the phosphoanhydride of nicotinic acid adenine dinucleotide (NaAD) releasing AMP and pyridinium 3,5-dicarboxylic acid mononucleotide (P2CMN). The carboxylic acids of P2CMN are converted to thioacids in pyridinium 3,5-dithiocarboxylic acid mononucleotide (P2TMN) by duplicate sacrificial sulfur transfer reactions from Cys side chains of two copies of LarE, generating dehydroalanine residues. LarC installs nickel into P2TMN to generate NPN in a reaction that requires CTP hydrolysis to CMP and pyrophosphate

#### 14.4.9.3 Other NPN-Binding Proteins

Approximately 10% of bacterial and archaeal genomes possess homologs to *larA*, *larB*, *larE*, and *larC* (Desguin et al. 2014), indicating a widespread ability to synthesize NPN for incorporation into lactate racemase-type enzymes. Significantly, many species possess more than one paralog of *larA*—up to eight copies in *Clostridium asparagiforme* and *Thermosinus carboxydivorans*—consistent with activities other than lactate racemase (Hausinger et al. 2018). Furthermore, *gntE*, a

*larA* homolog from *Thermotoga maritima*, is proposed to encode an epimerase that interconverts D-mannonate and D-gluconate (Rodionova et al. 2012). Biochemical studies with purified proteins confirm this suspicion and identify other 2-hydroxyacid racemases including those for malate, phenyllactate, 2-hydroxyglutarate, and less specific short-chain aliphatic 2-hydroxyacids (Desguin et al. 2020). Of additional interest, many cyanobacteria and some other microorganisms possess homologs of *larB*, *larE*, and *larC*, but lack any homologs of *larA*, suggesting these microorganisms may synthesize NPN for incorporation into proteins with a distinct architecture and possibly a unique function.

### 14.4.10 Methyl-S-Coenzyme M Reductase (MCR)

This chapter uses the name methyl-S-coenzyme M reductase (MCR) when referring to the enzyme of methanogenic archaea that forms methane as well as to the protein responsible for anaerobic oxidation of methane and short-chain alkanes in syntrophic methano(alkano)trophs. Excellent recent overviews of MCR including its proposed enzyme mechanism are available (Ragsdale et al. 2017; Thauer 2019).

#### 14.4.10.1 Nickel-Containing MCR of Methanogenic and Methanotrophic Archaea

Methanogenic archaea reduce CO<sub>2</sub> to methane by a pathway that includes the intermediate methyl-S-coenzyme M (methyl-S-CoM) (Taylor and Wolfe 1974). In addition, selected methanogen strains are capable of metabolizing CO, formate, methanol, methylamine, and acetic acid by pathways that also form this key chemical species (Thauer 1998). In all cases, methane release involves the action of MCR that reacts methyl-S-CoM with 7-mercaptoheptanoylthreonine phosphate (coenzyme B, HS-CoB) (Noll et al. 1986) to form the mixed disulfide CoM-S-S-CoB (Fig. 14.5j) (Bobik et al. 1987; Ellermann et al. 1988). The  $\alpha_2\beta_2\gamma_2$  enzyme associated with MCR activity (Fig. 14.6j) was first isolated from *Methanothermobacter thermoautotrophicus* (formerly *Methanobacterium thermoautotrophicum*  $\Delta$ H) and shown to contain nickel based on the incorporation of radioactive <sup>63</sup>Ni (Ellefson and Wolfe 1981; Ellefson et al. 1982). Numerous subsequent biochemical and spectroscopic studies of MCR have used the enzyme from this species and from *Methanothermobacter marburgensis* (formerly *Methanobacterium thermoautotrophicum* strain Marburg). Some methanogens possess multiple forms of MCR that are regulated differently (Rospert et al. 1990) and have distinct catalytic properties (Bonacker et al. 1993). The nickel of MCR is associated with a yellow organometallic cofactor named coenzyme F430 that occurs as protein-associated and free forms, with subtle differences in their spectra (Hausinger et al. 1984). An extensive series of studies ((Pfaltz et al. 1985) and earlier citations) identified the structure of coenzyme F430 as a highly reduced and

modified nickel-containing tetrapyrrole (see inset to Fig. 14.6j). Notably, derivatives of this cofactor exist in other methanogens and in anaerobic methanotrophs, as described below (Allen et al. 2014).

Microbial mats associated with anaerobic methane seeps in the Black Sea possess an abundant microorganism that contains an MCR-like protein with a nickel-containing cofactor resembling F430 (Krüger et al. 2003). This cofactor structure is the same as the methanogen-derived F430 except for the added presence of a methylthio group on the methylene carbon adjacent to the keto group in the carbocyclic ring (Mayr et al. 2008). The enzyme containing the modified cofactor is proposed to catalyze a reverse methanogenesis reaction (Shima and Thauer 2005), resulting in the anaerobic oxidation of methane. Indeed, *M. marburgensis* MCR also catalyzes this reverse reaction when subjected to appropriate experimental conditions (Scheller et al. 2010). Remarkably, MCR homologs in members of the *Candidatus* Syntrophoarchaeum, *Candidatus* Methanoliparia, *Candidatus* Ethanoperedens, and other genera of archaea are capable of specifically catalyzing the anaerobic oxidation of short chain alkanes, including butane and ethane (Chen et al. 2019; Hahn et al. 2020; Laso-Pérez et al. 2016, 2019; Wang et al. 2019, 2020).

#### 14.4.10.2 Structure of Methyl-S-Coenzyme M Reductase

The first reported MCR structure was that from *M. marburgensis* (Fig. 14.6j) (Ermler et al. 1997). Additional MCR structures have been elucidated from other methanogens [e.g. (Grabarse et al. 2000)] and from the Black Sea mat methanotroph (Shima et al. 2012). The structures are quite similar; e.g., each is an  $\alpha_2\beta_2\gamma_2$  enzyme with HS-CoB-binding channels that lead to the buried coenzyme F430. Of additional interest, multiple amino acid residues in these proteins are enzymatically derivatized, with at least some of the modifications affecting the activity of the enzyme (Lyu et al. 2020; Nayak et al. 2017, 2020; Selmer et al. 2000). Depending on the microbial source, highly specific changes include methylations (of histidine, arginine, glutamine, and cysteine), thioamidation (of glycine), desaturation (of aspartic acid), and hydroxylation (of tryptophan or methionine) [reviewed in (Chen et al. 2020)].

#### 14.4.10.3 Biosynthesis of Coenzyme F430

The biosynthetic pathway for coenzyme F430 has long been known to begin with L-glutamic acid, with initial steps progressing through glutamyl-tRNA, glutamate 1-semialdehyde, 5-aminolevulinic acid, porphobilinogen, uroporphyrinogen III, and dihydrosirohydrochlorin [reviewed in Thauer and Bonacker (1994)]. In addition, early studies reported the purification and mass spectrometric identification of the intermediate 15,17<sup>3</sup>-seco-F430-17<sup>3</sup>-acid (Pfaltz et al. 1987). A critical breakthrough in further understanding the pathway derived from genomic analyses that revealed a cluster of five genes in methanogens and anaerobic methanotrophs with potentially relevant functions. The genes within the *cfbAEDCB* cluster of

*Methanosarcina acetivorans* C2A or the alternately named *cfbABCDE* cluster of *M. barkeri* were demonstrated to encode enzymes catalyzing the reactions shown in Fig. 14.11 (Moore et al. 2017). Thus (using the nomenclature of the first report), CfbA incorporates nickel into sirohydrochlorin, CfbB converts two acetate side chains to acetamides, CfbC and CfbD together reduce the diamide-containing tetrapyrrole by six electrons and convert one amide to a lactam ring, and CfbE converts a propionate side chain into a cyclohexanone ring. In methanotrophs and some methanogens additional modifications occur by still unclear processes (Allen et al. 2014). It is uncertain how the resulting coenzyme species are incorporated into the corresponding MCR proteins.

#### 14.4.11 Other Nickel Enzymes

It is likely that other nickel-containing enzymes exist, and experimental evidence already points to some probable representatives. For example, *Bacillus subtilis* AraM is a glycerol-1-phosphate dehydrogenase that depends on nickel for greatest activity and co-purifies with nickel from cells grown on LB medium supplemented with 1 mM of this metal ion (Guldan et al. 2008). Two chromatographically-resolved proteins from cell-free extracts of *Pyrococcus furiosus* contain nickel, but no enzymatic activity has been demonstrated (Cvetkovic et al. 2010). PF0056, a possible sugar-binding protein, binds 0.47 Ni/subunit and is predicted to possess a cupin fold that coordinates the metal using three histidine and one glutamate residues (much like the quercetinase structure, Sect. 14.4.3). PF0086 is annotated as an alanyl-tRNA editing hydrolase and is predicted to bind its metal (0.86 Ni/subunit) using three histidine and one cysteine residue. None of these proteins has been extensively characterized and their structures have not been determined.

One must use caution when claiming an enzyme is nickel dependent. A nice illustration of this point is provided by peptide deformylase, the enzyme responsible for removal of the *N*-formyl group from the amino terminal methionine residue of newly synthesized proteins. Early studies had suggested the *E. coli* protein contains an active site zinc ion; however, substantial increases in enzyme activity occur when this enzyme is isolated from cells grown in the presence of nickel (Ragusa et al. 1998). The stable nickel-containing protein was extensively characterized, including determination of its structure (Becker et al. 1998). Nevertheless, compelling evidence was later generated that the native enzyme contains ferrous ion, which undergoes rapid inactivation by oxygen due to conversion to the non-functional ferric species (Rajagopalan and Pei 1998).



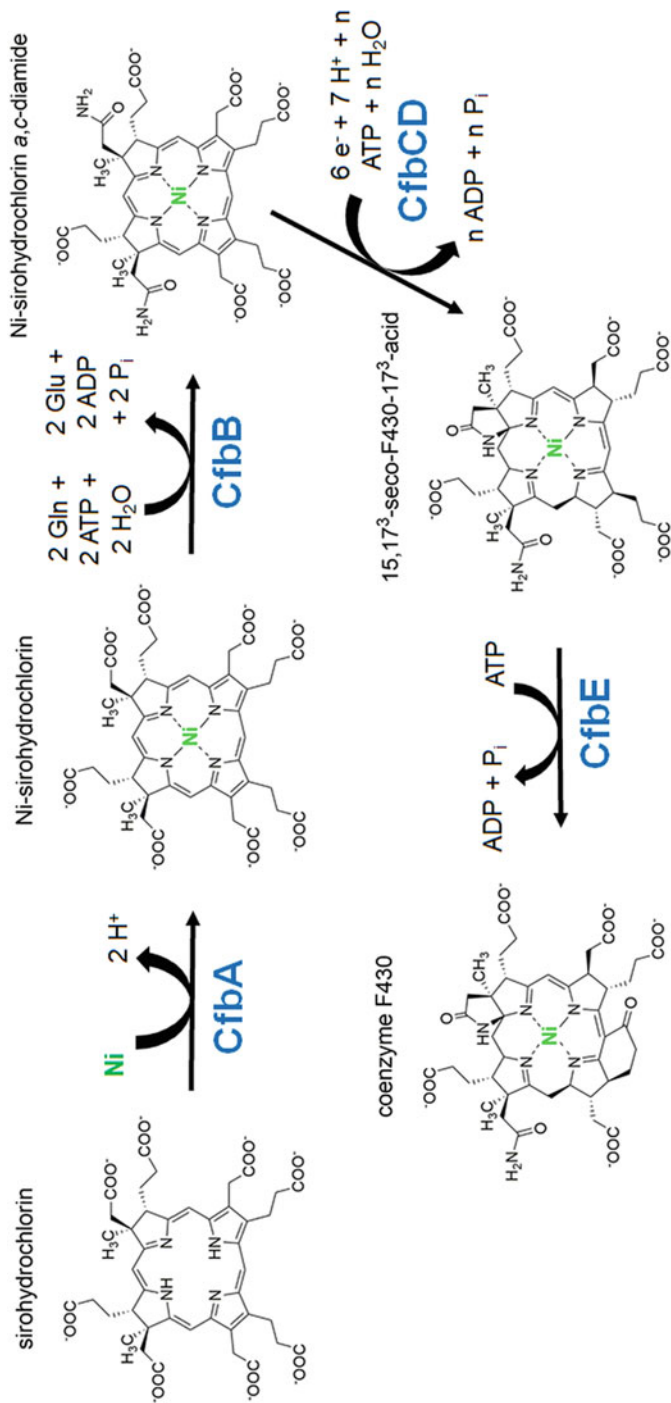


**Fig. 14.11** Biosynthesis of coenzyme F430. CfbA inserts nickel into sirohdrochlorin with the loss of two protons. CfbB converts two carboxylic acid side chains into amides via ATP-dependent activation and nitrogen transfer from glutamine. CfbC and CfbD catalyze a six-electron reduction of the nickel-sirohydrochlorin *a,c*-diamide and generate a lactam from one side chain. CfbE forms the carbocyclic ring of the coenzyme in an ATP-dependent reaction

### 14.4.12 Nickel Storage Proteins

Several proteins (HypB, UreE, LarC, SlyD, CooJ, etc.) bind nickel for eventual incorporation into metalloenzymes, and these proteins could also reasonably store the metal within the cell. Unfortunately, experimental support for a nickel storage function is lacking in most cases. The exception might be *B. japonicum* HypB (Sect. 14.4.6.2), named nickelin on the basis of studies that were consistent with such a role (Olson and Maier 2000).

The most extensively-studied and most convincing examples of nickel storage proteins are Hpn (alternatively called Hpn-1) and Hpn-like (Hpn1 or Hpn-2) proteins of *Helicobacter* species. First discovered in *H. pylori*, Hpn is a 60-amino acid long protein (7077 Da) that contains 28 His residues (47%) and tightly binds zinc or nickel (Gilbert et al. 1995). Hpn accounts for up to 2% of the *H. pylori* cellular protein, a feature that is compatible with a role in cellular nickel storage. Analogous proteins are present in *H. mustelae*, *H. felis*, and several other gastric species of this genus (Vinella et al. 2015). Biochemical and spectroscopic studies of the purified protein have demonstrated that *H. pylori* Hpn is multimeric (with the 20-mer being most prevalent), able to coordinate ~5 nickel ions per monomer ( $K \sim 7.1 \mu\text{M}$ ), and also capable of binding zinc and copper (~5 Zn/monomer, 19.3  $\mu\text{M}$ ; ~8.5 Cu/monomer, ~2.2  $\mu\text{M}$ ) (Ge et al. 2006a, b). Deletion of the gene encoding Hpn leads to increased toxicity from nickel ions, consistent with a protective role against nickel stress; furthermore, gene deletion reduces the nickel content of cells whereas gene overexpression results in increased cellular nickel content, indicative of a nickel storage function (Ge et al. 2006a; Vinella et al. 2015). A large subset of Hpn-containing *Helicobacter* strains also produce Hpn-2 (Vinella et al. 2015). This 72-amino acid long protein is rich in His (nearly 25%), but has an even greater percentage of Gln residues (42%) (Seshadri et al. 2007). Gene deletion studies suggested that it too functions in metal detoxification (in this case against nickel, cobalt, and cadmium) and a role in nickel storage was suggested. The purified Hpn-2 protein is oligomeric, like Hpn, and binds ~2 nickel ions per monomer ( $K \sim 3.8 \mu\text{M}$ ) (Zeng et al. 2008). The two nickel-binding sites are distinct, with the region involving His29 to His32 being critical for one binding site, whereas substitutions of other His residues do not affect nickel binding (Zeng et al. 2011). About one atom of copper, cobalt, or zinc also binds per Hpn-2 monomer, consistent with distinct environments for the two nickel sites. Chemical cross-linking studies show that Hpn and Hpn-2 interact with more than 100 proteins in *Helicobacter* cells, including UreA/UreB urease subunits, UreG GTPase, and HypB [NiFe] hydrogenase accessory protein (Saylor and Maier 2018). Overall, these studies reveal that Hpn-type proteins bind nickel, reduce toxicity to this metal, and facilitate activation of nickel enzymes, but a nickel storage role remains less compelling.

## 14.5 Conclusions and Perspectives

Microorganisms have developed a vast array of proteins that function to sense nickel concentrations, import the metal ion when cellular needs are deficient, and export the cation when internal levels are too high. The basis for cellular toxicity by nickel is partially understood, as are the mechanisms used by cells to defend against this harmful metal ion. A number of nickel-containing enzymes have been identified, with several of these enzymes dependent on accessory proteins for their biosynthesis. Nickel storage proteins exist in at least one bacterial genus. Further studies are likely to identify additional nickel-dependent enzymes and are certain to expand our understanding and provide more examples of proteins involved in sensing, transporting, and utilizing.

**Note Added in Proof** During the interval since this chapter was submitted, several relevant publications have appeared; selected examples are mentioned here. With regard to nickel-sensing transcription factors, additional structural and functional insights have been reported for SrnR (Mazzei et al. 2021). Nickel importers and exporters in *H. pylori* were reviewed (Camporesi et al. 2021). The maturation components responsible for activation of nickel-dependent hydrogenase and urease in *H. pylori* were summarized (Tsang and Wong 2022). Dynamics studies were carried out to better characterize a “bucket brigade” mode of nickel movement within the UreF and UreD/H proteins during urease activation (Masetti et al. 2021). Related to CODH activation, 150 homologues of CooJ were identified and three were characterized for nickel binding and other properties (Darrouzet et al. 2021). The structure and mechanism were revealed for LarB, catalyzing the first step of NPN cofactor biosynthesis (Rankin et al. 2021). Newly reported features of LarC, catalyzing the CTP-dependent nickel insertion during NPN cofactor biosynthesis, include formation of a novel reaction intermediate (Turmo et al. 2022). The structure was revealed for an MCR that functions in anaerobic ethane oxidation and contains a modified F430 cofactor (Hahn et al. 2021).

**Acknowledgements** Experimental investigations of microbial nickel metabolism in the Hausinger lab are supported by the National Institutes of Health (GM128959) and the National Science Foundation (CHE-1807073). I thank the many colleagues of my laboratory who have contributed to this work over the years.

## References

- Abreu IA, Cabelli DE (2010) Superoxide dismutases--a review of the metal-associated mechanistic variations. *Biochim Biophys Acta* 1804:263–274
- Adams MWW, Mortenson LE, Chen J-S (1981) Hydrogenase. *Biochim Biophys Acta* 594:105–176
- Addy C, Ohara M, Kawai F, Kidera A, Ikeguchi M, Fuchigami S, Osawa M, Shimada I, Park S-Y, Tame JRH, Heddle JG (2007) Nickel binding to NikA: an additional binding site reconciles spectroscopy, calorimetry and crystallography. *Acta Crystallogr D* 63:221–229

- Ahn B-E, Cha J, Lee E-J, Han A-R, Thompson CJ, Roe J-H (2006) Nur, a nickel-responsive regulator of the Fur family, regulates superoxide dismutases and nickel transport in *Streptomyces coelicolor*. *Mol Microbiol* 59:1848–1858
- Albareda M, Rodrigue A, Brito B, Ruiz-Argüeso T, Imperial J, Mandrand-Berthelot M-A, Palacios J (2015) *Rhizobium leguminosarum* HupE is a highly-specific diffusion facilitator for nickel uptake. *Metallomics* 7:691–701
- Alfano M, Cavazza C (2020) Structure, function, and biosynthesis of nickel-dependent enzymes. *Protein Sci* 29:1071–1089
- Alfano M, Pérard J, Miras R, Catty P, Cavazza C (2018) Biophysical and structural characterization of the putative nickel chaperone CooT from *Carboxydotherrmus hydrogenofmans*. *J Biol Inorg Chem* 23:809–817
- Alfano M, Pérard J, Carpentier P, Basset C, Zambelli B, Timm J, Crouzy S, Ciurli S, Cavazza C (2019a) The carbon monoxide dehydrogenase accessory protein CooJ is a histidine-rich multidomain dimer containing an unexpected Ni(II)-binding site. *J Biol Chem* 294:7601–7614
- Alfano M, Pérard J, Cavazza C (2019b) Nickel-induced oligomerization of the histidine-rich metallochaperone CooJ from *Rhodospirillum rubrum*. *Inorganics* 7:84
- Alfano M, Veronesi G, Musiani F, Zambelli B, Signor L, Proux O, Rovezzi M, Ciurli S, Cavazza C (2019c) A solvent-exposed cysteine forms a peculiar Ni<sup>II</sup>-binding site in the metallochaperone CooT from *Rhodospirillum rubrum*. *Chem Eur J* 25:15351–15360
- Allan CB, Wu L-F, Gu Z, Choudhury SB, Al-Mjeni F, Sharma ML, Mandrand-Berthelot M-A, Maroney MJ (1998) An X-ray absorption spectroscopic structural investigation of the nickel site in *Escherichia coli* NikA protein. *Inorg Chem* 37:5952–5955
- Allen KD, Wegener G, White RH (2014) Discovery of multiple modified F<sub>430</sub> coenzymes in methanogens and anaerobic methanotrophic archaea suggests possible new roles for F<sub>430</sub> in nature. *Appl Environ Microbiol* 80:6403–6412
- Al-Mjeni F, Ju T, Pochapsky TC, Maroney MJ (2002) XAS investigation of the structure and function of Ni in acireductone dioxygenase. *Biochemistry* 41:6761–6769
- An YJ, Ahn B-E, Han A-R, Kim H-M, Chung KM, Shin J-H, Cho Y-B, Roe J-H, Cha S-S (2009) Structural basis for the specialization of Nur, a nickel-specific Fur homolog, in metal sensing and DNA recognition. *Nucleic Acids Res* 37:3442–3451
- Arima J, Iwabuchi M, Hatanaka T (2004) Gene cloning and overproduction of an aminopeptidase from *Streptomyces septatus* TH-2, and comparison with a calcium-activated enzyme from *Streptomyces griseus*. *Biochem Biophys Res Commun* 317:531–538
- Ariza A, Vickers TJ, Greig N, Armour KA, Dixon MJ, Eggleston IM, Fairlamb AH, Bond CS (2006) Specificity of the trypanothione-dependent *Leishmania major* glyoxalase I: structure and biochemical comparison with the human enzyme. *Mol Microbiol* 59:1239–1248
- Ash PA, Kendall-Price SET, Vincent KA (2019) Unifying activity, structure, and spectroscopy of [NiFe] hydrogenases: combining techniques to clarify mechanistic understanding. *Acc Chem Res* 52:3120–3131
- Atherton JC (2006) The pathogenesis of *Helicobacter pylori*-induced gastro-duodenal diseases. *Annu Rev Pathol* 1:63–96
- Babich H, Stotzky G (1983) Toxicity of nickel to microbes: environmental aspects. *Adv Appl Microbiol* 29:195–265
- Balasubramanian A, Ponnuraj K (2010) Crystal structure of the first plant urease from jack bean: 83 years of journey from its first crystal to molecular structure. *J Mol Biol* 400:274–283
- Banaszak K, Martin-Diaconescu V, Bellucci M, Zambelli B, Rypniewski W, Maroney MJ, Ciurli S (2012) Crystallographic and x-ray absorption spectroscopic characterization of *Helicobacter pylori* UreE bound to Ni<sup>2+</sup> and Zn<sup>2+</sup> reveal a role for the disordered C-terminal arm in metal trafficking. *Biochem J* 441:1017–1026
- Barkay T, Miller SM, Summers AO (2003) Bacterial mercury resistance from atoms to ecosystems. *FEMS Microbiol Rev* 27:355–384
- Barondeau DP, Kassman CJ, Bruns CK, Tainer JA, Getzoff ED (2004) Nickel superoxide dismutase structure and mechanism. *Biochemistry* 43:8038–8047

- Bartha R, Ordal EJ (1965) Nickel-dependent chemolithotrophic growth of two *Hydrogenomonas* strains. *J Bacteriol* 89:1015–1019
- Beaton SE, Evans RM, Finney AJ, Lamont CM, Armstrong FA, Sargent F, Carr SB (2018) The structure of hydrogenase-2 from *Escherichia coli*: implications for H<sub>2</sub>-driven proton pumping. *Biochem J* 475:1353–1370
- Becker A, Schlichtling I, Kabsch W, Schultz S, Wagner AFV (1998) Structure of peptide deformylase and identification of the substrate binding site. *J Biol Chem* 273:11413–11416
- Bellucci M, Zambelli B, Musiani F, Turano P, Ciurli S (2009) *Helicobacter pylori* UreE, a urease accessory protein: specific Ni<sup>2+</sup>- and Zn<sup>2+</sup>-binding properties and interaction with its cognate UreG. *Biochem J* 422:91–100
- Benanti EL, Chivers PT (2010) *Geobacter uraniireducens* NikR displays a DNA binding mode distinct from other members of the NikR family. *J Bacteriol* 192:4327–4336
- Beniamino Y, Pesce G, Zannoni A, Roncarati D, Zambelli B (2020) SrnR from *Streptomyces griseus* is a nickel-binding transcriptional activator. *J Biol Inorg Chem* 25:187–198
- Benini S, Rypniewski WR, Wilson KS, Miletti S, Ciurli S, Mangani S (1999) A new proposal for urease mechanism based on the crystal structures of the native and inhibited enzyme from *Bacillus pasteurii*: why urea hydrolysis costs two nickels. *Structure* 7:205–216
- Benini S, Cianci M, Ciurli S (2011) Holo-Ni<sup>2+</sup> *Helicobacter pylori* NikR contains four square-planar nickel-binding sites at physiological pH. *Dalton Trans* 40:7831–7833
- Benoit SL, Maier RJ (2011) UreG (HP0868) is a nickel-binding protein that modulates urease activity in *Helicobacter pylori*. *mBio* 2:1–9
- Benoit SL, Mehta N, Weinberg MV, Maier C, Maier RJ (2007) Interaction between the *Helicobacter pylori* accessory proteins HypA and UreE is needed for urease maturation. *Microbiology* 153:1474–1482
- Benoit SL, McMurry JL, Hill SA, Maier RJ (2012) *Helicobacter pylori* hydrogenase accessory protein HypA and urease accessory protein UreG compete with each other for UreE recognition. *Biochim Biophys Acta* 1820:1519–1525
- Benoit SL, Seshadri S, Lamichhane-Khadka R, Maier RJ (2013) *Helicobacter hepaticus* NikR controls urease and hydrogenase activities via the NikABDE and HH0418 putative nickel import proteins. *Microbiology* 159:136–146
- Benvenuti M, Meneghello M, Guendon C, Jacq-Bailly A, Jeoung J-H, Dobbek H, Léger C, Fourmond V, Dementin S (2020) The two CO-dehydrogenases of *Thermococcus* sp. AM4. *Biochim Biophys Acta* 1861:148188
- Beveridge TJ, Murray RGE (1976) Uptake and retention of metals by cell walls of *Bacillus subtilis*. *J Bacteriol* 127:1502–1518
- Bienert GP, Desguin B, Chaumont F, Hols P (2013) Channel-mediated lactic acid transport: a novel function for aquaglyceroporins in bacteria. *Biochem J* 454:559–570
- Blahut M, Dzul S, Wang S, Kandedgedara A, Grosseohme NE, Stemmler TL, Outten FW (2018) Conserved cysteine residues are necessary for nickel-induced allosteric regulation of the metalloregulatory protein YqjI (NfeR) in *E. coli*. *J Inorg Biochem* 194:123–133
- Blériot C, Effantin G, Lagarde F, Mandrand-Berthelot M-A, Rodrigue A (2011) RcnB is a periplasmic protein essential for maintaining intracellular Ni and Co concentrations in *Escherichia coli*. *J Bacteriol* 193:3785–3793
- Blériot C, Gault M, Gueguen E, Arnoux P, Mandrand-Berthelot M-A, Rodrigue A (2015) Cu binding by the *Escherichia coli* metal-efflux accessory protein RcnB. *Metallomics* 6:1400–1409
- Blokesch M, Rohrmoser M, Rode S, Böck A (2004) HybF, a zinc-containing protein involved in NiFe hydrogenase biosynthesis. *J Bacteriol* 186:2603–2611
- Bloom SB, Zamble DB (2004) Metal-selective DNA-binding response of *Escherichia coli* NikR. *Biochemistry* 43:10029–10038
- Bobik TA, Olson KD, Noll KN, Wolfe RS (1987) Evidence that the heterodisulfide of coenzyme M and 7-mercaptoheptanoylthreonine phosphate is a product of the methylreductase reaction in *Methanobacterium*. *Biochem Biophys Res Commun* 149:455–460

- Böck A, King PW, Blokesch M, Posewitz MC (2006) Maturation of hydrogenases. *Adv Microb Physiol* 51:1–71
- Boer JL, Quiroz-Valenzuela S, Anderson KL, Hausinger RP (2010) Mutagenesis of *Klebsiella aerogenes* UreG to probe nickel binding and interactions with other urease-related proteins. *Biochemistry* 49:5859–5869
- Boer JL, Mulrooney SB, Hausinger RP (2014) Nickel-dependent metalloenzymes. *Arch Biochem Biophys* 544C:142–152
- Bonacker LG, Baudner S, Mörschel E, Böcher R, Thauer RK (1993) Properties of the two isoenzymes of methyl-coenzyme M reductase in *Methanobacterium thermoautotrophicum*. *Eur J Biochem* 217:587–595
- Bonam D, Ludden PW (1987) Purification and characterization of carbon monoxide dehydrogenase, a nickel, zinc, iron-sulfur protein, from *Rhodospirillum rubrum*. *J Biol Chem* 262:2980–2987
- Bonam D, McKenna MC, Stephens PJ, Ludden PW (1988) Nickel-deficient carbon monoxide dehydrogenase from *Rhodospirillum rubrum*: *in vivo* and *in vitro* activation by exogenous nickel. *Proc Natl Acad Sci U S A* 85:31–35
- Bossè JT, Gilmour HD, MacInnes JI (2001) Novel genes affecting urease activity in *Actinobacillus pleuropneumoniae*. *J Bacteriol* 183:1242–1247
- Brauer AL, Learman BS, Armbruster CE (2020) Ynt is the primary nickel import system used by *Proteus mirabilis* and specifically contributes to fitness by supplying nickel for urease activity. *Mol Microbiol* 114:185–199
- Braun V, Hantke K (2011) Recent insights into iron import by bacteria. *Curr Opin Chem Biol* 15:328–334
- Brito B, Prieto R-I, Cabrera E, Mandrand-Berthelot M-A, Imperial J, Ruiz-Argüeso T, Palacios J-M (2010) *Rhizobium leguminosarum hupE* encodes a nickel transporter required for hydrogenase activity. *J Bacteriol* 192:925–935
- Bryngelson PA, Arobo SE, Pinkham JL, Cabelli DE, Maroney MJ (2004) Expression, reconstitution, and mutation of recombinant *Streptomyces coelicolor* NiSOD. *J Am Chem Soc* 126:460–461
- Buan NR, Escalante-Semerena JC (2006) Purification and initial biochemical characterization of ATP: cob(I)alamin adenosyltransferase (EutT) enzyme of *salmonella enterica*. *J Biol Chem* 281:16971–16977
- Budnick JA, Prado-Sanchez E, Caswell CC (2018) Defining the regulatory mechanism of NikR, a nickel-responsive transcription regulator, in *Brucella abortus*. *Microbiology* 164:1320–1325
- Burne RA, Chen Y-YM (2000) Bacterial ureases in infectious diseases. *Microbes Infect* 2:533–542
- Bury-Moné S, Thiberg J-M, Contreras M, Maitournam A, Labigne A, De Reuse H (2004) Responsiveness to acidity via metal ion regulators mediates virulence in the gastric pathogen *Helicobacter pylori*. *Mol Microbiol* 53:623–638
- Busenlehner LS, Pennella MA, Giedroc DP (2003) The SmtB/ArsR family of metalloregulatory transcriptional repressors: structural insights into prokaryotic metal resistance. *FEMS Microbiol Rev* 27:131–143
- Campbell DR, Chapman KE, Waldron KJ, Tottey S, Kendall S, Cavallaro G, Andreini C, Hinds J, Stoker NG, Robinson NJ, Cavet JS (2007) Mycobacterial cells have dual nickel-cobalt sensors. Sequence relationships and metal sites of metal-responsive repressors are not congruent. *J Biol Chem* 282:32298–32310
- Campeciño JO, Maroney MJ (2017) Reinventing the wheel: the NiSOD story. In: Zamble D, Rowinska-Zyrek M, Kozlowski H (eds) *The biological chemistry of nickel*. The Royal Society for Chemistry, Cambridge
- Camporesi G, Minzoni A, Morasso L, Ciarli S, Musiani F (2021) Nickel import and export in the human pathogen *Helicobacter pylori*, perspectives from molecular modelling. *Metallomics* 13(12):mfab066. <https://doi.org/10.1093/mtomcs/mfab066>
- Can M, Armstrong FA, Ragsdale SW (2014) Structure, function, and mechanism of the nickel metalloenzymes, CO dehydrogenase, and acetyl-CoA synthase. *Chem Rev* 114:4149–4174

- Carr CE, Foster AW, Maroney MJ (2017a) An XAS investigation of the nickel site structure in the transcriptional regulator InrS. *J Inorg Biochem* 177:352–358
- Carr CE, Musiani F, Huang H-T, Chivers PT, Ciurli S, Maroney MJ (2017b) Glutamate ligation in the Ni(II)- and Co(II)-responsive *Escherichia coli* transcriptional regulator, RcnR. *Inorg Chem* 56:6459–6476
- Carter EL, Hausinger RP (2010) Characterization of *Klebsiella aerogenes* urease accessory protein UreD in fusion with the maltose binding protein. *J Bacteriol* 192:2294–2304
- Carter EL, Tronrud DE, Taber SR, Karplus PA, Hausinger RP (2011) Iron-containing urease in a pathogenic bacterium. *Proc Natl Acad Sci U S A* 108:13095–13099
- Cavet JS, Meng W, Pennella MA, Appelhoff RJ, Giedroc DP, Robinson NJ (2002) A nickel-cobalt sensing ArsR-SmtB family repressor: contributions of cytosol and effector binding sites to metal selectivity. *J Biol Chem* 277:38441–38448
- Chai SC, Ju T, Dang M, Goldsmith RB, Maroney MJ, Pochapsky TC (2008) Characterization of metal binding in the active sites of acireductone dioxygenase isoforms from *Klebsiella* ATCC 8724. *Biochemistry* 47:2428–2438
- Chaintreuil C, Rigault F, Moulin L, Jaffré T, Fardoux J, Giraud E, Dreyfus B, Bailly X (2007) Nickel resistance determinants in *Bradyrhizobium* strains from nodules of the endemic New Caledonia legume *Serianthes calycina*. *Appl Environ Microbiol* 73:8018–8022
- Chang Z, Kuchar J, Hausinger RP (2004) Chemical crosslinking and mass spectrometric identification of sites of interaction for UreD, UreF, and urease. *J Biol Chem* 279:15305–15313
- Chapot-Chartier M-P, Kulakauskas S (2014) Cell wall structure and function in lactic acid bacteria. *Microb Cell Factories* 13(Suppl 1):59
- Chen Y-YM, Burne RA (2003) Identification and characterization of the nickel uptake system for urease biosynthesis in *Streptococcus salivarius* 57.I. *J Bacteriol* 185:6773–6779
- Chen YP, Dilworth MJ, Glenn AR (1984) Aromatic metabolism in *Rhizobium trifolii* - protocatechuate 3,4-dioxygenase. *Arch Microbiol* 138:187–190
- Chen YP, Glenn AR, Dilworth MJ (1985) Aromatic metabolism in *Rhizobium trifolii* - catechol 1,2-dioxygenase. *Arch Microbiol* 141:225–228
- Chen S-C, Musat N, Lechtenfeld OJ, Paschke H, Schmidt M, Said N, Popp D, Calabrese F, Stryhanyuk H, Jaekel U, Zhu Y-G, Joye SB, Richnow H-H, Widdel F, Musat F (2019) Anaerobic oxidation of ethane by archaea from a marine hydrocarbon seep. *Nature* 568:108–111
- Chen H, Gan Q, Fan C (2020) Methyl-coenzyme M reductase and its post-translational modifications. *Front Microbiol* 11:578356
- Cheng Z, Wei YYC, Sung WWL, Glick BR, McConkey BJ (2009) Proteomic analysis of the response of the plant growth-promoting bacterium *Pseudomonas putida* UW4 to nickel stress. *Proteome Sci* 7:18
- Cheng T, Li H, Xia W, Jin L, Sun H (2016) Exploration into the nickel ‘microcosmos’ in prokaryotes. *Coord Chem Rev* 311:24–37
- Cherrier MV, Martin L, Cavazza C, Jacquamet L, Lemaire D, Gaillard J, Fontecilla-Camps JC (2005) Crystallographic and spectroscopic evidence for high affinity binding of FeEDTA (H<sub>2</sub>O)<sup>-</sup> to the periplasmic nickel transporter NikA. *J Am Chem Soc* 127:10075–10082
- Cherrier MV, Cavazza C, Bochet C, Lemaire D, Fontecilla-Camps JC (2008) Structural characterization of a putative endogenous metal chelator in the periplasmic nickel transporter NikA. *Biochemistry* 47:9937–9943
- Chivers PT (2015) Nickel recognition by bacterial importer proteins. *Metallomics* 7:590–595
- Chivers PT (2017) Nickel regulation. In: Zamble DB, Rowinska-Zyrek M, Kozłowski H (eds) *The biological chemistry of nickel*. Royal Society of Chemistry, Cambridge
- Chivers PT, Sauer RT (2000) Regulation of high affinity nickel uptake in bacteria. Ni<sup>2+</sup>-dependent interaction of NikR with wild-type and mutant operator sites. *J Biol Chem* 275:19735–19741
- Chivers PT, Sauer RT (2002) NikR repressor: high-affinity nickel binding to the C-terminal domain regulates binding to operator DNA. *Chem Biol* 9:1141–1148

- Chivers PT, Tahirov TH (2005) Structure of *Pyrococcus horikoshii* NikR: nickel sensing and implications for the regulation of DNA recognition. *J Mol Biol* 348:597–607
- Chivers PT, Benanti EL, Heil-Chapdelaine V, Iwig JS, Rowe JL (2012) Identification of Ni-(L-His)<sub>2</sub> as the substrate for NikABCDE-dependent nickel uptake in *Escherichia coli*. *Metallomics* 4:1043–1050
- Choudhury SB, Lee J-W, Davidson G, Yim Y-I, Bose K, Sharma ML, Kang S-O, Cabelli DE, Maroney MJ (1999) Examination of the nickel site structure and reaction mechanism in *Streptomyces seoulensis* superoxide dismutase. *Biochemistry* 38:3744–3752
- Chung H-Y, Choi J-H, Kim E-J, Cho Y-H, Roe J-H (1999) Negative regulation of the gene for Fe-containing superoxide dismutase by an Ni-responsive factor in *Streptomyces coelicolor*. *J Bacteriol* 181:7381–7384
- Clugston SL, Barnard JFJ, Kinach R, Miedema D, Ruman R, Daub E, Honek JF (1998) Overproduction and characterization of a dimeric non-zinc glyoxylase I from *Escherichia coli*: evidence for optimal activation by nickel ions. *Biochemistry* 37:8754–8763
- Cohen SE, Brignole EJ, Wittenborn EC, Can M, Thompson S, Ragsdale SW, Drennan CL (2020) Negative-stain electron microscopy reveals dramatic structural rearrangements in Ni-Fe-S-dependent carbon monoxide dehydrogenase/acetyl-CoA synthase. *Structure* 28:1–7
- Collins CM, D’Orazio SEF (1993) Bacterial ureases: structure, regulation of expression and role in pathogenesis. *Mol Microbiol* 9:907–913
- Colpas GJ, Hausinger RP (2000) *In vivo* and *in vitro* kinetics of metal transfer by the *Klebsiella aerogenes* urease nickel metallochaperone, UreE. *J Biol Chem* 275:10731–10737
- Colpas GJ, Brayman TG, McCracken J, Pressler MA, Babcock GT, Ming L-J, Colangelo CM, Scott RA, Hausinger RP (1998) Spectroscopic characterization of metal binding by *Klebsiella aerogenes* UreE urease accessory protein. *J Biol Inorg Chem* 3:150–160
- Colpas GJ, Brayman TG, Ming L-J, Hausinger RP (1999) Identification of metal-binding residues in the *Klebsiella aerogenes* urease nickel metallochaperone, UreE. *Biochemistry* 38:4078–4088
- Constant P, Chowdhury SP, Pratscher J, Conrad R (2010) *Streptomyces* contributing to atmospheric molecular hydrogen soil uptake are widespread and encode a putative high-affinity [NiFe]-hydrogenase. *Environ Microbiol* 12:821–829
- Constant P, Chowdhury SP, Hesse L, Pratscher J, Conrad R (2011) Genome data mining and soil survey for the novel group 5 [NiFe]-hydrogenase to explore the diversity and ecological importance of presumptive high-affinity H<sub>2</sub>-oxidizing bacteria. *Appl Environ Microbiol* 77:6027–6035
- Contreras M, Thiberge J-M, Mandrand-Berthelot M-A, Labigne A (2003) Characterization of the roles of NikR, a nickel-responsive pleiotropic autoregulator of *Helicobacter pylori*. *Mol Microbiol* 49:947–963
- Covacci A, Telford JL, Del Giudice G, Parsonet J, Rappuoli R (1999) *Helicobacter pylori* virulence and genetic geography. *Science* 284:1328–1333
- Cubillas C, Vinuesa P, Tabche ML, Garcia-de los Santos A (2013) Phylogenomic analysis of cation diffusion facilitator proteins uncovers Ni<sup>2+</sup>/Co<sup>2+</sup> transporters. *Metallomics* 5:1634–1643
- Cunha ES, Chen X, Sanz-Gaitero M, Mills DJ, Luecke H (2021) Cryo-EM structure of *helicobacter pylori* urease with an inhibitor in the active site at 2.0 Å resolution. *Nat Commun* 12:230
- Cussac V, Ferrero RL, Labigne A (1992) Expression of *Helicobacter pylori* urease genes in *Escherichia coli* grown under nitrogen-limiting conditions. *J Bacteriol* 174:2466–2473
- Cvetkovic A, Menon AL, Thorgersen MP, Scott JW, Poole FL II, Jenney FE Jr, Lancaster WA, Praissman JA, Shanmukh S, Vaccaro BJ, Trauger SA, Kalisiak E, Apon JV, Siuzdak G, Yannone SM, Tainer JA, Adams MWW (2010) Microbial metalloproteomes are largely uncharacterized. *Nature* 466:779–782
- Dai Y, Wensink PC, Abeles RH (1999) One protein, two enzymes. *J Biol Chem* 274:1193–1195
- Darnault C, Volbeda A, Kim EJ, Legrand P, Vernède X, Lindahl PA, Fontecilla-Camps JC (2003) NiZn[Fe<sub>4</sub>S<sub>4</sub>] and NiNi[Fe<sub>4</sub>S<sub>4</sub>] clusters in closed and open a subunits of acetyl-CoA synthase/carbon monoxide dehydrogenase. *Nat Struct Mol Biol* 10:271–279



- Darrouzet E, Rinaldi C, Zambelli B, Ciurli S, Cavazza C (2021) Revisiting the CooJ family, a potential chaperone for nickel delivery to [NiFe]-carbon monoxide dehydrogenase. *J Inorg Biochem* 225:111588. <https://doi.org/10.1016/j.jinorgbio.2021.111588>
- Davidson G, Clugston SL, Honek JF, Maroney MJ (2000) XAS investigation of the nickel active site structure in *Escherichia coli* glyoxalase I. *Inorg Chem* 39:2962–2963
- Davidson G, Clugston SL, Honek JF, Maroney MJ (2001) An XAS investigation of product and inhibitor complexes of Ni-containing GlxI from *Escherichia coli*: mechanistic implications. *Biochemistry* 40:4569–4582
- Davis GS, Flannery EL, Mobley HLT (2006) *Helicobacter pylori* HP1512 is a nickel-responsive NikR-regulated outer membrane protein. *Infect Immun* 74:6811–6820
- de Pina K, Navarro C, McWalter L, Boxer DH, Price NC, Kelly SM, Mandrand-Berthelot M-A, Wu L-F (1995) Purification and characterization of the periplasmic nickel-binding protein NikA of *Escherichia coli* K12. *Eur J Biochem* 227:857–865
- de Pina K, Desjardin V, Mandrand-Berthelot M-A, Giordano G, Wu L-F (1999) Isolation and characterization of the *nikR* gene encoding a nickel-responsive regulator in *Escherichia coli*. *J Bacteriol* 181:670–674
- Debussche L, Couder M, Thibaut D, Cameron B, Crouzet J, Blanche F (1992) Assay, purification, and characterization of cobaltochelatase, a unique complex catalyzing cobalt insertion in hydrogenobyrinic acid a,c-diamide during coenzyme B12 biosynthesis in *Pseudomonas denitrificans*. *J Bacteriol* 174:7445–7451
- Degen O, Kobayashi M, Shimizu S, Eitinger T (1999) Selective transport of divalent cations by transition metal permeases: the *Alcaligenes eutrophus* HoxN and the *Rhodococcus rhodochrous* NhlF. *Arch Microbiol* 171:139–145
- Delany I, Ieva R, Soragni A, Hillerlingmann M, Rappuoli R, Scarlato V (2005) In vitro analysis of protein-operator interactions of the NikR and Fur metal-responsive regulators of coregulated genes in *Helicobacter pylori*. *J Bacteriol* 187:7703–7715
- Denic M, Turlin E, Michel V, Fischer F, Khorasani-Motlagh M, Zamble D, Vinella D, de Reuse H (2021) A novel mode of control of nickel uptake by a multifunctional metallochaperone. *PLoS Pathog* 17:e1009193
- Desguin B, Goffin P, Viaene E, Kleerebezem M, Martin-Diaconescu V, Maroney MJ, Declercq J-P, Soumillion P, Hols P (2014) Lactate racemase is a nickel-dependent enzyme activated by a widespread maturation system. *Nat Commun* 5:3615
- Desguin B, Goffin P, Bakouche N, Diman A, Viaene E, Dandoy D, Fontaine L, Hallet B, Hols P (2015a) Enantioselective regulation of lactate racemization by LarR in *Lactobacillus plantarum*. *J Bacteriol* 197:219–330
- Desguin B, Zhang T, Soumillion P, Hols P, Hu J, Hausinger RP (2015b) A tethered niacin-derived pincer complex with a nickel-carbon bond in lactate racemase. *Science* 349:66–69
- Desguin B, Soumillion P, Hols P, Hausinger RP (2016) Nickel-pincer cofactor biosynthesis involves LarB-catalyzed pyridinium carboxylation and LarE-dependent sacrificial sulfur insertion. *Proc Natl Acad Sci U S A* 113:5598–5603
- Desguin B, Soumillion P, Hols P, Hu J, Hausinger RP (2017) Lactate racemase and its niacin-derived, covalently-tethered, nickel cofactor. In: Zamble DB, Rowinska-Zyrek M, Kozlowski H (eds) *The biological chemistry of nickel*. Royal Society of Chemistry, Cambridge
- Desguin B, Fellner M, Riant O, Hu J, Hausinger RP, Hols P, Soumillion P (2018) Biosynthesis of the nickel-pincer nucleotide cofactor of lactate racemase requires a CTP-dependent cyclometallase. *J Biol Chem* 293:12303–12317
- Desguin B, Urdiain-Arraiza J, Da Costa M, Fellner M, Hu J, Hausinger RP, Desmet T, Hols P, Soumillion P (2020) Uncovering a superfamily of nickel-dependent hydroxyacid racemases and epimerases. *Sci Rep* 10:18123
- Deshpande A, Pochapsky TC, Ringe D (2017) The metal drives the chemistry: dual functions of acireductone dioxygenase. *Chem Rev* 117:10474–10501
- Dian C, Schauer K, Kapp U, McSweeney SM, Labigne A, Terradot L (2006) Structural basis of the nickel response in *Helicobacter pylori*: crystal structures of HpNikR in apo and nickel-bound states. *J Mol Biol* 361:715–730

- Diederix REM, Fauquant C, Rodrigue A, Mandrand-Berthelot M-A, Michaud-Soret I (2008) Sub-micromolar affinity of *Escherichia coli* NikR for Ni(II). *Chem Commun* 1813–1815
- Dixon NE, Gazzola C, Blakeley RL, Zerner B (1975) Jack bean urease (EC 3.5.1.5). A metalloenzyme. A simple biological role for nickel? *J Am Chem Soc* 97:4131–4133
- Dobbek H, Svetlitchnyi V, Gremer L, Huber R, Meyer O (2001) Crystal structure of a carbon monoxide dehydrogenase reveals a [Ni-4Fe-5S] cluster. *Science* 293:1281–1285
- Dokpikul T, Chaoprasid P, Saninjuk K, Sirirakphaisarn S, Johnrod J, Nookabkaew S, Sukhawilit R, Mongkolsuk S (2016) Regulation of the cobalt/nickel efflux operon *dmeRF* in *Agrobacterium tumefaciens* and a link between the iron-sensing regulator RirA and cobalt/nickel resistance. *Appl Environ Microbiol* 82:4732–4742
- Domnik L, Merrouch M, Goetzl S, Jeoung J-H, Léger C, Dementin S, Fourmond V, Dobbek H (2017) CODH-IV: a high-efficiency CO-scavenging CO dehydrogenase with resistance to O<sub>2</sub>. *Angew Chem Int Ed* 56:15466–15469
- Dosanjh NS, West AL, Michel SL (2009) *Helicobacter pylori* NikR's interaction with DNA: a two-tiered mode of recognition. *Biochemistry* 48:527–536
- Doukov TI, Iverson TM, Seravalli J, Ragsdale SW, Drennan CL (2002) A Ni-Fe-Cu center in a bifunctional carbon monoxide dehydrogenase/acetyl-CoA synthase. *Science* 298:567–272
- Doukov TI, Blasiak LC, Seravalli J, Ragsdale SW, Drennan CL (2008) Xenon in and at the end of the tunnel of bifunctional carbon monoxide dehydrogenase/acetyl-CoA synthase. *Biochemistry* 47:3474–3483
- Drennan CL, Heo J, Sintchak MD, Schreiter E, Ludden PW (2001) Life on carbon monoxide: X-ray structure of *Rhodospirillum rubrum* Ni-Fe-S carbon monoxide dehydrogenase. *Proc Natl Acad Sci U S A* 98:11973–11978
- Dupont CL, Neupane K, Shearer J, Palenik B (2008) Diversity, function and evolution of genes coding for putative Ni-containing superoxide dismutases. *Environ Microbiol* 10:1831–1843
- Dupont CL, Johnson DA, Phillippy K, Paulsen IT, Brahamsha B, Palenik B (2012) Genetic identification of a high-affinity Ni transporter and the transcriptional response to Ni deprivation in *Synechococcus* sp. strain WH8102. *Appl Environ Microbiol* 78:7822–7832
- D'Urzo A, Santambrogio C, Grandori R, Ciurli S, Zambelli B (2014) The conformational response to Zn(II) and Ni(II) binding of *Sporosarcina pasteurii* UreG, an intrinsically disordered GTPase. *J Biol Inorg Chem* 19:1341–1354
- Eberz G, Eitinger T, Friedrich B (1989) Genetic determinants of a nickel-specific transport system are part of the plasmid-encoded hydrogenase gene cluster in *Alcaligenes eutrophus*. *J Bacteriol* 171:1340–1345
- Eitinger T (2004) In vivo production of active nickel superoxide dismutase from *Prochlorococcus marinus* MIT9313 is dependent on its cognate peptidase. *J Bacteriol* 186:7812–7825
- Eitinger T, Friedrich B (1991) Cloning, nucleotide sequence, and heterologous expression of the high-affinity nickel transport gene from *Alcaligenes eutrophus*. *J Biol Chem* 266:3222–3227
- Eitinger T, Friedrich B (1994) A topological model for the high-affinity nickel transporter of *Alcaligenes eutrophus*. *Mol Microbiol* 12:1025–1032
- Eitinger T, Mandrand-Berthelot M-A (2000) Nickel transport systems in microorganisms. *Arch Microbiol* 173:1–9
- Eitinger T, Wolfram L, Degen O, Anthon C (1997) A Ni<sup>2+</sup> binding motif is the basis of high affinity transport of the *Alcaligenes eutrophus* nickel permease. *J Biol Chem* 272:17139–17144
- Eitinger T, Degen O, Böhnke U, Müller M (2000) Nic1p, a relative of bacterial transition metal permeases in *Schizosaccharomyces pombe*, provides nickel ion for urease biosynthesis. *J Biol Chem* 275:18029–18033
- Eitinger T, Suhr J, Moore L, Smith JAC (2005) Secondary transporters for nickel and cobalt ions: theme and variations. *Biometals* 18:399–405
- Ellefson WL, Wolfe RS (1981) Component C of the methylreductase system of *Methanobacterium*. *J Biol Chem* 256:4259–4262
- Ellefson WL, Whitman WB, Wolfe RS (1982) Nickel-containing factor F<sub>430</sub>: chromophore of the methylreductase of *Methanobacterium*. *Proc Natl Acad Sci U S A* 79:3707–3710

- Ellermann J, Hedderich R, Böcher R, Thauer RK (1988) The final step in methane formation. Investigations with the highly purified methyl-CoM reductase (component C) from *Methanobacterium thermoautotrophicum* (strain Marburg). Eur J Biochem 172:669–677
- Englert DL, Adase CA, Jayaraman A, Manson MD (2010) Repellent taxis in response to nickel ion requires neither Ni<sup>2+</sup> transport nor the periplasmic NikA binding protein. J Bacteriol 192:2633–2637
- Ensign SA, Campbell MJ, Ludden PW (1990) Activation of the nickel-deficient carbon monoxide dehydrogenase from *Rhodospirillum rubrum*: kinetic characterization and reductant requirement. Biochemistry 29:2162–2168
- Ermler U, Grabarse W, Shima S, Goubeaud M, Thauer RK (1997) Crystal structure of methyl-coenzyme M reductase: the key enzyme of biological methane formation. Science 278:1457–1462
- Ernst FD, Kuipers EJ, Heijens A, Sarwari R, Stoof J, Penn CW, Kusters JG, van Vliet AH (2005) The nickel-responsive regulator NikR controls activation and repression of gene transcription in *Helicobacter pylori*. Infect Immun 73:7252–7258
- Ernst FD, Stoof J, Horrevoets WM, Kuipers EJ, Kusters JG, Van Vliet AHM (2006) NikR mediates nickel-responsive transcriptional repression of the *Helicobacter pylori* outer membrane proteins FecA3 (HP1400) and FrpB4 (HP1512). Infect Immun 74:6821–6828
- Eschweiler JD, Farrugia MA, Hausinger RP, Ruotolo BT (2018) A structural model of the urease activation complex derived from ion mobility-mass spectrometry and integrative modeling. Structure 26:599–606
- Farrugia MA, Han L, Zhong Y, Boer JL, Ruotolo BT, Hausinger RP (2013a) Analysis of a soluble (UreD:UreF:UreG)<sub>2</sub> accessory protein complex and its interactions with *Klebsiella aerogenes* urease by mass spectrometry. J Am Soc Mass Spectrom 24:1328–1337
- Farrugia MA, Macomber L, Hausinger RP (2013b) Biosynthesis of the urease metallocenter. J Biol Chem 288:13178–13185
- Farrugia MA, Wang B, Feig M, Hausinger RP (2015) Mutational and computational evidence that a nickel-transfer tunnel in UreD is used for activation of *Klebsiella aerogenes* urease. Biochemistry 54:6392–6401
- Fellner M, Desguin B, Hausinger RP, Hu J (2017) Structural insights into the catalytic mechanism of a sacrificial sulfur insertase of the N-type ATP pyrophosphatase family, LarE. Proc Natl Acad Sci U S A 114:9074–9079
- Fetzner S (2012) Ring-cleaving dioxygenases with a cupin fold. Appl Environ Microbiol 78:2505–2514
- Finkenwirth F, Eitinger T (2019) ECF-type ABC transporters for uptake of vitamins and transition metal ions into prokaryotic cells. Res Microbiol 170:358–365
- Fischer F, Robbe-Saule M, Turlin E, Mancuso F, Michel V, Richaud P, Veyrier FJ, De Reuse H, Vinella D (2016) Characterization in *Helicobacter pylori* of a nickel transporter essential for colonization that was acquired during evolution by gastric *Helicobacter* species. PLoS Pathog 12:e1006018
- Flannigan R, Choi WH, Chew B, Lange D (2014) Renal struvite stones--pathogenesis, microbiology, and management strategies. Nat Rev Urol 11:333–341
- Fong YH, Wong HC, Chuck CP, Chen YW, Sun H, Wong K-B (2011) Assembly of the preactivation complex for urease maturation in *Helicobacter pylori*: crystal structure of the UreF/UreH protein complex. J Biol Chem 286:43241–43249
- Fong YH, Wong HC, Yuen MH, Lau PH, Chen YW, Wong K-B (2013) Structure of UreG/UreF/UreH complex reveals how urease accessory proteins facilitate maturation of *Helicobacter pylori* urease. PLoS Biol 11:e1001678
- Fontecilla-Camps JC, Volbeda A, Cavazza C, Nicolet Y (2007) Structure/function relationships of [NiFe]- and [FeFe]-hydrogenases. Chem Rev 107:4273–4303
- Fortin D, Southam G, Beveridge TJ (1994) Nickel sulfide, iron-nickel sulfide and iron sulfide precipitated by a newly isolated *Desulfotomaculum* species and its relation to nickel resistance. FEMS Microbiol Ecol 14:121–132

- Forzi L, Sawers RG (2007) Maturation of [NiFe]-hydrogenases in *Escherichia coli*. *Biometals* 20: 565–578
- Foster AW, Patterson CJ, Pernil R, Hess CR, Robinson NJ (2012) Cytosolic Ni(II) sensor in cyanobacterium. Nickel detection follows nickel affinity across four families of sensors. *J Biol Chem* 287:12142–12151
- Foster AW, Pernil R, Patterson CJ, Robinson NJ (2014) Metal specificity of cyanobacterial nickel-responsive repressor InrS: cells maintain zinc and copper below the detection threshold for InrS. *Mol Microbiol* 92:797–812
- Foster AW, Pernil R, Patterson CJ, Scott AJP, Palsson LO, Pal R, Cummins I, Chivers PT, Pohl E, Robinson NJ (2017) A light tunable range for Ni(II) sensing and buffering in cells. *Nat Chem Biol* 13:409–414
- Fourcroy AF, Vauguelin LN (1799) Extrait d'un premier mémoire des cit. Fourcroy et Vaugueline poru servir a l'histoire naturelle, chimique et médicale de l'urine humaine, contentant quelques faits nouveaux sur son analyse et son altération spontanée. *Ann Chim* 31:48–71
- Fritsche E, Paschos A, Beisel H-G, Böck A, Huber R (1999) Crystal structure of the hydrogenase maturing endopeptidase HydD from *Escherichia coli*. *J Mol Biol* 288:989–998
- Fu C, Javedan S, Moshiri F, Maier RJ (1994) Bacterial genes involved in incorporation of nickel into a hydrogenase enzyme. *Proc Natl Acad Sci U S A* 91:5099–5103
- Fu C, Olson JW, Maier RJ (1995) HypB protein of *Bradyrhizobium japonicum* is a metal-binding GTPase capable of binding 18 divalent nickel ions per dimer. *Proc Natl Acad Sci U S A* 92: 2333–2337
- Fulkerson JF Jr, Mobley HLT (2000) Membrane topology of the NixA nickel transporter of *Helicobacter pylori*: two nickel transport-specific motifs within transmembrane helices II and III. *J Bacteriol* 182:1722–1730
- Fulkerson JF Jr, Garner RM, Mobley HLT (1998) Conserved residues and motifs in the NixA protein of *Helicobacter pylori* are critical for the high affinity transport of nickel ions. *J Biol Inorg Chem* 273:235–241
- Furukawa K, Ramesh A, Zhou Z, Weinberg Z, Vallery T, Winkler WC, Breaker RR (2015) Bacterial riboswitches cooperatively bind Ni<sup>2+</sup> or Co<sup>2+</sup> ions and control expression of heavy metal transporters. *Mol Cell* 57:1088–1098
- Gadd GM, Griffiths AJ (1978) Microorganisms and heavy metal toxicity. *Microb Ecol* 4:303–317
- García-Domínguez M, López-Maury L, Florencio FJ, Reyes JC (2000) A gene cluster involved in metal homeostasis in the cyanobacterium *Synechocystis* sp. strain PCC 6803. *J Bacteriol* 182: 1507–1514
- Garcin E, Vermede X, Hatchikian EC, Volbeda A, Frey M, Fontecilla-Camps JC (1999) The crystal structure of a reduced [NiFeSe] hydrogenase provides an image of the activated catalytic center. *Structure* 7:557–566
- Ge R, Watt RM, Sun X, Tanner JA, He Q-Y, Huang J-D, Sun H (2006a) Expression and characterization of the histidine-rich protein, Hpn: potential for nickel storage in *Helicobacter pylori*. *Biochem J* 393:285–293
- Ge R, Zhang Y, Sun X, Watt RM, He Q-Y, Huang J-D, Wilcox DE, Sun H (2006b) Thermodynamic and kinetic aspects of metal binding properties of the histidine-rich protein, Hpn. *J Am Chem Soc* 128:11330–11331
- Gencic S, Grahame DA (2003) Nickel in subunit b of the acetyl-CoA decarbonylase/synthase multienzyme complex in methanogens. Catalytic properties and evidence for a binuclear Ni-Ni site. *J Biol Chem* 278:6101–6110
- Geslin C, Llanos J, Prieur D, Jeanthon C (2001) The manganese and iron superoxide dismutases protect *Escherichia coli* from heavy metal toxicity. *Res Microbiol* 152:901–905
- Ghosh S, Sadhukhan PC, Chaudhuri J, Ghosh DK, Mandal A (1999) Purification and properties of mercuric reductase from *Azotobacter chroococcum*. *J Appl Microbiol* 86:7–12
- Ghssein G, Brutesco C, Ouerdane L, Fojcik C, Izaute A, Wang S, Hajjar C, Lobinski R, Lemaire D, Richaud P, Voulhoux R, Espaillet A, Cava F, Pignol D, Borezée-Durant E, Arnoux P (2016) Biosynthesis of a broad-spectrum nicotianamine-like metallophore in *Staphylococcus aureus*. *Science* 352:1105–1109

- Gilbert JV, Ramakrishna J, Sunderman FW Jr, Wright A, Plaut AG (1995) Protein Hpn: cloning and characterization of a histidine-rich metal-binding polypeptide in *Helicobacter pylori* and *Helicobacter mustelae*. *Infect Immun* 63:2682–2688
- Glass JB, Dupont CL (2017) Oceanic nickel biogeochemistry and the evolution of nickel use. In: Zamble DB, Rowinska-Zyrek M, Kozlowski H (eds) *The biological chemistry of nickel*. Royal Society of Chemistry, Cambridge
- Gong W, Hao B, Wei Z, Ferguson DJ Jr, Tallant T, Krzycki JA, Chan MK (2008) Structure of the  $a_2e_2$  Ni-dependent CO dehydrogenase component of the *Methanosarcina barkeri* acetyl-CoA decarbonylase/synthase complex. *Proc Natl Acad Sci U S A* 105:9558–9563
- Gourdon P, Liu X-Y, Skjorringe T, Morth JP, Moller LB, Pedersen BP, Nissen P (2011) Crystal structure of a copper-transporting PIB-type ATPase. *Nature* 475:59–64
- Grabarse W, Mahler F, Shima S, Thauer RK, Ermler U (2000) Comparison of three methyl-coenzyme M reductases from phylogenetically distant microorganisms: unusual amino acid modification, conservation, and adaptation. *J Mol Biol* 303:329–344
- Grahame DA (1991) Catalysis of acetyl-CoA cleavage and tetrahydrofarnesyl methylase by a carbon monoxide dehydrogenase-corrinoid enzyme complex. *J Biol Chem* 266:22227–22233
- Grass G, Grobe C, Nies D (2000) Regulation of the *cnr* cobalt and nickel resistance determinant from *Ralstonia* sp. strain CH34. *J Bacteriol* 182:1390–1398
- Grass G, Fan B, Rosen BP, Lemke K, Schlegel HG, Rensing C (2001) NreB from *Achromobacter xylosoxidans* 31A is a nickel-induced transporter conferring nickel resistance. *J Bacteriol* 183:2803–2807
- Greening C, Biswas A, Carere CR, Jackson CJ, Taylor MC, Stott MB, Cook GM, Morales SE (2016) Genomic and metagenomic surveys of hydrogenase distribution indicate  $H_2$  is a widely utilized energy source for microbial growth and survival. *ISME J* 10:761–777
- Gregg CM, Goetzl S, Jeong J-H, Dobbek H (2016) AcsF catalyzes the ATP-dependent insertion of nickel into the Ni<sub>2</sub>Ni-[4Fe4S] cluster of acetyl-CoA synthase. *J Biol Chem* 291:18129–18138
- Greig N, Wyllie S, Vickers TJ, Fairlamb AH (2006) Trypanothione-dependent glyoxalase I in *Trypanosoma cruzi*. *Biochem J* 400:217–223
- Griffith DP, Musher DM, Itin C (1976) Urease. The primary cause of infection-induced urinary stones. *Investig Urol* 13:346–350
- Grossoehme NE, Mulrooney SB, Hausinger RP, Wilcox DE (2007) Thermodynamics of Ni<sup>2+</sup>, Cu<sup>2+</sup>, and Zn<sup>2+</sup> binding to urease metallochaperone UreE. *Biochemistry* 46:10506–10516
- Guldán H, Sterner R, Babinger P (2008) Identification and characterization of a bacterial glycerol-1-phosphate dehydrogenase: Ni<sup>2+</sup>-dependent AraM from *Bacillus subtilis*. *Biochemistry* 47:7376–7384
- Guo H, Liu H, Wu H, Cui H, Fang J, Zuo Z, Deng J, Li Y, Wang X, Zhao L (2019) Nickel carcinogenesis mechanism: DNA damage. *Int J Mol Sci* 20:4690
- Ha N-C, Oh S-T, Sung JY, Cha KA, Lee MH, Oh B-H (2001) Supramolecular assembly and acid resistance of *Helicobacter pylori* urease. *Nat Struct Biol* 8:505–509
- Hadj-Saïd J, Pandelia M-E, Léger C, Fourmond V, Dementin S (2015) The carbon monoxide dehydrogenase from *Desulfovibrio vulgaris*. *Biochim Biophys Acta* 1847:1574–1583
- Hahn CJ, Laso-Pérez R, Vulcano F, Vaziourakis K-M, Stokke R, Steen IH, Teske A, Boetius A, Liebeke M, Amann R, Knittel K, Wegener G (2020) “*Candidatus* Ethanoperedens,” a thermophilic genus of *archaea* mediating the anaerobic oxidation of ethane. *mBio* 11:e00600–e00620
- Hahn CJ, Lemaire ON, Kahnt J, Engilberge S, Wegener G, Wagner T (2021) Crystal structure of a key enzyme for anaerobic ethane activation. *Science* 373(6550):118–121. <https://doi.org/10.1126/science.abg1765>
- Hall DR, Leonard GA, Reed CD, Watt CI, Berry A, Hunter WN (1999) The crystal structure of *Escherichia coli* class II fructose-1, 6-bisphosphate aldolase in complex with phosphoglycolohydroxamate reveals details of mechanism and specificity. *J Mol Biol* 287:383–394
- Happe RP, Roseboom W, Pierik AJ, Albracht SPJ, Bagley KA (1997) Biological activation of hydrogen. *Nature* 385:126

- Haritha A, Sagar KP, Tiwari A, Kiranmavi P, Rodrigue A, Mohan PM, Singh SS (2009) MrdH, a novel metal resistance determinant of *Pseudomonas putida* KT 2440, is flanked by metal-inducible mobile genetic elements. *J Bacteriol* 191:5976–5987
- Hausinger RP, Orme-Johnson WH, Walsh C (1984) Nickel tetrapyrrole cofactor F430: comparison of the forms bound to methyl coenzyme M reductase and protein free in cells of *Methanobacterium thermoautotrophicum* delta H. *Biochemistry* 23:801–804
- Hausinger RP, Desguin B, Fellner M, Rankin JA, Hu J (2018) Nickel pincer nucleotide cofactor. *Curr Opin Chem Biol* 47:18–23
- He MM, Clugston SL, Honek JF, Matthews BW (2000) Determination of the structure of *Escherichia coli* glyoxylase I suggests a structural basis for differential metal activation. *Biochemistry* 39:8719–8727
- Heddle J, Scott DJ, Unzai S, Park S-Y, Tame JRH (2003) Crystal structures of the liganded and unliganded nickel-binding protein NikA from *Escherichia coli*. *J Biol Chem* 278:50322–50329
- Herr CQ, Hausinger RP (2018) Amazing diversity in biochemical roles of Fe(II)/2-oxoglutarate oxygenases. *Trends Biochem Sci* 43:517–532
- Higgins K (2019) Nickel metalloregulators and chaperones. *Inorganics* 7:104
- Higgins KA, Carr CE, Maroney MJ (2012a) Specific metal recognition in nickel trafficking. *Biochemistry* 51:7816–7832
- Higgins KA, Chivers PT, Maroney MJ (2012b) Role of the N-terminus in determining metal-specific responses in the *E. coli* Ni- and Co-responsive metalloregulator, RcnR. *J Am Chem Soc* 134:7081–7093
- Higuchi Y, Yagi T, Yasuoka N (1997) Unusual ligand structure in Ni-Fe active center and an additional Mg site in hydrogenase revealed by high resolution X-ray structure analysis. *Structure* 5:1671–1680
- Honek JF (2015) Glyoxalase biochemistry. *Biomol Concepts* 6:401–414
- Honek JF (2017) Nickel glyoxalase I. In: Zamble D, Rowinska-Zyrek M, Kozłowski H (eds) The biological chemistry of nickel. The Royal Society of Chemistry, Cambridge
- Howlett RM, Hughes BM, Hitchcock A, Kelly DJ (2012) Hydrogenase activity in the foodborne pathogen *Campylobacter jejuni* depends upon a novel ABC-type nickel transporter (NikZYXWV) and is SlyD-independent. *Microbiology* 158:1645–1655
- Hu HQ, Huang H-T, Maroney MJ (2018) The *Helicobacter pylori* HypA-UreE<sub>2</sub> complex contains a novel high-affinity Ni(II)-binding site. *Biochemistry* 57:2932–2942
- Hurwitz J, Gold M, Anders M (1964) The enzymatic methylation of ribonucleic acid and deoxyribonucleic acid. IV. The properties of the soluble ribonucleic acid-methylating enzymes. *J Biol Chem* 239:3474–3482
- Inoue M, Nakamoto I, Omae K, Oguro T, Ogata H, Yoshida T, Sako Y (2019) Structural and phylogenetic diversity of anaerobic carbon-monoxide dehydrogenases. *Front Microbiol* 9:3353
- Iwig JS, Chivers PT (2009) DNA recognition and wrapping by *Escherichia coli* RcnR. *J Mol Biol* 393:514–526
- Iwig JS, Chivers PT (2010) Coordinating intracellular nickel--metal-site structure-function relationships and the NikR and RcnR repressors. *Nat Prod Rep* 27:658–667
- Iwig JS, Rowe JL, Chivers PT (2006) Nickel homeostasis in *Escherichia coli* - the *rcnR-rcnA* efflux pathway and its linkage to NikR function. *Mol Microbiol* 62:252–262
- Iwig JS, Leitch S, Herbst RW, Maroney MJ, Chivers PT (2008) Ni(II) and Co(II) sensing by *Escherichia coli* RcnR. *J Am Chem Soc* 130:7592–7606
- Iyaka YA (2011) Nickel in soils: a review of its distribution and impacts. *Sci Res Essays* 6:6774–6777
- Jabri E, Karplus PA (1996) Structures of the *Klebsiella aerogenes* urease apoprotein and two active-site mutants. *Biochemistry* 35:10616–10626
- Jabri E, Carr MB, Hausinger RP, Karplus PA (1995) The crystal structure of urease from *Klebsiella aerogenes*. *Science* 268:998–1004
- Jacobi A, Rossman R, Böck A (1992) The *hyp* operon gene products are required for maturation of catalytically active hydrogenase isoenzymes in *Escherichia coli*. *Arch Microbiol* 158:444–451

- Jeon WB, Cheng J, Ludden PW (2001) Purification and characterization of membrane-associated CooC protein and its functional role in the insertion of nickel into carbon monoxide dehydrogenase from *Rhodospirillum rubrum*. *J Biol Chem* 276:38602–38609
- Jeoung J-H, Giese T, Grünwald M, Dobbek H (2009) CooC1 from *Carboxydotherrmus hydrogenoformans* is a nickel-binding ATPase. *Biochemistry* 48:11505–11513
- Jeoung J-H, Giese T, Grünwald M, Dobbek H (2010) Crystal structure of the ATP-dependent maturation factor of Ni,Fe-containing carbon monoxide dehydrogenase. *J Mol Biol* 396:1165–1179
- Jeoung J-H, Nianios D, Fetzner S, Dobbek H (2017) Quercetin 2,4-dioxygenase activates dioxygen in a side-on O<sub>2</sub>-Ni complex. *Angew Chem Int Ed* 55:3281–3284
- Jia B, Jia X, Kim KH, Jeon CO (2017) Integrative view of 2-oxoglutarate/Fe(II)-dependent oxygenase diversity and functions in bacteria. *Biochim Biophys Acta* 1861:323–334
- Jiang D, Zhao Y, Wang X, Fan J, Heng J, Liu X, Feng W, Kang X, Huang B, Liu J, Zhang XC (2013) Structure of the YajR transporter suggests a transport mechanism based on the conserved motif A. *Proc Natl Acad Sci U S A* 110:14664–14669
- Johnson OE, Ryan KC, Maroney MJ, Brunold TC (2010) Spectroscopic and computational investigation of three Cys-to-Ser mutants of nickel superoxide dismutase: insight into the roles played by the Cys2 and Cys6 active-site residues. *J Biol Inorg Chem* 15:777–793
- Joho M, Inouhe M, Tohoyama H, Murayama T (1990) A possible role of histidine in a nickel resistant mechanism of *Saccharomyces cerevisiae*. *FEMS Microbiol Lett* 66:333–338
- Joho M, Ishikawa Y, Kunikane M, Inouhe M, Tohoyama H, Murayama T (1992) The subcellular distribution of nickel in Ni-sensitive and Ni-resistant strains of *Saccharomyces cerevisiae*. *Microbios* 71:149–159
- Jones MD, Zamble DB (2018) Acid-responsive activity of the *Helicobacter pylori* metalloregulator NikR. *Proc Natl Acad Sci U S A* 115:8966–8971
- Jones MD, Ademi I, Yin X, Gong Y, Zamble DB (2015) Nickel-responsive regulation of two novel *Helicobacter pylori* NikR-targeted genes. *Metallomics* 7:662–673
- Ju T, Goldsmith RB, Chai SC, Maroney MJ, Pochapsky SS, Pochapsky TC (2006) One protein, two enzymes revisited: a structural entropy switch interconverts the two isoforms of acireductone dioxygenase. *J Mol Biol* 393:823–834
- Jubier-Maurin V, Rodrigue A, Ouahrani-Bettache S, Layssac M, Mandrand-Bethelot M-A, Köhler S, Liautard J-P (2001) Identification of the *nik* gene cluster of *Brucella suis*: regulation and contribution to urease activity. *J Bacteriol* 183:426–434
- Kalliri E, Grzyska PK, Hausinger RP (2005) Kinetic and spectroscopic investigation of Co<sup>II</sup>, Ni<sup>II</sup>, and *N*-oxalylglycine inhibition of the Fe<sup>II</sup>/α-ketoglutarate dioxygenase, TauD. *Biochem Biophys Res Commun* 338:191–197
- Kaluarachchi H, Chan Chung KC, Zamble DB (2010) Microbial nickel proteins. *Nat Prod Rep* 27: 681–694
- Kaluarachchi H, Zhang JW, Zamble DB (2011) *Escherichia coli* SlyD, more than a Ni(II) reservoir. *Biochemistry* 50:10761–10763
- Kasprzak KS, Salnikow K (2007) Nickel toxicity and carcinogenesis. In: Sigel A, Sigel H, Sigel RKO (eds) *Metal ions in life sciences*. Wiley, New York
- Kerby RL, Ludden PW, Roberts GP (1997) In vivo nickel insertion into carbon monoxide dehydrogenase of *Rhodospirillum rubrum*: molecular and physiological characterization of *cooCTJ*. *J Bacteriol* 179:2259–2266
- Kidd SP, Djoko KY, Ng J, Argente MP, Jennings MP, McEwan AG (2011) A novel nickel responsive MerR-like regulator, NimR, from *Haemophilus influenzae*. *Metallomics* 3:1009–1018
- Kim E-J, Kim H-P, Hah YC, Roe J-H (1996) Differential expression of superoxide dismutases containing Ni and Fe/Zn in *Streptomyces coelicolor*. *Eur J Biochem* 214:178–185
- Kim E-J, Chung H-J, Suh B, Hah YC, Roe J-H (1998a) Expression and regulation of the *sodF* gene encoding iron- and zinc-containing superoxide dismutase in *Streptomyces coelicolor* Müller. *J Bacteriol* 180:2014–2020

- Kim E-J, Chung H-J, Suh B, Hah YC, Roe J-H (1998b) Transcriptional and post-transcriptional regulation by nickel of *sodN* gene encoding nickel-containing superoxide dismutase from *Streptomyces coelicolor* Müller. *Mol Microbiol* 27:187–195
- Kim I-K, Yim Y-I, Kim Y-M, Lee J-W, Yim H-S, Kang S-O (2003a) CbiX-homologous protein (CbiXhp), a metal-binding protein, from *Streptomyces seoulensis* is involved in expression of nickel-containing superoxide dismutase. *FEMS Microbiol Lett* 228:21–26
- Kim J-S, Kang S-O, Lee J-K (2003b) The protein complex composed of nickel-binding SrmQ and DNA binding motif-bearing SrmR of *Streptomyces griseus* represses *sodF* transcription in the presence of nickel ions. *J Biol Chem* 278:18455–18463
- Kim JK, Mulrooney SB, Hausinger RP (2005) Biosynthesis of active *Bacillus subtilis* urease in the absence of known urease accessory proteins. *J Bacteriol* 187:7150–7154
- Kim HM, Ahn B-E, Lee J-H, Roe J-H (2015) Regulation of a nickel-cobalt efflux system and nickel homeostasis in a soil actinobacterium *Streptomyces coelicolor*. *Metallomics* 7:702–709
- King GM, Weber CF (2007) Distribution, diversity and ecology of aerobic CO-oxidizing bacteria. *Nat Rev Microbiol* 5:107–118
- Koch D, Nies DH, Grass G (2007) The RcnRA (YohLM) system of *Escherichia coli*: a connection between nickel, cobalt, and iron homeostasis. *Biomaterials* 20:759–771
- Krüger M, Meyerdierks A, Glöckner FO, Amann R, Widdel F, Kube M, Reinhardt R, Kahnt J, Böcher R, Thauer RK, Shima S (2003) A conspicuous nickel protein in microbial mats that oxidize methane anaerobically. *Nature* 426:878–881
- Kulathila R, Kulathila R, Indic M, van den Berg B (2011) Crystal structure of *Escherichia coli* CusC, the outer membrane component of a heavy metal efflux pump. *PLoS One* 6:e15610
- Kumar V, Mishra RK, Kaur G, Dutta D (2017) Cobalt and nickel impair DNA metabolism by the oxidative stress independent pathway. *Metallomics* 9:1596–1609
- Kung Y, Drennan CL (2017) One-carbon chemistry of nickel-containing carbon monoxide dehydrogenase and acetyl-CoA synthase. In: Zamble D, Rowinska-Zyrek M, Kozłowski H (eds) *The biological chemistry of nickel*. Royal Society of Chemistry, Cambridge
- Kurzer F, Sanderson PM (1956) Urea in the history of organic chemistry. *J Chem Ed* 33:452–459
- Kusters JG, Van Vliet AHM, Kuipers EJ (2006) Pathogenesis of *Helicobacter pylori* infection. *Clin Microbiol Rev* 19:449–490
- Kwon S, Nishitani Y, Watanabe S, Hirao Y, Imanaka T, Kanai T, Atomi H, Miki K (2016) Crystal structure of a [NiFe] hydrogenase maturation protease HybD from *Thermococcus kodakarensis* KOD1. *Proteins* 84:1321–1327
- Kwon S, Watanabe S, Nishitani Y, Kawashima T, Kanai T, Atomi H, Miki K (2018) Crystal structures of a [NiFe] hydrogenase large subunit HyhL in an immature state in complex with a Ni chaperone HypA. *Proc Natl Acad Sci U S A* 115:7045–7050
- Labigne A, Cussac V, Courcoux P (1991) Shuttle cloning and nucleotide sequences of *Helicobacter pylori* genes responsible for urease activity. *J Bacteriol* 173:1920–1931
- Lacasse MJ, Zamble DB (2016) [NiFe]-hydrogenase maturation. *Biochemistry* 55:1689–1701
- Lam R, Romanov V, Johns K, Battaile K, Wu-Brown J, Guthrie JL, Hausinger RP, Pai E, Chirgadze NY (2010) Crystal structure of a truncated urease accessory protein UreF from *Helicobacter pylori*. *Proteins* 78:2839–2848
- Laso-Pérez R, Wegener G, Knittel K, Widdel F, Harding KJ, Krukenberg V, Meier DV, Richter M, Tegetmeyer HE, Riedel D, Richnow H-H, Adrian L, Reemtsma T, Lechtenfeld OJ, Musat F (2016) Thermophilic archaea activate butane via alkyl-coenzyme M formation. *Nature* 539:396–401
- Laso-Pérez R, Hahn C, van Vliet DM, Tegetmeyer HE, Schubotz F, Smit NT, Pape T, Sahling H, Bohrmann G, Boetius A, Knittel K, Wegener G (2019) Anaerobic degradation of non-methane alkanes by “*Candidatus* Methanoliparia” in hydrocarbon seeps of the gulf of Mexico. *mBio* 10:e01814–e01819
- Leach MR, Zamble DB (2007) Metallocenter assembly of the hydrogenase enzymes. *Curr Opin Chem Biol* 11:159–165
- Leach MR, Zhang JW, Zamble DB (2007) The role of complex formation between the *Escherichia coli* hydrogenase factors HypB and SlyD. *J Biol Chem* 282:16177–16186



- Lebrette H, Iannello M, Fontecilla-Camps JC, Cavazza C (2013) The binding mode of Ni-(L-His)<sub>2</sub> in NikA revealed by X-ray crystallography. *J Inorg Biochem* 121:16–18
- Lebrette H, Brochier-Armanet C, Zambelli B, de Reuse H, Borezée-Durant E, Ciurli S, Cavazza C (2014) Promiscuous nickel import in human pathogens: structure, thermodynamics, and evolution of extracytoplasmic nickel-binding proteins. *Structure* 22:1421–1432
- Lebrette H, Borezee-Durant E, Martin L, Richaud P, Boeri Erba E, Cavazza C (2015) Novel insights into nickel import in *Staphylococcus aureus*: the positive role of free histidine and structural characterization of a new thiazolidine-type nickel chelator. *Metallomics* 7:613–621
- Leclere V, Boiron P, Blondeau R (1999) Diversity of superoxide-dismutases among clinical and soil isolates of *Streptomyces* species. *Curr Microbiol* 39:365–368
- Lee MH, Mulrooney SB, Renner MJ, Markowicz Y, Hausinger RP (1992) *Klebsiella aerogenes* urease gene cluster: sequence of *ureD* and demonstration that four accessory genes (*ureD*, *ureE*, *ureF*, and *ureG*) are involved in nickel metallocenter biosynthesis. *J Bacteriol* 174:4324–4330
- Lee MH, Pankratz HS, Wang S, Scott RA, Finnegan MG, Johnson MK, Ippolito JA, Christianson DW, Hausinger RP (1993) Purification and characterization of *Klebsiella aerogenes* UreE protein: a nickel-binding protein that functions in urease metallocenter assembly. *Protein Sci* 2:1042–1052
- Lee CW, Chakravorty DK, Chang F-MJ, Reyes-Caballero H, Ye Y, Merz KM Jr, Giedroc DP (2012) Solution structure of *Mycobacterium tuberculosis* NmtR in the apo state: insights into Ni (II)-mediated allostery. *Biochemistry* 51:2619–2629
- Lemaire ON, Wagner T (2020) Gas channel rerouting in a primordial enzyme: structure insights of the carbon-monoxide dehydrogenase/acetyl-CoA synthase complex from the acetogen *Clostridium autoethanogenum*. *Biochim Biophys Acta* 1862:148330
- Lenz O, Friedrich B (1998) A novel multicomponent regulatory system mediates H<sub>2</sub> sensing in *Alcaligenes eutrophus*. *Proc Natl Acad Sci U S A* 95:12474–12479
- Li Y, Zamble DB (2009) Nickel homeostasis and nickel regulation: an overview. *Chem Rev* 109:4617–4643
- Li C, Vavra JW, Carr CE, Huang H-T, Maroney MJ, Wilmot CM (2020) Complexation of the nickel and cobalt transcriptional regulator RcnR with DNA. *Acta Crystallogr F* 76:25–30
- Liesegang H, Lemke K, Siddiqui RA, Schlegel HG (1993) Characterization of the inducible nickel and cobalt resistance determinant *cnr* from pMOL28 of *Alcaligenes eutrophus* CH34. *J Bacteriol* 175:767–778
- Loke H-K, Lindahl PA (2003) Identification and preliminary characterization of AcsF, a putative Ni-insertase used in the biosynthesis of acetyl-CoA synthase from *Clostridium thermoaceticum*. *J Inorg Biochem* 93:33–40
- Loke H-K, Bennett GN, Lindahl PA (2000) Active acetyl-CoA synthase from *Clostridium thermoaceticum* obtained by cloning and heterologous expression of *acsAB* in *Escherichia coli*. *Proc Natl Acad Sci U S A* 97:12530–12535
- Long F, Su C-C, Zimmermann MT, Boyken SE, Rajashankar KR, Jernigan RL, Yu EW (2010) Crystal structures of the CusA efflux pump suggest methionine-mediated metal transport. *Nature* 467:484–488
- Lopez-Maury L, Garcia-Dominguez M, Florencio FJ, Reyes JC (2002) A two-component signal transduction system involved in nickel sensing in the cyanobacterium *Synechocystis* sp. PCC 6803. *Mol Microbiol* 43:247–256
- Louwrier A, Knowles CJ (1996) The purification and characterization of a novel D(–)-specific carbamoylase enzyme from *Agrobacterium* sp. *Enzym Microb Technol* 19:562–571
- Lu M, Chai J, Fu D (2009) Structural basis for autoregulation of the zinc transporter YiiP. *Nat Struct Mol Biol* 16:1063–1068
- Lu M, Jiang Y-L, Wang S, Jin H, Zhang R-G, Virolle M-J, Chen Y, Zhou C-Z (2014) *Streptomyces coelicolor* SCO4226 is a nickel binding protein. *PLoS One* 9:e109660
- Lubitz W, Ogata H, Rüdiger O, Reijerse E (2014) Hydrogenases. *Chem Rev* 114:4081–4148
- Lutz A, Jacobi A, Schlenso V, Böhm R, Sawers G, Böck A (1991) Molecular characterization of an operon (*hyp*) necessary for the activity of the three hydrogenase isoenzymes in *Escherichia coli*. *Mol Microbiol* 5:123–135

- Lyu Z, Shao N, Chou C-W, Shi H, Patel R, Duin EC, Whitman WB (2020) Posttranslational modification of arginine in methyl coenzyme M reductase has a profound impact on both methanogenesis and growth of *Methanococcus maripaludis*. *J Bacteriol* 202:e00654–e00619
- Macomber L, Hausinger RP (2011) Mechanisms of nickel toxicity in microorganisms. *Metallomics* 3:1153–1162
- Macomber L, Elsey SP, Hausinger RP (2011) Fructose-1,6-bisphosphate aldolase (class II) is the primary site of nickel toxicity in *Escherichia coli*. *Mol Microbiol* 82:1291–1300
- Maeda M, Hidaka M, Nakamura A, Masaki H, Uozumi T (1994) Cloning, sequencing, and expression of thermophilic *Bacillus* sp. strain TB-90 urease gene complex in *Escherichia coli*. *J Bacteriol* 176:432–442
- Maillard AP, Girard E, Ziani W, Petit-Hartlein I, Kahn R, Covès J (2014) The crystal structure of the anti-s factor CnrY in complex with the s factor CnrH shows a new structural class of anti-s factors targeting extracytoplasmic function s factors. *J Mol Biol* 426:2313–2327
- Maillard AP, Künnemann S, Grobe C, Volbeda A, Schleuder G, Petit-Hartlein I, De Rosny E, Nies D, Covès J (2015) Response of CnrX from *Cupriavidus metallidurans* CH34 to nickel binding. *Metallomics* 7:622–631
- Manley OM, Myers PD, Toney DJ, Bolling KF, Rhodes LC, Gasparik JL, Grossoehme NE (2020) Evaluation of the regulatory model for Ni<sup>2+</sup> sensing by Nur from *Streptomyces coelicolor*. *J Inorg Biochem* 203:110859
- Maratea D, Young K, Young R (1985) Deletion and fusion analysis of the phage phi X174 lysis gene E. *Gene* 40:39–46
- Marcus EA, Scott DR (2001) Cell lysis is responsible for the appearance of extracellular urease in *Helicobacter pylori*. *Helicobacter* 6:93–99
- Maroney MJ, Ciurli S (2014) Nonredox nickel enzymes. *Chem Rev* 114:4206–4228
- Marques MC, Coelho R, De Lacey AI, Pereira IA, Matias PM (2010) The three-dimensional structure of [NiFeS] hydrogenase from *Desulfovibrio vulgaris* Hildenborough: a hydrogenase without a bridging ligand in the active site in its oxidized, “as isolated” state. *J Mol Biol* 396:893–907
- Marrero J, Auling G, Coto O, Nies DH (2007) High-level resistance to cobalt and nickel but probably no transenvelope efflux: metal resistance in the Cuban *Serratia marcescens* strain C-1. *Microb Ecol* 53:123–133
- Martin-Diaconescu V, Joseph C, Boer JL, Mulrooney SB, Hausinger RP, Maroney MJ (2017) Non-thiolate ligation of nickel by nucleotide-free UreG of *Klebsiella aerogenes*. *J Biol Inorg Chem* 22:497–503
- Masetti M, Bertazzo M, Recanatini M, Ciurli S, Musiani F (2021) Probing the transport of Ni (II) ions through the internal tunnels of the *Helicobacter pylori* UreDFG multimeric protein complex. *J Inorg Biochem* 223:111554. <https://doi.org/10.1016/j.jinorgbio.2021.111554>
- Matias PM, Soares CM, Saraiva LM, Coelho R, Morais J, Le Gall J, Carrondo MA (2001) [NiFe] hydrogenase from *Desulfovibrio desulfuricans* ATCC 27774: gene sequencing, three-dimensional structures determination and refinement at 1.8 Å and modeling studies of its interaction with the tetrahaem cytochrome c3. *J Biol Inorg Chem* 6:63–81
- Maynard EL, Lindahl PA (1999) Evidence of a molecular tunnel connecting the active sites for CO<sub>2</sub> reduction and acetyl-CoA synthesis in acetyl-CoA synthase from *Clostridium thermoaceticum*. *J Am Chem Soc* 121:9221–9222
- Mayr S, Latkoczy C, Krüger M, Günther D, Shima S, Thauer RK, Widdel F, Jaun B (2008) Structure of an F430 variant from archaea associated with anaerobic oxidation of methane. *J Am Chem Soc* 130:10758–10767
- Mazzei L, Musiani F, Ciurli S (2020) The structure-based reaction mechanism of urease, a nickel dependent enzyme: tale of a long debate. *J Biol Inorg Chem* 25:829–845
- Mazzei L, Musiani F, Žerko S, Koźminski W, Cianci M, Beniamino Y, Ciurli S, Zambelli B (2021) Structure, dynamics, and function of SrnR, a transcription factor for nickel-dependent gene expression. *Metallomics* 13(12):mfab069. <https://doi.org/10.1093/mtomcs/mfab069>

- McLean RJC, Nickel JC, Cheng K-J, Costerton JW (1988) The ecology and pathogenicity of urease-producing bacteria in the urinary tract. *Crit Rev Microbiol* 16:37–79
- McLean RJC, Beauchemin D, Clapham L, Beveridge TJ (1990) Metal-binding characteristics of the gamma-glutamyl capsular polymer of *Bacillus licheniformis* ATCC 9945. *Appl Environ Microbiol* 56:3671–3677
- McMillan DJ, Mau M, Walker MJ (1998) Characterization of the urease gene cluster in *Bordetella bronchiseptica*. *Gene* 208:243–251
- Mergeay M, Nies D, Schlegel HG, Gerits J, Charles P, van Gijssel F (1985) *Alcaligenes eutrophus* CH34 is a facultative chemolithotroph with plasmid-bound resistance to heavy metals. *J Bacteriol* 162:328–334
- Merloni A, Dobrovolska O, Zambelli B, Agostini F, Bazzani M, Musiani F, Ciarli S (2014) Molecular landscape of the interaction between the urease accessory proteins UreE and UreG. *Biochim Biophys Acta* 1844:1662–1674
- Merrouch M, Benvenuti M, Lorenzi M, Léger C, Fourmond V, Dementin S (2018) Maturation of the [Ni-4Fe-4S] active site of carbon monoxide dehydrogenases. *J Biol Inorg Chem* 23:613–620
- Meuer J, Bartoschek S, Koch J, Kunkel A, Hedderich R (1999) Purification and catalytic properties of Ech hydrogenase from *Methanosarcina barkeri*. *Eur J Biochem* 265:325–335
- Miki K, Atomi H, Watanabe B (2020) Structural insight into [NiFe] hydrogenase maturation by transient complexes between Hyp proteins. *Acc Chem Res* 53:875–886
- Miquel P (1890) *C R Acad Sci* 111:397
- Miraula M, Ciarli S, Zambelli B (2015) Intrinsic disorder and metal binding in UreG proteins from Archae hyperthermophiles: GTPase enzymes involved in the activation of Ni(II) dependent urease. *J Biol Inorg Chem* 20:739–755
- Mobley HLT, Hausinger RP (1989) Microbial ureases: significance, regulation, and molecular characterization. *Microbiol Rev* 53:85–108
- Mobley HLT, Garner RM, Bauerfeind P (1995a) *Helicobacter pylori* nickel-transport gene *nixA*: synthesis of catalytically active urease in *Escherichia coli* independent of growth conditions. *Mol Microbiol* 16:97–109
- Mobley HLT, Island MD, Hausinger RP (1995b) Molecular biology of microbial ureases. *Microbiol Rev* 59:451–480
- Moncrief MBC, Hausinger RP (1996) Purification and activation properties of UreD-UreF-urease apoprotein complexes. *J Bacteriol* 178:5417–5421
- Moncrief MBC, Hausinger RP (1997) Characterization of UreG, identification of a UreD-UreF-UreG complex, and evidence suggesting that a nucleotide-binding site in UreG is required for *in vivo* metallocenter assembly of *Klebsiella aerogenes* urease. *J Bacteriol* 179:4081–4086
- Moore SJ, Sowa ST, Schuchardt C, Deery E, Lawrence AD, Ramos JV, Billig S, Birkemeyer C, Chivers PT, Howard MJ, Rigby SE, Layer G, Warren MJ (2017) Elucidation of the biosynthesis of the methane catalyst coenzyme F<sub>430</sub>. *Nature* 543:78–82
- Muller C, Bahlawane C, Aubert S, Delay CM, Schauer K, Michaud-Soret I, De Reuse H (2011) Hierarchical regulation of the NikR-mediated nickel response in *Helicobacter pylori*. *Nucleic Acids Res* 39:7564–7575
- Mulrooney SB, Hausinger RP (1990) Sequence of the *Klebsiella aerogenes* urease genes and evidence for accessory proteins facilitating nickel incorporation. *J Bacteriol* 172:5837–5843
- Mulrooney SB, Ward SK, Hausinger RP (2005) Purification and properties of the *Klebsiella aerogenes* UreE metal-binding domain, a functional metallochaperone of urease. *J Bacteriol* 187:3581–3585
- Munkelt D, Grass G, Nies DH (2004) The chromosomally encoded cation diffusion facilitator proteins DmeF and FieF from *Wautersia metallidurans* CH34 are transporters of broad metal specificity. *J Bacteriol* 186:8036–8043
- Muraki N, Ishii K, Uchiyama S, Itoh SG, Okumura H, Aono S (2019) Structural characterization of HypX responsible for CO biosynthesis in the maturation of NiFe-hydrogenase. *Commun Biol* 2:385

- Musiani F, Zambelli B, Stola M, Ciurli S (2004) Nickel trafficking: insights into the fold and function of UreE, a urease metallochaperone. *J Inorg Biochem* 98:803–813
- Musiani F, Zambelli B, Bazzani M, Mazzei L, Ciurli S (2015) Nickel-responsive transcriptional regulators. *Metallomics* 7:1305–1318
- Navarro C, Wu L-F, Mandrand-Berthelot M-A (1993) The *nik* operon of *Escherichia coli* encodes a periplasmic binding-protein-dependent transport system for nickel. *Mol Microbiol* 9:1181–1191
- Nayak DD, Mahanta N, Mitchell DA, Metcalf WW (2017) Post-translational thioamidation of methyl-coenzyme M reductase, a key enzyme in methanogenic and methanotrophic archaea. *elife* 6:e29218
- Nayak DD, Liu A, Agrawal N, Rodriguez-Carero R, Dong S-H, Mitchell DA, Nair SK, Metcalf WW (2020) Functional interactions between posttranslationally modified amino acids of methyl-coenzyme M reductase in *Methanosarcina acetivorans*. *PLoS Biol* 18:e3000507
- Navarez JL, Turmo A, Hu J, Hausinger RP (2020) Biochemical pincer complexes. *ChemCatChem* 12:4242–4254
- Nianios D, Thierbach S, Steimer L, Lulchev P, Klostermeier D, Fetzner S (2015) Nickel quercetinase, a “promiscuous” metalloenzyme: metal incorporation and metal ligand substitution studies. *BMC Biochem* 16:10
- Nielubowicz GR, Mobley HLT (2010) Host-pathogen interactions in the urinary tract interaction. *Nat Rev Urol* 7:430–441
- Nies DH, Covès J, Sawers RG (2017) Cross-talk between nickel and other metals in microbial systems. In: Zamble DB, Rowinska-Zyrek M, Kozłowski H (eds) *The biological chemistry of nickel*. Royal Society of Chemistry, Cambridge
- Niki E, Yoshida Y, Saito Y, Noguchi N (2005) Lipid peroxidation: mechanisms, inhibition, and biological effects. *Biochem Biophys Res Commun* 338:668–676
- Nim YS, Wong K-B (2019) The maturation pathway of nickel urease. *Inorganics* 7:85
- Nishimura K, Igarashi K, Kakinuma Y (1998) Proton gradient-driven nickel uptake by vacuolar membrane vesicles of *Saccharomyces cerevisiae*. *J Bacteriol* 180:1962–1964
- Noll KN, Rinehart KL Jr, Tanner RS, Wolfe RS (1986) Structure of component B (7-mercaptoheptanoylthreonine phosphate) of the methylcoenzyme M methylreductase system of *Methanobacterium thermoautotrophicum*. *Proc Natl Acad Sci U S A* 83:4238–4242
- Norsworthy AN, Pearson MM (2017) From catheter to kidney stone: the uropathogenic lifestyle of *Proteus mirabilis*. *Trends Microbiol* 25:304–315
- Nriagu JO (1980) *Nickel in the environment*. Wiley, New York
- Ogata H, Kellers P, Lubitz W (2010) The crystal structure of the [NiFe] hydrogenase from the photosynthetic bacterium *Allochrochromatium vinosum*: characterization of the oxidized enzyme (Ni-A state). *J Mol Biol* 402:428–444
- Ogata H, Nishikawa K, Lubitz W (2015) Hydrogens detected by subatomic resolution protein crystallography in a [NiFe] hydrogenase. *Nature* 520:571–574
- Ogata H, Lubitz W, Higuchi Y (2016) Structure and function of [NiFe] hydrogenases. *J Biochem* 160:251–258
- Olson JW, Maier RJ (2000) Dual roles of *Bradyrhizobium japonicum* nickelin protein in nickel storage and GTP-dependent Ni mobilization. *J Bacteriol* 182:1702–1705
- Olson JW, Mehta NS, Maier RJ (2001) Requirement of nickel metabolism proteins HypA and HypB for full activity of both hydrogenase and urease in *Helicobacter pylori*. *Mol Microbiol* 39:176–182
- Outten CE, O’Halloran TV (2001) Femtomolar sensitivity of metalloregulatory proteins controlling zinc homeostasis. *Science* 292:2488–2492
- Padmanabhan PK, Mukherjee A, Singh S, Chattopadhyaya S, Gowri VS, Myler PJ, Srinivasan N, Mahubala R (2005) Glyoxylase I from *Leishmania donovani*: a potential target for anti-parasite drug. *Biochem Biophys Res Commun* 337:1237–1248
- Pal A, Paul AK (2010) Nickel uptake and intracellular localization in *Cupriavidus pauculus* KPS 201, native to ultramafic ecosystem. *Adv Biosci Biotechnol* 1:276–280
- Palmgren MG, Nissen P (2011) P-type ATPases. *Annu Rev Biochem* 40:243–266

- Palombo M, Bonucci A, Etienne E, Ciurli S, Uversky VN, Guigliarelli B, Belle V, Mileo E, Zambelli B (2017) The relationship between folding and activity in UreG, an intrinsically disordered enzyme. *Sci Rep* 7:5977
- Paraszkiewicz K, Bernat P, Naliwajski M, Dlugonski J (2010) Lipid peroxidation in the fungus *Curvularia lunata* exposed to nickel. *Arch Microbiol* 192:135–141
- Park I-S, Carr MB, Hausinger RP (1994) *In vitro* activation of urease apoprotein and role of UreD as a chaperone required for nickel metallocenter assembly. *Proc Natl Acad Sci U S A* 91:3233–3237
- Park JE, Schlegel H-G, Rhie HG, Lee HS (2004) Nucleotide sequence and expression of the *ncr* nickel and cobalt resistance in *hafnia alvei* 5-5. *Int Microbiol* 7:27–34
- Park J-S, Lee S-J, Rhie H-G, Lee H-S (2008) Characterization of a chromosomal nickel resistance determinant from *Klebsiella oxytoca* CCUG 15788. *J Microbiol Biotechnol* 18:1040–1043
- Pasteur L (1860) De l'origine des ferments, etc. *C R Acad Sci* 50:849
- Pearce DA, Sherman F (1999) Toxicity of copper, cobalt, and nickel salts is dependent on histidine metabolism in the yeast *Saccharomyces cerevisiae*. *J Bacteriol* 181:4774–4779
- Pearson MA, Michel LO, Hausinger RP, Karplus PA (1997) Structure of Cys319 variants and acetohydroxamate-inhibited *Klebsiella aerogenes* urease. *Biochemistry* 36:8164–8172
- Pennella MA, Shokes JE, Cospser NJ, Scott RA, Giedroc DP (2003) Structural elements of metal selectivity in metal sensor proteins. *Proc Natl Acad Sci U S A* 100:3713–3718
- Peters JW, Schut GJ, Boyd ES, Mulder DW, Shepard EM, Broderick JB, King PW, Adams MWW (2015) [FeFe]- and [NiFe]-hydrogenase diversity, mechanism, and maturation. *Biochim Biophys Acta* 1853:1350–1369
- Petkun S, Shi R, Li Y, Asinas A, Munger C, Zhang L, Waclawek M, Soboh B, Sawers RG, Cygler M (2011) Structure of hydrogenase maturation protein HypB with reaction intermediates shows two active sites. *Structure* 19:1773–1783
- Pfaltz A, Livingston DA, Jaun B, Diekert G, Thauer RK, Eschenmoser A (1985) Factor F430 from methanogenic bacteria: on the nature of the isolation artifacts of F430, a contribution to the chemistry of F430 and the conformational stereochemistry of the ligand periphery of hydroporphinoid nickel(II) complexes. *Helv Chim Acta* 68:1338–1358
- Pfaltz A, Kobelt A, Hüster R, Thauer RK (1987) Biosynthesis of coenzyme F430 in methanogenic bacteria. Identification of 15,17<sup>3</sup>-seco-F430-17<sup>3</sup>-acid as an intermediate. *Eur J Biochem* 170:459–467
- Phillips CM, Schreiter ER, Guo Y, Wang SC, Zamble DB, Drennan CL (2008) Structural basis of the metal specificity for nickel regulatory protein NikR. *Biochemistry* 47:1938–1946
- Phillips CM, Schreiter ER, Stultz CM, Drennan CL (2010) Structural basis of low-affinity nickel binding to the nickel-responsive transcription factor NikR from *Escherichia coli*. *Biochemistry* 49:7830–7838
- Pierik AJ, Roseboom W, Happe RP, Bagley KA, Albracht SPJ (1999) Carbon monoxide and cyanide as intrinsic ligands to iron in the active site of [NiFe]-hydrogenases -- NiFe(CN)<sub>2</sub>CO, biology's way to activate H<sub>2</sub>. *J Biol Chem* 274:3331–3337
- Pinkett HW, Lee AT, Lum P, Locher KP, Rees DC (2007) An inward-facing conformation of a putative metal-chelate-type ABC transporter. *Science* 315:373–377
- Pinske C, Sargent F, Sawers RG (2015) SlyD-dependent nickel delivery limits maturation of [NiFe]-hydrogenases in late-stationary phase *Escherichia coli* cells. *Metallomics* 7:683–690
- Pochapsky TC, Pochapsky SS, Ju T, Mo H, Al-Mjeni F, Maroney MJ (2002) Modeling and experiment yields the structure of acireductone dioxygenase from *Klebsiella pneumoniae*. *Nat Struct Biol* 9:966–972
- Pochapsky SS, Sunshine JC, Pochapsky TC (2008) Completing the circuit: direct-observe <sup>13</sup>C, <sup>15</sup>N double-quantum spectroscopy permits sequential resonance assignments near a paramagnetic center in acireductone dioxygenase. *J Am Chem Soc* 130:2156–2157
- Pompidor G, Maillard AP, Girard E, Gambarelli S, Kahn R, Covès J (2008) X-ray structure of the metal-sensor CnrX in both the apo- and copper-bound forms. *FEBS Lett* 582:3954–3958

- Quiroz-Valenzuela S, Sukuru SCK, Hausinger RP, Kuhn LA, Heller WT (2008) The structure of urease activation complexes examined by flexibility analysis, mutagenesis, and small-angle X-ray scattering. *Arch Biochem Biophys* 480:51–57
- Ragsdale SW, Rauegi S, Ginovska B, Wongnate T (2017) Biochemistry of methyl-coenzyme M reductase. In: Zamble D, Rowinska-Zyrek M, Kozlowski H (eds) *The biological chemistry of nickel*. Royal Society of Chemistry, Cambridge
- Ragusa S, Blanquet S, Meinel T (1998) Control of peptide deformylase activity by metal cations. *J Mol Biol* 280:515–523
- Rai R, Saraswat VA, Dhiman RK (2015) Gut microbiota: its role in hepatic encephalopathy. *J Clin Exp Hepatol* 5:S29–S36
- Raimunda D, Long JE, Sasseti CM, Argüello JM (2012) Role in metal homeostasis of CtpD, a  $\text{Co}^{2+}$  transporting  $\text{P}_{1\text{B4}}$ -ATPase of *Mycobacterium smegmatis*. *Mol Microbiol* 84:1139–1149
- Rajagopalan PT, Pei D (1998) Oxygen-mediated inactivation of peptide deformylase. *J Biol Chem* 273:22305–22310
- Randhawa VK, Zhou F, Jin X, Nalewajko C, Kushner DJ (2001) Role of oxidative stress and thiol antioxidant enzymes in nickel toxicity and resistance in strains of the green alga *Scenedesmus acutus* f. *alternans*. *Can J Microbiol* 47:987–993
- Rankin JA, Mauban RC, Fellner M, Desguin B, McCracken J, Hu J, Varganov SA, Hausinger RP (2018) Lactate racemase nickel-pincer cofactor operates by a proton-coupled hydride transfer mechanism. *Biochemistry* 57:3244–3251
- Rankin JA, Chatterjee S, Tariq Z, Lagishetty S, Desguin B, Hu J, Hausinger RP (2021) The LarB carboxylase/hydrolase forms a transient cysteinyl-pyridine intermediate during nickel-pincer nucleotide cofactor biosynthesis. *Proc Natl Acad Sci* 118(39):e2106202118. <https://doi.org/10.1073/pnas.2106202118>
- Ravichandran R, Hemaasri S, Cameotra SS, Jayaprakash NS (2015) Purification and characterization of an extracellular uricase from a new isolate of *Sphingobacterium thalpophilum* (VITPCB<sub>5</sub>). *Protein Expr Purif* 114:136–142
- Reissmann S, Hochleitner E, Wang H, Paschos A, Lottspeich F, Glass RS, Böck A (2003) Taming of a poison: biosynthesis of the NiFe-hydrogenase cyanide ligands. *Science* 299:1067–1070
- Remaut H, Safarof N, Ciurli S, Van Beeumen J (2001) Structural basis for  $\text{Ni}^{2+}$  transport and assembly of the urease active site by the metallo-chaperone UreE from *Bacillus pasteurii*. *J Biol Chem* 276:49365–49370
- Remy L, Carrière M, Derré-Bobillot A, Martini C, Sanguinetti M, Borezée-Durant E (2013) The *Staphylococcus aureus* Opp1 ABC transporter imports nickel and cobalt in zinc-depleted conditions and contributes to virulence. *Mol Microbiol* 87:730–743
- Reyes-Caballero H, Lee CW, Giedroc DP (2011) *Mycobacterium tuberculosis* NmtR harbors a nickel sensing site with parallels to *Escherichia coli* RcnR. *Biochemistry* 50:7941–7952
- Righetto RD, Anton L, Adaixo R, Jakob RP, Zivanov J, Mahi M-A, Ringler P, Schwede T, Maier T, Stahlberg H (2020) High-resolution cryo-EM structure of urease from the pathogen *Yersinia enterocolitica*. *Nat Commun* 11:5101
- Rodionov DA, Hebbeln P, Gelfand MS, Eitinger T (2006) Comparative and functional genomic analysis of prokaryotic nickel and cobalt uptake transporters: evidence for a novel group of ATP-binding cassette transporters. *J Bacteriol* 188:317–327
- Rodionova IA, Scott DA, Grishin NV, Osterman AL, Rodionov DA (2012) Tagaturonate-fructuronate epimerase UxaE, a novel enzyme in the hexuronate catabolic network in *Thermotoga maritima*. *Environ Microbiol* 14:2920–2934
- Rodrigue A, Effantin G, Mandrand-Bethelot M-A (2005) Identification of *rcnA* (*yohM*), a nickel and cobalt resistance gene in *Escherichia coli*. *J Bacteriol* 187:2912–2916
- Rodrigue A, Albareda M, Mandrand-Berthelot M-A, Palacios J (2017) Nickel in microbial physiology—from single proteins to complex trafficking systems: nickel import/export. In: Zamble DB, Rowinska-Zyrek M, Kozlowski H (eds) *The biological chemistry of nickel*. Royal Society of Chemistry, Cambridge

- Rospert S, Linder D, Ellermann J, Thauer RK (1990) Two genetically distinct methyl-coenzyme M reductases in *Methanobacterium thermoautotrophicum* strain Marburg and DH. *Eur J Biochem* 194:871–877
- Rubio-Sanz L, Prieto RI, Imperial J, Palacios JM, Brito B (2013) Functional and expression analysis of the metal inducible *dmeRF* system from *Rhizobium leguminosarum* bv. *viciae*. *Appl Environ Microbiol* 79:6414–6422
- Ryan KC, Johnson OE, Cabelli DE, Brunold TC, Maroney MJ (2010) Nickel superoxide dismutase: structural and functional roles of Cys2 and Cys6. *J Biol Inorg Chem* 15:795–807
- Sachs G, Scott D, Weeks D, Melchers K (2002) The compartment buffered by the urease of *Helicobacter pylori*: cytoplasm or periplasm? *Trends Microbiol* 10:217–219
- Saier MH Jr, Beatty JT, Goffeau A, Harley KT, Heijne WH, Huang SC, Jack DL, Jahn PS, Lew K, Liu J, Pao SS, Paulsen IT, Tseng TT, Virk PS (1999) The major facilitator superfamily. *J Mol Microbiol Biotechnol* 1:257–279
- San Martin-Uriz P, Mirete S, Alcolea PJ, Gomez MJ, Amils R, Gonzalez-Pastor JE (2014) Nickel-resistance determinants in *Acidiphilum* sp. PM identified by genome-wide functional screening. *PLoS One* 9:e95041
- Sar P, Kazy SK, Singh SP (2001) Intracellular nickel accumulation by *Pseudomonas aeruginosa* and its chemical nature. *Lett Appl Microbiol* 32:257–261
- Sargent F (2016) The model [NiFe]-hydrogenases of *Escherichia coli*. *Adv Microb Physiol* 68:433–507
- Sasaki D, Watanabe B, Matsumi R, Shoji T, Yasukochi A, Tagashira K, Fukuda W, Kanai T, Atomi H, Imanaka T, Miki K (2013) Identification and structure of a novel archaeal HypB for [NiFe] hydrogenase maturation. *J Mol Biol* 425:1627–1640
- Sato K, Okuba A, Yamazaki S (1998) Characterization of a multi-copper enzyme, nitrous oxide reductase, from *Rhodobacter sphaeroides* f. sp. *denitrificans*. *J Biochem* 124:51–54
- Sawers RG, Pinske C (2017) NiFe-hydrogenase assembly. In: Johnson MK, Scott RA (eds) *Encyclopedia of inorganic and bioinorganic chemistry*. Wiley
- Saylor Z, Maier R (2018) *Helicobacter pylori* nickel storage proteins: recognition and modulation of diverse metabolic targets. *Microbiology* 164:1059–1068
- Schaab MR, Barney BM, Francisco WA (2006) Kinetic and spectroscopic studies on the quercetin 2,3-dioxygenase from *Bacillus subtilis*. *Biochemistry* 45:1009–1016
- Schäfer C, Bommer M, Hennig SE, Jeoung J-H, Dobbek H, Lenz O (2016) Structure of an actinobacterial-type [NiFe]-hydrogenase reveals insight into O<sub>2</sub>-tolerant H<sub>2</sub> oxidation. *Structure* 24:285–292
- Schauer K, Gouget B, Carrière M, Labigne A, de Reuse H (2007) Novel nickel transport mechanism across the bacterial outer membrane energized by the TonB/ExbB/ExbD machinery. *Mol Microbiol* 63:1054–1068
- Scheller S, Goenrich M, Boecher R, Thauer RK, Jaun B (2010) The key nickel enzyme of methanogenesis catalyzes the anaerobic oxidation of methane. *Nature* 465:606–608
- Schneider J, Kaltwasser H (1984) Urease from *Arthrobacter oxydans*, a nickel-containing enzyme. *Arch Microbiol* 139:355–360
- Schreiter ER, Sintchak MD, Guo Y, Chivers PT, Sauer RT, Drennan CL (2003) Crystal structure of the nickel-responsive transcriptional factor NikR. *Nat Struct Biol* 10:794–799
- Schreiter ER, Wang SC, Zamble DB, Drennan CL (2006) NikR-operator complex structure and the mechanism of repressor activation by metal ions. *Proc Natl Acad Sci U S A* 103:13676–13681
- Schulz A-C, Frielingsdorf S, Pommerening P, Lauterbach L, Bistoni G, Neese F, Oestreich M, Lenz O (2020) Formyltetrahydrofolate decarboxylase synthesizes the active site CO ligand of O<sub>2</sub>-tolerant [NiFe] hydrogenase. *J Am Chem Soc* 142:1457–1464
- Sebbane F, Mandrand-Bethelot M-A, Simonet M (2002) Genes encoding specific nickel transport systems flank the chromosomal urease locus of pathogenic *Yersinia*. *J Bacteriol* 184:5706–5713
- Seffernick JL, McTavish H, Osbourne JP, de Souza ML, Sadowsky MJ, Wackett LP (2002) Atrazine chlorohydrolase from *pseudomonas* sp. strain ADP is a metalloenzyme. *Biochemistry* 41:14430–14437

- Selmer T, Kahn J, Goubeaud M, Shima S, Grabarse W, Ermler U, Thauer RK (2000) The biosynthesis of methylated amino acids in the active site region of methyl-coenzyme M reductase. *J Biol Chem* 275:3755–3760
- Senger M, Stripp ST, Soboh B (2017) Proteolytic cleavage orchestrates cofactor insertion and protein assembly in [NiFe]-hydrogenase biosynthesis. *J Biol Chem* 292:11670–11681
- Seravalli J, Ragsdale SW (2000) Channeling of carbon monoxide during anaerobic carbon dioxide fixation. *Biochemistry* 39:1274–1277
- Seshadri S, Benoit SL, Maier RJ (2007) Roles of His-rich Hpn and Hpn-like proteins in *Helicobacter pylori* nickel physiology. *J Bacteriol* 189:4120–4126
- Shafaat HS, Rüdiger O, Ogata H, Lubitz W (2013) [NiFe] hydrogenases: a common active site for hydrogen metabolism under diverse conditions. *Biochim Biophys Acta* 1827:986–1002
- Shaik MM, Cendron L, Salamina M, Ruzzene M, Zanotti G (2014) *Helicobacter pylori* periplasmic receptor CeuE (HP1561) modulates its nickel affinity via organic metallophores. *Mol Microbiol* 91:724–735
- Sheng Y, Abreu IA, Cabelli DE, Maroney MJ, Miller A-F, Teixeira M, Valentine JS (2014) Superoxide dismutases and superoxide reductases. *Chem Rev* 114:3854–3918
- Shi R, Munger C, Asinas A, Benoit SL, Miller E, Matte A, Maier RJ, Cygler M (2010) Crystal structures of apo and metal-bound forms of the UreE protein from *Helicobacter pylori*: role of multiple metal binding sites. *Biochemistry* 49:7080–7088
- Shima S, Thauer RK (2005) Methyl-coenzyme M reductase and anaerobic oxidation of methane in methanotrophic archaea. *Curr Opin Microbiol* 8:643–648
- Shima S, Krueger M, Weingert T, Demmer U, Kahnt J, Thauer RK, Ermler U (2012) Structure of a methyl-coenzyme M reductase from Black Sea mats that oxidize methane anaerobically. *Nature* 481:98–101
- Shomura Y, Higuchi Y (2012) Structural basis for the reaction mechanism of S-carbamoylation of HypE by HypF in the maturation of [NiFe]-hydrogenases. *J Biol Chem* 287:28409–28419
- Shomura Y, Yoon K-S, Nishihara H, Higuchi Y (2011) Structural basis for a [4Fe-3S] cluster in the oxygen-tolerant membrane-bound [NiFe]-hydrogenase. *Nature* 479:253–256
- Shomura Y, Taketa M, Nakashima H, Tai H, Nakagawa H, Ikeda H, Ishii M, Igarashi Y, Nishihara H, Yoon K-S, Ogo S, Hirota S, Higuchi Y (2017) Structural basis of the redox switches in the NAD<sup>+</sup>-reducing soluble [NiFe]-hydrogenase. *Science* 357:928–932
- Siddiqui RA, Schlegel HG (1987) Plasmid pMOL28-mediated inducible nickel resistance in *Alcaligenes eutrophus* strain CH34. *FEMS Microbiol Lett* 43:9–13
- Simitsopoulou M, Vafopoulou A, Choli-Papadopoulou T, Alichanidis E (1997) Purification and partial characterization of a tripeptidase from *Pediococcus pentosaceus* K9.2. *Appl Environ Microbiol* 63:4872–4876
- Slotboom DJ (2014) Structural and mechanistic insights into prokaryotic energy-coupling factor transporters. *Nat Rev Microbiol* 12:79–87
- Smith DH (1967) R factors mediate resistance to mercury, nickel and cobalt. *Science* 156:1114–1116
- Snavely MD, Gravina SA, Cheung TT, Miller CG, Maguire ME (1991) Magnesium transport in *Salmonella typhimurium*. Regulation of *mgtA* and *mgtB* expression. *J Biol Chem* 266:824–829
- Snow ET, Xu LS, Kinney PL (1993) Effects of nickel ions on polymerase activity and fidelity during DNA replication in vitro. *Chem Biol Interact* 88:155–173
- Song HK, Mulrooney SB, Huber R, Hausinger RP (2001) Crystal structure of *Klebsiella aerogenes* UreE, a nickel-binding metallochaperone for urease activation. *J Biol Chem* 276:49359–49364
- Song L, Zhang Y, Chen W, Gu T, Zhang S-Y, Ji Q (2018) Mechanistic insights into staphylopin-mediated metal acquisition. *Proc Natl Acad Sci U S A* 115:3942–3947
- Soriano A, Hausinger RP (1999) GTP-dependent activation of urease apoprotein in complex with the UreD, UreF, and UreG accessory proteins. *Proc Natl Acad Sci U S A* 96:11140–11144
- Soriano A, Colpas GJ, Hausinger RP (2000) UreE stimulation of GTP-dependent urease activation in the UreD-UreF-UreG-urease apoprotein complex. *Biochemistry* 39:12435–12440



- Stähler FN, Odenbreit S, Haas R, Wilrich J, Van Vliet AH, Kusters JG, Kist M, Bereswill S (2006) The novel *Helicobacter pylori* CznABC metal efflux pump is required for cadmium, zinc, and nickel resistance, urease modulation, and gastric colonization. *Infect Immun* 74:3845–3852
- Stoof J, Kuipers EJ, Klaver G, van Vliet AH (2010a) An ABC transporter and a TonB ortholog contribute to *Helicobacter mustelae* nickel and cobalt acquisition. *Infect Immun* 78:4261–4267
- Stoof J, Kuipers EJ, van Vliet AHM (2010b) Characterization of NikR-responsive promoters of urease and metal transport genes of *Helicobacter mustelae*. *Biometals* 23:145–159
- Su C-C, Long F, Zimmermann MT, Rajashankar KR, Jernigan RL, Yu EW (2011) Crystal structure of the CusBA heavy-metal efflux complex of *Escherichia coli*. *Nature* 470:558–562
- Sukdeo N, Clugston SL, Daub E, Honek JF (2004) Distinct classes of glyoxylase I: metal specificity of the *Yersinia pestis*, *Pseudomonas aeruginosa* and *Neisseria meningitidis* enzymes. *Biochem J* 384:111–117
- Sumner JB (1926) The isolation and crystallization of the enzyme urease. *J Biol Chem* 69:435–441
- Suttisansanee U, Honek JF (2019) Preliminary characterization of a Ni<sup>2+</sup>-activated and mycothiol-dependent glyoxalase I enzyme from *Streptomyces coelicolor*. *Inorganics* 7:99
- Suttisansanee U, Lau K, Lagishetty S, Rao KN, Swaminathan S, Sauder JM, Burley SK, Honek JF (2011) Structural variation in bacterial glyoxylase I enzymes. Investigation of the metalloenzyme glyoxalase I from *Clostridium acetobutylicum*. *J Biol Chem* 286:38367–38374
- Svetlitchnyi V, Dobbek H, Meyer-Klaucke W, Meins T, Thiele B, Römer P, Huber R, Meyer O (2004) A functional Ni-Ni-[4Fe-4S] cluster in the monomeric acetyl-CoA synthase from *Carboxydothermus hydrogenoformans*. *Proc Natl Acad Sci U S A* 101:446–451
- Symmonds MF, Marshall RL, Bavro VN (2015) Architecture and roles of periplasmic adaptor proteins in tripartite efflux assemblies. *Front Microbiol* 6:513
- Takeuchi T (1909) On the occurrence of urease in higher plants. *J Coll Agric Imp Univ Tokyo* i:1
- Tamagnini P, Leitao E, Oliveira P, Ferreira D, Pinto F, Harris DJ, Heidorn T, Lindblad P (2007) Cyanobacterial hydrogenases: diversity, regulation and applications. *FEMS Microbiol Rev* 31:692–720
- Tatum EL, Peterson WH, Fred EB (1936) CCLXVI. Enzymic racemization of optically active lactic acid. *Biochem J* 30:1892–1897
- Taylor CD, Wolfe RS (1974) Structure and methylation of coenzyme M (HSCH<sub>2</sub>CH<sub>2</sub>SO<sub>3</sub>). *J Biol Chem* 249:4879–4885
- Techtmann SM, Lebedinsky AV, Colman AS, Sokolova TG, Woyke T, Goodwin L, Robb FT (2012) Evidence for horizontal gene transfer of anaerobic carbon monoxide dehydrogenases. *Front Microbiol* 3:132
- Terlesky KC, Nelson MJ, Ferry JG (1986) Isolation of an enzyme complex with carbon monoxide dehydrogenase activity containing corrinoid and nickel from acetate-grown *Methanosarcina thermophila*. *J Bacteriol* 168:1053–1058
- Thauer RK (1998) Biochemistry of methanogenesis: a tribute to Marjory Stephenson. *Microbiology* 144:2377–2406
- Thauer RK (2019) Methyl (alkyl)-coenzyme M reductases: nickel F-430-containing enzymes involved in anaerobic methane formation and in anaerobic oxidation of methane or of short chain alkanes. *Biochemistry* 58:5198–5220
- Thauer RK, Bonacker LG (1994) Biosynthesis of coenzyme F430, a nickel porphyrinoid involved in methanogenesis. *Ciba Found Symp* 180:210–227
- Thauer RK, Kaster A-K, Goenrich M, Schick M, Hiromoto T, Shima S (2010) Hydrogenases from methanogenic archaea, nickel, a novel cofactor, and H<sub>2</sub> storage. *Annu Rev Biochem* 79:507–536
- Tian J, Wu N, Li J, Liu Y, Guo J, Yao B, Fan Y (2007) Nickel-resistant determinant from *Leptospirillum ferriphilum*. *Appl Environ Microbiol* 73:2364–2368
- Tibazarwa C, Wuertz S, Mergeay M, Wyns L, van der Lelie D (2000) Regulation of the *cnr* cobalt and nickel resistance determinant of *Ralstonia eutropha* (*Alcaligenes eutrophus*) CH34. *J Bacteriol* 182:1399–1409

- Timm J, Brochier-Armanet C, Perard J, Zambelli B, Ollganier-de-Choudens S, Ciurli S, Cavazza C (2017) The CO dehydrogenase accessory protein CooT is a novel nickel-binding protein. *Metallomics* 9:575–583
- Tominaga T, Watanabe S, Matsumi R, Atomi H, Imanaka T, Miki K (2012) Structure of the [NiFe]-hydrogenase maturation protein HypF from *Thermococcus kodakarensis*. *Acta Crystallogr F68*: 1153–1157
- Tominaga T, Watanabe S, Matsumi R, Atomi H, Imanaka T, Miki K (2013) Crystal structures of the carbamoylated and cyanated forms of HypE for [NiFe] hydrogenase maturation. *Proc Natl Acad Sci U S A* 110:20485–20490
- Trepreau J, de Rosny E, Duboc C, Sarret G, Petit-Hartlein I, Maillard AP, Imbert A, Proux O, Covès J (2011a) Spectroscopic characterization of the metal-binding sites in the periplasmic metal-sensor domain of CnrX from *Cupriavidus metallidurans* CH34. *Biochemistry* 50:9036–9045
- Trepreau J, Girard E, Maillard AP, de Rosny E, Petit-Hartlein I, Kahn R, Covès J (2011b) Structural basis for metal sensing by CnrX. *J Mol Biol* 408:766–779
- Tripathi VN, Srivastava S (2006) Extracytoplasmic storage as the nickel resistance mechanism in a natural isolate of *Pseudomonas putida* S4. *Can J Microbiol* 52:287–292
- Tsang KL, Wong KB (2022) Moving nickel along the hydrogenase-urease maturation pathway. *Metallomics*. <https://doi.org/10.1093/mtomcs/mfac003>
- Turmo A, Hu J, Hausinger RP (2022) Characterization of the nickel-inserting cyclometallase LarC from *Moorella thermoacetica* and identification of a CMPylated reaction intermediate. *Metallomics*. <https://doi.org/10.1093/mtomcs/mfac014>
- Valko M, Morris H, Cronin MT (2005) Metals, toxicity and oxidative stress. *Curr Med Chem* 12: 1161–1208
- Van der Linden P, Burgdorf T, Bernhard M, Belijlebens B, Friedrich B, Albracht SPJ (2004) The soluble [NiFe]-hydrogenase from *Ralstonia eutropha* contains four cyanides in its active site, one of which is responsible for the insensitivity towards oxygen. *J Biol Inorg Chem* 9:616–626
- Van Nostrand JD, Arthur JM, Kilpatrick LE, Neely BA, Bertsch PM, Morris PJ (2008) Changes in protein expression in *Burkholderia vietnamiensis* PR1 301 at pH 5 and 7 with and without nickel. *Microbiology* 154:3813–3824
- van Tieghem PEL (1984) Recherches sur la fermentation de l'urée. *C R Acad Sci* 58:40
- van Vliet AHM, Poppelaars SW, Davies BJ, Stoof J, Bereswill S, Kist M, Penn CW, Kuipers EJ, Kusters JG (2002) NikR mediates nickel-responsive transcriptional induction of urease expression in *Helicobacter pylori*. *Infect Immun* 70:2846–2852
- van Vliet AHM, Ernst FD, Kusters JG (2004) NikR-mediated regulation of *Helicobacter pylori* acid adaptation. *Trends Microbiol* 12:489–494
- Vannini A, Pinatel E, Constantini PE, Roncarati D, Puccio S, De Bellis G, Peano C, Danielli A (2017) Comprehensive mapping of the *Helicobacter pylori* NikR regulon provides new insights in bacterial responses. *Sci Rep* 7:45458
- Vickers TJ, Greig N, Fairlamb AH (2004) A trypanothione-dependent glyoxalase I with a prokaryotic ancestry in *Leishmania major*. *Proc Natl Acad Sci U S A* 101:13186–13191
- Vignais PM, Billoud B (2007) Occurrence, classification, and biological function of hydrogenases: an overview. *Chem Rev* 107:4206–4272
- Vignais PM, Billoud B, Meyer J (2001) Classification and phylogeny of hydrogenases. *FEMS Microbiol Rev* 25:455–501
- Vinella D, Fischer F, Vorontsov E, Gallaud J, Malosse C, Michel V, Cavazza C, Robbe-Saule M, Richaud P, Chamot-Rooke J, Brochier-Armanet C, De Reuse H (2015) Evolution of *Helicobacter*: acquisition by gastric species of two histidine-rich proteins essential for colonization. *PLoS Pathog* 11:e1005312
- Vitt S, Ma K, Warkentin E, Moll J, Pierik AJ, Shima S, Ermler U (2014) The F<sub>420</sub>-reducing [NiFe]-hydrogenase complex from *Methanothermobacter marburgensis*, the first X-ray structure of a group 3 family member. *J Mol Biol* 426:2813–2826

- Volbeda A, Fontecilla-Camps JC (2017) Crystallographic analyses of the active site chemistry and oxygen sensitivity of [NiFe(Se)]-hydrogenases. In: Zamble D, Rowinska-Zyrek M, Kozlowski H (eds) The biological chemistry of nickel. Royal Society of Chemistry, London
- Volbeda A, Charon M-H, Piras C, Hatchikian EC, Frey M, Fontecilla-Camps JC (1995) Crystal structure of the nickel-iron hydrogenase from *Desulfovibrio gigas*. *Nature* 373:580–587
- Volbeda A, Garcin E, Piras C, de Lacey AL, Fernandez VM, Hatchikian EC, Frey M, Fontecilla-Camps JC (1996) Structure of the [NiFe] hydrogenase active site: evidence for biologically uncommon Fe ligands. *J Am Chem Soc* 118:12989–12996
- Volbeda A, Martin L, Cavazza C, Matho M, Faber BW, Rosebloom W, Albracht SPJ, Garcia E, Rousset M, Fontecilla-Camps JC (2005) Structural differences between the ready and unready oxidized states of [NiFe] hydrogenases. *J Biol Inorg Chem* 10:239–249
- Volbeda A, Amara P, Darnault C, Mouesca J-M, Parkin A, Roessler MM, Armstrong FA, Fontecilla-Camps JC (2012) X-ray crystallographic and computational studies of the O<sub>2</sub>-tolerant [NiFe]-hydrogenase 1 from *Escherichia coli*. *Proc Natl Acad Sci U S A* 109:5305–5310
- Volbeda A, Darnault C, Parkin A, Sargent F, Armstrong FA, Fontecilla-Camps JC (2013) Crystal structure of the O<sub>2</sub>-tolerant membrane-bound hydrogenase 1 from *Escherichia coli* in complex with its cognate cytochrome *b*. *Structure* 21:184–190
- Voordouw G (2002) Carbon monoxide cycling by *Desulfovibrio vulgaris* Hildenborough. *J Bacteriol* 184:5903–5911
- Wang WC, Hsu WH, Chien FT, Chen CY (2001) Crystal structure and site-directed mutagenesis studies of N-carbamoyl-D-amino-acid amidohydrolase from *Agrobacterium radiobacter* reveals a homotetramer and insight into a catalytic cleft. *J Mol Biol* 306:251–261
- Wang SC, Dias AV, Bloom SL, Zamble DB (2004) The selectivity of metal binding and the metal-induced stability of *Escherichia coli* NikR. *Biochemistry* 43:10018–10028
- Wang SC, Li Y, Ho MY, Bernal M-E, Sydor AM, Kagzi WR, Zamble DB (2010a) The response of *Escherichia coli* NikR to nickel: a second nickel-binding site. *Biochemistry* 49:6635–6645
- Wang SC, Li Y, Robinson CV, Zamble DB (2010b) Potassium is critical for the Ni(II)-responsive DNA-binding activity of *Escherichia coli* NikR. *J Am Chem Soc* 132:1506–1507
- Wang S, Wu Y, Outten FW (2011) Fur and the novel regulator YqjI control transcription of the ferric reductase gene *yqjH* in *Escherichia coli*. *J Bacteriol* 193:563–574
- Wang S, Blahut M, Wu Y, Philipkosky KE, Outten FW (2014) Communication between binding sites is required for YqjI regulation of target promoters within the *yqjH-yqjI* intergenic region. *J Bacteriol* 196:3199–3207
- Wang Y, Branicky R, Noë A, Hekimi S (2018) Superoxide dismutases: dual roles in controlling ROS damage and regulating ROS signaling. *J Cell Biol* 217:1915–1928
- Wang Y, Wegener G, Hou J, Wang J, Xiao X (2019) Expanding anaerobic alkane metabolism in the domain of archaea. *Nat Microbiol* 4:595–602
- Wang Y, Wegener G, Ruff SE, Wang F (2020) Methyl/alkyl-coenzyme M reductase-based anaerobic alkane oxidation in archaea. *Environ Microbiol* 23:530–541
- Watanabe S, Matsumi R, Arai T, Atomi H, Imanaka T, Miki K (2007) Crystal structures of [NiFe] hydrogenase maturation proteins HypC, HypD, and HypE: insights into cyanation reaction by thiol redox signaling. *Mol Cell* 27:29–40
- Watanabe S, Arai T, Matsumi R, Atomi H, Imanaka T, Miki K (2009) Crystal structure of HypA, a nickel-binding metallochaperone for [NiFe] hydrogenase maturation. *J Mol Biol* 394:448–459
- Watanabe S, Matsumi R, Atomi H, Imanaka T, Miki K (2012) Crystal structures of the HypCD complex and the HypCDE ternary complex: transient intermediate complexes during [NiFe] hydrogenase maturation. *Structure* 20:2124–2137
- Watanabe S, Kawashima T, Nishitani Y, Kanai T, Wada T, Inaba K, Atomi H, Imanaka T, Miki K (2015) Structural basis of a Ni acquisition cycle for [NiFe] hydrogenase by Ni-metallochaperone HypA and its enhancer. *Proc Natl Acad Sci U S A* 112:7701–7706

- Watt RK, Ludden PW (1998) The identification, purification, and characterization of CooJ. A nickel-binding protein that is co-regulated with the Ni-containing CO dehydrogenase from *Rhodospirillum rubrum*. *J Biol Chem* 273:10019–10025
- Weeks DL, Eskandar S, Scott DR, Sachs G (2000) A H<sup>+</sup>-gated urea channel: the link between *Helicobacter pylori* urease and gastric colonization. *Science* 287:482–485
- Weimer PJ, Moen GN (2013) Quantitative analysis of growth and volatile fatty acid production by the anaerobic ruminal bacterium *Megasphaera elsdenii* T81. *Appl Microbiol Biotechnol* 97:4075–4081
- West AL, St John F, Lopes PEM, MacKerell AD Jr, Pozharski E, Michel SLJ (2010) Holo-Ni(II) HpNikR is an asymmetric tetramer containing two different nickel-binding sites. *J Am Chem Soc* 132:14447–14456
- Willecke K, Gries E-M, Oehr P (1973) Coupled transport of citrate and magnesium in *Bacillus subtilis*. *J Bacteriol* 218:807–814
- Wittenborn EC, Merrouch M, Ueda C, Fradale L, Léger C, Fourmond V, Pandelia M-E, Dementin S, Drennan CL (2018) Redoxdependent rearrangements of the NiFeS cluster of carbon monoxide dehydrogenase elife 7:e39451
- Wittenborn EC, Cohen SE, Merrouch M, Léger C, Fourmond V, Dementin S, Drennan CL (2019) Structural insight into the metallocofactor maturation in carbon monoxide dehydrogenase. *J Biol Chem* 294:13017–13026
- Wittenborn EC, Guendon C, Merrouch M, Benvenuti M, Fourmond V, Léger C, Drennan CL, Dementin S (2020) The solvent-exposed Fe-S D-cluster contributes to oxygen-resistance in *Desulfovibrio vulgaris* Ni-Fe carbon monoxide dehydrogenase. *ACS Catal* 10:7328–7335
- Wöhler F (1828) Ueber künstliche bildung des harnstoffs (On the artificial formation of urea). *Annalen der Physik (Berlin)* 12:253–256
- Wolfram L, Bauerfeind P (2002) Conserved low-affinity nickel-binding amino acids are essential for the function of the nickel permease NixA of *Helicobacter pylori*. *J Bacteriol* 184:1438–1443
- Wolfram L, Haas E, Bauerfeind P (2006) Nickel represses the synthesis of the nickel permease NixA of *Helicobacter pylori*. *J Bacteriol* 188:1245–1250
- Wray JW, Abeles RH (1993) A bacterial enzyme that catalyzes formation of carbon monoxide. *J Biol Chem* 268:21466–21469
- Wroblewski LE, Peek RM Jr, Wilson KT (2010) *Helicobacter pylori* and gastric cancer: factors that modulate disease risk. *Clin Microbiol Rev* 23:713–739
- Wu M, Ren Q, Durkin AS, Daugherty SC, Brinkac LM, Dodson RJ, Madupu R, Sullivan SA, Kolonay JF, Haft DH, Nelson WC, Tallon LJ, Jones KM, Ulrich LE, Gonzalez JM, Zhulin IB, Robb FT, Eisen JA (2005) Life in hot carbon monoxide: the complete genome sequence of *Carboxydotherrmus hydrogenoformans* Z-2901. *PLoS Genet* 1:e65
- Wuerges J, Lee J-W, Yim Y-I, Kang SO, Carugo KD (2004) Crystal structure of nickel-containing superoxide dismutase reveals another type of active site. *Proc Natl Acad Sci U S A* 101:8569–8574
- Wülfing C, Lombardero J, Plückthun A (1994) An *Escherichia coli* protein consisting of a domain homologous to FK506-binding proteins (FKBP) and a new metal binding motif. *J Biol Chem* 269:2895–2901
- Xu J, Cotruvo JA Jr (2020) The *czcD* (NiCo) riboswitch responds to iron(II). *Biochemistry* 59:1508–1516
- Yang F, Hu W, Xu H, Li C, Xia B, Jin C (2006) Structure and backbone dynamics of an endopeptidase HycI from *Escherichia coli*: implications for mechanism of the [NiFe] hydrogenase maturation. *J Biol Chem* 282:3856–3863
- Yang X, Li H, Cheng T, Xia W, Lai Y-T, Sun H (2014) Nickel translocation between metallochaperones HypA and UreE in *Helicobacter pylori*. *Metallomics* 6:1731–1736
- Yang X, Li H, Lai T-P, Sun H (2015) UreE-UreG complex facilitates nickel transfer and preactivates GTPase of UreG in *Helicobacter pylori*. *J Biol Chem* 290:12474–12485
- Youn H-D, Kim E-J, Roe J-H, Hah YC, Kang S-O (1996a) A novel nickel-containing superoxide dismutase from *Streptomyces* spp. *Biochem J* 318:889–896

- Youn H-D, Youn H, Lee J-W, Yim Y-I, Lee JK, Hah YC, Kang S-O (1996b) Unique isoenzymes of superoxide dismutase in *Streptomyces griseus*. Arch Biochem Biophys 334:341–348
- Yu Y, Zhou M, Kirsch F, Xu C, Zhang L, Wang Y, Jiang Z, Wang N, Li J, Eitinger T, Yang M (2014) Planar substrate-binding site dictates the specificity of ECF-type nickel/cobalt transporters. Cell Res 24:267–277
- Yuen MH, Fong YH, Nim YS, Lau PH, Wong K-B (2017) Structural insights into how GTP-dependent conformational changes in a metallochaperone UreG facilitate urease maturation. Proc Natl Acad Sci U S A 114:E10890–E10898
- Zadvornyy OA, Allen M, Brumfield SK, Varpness Z, Boyd ES, Zorin NA, Serebriakova L, Douglas T, Peters JW (2010) Hydrogen enhances nickel tolerance in the purple sulfur bacterium *Thiocapsa roseopersicina*. Environ Sci Technol 44:834–840
- Zambelli B, Stola M, Musiani F, De Vriendt K, Samyn B, Devreese B, Van Beeumen J, Dikiy A, Bryant DA, Ciurli S (2005) UreG, a chaperone in the urease assembly process, is an intrinsically unstructured GTPase that specifically binds  $Zn^{2+}$ . J Biol Chem 280:4684–4695
- Zambelli B, Bellucci M, Danielli A, Scarlato V, Ciurli S (2007a) The  $Ni^{2+}$  binding properties of *Helicobacter pylori* NikR. Chem Commun 3649–3651
- Zambelli B, Musiani F, Savini M, Tucker P, Ciurli S (2007b) Biochemical studies on *Mycobacterium tuberculosis* UreG and comparative modeling reveal structural and functional conservation among the bacterial UreG family. Biochemistry 46:3171–3182
- Zambelli B, Turano P, Musiani F, Neyroz P, Ciurli S (2009)  $Zn^{2+}$ -linked dimerization of UreG from *Helicobacter pylori*, a chaperone involved in nickel trafficking and urease activation. Proteins 74:222–239
- Zambelli B, Cremades N, Neyroz P, Turano P, Uversky VN, Ciurli S (2012) Insights in the (un)structural organization of *Bacillus pasteurii* UreG, an intrinsically disordered GTPase enzyme. Mol BioSyst 8:220–228
- Zambelli B, Banaszak K, Merloni A, Kiliszek A, Rypniewski W, Ciurli S (2013) Selectivity of Ni (II) and Zn(II) binding to *Sporosarcina pasteurii* UreE, a metallochaperone in the urease assembly: a calorimetric and crystallographic study. J Biol Inorg Chem 18:1005–1017
- Zamble D, Rowinska-Zyrek M, Kozłowski H (2017) The biological chemistry of nickel. Royal Society of Chemistry, Cambridge
- Zeer-Wanklyn CJ, Zamble DB (2017) Microbial nickel: cellular uptake and delivery to enzyme centers. Curr Opin Chem Biol 37:80–88
- Zeng Y-B, Zhang D-M, Li H, Sun H (2008) Binding of  $Ni^{2+}$  to a histidine- and glutamine-rich protein, Hpn-like. J Biol Inorg Chem 13:1121–1131
- Zeng Y-B, Yang N, Sun H (2011) Metal-binding properties of an Hpn-like histidine-rich protein. Chem Eur J 17:5852–5860
- Zhan G, Li D, Zhang L (2012) Aerobic bioreduction of nickel(II) to elemental nickel with concomitant biomineralization. Appl Microbiol Biotechnol 96:273–281
- Zhang JW, Butland G, Greenblatt JF, Emili A, Zamble DB (2005) A role for SlyD in the *Escherichia coli* hydrogenase biosynthetic pathway. J Biol Chem 280:4360–4366
- Zhu T, Tian J, Zhang S, Wu N, Fan Y (2011) Identification of the transcriptional regulator NcrB in the nickel resistance determinant of *Leptospirillum ferriphilum* UBK03. PLoS One 6:e17367
- Ziani V, Maillard AP, Petit-Hartlein I, Garnier N, Crouzy S, Girard E, Covès J (2014) The X-ray structure of NecX from *Cupriavidus metallidurans* 31A illustrates potential dangers of detergent solubilization when generating and interpreting crystal structures of membrane proteins. J Biol Chem 289:31160–31172
- Zielazinski EL, Gonzalez-Guerrero M, Subramanian P, Stemmler TL, Argüello JM, Rosenzweig AC (2013) *Sinorhizobium meliloti* Nia is a P-ATPase expressed in the nodule during plant symbiosis and is involved in Ni and Fe transport. Metallomics 5:1614–1623

# Chapter 15

## Microbial Transformation of Silicon in Soil



**Kalyanasundaram Geetha Thanuja, V. S. Reddy Kiran Kalyan, Subburamu Karthikeyan, and Savariappan Anthoniraj**

**Abstract** Silica (from Latin “silex” means to flint) is rarely found on its own and often combines with oxygen or other elements to form silicates which are regarded as the largest class of rock-forming materials. In nature, they occur as distinct polymorphs as silica or oxides of silica in either crystalline or amorphous form and their mineral weathering releases mono silicic acid which is assimilated by plants, adsorbed on minerals, transported to watersheds, or trapped in clay minerals. Being placed in group IV of the periodic table, carbon (C) and Si shares several characteristics and significance including that of C biotransformation and cycling. However, although Si compounds are abundant in soil, their availability to plants is limited. These compounds help to render resistance to plants against biotic and abiotic stress. Si is known to have a wide range of plant beneficial properties, yet regarded as a nonentity in plant nutritional aspect. This chapter details a suite of factors associated with silica in soil and plant systems.

---

K. Geetha Thanuja

Department of Agricultural Microbiology, Tamil Nadu Agricultural University, Coimbatore, Tamil Nadu, India

V. S. Reddy Kiran Kalyan

Department of Soil Science and Agricultural Chemistry, Tamil Nadu Agricultural University, Coimbatore, Tamil Nadu, India

S. Karthikeyan (✉)

Department of Agricultural Microbiology, Tamil Nadu Agricultural University, Coimbatore, Tamil Nadu, India

Department of Renewable Energy Engineering, Agricultural Engineering College and Research Institute, Tamil Nadu Agricultural University, Coimbatore, Tamil Nadu, India

e-mail: [skarthy@tnau.ac.in](mailto:skarthy@tnau.ac.in)

S. Anthoniraj

Rom Vijay Biotech Pvt. Ltd., Pondicherry, India

## 15.1 Introduction

Metalloids, being diagonally placed between metals and nonmetals in periodic table, also possess properties intermediate to them. They include boron (B), silicon (Si), arsenic (As), germanium (Ge), antimony (Sb), tellurium (Te), and polonium (Po). While metalloids like As and Sb are reported to be hazardous to plants and humans, silicon and boron serve as micro essential elements to plants. Silicon is widely recognized as a quasi-essential element to plants. Next to oxygen, silicon is the most abundant element found in the Earth's crust and serves as eighth most common element in nature. However, in nature, it does not occur in a free state, but its compounds are present abundantly. In biogeochemistry, silicon is commonly referred to as silica. Silica is silicon dioxide and silicon atoms are mostly found associated with oxygen, with the Si-O tetrahedron commonly serving as a building block. Being placed in the carbon family, Si can link to four additional atoms and can serve as transmuted source (Umamaheswari et al. 2016). Though Si is not considered an essential element, evidences are budding on their beneficial role especially under stress conditions (Luyckx et al. 2017). Silica is often termed as a quasi-essential element, whose absence does not hinder the plant growth and development but presence enhances the well-being of the plant. Silicon is the second most common element in earth's crust, and yet Si nevertheless often is either not available or available in small fractions to plants, because silicon atoms tend to be locked up as recalcitrant silicate minerals (Struyf et al. 2010). The importance of silicon has become widely accepted in recent years, rendering the resistance to plants against abiotic stress.

## 15.2 Silicon Research in India and the World

The history of silicon research dates back to eighteenth century across various parts of the globe. The earliest record on Si was given by European researcher de Saussure (1804), who showed a greater abundance of silica among members of the monocotyledonous Poaceae than in the dicotyledonous plants. The sayings "*the siliceous epidermis of the plants serves as a support, protects the bark from the action of the insects, and seems to perform a part in the economy of these feeble vegetable*" in the book *Elements of Agricultural chemistry* by European chemist Davy (1819) seeded knowledge in the protective role of Si. Liebig, a German chemist and agricultural scientist was the first to recommend sodium silicate as silica fertilizer to enhance crop productivity after his pioneering silicate effect greenhouse experiments on sugar beet. The recruitment of slag-based fertilizer has been extensively used for centuries in most of the countries. However, the first patent for using slag as fertilizer was acquired in the USA (Zippicotte 1881). In 1940s, it was recognized that soil Si could not be sufficient for the healthy growth of rice and the extensive use of slag-based fertilizer from iron industry was found in 1940s, especially after World War II

to ensure (staple) food security and crop productivity. Until then, Si was not applied to the field due to their natural presence in soil and was considered unnecessary. Studies on the physiological role of Si were initiated by Ohkawa (1936) and Ishibashi (1936) in growth of rice. They observed a decline in yield due to Si deficiency and their application alleviated brown spot and blast which was caused due to heavy application of nitrogen fertilizers. Further, several research efforts were attempted to reveal the significance of Si in plant biology. Recently various research has become engrossed in Si nanoparticles as a means of enhancing plants' disease resistance (El-Shetehy et al. 2021), improving fungicidal activity (Abdelrahman et al. 2021).

### 15.3 Silica in Plants

The significant difference in the Si accumulating ability of plants is their mechanism of Si uptake, which varies among the plant species. Plants uptake Si by diffusion in the form of ortho-silicic acid ( $\text{H}_4\text{SiO}_4$ ), which is the only molecular species known for plausible transfer to the membrane of root at physiological pH. The concentration of a plant's available silicic acid typically ranges from 0.1 to 0.6  $\text{mmol L}^{-1}$  in the soil solution which is even 100x higher than the available phosphorus (Epstein 1994; Gunnarsson and Arnórsson 2000). The uptake of Si in plants can be either passive along with the pore water or active by extraction of Si solute through the plant roots. Depending upon the amount of biogenic silica which they contain, plants are classified as either accumulators, excluders, or to be an intermediate type (Mitani and Ma 2005) as tabulated in Table 15.1. The exclusive survey of wide plant species from Bryophyta to Angiospermae was characterized by Takahashi et al. (1976–1981) to differentiate the silica accumulating and non-accumulating plants by their mineral composition. Plants possessing Si content and Si-Ca ratio greater than 1.0% and 1.0, respectively, are expounded as Si accumulators, while the plants with the Si content and Si-Ca ratio lesser than 0.5% and 0.5, respectively, are regarded as either non-accumulator or Si excluders. Plants with the halfway range are defined as intermediate-type plants. In monocots, Si content is found to be higher than in the dicots, and the level was found to increase in the order of legumes < fruits

**Table 15.1** Categorization of plants based on the accumulation of biogenic silica

Hyper accumulators	Intermediate accumulators	Non-accumulators (Excluders)
Rice	Wheat	Tomato
Sugarcane	Cucumber	Sunflower
Mosses	Chrysanthemum	Gymnosperms
Ferns	Pumpkin	
Bamboo		
Maize		
Sorghum		



crops < vegetables < grasses < grain crops (Thiagalasingam et al. 1977), which expounds that the level of Si accumulation tends to vary from plant species.

Being deposited on the walls of the epidermis and vascular tissues, silica are well-recognized for conferring strength, rigidity, and resistance to pests and diseases. It sustains the erectness of rice leaves and culms thereby resulting in increased photosynthetic activity. Silica in plants are evinced to filter harmful U-V radiation reaching leaf surface with leaf cells acting as “windows” transmitting more light energy to photosynthetic mesophyll and cortical tissues beneath the epidermis than would occur if silica were absent. It has been proposed that enzyme silicon complexes are formed to protect and regulate photosynthesis. Silicon not only contributes to increased photo-assimilation of carbon but also promotes movement of the assimilated carbon to the panicle in rice. It also plays a role in phosphorus nutrition and there is an interrelationship with phosphorus. The recognized oxidizing capability of rice roots coupled with tolerance to higher levels of iron and manganese are found to depend on silicon nutrition. With the addition of more and more nitrogen to high-yielding nitrogen responsive varieties, the silica requirements of rice tend to increase. Application of silica through silicate minerals also increases the grain yield of rice both in upland and water-logged conditions.

### ***15.3.1 Silica Requirement by Crops***

Silicon, though an element that is 146 times more represented in Earth’s crust and yet sharing scores of properties of carbon that forms the backbone of most organic molecules, hardly forms an integral part of any cellular component. The mineral composition of plants differs with the plant species and the growth environment even when grown in the same soil. Among the terrestrial plants, only horsetails were established to have utter requirements for Si (Epstein 1999). In general, leaf analysis could be an indicator of Si status and 0.6% of Si is the minimum leaf tissue concentration for optimum growth (McCray and Mylavarapu 2010).

In almost all the terrestrial plant species, Si is found in the shoot with concentrations ranging between 0.1 and 10% on a dry weight basis. Si content in plants is alike to major nutrients N, P, K, and several plants absorb more than they require. The seemingly excess amount of Si gets deposited in their tissue. The aerial plant parts have been found to accumulate more Si than the roots. Different plant parts accumulate various concentrations of Si, for example, rice accumulates 4–20% of Si in straw, and 90% of the plants silicic acid exists in rice leaf blades as silica gel, which is not from the added fertilizer. There is a variation in the Si accumulation of polished rice, rice bran, and hulls, typically contributing levels of  $0.5 \text{ g kg}^{-1}$ ,  $50 \text{ g kg}^{-1}$ , and  $230 \text{ g kg}^{-1}$ , respectively (Van Soest 2006). Sugarcane accumulates about 380 kg/ha of Si (Epstein 1994). The variation in existence, density, and localization of Si transport proteins would be responsible for marked capability of accumulation in the plant kingdom.

### ***15.3.2 Importance of Si to Plants***

Silica application to various plants such as sugarcane, rice, maize, sorghum, peanut, wheat, and barley are reported to increase plant yield (Guntzer et al. 2012; Liang et al. 2015). In soil and plants, Si is crucial in nutrient cycling and augments fertilization by improving both plant growth as well as N use efficiency. The enhanced yield responses in plants occur mainly due to stimulation of stress tolerance against biotic and abiotic stresses. Si is regarded as a biological inducer capable of accelerating physiological and biological plant responses (Kim et al. 2016) and its role in plant–pathogen interactions can be divided into three categories including physical, biochemical, and molecular mechanisms which perform structural reinforcement, production of signaling compounds, and transcriptomic regulation, respectively (Table 15.2).

### ***15.3.3 Si Nanoparticles in Plant Growth***

With the advent of nanoscale materials in agricultural application, the use of silica as a nanocarrier became likely looking. Since silica fertilizer availability is limited unlike conventional fertilizers, and silica fertilizers are too expensive, the use of mesoporous silica nanoparticles (SNP) and organosilica nanoparticles finds wide application. SNPs were observed to enhance growth, photosynthesis, and total protein in wheat seedlings (Sun et al. 2016). Furthermore, Si nanoparticles (SNP) efficiently function in alleviating abiotic stresses better than do the bulk materials. SNP (silicon dioxide/colloidal silica) are mesoporous particles with sizes ranging from 2 to 50 nm. Compared with the bulk crystalline silicon, SNPs have lower bulk density, higher specific surface area, and reactivity. The properties of SNP are postulated, that their access in plant cell walls is simple via Si transporters thereby increasing seed germination, growth, photosynthesis, nutrient availability, and so on as mentioned in Table 15.3.

## **15.4 Silica in Soils**

The aspect of silica in soil–plant–animal Si cycling is significant. Silica is abundantly available in soil but typically occurs in a polymerized form. Si-Si are frail than C-C bonds, while Si-H bonds are relatively unsteady and tend to react with oxygen. The larger size of the Si atom compared to C also renders it inappropriate as a building block despite the fact that it can also form bonds with four other atoms creating a three-dimensional network similar to carbon. Plants absorb only monosilicic acid and this could arise in soil solution only when depolymerization occurs in soil silicates. Organic acids resulting from the decomposition of organic

**Table 15.2** Reported role of Si in plants

Reported beneficial traits by Si	Possible mechanism	References
Mechanical support	Attachment to the cell wall, thereby increasing the rigidity	Raven (1983)
	Improves lodging resistance in rice by strengthening stem basis	Liang et al. (2013)
	Cross-links with pectic polysaccharides in cell wall of dicots and maintain integrity	He et al. (2013)
Anti-transpirant	Deposition in the epidermal tissues	Emadian and Newton (1989)
Heavy metal remediation	Cd-Decreased leachability and bioavailability Alleviation of oxidative stress caused by heavy metal by antioxidant enzyme production	Wang et al. (2020); Farooq et al. (2013)
	Cu-Upregulates the genes responsible for metallothioneins (MT) that can chelate toxic metals	Jiang et al. (2018)
	Pb-Increased antioxidant enzymes activity	Bharwana et al. (2013)
	Cr-Increased plant height, root length, and leaf size	Ali et al. (2013)
	Al-Hydroxy aluminosilicate formation in the apoplast thereby reducing mobility of Al	Wang et al. (2004)
	Zn-Establishment of less soluble zinc silicates	Collin et al. (2014)
Salt stress alleviation	Increased activities of guaiacol peroxidase, ascorbate peroxidase, superoxide dismutase, and glutathione reductase	Zhu et al. (2004)
	Reduces the bypass flow of ions to the shoot and accumulation in root apoplast	Thorne et al. (2020)
	Increased SOS and NHX (sodium/hydrogen antiporter) expression	Bosnic et al. (2018)
Drought tolerance	Formation of Si cuticle double layer to reduce water loss	Gong et al. (2003)
	Reduces stomatal conductance resulting in Si deposition with altered cell wall properties	Zhu and Gong (2014)
	Increases the level of glycine betaine	Saleh et al. (2017); Ahmad et al. (2019)
Protection against disease	Hard covering by SiO <sub>2</sub> polymerization in the cuticle	Rodrigues et al. (2003)
	Enhanced activity of chitinase, peroxidase, and polyphenol oxidase	Chérif et al. (1994)
	Accumulation of fungi toxic phenolic compounds and silica depositions	Ghanmi et al. (2004)

matter, metabolites from rhizosphere and non-rhizosphere microorganisms, root exudates, etc., might result in the breakdown of silicate minerals releasing the ionic component. It is well known that biological reactions involving silicon hinge around anabolic bond making and catabolic bond breaking reactions while soil reactions depend on ion exchange, their sorption and desorption. Soil solutions of

**Table 15.3** Reported role of SNP

Physiological process	Crop	Impact	References
Germination and growth	<i>Lycopersicon esculentum</i>	Improves shoot and root growth	Haghighi et al. (2012)
	<i>Thinopyrum intermedium</i>	Breaks seed dormancy and assists germination	Azimi et al. (2014)
	<i>Glycine max</i>	Increased nitrogen assimilation rate, leaf area index, relative growth rate, and yield	Suciaty et al. (2018)
Disease resistance	<i>Zea mays</i>	Renders resistance against <i>Fusarium</i> spp., <i>Aspergillus</i> spp.	Suriyaprabha et al. (2014)
	<i>Lycopersicon esculentum</i>	Displayed potential effect against <i>Alternaria solani</i>	Derbalah et al. (2018)
	<i>Citrullus lanatus</i>	Enhanced innate defense mechanism, and reduced disease severity against <i>Fusarium</i> wilt	Buchman et al. (2019)
Abiotic disease resistance	<i>Crataegus azarolus</i> subsp. <i>aronia</i>	Alleviates drought stress and decreases xylem water potential	Ashkavand et al. (2015)
	<i>Pisum sativum</i>	Upregulates defense system in the presence of Cr (VI)	Tripathi et al. (2015)
	<i>Oryza sativa</i>	Downregulation of Cd uptake genes	Cui et al. (2017)

Si are the initial point and serve as an immediate source to the soil-grown plants. Their presence in pasture plants results in the siliceous compounds ingested by grazing ruminants. With respect to biogeochemical weathering, plants play a pivotal role in silicate weathering, biosilicification, etc. A typical soil may contain 100-500  $\mu\text{mol L}^{-1}$  of silicic acid, however, its availability to plants gets hindered by soil type, temperature, and pH (Sommer et al. 2006). In soil, most Si exists in the form of insoluble aluminosilicates, which are not directly accessible to the plants. Further, the soluble fractions of Si rely on redox potential and pH.

### 15.4.1 Sources of Si in Soil

More than 90 percent of the Earth's crust is comprised of silicate minerals. Traces of Si are commonly found in carbonaceous rocks like limestone and carbonites, in basalt, and of course in such sedimentary rocks as orthoquartzite. The pedosphere of the Earth's crust is composed of approximately 28% Si by weight. Release of silicon into soil occurs from the weathering of silicate-containing minerals. Each kilogram of soil contains generally 50–400 g of Si. In general, there are three different fractions of Si in soil, and these namely are the solid phase, liquid phase, and adsorbed phase. All serve as key components in the soil silicon cycle. The solid

phase is inclusive of amorphous and crystalline forms. The most common form of Si in soil is silicon dioxide ( $\text{SiO}_2$ ), while the major Si components in soil structure include vermiculite, smectite, kaolin, orthoclase, feldspar, plagioclase, amorphous silica, and quartz. The finely dispersed secondary minerals in crystalline forms are mica, clay minerals, kaolinite, and smectite.  $\text{SiO}_2$  is the chief constituent of rock-forming minerals in metamorphic rocks. The coarsely dispersed primary minerals in crystalline form include feldspar and quartz (Matichenkov and Bocharnikova 2001). Free silica mainly occurs as quartz, constituting 12–14% of the lithosphere. The liquid phase of Si is complex and constitutes mainly mono silicic acid, poly silicic acid, and complexes with organic and inorganic compounds. Si as individual atoms are adsorbed to soil particles and as well to Fe and Al hydroxides.

### 15.4.2 Occurrence and Behavior of Si in Soil

Silica occurs in several distinct polymorphs including quartz, cristobalite, tridymite, coesite, silica glass, and opal; while the latter two are amorphous. Out of all the minerals, quartz is found copiously in the soil environment and cristobalite commonly occurs in soil. Figure 15.1 depicts the polymorphs of silica.

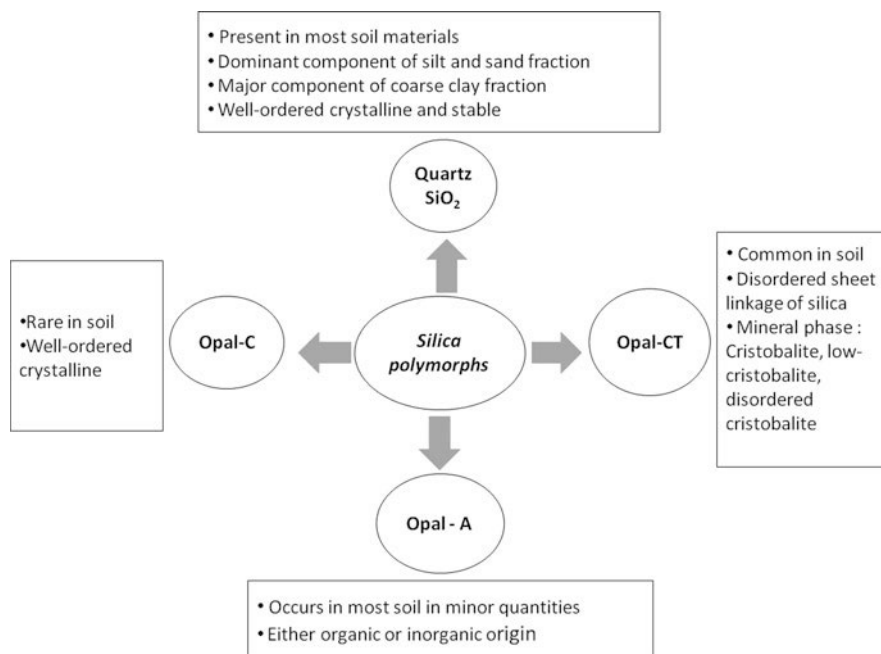


**Fig. 15.1** The common silica polymorphs and their characteristics

Silica is known to affect the uptake of several mineral nutrients (both micro and macronutrients) in soil, making it more or less available to the plants. In nature, silicon atoms are neither found in free form nor purely by themselves in crystalline form. Silicon is reactive at higher temperatures. Studies by Schaller et al. (2019) witnessed that silicon can increase phosphorus mobilization specifically the Fe (II)-P. At low pH, Si reduces the soil sorption of phosphorus (P), thereby increasing the plant available portion of P (Owino-Gerroh and Gascho 2005). P is mostly sorbed on Fe, Al, and Mn hydroxides, while Si associates with Fe and Mn thus reducing the hydroxide pools and alters the availability of Fe and Mn (Meharg and Meharg 2015). Si reduces soil acidification by involvement in soil buffering reactions, regulates atmospheric CO<sub>2</sub>, and promotes plant biomass C accumulation within phytoliths. Different soil Si fractions studied by Yang et al. (2020) of various soil layers in broadleaf forests revealed that the silicon components were composed of 97–98.5% of crystalline Si, versus 1.5–2.3% of noncrystalline silica.

### 15.4.3 *Si Pools in Soil and Availability*

The Si cycle in terrestrial ecosystems is quite complex due to the interactions among lithology and weathering, plant uptake, formation of secondary pedogenic phases, and various environmental factors like precipitation, temperature, and hydrology. The primary sources of Si released by weathering of bedrock silicates are governed by lithology and responsible for providing Si to the soil solution in the form of mono silicic acid (dissolved silicon). Part of the released Si is leached and forms secondary clay minerals upon reacting with Al, Fe, and Mg. Si pools in the soil are depicted in Fig. 15.2. The biogenic pool of Si is relatively soluble, and its compounds largely are of plant origin. Plants uptake Si in the form of silicic acid and re-translocate that to the shoots where it gets deposited as amorphous silica in the epidermal layer, often called opal phytoliths (Shakoor et al. 2014). Processes in the soil–plant Si cycle include not only dissolved Si (dSi) uptake, but also phytolith Si (pSi) formation and dissolution influences the Si mobility. These processes release mono silicic acid which is either adsorbed by the plants, or entrapped in neoformed clay minerals, or exported to watersheds representing the fluxes of bioavailable Si (Li et al. 2020). The clay minerals are constituted of 90–95% (amorphous) SiO<sub>2</sub> and traces of P, K, Ca, Na, Mg, Mn, and Fe. This form of silica returns to the soil by means of plant litter, accumulating within the biogenic pool throughout the topsoil (Cornelis et al. 2011). Several factors including pH, phytolith structure differences at plant species-level affect the dissolution rate of biogenic Si in soil. In general, the solubility rate of biogenic silicon compounds is 7–20 times higher than mineral silicates ensuing in efficient recycling of dissolved silicic acid. However, dSi exist in a dynamic equilibrium with various forms of solid silica.

Silicon availability to the plants becomes influenced by several factors such as soil type, age of the soil, and soil pH. Although sand is composed of silicon dioxide, it provides the least plant-available silicon. The soils which are highly weathered are

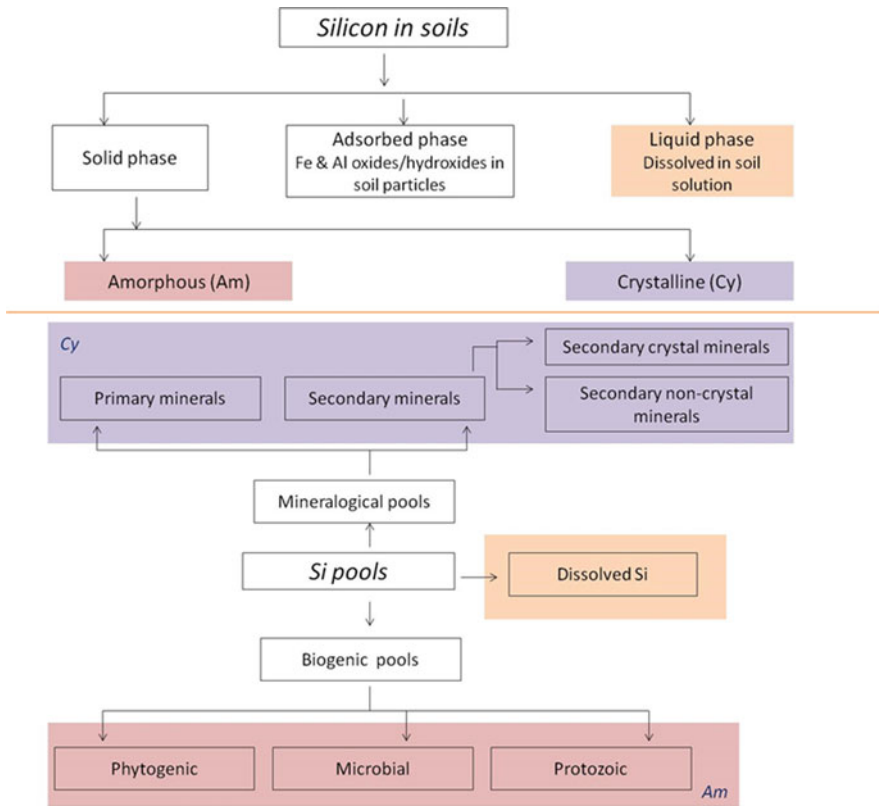


Fig. 15.2 Various fractions of silica in soil and their pools

more highly depleted of silicon than geologically young soils. Since Si does not owe to major component of soil organic matter, those soil types largely or entirely composed of humus and organic matter are devoid of the silicon minerals and possess low silicon content.

### 15.4.4 Weathering and Pedogenesis

Weathering encompasses various functions including precipitation, runoff, lithology, temperature, vegetation, and canopy cover. Land plants and their allied microbiome influence weathering of silicate minerals in various ways such as production of chelating ligands, pH alteration by production of CO<sub>2</sub> or organic acids and modification of soil physical properties (Hinsinger et al. 2001). Weathering processes transform silicate rocks into bicarbonate ions that precipitate into carbonates eventually sedimenting into oceans and chemical weathering leads to

removal of Si by leaching and erosion. The silicon released from the rocks by chemical weathering is taken up by land plants impacting photosynthesis. Disintegration of various rocks such as granites and sandstones releases an enormous quantity of quartz into the soil. The aging processes associated with chemical weathering eventually become less significant factors in silicon supply to the biosphere. The source of secondary silica is weathering of either primary silicate minerals or volcanic glass. Those water–rock interactions that accomplish chemical weathering of silicate minerals present in rocks and sediments create groundwater silica as the circulating groundwater dissolves Si (Hem 1959). Upon dissolution, siliceous limestone releases quartz into the soil.

As a pedogenic compound, opaline silica occurs in soils and is used as a marker of relative soil age. With increasing age, primary Si tends to decrease due to cumulative weathering of primary minerals and leaching of soluble Si. Since the weathering intensity and water flux are greater in the upper horizon, more primary Si gets leached from the upper horizon. The chronosequence of soil study conducted by Kendrick and Graham (2004) revealed that primary Si loss was equivalent to the accumulations of opal Si. The Si loss was concurrent with the dissipation of K and Na reflecting the dissolution of feldspar. Comparing the chronosequence of one of the oldest and the youngest soils in the world revealed that plant-available silicon was lowest in carbonate-rich young soils and increased in intermediate soils, but was decreased in the oldest, quartz-rich soils. The opal phytoliths are, in particular, stable in soils for thousands of years.

## 15.5 Biogeochemical Cycle of Si in Terrestrial and Aquatic Ecosystem

The accumulation and synthesis of biominerals containing  $\text{SiO}_2$  serve as a first foot in the terrestrial silica cycle. Hyper accumulators deposit major amount of amorphous Si in their tissues as phytoliths. The ecosystems encompassing copious accumulators such as tropical rainforests, grasslands, and bamboo forests are termed as “silica factories.” While in aquatic ecosystems, “silica bioengineers” are diatoms, sponges, and chrysophytes. Both play crucial roles in the silica biogeochemical cycle within their respective terrestrial and aquatic ecosystem. Si compounds resulted from the weathering of silicates and aluminosilicates in the bedrock and soil then enter natural waters such as rivers and lakes where they often typically are found in concentrations lower than  $120 \text{ mg SiO}_2\text{L}^{-1}$ . Those compounds serve as a substantial proportion of the Si absorbed by plants and influence the Si in soil solution. Rainwater also contains very little Si, contributing to accretion and input of  $<1 \text{ kg ha}^{-1} \text{ year}^{-1}$ . Rivers transport silicic acid (soluble product of weathering) to the oceans, where it is exploited by marine ecosystem. In the marine primary production, Si cycling is crucial.



The silicon which rivers transport to the oceans represents perhaps 80% of the ocean's total silicon. Dissolved silica (dSi) is significant in sustaining the riverine, coastal, and oceanic ecosystem since their primary productivity relies on the availability of dSi for phytoplankton. dSi varies in environmental concentration due to several factors such as land cover, evaporation, runoff in different rivers at a global scale (Wang et al. 2016). The oceanic reservoir and fluxes of its associated silicon are assumed to balance between inputs and sedimentation. The Si cycle in combined terrestrial and marine ecosystems is provided in Fig. 15.3. However, intense biogeochemical cycling occurs in both of those component ecosystems with recycling a dominant component. The annual production of terrestrial Bsi (biogenic silica) was found to be an order of magnitude higher than that of the annual inputs of dSi to the ocean (Tréguer et al. 1995).

### 15.5.1 Factors Influencing Biogeochemical Cycle of Si

Plants are the regulating factor in governing the silicon cycle shifts from geochemical process to biological control. On the order of nutrients in the soil like carbon and nitrogen, silica is also affected by soil warming due to global climate change (Gewirtzman et al. 2019). Among the reservoirs of amorphous Si, it is the pedogenic silica fraction that most easily gets influenced by soil pH. Si content in groundwater is dictated by several factors including permeability, lithology, and residence time of Si-groundwater interaction.

### 15.5.2 The Role of Microorganisms in Silicification

Soil dwelling bacteria bear the ability to depolymerize crystalline silicates in soil. Reports additionally suggest the release of Si from rocks and minerals by the soil heterotrophic fungi. Bacterial breakdown of naturally occurring and synthetic silicates was reported by several investigations (Webley et al. 1963; Malinovskaya et al. 1990). A *Pseudomonas* strain native of soil was known to dissolve most synthetic forms of silicate such as zinc, magnesium, and calcium, and the minerals of apophyllite, olivine, and wollastonite. Bacteria like *Proteus mirabilis*, [*Bacillus caldolyticus*, *Sporosarcina ureae*], and soil fungi like *Penicillium notatum* and *Penicillium simplicissimum* were also found to degrade silicates. *Paenibacillus mucilaginosus* was also reported to degrade silicate minerals. Several microorganisms like *Aspergillus niger*, *Methylobacterium extorquens*, and *Clostridium pasteurianum* were found to grow on muscovite, biotite, orthoclase, and micas in vitro (Reitemeier 1951).

Application of organominerals to crop plants increases the yield by an average of 18% in maize, wheat, potato, and tomatoes and a further 15% raise was obtained by the application of organominerals inoculated with silicate bacteria (Aleksandrov

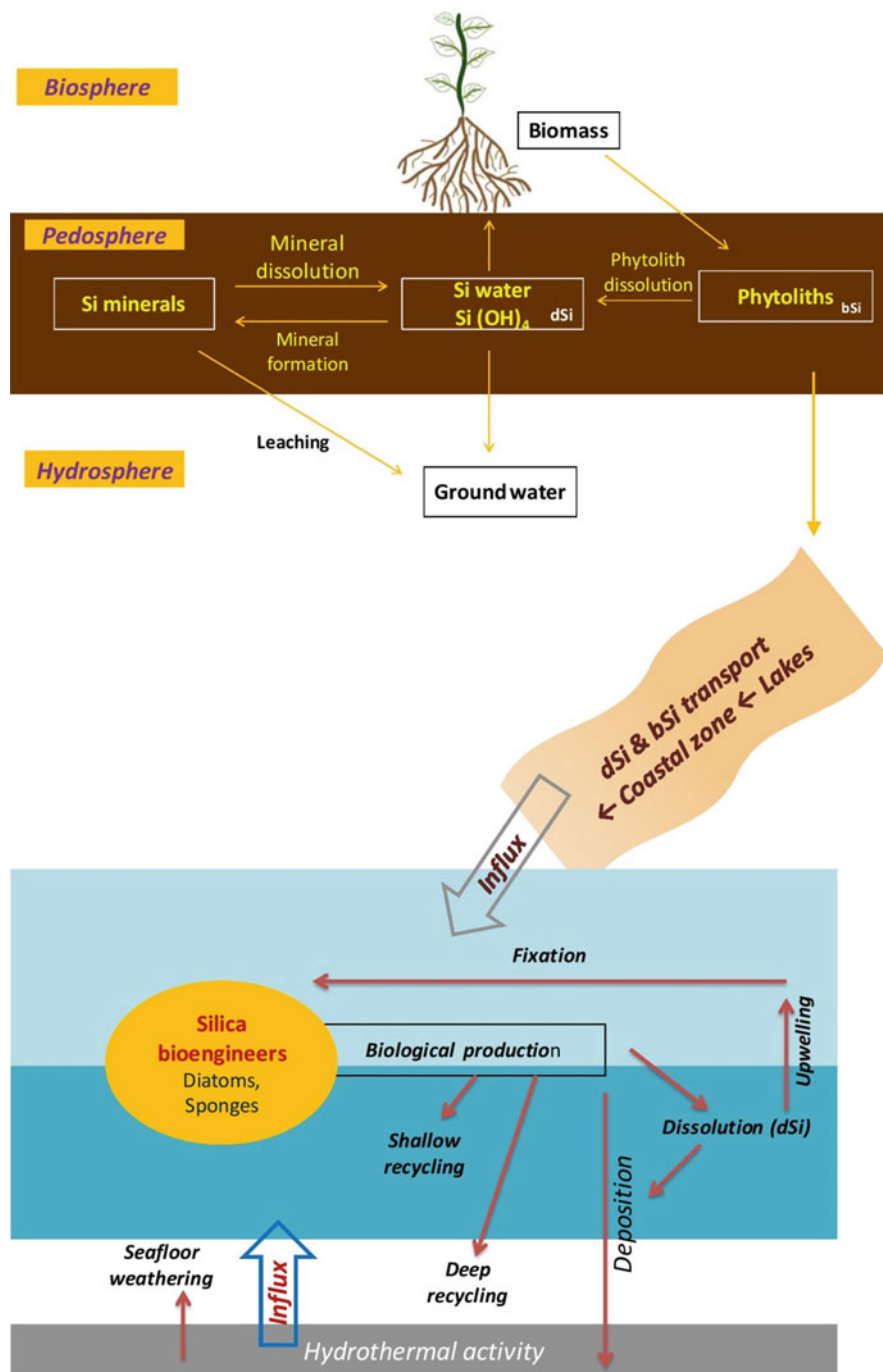


Fig. 15.3 Si biogeochemical cycle in terrestrial and aquatic ecosystem

1958). Ciobanu (1961) found that in degraded chernozem soils “Azotobacterin” (*Azotobacter*) and “silicabacterin” (*Silicibacter*) when applied simultaneously increased the yields of cotton. An efficient strain of silicate bacteria, currently designated *Nialliacirculans*, when used as a soil bioinoculant benefitted on the release of potassium and silicon from various minerals (Zahra et al. 1984). Soil contains silicate minerals that include potassium in them. Hence, when those silicates are acted upon, phosphorus will be solubilized and potassium will also be released. Thus, when silica is in solution it competes with the fixation sites for phosphorus thereby rendering phosphorus availability.

The direct role of microorganisms in the process of silica mobilization and precipitation involves several unknown factors and has been dubious. Microbial cell surfaces with their ultrastructure and extracellular polymeric substances (EPS) serve as a nucleation site thereby augmenting the precipitation of amorphous silica colloids and gels (Li et al. 2012). Sauro et al. (2018) have studied the microbial diversity in orthoquartzite caves to gain insight on subsurface silica cycle. The complex chemotropic microbial communities colonize and create chemical conditions appropriate for the quartz dissolution by i) increased amount of metal ions and inorganic cations as a consequence of biomineralization process and ii) increased pH moderated by microbial metabolism.

Several silica solubilizing bacteria like *Proteus mirabilis*, *Paenibacillus mucilaginosus*, [*Bacillus*] *caldolyticus*, *Pseudomonas*, and also the fungi *Penicillium*, have been found particularly effective at releasing silica from silicates (Lauwers and Heinen 1974; Avakyan et al. 1986).

### 15.5.2.1 Silica Solubilizing Bacteria and Sources of Silica in Soil

Silica solubilizing bacteria (SSB) have been isolated from paddy soil samples using Bunt and Rovira (1955) medium having 0.25 percent insoluble magnesium trisilicate, and the silicate-solubilizing colonies exhibit clear zones indicating that the magnesium trisilicate had been solubilized. The bacterial isolate from soil of a granite crusher yard showed a similar but larger clearing zone and was identified as *Bacillus* sp. Isolation of silica solubilizing bacteria was accomplished with Silicate minerals like feldspar, mica muscovite, biotite kaolin, vermiculite, quartz, and black ash (rice husk char). The silicate sources were pulverized and sieved through 60 mesh BSS and incorporated into basal medium at 0.25% level carefully avoiding the addition of dipotassium hydrogen phosphate to isolate silicate solubilizers alone. A clearing zone annule ranging between 2.64 cm<sup>2</sup> and 19.79 cm<sup>2</sup> was observed in modified Bunt and Rovira medium the highest with mica as silica source and the lowest with feldspar as silica source. An increase in the available silica content in the culture broth confirmed the same suggesting their release. Quartz and silica minerals were most solubilized with the release of 10.9 mg of SiO<sub>2</sub>.l<sup>-1</sup> after 20 days of inoculation. It was also found that autoclaving itself released some amount of silica from these organic siliceous materials. The effect of SSB on various organic and inorganic sources of silica may vary. Experiments with incorporation of varied silica

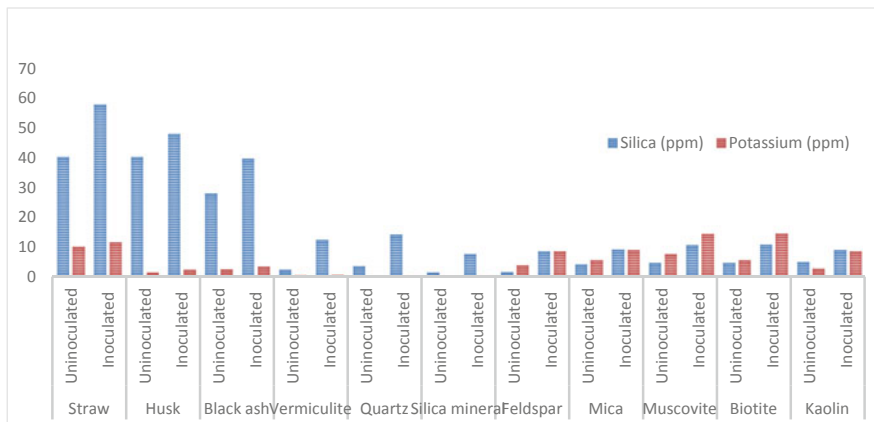


**Fig. 15.4** Solubilization of silica and potassium from silicates and organic siliceous materials by silica solubilizing bacteria

sources into mineral medium show that straw was more easily degraded releasing large quantities of silica as compared to the powdered minerals. The breakdown of organic siliceous materials also released phosphorus as evinced by an enhanced level of phosphorus in straw treatment in comparison with minerals. Unfortunately, no phosphorus was detected in media containing silicate minerals. There was a simultaneous release of potassium from silicate minerals and organic siliceous materials by SSB. The release of potassium increased with the incubation period. A higher potassium release was observed in straw incorporated medium. Higher release was also observed in the K-bearing silicate minerals like biotite, muscovite, mica, and feldspar. After 20 days of incubation as much as about 8–9 ppm increase was found in biotite incorporation. In vermiculite, quartz, and silica mineral incorporation, K release was almost negligible (Fig. 15.4).

### 15.5.2.2 Silica Solubilizing Bacteria (SSB) and Other Nutrient Availability in Soil

In another experiment, four different soils viz., red soil, clayey soil, sandy soils of a kg each and low bulk density forest soil of 700 g were filled in tubular pots (18 x 12 cm). The soil was moistened to 55 percent water holding capacity and one set was sterilized and the other left unsterile. The pots were inoculated with, SSB grown in nutrient broth (ca.  $10^9$  cells/ml) at the rate of 10 ml per 100 g soil. Analyses of water samples for available silica, phosphorus, and potassium, and silica in soil were done weekly. The available silica in sand and forest soil was higher as sand is primarily silica and SSB inoculation might have solubilized a larger proportion. Chinnaswamy and Chandrasekaran (1976) reported a higher available silica in clay soils than clayey loam and sandy loam. However, Nayar et al. (1982) reported that the available silica in rice soil was greatly influenced by flooding and the magnitude

of increase in silica was more in laterite soils than black soil. A mere submergence of soil released very little silica in sterile soils whereas in unsterile soil it was higher. This revealed the role of microorganisms in depolymerization of silicates. This view is also strengthened by the fact that inoculation of SSB augmented its level greatly in all these soils both under sterile and unsterile conditions. It is evident from these studies that SSB inoculation augmented silica content in soil solution and in soil of any type and this could be exploited as a bioinoculant.

The release of silica and potassium influenced by SSB and Phosphate solubilizing bacteria (PSB) are provided in Fig. 15.5(a and b). The potassium release was relatively higher in forest soil followed by clay, red and sandy soil due to SSB inoculation. This might be due to variation in K-bearing silicate minerals present in these soils and the organic matter content in the soils, which play a major role in the release of potassium (Tandon and Sekhon 1988). The K may be liberated to the immediately exchangeable form both by decomposition of K-bearing feldspar, and by replacement of interlayer K ions of micas. A part of this K may be fixed between the layers of particles of micaceous and montmorillonite minerals. The return of plant residue to soil will result in the liberation of their potassium to soluble and exchangeable ions by way of silicate solubilization. The release of K might be due to (i) Breakdown of K-bearing minerals and (ii) Si ions causing changes in the exchangeable ion status of minerals. This can occur irrespective of the soil upon SSB inoculation.

### 15.5.2.3 Silica Solubilizing Bacteria (SSB) and Phosphorus Dissolution in Soil

In the above experiment, when PSB was inoculated replacing SSB to the different soils, a higher solubilization of phosphorus was evident in forest soils followed by clay, red, and sandy soils. Unsterile soils had higher phosphorus levels in comparison to sterile soil. However, SSB inoculation simultaneously released the increased levels of potassium in forest soil followed by clay, red, and sandy soils after 4 weeks. A higher release was observed in unsterile set compared to sterilized set. The growth of SSB, *Bacillus* sp. on Bunt and Rovira medium supplemented with mica, quartz, silica mineral (sand), and magnesium trisilicate was quick and prominent. Lauwers and Heinen (1974) reported the ability of *Bacillus caldolyticus* and *Proteus mirabilis* to grow and solubilize quartz. Under studies with incorporation of various silica sources, a higher amount of silica was released from organic siliceous materials like straw, husk, and black ash than mineral sources. This might be due to their higher silica content itself, besides they are easily degraded and mineralized in nature. The solubilization of silica from silicates might be due to production of carbon dioxide, organic acids, exopolysaccharide production, alkali production, and H<sub>2</sub>S production (Ehrlich 1981; Malinovskaya et al. 1990). We also observed that autoclaving for sterilization itself released to some extent silica from both organic siliceous materials and silicate minerals suggesting the role of higher temperature similar to weathering.

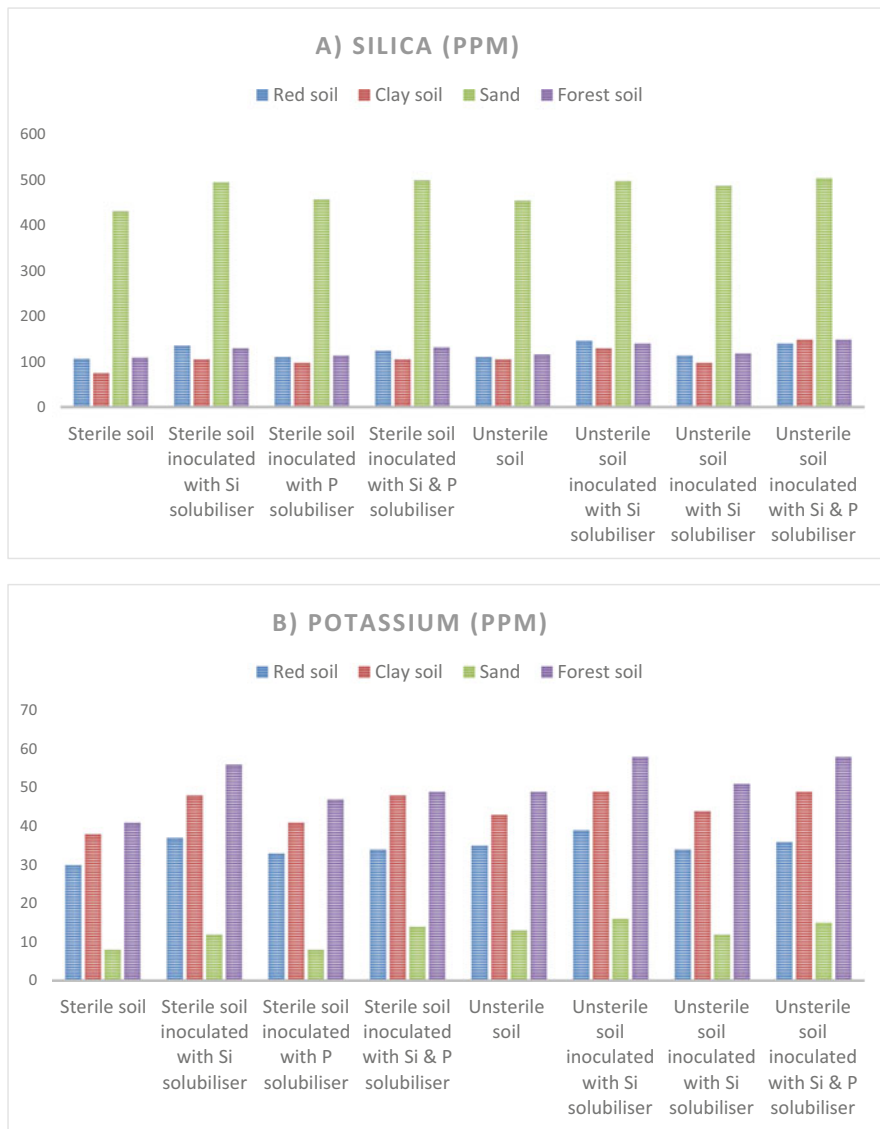


**Fig. 15.5** Release of available (a) silica and (b) Potassium in different soils inoculated with silicate and phosphorus solubilizing bacteria

The solubilization of P from different soils studied may not be solely due to the direct action of organic acids elaborated by the organisms as the silica solubilized by SSB can reverse P-fixation and keep the P-ion available in solution. The release of phosphate by silicate and the reversal of phosphorus fixation by silica was also reported (Jones and Handreck 1967). A higher release of phosphorus was noted in

soils treated with PSB or SSB. Bassitisse (1947) reported that silica mobilized phosphate anions by limiting the energy of fixation of soil colloids and precipitating the oxides of iron and aluminum in laterite soils. Roy et al. (1971) had also shown that silicic acid might compete against phosphate for a place on the hydrated hydroxides and such a mechanism might operate in the red soil in the study.

#### **15.5.2.4 Silica Solubilizing Bacteria (SSB) and Potassium Release in Soil**

The breakdown of silicate concurrently releases potassium. Upon progressive incubation of soil, there has been found higher release of K from K-bearing silicate minerals like muscovite, biotite, and feldspar by SSB. Reitemeier (1951) reported the growth of *Aspergillus niger* on cultivation medium containing muscovite, biotite, orthoclase, and microcline. The release of K observed might arise due to (i) leaching from the organic siliceous residues, (ii) decomposition of the organic matter, or (iii) breakdown of silicate in these materials. Soil incubation studies with and without inoculation of SSB, PSB, SSB, and PSB showed a varying intensity of dissolution of silica, phosphorus, and potassium, and this varied with the nature of soil and the inoculant. The survival of the inoculants over a period of time in sterile as well as unsterile soils indicated that the organic matter and the other nutrients available in the soils might have favored their survival even in the absence of plants that provide nutrients through root exudates, root decay, or leaf fall.

### **15.5.3 Silica Solubilizing Bacteria Application to Paddy Soil**

Silicate minerals are applied as fertilizers to acquire various direct and indirect effects. A desperately large amount of phosphorus fixation is prevented, thereby releasing fixed phosphorus and increasing the available P in the soil. Intensive cultivation of crops leads to Si removal and subsequently rejuvenation by external application of Si helps in maintaining soil Si status. It is to be recorded that farmers in the Cauvery delta in India hold a practice of applying 3–5 tons of SiO<sub>2</sub> (river sand) per hectare every 2 years.

There are a variety of siliceous materials available in rice paddy ecosystems. Rice stubbles (straw and root) left in the field constitute easily 1–2 t per ha depending upon the harvest and season. Rice straw rich in silica and potassium is left in the field uncollected when mechanical harvesting is done. Similarly, rice husk ash is available to the tune of 4–5 million tonnes annually. This contains 65% silica, 20–30% carbon, and a variety of micronutrients. Addition of these rice straws and rice husk ash can augment grain yield of rice particularly when the soil is inoculated with SSB. Black ash is available in rice mills scattered all over the rice growing area and is a renewable waste that can be used as a source of silica along with SSB. Raw sugarcane trash also can be used in rice culture with SSB so as to provide silica and other nutrients to rice.

## 15.6 Conclusion

The chemistry and the metabolism of silica in soil are outstretched due to their omnipresent nature and potential to form a wide range of compounds. In the realm of soil science, various developments and standardizations of procedures for extraction of the soil silicon fraction have allowed us to witness the significance of Si in soil fertility and management. However, although Si often does not come under the list of essential nutrient elements, their innumerable benefits exerted on the plants by direct and indirect means demonstrate the importance of Si fertilization. The recent advancements in several fields of knowledge have yielded effective production of Silica nanoparticles and eventually those advancements may prove beneficial to agriculture. Even so, many aspects of silicon availability in soil are understudied and need to further be explored for the purpose of enhancing plant growth and development, and those benefits will couple with the improvement of soil fertility.

## References

- Ali S, Farooq MA, Yasmeen T, Hussain S, Arif MS, Abbas F et al (2013) The influence of silicon on barley growth, photosynthesis and ultra-structure under chromium stress. *Ecotoxicol Environ Saf* 89:66–72. <https://doi.org/10.1016/j.ecoenv.2012.11.015>
- Abdelrahman TM, Qin X, Li D, Senosy IA, Mmby M, Wan H, Li J, He S (2021) Pectinase-responsive carriers based on mesoporous silica nanoparticles for improving the translocation and fungicidal activity of prochloraz in rice plants. *Chem Eng J* 404:126440. <https://doi.org/10.1016/j.cej.2020.126440>
- Ahmad P, Ahanger MA, Alam P, Alyemeni MN, Wijaya L, Ali S, Ashraf M (2019) Silicon (Si) supplementation alleviates NaCl toxicity in Mung Bean [*Vigna radiata* (L.) Wilczek] through the modifications of physio-biochemical attributes and key antioxidant enzymes. *J Plant Growth Regul* 38(1):70–82. <https://doi.org/10.1007/s00344-018-9810-2>
- Aleksandrov V (1958) Organo-mineral fertilizers and silicate bacteria. *Dokl Akad Nauk*:43–48
- Ashkavand P, Tabari M, Zarafshar M, Tomášková I, Struve D (2015) Effect of SiO<sub>2</sub> nanoparticles on drought resistance in hawthorn seedlings. *Leśne Prace Badawcze* 76(4):350–359
- Avakyan Z, Pivovarova T, Karavaiko G (1986) Properties of a new species, *Bacillus-mucilaginosus*. *Microbiology* 55(3):369–374
- Azimi R, Borzelabad MJ, Feizi H, Azimi A (2014) Interaction of SiO<sub>2</sub> nanoparticles with seed prechilling on germination and early seedling growth of tall wheatgrass (*Agropyron elongatum* L.). *Polish J Chem Technol* 16(3):25–29
- Bassittise K (1947) Studies on theoretical and practical conditions in which the availability of phosphoric acid as maintained in lateritic soils. *Annals Agronomy* 16:463–475
- Bharwana S, Ali S, Farooq M, Iqbal N, Abbas F, Ahmad M (2013) Alleviation of lead toxicity by silicon is related to elevated photosynthesis, antioxidant enzymes suppressed lead uptake and oxidative stress in cotton. *J Bioremed Biodegr* 4(4):187
- Bosnic P, Bosnic D, Jasnica J, Nikolic M (2018) Silicon mediates sodium transport and partitioning in maize under moderate salt stress. *Environ Exp Bot* 155:681–687. <https://doi.org/10.1016/j.envexpbot.2018.08.018>
- Buchman JT, Elmer WH, Ma C, Landy KM, White JC, Haynes CL (2019) Chitosan-coated mesoporous silica nanoparticle treatment of *Citrullus lanatus* (watermelon): enhanced fungal disease suppression and modulated expression of stress-related genes. *ACS Sustain Chem Eng* 7(24):19649–19659. <https://doi.org/10.1021/acssuschemeng.9b04800>



- Bunt B, Rovira S (1955) Isolation media for microbial analysis. *Nature* 56:156–158
- Chérif M, Asselin A, Bélanger R (1994) Defense responses induced by soluble silicon in cucumber roots infected by *Pythium* spp. *Phytopathology* 84(3):236–242
- Chinnaswamy K, Chandrasekaran S (1976) Effect of silica gel on rice in three soil types [India], Auara
- Ciobanu I (1961) Investigation on the efficiency of bacterial fertilizers applied to cotton. *Cent Exp Ingras Bact Lucrari Stiint* 3:203–214
- Collin B, Doelsch E, Keller C, Cazeville P, Tella M, Chaurand P et al (2014) Evidence of sulfur-bound reduced copper in bamboo exposed to high silicon and copper concentrations. *Environ Pollut* 187:22–30. <https://doi.org/10.1016/j.envpol.2013.12.024>
- Cornelis JT, Delvaux B, Georg RB, Lucas Y, Ranger J, Opfergelt S (2011) Tracing the origin of dissolved silicon transferred from various soil-plant systems towards rivers: a review. *Biogeosciences* 8(1):89–112. <https://doi.org/10.5194/bg-8-89-2011>
- Cui J, Liu T, Li F, Yi J, Liu C, Yu H (2017) Silica nanoparticles alleviate cadmium toxicity in rice cells: mechanisms and size effects. *Environ Pollut* 228:363–369. <https://doi.org/10.1016/j.envpol.2017.05.014>
- Davy H (1819) *Éléments de chimie agricole*. Ladrage, Paris
- Derbalah A, Shenashen M, Hamza A, Mohamed A, El Safty S (2018) Antifungal activity of fabricated mesoporous silica nanoparticles against early blight of tomato. *Egypt J Basic Appl Sci* 5(2):145–150. <https://doi.org/10.1016/j.ejbas.2018.05.002>
- Ehrlich HL (1981) *Geo microbiology*. Marcel Dekker Inc., New York, p 393
- El-Shetehy M, Moradi A, Maceroni M, Reinhardt D, Petri-Fink A, Rothen-Rutishauser B, Mauch F, Schwab F (2021) Silica nanoparticles enhance disease resistance in Arabidopsis plants. *Nat Nanotechnol* 16(3):344–353. <https://doi.org/10.1038/s41565-020-00812-0>
- Emadian SF, Newton RJ (1989) Growth enhancement of loblolly pine (*Pinus taeda* L.) seedlings by silicon. *J Plant Physiol* 134(1):98–103. [https://doi.org/10.1016/S0176-1617\(89\)80209-3](https://doi.org/10.1016/S0176-1617(89)80209-3)
- Epstein E (1994) The anomaly of silicon in plant biology. *Proc Natl Acad Sci* 91(1):11. <https://doi.org/10.1073/pnas.91.1.11>
- Epstein E (1999) SILICON. *Annu Rev Plant Physiol Plant Mol Biol* 50(1):641–664. <https://doi.org/10.1146/annurev.arplant.50.1.641>
- Farooq MA, Ali S, Hameed A, Ishaque W, Mahmood K, Iqbal Z (2013) Alleviation of cadmium toxicity by silicon is related to elevated photosynthesis, antioxidant enzymes; suppressed cadmium uptake and oxidative stress in cotton. *Ecotoxicol Environ Saf* 96:242–249. <https://doi.org/10.1016/j.ecoenv.2013.07.006>
- Gewirtzman J, Tang J, Melillo JM, Werner WJ, Kurtz AC, Fulweiler RW, Carey JC (2019) Soil warming accelerates biogeochemical silica cycling in a temperate forest. *Front Plant Sci* 10(1097). <https://doi.org/10.3389/fpls.2019.01097>
- Ghanmi D, McNally DJ, Benhamou N, Menzies JG, Bélanger RR (2004) Powdery mildew of *Arabidopsis thaliana*: a pathosystem for exploring the role of silicon in plant–microbe interactions. *Physiol Mol Plant Pathol* 64(4):189–199. <https://doi.org/10.1016/j.pmpp.2004.07.005>
- Gong HJ, Chen KM, Chen GC, Wang SM, Zhang CL (2003) Effects of silicon on growth of wheat under drought. *J Plant Nutr* 26(5):1055–1063. <https://doi.org/10.1081/PLN-120020075>
- Gunnarsson I, Arnórsson S (2000) Amorphous silica solubility and the thermodynamic properties of H<sub>4</sub>SiO<sub>4</sub> in the range of 0° to 350°C at Psat. *Geochim Cosmochim Acta* 64(13):2295–2307. [https://doi.org/10.1016/S0016-7037\(99\)00426-3](https://doi.org/10.1016/S0016-7037(99)00426-3)
- Guntzer F, Keller C, Meunier J-D (2012) Benefits of plant silicon for crops: a review. *Agron Sustain Dev* 32(1):201–213. <https://doi.org/10.1007/s13593-011-0039-8>
- Haghighi M, Afifipour Z, Mozafarian M (2012) The effect of N-Si on tomato seed germination under salinity levels. *J Biol Environ Sci* 6(16):87–90
- He C, Wang L, Liu J, Liu X, Li X, Ma J, Lin Y, Xu F (2013) Evidence for ‘silicon’ within the cell walls of suspension-cultured rice cells. *New Phytol* 200(3):700–709. <https://doi.org/10.1111/nph.12401>

- Hem JD (1959) Study and interpretation of the chemical characteristics of natural water. US Geological Survey, United States Government Printing Office, Washington, DC
- Hinsinger P, Fernandes Barros ON, Benedetti MF, Noack Y, Callot G (2001) Plant-induced weathering of a basaltic rock: experimental evidence. *Geochim Cosmochim Acta* 65(1): 137–152. [https://doi.org/10.1016/S0016-7037\(00\)00524-X](https://doi.org/10.1016/S0016-7037(00)00524-X)
- Ishibashi H (1936) Influence of silica on the growth of rice plant. *Jpn J Soil Sci Plant Nutr* 10:244–256
- Jiang N, Shang R, Heijman SGJ, Rietveld LC (2018) High-silica zeolites for adsorption of organic micro-pollutants in water treatment: a review. *Water Res* 144:145–161. <https://doi.org/10.1016/j.watres.2018.07.017>
- Jones LHP, Handreck KA (1967) Silica in soils, plants, and animals. In: Norman AG (ed) *Advances in agronomy*, vol 19. Academic Press, pp 107–149. [https://doi.org/10.1016/S0065-2113\(08\)60734-8](https://doi.org/10.1016/S0065-2113(08)60734-8)
- Kendrick KJ, Graham RC (2004) DIVISION S-5—PEDOLOGY. *Soil Sci Soc Am J* 68:1295–1303
- Kim Y-H, Khan AL, Lee I-J (2016) Silicon: a duo synergy for regulating crop growth and hormonal signaling under abiotic stress conditions. *Crit Rev Biotechnol* 36(6):1099–1109. <https://doi.org/10.3109/07388551.2015.1084265>
- Lauwers AM, Heinen W (1974) Bio-degradation and utilization of silica and quartz. *Arch Microbiol* 95(1):67–78. <https://doi.org/10.1007/BF02451749>
- Li J, Zhou H, Peng X, Wu Z, Chen S, Fang J (2012) Microbial diversity and biomineralization in low-temperature hydrothermal iron–silica-rich precipitates of the Lau Basin hydrothermal field. *FEMS Microbiol Ecol* 81(1):205–216. <https://doi.org/10.1111/j.1574-6941.2012.01367.x>
- Li Z, Cornelis J-T, Linden CV, Van Ranst E, Delvaux B (2020) Neoformed aluminosilicate and phytogenic silica are competitive sinks in the silicon soil–plant cycle. *Geoderma* 368:114308. <https://doi.org/10.1016/j.geoderma.2020.114308>
- Liang S, Li Z, Li X, Xie H, Zhu R, Lin J, Xie H, Wu H (2013) Effects of stem structural characters and silicon content on lodging resistance in rice (*Oryza sativa* L.). *Res Crops* 14(3):621–636
- Liang Y, Nikolic M, Bélanger R, Gong H, Song A (2015) *Silicon in agriculture*, vol 10. Springer, Dordrecht, pp 978–994
- Luyckx M, Hausman J-F, Lutts S, Guerriero G (2017) Silicon and plants: current knowledge and technological perspectives. *Front Plant Sci* 8:411. <https://doi.org/10.3389/fpls.2017.00411>
- Malinovskaya I, Kosenko L, Votselko S, Podgorsky V (1990) The role of *Bacillus mucilaginosus* polysaccharide in the destruction of silicate minerals. *Mikrobiologiya* 59(1):70–78
- Matichenkov VV, Bocharnikova EA (2001) Chapter 13: The relationship between silicon and soil physical and chemical properties. In: Datnoff LE, Snyder GH, Korndörfer GH (eds) *Studies in plant science*, vol 8. Elsevier, pp 209–219. [https://doi.org/10.1016/S0928-3420\(01\)80017-3](https://doi.org/10.1016/S0928-3420(01)80017-3)
- McCray JM, Mylavarapu R (2010) Sugarcane nutrient management using leaf analysis. *EDIS* 2010: 4
- Meharg C, Meharg AA (2015) Silicon, the silver bullet for mitigating biotic and abiotic stress, and improving grain quality, in rice? *Environ Exp Bot* 120:8–17. <https://doi.org/10.1016/j.envexpbot.2015.07.001>
- Mitani N, Ma JF (2005) Uptake system of silicon in different plant species. *J Exp Bot* 56(414): 1255–1261. <https://doi.org/10.1093/jxb/eri121>
- Nayar PK, Misara AK, Patnaik S (1982) Silica in rice and flooded rice soils. *Oryza* 19:34–40
- Ohkawa K (1936) Studies on plant physiological function of silica (1). *Jpn J Soil Sci Plant Nutr* 10: 96–101
- Owino-Gerroh C, Gascho GJ (2005) Effect of silicon on low pH soil phosphorus sorption and on uptake and growth of maize. *Commun Soil Sci Plant Anal* 35(15–16):2369–2378. <https://doi.org/10.1081/LCSS-200030686>
- Reitemeier RF (1951) Soil potassium. In: *Advances in agronomy*, vol III. (A.G. Norman, Ed.). Academic Prem Intl. Publ., New York, pp 113–164
- Raven JA (1983) The transport and function of silicon in plants. *Biol Rev* 58(2):179–207. <https://doi.org/10.1111/j.1469-185X.1983.tb00385.x>

- Rodrigues FÁ, Vale FXR, Korndörfer GH, Prabhu AS, Datnoff LE, Oliveira AMA, Zambolim L (2003) Influence of silicon on sheath blight of rice in Brazil. *Crop Prot* 22(1):23–29. [https://doi.org/10.1016/S0261-2194\(02\)00084-4](https://doi.org/10.1016/S0261-2194(02)00084-4)
- Roy AC, Ali MY, Fox RL, Silva JA (1971) Influence of calcium silicate on phosphate solubility and availability in Hawaiian latosols.
- Saleh J, Najafi N, Oustan S (2017) Effects of silicon application on wheat growth and some physiological characteristics under different levels and sources of salinity. *Commun Soil Sci Plant Anal* 48(10):1114–1122. <https://doi.org/10.1080/00103624.2017.1323090>
- Sauro F, Cappelletti M, Ghezzi D, Columbu A, Hong P-Y, Zowawi HM, Carbone C, Piccini L, Vergara F, Zannoni D, De Waele J (2018) Microbial diversity and biosignatures of amorphous silica deposits in orthoquartzite caves. *Sci Rep* 8(1):17569. <https://doi.org/10.1038/s41598-018-35532-y>
- Schaller J, Faucherre S, Joss H, Obst M, Goeckede M, Planer-Friedrich B, Peiffer S, Gilfedder B, Elberling B (2019) Silicon increases the phosphorus availability of Arctic soils. *Sci Rep* 9(1):449. <https://doi.org/10.1038/s41598-018-37104-6>
- Shakoor SA, Bhat MA, Mir SH, Soodan AS (2014) Investigations into phytoliths as diagnostic markers for the grasses (Poaceae) of Punjab. *Univers J Plant Sci* 2:107–122. <https://doi.org/10.13189/ujps.2014.020602>
- Sommer M, Kaczorek D, Kuzyakov Y, Breuer J (2006) Silicon pools and fluxes in soils and landscapes—a review. *J Plant Nutr Soil Sci* 169(3):310–329. <https://doi.org/10.1002/jpln.200521981>
- Struyf E, Smis A, Van Damme S, Garnier J, Govers G, Van Wesemael B, Conley DJ, Batelaan O, Frot E, Clymans W, Vandevenne F, Lancelot C, Goos P, Meire P (2010) Historical land use change has lowered terrestrial silica mobilization. *Nat Commun* 1(1):129. <https://doi.org/10.1038/ncomms1128>
- Suciaty T, Purnomo D, Sakya AT, Supriyadi (2018) The effect of nano-silica fertilizer concentration and rice hull ash doses on soybean (*Glycine max* (L.) Merrill) growth and yield. *IOP Conference Series: Earth and Environmental Science* 129:012009. <https://doi.org/10.1088/1755-1315/129/1/012009>
- Sun D, Hussain HI, Yi Z, Rookes JE, Kong L, Cahill DM (2016) Mesoporous silica nanoparticles enhance seedling growth and photosynthesis in wheat and lupin. *Chemosphere* 152:81–91. <https://doi.org/10.1016/j.chemosphere.2016.02.096>
- Suriyaprabha R, Karunakaran G, Kavitha K, Yuvakkumar R, Rajendran V, Kannan N (2014) Application of silica nanoparticles in maize to enhance fungal resistance. *IET Nanobiotechnol* 8(3):133–137. <https://doi.org/10.1049/iet-nbt.2013.0004>
- Tandon HLS, Sekhon GS (1988) Potassium research and agricultural production in India. *Fertiliser Development and Consultation Organisation, New Delhi*
- Thiagalangam K, Silva J, Fox R (1977) Effect of calcium silicate on yield and nutrient uptake in plants grown on a humic ferruginous latosol. In: *Conference on Chemistry and Fertility of Tropical Soils, Kuala Lumpur (Malaysia), 5–10 Nov 1973, PSTM*
- Thorne SJ, Hartley SE, Maathuis FJM (2020) Is silicon a panacea for alleviating drought and salt stress in crops? *Front Plant Sci* 11:1221. <https://doi.org/10.3389/fpls.2020.01221>
- Tréguer P, Nelson DM, Van Bennekom AJ, DeMaster DJ, Leynaert A, Quéguiner B (1995) The silica balance in the World Ocean: a Reestimate. *Science* 268(5209):375–379
- Tripathi DK, Singh VP, Prasad SM, Chauhan DK, Dubey NK (2015) Silicon nanoparticles (SiNp) alleviate chromium (VI) phytotoxicity in *Pisum sativum* (L.) seedlings. *Plant Physiol Biochem* 96:189–198. <https://doi.org/10.1016/j.plaphy.2015.07.026>
- Umamaheswari T, Srimeena N, Vasanthi N, Cibichakravarthy B, Anthoniraj S, Karthikeyan S (2016) Silica as biologically transmutated source for bacterial growth similar to carbon. *Matters Archive* 2(3):e201511000005
- Van Soest PJ (2006) Rice straw, the role of silica and treatments to improve quality. *Anim Feed Sci Technol* 130(3):137–171. <https://doi.org/10.1016/j.anifeedsci.2006.01.023>

- Wang B, Liu C-Q, Maberly SC, Wang F, Hartmann J (2016) Coupling of carbon and silicon geochemical cycles in rivers and lakes. *Sci Rep* 6(1):35832. <https://doi.org/10.1038/srep35832>
- Wang Y, Liu Y, Zhan W, Zheng K, Lian M, Zhang C, Ruan X, Li T (2020) Long-term stabilization of Cd in agricultural soil using mercapto-functionalized nano-silica (MPTS/nano-silica): a three-year field study. *Ecotoxicol Environ Saf* 197:110600. <https://doi.org/10.1016/j.ecoenv.2020.110600>
- Wang Y, Stass A, Horst WJ (2004) Apoplastic binding of aluminum is involved in silicon-induced amelioration of aluminum toxicity in maize. *Plant Physiol* 136(3):3762–3770. <https://doi.org/10.1104/pp.104.045005>
- Webley DM, Henderson MEK, Taylor IF (1963) The microbiology of rocks and weathered stones. *J Soil Sci* 14(1):102–112. <https://doi.org/10.1111/j.1365-2389.1963.tb00935.x>
- Yang X, Song Z, Yu C, Ding F (2020) Quantification of different silicon fractions in broadleaf and conifer forests of northern China and consequent implications for biogeochemical Si cycling. *Geoderma* 361:114036. <https://doi.org/10.1016/j.geoderma.2019.114036>
- Zahra MK, Monib M, Abdel-Al SI, Heggo A (1984) Significance of soil inoculation with silicate bacteria. *Zentralbl Mikrobiol* 139(5):349–357. [https://doi.org/10.1016/S0232-4393\(84\)80013-X](https://doi.org/10.1016/S0232-4393(84)80013-X)
- Zhu Y, Gong H (2014) Beneficial effects of silicon on salt and drought tolerance in plants. *Agron Sustain Dev* 34(2):455–472. <https://doi.org/10.1007/s13593-013-0194-1>
- Zhu Z, Wei G, Li J, Qian Q, Yu J (2004) Silicon alleviates salt stress and increases antioxidant enzymes activity in leaves of salt-stressed cucumber (*Cucumis sativus* L.). *Plant Sci* 167(3): 527–533. <https://doi.org/10.1016/j.plantsci.2004.04.020>
- Zippicotte J. (1881) Fertilizer. U.S. Patent No. 238240. Official Gazette of the United States Patent Office; p. 19, 9, and 496

# Chapter 16

## Microbial Interactions with Titanium



Lori Çobani and Ann M. Valentine

**Abstract** Titanium is an abundant element in the Earth's crust and is primarily found as Ti(IV) in slightly soluble mineral oxides. Even though it is avidly sequestered by some organisms, no essential biological role has been found yet. However, the element is unequivocally bioactive, including towards microbes. This chapter will cover how titanium interacts with select unicellular organisms and describe interactions it has with related biomolecules. It will further discuss the use of microbes as Ti nanoparticle producers, Ti antimicrobial function and the possibility of finding titanium in microbial metalloproteomes. Understanding the presence of titanium in diverse phyla of microbes and its different roles in them may pave the way towards discovering an essential biological role of this element in the future.

### 16.1 Abundance and Form of Titanium in the Environment

Titanium is the ninth most abundant element in the Earth's crust (Fig. 16.1) (Van Baalen 1993; Emsley 1998; Kaim et al. 2013). With a concentration of 5600 ppm, it is the second most abundant transition metal after iron but is generally considered inert (Buettner and Valentine 2012; Gallo et al. 2020). Ti(IV) is the most abundant form of titanium in the environment but Ti(III) is present as well. Much less common are the +2, 0 and -1 oxidation states (Valentine 2006). Most of the Ti available in nature exists as insoluble oxides (Van Baalen 1993; Buettner and Valentine 2012). Two common mineral oxides in which titanium can be found are ilmenite ( $\text{FeTiO}_3$ ) and titanite ( $\text{CaSiTiO}_5$ ), but it is also found as leucosene and perovskite (Closs 1983; Skrabal and Terry 2002; Yaroshevsky 2006). The primary crystal forms in which titanium oxide ( $\text{TiO}_2$ ) exists are anatase, rutile and brookite (Valentine 2006). Titanium dioxide makes up about 95% of the titanium found in nature and it also makes up 0.9% of Earth's crust and 1.4% of the oceanic crust (Van Baalen 1993).

---

L. Çobani · A. M. Valentine (✉)

Department of Chemistry, Temple University, Philadelphia, PA, USA

e-mail: [lori.cobani@temple.edu](mailto:lori.cobani@temple.edu); [ann.valentine@temple.edu](mailto:ann.valentine@temple.edu)

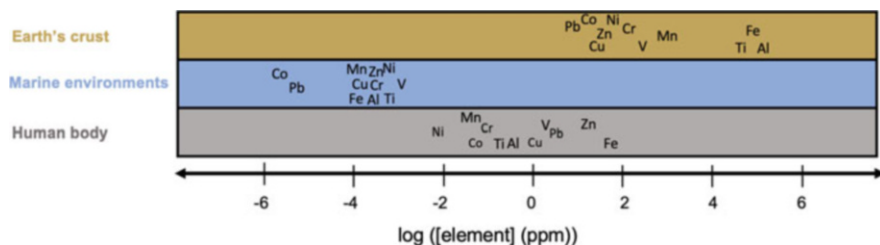


**Fig. 16.1** Abundance of some transition metals in the Earth's crust, in marine environments and in the human body. Adapted from the data of *The Elements* from J. Emsley (Emsley 1998)

Ti(IV) is a strong Lewis acid and is prone to hydrolysis and hydrolytic precipitation (Buettner and Valentine 2012). The hydrolytic behavior of metal complexes in general depends on factors including pH and concentration. The variation of these parameters leads to different species of titanium including many hydroxides and oxides (Baes and Mesmer 1981; Gaffney and Valentine 2011). Ti(IV) is widely favored in aerobic conditions and around neutral pH, while Ti(III) can be formed in reducing environments (Buettner and Valentine 2012). The first deprotonation of a water molecule bound to Ti(IV) occurs below pH 0, and the doubly hydrolyzed species,  $\text{Ti}(\text{OH})_2^{2+}$ , or as the hydrolytically equivalent titanyl ( $\text{Ti}=\text{O})^{2+}$ , exists even in conditions where the pH is below 2. By contrast, the first deprotonation of Fe(III) and Al(III) occur around pH 2 and pH 5, respectively (Baes and Mesmer 1981; Buettner and Valentine 2012). When hydrolyzed further,  $\text{Ti}(\text{OH})_2^{2+}$  gives  $\text{Ti}(\text{OH})_3^+$  and  $\text{Ti}(\text{OH})_4$ , whereas  $\text{Ti}(\text{OH})_5^-$  might also naturally occur at higher pH (Baes and Mesmer 1981; Buettner and Valentine 2012). The behavior of Ti in different conditions of aqueous chemistry helps guide our understanding of how nature has handled this metal. Even though it is fairly abundant, titanium has a low bioavailability due to the fact that it is only sparingly soluble in aqueous environments which may have prevented it from being widely used by different organisms (Zierden and Valentine 2016). Avid metal-binding ligands can support increased titanium metal ion solubility.

Titanium in its metallic form is well known for the high strength to weight ratio which enables its use as an alloy with other metals such as aluminum, molybdenum or vanadium (Hampel 1968). These strong and light alloys have diverse applications in fields like medicine for orthopedic or dental implants, metal plating for aerospace, industrial, military applications and many everyday objects like bicycles, tennis racquets and mobile phones (Li et al. 2021; Murr et al. 2009). Titanium metal tends to be coated by a passivating oxide that connects its activity to the chemistry of the metal oxides described above.

Titanium can be found in other environments besides earth's crust. Natural waters and the human body also contain significant amounts of titanium (Buettner and Valentine 2012). The amount of titanium in bodies of water from different geographical locations from all over the world ranges from 4 pM at the ocean surface to 100  $\mu\text{M}$  in hot springs (Orians et al. 1990; Van Baalen 1993). The concentration is

usually lower in fresh water at normal surface temperatures but it can reach up to 25  $\mu\text{M}$  in the surface water of rivers and lakes (Linnik and Zhezherya 2015; Wedepohl 1969). In the ocean, the concentration of titanium sometimes increases going from the surface of the water towards the seabed due to biotic and abiotic scavenging (Orians et al. 1990). The solubility of titanium is significantly enhanced in the presence of salts like alkaline fluorides and carbonates and other compounds like oxalic and citric acid (Linnik and Zhezherya 2015; Orians et al. 1990; Wedepohl 1969).

Even though Ti is very abundant in the environment, no organism has been reported yet to use it as an essential element and it is not known to appear natively in any metalloenzymes. Ti(IV) is a diamagnetic ion,  $d^0$ , and without any EPR signal (Buettner and Valentine 2012). The complexes it forms are mostly colorless or yellowish and there are sometimes no characteristic ligand-to-metal charge transfers in the UV region. Detecting Ti analytically can be challenging (Zierden and Valentine 2016). ICP-MS is sensitive enough to detect titanium, although there are limitations due to possible interferences especially in biological samples. Other modern mass spectrometry techniques like high-throughput tandem mass spectrometry (HT-MS/MS) are being used to characterize metalloenzymes and include Ti in the analysis (Buettner and Valentine 2012). In one proteomic study, for example, a high concentration of Ti was detected in the cytoplasm of *Pyrococcus furiosus* (Cvetkovic et al. 2010).

## 16.2 Microbial Dissolution and Weathering of Titanium Minerals

Weathering is a complex, slow geochemical process in which rocks, minerals and soils dissolve or decompose into smaller particles (Macheyeki et al. 2020). This process can be physical, chemical or biological. Physical weathering is the mechanical breakdown that rocks have to face first and is caused by processes like erosion, large temperature changes, frost and salt crystallization (Hazen et al. 2008). Chemical weathering changes the composition of rock minerals via oxidation, hydration, carbonation, hydrolysis and other reactions that can take place in the atmosphere with the help of oxygen, carbon dioxide and water (Holbrook et al. 2019). Physical and chemical weathering can be accompanied by biological weathering which utilizes soil microorganisms, plants and animals to disintegrate rocks into smaller particles. For example, lichens growing on rocks are a classic example of organisms accelerating the weathering of minerals. Lichens also impact chemical weathering by excreting oxalic acid which can dissolve minerals and chelate metals (Chen et al. 2000). Weathering often increases the bioavailability of metals by solubilizing them and making them ready to be taken up by different microorganisms. Titanium-bearing minerals are subject to each of these types of weathering. Geochemical

processes can break down titanium minerals through dissolution, fluid transport, and precipitation (Van Baalen 1993).

### 16.3 Metals in Biology

Bioinorganic chemistry is an interdisciplinary field that studies the role of inorganic elements in biological systems. In the 1940s it was believed that only about six elements had an importance in biology (Thomson 2016). Over the years, the biological roles of many other elements were explored and they were established as essential components of living systems (Kaim et al. 2013; Thomson 2016). Here we can mention Mg in chlorophyll, Fe in hemoglobin, Co in vitamin B12 and other metalloenzymes associated with transition metals like Cu, Mn, Mo, Ni, V, Cd and many more (Kaim et al. 2013; Maton 1993). The list of metals having an essential biological role continues to grow, which is also a result of the improvements achieved in developing analytical methods and instruments.

As mentioned in the examples above, nature has employed many inorganic elements to function in many metabolic pathways for different organisms. These elements must have a biological effect, and be abundant as well as being bioavailable, to be ready for use. Based on the standards above, it is reasonable to hypothesize that titanium could be a biological element, much like iron, zinc and copper which are frequently encountered in many organisms. However, no organism is found as of now that requires titanium as an essential element for any of its metabolic processes. The fact that titanium is used in many applications, for example as a catalyst, component of solar cells, part of alloys etc. (Buettner and Valentine 2012; Lütjering and Williams 2007) makes it even more intriguing to continue studying this element in living organisms. This review will cover current knowledge regarding the abundance of titanium in various microbial organisms, discuss the role of titanium minerals and describe the interaction it has with biomolecules from these organisms.

### 16.4 Microbial Adhesion to Titanium Minerals

Bacteria can colonize different environments including mineral surfaces in a process of biofilm formation (Di Martino 2018). This process can play a key role in mineral weathering, aggregate stability and degradation of other compounds found in soils (Huang et al. 2015; Di Martino 2018). Adhesion to inert surfaces is usually accompanied by nonspecific interactions. The molecular details are still not completely clear. However, it is thought that electrostatic forces and hydrophobicity are the major forces that direct this process (Huang et al. 2015). Adsorption is affected by other factors such as temperature, pH, salinity and minerals' composition. The survival and activity of microbes can depend strongly on adhesion (Hong et al.



2011). It has been determined that bacteria adhere more strongly to mineral surfaces under low nutrient levels as compared to high nutrient conditions (Huang et al. 2015). This finding might suggest that the molecules making up the minerals may play a role in any reactions of the living cycle of the bacteria studied.

Due to the fact that titanium and its alloys are extensively used for medical implants, and they make direct contact with living cells in the organisms where they are applied as well as with bacteria found nearby, studying the adhesion of microbes to titanium minerals has a notable interest (Bhadra et al. 2015).

A layer of  $\text{TiO}_2$  covers the surface of titanium based materials so adhesion normally takes place between a receptor on the surface of bacteria and the metal oxide (Li and Logan 2004). Bacteria can strongly adhere to  $\text{TiO}_2$  surfaces which increases the possibility of biofilm formation and might lead to infections in the case when the biofilm involves pathogens (Bhadra et al. 2015). Electrostatic interactions are the main forces that affect the bacterial-surface adhesion. Other factors include hydrophobic interactions and the specific type of macromolecule that makes up the bacterial receptor (Li and Logan 2004).

There is also evidence of nonelectrostatic specific interactions between microbes and  $\text{TiO}_2$ . The latter can adhere very strongly and selectively to bacteria like *Rhodococcus ruber* (Shabtai and Fleminger 1994). A protein purified from *R. ruber* binds to  $\text{TiO}_2$  at neutral pH, possibly using a Cys, His, Glu, Asp motif (Dayan et al. 2017).

Adhesion of bacteria to  $\text{TiO}_2$  surfaces and other titanium minerals is a wide area of research focused mainly on improving the biocompatibility of titanium implants in the medical field. Nevertheless it has other important applications in areas like bioenergy and biofouling, because titanium is bioactive in diverse organisms which will be explored below.

## 16.5 Microbes Associated with Titanium

### 16.5.1 Avid Marine Sequesterers of Titanium

Many marine organisms accumulate low levels of Ti, usually to levels less than 100 pm (Martin 1983; Vinogradov et al. 1953). Diatoms and ascidians are known as sequesterers of titanium, but there is no data yet to suggest the essentiality of Ti to these organisms. Other organisms like dinoflagellates and sponges show affinity for titanium too. Although titanium is associated with many different organisms ranging from unicellular to more complex, multicellular forms of life like sponges, ascidians, insects etc., this review will focus only on the interactions of titanium with microbes.

### 16.5.2 *Diatoms*

Diatoms can take up titanium from their growth media up to 940 ppm in the whole organism (Riley and Roth 1971). In their siliceous frustule, the concentration can reach 1254 ppm (Martin and Knauer 1973). The frustule is a highly patterned structure of the external layer of diatoms and is mainly composed of silica. It contains two parts named valves, where the small valve fits into the larger valve (Tamura et al. 2005). Ti can be taken up as  $\text{TiO}_2$  and incorporated into the silica frustules. It is distributed between both valves, reaching a tenfold increase of Ti in the valves as compared to the general concentration in the frustule (Chauton et al. 2015).  $\text{TiO}_2$  and silicic acid are captured by cells of diatoms simultaneously and Ti and Si have a similar rate of uptake and incorporation in the frustules (Basharina et al. 2012; Chauton et al. 2015). This fact might explain why dissolved Ti is depleted along with silicon during a spring diatom bloom (Skrabal et al. 1992). It may also contribute to the surface depleted profile of Ti in the ocean when the phenomenon of diatom blooming occurs (Orians et al. 1990). After the uptake into the frustule, the fate of Ti is not completely clear. It might precipitate there or be incorporated by other biomolecules of diatoms. Titanium, together with some other metals such as zirconium and tin, can penetrate into the silico deposition vesicles (SDV) and impede the genetically controlled process of valve formation (Basharina et al. 2012). This leads to different thickness and hardness of silica valves. The biomineralization process of frustules can be directed by enzymes called silaffins (Scheffel et al. 2011; Sumper and Kroger 2004). Beyond the biotechnological potential (Pamirsky and Golokhvast 2013), these proteins can serve as benchmarks for generation of synthetic peptides (Yan et al. 2014) and recombinant silaffins (Bedwell et al. 2015; Kröger et al. 2006; Van Eynde et al. 2016). This phenomenon provides a remarkable feature of diatoms where soluble titanium can be bioaccumulated (Cargnello et al. 2014; Van Eynde et al. 2016).  $\text{TiO}_2$  particles in the diatom frustule have bactericidal effects when irradiated with UV light. This activity occurs because of free radicals generated during the process (Lang et al. 2013).

### 16.5.3 *Dinoflagellates*

Dinoflagellates are unicellular eukaryotes that are usually considered algae. They are found in marine environments and fresh waters as well. In dinoflagellates, Ti has been reported at very high concentrations up to 33,700 ppm in blooms of the marine species *Karenia brevis* (Collier 1953). It is not clear whether the elevated titanium concentration is a cause or effect of the diatom bloom, or whether it is unrelated. The concentration of  $\text{TiO}_2$  nanoparticles in these habitats ranges from 0.2  $\mu\text{g/L}$  to 16  $\mu\text{g/L}$  (Peters et al. 2018; Xiao et al. 2019; Zhang et al. 2019). Since  $\text{TiO}_2$  nanoparticles are widely used in industry, they do inevitably end up in aquatic environments

(Li et al. 2020). The effects of these nanoparticles on algae can be toxic because the particles can interfere in some vital processes of the lifecycle of these species (Li et al. 2015). Experiments have shown that they inhibit the growth of some algae like *Karenia brevis* (Li et al. 2015, 2012). The mechanism by which this inhibition takes place includes the creation of oxidative stress and inhibition of photosynthesis by altering the chloroplast function (Li et al. 2015).

#### 16.5.4 Foraminifera

Foraminifera are amoeboid protists having a variety of morphologies, ranging from 100  $\mu\text{m}$  to 1 mm in length (Saraswati and Srinivasan 2016). Most are marine and live on or in the seafloor sediment. Many have foraminiferal shells or tests which serve to protect the organism and are also used to identify and classify them (Makled and Langer 2010; Gupta and Barun 1999). Some have tests incorporating different materials like tectin, calcium carbonate, iron (III) oxide, and silicate (Gupta and Barun 1999; Pawlowski et al. 2003). These tests sometimes have specific affinity for some minerals embedded in the shells.

One titanium-associated foraminiferan, *Bathysiphon argenteus* (Fig. 16.2), is an agglutinated species isolated from sedimentary rocks off the coast of Ireland (Landing et al. 2012). The species was originally characterized by the presence of rod-shaped needles in the wall of the test (Heron-Allen and Earland 1913). There was some debate about whether these needles were actively biomineralized by this species or instead were detrital in origin and selectively collected. Ultimately, these needles were concluded to be detrital, embedded in the shell and composed of  $\text{TiO}_2$

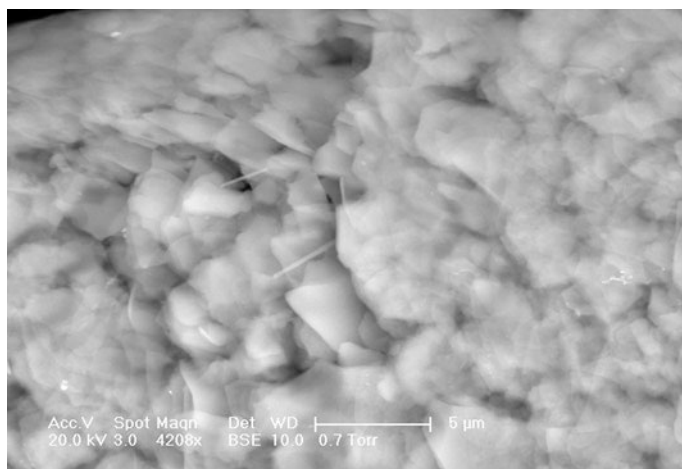


**Fig. 16.2** Scanning electron microscope image of the surface of the test of *Bathysiphon argenteus* showing the titania needles (Cole and Valentine 2006)

in rutile form (Waterston et al. 2006). The selectivity of *B. argenteus* for  $\text{TiO}_2$  might be due to the presence of a catechol functional group in the tectin, since catechols are known to favor adsorption onto  $\text{TiO}_2$  surfaces. Nevertheless it is clear that this species of foraminifera is strongly associated with, and in fact is characterized by, a titanium mineral in its test (Cole and Valentine 2006).

Titanium in several mineral forms has been associated with other species.  $\text{TiO}_2$  in anatase form is found in *Ammobaculites balkwilli* (Allen et al. 1999). It makes up about 10% of the shell, even though  $\text{TiO}_2$  is scarcely found in the local environment of this foraminifera (Allen et al. 1999). A further example is *Textularia hauerii* isolated in shallow waters in Mozambique (Makled and Langer 2010). It accumulates titanium in ilmenite form in its agglutinated test. Evidence suggests that there is a preferential uptake of the organism for ilmenite and selective agglutination of titanium minerals in this foraminifera (Makled and Langer 2010). Another example is *Psammophaga zirconia* found in the shallow parts of the Adriatic Sea as well as the Black Sea, which contains 27%  $\text{TiO}_2$  and 11% ilmenite in its test (Sabbatini et al. 2016). The sediment of the environment where this organism is found contains less than 4% of transition metals. A significant amount of crystals of zircon, about 51%, is found in the test too, although the environment contains less than 1% zircon (Sabbatini et al. 2016).

All the examples above suggest that there is a selectivity mechanism towards these titanium minerals at the expense of others. This selection might be based on electrostatic interactions between the biomolecules secreted in the shell of foraminifera and the inorganic materials like anatase, rutile, or ilmenite.

### 16.5.5 $\text{TiO}_2$ -Adhesive Bacteria

Particles of  $\text{TiO}_2$  were found to be adhered very strongly by some gram positive bacteria including species of genus *Rhodococcus*, found in the Mediterranean Sea near Israel (Shabtai and Fleminger 1994). The *Rhodococcus ruber* GIN-1 strain (Fig. 16.3) can adhere selectively to  $\text{TiO}_2$  and bind tightly to both anatase and rutile (Gertler et al. 2003; Shabtai and Fleminger 1994; Siegmann et al. 2009). *R. ruber* exhibits a significantly higher affinity towards  $\text{TiO}_2$  compared to other metal oxides and it has been determined that more than 85% of the cells adsorb to  $\text{TiO}_2$  within a minute (Shabtai and Fleminger 1994). Furthermore, this process takes place over a wide pH range, 1.0–9.0, and wide temperature range, 4°C to over 80°C (Shabtai and Fleminger 1994). Adhesion was resistant even in the presence of alcohols, mild acids or detergents which failed to remove *R. ruber* GIN-1 from the  $\text{TiO}_2$  particles (Gertler et al. 2003). The mechanism by which the bacteria adhere to  $\text{TiO}_2$  has not been fully elucidated yet. In some *Rhodococcus* strains, hydrophobic molecules like mycolic acid play an important role in the adhesiveness to solid surfaces (Bendinger et al. 1993; Gertler et al. 2003; Siegmann et al. 2009). *R. ruber* GIN-1 is able to accumulate appreciable Ti into its biomass after exposure to, and then desorption from, either anatase or rutile (Gallo et al. 2020). This titanium increase disrupts the

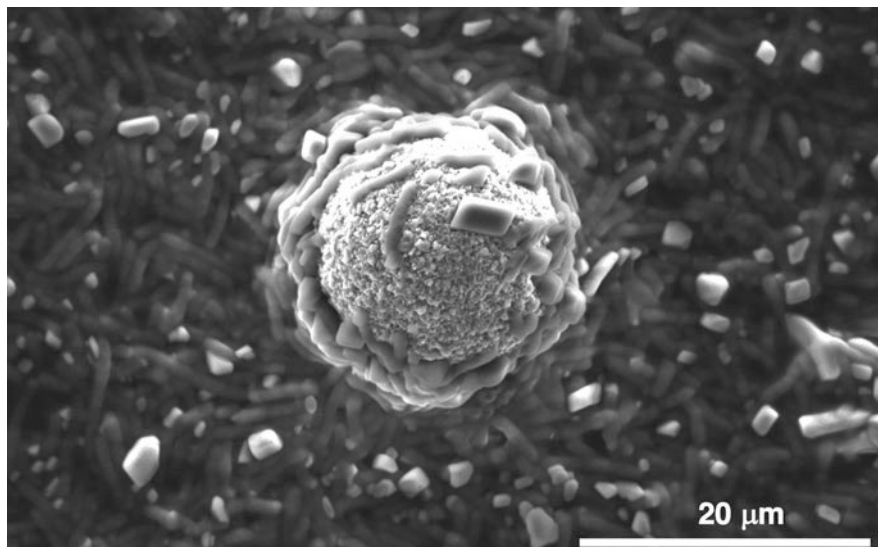


**Fig. 16.3** Scanning electron microscope image of *R. ruber* GIN-1 (rods) adsorbed to a Sachtopore rutile  $\text{TiO}_2$  particle (Gallo 2019)

metal ion quota of other biometals, especially iron, which significantly decreases in the biomass after titanium exposure.

Another important process is the biosorption of nanoparticles of  $\text{TiO}_2$ . It has been observed that *Escherichia coli* and *Pseudomonas aeruginosa* adsorb to  $\text{TiO}_2$  nanoparticles and this phenomenon can occur more broadly (Horst et al. 2010; Kiser et al. 2009, 2010; Li and Logan 2004; McWhirter et al. 2003; Petrone 2013). Agglomeration of particles on the bacteria has been observed too. Both of these interactions have been facilitated by siderophores and polysaccharides found on the cell surface.

Even as these titanium mineral-microbe interactions still are being discovered and explored, we might consider what driving force there might be for such an interaction. First, microbes may use a mineral as a source of metal ion for their metabolic needs. So far, we know that titanium is found in these organisms, and sometimes it is even selectively chosen by them, but no essentiality has been discovered yet. Alternatively, microbes can use metal ions in minerals as terminal electron acceptors for respiration. Again, there is no evidence that titanium is utilized as a terminal electron acceptor for any organism, but the  $\text{Ti(IV)/Ti(III)}$  redox potential is near 0 vs. the normal hydrogen electrode (NHE) and it is highly tunable by the metal ion coordination environment (Buettner and Valentine 2012). Titanium minerals could serve as a physical scaffold for selective microbial interaction, in which for example selective  $\text{TiO}_2$ -adhesive bacteria could find others of their kind. Microbes that are less sensitive to the deleterious effects of titanium might find a selective advantage relative to competitor microbes that are more sensitive. Another possible reason for interacting with minerals would be the ability to access depths in the ocean by

adsorption to or desorption from sinking particles. This ability would allow adhesive microbes to access different depths in response to nutrient or oxygen needs. One could even imagine adhesive microbes taking advantage of the photoactivity of natural TiO<sub>2</sub> particles in a sort of natural dye-sensitized solar cell.

## 16.6 Microbial Metalloproteomes and Titanium

Microbial metalloproteomes present many uncharacterized proteins with diverse coordination sites, most of which are not fully studied (Cvetkovic et al. 2010). We note that, because Ti is often not recognized as a “biological metal”, it may not be among the elements commonly analyzed. Together with the challenges in detection outlined above, this omission of appropriate detection efforts may be hindering further exploration of titanium’s role in the microbial realm. One key study did analyze for Ti, with intriguing results. Cvetkovic et al. (2010) describe an approach towards the identification of metalloproteins in microbes that is different from the traditional protein-based purification. Their study in the extremophilic archaea *Pyrococcus furiosus* presents a metal-based identification and purification method using high-throughput tandem mass spectrometry (HT-MS/MS) and inductively coupled plasma mass spectrometry (ICP-MS).

The samples examined in that study by Cvetkovic and coauthors were analyzed for 53 different metals, and 44 of those elements were detected in the *P. furiosus* growth medium. Titanium was not among the metals detected in the growth medium, suggesting that its concentration there was very low. However, titanium was among the 21 metals found in the cytoplasmic extract. At 1.58 μM, it was the fourth most abundant transition metal there (after Fe, Zn, and W, which are all known to be metal cofactors in this organism) (Cvetkovic et al. 2010). Its concentration was above those of Co, Mn, and V. When the cell extracts were subjected to chromatography to separate the macromolecules for further identification, the Ti was no longer found. It is not clear what happened to the Ti in the cytoplasmic extracts, but the high lability of Ti(IV) coupled with the propensity of this metal for hydrolysis and precipitation may have been responsible.

Extension of the method presented by Cvetkovic et al. might open the door for the identification of novel and uncharacterized metalloproteins, which increases the chances that there might be discovery of organisms that utilize titanium or other novel metals in any of their biological processes.

## 16.7 Microbial Synthesis of Metal-Containing Nanoparticles

Metal, metal oxide, and related nanoparticles are getting more and more attention due to their wide applications in agriculture, industry and medicine. This attention has recently shifted towards green nanotechnology by employing biological resources like bacteria, fungi, algae, viruses or yeast as more environmentally friendly and also cost effective ways to produce these particles (Gahlawat and Roy Choudhury 2019). These nanoparticles can be used in drug delivery, for waste treatment, as antimicrobial agents, in crop protection against pathogens and many more applications. The most common biosynthesized nanoparticles include those from gold, silver, copper as well as titanium oxide and zinc oxide (Gahlawat and Roy Choudhury 2019).

Bacteria are useful nanofactories because they can be engineered to synthesize nanoparticles of well-defined size and morphology. They can be easily grown and modified genetically for the biomineralization. One example is the biosynthesis of TiO<sub>2</sub> nanoparticles by *Bacillus mycooides* for the construction of green solar cells (Órdenes-Aenishanslins et al. 2014). In the presence of titanyl hydroxide, nanoparticles with anatase structure, spherical morphology and no display of phototoxicity were biosynthesized by the gram-positive bacteria, *B. mycooides*.

The thick coat of the capsid protein of viruses provides another favorable place where metals can interact with the virus and this property is utilized in the biosynthesis of nanoparticles by viruses (Gahlawat and Roy Choudhury 2019). One example is the production of 20–40 nm TiO<sub>2</sub> nanoparticles from M13 bacteriophage (Mao et al. 2003). Here the virus was used for the nucleation and orientation of semiconductor nanowires.

## 16.8 Titanium's Antimicrobial Activity

Biofilm formation and bacterial adhesion on different surfaces of biomaterials are sources of infections. Therefore reducing bacterial colonization of these surfaces is a necessity to improve the antibacterial activity in fabricated materials, implants, air and water purification systems. TiO<sub>2</sub> has been long studied for its antibacterial properties, including due to the photocatalytic effect it exhibits combined with its low cost, nontoxicity and ability not to get consumed in this reaction (Arango-Santander et al. 2018).

When TiO<sub>2</sub> is exposed to UV light in the presence of water, reactive oxygen species like peroxides, superoxides and hydroxyl radicals are generated which inactivate pathogenic bacteria, fungi and viruses (Han et al. 2016). The anatase form of titanium shows the greatest photocatalytic effect among all other forms (Tanaka et al. 1991).

Gram-positive bacteria are more resistant to photocatalytic disinfection than are Gram-negative bacteria because of the thick peptidoglycan layer possessed by Gram-positive bacteria and their lack of the outer membrane (Gerba 2013). The latter is where the attack by reactive oxygen species starts in Gram-negative bacteria. It continues to the peptidoglycan, then peroxidation of the lipid membrane takes place. Finally, the proteins in the membrane get oxidized and the cell wall breaks down causing the cell to burst (Gerba 2013). At the end of the disinfection process by photocatalysis, microbes are mineralized to CO<sub>2</sub> and H<sub>2</sub>O. Experiments with *Legionella pneumophila* suggest that the increase of the number of fatty acids in the membrane increases the sensitivity to TiO<sub>2</sub> photocatalysis (Gerba 2013). Other studies on *E. coli*, *Staphylococcus aureus*, and *Enterococcus faecalis* have demonstrated efficient disinfection by TiO<sub>2</sub>. Some pathogens which are often hard to destroy in the environment include *Cryptosporidium parvum* oocysts and *Giardia intestinalis* cysts, and many bacteria producing endospores. These pathogens were shown to be killed by TiO<sub>2</sub>-based materials (Foster et al. 2011).

The surface of titanium effectively inhibits microbial growth and prevents biofilm formation. Further studies of the interaction of TiO<sub>2</sub> with microbes on hard surfaces may lead to the development of better antimicrobials.

## 16.9 Conclusion

A wide variety of microbes interact with titanium in soluble or in mineral form. These interactions may be beneficial, neutral, or detrimental from the point of view of the microbes themselves or the humans and other organisms that share the microbes' environment. Even though there is no organism discovered to date that requires titanium for its biological processes, recent papers suggest that Ti is present in the biomass of many unicellular organisms and is bioactive. In addition to this, there are no proteins or other macromolecules found yet in any of the microbes studied that require titanium as a cofactor. But, by understanding how titanium interacts with microbes, it may be possible to come closer to identifying a specific organism or biomolecule that depends on this widely available and bioactive element.

**Acknowledgments** This work was supported by the United States National Science Foundation (CHE-1412373).

## References

Allen K, Roberts S, Murray JW (1999) Marginal marine agglutinated foraminifera: affinities for mineral phases. *J Micropalaeontol* 18(2):183–191. <https://doi.org/10.1144/jm.18.2.183>



- Arango-Santander S, Pelaez-Vargas A, Freitas SC, Garcia C (2018) A novel approach to create an antibacterial surface using titanium dioxide and a combination of dip-pen nanolithography and soft lithography. *Nature* 8(15818):1–10. <https://doi.org/10.1038/s41598-018-34198-w>
- Baes CF, Mesmer RE (1981) The thermodynamics of cation hydrolysis. *Am J Sci* 281(7):935–962. <https://doi.org/10.2475/ajs.281.7.935>
- Basharina TN, Danilovtseva EN, Zelinskiy SN, Klimenkov IV, Likhoshway YV, Annenkov VV (2012) The effect of titanium, zirconium and tin on the growth of diatom *Synedra Acus* and morphology of its silica valves. *Silicon* 4:239–249. <https://doi.org/10.1007/s12633-012-9119-x>
- Bedwell GJ, Zhou Z, Uchida M, Douglas T, Gupta A, Prevelige PE (2015) Selective biotemplated synthesis of TiO<sub>2</sub> inside a protein cage. *Biomacromolecules* 16(1):214–218. <https://doi.org/10.1021/bm501443e>
- Bendinger B, Rijnaarts HHM, Altendorf K, Zehnder AJB (1993) Physicochemical cell surface and adhesive properties of coryneform bacteria related to the presence and chain length of mycolic acids. *Appl Environ Microbiol* 59(11):3973–3977. <https://doi.org/10.1128/AEM.59.11.3973-3977.1993>
- Bhadra CM, Truong VK, Pham THV, Al Kobaisi M, Seniutinas G, Wang JY, Juodkasis S, Crawford RJ, Ivanova EP (2015) Antibacterial titanium nano-patterned arrays inspired by dragonfly wings. *Sci Rep* 5:16817. <https://doi.org/10.1038/srep16817>
- Buettner KM, Valentine AM (2012) Bioinorganic chemistry of titanium. *Chem Rev* 112(3):1863–1881. <https://doi.org/10.1021/cr1002886>
- Cargnello M, Gordon TR, Murray CB (2014) Solution-phase synthesis of titanium dioxide nanoparticles and nanocrystals. *Chem Rev* 114(19):9319–9345. <https://doi.org/10.1021/cr500170p>
- Chauton MS, Skolem LMB, Olsen LM, Vullum PE, Walmsley J, Vadstein O (2015) Titanium uptake and incorporation into silica nanostructures by the diatom *Pinnularia* sp. (*Bacillariophyceae*). *J Appl Phycol* 27(2):777–786. <https://doi.org/10.1007/s10811-014-0373-8>
- Chen J, Blume H-P, Beyer L (2000) Weathering of rocks induced by lichen colonization—a review. *Catena* 39(2):121–146. [https://doi.org/10.1016/S0341-8162\(99\)00085-5](https://doi.org/10.1016/S0341-8162(99)00085-5)
- Closs LG (1983) Book review: principles of geochemistry 4<sup>th</sup> edition. Brian Mason and Carleton B. Moore, John Wiley, New York, 1982, 344 p., 29.95. *Geochim Cosmochim Acta* 47:661–662. [https://doi.org/10.1016/0016-7037\(83\)90289-2](https://doi.org/10.1016/0016-7037(83)90289-2)
- Cole KE, Valentine AM (2006) Titanium biomaterials: Titania needles in the test of the Foraminiferan *Bathysiphon argenteus*. *Dalton Trans* 3:430–432. <https://doi.org/10.1039/B508989A>
- Collier A (1953) Titanium and zirconium in bloom of *Gymnodinium brevis* Davis. *Science* 118(3064):329–329. <https://doi.org/10.1126/science.118.3064.329>
- Cvetkovic A, Menon AL, Thorgersen MP, Scott JW, Poole FL, Jenney FE, Lancaster WA, Praissman JL, Shanmukh S, Vaccaro BJ, Trauger SA, Kalisiak E, Apon JV, Siuzdak G, Yannone SM, Tainer JA, Adams MWW (2010) Microbial metalloproteomes are largely uncharacterized. *Nature* 466(7307):779–782. <https://doi.org/10.1038/nature09265>
- Dayan A, Babin G, Ganath A, Kayouf NS, Eliza NN, Mukkala S, Tsfadia Y, Fleminger G (2017) The involvement of coordinative interactions in the binding of dihydrolipoamide dehydrogenase to titanium dioxide - localization of a putative binding site. *J Mol Recognit* 30:1–11. <https://doi.org/10.1002/jmr.2617>
- Di Martino P (2018) Bacterial adherence: much more than a bond. *AIMS Microbiol* 4(3):563–566. <https://doi.org/10.3934/microbiol.2018.3.563>
- Emsley SW (1998) *The elements*. Clarendon Press
- Foster HA, Ditta IB, Varghese S, Steele A (2011) Photocatalytic disinfection using titanium dioxide: spectrum and mechanism of antimicrobial activity. *Appl Microbiol Biotechnol* 90(6):1847–1868. <https://doi.org/10.1007/s00253-011-3213-7>
- Gaffney JP, Valentine AM (2011) The challenges of trafficking hydrolysis prone metals and ascidians as an archetype. *Dalton Trans* 40(22):5827–5835. <https://doi.org/10.1039/C1DT10092K>

- Gahlawat G, Roy Choudhury A (2019) A review on the biosynthesis of metal and metal salt nanoparticles by microbes. *RSC Adv* 9:12944–12967. <https://doi.org/10.1039/C8RA10483B>
- Gallo AD (2019) Homeostasis and trafficking of hydrolysis-prone metals in cells, proteins, and small molecules. PhD Thesis, Temple University, ProQuest. Identifier: TETDEDXGallo-temple-0225E-13636
- Gallo AD, Zierden MR, Proffitt LA, Jones KE, Bonafide CP, Valentine AM (2020) TiO<sub>2</sub> exposure alters transition metal ion quota in *Rhodococcus ruber* GIN-1. *Metallomics* 12(1):8–11. <https://doi.org/10.1039/C9MT00305C>
- Gerba CP (2013) Titanium dioxide as disinfectant. In: Krestinger RH, Uversky VN, Permyakov EA (eds) *Encyclopedia of metalloproteins*. [https://doi.org/10.1007/978-1-4614-1533-6\\_530](https://doi.org/10.1007/978-1-4614-1533-6_530)
- Gertler G, Brudo I, Kenig R, Fleminger G (2003) A TiO<sub>2</sub>-binding protein isolated from *Rhodococcus* strain GIN-1 (NCIMB 40340) – purification, properties and potential applications. *Mater Werkst* 34(12):1138–1144. <https://doi.org/10.1002/mawe.200300709>
- Gupta BKS, Barun K (1999) *Modern Foraminifera*. Springer Science & Business Media
- Hampel CA (1968) *The encyclopedia of the chemical elements*. Reinhold Book Corp, New York. <http://archive.org/details/encyclopediaofch00hamp>
- Han C, Lalley J, Namboodiri D, Cromer K, Nadagouda MN (2016) Titanium dioxide-based antibacterial surfaces for water treatment. *Curr Opin Chem Eng* 11:46–51. <https://doi.org/10.1016/j.coche.2015.11.007>
- Hazen RM, Papineau D, Bleeker W, Downs RT, Ferry JM, McCoy TJ, Sverjensky DA, Yang HY (2008) Mineral evolution. *Am Mineral* 93:1693–1720. <https://doi.org/10.2138/am.2008.2955>
- Heron-Allen E, Earland A (1913) *Proc R Irish Acad* 31 Section 3, Part 64, 1–81
- Holbrook WS, Marcon V, Bacon AR, Brantley SL, Carr BJ, Flinchum BA, Richter DD, Riebe CS (2019) Links between physical and chemical weathering inferred from a 65-m-deep borehole through Earth’s critical zone. *Sci Rep* 9(1):4495. <https://doi.org/10.1038/s41598-019-40819-9>
- Hong Z, Rong X, Cai P, Liang W, Huang Q (2011) Effects of temperature, pH and salt concentrations on the adsorption of *Bacillus subtilis* on soil clay minerals investigated by microcalorimetry. *Geomicrobiol J* 28(8):686–691. <https://doi.org/10.1080/01490451.2010.514025>
- Horst AM, Neal AC, Mielke RE, Sislian PR, Suh WH, Mädler L, Stucky GD, Holden PA (2010) Dispersion of TiO<sub>2</sub> nanoparticle agglomerates by *Pseudomonas aeruginosa*. *Appl Environ Microbiol* 76(21):7292–7298. <https://doi.org/10.1128/AEM.00324-10>
- Huang Q, Wu H, Cai P, Fein JB, Chen W (2015) Atomic force microscopy measurements of bacterial adhesion and biofilm formation onto clay-sized particles. *Sci Rep* 5:16857. <https://doi.org/10.1038/srep16857>
- Kaim W, Schwedereski B, Klein A (2013) *Bioinorganic chemistry - inorganic elements in the chemistry of life: an introduction and guide*, 2nd edn. Wiley
- Kiser MA, Westerhoff P, Benn T, Wang Y, Pérez-Rivera J, Hristovski K (2009) Titanium nanomaterial removal and release from wastewater treatment plants. *Environ Sci Technol* 43(17):6757–6763. <https://doi.org/10.1021/es901102n>
- Kiser MA, Ryu H, Jang H, Hristovski K, Westerhoff P (2010) Biosorption of nanoparticles to heterotrophic wastewater biomass. *Water Res* 44(14):4105–4114. <https://doi.org/10.1016/j.watres.2010.05.036>
- Kröger N, Dickerson MB, Ahmad G, Cai Y, Haluska MS, Sandhage KH, Poulsen N, Sheppard VC (2006) Bioenabled synthesis of rutile TiO<sub>2</sub> at ambient temperature and neutral pH. *Angew Chem Int Ed Engl* 45(43):7239–7243. <https://doi.org/10.1002/anie.200601871>
- Landing E, Reyes SP, Andreas AL, Bowser SS (2012) First discovery of early Palaeozoic Bathysiphon Foraminifera – test structure and habitat of a ‘living fossil’. *Geol Mag* 149(6):1013–1022. <https://doi.org/10.1017/S0016756812000155>
- Lang Y, del Monte F, Rodriguez BJ, Dockery P, Finn DP, Pandit A (2013) Integration of TiO<sub>2</sub> into the diatom *Thalassiosira weissflogii* during frustule synthesis. *Sci Rep* 3. <https://doi.org/10.1038/srep03205>
- Li B, Logan BE (2004) Bacterial adhesion to glass and metal-oxide surfaces. *Colloids Surf B Biointerfaces* 36(2):81–90. <https://doi.org/10.1016/j.colsurfb.2004.05.006>

- Li FM, Zhao W, Li YY, Tian ZJ, Wang ZY (2012) Toxic effects of nano-TiO<sub>2</sub> on *Gymnodinium breve*. Huan Jing Ke Xue 33(1):233–238. PMID: 22452216
- Li F, Liang Z, Zheng X, Zhao W, Wu M, Wang Z (2015) Toxicity of nano-TiO<sub>2</sub> on algae and the site of reactive oxygen species production. Aquat Toxicol 158:1–13. <https://doi.org/10.1016/j.aquatox.2014.10.014>
- Li Z, Juneau P, Lian Y, Zhang W, Wang S, Wang C, Shu L, Yan Q, He Z, Xu K (2020) Effects of titanium dioxide nanoparticles on photosynthetic and antioxidative processes of *Scenedesmus obliquus*. Plan Theory 9(12):1748. <https://doi.org/10.3390/plants9121748>
- Li M, Pan Y, Zou Y (2021) Application and optimization design of Titanium alloy in sports equipment. J Phys Conf Ser 1820(1):012011. <https://doi.org/10.1088/1742-6596/1820/1/012011>
- Linnik PN, Zhezherya VA (2015) Titanium in natural surface waters: the content and coexisting forms. Russ J Gen Chem 85(13):2908–2920. <https://doi.org/10.1134/S107036321513006X>
- Lütjering G, Williams JC (2007) Titanium, 2nd edn. Springer. <https://doi.org/10.1007/978-3-540-73036-1>
- Macheyeki AS, Li X, Kafumu DP, Yuan F (2020) Elements of exploration geochemistry. Applied Geochemistry, pp 1–43. <https://doi.org/10.1016/B978-0-12-819495-9.00001-3>
- Makled WA, Langer MR (2010) Preferential selection of titanium-bearing minerals in agglutinated Foraminifera: Ilmenite (FeTiO<sub>3</sub>) in *Textularia hauerii* d’Orbigny from the Bazaruto Archipelago, Mozambique. Revue de Micropaléontologie 53(3):163–173. <https://doi.org/10.1016/j.revmic.2009.11.001>
- Mao C, Flynn CE, Hayhurst A, Sweeney R, Qi J, Georgiou G, Iverson B, Belcher AM (2003) Viral assembly of oriented quantum dot nanowires. Proc Natl Acad Sci U S A 100(12):6946–6951. <https://doi.org/10.1073/pnas.0832310100>
- Martin JH (1983) Trace metal concentrations in marine organisms. Limnol Oceanogr 28(3): 600–600. <https://doi.org/10.4319/lo.1983.28.3.0600>
- Martin JH, Knauer GA (1973) The elemental composition of plankton. Geochim Cosmochim Acta 37(7):1639–1653. [https://doi.org/10.1016/0016-7037\(73\)90154-3](https://doi.org/10.1016/0016-7037(73)90154-3)
- Maton A (1993) Human biology and health. Prentice Hall, Englewood Cliffs. <http://archive.org/details/humanbiologyheal00scho>
- McWhirter MJ, Bremer PJ, Lamont IL, McQuillan AJ (2003) Siderophore-mediated covalent bonding to metal oxide surfaces during biofilm initiation by *Pseudomonas aeruginosa* bacteria. Langmuir 19(9):3575–3577. <https://doi.org/10.1021/la020918z>
- Murr LE, Quinones SA, Gaytan SM, Lopez MI, Rodela A, Martinez EY, Hernandez DH, Martinez E, Medina F, Wicker RB (2009) Microstructure and mechanical behavior of Ti–6Al–4V produced by rapid-layer manufacturing, for biomedical applications. J Mech Behav Biomed Mater 2(1):20–32. <https://doi.org/10.1016/j.jmbbm.2008.05.004>
- Órdenes-Aenishanslins NA, Saona LA, Durán-Toro VM, Monrás JP, Bravo DM, Pérez-Donoso JM (2014) Use of titanium dioxide nanoparticles biosynthesized by *Bacillus mycoides* in quantum dot sensitized solar cells. Microb Cell Factories 13(1):90. <https://doi.org/10.1186/s12934-014-0090-7>
- Orians KJ, Boyle EA, Bruland KW (1990) Dissolved titanium in the open ocean. Nature 348(6299): 322–325. <https://doi.org/10.1038/348322a0>
- Pamirsky IE, Golokhvast KS (2013) Silaffins of diatoms: from applied biotechnology to biomedicine. Mar Drugs 11(9):3155–3167. <https://doi.org/10.3390/md11093155>
- Pawlowski J, Holzmann M, Berney C, Fahrni J, Gooday AJ, Cedhagen T, Habura A, Bowser SS (2003) The evolution of early Foraminifera. Proc Natl Acad Sci 100(20):11494–11498. <https://doi.org/10.1073/pnas.2035132100>
- Peters RJB, van Bemmel G, Milani NBL, den Hertog GCT, Undas AK, van der Lee M, Bouwmeester H (2018) Detection of nanoparticles in Dutch surface waters. Sci Total Environ 621:210–218. <https://doi.org/10.1016/j.scitotenv.2017.11.238>
- Petrone L (2013) Molecular surface chemistry in marine bioadhesion. Adv Colloid Interf Sci 195–196:1–18. <https://doi.org/10.1016/j.cis.2013.03.006>

- Riley JP, Roth I (1971) The distribution of trace elements in some species of phytoplankton grown in culture. *J Mar Biol Assoc U K* 51(1):63–72. <https://doi.org/10.1017/S0025315400006457>
- Sabbatini A, Negri A, Bartolini A, Morigi C, Boudouma O, Dinelli E, Florindo F, Galeazzi R, Holzmann M, Lurcock PC, Massaccesi L, Pawlowski J, Rocchi S (2016) Selective zircon accumulation in a new benthic foraminifer, *Psammophaga zirconia*, sp. Nov. *Geobiology* 14(4):404–416. <https://doi.org/10.1111/gbi.12179>
- Saraswati PK, Srinivasan MS (2016) Calcareous-walled microfossils. In: *Micropaleontology*. Springer, Cham, pp 81–119. [https://doi.org/10.1007/978-3-319-14574-7\\_6](https://doi.org/10.1007/978-3-319-14574-7_6)
- Scheffel A, Poulsen N, Shian S, Kröger N (2011) Nanopatterned protein microrings from a diatom that direct silica morphogenesis. *Proc Natl Acad Sci* 108(8):3175–3180. <https://doi.org/10.1073/pnas.1012842108>
- Shabtai Y, Fleminger G (1994) Adsorption of *Rhodococcus* strain GIN-1 (NCIMB 40340) on titanium dioxide and coal Fly ash particles. *Appl Environ Microbiol* 60(9):3079–3088
- Siegmann A, Komarska A, Betzalel Y, Brudo I, Jindou S, Mor G, Fleminger G (2009) The titanium binding protein of *Rhodococcus ruber* GIN1 (NCIMB 40340) is a cell-surface homolog of the cytosolic enzyme dihydroliipoamide dehydrogenase. *J Mol Recognit* 22:138–145. <https://doi.org/10.1002/jmr.919>
- Skrabal SA, Terry CM (2002) Distributions of dissolved titanium in porewaters of estuarine and coastal marine sediments. *Mar Chem* 77(2):109–122. [https://doi.org/10.1016/S0304-4203\(01\)00077-9](https://doi.org/10.1016/S0304-4203(01)00077-9)
- Skrabal SA, Ullman WJ, Luther GW (1992) Estuarine distributions of dissolved titanium. *Mar Chem* 37(1):83–103. [https://doi.org/10.1016/0304-4203\(92\)90058-I](https://doi.org/10.1016/0304-4203(92)90058-I)
- Sumper M, Kroger N (2004) Silica formation in diatoms: the function of long-chain polyamines and silaffins. *J Mater Chem* 14:1–7. <https://doi.org/10.1039/B401028K>
- Tamura M, Shimada S, Horiguchi T (2005) *Galeidinium Rugatum* Gen. Et Sp. Nov. (Dinophyceae), a new coccoid dinoflagellate with a diatom endosymbiont1. *J Phycol* 41(3): 658–671. <https://doi.org/10.1111/j.1529-8817.2005.00085.x>
- Tanaka K, Capule MFV, Hisanaga T (1991) Effect of crystallinity of TiO<sub>2</sub> on its photocatalytic action. *Chem Phys Lett* 187(1–2):73–76. [https://doi.org/10.1016/0009-2614\(91\)90486-S](https://doi.org/10.1016/0009-2614(91)90486-S)
- Thomson AJ (2016) The science of RJP Williams. *J Biol Inorg Chem* 21(1):1–3. <https://doi.org/10.1007/s00775-015-1328-5>
- Valentine AM (2006) Titanium: inorganic & coordination chemistry based in part on the article Titanium: Inorganic & Coordination Chemistry by Charles A. McAuliffe & Neil Bricklebank which appeared in the *Encyclopedia of Inorganic Chemistry*, First Edition. In *Encyclopedia of Inorganic Chemistry*. American Cancer Society. <https://doi.org/10.1002/0470862106.ia246>
- Van Baalen MR (1993) Titanium mobility in metamorphic systems: a review. *Chem Geol* 110(1): 233–249. [https://doi.org/10.1016/0009-2541\(93\)90256-I](https://doi.org/10.1016/0009-2541(93)90256-I)
- Van Eynde E, Hu ZY, Tytgat T, Verbruggen SW, Watté J, Van Tendeloo G, Van Driessche I, Blust R, Lenaerts S (2016) Diatom silica–titania photocatalysts for air purification by bio-accumulation of different titanium sources. *Environ Sci Nano* 3(5):1052–1061. <https://doi.org/10.1039/C6EN00163G>
- Vinogradov AP, Efron J, Setlow JK (1953) Elementary composition of marine bacteria. In: Odum VW (ed) *Memoir II*. Yale University Press, pp 155–157. <https://doi.org/10.2307/j.ctvbc0gk.7>
- Waterston CD, Shearer AM, Royal Society of Edinburgh (2006) Former fellows of The Royal Society of Edinburgh, 1783–2002. The Royal Society of Edinburgh. [http://www.royalsoced.org.uk/fellowship/fells\\_indexp2.pdf](http://www.royalsoced.org.uk/fellowship/fells_indexp2.pdf)
- Wedepohl KH (1969) *Handbook of geochemistry*. Springer. <https://www.springer.com/gp/book/9783642463020>
- Xiao B, Zhang Y, Wang X, Chen M, Sun B, Zhang T, Zhu L (2019) Occurrence and trophic transfer of nanoparticulate Ag and Ti in the natural aquatic food web of Taihu Lake, China. *Environ Sci: Nano* 6(11):3431–3441. <https://doi.org/10.1039/C9EN00797K>

- Yan Y, Wang D, Schaaf P (2014) Fabrication of N-doped TiO<sub>2</sub> coatings on nanoporous Si nanopillar arrays through biomimetic layer by layer mineralization. *Dalton Trans* 43(22): 8480–8485. <https://doi.org/10.1039/C3DT53409J>
- Yaroshevsky A (2006) Abundances of chemical elements in the Earth's crust. *Geochem Int* 44:48–55. <https://doi.org/10.1134/S001670290601006X>
- Zhang M, Yang J, Cai Z, Feng Y, Wang Y, Zhang D, Pan X (2019) Detection of engineered nanoparticles in aquatic environments: current status and challenges in enrichment, separation, and analysis. *Environ Sci Nano* 6(3):709–735. <https://doi.org/10.1039/C8EN01086B>
- Zierden MR, Valentine AM (2016) Contemplating a role for titanium in organisms. *Metallomics* 8(1):9–16. <https://doi.org/10.1039/C5MT00231A>

# Chapter 17

## Microbial Tungsten Assimilation



Tetyana Milojevic

**Abstract** Hard and rare metal tungsten (W) with its extraordinary properties (high melting/boiling points and density) is one of the heaviest elements known to be used by living organisms and occur in biomolecules. Unique physical and mechanical properties of tungsten make this heavy metal indispensable in modern high-tech industry; however, in spite of extensive W utilization, the bio-inspired technological processing of tungsten resources is not yet established. Nowadays, our understanding of the possible role of microorganisms in natural environments enriched with tungsten is restricted by the lack of research into tungsten–microbial interactions. The biogeochemistry of tungsten is very limitedly presented in just a handful of publications. This chapter discusses the role of tungsten–microbial interactions in tungsten enriched biotopes and mineral environments resolved through fundamental and applied investigations. Tungsten is an essential element, constitutive, and functional part of tungstopterin cofactor of several bacterial and archaeal enzymes. In spite that functional tungsten-based microbial respiration has not yet been discovered, several newly described tungsten–microbial biomineralized interfaces have the potential for further biotechnological developments such as tungsten biosorption from wastewaters and bioleaching of tungsten ores. Tungsten encapsulation of archaeal cell surface has been proposed to function as a microbial radioprotective armor during interplanetary travel, enabling further studies of microbial survival in the outer space environment and helping answer fundamental questions of astrobiology. Newly described tungsten-containing biomolecules, tungsten–microbial interfaces and their corresponding biotechnological applications can further help unravel the biogeochemistry of tungsten.

---

T. Milojevic (✉)

Space Biochemistry Group, Department of Biophysical Chemistry, University of Vienna, Vienna, Austria

e-mail: [tetyana.milojevic@univie.ac.at](mailto:tetyana.milojevic@univie.ac.at)

## 17.1 Background

Hard, rare metal tungsten (W) (Swedish: “tung + sten” = heavy stone or German: “Wolfram” (W) = wolf-cream), with its extraordinary properties and the highest melting point of all metals is a rather unexpected choice in biological systems. It is one of the heaviest elements known to be used by any living organism. Tungsten is the only metal from the third transition series of the periodic table, which is shown to occur in biomolecules, where it is used in a few species of bacteria and methanogenic and hyperthermophilic archaea as an essential element, constitutive, and functional part of tungstopterin cofactor (Chan et al. 1995; Kletzin and Adams 1996; Andreesen and Makdessi 2008). Microbial assimilation of tungsten has been proposed in hydrothermal environments, where high concentrations of tungsten might be connected with the metabolic activity of hyperthermophilic archaea (Holden and Adams 2003). Based on several fundamental studies, tungsten was proposed to play a role of a phylogenetically ancient redox cofactor in ancestral microorganisms (Kletzin and Adams 1996).

However, investigations of tungsten–microbial interactions spread far beyond the scope of fundamental studies and nowadays fall into modern applied research. Passive tungstate biosorption recently shown for living or inactivated microbial cells has been suggested as an efficient strategy for tungsten recovery and recycling from aquatic systems (Malekzadeh et al. 2007; Ogi et al. 2013, 2016a, b). Based on recent findings of microbial tungsten solubilization (Blazevic et al. 2019), biohydrometallurgical processing of tungsten-bearing ores can be further explored. Such microbial-assisted solubilization of tungsten is useful for currently underrepresented and less studied biomining of tungsten ores, where biooxidative dissolution pre-treatment might be desirable. Furthermore, recently described microbial ability to build W-bearing armor on the cell surface (Blazevic et al. 2019; Milojevic et al. 2019; Kölbl et al. 2020) was proposed as a newly emerging approach for microorganisms to withstand harsh environments, such as during an interplanetary journey (Kölbl et al. 2020). Tungsten encapsulation can serve as a potent radioprotective armor against drastic environments, enabling the study of microbial survivability in an outer space environment (Kölbl et al. 2020).

Tungsten occurs naturally in ecosystems of soils and sediments usually in small concentrations (average lithospheric concentrations are 0.2–2.4 mg kg<sup>-1</sup>) (Strigul et al. 2005). However, anthropogenic activities (e.g., phosphate fertilizers, firing of tungsten projectiles, combustion used for waste disposal, thermal processing of ceramic materials, weaponry) significantly increase tungsten concentration in environmental systems, raising awareness of tungsten pollution (Strigul et al. 2005). Nowadays, our understanding of the possible role of microorganisms in natural environments enriched with tungsten is restricted by the lack of research into tungsten–microbial interactions. Certainly, new tungsten–microbial interfaces and corresponding microbial fingerprints can further help unravel the biogeochemistry of tungsten.

## 17.2 Tungsten–Microbial Interactions: Fundamental Investigations

### 17.2.1 Tungsten as an Enzymatic Cofactor

Around the late 1970s, it was found that the growth of certain prokaryotic microorganisms can be induced by the addition of tungstate into their cultivation medium. A decade later the first naturally occurring tungsten-containing protein was purified, and now an expanded variety of tungstoenzymes have been isolated from various microbial sources with a series resolved structures annotated in the RCSB PDB protein data bank. Today, it is evident that tungsten plays an essential role as a catalytic component of tungstoenzymes that have been thoroughly discussed in several reviews focusing on microbial physiology and structural biochemistry (Kletzin and Adams 1996; Andreesen and Makdessi 2008; Bevers et al. 2009; Seelmann et al. 2020). Naturally occurring tungsten-containing enzymes are present in a wide range of prokaryotic microorganisms, with most of them being found in obligate anaerobic bacteria and archaea, such as methanogens, acetogens, and hyperthermophiles. However, the occurrence of tungstoenzymes is not restricted to anaerobic organisms (e.g., a tungsten-dependent formate dehydrogenase from the aerobic methylotrophic *Methylobacterium extorquens* which is involved in the oxidation of reduced C1 compounds to CO<sub>2</sub> with O<sub>2</sub> as an electron acceptor) (Laukel et al. 2003).

This type of enzyme contains a catalytic moiety, where a single tungsten ion is coordinated by one or two pyranopterin dithiolene chelates called tungsten cofactors (WCo) (Fig. 17.1). The majority of these enzymes have similar catalytic properties and catalyze redox reactions converting carboxylic acids into aldehydes. Metalloenzymes containing WCo belong to distinct enzyme families based on different protein folds and functions, among which are oxidoreductases (archaeal aldehyde oxidoreductases family (Chan et al. 1995)), translocases (ModABC (Hollenstein et al. 2007)), and lyases (e.g., acetylene hydratase from *Syntrophotalea acetylenica* (Seiffert et al. 2007)) families. These tungstoenzymes harbor one or more Fe-S clusters next to the WCo, and additionally may contain a number of other redox-active centers, e.g., flavins or hemes.

The Gram-positive bacteria acetogens *Moorella thermoacetica* and *Clostridium formicoaceticum* grow either heterotrophically by sugar fermentation to produce acetate or autotrophically by consuming CO<sub>2</sub> in the presence of H<sub>2</sub>, thus converting CO<sub>2</sub> to acetate. In these acetogenes, the tungstoenzyme formate dehydrogenase (FDH) catalyzes the conversion of CO<sub>2</sub> to the methyl group of acetate. This FDH-catalyzed reaction generates formate, which is ultimately converted by a variety of enzymes to acetate as the end product. Tungsten containing FDHs have initially been described in a number of acetogenic clostridia such as *Moorella thermoacetica*, *C. formicoaceticum*, and *Clostridium carboxidivorans*. Another tungstoenzyme represented in acetogens is carboxylic acid reductase (CAR) from *Moorella thermoacetica*, which catalyzes the reduction of carboxylic acids to their



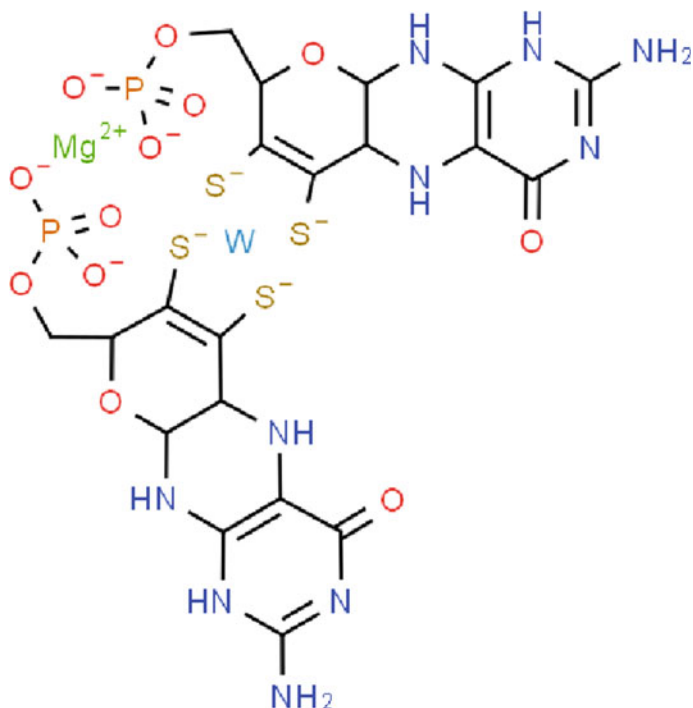


**Fig. 17.1** Tungsten cofactor (bis(molybdopterin)tungsten cofactor; magnesium; (2-amino-4-oxo-6,7-disulfido-1,5,5a,8,9a,10-hexahydropyrano[5,6-g]pteridin-8-yl)methyl phosphate; tungsten),  $C_{20}H_{20}MgN_{10}O_{12}P_2S_4W$  with average mass of 990.788 Da

corresponding aldehyde (White et al. 1989). Further WCo-containing FDHs are known from *Peptoclostridium acidaminophilum* (formerly *Eubacterium*) (Graentzdoerffer et al. 2003), *Campylobacter jejuni* (Taylor and Kelly 2019), and sulfate-reducing *Desulfovibrio* species (Mota et al. 2011).

Tungsten is well known to induce the growth of methanogenic archaea which produce methane using  $H_2$  and  $CO_2$ . Two kinds of FDH tungstoenzymes have been isolated from methanogen *Methanococcus vannielii*: one containing Mo and the other W (Jones and Stadtman 1981). Elevated tungstate concentrations in the cultivation medium are known to yield inactive Mo-dependent variants of FDHs from methanogen *Methanobacterium formicicum* (May et al. 1988). The other enzyme which shows a response to W in some methanogens is formylmethanofuran dehydrogenase (FMDH), a key enzyme in the methanogenic pathway. FMDH catalyzes the first step of methanogenesis, which is the reduction of  $CO_2$  to formaldehyde, yielding formate bound to the methanofuran cofactor. While in some methanogenic strains W is required for the expression of functional FMDH, the other methanogenic archaea have both W- and Mo-forms of this enzyme (Kletzin and Adams 1996). The tungsten-containing FMDH crystalized from *Methanothermobacter wolfeii* harbors two active sites which are separated by a

43 Å tunnel. The tunnel between those two active sites serves for the directed diffusion of the formate from the WCo center to the formylmethanofuran forming center (Wagner et al. 2016).

The discovery of hyperthermophilic archaea in the early 1990s facilitated fast progress in investigations of the biological role of tungsten. Tungsten was found to be an essential element for many of the hyperthermophilic archaea which optimally grow at temperatures  $>90$  °C. These heat-loving life forms require the addition of tungstate for growth due to its involvement in the formation of obligately tungsten-dependent enzymes with aldehyde oxidoreductase (AOR) activities. This family can be further divided into the subfamilies of archaeal AOR, formaldehyde oxidoreductases (FOR), glyceraldehyde-3-phosphate oxidoreductases (GAPOR), and tungsten-dependent oxidoreductases (WOR4 and WOR5). The genome of the hyperthermophilic archaeon *Pyrococcus furiosus* encodes four oxidoreductases of the AOR family, which have been well characterized. Tungsten in some of these proteins could not have been experimentally replaced with molybdenum (Mo) or vanadium (V), resulting in inactive variants. Structurally, the archaeal AORs form homodimers with a bridging iron atom and contain ferredoxin which serves as a physiological electron acceptor (Fig. 17.2). All characterized AOR enzymes oxidize a variety of aldehydes to their respective carboxylic acids, thus performing the detoxification of aldehydes which metabolically accumulate in various pathways. *P. furiosus* utilizes sugars as a carbon and energy source and its AOR tungstoenzyme catalyzes the oxidation of aldehydes (Chan et al. 1995). *P. furiosus* and other various hyperthermophilic archaea have FORs tungstoenzymes that show narrow specific activities toward short-chain aldehydes, e.g., diacid semialdehydes that serve as potential physiological substrates (Hu et al. 1999). According to the X-ray structural analysis, the FOR from *P. furiosus* has a homotetramer composition (Fig. 17.2) without a bridging iron atom. Instead, an additional  $\text{Ca}^{2+}$  ion is ligated to one of the WCo cofactors of this FOR, bearing a structural function. *Thermococcus litoralis* derives energy from the peptides fermentation and has the tungstoenzyme FOR that catalyzes the formaldehyde oxidation to formate (Mukund and Adams 1993).

GAPOR tungstoenzymes from archaea participate in glucose metabolism via a modified glycolytic pathway. They specifically catalyze the oxidation of glyceraldehyde-3-phosphate to 3-phosphoglycerate coupled to the reduction of ferredoxin. GAPORs are monomeric enzymes that contain  $\text{Zn}^{2+}$  as an additional metal (Scott et al. 2019). Tungsten-containing WOR4 and WOR5 from *P. furiosus* with no known function and no aldehyde-oxidizing activity contain a [3Fe-4S] cluster and have orthologous proteins in various hyperthermophilic archaea and anaerobic bacteria (Seelmann et al. 2020).

Anaerobic prokaryotes such as the denitrifying bacterium *Thauera aromatica* (Boll and Fuchs 1995), the Fe(III)-respiring *Geobacter metallireducens* (Huwiler et al. 2019) and the sulfate-respiring *Desulfosarcina cetonica* (Anselmann et al. 2019) degrade aromatic compounds using robust multimeric metalloenzymatic complexes called Benzoyl-CoA-reductases (BCRs). BCRs are macromolecular machineries comprised of 8 subunits ( $\text{Bam}[(\text{BC})_2\text{DEFGHI}]_2$ ), four WCo, four  $\text{Zn}^{2+}$  ions,  $>50$  Fe-S clusters, four selenocysteines, and six FADs. BCRs catalyze

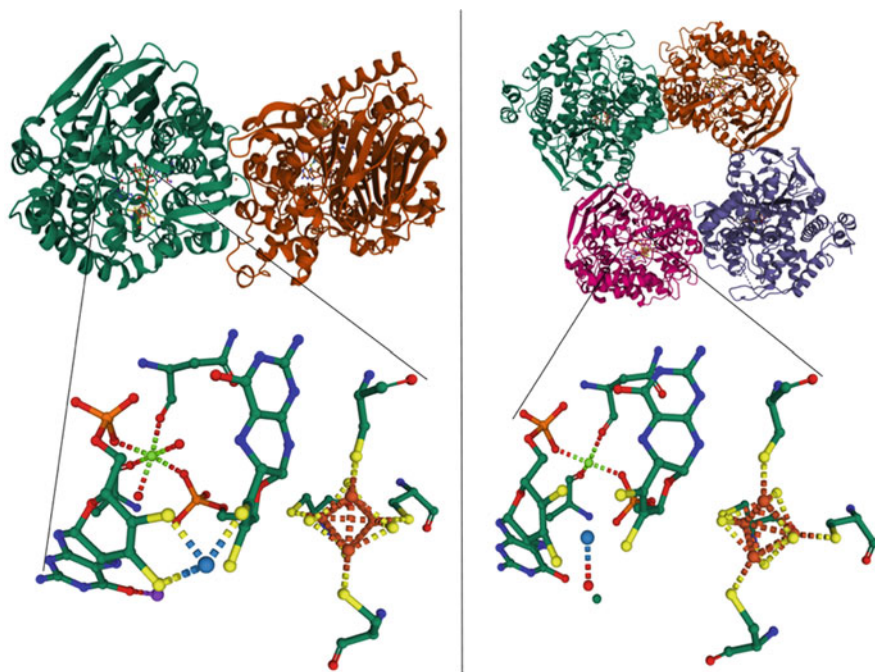


**Fig. 17.2** Structures of hyperthermophilic tungstoenzymes from *P. furiosus*. Left panel: overall homodimer structure of aldehyde oxidoreductase (pdb 1AOR) at 2.3 Å resolution; right panel: homotetramer of formaldehyde:ferredoxin oxidoreductase from *P. furiosus* (pdb 1B25) at 2.3 Å resolution. Corresponding enlarged WCo and [4Fe-4S] cofactors are given below each overall structure. The tungsten atom is shown in blue and  $Mg^{2+}$  is shown in green

the reduction of benzoyl-CoA, the central intermediate of benzoic acid metabolism (BAM) to dienoyl-CoA. The BamB subunit of these multimolecular complexes belongs to the AOR tungstoenzyme family and contains WCo,  $Zn^{2+}$  ion and a [4Fe-4S] cluster as cofactors (Kung et al. 2009). Strictly anaerobic bacteria use this tungsten-bearing BamB to reduce benzoyl-CoA when they grow on aromatic compounds.

The only one tungstoenzyme described to date that catalyzes a non-redox reaction is acetylene hydratase (AH) from *Syntrophotalea acetylenica* (previously designated *Pelobacter acetylenicus*, Seiffert et al. 2007). Apart from WCo, this enzyme contains a [4Fe-4S] cluster and use acetylene as a physiological substrate. AH is a member of the DMSO reductase family of tungstoenzymes which catalyzes the hydration of acetylene to acetaldehyde in an anaerobic degradation pathway of unsaturated hydrocarbons. High-resolution crystal structure studies of AH from *Syntrophotalea acetylenica* (Seiffert et al. 2007) have helped to unravel possible mechanisms of anaerobic acetylene degradation performed by this bacterium. The catalytically active W(IV) in WCo of AH was either suggested to directly coordinate acetylene for a nucleophilic attack by water (or hydroxide) or bind polarized water followed by

an electrophilic attack on the covalent carbon-carbon bond of acetylene (Seiffert et al. 2007).

Additionally, a lot of work has been done to understand the initial steps of microbial tungsten uptake and acquisition by prokaryotic cell. A class of tungsten-containing translocases has been reported, which are membrane-bound proteins involved in tungsten import system. Included among these translocases is the ABC transporter ModBC from *Archaeoglobus fulgidus* (Hollenstein et al. 2007). There also are ModABC, TupABC, and WtpABC transporter systems which help microbial cells acquire and transport tungsten in its highly soluble form of the tungstate oxyanion ( $\text{WO}_4^{2-}$ ), which is subsequently converted into the tungstopterin cofactor (Seelmann et al. 2020).

Discussing the essential role of tungsten in a variety of fundamental biological processes, it is worth noting that some of the tungstoenzymes can use exclusively tungsten (e.g., aldehyde oxidoreductase from hyperthermophiles), solely molybdenum (e.g., bacterial nitrate reductase), or both of these metals (e.g., FDH from *Methanococcus vannielii*). Although tungsten and molybdenum have much the same atomic and ionic radii and cognate coordination chemistry, a substitution of Mo by W may lead to an inactivation of the enzymes, and only in some cases was a substitution of W by Mo found to be possible without significant loss in enzyme activity (Buc et al. 1999; Stewart et al. 2000). The fundamental question that researchers have tried to solve was why some microorganisms utilize W and not Mo (Kletzin and Adams 1996). Indeed, while moderately thermophilic and mesophilic microorganisms usually are not obligatorily dependent on tungsten, and molybdenum can substitute tungsten both in the growth medium and in the pterin cofactor of their tungstoenzymes, hyperthermophiles have an obligatory requirement for tungsten, which plays an important role in their carbohydrate and peptide metabolism. Here, a unique exception has been reported for a thiosulfate reductase (TSR) involved in thiosulfate respiration in the archaeon *P. aerophilum*. TSR, which was recombinantly produced in *P. furiosus*, contained either Mo or W depending on the cultivation medium (Haja et al. 2020). Nevertheless, (hyper)-thermophily is regarded to be close to an ancestral phenotype (Stetter 2006; Akanuma et al. 2013) and WCo cofactor as the active site of tungstoenzymes has been proposed to be a precursor of the modern molybdenum cofactors. The interchangeable and labile function of Mo and W cofactors in many microbial tungstoenzymes may indicate the importance of Mo- and W-containing enzymes in the evolutionary process. Additionally, life has been proposed to have originated at extreme temperatures in deep-sea hydrothermal vents, where W is present in much higher concentrations than in the open ocean. It has been hypothesized that the earliest life forms were hyperthermophilic and also W-dependent. Presumably, on early Earth under anoxygenic conditions preceding to the availability of molecular oxygen due to photosynthesis, molybdenum and tungsten were represented as sulfides ( $\text{MoS}_2$  and  $\text{WS}_2$ ) rather than oxyanions ( $\text{MoO}_4^{2-}$  and  $\text{WO}_4^{2-}$ ). Out of these two sulfides,  $\text{WS}_2$  has higher water solubility than  $\text{MoS}_2$ , thus tungsten could have been more bioavailable to early life forms in primordial anoxygenic world (Kletzin and Adams 1996). Such W-dependent microbial life forms on early

Earth presumably would later have evolved into mesophilic molybdenum-dependent species and these evolutionary descendants now constitute the vast majority of different life forms. In conjunction to this, molybdenum is much more abundant than W in oxic, marine waters, where higher aerobic life forms might have evolved. In addition to W (bio)availability in volcanic areas (e.g., deep-sea hydrothermal systems) where hyperthermophiles can be found, W (but not Mo) is able to catalyze aldehyde oxidation and acid reduction at elevated temperatures. Based on all these afore-mentioned assumptions, tungsten has been proposed as a phylogenetically ancient redox cofactor (Kletzin and Adams 1996).

### ***17.2.2 From Tungsten Life-Sustainable Material Precursors to Microbial Tungsten Armor During Interplanetary Travel***

Certain microorganisms (chemolithotrophs) can respire by utilizing a variety of metals and metalloids as electron donors and acceptors to sustain microbial life and generate cellular proliferation. Among a variety of research studies, review papers, and chapters reporting the biochemistry of metal and metalloids, tungsten appears especially interesting, as there is no microbial respiration utilizing tungsten as terminal electron acceptor or primarily electron donor described in nature. Tungsten is the heaviest metal and has various biological functions, especially in thermophilic archaea (Chan et al. 1995; Kletzin and Adams 1996; Andreesen and Makdessi 2008), but functional tungsten-based microbial respiration has not yet been observed.

Our recent study (Milojevic et al. 2019) investigated whether complex inorganic systems based upon tungsten polyoxometalate (POM) clusters can sustain microbial chemolithotrophic life. POMs are artificial symmetric anionic macromolecules that contain oxidometalate polyhedra as building blocks, they are well suited as inorganic frameworks for complex self-assembling and -organizing systems and have been proposed as micelle-like structures in developing approaches to artificial inorganic life (Long et al. 2007; Cogdell et al. 2010; Gao et al. 2011; Yin et al. 2012; Symes et al. 2013). Analogously to mineral cells based on iron sulfide (Wächtershäuser 1992), POMs are considered as inorganic mineral cells in facilitating prelife chemical processes and displaying “life-like” characteristics (Miras et al. 2010; Cooper et al. 2011). However, the relevance of POMs to life-sustaining processes (e.g., microbial respiration) has not yet been addressed, whereas iron sulfides are very well known as ubiquitous mineral precursors and energy sources for chemolithotrophic metabolism. Investigating tungsten POMs as life-sustaining molecules, we showed that the use of tungsten-based inorganic POM clusters allows the possibility of incorporating tungsten redox heterogenous species by microbial cells (Milojevic et al. 2019). We detected the decomposition of W-POM macromolecular clusters and the appearance of low molecular weight W species (e.g., WO) in microbial

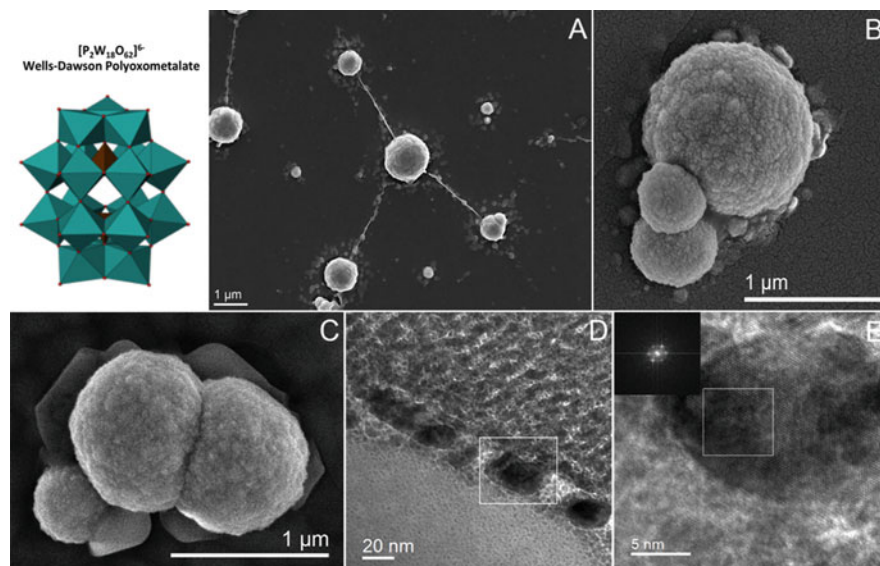


**Fig. 17.3** Microbial cultivation on supramolecular self-assemblages based on inorganic metal clusters of tungsten polyoxometalate (POM) (represented in green). Ancient archaea consume tungsten from an artificial inorganic compound, which previously was not associated with any living matter. Shown are microbial cells after 21 days of cultivation with W-POM (a–c) and tungsten deposits on the S-layer of microbial cell (d, e). This figure has been redrawn from Milojevic et al. (2019)

cultures. The presence of these W-POM decomposition products was not observed in abiotic controls after 21 days of incubation in growth medium in the absence of microorganisms. Furthermore, we documented the presence of metalloorganic assemblages at the W-POM-microbial interface resolved down to the nanometer scale using scanning and transmission electron microscopy tools (Fig. 17.3). High-resolution transmission electron microscopy indicated the deposition of redox heterogeneous tungsten species on the cell surface along with the accumulation of intracellular tungsten-bearing nanoparticles, i.e., clusters of tungsten atoms.

Among possible mechanisms of W-POM decomposition by microbial cells we can envisage respiration directly on electron flow generated by reduced W-POM species with unique electrochemical properties. Our results indicate that microbial cells form a tungsten-bearing mineralized S-layer via encrusting with tungsten carbide-like compounds. Whether the observed biomineralization occurs via a direct precipitation of tungsten from the cultivation medium or is coupled to active metabolic respiration is still unresolved issue. Hypothetically, it is possible that the accumulation of reduced W species might be utilized by microbial cells as a respiration source, although this kind of tungsten-based chemolithotrophy has not yet been demonstrated for any microbial entity. In this connection, the microbial molecular machinery responsible for tungsten binding, acquisition and assimilation is a topic that requires more thorough analysis in the future.

Here, of a special interest is a newly described tungsten–microbial biomineralized interface (Fig. 17.3). A few of our recent studies have indicated that microbial cells form tungsten-bearing mineralized cell surface via encrusting with tungsten carbide-like compounds (Milojevic et al. 2019; Blazevic et al. 2019). We also have proposed that the tungsten-encrusted S-layer represents a microbial strategy to withstand harsh environments, such as during an interplanetary journey (Kölbl et al. 2020). Numerous experimental studies of microbial transfer through space and between celestial bodies in the context of lithopanspermia hypothesis of life origin and transfer across the Universe have significantly proved the potential survival of microbial life in outer space (Rabbow et al. 2017; Kawaguchi et al. 2020; Ott et al. 2020). Tungsten encapsulation can serve as a potent radioprotective armor in outer space against drastic environmental conditions, enabling the further study of microbial survivability in outer space environment and helping answer fundamental questions of astrobiology (Kölbl et al. 2020). Tungsten exhibits a hardness of ~9–9.5 on the Mohs hardness scale (Tabor 1954) and can potentially provide an efficient barrier against water loss, supporting the preservation of cell integrity after desiccation (Kölbl et al. 2020). In this regard, tungsten incorporation by the cell envelope (Blazevic et al. 2019; Milojevic et al. 2019) may certainly serve as an efficient strengthening strategy, as this is a hard element with the highest melting point and extraordinary properties among all metals. Tungsten encrustation of the cell surface can potentially function as a microbial tungsten armor during interplanetary travel.

## 17.3 Tungsten–Microbial Interactions: Applied Studies

### 17.3.1 Tungsten Biosorption

In recent years, several investigations have been focusing on the development of environmentally friendly, cost-effective, and sustainable recycling techniques for the removal of tungsten from solutions. Tungsten is defined as a critical raw material by the European Union and a number of other countries (Chapman et al. 2013). W biosorption as an alternative to conventional processes of W removal from wastewaters has been attracting increasing attention to achieve environmental preservation and secure natural resources. A 97.1% removal of tungsten was described by introducing *E. coli* cells into a tungsten aqueous solution (Ogi et al. 2013) (Fig. 17.4). *E. coli* cells also have been shown to possess the potential for selective tungsten absorption from real wastewaters (Ogi et al. 2016a). That study with used tungsten carbide (WC) scrap demonstrated the feasibility of biosorption for WC recycling using microbial cells and enabled the establishment of a new, environmentally friendly recycling process. Another study suggested that *Bacillus* sp. strain MGG-83 isolated from Anzali lagoon in Iran is highly efficient in tungstate ( $WO_4^{2-}$ ) sorption, achieving 76% of tungstate adsorbed within 5 min of heterotrophic cultivation in laboratory conditions at 30 °C for 7 days (Malekzadeh et al. 2007). Those authors proposed an application of this strain in scavenging the tungstate from

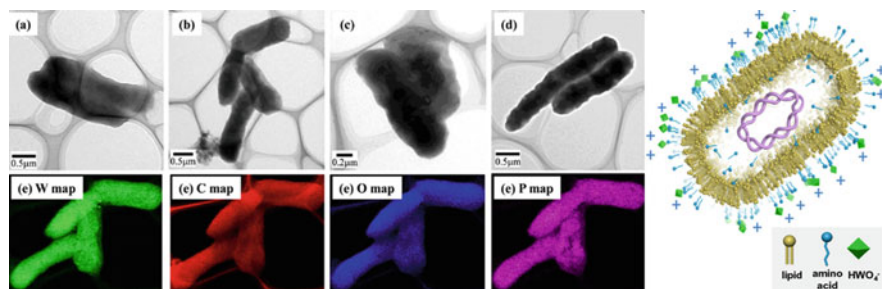


**Fig. 17.4** W adsorption by *E. coli* cells based on TEM analysis (a) before adsorption and after (b) 3 min, (c) 30 min, (d) 420 min and (e) elemental mapping analysis at 3 min followed by a schematic mechanism of W adsorption by *E. coli* cells. This figure has been modified from Ogi et al. (2013, 2016b)

radionuclide generators used for radio-therapeutic purposes. *Komagataeibacter xylinus* was able to uptake tungsten from the bacterial growth medium with W concentration up to 15 ppm and the authors suggested this bacterium as a promising agent for an eco-friendly recycling system (Nandiyanto et al. 2016).

Several tungsten biosorption studies have been reported, attempting to reveal the W biosorption mechanism which possibly occurs on the microbial cell surface (Ghazvini and Mashkani 2009; Ogi et al. 2016b, 2017) (Fig. 17.4). It has been found that amino acids exposed on the surfaces of heat-treated *E. coli* cells notably boosted the tungsten adsorption capacity (Ogi et al. 2016b). Based on Fourier transform infrared analysis, carboxyl and phosphate functional groups on the surface of the bacteria were proposed to play a crucial role in W adsorption (Ogi et al. 2013). Furthermore, the amino acid lysine has been suggested as a potentially efficient, nontoxic, and cost-effective adsorbent that has a minimum environmental impact (Ogi et al. 2017).

A very recent investigation by Coimbra et al. (2019) utilized a molecular bioengineering approach to construct an efficient microbial bioaccumulator of tungsten (EcotupW). The authors performed recombinant expression of the complete *tupBCA* gene cluster from *Sulfitobacter dubius* NA4 in *E. coli* cells and the obtained recombinant strains possessed a high bacterial capacity to accumulate W (Coimbra et al. 2019). Marine hydrothermal *S. dubius* strains isolated from the Lucky Strike hydrothermal vent field carrying a *tupBCA* cluster are known to tolerate and accumulate tungsten (Coimbra et al. 2017). The *tupBCA* gene cluster includes the genetic determinants which encode proteins responsible for W-binding and membrane transport into the bacterial cell. For instance, the protein TupA is involved in the recognition and highly specific binding of tungstate ( $WO_4^{2-}$ ). Further, by means of site-directed mutagenesis, the authors showed the importance of the valine amino acid residue in enhanced W-accumulation. The valine residue present in the VTTS motif located in the substrate-binding protein TupA was proposed to be responsible for efficient tungstate-binding (Coimbra et al. 2019). Such a recombinant microbial



bioaccumulator of tungsten was suggested as an alternative strategy to recover tungsten from natural and anthropogenic-impacted environments.

### 17.3.2 Tungsten Bioleaching

A great variety of evolutionarily diversified metallophilic microorganisms are equipped with unique capabilities and fascinating metabolic routes for manipulating minerals and dissolving them to access useful metals. Such microbial-assisted solubilization of metals is intensively used in industrial processes called biomining or bioleaching of mineral ores, in order to extract metals such as copper, nickel, gold, uranium, etc. This bioprocess is performed by chemolithoautotrophic microorganisms capable of oxidizing iron and sulfur. While microbial-mediated bioprocessing of Fe- and S-bearing minerals has been extensively studied and harnessed, exploitation of tungsten minerals still requires detailed investigations of tungsten–microbial interactions. One of the considerations which restricts the application of tungsten ore bioprocessing is the lack of research into tungsten–microbial interactions.

With its abundance of about 1.5 parts per million in the Earth's crust, tungsten never occurs as a free element in nature. Its most common naturally occurring ores are the minerals scheelite (calcium tungstate  $\text{CaWO}_4$ ) and wolframite (iron manganese tungstate  $\text{Fe, MnWO}_4$ , comprised of the two minerals ferberite  $\text{FeWO}_4$  and hübnerite  $\text{MnWO}_4$ ). Unique physical and mechanical properties of tungsten (high melting and boiling points plus its density) make this heavy metal indispensable in the modern high-tech industry. Tungsten is suitable for a great variety of industrial, civil and military applications, among which are high-temperature energy- and lighting technologies, radiation-shielding materials, and the space industry, where it is used as alloys or superalloys. In combination with carbon, tungsten exhibits diamond-like hardness and provides the basis of modern cutting and drilling tools (ranging from hair-like miniature drills to drills used in cutting, pressing, mining, and tunneling). The currently used hydrometallurgical and pyrometallurgical processes enable the breakage of the tungsten–oxygen bond and release of the associated tungsten; however, in spite of W extensive uses, the bioprocessing of tungsten-bearing minerals is not yet established.

Today, information on the biogeochemistry of tungsten and the role of microorganisms in natural tungsten mineral environments is very limited and has been presented in just a handful of publications. For instance, microbial colonies with morphology similar to that of cyanobacteria have been detected on the surface of scheelite via electron microscopy on the environmental samples taken from tungsten deposits near Lake Ladoga, Russia (Strigul et al. 2009). Some additional information on microbial-tungsten interactions has been obtained from laboratory investigations. Accelerated W mobilization from wolframite has been reported under aerobic conditions in liquid cultures of the autotrophic acidophilic bacteria *Thiobacillus ferrooxidans* and the heterotrophic bacteria *Pseudomonas putida* (previously

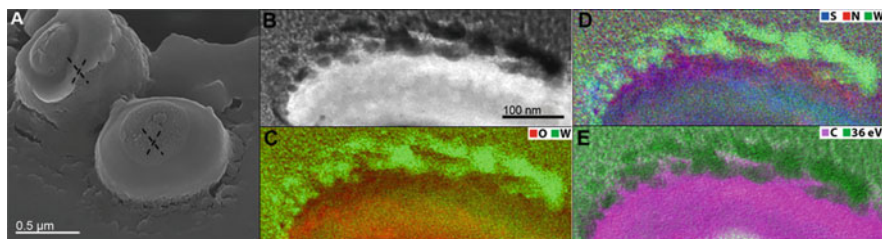


**Fig. 17.5** Elemental ultrastructural analysis of scheelite-grown cells of *Metallosphaera sedula*. (a) SEM image showing cells of *M. sedula* deposited over scheelite surface. (b) Scanning transmission electron microscopy (STEM) image of a cell fragment of *M. sedula* used for energy-filtered transmission electron microscopy (EFTEM) analysis. (c–e) Corresponding tungsten (W), oxygen (O), sulfur (S), nitrogen (N), and carbon (C) elemental maps. This figure has been redrawn from Blazevic et al. (2019)

identified as *Arthrobacter siderocapsulatus*, Chashchina and Lyalikova 1989). Those authors detected increased bioleaching of W, Fe, and Mn from the surface of polished pieces of wolframite and reported the formation of new mineral precipitates. After ~40 days of batch cultivation, a large quantity of newly formed minerals reduced the accessibility of the wolframite mineral surface and inhibited the bioleaching of tungsten. The authors proposed that the microbial biooxidation of Fe and Mn destroyed the wolframite structure and also reduced the pH of the cultivation media, which can be considered as an additional mineral breakdown factor in order to deliver W in solution. In the case of the heterotrophic bacteria *Pseudomonas putida*, W solubilization was suggested to be promoted by some of the organic acids biosynthesized by these bacteria (Chashchina and Lyalikova 1989).

Recently, microbial biotransformation of the tungsten mineral scheelite and active W bioleaching by the extreme thermoacidophile *Metallosphaera sedula* have been reported (Blazevic et al. 2019). *M. sedula* is a facultative chemolithotroph that is capable of bioleaching, and the key to its chemical attack of metal ores is the redox regeneration of  $\text{Fe}^{3+}$  from  $\text{Fe}^{2+}$ . Apart from Fe-oxidizing properties, metabolically versatile *M. sedula* has the ability to use a variety of electron donors (Huber et al. 1989; Auernik and Kelly 2008), including reduced inorganic sulfur compounds (Auernik and Kelly 2010), uranium ores (Mukherjee et al. 2012), as well as molecular hydrogen under microaerobic conditions (Auernik and Kelly 2010). Blazevic et al. (2019) showed that biooxidizing activity of *M. sedula* results in the breakage of scheelite structure, consequent tungsten solubilization in the leachate solution, and accumulation of W-bearing deposits on the cell surface (Fig. 17.5).

Biotransformation of scheelite was accompanied by biomineralization of the *M. sedula* S-layer with crystalline nanoparticles containing carbide-like tungsten. This process can be attributed to the highly ordered proteinaceous S-layer of *M. sedula* which promoted sorption of the metal ions serving as nucleation centers for crystallization and therefore facilitating the further growth of the nanoparticles. Moreover, *M. sedula* are grown on scheelite accumulated intracellular Mn and Fe redox heterogeneous inclusions that can represent a nanometer-sized energy storage

depot for microbial cells. The authors (Blazevic et al. 2019) proposed that the *M. sedula* mediated biooxidation of Fe and Mn destroyed the scheelite structure, leading to the release of W into solution. In addition to such a direct biooxidation of metals, the involvement of abiotic factors (e.g oxidizing attack of  $\text{Fe}^{3+}$ , acidic conditions, and calcium precipitation) may not be excluded as promoters of tungsten solubilization. Generally, the bioleaching mechanism always has a dual nature, combining microbiological and chemical components. In the case of scheelite biosolubilization, the authors also proposed that the combination of these two biogenic and abiotic factors results in the mobilization of tungsten from the solid mineral matrix of scheelite (Blazevic et al. 2019).

**Acknowledgments** This work was supported by the Austrian Science Fund (FWF) through an Elise-Richter Research fellowship V333 “Iron- and sulfur-oxidizing machinery of the bioleaching archaeon *Metallosphaera sedula*.” The author would like to thank Denise Kölbl (Space Biochemistry Group, University of Vienna) and Mihaela Albu (Graz Centre for Electron Microscopy) for many helpful suggestions and conversations over the years.

## References

- Akanuma S, Nakajima Y, Yokobori S et al (2013) Experimental evidence for the thermophilicity of ancestral life. *Proc Natl Acad Sci U S A* 110:11067–11072
- Andreesen JR, Makdessi K (2008) Tungsten, the surprisingly positively acting heavy metal element for prokaryotes. *Ann N Y Acad* 1125:215–229
- Anselmann SEL, Löffler C, Stärk H, Jehmlich N, Bergen M, Brüls T, Boll M (2019) The class II benzoyl-coenzyme A reductase complex from the sulfate-reducing *Desulfosarcina cetonica*. *Environ Microbiol* 21:4241–4252
- Auernik KS, Kelly RM (2008) Identification of components of electron transport chains in the extremely thermoacidophilic crenarchaeon *Metallosphaera sedula* through iron and sulfur compound oxidation transcriptomes. *Appl Environ Microbiol* 74:7723–7732
- Auernik KS, Kelly RM (2010) Impact of molecular hydrogen on chalcopyrite bioleaching by the extremely thermoacidophilic archaeon *Metallosphaera sedula*. *Appl Environ Microbiol* 76:2668–2672
- Bevers LE, Hagedoorn PL, Hagen WR (2009) The bioinorganic chemistry of tungsten. *Coord Chem Rev* 253:269–290
- Blazevic A, Albu M, Mitsche S, Rittmann SK-MR, Habler G, Milojevic T (2019) Biotransformation of scheelite  $\text{CaWO}_4$  by the extreme thermoacidophile *Metallosphaera sedula*: tungsten-microbial interface. *Front Microbiol* 10:1492
- Boll M, Fuchs G (1995) Benzoyl-coenzyme A reductase (dearomatizing), a key enzyme of anaerobic aromatic metabolism. *Eur J Biochem* 234:921–933
- Buc J, Santini C-L, Giordani R, Czjzek M, Wu L-F, Giordano G (1999) Enzymatic and physiological properties of the tungsten-substituted molybdenum TMAO reductase from *Escherichia coli*. *Mol Microbiol* 32:159–168
- Chan MK, Mukund S, Kletzin A, Adams MWW, Rees DC (1995) Structure of a hyperthermophilic tungstopterin enzyme, aldehyde ferredoxin oxidoreductase. *Science* 267:1463–1469
- Chapman A, Arendorf J, Castella T, Thompson P, Willis P, Espinoza L, Klug S, Wichmann E (2013) Study on critical raw materials at EU level. Oakdene Hollins, Buckinghamshire
- Chashchina NM, Lyalikova NN (1989) The role of bacteria in the transformation of tungsten minerals. *Mikrobiologiya* 58:122–126

- Cogdell RJ, Brotsudarmo TH, Gardiner AT, Sanchez PM, Cronin L (2010) Artificial photosynthesis – solar fuels: current status and future prospects. *Biofuels* 1:861–876
- Coimbra C, Farias P, Branco R, Morais PV (2017) Tungsten accumulation by highly tolerant marine hydrothermal Sulfitobacter dubius strains carrying a tupBCA cluster. *Syst Appl Microbiol* 40:388–395
- Coimbra C, Branco R, Morais PV (2019) Efficient bioaccumulation of tungsten by Escherichia coli cells expressing the Sulfitobacter dubius Tup BCA system. *Syst Appl Microbiol* 42:126001
- Cooper GJT, Kitson PJ, Winter R, Zagnoni M, Long DL, Cronin L (2011) Modular redox-active inorganic chemical cells: iCHELLs. *Angew Chem* 50:10373–10376
- Gao J, Yan J, Mitchell SG, Miras HN, Boulay AG, Long DL (2011) Self-assembly of a family of macrocyclic polyoxotungstates with emergent material properties. *Chem Sci* 2:1502–1508
- Ghazvini PTM, Mashkani SG (2009) Screening of bacterial cells for biosorption of oxyanions: application of micro-PIXE for measurement of biosorption. *Hydrometallurgy* 96:246–252
- Graentzdoerffer A, Rauh D, Pich A, Andreesen JR (2003) Molecular and biochemical characterization of two tungsten- and selenium-containing formate dehydrogenases from Eubacterium acidaminophilum that are associated with components of an iron-only hydrogenase. *Arch Microbiol* 179:116–130
- Haja DK, Wu CH, Poole FL, Sugar J, Williams SG, Jones AK, Adams MWW (2020) Characterization of thiosulfate reductase from Pyrobaculum aerophilum heterologously produced in Pyrococcus furiosus. *Extremophiles* 24:53–62
- Holden JF, Adams MW (2003) Microbe-metal interactions in marine hydrothermal environments. *Curr Opin Chem Biol* 2:160–165
- Hollenstein K, Frei DC, Locher KP (2007) Structure of an ABC transporter in complex with its binding protein. *Nature* 446:213–216
- Hu Y, Faham S, Roy R, Adams MW, Rees DC (1999) Formaldehyde ferredoxin oxidoreductase from Pyrococcus furiosus: the 1.85 Å resolution crystal structure and its mechanistic implications. *J Mol Biol* 286:899–914
- Huber G, Spinnler C, Gambacorta A, Stetter KO (1989) Metallosphaera sedula gen. and sp. nov. represents a new genus of aerobic, metal-mobilizing, thermoacidophilic archaeobacteria. *Syst Appl Microbiol* 12:38–47
- Huwiler SG, Löffler C, Anselmann SEL, Stärk HJ, von Bergen M, Flechsler J, Rachel R, Boll M (2019) One-megadalton metalloenzyme complex in Geobacter metallireducens involved in benzene ring reduction beyond the biological redox window. *Proc Natl Acad Sci U S A* 116:2259–2264
- Jones JB, Stadtman TC (1981) Selenium-dependent and selenium-independent formate dehydrogenases of Methanococcus vannielii. Separation of the two forms and characterization of the purified selenium-independent form. *J Biol Chem* 256:656–663
- Kawaguchi Y, Shibuya M, Kinoshita I, Yatabe J, Narumi I, Shibata H, Hayashi R, Fujiwara D, Murano Y, Hashimoto H, Imai E, Kodaira S, Uchihori Y, Nakagawa K, Mita H, Yokobori S, Yamagishi A (2020) DNA damage and survival time course of Deinococcal cell pellets during 3 years of exposure to outer space. *Front Microbiol* 11:2050
- Kletzin A, Adams MWW (1996) Tungsten in biological systems. *FEMS Microbiol Rev* 18:5–63
- Kölbl D, Blazevic A, Albu M, Fasching C, Milojevic T (2020) Desiccation of the extreme thermoacidophile Metallosphaera sedula grown on terrestrial and extraterrestrial materials. *Front Astron Space Sci* 7:41
- Kung JW, Löffler C, Dörner K, Heintz D, Gallien S, Van Dorsseleer A, Friedrich T, Boll M (2009) Identification and characterization of the tungsten-containing class of benzoyl-coenzyme A reductases. *Proc Natl Acad Sci U S A* 106:17687–17692
- Laukel M, Chistoserdova L, Lidstrom ME, Vorholt JA (2003) The tungsten-containing formate dehydrogenase from Methylobacterium extorquens AM1: purification and properties. *Eur J Biochem* 270:325–333
- Long DL, Burkholder E, Cronin L (2007) Polyoxometalate clusters, nanostructures and materials: from self assembly to designer materials and devices. *Chem Soc Rev* 36:105–121

- Malekzadeh F, Mashkani SG, Ghafourian H, Soudi MR (2007) Biosorption of tungstate by a *Bacillus* sp isolated from Anzali lagoon. *World J Microbiol Biotechnol* 23:905–910
- May HD, Patel PS, Ferry JG (1988) Effect of molybdenum and tungsten on synthesis and composition of formate dehydrogenase in *Methanobacterium formicicum*. *J Bacteriol* 170: 3384–3389
- Milojevic T, Albu M, Blazevic A, Gumerova N, Konrad L, Cyran N (2019) Nanoscale tungsten-microbial interface of the metal immobilizing thermoacidophilic archaeon *Metallosphaera sedula* cultivated with tungsten polyoxometalate. *Front Microbiol* 10:1267
- Miras HN, Cooper GJT, Long DL et al (2010) Unveiling the transient template in the self-assembly of a molecular oxide nanowheel? *Science* 327:72–74
- Mota CS, Valette O, González PJ, Brondino CD, Moura JGG, Moura I, Dolla A, Rivas MG (2011) Effects of molybdate and tungstate on expression levels and biochemical characteristics of formate dehydrogenases produced by *Desulfovibrio alaskensis* NCIMB 13491. *J Bacteriol* 93: 2917–2923
- Mukherjee A, Wheaton GH, Blum PH, Kelly RM (2012) Uranium extremophily is an adaptive, rather than intrinsic, feature for extremely thermoacidophilic *Metallosphaera* species. *Proc Natl Acad Sci U S A* 109:16702–16707
- Mukund S, Adams MW (1993) Characterization of a novel tungsten-containing formaldehyde ferredoxin oxidoreductase from the hyperthermophilic archaeon, *Thermococcus litoralis*. A role for tungsten in peptide catabolism. *J Biol Chem* 268:13592–13600
- Nandiyanto ABD, Halimatul HS, Rosyid NH, Effendi DB (2016) Effect of tungsten concentration on growth of *Acetobacter xylinum* as a promising agent for eco-friendly recycling system. International conference on innovation in engineering and vocational education. Book Series: IOP Conference Series-Materials Science and Engineering 128: 012041. <https://doi.org/10.1088/1757-899X/128/1/012041>
- Ogi T, Sakamoto Y, Nandiyanto ABD, Okuyama K (2013) Biosorption of tungsten by *Escherichia coli* for an environmentally friendly recycling system. *Ind Eng Chem Res* 52:14441–14448
- Ogi T, Makino T, Okuyama K, Stark WJ, Iskandar F (2016a) Selective biosorption and recovery of tungsten from an urban mine and feasibility evaluation. *Ind Eng Chem Res* 55:2903–2910
- Ogi T, Makino T, Iskandar F, Tanabe E, Okuyama K (2016b) Heat-treated *Escherichia coli* as a high-capacity biosorbent for tungsten anions. *Bioresour Technol* 218:140–145
- Ogi T, Makino T, Nagai S, Stark WJ, Iskandar F, Okuyama K (2017) Facile and efficient removal of tungsten anions using lysine-promoted precipitation for recycling high-purity tungsten. *ACS Sustain Chem Eng* 5:3141–3147
- Ott E, Kawaguchi Y, Kölbl D et al (2020) Molecular repertoire of *Deinococcus radiodurans* after 1 year of exposure outside the international Space Station within the Tanpopo mission. *Microbiome* 8:150
- Rabbow E, Rettberg P, Parpart A et al (2017) EXPOSE-R2: the astrobiological ESA mission on board of the international Space Station. *Front Microbiol* 8:1533
- Scott IM, Rubinstein GM, Poole FL, Lipscomb GL, Schut GJ, Williams-Rhaesa AM, Stevenson DM, Amador-Noguez D, Kelly RM, Adams MWW (2019) The thermophilic biomass-degrading bacterium *Caldicellulosiruptor bescii* utilizes two enzymes to oxidize glyceraldehyde 3-phosphate during glycolysis. *J Biol Chem* 294:9995–10005
- Seelmann CS, Willistein M, Heider J, Boll M (2020) Tungstoenzymes: occurrence, catalytic diversity and cofactor synthesis. *Inorganics* 8:44
- Seiffert GB, Ullmann GM, Messerschmidt A, Schink B, Kroneck PM, Einsle O (2007) Structure of the non-redox-active tungsten/[4Fe: 4S] enzyme acetylene hydratase. *Proc Natl Acad Sci U S A* 104:3073–3077
- Stetter KO (2006) Hyperthermophiles in the history of life. *Philos Trans R Soc Lond B* 361:1837–1842
- Stewart LJ, Bailey S, Bennett B, Charnock JM, Garner CD, McAlpine AS (2000) Dimethylsulfoxide reductase: an enzyme capable of catalysis with either molybdenum or tungsten at the active site. *J Mol Biol* 299:593–600

- Strigul N, Koutsospyros A, Arienti P, Christodoulatos C, Dermatas D, Braida W (2005) Effects of tungsten on environmental systems. *Chemosphere* 61:248–258
- Strigul N, Koutsospyros A, Christodoulatos C (2009) Tungsten in the former Soviet Union: review of environmental regulations and related research. *Land Contam Reclam* 17:1
- Symes MD, Cogdell RJ, Cronin L (2013) Designing artificial photosynthetic devices using hybrid organic-inorganic modules based on polyoxometalates. *Philos Trans A Math Phys Eng Sci* 371: 20110411
- Tabor D (1954) Mohs hardness scale – a physical interpretation. *Proc Phys Soc B* 67:249–257
- Taylor AJ, Kelly DJ (2019) The function, biogenesis and regulation of the electron transport chains in *Campylobacter jejuni*: new insights into the bioenergetics of a major food-borne pathogen. *Adv Microb Physiol* 74:239–329
- Wächtershäuser G (1992) Groundworks for an evolutionary biochemistry: the iron-Sulphur world. *Prog Biophys Mol Biol* 58:85–201
- Wagner T, Ermler U, Shima S (2016) The methanogenic CO<sub>2</sub> reducing-and-fixing enzyme is bifunctional and contains 46 [4Fe-4S] clusters. *Science* 354:114–117
- White H, Strobl G, Feicht R, Simon H (1989) Carboxylic acid reductase: a new tungsten enzyme catalyses the reduction of non-activated carboxylic acids to aldehydes. *Eur J Biochem* 184:89–96
- Yin P, Pradeep CP, Zhang B et al (2012) Controllable self-assembly of organic-inorganic amphiphiles containing Dawson polyoxometalate clusters. *Chem Eur J* 18:8157–8162

# Chapter 18

## Vanadium-Based Transformations Effected by Algae and Microbes



Dieter Rehder

**Abstract** Many algae and bacteria living in either aquatic or terrestrial environments are capable of transforming and in many ways utilizing inorganic vanadium—essentially vanadate(V) and oxidovanadium(IV)—in bio-transformations. These metabolic activities often are based on redox interactions between  $V^V$  and  $V^{IV}$  (and sometimes  $V^{III}$ ). Examples are (1) the oxidation of halides and pseudohalides by marine phytoplankton such as macroalgae (seaweeds), (2) the fixation of nitrogen (conversion of  $N_2$  to  $NH_4^+$ ) and the hydrogenation of alkynes by bacteria belonging to the genus *Azotobacter* and by cyanobacteria associated with bryophytes, and (3) the respiratory and dissimilatory reduction of  $H_2VO_4^-$  to  $V^{IV}$  (commonly insoluble  $VO(OH)_2$ ). Vanadate reduction can further be coupled with the nitrate to nitrite reduction process by *Thioalkalivibrio nitratireducens*, and to the oxidation of methane. Vanadate-reducing bacteria are of particular ecological interest for industrial areas where vanadium ores are processed with the release of (toxic) vanadate: Bacterially induced reduction of vanadate to insoluble  $VO(OH)_2$  is an increasingly probed object of research. In addition, bacterial reduction of vanadate does have implications in microbial fuel cells. Along with  $H_2VO_4^-/VO^{2+}$ , vanadium coordination compounds can exhibit antimicrobial activities related to health issues such as bacterial pneumonia. Decavanadate notably exerts growth inhibition against *Escherichia coli*.

### 18.1 General Role of Vanadium: Occurrence, Toxic and Beneficial Effects

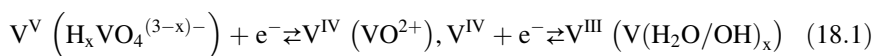
Vanadium, the 20th most abundant element on Earth, occurs in about 70 variants of minerals, in the form of oxidovanadium(IV) ( $VO^{2+}$ , “vanadyl”) in the porphyrins in crude oil and shales, and as hydrogenvanadate ( $H_2VO_4^-$ ) in water reservoirs. The concentration of vanadate in seawater (where vanadate is an essential source for

---

D. Rehder (✉)  
Chemistry Department, University of Hamburg, Hamburg, Germany  
e-mail: [rehder@chemie.uni-hamburg.de](mailto:rehder@chemie.uni-hamburg.de)

macro-algae and several sea organisms, tunicates and fan worms in particular) amounts to an average of ca. 35 nM. Vanadate ( $H_xVO_4^{(3-x)-}$ ,  $x = 1$  or 2, depending on the pH at about physiological conditions) is omnipresent in groundwater. Reductive processes can convert—and thus detoxify—vanadate into insoluble  $VO(OH)_2$ .

In either oxidation state,  $V^V$  and  $V^{IV}$  (and  $V^{III}$ ), vanadium can enter cellular compartments: in the form of vanadate via phosphate channels, and in the form of  $VO^{2+}$  via transport by transferrin. Supposedly, hydrogenvanadate—in trace amounts—is an essential element for the majority of living organisms. In part, this is due to its structural (and, to some extent, its chemical) similarity to hydrogen phosphate, a resemblance that induces—via its interference with physiologically relevant components—competitive behaviour in metabolic processes that are commonly governed by phosphatases and kinases. However, contrasting phosphate, vanadate(V) is labile with respect to reduction to  $V^{IV}$  ( $VO^{2+}$ , commonly in the form of VOL, where L is a biogenic ligand) and further to  $V^{III}$ , Eq. (18.1).



This redox lability makes vanadate more versatile than phosphate—but to some extent also potentially hazardous with respect to its functions in life: Vanadate is a competitor of phosphate, and vanadyl is a competitor of biologically relevant transition metal(2+) ions, which means that these vanadium ions can cause objectionable physiological side effects, and those effects potentially are ecotoxic. Another striking difference between vanadate and phosphate is the ability of vanadium (in all of its oxidation states) to attain the coordination numbers five, six (and even seven, in the vanabins of *Amanita* mushrooms), while phosphorous in phosphate at best undergoes intermediate and weak interactions with a fifth electron donor.

## 18.2 Oxidative Transformation of Halides and Pseudohalides by Vanadate-Dependent Haloperoxidases

Haloperoxidases catalyze the oxidative (normally by peroxide) transformation of halides, and usually pseudohalides as well, to hypohalous acid (hypohalite) that further are involved in the halogenation of organic substrates; Eq. (18.2a and 18.2b). Vanadate-dependent haloperoxidases (VHPOs) rely on hydrogenvanadate  $H_2VO_4^-$  bound into the catalytically active centre of the enzyme via a histidine- $N^e$ , plus hydrogen bonding interaction with additional N- and O-functional amino acid residues (Fig. 18.1). These peroxidases have been isolated from marine macroalgae (brown algae in particular, e.g. *Ascophyllum nodosum*; Fig. 18.1) (Vilter 1983, 1984; Wever et al. 2018), saprobes (such as the fungus *Curvularia inaequalis*) (Messerschmidt and Wever 1996), and from the terrestrial lichen *Xanthoria*



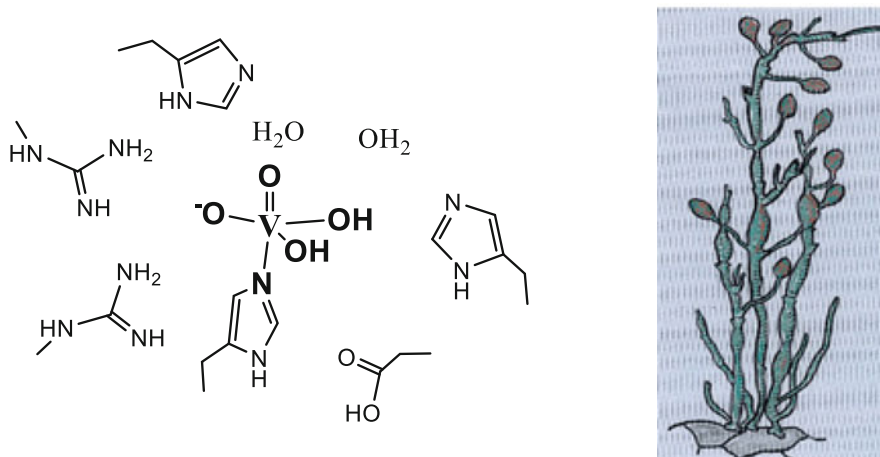


**Fig. 18.1** The active centre  $\text{H}_2\text{VO}_4(\text{His})^-$  (in bold) of the vanadate-dependent haloperoxidase of *Ascophyllum nodosum* (shown on the right), including a selection of nearby amino acid residues. In its inactive state, vanadium is in a distorted square pyramidal environment (McLauchlan et al. 2018). The central part (in bold) is conserved in all VHPOs; the second sphere (in hydrogen-bonding contact with the inner sphere) is subject to variations and responsible for the substrate specificity ( $\text{I}^-$ ,  $\text{Br}^-$ ,  $\text{Cl}^-$ , pseudohalides)

*parietina* (Plat et al. 1987). Vanadate-dependent iodoperoxidases are also present in some species of cyanobacteria (Bernroither et al. 2009); see also further down. Haloperoxidases “oxidatively” protect the algae against *parasitic* bacteria. More generally, many bacterial strains are sensitive to oxidative annihilation by hypohalite generated vanadium chloroperoxidase. An example is an antimicrobial effect against *Enterococcus faecalis* biofilms (Persoon et al. 2011). However, vanadate-dependent peroxidases can also be present in specific bacteria. Examples thereof include a chloroperoxidase detected in marine *Streptomyces* bacteria (Bernhardt et al. 2011; McKinnie et al. 2018), in cyanobacterial blooms responsible for the formation of halogenated methane derivatives (Johnson et al. 2015), and in flavobacteria associated with marine macroalgae (Fournier et al. 2014). The flavobacterium *Zobiella galactanivorans* (a marine bacterium associated with macroalgae) contains monomeric iodoperoxidases; more generally, the monomeric type of VHPOs is overrepresented in bacterial lineages. VHPOs likely derive from a marine bacterial ancestor; they are closely related to bacterial acid phosphatase (Fournier et al. 2014).

The active centre of these haloperoxidases is illustrated in a generalized form in Fig. 18.1. Figure 18.1 also pictures the brown alga *Ascophyllum nodosum*, where the enzyme has originally been detected and characterized (Vilter 1983, 1984). The active centre of the peroxidase in Eq. (18.1a) is symbolized by  $\{\text{H}_2\text{VO}_4^-\}$ . The mechanism of the halide peroxidation catalyzed by VHPOs is emblemized in Fig. 18.2.

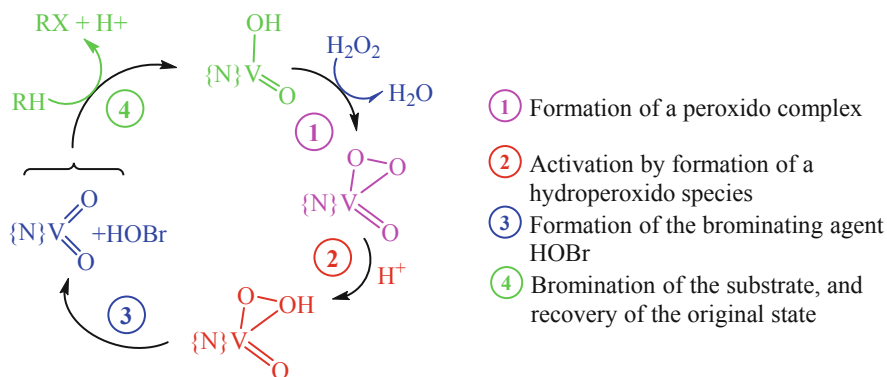
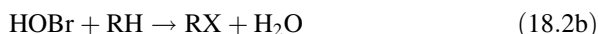
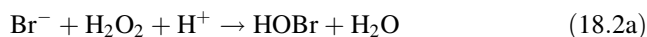
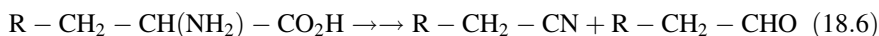
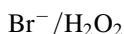
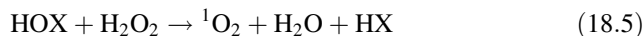
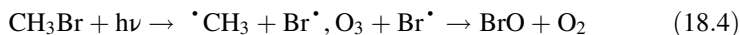
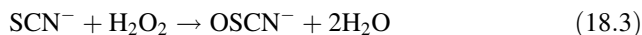


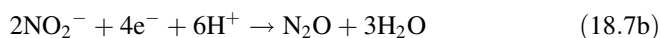
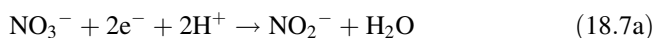
**Fig. 18.2** Mechanistic aspects of the bromination of an organic substrate (RH) by vanadium-based bromoperoxidase. The active centre is symbolized here by “ $\{N\}VO(OH)$ ” (top), where  $\{N\}$  stands for the directly ligated histidine (see Fig. 18.1) from the protein matrix



Along with halides, pseudohalides can also be subject to oxidative transformation by the haloperoxidases of marine phytoplankton. An example is the oxidation of thiocyanate to hypothiocyanite, Eq. (18.3). The formation of hypohalous acid in a marine environment does also have an impact on atmospheric chemistry: bromomethane, e.g., when released into the atmosphere, undergoes photolytic degradation to form bromine radicals, which can react with ozone and thus attribute to the atmospheric depletion of the ozone layer, Eq. (18.4) (Wever et al. 2018). Similarly, chloroform  $CHCl_3$  generated from organics by the enzymatically steered generation of  $HClO$  is split photolytically to form chlorine radicals. Additionally, initiated by the reaction of hypohalous acid and hydrogen peroxide, highly reactive singlet oxygen can be formed at higher pH, Eq. (18.5). The latter is likely the responsible oxidant in the peroxidase-catalyzed oxidative (by  $H_2O_2$ ) decarboxylation of amino acids such as phenylalanine, Eq. (18.6) (But et al. 2012).

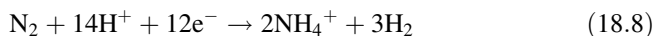


Haloperoxidase activity has also been detected for the (halo)alkaliphilic sulphur bacterium *Thioalkalivibrio nitratireducens*—living at extremely high pH and salinity (soda lakes). The main substrate for this chemolithoautotrophic bacterium, containing vanadium rather than molybdenum in its active centre, is the reduction of nitrate to nitrite (which can further be reduced to  $\text{N}_2\text{O}$ ), Eqs. (18.7a and 18.7b) (Antipov et al. 2003); electron donor is thiosulfate. Other substrates for the enzyme include chlorate, bromate, selenite and sulphite. The active centre of this periplasmic enzyme—a homotetramer of molecular mass 220 kDa—presumably contains three haeme-c groups and one vanadium. Other vanadate-reducing denitrifiers include *Pseudomonas isachenkovii* (Antipov et al. 1998). Additional substrates are, inter alia,  $\text{ClO}_3^-$ ,  $\text{BrO}_3^-$ ,  $\text{SeO}_4^{2-}$  and  $\text{SO}_3^{2-}$ .



### 18.3 Hydrogenation of Unsaturated Substrates by Vanadium-Dependent Nitrogenase

The nitrogen-fixing rhizobium bacterium *Azotobacter vinelandii* is responsible for the (proton- and ATP-supported) conversion of the comparably inactive (aerial) dinitrogen  $\text{N}_2$  to ammonium ions  $\text{NH}_4^+$ , and hence into a nitrogen source indispensable for a plethora of organisms for the synthesis of organic nitrogen compounds serving as building blocks for, e.g., amino acids and hence proteins. *A. vinelandii* is a soil bacterium, living symbiotically in the root nodules of members of the legume family (*Fabaceae*) such as clover, beans and sweet peas (e.g. *Lathyrus*, Fig. 18.3, right). The enzymes responsible for this ATP-driven conversion of  $\text{N}_2$  to  $\text{NH}_4^+$ , the nitrogenases, are comparatively complex iron-vanadium (or iron-molybdenum, or iron-only) proteins (Fig. 18.3, left); for the overall reaction see Eq. (18.8). The uptake of vanadate (and/or molybdate) is initiated by the siderophore azotobactin (Wichard et al. 2009).



Other unsaturated basic molecules, such as acetylene (Eq. 18.9),  $\text{CO}_2/\text{CO}$  (Eq. 18.10), and cyanide (Eq. 18.11) (Sippel and Einsle 2017; Sickerman et al. 2017) may equally be substrate for a reductive conversion based on vanadium-dependent nitrogenase. The reduction of  $\text{CO}$  by nitrogenases (Lee et al. 2018) is of particular interest in as far as  $\text{CO}$  and  $\text{N}_2$  are isoelectronic.

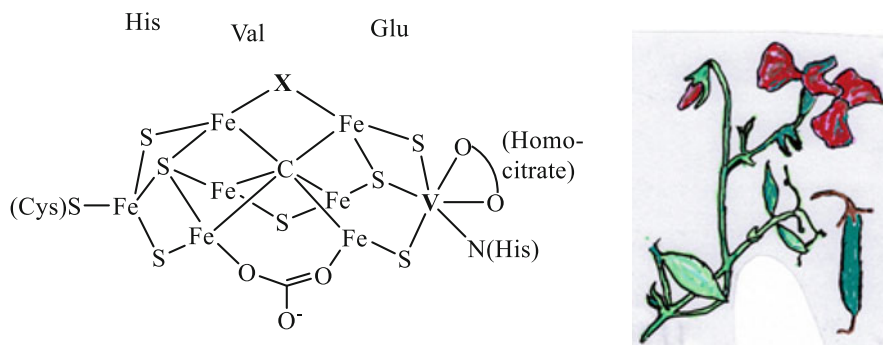
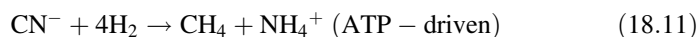
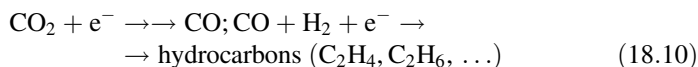
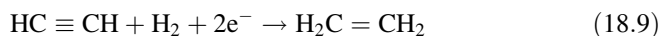
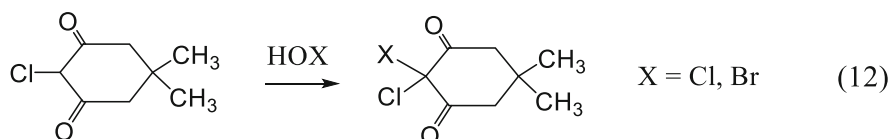


**Fig. 18.3** The iron-vanadium cofactor (M-cluster) of the vanadium nitrogenase from *A. vinelandii* (adapted from Benediktsson et al. 2018, modified). The bridging X can represent particularly labile  $S^{2-}$ , or OH, NH (Sippel et al. 2018), HCN,  $CN^-$ ,  $N_3^-$ , and CO (Eq. 18.10) (Rohde et al. 2020), and  $HC \equiv CH$  (Eq. 18.9), depending on the state of activation and on the substrate. The six irons surrounding the central carbon are arranged as a trigonal prism. The picture on the right represents the flour and fruit of *Lathyrus* (sweet pea), a member of the legume family



Along with *A. vinelandii*, associated with the legume family, the lichen-symbiotic cyanobacteria from the genus *Nostoc*, associated with lichen-forming fungal species of the genus *Peltigera*, contain (commonly along with a molybdenum and iron-only nitrogenase) a vanadate-dependent nitrogen fixing system that also catalyzes acetylene reduction (Hodkinson et al. 2014). Further, cyanobacteria (such as *Nostoc sp.*) associated with bryophytes (liverworts and hornworts) have been shown to employ—in addition to molybdenum nitrogenase—vanadium-nitrogenase (Nelson et al. 2019). As mentioned above, *Streptomyces* bacteria can also be involved—resorting to vanadate-dependent chloroperoxidase—in the biosynthesis of halogenated meroterpenoid products (McKinnie et al. 2018). An example is the chlorination/bromination of monochlorodimedone; Eq. (18.12).

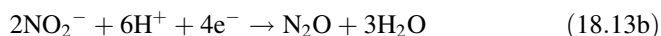
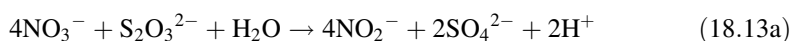


## 18.4 Accumulation and Redox Transformation of Vanadate(V) and Oxidovanadium(IV) by Bacteria and Protozoa

Several bacteria, archaea and fungi are able to reduce soluble vanadium (V) (hydrogenvanadate) to insoluble vanadium(IV) (commonly oxidovanadium hydroxide), eventually followed by geogenic conversion, i.e. formation of vanadium minerals. The reduction can be respiratory (the electron flow is coupled to the translocation of protons) or dissimilatory (anaerobic respiration; a proton-motive force is not involved). In tunicates, the reduction of vanadate is coupled to a symbiotic bacterium which previously was assigned the temporary name of *Pseudomonas isachenkovii* (Lyalkova and Yukova 1990; Lyalikova and Yukova 1992).

Intracellular and cell surface bioaccumulation of vanadium(V) and -(IV) (in concentrations up to 0.67 mM) by vanadium-resistant bacterial strains have been noted for the intestines of *Ascidia sydneiensis samea* (Romaidi 2016). The bacteria belong to the genera *Vibrio* and *Shewanella*. The maximum absorption (at pH 3) corresponds to an enrichment of twenty thousand times that of vanadate in seawater. A more recent study by Ueki et al. (2019) examined and compared the symbiotic bacteria (such as *Pseudomonas* and *Ralstonia*) associated with vanadium-rich ascidians (*Ascidia ahodori* and *A. sydneiensis samea*, with vanadium particularly accumulated in the branchial sacs) versus vanadium-poor ascidians (*Styela plicata*).

The chemolithoautotrophic bacterium *Thioalkalivibrio nitratireducens* has available a nitrate/nitrite reductase containing vanadium and haeme-c as cofactors (a homotetramer of the molecular mass 195 kDa; four identical subunits) (Antipov et al. 2003; Antipov 2013). Nitrate is reduced to nitrite and further to N<sub>2</sub>O (Eqs. 18.13a and 18.13b); electron donor is thiosulfate. *T. nitratireducens* is alkaliphilic and moderately halophilic, i.e. it exists at high pH and salinity (high soda levels). Substrates other than NO<sub>3</sub><sup>-</sup> include ClO<sub>3</sub><sup>-</sup>, BrO<sub>3</sub><sup>-</sup>, SeO<sub>4</sub><sup>2-</sup>, and SO<sub>3</sub><sup>2-</sup>. Interestingly, this enzyme does also have haloperoxidase activity (see above).

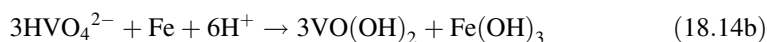


Microbial vanadate reduction (by *Methylomonas*) in particular in groundwater can also be coupled with anaerobic methane oxidation. The oxidation products are CO<sub>2</sub> along with fatty acids (Zhang et al. 2020); for a net reaction leading to fatty acids see Eq. (18.14a). Further reduction can result in the generation of methane. Nitrate essentially inhibits vanadate reduction, likely because (less toxic) nitrate is preferentially employed by the bacteria. Electron transfer to vanadate may occur directly, or via binding of vanadate to reductases of other electron acceptors, such as

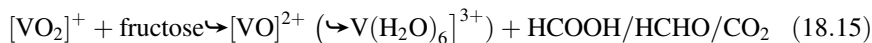
NADPH-dependent reductase. A similar situation applies to the competitive—vanadate vs. nitrate—behaviour in the bio-reduction of hydrogen (Jiang et al. 2018).



Vanadate(V)-reducing bacteria include the genera *Bacillus*, *Geobacter*, *Clostridium*, *Pseudomonas*, and the *Comamonadaceae* (a Gram-negative bacterial family commonly equipped with a flagella). Vanadate, at moderate to low concentrations, can effectively promote the growth of these bacteria (Wang et al. 2020). These bacterial strains dispose of a comparatively high vanadium resistance. An example is *Bacillus megaterium* (Rivas-Castillo et al. 2017). Since high concentrations of vanadate in the surface soil mainly of industrial areas are considered to exert ecological risks and, where appropriate, toxic effects [as noted previously, vanadate is an antagonist of phosphate], bacterial detoxification by reduction of  $\text{H}_2\text{VO}_4^-$  to  $\text{VO}^{2+}$ , and precipitation of the latter in the form of  $\text{VO}(\text{OH})_2$ , is ecologically (and consequently economically as well) important. Interestingly, elemental iron and sulphur can also reduce vanadate(V), in the presence of hydrogen carbonate and ammonium ions, to form insoluble vanadium(IV) hydroxide; see Eq. (18.14b) for the reduction by iron (Zhang et al. 2018). Bacteria responsible for these reductions belong to the strains *Geobacter* (for the reduction by iron) and *Spirochaeta* (for the reduction of sulphur).



The acidophilic obligatory heterotrophic bacterium *Acidocella aromatica* reduces vanadium(V) ( $\text{H}_2\text{VO}_4^-$ ), using fructose. Reduction takes place under microaerobic as well as anaerobic conditions, at vanadate concentrations up to 2 mM. Reduction is effective even under highly acidic (pH 2) conditions (Okibe et al. 2016) (where vanadium is present in the form of  $[\text{V}^{\text{V}}\text{O}_2(\text{H}_2\text{O})_4]^+$ ), and the potential oxidation products are formic acid, formaldehyde and  $\text{CO}_2$ , Eq. (18.15). The final (subtoxic) vanadium concentration is  $\sim 10 \mu\text{M}$ , hence a decrease of  $c(\text{V})$  by two orders of magnitude. The reduction product is blue  $\text{V}^{\text{IV}}\text{O}^{2+}\cdot\text{aq}$  (which, in part, can be further reduced to V(III)). With increasing pH, oxidovanadium hydroxide  $\text{VO}(\text{OH})_2$  precipitates, and temporarily becomes absorbed to the bacterial surface.



Bioreduction of vanadate(V) present in ground water, at about neutral pH and temperatures in the range between 15 and 40 °C, is also achieved by autohydrogenotrophic bacteria belonging to the  $\beta$ -proteobacteria such as *Rhodocyclus* (a denitrifying bacterium) and *Clostridium* (a fermenter); hydrogen gas  $\text{H}_2$  is used as the electron donor (Xu et al. 2015), Eq. (18.16).

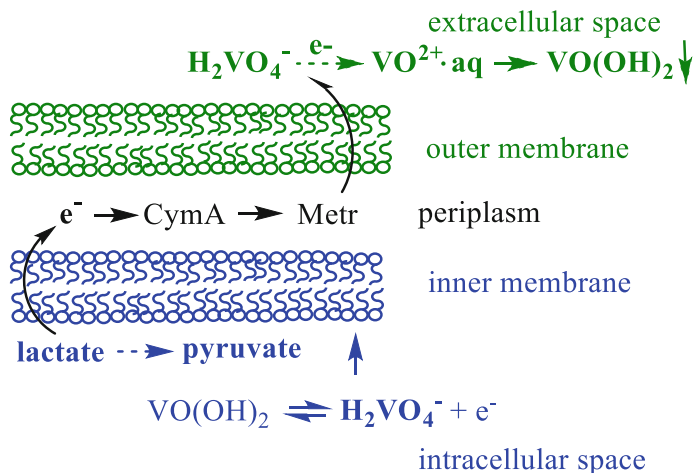
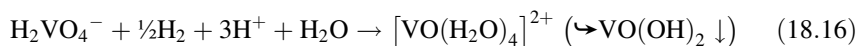


**Fig. 18.4** Electron transport from the intra-cellular to the extra-cellular space, exemplified for lactate as electron donor. CymA and Metr are heme-type iron proteins associated with the inner (CymA) and the outer (Metr) membrane. The main amount of vanadate is refined to the *extracellular* space



The potentiality of metal ion reduction (and vanadate in particular) by microbes such as *Geobacter metallireducens*, *Shewanella oneidensis*, *Pseudomonas*, *Lactococcus* and *Enterobacter* in (ground) water reservoirs (Ortiz-Bernard et al. 2004; Carpentier et al. 2005) has also been applied in microbial fuel cells to generate “bio-electricity”, and concomitantly detoxify groundwater (Hao et al. 2015). Organic substrates such as glucose and acetate effectively enhance microbial growth, *Lactococcus* (a lactic acid bacterium) being particularly effective in vanadate reduction.

The vanadium(V) reductase activity of bacteria takes place in the bacterial membrane, and is indirectly coupled to the oxidation of  $\text{H}_2$  or organics such as sugars and organic acids (e.g. lactate; Eq. 18.17a), and thus links carbon metabolism to the reduction of vanadate (and commonly other inorganics such as  $\text{Fe}^{3+}$  and  $\text{Mn}^{4+}$  as well) (Dundas et al. 2018, 2020). The  $\text{Fe}^{3+}/\text{Fe}^{2+}$  centres in the cytochrome-c type proteins CymA and MetrABC are involved in the transmembrane electron pathway, Eq. (18.17b): As illustrated in Fig. 18.4, electrons are delivered via the inner membrane by, e.g., lactate, to CymA( $\text{Fe}^{3+}$ ) to form CymA( $\text{Fe}^{2+}$ ). Further electron transport across the periplasm and the outer membrane involves MetrABC( $\text{Fe}^{3+}/\text{Fe}^{2+}$ ). The cytochromes have been symbolized, in Eq. (18.17b), by  $\{\text{Fe}^{3+}\}$  and  $\{\text{Fe}^{2+}\}$ . The reduction equivalents are finally taken up by extracellular hydrogenvanadate. Figure 18.4 provides an overview for this electron transfer pathway.

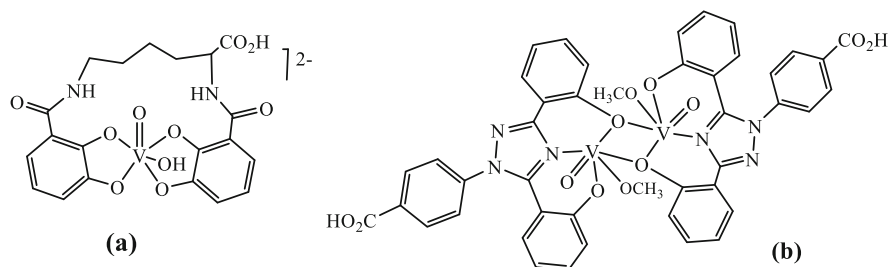
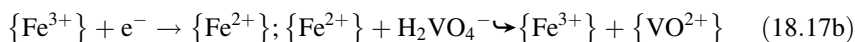
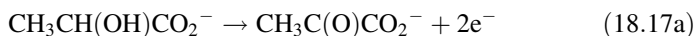


**Fig. 18.5** (a) Probable structure of the complex formed between oxidovanadium(V) and azotocheline. (b) A dinuclear antiamoebic vanadium complex with the ligand deferasirox (a medication commonly used to counteract iron overload in the blood)



Relating to vanadium-dependent nitrogenase (vide supra), the biosynthesis of the bis(catecholate) azotocheline by the soil bacterium *Azotobacter vinelandii* is of interest: azotocheline forms a strong coordination compound with  $\text{VO}^{3+}$  (Fig. 18.5a), a complex which supposedly acts as a vanadophore in supplying *A. vinelandii* with vanadium (Bellenger et al. 2007). Along with the bacterial reduction of vanadate(V) to oxidovanadium(IV) and thus insoluble  $\text{VO}(\text{OH})_2$ , further reduction of  $\text{VO}(\text{OH})_2$  to soluble  $[\text{V}^{\text{III}}(\text{OH})_{2/1}(\text{H}_2\text{O})_{4/5}]^{3+}$  has been noted to be performed, in hydrothermal environments, by several bacterial strains, such as *Pseudomonas aeruginosa* (Baysse et al. 2000).

Not surprisingly, bacteria can also be involved in the transformation of inorganic vanadium compounds. An example is the reductive conversion (and thus “detoxification”), by *Geobacter sulfurreducens*, of  $\text{V}^{\text{V}}$ -bearing ferrihydrites/magnetites. In this reaction, nano-particulate vanadium ferrite spinel  $(\text{Fe}, \text{V})_3\text{O}_4$  is produced (Coker et al. 2020; Liang et al. 2010), with a  $\text{V}^{\text{IV}}/\text{V}^{\text{III}}$  ratio around 0.3, and the iron (partially) reduced to  $\text{Fe}^{\text{II}}$ . These vanadium-substituted magnetites, with V predominantly at  $\text{Fe}^{\text{III}} \text{O}_h$  sites, are likely to have a potential as catalysts in electron transfer processes, e.g. in organic reactions. More generally, bacterial reduction of vanadium (V) to vanadium (IV) is an important issue as a response to vanadium pollution in the wake of mining and processing vanadium ores such as navajosite  $\text{Fe}^{\text{III}}\text{V}^{\text{V}}_9\text{O}_{24} \cdot 12\text{H}_2\text{O}$  (Wang et al. 2020).



## 18.5 Antimicrobial Effects of Vanadium Coordination Compounds

In conjunction with the bacterial *use* of vanadium (commonly, as noted above, in the form of vanadate(V) or oxidovanadium(IV)), *antibacterial* activity and interaction with unicellular organisms (protozoans) such as amoebae is of interest. A well-studied example is the antiamoebic activity (against *Entamoeba histolytica*) of specific vanadium coordination compounds such as the bis(oxidovanadium(V)) complex formed with deferasirox (4-[3,5-bis(2-hydroxylphenyl)-1,2,4-triazol-1-yl] benzoic acid; Fig. 18.6) (Maurya et al. 2016). That compound is more potent than the amoebicidal standard drug metronidazole.

Selected examples of vanadium coordination compounds that have turned out to be auspicious in antimicrobial (and antiviral) applications are depicted in Fig. 18.6.  $V^{IV}O(pic)(8HQ)$  (pic = picolinate, 8HQ = 8-hydroxyquinoline; **1** in Fig. 18.6) has been shown to counteract *Mycobacterium tuberculosis* (Correia et al. 2014), while the oxidovanadium(IV) complex VO(cefuroxime) (**2** in Fig. 18.6) exhibits antimicrobial activity against, e.g., pneumonia of bacterial origin, such as caused by *Klebsiella pneumoniae* (Datta et al. 2015). A likely mechanism of action of compound **1** is a release of the ligand at physiological conditions, causing binding (and thus depletion) of intracellular iron. The mechanism of action of compound **2** possibly roots in the hydrophobic interaction (docking through hydrophobic forces) between the vanadium complex and the protein receptor clathrin.

Along with mononuclear vanadium complexes, decavanadates such as depicted in Fig. 18.7, can have antimicrobial activity. The decavanadate **3** (with nicotinamide as the counter-ion) exerts growth inhibitory activity against *Escherichia coli* (Missina et al. 2018), the platinum and molybdenum substituted decavanadates **4** and **5** inhibit the growth of *Mycobacterium smegmatis* (Kostenkova et al. 2021) a generally non-pathogenic bacterium located in the genital areas.

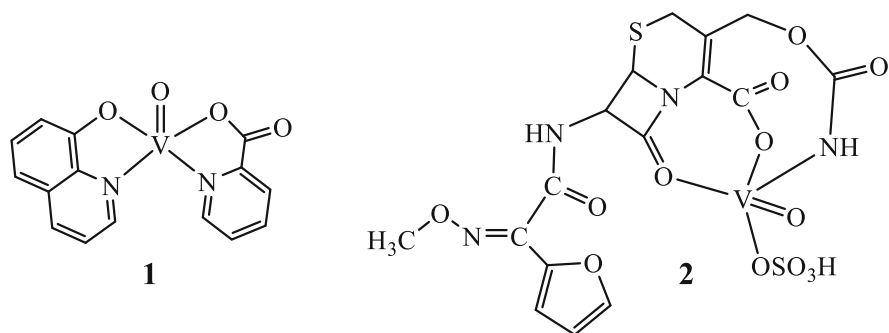


**Fig. 18.6** Examples of antimicrobial vanadium complexes: Compound **1** is effective against tuberculosis, compound **2** against bacterial pneumonia

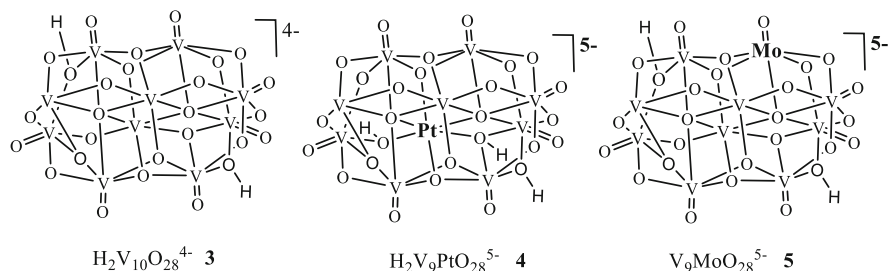


**Fig. 18.7** Decavanadate (left) (Missina et al. 2018) and substituted decavanadates (centre and right) (Kostenkova et al. 2021) that have been shown to exert antimicrobial activity. The counterions of compound **3** are nicotinamide and isonicotinamide

Similarly, octadecavanadates (IV/V) of composition such as  $[\text{V}^{\text{IV}}_{12}\text{V}^{\text{V}}_5\text{O}_{42}]^{7-}$  have been shown to exert chemo-protective activity, in *E. coli* cultures, towards alkylation by diethyl sulfate (Postal et al. 2021).

## References

- Antipov AN (2013) Vanadium in life organisms. In: Kestinger RH, Uversky VN, Permyakov EA (eds) Encyclopedia of metalloproteins. Springer, New York
- Antipov AN, Lyalikova NN, Khijniak TV, L'Vov NP (1998) Characterization of molybdenum-free nitrate reductase from Haloalkalophilic bacterium *Halomonas* sp. strain AGJ 1-3. FEBS Lett 441:257–260. <https://doi.org/10.1007/s10541-005-0186-0>
- Antipov AN, Sorokin DY, L'Vov NP, Kuenen JG (2003) New enzyme belonging to the family of molybdenum-free nitrate reductases. Biochem J 369:185–189. <https://doi.org/10.1042/BJ20021193>
- Baysse C, De Vos D, Naudet Y, Vandermonde A, Ochsner U, Meyer JM, Budzikiewicz H, Fuchs R, Cornelis P (2000) Vanadium interferes with siderophore-mediated iron uptake in *Pseudomonas aeruginosa*. Microbiology 146:2425–2434. [https://doi.org/10.1007/978-3-540-71160-5\\_9](https://doi.org/10.1007/978-3-540-71160-5_9)
- Bellenger J-P, Arnaud-Neu F, Asfari Z, Myneni SCB, Stiefel EI, Kraepiel AML (2007) Complexation of oxoanions and cationic metals by the biscatecholate siderophore azotochelin. J Biol Inorg Chem 12:367–376. <https://doi.org/10.1007/s00775-006-0194-6>
- Benediktsson B, Thorhallsson AT, Bjornsson R (2018) QM/MM calculations reveal a bridging hydroxo group in a vanadium nitrogenase crystal structure. Chem Commun 53:7265–7280. <https://doi.org/10.1039/C8CC03793K>
- Bernhardt P, Okino T, Winter JM, Miyanaga A, Moore BS (2011) A stereoselective vanadium-dependent chloroperoxidase in bacterial antibiotic biosynthesis. J Am Chem Soc 133:4268–4270. <https://doi.org/10.1021/ja201088k>
- Benroitner M, Zamocky M, Furtmüller PG, Peschek GA, Obinger C (2009) Purification and characterization of a hydroperoxidase from the cyanobacterium *Synechocystis* PCC 6803: identification of its gene by peptide mass mapping using matrix assisted laser desorption ionization time-of-flight mass spectrometry. J Exp Bot 60:423–440. <https://doi.org/10.1111/j.1574-6968.1999.tb13348.x>

- But A, Le Nôtre J, Scott EL, Wever R, JPM S (2012) Selective oxidative decarboxylation of amino acids to produce industrially relevant nitriles by vanadium chloroperoxidase. *ChemSusChem* 5: 1199–1202. <https://doi.org/10.1002/cssc.201200098>
- Carpentier W, Smet DL, Van Beeumen J, Brigé A (2005) Respiration and growth of *Shewanella oneidensis* MR-1 using vanadate as the sole electron acceptor. *J Bacteriol* 187:3293–3301. <https://doi.org/10.1128/JB.187.10.3293-3301>
- Coker VS, van der Laan G, Telling ND, Lloyd RL, Byrne JM, Arenholz E, Patrick RAD (2020) Bacterial production of vanadium ferrite spinel (Fe,V)<sub>3</sub>O<sub>4</sub> nanoparticles. *Mineralogical Magazine* 84:1–38. <https://doi.org/10.1180/mgm.2020.55>
- Correia I, Adão P, Roy S, Wahba M, Matos C, Maurya MR, Marques F, Pavan FR, Leite CQF, Aveçilla F, Costa Pessoa J (2014) Hydroxyquinoline derived vanadium(IV and V) and copper (II) complexes as potential anti-tuberculosis and ant-tumor agents. *J Inorg Biochem* 141:83–93. <https://doi.org/10.1016/j.jinorgbio.2014.07.019>
- Datta C, Das D, Mondal P, Chakraborty B, Sengupta M, Bhattacharjee CR (2015) Novel water soluble neutral vanadium(IV) antibiotic complex: Antioxidant, immunomodulatory and molecular docking studies. *Eur J Med Chem* 97:214–224. <https://doi.org/10.1016/j.ejmech.2015.05.005>
- Dundas CM, Graham AJ, Romanovicz DK, Keitz BJ (2018) Extracellular electron transfer by *Shewanella oneidensis* controls palladium nanoparticle phenotype. *Synth Biol* 7(12): 2726–2736. <https://doi.org/10.1021/acssynbio.8b00218>
- Dundas CM, Walker DJF, Keitz BK (2020) Tuning extracellular electron transfer by *Shewanella oneidensis* using transcriptional logic gates. *ACS Synth Biol* 9:2301–2315. <https://doi.org/10.1021/acssynbio.9b00517>
- Fournier J-B, Rebuffet E, Delage L, Grijol R, Meslet-Cladière L, Rzonca J, Potin P, Michel M, Czjzek M, Leblanc C (2014) The vanadium Iodoperoxidase from the marine *Flavobacteriaceae* species *Zobellia galactanivorans* reveals novel molecular and evolutionary features of halide specificity in the vanadium Haloperoxidase enzyme family. *Appl Environ Microbiol* 80:7561–7573. <https://doi.org/10.1128/AEM.02430-14>
- Hao L, Zhang B, Tian C, Liu Y, Shi C, Cheng M, Feng C (2015) Enhanced microbial reduction of vanadium (V) in groundwater with bioelectricity from microbial fuel cells. *J Power Sources* 287: 43–49. <https://doi.org/10.1016/j.jpowsour.2015.04.045>
- Hodkinson BP, Allen JL, Forrest LL, Goffinet B, Sérusiaux E, Andrésson OS, Mia V, Bellenger JP, Lutzoni F (2014) Lichen-symbiotic cyanobacteria associated with *Peltigera* have an alternative vanadium-dependent nitrogen fixation system. *Eur J Phycol* 49:11–19. <https://doi.org/10.1080/09670262.2013.873143>
- Jiang YF, Zhang BG, He C, Shi JX, Borthwick AGL, Huang XY (2018) Synchronous microbial vanadium (V) reduction and denitrification in groundwater using hydrogen as the sole electron donor. *Water Res* 141:289–296. <https://doi.org/10.1016/j.watres.2018.05.033>
- Johnson TL, Brahmsha B, Palenik B, Mühle J (2015) Halomethane production by vanadium-dependent bromoperoxidase in marine *Synechococcus*. *Limnol Oceanogr* 60:1823–1835. <https://doi.org/10.1002/lno.10135>
- Kostenkova K, Arhouma Z, Postal K, Rajan A, Kortz U, Nunes GG, Crick DC (2021) Pt<sup>IV</sup>- or Mo<sup>VI</sup>-substituted decavanadates inhibit the growth of *Mycobacterium smegmatis*. *J Inorg Biochem* 217:111356. <https://doi.org/10.1016/j.jinorgbio.2021.111356>
- Lee CC, Wilcoxon J, Hille CJ, Britt RD, Hu Y (2018) Evaluation of the catalytic relevance of the CO-bound states of V-nitrogenase. *Angew Chem Int Ed* 57:3411–3414. <https://doi.org/10.1002/anie.201800189>
- Liang XL, Zhu SY, Zhong YH, Zhu JX, Yuan P, He HP, Zhang J (2010) The remarkable effect of vanadium doping on the adsorption and catalytic activity of magnetite in the decolorization of methylene blue. *Appl Catal B Environ* 97:151–159. <https://doi.org/10.1016/j.apcatb.2010.03.035>
- Lyalkova NN, Yukova NA (1990) Role of microorganisms in vanadium concentration and dispersion. *Microbiologiya* 59:968–975. <https://doi.org/10.1080/01490459209377901>

- Lyalikova NN, Yukova NA (1992) *Geomicrobiology* 19:15–26
- Maurya MR, Sarkar B, Avecilla F, Tariq S, Azam A, Correia I (2016) Synthesis, characterization, reactivity, catalytic activity, and antiamebic activity of vanadium(V) complexes of ICL670 (Deferasirox) and a related ligand. *Eur J Inorg Chem* 2016:1430–1441. <https://doi.org/10.1002/ejic.201501336>
- McKinnie SMK, Miles ZD, Moore BS (2018) Characterization and biochemical assays of streptomycetes vanadium-dependent chloroperoxidases. *Methods Enzymol* 604:405–424. <https://doi.org/10.1016/bs.mie.2018.02.016>
- McLauchlan CC, Murakami HA, Wallace CA, Crans DC (2018) Coordination environment changes of the vanadium in vanadium-dependent haloperoxidase enzymes. *J Inorg Biochem* 186:267–279. <https://doi.org/10.1016/j.jinorgbio.2018.06.011>
- Messerschmidt A, Wever R (1996) X-ray structure of a vanadium-containing enzyme: chloroperoxidase from the fungus *Curvularia inaequalis*. *Proc Natl Acad Sci U S A* 93:392–396. <https://doi.org/10.1073/pnas.93.1.392>
- Missina JM, Gavinho B, Postal K, Santana FS, Valdameri G, de Souza EM, Hughes DL, Ramirez MI, Soares JF, Nunes GG (2018) Effects of decavanadate salts with organic and inorganic cations on *Escherichia coli*, *Giardia intestinalis*, and Vero cells. *Inorg Chem* 57:1193–1194. <https://doi.org/10.1021/acs.inorgchem.8b01298>
- Nelson JM, Hauser DA, Gudiño JA, Guadalupe YA, Meeks JC, Allen NS, Villarreal JC, Li FW (2019) Complete genomes of symbiotic cyanobacteria clarify the evolution of vanadium-nitrogenase. *Genome Biol Evol* 11:1959–1964. <https://doi.org/10.1093/gbe/evz137>
- Okibe N, Maki M, Nakayama D, Sasaki K (2016) Microbial recovery of vanadium by the acidophilic bacterium, *Acidocella aromatic*. *Biotechnol Lett* 38:1475–1481. <https://doi.org/10.1007/s10529-016-2131-2>
- Ortiz-Bernard L, Anderson RT, Vrionis HA, Lovely DR (2004) Vanadium respiration by *Geobacter metallireducens*: novel strategy for in situ removal of vanadium from groundwater. *Appl Environ Microbiol* 70:3091–3095. <https://doi.org/10.1128/AEM.70.5.3091-3095.2004>
- Persoon IF, Hoogenkamp MA, Bury A, Wesselink PR, Hartog AF, Wever R, Crielaard W (2011) Effect of vanadium chloroperoxidase on enterococcus faecalis biofilms. *J Endod* 38:72–74. <https://doi.org/10.1016/j.joen.2011.09.003>
- Plat H, Krenn BE, Wever R (1987) The bromoperoxidase from the lichen *Xanthoria parietina* is a novel vanadium enzyme. *Biochem J* 248:277–279. <https://doi.org/10.1042/bj2480277>
- Postal K, Santana FS, Hughes DL, Rüdiger AL, Ribeiro RR, Sá EL, de Souza EM, Soares JF, Nunes GG (2021) Stability in solution and chemoprotection by octadecavanadates (IV/V) in *E. coli* cultures. *J Inorg Biochem* 219:111438. <https://doi.org/10.1016/j.jinorgbio.2021.111438>
- Rivas-Castillo A, Orona-Tamayo D, Gomez-Remirez M, Rojas-Avelizapada NG (2017) Diverse molecular resistance mechanisms of *Bacillus megaterium* during metal removal present in a spent catalyst. *Biotechnol Bioprocess Eng* 22:296–307. <https://doi.org/10.1007/s12257-016-0019-6>
- Rohde M, Grunau K, Einsle O (2020) CO binding to the FeV cofactor of CO-reducing vanadium nitrogenase at atomic resolution. *Angew Chem Int Ed* 59:23626–23630. <https://doi.org/10.1002/anie.202010790>
- Romaidi UT (2016) Bioaccumulation of vanadium by vanadium-resistant bacteria isolated from the intestine of ascidia sydneyensis samea. *Mar Biotechnol* 18:359–371. <https://doi.org/10.1007/s10126-016-9697-5>
- Sickerman NS, Hu Y, Ribbe MW (2017) Activation of CO<sub>2</sub> by vanadium nitrogenase. *Chem Asian J* 12:1985–1996. <https://doi.org/10.1002/asia.201700624>
- Sippel D, Einsle O (2017) The structure of vanadium nitrogenase reveals an unusual bridging ligand. *Nat Chem Biol* 13:956–951. <https://doi.org/10.1038/nchembio.2428>
- Sippel D, Rohde M, Netzer J, Trneik C, Gies J, Grunau K, Djurdjevic I, DeCamps L, Andrade SLA, Einsle O (2018) A bound reaction intermediate sheds light on the mechanism of nitrogenase. *Science* 359:1484–1489. <https://doi.org/10.1126/science.aar2765>

- Ueki T, Fujie M, Romaidi SN (2019) Symbiotic bacteria associated with ascidian vanadium accumulation identified by 16S rRNA amplicon sequencing. *Mar Genomics* 43:33–42. <https://doi.org/10.1016/j.margen.2018.10.006>
- Vilter H (1983) Peroxidases from Phaeophyceae III: catalysis of halogenation by peroxidases from *Ascophyllum nodosum* (L.). *Bot Mar* 26:429–435. <https://doi.org/10.1515/botm.1983.26.9.429>
- Vilter H (1984) Peroxidases from phaeophyceae: A vanadium(V)-dependent peroxidase from *Ascophyllum nodosum*. *Phytochemistry* 23:1387–1390. [https://doi.org/10.1016/S0031-9422\(00\)80471-9](https://doi.org/10.1016/S0031-9422(00)80471-9)
- Wang S, Zhang B, Li T, Li Z, Fu J (2020) Soil vanadium (V)-reducing related bacteria drive community response to vanadium pollution from a smelting plant over multiple gradients. *Environ Int* 138:105630. <https://doi.org/10.1016/j.envint.2020.105630>
- Wever R, Krenn BE, Renirie R (2018) Marine vanadium-dependent Haloperoxidases, their isolation, characterization, and application. *Methods Enzymol* 605:141–201. <https://doi.org/10.1016/bs.mie.2018.02.026>
- Wichard T, Bellenger J-B, Morel FFM, Kraepiel AML (2009) Role of the siderophore azotobactin in the bacterial acquisition of nitrogenase metal cofactors. *Environ Sci Technol* 43:7218–7224. <https://doi.org/10.1021/es8037214>
- Xu X, Xia S, Zhou L, Zhang Z, Rittmann B (2015) Bioreduction of vanadium (V) in groundwater by autohydrogenotrophic bacteria: mechanisms and microorganisms. *J Environ Sci* 30:122–128. <https://doi.org/10.1016/j.jes.2014.10.011>
- Zhang B, Qiu R, Lu L, Chen X, He C, Lu J, Ren ZJ (2018) Autotrophic vanadium (V) bioreduction in groundwater by elemental Sulfur and zerovalent iron. *Environ Sci Technol* 52:7434–7442. <https://doi.org/10.1021/acs.est.8b01317>
- Zhang B, Jiang Y, Zuo K, He C, Dai Y (2020) Disassembly of lignocellulose into cellulose, hemicellulose, and lignin for preparation of porous carbon materials with enhanced performances. *J Hazardous Mat* 392:121228. <https://doi.org/10.1016/j.jhazmat.2020.124956>

# Chapter 19

## How is a Zinc Ion Correctly Allocated to a Zinc-dependent Protein?



Dietrich H. Nies

**Abstract** This book chapter tries to visualize how a bacterial cell manages to bring zinc and no other transition metal cation to a zinc-dependent protein. Based upon the chemical constraints described in an introductory part of this book (“Chemical constraints for transition metal cation allocation” by author Dietrich H. Nies), a zinc allocation hypothesis was derived and tested on a theoretical level. The number of Lewis acids and bases were determined in the bacterium *Cupriavidus metallidurans* to define the stage. Molecular crowding and the Debye–Hückel equation describes how close the interacting Lewis bases and acids approach each other under cellular conditions. As one path for metal allocation, pre-discriminated cations may move along in the crowded areas from binding site to binding site, until “node” sites are reached that allow metal storage and discrimination by the formation of complex compounds. An inventory of motifs for such sites in *C. metallidurans* was derived. These may contribute to the movement of pre-discriminated ions or may be binding sites for already discriminated metals. As can be expected such motifs were found in proteins that are part of the three pillars of multiple metal homeostasis. First is the transportome, which adjusts the concentrations of metal cations and the composition of the mélange. Second is the repository, especially the zinc repository in the ribosome and RNA polymerase, which interacts with the transportome and buffers the cellular metal content. Third is a preference setting with iron first and sigma factors of the ECF (extracytoplasmic functions) family of sigma factors. This process is not completely understood at present.

### 19.1 A Hypothesis for Cellular Zinc Allocation

How is a zinc ion correctly allocated to its zinc-binding enzyme? The chemical constraints for this process have been outlined in an introductory part of this book (“Chemical constraints for transition metal cation allocation” by author Dietrich

---

D. H. Nies (✉)

Martin-Luther-University Halle-Wittenberg, Molecular Microbiology, Halle (Saale), Germany  
e-mail: [d.nies@mikrobiologie.uni-halle.de](mailto:d.nies@mikrobiologie.uni-halle.de)

H. Nies). Discrimination between metal cations is needed for the successful formation of complex compounds. In case of zinc with its completely filled d-orbital, only tetrahedral complexes are stable; however, these complexes can also accept other metal cations. Fe(II), Ni(II), and Co(II) are able to bind more ligands than Zn(II). Formation of such complexes can be used to spirit iron, nickel, and cobalt away from any zinc allocation pathway. Discrimination processes may also use the different redox potential of metal cations. A change of the oxidation state under physiological conditions is not possible for Zn(II) but can occur for Fe(III)/Fe(II), Cu(II)/Cu(I), Mn(IV)/Mn(II), and within complex compounds Co(III)/Co(II). Finally, Cu(I) and some characteristically toxic metal cations such as Cd(II) are soft Lewis acids with a high tendency to accept thiol compounds such as Cys as a ligand. Mn(II) is a hard Lewis acid with a high affinity for ligands such as Asp and Glu. Zn(II) is a borderline Lewis acid and its high affinity for His as a ligand is between those affinities of Asp, Glu, and Cys.

Work with the bacterium *Cupriavidus metallidurans* and many other organisms identified at least two different zinc pools in cells. One pool is composed of zinc ions firmly bound to proteins without access to the outside, while zinc ions residing in another pool are “loosely bound” and still have contact to solvent outside of a zinc-binding protein (see “Chemical constraints for transition metal cation allocation” by author Dietrich H. Nies). In *C. metallidurans*, some metal efflux systems may acquire their substrate for export from both pools, others are only able to reach Zn(II) located in one pool and not another one (Scherer and Nies 2009). A zinc-specific uptake system named ZupT in *C. metallidurans* is essential for an efficient allocation of zinc to beta-prime subunit RpoC of the RNA polymerase (Herzberg et al. 2014a). In the absence of this importer, other metal uptake systems can also provide zinc to the cytoplasm in similar numbers of zinc atoms per cell as would this importer. Growth is not retarded, and transcription not impaired in the absence of functional RpoC. However, misfolded RpoC unusually accumulates in inclusion bodies, indicating a lower efficiency of zinc allocation in the absence of this specific zinc import system. Since there is evidence for two cellular zinc pools, Ockham’s razor prohibits the assumption of a third zinc pool. The two theoretical zinc pools have been known in literature (Krezel and Maret 2016; Colvin et al. 2010) as “loosely bound” or “mobile” and “tightly bound” zinc, so that the zinc importer in *C. metallidurans* should feed zinc directly into the “tightly bound” zinc pool. One group of metal efflux systems in *C. metallidurans* acquires their substrate from both pools, and the other group only from the “loosely bound” zinc pool.

When the evidence for two zinc pools and their associated chemical constraints are combined, the “tightly bound” zinc pool should be composed of zinc complexes with a higher number of His and Cys ligands than Asp and Glu ligands. In a perfect arrangement of the ligand field, zinc-binding sites stabilize the remainder of a proteins conformation and at the same time those binding sites are stabilized by the remainder of the protein conformation, and the binding may occur in sites occluded from the surface of the protein. The “loosely bound” zinc pool should be composed of metal complexes with a low number of ligands, more Asp and Glu than His and Cys, with those binding sites tending to occur at the surface of proteins and

eventually in metal-promiscuous (those which bind less selectively with metals) enzymes. Zinc discrimination is the process that connects both pools. Since in reality a huge number of zinc-binding sites with a broad range of binding energies may exist, a better expression for “loosely bound” or “mobile” zinc would be “pre-discriminated” zinc, and “already discriminated” zinc instead of “tightly bound” zinc. Pre-discriminated zinc ions could be released again from their zinc-binding site due to a rather low binding energy and should be allowed to roam freely in the cell. The energetic valley of complexed, already discriminated zinc prevents a rapid release of the ion. Movement of discriminated zinc should no longer be the migration of the zinc ion but transfer of the zinc ion from one zinc-binding site to another one. Pre-discriminated zinc should move as ion, discriminated zinc with proteins. Movement of zinc by direct protein–protein contact may also need additional energy to split the interacting proteins.

The results obtained by studying the zinc importer protein in *C. metallidurans* cytoplasmic membrane indicate the presence of at least two modes of zinc discrimination within the cell. In one of these two modes, zinc brought into the cell by the importer ZupT should be already discriminated. Proteins are subsequently needed to transport the discriminated zinc from this importer in the cytoplasmic membrane to ribosomes that will be translating RpoC. In the second mode, zinc imported by other uptake systems should be pre-discriminated. It should move as a metal ion from binding site to binding site along a thermodynamic gradient until nodes are reached that bind the zinc ion more tightly and retard further movement of the zinc ion. Together, these node sites may mediate a stepwise discrimination process. Zinc ion starts as pre-discriminated and ends as discriminated zinc along this road. Discriminators may interfere and discriminate ions more efficiently and such discriminators may exist for Cu(I), Fe(II), Co(II), Ni(II), and Zn(II). Some of these discriminators may also be track switches, starting points for allocation paths of two or more different and already discriminated metal ions.

The outlined hypothesis predicts a pool of pre-discriminated, freely roaming metal cations inside the cell, interfering with a small number of Lewis bases per binding site, and pools of already discriminated metal cations moving within proteins. This book chapter collects evidence to investigate the bearing capacity of this hypothesis. Which cytoplasmic components are the containers of and interaction partners for discriminated and pre-discriminated metal cations? Which proteins may serve as discriminator and which proteins as carriers of discriminated zinc and other metal cations? If the hypothesis is not falsified at this stage and can indeed be envisioned, the next step would be an experimental verification, which, unfortunately, cannot be part of this book chapter.



## 19.2 *Cupriavidus metallidurans*: What is in the Cell?

### 19.2.1 Cellular Content of Lewis Acids and Bases

*C. metallidurans* strain CH34 is a Gram-negative beta-proteobacterium that lives in mesophilic metal-rich environments (Nies 2016; Mergeay et al. 1985; Janssen et al. 2010). Examples are auriferous soils in Australia or zinc deserts (Diels and Mergeay 1990; Reith et al. 2007; Reith et al. 2006). It is able to conserve energy as heterotrophic degrader of organic acids and facultatively also as a chemolithotrophic hydrogen-oxidizing bacterium (Mergeay et al. 1985; Herzberg et al. 2015). The proteins required for hydrogen oxidation and fixation of CO<sub>2</sub> are located on genomic islands, which were obtained by horizontal gene transfer (Van Houdt et al. 2009; Van Houdt et al. 2018; Van Houdt et al. 2012). The bacterium is also able to grow mixotrophically on organic acids, molecular hydrogen, and CO<sub>2</sub> (Mergeay et al. 1985). Since weathering minerals often produce molecular hydrogen and release transition metal cations during this process (Brazelton et al. 2013; Schulte et al. 2006; Sleep et al. 2004), *C. metallidurans* may have specifically evolved to harvest molecular hydrogen during mixotrophic growth on organic acids. The prize for such an attractive ecological niche would be to handle high concentrations of transition metals.

*C. metallidurans* obtained genes for chemolithoautotrophic growth, degradation of some organic substrates, and a broad variety of metal-handling transport, periplasmic or cytoplasmic proteins by horizontal gene transfer (Nies 2016). The respective genes are located on its chromosome, a chromid, and two large plasmids that are jammed with metal resistance determinants (Janssen et al. 2010). For many of these metal-handling proteins, *C. metallidurans* has two, three, or even four paralogs while other bacteria may have just one member of a given protein family (Nies et al. 2006). *C. metallidurans* has it all and understanding the accomplishment of metal homeostasis by other bacteria can be derived from that of *C. metallidurans* by simplification.

A large amount of genomic, proteomic, transcriptomic, mutant, physiological, and biochemical data has been published during the last 40 years that describe metal homeostasis and other processes in *C. metallidurans* (Nies 2016; Janssen et al. 2010; Mergeay et al. 2003; Mergeay 2000). These data can be connected to derive a hypothesis, a metal allocation model, as outlined above. To set the stage for a model of the subsequent metal allocation events, the sum of the negative and positive charges provided by all Lewis bases and acids, respectively, per *C. metallidurans* cell were calculated (Table 19.1).

The number of charged amino acid residues was derived from a measured protein content of 1.88 M copies per cell (Herzberg et al. 2014b), the average length, and amino acid composition of the predicted proteome. The charges contributed from the proteins mainly stem from Lys, Arg, Glu, and Asp residues with small contributions from de-protonated, negatively charged Cys residues and protonated, positively

**Table 19.1** Charges from Lewis bases and acids per cell of *C. metallidurans*<sup>a</sup>

Positive	Million/cell	Negative	Million/cell
Lys	17.9	Glu	29.8
Arg	45.2	Asp	31.5
His <sup>b</sup>	0.8	His	0
Cys	0	Cys <sup>b</sup>	0.9
PROTEINS	63.9	+1.72	62.2
<u>Ions (ICP-MS values<sup>c</sup>)</u>			
Na(I)	96.2±45.3	P@IM	57.2
K(I)	33.5±9.5	P@DNA	13.8
Mg(II)	27.4±1.6	P@RNA	40.6
Ca(II)	1.75±0.27	Sum P	112
TMetals	1.41±0.28	P (ICP-MS)	132±2
<u><sup>d</sup>Other components</u>			
		GSH	0.27
		Murein	1.88
		LPS	9.03
All	224±57	All max	205±2

<sup>a</sup>The charges per cell of *C. metallidurans* were predicted or determined by ICP-MS (Herzberg et al. 2014b; Große et al. 2019; Herzberg et al. 2014a; Kirsten et al. 2011). The total number of proteins per *C. metallidurans* cell of 1.88 million comes from a biochemical determination (Herzberg et al. 2014b) and was used to calculate the proteome from a proteomic experiment. The data for some proteins such as F<sub>1</sub>F<sub>0</sub> ATPase, RNA polymerase, and ribosomes were verified with literature data. As calculated from the dry mass of 615 fg per cell derived from the cell dimensions (Goris et al. 2001), the cell could contain twice as many protein copies. The amino acid content of the predicted proteome was multiplied by the 1.88 million protein copies per cell and the average length of 316.51 amino acids per protein to generate the estimated number of Lys, Arg, His, Cys, Glu, and Asp residues per cell. <sup>b</sup>The number of charges provided comes from the pK<sub>a</sub> values of Cys and His, the internal pH of 7.6 (Hunte et al. 2005) and the use of the Henderson–Hasselbalch equation. <sup>c</sup>The number of metal cations and transition metal cations (TMetals) were determined by ICP-MS and multiplied with the charge of the respective metal. Phosphate of the inner membrane and inner layer of the outer membrane (P@IM) comes from the cellular dimensions, including estimates of the DNA from the genome size, and the RNA content from the sizes of the rRNAs, the number of ribosomes and an 80% ratio of rRNA compared to total RNA. <sup>d</sup>GSH comes from the net de-protonation of the Cys residue, the cell dimensions and a content of 5 mM. Murein and LPS data come from the cellular dimensions compared to the content of these components in *Escherichia coli* and the mass ratio *C. metallidurans* (615 pg) to *E. coli* (283 pg) as taken from the cell dimensions (Goris et al. 2001). The shaded box gives the difference between negatively and positively charged amino acid residues per cell

charged His residues. In total, the predicted proteome is nearly neutral with a slight 2.7% higher positive charge of +1.72 M residues (Table 19.1).

The phosphate content of *C. metallidurans* was measured with a refined protocol to eliminate the interference of argon with the phosphate signal (Große et al. 2019). The cells contained 132 million phosphate residues. An older ICP-MS result of

110 million P (Kirsten et al. 2011) matched the calculated number of residues in the membranes and nucleic acids (Table 19.1). The phosphate entities provide two-third of the negative charge of the *C. metallidurans* cells and are located in the membranes, the nucleoid, and in polyphosphate granules. Together with the negative charges of the proteins, the total negative charges per cell are 205 M, neutralized by 224 M Lys, Arg residues and charges coming from the metal cations. Due to the experimental error of the ICP-MS experiments, the difference between the number of positive and negative charges is not significant. It cannot be stated at this stage if the cell carries a total negative or positive charge (Table 19.1). But should the cytoplasm not contain a high number of negative charges as part of the proton motive force across the cytoplasmic membrane?

From the chemiosmotic theory (Lehninger 1977), the inner face of the cytoplasmic membrane should indeed be negatively charged and the outer face positively charged. Calculated from the capacity of the cytoplasmic membrane area as derived from the cellular dimensions, a number of 6888 negative charges is needed to generate a charge gradient of 150 mV. This is a very small number compared to the 205 million total negative charges per cell (Table 19.1). A cytoplasmic pH of 7.6 (Zilberstein et al. 1984), a periplasmic pH of 6.6, and a volume of the periplasm of 5% of the cytoplasm would result in only 8.6 individual protons (as  $\text{H}_3\text{O}^+$ ) and 137  $\text{OH}^-$  in the cytoplasm, and 4.3 protons in the periplasm. From the growth yield of *C. metallidurans* of about 2 g gluconate per 1 g of dry weight and the KDPG degradation pathway (Legatzki et al. 2003b), a number of 13.8 million protons have to be transported through all 3000  $\text{F}_1\text{F}_0$  ATPases (Herzberg et al. 2014b) per cell per second to allow a doubling time of 240 min. A number of 6888 negative charges at the cytoplasmic face of the cytoplasmic membrane plus 4.3 single protons in the periplasm thus correspond to 13.8 million protons moved per second from the cytoplasm to the periplasm and back again.

This clearly shows that the proton motive force is not directly coupled to the cellular net charge, pH homeostasis, or proton content. The chemiosmotic energy conservation seems to result from moving positive charges in a charge relay net. Individual protons are only moved during a few instances, e.g., during the Q cycle or when the subunits of the c-ring of the  $\text{F}_1\text{F}_0$  ATPase are being protonated to drive the c-ring rotation (Junge et al. 2009). This is very similar to electric currency. Electrons separated from the positive charges in an electric power generator also do not travel all the way to a device driven by electricity such as a bulb in a lamp. The respiratory chain components use the energy of a redox reaction to generate a charge separation with positive charges outside of the cytoplasm. This inverse proton motive force voltage is transformed into a rotation movement in the  $\text{F}_1\text{F}_0$  ATPase, and the rotatory force is used to produce ATP from ADP and phosphate. This allows the chemiosmotic mode of energy conservation to function with a small number of calculated negative and positive charges, despite a background of millions of negative and positive charges in the cytoplasm.

Table 19.1 shows also that both Na(I) and K(I) are required in the cytoplasm to neutralize the charge of the phosphate residues, although Na(I) was expected to be predominantly outside the cell (Hunte et al. 2005; Wilson and Ding 2001). The total

positive charges of the monovalent and divalent metal cations summarize to  $+160 \pm 57$  million charges, which over-compensates the  $-132 \pm 2$  million negative charges of the phosphate residues. Both ions play important roles in two different global regulatory processes, K(I) in rapid adaptation to changing osmotic conditions that are compensated by K(I) uptake or efflux, depending on how the osmotic conditions have been changed (Altendorf and Epstein 1996; Walderhaug et al. 1992), and Na(I) is needed to balance the cytoplasmic pH values by sodium-proton exchange (Padan et al. 2001; Zilberstein et al. 1984). This pH homeostasis needs a buffer. The 14.88 million His residues of the proteome, which are predominantly neutral, are perfect for this job. That way, the Na(I), K(I) ions, and His residues may be deeply involved in the neutralization of the negative charges of the phosphate residues, osmo-adaptation, and homeostasis of the cytoplasmic pH value. As stated in the introductory part of this book, the His residues are ideal ligands for complex compounds formed by borderline transition metal cations such as Zn(II). His residues may work together with the Cys residues, which interfere with the redox homeostasis. That way, metal-binding sites in proteins, which variously are composed of Cys and His residues and supplemented by Asp and Glu residues, may be at the center of transition metal cation homeostasis and at the same time involved in other essential global homeostatic processes.

In summary, the number of Lewis acids and bases in the cell of the model bacterium *C. metallidurans* can be estimated, summing up to more than 200 million negative charges per cell, mainly provided by phosphate, Glu, and Asp, and compensated by more than 200 million positive charges per cell coming from Lys, Arg, and metal cations.

### 19.2.2 Debye–Hückel Equation and Macromolecular Crowding

To understand how the Lewis acids and bases inside the *C. metallidurans* cell may interact, the number of charged ions in the *C. metallidurans* cell was divided by the Avogadro constant and the cell volume of *C. metallidurans* of 0.57 fL (Goris et al. 2001) to calculate the concentrations of these ions and subsequently the ionic strength of the cytoplasm: 711 mM. Using the Debye–Hückel limiting law (Debye and Hückel 1923), this calculates to a Debye radius of 361 pm at 293 K (Israelachvili 1985). This means that the average distance between a central charged ion and a cloud of ions of the opposite charge in the cytoplasm of *C. metallidurans* is 361 pm. For Mg(II) or a transition metal cation with an ionic radius of between 65 pm and 80 pm and a divalently charged oxygen atom of 140 pm (Weast 1984), this leaves 140–160 pm free space for the water molecules, more exactly, only one water molecule between each cation and anion on the average.

The Debye–Hückel model (Debye and Hückel 1923) was developed for fully solvated ions but ions do also form ion-pairs (Fig. 19.1), solvent-shared ion-pairs

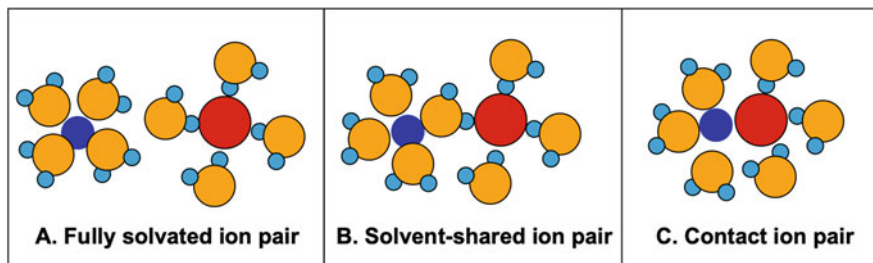


**Fig. 19.1** Schematic representation of ion pairs. Fully solvated (a), solvent-shared (b) and contact ion pairs (c) are shown. Cations in blue, anions in red, water with oxygen in orange and hydrogen in light blue. Not drawn to the scale

with exactly one solvent molecule of the primary solvent shell between both ions, which corresponds to the average distance between an ion pair as predicted by the Debye–Hückel limiting law, and contact ion-pairs with both ions directly adjacent to each other in a solvent shell shared by both ions (Bjerrum 1926). Due to the Coulomb law, the charge and dielectric constant of the solvent determines which mode of ion association is formed by an ion pair. Water with a high dielectric constant yields fully solvated ion-pairs of a monovalent cation and a monovalent anion, for instance, Na(I) or K(I) and a de-protonated carboxyl-group of Asp or Glu. In the high ionic strength of the cytoplasm, alkali cations should stay fully solvated (Fig. 19.1a) or at a maximum form a solvent-shared ion-pair with the monovalent anions of Asp, Glu or the phosphate backbones of RNA or DNA (Fig. 19.1b).

Due to the higher Coulomb force between an ion-pair composed of a divalent cation and a divalent anion compared to a monovalent couple, a divalent pair should switch between a solvent-shared and a contact ion-pair (Fig. 19.1b, c), as shown for magnesium sulfate in seawater (Burgess 1978). The Coulomb force for a divalent cation and a monovalent anion is twice as high as that of a monovalent couple but half as high as that of a divalent pair so that such a pair should be present in all three ion-pair configurations but mostly as a solvent-shared ion-pair (Fig. 19.1b).

This fits exactly to the Debye radius of ions in the cytoplasm, which leaves space for exactly one water molecule as shared first-shell solvent molecule between both ions (Fig. 19.1b), and the increase in the percentage of the covalent bond character between a metal cation and an oxygen anion from  $K(I) < Na(I) < Ca(II) < Mg(II) < Mn(II) < Zn(II) < Fe(II) = Ni(II) = Co(II) < Cu(II)$ . This indicates an increasing tendency to form short-living direct contact ion-pairs with a covalent bond character with Asp or Glu (Fig. 19.1b, c). This model explains also the formation of contact ion pairs of Mg(II) with ATP, other NTPs or polyphosphate, and the uptake of Mg(II) as Mg(II)-phosphate as contact ion-pair by PitA-type phosphate transporters (Herzberg et al. 2016; Grosse et al. 2016).

A His or Cys residue directly adjacent to an Asp or Glu, or in the vicinity of such a residue in an alpha-helix, beta-sheet, or coil structure should stabilize the direct contact ion-pair between a divalent metal cation and the Asp or Glu carboxylic group, retarding the metal at the surface of the respective protein. Cys should only

retard soft and borderline metals, His all metals in the order transition metals > Mg (II) > Ca(II) > Na(I) > K(I) (Hashemian 2011; Kumar et al. 2015). Consequently, the alkali cations Na(I) and K(I) stay as fully solvated ions away from proteins and nucleic acids and approach surface anions at a maximum as a solvent-shared ion-pair within the distance of a Debye length (Fig. 19.1a, b). Mg(II) and the transition metal cations should form solvent-shared ion-pairs and approach also into contact ion-pair associations (Fig. 19.1b, c), which may be even more stabilized by His residues adjacent to Asp and Glu, and, in case of all transition metal cations except the “hard” Mn(II), even more by a Cys residue. Pre-discriminated divalent metal cations should move inside the cytoplasm from one reversible contact ion pair with an Asp/Glu plus His/Cys amino acid residue at the surface of a protein to the next site. Solvent-shared ion-pairs are intermediates formed during approach of a metal cation to the protein surface and during the cation release process.

Additionally, the bacterial cytoplasm is not unstructured like the contents of a “tea bag” but can be visualized as a highly ordered, crowded structure composed of transiently interaction proteins or hyper-structures up to cellular compartments defined by crowding, mainly the nucleoid containing the DNA and the remaining cytoplasm outside of the nucleoid (Norris et al. 2007; Spitzer 2011; Spitzer and Poolman 2009). Transient interactions in crowded areas of the cytoplasm result from repulsive excluded volume interactions and may be modulated by the pH value and metal ions. The cytoplasmic proteins aggregate in crowded areas, leaving small channels between them and larger free areas between the crowded volume portions (Fig. 19.2). The negative charges at the surface of proteins also cause a re-distribution of the cations around them, so that on the scale of microseconds, this results in a conducting fluid involved in transport of organic and inorganic ions throughout the cell (Spitzer 2011; Spitzer and Poolman 2009). This conducting fluid is composed of fully solvated alkali metal cations plus Mg(II) and transition metal cations that will approach the proteins more closely by the formation of transient solvent-shared and contact ion-pairs, which are themselves stabilized by adjacent His and Cys residues that act to retard the metal cation at the surface of the protein. Eventually, stable metal complexes are formed when an increasing number of ligands bond with the metal. Pre-discriminated metal cations move inside the channels along the surface of the crowded proteins as part of the conducting fluid until they reach sites that may discriminate them.

The conducting fluid of ions is, at the level of cellular crowding, driven by transcription. When the cell starts to divide the conducting fluid is driven by DNA replication. On the cellular level, there is a constant flow of MgATP, other MgNTPs or Mg-dNTPs from the remaining cytoplasm into the nucleoid since the MgNTPs and MgdNTPs are needed there for transcription and DNA replication. Mg-pyrophosphate flows back from the nucleoid into the remaining cytoplasm. ATP should carry 3 to 4 negative charges under cytoplasmic conditions as calculated from the pKa value (Dawson et al. 1969) and the Mg(II)ATP contact ion pair 1 to 2 net negative charges. Pyrophosphate with the pKa values 0.91, 2.10, 6.7, and 9.32 should consequently carry in the cytoplasm 2 to 3 charges and Mg(II)-pyrophosphate 0 to 1 net negative charges. When MgNTPs and MgdNTPs are

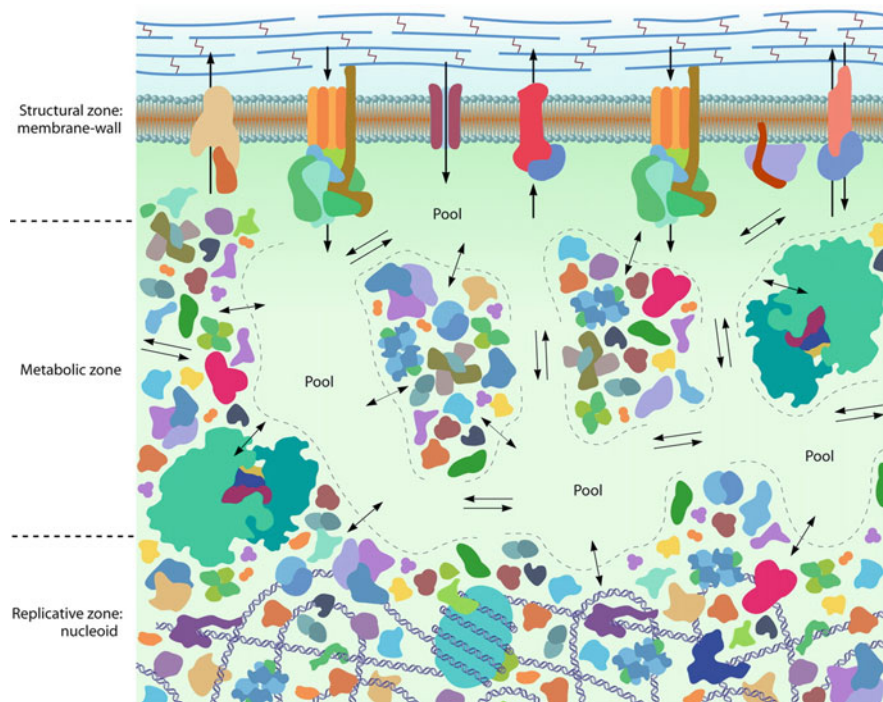


**Fig. 19.2** Cellular areas with crowded macromolecules as stage for metal allocation. A bacterial cell is composed of a nucleoid zone at the center, containing the DNA, a remaining cytoplasm and the area adjacent to the cytoplasmic membrane. Cytoplasmic and the cytoplasmic parts of membrane proteins form crowded areas by attractive non-covalent bonds. These are separated from but connected by non-crowded lagunes containing electrolytes such as ATP. Metal cations can be expected to interact with the Asp and Glu sites at the surface of proteins to form short-living solvent-shared or contact ion pairs, which may be stabilized by an adjacent His or Cys residue. The cations may move within the crowded areas from contact site to contact site until they reached proteins supplying sufficient residue to form a metal complex. On a larger time-scale, the metal cations may move along via the contact sites from metal complex to metal complex down a thermodynamic gradient, which leads to metal discrimination and allocation. Figure taken with permission from Spitzer and Poolman (Spitzer and Poolman 2009)

polymerized during transcription and replication into RNA and DNA, respectively, plus Mg-pyrophosphate, one net negative charge remains in the nucleoid. Eventually, used mRNA is exported back into the remaining cytoplasm and degraded here. Until this occurs, there is a constant increase in the net negative charge of the nucleoid that has to be neutralized by a parallel import of metal cations into this cellular compartment.

In summary, molecular crowding and the Debye–Hückel considerations can be used to define the stage of cellular metal homeostasis more closely. The cell contains crowded and super-crowded areas of proteins and nucleic acids, allowing small molecules only passage within channels between the macromolecules. An ion

current, driven by transcription and DNA replication, moves within these channels from the remaining cytoplasm into the nucleoid. The alkali metal cations stay fully solvated or approach a negative charge at a maximum in the form of a solvent-shared ionic pair. Divalent metal cations form solvent-shared pairs and even approach into contact ion pairs with a tendency of  $\text{Mg(II)} < \text{Mn(II)} < \text{other transition metal cations}$ . A His residue adjacent to an Asp or Glu residue may form an additional bond especially to transition metal cations, a Cys, especially to soft cations. Pre-discriminated divalent metal cations may move onward from one short-living but His-stabilized direct ion pair with Asp or Glu until node sites with more Asp, Glu, His, and Cys ligands are reached, which retain the metals longer and discriminate the metals by their different abilities to accept four or more ligands.

### ***19.2.3 Inventory of Possible Metal Binding Sites in the Proteome of *C. metallidurans****

Asp and Glu residues adjacent to His or Cys residues are thus essential to control the movement of Mg(II) and of pre-discriminated transition metal cations as shared-solvent ion pairs within the narrow channels between crowded proteins. The formation of contact ion-pairs additionally stabilized by a bond to an adjacent His or Cys assists in the task of retarding the cations, plus helps to discriminate transition metal cations against Mg(II). There can be additional help to discriminate metal cations against each other by using additional His, Cys, Asp, or Glu residues to form metal-selective complexes. Once discrimination has occurred, the discriminated metal cation may only move bound to a protein.

To create an inventory of all candidates for metal-binding sites, the complete predicted proteome of *C. metallidurans* was analyzed. Amino acid sequences were selected that contained histidine or cysteine residues in a distance of one to four amino acids from at least one additional His, Cys, Asp, Glu, or the carboxy-terminus that may also attract a metal cation. A distance of four amino acids means 3 nonspecified amino acids between the (H, C, D, E) and (H, C), which is slightly more than one turn in an alpha helix or two positions apart in the same plane of a beta-sheet.

This approach generated 27,926 candidates for potential metal-binding motifs in 6345 predicted gene products of *C. metallidurans* (Große et al. 2022). These motifs could be stand-alone metal-binding sites, but in most cases, amino acid residues from other parts of the protein or other proteins may contribute to the actual metal-binding site. For each possible site, the metal capacity was calculated as “number of metal binding residues” divided by 4 (four ligands in a tetrahedral complex). Motifs with two residues and a metal capacity of 0.5 could be simple “flow sites” facilitating the movement of pre-discriminated metal cations close to the protein in the channels of the crowded protein areas, in case they are not part of a larger metal-binding site together with residues from other parts of the polypeptide chain. In total, 13,905 of



the motifs corresponded to possible “flow sites,” especially the 8726 motifs with one His plus one Asp or Glu. Motifs with two His numbered 1084; 866 motifs contained His and Cys, 2805 motifs were Cys and Asp or Glu, 424 motifs were double-Cys. In total, 161 proteins contained a His adjacent to the C-terminal carboxy-site and 25 proteins a Cys at this position (Große et al. 2022). Since His-His, His-Cys, and Cys-Cys motifs do not contain a negatively charged Asp or Glu to attract an anion, these motifs may represent parts of metal-complexing metal-binding sites for already discriminated metal cations.

Motifs with three ligands and a capacity of 0.75 may be at the edge between a metal binding and a “flow site.” In proteins quantified in the proteome of *C. metallidurans*, 4393 of these candidate sites were found. Multiplied by the respective number of proteins per cell that contains these motifs, this leads to nearly 2 million possible sites per cell within the total proteome. A similar number, 4268 possible sites, were in proteins not identified in the total proteome of *C. metallidurans*. Motifs with already four ligands in close proximity may represent binding sites, or parts thereof, for Zn(II) and other transition metal cations. The proteome contained nearly 1.4 million possible sites with four or five metal ligands composed of 2131 motifs, 2199 motifs were in proteins not identified or not quantified. A number of 307 motifs with 6 to 7 ligands were in quantified proteins, summing up to 305,000 possible sites per cell, and 373 motifs were in proteins not found (Große et al. 2022).

Most interesting were the motifs that could accommodate alone at least 2 metal cations with 8 ligands or more, possible “big sites.” The corresponding metal-binding proteins could be major nodes in the zinc allocation and discrimination network. There were 69 big sites in quantified proteins, theoretically able to bind 105,000 metal cations, and 95 big sites in proteins not found in the proteome. There was always a similar number of motifs of the same group in quantified and not identified proteins indicating that the cell had the genomic capacity to double the binding sites of each group should the need arise. Secondly, there was a gradient of a large number of mere “flow sites” to a lower number of sites with more and more ligands as evidence for a stepwise transformation of pre-discriminated into discriminated metals. Mg(II) and the transition metal cations may flow through the narrow channels of crowded proteins (Fig. 19.2), attracted to the surface of these proteins, discriminated during this flow until they migrate from one metal-binding complex to the next one down the thermodynamic gradient (Banci et al. 2010). Proteins with “big sites” could thus be important contributors to metal homeostasis as flow nodes, sensors, switches, track switches, discriminators, buffers, or containers of already discriminated metal cations.

The metal capacity of a predicted protein was the sum of the capacities of its metal-binding motifs. The 27 proteins with the biggest big sites exhibited a predicted potential to bind 15 metals per polypeptide or more with UvrA2 from the main base excision DNA repair system on the top with 33 sites (Table 19.2). Half of the 27 proteins with the largest metal-binding capacity could be quantified in *C. metallidurans*. On top of the expression level was the 2-oxoglutarate dehydrogenase of the tricarboxylic acid (TCA) cycle Kdg, followed by the glutamate synthase

**Table 19.2** Proteins with the largest metal-binding capacity per protein<sup>a</sup>

Rmet	Gene	KO	P(AE 04)	Kap/Prot	Description
<b>Rmet_4549</b>	<i>uvrA2</i>	<b>GIP-REP-Recomb</b>	<b>545</b>	<b>33.00</b>	<b>QILEL2 UvrA family protein</b>
Rmet_4797	–	NA	NeF	27.00	QILDW7 YD repeat
Rmet_0591	–	NA	NeF	21.25	QILQU9 Diguanylate cyclase/with PAS/PAC sensor(S)
Rmet_0555	<i>fdxA</i>	MET-CAH-DiCarb	NeF	20.75	QILQY5 Formate dehydrogenase, alpha subunit
Rmet_5407	–	NA	NeF	20.00	QILC60 Putative uncharacterized protein
Rmet_5309	–	NA	NeF	20.00	QILCF8 Sensor protein
<b>Rmet_0367</b>	–	NA	<b>960</b>	<b>19.50</b>	<b>QILRH3 FAD linked oxidase-like protein</b>
Rmet_5349	–	NA	NeF	19.00	QILCB8 Sigma-54 factor, interaction region
<b>Rmet_1181</b>	<i>gdhB</i>	MET-EN-Nitrog	<b>89</b>	<b>18.75</b>	<b>QILP59 Glutamate dehydrogenase (NAD)</b>
Rmet_2074	<i>narG</i>	MET-EN-Nitrog	NeF	18.50	QILLM3 Respiratory nitrate reductase alpha subunit apoprotein
<b>Rmet_3396</b>	–	MET-CAH-PyrOx	<b>68</b>	<b>18.00</b>	<b>QILHV8 Pyruvate ferredoxin/flavodoxin oxidoreductase</b>
Rmet_4932	–	NA	NeF	17.75	QILD12 Ferredoxin
Rmet_0198	<i>dmeF</i>	EIP-TRA-Ion	NeF	17.50	QILRZ2 Cation diffusion facilitator family transporter
Rmet_4821	<i>nasA</i>	MET-EN-Nitrog	NeF	17.00	QILDU3 Assimilatory nitrate reductase (NADH) alpha subunit apoprotein
<b>Rmet_3263</b>	<i>glbB</i>	MET-EN-Nitrog	<b>4010</b>	<b>16.75</b>	<b>QIL191 Glutamate synthase (NADH) large subunit</b>
<b>Rmet_0313</b>	<i>uvrA1</i>	<b>GIP-REP-Recomb</b>	<b>814</b>	<b>16.50</b>	<b>QILRM7 Excinuclease ABC subunit A</b>
<b>Rmet_1870</b>	<i>purL</i>	MET-NUC-Pur	<b>1505</b>	<b>16.25</b>	<b>QILM77 Phosphoribosylformylglycinamide synthase</b>
<b>Rmet_2050</b>	<i>kgd</i>	NA	<b>4358</b>	<b>16.00</b>	<b>QILLP7 2-oxoglutarate dehydrogenase E1 component</b>
<b>Rmet_2885</b>	<i>ileS</i>	MET-AA-VaiLeulle	<b>1261</b>	<b>16.00</b>	<b>QILJB8 Isoleucyl-tRNA synthetase</b>
<b>Rmet_0673</b>	<i>pill2</i>	<b>GIP-PTL-T2S</b>	<b>1036</b>	<b>15.50</b>	<b>QILQL7 Histidine kinase/response regulator hybrid</b>
<b>Rmet_0125</b>	<i>cobW3</i>	NA	<b>263</b>	<b>15.50</b>	<b>QILS65 Cobalamin synthesis CobW-like protein</b>
<b>Rmet_0993</b>	–	NA	<b>385</b>	<b>15.50</b>	<b>QILPP7 Putative uncharacterized protein</b>
<b>Rmet_2131</b>	–	<b>GIP-REP-Recomb</b>	<b>261</b>	<b>15.50</b>	<b>QILLG6 DNA helicase/exodeoxyribonuclease V, subunit A</b>
<b>Rmet_3482</b>	<i>gcvP</i>	MET-AA-GlySerThr	<b>372</b>	<b>15.25</b>	<b>QILHM2 Glycine dehydrogenase, decarboxylating</b>
Rmet_4818	<i>nirB</i>	MET-EN-Nitrog	NeF	15.25	QILDU6 Assimilatory nitrite reductase (NAD(P)H) large subunit

(continued)

Table 19.2 (continued)

Rmet	Gene	KO	P(AE104)	Kap/Prot	Description
<b>Rmet_2069</b>	–	<b>GIP-REP-Recomb</b>	<b>65</b>	<b>15.00</b>	<b>QILLM8 ATP-dependent helicase HrpA</b>
Rmet_4657	–	NA	NQ	15.00	QILEA7 Diguanylate cyclase/phosphodiesterase

<sup>a</sup>All proteins with 15 or more predicted metal-binding sites are shown. The Rmet number is provided and the gene name, if it exists. The proteins were sorted into the KEGG orthology (KO) first-level groups cell division and motility (DIV), environmental signal processing (EIP), genetic information processing (GIP), metabolism (MET) and not assigned in the current KEGG database (NA) and the total metal capacity and protein number in all these sites was summarized (Kanehisa et al. 2006; Kanehisa and Sato 2020). This was also done for the second level categories such as division, motility, protein translation, replication, transcription, translation, metabolism of amino acids, carbohydrates, cofactors, energy, membrane, lipids, nucleic acid bases, other amino acids including GSH, secondary metabolites of xenobiotics, from the top. The subsequent rows indicate the number of proteins P(AE104) per cell in *C. metallidurans* AE104 and the capacity per protein. NeF, never found, NQ, found but not quantified. Bold, proteins quantified in *C. metallidurans* AE104 (Herzberg et al. 2014b)

GltB (Table 19.2). Enzymes of the TCA cycle and the attached metabolic pathways for nitrogen assimilation seem to be major nodes of metal homeostasis.

The metal capacity of each protein was multiplied with the copy number of these proteins in the cells of *C. metallidurans*, yielding the total metal binding capacity of the proteome of this cell for pre-discriminated and discriminated metals: 5.77 million divalent metal cations (Große et al. 2022). When *Escherichia coli* cells were inactivated on metallic copper surfaces (Bleichert et al. 2021), the cells contained after 30 seconds of incubation 5 million copper atoms per cell could not produce colonies after 1 minute and contained 10 million copper atoms after 5 minutes. These cells had no longer a proton motive force and were consequently dead after 15 min. They contained at this point of time 51 million copper ions per cell, before they disintegrated and released the copper again. These data clearly show that the total metal-binding capacity of a bacterial cell may be indeed in the range of millions of metal cations per cell, although the cells do not survive such a high metal load, especially when this metal was copper (Bleichert et al. 2021).

The total capacity of 5.77 million divalent cations per cell is more than the total number of transition metal cations per cell, 700,000, and most of these transition metal cations are iron. This number of 700,000 transition metal cations can be easily accommodated by the 105,000 “big sites” in quantified proteins, 305,000 sites with 6 or 7 ligands, and 400,000 of the 1.4 million sites with 4 or 5 ligands, even leaving 1 million sites with 4 or more ligands empty. In *C. metallidurans* cells overloaded with metal cations, several 100,000 more ions were present in the cell (Bütöf et al. 2018; Wiesemann et al. 2017) so that a maximum cellular capacity of 1.8 million binding sites for pre-discriminated and discriminated transition metal cations should not be too far away from reality.

This huge metal-binding total capacity of the cytoplasmic proteome should also be sufficient to keep most of the transition metal cations away from the glutathione pool. The capacity of all flow and binding sites would also be sufficient to accommodate half of the 13.7 million magnesium ions, leaving sufficient numbers of Mg(II) to bind to NTPs and pyrophosphate and to allow a conductive fluid of the metal cation. Mg(II) seems to be indeed part of a conductive ion fluid within the cell (Spitzer 2011). Mg(II) binds to phosphate-containing compounds with  $\lg(K)$ -values of 5.7 (pyrophosphate) > 4.58 (ATP) > 3.34 (ADP) > 2.5 (phosphate) > 2.32 (RNA) > 2.10 (DNA) (Dawson et al. 1969). With the 3.5 negative charges of ATP, the 2.5 of ADP, the 1.5 of phosphate and 1 per RNA or DNA base pair backbone, the Coulomb force decreases from six- or eightfold, via an intermediate range of four- or sixfold, down to threefold of the electrostatic attraction of Mg(II) to RNA or DNA. The result is a close ion pairing of Mg(II)ATP, an increased tendency to form a solvent-shared ion-pair with ADP and phosphate, and a solvent-shared ion-pair with RNA or DNA. Together with the decreasing affinity of Mg(II) to RNA or DNA, this prevents Mg(II) from binding to RNA or DNA during the RNA polymerase action. Instead, Mg(II) leaves as a tightly bound contact ion pair with pyrophosphate. In the active site of the RNA polymerase, Mg(II) is attracted to Asp and Glu residues in the active site of the enzyme (Svetlov and Nudler 2013). This is an example that illustrates how the different ion associations and binding affinities

cooperate to mediate central biochemical processes, highlights the essential role of metal cations herein and is the chemical basis for the constant flow of negative net charges from the remaining cytoplasm into the cellular nucleoid compartment.

The proteins responsible for the cellular metal capacity can be sorted into the KEGG orthology levels division (DIV), environmental signal processing (EIP), genetic information processing (GIP), metabolism (MET) or yet not listed in the KEGG encyclopedia (NA) from the first to the third level (Table 19.3). Proteins involved in metabolism (MET) and transcription (GIP-TK) have been found to contribute more greatly per polypeptide to the cellular metal capacity than did proteins involved in either environmental signal processing or translation (GIP-TL). A high metal-binding capacity seems to be especially needed in proteins that may be involved in the ion current from the cytoplasm into the cellular nucleoid compartment.

All proteins were listed that provided more than 20,000 possible metal binding sites to the cell (Table 19.4). These proteins provided 22% or 1.25 million sites to the total metal-binding capacity of the cell. Again, enzymes of the tricarboxylic acid cycle and nitrogen assimilation stood out (green and purple, respectively) but also components of the genetic information processing group: elongation factors Tu and G, three ribosomal proteins RplB, RpsA, RplY, and the components of the RNA polymerase core RpoA, RpoB, RpoC. While the components of the RNA polymerase were responsible for the large contribution of metal-binding capacity within the KEGG orthology group GIP-TK, contribution of the ribosomal components was specifically provided by a few selected proteins. Elongation factor Tu was not listed in the KEGG encyclopedia of *C. metallidurans*. The ribosomes contributed 240,000 metal-binding sites to the cell (Table 19.5) and four ribosomal proteins were predicted to bind three or more metal cations. The proteins L2, S2, S9, S15, and S17 were zinc-binding ribosomal proteins (Herzberg et al. 2014b). The sequence of these proteins and additional ribosomal proteins contained identified zinc-binding sites (Fig. 19.3). Additionally, L31 type B, which has a capacity of 2.5 metals per protein, may be an important zinc-binding protein (Fig. 19.3) of the ribosome (Akanuma et al. 2006).

While metabolic enzymes and those involved in transcription contain a high number of general metal-binding motifs, proteins needed for translation are especially rich in zinc-binding sites. The ribosome seems to be central for zinc homeostasis. Some bacteria contain paralogs of zinc-binding ribosomal proteins that do not contain zinc-binding sites (Akanuma et al. 2006). The genes for the zinc-free paralogs are expressed under the control of the Zur repressor under zinc starvation conditions and replace their zinc-binding paralogs (Gabriel and Helmann 2009; Owen et al. 2007; Shin et al. 2007). The resulting ribosome could be transformed by hibernating factors to hibernating ribosomal dimers, leading to slow-growing persister sub-populations (Li et al. 2021). *C. metallidurans* does not contain zinc-free paralogs of ribosomal proteins under Zur control and its hibernation-mediating protein RaiA or RpoX is encoded downstream of the gene for the nitrogen-starvation sigma factor RpoN, although under control of at least three *rpoX*-specific promoters (Große et al. 2022). Hibernating ribosomes in *C. metallidurans* seem to be a matter

**Table 19.3** Metal capacity of *C. metallidurans* with respect to KEGG orthology levels<sup>a</sup>

KEGG level	Capacity	% capacity	Proteins	% proteins	%cap/%prot
<b>DIV</b>	<b>43,994</b>	<b>0.75%</b>	<b>15,900</b>	<b>0.83%</b>	<b>0.90</b>
DIV-Division	33,718	0.57%	12,690	0.66%	0.86
DIV-MOT	9,382	0.16%	3,104	0.16%	0.98
<b>EIP</b>	<b>172,798</b>	<b>2.94%</b>	<b>97,500</b>	<b>5.09%</b>	<b>0.58</b>
EIP-SIG	21,636	0.37%	11,129	0.58%	0.63
EIP-TRA	15,1162	2.57%	86,322	4.51%	0.57
<b>GIP</b>	<b>1,047,531</b>	<b>17.80%</b>	<b>510,000</b>	<b>26.68%</b>	<b>0.67</b>
GIP-PTL	329,899	5.61%	128,923	6.74%	0.83
GIP-REP	169,563	2.88%	47,305	2.47%	1.17
GIP-TK	178,704	3.04%	33,680	1.76%	1.72
GIP-TL	369,365	6.28%	300,522	15.71%	0.40
<b>MET</b>	<b>2,626,926</b>	<b>44.64%</b>	<b>601,000</b>	<b>31.40%</b>	<b>1.42</b>
MET-AA	679,382	11.54%	144,920	7.58%	1.52
MET-CAH	841,441	14.30%	197,121	10.30%	1.39
MET-COF	180,521	3.07%	42,662	2.23%	1.38
MET-EN	435,848	7.41%	93,996	4.91%	1.51
MET-GLYC-LPS	22,829	0.39%	7,465	0.39%	0.99
MET-LIP	96,612	1.64%	34,318	1.79%	0.92
MET-NUC	29,4426	5.00%	59,914	3.13%	1.60
MET-OAA	39,820	0.68%	9,885	0.52%	1.31
Met-SecMetab	7684	0.13%	2855	0.15%	0.87
MET-XEN	27445	0.47%	6778	0.35%	1.32
<b>NA</b>	<b>1,990,415</b>	<b>33.82%</b>	<b>688,000</b>	<b>35.94%</b>	<b>0.94</b>

<sup>a</sup>The calculated capacity of all predicted metal-binding proteins in the predicted proteome of *C. metallidurans* was multiplied with the actual content in *C. metallidurans* AE104 cells (Herzberg et al. 2014b). The proteins were sorted into the KEGG orthology first level groups cell division and motility (DIV), environmental signal processing (EIP), genetic information processing (GIP), metabolism (MET), and not assigned in the current KEGG database (NA) and the total metal capacity and protein number in all these sites was summarized (Kanehisa et al. 2006; Kanehisa and Sato 2020). This was also done for the second level categories such as division, motility, protein translation, replication, transcription, translation, metabolism of amino acids, carbohydrates, cofactors, energy, membrane, lipids, nucleic acid bases, other amino acids including GSH, secondary metabolites of xenobiotica, from the top. Only KEGG-orthology groups with >0.05% of the total cellular metal capacity are listed. Green, ratio capacity/proteins >1.3 (enriched in sites); red, < 0.67; black in-between; bold, first-level categories

**Table 19.4** Proteins responsible for the largest metal-binding capacity per cell<sup>a</sup>

Rmet	Gene	KO	P(AE104)	Kap/Prot	Total	Description
Rmet_3324	<i>Tuf1</i>	NA	14226	5.25	74686	Q1L113 Elongation factor Tu
Rmet_2050	<i>Kgd</i>	NA	4358	16.00	69729	Q1LLP7 2-oxoglutarate dehydrogenase E1 component
Rmet_3263	<i>glfB</i>	MET-EN-Nitrog	4010	16.75	67159	Q1LI91 Glutamate synthase (NADH) large subunit
Rmet_3333	<i>rpoC</i>	GIP-TK-RNAP	4709	12.50	58859	Q1LI21 DNA-directed RNA polymerase subunit beta'
Rmet_3729	<i>icdA</i>	MET-CAH-TCA	7557	7.50	56677	Q1LGX5 Isocitrate dehydrogenase, NADP-dependent
Rmet_2481	<i>glfA</i>	MET-CAH-TCA	8951	6.00	53705	Q1LKG8 Citrate synthase
Rmet_3334	<i>rpoB</i>	GIP-TK-RNAP	4908	10.50	51534	Q1LI20 DNA-directed RNA polymerase subunit beta
Rmet_3046	<i>maeB1</i>	MET-CAH+Pyr	4352	11.00	47867	Q1LIV8 Malic enzyme, NAD-binding
Rmet_2484	<i>sdhA</i>	MET-CAH-TCA	6561	7.00	45925	Q1LKG5 Succinate dehydrogenase subunit A
Rmet_2680	<i>glvA</i>	MET-EN-Methane	4867	8.00	38939	Q1LJX3 Serine hydroxymethyltransferase
Rmet_1950	<i>atpC</i>	GIP-PTL-Fold	9824	3.50	34385	Q1LLZ7 Alkyl hydroperoxide reductase
Rmet_3325	<i>fusA1</i>	NA	7986	4.25	33939	Q1LI29 Elongation factor G 1
Rmet_0923	<i>prp</i>	MET-NUC-Pur	5723	5.75	32908	Q1LPW7 Polyribonucleotide nucleotidyltransferase
Rmet_0933	<i>nuoG</i>	MET-EN-OxPhos	3570	9.00	32126	Q1LPV7 NADH-quinone oxidoreductase
Rmet_3314	<i>rplB</i>	GIP-TL-Ribo	8352	3.75	31321	Q1LI40 50S ribosomal protein L2
Rmet_0722	<i>rpsA</i>	GIP-TL-Ribo	9093	3.25	29551	Q1LQG8 SSU ribosomal protein S1P
Rmet_1196	<i>aceE</i>	MET-CAH+FbP	3692	8.00	29538	Q1LP44 2-oxo-acid dehydrogenase E1 component
Rmet_0288	<i>rplY</i>	GIP-TL-Ribo	7358	4.00	29433	Q1LRQ2 50S ribosomal protein L25
Rmet_4564	<i>meE</i>	MET-AA-Met	3887	7.50	29154	Q1LEK0 Methionine synthase (B12-independent)
Rmet_3494	<i>atpD</i>	MET-EN-OxPhos	7664	3.75	28740	Q1LHL0 ATP synthase subunit beta
Rmet_0117	<i>bioB</i>	MET-COF-Biotine	4380	6.50	28473	Q1LS73 Biotin synthase
Rmet_0156	<i>metK</i>	MET-AA-Met	5195	5.25	27271	Q1LS34 S-adenosylmethionine synthetase
Rmet_0137	-	NA	4951	2.50	27231	Q1LS53 Putative uncharacterized protein
Rmet_3262	<i>glfD</i>	MET-EN-Nitrog	4014	6.75	27091	Q1LI92 Glutamate synthase (NADH) small subunit
Rmet_2031	<i>infB</i>	NA	2797	9.00	25171	Q1LLR6 Translation initiation factor IF-2
Rmet_0878	<i>maeB</i>	MET-CAH+Pyr	2938	8.50	24974	Q1LQ12 Malic enzyme, NAD-binding

(continued)

Table 19.4 (continued)

Rmet_1870	<i>purL</i>	MET-NUC-Pur	1505	16.25	24455	Q1LM77 Phosphoribosylformylglycinamide synthase
Rmet_2062	<i>glnA</i>	MET-EN-Nitrog	3848	6.00	23090	Q1LLN5 Glutamine synthetase
Rmet_0539	<i>sodB</i>	NA	6581	3.50	23033	Q1LR01 Superoxide dismutase
Rmet_3291	<i>rpoA</i>	GIP-TK-RNAP	6895	3.25	22410	Q1LI63 DNA-directed RNA polymerase subunit alpha
Rmet_0170	<i>ahcY</i>	MET-AA-Met	4288	5.00	21440	Q1LS20 Adenosylhomocysteinase
Rmet_3118	<i>secA</i>	GIP-PTL-Exp	1754	12.00	21047	Q1LIN6 Protein translocase subunit secA
Rmet_1146	-	NA	2133	9.75	20795	Q1LP94 Electron transfer flavoprotein-ubiquinone oxidoreductase
Rmet_0127	<i>cobW2</i>	NA	1755	11.50	20181	Q1LS63 Cobalamin synthesis protein, P47K
Rmet_2885	<i>lfeS</i>	MET-AA-ValLeulle	1261	16.00	20176	Q1LJB8 Isoleucyl-tRNA synthetase
Rmet_2483	<i>sdhB</i>	MET-CAH-TCA	4739	4.25	20140	Q1LKG6 Succinate dehydrogenase subunit B

<sup>a</sup>All proteins providing more than 20,000 predicted metal-binding sites per cell are shown. The Rmet number is provided, the gene, the KEGG orthology membership down to the third level (Kanehisa et al. 2006; Kanehisa and Sato 2020), the number of proteins per cell in *C. metalliturgans* AE104 (Herzberg et al. 2014b), the capacity per protein and, as a product, the capacity per cell. Genetic information processing in red, carbohydrate metabolism in green, nitrogen assimilation in purple



**Table 19.5** Total metal-binding capacity of the ribosome<sup>a</sup>

Rmet	Gene	P (AE104)	Kap/ Prot	Total	Descr
Rmet_0288	<i>rplY</i>	7358	4.00	29,433	Q1LRQ2 50S ribosomal protein L25
<b>Rmet_3314</b>	<b><i>rplB</i></b>	<b>8352</b>	<b>3.75</b>	<b>31,321</b>	<b>Q1LI40 50S ribosomal protein L2</b>
Rmet_0722	<i>rpsA</i>	9093	3.25	29,551	Q1LQG8 SSU ribosomal protein S1P
Rmet_1979	<i>rpsF</i>	4861	3.00	14,584	Q1LLW8 30S ribosomal protein S6
Rmet_2137	<i>rpmE</i>	4997	2.50	12,492	Q1LLG0 50S ribosomal protein L31 type B
Rmet_0410	<i>rplM2</i>	4679	2.50	11,697	Q1LRD0 50S ribosomal protein L13
<b>Rmet_1435</b>	<b><i>rpsB</i></b>	<b>6441</b>	<b>2.25</b>	<b>14,493</b>	<b>Q1LNF8 30S ribosomal protein S2</b>
Rmet_3316	<i>rplD</i>	7471	2.00	14,942	Q1LI38 50S ribosomal protein L4
Rmet_2432	<i>rpmF</i>	3633	2.00	7267	Q1LKL7 50S ribosomal protein L32
<b>Rmet_0410</b>	<b><i>rpsI</i></b>	<b>7992</b>	<b>1.75</b>	<b>13,986</b>	<b>Q1LRC9 30S ribosomal protein S9</b>
Rmet_3313	<i>rpsS</i>	3671	1.75	6424	Q1LI41 30S ribosomal protein S19
Rmet_3327	<i>rpsL</i>	4440	1.50	6660	Q1LI27 30S ribosomal protein S12
Rmet_3293	<i>rpsK</i>	5353	1.25	6691	Q1LI61 30S ribosomal protein S11
<b>Rmet_0921</b>	<b><i>rpsO</i></b>	<b>4847</b>	<b>1.25</b>	<b>6058</b>	<b>Q1LPW9 30S ribosomal protein S15</b>
Rmet_3295	<i>rpmJ</i>	NeF	1.25	0	Q1LI59 50S ribosomal protein L36
Rmet_3302	<i>rplF</i>	7732	1.00	7732	Q1LI52 50S ribosomal protein L6
Rmet_3317	<i>rplC</i>	7040	1.00	7040	Q1LI37 50S ribosomal protein L3
Rmet_3303	<i>rpsH</i>	5099	1.00	5099	Q1LI51 30S ribosomal protein S8
Rmet_3338	<i>rplK</i>	4798	1.00	4798	Q1LI16 50S ribosomal protein L11
<b>Rmet_3308</b>	<b><i>rpsQ</i></b>	<b>3251</b>	<b>1.00</b>	<b>3251</b>	<b>Q1LI46 30S ribosomal protein S17</b>
Rmet_3105	<i>rpmA</i>	2121	1.00	2121	Q1LIP9 50S ribosomal protein L27
Rmet_1163	<i>rplT</i>	5230	0.75	3923	Q1LP77 50S ribosomal protein L20
Rmet_3294	<i>rpsM</i>	4610	0.75	3458	Q1LI60 30S ribosomal protein S13
Rmet_3299	<i>rpmD</i>	1634	0.75	1226	Q1LI55 50S ribosomal protein L30
Rmet_1162	<i>rpmI</i>	968	0.75	726	Q1LP78 50S ribosomal protein L35
Rmet_1976	<i>rplI</i>	8849	0.50	4425	Q1LLX1 50S ribosomal protein L9
Rmet_3298	<i>rplO</i>	6201	0.50	3100	Q1LI56 50S ribosomal protein L15
Rmet_3307	<i>rplN</i>	4613	0.50	2306	Q1LI47 50S ribosomal protein L14
Rmet_2871	<i>rpmG</i>	NeF	0.00	0	Q1LJD2 50S ribosomal protein L33

<sup>a</sup>The Rmet number is provided, the number of proteins per cell in *C. metallidurans* AE104 (Herzberg et al. 2014b), the capacity per protein and, as a product, the capacity per cell. NeF, never found. Bold, zinc-binding ribosomal proteins

of nitrogen supply and not of zinc. Nevertheless, the allocation of zinc to the translating ribosome is of global importance for the growth of many bacteria. This agrees with the fact outlined in the introductory part of this book (“Chemical constraints for transition metal cation allocation” by author Dietrich H. Nies) that due to the negative electron affinity of zinc, the metal needs to be inserted into structural zinc sites immediately after translation. The cells have to manage a flow of MgNTPs to transcription and of zinc to translation. Interruption of zinc allocation to the ribosome can be compensated as a first step by decreasing the zinc-binding and

>KWW39963.1 50S ribosomal protein L36 (Cupriavidus metallidurans)  
MKVLASVKRI**CRNCKI**IKRNGVVRVIC**SSDPRH**KQRQG

>KWW37692.1 50S ribosomal protein L31 type B (Cupriavidus metallidurans)  
MKEGI**H**PNYREVL**FD**VSNDFK~~FVTR~~STIQTKDTIE**HEG**KTYPLAKIEVSS**ESH**PFYTGTKIMDTAGRV  
EKFRQKFGSKLGAACK

>KWW36056.1 50S ribosomal protein L13 (Cupriavidus metallidurans)  
MKTFSAKPAEVKRDWYVIDATDKVLGRVASEVARRLRGK**HKPEFTPHVD**TGDFIIIVNAAKLRVGTGKEQ  
DKKYYR**HSGYPGGIYE**TFGKMQQRFPGRALEKAVKGMPLKGPLGYAMIKKLVYA**EA**E**HPH**SAQQPKVL  
EI

>KWW39982.1 50S ribosomal protein L2 (Cupriavidus metallidurans)  
MALVKTTPKTPSGRRSMVKVNVN**DLHKGAPH**APLLEKQFOKSGRNNNG**HITTRHKG**GGH**KHH**YRVVDFKRN  
DKDGIAAKVERLEYPDNRSANIALVLFADGERRYIATKGMVAGQALMNGSEAPIKAGNNLPINIPVGT  
TINNVEILPGKAQVARAAGGSAVLLAREGLYAQVRLRSGEVRRV**HIE**CRATIGEV**GN**E**HEH**SLRVIGKAG  
ATRWGRIRPTVRGVMM**PVDHPHGGEGE**GKTAAGRDPVSPWGT**PAKGYR**TRSNKRTDSMIVQRRHKR

>KWW36057.1 30S ribosomal protein S9 (Cupriavidus metallidurans)  
MIGNWNYGTGRRKSAVARVFIKSGKGDIVNGKPIKEYFARETSLMIVRQ**PLELTAHAETFD**IKVNVTTGG  
GETGQAGAVRHGITRALIDYD**ATL**KPTLSKAGYVTRDAREVERKKVGLHKARRRKQFSKR

>KWW39976.1 30S ribosomal protein S17 (Cupriavidus metallidurans)  
MTEAAKTETSLRRTLVRGVVSDKMDKTVTVLIENRV**KHPL**YGYVLRSKKY**HAHDE**ANQYKEGDKVEIQE  
TRPLSR**TKS**WVVSRLVEAARVI

>KWW36616.1 30S ribosomal protein S15 (Cupriavidus metallidurans)  
MATANTNKSEIIAKFARGTNDTGSPEVQVALLTRINEL**TPHF**KANMK**DHHS**RRGLLRMVSRRLRLDYL  
KASADRYRALIEALGLRK

>KWW37010.1 30S ribosomal protein S2 (Cupriavidus metallidurans)  
MSVTMREMLEAG**CHF**GHQTRFWNPKMAPFIF**GRN**KI**HI**INLEKTLPMFQDALKYVRQLAANRGTVLVFG  
TKRQSREILAAEEAGRAGMPYVDARWLGGMLTNFKTVKISIKRLKDMEAAKEAGALETMSKKEALMFEREM  
EKLEKSIGGIKDMGGIPDAIFVV**DVGYH**KIAVTEANKLGIPIVIGVV**DTNHS**PEGIDYVIPGNDSSKAVA  
LYVRGVADAIILEGRANAVQEVVEAARGDDEFVEVQEG

**Fig. 19.3** Amino acid sequence of metal-binding ribosomal proteins in *C. metallidurans*. The amino acid of some ribosomal proteins from *C. metallidurans* is shown. Motifs found during the search in bold, site involved in binding in red. These were identified in the respective structures of the orthologs in *E. coli* (Fischer et al. 2015). Underlined are zinc-binding ribosomal proteins (Herzberg et al. 2014b)

zinc-buffering capacity of the ribosome, so that ribosomal zinc-binding sites do not compete with zinc-binding sites in just translated proteins. As a second step, ribosome hibernation occurs, growth is retarded and the cells may enter a persist state.

The large binding capacity for metal cations to the cell provided by cytoplasmic proteins may allow general cation flows and serves as binding sites for pre-discriminated transition metal cations to keep them apart from compounds, protein sites, or biochemical reactions that are sensitive to an inhibitory action of a transition metal cation. Examples would be a disturbance of redox homeostasis by binding of the metal cations to glutathione or other thiols, formation of ZnATP (lg ( $K$ ) = 4.8), CoATP (4.71), NiATP (4.54) instead of MgATP (4.58), binding to tri- or dicarboxy acids of the TCA cycle such as zinc citrate (6.2), zinc oxalate (4.9) or zinc

succinate (1.8) (Weast 1984), to DNA or RNA, to inactive reaction centers that are Mg-dependent such as transcription, sensitive iron-containing important enzymes such as aconitase or lipoamide-dependent reactions such as in 2-oxoglutarate or pyruvate dehydrogenase complexes.

As shown with the drastic example of *E. coli* cells overwhelmed by a huge content of copper ions stemming from metallic copper surfaces in the direct vicinity (Bleichert et al. 2021), the cells are dead when their metal-binding capacity is completely filled with transition metal cations. It is the task of the metal transportome to supply the required metals to the cell, to adjust their concentration so that sufficient metal-binding capacity is left to allow cation fluids and to keep transition metal cations from binding to “wrong” sites and substances, and also to arrange the composition of the transition metal mélange to minimize negative inference between the various cations. The transport proteins of the transportome (Nies 2016) are thus at the beginning of the sorting and discriminating flow of cations through the cell, and in case of efflux system also at its end.

In summary, the proteome of *C. metallidurans* contains a huge number of possible metal-binding sites, from small “flow-sites” with an Asp or Glu in combination with a His up to big sites with dozens of Asp, Glu, His, or Cys residues. The small sites may allow a current of pre-discriminated metal cations in crowded areas by the formation of transient contact ion pairs. The metal current connects the more elaborated metal-binding sites that may serve as nodes in the metal allocation and discrimination process, or sequester transition metal cations away from sensitive biochemical processes.

## 19.3 The Transition Metal Transportome

### 19.3.1 *Constraints: Energetics, Flow Equilibrium, Rate Versus Affinity*

To further understand transition metal homeostasis on the chemical basis as described above, three concepts should be considered which describe different aspects of the process: (i) the transition metal transportome; (ii) the zinc repository interacting with the transportome; (iii) and the possible setting of preferences in transition metal homeostasis with “iron first.”

The transition metal transportome is the totality of all metal uptake and efflux systems of the cell (Nies 2016). In a kinetical flow equilibrium of import and export reactions (Legatzki et al. 2003b), the composition of the cellular transition metal cation mélange is adjusted and the concentration of the individual metals controlled so that sufficient metals are present to fulfill their essential function but not too much metal is present because of the necessity to avoid toxic effects. The transportome interacts with the metal-binding capacity of the cell and is also part of it. In general, the concentration of essential-but-toxic metals of the first transition period is kept at

an optimum cellular amount whereas toxic-only metals are removed when their concentration increases above a toxicity threshold. That way, the transportome is the part of the cellular ion current that connects the interior of the cell to the outside.

Metal cations as charged ions cannot diffuse through the hydrophobic core of the bacterial inner or outer membrane. Exceptions are neutral metal compounds with a very small difference between the electronegativity of the cation and its ligands such as di-methyl mercury or even mercury di-chloride. All other metals need a carrier-mediated process to allow passage through these membranes. Carriers are often integral membrane proteins, organized as beta barrels in the outer membrane and transmembrane alpha-helices in the inner membrane. Additionally, smaller molecules may serve as carriers too, binding a metal at one side, passing that metal through the membrane by diffusion or a transport protein, and releasing the metal on the opposite side of the membrane. Carrier-mediated transport is the general rule for transport processes involving transition metal cations.

Carrier-mediated transport processes could be driven solely by the concentration gradient between the compartments on either side of the membrane. The energy of the concentration difference is  $\Delta G = -RT \ln(c_i/c_o)$  with R (general gas constant, 8.3141 J/mol·K), T (absolute temperature, e.g., 303 K = 30 °C),  $c_i$  concentration inside and  $c_o$  concentration outside a compartment. A concentration difference of  $c_i/c_o = 10$  thus represents an energy of  $-5.8$  kJ/mol, meaning,  $+5.8$  kJ/mol are needed to create such a concentration gradient or  $-5.8$  kJ/mol can be used to transport the gradient-forming substance in the direction that decreases the concentration difference. A difference of  $c_i/c_o = 100$  represents  $-11.6$  kJ/mol, 1000 represents  $-17.4$  kJ/mol and so on. Since the number of carriers in a given system is limited, all kinds of carrier-mediated transport processes show substrate saturation while simple diffusion processes are not limited by substrate saturation, however, until substrate saturation is reached, the transport rate of carrier-mediated transport processes is much higher than that obtained by simple diffusion. Carrier-mediated transport processes that are driven only by a concentration difference and no other driving force are designated “facilitated diffusion.” This process is used to transport metal cations through general porin proteins of the outer membrane {further explained in (Nies 2014)}.

The cytoplasmic or inner membrane of bacterial cells carries a proton motif force (pmf) of about 200 mV in aerobically respiring bacteria. The pmf is composed of a charge difference between inside and outside plus the concentration difference of the protons,  $\Delta pH$  with a negative charge inside, and a positive charge outside of the cytoplasm. Transport of metal cations interferes with this pmf. Import of a cation decreases the charge difference of the pmf and is thus driven by the pmf, export of a cation from the cytoplasm is against the charge gradient of the pmf and an endergonic process. This can be described by  $\Delta G = -nF \cdot \Delta E$  with  $\Delta E$  being the charge difference, F the Faraday constant (96,484 J/mol C, the charge of one mol electrons) and n the charge that is transported. Since  $\Delta G = -n F \Delta E$  and  $\Delta G = -R T \ln(K)$ ,  $-n F \Delta E = -R T \ln(K)$  and consequently  $\Delta E = (R T/n F) \ln(K)$  {further explained in (Nies 2014)}.

For this reason, the transport of a cation across the pmf-carrying inner membrane can never be by a facilitated diffusion. Transport processes depending on a concentration gradient and additionally another energy source are designated “active transport processes.” They are a sub-category of carrier-mediated transport processes and show as such substrate saturation. In contrast to facilitated diffusion, active transport processes are able to increase concentration differences to accumulate a given substrate in one compartment or, alternatively, to decrease its concentration. Active transport processes can be sub-grouped on the next level into primary and secondary active transport processes. Secondary transport processes use one (driving) concentration gradient to create a concentration gradient of another substance. For instance, the pmf or a sodium gradient can be driving gradients on the one hand but a pmf can also be used to build a sodium gradient and vice versa. If the substance associated to the driving gradient is transported in the same direction as the substance associated with the secondary gradient, the secondary active transport process is a symport. If both substances are transported into opposite directions, the transport process is an antiport. In the case of a uniport, the secondary concentration gradient is created just by the charge portion of the pmf. Only the driven substrate is transported and decreases the charge gradient. A lot of cations are just driven by uniport, which is very often confused with facilitated diffusion. Uniport is the active transport of a charged ion and is driven by the charge gradient part of the pmf. Facilitated diffusion occurs when either the substrate is not charged or no pmf or other charged gradient exists, and if no other energy transformation is coupled to the transport process {further explained in (Nies 2014)}.

Primary active transport processes use another energy form than a driving gradient to produce a gradient. Driving forces can be absorbed light photons, cleavage of an energy-rich compound such as ATP, GTP or phosphoenol-pyruvate, even a simple exergonic decarboxylation, or an exergonic redox reaction. In a way, the respiratory chain is a redox reaction-driven primary active transport system that creates the pmf. The  $F_1F_0$ -ATPase working in the ATPase direction is an ATP-driven primary active transport system. The electron transport chain of photosynthetic bacteria is likewise a light-driven primary active transport reaction {further explained in (Nies 2014)}. Both, primary and secondary active transport systems are the most important constituents of the bacterial transition metal transportome (Nies 2016).

Not yet included in the energetics of transport reactions is the binding energy of a to-be-transported metal to a ligand and the energy that is released when the just-transported metal binds to metal-binding components after the transport process. Outside of the bacterial cell, metals may be constituents of minerals, bound to minerals, to negatively charged biogenic polymers such as in humus, or to phosphate. Phosphate is also the most important metal-binding substance of mineral salts media used for the cultivation of most bacteria (Nies 2016). When complex media are being used, the thiol-containing substances, however, are even more important complexing ingredients. Inside the cell, the transition metal cation may be bound to the putative metal-binding sites of the cytoplasmic proteins. Consequently, metals are not just transported from one side of the membrane to the other side but from a

complex on one side of the membrane to a complex on the other side, or simply the complete complex is transported.

Since metal uptake and efflux processes are usually both active transport processes, entropy is being released when a metal cation is first imported and subsequently exported. This entropy, however, is needed to over-compensate order or negentropy that is created by the import and export processes: the desired optimal concentration of a metal cation and the composition of the overall metal cation mélange. If the change of a concentration in the cytoplasm  $dc/dt = v_{in} - v_{out}$  and both transport reactions would follow Michaelis–Menten kinetics, a kinetical flow equilibrium would be reached if  $dc/dt = 0$  or  $v_{in} - v_{out} = 0$  or  $v_{in} = v_{out}$ . If the respective Michaelis–Menten equations are inserted,

$$v_{in} = v_{max-up} * c_o / (K_{up} + c_o) \text{ and } v_{out} = v_{max-ef} * c_i / (K_{ef} + c_i).$$

this transforms to.

$$v_{max-ef} * c_i / (K_{ef} + c_i) = v_{max-up} * c_o / (K_{up} + c_o). \quad (19.1)$$

Equation 19.1 can be transformed in a series of steps:

$$c_i / (K_{ef} + c_i) = v_{max-up} / v_{max-ef} * c_o / (K_{up} + c_o). \quad (19.2)$$

$$(K_{ef} + c_i) / c_i = v_{max-ef} / v_{max-up} * (K_{up} + c_o) / c_o. \quad (19.3)$$

$$K_{ef} / c_i + 1 = v_{max-ef} / v_{max-up} * (K_{up} / c_o + 1). \quad (19.4)$$

$$K_{ef} / c_i = v_{max-ef} / v_{max-up} * (K_{up} / c_o + 1) - 1. \quad (19.5)$$

$$c_i / K_{ef} = v_{max-up} / v_{max-ef} * [(K_{up} / c_o + 1) - 1]^{-1}. \quad (19.6)$$

$$c_i = K_{ef} * v_{max-up} / v_{max-ef} * [(K_{up} / c_o + 1) - 1]^{-1}. \quad (19.7)$$

Equation 19.7 means that the concentration inside the cell can be adjusted by three mechanisms (Legatzki et al. 2003b). First, the rate-limiting efflux system can be changed. An efflux system with a higher affinity (lower  $K_{ef}$ ) decreases  $c_i$ . Second, the rate-limiting uptake system should be adapted so that its  $K_{up}$  fits to  $c_o$ . Since the term “ $(K_{up}/c_o + 1) - 1$ ” is in the denominator, a value  $K_{up} \ll c_o$  would lead to a denominator approaching zero and consequently a  $c_i$  approaching infinite, meaning a complete loss of control of import, if such a condition is not prevented by a low  $v_{max-up}$  and sufficiently high  $v_{max-ef}$ . A low  $c_o$  requires a high-affinity uptake system with a low  $K_{up}$  and a high  $c_o$  value a low-affinity uptake system with a higher  $K_{up}$ . Third,  $c_i$  can be influenced by changing the  $v_{max-up}/v_{max-ef}$  ratio of the import and export systems (Legatzki et al. 2003b). This can be accomplished by changing such parameters as either the total number or the specific activity of already existing transport proteins.

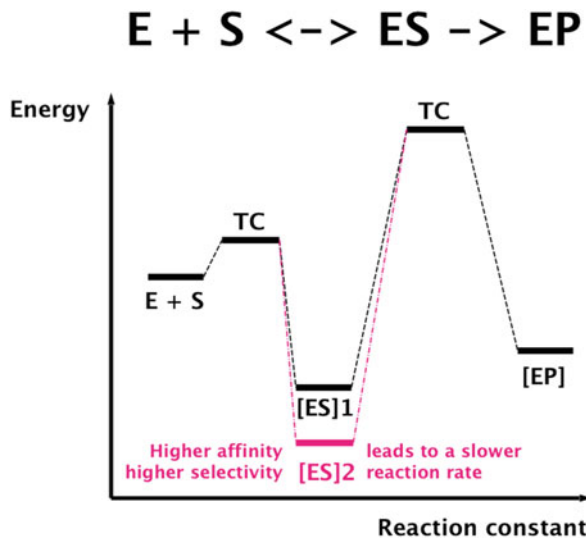


**Fig. 19.4** Selectivity and substrate affinity of biochemical reactions are antagonists of the reaction rate. TC, transition compound; ES, enzyme–substrate complex; EP, enzyme–product complex. Taken from (Nies 2016), published by the Royal Society for Chemistry. Enzymes that exhibit both high affinity and high selectivity have a comparatively slow reaction rate when compared with the faster reaction rates of enzymes that exhibit low affinity and low selectivity. Tighter binding of a substrate combined with high selectivity results in an [ES]2 complex that has an especially low energy in addition to being associated with a slower reaction rate. There consequently is a larger energetic difference and a greater energetic barrier that must be overcome between [ES]2 and the transition state. On the other hand, a lower substrate affinity and selectivity means a smaller energetic difference between the [ES]1 complex and the transition state. According to Boltzmann, the energetic barrier associated with a transition state determines the rate of substrate formation

In reality, many import systems with different kinetic parameters contribute to the overall uptake reaction but the efflux systems are assigned to one or a few substrates only. This results from a unique constraint important for enzymatic as well as transport reactions. Enzymes bind a substrate and catalyze the formation of a product (Fig. 19.4). The enzyme–substrate complex ES is a state of low energy but the enzyme product complex EP is separated from ES by the energetic barrier of the transition state between ES and EP. Tight binding of a substrate with high selectivity results in an especially low energy of the ES2 complex and consequently a large energetic difference between ES2 and the energetic barrier of the transition state. On the other hand, a lower substrate affinity and selectivity means a smaller energetic difference between the ES1 complex and the transition state. According to Boltzmann (Housecroft and Constable 2006), the energetic barrier of the transition state determines the rate of substrate formation. Consequently, high affinity and selectivity enzymes have a comparable low reaction rate whereas low affinity and selectivity systems exhibit a higher reaction rate per enzyme.

The same rules apply to transport systems since the transition state is the actual transport process through the biological membrane. Consequently, metals can be

transported by either high-rate low-selectivity or low-rate high-selectivity transport systems. According to Eq. 19.7, high-rate low-selectivity systems would allow controlled import of substrates at high external substrate concentrations and low-rate high-selectivity systems at low external concentrations. In case of transition metal cations with similar ionic diameters, an exact discrimination of an individual transition metal cation by a transport system would require the formation of a discriminating and specific metal complex as ES complex. This would create an extremely large energetic barrier for the actual transport process and a very low transport rate. The barrier can be lowered by coupling the transport process with an exergonic reaction. This means that discriminating and metal-specific transport processes must be primary active systems, which are energy-expensive and should be only produced by the cell when needed.

Alternatively, metal transport systems with a low degree of discrimination would transport a bunch of transition metal cations with similar ionic diameters as active secondary transporters with a much lower expense of energy. The task of discrimination needs to be accomplished after such a low-selectivity process, and also the task of controlling the concentration of a specific metal cation, which is performed by efflux of surplus transition metal cations. When, however, the total  $v_{\max\text{-ef}}$  of the efflux reaction for a given metal cation becomes too low, the denominator of Eq. 19.7 would be decreased to zero and the equation approaches infinite, as in case of  $K_{\text{up}} \ll c_0$ . In both cases, the cell then would become overcrowded with the metal. The  $v_{\max\text{-ef}}$  is the product of the number of mono- or multimeric transport systems per cell multiplied with the transport rate of each protein or protein complex. Increasing its selectivity would decrease the turn-over number and increase the number of proteins per cell needed to reach a sufficient  $v_{\max\text{-ef}}$ . Since protein synthesis is an energy-expensive process, the turn-over-number of an efflux system must be sufficiently high to allow an energy-efficient overall efflux process, meaning that the substrate selectivity of efflux systems cannot be too high.

In summary, metal cation uptake systems are in many cases high-rate low-selectivity secondary active transporters that provide with a high rate a mélange of pre-discriminated metals to the cell at a low energetic cost. These systems allow efficient and controlled metal import at high external substrate concentrations. In many bacteria, low-rate high-selectivity primary active transport systems, which are energy-intensive transporters, give additional support in conditions of low metal availability. Metal efflux systems adjust the cellular metal mélange by removing surplus essential-but-toxic ions and potentially a selective removal of toxic-only ions.

### 19.3.2 Control

Efflux systems presumably are required to remove specifically one transition metal cation to control its concentration and thus favorably improve the overall transition metal cation mélange, however, they cannot increase their substrate specificity too



much because this would lower the transport rate. This apparent contradiction can be solved by delegating the task of metal discrimination to regulators of gene expression. These regulators are able to bind a specific metal cation with a high selectivity and subsequently use this information to control the expression of the gene for the efflux system (Waldron et al. 2009). Consequently, the selective efflux system proteins are only synthesized when the concentration of a given metal is high enough. In this case, transport of alternative substrates by components of the efflux system that have rather broad substrate ranges could be competitively inhibited by the metallic substrate that induced synthesis of the selective efflux system. This is a very elegant solution to the contradiction between the required transport range and substrate selectivity of efflux systems. Genes for transition metal efflux systems of the inner membrane are very often controlled by transcriptional regulators belonging to the MerR or ArsR/CadC protein families (Helmann et al. 2007; Hobman et al. 2007; Tottey et al. 2007). Genes for transenvelope efflux systems that export cations from the periplasm to the outside are very often controlled by two-component systems composed of either a membrane-bound histidine kinase sensor protein plus a cytoplasmic response regulator (Nies and Brown 1998; Affandi et al. 2016; Gudipaty and McEvoy 2014; Choi et al. 2009; Yamamoto et al. 2005), or by sigma factors belonging to the extracytoplasmic function (ECF) sigma factor family (Staron et al. 2009; Helmann 2002; Lonetto et al. 1994; Große et al. 2019; Egler et al. 2005).

Regulation of the expression of import systems follows a different rule. Here, high-rate, low-selectivity secondary active transport systems supply a range of pre-discriminated transition metal cations to the cell, leaving the task of discrimination and concentration control to the cytoplasmic factors and efflux system. This seems to be a very efficient mode of supplying transition metal cations to the cell. Low-rate, high-selectivity primary active transport systems are only needed when the cell is threatened by metal starvation. They may provide already discriminated metals. Regulators that control the expression of these systems should become activated by sensing a much lower cytoplasmic availability of a target metal than is required for expression of the corresponding efflux systems. Often, these regulators belong to the Fur (ferric uptake regulator) family of proteins (Hantke 1987; Fontenot et al. 2020; Hobman et al. 2007; Helmann et al. 2007).

Expression of a gene to produce a protein takes a few minutes (Thieme et al. 2008) and removal of a protein may take even longer. Such a process may be too slow to respond to a rapid change in the concentration of a metal in the cellular environment. In addition to control of transcription or degradation, a quick response mechanism is needed. This is accomplished by flux control (Nies 2007b). Binding of a primary substrate to cytoplasmic binding sites of an uptake system decreases the import rate when sufficient metal resides inside the cell. Additionally, binding of a primary substrate to the cytoplasmic site of an efflux system of the inner membrane or periplasmic sites of a transenvelope efflux system increases the export rate. These sites also accumulate the substrate in the vicinity of the efflux system and contribute to substrate selectivity.

**Table 19.6** Metal content of *C. metallidurans* CH34 cells cultivated in non-complexing mineral salts medium with only trace concentrations of transition metal cations<sup>a</sup>

Metal ion	Atoms per CH34 cell	Examples
Mg(II)	13,700,000	Counterion for ATP, nucleic acids and protein
Ca(II)	875,000	Cell wall and membranes
Mn(II)	993	Not used in <i>C. metallidurans</i>
Fe(II/III)	537,000	FeS-centers and cytochromes
Co(II)	3970	B12-dependent reactions
Ni(II)	10,800	Hydrogenase, urease
Cu(I/II)	60,700	Cytochrome oxidase, periplasmic CuZn SOD
Zn(II)	90,900	RNA polymerase
Cd(II)	221	Toxic only in <i>C. metallidurans</i>
K(I)	33,500,000	Osmoregulation
Na(I)	96,200,000	Gradients, major counterion of the cell

<sup>a</sup>Taken from (Kirsten et al. 2011)

A transition metal cation may enter the cell through a high-rate, low-selectivity secondary active import system. Inside, it enters the huge pool of possible metal-binding sites of the cellular proteins and will be passed along following a thermodynamic gradient to a higher number and quality (Cys > His > Asp, Glu) of ligands. This process may also be used for discrimination and allocation of Zn(II), Co(II), and Ni(II), after Fe(II) and Cu(I) have been removed up-front as outlined in an introductory chapter of this book (“Chemical constraints for transition metal cation allocation” by author Dietrich H. Nies). The metal-binding sites of regulators needed for flux control, and the substrate-binding sites of the efflux systems, are also part of the overall pool of cellular metal-binding sites. But they are located at different positions in the thermodynamic gradient used for discrimination and allocation (Banci et al. 2010). Starting with the smallest binding energy, smallest number, and quality of ligands, sites in regulators for efflux gene expression should come first, followed by sites involved in flux control of the efflux systems, the substrate-binding sites of efflux systems, sites involved in flux control of high-rate, low specificity secondary active uptake systems, and finally sites in regulators for the expression of genes for low-rate, high specificity primary uptake systems.

The outcome of the action of the transition metal transportome is the cellular metal composition found under “standard” conditions, meaning that which is achieved during cultivation in non-complexing mineral salts medium without added metals except for the supplemental presence of a trace element solution (Table 19.6). The transition metal cations with the highest number per cell are iron and zinc. The zinc content is kept between 20,000 Zn(II) per cell, which seems to be the lowest possible level that allows growth, and 120,000 Zn(II) per cell. Above this number per cell, the efflux systems for zinc remove additional zinc ions. In a deletion mutant of *C. metallidurans* without these efflux systems, the zinc content increases to about 250,000 Zn(II) cell at low  $\mu\text{M}$  zinc concentration and cellular growth is impaired (Herzberg et al. 2014b). The total metal-binding capacity of the cell with

5.77 million possible cations bound can thus only accommodate a maximum of 250,000 Zn(II) before it spills over and zinc can no longer be kept from binding to “wrong” sites.

The number of Cu(I/II) follows that of Zn(II), however, copper ions seem to be used only in sites located in the periplasm (Changela et al. 2003; O’Halloran and Culotta 2000). The intracellular numbers of Ni(II) and Co(II) are very low, probably to avoid interference with iron and zinc homeostasis. The following sections of this chapter describe which transport systems are involved in maintaining the cellular transition metal mélange and which metal-binding sites contribute to this process.

In summary, since tight substrate binding and discrimination by an efflux system would decrease its transport rate, the substrate-specificity of metal efflux systems remains rather broad. They are assigned to their tasks by regulators of gene expression, which can perform the tedious task of substrate discrimination without interfering with the transport rate. Moreover, while regulation of gene expression takes minutes, flux control of the activity of the transport protein can occur much more rapidly.

### 19.3.3 *Import Across the Outer Membrane*

Import of metal cations in a Gram-negative bacterium such as *C. metallidurans* requires as a first step import across the outer membrane. The outer membrane contains beta-barrel-shaped trimeric porins that allow passage for a number of substances by facilitated diffusion. Since this is no barrier for protons, no proton motif force exists across the outer membrane. Nevertheless, active transport across the outer membrane is possible. A complex composed of the proteins ExbB, ExbD, and TonB uses the energy of the pmf to obtain an energy-rich conformation of the TonB protein, which reaches across the periplasmic space and makes contact with the “plug”-domain of a TonB-dependent outer membrane receptor protein. Relaxation of the energy-rich conformation of TonB is coupled to the transport of a substrate through the outer membrane receptor from the outside to the periplasm (Braun 1995; Koebnik et al. 2000; Mazzon et al. 2014; Noinaj et al. 2010; Higgs et al. 1998).

TonB-dependent outer membrane receptors are involved in the import of large compounds that do not diffuse through the porins, or of compounds with low availability. Such large compounds are for instance cobalamin derivatives, siderophores, or other metal-complexing compounds (Bobrov et al. 2014; Braun and Braun 2002; Coulton et al. 1986; Hantke 1983; Schauer et al. 2007; Schauer et al. 2008). Siderophores as Fe(III)-complexing substances are required for an efficient import of iron since the solubility of Fe(III)-hydroxide complexes at a neutral pH value is close to zero (Weast 1984). TonB-dependent outer membrane receptors usually interact with low-rate, high affinity primary active transport systems of the inner membrane, which transport the already discriminated substance or metal further on from the periplasm to the cytoplasm.

**Table 19.7** Porins and TonB-dependent receptor proteins identified in the proteome of *C. metallidurans*<sup>a</sup>

Rmet	ProtNum	Gene	Total
<b>TonB-dependent receptor proteins</b>			
Rmet_2789	535	<i>btuB</i>	HXE-EX3H-DHXE-DX3H-DHX2D-HX3D
<b>Rmet_1118</b>	209	<i>yncD</i>	DX3HXE-DX2H-DX2HX3D-HXD-EHXD-HX3E-DHE
Rmet_3055	112	–	HX2E-EHD
Rmet_4565	91	<i>cirA</i>	HXE-HXD
<b>Rmet_5373</b>	72	<i>fepA</i>	EX2H-EXH-DHXE-HXD-DXHXE- <b>HDXDX3H-EXHX3DH</b> -HX2D
<b>Rmet_2277</b>	44	–	<b>CHXD</b> -EX2C-DEX2H
<b>Rmet_0837</b>	20	<i>fu</i>	DHXDDD-EXH-DXH-DHXD-DX2H
Rmet_5806	19	<i>fecA</i>	X2HX2H- <b>HX2DXH</b> -HXD-HX2D-EX3HXD-HX3E
<b>Porins</b>			
Rmet_3704	932	–	EX3H-CX2E-CXE-HX3D
Rmet_3234	792	–	<b>H2X2D</b> -EX3H-HX3E
Rmet_5288	180	–	<b>CXC</b> -EX3H
Rmet_4834	61	–	EX3H-DXHE
Rmet_4991	37	–	EX3H-DXH

<sup>a</sup>**Bold faced Rmet number:** respective gene up-regulated in the presence of EDTA (Herzberg et al. 2015); **bold-faced motif:** more than one H or C. Protein numbers per cell taken from (Herzberg et al. 2014b)

The genome of *C. metallidurans* contains the genes for 21 TonB-dependent outer membrane proteins and 31 porins with 18 of those porins possessing metal-binding motifs. Eight of those TonB-dependent proteins and 10 of those porins have been quantified in the proteome with 5 of the porins known to be carrying metal-binding motifs (Table 19.7). Half of the porins but all TonB-dependent proteins thus carry metal-binding motifs. Among the TonB-dependent proteins, BtuB is involved in the import of cobalamin-like compounds, the other proteins probably in the import of various siderophores. The metal-binding motifs are mostly flow sites with only one His or Cys adjacent to an Asp or Glu. Five sites stand out. Double-His sites are in the siderophore-specific TonB-dependent proteins FepA and FecA that could be involved in the recognition of an iron-loaded siderophore against an empty or mis-loaded siderophore. Porin Rmet\_3234 also carries a HHXXD-site that may discriminate transition metal cations against other metal cations. The TonB-dependent receptor Rmet\_2277, up-regulated under conditions of metal starvation, contains a CHXD-site and the porin Rmet\_5288 contains a paired CXC site, which both may also discriminate transition metal cations. The function of these proteins is currently unknown.

In summary, half of the porins and all TonB-dependent outer membrane proteins, which connect the cellular periplasm with the outside, contain metal-binding motifs. These are in most cases small “flow sites” that allow a transient, His-stabilized direct ion pair between a transported metal cation and an Asp or Glu residue. The ion cellular ion current within the cell may thus start already at the outside.

### 19.3.4 Import Across the Inner or Cytoplasmic Membrane

Transition metal cations are usually imported into the cell across the cytoplasmic membrane by high-rate, low-affinity secondary active import systems. These importers include uniporters driven by the charge gradient that exists across the inner membrane, metal-proton symporters that reach a higher possible accumulation due to the additionally imported proton, and metal-phosphate symporters such as PitA (Harris et al. 2001). These high-rate, low-affinity systems provide a mélange of pre-discriminated transition metal cations to the cell, leaving the discrimination process to cytoplasmic components and the adjustment of the concentration of individual metals to the efflux systems (Fig. 19.5).

In addition to this very efficient mode of metal cation acquisition, low-rate, high-affinity primary and secondary transport systems are used in many bacterial strains under conditions of metal starvation. These systems belong to the family of ATP-binding cassette transport proteins that also are called the ABC system, each of which is composed of four modules, two of them membrane-bound and two

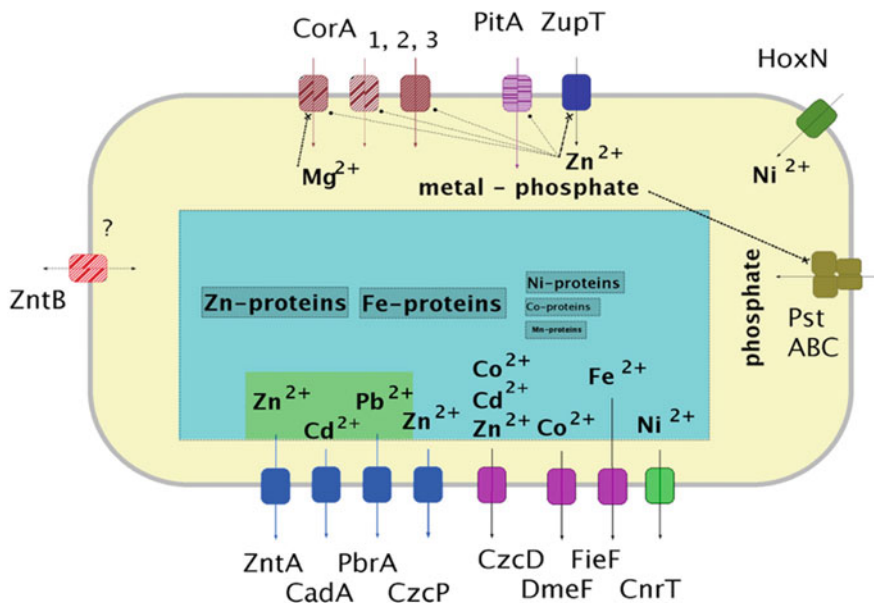


**Fig. 19.5** The metal cation transportome of *C. metallidurans*. Seven secondary, high-rate and low selectivity importers plus the primary Pst system for phosphate import are shown on the top, left and right side of the schematic cell. Only ZupT is influenced by zinc availability via the Zur regulator, CorA<sub>1</sub> by magnesium and Pst by phosphate availability (dashed line), the other systems are only weakly influenced (dotted lines). The two P-type importers for Mg/Ca are not shown. These supply metals to the cell, which move around in the stage shown in Fig. 19.2 to reach their metal-specific proteins (turquoise field). Surplus metals are removed by efflux systems, four P-type ATPases (blue), three CDF proteins (magenta) and CnrT (green) are from yet another protein family. Copper-exporting P-type ATPases are not shown. Details were reviewed recently (Nies 2016)

others that are ATP-binding modules associated with the membrane-bound components (Rice et al. 2014; Hantke 2005; Patzer and Hantke 1998; Fath and Kolter 1993; Higgins 1992). Depending on the individual transport system, all four modules either may reside as domains on one polypeptide chain, or be represented by individual polypeptide chains, or anything in-between these possibilities. The central ABC component can be upgraded by either a periplasmic adapter or membrane-fusion proteins in combination with outer membrane export proteins to form ABC-dependent transenvelope efflux systems, or by containing an energy-coupling device resulting in an ECF-ABC import system (Eitinger et al. 2011; Siche et al. 2010), or by interacting with a periplasmic substrate-binding component. In this latter case, the task of substrate discrimination is “outsourced” to the periplasmic component so that each import system relies on more than one substrate-binding site located in the periplasmic component. Since the substrate cation has already been discriminated in the periplasm, ABC importers may interact with cytoplasmic metal chaperones that keep the valuable metal cation in the discriminated state and forward it to its metal-depending enzyme.

*C. metallidurans* contains ABC import systems for cobalamin derivatives and siderophores but no ABC import system for zinc such as the ZnuABC importer in *E. coli* (Patzer and Hantke 1998). If iron cannot be imported as part of a siderophore compound and cobalt not as cobalamin, these metals as well as zinc and nickel have to rely on the high-rate, low-affinity secondary active transport systems. *C. metallidurans* possesses four members of the MIT protein family (CorA<sub>1</sub>, CorA<sub>2</sub>, CorA<sub>3</sub>, ZntB) which usually also import Mg(II) in case of either the CorAs, or ZupT of the ZIP protein family, HoxN of the nickel-cobalt-transporting NiCoT protein family, PitA for metal-phosphate import, the potential iron import systems FeoB and PbrT, plus additionally two primary active magnesium-importing P-type ATPases, MgtA and MgtB (Fig. 19.5, Table 19.8). *C. metallidurans* does not contain an Mn-importer of the NRAMP protein family (Garrick et al. 2006; Makui et al. 2000; Kehres et al. 2000) of metal-proton-symporters, which may be fortunate since these are also notorious cadmium importers, and that noted absence of a Mn-importer seems in agreement with the low Mn content of the *C. metallidurans* cell (Table 19.6) and the absence of an Mn-type superoxide dismutase (Roux and Coves 2002; Juhnke et al. 2002).

The four MIT proteins, PitA, ZupT, HoxN and the two P-type import ATPases are all involved in zinc uptake (Herzberg et al. 2016; Grosse et al. 2016; Herzberg et al. 2014a; Kirsten et al. 2011). None of them is essential for this process but with an increasing number of deletions, the cells are losing their fitness and metal tolerance, although efflux systems for all kinds of metal were still present in the mutant cells. This indicates quite clearly that the import systems for metals are also very important for metal homeostasis and interact closely with metal efflux systems in a flux-controlled kinetical flow equilibrium to accomplish the net process of metal ion management. This led to the concept of a transition metal transportome as the totality of all transition metal cation uptake and efflux system (Nies 2016), which together create transition metal homeostasis as an emergent feature. The transportome is the first pillar of metal homeostasis.

**Table 19.8** Metal import systems in *C. metallidurans*<sup>a</sup>

Rmet	ProtNum	Gene	Total
Rmet_3052	117	<i>corA1</i>	EX3H-EDEX2HX3D-HDED-EXH
Rmet_0036	38	<i>corA2</i>	<b>HX2C</b> -EXH-EXH-EXCEED-DX2HDE-HED-EX3H
Rmet_3287	37	<i>corA3</i>	HX2D-DXHX2D-DX2HX2D-EXC-EHX2EE
Rmet_0549	NeF	<i>zntB</i>	<b>HXH-HX2CE-HXDH</b> -DX3HX3D-DHXH
Rmet_2621	NeF	<i>zupT</i>	EX3H-HX3E- <b>HXH3EXDXH5XHD</b> -DX2HX3D- <b>HEXHXHXH</b>
Rmet_1973	NeF	<i>pitA</i>	<b>H2</b> -HX3D-CXE
Rmet_1533	NeF	<i>hoxN</i>	<b>HX2DXDH</b> -HDE- <b>HX2H</b>
Rmet_5396	NeF	<i>mgtA</i>	EEX3H-CXD-CXD- <b>EHCDDH</b> -ECHE-ECX2E-EXHE-HX3DE-HX2E
Rmet_2211	51	<i>mgtB</i>	<b>H2XE</b> -HX3D-HX2D-DX3HE-HX3D-CXD- <b>CX2HX2D-DXHX2DX2HC</b> -CXD-DDX3HXE- <b>EHX3EX3HX2D-H2DXDH-ECH2</b> -DXHE-HX3E-EXC-CX2E
Rmet_5890	100	<i>feoB</i>	EXC-DXHXE-EX3HX3E- <b>DHXEH</b>
Rmet_5945	#NV	<i>pbrT</i>	DXHX3E- <b>CX2CH</b> -HXD-DHE-EX2HE
<u>Regulators of uptake</u>			
Rmet_2976	1706	<i>furA</i>	EX2HX3 <b>ED</b> -EHXD-EX2 <b>HHDHX2CXDCX3EE-CX2DDCXH</b>
Rmet_5746	23	<i>furB</i>	HX2E-EX2HX3 <b>ED-HX2EXDXH3EX2EX2HHDHX2CXECX3EE-CXDC</b>
Rmet_0128	77	<i>zur</i>	<b>CX2EX2EX3H</b> -DXHX3E-EHE-EXHX2HXHX <b>CX2CDX3CXE-EHXE-CXECX3HXDX3H/</b>

<sup>a</sup>Some of the proteins were never found (NeF) in the proteome of *C. metallidurans* strain AE104 (Herzberg et al. 2014b), which is plasmid-free (Mergeay et al. 1985), although they are encoded by chromosomal or chromid genes. Others could not be found (#NV) because they are plasmid-encoded genes. **Bold-faced** motifs contain more than one His or Cys residue, sites in red complex the structural zinc in Zur-type proteins or FeS-site in Fur-type proteins. Green and blue residues indicate components of additional zinc-binding sites. A “/” indicates the C-terminus of the protein

All import proteins contain metal-binding motifs (Table 19.8). MIT family members (CorAs, ZntB) form homo-pentamers. Each protomer begins with a large amino-terminal part that is located at the cytoplasmic face of the inner membrane, followed by two transmembrane alpha-helices (Eshaghi et al. 2006; Guskov et al. 2012; Kean et al. 2008; Lunin et al. 2006; Papp-Wallace et al. 2008; Pfoh et al. 2012). With the exception of the terminal EX3H and DHXH motifs of CorA2 and ZntB, respectively, which are located in the periplasm between the two transmembrane spans, all metal-binding motifs are located in the cytoplasmic amino-terminal domain. This part of the protein is supposed to contain metal-binding sites involved in flux control (Eshaghi et al. 2006; Nordin et al. 2013; Pfoh et al. 2012), which involves a DX2DH motif in CorA from *Thermotoga maritima* (Nordin et al. 2013). With exception of a HXXC motif of CorA<sub>2</sub>, all motifs in the CorAs may be flow sites for metal cations; however, these sites are different between the three CorAs. In *C. metallidurans*, the copy numbers of CorA<sub>1</sub>:CorA<sub>2</sub>:CorA<sub>3</sub> are in a 3:1:1 ratio (Herzberg et al. 2016; Grosse et al. 2016) leading to the speculation that the CorA pentamer in this bacterium could be in fact a hetero- instead of a homo-pentamer. All three CorAs are involved in cobalt import but only CorA<sub>1</sub> and CorA<sub>3</sub> are connected

to cobalt toxicity while CorA<sub>1</sub> and CorA<sub>2</sub> are involved in nickel import (Herzberg et al. 2016). Only CorA<sub>1</sub> is regulated by magnesium availability (Kirsten et al. 2011).

A major flux control of a hypothetical CorA<sub>1,1,1,2,3</sub> heteropentamer by magnesium via CorA<sub>1</sub> with minor flux control contributions by nickel via CorA<sub>2</sub> and by cobalt via CorA<sub>3</sub> would explain the results obtained by mutant studies (Herzberg et al. 2016). CorA<sub>1</sub> contains only four metal-binding motifs but CorA<sub>2</sub> contains 7 with one HX2C at the amino-terminal part and CorA<sub>3</sub> five sites including an EXC (Table 19.8). This would link these possible metal-binding sites to the function of being an importer that is flux-controlled by nickel or by cobalt, respectively, for CorA<sub>2</sub> and CorA<sub>3</sub>. The HX2C and EXC sites in CorA<sub>2</sub> and CorA<sub>3</sub>, respectively, are noticeable and indicate an affinity for a transition metal cation rather than for Mg (II) (Table 19.8).

The MIT protein ZntB of *C. metallidurans* is a zinc importer (Herzberg et al. 2016) and not a zinc efflux system (Tan et al. 2009; Wan et al. 2011; Worlock and Smith 2002). In agreement with this function, ZntB contains sites that may be involved in transition metal binding rather than serving as mere flow sites. ZntB has a DPH motif in the periplasmic part between the two transmembrane alpha-helices that are not conserved between ZntB and the three CorAs. This motif stands out as a possible periplasmic zinc-binding site of ZntB. Moreover, with the exception of the HX2C of CorA<sub>2</sub>, there is neither a motif with a paired His-His nor a His-Cys motif in the other CorAs. ZntB contains a HXH, a HX2CE instead of the EXC of CorA<sub>2</sub>/CorA<sub>3</sub>, a HXDH and the mentioned DPH motif (Table 19.8), which all might be involved in zinc uptake or zinc-dependent flux control. Nevertheless, neither the three CorAs nor ZntB nor all four systems are essential for the import of zinc into *C. metallidurans* cells (Herzberg et al. 2016).

Due to either the ionic strength of growth media or the inside of cells, Mg (II) phosphate and the phosphates of divalent transition metal cations are present in a state between a solvent-shared and a contact ion-pair. The PitA import system consequently imports a divalent metal cation – tri-phosphate pair as proton-symporter (McCarthy et al. 2014; Jackson et al. 2008; Harris et al. 2001; Beard et al. 2000; Herzberg et al. 2016; Grosse et al. 2016). PitA has a paired His close to the amino terminus and a CXE instead of the EXC of CorA<sub>2</sub>/CorA<sub>3</sub>.

The HoxN (High-affinity nickel transport) protein is encoded by a gene of an autotrophic genomic island in *C. metallidurans*, which is needed to synthesize both a soluble nickel-containing hydrogenase and the enzymes of the Calvin cycle (Herzberg et al. 2015). The HoxN protein supplies nickel both to this hydrogenase and also to a second, membrane-bound enzyme (Eitinger et al. 2005; Eitinger et al. 1997; Eitinger and Friedrich 1994; Wolfram et al. 1991; Eitinger and Friedrich 1991; Eberz et al. 1989; Herzberg et al. 2015). Due to the expected low substrate affinity of these importers, HoxN can also be recruited as a zinc importer (Grosse et al. 2016). HoxN contains one motif with three His, one with two His, and sufficient adjacent Asp or Glu residues to form a nickel-specific binding site (Trepreau et al. 2014) without preventing import of Co(II) or Zn(II) (Table 19.8). All sites are located in cytoplasmic parts of the protein, the first motif at the N-terminus, the others between



the first and second pairs of transmembrane alpha-helices. Two additional import systems, FeoB and PbrT, may be involved in the uptake of ionic iron.

Two P-type ATPases of the Mg/Ca transporter group are also involved in zinc transport (Herzberg et al. 2016; Grosse et al. 2016). MgtB was found in the proteome, although MgtA was not (Herzberg et al. 2014b). MgtA contains besides putative flow sites plus an EDCDH motif (Table 19.8) located in the nucleotide-binding domain of the protein (Kühlbrandt 2004), one residue downstream of the nucleotide-binding KGAX<sub>3</sub>I. MgtA and MgtB contain two CXD sites, the aspartate of the first of these domains is the strictly conserved residue that is phosphorylated during the catalytic cycle (Table 19.8). MgtB additionally contains 6 metal-binding motifs, an HHTE at the N-terminus and five Cys- and His-rich stretches in the nucleotide-binding domains. This indicates that MgtB may not only be an Mg(II)/Ca (II) transporter with some activity for transition metal cations, but it may also be flux-controlled in its activity by transition metal cations. There is more to MgtB than visible from the currently available data.

ZupT of the ZIP protein family is special (Herzberg et al. 2014b; Herzberg et al. 2014a; Kirsten et al. 2011). ZupT proteins combine a broad substrate range with a high transport rate and are probably uniporters (Cerasi et al. 2014; Taudte and Grass 2010; Grass et al. 2002; Grass et al. 2005a). While expression of *zupT* in *E. coli* is constitutive (Grass et al. 2002), *zupT* in *C. metallidurans* is under the control of the zinc uptake regulator Zur (Kirsten et al. 2011; Bütof et al. 2019; Bütof et al. 2017; Schmidt et al. 2014). Deletion of *zupT* in *C. metallidurans* has no effect on zinc uptake at the first glance but strong pleiotropic effects at the second. In the absence of ZupT, even when sufficient zinc ions can be imported into the *C. metallidurans* cell, zinc cannot be efficiently allocated to zinc-dependent proteins such as the beta-prime subunit RpoC of the RNA polymerase (Herzberg et al. 2014a). ZupT thus provides Zn(II) directly to an efficient zinc allocation pathway while zinc imported by other transport systems cannot enter this pathway easily. The ZupT protein was not found in the proteome of *C. metallidurans*, probably due to a low copy number (Herzberg et al. 2014b).

ZupT has some long His-rich stretches HXHHHEXDXHHHHHXHD and HEXHXHXH (Table 19.8), which are located on the cytoplasmic part of the protein between the first and second pair of transmembrane alpha-helices. These metal-binding domains are probably involved in the discrimination of zinc, possible flux control, keeping zinc apart from glutathione, and could be the starting point for the efficient allocation of already discriminated zinc. It may interact with a cytoplasmic zinc chaperone to allocate zinc efficiently to zinc-depending proteins. Such a protein can be expected to possess metal-binding sites with a high number of His and Cys residues to remove Zn(II) from ZupT.

Iron and zinc uptake in *C. metallidurans* is regulated by three proteins of the Fur family of regulators. FurA is the main regulator for iron uptake, FurB regulates the uptake of divalent metal cations with a preference for iron, and Zur (formerly FurC) has involvement with uptake and homeostasis of Zn(II) (Schmidt et al. 2014). FurA and FurB contain two strong metal-binding motifs each, EX2HHDHX2CXDCX3EE plus CX2DDCXH and HX2EXDHX3EX2EX2HHDHX2CXECX3EE plus CXDC,

respectively. Zur contains a CX<sub>2</sub>EX<sub>2</sub>EX<sub>3</sub>H 44 residues downstream of the N-terminus, EXHX<sub>2</sub>HXHXHCX<sub>2</sub>CDX<sub>3</sub>CXE in the middle of the protein and CXECX<sub>3</sub>HXD<sub>3</sub>H/ at the C-terminus (Table 19.8). Fur-type proteins, even iron uptake regulators, usually contain a structurally important Zn(II) (Ma et al. 2011; Helmann et al. 2007; Baichoo and Helmann 2002; Gaballa and Helmann 1998). Since only zinc-bound Fur proteins were studied it was imagined that this tightly bound zinc was complexed by four Cys residues. This picture was recently turned upside down. Fontenot et al. identified that ability to insert iron–sulfur clusters into the Fur protein was the actual regulatory process (Fontenot et al. 2020). The 2Fe-2S-cluster was bound by the cysteine residues previously imagined as a tight zinc-binding site. Nevertheless, structural zinc ions are required but bound to a H, D, E, H and H, E, H, H ligand field, respectively (Fontenot et al. 2020).

All three sites are also conserved in Zur proteins. In the Zur-ortholog of *Mycobacterium tuberculosis*, these are D62-C76-H81-H83, H80-H82-E101, and H118 while the four ligands of the structural zinc site are C86-C89 and C126-C129; typical CX<sub>2</sub>X motifs (Lucarelli et al. 2007). In Zur from *C. metallidurans*, the His residues for the two additional sites are also located upstream of the first CX<sub>2</sub>C, but as a EXHX<sub>2</sub>HXHXH instead of an HHDH (Table 19.8). The new results leave many questions open. Do the CX<sub>2</sub>C sites of all Fur proteins receive 2Fe-2S clusters to signal enough iron but not enough zinc? Or do the occupation of the Cys-sites indicate sufficient zinc in the pool of already discriminated zinc within the cell? Does zinc stabilize the Cys sites of the Furs when the 2Fe-2S cluster is absent to indicate strong iron starvation or disturbance of FeS-clusters by zinc ions? The Fur and Zur proteins may be more than just iron and zinc uptake regulators.

In summary, *C. metallidurans* contains six uniporters, a metal phosphate proton symporter, two primary active, and at least one unknown importer for divalent cations including zinc. While none is essential for zinc import, stepwise loss of these 9 systems results in decreased cellular fitness and metal resistance despite the presence of metal efflux systems. This highlights the importance of the cooperation of metal uptake and efflux system for metal homeostasis, leading to the concept of the metal transportome as an emergent cellular feature. ZupT is under control of the zinc uptake regulator Zur and is required for efficient zinc allocation. All 9 uptake systems have metal-binding motifs, from simple “flow site” to a Cys/Glu-site for a possible identification of borderline transition metal cations up to two His-rich stretches of ZupT, which may constitute the portal node of the cytoplasmic zinc-allocating ion current.

### 19.3.5 Efflux Across the Inner Membrane

*C. metallidurans* contains more than a dozen inner membrane efflux systems for transition metal cations (Nies 2016), 8 P<sub>IB</sub>-type ATPases, 3 CDF proteins, and 2 exporters from other protein families (Table 19.9, Fig. 19.5). The 8 P<sub>IB</sub>-type ATPase are from three different groups of these proteins (Argüello et al. 2007),

**Table 19.9** Inner membrane efflux systems in *C. metallidurans*<sup>a</sup>

Rmet	ProtNum	Gene	Total
<u>P-type ATPases</u>			
Rmet_4594	396	<i>zntA</i>	<b>HX3HDHDXHX2DHXHDHXHEHXHXHXHDHDXHE-C2X3C-CX2EE-H2X2D-HX2E-CXC-CX3HX3HDX3C-EX2HE-DX2H-DX2HXH</b>
Rmet_2303	82	<i>cadA</i>	<b>CXC-CX2E-CX2EE-HXE-CX2EE-CX2EE-CX2EE-HX2D-DX2H-HX2E-HX2E-CXC-HX3E-HX3H-DX2H</b>
Rmet_5947	#NV	<i>pbrA</i>	X2EC-CXC-CX2EE-HX2DCX2EE-HX2HX2DX3H-HX3H-HX2E-HX2E-CXC-DDHX2HX3HX3EEX3CX2E-DXH-DX2H
Rmet_5970	#NV	<i>czcP</i>	CXE-EX2H-CXHXD-HXDHEHXEX3DHXHXEXEXHXHXH-HX2EH-EX2H-DDX2H
Rmet_3524	75	<i>cupA</i>	<b>EX3CX2C-CX2C-DX3HX3E-EX3HXDE-CXC-EX2H-HX2D-DX3H-HXE</b>
Rmet_6119	#NV	<i>copF</i>	<b>HEHX2H-DHDHX2DHX2HX3CD-EHD-CX3CH-CX2HXE-CX2C-EXC-HXHX2D-CXC-DX3HX3E</b>
Rmet_2379	NF/NF	<i>ctpA</i>	<b>CX2C-EXHX3E-CXC-CXE-HX3E-HX3H-EXH-CX2EE</b>
Rmet_2046	NF/NF	<i>rdxI</i>	<b>HCXHC-C2X2C-HX3D-EX3CX2C-EXH-DXHD-HX3D-CXC-HX2E-DHXE-EXH-CH</b>
<u>Chaperones</u>			
Rmet_3525	845	<i>cupC</i>	<b>HCEX2H2-EX2H-EX3CXHC</b>
<u>CDF proteins</u>			
Rmet_0198	NeF	<i>dmeF</i>	<b>DX2HXDCX3H-HXHX2D-DX2HX3H-HX2E-H2XHDHXHXHDHXHX2HXHDH2DHHXHXHXHX2HDDHXHXH2D-HX3D-DHX3EE-HXED-DXH-EX3C-HDEX2HX3EX3CDDX2DXHDXHX2HX2HXH/HXD-EX3HDE-DX2HX3D-H2X3D-DHX3HX3E-HX3D-HX2D-DXHXE-EX2H-HXD</b>
Rmet_3406	42	<i>fieF</i>	<b>HXHDH-DX2HX3D-HDXH-HX3D-DX2H-EX3CEX2DX3H</b>
Rmet_5979	#NV	<i>czcD</i>	
<u>Other efflux systems</u>			
Rmet_6144	#NV	<i>nreB</i>	HXC-HED
Rmet_6211	#NV	<i>cnrT</i>	<b>CXCX3D-HX2EXHEHEHXHEX2EHXHXHXHDEH2XHEHD-EXHXHXHXHEX3HXHXHX2DXH2HXHXH/</b>
<u>Regulators</u>			
Rmet_2302	NF/NF	<i>cadR</i>	DEXH-CX3D-EX2CXE-DXH
Rmet_3456	87	<i>zntR</i>	<b>EX3HX2CD-DXH-HC-CDD-EX2H-HXCE-HX3EC- EX3CECHX2H/</b>
Rmet_3523	246	<i>cupR</i>	HXE-DEX3H-HX2D-EXCX2DD- <b>CH2/</b>
Rmet_5946	#NV	<i>pbrR</i>	EEHXE- <b>HCX3D-CXE-DEH-EX2H2X2EX2EXC-CXCD- HX2D/</b>

<sup>a</sup>Some of the proteins were never found (NeF) in the proteome of *C. metallidurans* strain AE104 (Herzberg et al. 2014b), which is plasmid-free (Mergeay et al. 1985), although they are encoded by chromosomal or chromid genes. Others could not be found (#NV) because they are plasmid-encoded genes. “CPC” motif on a yellow field, strong metal-binding motifs in bold-faced letters, HMA motif (cd00371) underlined

four of them are P<sub>IB1</sub>-type Cu(I)/Ag(I)-, three are P<sub>IB2</sub>-type Zn(II)/Cd(II)/Pb(II)- and one is a P<sub>IB4</sub>-type Zn(II) exporter.

The three P<sub>IB2</sub>-type Zn(II)/Cd(II)/Pb(II)-exporter ZntA, CadA, and PbrA all export Zn(II) and Cd(II) in vitro with similar kinetical parameters (Scherer and Nies 2009). This, to some degree, broad substrate range may be required to keep

the transport rate high enough to compensate for the import rate of the individual substrates by the high-rate low-specificity import systems. All three systems are assigned to their respective physiological function by their individual MerR-type regulators of gene expression, ZntR, CadR, and PbrR (Borremans et al. 2001; Schulz et al. 2021). Control is exerted by the cytoplasmic concentration of the respective substrates. ZntA is also responsible for the efflux of Cd(II) while CadA is up-regulated when the removal rate of Cd(II) by ZntA is not sufficient (Legatzki et al. 2003a; Scherer and Nies 2009). All three systems substitute each other with respect to zinc and cadmium resistance. At least one of these three  $P_{IB2}$ -type ATPases is needed for full zinc and cadmium resistance. Other efflux systems, the  $P_{IB4}$ -type ATPase CzcP and the CDF protein CzcD, are not sufficient to mediate full resistance to these two ions. The three  $P_{IB2}$ -type ATPases may be able to remove especially zinc and cadmium ions bound tightly to “wrong” sites or already discriminated surplus zinc ions, which other efflux systems cannot reach (Scherer and Nies 2009).

All three  $P_{IB2}$ -type ATPases possess the typical CXC (yellow, as CPC) motif of  $P_{IB1}$ -/ $P_{IB2}$ -type ATPases (Table 19.9) (Argüello et al. 2007; Fagan and Saier 1994; Nies 2003). Despite the fact that they all transport Zn(II) and Cd(II) with equal ease in vitro, they differ remarkably in their metal-binding motifs. ZntA starts with a long His-rich stretch of 20 amino acids downstream of the amino terminus, followed by a triple-Cys site C2X3C (as CCGSAC) and an HMA motif (heavy-metal associated motif cd00371). Another metal-binding motif is located in a cytoplasmic domain upstream of the last pair of transmembrane alpha-helices. This provides a huge metal capacity to ZntA, which just barely did not make it among the top 15 metal-binding proteins (Table 19.2). The tasks of all these sites may be to sequester Zn(II) and Cd(II) as a preparation for efflux. The His-rich site could also have a dual role as part of the zinc repository and flux-control site for ZntA, allowing efflux of the essential ion only when it is present in sufficient numbers. This site alone could store 6 zinc ions, with 400 ZntA per cell a capacity of 2400 zinc ions or 10% of the minimum number of zinc ions per cell.

CadA has four HMA motifs in the amino-terminal part (CX2EE, the methionine residues of typical HMA motifs were not considered by the searching algorithm used), serving as metal-shuffling and possibly flux-control sites. PbrA has a paired CXC (as CGC) close to the amino-terminus and two HMA sites, the second with a preceding His. PbrA has three additional His-rich sites, one in the amino-terminal part, one (HGGNH) after the first transmembrane alpha-helix, and one in the carboxy-terminal cytoplasmic part. Despite the similar in vitro function of the three proteins, these differences in the equipment of metal-binding motifs may indicate that they may have been specialized in vivo to handle their specific substrate ions, Zn(II), Cd(II), or Pb(II), respectively, efficiently. Zinc is essential-but-toxic, cadmium and lead are toxic-only.

The  $P_{IB4}$ -type ATPase CzcP alone cannot mediate full zinc and cadmium resistance and needs at least one of the  $P_{IB2}$ -type ATPase to accomplish this task (Scherer and Nies 2009). The explanation could be that CzcP reaches only pre-discriminated zinc ions. On the other hand, CzcP has a higher transport rate as the three  $P_{IB2}$ -type

ATPase. Expression of the *czcP* gene is under the control of the two-component regulatory system CzcSR (Scherer and Nies 2009). CzcP is probably needed to remove zinc ions at a high rate when those ions occur at high concentrations in the periplasm, and thus this enzyme helps to preclude the zinc ions from potentially overwhelming the cell should those ions eventually enter the cytoplasm. The goal of this enzyme is to accomplish that removal before the metal can reach more tightly-binding zinc-binding sites. CzcP has no CPC central substrate-binding site but an SPC instead (not shown in Table 19.9 since single C sites were not considered by the algorithm). This may allow a higher transport rate because the energy of the enzyme-substrate complex during the transport process is lower in the case of a CPC site than in the case of an SPC site. Additionally, CzcP contains three His-rich stretches in the amino-terminal cytoplasmic part.

The four  $P_{IB1}$ -type ATPases all export Cu(I) (Wiesemann et al. 2017). CupA and CopF remove cytoplasmic Cu(I) to prevent the toxic action of the metal, CtpA and RdxI provide cytoplasmic Cu(I) to periplasmic copper-requiring sites. Obviously, aerobic bacterial cells loop copper through the cytoplasm to discriminate the metal by its ability to be reduced to Cu(I). The *cupA* gene is under the control of the MerR-type regulator CupR which also binds Au(I) (Jian et al. 2009). The *copF* gene is part of a large plasmid-encoded copper resistance determinant, while the other two genes are co-transcribed with genes for periplasmic copper-requiring proteins (Monchy et al. 2006). CupA interacts with the cytoplasmic copper chaperone CupC (Table 19.9). The contribution to copper resistance of the four proteins is CupA > CopF > CtpA > RdxI (Wiesemann et al. 2017).

All four  $P_{IB1}$ -type ATPases have the central CPC substrate-binding site but differ in the remaining metal-binding sites (Table 19.9). CupA possesses two double Cys-sites at the amino-terminal cytoplasmic part of the protein, which should correspond with the Cys-sites in CupC. The plasmid-encoded CopF starts with a triple-His site at the amino-terminus, followed by a second His-rich stretch, which is followed by a double-Cys site in a unique metal-binding domain YHS (pfam04945), plus there are both a Cys-His and another double-Cys site upstream of the first transmembrane span. The difference in structure between CupA and CopF is noteworthy, especially the His-rich sequences. Cu(I) tends to bind to methionine-rich sequence motifs and Cys sites. Could it be that CopF is able to bind also Cu(II) that just has arrived in the cytoplasm, keeping Cu(II) for reduction to Cu(I) and subsequent efflux?

Among the two “anabolic”  $P_{IB1}$ -type ATPases (Gonzalez-Guerrero et al. 2010), which allocate Cu(I) to copper-depending proteins with copper sites located in the periplasm, CtpA possesses a smaller number of metal-binding motifs than do the two enzymes CupA and CopF involved in resistance (Table 19.9). In addition to the “CPC” motif, CtpA has a double-Cys only in its amino-terminal part plus a few flow sites. The *ctpA* gene is in an operon region with genes for a putative cytochrome-c oxidase. RdxI again has a surprisingly elaborated repertoire of metal-binding motifs at its amino-terminal part. Yet another type of metal-binding domain, “ATPase-cat\_bd” (pfam12156), starts with a double-Cys-double-His motif. The pfam12156-type domain has a triple Cys-motif in the middle and is followed by a double-Cys

site. The *rdxI* gene is in an operon with genes encoding a *cbb3*-type cytochrome oxidase.

The differences in the metal-binding motifs and domains indicate an evolutionary adaptation of the four  $P_{IB1}$ -type ATPases to different functions. All of them rapidly remove cytoplasmic copper ions after these have entered the cell. CupC roams in the cytoplasm to sequester copper ions that have diffused away from the cytoplasmic membrane. Copper is thus prevented from binding to thiol residues, doing Fenton-type reactions and disturbing iron and zinc homeostasis. CupC and the four  $P_{IB1}$ -type ATPases perform the Cu(I) discrimination process, couple this process to copper export and provide already discriminated Cu(I) to the periplasm. Here, Cu(I) may be accepted by periplasmic copper chaperones.

CDF proteins (Paulsen and Saier 1997) (cation diffusion facilitators) were misnamed before their energetics were clear (Nies 1992; Nies and Silver 1995) (and I am sorry for that!). They are not “diffusion facilitators” since the transport of an ion across a pmf-charged membrane can never ever be by facilitated diffusion. In fact, these proteins are probably proton-cation-antiporters (Nies 2003). *C. metallidurans* contains three CDF proteins, DmeF, FieF, and CzcD.

DmeF is the most important factor for cobalt resistance in *C. metallidurans* and may also export nickel (Scherer and Nies 2009; Munkelt et al. 2004). The protein possesses a large number of His residues (Table 19.9), leading to ranking position number 13 of the proteins with the largest metal-binding capacity in *C. metallidurans* (Table 19.2). There is no involvement in zinc resistance (Scherer and Nies 2009), so that the large number of His residues lead to a preference of cobalt binding over zinc binding. This binding preference should be accomplished by a distinction of the ligands that Co(II) can accept, which would also lead to a slight preference of Co(II) over Ni(II). Similar to most CDF proteins, DmeF possesses three pairs of transmembrane alpha-helices and a large carboxy-terminal cytoplasmic region involved in metal binding and possibly flux control. Two additional cytoplasmic parts are larger than in other CDF proteins, these are an N-terminal region of 50 aa length and a unique region after the first four transmembrane spans. This unique region contains the largest His-rich stretch of DmeF with 22 His separated by Asp and Gly residues, making the motif into a flexible coil structure. This region looks like a cobalt sponge. The N-terminal cytoplasmic part contains both a double-His-single-Cys site plus a double-His site and is followed by a first pair of transmembrane alpha-helices. Between both alpha-helices, and therefore in the periplasm, is another double-His site. The very C-terminus of 32 aa contains a last His-rich stretch with one Cys residue. As with ZntA and zinc, this leaves the impression that DmeF is also a repository for its substrate cobalt. Both efflux systems may only be allowed to export zinc or cobalt, respectively, when their metal-specific repository sponge is full.

The structure of the FieF ortholog (Munkelt et al. 2004) from *E. coli* YiiP has been solved (Lu et al. 2009; Lu and Fu 2007). While the protein transports Zn (II) in vitro, FieF/YiiP from *E. coli* transports Fe(II) in vivo (Grass et al. 2005c; Chao and Fu 2004; Wei and Fu 2005). FieF from *C. metallidurans* does not contribute to zinc resistance but has a very small effect on cadmium and cobalt resistance (Scherer

and Nies 2009). The protein has two double-His sites in a cytoplasmic part following the first two transmembrane alpha-helices but no additional His-stretch, neither in the N- nor in the C-terminal cytoplasmic domain (Table 19.9). When the FieF proteins were described (Grass et al. 2005c), the concept that bacteria might efflux Fe(II) had not been universally accepted, an opinion which has now changed (Guan et al. 2015).

CzcD is, together with ZRC1 from yeast, the founder of the CDF protein family (Nies 1992; Nies and Silver 1995; Nies et al. 1989; Nies et al. 1987; Kamizomo et al. 1989). The protein is part of the plasmid-encoded cobalt-zinc-cadmium resistance system of *C. metallidurans*. Reminiscent of CzcP, it seems to export pre-discriminated cytoplasmic zinc ions to the periplasm for further removal by the CzcCBA transenvelope efflux gun (Scherer and Nies 2009). CzcD has a triple-His site at its short cytoplasmic N-terminal part, a double-His, and a Cys-His-site in the C-terminal cytoplasmic part (Table 19.9). These three sites may perform shuffling or serve as flux-control sites. CzcD contributes mainly to achieving regulation of zinc and also contributes to cobalt and cadmium resistance (Scherer and Nies 2009).

The plasmid-encoded NreB protein is part of an inactivated determinant, which has never been found to be expressed (Große et al. 2019). CnrT is part of the plasmid-encoded nickel-cobalt resistance determinant *cnr* (Liesegang et al. 1993). The CnrT protein exports cytoplasmic Ni(II) to the periplasm for further export by the transenvelope efflux gun CnrCBA. CnrT has ten transmembrane alpha-helices. A double-Cys motif is located in a small cytoplasmic part after the first three helix pairs, CnrT also has two large His-rich stretches at the C-terminal cytoplasmic domain, one with 13 and the second with 10 His residues, which are separated by Glu residues, a few Pro, but no Gly residues (Table 19.9). This region could again serve as nickel sponge, effectively acting as part of the nickel repository, or be a cation shuffling site and possibly have involvement in flux control.

In summary, *C. metallidurans* contains the genes for 13 inner-membrane efflux systems for transition metal cations. Together, this arsenal is able to remove all surplus transition metal cations from the cytoplasm. When two or more efflux pumps share the same primary substrate as in the case of Cu(I) and Zn(II), the proteins have different functions with respect to the targeted substrate pool or physiological role of the export. These differences are always visible in the outfit of the protein with metal-binding motifs. The most important exporters for essential-but-toxic metal cations may also be part of the repository of the respective substrate, so that via flux control the respective metal is only exported when the repository at the exporter is filled. Examples are here ZntA for Zn(II), DmeF for Co(II), and CnrT for Ni(II).

### 19.3.6 *Transenvelope Efflux*

Gram-negative bacteria possess within their periplasm a second compartment for metal homeostasis, which is especially important for copper homeostasis. Cu(II), the

predominant ionic form under oxic conditions, is transported into the cytoplasm of *C. metallidurans* or *E. coli* only at a low rate, such as by ZupT (Taudte and Grass 2010) or as phosphate complex by PitA (Herzberg et al. 2016; Grosse et al. 2016). Cu(II) can be reduced in the periplasm by contact with components of the respiratory chain to Cu(I) (Volentini et al. 2011), which is rapidly imported into the cytoplasm (Thieme et al. 2008). Indirect evidence suggests that Cu(I) may use Na(I)-dependent transport systems in *E. coli* (Große et al. 2014). One way to prevent a rapid import of Cu(I) is oxidation back to the “bad” import substrate Cu(II) by CueO/CopA-type periplasmic copper oxidases (Magnani and Solioz 2007; Grass and Rensing 2001; Williams et al. 1993; Brown et al. 1995; Cooksey 1993; Cha and Cooksey 1991; Mellano and Cooksey 1988; Bender and Cooksey 1985). *C. metallidurans* possesses chromosomal and plasmid-encoded genes for such enzymes plus a variety of helper proteins (Janssen et al. 2010; Bersch et al. 2008; Monchy et al. 2006; Mergeay et al. 2003). Since molecular oxygen is the electron acceptor for copper oxidases, CueO/CopA-type enzymes do not function under anoxic conditions. Instead and under oxic conditions there exist additional, transenvelope efflux systems that operate to pump Cu(I) from the periplasm to the outside (Outten et al. 2001).

The first transenvelope efflux system for metal cations described was the CzcCBA efflux gun: phenotype (Mergeay et al. 1985), cloned (Nies et al. 1987), basic mechanism figured out (Nies and Silver 1989), sequenced (Nies et al. 1989), energy-coupling (Nies 1995), contribution of the subunits (Rensing et al. 1997), regulation (van der Lelie et al. 1997), function of the central component (Goldberg et al. 1999), transcription (Große et al. 1999), along with a definition of the CDF (Nies 1992; Paulsen and Saier 1997) and RND (resistance-nodulation-cell division protein family) (Tseng et al. 1999; Paulsen et al. 1997; Saier et al. 1994) protein families. RND-containing protein complexes are able to perform transenvelope efflux of metals and these protein complexes are composed of three subunits. The actual pmf-driven device is the trimeric RND protein, which is located in the inner membrane and extends into the periplasm (Saier et al. 1994; Nies 2013; Tseng et al. 1999). RND proteins are the result of an ancient gene duplication and each individual molecule contains twelve transmembrane alpha-helices plus two large periplasmic domains. CzcA was the first RND protein described in detail. An additional outer membrane factor, OMF, is also a trimeric outer membrane protein with the trimers constituting one common beta-barrel. OMF trimers also extend from the outer membrane into the periplasm, examples being CzcC, CusC, and TolC. A hexameric membrane fusion, MFP or adaptor protein (Saier et al. 1994; Higgins et al. 2004), makes contact between RND and OMF trimers, creating a membrane fusion for the transport event. Examples of such proteins are CzcB, CusB, and AcrA (Nies 2013; Tseng et al. 1999).

One transmembrane alpha-helix of the RND protein is central to the import of the driving protons into the cytoplasm. This helix ends with strictly conserved Glu residues, often followed by an asparagine (EN), at the cytoplasmic end of the helix. When divalent metals are used as substrates, an aspartate is located in the middle of this helix and a “DFG” motif at its periplasmic beginning. Copper-transporting proteins often contain an “AIG” instead of the “DFG.” RND proteins



involved in the transport of organic substances such as AcrB from *E. coli* usually exhibit a “DD” motif instead of the “DFG” and the inner-membrane aspartate is missing (Nies 2013; Tseng et al. 1999; Nies 2007a, 2003; Goldberg et al. 1999).

Proton import drives a conformational change of the RND trimer in a way that all three protomers rotate between three conformations, but it always is the case that the trimer simultaneously has all three conformations present (Seeger et al. 2006). One conformation allows binding of substrate from the periplasm or, in case of hydrophobic substrates, the interior of the inner membrane, one conformation is closed, and the third open to the export channel from the RND trimer through the interior of the OMF protein directly to the outside (Nies 2013).

It is a long-standing debate if RND-driven transmembrane efflux complexes such as CzcCBA export their substrate from the cytoplasm versus the periplasm to the outside (Nies 2013). The two RND proteins CzcA and CusA could transport metals *in vitro* across a membrane (Su et al. 2011; Long et al. 2010; Goldberg et al. 1999), which would correspond to the inner membrane. On the contrary, no evidence exists that the respective CzcCBA or CusCBA complexes do export their substrates from the cytoplasm to the outside *in vivo* (Scherer and Nies 2009; Rensing and Grass 2003). Neither of these two systems is able to functionally substitute for an inner membrane efflux system. Instead, these two systems essentially rely on an inner membrane system to first remove a substrate from the cytoplasm to the periplasm before the transenvelope efflux complex is able to successfully continue the removal of the substrate. CusCBA does functionally substitute for missing or, under anaerobic conditions, enzymatically inactive periplasmic copper oxidases (Rensing and Grass 2003; Outten et al. 2001).

Transport of metals by RND-driven transenvelope systems is *in vivo* from the periplasm to the outside (Nies 2013). Both modes of action, from the cytoplasm and periplasm, however, cannot be allowed to run in parallel because this would lead to an immediate function of the RND protein as a uniporter, which by definition imports a specific cation driven by the charge gradient from the periplasm into the cytoplasm (Nies 2013). This clear contradiction between the *in vitro* and *in vivo* data, transport from the cytoplasm or from the periplasm to the outside, maybe explained by an idea. The very first cation that is exported may be required to come from the cytoplasm to start the rotational or “periplasmic pump” mechanism of the RND protein. This may happen after assembly of the complex, or after a membrane fusion to the OMF protein has been newly established after a pause. After such an “ignition”, achieved by a first proton-cation antiport across the inner membrane, this path must be blocked to prevent a cation uniport mechanism by an RND trimer with arrested conformations. That way, the “ignition” could also be used as a measure of flux control, allowing the export of copper or zinc to the outside only when a sufficient number of these ions is present in the cell. One of the many pleiotropic consequences of the zinc starvation phenotype of  $\Delta zupT$  mutants is an instability of CzcA (or prevention of translation of the *czcA*-mRNA) (Herzberg et al. 2014a). This could mean that RND proteins that cannot be “ignited” are unstable and rapidly degraded.

*C. metallidurans* contains twelve determinants encoding RND-driven transenvelope efflux systems for metals but only four are active and required (Nies 2013; von Rozycki and Nies 2009; von Rozycki et al. 2005; Nies et al. 2006): (i) *Czc* for zinc and some activity for cobalt and cadmium; (ii) *Cnr* for nickel and some activity for cobalt too; and (iii) *Cus* and *Sil* for copper and silver. The other eight systems are on different levels of un-importance. While *czc* is located on one of the plasmids, the chromid of *C. metallidurans* carries an ancestral, second *czc2* determinant (von Rozycki and Nies 2009), which is interrupted in the middle of the *czcB2* gene. Both parts of the ancient *czc2* determinant became additionally separated by a large re-arrangement of the chromid. The active *zntA* gene, with *ZntA* being the most important inner membrane efflux pump for zinc under all conditions, is part of this ancient *czc2* determinant. The chromid contains also the *zni/zne* region for two additional RND-driven systems with a low-level expression of these components (De Angelis et al. 2010; Große et al. 2019). The *czc*-plasmid pMOL30 also contains a *ncc* nickel-cobalt-cadmium determinant, which is not expressed and has a mutation within the *nccB* gene. The *hmv* determinant on the chromid is expressed but with an inactivating mutation in the *hmvA* gene. The *hmyA*-gene on the chromid carries a transposon-insertion, as does *nimA* on the chromid and *hmz* on a genomic island on the chromosome. With *czc* and *sil* on plasmid pMOL30, *cnr* on plasmid pMOL28, and *cus* on the chromid, it is interesting to note that all of these 12 active or inactive RND-driven systems have been acquired by horizontal gene transfer, which is also true for *zntA*, *cadA*, *pbrA*, *czcP*, *copF*, and both determinants for copper oxidases. Only *cupA* and the two genes for the two “anabolic” copper-exporting P<sub>IB1</sub>-type ATPases are on genes not associated with “recent” horizontal gene transfer (Große et al. 2022).

The metal-binding motifs in most RND proteins appear to be simple “flow sites” required to pass the metal substrate along by the formation of solvent-shared or transient direct ion pairs (Table 19.10). Three RND proteins stand out. *CzcA* possesses a Cys adjacent to the EN directly adjacent to the crucial, proton-transporting transmembrane alpha-helix with the “DFG...D...EN” motif. Moreover, that motif is followed by a small cytoplasmic part of 61 amino acids in length, which contains a triple-His motif HAQEHH (HX2EH2, Table 19.10). This triple-His motif site may be an important flux-control site, allowing *CzcCBA* to remove periplasmic zinc only when sufficient cytoplasmic zinc is present. The site could also be involved in the instability of *CzcA* under conditions of zinc starvation or the hypothetical first “ignition” zinc export. The MFP protein *CzcB* also stands out because it contains two important metal-binding motifs right after the N-terminal membrane anchor of *CzcB*, and those metal-binding motifs are involved in transport (Rensing et al. 1997). These metal-binding sites could be shuffling sites, metal-concentrating sites, and maybe also involved in flux control (Kim et al. 2011).

Both *CusA* and *SilA*, which are Cu(I)-transporting RND proteins, also contain metal-binding motifs and these are directly adjacent to the “EN” motif. The membrane fusion protein *SilB* has a double-His site in the N-terminal part (Table 19.10) so that the *Cus* and *Sil* systems may only remove periplasmic copper when sufficient metal is present.

**Table 19.10** Transenvelope efflux systems in *C. metallidurans*<sup>a</sup>

Rmet	ProtNum	Gene	
<u>RND proteins</u>			
Rmet_5980	#NV	<i>czcA</i>	EXC- <b>HX2EH2</b> -EX2HE-HXE-EEXHX2D-HX2DED-HX2D
Rmet_4468	-	<i>czcA2</i>	EX3H-EXC-HX2E
Rmet_6210	#NV	<i>cnrA</i>	HX2DD-HX2E-HX3D-EX2HX3E-EX2HXE
Rmet_6145	#NV	<i>nccA</i>	EX2HX3E-HXE
Rmet_5033	NeF	<i>cusA</i>	<b>EX2HXHXEX2HXDH</b> -HX2ED
Rmet_6136	#NV	<i>silA</i>	<b>EX2HXHXEHXHX2HX3E-HX2HD</b>
Rmet_3838	0	<i>hmvA</i>	DX3H-CH-HED-EEX2H-EXH
Rmet_5319	76	<i>zniA</i>	DXHX2D- <b>HX3H</b> -HXEE-HX3E-HXE-HX3DD-DX3HE
Rmet_5329	NeF	<i>zneA</i>	EX2H-DX3H-H2-EXHX2D-HXE-HXD-DX2H
Rmet_5678	NeF	<i>nimA</i> "	HX3D-HED-DEXHD
Rmet_5681	0	<i>nimA</i> "	DEH-EEXH-HXDE-C/
Rmet_3011	NeF	<i>hmzA</i>	EX3HX2DD-DXH-EHXHXE-EX3H2-EX2H-DXHX2D-HX3D-DEHXD
<u>Membran fusion or adaptor proteins</u>			
Rmet_5981	#NV	<i>czcB</i>	<b>EEX3HXEX3HXDXEH2-DHXDDX2HXDXEH2E</b> -EXHX2D-EDX3H-EXH-EHXH/
Rmet_4469	0	<i>czcB2'</i>	EXH-DX2H-EHXH/
Rmet_5032	48	<i>cusB</i>	EHE-DX3HD-HX2ED
Rmet_6135	#NV	<i>silB</i>	HX2D- <b>HDXHD</b> -DXH
Rmet_3837	194	<i>hmvB</i>	XHX3D-CX3E-DX2H-H/
Rmet_5320	328	<i>zniB</i>	EX2HX3E-DX3H-DX2HE
Rmet_5330	NeF	<i>zneB</i>	DX2H-DX2H
Rmet_5682	182	<i>nimB</i>	EX3H-HX2E
Rmet_3012	NeF	<i>hmzB</i>	DXHX3E-DXHXD
<u>Two-component sensors</u>			
Rmet_1752	NeF	<i>agrS</i>	<b>DX2HD</b> -EEXHX3D- <b>HX2H-DXH2</b>
Rmet_4466	NF/NF	<i>czcS2</i>	<b>DX3HX2EXHXD-HX3E</b> -DXHX3D-EXH- <b>DX2HD</b> -EX3H
Rmet_5327	38	<i>zneS</i>	DX2H-HX2D-HXDDEE-DHE-EHE- <b>DX2HE</b> -DX2HXD-HX3D- <b>CXDXC</b>
Rmet_5332	17	<i>zneS2</i>	HX3D-EXH-DDXHX3E-EX3H- <b>DX2HE-CXDE-CX2DXH</b>
Rmet_5673	NeF	<i>copS2</i>	<b>DX2HX3DX2H</b> -DXHX3ED-DX3H2-HX2DDD-EXHEHX2H-DX2HE- <b>DX2HE-EHX2DX2HXE</b> -EXHXE
Rmet_5977	#NV	<i>czcS</i>	DX3HX3D-EHX3E-HX2DD-EX2H- <b>DX2HD</b> -HXE- <b>EX2HC2XD</b> -EXHX2D
Rmet_6110	#NV	<i>copS1</i>	DXHX3ED- <b>EH2</b> -EX2H- <b>EXHXHX2H-DX2HE</b> -EXHX2D

<sup>a</sup>Some of the proteins were never found (NeF) in the proteome of *C. metallidurans* strain AE104 (Herzberg et al. 2014b), which is plasmid-free (Mergeay et al. 1985), although they are encoded by chromosomal or chromid genes. Other could not be found (#NV) because they are plasmid-encoded genes. The putative metal-binding motifs in red letters contain the conserved His residue of sensory histidine kinases

Expression of the genes for transenvelope efflux systems is under the control of the periplasmic substrate concentrations. In most cases, control is exerted by a two-component regulatory system composed of a membrane-bound histidine kinase and a cytoplasmic response regulator of gene expression (Nies and Brown 1998; Yamamoto et al. 2005). The exception is *cnr*. Here, the sigma factor CnrH of the extracytoplasmic functions (ECF) family of sigma factors, actually one of the founding members of this family, activates *cnr* expression. Availability of CnrH is controlled by a membrane-bound anti-sigma factor complex CnrYX. CnrX is the nickel sensor and binds Ni(II) in a degenerated octahedral complex with a carboxylic group at two corners of the octahedral plain, which perfectly interacts with the two anti-binding d-electrons of the nickel atom. The complex discriminates against Zn (II), plus has some activity for binding of Co(II) (Grass et al. 2005b; Grass et al. 2000; Maillard et al. 2015; Trepreau et al. 2014; Tibazarwa et al. 2000; Ziani et al. 2014; Maillard et al. 2014; Trepreau et al. 2011; Pompidor et al. 2008).

Sensory histidine kinases such as CusS are usually membrane-bound dimers, each composed of an N-terminal first transmembrane alpha-helix, a periplasmic sensory domain, a second transmembrane alpha-helix, and the cytoplasmic ATP-binding domain which also contains the essential His site that is phosphorylated (Affandi et al. 2016; Gudipaty and McEvoy 2014; Gudipaty et al. 2012; Quaranta et al. 2009). The conserved motif containing the His site usually appears as minor metal-binding motif “DX2HD” or “DX2HE” in the motif-search algorithm used (Table 19.10). Those histidine kinases which serve as determinants for RND-driven efflux systems may contain metal-binding domains in the periplasmic sensory parts, as expected, but also surprisingly contain metal-binding domains in their cytoplasmic parts, for instance, an EX2HC2XD His-double-Cys motif in CzcS. This could indicate that these histidine kinases may compare the periplasmic and cytoplasmic metal content and use this information for control of the actual phosphorylation event.

In summary, *C. metallidurans* contains twelve horizontally acquired determinants for transenvelope efflux systems. Six of those are inactivated by native mutation, *zni/zne* is active only on a low level, *cus/sil* involved in export of copper and silver, *cnr* mainly for nickel export, and *czc* mainly for zinc export. The transenvelope efflux systems are large protein complexes spanning the complete cell wall from the inner to the outer membrane. They are composed of the inner membrane trimeric RND protein, which uses the import of protons as a driving force to sequester periplasmic substrate ions. A trimeric OMF protein forms a beta-barrel passage through the outer membrane. The hexameric MFP or adapter protein fuses together with the RND and OMF proteins to allow transport from the periplasm through the OMF to the outside. Expression of genes for the transenvelope efflux systems is under the control of periplasmic substrates and mediated by two-component histidine kinases/response regulators or ECF sigma factors. Often, additional periplasmic components or inner membrane efflux systems are encoded alongside with the genes for the transenvelope efflux systems. These transenvelope efflux systems rely on inner membrane efflux systems to export a substrate ion first from the cytoplasm to the periplasm for further export by the RND system, they compete with the uptake systems for periplasmic

ions as substrate for transport, and they are antagonists of the outer membrane porins which import metals or their complexes by facilitated diffusion into the periplasms.

## 19.4 The Zinc Repository

### 19.4.1 *The Zinc Repository and the Expressome*

The transportome thus adjusts the periplasmic and cytoplasmic transition metal concentration and composition in *C. metallidurans* (Nies 2016). Already beginning in the periplasm, the CzcCBA transenvelope efflux system removes surplus zinc ions that have entered by facilitated diffusion through outer membrane porins. CzcCBA competes with the uptake systems for zinc and its activity is buffered by periplasmic metal-binding proteins such as CzcI, CzcE, CzcJ, which are also components of the Czc system. Surplus cytoplasmic zinc ions have to be removed first by inner membrane efflux systems, mainly ZntA, before they can be transported to the outside by CzcCBA. When ZntA is not sufficient to export all surplus zinc ions, the additional inner membrane efflux systems CzcP and CzcD are up-regulated. All these export processes seem to be tightly controlled to prevent over-pumping of zinc: removal of so much zinc that the cell runs into zinc starvation. This is accomplished by regulation of gene expression, of *czc* by a two-component regulatory system sensing periplasmic zinc ions and additional regulatory circuits, of *zntA* by a MerR-type regulator, and all signatures of flux control as a rapid response by ZntA, CzcB, and CzcA. Similar mechanisms adjust the concentrations of nickel (CnrT, CnrCBA), of cobalt (DmeF, CnrCBA, and CzcCBA), of cadmium (CadA, CzcCBA), of copper (periplasmic copper oxidases, CupA, CupC, CopF, CusCBA, SilCBA), of lead (PbrA), and iron (FieF); not considering here chromate, arsenate, and mercury (Nies 2016).

A transportome needs a buffer. Otherwise, the effects of the flux controls of import and export systems will result in strong fluctuations in the cytoplasmic metal concentrations. Moreover, the transportome adjusts the metal concentration in the region adjacent to the inner membrane. Diffusion of metals through the crowded and super-crowded protein areas to the central nucleoid-containing part of the cell needs some time. Gene expression starts throughout the nucleoid by the initiation of transcription by the RNA polymerase (RNAP) holoenzyme, composed of the two RpoA, one RpoC, RpoD, RpoZ subunits, and a sigma factor to identify the promoter regions (Kohler et al. 2017; Sarkar et al. 2013; Markov et al. 1999; Ishihama 1988; Helmann 2002; Missiakas and Raina 1998; Feklistov et al. 2014). In 70% of the expression events, the sigma factor of the transcribing RNAP is exchanged after the promoter escape by elongation factors, Nus and Gre proteins (Harden et al. 2016). This allows immediate physical contact with a first leader ribosome, which immediately starts to translate the nascent mRNA (Kohler et al. 2017; Burmann et al. 2010; Proshkin et al. 2010). This close coupling of transcription and translation allows a multitude of regulatory events during transcription elongation. If the sigma

factor stays on, different kinds of regulatory events take place. A strong gene expression event, meaning that there may be many RNA polymerases transcribing the same gene region and possibly many ribosomes translating newly synthesized RNA, leads to a re-organization of the nucleoid so that these strong gene expression events are pushed to the surface of the nucleoid, to the border between nucleoid and the remaining cytoplasm (Mohapatra and Weisshaar 2018).

The nucleoid carries most of the negative net charges of the cell (Table 19.1), with half of the phosphate residues present in the DNA and RNA. The remaining half are located in the phospholipids. The ribosomal RNA represents the largest part of the total RNA pool so that the ribosomes are in fact large RNA complexes garnished with a few proteins. The negative charges of the DNA and RNA inside the nucleoid should be neutralized by potassium and sodium ions, which, however, keep their distance and approach the phosphate residues at a maximum as shared-solvent ion pairs. Magnesium may approach more closely as a shared-solvent or direct ion pair. It is not a surprise that the ribosome is packed with magnesium ions, 317 in the ribosome plus elongation factor Tu (Fischer et al. 2015).

Except for zinc, transition metal cations are mostly inserted into proteins after translation and folding; iron as iron-sulfur center or cytochromes, copper into periplasmic sites either after export of the protein or after insertion into the folded protein and subsequent TAT-transport, nickel into folded urease and hydrogenase, cobalt mostly as cobalamin-derivative (Nies 2016).

Zinc should also be able to enter catalytic sites close to the surface of the protein with 3 or 4 ligand amino acyl residues after the protein has been folded; however, due to the negative electron affinity and nearly covalent bond with sulfur, tetrahedral sites with 3 or 4 Cys residues and also CCHH sites (Table 19.3, and chapter “Chemical constraints for transition metal cation allocation” by author Dietrich H. Nies) need to have their zinc inserted co-translationally or immediately after translation to allow a proper folding of the respective protein with such a structurally important, firmly bound zinc ion. Zinc, therefore, needs to be present at the ribosome during translation (Hensley et al. 2011; Panina et al. 2003). Since it may be used up during translation by insertion into folding proteins, zinc also needs to be transported to ribosomes inside the nucleoid. Nevertheless, under certain conditions, cobalt may be able to substitute for zinc as has recently been suggested (Ammendola et al. 2020).

*C. metallidurans* contains 70,000 zinc ions per cell after cultivation in Tris-buffered mineral salts medium with 200 nM zinc (Kirsten et al. 2011). When the cellular zinc homeostasis is disturbed by the deletion of the *zupT* gene for the major zinc importer, *C. metallidurans* can function with 20,000 zinc ions per cell (Herzberg et al. 2014a). By adding  $\mu\text{M}$  concentration of zinc to the growth medium, the cells accumulate about 120,000 zinc ions per cell. At this concentration, the efflux systems, mainly ZntA, kick in and keep the number of zinc atoms per cell at this level. When all known inner membrane efflux systems for zinc are deleted, low  $\mu\text{M}$  concentrations of zinc outside result in about 250,000 zinc per cell, and at higher concentrations, the cells stop growing (Herzberg et al. 2014b). The capacity range of

*C. metallidurans* for zinc ions thus is between 20,000 and about 250,000 zinc ions per cell. The optimum is a 50% capacity of about 120,000 ions per cell.

The number of zinc-binding proteins of *C. metallidurans* cells was estimated to be 110,000–120,000 proteins per cell (Herzberg et al. 2014b), with some of the proteins binding more than 1 zinc per polypeptide. The optimum zinc quota of the cell is therefore at an average of one zinc per zinc-binding protein. The totality of these proteins is the central zinc repository of the bacterial cell. At 70,000 or 20,000 zinc ions per cell, most of these proteins do not contain a zinc ion. When the optimum is reached, ZntA starts to remove zinc. ZupT, its regulator of gene expression Zur, ZntA, and its regulator ZntR (Schulz et al. 2021) all contain His-rich stretches that may be part of the repository (Tables 19.8 and 19.9), and these stretches allow a read-out of the status of the repository to yield regulatory events, gene expression, and flux control.

Half of the cellular zinc-binding proteins of *C. metallidurans* belong to the KEGG category “genetic information processing” (Herzberg et al. 2014b). About 17,000 zinc can be associated with the RNA polymerase (Herzberg et al. 2014b) but only the structural zinc in a tetra-Cys site of RpoC should be firmly bound (Markov et al. 1999). About 31,000 zinc atoms can be associated with four ribosomal proteins, L2, S9, S2, S15, and S17 (Herzberg et al. 2014b), which also have a considerable metal-binding capacity (Table 19.5, Fig. 19.3). The ribosome of *E. coli* may bind 8 equivalents of zinc, which are required for the proper synthesis of zinc-requiring proteins (Hensley et al. 2011). The expressome, a transcribing RNA polymerase and a leader ribosome in physical contact, thus is part of the zinc repository and can contain a large part of the total cellular zinc repository. It cannot be derived at this stage which part of the zinc repository contains pre-discriminated and which part already discriminated zinc ions. The minimum number of 20,000 zinc ions per cell should be discriminated ions, anything above 120,000 ions per cell may be pre-discriminated ions. Further experimental evidence is needed here.

How does the zinc get to a ribosome that spends zinc during translation and is located in the middle of the nucleoid? The possible ion current in crowded and supercrowded cellular areas (Spitzer 2011; Spitzer and Poolman 2009) can involve all metal cations but only Mg(II) approaches closely to negatively charged amino acid residues at the surface of a protein to form transient direct ion pairs, and transition metal cations may approach even more closely. Since copper and iron are removed from this flow and the number of cobalt and nickel ions remains low and strictly controlled, only zinc could be allowed to move within the magnesium current when sufficient zinc is present in the cells, closely to the surface of proteins in crowded areas. The proteins providing the largest metal-binding capacity to the cell are components of the expressome, and significant metal capacity also exists with components of the tricarboxylic acid cycle. On top of the list (Table 19.4) for metal binding capacity are elongation factor Tu, the RNA polymerase subunits RpoC and RpoD, the enzyme-producing 2-oxoglutarate, glutamate from 2-oxoglutarate and glutamine from glutamate (Table 19.7). These are the amino donors for aminotransferases, usually the last step in amino acid synthesis. Many aminotransferases and tRNA synthetases contain a large number of metal-binding motifs (Table 19.11).

**Table 19.11** Motifs in enzymes involved in amino acid processing<sup>a</sup>

Rmet	ProtNum	Gene	Total	Description
<b>Elongation factors</b>				
Rmet_1436	4224	<i>tsf</i>	EX2CE-DX3H	QILNF7 Elongation factor Ts
Rmet_3324	14,226	-	EX3H-HXDH-HXE- <b>HX2HXDCX2HXD</b> -CX3D-CX3E- <b>HXHX3E</b> -DEX3H	QILJ13 Elongation factor Tu
Rmet_3325	7986	<i>fusA1</i>	HXD- <b>HX3EXHD</b> -DX3HXD- <b>CX3C</b> -EXHXE-EX2HX2E	QILJ29 Elongation factor G 1
Rmet_5930	1980	<i>fusA2</i>	HXD- <b>HX3EXHD</b> -DX3HXD-CX3D-EDH-EXHD-HXEDD-EXHX2DDE-EXHXE-HX3D-HX2ED-EX2HX2E	QILAN7 Elongation factor G 2
<b>tRNA synthetases</b>				
Rmet_0096	1155	<i>argS</i>	HXD2C-HX2H-HXE-DX3H-DH2-DX3H-CXE-DX3H-HX3CX3E-EX3H-DXH	QILS94 Arginyl-tRNA synthetase
Rmet_0378	2206	<i>aspS</i>	HXC-EXC-EX2CHE-HX3D-CX2DED-HXE-H2-DEH-EXH	QILRG2 Aspartyl-tRNA synthetase
Rmet_0416	224	-	DXHXE-DXH2D-DHX2H2-HX3D-DX2H-HXHXE	QILRC3 Tyrosyl-tRNA synthetase
Rmet_0440	807	<i>trpS</i>	HX2H-EXH-DX2HD-EX2H-DX2H	QILRA0 Tryptophanyl-tRNA synthetase
Rmet_0446	1003	<i>glyS</i>	EX2HX2E-CHXEE-EXH-HX2D-HDDE-CXEH-EX3HE	QILR94 Glycyl-tRNA synthetase, beta subunit
Rmet_0448	469	<i>glyQ</i>	HXH-DX2HX2E-EHX3E-HX2EHE-CX2E	QILR92 Glycyl-tRNA synthetase alpha subunit
Rmet_0695	1215	<i>serS</i>	DHXD-DXHX2EHX3E-HX2CX3E-HX2D-HXE-CX2D-EX3C-EX2H	QILQJ5 Seryl-tRNA synthetase
Rmet_0818	759	<i>glnS</i>	X2HD-HX2H-CHX3DD-DX2H-HXH3X3DX2C-DX2HCX2DX2EX3HX2CX2E-EHX2D-HX2E-EEC-ECX3D-HXCE-EXH	QILQ72 Glutaminyl-tRNA synthetase
Rmet_0831	1794	<i>alaS</i>	EX3H-HXD-H2X3E-CX2CXEX3DHX2D-CXD-HXHX3E-EXHX2D-DHX3C-HX2D-DX3H-HX3HX2H-DX2H-EXCX3H-DX3H	QILQ59 Alanyl-tRNA synthetase
Rmet_1034	1320	<i>fysS</i>	HX3ED/-HXD-DX2HX3D-HX2D-H2X3D-HX2E	QILPK6 Lysyl-tRNA synthetase
Rmet_1085	748	<i>cysS</i>	EXH-HXHX3C-CHX2H-DX2H-HED-HXEC-EHXDXXH-H2E-DXHXDDX2H-CX2DXEEXH-DXH	QILPF5 Cysteinyl-tRNA synthetase

(continued)



Table 19.11 (continued)

Rmet	ProtNum	Gene	Total	Description
Rmet_1160	1119	<i>thrS</i>	EX2C-EXC-DX3HX3H-CX3H-DX3HX2EE-DX2HX2EE-EX3HXD-CX2H-EX3CHX2E-DDXHX2CXEE-DHXED-CX2E-EXHX2D-EXH	Q1LP80 Threonyl-tRNA synthetase / Ser-tRNA (Thr) hydrolase
Rmet_1164	1471	<i>pheS</i>	EX2HXE-DXHE-DX3HD-DXH-HXE-DX2H	Q1LP76 Phenylalanyl-tRNA synthetase alpha chain
Rmet_1165	1532	<i>pheT</i>	DX3H-EXHX3D-CX2D-CX3E-EDH-CX3H-HX2DXDX2HX3D-DX2HX2E-EHXE-HX3H-HXD-EX3H-EX3HX3H-EXH-CX2D	Q1LP75 Phenylalanyl-tRNA synthetase beta subunit
Rmet_2105	1441	<i>hisS</i>	DHX2DD-HEX3HXE-EEX3HXE-HX2E-DX3HX3D	Q1LLJ2 Histidyl-tRNA synthetase
Rmet_2140	1047	<i>glx</i>	EX3HC-CX3DD-DDH-HXD-EHX2DE	Q1LLF7 Glutamyl-tRNA synthetase
Rmet_2630	1578	<i>valS</i>	HX2H-HXH-HXEDEX3H-EX3H-EX2H-EXHDC-CX2DCX2DX3H-DEXCD-DX2H-EX3C	Q1LK19 Valyl-tRNA synthetase
Rmet_2769	2075	<i>metG</i>	HX2HX2E-DDXH-EHX2D-ECX2CX3D-CEXC-HX3EX2H-DX2HX2C-EXH	Q1LJN4 Methionyl-tRNA synthetase
Rmet_2885	1261	<i>ileS</i>	DXHX2H-CH-CXDC-DX3HX2H-HXE-EX3H2-CX2HX3D-HX2EHX3HCX2H-HXE-EXHX2E-HXDE-DXH-DHX2H-EX3H-EXH-CXED-HX2EHXD-HX2CEXCXHX3DX2HX2EHX3CX2CD-EHX2H	Q1LJB8 Isoleucyl-tRNA synthetase
Rmet_2973	1098	<i>leuS</i>	CX2H-HX2H-EX3CX2E-HX2E-EECXH-HDE-EHX2CXH-HCDXC-ECXCX2C-CXD-EHX3H-EXH-HX2H	Q1LJ30 Leucyl-tRNA synthetase
Rmet_3100	1624	<i>proS</i>	HX2D-EX3H-DXHE-HEHX3D-CX3D-EX3CEHX2E-DHE-C2X3DXDXH-CX3EX2H-DX2HXE-DX3H	Q1LJQ4 Prolyl-tRNA synthetase
Rmet_3564	624	<i>fnt</i>	EX2H-EX3HXCX3H-HX3E	Q1LHE0 Methionyl-tRNA formyltransferase
Aminotransferases				
Rmet_0493	1339	<i>thrE</i>	DX3HX3HX2H-EXC-H2-CXD-DEX2CXDE	Q1LR47 Branched chain amino acid aminotransferase
Rmet_0715	1030	<i>serC</i>	EX2HX3EE-EX2HX3EXEX2HXE-DX3HX3D-HXCX2E-DX3H-HX2C	Q1LQH5 Phosphoserine aminotransferase
Rmet_1018	5021	<i>tyrB</i>	EXH-DX3H-HXC2H-HX3D	Q1LPM2 Aminotransferase

Rmet_2249	409	<i>dat</i>	CX3ED-EEXCX3D	Q1LL48 Branched chain amino acid aminotransferase
Rmet_2862	1453	<i>argD</i>	HX2E-CXD-DHX2H-DXH-CX2C-CX2D	Q1LJE1 Acetylornithine aminotransferase
Rmet_3247	1177	<i>hisC</i>	HX2DXH-EXC	Q1LJA7 Histidinol phosphate aminotransferase
Rmet_4927	935	<i>tyrB</i>	X2EHXE-EXH-HXC2H-EXC-CX3DE-HDHX2EHX3E	Q1LDJ7 Aminotransferase
<u>Glutamine synthetase</u>				
Rmet_2062	3848	<i>glnA</i>	CX3D-EXH-HXDEDX2EX2HX2D-EXCX3E-EXH3E-HXH-HX2E-CX3D-HX2E	Q1LLN5 Glutamine synthetase

<sup>a</sup>The Rmet number is provided, the number of proteins per cell in *C. metallidurans* AE104 (Herzberg et al. 2014b), the capacity per protein and, as a product, the capacity per cell

Elongation factor Tu, which binds the loaded tRNAs to bring them to the ribosome, also is on top of the metal capacity list (Table 19.4) and the GDP-GTP exchange factor for Tu, elongation factor Ts, is part of the zinc repository (Herzberg et al. 2014b). This sums up the attractive picture that pre-discriminated zinc moves close to the surface of proteins that are producing precursors of amino acids, subsequently amino acids, proteins which load amino acids to tRNA and which transport the loaded tRNA to translating ribosomes. Elongation factor Ts may especially steer zinc to Tu, and the RNA polymerase subunits as well as some ribosomal proteins serve as a sink for the zinc ions arriving with ready-to-go loaded tRNAs. In addition, zinc chaperones may provide already discriminated zinc ions to the ribosome and to other important zinc-depending proteins.

In summary, *C. metallidurans* contains a zinc repository composed of about 120,000 zinc-binding proteins, most of them the expressome components ribosome and RNA polymerase. His-rich stretches indicate that ZupT, ZntA and the associated regulators of gene expression are also components of the zinc repository. That way, the status of the repository can influence gene expression and flux control of import and export systems for zinc. The cell accumulates zinc ions until the repository is filled, removes zinc ions above this quota, and stops growth when the zinc repository flows over. In a picture that combines the need for zinc of translating ribosomes in the inside of the nucleoid with the crowded model of the cell and the ion current at the surface of the proteins in these areas, zinc may move along with magnesium from enzymes involved in amino acid synthesis, tRNA synthetases and elongation factors Tu and Ts from the outside into the inside of the nucleoid, allowing a constant supply of pre-discriminated zinc to the translating ribosome. Additionally, zinc chaperones may provide already discriminated zinc ions.

### 19.4.2 GTPases as Acting Component of the Zinc Repository

Unfortunately, the supply of pre-discriminated zinc moving in parallel with amino acids via tRNAs, Tu, and Ts to the translating ribosome is not an efficient allocation path of zinc to the ribosome. Without ZupT, even when additional zinc is provided to the cells and they contain 120,000 zinc ions bound to the cell, these zinc ions do not arrive in sufficient numbers at the ribosomes that translate RpoC (Herzberg et al. 2014a). In RpoC zinc has an essential structural role and is complexed in a tetra-Cys environment (Markov et al. 1999). RpoZ verifies a proper zinc-mediated folding of RpoC before RpoC is allowed to assemble with RpoA<sub>2</sub>RpoB to create the mature RNA polymerase core enzyme (Sarkar et al. 2013). Not properly folded RpoC is secreted into inclusion bodies (Herzberg et al. 2014a).

The supply of pre-discriminated zinc to the ribosome should be complemented by a supply of discriminated zinc. Candidates for discriminators are the products of genes that are co-regulated with *zupT* by the Zur protein (Bütöf et al. 2017). Zur controls beside the *zupTp* promoter three additional operons, a *zur-cobW2* and *cobW3* promoter with one binding site and a large operon beginning with the gene

*cobW1* with two binding sites. Consequently, *zupT*, *zur*, *cobW2*, and *cobW3* are produced at medium zinc concentration while *cobW1* and the six genes following *cobW1* are synthesized only under conditions of severe zinc starvation (Bütöf et al. 2017).

In hierarchical protein taxonomy, the three CobW proteins belong to: (i) the COG0523 group of the (ii) G3E family of GTPases, (iii) SIMIBI protein class and (iv) GTPase superclass of (v) P-loop NTPases (Leipe et al. 2002; Verstraeten et al. 2011). All proteins binding NTP or related compounds can be categorized according to their central folding type. This is in the case of P-loop NTPases a central beta-sheet surrounded by alpha-helices. The N-terminal part of these proteins contains the “Walker A” NTP-binding motif in a flexible phosphate-binding or “P-loop,” and a “Walker B” motif with a conserved negatively charged amino acid (Leipe et al. 2002). A large number of protein superclasses belong to these P-loop NTPases, among them the  $F_1$ -components of the  $F_1F_0$ -ATPase, ABC proteins, AAA+ proteins and GTPases such as the three CobW proteins. These GTPases usually cycle between a GTP- or “on”-state and a GDP- or “off”-state and interact in the “on”-state with other proteins (Leipe et al. 2002). They contain in addition to the two Walker motifs a switch “G2” motif and two binding motifs for the guanine residue (Verstraeten et al. 2011). The switch coordinates the magnesium ion of the MgGTP complex and couples the interaction with an effector of GTP hydrolysis. In the case of the CobW-related protein YkiA, the switch contains a metal-binding triple-Cys motif GCICC (Khil et al. 2004; Sydor et al. 2013), which is also present in CobW1 and CobW2 (CXC2, Table 15) but not in CobW3. Binding of a metal to the metal-binding motif at the switch site may trigger interaction with an effector and GTP hydrolysis.

The P-loop GTPases in general assemble with interaction partners, exchange GDP for GTP, hydrolyze GTP, and the interacting complex is dissolved again. This process activates the interaction partner. There are two protein classes of the P-loop GTPases, the translation factors (TRAFAC class, e.g., elongation factors TU and G) and a class of signal recognition particles (SIMIBI class), which differ with respect to the fold of the protein and the location of the Walker motifs (Verstraeten et al. 2011; Leipe et al. 2002). Within the SIMIBI class of proteins, CooC-like proteins of the MinD-type SIMIBI proteins insert nickel ions into the carbon monoxide dehydrogenase and acetyl CoA synthase in anaerobic bacteria (Kerby et al. 1997; Jeon et al. 2001; Gregg et al. 2016) (Leipe et al. 2002; Jeoung et al. 2009). Another SIMIBI protein family named “G3E” contains a conserved glutamate residue at the Walker B (or G3) motif. Four subfamilies of G3E-SIMIBI P-loop GTPases all contain members that interact with transition metals: (i) ArgK/MeaB proteins help to assemble B12-dependent methyl-malonyl-CoA mutase (Hubbard et al. 2007), maybe by inserting cobalt; (ii) HypB- and (iii) UreG-proteins deliver Ni to hydrogenase and urease, respectively, while (iv) the CobW proteins belong to the COG0523 group of enzymes that interact with zinc (Haas et al. 2009). These proteins may all be providers of already discriminated metal cations. UreG and HypB proteins are excellent models for the function of COG0523 proteins.

UreG should cycle between assembly with an interaction partner on the one hand, and GTPase-triggered metal delivery and dis-assembly on the other hand. *C. metallidurans* contains also genes for an urease and its assembly, although in Tris-buffered mineral salts medium there is sufficient ammonium present that the urease is not produced. Interestingly, UreG and the nickel chaperone UreE are present in the cells nevertheless, maybe serving as nickel storage compounds to keep nickel in case urease might be required in the future. UreG shows two putative metal-binding motifs (Table 19.12), one with a Cys and one with a CXH motif. UreE exhibits a triple His-site and a large C-terminal His-rich stretch with 19 His residues, mostly with one aminoacyl residue in-between the His, plus one Cys (Table 19.12).

The function of UreG was mainly studied in *Helicobacter pylori* and *Klebsiella aerogenes*. Loss of UreG leads to a clear-cut phenotype: urease apoproteins without nickel, consequently no enzymatic activity and mutants unable to use urea as nitrogen source or, in the case of *H. pylori*, unable to buffer its microenvironment in the stomach to survive the low pH value (Farrugia et al. 2013).

To deliver nickel, UreG interacts with the tri-trimeric (UreABC)<sub>3</sub> apo protein complex as target protein, the docking protein UreD that is named “UreH” in *H. pylori*, the metal-fidelity checkpoint UreF (Zambelli et al. 2014), and the nickel chaperone UreE (Farrugia et al. 2013; Yang et al. 2015). Two Ni ions are inserted per UreABC trimer, which explains why the nickel-delivering protein complex is in the dimeric (UreDFG)<sub>2</sub> form. The second task of this complex is connected to the carbamylation of an active site lysine residue of the urease, which is a prerequisite for nickel delivery because it bridges the two cations (Farrugia et al. 2013). So, while the CobWs might be required to deliver one tightly bound zinc ion for instance to the nascent RpoC subunit of the RNA polymerase (Wu et al. 1992; Markov et al. 1999), UreG is involved in the delivery of two nickel ions plus a carbamylation reaction, which explains why dimerization is more important for UreG than for the CobWs as demonstrated for CobW1 (Bütof et al. 2019).

Carbamylation and nickel delivery seems to be initiated by binding of UreD docking protein to the (UreABC)<sub>3</sub> apoprotein complex although there first may be the formation of the (UreDFG)<sub>2</sub> di-trimer that subsequently binds to (UreABC)<sub>3</sub> (Farrugia et al. 2013). Since the metallation of urease apo-protein is not finished by a covalent modification or proteolytic action, the task of UreD could be to differentiate between correctly metallated urease and wrongly or under-metallated protein forms, indicating that metallation of mature proteins may need a docking protein. In any case, two UreDs interact with an UreF<sub>2</sub> dimer (Fong et al. 2011). This homo-dimerization to (UreDF)<sub>2</sub> is essential for urease maturation (Fong et al. 2013) and may provide a nickel-specific funnel to under-metallated apo-ureases. Since the ratio of Zn:Ni for instance in *E. coli* is >9:1 (Kirsten et al. 2011), the funnel may serve as a last quality checkpoint to prevent metallation of urease by zinc despite previous discrimination steps. In the opposite case of zinc insertion, the lower nickel content and the presence of nickel-binding proteins make mis-metallation of zinc proteins by nickel an event of low probability, possibly making a last checkpoint not necessary.

Free UreG may be partly an intrinsically disordered protein either without or having only a low GTPase activity, is a monomer in the absence of metals, and binds

Table 19.12 GTPases and associated proteins<sup>a</sup>

Rmet	ProtNum	Gene	Total
<b>Urease</b>			
Rmet_0959	NeF	<i>ureJ</i>	<b>HX2HD-HX3HX2E</b>
Rmet_0962	78	<i>ureE</i>	DXH-HX3E-HXHXHD-HEH2XHXHXHXHXHXHDHDDHDDHDXHDEHCXHXH/
Rmet_0963	NQ/NF	<i>ureF</i>	DX3H-DX2HX3E-DEX2CX2D
<b>Rmet_0964</b>	179	<i>ureG</i>	<b>EX2C-EX3CXH</b>
<b>SlyD-type</b>			
Rmet_1073	2029	<i>slyD</i>	HX3D-DXHD-DX2H-H/
<b>Membrane-bound hydrogenase</b>			
<b>Rmet_1285</b>	NF/NF	<i>hypB1</i>	<b>XCX2CXCD-HX2H-DXH-HXEXH-CX3E-CHXD-HXHEHXDXHXHDHDXHDH4XDXXH-DX3HX3DX3C-DX3HX2DH-HSDE</b>
Rmet_1286	NF/NF	<i>hypA1</i>	XHE-CX2C-CX2C
Rmet_1296	NeF	<i>hypE</i>	HXHE-HX2H-EX3H-HX3HX2E
<b>Soluble hydrogenase</b>			
Rmet_1535	NF/NF	<i>hypA2</i>	XHE-CXD-, Although
<b>Rmet_1536</b>	NF/NF	<i>hypB2</i>	<b>XCX2CXCX3E-EHXHEHXHXDX3HXHXHX2HEXDXH2X2DHDHDXHXHXH-DHXHX2H-DEH-CHXD-HX2E-EXH-CDX3HX3D</b>
<b>CobWs and proteins encoded downstream of <i>cobW1</i></b>			
<b>Rmet_0125</b>	263	<i>cobW3</i>	HXE-DXHXD-DHX3E-EDEHXE-HXD-DXHD-HDDDD-EXCD-HX3H-DX2H-DX2HXE3EHXD-DXHX2E-CX3DDE-DDDDHDDHDXHDHDXDX2CDCXHXH/
<b>Rmet_0127</b>	1755	<i>cobW2</i>	EXH-CXC2-DX2H-DX2HX3H-HX2E-DEHDHEHDHEHEHEHCX2DCXHDHXHEHXHDHXXHXHDH7XD-DX3H
<b>Rmet_1098</b>	NeF	<i>cobW1</i>	<b>HX2H-HX2HX2E-CX2X3ED-EX2HXD-EXCD-HX2E-EX3CXDXCX3DDE</b>
Rmet_1099	NeF	<i>foIE_IB2</i>	<b>HX2C-HX3DXHXD-DXHXDCE-CXC-DHXE-HX2HXEX2HXHD-HX2E</b>
Rmet_1100	NeF	<i>cysS</i>	DX2HED-DHX3H-HXECDXKH-H2E-CX3EX2C-HX2HX2D-EHXE-DHX3E
Rmet_1101	NeF	-	X2CDE-EX2H-CXHX2HXH-EXHX2DH-HXE-DX3H-CX2ED

(continued)

Table 19.12 (continued)

Rmet	ProtNum	Gene	Total
Rmet_1102	NF/NF	-	<b>HX2C-CX2EDXC-CH</b>
Rmet_1103	NeF	<i>allB</i>	HXD-DX3HX2E-HXE- <b>CDH-EHXE-DDDEX2C-HXEDE-DX3H-HX2H-EX3H2X3EX2FCXF-EXCH-DHX2HX3E-DHXH</b>

<sup>a</sup>The Rmet number is provided, the number of proteins per cell in *C. metallidurans* AE104 (Herzberg et al. 2014b), the capacity per protein and, as a product, the capacity per cell

nickel only with low affinity without leading to dimerization (Bellucci et al. 2009). UreG alone may dimerize in the presence of nickel plus MgGTP but the (UreDF)<sub>2</sub> complex facilitates dimerization of UreG at this scaffold (Fong et al. 2013). Following binding of GTP, a Cys and a His residue from each of the UreG protomers move toward each other to pre-form a square-planar binding site for nickel with nickel-binding to this site being a pre-requisite for dimerization (Yuen et al. 2017). These amino acid residues in a CPH motif are directly downstream of the Walker B motif (EX3CXH = ETGGCPH, Table 19.12). There is no such motif in the CobWs (Bütöf et al. 2019), again indicating a less pronounced interaction between metal binding and dimerization in agreement with the fact that only one zinc ion is required to be delivered in most cases, compared to two nickel ions.

In the presence of MgGTP and Ni, Ni-(UreG-MgGTP)<sub>2</sub> is also ready to dissociate from this complex again. In the additional presence of bicarbonate, required for carbamylation, the GTPase activity of UreG within the (UreDFG)<sub>2</sub> complex seems to be activated, leading to monomerization of UreG and nickel delivery through a nickel tunnel through UreF that exits at UreD (Farrugia et al. 2015; Fong et al. 2013; Farrugia et al. 2013). So, the (UreDFG)<sub>2</sub> di-trimer assembles and binds to the target protein or assembles at the target protein, and presence of nickel plus bicarbonate triggers GTP hydrolysis, nickel delivery through UreFD to the target and UreG release, following the SIMIBI scheme but with a sophisticated nickel delivery tunnel.

The nickel ion delivered to urease initiates from UreE (Farrugia et al. 2015). The C-terminus of UreE is disordered and acquires structure upon metal binding. Nickel and zinc ions are both bound but in a different complex. Zinc is bound by a UreE tetramer in a tetrahedral complex by histidine residues coming from three UreE polypeptides, nickel is penta-coordinated by histidine residues and a glutamate is provided by another protomer (Banaszak et al. 2012; Zambelli et al. 2013) so that the identity of the bound metal is mirrored in the dimeric or tetrameric form of UreE (Merloni et al. 2014). UreE is thus responsible for the first discrimination of nickel. The C-terminal His-rich stretch of UreE (Table 19.12) is central to this process and the typically 78 UreE proteins present per *C. metallidurans* cell serve as part of the cellular nickel repository that gets Ni(II) away from the zinc allocation pathway. The role of the glutamate to discriminate nickel is reminiscent to the CnrX nickel-binding protein involved in the regulation of the CnrCBA nickel efflux system of *C. metallidurans* (Nies et al. 2017; Maillard et al. 2015; Trepreau et al. 2014). Dimeric UreE binds UreG to form a (UreEG)<sub>2</sub> hetero-tetramer in the presence of MgGTP. The GTPase activity is activated in the presence of hydrogen carbonate, and thus the UreG is able to bind nickel (Yang et al. 2015).

Similar to other GTPases, the GTP-bound state of UreG is “on.” Activity of UreG requires interaction with at least three other proteins for docking, quality control, and as nickel chaperone. UreG does not discriminate nickel. Correct folding of UreG and activation of the GTPase activity is mediated by the (UreDFG)<sub>2</sub> nickel delivery complex. In the GDP-bound “off” state, monomeric UreG seems to be released from the (UreDF) nickel delivery scaffold. The absence of extensive His-rich sequences in UreG could make UreE and maybe also both SlyD and UreJ serve as additional



nickel chaperones when necessary (Haas et al. 2009; Farrugia et al. 2013). As in the case of the CooC-proteins of the MinD family, the dimeric nickel delivery complex assembles at the target protein, binds a metal substrate, and metal delivery and release of the delivering proteins then is triggered by NTP hydrolysis.

Chemolithoautotrophic growth of some hydrogen-oxidizing bacteria depends on the presence of nickel (Bartha and Ordal 1965) because one class of hydrogenases contains a complex iron-nickel active center. The products of such accessory genes are required to insert both metals and their ligands (Sankar et al. 1985), first the iron followed by the nickel center (Lacasse and Zamble 2016). Nickel incorporation is accomplished by HypA, HypB, maybe an additional nickel chaperone such as HupE and, not encoded by the auxiliary hydrogenase maturation gene cluster, SlyD (Lacasse and Zamble 2016). *C. metallidurans* CH34 wild type with both plasmids synthesizes both a membrane-bound and a soluble nickel-containing hydrogenase, however, the plasmid-free mutant strain AE104 suffers a mild zinc stress in Tris-buffered mineral salts medium, leading to a deletion of various genomic islands, including both islands that encode for the hydrogenases (Herzberg et al. 2015; Große et al. 2022). That corresponds to the discovery that no hydrogenases or maturation factors for these enzymes were found in the proteome of strain AE104 (Herzberg et al. 2014b, Table 15).

Reminiscent to UreG, HypB from *E. coli* acts as dimer and has a low-level GTPase activity (Maier et al. 1993), as does its ortholog from *Bradyrhizobium japonicum*. This protein is able to bind 18 Ni per dimer to a His-rich region (Fu et al. 1995), while the ortholog from *Rhizobium leguminosarum* binds only 8 Ni per dimer, mostly to its His-rich N-terminus (Rey et al. 1994). The number of nickel atoms bound and the size of the His-rich stretch varies among the HypB proteins. *C. metallidurans* contains a HybB for each hydrogenase and both contain large His-rich stretches that could compete with UreE and CnrT for nickel-binding capacity. Please note that the GTPase for urease maturation, UreG, does not contain a large nickel-binding site and this task is performed by an extra protein, UreE, while both HypBs may have the ability to be also nickel-storage compounds (Table 19.12).

The structure of HypB from the archaeon *Methanocaldococcus jannaschii* shows that dimerization depends on the presence of the nucleotides, which are bound to sites at the dimer interfaces. Since the nucleotides bind to amino acid residues of both protomers, dimerization and nucleotide binding go hand-in-hand, and are a pre-requisite of the subsequent GTP hydrolysis. This situation is different in the case of CobW1, because dimerization was not influenced by the presence of zinc or MgGTP (Bütöf et al. 2019). Of the two metal-binding sites of the archaeal HybB ortholog, one is relayed to the nucleotide-binding site via the switch region (Gasper et al. 2006). HypB from *H. pylori* dimerizes only in the presence of nickel but not zinc, and zinc inhibits its GTPase activity (Sydor et al. 2011). Both metals bind to HypB but as in the case of UreE, zinc forms the “wrong” ternary complex, only nickel the correct complex, which is a pre-requisite for GTP hydrolysis. This agrees fully with the ability of Ni(II) to accommodate one ligand (or two half ligands) more than Zn(II). In HypB from *H. pylori*, GTP or GDP affect a different coordination geometry of the nickel ion via a histidine residue and a cysteine of the switch II

GTPase domain, which is also involved in the interaction between metal binding and GTPase activity (Sydor et al. 2014). So, HypB is able to discriminate nickel, which allows dimerization and activates GTPase activity. Consequently, nickel-mediated dimerization is an important nickel-against-zinc discrimination process, which is used by HypB and UreE. Since the CobWs may not need to discriminate zinc against nickel or cobalt, due to the lower numbers of these ions in the cell, this could be another reason for a low importance of dimerization in the CobWs (Bütof et al. 2019).

SlyD contains three domains, a peptidylprolyl isomerase, a molecular chaperone and a C-terminal metal-binding domain. The chaperone domain of SlyD and a linker region between the GTPase domain and the N-terminal nickel-binding site of HypB interact to form a HypB-SlyD complex. The C-terminal metal-binding domain is required to stimulate the release of nickel from the high-affinity site of HypB, so that SlyD could activate nickel release from HypB to the maturing hydrogenase in *E. coli* (Leach et al. 2007; Khorasani-Motlagh et al. 2017), especially in late-stationary phase cells (Pinske et al. 2015). In *H. pylori*, the chaperone domain of SlyD is also required for interaction with HypB but in this bacterium, SlyD additionally delivers nickel to HypB, which leads to activation of the GTPase activity (Cheng et al. 2013). SlyD enhances the ability of HypB to acquire and discriminate nickel. With this respect, SlyD interacts with HypB to form another checkpoint for correct discrimination of nickel, comparable to the interaction of UreG and the UreF funnel. Nevertheless, there are no outstanding metal-binding motifs in SlyD from *C. metallidurans* (Table 19.12).

HypA from *E. coli* contains a structural zinc atom, binds nickel only weakly, and interacts with HypB (Atanassova and Zamble 2005). The ortholog from *H. pylori* contains two domains, one with a rigid structural zinc-binding site composed of a tetrahedral zinc-Cys4 complex, and an N-terminal site where nickel is bound by four nitrogen atoms possibly in a square-planar geometry (Xia et al. 2009). Both HypAs from *C. metallidurans* possess two double-Cys sites required for the binding of zinc in a tetrahedral CCCC site (Table 19.12).

HypA and HypB interact (Xia et al. 2012). Although both proteins are dimers, a HypAB heterodimer is formed when both proteins are present (Mehta et al. 2003). In *E. coli*, HypA can efficiently remove nickel from HypB-GDP and to a smaller extent from HypB-GTP (Douglas et al. 2013). A mutant HypA that cannot bind nickel still can bind to HypB-GDP but not HypB-GTP so that formation of the Ni-GTP-dimer of HypB triggers GTP hydrolysis, followed by binding of HypA and transfer of nickel to HypA (Lacasse et al. 2016). HypB from the thermophilic euryarchaeon *Thermococcus kodakarensis* is an ATPase instead of a GTPase. Only ATP-HypB binds HypA, which forms the square-planar nickel binding site, which leads to ATP hydrolysis, disruption of the HypAB complex, and maybe insertion of nickel into the apo-hydrogenase (Watanabe et al. 2015).

UreG and HypB act as a dimer, may receive nickel from other proteins (UreE, SlyD), achieve binding of nickel and of the nickel receiver protein (UreF, HypA), then activates GTPase action, which leads to nickel delivery. In *H. pylori*, these nickel delivery pathways are interwoven, since the HypA and HypB proteins are also

needed for the formation of an active urease (Olson et al. 2001). Nickel but not zinc is transferred from HypA in a HypA-(UreE)<sub>2</sub> complex by protein–protein interaction (Yang et al. 2014) so that in *H. pylori*, UreE discriminates nickel and serves as a bridge to deliver the metal from HypA through the UreGF tunnel to urease in the presence of carbonate. HypA of *H. pylori* switches its nickel-binding site from a Cys4 environment at neutral pH values to a Cys2His2 at pH = 6.3, which may result in the allocation of nickel to urease rather than hydrogenase and subsequently increased release of ammonium from urease to buffer the acidic pH value outside of the bacterial cell (Johnson et al. 2015). HypA may act as track switch for nickel allocation. Subsequently, UreE serves as a bridge allowing UreG to grasp nickel from HypA (Yang et al. 2015). A zinc ion bound to a conserved CPH motif at the dimerization interface of UreG from *H. pylori* may keep UreG as dimer until nickel is delivered by this multi-step delivery pathway. This feature is absent in UreG from *Klebsiella* (Martin-Diaconescu et al. 2017).

Additional components for urease-specific nickel delivery may be the SlyD protein (Benanti and Chivers 2009) and UreJ/HupE-type proteins (McMillan et al. 1998). *C. metallidurans* contains all these proteins, two HypAs, HypBs and HupE/UreJs, SlyD (Rmet\_1073), and an *ureDAJBCEFG* operon, together with providing an extensive cellular network for nickel delivery. Since CobW2 contains a firmly bound nickel ion, probably stemming from the nickel-NTA column used for the purification of this protein, CobW2 possibly could interact with all these proteins involved in nickel delivery, although a role of CobW2 in nickel homeostasis has not been demonstrated.

CobW2 and CobW3 both contain large His-rich stretches, at the C-terminus in CobW3 and in the middle of the protein in the case of CobW3 (Table 19.12). CobW3 is no longer a GTPase. The protein seems to “titrate” zinc by increasing its zinc content with the cellular zinc concentration and interacts with zinc uptake systems other than ZupT (Bütöf et al. 2019). That way, it is responsible for the low zinc content of 20,000 zinc per cell in  $\Delta zupT$  cells (Bütöf et al. 2019). CobW3 blocks import by other uptake systems and the zinc content is kept at the absolute minimum as the result of this misregulation. CobW3 is ranked number 21 of the *C. metallidurans* proteins with the highest metal-binding capacity (Table 19.2).

CobW2 is still a GTPase and is responsible for the increased zinc content of  $\Delta zur$  cells, which express the Zur regulon at a high level (Bütöf et al. 2019; Bütöf et al. 2017; Schmidt et al. 2014). CobW2 may occur in a “closed” zinc-storing conformation and an “open” zinc-presenting conformation, and GTP-hydrolyzation may be connected to a switch between these two conformations. CobW2 is among the proteins with the largest overall metal-binding capacity of the cell (Table 19.4). The 1755 CobW2 copies per cell may bind up to 20,000 divalent transition metal cations per cell, 20% of the zinc repository, and this value has been experimentally verified (Bütöf et al. 2019).

While CobW3 may be a zinc transmitter and flux control regulator of zinc import systems and CobW2 a zinc sponge, CobW1, which is produced only under conditions of severe zinc starvation, is able to bind a lower number of zinc ions per protein (Table 19.12). CobW1 is still a GTPase (Bütöf et al. 2019) with a metal-binding

switch site plus two double His sites upstream of the switch CXCCX3ED (Table 19.12). Proteins closely related to CobW1 are YjiA and YeiR from *E. coli* and YciC from *Bacillus subtilis*. All of these proteins have a switch domain consisting of 10 or 11 amino acyl residues downstream of the Walker A motif, an internal metal-binding site with a triple Cys between their switch and a Walker B motif, a Guanine-binding site, but no long His-rich stretches as CobW2 and CobW3 possess (Bütöf et al. 2019).

YciC has been recently renamed as ZagA for “ZTP-activated GTPase A” as a response to a newly found connection between the zinc and folate metabolism in *B. subtilis* and maybe other bacteria (Chandrangsu et al. 2019). ZTP (Z nucleotide-5' triphosphate) is an alarmone that signals a shortage of tetrahydrofolate (THF) carrying a C1 compound such as a formyl, methenyl, methylene or methyl group. In a central step of cellular purine biosynthesis (Fig. 19.6), ZMP (AICAR, 5'-phosphoribosyl- 4-carboxyamido-5-aminoimidazole) and N<sup>10</sup>-formyl-THF react to form inosine monophosphate IMP, which is the direct precursor of GMP and GTP. The first step of this synthesis pathway is the ATP-dependent pyrophosphorylation of ribose-5-phosphate to 5-phosphoribosyl-1-pyrophosphate PRPP. A lack of N<sup>10</sup>-formyl-THF results in the accumulation of PRPP and ZMP. Both react to yield ribose-5-phosphate and ZTP until N<sup>10</sup>-formyl-THF becomes available again and can react back to PRPP and ZMP, which can now be processed to IMP and finally to GMP and GTP (Fig. 19.6).

Accumulation of ZTP indicates a shortage of C1-carrying THF, which could mean a lack of either C1 moieties or THF. C1 compounds can be generated from the amino acids serine and glycine (Lehninger 1977). Serine can be produced from the central metabolic component 3-phosphoglycerate via 3-phosphohydroxypyruvate, and cleaved into glycine and N<sup>5</sup>-N<sup>10</sup>-methylene-THF by the serine hydroxymethyltransferase GlyA. Glycine can be subsequently degraded into N<sup>5</sup>-N<sup>10</sup>-methylene-THF, ammonium and carbon dioxide by glycine dehydrogenase. GlyA is interestingly number 10 in the ranking list of proteins in *C. metallidurans* providing the largest metal capacity (Table 19.7). N<sup>5</sup>-N<sup>10</sup>-methylene-THF can be converted into N<sub>10</sub>-formyl-THF, the co-substrate for the synthesis of IMP from ZMP. The *glyA* gene in *C. metallidurans* is under the control of the *pfl* riboswitch, which is activated by ZTP so that more C1-carrying THF is produced as a response to ZTP accumulation.

Producing more C1-carrying THF is one possibility to solve the problem of interrupted purine biosynthesis due to a shortage of formyl-THF. The second would be to produce more folate and THF. Folate biosynthesis starts with GTP, which is cleaved by a cyclo-hydrolase. Depending on the particular cleavage reaction, the precursor for folate or other co-enzymes is produced (Sankaran et al. 2009; Ren et al. 2005; Karp et al. 2014). Fole\_I-type GTP cyclohydrolases initiate folate biosynthesis. Fole\_I GTP-cyclohydrolases belong either to the strictly zinc-dependent Fole\_IA or the metal-promiscuous Fole\_IB group (Sankaran et al. 2009). In *B. subtilis*, a combined shortage of formyl-THF and of zinc leads to the synthesis of ZTP on the one hand and Zur-dependent synthesis of ZagA on the other hand.

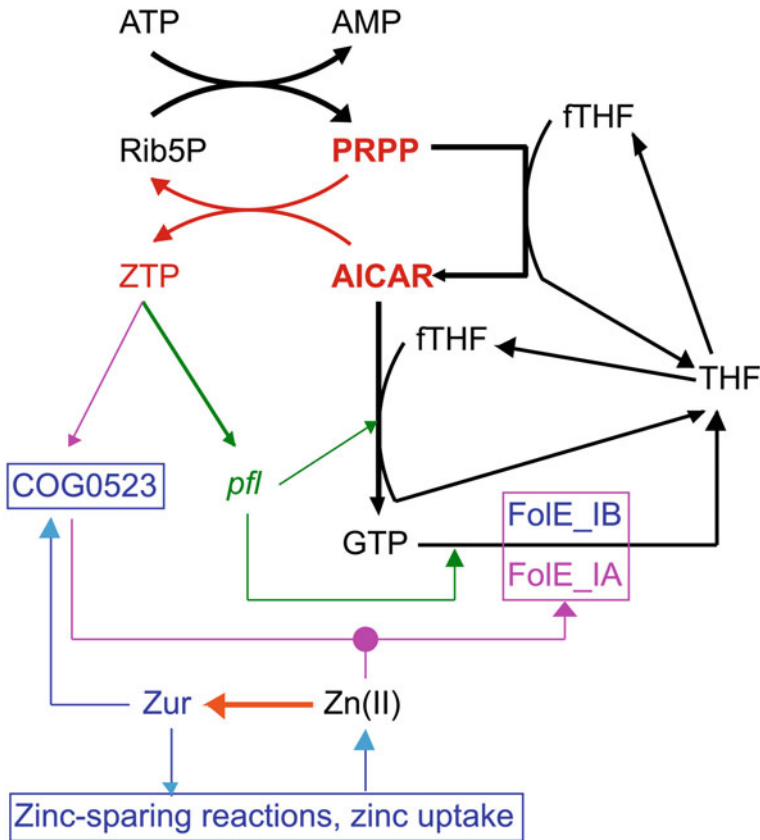


**Fig. 19.6** ZTP regulatory circuits. **Black:** GTP is a product of the bacterial purine biosynthesis pathway, which starts with an ATP-dependent pyrophosphorylation of ribose-5-phosphate (Rib5P) to 5-phosphoribosyl-1-pyrophosphate (PRPP), and continues via intermediates to GTP. Two of the biochemical reactions on this pathway depend on  $N^5,N^{10}$ -methenyl- or  $N^{10}$ -formyl-tetrahydrofolate (fTHF). **Red:** During THF starvation, transformation of AICAR to IMP by the strictly fTHF-dependent PurH enzyme is decreased, AICAR accumulates and is pyrophosphorylated by PRPP to ZTP. **Green:** Using the *pfl* riboswitch, ZTP activates operons involved in purine, THF biosynthesis, and/or interconversion of THF derivatives such as fTHF to compensate for fTHF starvation; different genes are used in different bacteria. An increased transformation of AICAR to GTP and further on to THF may cause as a back-reaction ZTP-dependent pyrophosphorylation of Rib5P to AICAR, consuming ZTP and switching-off the response. **Blue:** Under conditions of cellular zinc sufficiency the Zur regulator is activated by Zn(II) and prevents expression of genes involved in zinc uptake and consumption. These Zur-controlled operons are de-repressed when zinc ions are lacking in the cytoplasm (orange arrow). Some of these genes encode proteins of the COG0523 protein group, which are zinc chaperones, some *FoIE<sub>IB</sub>*-type GTP-cylohydrolases that do not strictly depend on zinc for activity. **Purple:** This sophisticated ZTP-dependent regulation of purine and THF biosynthesis is also exploited in *B. subtilis* to influence zinc homeostasis by recruiting the THF-influenced AICAR pool as sensor for zinc availability. If not compensated by the *FoIE<sub>IB</sub>*, decreased activity of the zinc-dependent *FoIE<sub>IA</sub>* enzyme due to zinc under-metallation leads to a diminished THF concentration, reduced activity of the fTHF-dependent PurA enzyme, and accumulation of AICAR and ZTP. The publication by the Helmann group (Chandrangsu et al. 2019) demonstrates that the COG0523 protein YciC from *B. subtilis* is activated by ZTP, which may result

ZTP activates ZagA, which consequently may deliver zinc to FolE<sub>IA</sub> to stimulate folate biosynthesis from GTP (Chandrangsu et al. 2019).

*C. metallidurans* contains three FolE-type enzymes, a FolE<sub>IA</sub> and two FolE<sub>IB</sub>-type proteins (Sankaran et al. 2009). One, FolE<sub>IB2</sub> or Rmet\_1099, is encoded directly downstream of *cobW1* in the *cobW1*-zinc starvation operon. CobW1 binds to FolE<sub>IB2</sub> although FolE<sub>IB2</sub> should be metal-promiscuous (Bütöf et al. 2019). The interaction of the three FolEs in *C. metallidurans* and the function of CobW1, also its interaction with ZTP, are the subject of current investigations.

In summary, metal-binding G3E-SIMIBI proteins of P-loop GTPases play an important role in the delivery of metals to metal-dependent proteins. They may be discriminators and providers for already discriminated metal cations. The interaction of the UreG GTPase with the nickel chaperone UreE and other factors to deliver nickel into urease and of the GTPase HybB to allocate nickel to hydrogenase has been well investigated. The COG0523 group of zinc-allocating GTPases has not been studied in such detail. *C. metallidurans* possesses three COG0523 proteins. CobW3 is present also in cells well provisioned with zinc, where it is no longer a GTPase but seems to interact with zinc uptake systems to control the influx of zinc. CobW2 is a zinc-storage compound that also is found in cells with sufficient zinc supply. CobW1 is encoded in an operon with six paralogs of zinc-dependent proteins, which are all expressed only under conditions of severe zinc starvation. The CobW1 ortholog ZagA from *B. subtilis* is activated by the alarmone ZTP and may deliver zinc to the zinc-dependent GTP-cyclohydrolase FolE<sub>IA</sub> to stimulate folate biosynthesis from GTP, with subsequent conversion of ZTP to ZMP and there might further be some conversion in a formyl-THF-dependent step to IMP, GMP, GTP. A gene for a metal-promiscuous GTP-cyclohydrolase FolE<sub>IB2</sub> is encoded downstream of *cobW1*. CobW1 and FolE<sub>IB2</sub> interact. It is currently under investigation how the FolE-type enzymes and the three CobWs in *C. metallidurans* interact, and which role ZTP might play at this point.

## 19.5 Sigma Factors Mollify the Effect of Allocation Preferences

The first pillar of multiple transition metal cation homeostasis is the transportome, which connects the outside, periplasm, and inside of the cell, and adjusts the transition metal cation concentrations and relative composition of the cell's metal supply. The second pillar is the cellular metal repository, which serves as a buffer for the transportome. Magnesium ions and transition metal cations may flow throughout



**Fig. 19.6** (continued) in an enhanced delivery of the zinc to FolE<sub>IA</sub>. Consequently, YciC was renamed “ZTP-activated GTPase A,” ZagA (Chandrangsu et al. 2019). Figure from (Nies 2019) with permission

the cell by a process of stepwise discrimination, beginning as pre-discriminated ions associated with repository parts on the surfaces of transport proteins in crowded and supercrowded cellular areas until, finally, the ions reach their eventual target proteins. Cu(I) is rapidly removed from the cytoplasm by CupC and P<sub>IB1</sub>-type ATPases to prevent its interference with interactions of other metals and their proteins. Iron could be discriminated by synthesis of iron-sulfur clusters and stored as Fe(III) in ferritin-like proteins. Zinc moves alongside magnesium until its repository has been reached. The repositories for zinc are located in the ribosome, RNA polymerase, CobW2 and CobW3 in *C. metallidurans*. Feedback control between the transportome and repository is exerted by the repository parts that are located in transport proteins and by metal-associated regulators of gene expression. These repository parts control the number of transport proteins per cell and fine-tune the transport activity by establishing flux control. The low numbers of nickel and cobalt ions per cell are directed to their target proteins such as urease and hydrogenase, and cobalamin compounds, respectively, by other members of the protein family of G3E-SIMIBI P-loop GTPases, which may efficiently remove nickel and cobalt from the zinc allocation pathway.

A third pillar seems to orchestrate all of this metal-associated activity and it is currently completely unclear how that orchestration works (Große et al. 2019). Responsibility for this third pillar in *C. metallidurans* rests with 11 sigma factors of the extracytoplasmic functions, or ECF family, of sigma factors (Staron et al. 2009; Helmann 2002; Lonetto et al. 1994). These ECF sigma factors are present in the cell in different numbers (Große et al. 2019). They can be grouped by the similarity of their amino acid sequences into four clusters named FecI1, FecI2, RpoE, and “ECF,” with each cluster containing 3 or 2 ECF sigma factors (Nies 2004; Große et al. 2007). These are involved in a hierarchical setting of preferences in transition metal cation homeostasis, with iron first and on top of the hierarchy (Fig. 19.7). This means that the required number of iron atoms per cell is maintained even at the cost of a disturbed homeostasis of other transition metal cations, magnesium, and also phosphate (Große et al. 2019). The consequences of pushing through “iron first” are reminiscent to the effect of multiple deletions of metal uptake systems (Herzberg et al. 2016; Grosse et al. 2016): despite the presence of their metal efflux systems, some metal cations other than iron do accumulate and become toxic. When “iron first” is challenged or uptake systems are absent, the cell seems to open new import and metal-distribution pathways, which cannot be sufficiently fine-tuned.

The FecI1-type sigma factors are RpoI, RpoJ, and RpoK. RpoI controls the synthesis and maybe transport of the siderophore of *C. metallidurans*, staphyloferrin B (Große et al. 2007). Despite the energetic cost of the synthesis of a complicated organic compound, its excretion and import of the iron-siderophore complex, this import pathway seems to be a well-controlled possibility to get a large part of the 500,000–700,000 needed iron ions into the cell. Lack of RpoI immediately lowers resistance to all divalent cations with an ionic diameter similar to Fe(II), namely Cu(II), Co(II), Ni(II), and Zn(II), plus Mg(II) and phosphate (Große et al. 2019). Gene arrays did not reveal which gates have been opened when staphyloferrin B cannot be

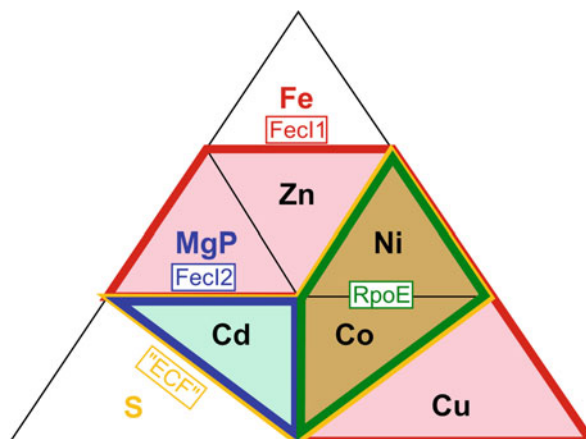


**Fig. 19.7** Preference formation by ECF sigma factors in *C. metallidurans*. The FecI1-type sigma factors mollify the effect of the “iron first” rule on homeostasis of the other transition metals, thereby influencing homeostasis of Zn, Ni, Co, Cu and the macro-bioelements Mg and P (fields framed in red). The FecI2-type sigma factors are involved in Mg and P homeostasis, which influences also cadmium resistance (blue field). The RpoE-type sigma factors are responsible for Ni and Co, “ECF”-type probably for sulfide/thiol/redox stress. The influences of “ECF” and FecI2 overlap with the Cd field (light blue color), “ECF”-, FecI1-, and RpoE-type with the Ni and Co field (brown). With permission from (Große et al. 2019)

used but the new import pathway seems to be a high-rate, low-selectivity, and difficult to control. Since cadmium resistance is not touched, the staphyloferrin B substitute is different from the metal import pathway upregulated in the  $\Delta 7$  and  $\Delta 9$  multiple uptake deletion mutants, which even accumulate more gold (Herzberg et al. 2016; Grosse et al. 2016; Wiesemann et al. 2013).

RpoJ and RpoK functionally substitute for RpoI to some extent, and all three FecI1-type sigma factors cooperate with FurA and FurB. There is also a cross-substitution of missing FecI1-type sigma factors by sigma factors of other ECF groups or even other sigma factors at all (Große et al. 2019). At the moment, a large data set of RNASeq and transcriptional start sites is being processed to assign the sigma factors of *C. metallidurans* to overlapping consensus sequences (Große et al. 2022). When this has been accomplished, it will reveal, how the FecI1-type sigma factors mollify the effect of “iron first” on homeostasis of the other transition metal cations of the first transition group, plus magnesium and phosphate, and which genes are up-regulated in response to a challenged “iron first.”

The FecI2-type ECF sigma factors RpoO, RpoL, and RpoM are connected to the balance between phosphate and metal-phosphate (Fig. 19.7). Disturbance here leads to over-accumulation of magnesium and phosphate, together with cadmium and partly also zinc (Große et al. 2019). Among the RpoE-type sigma factors RpoE, RpoP, and CnrH, RpoE is responsible for the integrity of the cell wall in *C. metallidurans* as in other bacteria (Ades et al. 2003; Rouviere et al. 1995; Egler et al. 2005), and CnrH for expression of the *cnr* cobalt-nickel resistance determinant



(Tibazarwa et al. 2000). All three sigma factors control nickel and cobalt homeostasis (Grass et al. 2005b; Grass et al. 2000). Since nickel and cobalt should inhibit the synthesis of iron-sulfur clusters (Ranquet et al. 2007; Thorgersen and Downs 2007; Fantino et al. 2010), the role of the periplasm in this process remains unclear. Lastly, the “ECF”-type sigma factors RpoQ and RpoR are connected to thiol homeostasis, maybe influencing the synthesis of iron-sulfur clusters to increase tolerance to nickel and cobalt, so that nickel and cobalt are controlled by three groups of ECF sigma factors, FecI1-, RpoE-, and “ECF”-type (Große et al. 2019). The 11 ECF sigma factors are thus involved in the preference setting of cellular transition metal cation, magnesium, phosphate, and thiol homeostasis (Fig. 19.7) but an understanding of how this all is functioning needs more work.

In summary, the 11 ECF sigma factors of *C. metallidurans* are involved in preference setting for metal homeostasis. The three FecI1-type sigma factors mollify the negative effect of “iron first” on the homeostasis of the remaining transition metal cations Co(II), Ni(II), Cu(II), Zn(II) plus magnesium and phosphate. The three FecI2-type sigma factors control phosphate versus metal-phosphate homeostasis. The three RpoE-type sigma factors are connected to the periplasm, plus associated with nickel and cobalt. Lastly, the two “ECF”-type sigma factors have thiol homeostasis as a common ground. How this all functions by a collective coordination is yet unclear but a large data set of RNASeq and transcriptional start site data is currently being analyzed which hopefully will further our understanding of these integrated systems.

## References

- Ades SE, Grigorova IL, Gross CA (2003) Regulation of the alternative sigma factor sigma (E) during initiation, adaptation, and shutoff of the extracytoplasmic heat shock response in *Escherichia coli*. *J Bacteriol* 185(8):2512–2519. <https://doi.org/10.1128/Jb.185.8.2512-2519.2003>
- Affandi T, Issaian AV, McEvoy MM (2016) The structure of the periplasmic sensor domain of the histidine kinase CusS shows unusual metal ion coordination at the dimeric interface. *Biochemist* 55(37):5296–5306. <https://doi.org/10.1021/acs.biochem.6b00707>
- Akanuma G, Nanamiya H, Natori Y, Nomura N, Kawamura F (2006) Liberation of zinc-containing L31 (RpmE) from ribosomes by its paralogous gene product, YtiA, in *Bacillus subtilis*. *J Bacteriol* 188:2715–2720
- Altendorf K, Epstein W (1996) The Kdp-ATPase of *Escherichia coli*. In: Dalbey RE (ed) *Advances in cell and molecular biology of membranes and organelles*, vol 5. JAI Press, Greenwich, pp 401–418
- Ammendola S, Ciavardelli D, Consalvo A, Battistoni A (2020) Cobalt can fully recover the phenotypes related to zinc deficiency in *Salmonella typhimurium*. *Metallomics* 12(12): 2021–2031. <https://doi.org/10.1039/d0mt00145g>
- Argüello JM, Eren E, Gonzalez-Guerrero M (2007) The structure and function of heavy metal transport P-1B-ATPases. *Biometals* 20:233–248
- Atanassova A, Zamble DB (2005) *Escherichia coli* HypA is a zinc metalloprotein with a weak affinity for nickel. *J Bacteriol* 187(14):4689–4697

- Baichoo N, Helmann JD (2002) Recognition of DNA by Fur: a reinterpretation of the Fur box consensus sequence. *J Bacteriol* 184:5826–5832
- Banaszak K, Martin-Diaconescu V, Bellucci M, Zambelli B, Rypniewski W, Maroney MJ, Ciorli S (2012) Crystallographic and X-ray absorption spectroscopic characterization of *Helicobacter pylori* UreE bound to Ni<sup>2+</sup> and Zn<sup>2+</sup> reveals a role for the disordered C-terminal arm in metal trafficking. *Biochem J* 441:1017–1026. <https://doi.org/10.1042/bj20111659>
- Banci L, Bertini I, Ciofi-Baffoni S, Kozyreva T, Zovo K, Palumaa P (2010) Affinity gradients drive copper to cellular destinations. *Nature* 465(7298):645–648. <https://doi.org/10.1038/nature09018>
- Bartha R, Ordal EJ (1965) Nickel-dependent chemolithotrophic growth of two *Hydrogenomonas* strains. *J Bacteriol* 89:1015–1019
- Beard SJ, Hashim R, Wu GH, Binet MRB, Hughes MN, Poole RK (2000) Evidence for the transport of zinc(II) ions via the Pit inorganic phosphate transport system in *Escherichia coli*. *FEMS Microbiol Lett* 184(2):231–235
- Bellucci M, Zambelli B, Musiani F, Turano P, Ciorli S (2009) *Helicobacter pylori* UreE, a urease accessory protein: specific Ni<sup>2+</sup>- and Zn<sup>2+</sup>-binding properties and interaction with its cognate UreG. *Biochem J* 422:91–100. <https://doi.org/10.1042/bj20090434>
- Benanti EL, Chivers PT (2009) An intact urease assembly pathway is required to compete with NikR for nickel ions in *Helicobacter pylori*. *J Bacteriol* 191(7):2405–2408. <https://doi.org/10.1128/jb.01657-08>
- Bender CL, Cooksey DA (1985) Plasmid-mediated copper resistance in *Pseudomonas syringae* pv *tomato*. *Phytopathology* 75(11):1325–1325
- Bersch B, Favier A, Schanda P, van Aelst S, Vallaeyts T, Coves J, Mergeay M, Wattiez R (2008) Molecular structure and metal-binding properties of the periplasmic CopK protein expressed in *Cupriavidus metallidurans* CH34 during copper challenge. *J Mol Biol* 380(2):386–403
- Bjerrum N (1926) Untersuchungen über Ionenassoziation. In: I. Der Einfluss der Ionenassoziation auf die Aktivität der Ionen bei Mittleren Assoziationsgraden. Publisher B. Lunos, Copenhagen
- Bleichert P, Bütof L, Rückert C, Herzberg M, Francisco R, Morais P, Grass G, Kalinowski J, Nies DH (2021) Mutant strains of *Escherichia coli* and methicillin-resistant *Staphylococcus aureus* obtained by laboratory selection to survive on metallic copper surfaces. *Appl Environ Microbiol* 87(1):e01788–e01720. <https://doi.org/10.1128/AEM.01788-20>
- Bobrov AG, Kirillina O, Fetherston JD, Miller MC, Burlison JA, Perry RD (2014) The *Yersinia pestis* siderophore, yersiniabactin, and the ZnuABC system both contribute to zinc acquisition and the development of lethal septicaemic plague in mice. *Mol Microbiol* 93(4):759–775. <https://doi.org/10.1111/mmi.12693>
- Borreman B, Hobman JL, Provoost A, Brown NL, Van der Lelie D (2001) Cloning and functional analysis of the *pbr* lead resistance determinant of *Ralstonia metallidurans* CH34. *J Bacteriol* 183(19):5651–5658
- Braun V (1995) Energy-coupled transport and signal transduction through the gram-negative outer membrane via TonB-ExbB-ExbD-dependent receptor proteins. *FEMS Microbiol Rev* 16(4):295–307
- Braun V, Braun M (2002) Active transport of iron and siderophore antibiotics. *Curr Opin Microbiol* 5:194–201
- Brazelton WJ, Morrill PL, Szponar N, Schrenk MO (2013) Bacterial communities associated with subsurface geochemical processes in continental serpentinite springs. *Appl Environ Microbiol* 79(13):3906–3916. <https://doi.org/10.1128/AEM.00330-13>
- Brown NL, Barrett SR, Camakaris J, Lee BT, Rouch DA (1995) Molecular genetics and transport analysis of the copper-resistance determinant (*pco*) from *Escherichia coli* plasmid pRJ1004. *Mol Microbiol* 17(6):1153–1166
- Burgess J (1978) Chapter 12: Kinetics and mechanism: complex formation. In: Metal ions in solution. Ellis Horwood, Chichester

- Burmann BM, Schweimer K, Luo X, Wahl MC, Stitt BL, Gottesman ME, Rosch P (2010) A NusE: NusG complex links transcription and translation. *Science* 328(5977):501–504. <https://doi.org/10.1126/science.1184953>
- Bütof L, Schmidt-Vogler C, Herzberg M, Große C, Nies DH (2017) The components of the unique Zur regulon of *Cupriavidus metallidurans* mediate cytoplasmic zinc handling. *J Bacteriol* 199(21):e00372–e00317., spotlight article. <https://doi.org/10.1128/JB.00372-17>
- Bütof L, Wiesemann N, Herzberg M, Altzschner M, Holleitner A, Reith F, Nies DH (2018) Synergetic gold-copper detoxification at the core of gold biomineralisation in *Cupriavidus metallidurans*. *Metallomics* 10:278–286. <https://doi.org/10.1039/c7mt00312a>
- Bütof L, Große C, Lilie H, Herzberg M, Nies DH (2019) Interplay between the Zur regulon components and metal resistance in *Cupriavidus metallidurans*. *J Bacteriol* 201(15):e00192–e00119. <https://doi.org/10.1128/JB.00192-19>
- Cerasi M, Liu JZ, Ammendola S, Poe AJ, Petrarca P, Pesciaroli M, Pasquali P, Raffatellu M, Battistoni A (2014) The ZupT transporter plays an important role in zinc homeostasis and contributes to *Salmonella enterica* virulence. *Metallomics* 6(4):845–853. <https://doi.org/10.1039/c3mt00352c>
- Cha JS, Cooksey DA (1991) Copper resistance in pseudomonas-syringae mediated by periplasmic and outer-membrane proteins. *Proc Natl Acad Sci U S A* 88(20):8915–8919. <https://doi.org/10.1073/pnas.88.20.8915>
- Chandrangsu P, Huang X, Gaballa A, Helmann JD (2019) *Bacillus subtilis* FoIE is sustained by the ZagA zinc metallochaperone and the alarmone ZTP under conditions of zinc deficiency. *Mol Microbiol* 112:751–765
- Changela A, Chen K, Xue Y, Holschen J, Outten CE, O’Halloran TV, Mondragon A (2003) Molecular basis of metal-ion selectivity and zeptomolar sensitivity by CueR. *Science* 301(5638):1383–1387
- Chao Y, Fu D (2004) Thermodynamic studies of the mechanism of metal binding to the *Escherichia coli* zinc transporter YjiP. *J Biol Chem* 279(17):17173–17180
- Cheng TF, Li HY, Yang XM, Xia W, Sun HZ (2013) Interaction of SlyD with HypB of *Helicobacter pylori* facilitates nickel trafficking. *Metallomics* 5(7):804–807. <https://doi.org/10.1039/c3mt00014a>
- Choi E, Groisman EA, Shin D (2009) Activated by different signals, the PhoP/PhoQ two-component system differentially regulates metal uptake. *J Bacteriol* 191(23):7174–7181. <https://doi.org/10.1128/JB.00958-09>
- Colvin RA, Holmes WR, Fontaine CP, Maret W (2010) Cytosolic zinc buffering and muffling: Their role in intracellular zinc homeostasis. *Metallomics* 2(5):306–317. <https://doi.org/10.1039/b926662c>
- Cooksey DA (1993) Copper uptake and resistance in bacteria. *Mol Microbiol* 7(1):1–5. <https://doi.org/10.1111/j.1365-2958.1993.tb01091.x>
- Coulton JW, Mason P, Cameron DR, Carmel G, Jean R, Rode HN (1986) Protein fusions of beta-galactosidase to the ferrichrome-iron receptor of *Escherichia coli* K-12. *J Bacteriol* 165(1):181–192
- Dawson RMC, Elliott DC, Elliott WH, Jones KM (1969) Data for biochemical research, 2nd edn. At The Clarendon Press, Oxford
- De Angelis F, Lee JK, O’Connell JD, Miercke LJW, Verschuieren KH, Srinivasan V, Bauvois C, Govaerts C, Robbins RA, Ruyschaert JM, Stroud RM, Vandebussche G (2010) Metal-induced conformational changes in ZneB suggest an active role of membrane fusion proteins in efflux resistance systems. *Proc Natl Acad Sci U S A* 107(24):11038–11043. <https://doi.org/10.1073/Pnas.1003908107>
- Debye P, Hückel E (1923) Zur Theorie der Elektrolyte. I. Gefrierpunktserniedrigung und verwandte Erscheinungen. *Phys Z* 24:185–206
- Diels L, Mergeay M (1990) DNA probe-mediated detection of resistant bacteria from soils highly polluted by heavy metals. *Appl Environ Microbiol* 56:1485–1491

- Douglas CD, Ngu TT, Kaluarachchi H, Zamble DB (2013) Metal transfer within the *Escherichia coli* HypB-HypA complex of hydrogenase accessory proteins. *Biochemist* 52(35):6030–6039. <https://doi.org/10.1021/bi400812r>
- Eberz G, Eitinger T, Friedrich B (1989) Genetic determinants of a nickel-specific transport system are part of the plasmid-encoded hydrogenase gene cluster in *Alcaligenes eutrophus*. *J Bacteriol* 171:1340–1345
- Egler M, Große C, Grass G, Nies DH (2005) Role of ECF sigma factor RpoE in heavy metal resistance of *Escherichia coli*. *J Bacteriol* 187:2297–2307
- Eitinger T, Friedrich B (1991) Cloning, nucleotide sequence, and heterologous expression of a high-affinity nickel transport gene from *Alcaligenes eutrophus*. *J Biol Chem* 266(5):3222–3227
- Eitinger T, Friedrich B (1994) A topological model for the high-affinity nickel transporter of *Alcaligenes eutrophus*. *Mol Microbiol* 12(6):1025–1032
- Eitinger T, Wolfram L, Degen O, Anthon C (1997) A Ni<sup>2+</sup> binding motif is the basis of high affinity transport of the *Alcaligenes eutrophus* nickel permease. *J Biol Chem* 272(27):17139–17144
- Eitinger T, Suhr J, Moore L, Smith JAC (2005) Secondary transporters for nickel and cobalt ions: Theme and variations. *Biometals* 18(4):399–405
- Eitinger T, Rodionov DA, Grote M, Schneider E (2011) Canonical and ECF-type ATP-binding cassette importers in prokaryotes: diversity in modular organization and cellular functions. *FEMS Microbiol Rev* 35(1):3–67. <https://doi.org/10.1111/j.1574-6976.2010.00230.x>
- Eshaghi S, Niegowski D, Kohl A, Molina DM, Lesley SA, Nordlund P (2006) Crystal structure of a divalent metal ion transporter CorA at 2.9 angstrom resolution. *Science* 313(5785):354–357
- Fagan MJ, Saier MH Jr (1994) P-type ATPases of eukaryotes and bacteria: sequence comparisons and construction of phylogenetic trees. *J Mol Evol* 38:57–99
- Fantino JR, Py B, Fontecave M, Barras F (2010) A genetic analysis of the response of *Escherichia coli* to cobalt stress. *Environ Microbiol* 12(10):2846–2857. <https://doi.org/10.1111/j.1462-2920.2010.02265.x>
- Farrugia MA, Macomber L, Hausinger RP (2013) Biosynthesis of the urease metallocenter. *J Biol Chem* 288(19):13178–13185. <https://doi.org/10.1074/jbc.R112.446526>
- Farrugia MA, Wang BB, Feig M, Hausinger RP (2015) Mutational and computational evidence that a nickel-transfer tunnel in UreD is used for activation of *Klebsiella aerogenes* urease. *Biochemist* 54(41):6392–6401. <https://doi.org/10.1021/acs.biochem.5b00942>
- Fath MJ, Kolter R (1993) ABC-transporters: the bacterial exporters. *Microbiol Rev* 57:995–1017
- Feklistov A, Sharon BD, Darst SA, Gross CA (2014) Bacterial sigma factors: a historical, structural, and genomic perspective. *Annu Rev Microbiol* 68:357–376. <https://doi.org/10.1146/annurev-micro-092412-155737>
- Fischer N, Neumann P, Konevega AL, Bock LV, Ficner R, Rodnina MV, Stark H (2015) Structure of the *E. coli* ribosome-EF-Tu complex at <3 Å resolution by Cs-corrected cryo-EM. *Nature* 520(7548):567–570. <https://doi.org/10.1038/nature14275>
- Fong YH, Wong HC, Chuck CP, Chen YW, Sun HZ, Wong KB (2011) Assembly of preactivation complex for urease maturation in *Helicobacter pylori*. Crystal structure of the UreF-UreH protein complex. *J Biol Chem* 286(50):43241–43249. <https://doi.org/10.1074/jbc.M111.296830>
- Fong YH, Wong HC, Yuen MH, Lau PH, Chen YW, Wong KB (2013) Structure of UreG/UreF/UreH complex reveals how urease accessory proteins facilitate maturation of *Helicobacter pylori* urease. *PLoS Biol* 11(10):e100167810
- Fontenot CR, Tasnim H, Valdes KA, Popescu CV, Ding H (2020) Ferric uptake regulator (Fur) reversibly binds a [2Fe-2S] cluster to sense intracellular iron homeostasis in *Escherichia coli*. *J Biol Chem* 295(46):15454–15463. <https://doi.org/10.1074/jbc.RA120.014814>
- Fu CL, Olson JW, Maier RJ (1995) HypB protein of *Bradyrhizobium japonicum* Is a metal-binding GTPase capable of binding 18 divalent nickel ions per dimer. *Proc Natl Acad Sci U S A* 92(6):2333–2337. <https://doi.org/10.1073/pnas.92.6.2333>
- Gaballa A, Helmann JD (1998) Identification of a zinc-specific metalloregulatory protein, Zur, controlling zinc transport operons in *Bacillus subtilis*. *J Bacteriol* 180(22):5815–5821

- Gabriel SE, Helmann JD (2009) Contributions of Zur-controlled ribosomal proteins to growth under zinc starvation conditions. *J Bacteriol* 191(19):6116–6122. <https://doi.org/10.1128/jb.00802-09>
- Garrick MD, Singleton ST, Vargas F, Kuo HC, Zhao L, Knopfel M, Davidson T, Costa M, Paradkar P, Roth JA, Garrick LM (2006) DMTI: Which metals does it transport? *Biol Res* 39(1):79–85
- Gasper R, Scrima A, Wittinghofer A (2006) Structural insights into HypB, a GTP-binding protein that regulates metal binding. *J Biol Chem* 281(37):27492–27502
- Goldberg M, Pribyl T, Juhnke S, Nies DH (1999) Energetics and topology of CzcA, a cation/proton antiporter of the RND protein family. *J Biol Chem* 274:26065–26070
- Gonzalez-Guerrero M, Raimunda D, Cheng X, Argüello JM (2010) Distinct functional roles of homologous Cu plus efflux ATPases in *Pseudomonas aeruginosa*. *Mol Microbiol* 78(5): 1246–1258. <https://doi.org/10.1111/j.1365-2958.2010.07402.x>
- Goris J, De Vos P, Coenye T, Hoste B, Janssens D, Brim H, Diels L, Mergeay M, Kersters K, Vandamme P (2001) Classification of metal-resistant bacteria from industrial biotopes as *Ralstonia campinensis* sp. nov., *Ralstonia metallidurans* sp. nov. and *Ralstonia basilensis* Steinle et al. 1998 emend. *Int J Syst Evol Microbiol* 51:1773–1782
- Grass G, Rensing C (2001) CueO is a multi-copper oxidase that confers copper tolerance in *Escherichia coli*. *Biochem Biophys Res Commun* 286(5):902–908
- Grass G, Große C, Nies DH (2000) Regulation of the *cnr* cobalt/nickel resistance determinant from *Ralstonia* sp. CH34. *J Bacteriol* 182(5):1390–1398
- Grass G, Wong MD, Rosen BP, Smith RL, Rensing C (2002) ZupT Is a Zn(II) uptake system in *Escherichia coli*. *J Bacteriol* 184:864–866
- Grass G, Franke S, Taudte N, Nies DH, Kucharski LM, Maguire ME, Rensing C (2005a) The metal permease ZupT from *Escherichia coli* is a transporter with a broad substrate spectrum. *J Bacteriol* 187:1604–1611
- Grass G, Fricke B, Nies DH (2005b) Control of expression of a periplasmic nickel efflux pump by periplasmic nickel concentrations. *Biometals* 18:437–448
- Grass G, Otto M, Fricke B, Haney CJ, Rensing C, Nies DH, Munkelt D (2005c) FieF (YiiP) from *Escherichia coli* mediates decreased cellular accumulation of iron and relieves iron stress. *Arch Microbiol* 183(1):9–18
- Gregg CM, Goetzl S, Jeoung JH, Dobbek H (2016) AcsF catalyzes the ATP-dependent insertion of nickel into the Ni<sub>2</sub>Ni-[4Fe4S] cluster of acetyl-CoA synthase. *J Biol Chem* 291(35): 18129–18138. <https://doi.org/10.1074/jbc.M116.731638>
- Große C, Grass G, Anton A, Franke S, Navarrete Santos A, Lawley B, Brown NL, Nies DH (1999) Transcriptional organization of the *czc* heavy metal homeostasis determinant from *Alcaligenes eutrophus*. *J Bacteriol* 181:2385–2393
- Große C, Friedrich S, Nies DH (2007) Contribution of extracytoplasmic function sigma factors to transition metal homeostasis in *Cupriavidus metallidurans* strain CH34. *J Mol Microbiol Biotechnol* 12:227–240
- Große C, Schleuder G, Schmöle C, Nies DH (2014) Survival of *Escherichia coli* cells on solid copper surfaces is increased by glutathione. *Appl Environ Microbiol* 80(22):7071–7078. <https://doi.org/10.1128/AEM.02842-14>
- Grosse C, Herzberg M, Schüttau M, Nies DH (2016) Characterization of the Δ7 mutant of *Cupriavidus metallidurans* with deletions of seven secondary metal uptake systems. *mSystems* 1(1):e00004–e00016. <https://doi.org/10.1128/mSystems.00004-16>
- Große C, Poehlein A, Blank K, Schwarzenberger C, Schleuder G, Herzberg M, Nies DH (2019) The third pillar of metal homeostasis in *Cupriavidus metallidurans* CH34: Preferences are controlled by extracytoplasmic functions sigma factors. *Metallomics* 11:291–316. <https://doi.org/10.1039/C8MT00299A>
- Große C, Kohl T, Herzberg M, Nies DH (2022) Loss of mobile genomic islands in metal resistant, hydrogen-oxidizing *Cupriavidus metallidurans*. *Appl Environ Microbiol* 88:e02048-21. <https://doi.org/10.1128/aem.02048-21>
- Guan G, Pinochet-Barros A, Gaballa A, Patel SJ, Arguello JM, Helmann JD (2015) PfeT, a P1B4 -type ATPase, effluxes ferrous iron and protects *Bacillus subtilis* against iron intoxication. *Mol Microbiol* 98(4):787–803. <https://doi.org/10.1111/mmi.13158>

- Gudipaty SA, McEvoy MM (2014) The histidine kinase CusS senses silver ions through direct binding by its sensor domain. *Biochimica Et Biophysica Acta-Proteins and Proteomics* 1844(9): 1656–1661. <https://doi.org/10.1016/j.bbapap.2014.06.001>
- Gudipaty SA, Larsen AS, Rensing C, McEvoy MM (2012) Regulation of Cu(I)/Ag(I) efflux genes in *Escherichia coli* by the sensor kinase CusS. *FEMS Microbiol Lett* 330(1):30–37. <https://doi.org/10.1111/j.1574-6968.2012.02529.x>
- Guskov A, Nordin N, Reynaud A, Engman H, Lundback AK, Jong AJO, Cornvik T, Phua T, Eshaghi S (2012) Structural insights into the mechanisms of  $Mg^{2+}$  uptake, transport, and gating by CorA. *Proc Natl Acad Sci U S A* 109(45):18459–18464. <https://doi.org/10.1073/pnas.1210076109>
- Haas CE, Rodionov DA, Kropat J, Malasarn D, Merchant SS, de Crecy-Lagard V (2009) A subset of the diverse COG0523 family of putative metal chaperones is linked to zinc homeostasis in all kingdoms of life. *BMC Genomics* 10:470. <https://doi.org/10.1186/1471-2164-10-470>
- Hantke K (1983) Identification of an iron uptake system specific for coprogen and rhodotorulic acid in *Escherichia coli* K12. *Mol Gen Genet* 191(2):301–306
- Hantke K (1987) Selection procedure for deregulated iron transport mutants (*fur*) in *Escherichia coli* K12: *fur* not only affects iron metabolism. *Mol Gen Genet* 210:135–139. <https://doi.org/10.1007/BF00337769>
- Hantke K (2005) Bacterial zinc uptake and regulators. *Curr Opin Microbiol* 8(2):196–202
- Harden TT, Wells CD, Friedman LJ, Landick R, Hochschild A, Kondev J, Gelles J (2016) Bacterial RNA polymerase can retain sigma70 throughout transcription. *Proc Natl Acad Sci U S A* 113(3):602–607. <https://doi.org/10.1073/pnas.1513899113>
- Harris RM, Webb DC, Howitt SM, Cox GB (2001) Characterization of PitA and PitB from *Escherichia coli*. *J Bacteriol* 183(17):5008–5014. <https://doi.org/10.1128/Jb.183.17.5008-5014.2001>
- Hashemian S (2011) Interaction energies of histidine with cations (H<sup>+</sup>, Li<sup>+</sup>, Na<sup>+</sup>, K<sup>+</sup>, Mg<sup>2+</sup>, Ca<sup>2+</sup>). *Russ J Inorg Chem* 56(3):397–401. <https://doi.org/10.1134/s0036023611020082>
- Helmann JD (2002) The extracytoplasmic function (ECF) sigma factors. *Adv Microb Physiol* 46: 47–110
- Helmann JD, Soonsange S, Gabriel S (2007) Metallalloregulators: arbiters of metal sufficiency. In: Nies DH, Silver S (eds) *Molecular microbiology of heavy metals*, Microbiology Monographs, vol 6. Springer-Verlag, Berlin, pp 37–71
- Hensley MP, Tierney DL, Crowder MW (2011) Zn(II) binding to *Escherichia coli* 70S ribosomes. *Biochemist* 50(46):9937–9939. <https://doi.org/10.1021/bi200619w>
- Herzberg M, Bauer L, Nies DH (2014a) Deletion of the *zupT* gene for a zinc importer influences zinc pools in *Cupriavidus metallidurans* CH34. *Metallomics* 6:421–436. <https://doi.org/10.1039/C3MT00267E>
- Herzberg M, Dobritzsch D, Helm S, Baginski S, Nies DH (2014b) The zinc repository of *Cupriavidus metallidurans*. *Metallomics* 6:2157–2165. <https://doi.org/10.1039/C4MT00171K>
- Herzberg M, Schütttau M, Reimers M, Grosse C, Schlegel HG, Nies DH (2015) Synthesis of nickel-iron hydrogenase in *Cupriavidus metallidurans* is controlled by metal-dependent silencing and un-silencing of genomic islands. *Metallomics* 7:632–649. <https://doi.org/10.1039/C4MT00297K>
- Herzberg M, Bauer L, Kirsten A, Nies DH (2016) Interplay between seven secondary metal transport systems is required for full metal resistance of *Cupriavidus metallidurans*. *Metallomics* 8:313–326. <https://doi.org/10.1039/C5MT00295H>
- Higgins CF (1992) ABC-transporters: from microorganisms to man. *Annu Rev Cell Biol* 8:67–113
- Higgins MK, Bokma E, Koronakis E, Hughes C, Koronakis V (2004) Structure of the periplasmic component of a bacterial drug efflux pump. *Proc Natl Acad Sci U S A* 101(27):9994–9999
- Higgs PI, Myers PS, Postle K (1998) Interactions in the TonB-dependent energy transduction complex: ExbB and ExbD form homomultimers. *J Bacteriol* 180(22):6031–6038

- Hobman JL, Yamamoto K, Oshima T (2007) Transcriptomic responses of bacterial cells to sublethal metal ion stress. In: Nies DH, Silver S (eds) *Molecular microbiology of heavy metals*, vol 6. Springer-Verlag, Berlin, pp 73–116
- Housecroft CE, Constable EC (2006) *Chemistry*, 3rd edn. Pearson Education, Essex
- Hubbard PA, Padovani D, Labunska T, Mahlstedt SA, Banerjee R, Drennan CL (2007) Crystal structure and mutagenesis of the metallochaperone MeaB - Insight into the causes of methylmalonic aciduria. *J Biol Chem* 282(43):31308–31316
- Hunte C, Srepani E, Venturi M, Rimon A, Padan E, Michel H (2005) Structure of a Na<sup>+</sup>/H<sup>+</sup> antiporter and insights into mechanism of action and regulation by pH. *Nature* 435:1197–1202
- Ishihama A (1988) Promoter selectivity of prokaryotic RNA polymerases. *Trends Genet* 4:282–286
- Israelachvili J (1985) *Intermolecular and surface forces*. Academic Press, Cambridge MA
- Jackson RJ, Binet MRB, Lee LJ, Ma R, Graham AI, McLeod CW, Poole RK (2008) Expression of the PitA phosphate/metal transporter of *Escherichia coli* is responsive to zinc and inorganic phosphate levels. *FEMS Microbiol Lett* 289(2):219–224. <https://doi.org/10.1111/j.1574-6968.2008.01386.x>
- Janssen PJ, Van Houdt R, Moors H, Monsieurs P, Morin N, Michaux A, Benotmane MA, Leys N, Vallaes T, Lapidus A, Monchy S, Medigue C, Taghavi S, McCorkle S, Dunn J, van der Lelie D, Mergeay M (2010) The complete genome sequence of *Cupriavidus metallidurans* strain CH34, a master survivalist in harsh and anthropogenic environments. *PLoS One* 5(5): e10433. <https://doi.org/10.1371/journal.pone.0010433>
- Jeon WB, Cheng JJ, Ludden PW (2001) Purification and characterization of membrane-associated CooC protein and its functional role in the insertion of nickel into carbon monoxide dehydrogenase from *Rhodospirillum rubrum*. *J Biol Chem* 276(42):38602–38609
- Jeoung JH, Giese T, Grunwald M, Dobbek H (2009) CooC1 from *Carboxydotherrmus hydrogenoformans* is a nickel-binding ATPase. *Biochemist* 48(48):11505–11513. <https://doi.org/10.1021/bi901443z>
- Jian X, Wasinger EC, Lockard JV, Chen LX, He C (2009) Highly sensitive and selective gold (I) recognition by a metalloregulator in *Ralstonia metallidurans*. *J Amer Chem Soc* 131:10869–10871
- Johnson RC, Hu HQ, Merrell DS, Maroney MJ (2015) Dynamic HypA zinc site is essential for acid viability and proper urease maturation in *Helicobacter pylori*. *Metallomics* 7(4):674–682. <https://doi.org/10.1039/c4mt00306c>
- Juhnke S, Peitzsch N, Hübener N, Große C, Nies DH (2002) New genes involved in chromate resistance in *Ralstonia metallidurans* strain CH34. *Arch Microbiol* 179:15–25
- Junge W, Sielaff H, Engelbrecht S (2009) Torque generation and elastic power transmission in the rotary F(O)F(1)-ATPase. *Nature* 459(7245):364–370. <https://doi.org/10.1038/nature08145>
- Kamizomo A, Nishizawa M, Teranishi A, Murata K, Kimura A (1989) Identification of a gene conferring resistance to zinc and cadmium ions in the yeast *Saccharomyces cerevisiae*. *Mol Gen Genet* 219:161–167
- Kanehisa M, Sato Y (2020) KEGG Mapper for inferring cellular functions from protein sequences. *Protein Sci* 29(1):28–35. <https://doi.org/10.1002/pro.3711>
- Kanehisa M, Goto S, Hattori M, Aoki-Kinoshita KF, Itoh M, Kawashima S, Katayama T, Araki M, Hirakawa M (2006) From genomics to chemical genomics: new developments in KEGG. *Nucleic Acids Res* 34:D354–D357
- Karp P, Weaver D, Paley S, Fulcher C, Kubo A, Kothari A, Krummenacker M, Subhraveti P, Weerasinghe D, Gama-Castro S, Huerta A, Muñoz-Rascado L, Bonavides-Martinez C, Weiss V, Peralta-Gil M, Santos-Zavaleta A, Schröder I, Mackie A, Gunsalus R, Collado-Vides J, Keseler I, Paulsen I (2014) The EcoCyc Database. *EcoSal Plus*. <https://doi.org/10.1128/ecosalplus.ESP-0009-2013>
- Kean J, Cleverley RM, O’Ryan L, Ford RC, Prince SM, Derrick JP (2008) Characterization of a CorA Mg<sup>2+</sup> transport channel from *Methanococcus jannaschii* using a thermofluor-based stability assay. *Mol Membr Biol* 25(8):653–661. <https://doi.org/10.1080/09687680802541169>

- Kehres DG, Zaharik ML, Finlay BB, Maguire ME (2000) The NRAMP proteins of *Salmonella typhimurium* and *Escherichia coli* are selective manganese transporters involved in the response to reactive oxygen. *Mol Microbiol* 36(5):1085–1100
- Kerby RL, Ludden PW, Roberts GP (1997) In vivo nickel insertion into the carbon monoxide dehydrogenase of *Rhodospirillum rubrum*: Molecular and physiological characterization of *cooCTJ*. *J Bacteriol* 179(7):2259–2266. <https://doi.org/10.1128/jb.179.7.2259-2266.1997>
- Khil PP, Obmolova G, Teplyakov A, Howard AJ, Gilliland GL, Camerini-Otero RD (2004) Crystal structure of the *Escherichia coli* YjiA protein suggests a GTP-dependent regulatory function. *Proteins* 54(2):371–374. <https://doi.org/10.1002/prot.10430>
- Khorasani-Motlagh M, Lacasse MJ, Zamble DB (2017) High-affinity metal binding by the *Escherichia coli* [NiFe]-hydrogenase accessory protein HypB is selectively modulated by SlyD. *Metallomics* 9(5):482–493. <https://doi.org/10.1039/c7mt00037e>
- Kim E-H, Nies DH, McEvoy M, Rensing C (2011) Switch oder funnel: how RND-type transport systems control periplasmic metal homeostasis. *J Bacteriol* 193:2381–2387. <https://doi.org/10.1128/JB.01323-10>
- Kirsten A, Herzberg M, Voigt A, Seravalli J, Grass G, Scherer J, Nies DH (2011) Contributions of five secondary metal uptake systems to metal homeostasis of *Cupriavidus metallidurans* CH34. *J Bacteriol* 193(18):4652–4663
- Koebnik R, Locher KP, Van Gelder P (2000) Structure and function of bacterial outer membrane proteins: barrels in a nutshell. *Mol Microbiol* 37(2):239–253. <https://doi.org/10.1046/j.1365-2958.2000.01983.x>
- Kohler R, Mooney RA, Mills DJ, Landick R, Cramer P (2017) Architecture of a transcribing-translating expressome. *Science* 356(6334):194–197. <https://doi.org/10.1126/science.aal3059>
- Krezel A, Maret W (2016) The biological inorganic chemistry of zinc ions. *Arch Biochem Biophys* 611:3–19. <https://doi.org/10.1016/j.abb.2016.04.010>
- Kühlbrandt W (2004) Biology, structure and mechanism of P-type ATPases. *Nat Rev Mol Cell Biol* 5:282–295. <https://doi.org/10.1038/nrm1354>
- Kumar BA, Naik KB, Raju S, Rao GN (2015) Formation and confirmation of binary complexes of calcium(II), magnesium(II) and zinc(II) with L-histidine in dioxan-water media. *Chem Spec Bioavailability* 24(3):139–146. <https://doi.org/10.3184/095422912x13406452149755>
- Lacasse MJ, Zamble DB (2016) [NiFe]-Hydrogenase Maturation. *Biochemist* 55(12):1689–1701. <https://doi.org/10.1021/acs.biochem.5b01328>
- Lacasse MJ, Douglas CD, Zamble DB (2016) Mechanism of selective nickel transfer from HypB to HypA, *Escherichia coli* [NiFe]-hydrogenase accessory proteins. *Biochemist* 55(49):6821–6831. <https://doi.org/10.1021/acs.biochem.6b00706>
- Leach MR, Zhang JW, Zamble DB (2007) The role of complex formation between the *Escherichia coli* hydrogenase accessory factors HypB and SlyD. *J Biol Chem* 282(22):16177–16186
- Legatzki A, Anton A, Grass G, Rensing C, Nies DH (2003a) Interplay of the Czc-system and two P-type ATPases in conferring metal resistance to *Ralstonia metallidurans*. *J Bacteriol* 185:4354–4361
- Legatzki A, Franke S, Lucke S, Hoffmann T, Anton A, Neumann D, Nies DH (2003b) First step towards a quantitative model describing Czc-mediated heavy metal resistance in *Ralstonia metallidurans*. *Biodegradation* 14:153–168
- Lehninger AL (1977) *Biochemistry*. Worth Publishers, New York
- Leipe DD, Wolf YI, Koonin EV, Aravind L (2002) Classification and evolution of P-loop GTPases and related ATPases. *J Mol Biol* 317(1):41–72. <https://doi.org/10.1006/jmbi.2001.5378>
- Li Y, Sharma MR, Koripella RK, Banavali NK, Agrawal RK, Ojha AK (2021) Ribosome hibernation: a new molecular framework for targeting nonreplicating persisters of mycobacteria. *Microbiology* 167(2):001035. <https://doi.org/10.1099/mic.0.001035>
- Liesegang H, Lemke K, Siddiqui RA, Schlegel H-G (1993) Characterization of the inducible nickel and cobalt resistance determinant *cnr* from pMOL28 of *Alcaligenes eutrophus* CH34. *J Bacteriol* 175:767–778



- Lonetto MA, Brown KL, Rudd KE, Buttner MJ (1994) Analysis of the *Streptomyces coelicolor* *sigF* gene reveals the existence of a subfamily of eubacterial RNA polymerase  $\sigma$  factors involved in the regulation of extracytoplasmic functions. *Proc Natl Acad Sci U S A* 91:7573–7577
- Long F, Su CC, Zimmermann MT, Boyken SE, Rajashankar KR, Jernigan RL, Yu EW (2010) Crystal structures of the CusA efflux pump suggest methionine-mediated metal transport. *Nature* 467(7314):484–488. <https://doi.org/10.1038/Nature09395>
- Lu M, Fu D (2007) Structure of the zinc transporter YiiP. *Science* 317(5845):1746–1748
- Lu M, Chai J, Fu D (2009) Structural basis for autoregulation of the zinc transporter YiiP. *Nature Struct Mol Biol* 16(10):1063–1068. <https://doi.org/10.1038/nsmb.1662>
- Lucarelli D, Russo S, Garman E, Milano A, Meyer-Klaucke W, Pohl E (2007) Crystal structure and function of the zinc uptake regulator FurB from *Mycobacterium tuberculosis*. *J Biol Chem* 282(13):9914–9922
- Lunin V, Dobrovetsky E, Khutoreskaya G, Zhang R, Joachimiak A, Doyle DA, Bochkarev A, Maguire ME, Edwards AM, Koth CM (2006) Crystal structure of the CorA Mg<sup>2+</sup> transporter. *Nature* 440:833–837
- Ma Z, Gabriel SE, Helmann JD (2011) Sequential binding and sensing of Zn(II) by *Bacillus subtilis* Zur. *Nucleic Acids Res* 39(21):9130–9138. <https://doi.org/10.1093/nar/gkr625>
- Magnani D, Solioz M (2007) How bacteria handle copper. In: Nies DH, Silver S (eds) *Molecular microbiology of heavy metals*, Microbiology monographs, vol 6. Springer-Verlag, Berlin, pp 259–285
- Maier T, Jacobi A, Sauter M, Böck A (1993) The product of the *hypB* gene, which is required for nickel incorporation into hydrogenases, is a novel guanine nucleotide-binding protein. *J Bacteriol* 175(3):630–635
- Maillard AP, Girard E, Ziani W, Petit-Hartlein I, Kahn R, Coves J (2014) The crystal structure of the anti-sigma factor CnrY in complex with the sigma factor CnrH shows a new structural class of anti-sigma factors targeting extracytoplasmic function sigma factors. *J Mol Biol* 426(12):2313–2327. <https://doi.org/10.1016/j.jmb.2014.04.003>
- Maillard AP, Kuennemann S, Grosse C, Volbeda A, Schleuder G, Petit-Härtlein I, de Rosny E, Nies DH, Coves J (2015) Response of CnrX from *Cupriavidus metallidurans* CH34 to nickel binding. *Metallomics* 7:622–631. <https://doi.org/10.1039/c4mt00293h>
- Makui H, Roig E, Cole ST, Helmann JD, Gros P, Cellier MF (2000) Identification of the *Escherichia coli* K-12 Nramp orthologue (MntH) as a selective divalent metal ion transporter. *Mol Microbiol* 35(5):1065–1078
- Markov D, Naryshkina T, Mustaev A, Severinov K (1999) A zinc-binding site in the largest subunit of DNA-dependent RNA polymerase is involved in enzyme assembly. *Genes Dev* 13(18):2439–2448
- Martin-Diaconescu V, Joseph CA, Boer JL, Mulrooney SB, Hausinger RP, Maroney MJ (2017) Non-thiolate ligation of nickel by nucleotide-free UreG of *Klebsiella aerogenes*. *J Biol Inorg Chem* 22(4):497–503. <https://doi.org/10.1007/s00775-016-1429-9>
- Mazzon RR, Braz VS, da Silva Neto JF, do Valle Marques M (2014) Analysis of the *Caulobacter crescentus* Zur regulon reveals novel insights in zinc acquisition by TonB-dependent outer membrane proteins. *BMC Genomics* 15:1–14
- McCarthy S, Ai C, Wheaton G, Tevatia R, Eckrich V, Kelly R, Blum P (2014) Role of an archaeal PitA transporter in the copper and arsenic resistance of *Metallosphaera sedula*, an extreme thermoacidophile. *J Bacteriol* 196(20):3562–3570. <https://doi.org/10.1128/jb.01707-14>
- McMillan DJ, Mau M, Walker MJ (1998) Characterisation of the urease gene cluster in *Bordetella bronchiseptica*. *Gene* 208(2):243–251. [https://doi.org/10.1016/S0378-1119\(97\)00651-3](https://doi.org/10.1016/S0378-1119(97)00651-3)
- Mehta N, Olson JW, Maier RJ (2003) Characterization of *Helicobacter pylori* nickel metabolism accessory proteins needed for maturation of both urease and hydrogenase. *J Bacteriol* 185(3):726–734
- Mellano MA, Cooksey DA (1988) Nucleotide sequence and organization of copper resistance genes from *Pseudomonas syringae* pv. tomato. *J Bacteriol* 170(6):2879–2883

- Mergeay M (2000) Bacteria adapted to industrial biotopes: metal-resistant *Ralstonia*. In: Storz G, Hengge-Aronis R (eds) Bacterial stress responses. ASM Press, Washington DC, pp 403–414
- Mergeay M, Nies D, Schlegel HG, Gerits J, Charles P, van Gijsegem F (1985) *Alcaligenes eutrophus* CH34 is a facultative chemolithotroph with plasmid-bound resistance to heavy metals. J Bacteriol 162:328–334
- Mergeay M, Monchy S, Vallaeyts T, Auquier V, Benotmane A, Bertin P, Taghavi S, Dunn J, van der Lelie D, Wattiez R (2003) *Ralstonia metallidurans*, a bacterium specifically adapted to toxic metals: towards a catalogue of metal-responsive genes. FEMS Microbiol Rev 27(2–3):385–410
- Merloni A, Dobrovolska O, Zambelli B, Agostini F, Bazzani M, Musiani F, Ciurli S (2014) Molecular landscape of the interaction between the urease accessory proteins UreE and UreG. Biochimica Et Biophysica Acta-Proteins and Proteomics 1844(9):1662–1674. <https://doi.org/10.1016/j.bbapap.2014.06.016>
- Missiakas D, Raina S (1998) The extracytoplasmic function sigma factors: role and regulation. Mol Microbiol 28:1059–1066
- Mohapatra S, Weissshaar JC (2018) Functional mapping of the *E. coli* translational machinery using single-molecule tracking. Mol Microbiol 110(2):262–282. <https://doi.org/10.1111/mmi.14103>
- Monchy S, Benotmane MA, Wattiez R, van Aelst S, Auquier V, Borremans B, Mergeay M, Taghavi S, van der Lelie D, Vallaeyts T (2006) Transcriptomics and proteomic analysis of the pMOL30-encoded copper resistance in *Cupriavidus metallidurans* strain CH34. Microbiology 152:1765–1776
- Munkelt D, Grass G, Nies DH (2004) The chromosomally encoded cation diffusion facilitator proteins DmeF and FieF from *Wautersia metallidurans* CH34 are transporters of broad metal specificity. J Bacteriol 186:8036–8043
- Nies DH (1992) CzcR and CzcD, gene products affecting regulation of resistance to cobalt, zinc and cadmium (*czc* system) in *Alcaligenes eutrophus*. J Bacteriol 174:8102–8110
- Nies DH (1995) The cobalt, zinc, and cadmium efflux system *CzcABC* from *Alcaligenes eutrophus* functions as a cation-proton-antiporter in *Escherichia coli*. J Bacteriol 177:2707–2712
- Nies DH (2003) Efflux-mediated heavy metal resistance in prokaryotes. FEMS Microbiol Rev 27(2/3):313–339
- Nies DH (2004) Incidence and function of sigma factors in *Ralstonia metallidurans* and other bacteria. Arch Microbiol 181:255–268
- Nies DH (2007a) Bacterial transition metal homeostasis. In: Nies DH, Silver S (eds) Molecular microbiology of heavy metals, Microbiology monographs, vol 6. Springer-Verlag, Berlin, pp 118–142
- Nies DH (2007b) How cells control zinc homeostasis. Science 317:1695–1696
- Nies DH (2013) RND-efflux pumps for metal cations. In: Yu EW, Zhang Q, Brown MH (eds) Microbial efflux pumps: current research. Caister Academic Press, Norfolk, pp 79–122. ISBN: 978-1-908230-21-8
- Nies DH (2014) Basic biochemical roots. In: Ecological biochemistry: environmental and inter-species interactions. Wiley-VCH, Weinheim
- Nies DH (2016) The biological chemistry of the transition metal “transportome” of *Cupriavidus metallidurans*. Metallomics 8:481–507. <https://doi.org/10.1039/C5MT00320B>
- Nies DH (2019) The ancient alarmone ZTP and zinc homeostasis in *Bacillus subtilis*. Mol Microbiol 112:741–746. <https://doi.org/10.1111/mmi.14332>
- Nies DH, Brown N (1998) Two-component systems in the regulation of heavy metal resistance. In: Silver S, Walden W (eds) Metal ions in gene regulation. Chapman Hall, New York, pp 77–103
- Nies DH, Silver S (1989) Plasmid-determined inducible efflux is responsible for resistance to cadmium, zinc, and cobalt in *Alcaligenes eutrophus*. J Bacteriol 171:896–900
- Nies DH, Silver S (1995) Ion efflux systems involved in bacterial metal resistances. J Ind Microbiol 14:186–199
- Nies D, Mergeay M, Friedrich B, Schlegel HG (1987) Cloning of plasmid genes encoding resistance to cadmium, zinc, and cobalt in *Alcaligenes eutrophus* CH34. J Bacteriol 169:4865–4868

- Nies DH, Nies A, Chu L, Silver S (1989) Expression and nucleotide sequence of a plasmid-determined divalent cation efflux system from *Alcaligenes eutrophus*. Proc Natl Acad Sci U S A 86:7351–7355
- Nies DH, Rehbein G, Hoffmann T, Baumann C, Grosse C (2006) Paralogs of genes encoding metal resistance proteins in *Cupriavidus metallidurans* strain CH34. J Mol Microbiol Biotechnol 11: 82–93
- Nies DH, Coves J, Sawers G (2017) Cross-talk between nickel and other metals in microbial systems. In: Kozłowski H, Zamble D, Rowińska-Żyrek M (eds) The Biochem of Nickel. The Royal Society of Chemistry, London, pp 306–338
- Noinaj N, Guillier M, Barnard TJ, Buchanan SK (2010) TonB-dependent transporters: regulation, structure, and function. Annu Rev Microbiol 64:43–60. <https://doi.org/10.1146/annurev.micro.112408.134247>
- Nordin N, Guskov A, Phua T, Sahaf N, Xia Y, Lu SY, Eshaghi H, Eshaghi S (2013) Exploring the structure and function of *Thermotoga maritima* CorA reveals the mechanism of gating and ion selectivity in Co<sup>2+</sup>/Mg<sup>2+</sup> transport. Biochem J 451:365–374. <https://doi.org/10.1042/bj20121745>
- Norris V, den Blaauwen T, Cabin-Flaman A, Doi RH, Harshey R, Janniere L, Jimenez-Sanchez A, Jin DJ, Levin PA, Mileyskova E, Minsky A, Saier M Jr, Skarstad K (2007) Functional taxonomy of bacterial hyperstructures. Microbiol Mol Biol Rev 71(1):230–253. <https://doi.org/10.1128/MMBR.00035-06>
- O'Halloran TV, Culotta VC (2000) Metallochaperones, an intracellular shuttle service for metal ions. J Biol Chem 275(33):25057–25060
- Olson JW, Mehta NS, Maier RJ (2001) Requirement of nickel metabolism proteins HypA and HypB for full activity of both hydrogenase and urease in *Helicobacter pylori*. Mol Microbiol 39(1):176–182
- Outten FW, Huffman DL, Hale JA, O'Halloran TV (2001) The independent *cue* and *cus* systems confer copper tolerance during aerobic and anaerobic growth in *Escherichia coli*. J Biol Chem 276(33):30670–30677
- Owen GA, Pascoe B, Kallifidas D, Paget MSB (2007) Zinc-responsive regulation of alternative ribosomal protein genes in *Streptomyces coelicolor* involves Zur and sigma(R). J Bacteriol 189(11):4078–4086
- Padan E, Venturi M, Gerchman Y, Dover N (2001) Na<sup>+</sup>/H<sup>+</sup> antiporters. Biochim Biophys Acta 1505:144–157
- Panina EM, Mironov AA, Gelfand MS (2003) Comparative genomics of bacterial zinc regulons: enhanced ion transport, pathogenesis, and rearrangement of ribosomal proteins. Proc Natl Acad Sci U S A 100(17):9912–9917
- Papp-Wallace KM, Nartea M, Kehres DG, Porwollik S, McClelland M, Libby SJ, Fang FC, Maguire ME (2008) The CorA Mg<sup>2+</sup> channel is required for the virulence of *Salmonella enterica* serovar Typhimurium. J Bacteriol 190(19):6517–6523. <https://doi.org/10.1128/JB.00772-08>
- Patzter SI, Hantke K (1998) The ZnuABC high-affinity zinc uptake system and its regulator Zur in *Escherichia coli*. Mol Microbiol 28(6):1199–1210
- Paulsen IT, Saier MH Jr (1997) A novel family of ubiquitous heavy metal ion transport proteins. J Membr Biol 156(2):99–103
- Paulsen IT, Park JH, Choi PS, Saier MHJ (1997) A family of Gram-negative bacterial outer membrane factors that function in the export of proteins, carbohydrates, drugs and heavy metals from Gram-negative bacteria. FEMS Microbiol Lett 156:1–8
- Pföh R, Li A, Chakrabarti N, Payandeh J, Pomes R, Pai EF (2012) Structural asymmetry in the magnesium channel CorA points to sequential allosteric regulation. Proc Natl Acad Sci U S A 109(46):18809–18814. <https://doi.org/10.1073/pnas.1209018109>
- Pinske C, Sargent F, Sawers RG (2015) SlyD-dependent nickel delivery limits maturation of [NiFe]-hydrogenases in late-stationary phase *Escherichia coli* cells. Metallomics 7(4): 683–690. <https://doi.org/10.1039/c5mt00019j>

- Pompidor G, Maillard AP, Girard E, Gambarelli S, Kahn R, Coves J (2008) X-ray structure of the metal-sensor CnrX in both the apo- and copper-bound forms. *FEBS Lett* 582(28):3954–3958. <https://doi.org/10.1016/j.febslet.2008.10.042>
- Proshkin S, Rahmouni AR, Mironov A, Nudler E (2010) Cooperation between translating ribosomes and RNA polymerase in transcription elongation. *Science* 328(5977):504–508. <https://doi.org/10.1126/science.1184939>
- Quaranta D, McEvoy MM, Rensing C (2009) Site-directed mutagenesis identifies a molecular switch involved in copper sensing by the histidine kinase CinS in *Pseudomonas putida* KT2440. *J Bacteriol* 191(16):5304–5311. <https://doi.org/10.1128/jb.00551-09>
- Ranquet C, Ollagnier-de-Choudens S, Loiseau L, Barras F, Fontecave M (2007) Cobalt stress in *Escherichia coli*. *J Biol Chem* 282:30442–30451
- Reith F, Rogers SL, McPhail DC, Webb D (2006) Biomineralization of gold: biofilms on bacterioform gold. *Science* 313:233–236
- Reith F, Lengke MF, Falconer D, Craw D, Southam G (2007) The geomicrobiology of gold. *ISME J* 1:567–584
- Ren J, Kotaka M, Lockyer M, Lamb HK, Hawkins AR, Stammers DK (2005) GTP cyclohydrolase II structure and mechanism. *J Biol Chem* 280(44):36912–36919. <https://doi.org/10.1074/jbc.M507725200>
- Rensing C, Grass G (2003) *Escherichia coli* mechanisms of copper homeostasis in a changing environment. *FEMS Microbiol Rev* 27(2–3):197–213. [https://doi.org/10.1016/S0168-6445\(03\)00049-4](https://doi.org/10.1016/S0168-6445(03)00049-4)
- Rensing C, Pribyl T, Nies DH (1997) New functions for the three subunits of the CzcCBA cation-proton-antiporter. *J Bacteriol* 179(22):6871–6879
- Rey L, Imperial J, Palacios JM, Ruizargueso T (1994) Purification of *Rhizobium leguminosarum* HypB, a nickel-binding protein required for hydrogenase synthesis. *J Bacteriol* 176(19):6066–6073. <https://doi.org/10.1128/jb.176.19.6066-6073.1994>
- Rice AJ, Park A, Pinkett HW (2014) Diversity in ABC transporters: Type I, II and III importers. *Crit Rev Biochem Mol Biol* 49(5):426–437. <https://doi.org/10.3109/10409238.2014.953626>
- Rouviere PE, De Las PA, Meccas J, Lu CZ, Rudd KE, Gross CA (1995) *rpoE*, the gene encoding the second heat-shock sigma factor, sigma E in *Escherichia coli*. *Embo J* 14(5):1032–1042
- Roux M, Coves J (2002) The iron-containing superoxide dismutase of *Ralstonia metallidurans* CH34. *FEMS Microbiol Lett* 210(1):129–133
- Saier MH Jr, Tam R, Reizer A, Reizer J (1994) Two novel families of bacterial membrane proteins concerned with nodulation, cell division and transport. *Mol Microbiol* 11:841–847
- Sankar P, Lee JH, Shanmugam KT (1985) Cloning of hydrogenase genes and fine-structure analysis of an operon essential for H<sub>2</sub> metabolism in *Escherichia coli*. *J Bacteriol* 162(1):353–360
- Sankaran B, Bonnett SA, Shah K, Gabriel S, Reddy R, Schimmel P, Rodionov DA, de Crécy-Lagard V, Helmann JD, Iwata-Reuyl D, Swairjo MA (2009) Zinc-independent folate biosynthesis: genetic, biochemical, and structural investigations reveal new metal dependence for GTP cyclohydrolase IB. *J Bacteriol* 191:6936–6949
- Sarkar P, Sardesai AA, Murakami KS, Chatterji D (2013) Inactivation of the bacterial RNA polymerase due to acquisition of secondary structure by the omega subunit. *J Biol Chem* 288(35):25076–25087. <https://doi.org/10.1074/jbc.M113.468520>
- Schauer K, Gouget B, Carriere M, Labigne A, de Reuse H (2007) Novel nickel transport mechanism across the bacterial outer membrane energized by the TonB/ExbB/ExbD machinery. *Mol Microbiol* 63(4):1054–1068
- Schauer K, Rodionov DA, de Reuse H (2008) New substrates for TonB-dependent transport: do we only see the ‘tip of the iceberg’? *Trends Biochem Sci* 33(7):330–338
- Scherer J, Nies DH (2009) CzcP is a novel efflux system contributing to transition metal resistance in *Cupriavidus metallidurans* CH34. *Mol Microbiol* 73(4):601–621. <https://doi.org/10.1111/j.1365-2958.2009.06792.x>
- Schmidt C, Schwarzenberger C, Grosse C, Nies DH (2014) FurC regulates expression of *zupT* for the central zinc importer ZupT of *Cupriavidus metallidurans*. *J Bacteriol* 196:3461–3471

- Schulte M, Blake D, Hoehler T, McCollom T (2006) Serpentinization and its implications for life on the early Earth and Mars. *Astrobiology* 6(2):364–376. <https://doi.org/10.1089/ast.2006.6.364>
- Schulz V, Schmidt-Vogler C, Strohmeier P, Weber S, Kleemann D, Nies DH, Herzberg M (2021) Behind the shield of Czc: ZntR controls expression of the gene for the zinc-exporting P-type ATPase ZntA in *Cupriavidus metallidurans*. *J Bacteriol* 203(11):e00052–e00021
- Seeger MA, Schiefner A, Eicher T, Verrey F, Diederichs K, Pos KM (2006) Structural asymmetry of AcrB trimer suggests a peristaltic pump mechanism. *Science* 313(5791):1295–1298
- Shin JH, Oh SY, Kim SJ, Roe JH (2007) The zinc-responsive regulator Zur controls a zinc uptake system and some ribosomal proteins in *Streptomyces coelicolor* A3(2). *J Bacteriol* 189(11):4070–4077
- Siche S, Neubauer O, Hebbeln P, Eitinger T (2010) A bipartite S unit of an ECF-type cobalt transporter. *Res Microbiol* 161(10):824–829. <https://doi.org/10.1016/j.resmic.2010.09.010>
- Sleep NH, Meibom A, Fridriksson T, Coleman RG, Bird DK (2004) H<sub>2</sub>-rich fluids from serpentinization: geochemical and biotic implications. *Proc Natl Acad Sci U S A* 101:12818–12823
- Spitzer J (2011) From water and ions to crowded biomacromolecules: in vivo structuring of a prokaryotic cell. *Microbiol Mol Biol R* 75(3):491–506. <https://doi.org/10.1128/Mmbr.00010-11>
- Spitzer J, Poolman B (2009) The role of biomacromolecular crowding, ionic strength, and physicochemical gradients in the complexities of life's emergence. *Microbiol Mol Biol Rev* 73(2):371–388. <https://doi.org/10.1128/mmbr.00010-09>
- Staron A, Sofia HJ, Dietrich S, Ulrich LE, Liesegang H, Mascher T (2009) The third pillar of bacterial signal transduction: classification of the extracytoplasmic function (ECF) sigma factor protein family. *Mol Microbiol* 74(3):557–581. <https://doi.org/10.1111/j.1365-2958.2009.06870.x>
- Su CC, Long F, Zimmermann MT, Rajashankar KR, Jernigan RL, Yu EW (2011) Crystal structure of the CusBA heavy-metal efflux complex of *Escherichia coli*. *Nature* 470:558–563. <https://doi.org/10.1038/nature09743>
- Svetlov V, Nudler E (2013) Basic mechanism of transcription by RNA polymerase II. *Biochim Biophys Acta* 1829(1):20–28. <https://doi.org/10.1016/j.bbagr.2012.08.009>
- Sydor AM, Liu J, Zamble DB (2011) Effects of metal on the biochemical properties of *Helicobacter pylori* HypB, a maturation factor of [NiFe]-hydrogenase and urease. *J Bacteriol* 193(6):1359–1368. <https://doi.org/10.1128/jb.01333-10>
- Sydor AM, Jost M, Ryan KS, Turo KE, Douglas CD, Drennan CL, Zamble DB (2013) Metal binding properties of *Escherichia coli* YjiA, a member of the metal homeostasis-associated COG0523 family of GTPases. *Biochemist* 52(10):1788–1801. <https://doi.org/10.1021/Bi301600z>
- Sydor AM, Lebrette H, Ariyakumaran R, Cavazza C, Zamble DB (2014) Relationship between Ni (II) and Zn(II) coordination and nucleotide binding by the *Helicobacter pylori* [NiFe]-hydrogenase and urease maturation factor HypB. *J Biol Chem* 289(7):3828–3841. <https://doi.org/10.1074/jbc.M113.502781>
- Tan KM, Sather A, Robertson JL, Moy S, Roux B, Joachimiak A (2009) Structure and electrostatic property of cytoplasmic domain of ZntB transporter. *Protein Sci* 18(10):2043–2052. <https://doi.org/10.1002/pro.215>
- Taudte N, Grass G (2010) Point mutations change specificity and kinetics of metal uptake by ZupT from *Escherichia coli*. *Biometals* 23(4):643–656. <https://doi.org/10.1007/s10534-010-9319-z>
- Thieme D, Neubauer P, Nies DH, Grass G (2008) Sandwich hybridization assay for sensitive detection of dynamic changes in mRNA transcript levels in crude *Escherichia coli* cell extracts in response to copper ions. *Appl Environ Microbiol* 74(24):7463–7470. <https://doi.org/10.1128/aem.01370-08>
- Thorghersen MP, Downs DM (2007) Cobalt targets multiple metabolic processes in *Salmonella enterica*. *J Bacteriol* 189:7774–7781

- Tibazarwa C, Wuertz S, Mergeay M, Wyns L, van der Lelie D (2000) Regulation of the *cnr* cobalt and nickel resistance determinant of *Ralstonia eutropha* (*Alcaligenes eutrophus*) CH34. *J Bacteriol* 182(5):1399–1409
- Totley S, Harvie DR, Robinson NJ (2007) Understanding how cells allocate metals. In: Nies DH, Silver S (eds) *Molecular microbiology of heavy metals*, Microbiology monographs, vol 6. Springer-Verlag, Berlin, pp 3–36
- Trepreau J, Girard E, Maillard AP, de Rosny E, Petit-Haertlein I, Kahn R, Coves J (2011) Structural basis for metal sensing by CnrX. *J Mol Biol* 408(4):766–779. <https://doi.org/10.1016/j.jmb.2011.03.014>
- Trepreau J, Grosse C, Mouesca J-M, Sarret G, Girard E, Petit-Haertlein I, Kuennemann S, Desbourdes C, de Rosny E, Maillard AP, Nies DH, Coves J (2014) Metal sensing and signal transduction by CnrX from *Cupriavidus metallidurans* CH34: role of the only methionine assessed by a functional, spectroscopic, and theoretical study. *Metallomics* 6:263–273
- Tseng T-T, Gratwick KS, Kollman J, Park D, Nies DH, Goffeau A, Saier MHJ (1999) The RND superfamily: an ancient, ubiquitous and diverse family that includes human disease and development proteins. *J Mol Microbiol Biotechnol* 1:107–125
- van der Lelie D, Schwuchow T, Schwidetzky U, Wuertz S, Baeyens W, Mergeay M, Nies DH (1997) Two component regulatory system involved in transcriptional control of heavy metal homeostasis in *Alcaligenes eutrophus*. *Mol Microbiol* 23:493–503
- Van Houdt R, Monchy S, Leys N, Mergeay M (2009) New mobile genetic elements in *Cupriavidus metallidurans* CH34, their possible roles and occurrence in other bacteria. *Antonie Van Leeuwenhoek* 96(2):205–226. <https://doi.org/10.1007/s10482-009-9345-4>
- Van Houdt R, Monsieurs P, Mijndonckx K, Provoost A, Janssen A, Mergeay M, Leys N (2012) Variation in genomic islands contribute to genome plasticity in *Cupriavidus metallidurans*. *BMC Genomics* 13:111. <https://doi.org/10.1186/1471-2164-13-111>
- Van Houdt R, Provoost A, Van Assche A, Leys N, Lievens B, Mijndonckx K, Monsieurs P (2018) *Cupriavidus metallidurans* strains with different mobilomes and from distinct environments have comparable phenomes. *Genes-Basel* 9(10):ARTN 507. <https://doi.org/10.3390/genes9100507>
- Verstraeten N, Fauvart M, Versees W, Michiels J (2011) The universally conserved prokaryotic GTPases. *Microbiol Mol Biol Rev* 75(3):507–542. <https://doi.org/10.1128/MMBR.00009-11>
- Volentini SI, Farias RN, Rodriguez-Montelongo L, Rapisarda VA (2011) Cu(II)-reduction by *Escherichia coli* cells is dependent on respiratory chain components. *Biometals* 24(5): 827–835. <https://doi.org/10.1007/s10534-011-9436-3>
- von Rozycki T, Nies DH (2009) *Cupriavidus metallidurans*: evolution of a metal-resistant bacterium. *Antonie Van Leeuwenhoek* 96:115–139
- von Rozycki T, Nies DH, Saier MHJ (2005) Genomic analyses of transport proteins in *Ralstonia metallidurans*. *Comp Func Genom* 6:17–56
- Walderhaug M, Polarek J, Voelkner P, Daniel J, Hesse J, Altendorf K, Epstein W (1992) KdpD and KdpE, proteins that control expression of the *kdpABC* operon, are members of the two-component sensor-effector class of regulators. *J Bacteriol* 174:2152–2159
- Waldron KJ, Rutherford JC, Ford D, Robinson NJ (2009) Metalloproteins and metal sensing. *Nature* 460(7257):823–830. <https://doi.org/10.1038/nature08300>
- Wan Q, Ahmad MF, Fairman J, Gorzelle B, de la Fuente M, Dealwis C, Maguire ME (2011) X-ray crystallography and isothermal titration calorimetry studies of the *Salmonella* zinc transporter ZntB. *Structure* 19(5):700–710. <https://doi.org/10.1016/j.str.2011.02.011>
- Watanabe S, Kawashima T, Nishitani Y, Kanai T, Wada T, Inaba K, Atomi H, Imanaka T, Miki K (2015) Structural basis of a Ni acquisition cycle for [NiFe] hydrogenase by Ni-metallochaperone HypA and its enhancer. *Proc Natl Acad Sci U S A* 112(25):7701–7706. <https://doi.org/10.1073/pnas.1503102112>
- Weast RC (1984) *CRC handbook of chemistry and physics*, 64th edn. CRC Press, Boca Raton, FL
- Wei YN, Fu D (2005) Selective metal binding to a membrane-embedded aspartate in the *Escherichia coli* metal transporter YiiP (FieF). *J Biol Chem* 280(40):33716–33724

- Wiesemann N, Mohr J, Grosse C, Herzberg M, Hause G, Reith F, Nies DH (2013) Influence of copper resistance determinants on gold transformation by *Cupriavidus metallidurans* strain CH34. *J Bacteriol* 195:2298–2308. <https://doi.org/10.1128/JB.01951-12>
- Wiesemann N, Bütof L, Herzberg M, Hause G, Berthold L, Etschmann B, Brugger J, Martínéz-Criado G, Dobritzsch D, Baginski S, Reith F, Nies DH (2017) Synergistic toxicity of copper and gold compounds in *Cupriavidus metallidurans*. *Appl Environ Microbiol* 83(23):e01679–e01617. <https://doi.org/10.1128/AEM.01679-17>
- Williams JR, Morgan AG, Rouch DA, Brown NL, Lee BTO (1993) Copper-resistant enteric bacteria from United Kingdom and Australian piggeries. *Appl Environ Microbiol* 59(8): 2531–2537
- Wilson TH, Ding PZ (2001) Sodium-substrate cotransport in bacteria. *Biochim Biophys Acta* 1505(1):121–130
- Wolfram L, Eitinger T, Friedrich B (1991) Construction and properties of a triprotein containing the high-affinity nickel transporter of *Alcaligenes eutrophus*. *FEBS Lett* 283(1):109–112
- Worlock AJ, Smith RL (2002) ZntB is a novel Zn<sup>2+</sup> transporter in *Salmonella enterica* serovar typhimurium. *J Bacteriol* 184(16):4369–4373
- Wu FYH, Huang WJ, Sinclair RB, Powers L (1992) The structure of the zinc sites of *Escherichia coli* DNA-dependent RNA polymerase. *J Biol Chem* 267(35):25560–25567
- Xia W, Li HY, Sze KH, Sun HZ (2009) Structure of a nickel chaperone, HypA, from *Helicobacter pylori* reveals two distinct metal binding sites. *J Amer Chem Soc* 131(29):10031–10040. <https://doi.org/10.1021/ja900543y>
- Xia W, Li HY, Yang XM, Wong KB, Sun HZ (2012) Metallo-GTPase HypB from *Helicobacter pylori* and its interaction with nickel chaperone protein HypA. *J Biol Chem* 287(9):6753–6763. <https://doi.org/10.1074/jbc.M111.287581>
- Yamamoto K, Hirao K, Oshima T, Aiba H, Utsumi R, Ishihama A (2005) Functional characterization in vitro of all two-component signal transduction systems from *Escherichia coli*. *J Biol Chem* 280(2):1448–1456. <https://doi.org/10.1074/jbc.M410104200>
- Yang XM, Li HY, Cheng TF, Xia W, Lai YT, Sun HZ (2014) Nickel translocation between metallochaperones HypA and UreE in *Helicobacter pylori*. *Metallomics* 6(9):1731–1736. <https://doi.org/10.1039/c4mt00134f>
- Yang X, Li H, Lai TP, Sun H (2015) UreE-UreG complex facilitates nickel transfer and preactivates GTPase of UreG in *Helicobacter pylori*. *J Biol Chem* 290(20):12474–12485. <https://doi.org/10.1074/jbc.M114.632364>
- Yuen MH, Fong YH, Nim YS, Lau PH, Wong KB (2017) Structural insights into how GTP-dependent conformational changes in a metallochaperone UreG facilitate urease maturation. *Proc Natl Acad Sci U S A* 114(51):E10890–E10898. <https://doi.org/10.1073/pnas.1712658114>
- Zambelli B, Banaszak K, Merloni A, Kiliszek A, Rypniewski W, Ciurli S (2013) Selectivity of Ni(II) and Zn(II) binding to *Sporosarcina pasteurii* UreE, a metallochaperone in the urease assembly: a calorimetric and crystallographic study. *J Biol Inorg Chem* 18(8):1005–1017. <https://doi.org/10.1007/s00775-013-1049-6>
- Zambelli B, Berardi A, Martin-Diaconescu V, Mazzei L, Musiani F, Maroney MJ, Ciurli S (2014) Nickel binding properties of *Helicobacter pylori* UreF, an accessory protein in the nickel-based activation of urease. *J Biol Inorg Chem* 19(3):319–334. <https://doi.org/10.1007/s00775-013-1068-3>
- Ziani W, Maillard AP, Petit-Hartlein I, Garnier N, Crouzy S, Girard E, Coves J (2014) The X-ray structure of NecX from *Cupriavidus metallidurans* 31A illustrates potential dangers of detergent solubilization when generating and interpreting crystal structures of membrane proteins. *J Biol Chem* 289(45):31160–31172. <https://doi.org/10.1074/jbc.M114.586537>
- Zilberstein D, Agmon V, Schuldiner S, Padan E (1984) *Escherichia coli* intracellular pH, membrane potential, and cell growth. *J Bacteriol* 158:246–252